

Regd. No. C-8911

# INDIAN JOURNAL OF PHYSICS

VOL. 40

AND

PROCEEDINGS

OF THE

Indian Association for the Cultivation of Science, Vol. 49  
(*Edited in Collaboration with the Indian Physical Society*)

Secretary Board of Editors.  
INDIAN JOURNAL OF PHYSICS.

(With Four Plates).

Published by the Registrar, Indian Association for the Cultivation of Science,  
Jadavpur, Calcutta 32 and printed by Prakesh Chandra Chakroberty  
Eka Press, 204/1, B. T. Road, Calcutta

1966

## BOARD OF EDITORS

K. BANERJEE	S. R. KHASTGIR
G. N. BHATTACHARYA	D. S. KOTHARI
D. M. BOSE	B. D. NAG CHOUDHURI
S. N. BOSE	K. R. RAO
S. D. CHATTERJEE	R. RAMANNA
P. S. GILL	D. B. SINHA
B. N. SHIVASTAVA	S. C. SIRKAR
A. BOSE ( <i>Secretary</i> )	

## EDITORIAL COLLABORATORS

R. K. ASUNDI  
D. BASU  
J. N. BHAR  
V. G. BHIDE  
H. N. BOSE  
S. K. CHAKRABORTY  
J. S. CHATTERJEE  
K. DAS GUPTA  
N. N. DAS GUPTA  
J. DHAR  
A. K. DUTTA  
S. DUTTA MAZUMDAR  
C. S. GHOSH  
S. GHOSH  
S. N. GHOSH  
S. GUPTA  
D. N. KUNDU  
R. C. MAZUMDAR  
A. MOOKHERJEE  
Y. G. NAIK  
S. R. PALIT  
H. RAKSHIT  
A. SAHA  
VIKRAM A. SARABHAI  
A. K. SENGUPTA  
NAND LAL SINGH  
M. S. SINHA  
N. R. TAWDE  
P. VENKATESWARLU.



# INDIAN JOURNAL OF PHYSICS VOL. 40, 1966

## CONTENTS

### No. 1. January

	PAGE
1. Relaxation Technique as Applied to Electrical Network Problem of "Ring Distributor"—S. N. Dutta ... ..	1
2. Relaxation Method of Solving Electrical Network Problem of "Two Wire D.C. Transmission Lines"—S. N. Dutta ... ..	7
3. Intermolecular Potential of Krypton and Xenon on the Core Model—A. N. Roy and S. K. Deb ... ..	12
4. Deduction of Generalised Krichhoff's Laws from the Basic Principles of Electromagnetism—S. K. Mitra and T. Roy ... ..	19

#### LETTERS TO THE EDITOR—

1 On the Transfer of Electromagnetic Excitation Energy in Liquids—M. K. Machwe, J. Kishore and K. Gopala Krishnan ... ..	45
2. Study of Electron Affinity from Gaussian form Repulsion Term Potential Function for Polar Diatomic Molecules—S. P. Tandon, M. P. Bhutra and K. Tandon ... ..	49
BOOK REVIEW ... ..	52

### No. 2. February

5. The Near Ultraviolet Absorption Spectra of Ortho, Meta-, and Para-Fluoroanilines—M. A. Shashidhar and K. Sruyanarayana Rao ... ..	53
6. A Generalised Direct Exchange Interaction: Application to Heusler Alloys—Narendra Kumar and K. P. Sinha... ..	62
7. An Improved Method of Measuring Magnetic Anisotropy of Paramagnetic Crystals from 303°K to 68°K, and New Data of Some Co <sup>2+</sup> and Fe <sup>2+</sup> Tutton Salts—Debjani Guha Thakurta and Deepti Mukhopadhyay ... ..	69
8. Probability-Distribution of States in Rational Thermodynamics—M. Dutta ... ..	85

#### LETTERS TO THE EDITOR—

3. X-Ray Measurements of Stacking Faults in $\alpha$ -AgMn Alloys—S. P. Sen Gupta and K. N. Goswami ... ..	97
BOOK REVIEW ... ..	100

## No. 3. March

	PAGE
9. Studies on the Dielectric Loss at 7.7 mm. Microwaves of some Substituted Benzene and Naphthalene Compounds—(Miss) B. Sinha, S. B. Roy and G. S. Kastha ... ..	101
10. Different Classes of Solar and Solar-Terrestrial Events in Relation to the Phase of the Solar Cycle—D. Basu and M. K. Das Gupta ...	117
11. Covalency Reduction Factors in the Case of Tetrahedral Complexes R. Rai and R. K. Mukherjee ... ..	126
12. Dynamics of the Extensional Vibration of a Free-Free Bar—S. K. Ghosh and Sunil Kumar Banerjee ... ..	135
13. Light Absorption of $\text{Cu}^{++}$ Ion in Crystal—A. Mookherji and N. S. Chhonkar ... ..	143

## LETTERS TO THE EDITOR—

4. Some Probe Data of Duoplasmatron Plasma—D. K. Bose, N. K. Majumdar and S. N. Sengupta ... ..	147
5. Determination of Ionization Potential of Gd and Ho by Surface Ionization Method—S. D. Dey and S. B. Karmohapatro ...	151
BOOK REVIEW ... ..	154

## No. 4. April

14. On the Theory of Specific Heat of Liquids—S. C. Misra ...	157
15. Relaxation Method Applied to Network Problem Involved in Electric Railway System—S. N. Dutta ... ..	163
16. L Subshell Ratios of E2 Transitions in Deformed Rare Earth Nuclei—W. H. Brantley, S. C. Pancholi and J. H. Hamilton ...	169
17. A-Binding Energy of Hypernuclei. (I)—A. K. Dutta, D. Banerjee and P. Ganguly ... ..	178
18. Non-Degenerate Statistical Approach to the Binding Energy of Nuclei and of $\Lambda$ -Hypernuclei (II)—A. K. Dutta ... ..	181
19. Dielectric Absorption of 3.14 cm Microwaves in some Polar Liquids—Part II. Substituted Halo-Benzene and Naphthalene—J. Bhattacharyya, S. B. Roy and G. S. Kastha ... ..	187
20. Dynamics of Vibration of a Cantilever under Lateral Impact of an Elastic Load (General Theory—Part I)—B. B. Banerjee ...	198
21. Dynamics of Vibration of a Cantilever under Lateral Impact of an Elastic Load (General Theory—Part II)—B. B. Banerjee ...	208
BOOK REVIEW ... ..	214

## No. 5. May

22. Dynamics of Vibration of a Cantilever under Lateral Impact of an Elastic Load—(Part II) General Theory—B. B. Banerjee ...	215
---	-----

# Contents

iii

	PAGE
23. Dynamics of Vibration of a Cantilever under Lateral Impact of an Elastic Load —(Part IV) Energy of the Bar—B. B. Banerjee ...	221
24. Dielectric Constant and Interatomic Forces—C. M. Kachhava and S. C. Saxena ...	252
25. Electron Collision with Caesium Atom—(Mrs.) R. Basu and N. C. Sil ...	233
26. Influence of Limits Set to Lateral Displacement on the Determination of mean Multiple Coulomb Scattering in Nuclear Emulsions —P. K. Aditya ...	238
27. Locking Phenomena in Injection Synchronised Pulsed Oscillators —B. N. Biswas and G. Dutta ...	244
28. Dielectric Function of a Degenerate Electron Gas in the Presence of a Steady Magnetic Field—P. Misra ...	253
29. Variational Treatment of Slow Electron Scattering by a Helium Atom—S. N. Banerjee, R. Jha and N. C. Sil ...	258

## LETTER TO THE EDITOR—

6. Wigner Quarks—T. Roy ...	265
7. X-Ray Study of Nickel Biguanide Chloride $[Ni((C_2N_6N_7) Cl)_2 \cdot 2H_2O]$ —S. K. Roy and S. C. Chakraborty ...	267
8. Stationary Spherically Symmetric Dust Distribution in a Steady State Universe—Asit Banerjee ...	269
9. X-Ray Study of <i>p</i> -Aniside—M. Y. Khan and Y. Misra ...	271
10. Gruneisen Constant, Thermal Expansion of Crystals and the Law of Interatomic Forces—C. M. Kachhava and S. C. Saxena ...	273
BOOK REVIEW ...	278

## No. 6 June

30. Reciprocity Equations for Isotropic Opalescent Scattering Media' —S. P. Tewarson ...	281
31. The 60 MeV Grenoble Isochronous Cyclotron—N. C. Sen ...	294
32. Electrolytic Effect on a Current Carrying Conductor—G. P. Bhatnagar, M. S. Gaur and V. S. Dubey ...	303
33. Luminescence Spectra of Benzyl Acetate in the Solid State at Low Temperatures—S. C. Bag ...	133
34. Molecular Polarizability and Absolute Raman Intensities of Modes in Mercury Dicyanide and Mean Amplitudes of Vibration in Linear Dicyanides—G. Nagarajan ...	319
35. Low Energy Scattering of Electron by Atomic Potential with a Long-Range Tail—S. B. Gupta and N. C. Sil ...	333
36. Electronic Energy States in one Dimensional Crystals—C. L. Roy ...	345
37. Influence of $^3He$ on the Lambda Temperature—D. G. Kapadnis ...	355

## LETTERS TO THE EDITOR—

6. Applications of the Non-Degenerate Statistical Relation to Binding Energy Characteristics in Nuclei—A. K. Dutta ... 362

## BOOK REVIEW 365

## No. 7. July

38. On the Elastic Scattering Cross Sections of Gamma Rays from Different Elements—M. Singh, S. Anand and B. S. Sood ... 367
39. Elementary Investigations of Polarization Characteristics, Electron Number Density and Electron Collisional Frequency of Down-Coming Radio-Waves at Oblique Incidence—S. R. Khastgir and Y. S. N. Murty ... 373
40. Scattering of the Radiation Field of a Loop Antenna by a Conducting Cylinder Immersed in a Cold Plasma—T. D. Shockley and C. R. Haden ... 393
41. On the Measurement of Equivalent Focal Length of Telescope Lenses—J. Prasad and M. S. R. S. Sarma ... 398
42. Dimerization in Polar Gases—A. N. Roy and A. Das Gupta ... 404
43. On the Raman and Infrared Spectra of Benzyl Acetate—S. Chattopadhyay and D. K. Mukherjee ... 409
44. On the Raman Spectra of Dilute Solutions of Para- and Metachlorotoluene—S. K. Nandy ... 415
45. Development of Neon Tube Hodoscope Chamber as a Detector of Ionising Particles—B. K. Bandyopadhyay, Subhra Bhattacharya and R. L. Sengupta ... 419
46. On a New Distribution Formula for Molecules of Real Gases and for Ions of Strong Electrolytes in Solution—M. Dutta ... 422
47. Lifetimes of  $2^1$  and  $4^1$  States of Dy-160—K. M. M. S. Ayyangar, V. Lakshminarayana and Swami Jnanananda ... 432

## No. 8 August

48. Rectifier action of a Gas Discharge and its Dependence on the V-I Characteristics in Forward and the Reverse Direction—V. T. Chiplonkar and N. M. A. Kukshiwal ... 344
49. Transient Heat Conduction in a Finite Wedge—K. C. Sabherwal ... 448
50. A Study of Thermodynamic Behaviour of Imperfect Gases Assuming Association—S. P. Pal ... 451
51. A Simple Method of Finding Principal Ionic Susceptibilities of Crystals—J. K. Ghose ... 457
52. Non-Analytic Spinor Representation of 4-Dimensional Lorentz Transformation—N. N. Ghosh ... 471

# Contents

v

	PAGE
53. A Photochemical Model of the Martian Atmosphere—S. N. Ghosh and A. Sharma ... ..	475

## LETTERS TO THE EDITOR—

12. Notes on High Voltage Thyatron Pulsar and on Filling Gas for Neon Tube Hodoscope Chamber—B. K. Bandyopadhyay and Subhra Bhattacharya ... ..	487
13. Elastic Scattering of Electrons by Helium Atom in Ochkur Approximation—S. N. Banerjee, R. Jha and N. C. Sil ... ..	480
14. Elastic and Inelastic Scattering of Electrons by Atomic Hydrogen in Ochkur Approximation—R. Jha, S. N. Banerjee and N. C. Sil ... ..	491
15. An X-Ray Study of Chakrasine Iodine—S. C. Biswas and S. K. Talapatra ... ..	492
16. Magnetic Susceptibility of Graphite Along Directions in the Basal Plane—Miss D. Das ... ..	493

## No. 9 September

54. The Visible Absorption Spectrum of the SnS Molecule—R. Yamdagni and M. M. Joshi ... ..	495
55. Coherent Reception using Carrier Lock and Sideband Lock Techniques (Part I)—N. B. Chakrabarti and A. K. Dutta ... ..	501
56. On the Magnetic Susceptibility of Pure and Impure Copper Metal—A. V. Subrahmanyam ... ..	527
57. Counter/Frequency Meter—S. S. Agarwal and P. S. Gill ... ..	534

## LETTERS TO THE EDITOR—

17. Fluctuations and Thermal Conductivity of CO <sub>2</sub> in the Critical Region—A. K. Barua and T. K. Rai Dastidar ... ..	541
---	-----

## No. 10. October

58. Effects of Polarisation on the Elastic Electron Scattering by Helium Atom—R. Jha, S. N. Banerjee and N. C. Sil ... ..	543
59. Ligand Field Theory of Trigonal Distorted Octahedral Ni <sup>2+</sup> Salts—B. D. Bhattacharyya and Manju Majumdar ... ..	549
60. Validity of the Generalized Reciprocity Equation Involving Circular Polarization—S. P. Tewarson ... ..	562
61. Simple Properties of Crystals and Reststrahlen Frequency—C. M. Kachhava and S. C. Saxena ... ..	567
62. Crystallographic Data for Complex Copper Lutidine Chloride—T. Ratho and Mrs. M. Krishnaswamy ... ..	576

	PAGE
63. Relaxation Method of Solving the Circuit of an Induction Motor with a Phase Advancer—S. N. Dutta ... ..	581
LETTERS TO THE EDITOR—	
18. On a Hole Theory of Liquids—S. C. Misra ... ..	589
<b>No. 11 November</b>	
64. Relaxation Technique as Applied to Wheatstone Bridge Network Problem—S. N. Dutta ... ..	591
65. Measurement of Thermal Conductivity of Gases using Thermal Diffusion Column : Neon—V. K. Saxena, M. P. Saxena and S. C. Saxena ... ..	597
66. Light-Scattering Studies in Solutions of Acacia Catechuic Acid—J. N. Chakravorty ... ..	605
67. The Study of the Vibration of a Cantilever under Lateral Impact of an Elastic Load, Part V (Experiment)—B. B. Banerjee ...	609
68. A New Laboratory Model Harmonic Analyser—G. Lakshman and Syed Ziauddin ... ..	617
69. S-Wave Neutron Strength Function and the Optical Model with Volume and Surface Absorption—Chhaya Ganguly and N. C. Sil ...	623
LETTERS TO THE EDITOR—	
19. Asymmetrical Raman Scattering by Water and Sulphuric Acid—N. Rajeswar Rao and K. V. Ramanaiah ... ..	627
20. Influence of Inter-Electrode Separation in High Frequency Titration—I. N. Chakravorty ... ..	630
21. On a Conditional Aspect of the J-Phenomenon in X-Rays—H. K. Pal ... ..	633
BOOK REVIEW ... ..	636
<b>No. 2. December</b>	
70. Electronic Energy-States of One-Dimensional Mixed Crystals—C. L. Roy ... ..	639
71. Phase Following behavior of an Automatic Phase Control Circuit with Respect to a Signal in Presence of a Random Noise—B. N. Biswas ... ..	648
LETTERS TO THE EDITOR—	
22. Study of Light Absorption in 8-Hydroxy-1-Methyl Quinolinium Hydroxide Anhydro-Salt in State of Solution—S. P. Tandon, K. Tandon and J. P. Saxena ... ..	669

# Contents

vii

## PAGE

23. A Note on the Abnormal Magnetic behaviour of a Tetrahedral Copper (II) Compound at Low Temperature—S. Lahiry, D. Ghosh (née Guha Thakurta) and D. Mukhopadhyay ... ..	671
24. Anomalous Magnetic Behaviour of Copper Acetate Monohydrate—R. N. Bagchi, P. Sengupta ... ..	675
25. $r$ -Centroids and Frank-Condon Factors for the Bands $A_2\Sigma-X^2\pi$ System of PO Molecule—S. Sankaranarayanan ... ..	678
26. Preliminary Crystal Structure Data of some Amino Acids Derivatives and Metal Complexes—N. N. Saha, S. K. Majumdar, S. C. Bhattacharya, P. N. Roy, R. Handa and S. Guha ... ..	681
27. Magnetic Properties of $\alpha$ -Silicon Carbide Crystals—D. Das ... ..	684
BOOK REVIEW ... ..	687

# AUTHOR INDEX

AUTHOR	SUBJECT	PAGE
Aditya, P. K.	Influence of limits set to lateral displacement on the determination of mean multiple Coulomb scattering in nuclear emulsions ...	238
Anand, S.	See Singh, M.	
Agarwal, S. S. and Gill, P. S.	Counter/frequency meter ...	534
Ayyangar, K. M. M. S., Lakshminarayana, V. and Jnanananda, Swami	Lifetimes of $2^+$ and $4^+$ states of Dy-160...	432
Bag, S. C.	Luminescence spectra of benzyl acetate in the solid state at low temperatures	313
Bagchi, R. N. and Sengupta, P.	Anomalous magnetic behaviour of copper acetate monohydrate (L) ...	675
Bandyopadhyay, B. K. and Bhattacharya, Subhra	Notes on high voltage thyratron pulser and on filling gas for neon tube hodoscope chamber (L) ...	487
Bandyopadhyay, B. K., Bhattacharya, Subhra and Sengupta, R. L.	Development of neon tube hodoscope chamber as a detector of ionising particles ...	419
Banerjee, Asit	Stationary spherically symmetric dust distribution in a steady state universe (L) ...	269
Banerjee, B. B.	. Dynamics of vibration of a cantilever under lateral impact of an elastic load (General theory—Part I) ...	198
	. Dynamics of vibration of a cantilever under lateral impact of an elastic load (General theory—Part II) ...	208
	. Dynamics of vibration of a cantilever under lateral impact of an elastic load —(Part III) General theory ...	215
	.. Dynamics of vibration of a cantilever under lateral impact of an elastic load —(Part IV) energy of the bar ...	221
	.. The study of the dynamics of vibration of a cantilever under lateral impact of an elastic load. Part V (Experiment) ...	609
Banerjee, D.	.. See Dutta, A. K.	



AUTHOR	SUBJECT	PAGE
Banerjee, S. K.	See Ghosh, S. K.	
Banerjee, S. N., Jha, R. and Sil, N. C.	Variational treatment of slow electron scattering by a helium atom ... Elastic scattering of electrons by helium atom in Ochkur approximation (L) ...	258 489
Banerjee, S. N.	See Jha, R.	
Barna, A. K. and Rai	Fluctuations and thermal conductivity of CO <sub>2</sub> in the critical region (L) ...	541
Dastidar, T. K.		
Basu, D. and Das Gupta, M. K.	Different classes of solar and solar- terrestrial events in relation to the phase of the solar cycle ...	117
Basu, R. (Mrs.) and Sil, N. C.	Electron collision with Caesium atom ...	233
Bhattacharyya, B. D. and Majumdar, Manju	Ligand field theory of trigonally dis- torted octahedral Ni <sup>2+</sup> salts ...	549
Bhatnagar, G. P., Gaur, M. S. and Dubey, V. S.	Electrolytic effect on a current carrying conductor ...	303
Bhattacharyya, J., Roy, S. B. and Kashta, G. S.	Dielectric absorption of 3.14 cm micro- waves in some polar liquids—Part II substituted halo-benzenes and naph- thalene ...	187
Bhattacharya, S. C.	See Saha, N. N.	
Bhattacharya, Subhra	See Bandyopadhyaya, B. K.	
Biswas, B. N.	Phase following behaviour of an auto- matics phase control circuit with res- pect to a signal in presence of a random noise ...	648
Biswas, B. N. and Dutta, G.	Locking phenomena in injection syn- chronised pulsed oscillators ...	244
Biswas, S. C. and Talapatra, S. K.	An X-ray study of chaksine iodine (L) ...	492
Bhutra, M. P.	See Tandon, S. P.	
Rose, D. K., Majumdar, N. K. and Sengupta, S. N.	Some probe data of duoplasmatron plasma (L) ...	147
Brantley, W. H., Pancholi S. C. and Hamilton, J. H.	L subshell ratios of E2 transitions deformed rare earth nuclei ...	169
Chakraborty, J. N.	Light-scattering studies in solutions of acacia catechuic acid ... Influence of inter-electrode separation in high frequency titration (L) ...	605 630
Chakrabarti, N. B. and Dutta, A. K.	Coherent reception using carrier lock and sideband lock techniques (Part I) ...	501
Chakraborty, S. C.	See Roy, S. K.	
Chattopadhyay, S. and Mukherjee, D. K.	On the Raman and infrared spectra of benzyl acetate ...	409

AUTHOR	SUBJECT	PAGE
Chiplonkar, V. T. and Kukshiwala, N. M. A.	Rectifier action of a gas discharge and its dependence on the V-I character- istics in the forward and the reverse direction ... ..	443
Chhonkar, N. S.	See Mookherji, A.	
Das, D.	Magnetic properties of $\alpha$ -silicon carbide crystal (L) ... ..	684
	Magnetic susceptibility of graphite along directions in basal plane (L) ... ..	493
Das Gupta, A.	See Roy, A. N.	
Das Gupta, M. K.	See Basu, D.	
Dutta, A. K.	See Chakrabarti, N. B.	
Deb, S. K.	See Roy, A. N.	
Dey, S. D. and Karmohapatro, S. B.	Determination of ionization potential of Gd and Ho by surface ionization method (L) ... ..	151
Dutta, A. K., Banerjee, D. and Ganguly, P.	$\Lambda$ -binding energies of hypernuclei (I) ... ..	178
Dutta, A. K.	Non-degenerate statistical approach to the binding energy of nuclei and of $\Lambda$ -hypernuclei (II) ... ..	181
	Application of the non-degenerate statis- tical relation to binding energy cha- racteristics in nuclei (L) ... ..	362
Dutta, G.	See Biswas, B. N.	
Dutta, M.	On probability-distribution of states in rational thermodynamics ... ..	85
	On a new distribution formula for mole- cules of real gases and for ions of strong electrolytes in solution ... ..	422
Dutta, S. N.	Relaxation technique as applied to electrical network problem of "Ring Distribution" ... ..	1
	Relaxation method of solving electrical network problem of "Two wire D.C. transmission lines" ... ..	7
	Relaxation method applied to network problem involved in electric railway system ... ..	163
	Relaxation method of solving the circuit of an induction motor with a phase advancer ... ..	581

AUTHOR	SUBJECT	PAGE
Dutta, S. N	Relaxation technique as applied to wheatstone bridge network problem...	591
Dubey, V. S.	See Bhatnagar, G. P.	
Ganguly, Chhaya and Sil, N. C.	S-wave neutron strength function and the optical model with volume and surface absorption ...	623
Ganguly, P.	.. See Dutta, A. K.	
Gaur, M. S.	.. See Bhatnagar, G. P.	
Ghosh, D. (née Guha Thakurta).	See Lahiry, S.	
Ghose, J. K.	. . A simple method of finding the principal ionic susceptibilities of crystal ...	457
Ghosh, N. N.	. . Non-analytic spinor representation of 4- dimensional Lorentz transformation ...	471
Ghosh, S. K. and Banerjee, S. K.	Dynamics of the extensional vibration of a free-free bar. ...	135
Ghosh, S. N. and Sharma, A.	. . A photochemical model of the Martian atmosphere ...	475
Gill, P. S.	. . See Agarwal, S. S.	
Gopala Krishnan, K.	. . See Machwe, M. K.	
Goswami, K. N.	. . See Sen Gupta, S. P.	
Guha, S.	. . See Saha, N. N.	
Guha Thakurta, Debjani and Mukhopadhyay, Deepti	An improved method of measuring magnetic anisotropy of paramagnetic crystals from 303°K to 68°K and new data of some Co <sup>2+</sup> and Fe <sup>2+</sup> tutton salts ...	69
Gupta, S. B. and Sil, N. C.	. Low-energy scattering of electron by atomic potential with a long-range tail ...	333
Haden, C. R.	. See Shockley, T. D.	
Hamilton, J. H.	. See Brantley, W. H.	
Handa, P. N.	. See Saha, N. N.	
Jha, R.	. See Banerjee, S. N.	
Jha, R., Banerjee, S. N. and Sil, N. C.	Effect of polarisation on the elastic electron scattering by helium atom ...	543
Jnanananda, Swami	.. See Ayyangar, K. M. M. S.	
Joshi, M. M.	. See Yamdagni, R.	
Kachhava, C. M. and Saxena, S. C.	Dielectric constant and interatomic forces ...	225
	Gruneisen constant, thermal expansion of crystals and the law of interatomic forces (L) ...	273

AUTHOR	SUBJECT	PAGE
Kachhava, C. M. and Saxena, S. C.	Simple properties of crystals and Resistahelen frequency ...	567
Kapadnis, D. G.	The influence of $^3\text{He}$ on the lambda temperature ...	355
Karmohapatro, S. B.	See Dey, S. D.	
Khastgir, S. R. and Murty, Y. S. N.	Experimental investigations on polarization characteristics, electrons number density and electrons collisional frequency of down-coming radio-waves at oblique incidence ...	37½
Khastha, G. S.	... See Sinha, B. (Miss)	
"	... See Bhattacharyya, J.	
Khan, M. Y. and Misra, Y.	... X-ray study of <i>p</i> -aniside (L) ...	271
Kishore, J.	... See Machwe, M. K.	
Krishnaswamy, (Mrs.) M.	.. See Ratho, T.	
Kushiwalu, N. M. A.	... See Chiplonkar, V. T.	
Kumar Narendra and Sinha, K. P.	A generalised direction exchange interaction : application to Heusler alloys	62
Lahiry, S., Ghosh, D. (née Guha Thakurta) and Mukhopadhyay, D	A note on the abnormal magnetic behaviour of a tetrahedral copper (II) compound at low temperature (L) ...	671
Lakshminarayana, V.	... See Ayyangar, K. M. M. S.	
Lakshman, G. and Ziauddin, Syed	A new laboratory model harmonic analyser ...	617
Machwe, M. K., Kishore, J. and Gopala Krishnan, K.	On the transfer of electronic excitation energy in liquids (L) . .	45
Majumdar, Manju	... See Bhattacharyya, B. D.	
Majumdar, N. K.	... See Bose, D. K.	
Mazumdar, S. K.	... See Saha, N. N.	
Misra, P.	. Dielectric function of a degenerate electron gas in the presence of a steady magnetic field ...	253
Misra, S. C.	. On a hole theory of liquids (L) ...	589
"	. On the theory of specific heat of liquids	157
Misra, Y.	.. See Khan, M. Y.	
Mitra, S. K. and Roy, T.	.. Deduction of generalised Krichhoff's laws from the basic principles of electromagnetism. ...	19
Mookerji, A. and Chhonkar, N. S.	Light absorption of $\text{Cu}^{++}$ ion in crystal...	143
Mukherjee, D. K.	... See Chattopadhyay, S.	
Mukherjee, R. K.	... See Rai, R.	
Mukhopadhyay, D.	... See Lahiry, S.	
Mukhopadhyay, Deepti	... See Guha Thakurta, Debjani	

AUTHOR	SUBJECT	PAGE
Murty, Y. S. N.	See Khastgir, S. R.	
Nagarajan, G.	Molecular polarizability and absolute Raman intensities of modes in mercury dicyanide and mean amplitudes of vibration in linear dicyanides ...	319
Nandy, S. K.	... On the Raman spectra of dilute solutions of para- and meta-chlorotoluene ...	415
Pal, H. K.	... On a conditional aspect of the J-phenomenon in X-rays (I) ...	633
Pal, S. P.	... A study of thermodynamic behaviour of imperfect gases assuming association ...	451
Pancholi, S. C.	... See Brantley, W. H.	
Prasad, J. and Sharma, M.S.R.S.	On the measurement of equivalent focal length of telescope lenses ...	308
Rai, R. and Mukherjee, R. K.	... Covalency reduction factors in the case of tetrahedral complexes ...	126
Rai Dastidar, T. K.	See Barua, A. K.	
Ramanaiah, K. V.	... See Rajeswara, Rao, N.	
Rajeswara, Rao, N. and Ramanaiah, K. V.	Asymmetrical Raman scattering by water and sulphuric acid (L) ...	627
Rao, Suryanarayana, K.	... See Shashidhar, M. A.	
Ratho, T. and Krishnaswamy, (Mrs.) M.	Crystallographic data for complex copper lutidine chloride ...	576
Roy, A. N. and Deb, S. K.	... Intermolecular potential of krypton and xenon on the core model ...	12
Roy, A. N. and Das Gupta, A.	... Dimerization in polar gases ...	404
Roy, C. L.	... Electronic energy states in one dimensional crystal ...	345
"	... Electronic energy-state of one-dimensional mixed crystal ...	639
Roy, P. N.	... See Saha, N. N.	
Roy, S. B.	... See Sinha, B. (Miss).	
"	... See Bhattacharyya, J.	
Roy, S. K. and Chakraborty, S.C.	An X-ray study of nickel biguanide chloride $[\text{Ni}(\text{C}_2\text{N}_5\text{N}_7)_2]\text{Cl}_2 \cdot 2\text{H}_2\text{O}$ (L) ...	267
Roy, T.	... See Mitra, S. K.	
"	... Wigner Quarks (L) ...	265
Sabherwal, K. C.	... Transient heat conduction in a finite ...	448
Saha, N. N., Mazumdar, S. K., Bhattacharya, S. C., Roy, P. N., Handa, R. and Guha, S.	Preliminary crystal structure data of some amino acids derivatives and metal complexes (I) ...	681
Saksena, M. P.	... See Saxena, V. K.	

AUTHOR	SUBJECT	PAGE
Sankaranarayanan, S.	$r$ -centroids and Frank-Condon factors for the bands $A \ ^2\Sigma-X \ ^2\pi$ system of PO molecule (L) ...	678
Saxena, J. P.	... See Tandon, S. P.	
Sarma, M. S. R. S.	... See Prasad, J.	
Saxena, S. C.	... See Kachhava, C. M.	
"	... See Saxena, V. K.	
Saxena, V. K., Saksena, M. P. and Saxena, S. C.	Measurement of thermal conductivity of gases using thermal diffusion column : neon ...	597
Sen, N. C.	The 60 Mev grenoble Isochronous Cyclotron ...	294
Sengupta, P.	... See Bagchi, R. N.	
Sengupta, S. N.	... See Bose, D. K.	
Sen Gupta, S. P. and Goswami, K. N.	X-ray measurements of stacking faults in $\alpha$ -AgMn alloys (L) ...	97
Sengupta, R. L.	... See Bandhopadhyay, B. K.	
Sharma, A.	... See Ghosh, S. N.	
Shashidhar, M. A. and Rao, Suryanarayana, K.	The near ultraviolet absorption spectra or ortho, meta-, and para- fluoro-anilines ...	53
Shockley, T. D. and Haden, C. R.	Scattering of the radiation field of a loop antenna by a conducting cylinder immersed in a cold plasma ...	393
Sil, N. C.	. See Basu R. (Mrs.) . See Gupta, S. B. . See Jha, R. . See Ganguly, Chhaya . See Banerjee, S. N.	
Singh, M., Anand, S. and Sood, B. S.	On the estimation of elastic scattering cross sections of gamma rays from different elements ...	367
Sinha, B. (Miss), Roy, S. B. and Kastha, G. S.	Studies on the dielectric loss at 7.7 mm. microwaves of some substituted benzene and naphthalene compounds ...	101
Sinha, K. P.	. See Kumar, Narendra	
Sood, B. S.	. See Singh, M.	
Subrahmanyam, A. V.	. On the magnetic susceptibility of pure and impure copper metal... ..	527
Talapatra, S. K.	. See Biswas, S. C.	
Tandon, K.	.. See Tandon, S. P.	

# *Author Index*

*xv*

AUTHOR	SUBJECT	PAGE
Tandon, S. P., Bhutra, M. P. and Tandon, K.	Study of electron affinity form Gaussian form repulsion term potential func- tion for polar diatomic molecules (L)	49
Tandon, S. P., Tandon, K. and Saxena, J. P.	Study of light absorption in 8-hydroxy- 1-methyl quinolinium hydroxide an- hydro-salt in state of solution (L) ...	669
Tewarson, S. P.	Reciprocity equations for isotropic opal- escent scattering media ...	281
	Validity of the generalized reciprocity equation involving circular polariza- tion ...	562
Yamdagni, R. and Joshi, M. M.	The visible absorption spectrum of the SnS molecule ...	495
Ziauddin, Syed	See Lakshman, G.	

# SUBJECT INDEX

SUBJECT	AUTHOR	PAGE
Absorption spectrum of the SnS molecule.—The visible ...	R. Yamdagni and M. M. Joshi ...	495
Automatic phase control circuit with respect to a signal in presence of a random noise.—Phase flowing behaviour of an ...	B. N. Biswas ...	648
A-Binding energies of hypernuclei (I)	A. K. Dutta, D. Banerjee and P. Ganguly ...	178
Binding energy of nuclei and of $\Lambda$ -hyper-nuclei (II).—Non-degenerate statistical approach to the ...	A. K. Dutta ...	181
Coherent reception using Carrier lock and sideband lock techniques.		
Part-I ...	N. B. Chakrabarti and A. K. Dutta ...	501
Counter/frequency meter ...	S. S. Agarwal and P. S. Gill ...	534
Covalency reduction factors in the case of tetrahedral complexes ...	R. Rai and R. K. Mukherjee ...	126
Crystal and reststrahlen frequency.—Simple properties of ...	C. M. Kachhava and S. C. Saxena ...	567
Crystallographic data for complex copper lutidine chloride ...	T. Ratho and Mrs. M. Krishnaswami ...	576
Crystal structure data of some amino acids derivatives and metal complexes.—Preliminary (I) ...	N. N. Saha, S. K. Majumdar, S. C. Bhattacharya, P. N. Roy, R. Handa and S. Guha ...	681
Dielectric absorption of 3.14 cm microwaves in some polar liquids—Part II substituted halo-benzenes and naphthalene ...	J. Bhattacharyya and S. B. Roy ...	187
Dielectric constant and interatomic forces ...	C. M. Kachhava and S. C. Saxena ...	225
Dielectric loss at 7.7 mm microwaves of some substituted benzene and naphthalene compounds.—Studies on the ...	B. Sinha, S. B. Roy and G. S. Kastha ...	101
Dielectric function of a degenerate electron gas in the presence of a steady magnetic field ...	P. Misra ...	253



# Subject Index

xvii

SUBJECT	AUTHOR	PAGE
Dimerization in polar gases ...	A. N. Roy and A. Das Gupta ...	404
Distribution formula for molecules of real gases and for ions of strong electrolytes in solution.—On a new	M. Dutta ...	422
Duoplasmatron plasma.—Some probe data of (L) ...	D. K. Bose, N. K. Majumdar and S. N. Sengupta ...	147
Elastic scattering cross section of Gamma rays from different elements.—On the estimation of ...	M. Singh, S. Anand and B. S. Sood ...	367
Elastic scattering of electrons by helium atom in Ochkur approximation (L) ...	S. N. Banerjee, R. Jha and N. C. Sil ...	489
Electrolytic effect on a current carrying conductor ...	G. P. Bhatnagar, M. S. Gaur and V. S. Dubey ...	303
Electron affinity form Gaussian form repulsion term potential function for polar diatomic molecules.—Study of (L) ...	S. P. Tandon, M. P. Bhutra and K. Tandon ...	49
Electron collision with caesium atom	(Mrs.) R. Basu and N. C. Sil ...	233
Electronic energy-states of one dimensional mixed crystals ...	C. L. Roy ...	639
Electronic energy states in one dimensional crystals ...	C. L. Roy ...	345
Extensional vibration of a free-free bar.—Dynamics of the ...	S. K. Ghose and S. K. Banerjee ...	135
Gas Discharge and its dependence on the V-I characteristics in the forward and the reverse direction.—Rectifier action of a ...	V. T. Chiplonkar and N. M. A. Kukshiwal ...	443
Generalised direction exchange interaction : application to Heusler alloys.—A ...	N. Kumar and K. P. Sinha ...	62
Generalised Krichhoff's laws from the basic principles of electromagnetism.—Deduction of ...	S. K. Mitra and T. Roy ...	19
Generalised reciprocity equation involving circular polarization.—Validity of the ...	S. P. Tewarson ...	562

SUBJECT	AUTHOR	PAGE
Grüneisen constant, thermal expansion of crystals and the law of interatomic forces (L) ...	C. M. Kachhava and S. C. Saxena	273
Harmonic analyser.—A new laboratory model ...	G. Lashman and Syed Ziauddin	617
Hole theory of liquids.—On a (L) ...	S. C. Misra	589
Influence of $^3\text{He}$ on the lambda temperature.—The ...	D. G. Kapadnis	355
Inter-electrode separation in high frequency titration.—Influence of (L) ...	J. N. Chakravorty	630
Intermolecular potential of krypton and xenon on the core model ...	A. N. Roy and S. K. Deb	12
Ionization potential of Gd and Ho by surface ionization method.—Determination of (L) ...	S. D. Dey and S. B. Karmohapatro	151
Isochronous electron.—The 60 Mev Grenoble ...	N. C. Sen	294
J-phenomenon in X-rays.—On a conditional aspects of the (L) ...	H. K. Pal	633
Lifetime of $2^+$ and $4^+$ states of Dy-160 ...	K. M. M. S. Ayyangar, V. Lakshminarayana and Swami Jnanananda	432
Ligand field theory of the trigonally distorted octahedral $\text{Ni}^{+2}$ salts ...	B. D. Bhattacharyya and Manju Majumdar	549
Light absorption in 8-hydroxy-1-methyl quinolinium hydroxide anhydro-salt in state of solution.—Study of (L) ...	S. P. Tandon, K. Tandon, and J. P. Saxena	669
Light absorption of $\text{Cu}^{+}$ ion in crystal ...	A. Mookherji and N. S. Chhonkar	143
Light scattering studies in solutions of acacia catechuic acid ...	J. N. Chakravorty	605
Limits set to lateral displacement on the determination of mean multiple Coulomb scattering in nuclear emulsions.—Influence of ...	P. K. Aditya	238
Locking phenomena injection synchronised pulsed oscillators...	B. N. Biswas and G. Dutta	244
L subshell ratios of E2 transitions in deformed rare earth nuclei ...	W. H. Brantley, S. C. Pandhori and J. H. Hamilton	169

# Subject Index

xix

SUBJECT	AUTHOR	PAGE
Luminescence spectra of benzyl acetate in the solid state at low temperatures ...	S. C. Bag ...	313
Magnetic anisotropy of paramagnetic crystals from 303°K to 68°K and new data of some $\text{Co}^{2+}$ and $\text{Fe}^{2+}$ tutton salts.—An improved method of measuring ...	D. Guha Thakurta and D. Mukhopadhyay ...	69
Magnetic behaviour of a tetrahedral copper (II) compound at low temperature.—A note on the abnormal (L) ...	S. Lahiry, D. Ghose (née Guha Thakurta) and D. Mukhopadhyay	671
Magnetic behaviour of copper acetate monohydrate.—Anomalous (L) ...	R. N. Bagchi and P. Sengupta ...	675
Magnetic properties of $\alpha$ -silicon carbide crystal (L) ...	D. Das ...	684
Magnetic susceptibility of graphite along direction in the basal plane (L) ...	D. Das ...	493
Magnetic susceptibility of pure and impure copper metal.—On the ...	A. V. Subrahmanyam ...	527
Measurement of equivalent focal length of telescope lenses.—On the ...	J. Prasad and M. S. R. S. Sarma ...	398
Molecular polarizability and absolute Raman intensities of $\Sigma_g^+$ modes in mercury dicyanide and mean amplitudes of vibration in linear dicyanides ...	G. Nagarajan ...	319
Non-analytic spinor representation of 4-dimensional Lorentz transformation ...	N. N. Ghosh ...	471
Non-degenerate statistical relation to binding energy characteristics in nuclei.—Application of the (L) ...	A. K. Dutta ...	362
Neon tube hodoscope chamber as a detector of ionising particles.—Development of ...	B. K. Bandhopadhyay, Subhra Bhattacharya and R. L. Sengupta...	419
Photochemical model of the martian atmosphere.—A ...	S. N. Ghosh and A. Sharma ...	475

SUBJECT	AUTHOR	PAGE
Polarisation on the elastic electron scattering by helium atom.—Effect of ...	Sharma ... R. Jha, S. N. Banerjee and N. C. Sil ...	... 543
Polarization characteristics, electron number density and electron collisional frequency of down-coming radiowaves at oblique incidence.—Experimental investigations on	S. R. Khastgir and Y. S. M. Murty	373
Principal ionic susceptibilities of crystals.—A simple method of finding the ...	J. K. Ghose ..	457
Probability-distribution of states in rational thermodynamics.—On	M. Dutta ..	85
r-Centroids and Frank-Condon factors for the bands $A^2\Sigma-X^2\Pi$ system of Po molecule	S. Sankaranarayan ..	578
Raman and infrared spectra of benzyl acetate.—On the ...	S. Chattopadhyay and D. K. Mukherjee ..	409
Raman scattering by water and sulphuric acid.—Asymmetrical (L) ...	N. Rajeswara Rao and K. V. Ramanaiah ..	627
Raman spectra of dilute solutions of para- and metachlorotoluene.—On the ...	S. K. Nandy .	415
Reciprocity equations for isotropic opalescent scattering media	S. P. Tewarson .	281
Relaxation method applied to network problem involved in electric railway system	S. N. Dutta .	163
Relaxation method of solving electrical network problem of "Two wire D.C. Transmission Lines"	S. N. Dutta .	
Relaxation method of solving the circuit of an induction motor with a phase advancer	S. N. Dutta .	581
Relaxation technique as applied to electrical network problem of 'Ring distributor'	S. N. Dutta .	1
Relaxation technique as applied to wheatstone bridge network problem	S. N. Dutta .	591

# Subject Index

xxi

SUBJECT	AUTHOR	PAGE
Scattering of electron by atomic potential with a long-range tail.—Low-energy ... ..	S. B. Gupta and N. C. Sil	333
Scattering of the radiation field of a loop antenna by a conducting cylinder immersed in a cold plasma	T. D. Shockley and C. R. Haden	303
Solar and solar-terrestrial events in relation to the phase of the solar cycle.—Different classes of	D. Basu and M. K. Das Gupta	117
Specific heat of liquids.—On the theory of ... ..	S. C. Misra	157
Stationary spherically symmetric dust distribution in a steady state universe (L) ... ..	Asit Banerjee	269
S-wave neutron strength function and the optical model with volume and surface absorption ... ..	Chhaya Ganguly and N. C. Sil	623
Thermal conductivity of gases using thermal diffusion column: neon.—Measurement of ... ..	V. K. Saxena, M. P. Saxena and S. C. Saxena	597
Thermal conductivity of CO <sub>2</sub> in the critical region.—Fluctuations and (L) ... ..	A. K. Barua and T. K. Rai Dastidar	541
Thermodynamic behaviour of imperfect gases assuming association.—A study of ... ..	S. P. Pal	451
Thyratron pulser and on filing gas for neon tube hodoscope chamber.—Notes on high voltage (L) ... ..	B. K. Bandhopadhyay and Subhra Bhattacharya	487
Transient heat conduction in a finite wedge ... ..	K. C. Sabherwal	448
Transfer of electronic excitation energy in liquids.—On the (L) ... ..	M. K. Machwe, J. Kishore and K. Gopala Krishnan	45
Ultraviolet absorption spectra of ortho, meta-, and para-fluoroanilines.—The near ... ..	M. A. Shashidhar and K. Suryanarayana Rao	53

SUBJECT	AUTHOR	PAGE
Variational treatment of slow electron scattering by a helium atom ...	S. N. Banerjee, R. Jha and N. C. Sil ...	258
Vibration of a cantilever under lateral impact of an elastic load (General theory—Part I)—Dynamics of ...	B. B. Banerjee ...	198
Vibration of a cantilever under lateral impact of an elastic load (General theory—Part II)—Dynamics of ...	B. B. Banerjee ...	208
Vibration of a cantilever under lateral impact of an elastic load (Part III) general theory.—Dynamics of ...	B. B. Banerjee ...	215
Vibration of a cantilever under lateral impact of an elastic load (Part IV)	B. B. Banerjee ...	221
Vibration of a cantilever under lateral impact of an elastic load. Part V (experiment).—The study of the dynamics of ...	B. B. Banerjee ...	609
Wigner Quarks (I) ...	T. Roy ...	265
X-ray measurements of stacking faults in $\alpha$ -AgMn alloys (L) ...	S. P. Sen Gupta and K. N. Goswami	97
X-ray study of nickel biguanide chloride. $[\text{Ni}(\text{C}_2\text{H}_5\text{N}_7)_2]\text{Cl}_2 \cdot 2\text{H}_2\text{O}$ —An (L) ...	S. K. Roy and S. C. Chakraborty ...	267
X-ray study of p-aniside (L) ...	M. Y. Khan and Y. Misra ...	271
X-ray study of chaksine iodine.—An (L) ...	S. C. Biswas and S. K. Talapatra ...	492
BOOK REVIEWS ...	... 52, 100, 154, 214, 278, 365, 636, 687	

# RELAXATION TECHNIQUE AS APPLIED TO ELECTRICAL NETWORK PROBLEM OF "RING DISTRIBUTOR"

S. N. DUTTA

DEPARTMENT OF APPLIED PHYSICS, CALCUTTA UNIVERSITY

(Received November 10, 1965)

**ABSTRACT** This paper deals with the relaxational solution of the problem of a "Ring Distributor". In this method a set of linear simultaneous equations is obtained using Kirchhoff's laws of networks, and these equations are solved by relaxation method. It reveals the usefulness of the relaxational solution of any problem for which a number of linear simultaneous equations can be developed and further it yields a number of required informations simultaneously. This is illustrated with an example and the results thus obtained are compared with those calculated by conventional method of network analysis.

## INTRODUCTION

In low voltage D.C. power distribution, the Ring Distributor (Starr, 1946 Cotton, 1948), is used in preference to other systems for having uninterrupted supply with a minimum expenditure on transmission lines or feeders. Because in this system any load may be supplied even if there is a break in transmission lines. This problem can be solved by the conventional methods used in network analysis. But those methods become laborious with the increase of the loading points. This paper suggests a method based on relaxation technique (Allen, 1954), and shows the utility of its application for such problems.

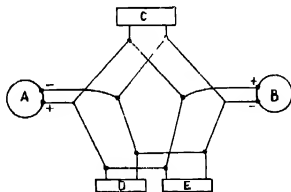


Fig. 1

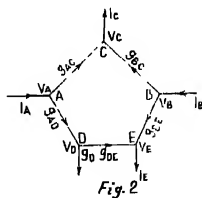


Fig. 2

Here a case of a symmetrical circuit i.e. each wire of each pair of lines having the same resistance as shown in Fig. 1, is dealt with. It can be further simplified by assuming that one wire ring has zero resistance and that each wire in the other ring has twice its actual value of the resistance, so that the equivalent circuit diagram can be drawn as shown in fig. 2.

$q_D = 1/R_D$ ,  $R_D$  being the resistance of the load  $D$



The above set of equations after simplification may be written as follows.

$$\left. \begin{aligned} I_A - V_A(g_{AC} + g_{AD}) + V_C g_{AC} + V_D g_{AD} &= 0 = F_1 \\ V_A g_{AC} - V_C(g_{AC} + g_{BC}) + V_B g_{BC} - I_C &= 0 = F_2 \\ I_B - V_B(g_{BC} + g_{BE}) + V_C g_{BC} + V_E g_{BE} &= 0 = F_3 \\ V_B g_{BE} - V_E(g_{BE} + g_{DE}) + V_D g_{DE} - I_E &= 0 = F_4 \\ V_A g_{AD} - V_D(g_{AD} + g_{DE} + g_D) + V_E g_{DE} &= 0 = F_5 \end{aligned} \right\} \dots (2)$$

where  $F_1, F_2, F_3, F_4$  and  $F_5$  are the residuals, the liquidation of which yields the unknown quantities contained in the relation (2). In liquidating them the required basic unit block, group operation tables and the relaxation table can be prepared (Allen 1954). In basic unit operation table the changes of the residuals due to unit positive increment to the value of the unknown are written (Table I, operation number 1 to 5). In block operation equal increments to more than one unknown are applied simultaneously (Table I, operation number 6 and 7) and in group operation unequal increments are added simultaneously to the various unknowns (Table I operation number 8). So the suitable operation blocks or groups to bring about the changes in one or more residuals without affecting the remaining residuals can be easily written and with the help of this operation table (Table I) the relaxation table (Table II) can be obtained to get the residuals liquidated quickly. This is clearly shown with an illustration given below.

#### ILLUSTRATION

An example worked out by the conventional method (Mem. Staff Dept. Elect. Eng. M I T, 1953) is taken for illustration where  $V_A = 230$  volts,  $V_B = 220$  volts,  $I_C = 1000$  amps,  $I_E = 1500$  amps,  $R_D = 0.4$  ohm,  $R_{AD} = 0.008$  ohm,

$R_{BC} = 0.006$  ohm,  $R_{BE} = 0.006$  ohm,  $R_{DE} = 0.01$  ohm,  $R_{ED} = 0.008$  ohm are given. It is required to calculate the line currents, load currents, voltages, resistances and generator currents.

Substituting the numerical values in the relation (2) it can be written as follows

$$\left. \begin{aligned} I_A + 125V_C + 125V_D - 57500 &= 0 = F_1 \\ -292V_C + 64490 &= 0 = F_2 \\ I_B + 167V_C + 167V_E - 73480 &= 0 = F_3 \\ 100V_D - 267V_E + 35240 &= 0 = F_4 \\ -227.5V_D + 100V_E + 28750 &= 0 = F_5 \end{aligned} \right\} \dots (3)$$

In the above illustration the block and group operations are performed after careful study and observation of the unit operation table. From those operation tables final relaxation table is obtained. The actual procedure followed to obtain the block and group operation or liquidation of the residuals is shown within the bracket [ ] and the operation number in unit, block, or group operation tables and liquidation step in relaxation tables are shown within the bracket ( ).

After liquidation of the residuals the generator currents and the load voltages are obtained directly from the relaxation table. From those and the supplied values of the generator voltages, load currents and the line resistances, the required line currents and load resistances and also the load current can be calculated as shown below

$$I_A = 2302.074 \text{ amps}$$

$$I_B = 749.736 \text{ "}$$

$$V_C = 220.856 \text{ volts}$$

$$V_D = 220.727 \text{ "}$$

$$V_E = 214.654 \text{ "}$$

$I_{AC} = 1142.875$  amps, where  $I_{AC}$  is the current flowing in the line joining the generator  $A$  and the load  $C$

$$I_{AD} = 1159.875 \text{ " , , , } I_{AD} \text{ ..... } D$$

$$I_{DE} = 607.290 \text{ " , , , } I_{DE} \text{ ..... load } D \text{ , ..... } E$$

$$I_{BC} = -142.700 \text{ " , , , } I_{BC} \text{ ..... generator } B \text{ , ..... } C.$$

$$I_D = 551.818 \text{ " , , , } I_D \text{ ..... of the load } D$$

$$R_C = 0.221 \text{ ohm, where } R_C \text{ is the resistance of the load } C$$

$$R_E = 0.143 \text{ " , , , , } R_E \text{ ..... } E.$$

The above values are seen to be in very good agreement with those obtained by conventional methods of network analysis shown in the table below (Table III)

In the Table III methods I, II and III mean the Relaxation method, conventional method of network analysis and the conventional method followed (with some approximations) in the book (Mom. Staff Dept Elec. Eng., M.I.T., 1953) respectively.

TABLE I  
Operation Table

Operation number	$\delta I_A$	$\delta I_B$	$\delta V_C$	$\delta V_D$	$\delta V_E$	$\delta F_1$	$\delta F_2$	$\delta F_3$	$\delta F_4$	$\delta F_5$
<i>Unit Operation</i>										
(1)	1	—	—	—	—	—	1	0	0	0
(2)	—	1	—	—	—	0	0	1	0	0
(3)	—	—	1	—	—	125	-292	167	0	0
(4)	—	—	—	1	—	125	0	0	100	-227.5
(5)	—	—	—	—	1	0	0	167	-267	100
<i>Block operation</i>										
(6) [(1)+(2)]	1	1	—	—	—	1	0	1	0	0
(7) [(3)+(4)-(5)]	—	—	1	1	1	250	-292	334	-167	-127.5
<i>Group operation</i>										
(8) [2.67 × (4) - (5)]	—	—	—	2.67	1	333.75	0	167	0	507.425

 TABLE II  
Relaxation

	$\delta I_A$	$\delta I_B$	$\delta V_C$	$\delta V_D$	$\delta V_E$	$F_1$	$F_2$	$F_3$	$F_4$	$F_5$
	$I_A =$	$I_B =$	$V_C =$	$V_D =$	$V_E = 0$	-37500	6450	-78540	37240	28750
(1) [220 × (7)]	—	—	200	220	220	-2500	250	0	-1500	700
(2) [15 × (4)]	—	—	—	15	—	625	250	0	0	2712.5
(3) [-5 3456 × (8)]	—	—	—	-14 2727	-5 3456	-2409 0.40	250	-802 7152	0	0
(4) [0 8562 × (3)]	—	—	0 8562	—	—	-2302 0740	0	-749 7365	0	0
(5) [2302 074 × (1) + 749 7365 × (2)]	2302 0740	749 7365	—	—	—	0	0	0	0	0
	2302 0740	749 7365	220 8562	220 7273	214 6544	0	0	0	0	0

TABLE III

Unknown quantities	Values of the unknown quantities obtained by		
	Method I	Method II	Method III
$I_A$	2302.074 Amps	2301.600 Amps	2300.000 Amps
$I_B$	749.736 ..	747.600 ..	700.000 ..
$I_{AC}$	1142.785 ..	1143.000 ..	1100.000 ..
$I_{AD}$	1159.875 ..	1157.785 ..	1170.000 ..
$I_{DE}$	607.290 ..	607.900 ..	620.000 ..
$I_{BC}$	--142.700 ..	142.607 ..	--200.000 ..
$I_{BE}$	890.933 ..	890.330 ..	880.000 ..
$I_D$	551.818 ..	551.862 ..	550.000 ..
$V_C$	220.856 Volts	220.856 Volts	221.000 Volts
$V_D$	220.727 ..	220.737 ..	221.000 ..
$V_E$	211.651 ..	214.658 ..	215.000 ..
$R_C$	0.221 ohm	0.221 ohm	0.221 ohm
$R_L$	0.113 ..	0.113 ..	0.113 ..

## DISCUSSION

This paper shows the utility of relaxation method in the sense that it yields a number of useful informations (generator voltage, load voltage, etc.) simultaneously. Also this method proves to be of great advantage over the other methods when the number of nodal points increases by the change of network conditions such as increase of the loading points etc. Some differences in the values obtained by this method and that in the book (Mem. Staff, Dept. Elec. Eng. MIT, 1953), can be accounted for by the fact that in the conventional method followed in that book the values are rounded off considering the practical aspect of the illustrating problem.

## ACKNOWLEDGMENT

The author takes this opportunity to convey his deep appreciation and gratefulness to Prof. A. K. Sengupta D.Sc. AMIEE, (London), Head of the Department of Applied Physics, Calcutta University, for his guidance and help throughout the progress of the work. He is also thankful to Dr. R. N. Basu and Dr. S. K. Basu, both of the above department (now in Canada) for their valuable discussions.

## REFERENCES

- Allen, D. N. deG., 1954 *Relaxation Method*, Chapter 1 & 2, (McGraw-Hill, New York)
- Cotton, H., 1948, *The Transmission and Distribution of Electrical Energy*, Chapter II, The English Universities Press Ltd., London.
- Members of the Staff of the Department of Electrical Engineering, Massachusetts Institute of Technology, 1953 *Electric Circuits*, 150, (The Technology Press, MIT)
- Staff, A. T. 1946, *Generation, Transmission and Utilisation of Electrical Power*, Chapter II, Sir Isaac Pitman & Sons Ltd., London.

# RELAXATION METHOD OF SOLVING ELECTRICAL NETWORK PROBLEM OF "TWO WIRE D. C. TRANSMISSION LINES"

S. N. DUTTA

DEPARTMENT OF APPLIED PHYSICS, CALCUTTA UNIVERSITY

(Received November 10, 1965)

**ABSTRACT** The present paper shows the application of relaxation method in the solution of D. C. Two Wire Transmission of Electrical Power with an illustration. The principle of relaxational solution of D. C. networks having usual circuit conditions is utilised. The results obtained thereby are compared with those calculated by the conventional method of network analysis. It also points out the utility of relaxation method in cases where a number of informations are wanted simultaneously.

## INTRODUCTION

The calculations of D.C. Two Wire Transmission lines when conditions at the sending and receiving ends are given, are quite familiar. There are different methods for such calculations and the problems can be solved according to the supplied informations of the sending and receiving end conditions.

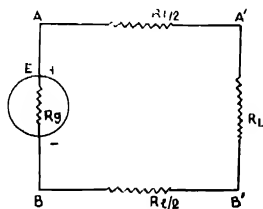


Fig. 1

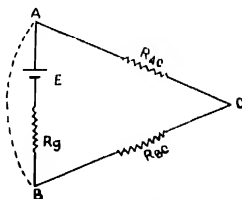


Fig. 2

When the receiving end terminals of a D.C. Two Wire Transmission line network are terminated by load resistance as shown in Fig. 1, the same network can be transformed into a convenient form as shown in Fig. 2. This form of network is solved by relaxation method and it is shown that such a relaxational solution gives a number of useful informations simultaneously.

Relaxation method was applied by Southwell and Black (1938), to solve the problem of D. C. networks and the utility of the application of relaxation technique for solving the network shown in Fig. 2., is clearly shown here.

## PRINCIPLE OF THE METHOD

In this method an electrical theorem in regard to the heating effects of steady currents has been used (Southwell and Black, 1938), which is enunciated below:

"In a network of conductors to which specified currents are supplied at two or more nodal points, the actual distribution of currents is such that the total generation of heat less twice the energy expended in supplying the specified currents from a source at datum potential has its minimum value consistent with the satisfaction of Kirchhoff's second law."

Let two nodal points  $A$  and  $C$ , joined by a conductor of resistance  $R_{AC}$ , be considered as shown in the network diagram represented by Fig. 2. If  $V_A$  and  $V_C$  be the potential at  $A$  and  $C$ , by Ohm's law a current  $\frac{V_A - V_C}{R_{AC}}$  will flow from  $A$  to  $C$ . Denoting the currents flowing towards  $A$  and  $C$  by  $I_A$  and  $I_C$  respectively, it can be written as

$$I_A = I_C = g_{AC}(V_A - V_C), \text{ where } g_{AC} = 1/R_{AC}$$

Considering all the conductors connected to  $A$ , it is obtained as,

$$\sum_A g_{AC}(V_C - V_A) + I_{A0} = 0 \quad (1)$$

where  $I_{A0}$  stands for the current supplied to  $A$  from outside. The heat generated in  $AC$  is measured by  $g_{AC}(V_A - V_C)^2$  and so the total generation of heat in the network is given by,

$$2H = \sum_m g_{AC}(V_A - V_C)^2 \quad \dots (2)$$

where  $\sum_m$  denotes a summation extending to every conductor. Also if the current is supplied to  $A$  from an outside source at datum potential  $V_0$  the rate of expenditure of energy is measured by  $I_{A0}(V_A - V_0)$  and the total expenditure of energy is measured by,

$$\sum_n \{I_{A0}(V_A - V_0)\} = -E \quad \dots (3)$$

where  $\sum_n$  denotes a summation extending to every nodal point. So equation (1) is typical of the conditions for a minimum value of the quantity,

$$Q = H + E = \frac{1}{2} \sum_m \{g_{AC}(V_A - V_C)^2\} + \sum_n \{I_{A0}(V_A - V_0)\} \quad \dots (4)$$

as it is equivalent to,

$$\frac{\partial Q}{\partial V_A} = - \frac{\delta}{\delta V_A} (H + E) = 0$$

As the source of E.M.F., i.e. generator is involved it may be assumed that the whole E.M.F. of the source is utilized to pass current to earth through its own

resistance and the datum distribution for the known current to enter and to leave the network at nodal points is obtained. Afterwards it is simply required to calculate and superpose the effects of neutralising currents at those points. With this modification the problem can be solved conveniently by relaxation method taking the help of the above theorem.

If  $A$  and  $B$  be joined by a wire of zero resistance, shown by dotted line, the current passing through the source  $E$  from  $A$  to  $B$  would return by that wire and hence in the datum distribution a current of  $E/R_G$  enters the system at  $A$  and leaves at  $B$  where  $R_G$  is the internal resistance of the generator. Now it is required to calculate and superpose the current distribution which when the neutralising currents  $+E/R_G$  and  $-E/R_G$  are supplied at  $B$  and  $A$  to the network after the source of E M F is removed.

Using equation (4), the expression for  $Q$  and the residuals can be written as follows :

$$2Q = \frac{(V_C - V_A)^2}{R_{AC}} + \frac{(V_C - V_B)^2}{R_{BC}} + \frac{(V_A - V_B)^2}{R_G} + 2 \frac{E}{R_G} \{V_0 - V_B - (V_0 - V_A)\} \quad \dots \quad (5)$$

where  $R_{AC} = \frac{R_I + R_L}{2} = R_{BC}$

Hence,

$$\left. \begin{aligned} \frac{\partial Q}{\partial V_C} &= \frac{V_C - V_A}{R_{AC}} - \frac{V_C - V_B}{R_{BC}} = 0 = F_C \text{ initially} \\ \frac{\partial Q}{\partial V_A} &= \frac{V_C - V_A}{R_{AC}} - \frac{V_A - V_B}{R_G} = -\frac{E}{R_G} = -F_A \text{ initially} \\ \frac{\partial Q}{\partial V_B} &= \frac{V_C - V_B}{R_{BC}} + \frac{V_A - V_B}{R_G} = +\frac{E}{R_G} = F_B \text{ initially} \end{aligned} \right\} \quad (6)$$

Now on liquidating the residuals obtained initially the required values of voltages at  $A$ ,  $B$  and  $C$  can be found out. The method is illustrated by the following example.

#### ILLUSTRATION

For illustration the following example worked by Corcoran (1949), using a different method is considered.

In the arrangement of the Two Wire D.C. Transmission of Electrical Power shown in Fig. 1, the generated voltage  $E = 110$  volts, internal resistance of the

generator  $R_G = 0.1$  ohm and the line resistance  $R_L = 0.9$  ohm and the load resistance  $R_L$  is so adjusted that  $V_{A'E'} = 100$  volts. The efficiency of transmission and the voltage regulation of the transmission line are to be found out.

The value of the load resistance  $R_L$  can be calculated to be 10 ohms from the supplied data. Then using the relations (5) and (6) the basic operation table (Table I) can be easily obtained (Allen 1954).

In the basic operations suitable positive increments are given to the unknowns and the corresponding changes in the residuals are found out (Table I, operation number 1 to 3). The block operation (Table II, operation number 2) in which equal increments are added to more than one unknown simultaneously to bring about the changes in the residuals quickly is carried on with the help of the basic operations. In preparing the relaxation table (Table II) both the basic operation and the block operation are used and the residuals are liquidated in only two steps (Table II operation number 1 and 2).

TABLE I  
Basic Operation Table

Operation Number	$\delta V_G$	$\delta V_L$	$\delta V_R$	$\delta E_G$	$\delta E_A$	$\delta E_B$
1	5.45			2	53.5	1
2		5.45		1	55.5	54.5
3			5.45	1	54.5	-55.5

TABLE II  
Relaxation Table

Operation Number	$\delta V_G$	$\delta V_L$	$\delta V_R$	$E_G$	$E_A$	$E_B$
	$V_G$	$V_L$	$V_R$	0	-1100	1100
1	0	-100	0	20	10	10
2	0	54.5	54.5	0	0	0
	0	54.5	54.5	0	0	0



TABLE III  
Comparison of values

	Values Calculated by Relaxation Method	Values Calculated by Conventional Method of Network Analysis
Efficiency Transmission	0.918	0.918
Voltage Regulation	0.09	0.09

Hence the potential of  $B$  with respect to  $A$  is 109 volts and that of  $C$  relative to  $A$  is 54.5 volts. Therefore  $V_{AB} = 109$  volts so that the efficiency of transmission is 0.918 and the voltage regulation of transmission line is 0.09. These values are exactly the same as those obtained by the conventional method of network analysis shown by Table III.

#### DISCUSSION

The method described in this paper is a useful one as it gives out a number of informations at a time viz. potentials at  $A$ ,  $B$  and  $C$  simultaneously. Also with some practice of relaxation method, the table can be obtained with little difficulty and hence little time is required for the whole operation compared to other methods. But this method requires the value of the internal resistance of the source of  $E M F$  or the resistance of the path  $AB$  to calculate the current in the datum distribution.

#### ACKNOWLEDGMENT

The author takes this opportunity to record his deep appreciation and gratitude to Prof. A. K. Sengupta, D.Sc., A.M.I.E.E. (London), Head of the Department of Applied Physics, Calcutta University, for his help and guidance throughout the progress of the work. He is also thankful to Dr. R. N. Basu and Dr. S. K. Basu, both of the above department (now in Canada) for their valuable discussions.

#### REFERENCES

- Allen, D. N. deG., 1954, *Relaxation Method*, Chapter 1 & 2 (McGraw Hill Book Co., New York).
- Black, A. N. and Southwell, R. V., 1938, *Relaxation Methods Applied to Engineering Problems II Basic Theory with Application to Surveying and to Electrical (Networks and Extension to Gyrostatic Systems)* Proc. Roy. Soc. (A) **164**, p. 447.
- Corenau, G. F., 1949, *Basic Electrical Engineering*, Chapter VI John Wiley & Sons, New York.
- Southwell, R. V., 1951, *Relaxation Methods in Engineering Science*, Chapter VI, Oxford University Press, London.

# INTERMOLECULAR POTENTIAL OF KRYPTON AND XENON ON THE CORE MODEL

A. N. ROY AND S. K. DEB

INDIAN ASSOCIATION FOR THE CULTIVATION OF SCIENCE, CALCUTTA-32.

(Received November 10, 1965)

**ABSTRACT** The potential parameters for the core model have been obtained for krypton and xenon by using simultaneously the viscosity and the second virial coefficient data. The potential energy curves thus obtained are quite close to the elaborate six-parameter of Guggenheim and McGlashan. The satisfactory agreement between the experimental data and the calculated values and the comparatively simple form of the core potential raise the possibility of using it in the place of more commonly used Lennard-Jones (12-6) and exp-6 potentials.

The limitations of the comparatively simple intermolecular potentials like Lennard-Jones (12-6) and the exp-6 models are now well recognised (Kihara 1953, 1955; Guggenheim and McGlashan 1960). However, more elaborate and complicated potentials (e.g. six-parameter potential of Guggenheim and McGlashan) are not convenient particularly for the calculation of collision integrals for representing transport properties of gases. Consequently it is necessary to obtain an intermolecular potential model which is comparatively simple in form and at the same time represent the potential adequately. Recent calculation by Barker (1964) for argon on the core model of Kihara is fairly successful in these regards. The core potential with a spherical core of diameter  $2a$  may be represented as,

$$\phi(r) = 4\epsilon \left[ \left( \frac{\sigma - 2a}{r - 2a} \right)^{12} - \left( \frac{\sigma - 2a}{r - 2a} \right)^6 \right] \quad r > 2a \quad \dots \quad (1a)$$

$$\phi(r) = \infty \quad r \leq 2a \quad \dots \quad (1b)$$

where  $\sigma$  is the value of  $r$  for which  $\phi(r) = 0$  and  $\epsilon$  is the depth of the potential well. The addition of the term  $a$  makes the core potential more flexible than the Lennard-Jones (12-6) potential and at the same time the mathematical simplicity is retained. Kihara (1953) obtained the second virial coefficient  $B(T)$  on the core model and very recently Barker (1964) has obtained the collision integrals on this model. By combining  $B(T)$  and the viscosity data Barker (1961) has obtained the force constants for argon on the core model and the potential energy curve thus obtained is quite close to the elaborate six-parameter potential of Guggenheim and McGlashan (1960). The constants thus obtained can explain all the gaseous properties of argon satisfactorily. The success achieved for argon with the core model raises the possibility of replacing the Lennard-Jones (12-6) potential by

the core potential. Consequently, we have thought it worthwhile to obtain the intermolecular potentials of Kr and Xe on the core model and test its suitability. Recently, Sherwood and Prausnitz (1964) have obtained the force constants for the inert gases on the core model. However as shown by Keller and Zurno (1959)  $B(T)$  data alone cannot determine the force parameters uniquely. In this paper we have calculated the force parameters for krypton and xenon by utilising both second virial coefficient and viscosity data. The constants thus obtained have been checked by calculating various other properties.

# CALCULATION AND RESULTS

For the determination of the force parameters we shall use simultaneously the second virial coefficient and the viscosity data. The viscosity  $\eta$  may be represented as (Hirschfelder, Curtiss and Bird)

$$\eta \times 10^7 = 226.93 \frac{\sqrt{MT}}{\sigma^2 \Omega^{(2,2)}(T^*)} \quad \dots (2)$$

where  $M$  is the molecular weight and  $\Omega^{(2,2)}(T^*)$  is a collision integral as calculated by Barker (1964). The second virial coefficient  $B(T)$  may be written as,

$$B(T) = b_0 B^*(a^*, T^*) \quad (3)$$

$$\text{where} \quad b_0 = \frac{2\pi N \sigma^3}{3} \cdot a^{*3} \cdot \frac{2a}{\sigma - 2a}, \quad T^* = \frac{KT}{\epsilon} \quad (4)$$

$$\text{and} \quad B^*(a^*, T^*) = [2^{1/2} F_3(T^*) + 3 \cdot 2^{1/3} \cdot a^* F_2(T^*) + 3 \cdot 2^{1/6} \cdot a^{*2} \cdot F_1(T^*) \\ + a^{*3}] (1 + a^*)^{-3} \quad (5)$$

$$F_s(T^*) = - \frac{\pi}{12} \sum_{j=0}^s \frac{2^j}{j!} \Gamma \left( \frac{6j-8}{12} \right) T^{* - \frac{6j+8}{12}} \quad (6)$$

From Eqs. (2) and (3)

$$\log_{10} \left( \frac{\eta \beta}{T^3} \right) = \log_{10} \frac{B^*(a^*, T^*)}{\Omega^{(2,2)}(a^*, T^*)} + \log \sigma + \log c \quad (7)$$

$$\text{where} \quad c = 226.93 \times \frac{2}{3} \pi N \sqrt{M} \times 10^{-7}$$

$$\text{and} \quad \log T = \log T^* + \log \frac{\epsilon}{K} \quad \dots (8)$$

For a chosen value of  $a^*$  it is possible to determine  $\sigma$  and  $\epsilon/K$  from Eqs (7) and (8) by the graphical method (Mason and Rice 1954). The set of values of  $a^*$ ,  $\epsilon/K$ ,  $\sigma$  which represented the experimental data best were taken as the correct force parameters. The results thus obtained are shown in Table 1. The potential energy curves for krypton and xenon as obtained on the core model are shown together with those for the Lennard-Jones (12-6) and the six-parameter potentials are shown in Figs. 1 and 2.

#### COMPARISON WITH EXPERIMENT

##### (a) Krypton

The average deviation between the experimental and the calculated values of the thermal conductivity (Kannulnik and Garmann, 1952; temperature range 195° to 579°K) and viscosity (Chilton 1963; temperature range 300° to 690°K) is 0.8% and 2% respectively. Up to 473°K the agreement with the experimental second virial coefficient data is within 2%. The agreement becomes worse at higher temperatures. This probably means that the effective core diameter is changed at higher temperatures. For all these properties the agreement with the experimental values is better than that obtained by using the constants obtained by Sherwood and Prausnitz (1964) from the second virial coefficient data only.

##### (b) Xenon

For xenon the average deviation between the experimental and the calculated values of thermal conductivity (Kannulnik and Garmann, 1952) and viscosity (Trantz, Marx and Roberg Heberling, 1934) is within 4% and 2% respectively. In both the cases the calculated values are lower than the experimental values which may be partly due to the fact that xenon always contains a certain percentage of krypton as impurity. For second virial coefficient the agreement between experimental and the calculated values is excellent (average deviation 2%) over the temperature range 290°-573°K. It is interesting to note that the agreement with the experimental  $B(T)$  data is better than those obtained by using Sherwood and Prausnitz (1964) who used  $B(T)$  data for calculating the force parameters.

##### (c) Third Virial Coefficient

It has been pointed out by Graben and Present (1962) that three-body interactions cannot be neglected in the calculation of the third virial coefficient. The three body interaction effect has been calculated approximately by Sherwood and Prausnitz (1964) for the core potential. The third virial coefficient  $C$  may be expressed as the sum of the contributions of pair-wise interactions and the non-additive interactions i.e.

$$C = C^a + \Delta C \quad \dots (9)$$

$$\text{where} \quad C^a = -\frac{8\pi^2 N^2}{3} \int \int \int f_{12} f_{13} f_{23} r_{12}^2 r_{13}^2 r_{23}^2 dr_{12} dr_{13} dr_{23} \quad \dots (10)$$

$$\Delta U = \frac{8\pi^2 N^2}{3} \int \int \int \exp - \frac{\Sigma \phi_{ij}}{kT} \left[ \exp \left( - \frac{\Delta \phi}{kT} \right) - 1 \right] r_{12}^2 r_{13}^2 dr_{12} dr_{13} dr_{23} \quad (11)$$

$$f_{ij} = \exp \left( - \frac{\phi_{ij}}{kT} \right) - 1$$

$$\Sigma \phi_{ij} = \phi_{12} + \phi_{13} + \phi_{23} \quad (12)$$

$r_{ij}$  being the distance between molecules  $i$  and  $j$ .  $\Delta \phi$  represent the difference between the three-body interaction energy and the sum of pair energies.

For obtaining  $\Delta U$  Kihara (1958) has expanded  $\Delta U$  in terms of the polarizability  $\alpha$  which may be written as

$$\Delta U = \alpha \cdot \left( \frac{\partial \Delta U}{\partial \alpha} \right)_{\alpha=0} + \dots \quad (13)$$

neglecting higher terms.

Consequently  $U$  in the reduced form is given by

$$U^* = \frac{U}{b_0^2} = U^{**} + \alpha^* \left( \frac{\partial \Delta U^*}{\partial \alpha^*} \right) \quad (14)$$

The quantities  $U^{**}$  and  $\alpha^* \cdot \left( \frac{\partial \Delta U^*}{\partial \alpha^*} \right)$  have been tabulated by Sherwood and Praesnitz (1964) for the core potential. The results obtained by us for the third virial coefficient by using the calculated constants are shown in Table II.

TABLE I  
Force constants for krypton and xenon

Potential form	krypton			xenon		
	$\sigma$ in Å	$\epsilon/k$ in °K	$a^*$	$\sigma$ in Å	$\epsilon/k$ in °K	$a^*$
Core potential	3.570	204.0	0.125	3.922	360.6	0.2
Lennard-Jones (12-6)	3.61	190	0	4.055	229	0

**TABLE II**  
Third virial coefficient

$T^{\circ}K$	Krypton		Xenon	
	Calculated (cc/mole) <sup>2</sup>	Experimental (cc/mole) <sup>2</sup> (a)	Calculated (cc/mole) <sup>2</sup>	Experimental (cc/mole) <sup>2</sup> (b)
298	2626	2611	7941	6077
323	2383	2262	7109	5314
348	2186	2079	6309	4641
373	2033	1945	5721	4120
398	1908	1845	5233	3744
423	1811	1759	4777	3474
448	1721	1671	4444	3244
473	1659	1584	4170	3035
498	1601	1642	3907	2873
523	1553	1579	3710	2688
548	1513	1563	3510	2528
573	1476	1612	3378	2426

(a) Bontas, J. A., Burley, J. S. and Barnauli, R. J., 1952.

(b) Bontas, J. A., Barnauli, R. J., Burley, J. S., 1951.

#### DISCUSSION OF RESULTS

From Figs. 1 and 2 it may be seen that the core potential as derived from the gaseous properties is close to the elaborate six-parameter potential of Guggenheim and McGlashan (1960). As also observed by Barker (1964) for argon the potential energy curve as obtained on the core potential is quite different from that on the Lennard-Jones (12-6) potential. The concept of introducing a hard core most probably makes the potential function more flexible and realistic than the more commonly used Lennard-Jones (12-6) and exp-6 potentials. However, since the effective diameter of the hard core should depend on the energy of the colliding molecules i.e. on temperature, the same set of parameters cannot probably represent potential energy curve over a wide range of temperatures.

The calculations performed for krypton and xenon together with results obtained by Barker (1964) for argon show that the core potential can represent the various macroscopic properties satisfactorily. In view of the comparatively simple form of the core potential, it may be possible to use it in place of usual Lennard-Jones (12-6) potential which is too much restricted as pointed out by Guggenheim and McGlashan (1960).

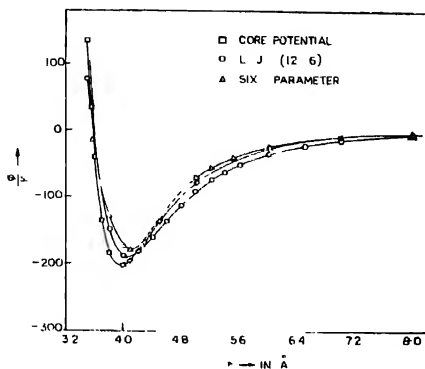


Fig. 1. Potential energy curves for krypton on different models.

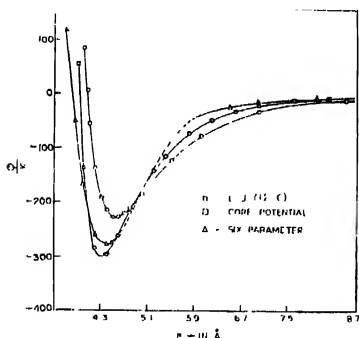


Fig. 2. Potential energy curves for xenon on different models.

From Table II it may be seen that by considering non-additive interactions it is possible to represent very satisfactorily the third virial coefficient data of krypton. The disagreement between the experimental and the calculated values of  $C$  for xenon is quite large. One reason for this disagreement may be due to presence of krypton as an impurity in xenon. Another factor which is probably more important is that in calculating the non-additive part of  $C$  the repulsive part of the potential has not been considered (Sherwood and Prausnitz, 1964).

## ACKNOWLEDGEMENT

The authors wish to thank Dr. A. K. Bania for suggesting the problem and helpful guidance and to Prof. B. N. Srivastava D.Sc., F.N.I., for his kind encouragement and interest in the work

## REFERENCES

- Barlow, J. A., Fock, W., and Smith, F., 1964, *Phys. Fluids*, **7**, 897.  
Beattie, J. A., Brerley, J. S. and Burdett, R. J., 1951, *J. Chem. Phys.* **19**, 1222, **20**, 1615  
Chilton David, G., 1963, *J. Chem. Phys.*, **28**, 1123  
Graben, H. W. and Pressent, R. D., 1962, *Phys. Rev. Letters*, **9**, 247  
Guggenheim, E. A. and McGlashan, M. L., 1960, *Proc. Roy. Soc., A* **255**, 456  
Hirschfelder, Curtiss and Bird, 1954, *Molecular Theory of Gases and Liquids*, John Wiley & Sons, N. Y., 528  
Kamanduk, G. and Gorman, E. G., 1952, *Proc. Phys. Soc.*, **65**, 706  
Koller, J. B. and Zuanno, B., 1959, *J. Chem. Phys.*, **30**, 1351  
Kilham, T., 1953, *Rev. Mod. Phys.*, **25**, 831, 1955, *Rev. Mod. Phys.*, **27**, 412  
Mason, E. A. and Rice, W. E. 1954, *J. Chem. Phys.*, **22**, 843  
Shawwood, A. E. and Prinsnitz, J. M., 1964, *J. Chem. Phys.* **41**, 429  
Touatz, Max, Heberling Robert, 1934, *Ann. Physic*, **20**, 118



# DEDUCTION OF GENERALISED KRICHHOFF'S LAWS FROM THE BASIC PRINCIPLES OF ELECTROMAGNETISM

S. K. MITRA AND T. ROY\*

INDIAN STATISTICAL INSTITUTE

(Received December 18, 1964 ; Resubmitted Sept. 22, 1965)

**ABSTRACT** The existence of solution of the classical boundary value problem of steady current flow in a continuous semi-conducting medium under Ohm's Law is proved from the Fredholm Theory of Integral Equations. Though the solution of the integral equations remains arbitrary, the solution of the boundary value problem has been shown to be unique as it should be from *prima facie* arguments. A unique relation between the currents through the electrodes and their potentials is also established. Further, an expression for the cross-currents flowing between two electrodes is deduced from theory leading to the usual Kirchhoff's Laws for line conductors.

## INTRODUCTION

The well-known Kirchhoff's Laws describe the current voltage relationships in a net-work containing resistors. These laws are based on (a) the macroscopic (Jenns, 1923) Ohm's Law which says that the total current flowing across a resistor is proportional to the difference of potential at its ends, and secondly (b) on the principle of steady state condition of electromagnetism under which any free volume charge does not appear. The two laws of Kirchhoff are obvious consequences of these two principles. The question of deduction of these two accepted 'laws' of Kirchhoff appears to be somewhat preposterous at first sight. But there are two things which are normally overlooked, viz. the resistors in Kirchhoff's Laws are 'wires' which are idealised one-dimensional lines and Ohm's Law which is applied to these 'wires' is but a limiting approximation of the microscopic Ohm's Law for continuous media. Strictly speaking, the Laws are to be deduced from the fundamental electromagnetic equations for a continuous resistive medium under the steady state conditions and then extended to the 'line' conductors as a limiting case. As this was not done before, the natural form of the Kirchhoff's Laws never became apparent. As a result in the accepted form of Kirchhoff's Laws there are numerous redundant variables, which are difficult to eliminate in actual calculations. The powerful topological tool of Graph Theory has in recent years been extensively employed by circuit analysts to remove this difficulty. We shall show in this paper that the Kirchhoff's Laws take a simple natural form if deduced as a particular case of the more general laws for the continuous medium, which we have

---

\*Jadavpur University

established from the fundamental equations of electromagnetism. The laws take a neater and convenient form from which all the redundant variables disappear. The accepted form of the Kirchhoff's Laws can at once be deduced from these general relationships as a special case, but the reverse process is not at all obvious, because of the presence of the redundant variables.

The problem of steady current flow in a semi-conducting medium obeying Ohm's Law was first formulated by Krichhoff (1893). He showed from physical principles that the currents through the electrodes and then potentials are connected through linear relations, as in the case of charges and potentials for a system of conductors shown earlier by Maxwell. The main purpose of this work is to show rigorously that the solution of the boundary value problem of Kirchhoff always exists and though the fundamental solution has some irremovable arbitrariness, there exists a unique linear relation between the currents and potentials on the electrodes. The existence of cross-currents between any two electrodes and their relation with the potentials are also deduced as a consequence from the existence theorem.

#### STATEMENT OF THE PROBLEM

In a finite semi-conducting medium of uniform specific conductivity  $\kappa$  let there be  $m$  electrodes. The electrodes are perfect conductors by definition. Let

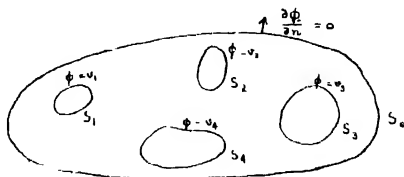


FIG. 1

the bounding surfaces of the electrodes be  $S_1, S_2, \dots, S_m$ . Let  $S_0$  be the bounding surface of the medium. The surfaces  $S_1, S_2, \dots, S_m$  are all enclosed within the outer surface  $S_0$ . Let  $v_1, v_2, v_3, \dots, v_m$  be the constant potentials on the respective electrode surfaces. Let  $\vec{c}$  be the current density at any point  $P$  of the medium and  $\phi(P)$  be the potential at  $P$ . The steady state condition gives,

$$\operatorname{div} \vec{c} = 0 \quad \dots (1)$$

and Ohm's Law gives,

$$\vec{c} = -\kappa \operatorname{grad} \phi \quad \dots (2)$$

From these equations, follows the Laplace's Equation

$$\nabla^2 \phi = 0 \quad \dots (3)$$

The boundary conditions for the problem are

$$\phi = \text{constant} = v_1, v_2, \dots, v_m \quad \dots (4.1)$$

on the electrode surfaces  $S_1, S_2, \dots, S_m$  and the normal component of the current density  $c_n$  on the enclosing surface  $S_0$  shall vanish because no current can go out of the medium that is

$$c_n = -\kappa \left( \frac{\partial \phi}{\partial n} \right)_{S_0} = 0 \quad \text{on } S_0 \quad \dots (4.2)$$

If a solution of this boundary values problem exists then it can be shown by Green's Theorem that this must be unique (see Appendix I). Further it must satisfy the equation of constraint, viz

$$\sum_{i=1}^m \iiint_{S_i} \left( \frac{\partial \phi}{\partial n} \right)_{S_i} dS - \iiint \nabla^2 \phi \, d\tau = 0 \quad (5)$$

#### PROOF OF THE EXISTENCE OF SOLUTION

Following the well-known method of Fredholm for the proof of existence of solution of the Dirichlet and Neumann's problems in Potential Theory, we shall show that the solution of the boundary value problem exists. In the following we shall follow the notation of Sternberg (1952). Let us assume that the potential is due to a surface distribution  $\sigma(Q)$  on the surfaces where  $\sigma_0(Q)$  shall indicate the surface density on the outer enclosing surface  $S_0$ ,  $\sigma_1(Q)$  be the same on the electrode surface  $S_1$  and so on. Obviously,  $\sigma(Q)$  can be looked upon as an  $(m+1)$  dimensional vector having the  $(m+1)$  components  $\sigma_0(Q), \sigma_1(Q), \dots, \sigma_m(Q)$  on the surfaces and has values only if  $Q$  is a point on the surfaces. If such a surface distribution exists in general, which satisfies the boundary conditions then the solution of the problem exists also. Further, such a solution has to be unique.

The potential at any point  $P$  inside the region is given by,

$$\phi(P) = \sum_{i=0}^m \iint_{S_i} \int_{V_P} \sigma_i(Q) \, dS \quad \dots (6)$$

This potential is continuous in crossing the surfaces  $S_1, S_2, \dots, S_m$ . Further by a well-known theorem of the Newtonian Potential Theory, the discontinuity of the normal derivative of the potential is given by (Sternberg et al. 1952).

$$\frac{\partial \phi_-}{\partial n} = \frac{\partial \phi}{\partial n_s} + 2\pi\sigma(s) \quad \dots (7.1)$$

$$\frac{\partial \phi_+}{\partial n} = \frac{\partial \phi}{\partial n_s} - 2\pi\sigma(s) \quad \dots (7.2)$$

where  $\frac{\partial \phi_-}{\partial n}$  means the normal derivative from inside a closed surface,  $\frac{\partial \phi_+}{\partial n}$  meaning from outside the surface, and  $\frac{\partial \phi}{\partial n_s}$  means the value of the normal derivative on the surface. Thus, for any surface  $S_j$

$$\left( \frac{\partial \phi_-}{\partial n} \right)_{S_j} = 2\pi \sigma_j(s) + \sum_{i=0}^m \frac{\partial}{\partial n_s} \int \int_{S_i} \frac{\sigma_i(Q)}{r_{sQ}} dS$$

Now, by the boundary conditions (4.2),

$$0 = \left( \frac{\partial \phi_-}{\partial n} \right)_{S_0} = 2\pi \sigma_0(s) + \sum_{i=0}^m \frac{\partial}{\partial n_s} \int \int_{S_i} \frac{\sigma_i(Q)}{r_{sQ}} dS$$

Further, since the potential function  $\phi(P)$  is constant on the surfaces  $S_1, S_2, \dots, S_m$  by the boundary condition (4.1), then it must be constant throughout the volume enclosed by each of these closed surfaces according to the continuity property of the potential function for a surfaces distribution. Therefore,

$$\left( \frac{\partial \phi_-}{\partial n} \right)_{S_i} = 0, \quad i = 0, 1, 2, \dots, m \quad \dots (8)$$

for each surface.

Thus by (7.1)  $\sigma_j(s)$  must satisfy the same homogeneous integral equation on all the surfaces.

$$2\pi \sigma_i(s) + \sum_{i=0}^m \frac{\partial}{\partial n_s} \int \int_{S_i} \frac{\sigma_i(Q)}{r_{sQ}} dS = 0 \quad \dots (9)$$

If non-trivial solution of this system of homogeneous integral equations exists, then the potential formed from this surface distribution will automatically satisfy the boundary conditions (4.1) and (4.2), as also the equation of constraint (5). For integrating the surface density  $\sigma_0(Q)$  over the enclosing surface  $S_0$  in (9) gives

$$2\pi \int \int_{S_0} \sigma_0(s) dS + \sum_{i=0}^m \int \int_{S_i} \sigma_i(Q) dS \int \int_{S_0} \frac{\partial}{\partial n_s} \left( \frac{1}{r_{sQ}} \right) dS =$$

$$\text{Now, by Gauss Theorem, } \frac{1}{2\pi} \int \int_{S_0} \frac{\partial}{\partial n_s} \left( \frac{1}{r_{sQ}} \right) dS = -1 \text{ when } Q \text{ is an } S_0$$

$$= -2 \quad " \quad " \quad " \quad " \quad S_i$$

Thus,

$$\sum_{i=1}^m \int \int_{S_i} \sigma_i(Q) dS = 0$$

But,

$$\sigma_i(Q) = -\frac{1}{4\pi} \left( \frac{\partial \phi_i}{\partial n} \right)_{S_i}$$

$$i = 1, 2, 3, \dots, m$$

Or,

$$\sum_{i=1}^m \int_{S_i} \left( \frac{\partial \phi_i}{\partial n} \right) dS = 0$$

The problem is thus nearly analogous to the Neumann's Interior Problem of Potential Theory. Following the steps of Fredholm we shall now show that the solution of these coupled system of  $(m+1)$  homogeneous integral equations exists in general and there are exactly  $(m+1)$  linearly independent solutions corresponding to the eigen value  $= 1$ .

Following Sternberg (1952) let us denote by

$$K(Q, s) = \frac{1}{2\pi} \frac{\partial}{\partial n_s} \left( \frac{1}{r_{sQ}} \right) \quad \dots (10)$$

$$K(s, Q) = \frac{1}{2\pi} \frac{\partial}{\partial n_Q} \left( \frac{1}{r_{sQ}} \right) \quad \dots (10)$$

then the equation (9) takes the form

$$\sigma_j(s) + \sum_{i=1}^m \int_{S_i} K(Q, s) \sigma_i(Q) dS = 0 \quad \dots (11)$$

The corresponding transposed system of integral equations is,

$$\mu_j(s) + \sum_{i=1}^m \int_{S_i} K(s, Q) \mu_i(Q) dS = 0 \quad \dots (12)$$

By Gauss's Theorem,

$\mu_j(s) = 1$  and  $\mu_i(s) = 0$  is a non-trivial solution. Thus,

$$i \neq j$$

$$\vec{\mu}(s) = \begin{bmatrix} 1 \\ 0 \\ 0 \\ \vdots \\ 0 \end{bmatrix}, \begin{bmatrix} 0 \\ 1 \\ 0 \\ \vdots \\ 0 \end{bmatrix}, \dots, \begin{bmatrix} 0 \\ 0 \\ \vdots \\ 1 \end{bmatrix} \quad \dots (13)$$

are  $(m-1)$  linearly independent solutions corresponding to the eigen value  $-1$ . Therefore by Fredholm's theorem  $(m+1)$  linearly independent solutions of the transposed homogenous integral equation (11) always exist. Thus  $(m+1)$  linearly independent solutions of the fundamental integral equation (9) exist

General solution will be a linear combination of these  $(m+1)$  linearly independent solutions, with  $(m+1)$  arbitrary constants to be determined from the values of the potential given on the  $m$  electrode surfaces. One arbitrary constant cannot be determined because the boundary condition on the enclosing surface (0th surface) is satisfied automatically through the integral equations (9). But by the Uniqueness Theorem the potential function should be independent of this undeterminable constant

Further each fundamental solution of the integral equation (11) must satisfy the equation of constraint (5) automatically because expression (6) satisfies Laplace's Equation

$$\text{Let } \overrightarrow{v_0(s)}, \overrightarrow{v_1(s)}, \overrightarrow{v_2(s)}, \dots, \overrightarrow{v_m(s)} \quad \dots (14)$$

be the  $(m+1)$  linearly independent vector solutions of the integral equation (11). Each of these solutions satisfies the equation of constraint (5). Let us call by  $N(s)$  the  $(m-1) \times (m+1)$  matrix,

$$N(s) = \left( \overrightarrow{v_0(s)}, \overrightarrow{v_1(s)}, \dots, \overrightarrow{v_m(s)} \right) \quad \dots (15)$$

The surface density  $\overrightarrow{\sigma}(s)$  will be a linear combination of these solutions, viz.,

$$\begin{aligned} \overrightarrow{\sigma}(s) &= x_0 \overrightarrow{v_0(s)} + x_1 \overrightarrow{v_1(s)} + \dots + x_m \overrightarrow{v_m(s)} \\ &= N(s) \vec{x} \end{aligned} \quad \dots (16)$$

where  $x_0, x_1, x_2, \dots, x_m$  are  $(m+1)$  arbitrary constants to be determined from the boundary conditions of the problem. The potential at any point  $P$  is thus

$$\begin{aligned} \phi(P) &= \left[ \iint \left( \frac{1}{r_{PQ_0}} + \frac{1}{r_{PQ_1}} + \dots + \frac{1}{r_{PQ_m}} \right) N(Q) dS \right] \vec{x} \\ &= \vec{\rho}'(P) \vec{x} \quad \text{say,} \end{aligned} \quad \dots (17)$$

where  $\left( \frac{1}{r_{PQ_0}} + \frac{1}{r_{PQ_1}} + \dots + \frac{1}{r_{PQ_m}} \right)$  is a row vector and the row vector

$$\vec{\rho}'(P) = \iint \left( \frac{1}{r_{PQ_0}}, \frac{1}{r_{PQ_1}}, \dots, \frac{1}{r_{PQ_m}} \right) N(Q) dS \quad \dots (18)$$

is the fundamental solution of the problem from which particular solutions are formed with different values of  $\vec{x}$ . According to the boundary conditions (4.1)  $\phi(P)$  assumes the values  $v_1, v_2, \dots, v_m$  on the electrodes. This can be expressed vectorially as

$$\vec{v} = \begin{bmatrix} v_1 \\ v_2 \\ \vdots \\ v_m \end{bmatrix} = \begin{bmatrix} \int \int R(Q) N(Q) dS \\ \vdots \\ \int \int R(Q) N(Q) dS \end{bmatrix} \vec{x} \quad \dots (19)$$

where  $R(Q)$  is a rectangular matrix of  $m$  rows and  $(m+1)$  columns, viz.,

$$R(Q) = \begin{bmatrix} 1 & 1 & \dots & 1 \\ rs_1 Q_0 & rs_1 Q_1 & \dots & rs_1 Q_m \\ \\ 1 & 1 & \dots & 1 \\ rs_2 Q_0 & rs_2 Q_1 & \dots & rs_2 Q_m \\ \vdots & \vdots & \ddots & \vdots \\ 1 & 1 & \dots & 1 \\ rs_m Q_0 & rs_m Q_1 & \dots & rs_m Q_m \end{bmatrix} \quad \dots (20)$$

Let us denote the matrix with constant coefficients

$$\int \int R(Q) N(Q) dS = P$$

$$m \times (m+1) \quad (21)$$

for brevity. Here  $P$  is obviously a rectangular matrix of  $m$  rows and  $(m+1)$  columns. The coefficients of this matrix are completely determined from the fundamental solutions of the integral equation and from the geometry of the system. The  $(m+1)$  arbitrary constants are to be determined from the  $m$  equations (19) viz.,

$$\vec{v} = \begin{bmatrix} v_1 \\ v_2 \\ \vdots \\ v_m \end{bmatrix} = P \begin{bmatrix} x_0 \\ x_1 \\ \vdots \\ x_m \end{bmatrix} = P\vec{x} \quad \dots (22)$$

It is obvious that only  $m$  of the  $(m+1)$  arbitrary constants  $(x_0, x_1, x_2, \dots, x_m)$  can be determined from these  $m$  equations in terms of  $v_1, v_2, v_3, \dots, v_m$ . One arbitrary constant will remain undetermined. The solution therefore remains apparently arbitrary for one arbitrary constant, which it should not according to the uniqueness theorem.

We shall show later, that though the surface densities cannot be uniquely determined, the matrix  $P$  satisfies some general conditions so that the potential function becomes unique. Before doing this, we shall show that a unique relation between the total currents through the electrodes and their potentials exists, if we make use of the Green's Reciprocal Theorem. The total current  $i_l$  on the  $l$ -th electrode is given by,

$$\begin{aligned} i_l &= - \frac{\kappa}{4\pi} \iint_{S_l} \left( \frac{\partial \phi_l}{\partial n} \right) dS = \kappa \iint_{S_l} \sigma_l(Q) dS \\ &= \kappa \left( \iint N(Q) d\vec{S} \right)_l \end{aligned} \quad \dots (23)$$

Let us call the  $m \times (m+1)$  matrix

$$\iint N^0(Q) dS = Q \quad \dots (24)$$

$N^0(Q)$  being formed from  $N(Q)$  by removing its first row.

Thus, 
$$\vec{i} = \kappa Q \vec{x} \quad \dots (25)$$

By the equation of constraint (5) the sum of the elements of a column of must be zero, that is, the rows of  $Q$  are linearly dependent.

That is

$$(1, 1, \dots, 1)Q = 0 \quad \dots (26)$$

or 
$$Q' \begin{bmatrix} 1 \\ 1 \\ \vdots \\ 1 \end{bmatrix} = 0 \quad \dots (26')$$

#### UNIQUE RELATION BETWEEN CURRENTS AND POTENTIALS

Let  $\vec{w}$  be another system of potentials and  $\vec{j}$  the corresponding currents and  $\psi(P)$  be the corresponding potential at a point  $P$ .

Then by Green's Theorem,

$$\begin{aligned} 0 &= \iiint (\psi \nabla^2 \phi - \phi \nabla^2 \psi) d\tau = \sum_{l=1}^m \iint_{S_l} \left( \chi \frac{\partial \phi}{\partial n} - \phi \frac{\partial \psi}{\partial n} \right) dS \\ &= - \frac{4\pi}{\kappa} \sum_{l=1}^m (w_l i_l - \psi_l j_l) \end{aligned}$$



Therefore

$$\sum_i w_{ij} v_i = \sum_j v_j j$$

or 
$$w_{ij} = i \quad w = v' \quad j = j' \quad v$$

Now 
$$\vec{r} = P\vec{x} \quad \text{and} \quad \vec{w} = P\vec{y} \quad (\text{say})$$

$$\vec{i} = \kappa \vec{Q}\vec{x} \quad \text{and} \quad \vec{j} = \kappa \vec{Q}\vec{y} \quad (\text{say})$$

Thus, 
$$\vec{w}'\vec{i} = \kappa \vec{y}'P'Q\vec{x} \quad \vec{j}'\vec{r} = \kappa \vec{y}'Q'P\vec{x}$$

or 
$$\vec{y}'P'Q\vec{x} = \vec{y}'Q'P\vec{x}$$

for any arbitrary  $\vec{x}$  and  $\vec{y}$ . Therefore

$$P'Q = Q'P \quad (P'Q)'$$
(27)

or  $P'Q$  is a symmetric matrix of  $(m+1) \times (m+1)$  order.

Again from (22) (25) and (27)

$$Q'\vec{r} = Q'P\vec{x} = P'Q\vec{x} = I \quad P\vec{i}$$

Thus we obtain the important result.

$$\kappa Q'\vec{r} = P\vec{i}$$
(28)

That is, the relation between the potentials on the electrodes and the currents flowing through them is unique and free from the inherent arbitrariness.

The currents  $\vec{i}$  can be linearly expressed in terms of the potentials  $\vec{v}$  from this equation (28). Multiplying both sides of equation (28) by  $P$  and denoting by  $U$  the Legendre Transform of  $P$  i.e.,

$$U \equiv P \quad P'$$
... (29)

we obtain

$$\kappa P Q' \vec{v} = P \quad P' \vec{i}$$

The  $(m \times m)$  matrix  $U$  is non-singular (See Appendix II), and thus

$$\vec{i} = \kappa U^{-1} P Q' \vec{v}$$
... (30)

It can also be shown that the matrix  $U^{-1}PQ'$  is symmetric (Appendix II). Thus,

$$\vec{i} = \kappa U^{-1}PQ'\vec{v} = \kappa QP'U^{-1}\vec{v} \quad \dots (31)$$

When the potentials  $v_1, v_2, \dots, v_m$  on the electrodes have the same value, say  $v_0$  then it follows from (26') that

$$\vec{i} = \kappa U^{-1}PQ' \begin{bmatrix} 1 \\ 1 \\ \vdots \\ 1 \end{bmatrix} \vec{v}_0 = 0$$

which means physically that no current will flow through the electrodes, if they are kept at the same potential

#### COMPLETE SOLUTION OF THE PROBLEM

It has been shown in Section 3, that all the  $(m+1)$  arbitrary constants  $x_0, x_1, x_2, \dots, x_m$  cannot be determined from the boundary conditions and one of these will remain arbitrary. Instead of choosing any particular one of these constants  $x_0, x_1, \dots, x_m$  as arbitrary we can introduce a new arbitrary constant which appears in a natural way. There are  $m$  equations in (22), and there are  $(m+1)$  unknowns to be determined. Multiplying both sides of equation (22) by  $P'$  which is a  $(m+1) \times m$  matrix, we get  $(m+1)$  linear equations.

$$P'\vec{v} = P'\vec{P}x$$

Here  $P'P$  is a  $(m+1) \times (m+1)$  matrix and is of rank  $m$ . It can be shown that the solution of these equations always exists (See Appendix III) and the solution is,

$$\vec{x} = P'U^{-1}\vec{v} + \alpha\vec{g} \quad \dots (32)$$

where  $\alpha$  is an arbitrary constant and the vector  $\vec{g}$  having  $(m+1)$  elements satisfies the homogeneous equation

$$P'\vec{P}g = 0 \quad \dots (33)$$

Further  $\vec{g}$  is not a null-vector

This vector  $\vec{g}$  has some interesting properties. Let us form a particular surface distribution  $\vec{\omega}(s)$  by putting  $\vec{x} = \vec{g}$  in (16),

$$\vec{\omega}(s) = N(s)\vec{g} \quad \dots (34)$$

Since (See Appendix III)

$$\vec{P}g = 0, \quad \vec{Q}g = 0 \quad \dots (35)$$

$$\vec{v} = \vec{P}g = 0 \quad \text{and} \quad \vec{i} = \kappa\vec{Q}g = 0$$

This means that this particular non-trivial surface-distribution  $\vec{\omega}(s)$  gives rise to null potentials on the electrode surfaces  $S_1, S_2, \dots, S_m$  at the same time the currents flowing through the electrodes also vanish. This appears to be paradoxical at first sight. But we can identify this peculiar distribution with the help of relations (7.1) and (7.2). Since the potential  $\phi(s)$  vanishes on the electrode surfaces, so by Green's Theorem,

$$\begin{aligned} \iiint (|\text{grad } \phi|^2 + \phi \nabla^2 \phi) d\tau &= \iiint \text{div } (\phi \text{ grad } \phi) d\tau \\ &= - \sum_{i=1}^m \int_0 \int_{S_i} \phi \frac{\partial \phi}{\partial n} dS \\ &= 0 \end{aligned}$$

Thus,  $|\text{grad } \phi|^2 = 0$  everywhere which means that  $\phi = 0$  everywhere inside  $S_0$ . This means particularly,

$$\left( \frac{\partial \phi}{\partial n} \right)_{S_i} = 0$$

From (7.1) and (7.2) it follows,

$$\omega_i(s) = 0, \quad i = 1, 2, 3, \dots, m \quad (36)$$

and from (11),

$$\omega_0(s) + \int_{S_n} K(Q, s) \omega_0(Q) dS = 0 \quad (37)$$

This integral equation has a non-trivial solution according to the Fredholm Theory.\*  $\omega_0(s)$  therefore exists mathematically. Since the potential function vanishes throughout the region inside  $S_0$  and as it is continuous on  $S_0$ , the enclosing surface  $S_0$  becomes an equipotential surface with zero potential due to this particular distribution. The surface distribution  $\omega_0(s)$  is identical to the distribution which will be formed if the surface  $S_0$  were a perfect conductor, grounded and subject to inductive influences of the field due to outside bodies or in other words if  $S_0$  were an electrical shield for the internal conductors. Thus such a surface distribution physically can exist. Since this surface distribution  $\vec{\omega}(s)$  gives rise to zero potential throughout the region inside  $S_0$  then from (17)

$$\vec{\rho'}(P)\vec{g} = \phi(P) = 0 \quad (38)$$

for this particular surface distribution. Now, when the potentials on the electrodes are given to be  $v_1, v_2, v_3, \dots, v_m$ , the arbitrary constants  $x_0, x_1, x_2, \dots, x_m$ , can be determined completely from the equation (29) but for an arbitrary constant

$\sigma$ . From (16) the surface density  $\vec{\sigma}(s)$  can be expressed in terms of the electrode

\*As a non-trivial solution of its Transposed equation exists,

potentials  $v_1, v_2, \dots, v_m$  but not uniquely because the arbitrary constant  $\alpha$  remains undetermined from the boundary conditions, thus

$$\overrightarrow{\sigma}(s) = N(s)\overrightarrow{x} - N(s)P'U^{-1}\overrightarrow{v} + \alpha N(s)\overrightarrow{g} \quad \dots \quad (39)$$

From (17), the potential function  $\phi(P)$  at the point  $P$  is

$$\begin{aligned} \phi(P) &= \overrightarrow{\rho'}(P)\overrightarrow{x} \\ &= -\overrightarrow{\rho'}(P)P'U^{-1}\overrightarrow{v} + \alpha\overrightarrow{\rho'}(P)\overrightarrow{g} \\ &= \overrightarrow{\rho'}(P)P'U^{-1}\overrightarrow{v} \quad \dots \quad (40) \end{aligned}$$

the second term vanishes as has been shown just now. This is the complete solution of the boundary value problem and it is also unique. The apparent paradox is thus removed. Though the surface distribution cannot be determined uniquely, the potential function can be determined uniquely from the boundary conditions.

Since  $\overrightarrow{\rho'}(P)$  assumes the values  $\overrightarrow{\rho'_1}, \overrightarrow{\rho'_2}, \dots, \overrightarrow{\rho'_m}$  when the point  $P$  lies on the electrodes, the scalar products  $\overrightarrow{\rho'_1}\overrightarrow{g_1}, \overrightarrow{\rho'_2}\overrightarrow{g_2}, \dots, \overrightarrow{\rho'_m}\overrightarrow{g_m}$  should vanish according to (35). Or in other words

$$P'\overrightarrow{g} = 0$$

which has been proved independently in Appendix III.

#### INFINITELY EXTENDED MEDIUM AND CORRESPONDENCE WITH THE MAXWELL'S COEFFICIENTS OF CAPACITY

When the semi-conducting medium extends to infinity, the problem becomes somewhat modified. The bounding surface  $S_0$  no longer exists and therefore the boundary condition (4.2) is not material in this case, and has to be replaced by the usual regularity conditions for the Newtonian Potential at infinity. Accordingly, the equation of constraint (5), does not exist for this case. Hence the problem becomes identical with the Dirichlet's Exterior Problem for many bodies and its solution is well known (Maxwell). Thus it reduces to the electrostatic problem for many bodies discussed by Maxwell. The matrices  $P$  and  $Q$  both become regular square matrices of  $m \times m$  order. Consequently,

$$\overrightarrow{v} = \alpha QP^{-1}\overrightarrow{v}, \quad \overrightarrow{v} = \frac{1}{\alpha} PQ^{-1}\overrightarrow{v}$$

in this case. The matrix  $QP^{-1}$  however, still remains symmetric, because Green's

Reciprocal Theorem can still be applied. The elements of  $QP^{-1}$  are obviously the usual Maxwell's Coefficients of capacity (Jeans, 1923)

THE PHYSICAL INTERPRETATION OF THE SOLUTION AND CROSS-CURRENTS BETWEEN ELECTRODES

The currents flowing through the electrodes and the potentials of the electrodes are the only observable physical quantities. The natural question is how to determine the matrices  $P$  and  $Q$  or their functions from those observable quantities. First following Krichhoff (1893) let us give the first electrode unit potential keeping the rest at zero potential and designate the corresponding currents through them as  $c_{11}, c_{21}, c_{31}, \dots, c_{m1}$ . These currents must satisfy the fundamental property that their sum is zero, that is,

$$\begin{aligned} c_{11} + c_{21} + c_{31} + \dots + c_{m1} &= 0 \\ c_{11} &= -c_{21} - c_{31} - \dots - c_{m1} \end{aligned}$$

Physically it is obvious that no cross-currents (which have not yet been defined mathematically) can flow between the second and the third electrodes and so on, because they are at the same potential. Actually, the current which enters the first electrode leaves through the other electrodes. The current that enters through the second electrode is  $c_{21}$  and therefore the 'cross-current' between the first and the second electrode is  $-c_{21}$  and so on. Let us call  $c_{12}, c_{22}, c_{32}, \dots, c_{m2}$  the currents flowing through the electrodes when the second is kept at unit potential and the rest at zero potential and so on. Then from the fundamental relation (28),

$$\kappa Q' \begin{bmatrix} 1 \\ 0 \\ \vdots \\ 0 \end{bmatrix} = P' \begin{bmatrix} c_{11} \\ c_{21} \\ \vdots \\ c_{m1} \end{bmatrix}, \quad \kappa Q' \begin{bmatrix} 0 \\ 1 \\ \vdots \\ 0 \end{bmatrix} = P' \begin{bmatrix} c_{12} \\ c_{22} \\ \vdots \\ c_{m2} \end{bmatrix} \text{ etc.}$$

$$\kappa Q' \begin{bmatrix} 1 & 0 & 0 \dots 0 \\ 0 & 1 & 0 \dots 0 \\ \dots & \dots & \dots & \dots \\ 0 & 0 & 0 \dots 1 \end{bmatrix} = P' \begin{bmatrix} c_{11} & c_{12} & \dots & c_{1m} \\ c_{21} & c_{22} & \dots & c_{2m} \\ \dots & \dots & \dots & \dots \\ c_{m1} & c_{m2} & \dots & c_{mm} \end{bmatrix}$$

that is, where  $\kappa Q' = P' C$  say, where  $C = (c_{ij})$  ... (41)

Physically, the non-diagonal elements of this matrix represent the reverse cross-currents.

Again from (41) and (29) and Appendix II,

$$\kappa PQ' = PP' C \equiv UC$$

$$\text{or} \quad C = \kappa U^{-1} PQ' = \kappa (U^{-1} PQ')' = C' \quad \dots (42)$$

and from (26')

$$C \begin{bmatrix} 1 \\ 1 \\ 1 \end{bmatrix} = \kappa U^{-1} PQ' \begin{bmatrix} 1 \\ 1 \\ 1 \end{bmatrix} = 0 \quad \dots (43)$$

Thus  $C$  is a symmetric matrix. Physically this means that the cross-current that flows from the second electrode to the first when the first is at unit potential is equal to the cross-current that flows from the first to the second when the second is kept at unit potential and so on.

So far the concept of cross-currents is quite obvious and simple. The next question is what are the cross currents when the first, second, ... electrodes have any potentials  $v_1, v_2, v_3 \dots v_m$ . Physically such cross currents must exist and shall have the property that the current which enters an electrode must branch out as cross-currents to other electrodes. Further they will have anti-symmetric property that is, cross-current from the first to the second electrode will be equal and opposite to that from the second to the first. Our task is to spot this cross-current matrix. Now from (31)

$$\begin{aligned} \vec{i} &= \kappa U^{-1} PQ' \vec{v} = C \vec{v} \\ &= C \begin{bmatrix} v_1 & 0 & 0 & \dots & 0 \\ 0 & v_2 & 0 & \dots & 0 \\ \dots & \dots & \dots & \dots & \dots \\ 0 & 0 & 0 & \dots & v_m \end{bmatrix} \begin{bmatrix} 1 \\ 1 \\ \vdots \\ 1 \end{bmatrix} \\ &= CV \begin{bmatrix} 1 \\ 1 \\ \vdots \\ 1 \end{bmatrix} \quad \dots (44) \end{aligned}$$

where  $V$  is the diagonal matrix

$$V_{m \times m} = \begin{bmatrix} v_1 & 0 & 0 & \dots & 0 \\ 0 & v_2 & 0 & \dots & 0 \\ 0 & 0 & v_3 & \dots & 0 \\ \dots & \dots & \dots & \dots & \dots \\ 0 & 0 & 0 & \dots & v_m \end{bmatrix} \quad \dots (45)$$

$$\text{Let } J_{m \times m} \equiv CV - VC \quad \dots (46)$$

This is a skew-symmetric matrix and

$$\begin{bmatrix} 1 \\ 1 \\ 1 \end{bmatrix} = CV \begin{bmatrix} 1 \\ 1 \\ 1 \end{bmatrix} - VC \begin{bmatrix} 1 \\ 1 \\ 1 \end{bmatrix}$$

$$\bar{C}r \quad \text{from (43)}$$

$$\vec{i} \quad \text{from (44)}$$

or

$$J_{12} + J_{13} + \dots + J_{1m} = i_1, \quad J_{21} + J_{23} + \dots + J_{2m} = i_2$$

That is, the matrix  $J$  has the requisite fundamental property that the sum of the cross currents branching out from an electrode is equal to the current that enters it. Further the matrix  $J$  reduces to the column vectors of  $C$  when  $v_1 = 1, v_2 = 0, v_3 = 0, \dots, v_m = 0$  etc., that is, they become identical with the cross-currents for the physically obvious fact mentioned at the beginning of this section. More explicitly, the cross-current matrix  $J$  is

$$\begin{aligned} 0 & \quad c_{12}(v_2 - v_1) \quad c_{13}(v_3 - v_1) \quad \dots \quad c_{1m}(v_m - v_1) \\ c_{21}(v_1 - v_2) & \quad 0 \quad c_{23}(v_3 - v_2) \quad \dots \quad c_{2m}(v_m - v_2) \end{aligned} \quad (47)$$

$$c_{m1}(v_1 - v_m) \quad c_{m2}(v_2 - v_m) \quad \dots \dots \dots 0$$

The skew symmetry is consistent with the physical property of cross-currents, viz. the cross-current from the first electrode to the second is the reverse of that flowing from the second to the first.

The Kirchhoff's Laws take the following form for continuous media :

$$J = CV - VC \quad (48)$$

$$J \begin{bmatrix} 1 \\ 1 \\ \vdots \\ 1 \end{bmatrix} = \vec{i} \quad \dots (59)$$

where  $C$  is the conductivity and  $V$  the diagonal matrix defined earlier.

Physically, the Ohmic heat generated by the hypothetical cross-currents will be

$$\begin{aligned}
 \frac{1}{2} \sum_{p=1}^m \sum_{q=1}^m j_{pq} (v_p - v_q) &= \frac{1}{2} \sum_{p=1}^m v_p \sum_{q=1}^m j_{pq} - \frac{1}{2} \sum_{q=1}^m v_q \sum_{p=1}^m j_{pq} \\
 &= \frac{1}{2} \sum_{p=1}^m v_p \sum_{q=1}^m j_{pq} + \frac{1}{2} \sum_{q=1}^m v_q \sum_{p=1}^m j_{qp} \\
 &= \frac{1}{2} \sum_{p=1}^m v_p i_p + \frac{1}{2} \sum_{q=1}^m v_q i_q \\
 &= \sum_{p=1}^m v_p i_p
 \end{aligned}$$

which is identical with the expression for the actual heat generated. Thus, physically the cross-currents can replace the electrode currents for all purposes

#### MATHEMATICAL INTERPRETATION OF THE SOLUTION AND EXISTENCE OF CROSS-CURRENTS

In the preceding section we demonstrated the existence of cross-currents from purely physical considerations. The cross-current matrix did not come out automatically from the solution of the integral equations (11). We shall now prove, by suitable choice of the solution of the integral equations (14), the existence of cross-currents as also the matrix equation (48) satisfied by them.

Any linear combination of the  $(m+1)$  linearly independent solutions  $\vec{v}_0(s)$ ,  $\vec{v}_1(s)$ , ...,  $\vec{v}_m(s)$  of the simultaneous homogeneous integral equations (11) is a solution. Since these  $(m+1)$  solutions are all linearly independent exactly  $(m+1)$  linearly independent solutions can be constructed through linear combinations of these solutions. This new set of solutions can be taken as the fundamental set. We choose for the first solution  $\vec{v}_0(s)$  the peculiar characteristic solution  $\vec{\omega}(s)$  of the problem (34). Thus,

$$v_{00}(s) = \omega_0(s), v_{10}(s) = \omega_1(s) = 0 \quad v_{m0}(s) = \omega_m(s) = 0$$

Through this choice of solution the 0-th columns of the both the  $m \times (m+1)$  matrix  $P$  and  $Q$  become null vectors. Let us denote by  $\Pi$  the  $m \times m$  square matrix which is formed from  $P$  leaving the 0-th column which has become a null vector. The rank of this  $m \times m$  matrix  $\Pi$  is full as the rank of the  $m \times (m+1)$  matrix  $P$  was proved to be  $m$ . Let us form a new set of linearly independent solutions

$$\Lambda(s) \equiv (\vec{\omega}(s), \vec{\lambda}_1(s), \vec{\lambda}_2(s), \dots, \vec{\lambda}_m(s))$$



by linear combinations of  $\vec{v}_1(s), \vec{v}_2(s), \dots, \vec{v}_m(s)$

$$\wedge(s)_{(m+1) \times (m+1)} = \begin{pmatrix} \vec{\omega}(s).N(s)\Pi^{-1} \\ (m+1) \times m \end{pmatrix}$$

For this fundamental solution let us denote by the matrix  $\Theta$  the integral,

$$\Theta = \iint \wedge^0(Q) dS$$

By choice of this fundamental solution  $\wedge(s)$  the matrix  $P$  defined in (21) becomes the identity matrix  $I_m$  with null vector as its 0-th column. Thus the symmetry relation (27),

$$P'Q = Q'P$$

reduces in this case to

$$\Theta = \Theta'$$

and the relation (32) reduces simply to

$$\vec{x} = \begin{pmatrix} 0 \\ v_1 \\ v_2 \\ \vdots \\ v_m \end{pmatrix} + \alpha \begin{pmatrix} 1 \\ 0 \\ 0 \\ \vdots \\ 0 \end{pmatrix}$$

Thus the vector

$$\begin{pmatrix} x_1 \\ x_2 \\ \vdots \\ x_m \end{pmatrix} = \begin{pmatrix} v_1 \\ v_2 \\ \vdots \\ v \end{pmatrix}$$

The diagonal matrix  $\text{dia}(x_1, x_2, \dots, x_m)$  is

$$\text{dia}(x_1, x_2, \dots, x_m) = \text{dia}(v_1, v_2, \dots, v_m) \equiv V$$

and from (41)

$$C = \kappa \mathbb{1}$$

By this transformation, the  $Q$  matrix becomes a square and symmetric matrix  $\Theta$ . The current  $i_1$  flowing through the first electrode is given by

$$\begin{aligned} \kappa \int_{S_1} \sigma_1(Q) dS = i_1 &= \kappa \{ x_1 \int_{S_1} \lambda_{11}(Q) dS + x_2 \int_{S_1} \lambda_{12}(Q) dS + \dots \} \\ &= \kappa \{ \theta_{11}x_1 + \theta_{12}x_2 + \dots + \theta_{1m}x_m \} \\ &= \kappa \{ -(c\theta_{21} + \theta_{31} + \dots + \theta_{m1})x_1 + \theta_{21}x_2 + \theta_{31}x_3 + \dots + \theta_{m1}x_m \} \\ &= \kappa \{ \theta_{21}(x_2 - x_1) + \theta_{31}(x_3 - x_1) + \dots + \theta_{m1}(x_m - x_1) \} \\ &= \kappa \{ (x_2 - x_1) \int_{S_2} \lambda_{21}(Q) dS + (x_3 - x_1) \int_{S_3} \lambda_{31}(Q) dS + \dots \} \end{aligned}$$

Mathematically this relation means that the surface integral over the first electrode surface is contributed by a sum of surface integrals over all the electrodes surfaces excepting the first one. The surface integral  $\kappa \iint_{S_1} \sigma_1(Q) dS$  represents the total current flowing from the first electrode which equals the sum of currents flowing through the other electrode surfaces. Thus,

$$\kappa(i_2 - i_1) \iint_{S_2} \lambda_{21}(Q) dS = \kappa(i_2 - i_1) i_{21}$$

represents the cross-current flowing from the first to the second electrode surface which has been denoted by  $i_{21}$ . The cross-current matrix is obviously,

$$J = \kappa \{ \text{dia}(x_1, x_2, \dots, x_m) - I \text{ dia}(x_1, x_2, \dots, x_m) \}$$

$$C' = VC'$$

#### DISCUSSION OF THE MAIN RESULTS

Before attempting to deduce the usual Kirchhoff's Laws it will be profitable to recapitulate the important results already deduced.

(a) We have deduced in Section 4, that when the electrodes are kept at the same potential no currents will flow from them. This confirms to the physical fact.

(b) The algebraic sum of the currents flowing through all the electrodes is nil.

(c) The algebraic sum of the currents flowing in and flowing out from an electrode is nil. Equation (49).

(d) The cross-current flowing between any two electrodes is proportional to the difference of potentials between these electrodes. Equation (48).

These are summarised in the following formulae already deduced which correspond to Kirchhoff's Laws for a continuous medium.

$$J = C'V - VC' \quad \dots (48)$$

$$\sum_i i = J \begin{pmatrix} 1 \\ 1 \\ \vdots \\ 1 \end{pmatrix} = 0 \quad \dots (49)$$

$$\text{where } C' = C'', \quad \Gamma = \text{dia}(v_1, v_2, \dots, v_m) \quad \dots (50)$$

$$\text{and } (1, 1, \dots, 1)C = 0 \quad \dots (51)$$

The coefficients of the conductivity matrix  $C$  are difficult to calculate mathematically from the geometry of the system. Experimentally each coefficient  $c_{ik}$  of the matrix can be determined by keeping the  $i$ -th electrode at unit potential and the remaining electrodes connected to ground through ammeters. The current

flowing from the  $k$ -th electrode through the ammeter to the ground is the cross-current from the  $l$ -th electrode to the  $k$ -th electrode and is  $c_{lk}$ . In this way all the elements of  $C$  can be experimentally determined.

The boundary value problem can likewise be solved when the total currents flowing through the electrodes are specified instead of the potentials on the electrodes. It can also be solved when potentials are specified on some of the electrodes and the total currents are specified for the remaining electrodes. As it will make this paper too lengthy the solutions are not presented here.

For discussing the usual Kirchhoff's Laws it is necessary to consider a special case of the problem. It is quite possible that only a few of the  $m$  electrodes are kept 'live' that is connected to sources of constant potential, the remaining are kept floating. This will not affect the conductivity matrix  $C$  which is entirely governed by the geometry of the system. Since these 'dead' electrodes cannot draw any current from any source, no current can flow into them. If we enumerate these dead electrodes from  $k$  onwards up to  $m$ , then

$$i_k = 0, \quad i_{k+1} = 0, \quad \dots, \quad i_m = 0$$

However, cross-currents will flow from them according to equation (48). The potential on these dead electrodes can be determined from the equation,

$$\begin{bmatrix} i_1 \\ i_2 \\ \vdots \\ i_{k-1} \\ 0 \\ 0 \\ \vdots \\ 0 \end{bmatrix} = C \begin{bmatrix} v_1 \\ v_2 \\ \vdots \\ v_{k-1} \\ v_k \\ \vdots \\ v_m \end{bmatrix}$$

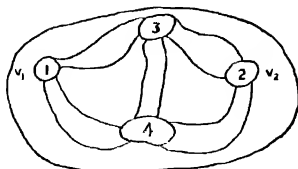
in terms of the given  $v_1, v_2, \dots, v_{k-1}$ . If the currents  $i_1, i_2, \dots, i_{k-1}$  are specified, the potentials can also be determined by partitioning the matrix  $C$ .

#### DEDUCTION OF THE USUAL KIRCHHOFF'S LAWS FOR LINE CONDUCTORS

Any net-work of resistors is actually some continuous media having some geometrical form. If we imagine the typical Wheatstones Bridge Network as a continuous medium, it will be somewhat like the following diagram :

There are four electrodes embedded in the semi-conducting medium having five lobes. The two electrodes (1) and (2) are connected to batteries and are at potentials  $v_1$  and  $v_2$ , the two others (3) and (4) are 'dead' electrodes, but are at unknown potentials  $v_3$  and  $v_4$  to be determined. The cross-currents flowing between the

electrodes (1) and (3) is  $j_{13} = c_{13}(v_1 - v_3)$ . Mathematically,  $c_{13}$  is difficult to determine from this geometry of the system. Since we are not interested in the micro-



scopic distribution of currents in the material we take the macroscopic Ohm's Law. If  $R_{13}$  be the lumped resistance of the lobe, then macroscopic Ohm's Law states that the current between the electrodes (1) and (3) is  $(v_1 - v_3)/R_{13}$ , that is,

$$j_{13} = \frac{v_1 - v_3}{R_{13}}$$

From this relation we can at once get the value of the coefficient  $c_{13}$  of the conductivity matrix  $C$  for this case. Thus

$$c_{13} = \frac{1}{R_{13}}$$

which is identical with the total conductance of the lobe. Similarly, we can find the other elements of the  $C$  matrix. If two electrodes are not connected through a lobe, then the corresponding coefficient will be zero, i.e.  $c_{12} = 0$  in this case, because the electrodes (1) and (2) are not connected by any lobe of the material. Thus the conductivity matrix in this case is

$$C = \begin{bmatrix} \left( \frac{1}{R_{13}} + \frac{1}{R_{14}} \right) & 0 & \frac{1}{R_{13}} & \frac{1}{R_{14}} \\ 0 & \left( \frac{1}{R_{23}} + \frac{1}{R_{24}} \right) & \frac{1}{R_{23}} & \frac{1}{R_{24}} \\ \frac{1}{R_{13}} & \frac{1}{R_{23}} & -\left( \frac{1}{R_{13}} + \frac{1}{R_{23}} + \frac{1}{R_{24}} \right) & \frac{1}{R_{34}} \\ \frac{1}{R_{14}} & \frac{1}{R_{24}} & \frac{1}{R_{34}} & -\left( \frac{1}{R_{14}} + \frac{1}{R_{24}} + \frac{1}{R_{34}} \right) \end{bmatrix}$$

The number of independent current variables is  $2 - 1 = 1$  in this case.

All the equations deduced for the continuous media remain the same. It is now apparent that equation (49) expresses Kirchhoff's Nodal Law. The usual Mesh Law follows as an obvious consequence of the matrix equation (48) if the conductances are replaced by resistances.

For alternating current circuits containing capacitors and inductances besides resistors, the usual Kirchhoff's Laws are extended by analogy. Through analogy the equations (48) and (49) can also be extended to the case of alternating currents. The only difference will be that the potentials and currents will be complex quantities and the elements of the conductivity matrix  $C$  will also be complex. This admittance matrix  $C$  will, however, remain symmetric and all other equations will remain the same. The complex elements of this admittance matrix can likewise be calculated from the branch impedances. This will be discussed in a future communication.

The number of independent variables are at once apparent from the generalised form of Kirchhoff's Laws. If there are  $n$  live electrodes, the number of independent voltage variables is  $n$  and the number of independent current variables is  $n - 1$ .

## APPENDIX I

### UNIQUENESS OF SOLUTION

Suppose  $\psi$  be another solution besides  $\phi$

$$\text{Let } \chi = \phi - \psi$$

$$\text{Thus, } \nabla^2 \chi = 0$$

$$\text{and } \chi = 0 \quad \text{on } S_1, S_2, \dots, S_m \quad \text{also}$$

$$\left( \frac{\partial \chi}{\partial n} \right)_{S_0} = 0 \quad \text{on } S_0$$

Now

$$\operatorname{div}(\chi \operatorname{grad} \chi) = (\operatorname{grad} \chi)^2 + \chi \nabla^2 \chi (\operatorname{grad} \chi)^2$$

By Green's Theorem,

$$\iiint (\operatorname{grad} \chi)^2 d\tau = \iiint \operatorname{div}(\chi \operatorname{grad} \chi) d\tau$$

$$= \sum_{i=0}^m \iint_{S_i} \chi \left( \frac{\partial \chi}{\partial n} \right)_{S_i} dS$$

$$= 0$$

Therefore

$$\text{grad } \chi = 0$$

Or,

$$\phi - \psi = \chi = \text{constant} = 0$$

since

$$\chi = 0, \text{ on } S_1, S_2, \dots, S_m$$

Hence

$$\phi = \psi$$

*Equation of constraint*

Since  $\nabla^2 \phi = 0$  in the region formed by the surfaces  $S_0, S_1, S_2, \dots, S_m$  then by Green's Theorem,

$$0 = \iiint \nabla^2 \phi d\tau = \sum_{i=0}^m \iint_{S_i} \left( \frac{\partial \phi}{\partial n} \right)_{S_i} dS$$

$$= \sum_{i=1}^m \iint_{S_i} \left( \frac{\partial \phi}{\partial n} \right)_{S_i} dS + \iint_{S_0} \left( \frac{\partial \phi}{\partial n} \right)_{S_0} dS$$

since by the boundary condition (4.2)  $\left( \frac{\partial \phi}{\partial n} \right)_{S_0} = 0$

$$\sum_{i=1}^m \iint_{S_i} \left( \frac{\partial \phi}{\partial n} \right)_{S_i} dS = 0$$

Every solution of the boundary value problem has to satisfy this equation of constraint. Physically this means that the algebraic sum of the total currents flowing through the electrode must vanish.

## APPENDIX II

### REGULARITY OF THE MATRIX

Since  $P'$  is a matrix of  $(m+1)$  rows and  $m$  columns, the matrix  $P'P' \equiv U$  has  $m$  rows and  $m$  columns and is symmetric square matrix. Let  $\vec{p}_1, \vec{p}_2, \dots, \vec{p}_m$  denote the  $m$  row vectors of  $P'$ . Let us suppose that there is a linear dependence amongst them, viz.,

$$c_1 \vec{p}_1 + c_2 \vec{p}_2 + \dots + c_m \vec{p}_m = 0$$

But from the boundary conditions (22),

$$c_1 = p_{10}x_0 + p_{11}x_1 + \dots + p_{1m}x_m$$

$$c_2 = p_{20}x_0 + p_{21}x_1 + \dots + p_{2m}x_m$$

$$c_m = p_{m0}x_0 + p_{m1}x_1 + \dots + p_{mm}x_m$$

Multiplying by  $c_1, c_2, \dots, c_m$  respectively these equations and adding,

$$c_1 v_1 + c_2 v_2 + \dots + c_m v_m = (c_1 p_{10} + c_2 p_{20} + \dots + c_m p_{m0})x_0 + (c_1 p_{11} + c_2 p_{21} + \dots + c_m p_{m1})x_1$$

$= 0$  by the above assumption

If the assumption is true then there must always be a definite linear relation between the potentials of the electrodes, which is absurd. This will mean that if we give a potential to one electrode keeping the remaining at zero potential the solution will not exist. The potentials on the electrodes, however can be arbitrarily given. This is contradictory to the Existence Theorem already proved. Thus there cannot be any linear dependence amongst the  $m$  row vectors of  $P$ . The rank of  $P$  is therefore full. Consequently, the rank of its Legendre Transform  $PP'$  is also full, that is  $PP'$  is a nonsingular matrix. Thus  $U^{-1}$  exists.

*Symmetry of  $U^{-1}PQ'$*

Since from (27)

$$P'Q = Q'P$$

$$UQ = PP'Q = PQ'P$$

thus,

$$Q = U^{-1}PQ'P \text{ since } U^{-1} \text{ exists}$$

Or,

$$QP' = U^{-1}PQ'PP' = U^{-1}PQ'U$$

Thus,

$$QP'U^{-1} = U^{-1}PQ' = (QP'U^{-1})'$$

Again,

$$(U^{-1}PQ')' = QP'U^{-1} = U^{-1}PQ'$$

Therefore, the matrices  $QP'U^{-1}$  and  $U^{-1}PQ'$  are symmetric and identical. Moreover  $QP'$  and  $PQ'$  are connected by a similarity transformation

### APPENDIX III

As has been proved in Appendix II the rank of the  $m \times (m+1)$  matrix  $P$  is  $m$ , and therefore the equation

$$\vec{v} = \vec{P}\vec{x}$$

can always be solved for  $x_0, x_1, x_2, \dots, x_m$ , but with an arbitrary constant. Multiplying the above equation by  $P'$  we get

$$\vec{P}'\vec{v} = P'\vec{P}\vec{x}$$

Here  $P'P$  is a  $(m+1) \times (m+1)$  square matrix but of rank  $m$ . Thus one and only one non-trivial solution of the homogeneous equation,

$$P'P\vec{x} = 0$$

exists according to the Fundamental Theorem of Linear Algebra.) Let us

denote this non-trivial solution by  $\vec{y}$  which has  $(m+1)$  elements. Now,

$$UP = PP'P$$

thus

$$U\vec{P}\vec{y} = P(P'\vec{P})\vec{y} = 0$$

Since  $U^{-1}$  exists as shown in Appendix II, therefore,

$$\vec{P}\vec{y} = 0$$

Or in other words the vector  $\vec{y}$  is orthogonal to the  $m$  row vectors of  $P$ , viz.,  $\vec{p}_1, \vec{p}_2, \dots, \vec{p}_m$ , which have  $(m+1)$  elements each. Obviously, the elements of  $\vec{y}$  are proportional to the determinants,

$$\begin{vmatrix} p_{11} & p_{12} & \dots & p_{1m} \\ p_{21} & p_{22} & \dots & p_{2m} \\ \dots & \dots & \dots & \dots \\ p_{m1} & p_{m2} & \dots & p_{mm} \end{vmatrix}, \dots, \begin{vmatrix} p_{10} & p_{12} & \dots & p_{1m} \\ p_{20} & p_{22} & \dots & p_{2m} \\ \dots & \dots & \dots & \dots \\ p_{m0} & p_{m2} & \dots & p_{mm} \end{vmatrix}$$

because by the well-known theorem of determinants,

$$0 = \begin{vmatrix} p_{10} & p_{11} & p_{12} & \dots & p_{1m} \\ p_{10} & p_{11} & p_{12} & \dots & p_{1m} \\ p_{20} & p_{21} & p_{22} & \dots & p_{2m} \\ \dots & \dots & \dots & \dots & \dots \\ p_{m0} & p_{m1} & p_{m2} & \dots & p_{mm} \end{vmatrix} = p_{10} \times \begin{vmatrix} p_{11} & p_{12} & \dots & p_{1m} \\ p_{21} & p_{22} & \dots & p_{2m} \\ \dots & \dots & \dots & \dots \\ p_{m1} & p_{m2} & \dots & p_{mm} \end{vmatrix} - p_{11} \times \begin{vmatrix} p_{10} & p_{12} & \dots & p_{1m} \\ p_{20} & p_{22} & \dots & p_{2m} \\ \dots & \dots & \dots & \dots \\ p_{m0} & p_{m2} & \dots & p_{mm} \end{vmatrix}$$



as the two rows are identical

Further,

$$\begin{aligned} U\vec{Qg} &= (PP'Q)\vec{g} \\ &\quad - (PQ'P)\vec{g} \end{aligned}$$

because from (27)  $P'Q = Q'P$  and from the result just proved, viz.,  $P\vec{g} = 0$ ,

$$U\vec{Qg} = 0$$

Since,  $U^{-1}$  exists,

$$\vec{Qg} = 0$$

therefore the vector  $\vec{g}$  is also orthogonal to the  $m$  row vectors of  $Q$ .

Again, since  $P'P$  is a symmetric matrix,  $\vec{g}$  is also a solution of the transposed equation that is

$$(P'P)\vec{g} = P'\vec{Pg} = 0$$

Further the scalar product,

$$\vec{g}'P'\vec{r} = (P\vec{g})'\vec{r} = 0$$

because  $P\vec{g} = 0$ . By the Fundamental Theorem of Linear Algebra the solution of the inhomogeneous equation

$$P'\vec{v} = P'\vec{P}$$

always exists whatever  $\vec{v}$  is

Since all the  $m$  rows of the rectangular matrix  $P$  are linearly independent, the right inverse of  $P$  exists (Zornuhl, 1962). Let this be  $W$ , that is

$$PW = I_m$$

where  $I_m$  is the identity matrix of  $m$  elements, and  $W$  is a  $(m+1) \times m$  matrix. Obviously,

$$W = P'U^{-1}$$

because,

$$PW = PP'U^{-1} \equiv UU^{-1} = I_m$$

Thus the general solution of the inhomogeneous equation is,

$$\begin{aligned}\vec{x} &= W\vec{v} + \alpha\vec{g} \\ &= P'U^{-1}\vec{v} + \alpha\vec{g}\end{aligned}$$

where  $\alpha$  is any arbitrary constant which cannot be determined from the boundary conditions

#### REFERENCES

- Courant and Hilbert, *Methoden der Mathematischen Physik*, Bd I, 2nd edition 1931, pp 5-6
- Journs, *Mathematical Theory of Electricity and Magnetism* 4th edition, 1923, p 312, 350-352
- Kuchhoff, *Gesammelte Abhandlungen* pp 33, 151 (Also the articles by F. Auerbach in Winkelmann's *Handbuch der Physik* Vol 3, Part I, 1893 p 204. and article by P. Debye in the *Encyclopaedie der mathematischen Wissenschaften*, Bd V. 2, p 395 et seq
- Maxwell, *Treatise on Electricity & Magnetism* 3rd edition, Vol I, Chapter III.
- Zumahl, *Matrizen*, 3rd edition 1962, pp 116-117.
- Sternberg and Smith, *Theory of Potential and Spherical Harmonics*, 1952, Chap V, p 145, Chap XI.

# Letters to the Editor

*The Board of Editors does not hold itself responsible for opinions expressed in the letters published in this section. The notes containing short reports of original investigations communicated to this section should not contain many figures and should not exceed 500 words in length. The contributions reaching the Secretary by the 15th of any month may be expected to appear in the issue for the next month. No proof will be sent to the author.*

## 1

### ON THE TRANSFER OF ELECTRONIC EXCITATION ENERGY IN LIQUIDS

M. K. MACIWE, J. KISHORE AND K. GOPALA KRISHNAN

DEPARTMENT OF PHYSICS AND ASTROPHYSICS, UNIVERSITY OF DELHI, DELHI

(Received July 26, 1965; Resubmitted Oct. 18, 1965)

Concentration quenching of fluorescence in solutions gives a convenient method for the study of transfer of electronic excitation energy. The diffusion theory of concentration extinction of fluorescence worked out by Frank Wawilow and Sveshniko taking into account the Brownian motion of the particles and collisions of the second kind, gives the following equation.

$$\frac{L_0}{L} = 1 + \frac{2p\tau_0 ckTR(\sigma_1 + \sigma_2)}{3\eta\sigma_1\sigma_2} \quad (1)$$

$L_0$  and  $L$  are the yields of fluorescence in the unextinguished and extinguished solutions,  $p$  the probability of extinction during one collision,  $K$  the Boltzmann Constant,  $T$  the absolute temperature,  $C$  the number of molecules in unit volume,  $R$  radius of the sphere of activity,  $\sigma_1$  and  $\sigma_2$  the kinetic radii of the colliding molecules and  $\eta$  the coefficient of viscosity. However, the experimental results on the quenching of fluorescence indicate that the above mechanism of the transfer of energy by itself is not adequate to explain the phenomenon. Forster has shown that as a consequence of the fluctuations in the distribution of the molecules of the fluorescent material in solutions which are viscous, the concentration extinction of fluorescence for individual excited molecules takes place with different probabilities. The contribution due to this towards quenching is termed 'statistical extinction'. The present measurements of fluorescence yield with varying concentrations of dye stuffs in solutions having different viscosities have been undertaken to confirm the above.

The experimental set-up is the same as described earlier (Machwe *et al.*, 1964). The dyes used in the present investigation are sodium fluorescein and acraflavin. The solvent viscosity is varied by taking suitable glycerine-water mixtures. The exciting radiation is the unpolarised Hg line  $\lambda$  4358Å. In Figs 1, 2, 3 and 4

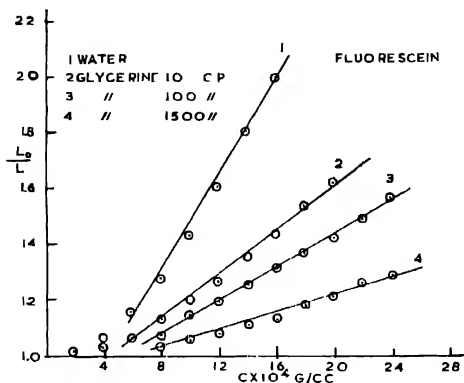


Fig. 1 Fluorescein. Dependence of yield on concentration in (1) water, (2) water glycerine 10 cp, (3) water + glycerine 100 cp and (4) glycerine 1500 cp.

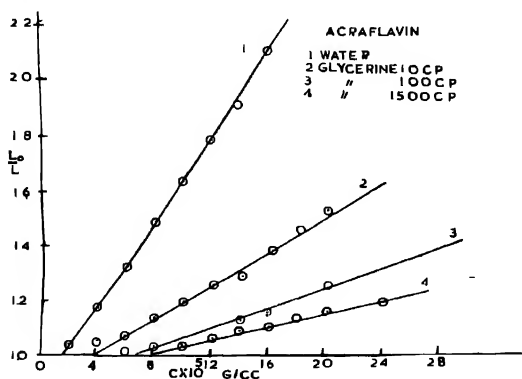


Fig. 2 Acraflavin. Dependence of yield on concentration in the same solvents as fig. 1.

are reproduced the data obtained by us. Figs 1 and 2 show the dependence of fluorescence yield ( $L_0/L$ ) on the concentration ( $C$ ) of the dissolved substance in different solvents having viscosities in the range of 1 cp to 1500 cp. Figs 3 and 4 show the dependence of yield ( $L_0/L$ ) on the viscosity ( $\eta$ ) of the solvent

It will be seen from the graph that, in the concentration region selected, a linear relationship exists between the fluorescence yield ( $I_0/L$ ) and concentration ( $C$ ). This agrees well with the results obtained on the basis of the diffusion theory and indicates the occurrence of collisions of the second kind. For a fixed value of  $\eta$ ,  $\rho$  in Eqn. 1 remains constant and therefore, the statical extinction will have no effect on the linear relation between  $I_0/L$  and  $C$ .

The diffusion theory, Eqn 1, also predicts a linear relationship between  $I_0/L$  and  $1/\eta$ , but our measurements (Figs. 3 and 4) show a deviation from such a rela-

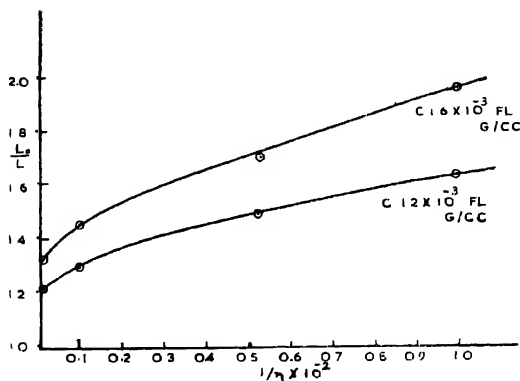


Fig. 3. Fluorescein : Dependence of yield on viscosity of solvent.

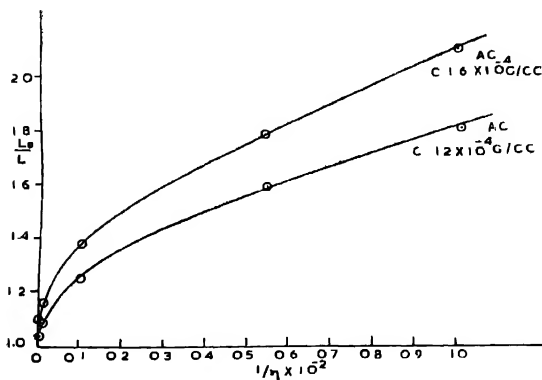


Fig. 4. Acraflavin : Dependence of yield on viscosity of solvent.

tionship. This shows that the diffusion theory is not adequate by itself in explaining the results, when  $p$  in Eqn. 1 is assumed constant. But if one considers in addition a statical extinction, the value of  $p$  will change with  $\eta$  and can explain the nonlinear relationship between  $L_0/L$  and  $1/\eta$ . Similar results were obtained by us in the case of rhodamm (Machwe *et al.*, 1964) and of anthracene by Sveshnikov *et al.* (1956). So it is reasonable to assume that in the case of fluorescein and acraflavin solutions also the transfer of excitation energy takes place through the mechanism of diffusion theory as modified by considerations of fluctuations in the distribution of the solute molecules in solutions.

## REFERENCES

- Forster, T., 1949, *Zs. Naturforsch.*, **4a**, 321.  
Machwe, M. K., *et al.*, 1964, *Chem. Sci.*, **10**, 301.  
Sveshnikov, B. Ya., and Tishchenko, G. A., 1956, *Optika Spektroskopii*, **2**, 155.

# STUDY OF ELECTRON AFFINITY FROM GAUSSIAN FORM REPULSION TERM POTENTIAL FUNCTION FOR POLAR DIATOMIC MOLECULES

S. P. TANDON, M. P. BHUTRA AND K. TANDON\*

PHYSICAL LABORATORIES, UNIVERSITY OF JODHPUR, JODHPUR, INDIA

(Received June 11, 1965; Resubmitted September 1, 1965 and Nov. 3, 1965)

Theoretical methods (Pritchard, 1953) yield very divergent values of electron affinity of elements, which are also not in good agreement with the experimental values. Present communication reports a method of calculating the electron affinity of an element in the case of polar molecules using gaussian form repulsion term potential function.

The study of potential functions (Bleick and Mayer, 1934; Kunnium, 1950; Rice and Klemperer, 1957; Varshni, 1957; Varshni and Shukla, 1961) reveals that gaussian form repulsion term adequately includes the polarization, Vander wall and short range repulsion effects. Such a function may be represented by

$$U(r) = (e^2/r) + A \exp(-br^2) \quad \dots (1)$$

where  $A$  and  $b$  are constants and other symbols have usual meaning. Applying the following condition of suitability to equation (1)

$$\left. \begin{aligned} U(r)_{r=r_e} &= -D_e \\ (dU/dr)_{r=r_e} &= 0 \\ (d^2U/dr^2)_{r=r_e} &= k_e \end{aligned} \right\} \quad \dots (2)$$

and

and then using the relation equation (3) (Gaydon, 1953)

$$D_e = D_e - I + E \quad \dots (3)$$

we get the relation, equation (4), connecting the electron affinity ( $E$ ), dissociation energy ( $D_e$ ), ionization potential ( $I$ ), force constant for infinitesimal amplitude ( $k_e$ ) and equilibrium internuclear distance ( $r_e$ )

$$E = D_e + I - \frac{e^2}{r_e} \left[ 1 - \left\{ \frac{ke}{e^2} r_e^3 + 3 \right\}^{-1} \right] \quad \dots (4)$$

To show the applicability of this relation, the electron affinity of chlorine atom in the case of NaCl molecule has been calculated. The  $K_e$ ,  $r_e$  and  $D_e$  values have

---

\*Chemical laboratories, University of Jodhpur, Jodhpur, India.

been taken from the data of Tandon and Tandon (1964). The values of ionization potential are taken from Hodgman's data (1963). The result obtained is compared with that obtained by other theoretical and experimental methods (Table I). It is of interest to note that the linear extrapolation methods yield higher values whereas the quadratic ones yield lower ones. The values obtained by equation (4) are in close agreement with the observed magnetron and electron impact methods.

This method has been applied to calculate electron affinities of twenty elements in about one hundred and fifty diatomic molecules. The results are in good agreement with experimental values (Pritchard, 1953, Page, 1965).

TABLE I

(Comparison of values of electron affinity  $E(e.v)$  of chlorine atom by different methods)

$E(e.v)$	Method	Author
$3.9183 \pm 0.05$	by equation (4)	Present
4.8	linear extrapolation of ionization potential	Pritchard (1953)
3.7	quadratic extrapolation of ionization potential.	Glockler*
3.1	do	Bates*
3.05	do	Pritchard (1953)
$3.58 \pm 0.13$	surface ionization measurements	Dukel'skil and Tonov
3.913	lattice energies	Pritchard (1953)
$3.93 \pm 0.174$	magnetron	Mitchell and Mayer (1940)
$3.724 \pm 0.434$	do	James <i>et al.</i> (1943)
$3.999 \pm 0.26$	electron impact	Hanson*

\*From Pritchard (1953)

The authors wish to express heart-felt thanks to Prof. R. C. Kapoor, D Phil., D Sc., and Prof. A. Mookherji, D Sc., for helpful discussions and suggestions.

## REFERENCES

- Bloch, W. E. and Mayer, J. E., 1934, *J. Chem. Phys.* **2**, 252  
 Gaydon, A. G., 1953, *Dissociation energy and Spectra of Diatomic molecules*, Chapman and Hall Ltd., London, Ed. II.



- Hodgman, C. D., 1963, *Hand Book of Chemistry and Physics*, The Chemical Publishing company, Ohio, Ed. 44
- Jones, K., McCallum and Mayer, J. E., 1917, *J. Chem Phys.*, **11**, 56
- Kanumura, M., 1950, *Prog Theoret Phys. (Kyoto)*, **5**, 412
- Mitchell, J. J. and Mayer, J. E., 1940, *J. Chem Phys.*, **8**, 282
- Page, F. M., 1955, *Tech Report on Electron Affinities of Inorganic Radicals*, College of Advanced Technology, Birmingham.
- Pritchard, H. O., 1953, *Chem. Rev.*, **53**, 529.
- Rice, S. A. and Klempeter, W., 1957, *J Chem Phys.*, **27**, 573
- Tandon, S. P. and Tandon, K., 1964, *Indian J. Phys.*, **38**, 460
- Varshni, Y. P., 1957, *Trans. Faraday Soc., London*, **53**, 132.
- — —, 1957, *Rev. Mod Phys.*, **29**, 664.
- Varshni, Y. P. and Shukla, R. C., 1961, *J. Chem. Phys.*, **35**, 582.

## BOOK REVIEW

VARIATIONAL PRINCIPLES IN THE THEORY OF COLLISIONS.—by  
Y. N. Demkov and translated from the Russian by N. Kemmer. Published  
by Pergamon Press in 1963.

This monograph is devoted solely to the application of variational principles to scattering phenomena. Though the variational method has proved to be a well tested procedure of quantum mechanics since 1928 or even earlier, yet its consideration was mainly confined to the discrete spectrum. It is only in 1944 when Hulten was the first to recognize its application to the collision phenomena. In 1955, Mott and Massey published a monograph in fact the first monograph in this subject, entitled "The Theory of Atomic Collisions" where however, they devoted very little on the variational problems. This monograph, therefore, serves a very good purpose of a comprehensive review on this entire field. But unfortunately, this monograph is not a complete one since many important works in this field have appeared after the Russian edition was prepared. chiefly the works by Kato, Spruch and Rosenberg are worth mentioning. Although the Author recognized this gap in this foreword to the English editors, he did not attempt at incorporating these works in the body of this monograph, though an inclusion of these works would have greatly added to the value of the book.

There are many good features of this book which deserve mentioning, for instance, the extent of material covered here are simply enormous. mathematical proofs are given with the degree of accuracy that is usually considered sufficient for physicists working in this field. This book selects only some, out of the large number of problems in the theory of collisions that are related to variational principles, confining its attention to non-relativistic stationary problems and hardly discusses non-stationary problems at all. Here the Author has presented, in a lucid manner the formulation of the variational principle, the connection between various formulations of variational principles and subsequently their application in the theory of collisions. The optical theorem, the principle of detailed balance or the virial theorem etc., have been arrived at by consideration of functionals obeying variational principles. This book deals with concrete problems that are sufficiently general to make the extension to more complicated problems such as the scattering of electrons by atoms a matter of no fundamental difficulty and with a clarity that is not evident by more conventional procedures.

Lastly, the English translation is very well done. On the whole, it is a very well written book which is absolutely essential to all working in this field.

A. S. Chakravarty

# THE NEAR ULTRAVIOLET ABSORPTION SPECTRA OF ORTHO-, META-, AND PARA-FLUOROANILINES

M. A. SHASHIDHAR AND K. SURYANARAYANA RAO

DEPARTMENT OF PHYSICS, KARNATAK UNIVERSITY, DHARWAD-3

(Received August 23, 1965; Re-submitted October 18, 1965)

## Plate 1 & 2

**ABSTRACT.** The near ultraviolet absorption spectra of the vapours of the ortho-, meta-, and para-fluoroanilines were photographed and analysed. The spectrum of the ortho-fluoroaniline consists of about 25 red-degraded bands in the region 3065–2750 Å and with the band at 31584  $\text{cm}^{-1}$  as (0,0), these bands can be interpreted in terms of ten ground state and eight upper state fundamentals. About 35 red-degraded bands are recorded in the spectrum of the meta-isomer in the region 2950–2685 Å and are explained on the basis of nine ground state and twelve upper state fundamentals with the band at 31620  $\text{cm}^{-1}$  chosen as (0,0). In the spectrum of the para-molecule, about 25 red-degraded bands are observed in the region 3100–2710 Å and are interpreted in terms of two ground state and nine upper state frequencies, taking the band at 32669  $\text{cm}^{-1}$  as the (0,0) band. The assignments of the fundamentals chosen in these molecules are correlated with the Raman data where available.

## INTRODUCTION

Although the ultraviolet absorption spectra of aniline and of some substituted anilines were investigated, substituted anilines still require a systematic study. In view of this, a study of the near ultraviolet absorption spectra of fluorinated anilines, namely, ortho-, meta-, and para-fluoroanilines, was carried out. A preliminary note giving the results has already been published (Shashidhar and Suryanarayana Rao, 1965). In this paper are reported the details of the investigation. The Raman spectrum of para-compound has been studied by Kohlrausch and Ypsilanti (1935). The Raman spectra of the other two molecules, namely, ortho- and meta-molecules do not seem to have been observed yet. There are, however, interpolated Raman spectra of these molecules (Kohlrausch and Vogel & Hertey 1947). There do not seem to be any infra-red spectral data available yet on these molecules.

## EXPERIMENTAL

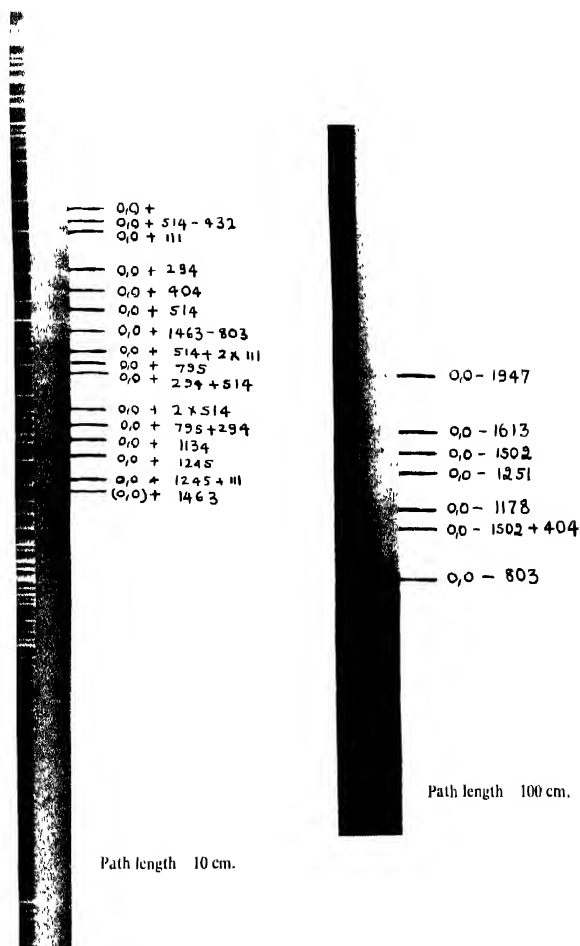
The samples of ortho-, meta-, and para-fluoroanilines used in this investigation were obtained from Light Co, England. The boiling points of ortho-, meta-, and para-fluoroanilines are 175°C, 186°C, and 187.6°C respectively. They

were purified by distilling three times in vacuum sealed tubes and this distilled product was used for further work. The absorption tube was an all quartz one of different lengths with fused plane quartz windows (lengths 5 cms, 10 cms, 25 cms and for higher path lengths quartz to pyrex graded seals were used). The absorption cell was evacuated continuously with intermittent heating so as to degas the tube. The distilled product was then introduced into the side limb of the absorption tube and then suddenly the temperature of the side limb was lowered by immersing it in a cooling mixture and the whole system was then evacuated for about half an hour and the tube was sealed off. Under these conditions, the substance in the absorption tube would be approximately at its saturated vapour pressure. For temperatures higher than the room temperature it was found desirable to keep the main body of the absorption tube at about  $10^{\circ}\text{C}$  higher in temperature than the container so as to eliminate the possibility of the vapour condensing on the inside and the windows of the tube. Hilger hydrogen lamp run on a stabilised direct current hydrogen lamp power supply unit FL16 was used as a source of continuum. Spectrograms were taken on Ilford R-40 and (4-30) plates employing a Hilger medium quartz spectrograph. Exposure times varied from 30 minutes to 7 hours. Absorption path lengths 5 cms, 10 cms, 25 cms, 50 cms, 75 cms, 100 cms were used. The temperature of the absorption cell was varied from  $-10^{\circ}\text{C}$  to  $150^{\circ}\text{C}$ . Each band was measured on three different spectrograms using a Hilger comparator with reference to the standard iron arc lines and using Hartmann's dispersion formula, and the mean value of the different determinations was taken for the wavelength of each band. Band heads were measured in the case of sharp bands and centres in the case of diffuse bands. Intensities are visual estimates. The accuracy of measurements has been estimated to be about  $5\text{ cm}^{-1}$  for the sharp bands and about  $10\text{ cm}^{-1}$  for broad or diffuse bands.

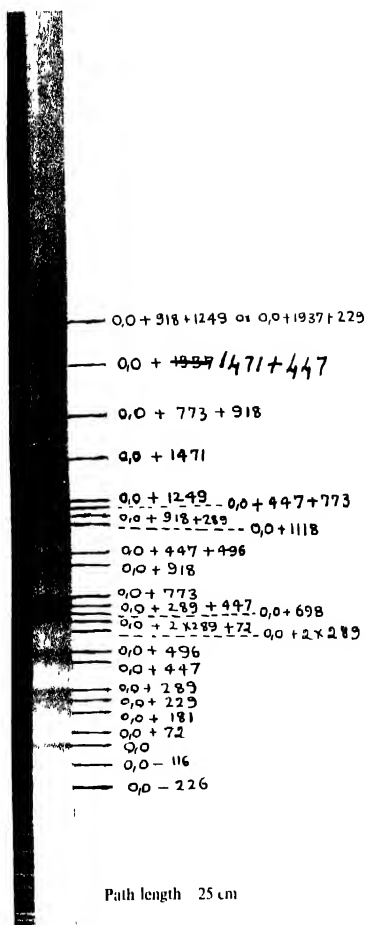
## RESULTS

*Ortho-fluoronitroline*. The absorption spectrum of this molecule lies in the region  $3065.1-2750\text{\AA}$ . The bands are rather sharp and degraded to the red. The spectra were photographed with path lengths 5 cm, 10 cm, 50 cm, 75 cm, and 100 cm at room temperature and at temperatures between  $-10^{\circ}\text{C}$  to  $150^{\circ}\text{C}$ . The maximum number of bands are obtained with a 10 cm cell at room temperature. At higher temperatures the absorption on the violet side grows stronger and becomes continuous and more bands gradually appear on the red end of the continuum. The amount of vapour in the absorption cell was adjusted as described earlier. The longest wavelength side band at  $3063\text{\AA}$  is recorded at room temperature using a  $100\text{ cm}$  cell.

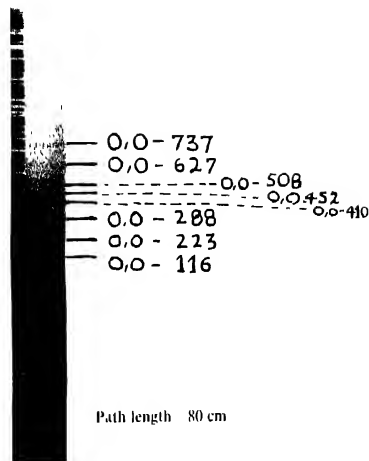
*Meta-fluoronitroline*. The absorption spectrum lies in the region  $2950\text{\AA}$  to  $2685\text{\AA}$ . The bands are sharp and degraded to the red. The maximum number



Ultraviolet absorption spectrum of ortho-fluoroaniline vapour at room temperature

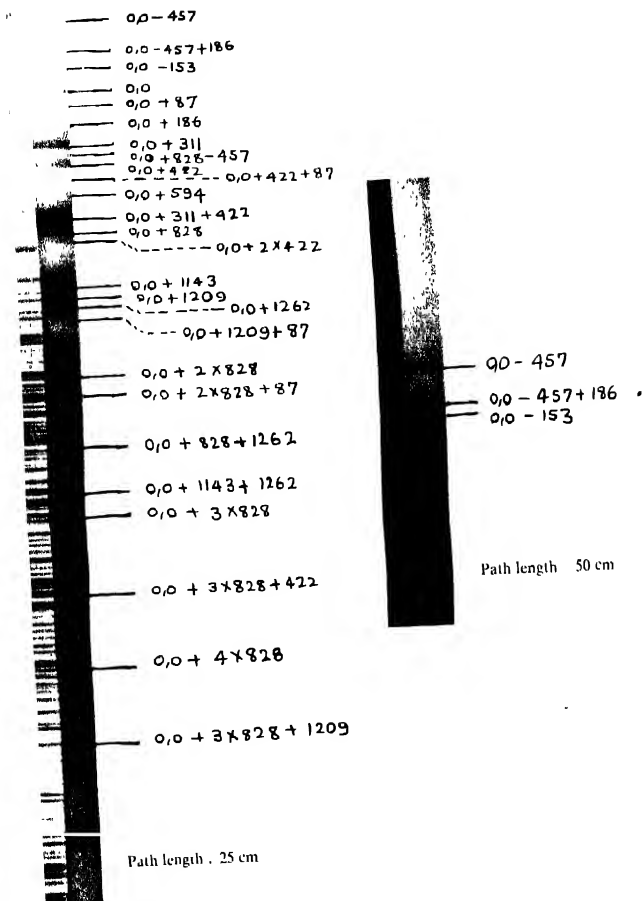


Ultraviolet absorption spectrum of meta fluoroaniline vapour  
at room temperature.



Ultraviolet absorption spectrum of meta fluoroaniline  
 vapour at room temperature

M. A. Sashidhar and K. Surjanaryan Rao



Ultraviolet absorption spectrum of Para fluoroaniline vapour at room temperature.



of bands are recorded with a 25 cm at room temperature. The effect of increasing temperature and path length is the same as in the case of ortho-compound.

*Para-fluoroaniline*. The bands of the para-isomer lie in the region 3100 Å to 2710 Å. Some of the bands are somewhat sharp and the others are rather broad and they are all degraded to the red. The effect of increasing temperature and path length is the same as in the case of ortho- and meta-fluoroanilines. The maximum number of bands are recorded with a 25 cm cell at room temperature.

The first two columns of each of tables I, II and III give the wave numbers in vacuum of the bands and their visually estimated intensities respectively of ortho-, meta-, and para-fluoroanilines.

#### ANALYSIS AND DISCUSSION

*Ortho-fluoroaniline*. This molecule belongs to the point group  $C_2$ . The molecule has only one element of symmetry namely, the plane of molecule assuming  $\text{NH}_2$  to be a single unit and the whole molecule to be planar, which is a plane of symmetry. The transition, which is  $A' \rightarrow A''$ , is an allowed one with the transition moment lying in the molecular plane.

The minimum number of bands for this isomer are recorded with a 5 cm cell at  $-10^\circ\text{C}$ . Of these, the one lying at the longest wave length side at  $34584\text{ cm}^{-1}$  is chosen as the (0, 0) band of the system. The strong bands on its long wavelength side with separations 261, 350, 432, 564, 803, 1178, 1251, 1502, 1613 and  $1947\text{ cm}^{-1}$  are identified as the ground state fundamentals, while the strong bands on its short wavelength side with shifts 111, 294, 404, 514, 795, 1134, 1245,  $1463\text{ cm}^{-1}$  are assigned as the fundamentals of upper electronic state of the system. These ten ground state and eight upper state fundamentals can account for almost all the bands of the system. The separations of the bands of the ortho-fluoroaniline from the (0, 0) band and their assignments are given in columns 3 and 4 respectively of table I.

*Meta-fluoroaniline*. Meta-fluoroaniline like the ortho-isomer, belongs to the point group  $C_2$ . The minimum number of bands for this isomer are recorded with a 5 cm cell at  $-10^\circ\text{C}$ . Of these, the one lying on the long wavelength side at  $34620\text{ cm}^{-1}$  is taken as the (0, 0) band of the system. The strong bands with separations 116, 223, 288, 410, 452, 508, 627, 737,  $846\text{ cm}^{-1}$  from the (0, 0) band towards the longer wavelength side are assigned as the ground state fundamentals. The strong bands with shifts 72, 181, 229, 289, 447, 496, 698, 773, 918, 1118, 1249 and  $1471\text{ cm}^{-1}$  from (0, 0) on its violet side are taken as the fundamentals of the upper state. On the basis of these nine ground state and twelve upper state fundamentals, all the bands of this isomer can be assigned. Columns 3 and 4 of table II respectively give the shifts of the bands from the (0, 0) band and their assignments,

TABLE I

Ultraviolet absorption bands of ortho-fluoroaniline

Wave number (vacuum) in $\text{cm}^{-1}$	Relative Intensity	Shift from 0,0 band in $\text{cm}^{-1}$	Assignment
32637	2	-1947	0,0-1947
32917	2	-1613	(0,0-350-2 $\times$ 803)
33082	2	-1502	0,0-1613
33333	0	-1251	(0,0-2 $\times$ 803)
33406	2	-1178	0,0-1502
33480	2	-1104	0,0-1251
33781	3	-803	0,0-1178
34020	1	-564	0,0-1104
34152	1	-432	0,0-803
34234	1	-350	0,0-564
34323	1	-261	0,0-432
34584	5	0	0,0-350
34657	0	73	0,0-261
34695	4	111	0,0
34878	4	294	0,0+514-432
34988	4	404	0,0+111
35098	3b	514	0,0+294
35249	1b	665	0,0+404
35338	0bd	754	0,0+514
35379	1	795	0,0+1463-803
35406	1	822	0,0+795
35617	0b	1033	0,0+294+514
35653	0bd	1069	0,0+2 $\times$ 514
35718	0bd	1134	0,0+795+294
35829	0b	1245	0,0+1134
35947	1b	1363	0,0+1245
36047	0b	1463	0,0+1245+111

b = broad;  
bd = broad and diffuse.

TABLE II

Ultraviolet absorption bands of meta-fluoroaniline

Wave number (vacuum) in $\text{cm}^{-1}$	Relative Intensity	Shift from 0,0 band in $\text{cm}^{-1}$	Assignment
33774	0	— 846	0,0—846
33883	0	— 737	0,0—737
33993	1	— 627	0,0—627
34046	0	— 571	0,0—288
34112	3	— 508	0,0—508
34168	1	— 452	0,0—452
34210	5	— 410	0,0—410
34332	2b	— 288	0,0—288
34397	4	— 223	0,0—223
34504	2	— 116	0,0—116
34620	7	0	0,0
34692	0	72	0,0+72
34801	2	181	0,0+181
34849	4	229	0,0+229
34909	5	289	0,0+289
35067	3	447	0,0+447
35116	4	496	0,0+496
35208	0d	588	0,0+2×289
35269	1d	649	0,0+2×289+72
35318	2	698	0,0+698
35360	1	740	0,0+289+447
35393	5	773	0,0+773
35474	0b	854	0,0+773+72
35538	2	918	0,0+918
35588	2	968	0,0+447+496
35738	2	1118	0,0+1118
35817	2	1197	0,0+918+289
35837	1	1217	0,0+447+773
35869	2	1249	0,0+1249

TABLE II—*contd.*

Wave number (vacuum) in $\text{cm}^{-1}$	Relative Intensity	Shift from 0,0 band in $\text{cm}^{-1}$	Assignment
36091	2b	1471	0,0-  1471
36300	1b	1680	0,0-  773+918
36164	0b	1844	0,0+2 $\times$ 918
36557	0b	1937	0,0-  1471+147
36786	0b	2166	0,0-  918+1249
36902	0b	2282	0,0-  2 $\times$ 918+447 or 0,0+2 $\times$ 1249-223
37036	0b	2416	0,0+1471   447+496
37186	0bd	2566	0,0   2 $\times$ 1249-  72
37249	0bd	2629	0,0-  2 $\times$ 918   773

b = broad; bd = broad and diffuse.

TABLE III

Ultraviolet absorption bands of para-fluoroaniline

Wave number (vacuum) in $\text{cm}^{-1}$	Relative Intensity	Shift from 0,0 band in $\text{cm}^{-1}$	Assignment
32212	1	- 457	0,0-457
32407	1	- 262	0,0-457+186
32516	2	- 153	0,0-153
32669	7	0	0,0
32756	0	87	0,0   87
32855	0	186	0,0+186
32980	7	311	0,0+311
33025	0	356	0,0+828-457
33091	6	422	0,0+422
33193	0	524	0,0+422+87
33263	1	594	0,0-  594
33418	7	749	0,0+311+422
33497	6	828	0,0-  828
33523	1	854	0,0+2 $\times$ 422

TABLE III—*contd.*

Wave number (vacuum) in cm	Relative Intensity	Shift from (0, 0) band in cm	Assignment
33812	3	1113	0, 0 + 1113
33877	2	1209	0, 0 + 1209
33931	2	1262	0, 0 + 1262
33988	2	1319	0, 0 + 1209 + 87
34325	2b	1656	0, 0 + 2 × 828
34421	1	1752	0, 0 + 2 × 828 + 87
34751	1b	2082	0, 0 + 828 + 1262
35055	1b	2386	0, 0 + 1143 + 1262
35168	2bd	2499	0, 0 + 3 × 828
35518	1bd	2879	0, 0 + 3 × 828 + 422
35995	0bd	3326	0, 0 + 4 × 828
36362	0bd	3693	0, 0 + 3 × 828 + 1209

b = broad, bd = broad and diffuse

*Para-fluoroaniline* This molecule belongs to the point group  $C_{2v}$ . The bands belong in this case, to the transition  $A_1 \rightarrow B_1$ , with the transition moment lying in the molecular plane and perpendicular to the para-axis.

The minimum number of bands for this molecule are recorded with a 5 cm cell at  $-10^\circ\text{C}$  and of these, the one which lies on the longer wavelength side at  $32669\text{ cm}^{-1}$  is chosen as (0, 0) band. On the red side of the (0, 0) band are two bands with shifts 153,  $457\text{ cm}^{-1}$ . These may be assigned as ground state fundamentals and correlated with Raman frequencies 164 and  $452\text{ cm}^{-1}$ . The following strong bands on the violet side of the (0, 0) band at 87, 186, 311, 422, 594, 828, 1143, 1209,  $1262\text{ cm}^{-1}$  are identified as the upper state fundamentals. Almost all the observed bands can be explained in terms of these two ground state and nine upper state fundamentals. Column 3 of table III gives the shifts of the observed bands from the (0, 0) band while column 4 gives their assignments.

It may be mentioned that in this molecule despite the fact that the spectra were taken under different possible experimental conditions, not more than three bands have been obtained on the red side of the (0, 0) band. Two of these bands have been assigned as ground state fundamentals. In contrast, in the ortho-, and meta- isomers, many ground state fundamentals have been obtained. We have no explanation for this rather strange feature in the para-molecule.

The assignments of most of the bands are indicated on reproductions in plates 1, 2 and 3. Since the preliminary note on this investigation, referred to earlier, was sent up for publication, the analyses have been slightly revised and with these slightly revised analyses, it has been possible to assign almost all bands

TABLE IV  
Fundamental frequencies of ground and excited states of ortho-, meta-para-fluoroanilines

Ground State frequencies in cm <sup>-1</sup>				Excited State frequencies in cm <sup>-1</sup>			
Ultraviolet absorption (present work)				Ultraviolet absorption (present work)			
ortho-	meta-	para-	ortho- (Interpolated Raman Spectrum)	meta-	para- (Observed)	ortho-	meta- para-
—	116 (2)	133 (2)	—	—	164 (2)	111 (4)	72 (6) 87 (1)
—	223 (4)	—	195 (St)	220 (met)	197 (6)	—	181 (6) 186 (1)
261 (1)	298 (2b)	—	285 (met)	240 (met)	—	—	229 (1) —
350 (1)	416 (5)	—	330 (m)	350 (m)	362 (3)	294 (4)	289 (5) 311 (7)
564 (1)	508 (3)	—	595 (met) 586 (St)	530 (St) 515 (m)	635 (1)	514 (3b)	406 (4) 594 (1)
432 (1)	452 (1)	457 (1)	448 (m)	—	452 (4)	404 (4)	447 (3) 422 (6)
—	627 (1)	—	—	605 (m)	—	—	—
—	737 (6)	—	765 (St)	740 (St)	—	—	698 (2) —
803 (3)	846 (6)	—	860 (St)	—	844 (4b)	705 (1)	773 (5) 828 (6)
—	—	—	1030 (St)	1000 (St)	—	—	918 (2) —
1178 (2)	—	—	—	—	1150 (6)	1134 (obsd)	1118 (2) 1143 (3)
—	—	—	—	—	1218 (6)	—	— 1209 (2)
1251 (6)	—	—	1270 (St)	1293 (St)	1265 (4)	1245 (6b)	1249 (2) 1262 (2)
1502 (2)	—	—	—	—	—	1463 (6b)	1471 (2b) —
1613 (2)	—	—	1580 (m) 1600 (m)	1590 (m)	1510 (6)	—	—
1947 (2)	—	—	—	—	—	—	—

in the spectra. It may be seen that the fundamentals, however, remain nearly the same.

Some alternative assignments for some of the bands in these spectra as overtones and combinations may be possible, as indeed we find they are. But we prefer the assignments given in the tables because we feel that the bands we have chosen as fundamentals are a little too intense to be regarded as combinations or overtones. This argument also applies to the band  $1947\text{ cm}^{-1}$  in the ortho-molecule. Further, along with the ultra-violet absorption work we have also recorded and analysed the infra-red spectra in the liquid state of these molecules (communicated) and the analyses of these infra-red spectra confirm our assignments of the fundamentals in the present work.

The correlations between the ground state fundamentals from Raman spectra and the present work and the upper state fundamentals obtained from the present work are indicated in table IV for the three molecules.

It may be mentioned that the agreement between the ground state fundamentals observed in ultra violet absorption in the present work and the interpolated Raman spectra in the case of ortho-, and meta-isomers is, in some cases, not satisfactory but it may not be too surprising, considering that the available Raman spectra of these molecules are not observed ones but only interpolated ones.

The shifts of the (0, 0) bands from that of benzene are 3506, 3469 and 4520  $\text{cm}^{-1}$  in ortho-, meta- and para-molecules respectively. The shifts in the ortho-, and meta-isomers are nearly equal whereas the para-molecules exhibits a markedly large shift. This influence of the para-position fluorine atom on the shift of the (0, 0) band is also displayed by para-fluorotoluene, (Cave and Thompson, 1950) where the shift is  $1212\text{ cm}^{-1}$  as compared to  $691\text{ cm}^{-1}$  in meta-, and  $513\text{ cm}^{-1}$  in ortho-isomers. This is observed also in para-difluorobenzene (Cooper, 1954), para-fluorobenzonitrile (Cooper, 1953), para-fluorobenzobenzene (Krishnamachari, 1957).

#### ACKNOWLEDGMENTS

One of the authors (K.S.R.) wishes to thank the University Grants Commission Delhi, for the kind financial assistance given towards the cost of the chemicals used in this investigation.

#### REFERENCES

- Cave and Thompson, 1950, *Faraday Soc. Discussions*, **9**, 35.  
Cooper, C. D., 1953, *J. Chem. Phys.*, **21**, 379.  
——— 1954, *J. Chem. Phys.*, **22**, 503.  
Kohlrausch, K. W. F. and Vogel, R. & Herty, E. 1947, *Monatsh*, **76**, 200.  
Kohlrausch, K. W. F. and Ypsilanti, 1935, *Monatsh*, **66**, 285.  
Krishnamachari, S. L. N. G., 1957, *Indian J. Phys.*, **31**, 447.  
Shashidhar, M. A. and Suryanarayana Rao, K., 1965, *Current Science*, **34**, 470

# A GENERALISED DIRECT EXCHANGE INTERACTION: APPLICATION TO HEUSLER ALLOYS

NARENDRA KUMAR AND K. P. SINHA

NATIONAL CHEMICAL LABORATORY, POONA-8, INDIA

(Received September 30, 1965)

**ABSTRACT.** A generalised Heisenberg-type exchange interaction is discussed. This arises from a combination of  $s$ - $d$  mixing effects as well as  $s$ - $d$  exchange. It is shown that the effective coupling shows an oscillatory behaviour. This mechanism is applicable to magnetic alloys where paramagnetic atoms are far separated from each other. A qualitative comparison with some Heusler alloys is made.

## INTRODUCTION

In magnetically ordered solids where the paramagnetic ions are far separated from each other, the direct exchange interaction between their localised magnetic carriers is extremely feeble to bring about any appreciable coupling. One usually invokes mechanisms such as superexchange or indirect exchange, involving the role of the diamagnetic ions in magnetic compounds (Anderson, 1959; Korde, Sinha and Tanabe, 1959). In magnetic metals and alloys the indirect exchange via the polarisation of conduction electron is often treated as the important mechanism. This is essentially a second order process involving  $s$ - $d$  exchanges mechanism (Kasuya, 1956). The magnitude of this indirect exchange interaction decreases as the inverse third power of the distance between the magnetic ions in question (Ruderman and Kittel, 1954; Yoshida, 1957). However the sign of the interaction depends on the functions  $F(x) = (x \cos x - \sin x)/x^4$  where  $r = 2k_F R_{lm}$ ,  $k_F$  is the magnitude of the Fermi wave vector of conduction electrons and  $R_{lm}$  is the distance between the magnetic ion at  $R_l$  and  $R_m$ . In effect this gives a sort of oscillating behaviour with distance.

In the present paper we intend to generalise the direct exchange interaction by including  $s$ - $d$  mixing effect as distinct from pure  $s$ - $d$  exchange. We shall see that it incorporates both the effect of  $s$ - $d$  exchange and  $s$ - $d$  mixing. The  $s$ - $d$  mixing is one electron effect and emanates from crystal field effects which can cause mixing of  $s$  and  $d$  orbitals on the same atom (intra-atomic mixing, Sinha and Upadhyaya, 1964), or between two different atoms (inter-atomic mixing, Anderson, 1961). The former will be present if the local symmetry at the site of the magnetic atoms is such that the crystal field has the appropriate

\* Communication No 836 from National Chemical Laboratory, Poona-8



symmetry to admit  $s$  and  $d$  states. The latter is present even in ideally cubic crystal and connects  $s$  and  $d$  states on neighbouring atoms. Owing to these effects, we cannot talk in terms of pure  $d$  and pure  $s$  orbitals. The mixing effects ought to be taken into account in the description of the magnetic coupling.

In what follows, we formulate Heisenberg-like direct exchange interaction by taking cognizance of the mixing effects mentioned above. For its application we have in view Heusler alloys  $\text{Cu}_2\text{MnX}$ , where  $X$  may be Al, In, Sn, Ge, Sb, etc. Other types of exchange interactions involving this type of mixing for magnetically dilute alloys have been considered by a few workers (Kim and Nagaoka 1963; Alexander and Anderson 1964, see also Moriya 1965).

It will be shown that like the Ruderman-Kittel mechanism here also one gets some sort of oscillating behaviour.

#### FORMULATION OF GENERALISED DIRECT EXCHANGE

Let us consider a magnetic crystal e.g.  $\text{Cu}_2\text{MnX}$  which has paramagnetic ions far separated from each other along with other-nonmagnetic atoms. The magnetic atoms have unpaired electrons in the  $d$  or  $f$  like orbitals unfilled shells. The non magnetic as well as the magnetic atoms contribute  $s$  like electrons which are in the conduction band in the system. Thus the total Hamiltonian for the  $d$ (localised) and conduction electrons can be expressed as

$$H = \sum_i H_{od}^{(i)} + \sum_j H_{os}^{(j)} + H_{sd} + \sum_{l < m} H_{lm} + H' \quad (1)$$

where  $H'$  contains the Zeeman, lattice and electron-lattice parts of the Hamiltonian and will not be considered in the present formulation.  $\sum_{l < m} H_{lm}$  are the two particle interaction terms and are responsible for  $d-d$  and  $s-d$  exchange process.  $H_{sd}$  is the one electron interaction term which may arise due to local distortion at atomic site or crystal field effect of the neighbouring atoms in the undistorted situation. We will see that they will lead to mixing of  $s$  and  $d$  orbital states. We will exploit these terms as perturbations over pure  $d$  and  $s$  states. The pure  $d$  and  $s$  states are the solutions of the one electron Hamiltonians  $H_{od}$  and  $H_{os}$  more or less explicitly

$$H_{od} \phi_{dl} = E_{ol} \phi_{dl} \quad \dots \quad (2)$$

$$H_{os} \phi_k = E_k \phi_k \quad \dots \quad (3)$$

Here,  $\phi_{dl}$  represents the localised  $d$  function in the field of atom at site  $R_l$ .  $\phi_k$  is Bloch function for the band. We shall represent this as

$$\phi_k = \frac{1}{\sqrt{V}} \sum_r u_k(r) e^{ik \cdot r} \quad (4)$$

For present purposes we consider a cubic crystal i.e. the field at the magnetic atoms has cubic symmetry. Thus the  $s$ - $d$  mixing for this case is confined to inter-atomic processes. The  $d$  orbital of atom at  $R_l$  is mixed with the  $s$  orbital at site  $R_m$ . We represent the solution of the reduced one electron Hamiltonian

$$(H_{0d} + H_{sd})\psi_l = E_l \psi_l \quad \dots (5)$$

where

$$\psi_l = \phi_{dl} + \sum_k e^{ik \cdot R_l} t_{kdl} \phi_k \quad \dots (6)$$

$$t_{kdl} = \frac{1}{\sqrt{N}} \frac{V_{kdl}}{\Delta E_{kd}} = \frac{1}{\sqrt{N}} \frac{\langle \phi_k | H_{d-s} e^{-ik \cdot R_l} | \phi_{dl} \rangle}{\Delta E_{kd}}$$

Likewise, the conduction electron wave function is also modified from  $\phi_k$  owing to this interaction. They can be designated by

$$\psi_k = \phi_k - \sum_l e^{-ik \cdot R_l} t_{dkl} \phi_{dl}$$

which are nearly orthogonal to  $\psi_l$ . However, we shall not require these explicitly in the present formulation.

Let us now evaluate the two particle exchange interactions in terms of the localised states given by  $\psi_l$  etc. In doing so we make use of the second quantized representation (Landau and Lifshitz, 1958). We make use of the particle field operators.

$$\chi(\xi) = \sum_{j\sigma} \psi_{j\sigma} C_{j\sigma}, \quad \chi^\dagger(\xi) = \sum_{i\sigma} \psi_{i\sigma}^\dagger C_{i\sigma}^\dagger \quad \dots (7)$$

The two particle interaction is then given as

$$\int \chi^\dagger(\xi) \chi^\dagger(\xi') \left( \sum_{l < m} H_{lm} \right) \chi(\xi) \chi(\xi') d\xi d\xi'$$

Making use of the operator (7), this is written as

$$\sum_{l < m} C_{l\sigma}^\dagger C_{m\sigma'}^\dagger \langle \psi_{l\sigma} \psi_{m\sigma'} | H_{12} | \psi_{m\sigma} \psi_{l\sigma'} \rangle C_{m\sigma} C_{l\sigma} \quad \dots (8)$$

In these expressions  $C_{i\sigma}^\dagger$ ,  $C_{i\sigma}$  etc. are the fermion creation and annihilation operators with respect to states  $\psi_{i\sigma}$  and  $\psi_{i\sigma}$  respectively;  $\sigma$  is the spin index.

We now re-express the matrix elements in (8) involving  $\psi_{i\sigma}$  and  $\psi_{m\sigma'}$  etc. in terms of the explicit expressions like (6).

The expanded form will contain sixteen terms. However, this can be reduced on the basis of the following arguments. We select  $\phi_l$  and  $\phi_m$  as extremely localised functions and hence their overlap is negligible. Thus those matrix elements which involve pure  $\phi_l(1) \phi_m(1)$  as factors will be neglected. This rules out all the first and second order terms. In the third order terms the strongest will be those which involve intra-atomic exchange along with the transfer processes.

Processes other than this and of higher order in perturbation are neglected. Thus, we concentrate on the processes such as

$$\frac{2\Sigma}{l,m} \frac{\Sigma}{kk'} \frac{\Sigma}{\sigma\sigma'} t_{dlk'} \langle \phi_k \phi_m | H_{12} | \phi_m \phi_k \rangle t_{kdl} C_{l\sigma}^+ C_{m\sigma'}^+ C_{m\sigma} C_{l\sigma} \quad \dots \quad (9)$$

Let us carry out the summation over the spin indices, and write the above expression in terms of the spin operators. For this we have to utilise the relations (Sinha and Upadhyaya 1962),

$$\begin{aligned} C_{l(+)}^+ C_{l(-)} &= S_{lx} + iS_{ly} \\ C_{l(+)}^+ C_{l(+)} &= S_{lx} - iS_{ly} \\ C_{l(+)}^+ C_{l(+)} - C_{l(-)}^+ C_{l(-)} &= 2S_{lz} \\ C_{l(+)}^+ C_{l(+)} + C_{l(-)}^+ C_{l(-)} &= 1 \end{aligned} \quad \dots \quad (10)$$

The equation (9) then reduces to

$$-2\Sigma_{l,m} \frac{\Sigma}{kk'} e^{ik'R_l} t_{dlk} \langle \phi_k \phi_m | H_{12} | \phi_m \phi_k \rangle t_{kdl} e^{-ik'R_l} \times \frac{1}{2} (1 + 4S_{lx} S_{mx}) \quad \dots \quad (11)$$

where  $S_l, S_m$  are the vector spin operators of an electron associated with states  $\phi_l, \phi_m$  etc. We now concentrate on summation over  $k$  and  $k'$  and it would therefore suffice to consider the matrix elements,

$$\begin{aligned} \Sigma_k \Sigma_{k'} e^{ik'R_l} t_{dlk'} \langle \phi_{k'} \phi_{dm} | H_{12} | \phi_{dm} \phi_k \rangle t_{kdl} e^{-ik'R_l} \\ = \frac{1}{N^2} \Sigma_{k,k'} e^{ik' \cdot R_l} \left( \frac{V_{dlk'}}{\Delta E_{lk}} \right) J(k-k') e^{i(k-k') \cdot R_m} \left( \frac{V_{kdl}}{\Delta E_{kd}} \right) e^{-ik \cdot R_l} \quad \dots \quad (12) \end{aligned}$$

where

$$J(k-k') = N \int e^{-i(k-k') \cdot R_m} \frac{\phi_{k'}^*(r_1) \phi_{dm}^*(r_2 \dots R_m) e^2 \phi_k(r_1 - (r_0) R_l) \phi_{dlm}}{r_{12}} d\tau_1 d\tau_2 \quad \dots \quad (13)$$

As done by others (Yosida, 1957), we shall assume that  $J(k-k')$  does not depend strongly on  $k$  and  $k'$ . It is customary to replace this by the intra-atomic  $s-d$  exchange integral which gives the maximum contribution at one site. The denominators in (12) are of the form

$$\Delta E_{kd} = E_k - E_d = \frac{\hbar^2 k^2}{2m^*} - E_l \equiv \frac{\hbar^2}{2m^*} (k^2 + a^2) \quad \dots \quad (14)$$

where  $\hbar^2 k^2/2m^*$  is the energy of the conduction electron in state  $k$ ,  $E_d$  is that which corresponds to localised pure  $d$  states; and  $a^2 = (2m/\hbar^2)\Delta$  where  $\Delta$  is the energy gap between the bound  $d$ -state and the bottom of the conduction band.

Thus the integral in (12) reduces to

$$\frac{1}{N^2} \sum_{kk'} \frac{V_{dl,k'} J(k' - k) V_{ld,l'} (k - k'), (R_l - R_m)}{(\hbar^4/(2m^*)^2)(k^2 + a^2)(k'^2 + a^2)} \quad (15)$$

Next, we change from summation to integration, we get

$$\frac{1}{N^2} \frac{(V_{sd})^2}{\hbar^4/(2m^*)^2} \frac{V^2}{8\pi^3} \int_0^{k_F} \int_{k_F}^{\infty} \frac{e^{-i(k-k') \cdot R_{lm}}}{(k^2 + a^2)(k'^2 + a^2)} d^3k d^3k' \quad (16)$$

In putting the limits of integration, we are guided by the exclusion principle;  $k_F$  is the wave-vector at the Fermi surface. This is evaluated below. We do not make any approximation regarding  $k^2 + a^2$  and  $k'^2 + a^2$ . The value of the integral is then

$$16\pi^2 k_F^2 \left[ \frac{\pi}{2} e^{-\lambda} x \frac{\cos x}{x^3(1+\lambda^2)} - \frac{\cos^2 x}{x^4(1+\lambda^2)^2} - \frac{\pi}{2} e^{-\lambda} x \frac{\sin x}{x^4(1+\lambda^2)} \left( 1 - \frac{2}{1+\lambda^2} \right) + \dots \right] \quad (17)$$

where  $\lambda = \frac{a}{k_F}$  and  $x = k_F R$

The final expression (cf. equation 17) is most general. One point which can be easily inferred from this is that the function is oscillating and changes sign periodically in a damped manner as a function of  $Rk_F$ .

The complete expression for the exchange interaction between the magnetic atoms is then given by (cf. equation (11))

$$= \sum_{(l,m)} \frac{V_{sd}^2 J_{sd}^2}{\hbar^4/(2m^*)^2} \frac{V^2}{N^2} 16\pi^2 k_F^2 \left[ \frac{\pi}{2} e^{-\lambda} x \frac{\cos x}{x^3(1+\lambda^2)} - \frac{\cos^2 x}{x^4(1+\lambda^2)^2} - \frac{\pi}{2} e^{-\lambda} x \frac{\sin x}{x^4(1+\lambda^2)} \left( 1 - \frac{2}{1+\lambda^2} \right) + \dots \right] S_l \cdot S_m \dots \quad (18)$$

where the summation over  $l, m$  involves nearest neighbours only. The function given in the square bracket of (18) has been plotted in Fig.1. against the parameter  $Rk_F$  which involves the separation between magnetic atoms. We have shown the

various curves with different values of the gap parameter, namely,  $(\lambda = (a/k_F))$ . For comparison the Ruderman-Kittel ( $R-K$ ) function in the form

$$(2x \cos 2x - \sin 2x)/(2x)^4, \text{ where } x = k_F R,$$

has also been plotted. It can be seen that for the initial values of the argument the two prediction differ, whereas R-K curve indicates ferromagnetic coupling

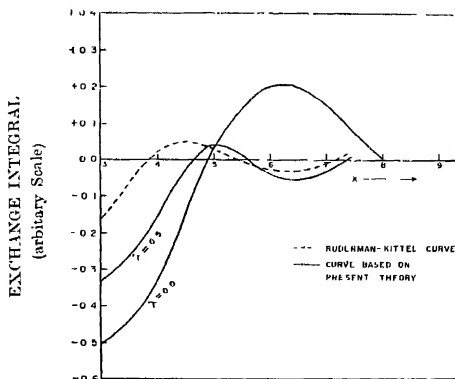


Fig. 1. Plot of exchange integral vs.  $X$  with  $\lambda$  as gap parameters.

the present curve gives antiferromagnetic coupling. Later on the oscillation periods are similar. However, the curve based on the present analysis is more flexible and the ferromagnetic and antiferromagnetic regions contract or expand depending on the gap parameter. This has been displayed clearly.

#### APPLICATION TO HEUSLER ALLOYS

For actual comparison with experimental results we select some magnetic alloys of the form  $\text{Cu}_2\text{MnX}$  with  $X$  standing for Al, Sn, In, Sb, etc. This system in the ordered phase (which is of interest at present) has a body centred cubic structure with a face centred superstructure (Bradley and Rodgers, 1934). The copper atoms are at the cube corners and Mn and  $X$  alternate at the body centres. The magnetic moment is localised at the Mn atoms which are supposed to have four unpaired  $d$  electrons. As can be seen from the structure, there is no direct overlap between two Mn atoms owing to the presence of the intervening diamagnetic atoms. The distance between nearest Mn-Mn neighbour is about  $4.2\text{\AA}$ . We shall select the system  $\text{Cu}_2\text{MnSb}$  which is an antiferromagnetic and for which some data have been reported by Oxley *et al* (1963). From their data the order of the parameter  $Rk_F$  turns out to be 4.35. This falls in the antiferromagnetic region in our graph whereas this corresponds to ferromagnetic region of

R-K curve. It may, however, be noted that the actual coupling will be due to the overall effective exchange i.e. arising from the R-K mechanism, generalised Heisenberg type interaction discussed here and other superexchange type processes. An exact comparison with experimental results with many systems does not seem to be possible owing to a lack of knowledge of  $k_1$  and other parameters. We do not know as to how many conduction electrons per atom are to be taken for each system. We must await some experimental work in this direction.

## REFERENCES

- Alexander, S., and Anderson, P. W., 1964, *Phys. Rev.*, **133**, A1594.  
 Anderson, P. W., 1959, *Phys. Rev.*, **115**, 2.  
 Anderson, P. W., 1961, *Phys. Rev.*, **124**, 41.  
 Bradley, A. J. and Rodgers, J. W., 1934, *Proc. Roy. Soc. (London)*, **A144**, 340.  
 Kasuya, T., 1956, *Prog. Theoret. Phys. (Kyoto)*, **16**, 45.  
 Kim, D. J. and Nagaoka, Y., 1963, *Prog. Theoret. Phys.*, **30**, 743.  
 Koide, S., Sinha, K. P. and Tanabe, Y., 1959, *Prog. Theoret. Phys.*, **22**, 647.  
 Landau, L. D., Lifshitz, L. P., 1958, *Quantum Mechanics*, Pergamon Press.  
 Moriya, T., 1965, *Prog. Theoret. Phys.*, **33**, 157.  
 Osley, D. P., Tobble, R. S. and Williams, K. C., 1963, *J. Appl. Phys.*, **34**, 1362.  
 Sinha, K. P. and Upadhyaya, U. N., 1962, *Phys. Rev.*, **127**, 432.  
 ———— 1964, *Ind. J. Pure & Appl. Phys.*, **2**, 273.  
 Yoshida, K., 1957, *Phys. Rev.*, **106**, 893.

# AN IMPROVED METHOD OF MEASURING MAGNETIC ANISOTROPY OF PARAMAGNETIC CRYSTALS FROM 303°K TO 68°K AND NEW DATA OF SOME $\text{Co}^{2+}$ AND $\text{Fe}^{2+}$ TUTTON SALTS

DEBJANI GUHA THAKURTA AND DEEPTI MUKHOPADHYAY

DEPARTMENT OF MAGNETISM,

INDIAN ASSOCIATION FOR THE CULTIVATION OF SCIENCE, CALCUTTA-32

(Received November 30, 1965)

**ABSTRACT** With a view to increasing considerably the accuracy of the experimental data for the magnetic anisotropies of paramagnetic crystals considerable changes in the design of the existing apparatus, originally constructed by Bose (1947) and later modified by Dutta (1956), was necessary. The main improvements aimed at and achieved in the present set-up are:

1. More than tenfold increase in the sensitivity of the detection (i.e., up to 01%) and measurement of the rotational motion of a freely suspended paramagnetic crystal, by using a photo-electric detecting device and an accurately graduated double-venner torsion head.
2. A hundred times increase in the stabilization of the magnetic field, i.e., up to 0.01 oersteds.
3. A tenfold increase in the stabilization and accuracy of the temperature of the crystal (i.e., up to 0.01° K), by using additional calibration points, a sensitive potentiometric device for measuring the e.m.f. of the thermocouple eliminating spurious e.m.f.'s, and finally using a new type of gas flow cryostat.

The experimental data thus obtained with some ferrous and cobalt Tutton salts, in the temperature range of 303° K to 68° K, show a general deviation from the already existing data of Bose (1947).

## INTRODUCTION

In recent years anisotropic ligand field theories of most of the salts of the non-group elements have been developed by Bose *et al.* (1961-'62, '63-'64), Chakravorty (1964) and others in our laboratory and elsewhere with great rigour. In the case of  $\text{Fe}^{2+}$  and  $\text{Co}^{2+}$  Tutton salts, theoretical formulation enables one to express the mean and principal susceptibilities of the paramagnetic complexes in terms of certain parameters connected with the anisotropic ligand field splitting, covalency effect and admixtural effect from the upper orbital levels. In order to evaluate the above mentioned theoretical parameters very accurately and to observe the finer features in their thermal and other behaviors, it was necessary to determine the mean susceptibility and magnetic anisotropy as accurately as possible. Earlier measurements on anisotropies and susceptibilities of some of

these salts are in the nature of pioneering work and the accuracy of the room temperature value as well as at low temperatures are not quite up to the mark of the rigorous theory developed.

With a view to supplying such data, the present anisotropy balance and a new gas flow cryostat have been set up to increase the sensitivity of the measurement, at least ten times the earlier ones, by avoiding carefully the usual sources of errors. In the present paper the crystalline and ionic magnetic anisotropies of the Tutton salts,  $\text{Co}(\text{NH}_4\text{SO}_4)_2 \cdot 6\text{H}_2\text{O}$ ,  $\text{Co}(\text{KSO}_4)_2 \cdot 6\text{H}_2\text{O}$ ,  $\text{Fe}(\text{NH}_4\text{SO}_4)_2 \cdot 6\text{H}_2\text{O}$ ; and  $\text{Fe}(\text{KSO}_4)_2 \cdot 6\text{H}_2\text{O}$  measured with above set-up are given in the range 68°K to 303°K. These crystals are isomorphous and belong to the monoclinic system with space group  $P_{21}/a$ , the unit cell containing two magnetically equivalent ions at  $(0, 0, 0)$  and  $(\frac{1}{2}, \frac{1}{2}, 0)$ .

#### MEASUREMENT OF MAGNETIC ANISOTROPY

The method used for the measurement of magnetic anisotropy is the 'Static torque' method of Stout and Griefel (1950), and Dutta (1956) which is a very useful modification of the 'Critical torque' method of Krishnan *et al.* (1935). In this method, the maximum magnetic couple acting on the crystal at 45° position due to the horizontal homogeneous magnetic field  $H$  is kept balanced by the torsion of the vertically suspended fibre. The magnetic anisotropy  $\Delta\chi$  per gm. mole. in the horizontal plane is related to the maximum torsion angle  $\alpha_m$  according to the following expression

$$\Delta\chi = \frac{2MC}{mH^2} \alpha_m$$

where  $M$  and  $m$  are, respectively, the molecular weight and mass of the crystal, and  $C$  is the torsion constant of the fibre.

The angle  $\alpha_m$  is noted from the vernier torsion disc, from which the crystal is suspended, and the mass  $m$  is measured with the help of a Mettler micro-balance (0.5–10  $\mu$ gms). To determine the constant  $C/H^2$ , the value of  $\alpha_m$  is measured for a  $\text{NiSO}_4 \cdot 6\text{H}_2\text{O}$  (tetragonal system) crystal of known mass. The  $\text{NiSO}_4 \cdot 6\text{H}_2\text{O}$  crystal is suspended with its  $c$ -plane vertical and the shape is chosen such that the cross-section in the horizontal plane is approximately a square, to avoid shape effect (M. Mazumdar 1962). The exact value of  $\Delta\chi_s$  of this standard crystal at the temperature of the experiment is obtained from an already calibrated graph of  $\Delta\chi_s$  vs temperature round about room temperatures, (Dutta 1956) and substitution of  $\Delta\chi_s$  in the above equation determines  $C/H^2$ .

The anisotropy of a given crystal at any temperature is determined by noting the corresponding  $\alpha_m$  at that temperature. In most cases we have observed  $\alpha_m$  at intervals of about 20°K between room temperature and 68°K.



In the present work, the crystals to be investigated being monoclinic the crystalline anisotropies are determined by measuring first the anisotropies with (1) "b" axis vertical and then with (2) "a" axis vertical or the (001) plane horizontal the planes being well developed in these crystals. The "b" axis coincides with the principal susceptibility  $\chi_3$  so that the first measurement directly gives the difference  $\chi_1 - \chi_2$  from the above eqn. The second measurement gives  $\chi_1 \sim \chi_3$  using the eqn.

$$\Delta\chi = \pm[(\chi_1 - \chi_3) - (\chi_1 - \chi_2) \sin^2 \theta]$$

or

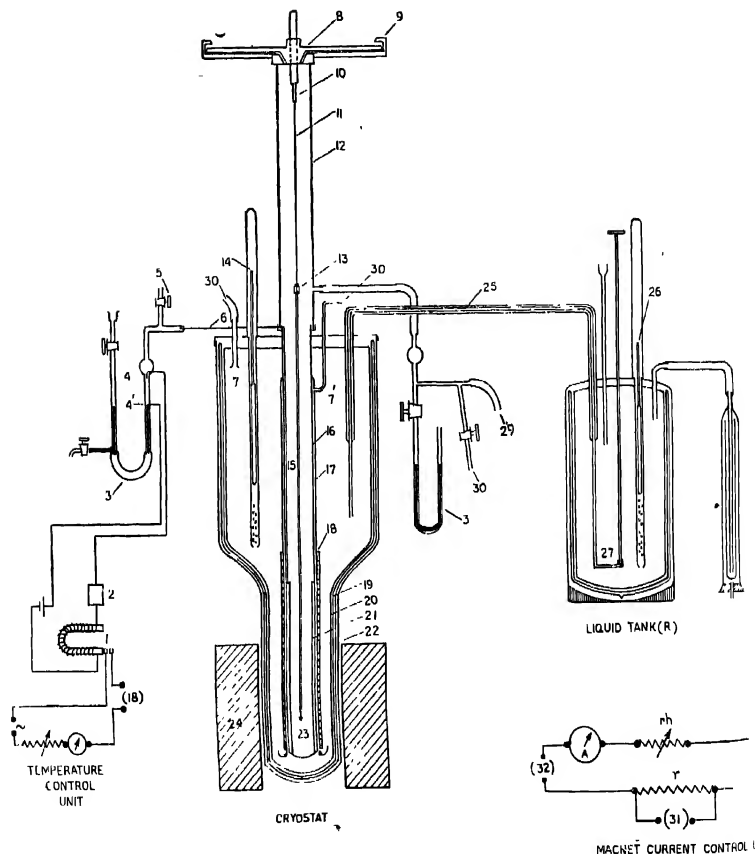
$$\Delta\chi = \pm[(\chi_1 - \chi_3) - (\chi_1 - \chi_2) \cos^2 \theta]$$

according as the "a" axis is vertical or the (001) plane horizontal is considered. The +ve or -ve sign is taken as "b" axis sets perpendicularly or parallel to the magnetic field in these latter suspensions. The angle  $\theta$  between  $\chi_2$  and "a" axis is determined as described by previous workers Dutta (1954), in this laboratory.

#### THE IMPROVEMENTS IN THE PRESENT SET-UP FOR MAGNETIC ANISOTROPY MEASUREMENT AS COM- PARED TO THE PREVIOUS WORKS

The magnetic anisotropy of any paramagnetic crystal is determined by comparison with the magnetic anisotropy of  $\text{NiSO}_4 \cdot 6\text{H}_2\text{O}$  taken as standard, and as such it is essential that the magnetic field should remain constant during the comparison. Furthermore since the magnetic couple on the crystal due to the magnetic field depends upon the square of the magnetic field, even a small fluctuation in the field during measurement of the rotation of the crystal affects the observed values of anisotropies appreciably. In earlier experiments here the magnetic field was kept constant only within 0.1%. For keeping the field constant to a much better degree, a potentiometric device is used to stabilize the d.c. feeding the magnet. The magnet current is obtained from a compound wound 220 d.c. generator, the 15 K.W. 440 A.C. motor of which is stabilized with a suitable saturation core transformer so that the voltage of the generator is constant within  $\pm 1$  volt. For the final stabilization of the magnet current a small standard resistance 'r' is added in series with the coils of the electromagnet. The p.d. across this standard resistance 'r' is maintained constant within 1 micro-volt by the usual potentiometric balancing method, controlling the current through 'r' by adjusting a fine control wire rheostat 'rh' in series with it (see Fig.).

The maximum current that can flow through the coils in series with the magnet is 1.6 amps. and hence the value of the standard resistance was chosen so as to create a p.d. of exactly 1.01830 volts across it when a current of about 1.56 amps (it is not necessary to measure this current exactly) flows through it. The standard resistance ( $\sim 65$  ohms) was prepared by winding a Eureka wire (1.5mm dia.) over an ebonite core and the ends soldered to the leads.



- (1) relay magnet (2) transistorised amplifier (3) mercury manometer (4,4') platinum electrode  
 (5) stop cock (6) stainless-steel capillary tube (7,7') outlets for oxygen (8) torsion-head (9) vent  
 (10) pin-holder (11) quartz-fibre (12) experimental chamber (glass portion) (13) mirror-system  
 (14) indenter (15) suspension system (16) experimental chamber (metallic portion) (17) co-axial lead  
 (18) heater coil (19) glass-dewar (20) minor-casing (21) constant volume gas thermometer (22) outer  
 casing (23) crystal (24) pole-pieces (25) siphon (26) indicator (27) pin-valve (28) air inlet  
 (29) to Kipp's apparatus (30) to pump (31) to potentiometric circuit (32) to magnet coils.

The low frequency fluctuation of the magnet current are automatically damped by the magnet inductance and any residual effect of the same upon the crystal is damped by the low (non-resonant) natural time period of the suspension system. Hence the magnetic couple balance reading and the magnet current balance reading can be synchronized to within a fraction of a second depending upon the personal reflex action of the observer so that if the observer is at all the while assured that neither the potentiometric current balance nor the magnetic couple balance has fluctuated from the desired value appreciably over several seconds during the final adjustments of the controls it is easy to see that the steadiness of the magnet current is limited only by the error of the least reading of the balancing current microammeter (of small resistance). Estimating this it is found that the stabilization of the magnet current during measurement is attained to within 1 part in 100,000. Of course, it should be remembered that owing to leakage currents the absolute value of the magnetic field may not be obtained with the same degree of accuracy, but since our anisotropy measurements is a relative one this will not matter unless the leakage current has different values during a set of measurements, which is rather unlikely.

#### PREPARATION AND MOUNTING OF CRYSTALS

Single crystals of ferrous and cobalt Tutton salts  $[M^2(MSO_4)_2 \cdot 6H_2O]$  were prepared by slow evaporation from a saturated solution containing equimolecular weights of analytically pure component salts of Merck or BDH quality in double-distilled water. The solution was allowed to evaporate in a dust-free air-conditioned room on a vibration-proof stand. Out of successive crops of crystals from the same mother liquor only the middle ones were chosen. Single crystals thus obtained were allowed to crystallise for the second or even the third time if thought necessary. Such repeated crystallisation reduced the impurities in the crystal to a minimum. The crystals selected were next tested under a polarising microscope so as to reject any twinned or defective crystals. One of the best crystals thus obtained was next attached to the end of a thin and light glass-rod with 'Quick-fix' adhesive (diamagnetic and non-crystalline), in the required orientation with reference to the rod, correctly to 0.1 degree by mounting the whole on a two-circle goniometer. The rod bearing the crystal was next attached to the lower end of a thin and long glass tube, fitted at the top with a small light hexagonal mirror system (13) (fig.) with the hexagonal axis vertical. This whole suspension system (15) was next attached to quartz-fibre (11), of suitable diameter depending on the magnetic anisotropy of the crystal, from the pin (10) fixed axially to the torsion head (8). The torsion head is a brass disc of 16cms diameter, fitted on a smooth taper collar, and very accurately graduated into 500 equal divisions, the two verniers (9) (with vernier constant 0.02 of each main scale division, i.e.  $\sim 0.014$  degrees, in earlier experiments this was 0.1 degree) are carried on a pair of radially projecting arms connected to the collar, diametrically opposite each

other on the outer edge of the disc. A pyrex glass tube (diameter 3 cms, length 24 cms) is fitted into a circular groove on the lower end of the collar, and cemented air tight by araldite adhesive. The other end of this glass tube is fitted air tight to the german silver end of the experimental tube (16), inside the cryostat by a metal glass joint. Thus the experimental chamber is composed of a glass portion (12) above, through which the hexagonal mirror attached to the crystal suspension is visible, and a metallic portion inside the cryostat. The crystal to be measured, hangs near the lower end of metallic portion

To prevent condensation of the atmospheric moisture, or carbon dioxide upon the sample crystal at low temperatures (down to about 65°K), the experimental tube was evacuated and filled with hydrogen gas at atmospheric pressure through a side tube from a Kipp's apparatus, after passing through a series of purifying and drying towers. The pressure inside the experimental chamber was kept constant at low temperatures

#### DETECTION OF CRYSTAL MOTION BY PHOTO-CELL ARRANGEMENT

It has been seen in earlier experiments that the rotational motion of the crystal in the magnetic field is considerably magnified by the motion of a collimated beam of light from a stabilized a.c. source, reflected from one or the other mirrors of the hexagonally arranged mirror system attached to the suspension rod. But, since the maximum angular motion of the crystal is through 45° from the no-torque position to the maximum torque position in the magnetic field, it is essential that both these angular positions should be adjusted and measured so accurately so as to keep the error in  $\sin 2\phi$  (Dutta, 1956) to less than one part in 10,000. For this purpose now, a pair of barrier-photo-voltaic cells, connected in opposition through a suitably shunted sensitive galvanometer, are mounted very close to each other and kept inside a long blackened wooden box with a small window in front, through which the light spot falls on the cells

The position of the photo cells, placed at a distance of about 50 cms from the mirror system, is adjusted in such a way that the cells are very nearly equally illuminated, so that no resultant e.m.f. is observed in the galvanometer. Now, if the mirror rotates even by a small amount by applying the magnetic field on the crystal, the balance of the photo-cell e.m.f. is destroyed and a large deflection is observed in the galvanometer. The balance is restored by applying a sufficient torque upon the quartz fibre bearing the crystal, with the help of the torsion head.

The magnification was adjusted in such a way that even if the crystal rotates through 0.01°, (which is roughly equal to the value of one vernier division of the torsion head), the galvanometer deflection on the scale is about 10 cms. The current into the galvanometer is controlled by a 5 K  $\Omega$  potentiometer. It will be seen that, even with a heavily shunted galvanometer, the sensitivity of the detection of the rotation of the crystal is more than 20 times the earlier lamp and scale

method and more than 100 times as can be measured with the present torsion head. There is thus scope for further increase in accuracy of measurement, if needed in future works.

#### CRYOSTATIC ARRANGEMENT

The cryostat is really a combination of gas flow type (Bose 1947) and liquid bath type (Bose *et al.* 1963). At temperatures between 303°K and 90°K, it acts as a continuous gas flow type, the flow of cold gas from evaporated liquid oxygen being controlled by an adjustable speed pumping arrangement. After reaching the liquid oxygen temperature i.e. 90°K, a quantity of liquid oxygen is collected inside the cryostat and made to boil inside it under reduced pressure, whereby ~8°K is obtained in the experimental chamber.

The present cryostatic arrangement differs considerably in details of construction from the earlier types. The cryostatic arrangement broadly consists of three main sections, (Figure)

- i) The liquid oxygen reservoir tank R, with vacuum jacket cover.
  - ii) The cryostatic chamber, connected to the pumping unit
  - iii) The temperature controlling unit
- i) *Liquid oxygen reservoir tank R*

The tank R is a cylindrical chamber of german silver of capacity 2 litres and fitted with a cap packed with a lining of cotton and felt, and placed inside a wide-mouthed hard glass thermo-flask. The cap has two openings, through one of which liquid oxygen is poured, and through the other dry air is allowed into the tank, to replace the liquid air sucked out. A light glass bulb (26) ending in a long thin capillary stem with an index at the top passes through a perforated german silver tube extending nearly to the bottom. It floats in liquid oxygen, the end of the stem being visible through a gauge glass tube, fitted to the upper end of german silver tube. It serves as the liquid level indicator.

Liquid oxygen is sucked into the cryostat chamber with the help of a two-stage rotary oil pump of 50 litres/min. gas capacity through a vacuum jacketted german silver siphon, the flow being controlled by a needle valve (27). The siphon is a double-walled tube of german silver, the interspace being evacuated and sealed permanently and is bent twice at right angles as shown in the figure. To obtain temperatures below liquid oxygen b.pt the needle valve is operated with a long thin stainless steel tube stem and can be used to regulate the flow of liquid into the cryostat, as also to cut off completely the supply after a sufficient quantity of liquid has been sucked into the cryostat, when it can be made to boil under reduced pressure inside the cryostat

#### iv) *Cryostat*

The cryostat is a wide mouthed (inner dia. ~10 cms.) double-walled silvered glass Dewar (19) with a narrow tail (inner dia. ~3.5 cms.) which passes into the

space between the polepieces (24) of the magnet. An outer brass casing (22) protects the glass dewar from external mechanical shocks another inner german silver casing (20) serves to protect it from breakage due to sudden local cooling when oxygen is pumped into it. Both are fitted with leak-tight caps, the space between the caps being lined with aluminum foil and packed with felt to prevent heat leakage. One bent of the siphon (25) passes through the caps into the inner chamber, the other bent end passing into the reservoir R, its inner tube passing to the bottom. A glass float-indicator (14) as used in the tank R is also fitted to the cryostat chamber to see the level of the liquid oxygen when the cryostat is used as a bath type one as earlier mentioned.

The experimental chamber (16) as mentioned earlier reaches up to 2 mm from the bottom of the narrow tail end of the cryostat. The portion of (16) above the tail of the dewar is made of german silver to prevent conduction of heat through the neck into the dewar. The remaining portion lying inside the tail of the dewar is made of copper to help temperature uniformity, the two parts being silver soldered. The copper tube has an annular chamber near the lower end which acts as the bulb for a constant volume gas-thermometer (21). A stainless steel capillary tube (6) from this bulb passes out of the experimental chamber and is connected to a mercury-in-glass manometer (3), the junction of the two being made leak-tight with araldite. The composite experimental tube (16) is surrounded by a coaxial copper jacket (17) open at the lower end and soldered to (16) at the top, an inch below the inner cap, and a side tube (7') of stainless steel, leads from this jacket to the pump. A fine nichrome coil (18) insulated with thin mica sheet is wound non-inductively for about 10 cms. of the lower end of this tube (17), and fed by a small a.c. from the mains through a variac. This acts as a heater, the insulated leads of which are brought out through the caps and sealed leak-tight with araldite cement (not shown in the fig.). Thin copper gauze of about 20 mesh per inch, is loosely packed over the heater and also in the wider portion of the dewar to facilitate rapid and uniform evaporation of liquid oxygen and quick and uniform distribution of heat over the experimental chamber. The cold vapour from liquid oxygen after exchanging heat with the heater and arriving at a desired low temperature is sucked into the narrow space between the experimental chamber and the coaxial jacket, cooling the former and finally goes out of the cryostat through the suction line (7'). The heat-exchange between the experimental chamber and the vapour depends on the rate of pumping so that different steady temperatures are obtained in (16) with a fair degree of accuracy, by regulating this rate. The temperature regulation is further helped by adjusting the heater current. Since the rate of pumping cannot be adjusted beyond a certain limit owing to the irregular spurts of liquid oxygen through the siphon, caused by the somewhat intermittent suction of the rotary pump and also by the back pressure developed in the siphon line by the evaporation of the liquid a relay

system worked by a gas thermometer is utilized for fine control of temperature, as will be described later

For obtaining temperatures below 90°K. outlet (7') is nearly closed and the alternative outlet (7) is fully opened. The outlet (7) is connected to the pump in parallel to (7'), and reaches only an inch below the cap of the inner casing of the dewar. Liquid oxygen is now pumped into the cryostat by opening the pin valve (27) full, and then closing it tightly after a sufficient amount of the liquid is collected as shown by the level indicator. Liquid begins to boil under the reduced pressure which can be noted by a manometer (not shown in the fig.) connected to the cryostat chamber. A steady temperature is soon reached depending on the steady pressure over the liquid. The heat leakage in our system being fairly large it was not possible with the given pump to go below about 68°K by reducing the vapour pressure.

(iii) *Temperature control*

The temperature inside the experimental tube (16) is very accurately controlled by means of a gas thermometer ( $H_2$  gas from a Kipps can be used over the entire range) relay system. The bulb of the constant-volume-gas thermometer connected to the manometer as mentioned earlier (fig.) can be opened to the source of gas through the stop-cock (5). Two platinum electrodes (4) and (4') are fused into the capillary glass tube forming one limb of the manometer (3), (4') always dips into the mercury. When the mercury level touches the other contact (4) the relay magnet circuit is completed, which in its turn closes the heater circuit.

Initially by adjusting the pumping rate, while keeping the stop-cock (5) open to the atmosphere, the temperature required is nearly attained with a slight preponderance of cooling, and then the stop-cock is closed, shutting off the bulb from the atmosphere. The enclosed gas in the bulb now contracts due to the small tendency for over cooling, the mercury level rises and makes the contact when the heater is adjusted as far as possible to just balance the overcooling so that a fine control of temperature, to less than  $0.01^\circ K$  is obtained.

This adjustment is however laborious and is likely to be upset by fluctuations in the pumping rate or the heater current, and hence need not be made very critical. What is done in practice is that with a slight cooling tendency the heater current is adjusted to just overbalance it, so that the relay, actuated by the gas thermometer makes and breaks the heater circuit repeatedly, to just maintain the balance of temperature. With suitable adjustments the alternate peak of rise and fall in temperature can be narrowed down to less than  $0.01^\circ K$  as indicated by the fluctuation in the light spot in the galvanometer (not shown in fig.) used to indicate the balance of the copper-constantan thermo-couple c.m.f. in the potentiometric circuit for the temperature measurement.

## TEMPERATURE MEASUREMENT

The temperature of the crystal is measured by means of a very accurately calibrated copper-constantan thermo-couple junction placed very near it, the temperature gradient in this region being found to be less than  $0.01^{\circ}\text{K}$ . The thermo-couple leads come out of the experimental chamber through a leak tight side tube (not shown in the fig.)

The thermo-couple was calibrated using a 5 constant formula relating the thermo-e.m.f.  $E'$  to the centigrade temperature  $t$  of the measuring junction, (the standard junction being kept in melting ice), as follows :--

$$E' = a + bt + ct^2 + dt^3 + et^4$$

where  $a, b, c, d, e$ , are constants determined by noting the thermo e.m.f. at the standard temperatures of ice steam, solid  $\text{CO}_2$ , room temperature (given by a standard mercury glass thermometer), and liquid oxygen boiling point at atmospheric pressure. When both junctions are put in melting ice mixed with distilled water in a thermo-flask, then

$$E = a = 0$$

showing there were no spurious e.m.f's. For obtaining the temperature of pure liquid oxygen, a miniature rectifier column was constructed and used for purifying the commercially obtained liquid oxygen containing some dissolved nitrogen. Oxygen gas from a cylinder of 99.5% purity at  $\sim 100$  atmos pressure, was pre-cooled by circulating through a cooling spiral immersed in a reservoir of commercial liquid oxygen at the bottom of the rectifier column and after liquefaction by Joule-Thomson expansion at the top of the column, is made to trickle down a series of perforated discs made out of fine mesh of copper gauze, thereby exchanging its nitrogen content with the oxygen content of the upstreaming vapour mixture of oxygen and nitrogen from the reservoir. Thus the escaping gas becomes progressively richer in nitrogen, while the down flowing liquid richer in oxygen, until the liquid in the reservoir is practically all pure oxygen. The thermo-couple immersed in this liquid shows a gradual reduction in e.m.f. until at the end it becomes steady at pure oxygen temperature. The corresponding pressure inside the rectifier over the liquid is noted, as also the barometric pressure on a standard Fortin's barometer, for correcting to the normal boiling point.

Solid  $\text{CO}_2$  temperature is obtained with a mixture of ether and solid  $\text{CO}_2$  made by expansion from a commercial cylinder of the gas of sufficient purity. Steam temperature is obtained in the usual manner in a hypsometer. Both temperatures are corrected for the atmospheric pressure in the usual way.

To calibrate the thermo-couple from  $90^{\circ}\text{K}$  to  $68^{\circ}\text{K}$ , we have measured thermo-e.m.f. at different vapour pressure of liquid nitrogen. The corresponding temperatures are obtained from the International Critical Table (Vol. III). The

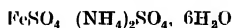


vapour pressure of the boiling liquid was measured by means of a Torricelli type of Hg manometer, capable of reading up to 0.5 mm of the mercury level. Near the temperature 68°K, 1 mm change of the level corresponds to 0.03 K, so that the accuracy of the temperature is 0.015°K. For temperatures above, the accuracy increases as can be shown from the vapour pressure chart.

TABLE I

Serial no of crystals	Mass of crystal in (gm)	Maximum torsional angle $\alpha_m$ (degree)	$\alpha_m/m$ at 301.23°K
1	0.043495	67.22	1545.46
2	0.022043	34.02	1543.42
3	0.043200	67.70	1547.23
4	0.025009	37.34	1546.64
5	0.039194	60.52	1544.11

TABLE II



Temp (°K)	Angle $\theta^\circ$ between 'a' & $X_2$ axes	$(X_1 - X_2)$ $\times 10^6$	$(X_1 - X_3)$ $\times 10^6$	$(K_{11} - K_{33})$ $\times 10^6$	$(\Delta K T)$ $\times 10^4$	$\phi^\circ$ Angle
303	-36.92	2381.6	180.45	4582.7	1388.8	43.86
280	-36.74	2826.5	234.69	5418.3	1517.1	43.75
260	-36.54	3278.1	288.46	6267.7	1629.6	43.68
240	-36.35	4038.2	351.56	7724.8	1853.9	43.70
220	-36.22	4942.2	419.42	9464.9	2082.3	43.75
200	-36.18	6040.0	502.50	11577	2315.5	43.75
180	-36.15	7413.6	604.94	14222	2560.0	43.78
160	-36.11	9246.1	737.50	17755	2840.7	43.80
140	-36.10	11750	908.16	22592	3162.8	43.85
120	-36.09	15377	1151.4	29404	3528.5	43.85
100	-36.08	20520	1518.0	39522	3952.2	43.90
80	-36.08	29062	2125.0	50000	4480.0	43.91
68	-36.08	37737	2724.9	73751	5015.0	43.93

TABLE III  
FeSO<sub>4</sub>, K<sub>2</sub>SO<sub>4</sub>, 6H<sub>2</sub>O

Temp. (°K)	Angle θ° between 'a' & χ <sub>2</sub> axis	(χ <sub>1</sub> - χ <sub>2</sub> ) × 10 <sup>3</sup>	(χ <sub>1</sub> - χ <sub>3</sub> ) × 10 <sup>3</sup>	(K <sub>  </sub> - K <sub>⊥</sub> ) × 10 <sup>3</sup>	(ΔKT) × 10 <sup>4</sup>	φ° Angle
303	-43.90	1768.2	-301.18	3837.6	1102.8	42.75
280	-44.00	2028.1	-391.32	4417.5	1245.3	42.46
260	-44.11	2304.7	-485.65	5095.1	1324.7	42.23
240	-44.25	2644.9	-601.73	5891.5	1413.9	42.06
220	-44.45	3065.1	-753.51	6883.7	1514.4	41.85
200	-44.75	3597.5	-948.50	8143.5	1628.7	41.65
180	-45.02	4274.7	-1214.5	9763.9	1757.3	41.41
160	-45.44	5171.9	-1544.9	11889	1902.2	41.26
140	-45.85	6397.9	-1922.4	14718	2060.5	41.25
120	-46.18	8125.0	-2438.2	18688	2242.5	41.25
100	-46.25	10707	-3054.0	24469	2446.9	41.41
80	-46.30	14847	-3570.0	33265	2661.2	41.01
68	-46.30	18386	-4300.1	41071	2792.3	42.00

TABLE IV  
CoSO<sub>4</sub>, (NH<sub>4</sub>)<sub>2</sub>SO<sub>4</sub>, 6H<sub>2</sub>O

Temp. (°K)	Angle θ° between 'a' & χ <sub>2</sub> axis	(χ <sub>1</sub> - χ <sub>2</sub> ) × 10 <sup>3</sup>	(χ <sub>1</sub> - χ <sub>3</sub> ) × 10 <sup>3</sup>	(K <sub>  </sub> - K <sub>⊥</sub> ) × 10 <sup>3</sup>	(ΔKT) × 10 <sup>4</sup>	φ° Angle
303	60.10	3011.8	1715.4	4308.2	1305.3	33.26
280	60.04	3565.7	2108.4	5023.0	1406.4	32.58
260	60.03	4156.8	2510.3	5803.3	1508.8	32.18
240	59.98	4878.5	3001.7	6755.3	1621.2	31.80
220	59.90	5760.3	3617.7	7902.9	1738.6	31.36
200	59.80	6872.5	4400.0	9345.0	1869.0	30.95
180	59.65	8283.9	5401.2	11166	2009.8	30.53
160	59.38	10105	6742.2	13468	2154.8	29.98
140	59.07	12515	8576.5	16453	2303.4	29.28
120	58.07	15652	10930	20374	2444.8	28.75
100	58.35	19550	14502	24598	2459.8	26.93
80	58.27	24500	18300	30700	2456.0	26.23
68	58.25	27898	21622	34174	2323.8	25.33

TABLE V  
CoSO<sub>4</sub>, K<sub>2</sub>SO<sub>4</sub> · 6H<sub>2</sub>O

Temp (°K)	Angle $\theta^\circ$ between 'a' & $\chi_2$ axes	( $\chi_1 - \chi_2$ ) $\times 10^6$	( $\chi_1 - \chi_3$ ) $\times 10^6$	( $K_{  } - K_{\perp}$ ) $\times 10^6$	( $\Delta KT$ ) $\times 10^4$	$\phi^\circ$ Anglo
303	30 20	2490.5	1835.2	3145.8	953.17	27 15
280	29.90	2913.9	2152.0	3677.8	1029.7	27 08
260	29.65	3357.9	2502.3	4213.5	1095.5	26.78
240	29.45	3890.6	2940.2	4861.2	1166.6	26.30
220	29.25	4532.2	3530.0	5552.1	1221.4	25.16
200	29.06	5317.5	4306.4	6328.6	1265.7	23.55
180	29.00	6311.7	5185.1	7138.3	1338.9	22.90
160	29.00	7562.9	6190.2	8934.8	1429.5	23.06
140	29.00	9198.9	7538.8	11059	1548.2	23.51
120	29.00	11451	9218.9	13653	1638.3	23.68
100	29.00	14320	11501	17139	1713.9	23.91
80	29.00	18328	14403	22253	1780.2	24.83
68	29.00	21907	16552	27262	1853.8	26.30

## SENSITIVITY OF THE APPARATUS

To check the reproducibility and accuracy of our measurement, we have measured the magnetic anisotropy of 5 crystals of NiSO<sub>4</sub> · 6H<sub>2</sub>O. The ratio of  $\chi_m/m$  of these crystals were found to be constant to about 2 parts in a thousand, (Table I). This variation is more due to lack of perfection in the different crystals rather than due to inaccuracy in other experimental parameters, since it was found that for the same crystal the said ratio is constant up to 2 parts in 10 000 when the same crystal is measured by varying other conditions such as detaching and remounting it, changing the torsion fibre and also the magnetic field, taking into consideration the changes in C and H.

## TABLES OF RESULT

The method of calculation of the principal crystalline anisotropies at different temperatures is already described earlier. The first 4 columns of the Table II to V respectively, give (i) the temperatures in degrees Kelvin, of the experimental measurements, (ii) the angles between "a" axis and  $\chi_2$  direction of the crystals, (iii) the values of  $\chi_1 - \chi_2$  and (iv) values of  $\chi_1 - \chi_3$  calculated from the extrapolated graphs at 20°K intervals, starting with 303°K and ending at 68°K, the lowest available temperatures.

It has been shown from earlier works, (Bose *et al.* 1960, Bleaney and Ingram 1951) that the complexes Fe<sup>2+</sup> · 6H<sub>2</sub>O and Co<sup>2+</sup> · 6H<sub>2</sub>O in the Tutton salts have nearly tetragonal symmetry and moreover, the symmetry axes of the two octahedra in the unit cell are inclined at an angle which is bisected by  $\chi_1$  axis of

the crystal. Hence the principal g.m. ionic anisotropy of the complexes is given by

$$K_{\parallel} - K_{\perp} = 2(\chi_1 - \chi_2) - (\chi_1 - \chi_3) \quad \text{for } K_{\parallel} > K_{\perp},$$

$$\text{and} \quad \cos 2\phi = \frac{\chi_1 - \chi_3}{2(\chi_1 - \chi_2) - (\chi_1 - \chi_3)}$$

where  $K_{\parallel}$  and  $K_{\perp}$  are the principal g.m. ionic susceptibilities parallel and perpendicular to the tetragonal axis of the complex. The values of  $(K_{\parallel} - K_{\perp})$  and  $\phi$  calculated in this way at different temperatures are given in the next two columns of the tables. The overall accuracy of these values is estimated to be better than 0.1%. This is at present limited by the method of graphical extrapolation adopted but can be very much improved by using a more laborious least square method. But since our approximation in respect of the symmetry of the complexes has already been assumed it was not thought worth while for the present to perform this extra labour in the absence of more accurate structural data.

#### RESULTS AND DISCUSSION

##### (a) *The shape of the magnetic ellipsoid of the crystals*

From the values of  $(\chi_1 - \chi_2)$  and  $(\chi_1 - \chi_3)$  it will be observed that in the  $\text{Fe}^{2+}$  salts the magnetic ellipsoid of the crystals are roughly reduced to oblate spheroids about the  $\chi_2$  axis, which has thus the minimum susceptibility. This is evidently a consequence of the fact that  $K_{\parallel} \gg K_{\perp}$  and the angle  $\phi$  is close upon  $45^\circ$ . The former conclusion that  $K_{\parallel} > K_{\perp}$  in the case of potassium salt is directly a consequence of our observation that  $\chi_1 - \chi_3$  is negative for this salt at all temperatures. In consequence, in this case the condition that  $\phi$  is nearly  $45^\circ$  is also automatically fulfilled as is shown from our calculations of  $\phi$ . The alternative assumption of  $K_{\perp} > K_{\parallel}$  leads to a value of  $\cos 2\phi < 1$ , which is impossible. For the ammonium salt, however, the conclusion is not so straightforward, and we assume the same to be true also in this salt, not only because this is more likely for an isomorphous salt with the same paramagnetic ion, but because, as shown by Bose *et al.* (1961) such an assumption (i.e.  $K_{\parallel} > K_{\perp}$ ) will lead to a particular energy level scheme in this salt leading to the anisotropic spectroscopic splitting factors to be  $g_{\parallel} \approx 9$ ,  $g_{\perp} \approx 0$ . (Bose *et al.*, 1960) which agrees with the experimental result.

For the  $\text{Co}^{2+}$  salts the crystalline tensor ellipsoid is more or less triaxial as can be seen from the anisotropic data and hence the ambiguity is more difficult to remove normally. But in this case for both the Tutton salts paramagnetic resonance gives clear indication that the ionic ellipsoid is nearly uniaxial, also,  $K_{\parallel} > K_{\perp}$  and the values of  $\phi$  obtained from resonance, (Bleaney, 1951) are close to ours, calculated from magnetic anisotropy. It is, however, necessary that we should make more extensive trial and error calculations for finding the actual scheme of energy levels in the individual Tutton salts with the present new and

very accurate data for then we can make a definite decision in favour of one or the other.

The detailed discussion of the results in reference to the theory of octahedral  $\text{Co}^{2+}$  and  $\text{Fe}^{2+}$  ions will be given in the next part of the paper only after the mean susceptibilities are measured with comparative degree of accuracy which are in progress. It will be, however, interesting to give here some broad features of the thermal magnetic behavior of the crystals.

(b) *Large ionic anisotropies*

Due to the predominant cubic component of the electric field of the 6 surrounding charges, the free-ion ground state  ${}^2D(3d^6)$  of  $\text{Fe}^{2+}$  breaks up into an orbital triplet and a doublet, and the free-ion ground state  ${}^4F(3d^7)$  of  $\text{Co}^{2+}$  splits into 2 orbital triplets and a singlet, a triplet lying lowest in both cases. The axial component of the ligand field and spin-orbit interaction, considered together, breaks up partially the remaining spin and orbital degeneracies. Thus spin-orbit interaction has got a definite effect on the cubic ground level. In the first order, unlike some other octahedrally coordinated salts of the iron group such as of  $\text{Cr}^{2+}$ ,  $\text{Ni}^{2+}$ ,  $\text{Cr}^{3+}$  and  $\text{Mn}^{3+}$ . This explains the large value of the ionic anisotropy of the octahedrally coordinated  $\text{Fe}^{2+}$  and  $\text{Co}^{2+}$  ions in comparison to that of the latter ions, the values at 303°K being respectively 4583, 3838, 4308, and 4146 units for  $\text{Fe}(\text{NH}_4\text{SO}_4)_2 \cdot 6\text{H}_2\text{O}$ ,  $\text{Fe}(\text{KSO}_4)_2 \cdot 6\text{H}_2\text{O}$ ,  $\text{Co}(\text{NH}_4\text{SO}_4)_2 \cdot 6\text{H}_2\text{O}$  and  $\text{Co}(\text{KSO}_4)_2 \cdot 6\text{H}_2\text{O}$ . These results agree in general with those of earlier works (Bose 1947, Dutta 1956) but are more accurate as to the actual values as already stated.

(c) *Temperature variation of anisotropies*

From the results it is apparent that the ionic anisotropy does not follow a simple linear inverse temperature dependence. In many salts of the iron group, previous workers (Bose *et al.* 1948, Dutta, 1956), have represented the ionic anisotropy by a 3-constant formula as follows

$$K_{||} \sim K_{\perp} = A + B/T + C/T^2.$$

Although we cannot assume that the 3-constant formula is sufficient to fit our experimental results, we expect that the same formula will also hold good in our case. The constant  $A$ ,  $B$ ,  $C$  are very much structure sensitive and varies from salt to salt even for the same ion. It is known that the effect of the distant atoms outside the primary ligand cluster, the disposition of which is determined by packing of the atoms consistent with the space group symmetry of the crystal, is more pronounced in the anisotropy value than in the mean susceptibility (Van Vleck 1939, Bose *et al.*, 1957, 1958). The members of  $\text{Co}^{2+} \cdot 6\text{H}_2\text{O}$  or  $\text{Fe}^{2+} \cdot 6\text{H}_2\text{O}$  clusters are rigidly bound together as shown by the persistence of the cluster under extreme conditions, but not so for the distant atoms which are weakly bound. Consequently even a small anisotropic thermal expansion of the lattice, affects more the effect of the distant atoms i.e., the anisotropic component rather

than the cubic component of the field. The increase of the anisotropy between 303°K and 68°K is observed to be maximum in  $\text{Fe}(\text{NH}_4\text{SO}_4)_2 \cdot 6\text{H}_2\text{O}$ , being 16 times, and a minimum in  $\text{Co}(\text{NH}_4\text{SO}_4)_2 \cdot 6\text{H}_2\text{O}$ , being 7 times.

(d) *Variation from salt to salt*

The above effect of the distant atoms also explains the variation of anisotropy values for the same ionic cluster but with a different alkali radical outside it. The difference in the anisotropy value between the two ferrous ions is 20% and between that of cobalt is 36 %

(e) *Change of orientation of the magnetic ellipsoid with temperature*

The change in the angle  $\theta$  between the  $\chi_2$  axis and the  $z$  axis over the entire temperature range is different for each of these Tutton salts, a minimum for  $\text{Fe}(\text{NH}_4\text{SO}_4)_2 \cdot 6\text{H}_2\text{O}$  ( $\Delta\theta = 0.87^\circ$ ) and maximum for  $\text{Fe}(\text{KSO}_4)_2 \cdot 6\text{H}_2\text{O}$  ( $\Delta\theta = 2.4^\circ$ ), for the  $\text{Co}^{2+}$  salts,  $\Delta\theta = 1.85^\circ$  and  $1.20^\circ$  respectively for ammonium and potassium radicals. This indicates a small rotation with temperature, of the crystalline magnetic ellipsoid about the crystalline symmetry axis

From the table it is observed that the angle  $2\phi$  between the 2 tetragonal axes of the differently oriented ions in the unit cell changes with temperature differently for different salts. For ferrous ammonium, ferrous potassium and cobalt potassium salts,  $\phi$  decreases to a minimum at temperatures 260°K, 140°K and 180°K respectively. However, for cobalt ammonium salt  $\phi$  continuously decreases with temperature. The maximum changes  $\Delta\phi$  for the above salts taken in the same order, are respectively  $0.16^\circ$ ,  $1.50^\circ$ ,  $7.90^\circ$  and  $4.25^\circ$ . The appreciable changes in  $\phi$  for the cobalt ions may be due to the lack of a perfect uniaxial symmetry which we have assumed for calculating  $\phi$ . The changes in  $\theta$  and  $\phi$  angles are due to anisotropic thermal expansion of the lattice, the  $\phi$  angle being more sensitive to temperature variation

#### ACKNOWLEDGMENT

The authors are deeply grateful to Prof. A. Bose, D.Sc., F.N.I., for his guidance and help. Thanks are due to the Council of Scientific and Industrial Research for offering a fellowship to D. Guha Thakurta one of the authors. They are also thankful to the Workshop for efficient construction of the apparatus

#### REFERENCES

- Bleaney, B. and Ingram, D. J. R., 1951, *Proc. Roy. Soc.*, **A208**, 143.  
 Bose, A., 1947, *Indian J. Phys.*, **21**, 275.  
 Bose, A., 1948, *Indian J. Phys.*, **22**, 275, 483.  
 Bose, A., Chakravarty, A. S. and Chatterjee, R., 1961, *Proc. Roy. Soc.*, **A261**, 43, 207  
 Bose, A., Dutta Roy, S. K., Ghosh, P. K. and Mitra, S., 1963, *Indian J. Phys.*, **37**, 505  
 Datta, S. K., 1954, *Indian J. Phys.*, **28**, 239.  
 Datta, S. K., 1956, *D Phil Thesis* (Calcutta University).  
 Krishnan, K. S. and Banerjee, S., 1936, *Phil. Trans. Roy. Soc.*, **A235**, 843.  
 Majumdar, M., 1962, *Indian J. Phys.*, **36**, 111.  
 Stout, J. W. and Griefel, M., 1950, *J. Chem. Phys.*, **18**, 1449

# ON PROBABILITY-DISTRIBUTION OF STATES IN RATIONAL THERMODYNAMICS\*

M. DUTTA

A/31, C.I.T. BUILDINGS, SINGHEEBAGAN, CALCUTTA-7, INDIA.

(Received November 25, 1965)

**ABSTRACT.** In an essential statistical approach to thermodynamic problems, Dutta started with two observable entities, taken to be additive and having then numerical measures  $M$  and  $E$ . These quantities,  $M$  and  $E$ , corresponding to an instantaneous state (complexion), were assumed to be random variables. The probability-distribution for those  $M$  and  $E$  was taken to be exponential and written from arguments similar to those used for deduction of the Bayes rule. Then, the parameters of distribution were estimated by a method practically same as that of maximum likelihood. For an essentially statistical model, conceived in this way, all known results of statistical thermodynamics were obtained for equations of conservation of  $M$  and of  $E$ .

Here attempts are made to scrutinise earlier works to ascertain those properties of the above entities which play really fundamental roles in the development. It is seen that additivity (with usual physical assumption of continuity) implies and is implied by the exponential distribution, which is practically same as the Gibbs canonical (or, grand canonical) distribution in the terminology of orthodox statistical mechanics. Gibbs, starting from Liouville's theorem, proposed the canonical distribution as a distribution sufficient (not necessary) for constructing a mathematical model similar to thermodynamic systems. Here it is seen that it is necessary too. Then, how the statistical method of Dutta is related to the orthodox method of maximum likelihood of Fisher is investigated. Finally, the laws of probability-distributions for temperature, chemical potential etc., and expressions for their fluctuations are obtained.

## INTRODUCTION

In last fifteen years some attempts have been made to formulate and solve the problem of rational thermodynamics from essentially statistical and probabilistic methods with statistical model. The advantages of these attempts appears to be two-fold. Firstly, the methods are expected to be applicable also to systems which are not of thermodynamics nor even of physics. Secondly, it will be possible to interpret the equations and other results, commonly discussed in thermodynamics, in various ways in context of other branches of science thus, their real deeper significances will be revealed.

Starting with statistical model and using statistical arguments similar to Bayes rule, Dutta (1951, 1953, 1955, 1959, 1960, 1965a, 1965b), wrote down the

\* This research work was supported by the National Professor, S. N. Bose's Research Scheme of the Government of India at the Indian Association for the Cultivation of Science, Calcutta-32, India.

probability distribution for states of a thermodynamic system and estimated the parameters, involved in the distribution by a method, closely related to that of maximum likelihood of Gauss and Fisher. Then, from the equation of conservation of any of the fundamental entities, written down suitably, all the known results of that of phenomenological thermodynamic in forms quite similar to those, obtained by Gibbs (1902) and Fowler (1936)

With some objectives, Jaynes (1957a, 1957b) obtained the probability distribution of states by the method, named by him as the maximum entropy estimation, by maximising the information theoretic entropy which came into great prominence after the development of information theory (Shannon and Weaver, 1949, Goldmann 1953; Khinchin, 1957). Then, he obtained the commonly known results of statistical thermodynamics by identifying some of the quantities, entered in his calculations with usual thermodynamic quantities after Schrodinger (1948).

Recently Mandelbrot (1963) also tried to study the statistical mechanics of Gibbs as a branch of statistics. In his opinion, in statistical mechanics the physicists, and in mathematical statisticians the theoretical statisticians have been developing practically same methods from similar ideas in different symbols and different terminology without knowing and understanding works of one another.

Dutta (1960) showed that the laws of probability distribution of states, obtained by Dutta, and by Jaynes (1957a) were identical. As in both the developments, models, started with, are same and, also, the results obtained are same, so, it is quite natural to think that there must be deeper interrelations between these two for finding out the probability distribution of states. Recently, Mukerjee (1965) just touched this point from considerations of stochastic processes by simple mathematics. Dutta (1965a) also established that the method of maximum entropy estimation as used by Jaynes implies and is implied by an exponential distribution with parameters, estimated by the method, used by Dutta, and practically same as that of maximum likelihood of Gauss and Fisher. That the maximum entropy estimation leads to an exponential distribution is known (Kullback 1959), but that the parameters of the distribution by maximum likelihood has not been noticed earlier. Also, Dutta (1965) has been able to establish the deep interrelation even between the definition of likelihood function and that of information-theoretic entropy, particularly for ergodic samples, and between these two methods considered purely as methods of statistical estimation. In this connection, it is to be noted that if the frequency approach to probability as put forward by Venn, Mises, Craumer and others be accepted as most fundamental to start with the above results will be evident.

The aim of the present discussion is to investigate what basic properties of the entities, introduced by Dutta as most fundamental in his essentially statistical approach, leads to the exponential distribution and how. It is seen that it is not necessary that the exponential distribution should be introduced by advancing



the arguments, similar to the Bayes's rule. It is a simple and direct consequence of additivity (also known as, the extensive property)

Another object of this paper is to show clearly how the method of estimation, used by Dutta, is fitted in with the orthodox method of maximum likelihood of Fisher. In this connection the role of ergodic theory in these statistical developments has been pointed out clearly. The assertion of Jaynes (1957) that in essential statistical development the ergodic hypothesis is not at all necessary is not a fact. This point has just been mentioned by Dutta earlier (1965a). Here, this point has been dealt with in some details

At the end, the probability distribution of the parameters of distribution (which are related to the temperature and the chemical potential) and then the expressions for functions of the temperature and the chemical potential have been deduced. These are quite in agreement with those given by Landau and Lifschitz (1958)

#### FUNDAMENTAL ENTITIES

Dutta in his essentially statistical approach (1951, 1953, 1956 and 1959), started with two entities, denoted by  $M$  and  $E$  which were supposed to be two observable entities specifying the system, under consideration in a state. The system considered was taken to be open, i.e., to be able to exchange these entities freely with the environment (in the orthodox language of thermodynamics, in a heat and matter both). As the fluctuations were also supposed to be fundamental for the system in a state, so the instantaneous numerical measures of  $M$  and  $E$  are random variables. The probability distribution of these quantities were written from arguments, similar to those used in discussions of Bayes rule and normalisation. The parameters of the distribution were estimated by method similar to that of maximum likelihood. How the method, actually used by Dutta, fits in with the orthodox method of maximum likelihood of Fisher is investigated in the section 5.

Besides the randomness, the additivity of  $M$  and  $E$  was postulated as the basic property. By additivity, it is meant that the instantaneous value of any of the quantities  $M$  and  $E$ , of a system consisting of a number of mutually non-interacting (statistically independent) part-systems is equal to the algebraic sum of its instantaneous values of the part-systems. The discussion of additivity can be seen in some standard literature of classical thermodynamics (Epstein, 1948). In a recent new axiomatic development of thermodynamics (Giles, 1964) the significance of the concept of additivity has been fully emphasized. The additivity is really the basic property of thermodynamic variable in standard literatures of thermodynamics (e.g., see Epstein, 1948, Guggenheim, 1950). In a recent paper (Dutta, 1965a), it has been explicitly asserted that for determining the correct law of distribution of states, the measurable quantities should be fundamental,

i.e., satisfying the additivity law and the conservation law'. The work 'correct,' in this assertion signifies just sufficient for probabilistic consideration and also 'just meeting thermodynamic requirements'. In the next section, it will be shown that randomness and additivity are just sufficient for complete determination (i.e., specification and estimation) of the probability distribution of states of the system.

For thermodynamic requirements i.e., for constructing functions having fundamental properties similar those of entropy, temperature and the like, and equation of conservation of any one these entities should be written. This equation is written by equating the total (small) increment of any of these entities due to small changes in the system and/or environment to the (algebraic) sum of the small changes in the coordinates, explicitly used for the system and environment along with changes due to flow or caused by changes of uncontrollable or hidden variables associated with the system or the environment. In the statistical approach, proposed by Dutta it is seen that the same expression of entropy is obtained as the integral of Paffian equation for conservation of any one of these entities after identification of these equations for interpretation with usual equations for conservation in physics, viz. the first law of thermodynamics, the equation of continuity, etc., but, the integrating factors are different and correspond to different physical quantities, viz. temperature, chemical potential, etc., which are the intensive variables of thermodynamic.

In the statistical approach by Dutta, entities, which are random, additive and conserving, are called 'fundamental'. Instantaneous values of mass, energy, charge momentum, etc. of a microscopic physical system are examples of the fundamental quantities. In the terminology of Giles (1964), additive conserving quantities are 'components of contents'. In the axiomatic discussion of Giles, it is seen that any components of contents may be taken as the basis for introduction of entropy. In Jaynes' approach (1963), it is also noted that the probability discussion can be made with any measurable quantity, but, the use of energy (not temperature) is most convenient for the purpose of thermodynamics. Some explanations for the necessity of taking energy as the basis in the statistical formulation of thermodynamics, put forward by Jaynes, are from mechanical consideration. This explanation, based on mechanical consideration defeats the very objectives of the essential statistical approach to thermodynamics for deducing everything from statistical model by statistical reasoning only.

#### ADDITIVITY RANDOM VARIABLE AND EXPONENTIAL DISTRIBUTION

Let  $M$ ,  $E$  be numerical measures of two additive random entities of a system composed of two non-interacting (statistically independent) part systems, of which the corresponding quantities are  $M_1$ ,  $E_1$  and  $M_2$ ,  $E_2$  where

$$M = M_1 + M_2, \quad E = E_1 + E_2 \quad \dots \quad (3.01)$$

As all these quantities are random variables so a probability distributions are associated with them. From additivity of  $M$  and  $E$ , and from the multiplicativity of the probability, we have

$$P(M_1 + M_2, E_1 + E_2) = P(M_1, E_1) P(M_2, E_2) \quad \dots \quad (3.02)$$

or

$$\log P(M_1 + M_2, E_1 + E_2) = \log P(M_1, E_1) + \log P(M_2, E_2) \quad \dots \quad (3.03)$$

where

$$\sum_{M, E} P(M, E) = 1 \quad \dots \quad (3.04)$$

the summation being taken over all values of  $M$  and  $E$

$$\sum P(M, E) = 1 \quad \dots \quad (3.04)$$

the summation being taken over all values of  $M$  and  $E$

*Prop.* If  $g(x, y)$  be a continuous function of  $x$  and  $y$  satisfying the functional relations given by

$$g(x_1 + x_2, y_1 + y_2) = g(x_1, y_1) + g(x_2, y_2) \quad \dots \quad (3.05)$$

then,  $g(x, y)$  must be an exponential function.

*Proof.* Taking  $x_1 = 0, x_2 = 0, y_1 = 0, y_2 = 0$  we get

$$g(0, 0) = g(0, 0) + g(0, 0) \quad \dots \quad (3.06)$$

i.e.,

$$g(0, 0) = 0 \quad \dots \quad (3.07)$$

Obviously  $g(x, y) = 0$

is a trivial solution of (3.05)

Now, from the relation (3.05), it is easy to see that

$$g(na, 0) = ng(a, 0), \quad g(0, mb) = mg(0, b) \quad \dots \quad (3.08)$$

for any two numbers  $a$  and  $b$  and for any two positive integers  $n$  and  $m$ . Then, for integral  $n$  and  $m$ , we also have

$$\frac{1}{n} g(a, 0) = \frac{1}{n} g\left(n \cdot \frac{a}{n}, 0\right) = g\left(\frac{a}{n}, 0\right), \text{ and, } \frac{1}{m} g(0, b) = g\left(0, \frac{b}{m}\right) \dots \quad (3.9)$$

From these two relations, for integral  $p, q, p', q'$ , we have

$$g\left(\frac{p}{q} a, 0\right) = \frac{p}{q} g(a, 0), \quad g\left(0, \frac{p'}{q'} b\right) = \frac{p'}{q'} g(0, b) \quad \dots \quad (3.10)$$

Then, from continuity of  $g(x, y)$  we get

$$g(x'a, 0) = x'g(a, 0) \text{ and } g(0, y'b) = y'g(0, b) \quad \dots \quad (3.11)$$

for real  $x', y'$ . Thus, we can write

$$g(x, y) = g(x+0, 0+y) = g(x, 0) + g(0, y) = xg(1, 0) + yg(0, 1) \quad \dots \quad (3.12)$$

If  $x, y$  be negative, we have

$$0 = g(0, 0) = g(x+(-x), y+(-y)) = g(x, y) + g(-x, -y) \quad \dots \quad (3.13)$$

$$\text{or} \quad g(x, y) = -g(-x, -y) = -yg(1, 0) - xg(0, 1) \quad \dots \quad (3.14)$$

*Note.* In the above proof, it is to be noted that it is sufficient to take  $g(x, y)$  continuous with respect to  $x$  and  $y$  separately.

Now, as  $P(M, E)$  is a probability distribution, so,

$$P(M, E) = \frac{t^M z^E}{\sum t^M z^E} = \frac{f(t, z)}{f(t, z)} \quad (3.15)$$

where

$$f(t, z) = \sum_{n, E} t^M z^E \quad (3.16)$$

and in the summation  $\Sigma$ , the term is to be repeated if there be multiplicity of states specified by  $M$  and  $E$  (in the terminology of physics, degeneracy of states). It is to be noted in this connection that as  $P(M, E)$  is multiplicative, we should have

$$f(t, z) = f_1(t, z) \cdot f_2(t, z) \quad (3.17)$$

where  $f(t, z)$  is associated with the entire system and  $f_1(t, z)$  and  $f_2(t, z)$  are associated with part-systems. The validity of relations and its significance were considered in earlier papers (Dutta, 1953, 1956, 1965a),  $f(t, z)$  is the partition function.

The probability distribution given by (3.15), (3.16), and of course, originally written from different arguments was the starting point of the essential statistical approach of Dutta.

In the above deduction, same set of  $t$  and  $z$  has been taken for both the part-systems. This means that they have been taken from the same (statistical) population, and in the language of statistical mechanics after Gibbs, the systems are known to be in statistical (thermodynamic) equilibrium.

#### THE FORMULATION OF GIBBS AND EXPONENTIAL DISTRIBUTION

Starting from Liouville's theorem,

$$\frac{dP}{dt} = [P, H] \quad \dots \quad (4.01)$$

Gibbs (1900) argued that for statistical equilibrium,

$$\frac{dP}{dt} = 0, \quad \text{i.e.,} \quad [H, P] = 0 \quad \dots \quad (4.02)$$

For any constant  $C$  of motion of a dynamical system

$$[H, C] \quad \dots \quad (4.03)$$

and also, for any (differentiable) function  $F(c)$  of the constant  $C$  of motion

$$[H, F(c)] = 0 \quad \dots \quad (4.04)$$

Thus, from (4.02), it is sufficient to take that

$$P = f(C_1, C_2, \dots) \quad \dots \quad (4.05)$$

where  $C_1, C_2, \dots$  are constants of motion. Gibbs, for simplicity, assumed the index of probability as a linear functions of constants. As in thermodynamics, energy is the most important concept and no other quantity associated with any other constant of a motion is generally introduced so in the major part of the development of statistical mechanics due to Gibbs, the canonical distribution (which is nothing but a general exponential distribution) is given by

$$P = \frac{\psi - \epsilon}{\theta} \quad \dots \quad (4.05)$$

where  $\psi$  and  $\theta$  are parameters of distribution and  $\epsilon$  is the energy of the system is taken as the starting point of discussion. In this development, one can also find a bit more general distribution, named by him as 'grand canonical distribution' and given by

$$P = e^{(\psi - \epsilon + \sum \mu_l N_l)/\theta} \quad \dots \quad (4.07)$$

where  $\psi, \theta, \mu_l$ s are parameters of distribution,  $\epsilon$  is the energy and  $N$ 's are the number of  $l$ -th type of particles. This is also an exponential distribution and can be written by same simple transformation of variables in the form (3.15). Besides these canonical distributions, in the entire development of Gibbs, the only other distribution considered is the uniform surface distribution on an energy-surface. But this is considered after Gibbs as a truncated canonical distribution and named as a micro-canonical distribution. In Gibbs' development, all these distributions are introduced as soon as possible distributions to suitable for construction mathematical models for thermodynamic systems, but, a little scrutiny will show that the canonical (exponential) distributions are only fundamental distribution for this purpose. Thus, canonical distributions are necessary and sufficient. Sufficiency was stressed by Gibbs himself. Necessity of the distribution is implied by additivity of energy and other significant constant of motion when required in particular cases.

#### METHOD USED BY DUTTA AND THE ORTHODOX METHOD OF MAXIMUM LIKELIHOOD OF FISHER

Thermodynamic and similar other microscopic measurements are generally taken for a time  $T$ , sufficiently large, compared to the least time  $\tau$  required by a

[sense or a machine to get any impression (as for example, the time for eye is 1/10th. of a second). Thus the actually measured values are really over time intervals.

Let  $n_i$  be the frequency of realisation of a set of values of  $M$  and  $E$  in  $N = T/\tau$  intervals. If  $M_0, E_0$  be the observed values (i.e. the average values), thus,

$$M_0 = \frac{1}{N} \sum n_i M_i \quad \dots \quad (5.01)$$

$$E_0 = \frac{1}{N} \sum n_i E_i \quad \dots \quad (5.02)$$

In the essentially statistical approach proposed by Dutta, the expression.

$$P(M_0, E_0, t, z) = \frac{t^{M_0 z E_0}}{f(t, z)} = \left[ \Pi_l \left\{ \frac{t^{M_{lz} E_l}}{f(t, z)} \right\}^{n_l} \right]^{1/N} \quad \dots \quad (5.03)$$

has been maximised, where as in the orthodox method of Fisher, the likelihood functions,

$$L = \Pi_l \left\{ \frac{t^{M_{lz} E_l}}{f(t, z)} \right\} = P^N$$

is maximised. As  $N$  the sample size, remain constant in the variations considered and, evidently  $P = L^{1/N}$  and  $L$  attains maximum simultaneously, so the equations for determining are same.

In the statistical approach of Dutta, it is seen that these observed values are also the mean values of these two fundamental entities, calculated from distribution, and for other entities, mean values calculated from the distributions, have been taken to be equal to the observed values. In other statistical approaches, also, mean values calculated from the distributions are postulated to be equal to those observed values. Now, the postulate, by which mean values are equated to observed values (time-averages), is an ergodic hypothesis. Only, the form of this hypothesis may change when the mechanical model is replaced by a statistical model. Beside this hypothesis, as in usual statistical mechanics here also, we have to introduce another hypothesis for equating the short time-average (actually observed) values to the above long time averages. (Dutta, 1966). Thus, Jaynes impression that in these statistical approaches the discussions of ergodicity can be avoided appear not to be justified.

#### DISTRIBUTION OF $t, z$ AND FLUCTUATIONS OF TEMPERATURE ETC.

For the fixed observed values of  $M$  and  $E$ , the law of distribution for  $t, z$ , can be taken as usual as

$$p(t, z; M_0, E_0) = \frac{t^{M_0 z E_0}}{f(t, z)} = g(t, z; M_0, E_0) = e^{G(t, z)} \quad \dots \quad (6.01)$$

Now by Taylor's expansion of  $G(t, z)$  about  $(t_0, z_0)$  the set of values of  $t$  and  $z$  estimated from likelihood equations we get

$$G(t, z) = G(t_0, z_0) + \frac{1}{2} \left\{ (t-t_0)^2 \left( -\frac{\partial^2 G}{\partial t^2} \right)_0 - 2(t-t_0)(z-z_0) \left( \frac{\partial^2 G}{\partial t \partial z} \right)_0 + (z-z_0)^2 \left( \frac{\partial^2 G}{\partial z^2} \right)_0 \right\} \\ + \{\text{terms containing higher powers of } (t-t_0) \text{ and } (z-z_0)\} \quad \dots \quad (6.02)$$

$$p(t, z | M_0, E_0) = \frac{C \cdot t_0^{\overline{M_0 z_0 E_0}}}{f(t_0, z_0)} \exp \left[ -\frac{1}{2} \{ (t-t_0) \left( -\frac{\partial^2 \log g}{\partial t^2} \right)_0 + \dots \} \right] \quad \dots \quad (6.03)$$

$C$  being the factor to be determined by normalisation ... (6.03)

Now from well-known results of statistics, fluctuations are given by

$$\text{Exp} \{ (t-t_0)^2 \} = \text{var}(t) = \frac{1}{\left( -\frac{\partial^2 \log g}{\partial t^2} \right)_0} \Delta \quad \dots \quad (6.04)$$

$$\text{Exp} \{ (z-z_0)^2 \} = \text{Var}(z) = \frac{1}{\left( -\frac{\partial^2 \log g}{\partial z^2} \right)_0} \Delta \quad \dots \quad (6.05)$$

$$\text{Exp} \{ (t-t_0)(z-z_0) \} = \text{cov}(t, z) = \left( -\frac{\partial^2 \log g_0}{\partial t \partial z} \right)_0 \left\{ \left( -\frac{\partial^2 \log}{\partial t^2} \right)_0 \left( -\frac{\partial^2 \log}{\partial z^2} \right)_0 \right\} \Delta$$

where

$$\Delta = 1 - \left\{ \left( -\frac{\partial^2 \log g}{\partial t \partial z} \right)_0 \right\}^2 / \left\{ \left( -\frac{\partial^2 \log g}{\partial t^2} \right)_0 \left( -\frac{\partial^2 \log g}{\partial z^2} \right)_0 \right\} \quad \dots \quad (6.07)$$

Now, the expressions for the partial derivatives of  $\log g$  can be calculated as in an earlier paper (Dutta, 1965b). They are the following

$$\left( -\frac{\partial^2 \log g}{\partial t^2} \right)_0 = \frac{(M - \overline{M_0})^2}{t_0^2} \quad \dots \quad (6.08)$$

$$\left( -\frac{\partial^2 \log g}{\partial Z_0^2} \right)_0 = \frac{(E - \overline{E_0})^2}{z_0} \quad \dots \quad (6.09)$$

$$\left( -\frac{\partial^2 \log g}{\partial t \partial z} \right)_0 = \frac{(\overline{M - M_0})(\overline{E - E_0})}{t_0 z_0} \quad \dots \quad (6.10)$$

It can be easily seen (Dutta, 1953) that  $\overline{M_0}$ ,  $\overline{E_0}$  are the average values of  $M$  and  $E$ .

Utilising the above results, we get

$$\text{Var}(t) = \frac{t}{(M - M_0)^2} \Delta \quad \dots \quad (6.11)$$

$$\text{Var}(z) = \frac{z_0^2}{(E - E_0)^2} \Delta \quad \dots \quad (6.12)$$

$$\text{Cov}(t, z) = \frac{t_0 z_0}{(E - E_0)(M - M_0)} \Delta \quad \dots \quad (6.13)$$

and

$$\Delta = 1 - \frac{\{(M - M_0)(E - E_0)\}^2}{(M - M_0)^2 \cdot (E - E_0)^2} = 1 - r_{M,E}^2 \quad \dots \quad (6.14)$$

$r_{M,E}$  denoting the correlation between  $M$  and  $E$ .

Now the correlation between  $t$  and  $z$  is given by

$$r_{t,z} = \frac{\text{Cov}(t, z)}{\{\text{Var}(t) \text{Var}(z)\}^{1/2}} = \frac{\left( -\frac{\partial^2 \log g}{\partial t \partial z} \right)_0}{\left\{ \left( -\frac{\partial^2 \log g}{\partial t^2} \right)_0 \left( -\frac{\partial^2 \log g}{\partial z^2} \right)_0 \right\}^{1/2}} \quad \dots \quad (6.15)$$

$$= \frac{(M - M_0)(E - E_0)}{(M - M_0)^2 (E - E_0)^2} = r_{M,E}$$

$$z_0 = e^{1/kT} \quad \dots \quad (6.16)$$

and

$$t_0 = e^{\mu/RT} \quad \dots \quad (6.17)$$

Then,

$$\frac{dT}{dz_0} = \frac{1}{k(\log z_0)^2} \cdot z_0 = \frac{kT^2}{z_0} \quad \dots \quad (6.18)$$

and similarly,

$$\left( \frac{\partial \mu}{\partial t_0} \right)_{z_0} = \frac{kT}{t_0} \quad \dots \quad (6.19)$$

Then,

$$\text{Var } T = \left( \frac{dT}{dz_0} \right)^2 \text{Var}(z)$$



$$\frac{k^2 T^4}{z_0^2} \cdot \frac{z_0^2}{(E - E_0)^2 \cdot (1 - r_{E,M}^2)} \\ - \frac{k^2 T^4}{k^2 T^2 C_v} \cdot \frac{1}{(1 - r_{E,M}^2)} - \frac{k T^2}{C_v} \cdot (1 - r_{E,M}^2)^{-1} \quad (6.20)$$

after substituting the value of  $(E - E_0)^2$  from previous calculations (Dutta, 1953, 1959, 1965a). This is the expression given by Landau and Lifschitz (1958) for the temperature fluctuations multiplied by the factor  $(1 - r_{E,M}^2)^{-1}$ . Similarly expression for fluctuation of  $\mu$  can be obtained.

The expression for fluctuation for  $T$  reduces to the value given by Landau and Lifschitz (1958) when

$$r_{M,E} = 0 \quad \dots (6.21)$$

i.e., random variables  $M$  and  $E$  are uncorrelated. Actually the value,  $\frac{kT^4}{C_v}$ , has been obtained when  $T$  and  $V$  are taken as independent variable so that  $r_{T,V} = 0$ . Thus the expression (6.20) yield a general form

The law of probability distribution of and so of temperature and chemical potential are given by (6.03) when the values of the coefficients of exponential quadratic form is given by (6.08), (6.09) and (6.10). The distribution is approximately Gaussian. Landau and Lifschitz (1958) have also used the Gaussian distribution for finding out expressions for fluctuations of thermodynamic quantities. Here, the distribution is obtained from the fact that and have been estimated from the principle of maximum likelihood.

#### CONCLUDING REMARKS

Now, in quantum mechanical formulation particularly in axiomatic representation states of a system are represented by vectors in Hilbert space and physically observable quantities correspond to Hermitian linear (additive homogeneous) operators in this space (Dirac, 1947, Ludwig 1954). So the probability distributions, associated with these physically observable quantities appears to be deducible as exponential distribution of this linear operators by extension of above arguments. This deduction appears to be interesting and will be investigated fully in future.

The probability distribution of parameters estimated by methods similar to that of maximum likelihood as seen in the above discussion is Gaussian approximately. It is in conformity with Fisher's idea. He always took the Gaussian distribution for parameters estimated by the principle of maximum likelihood (1925).

From this paper and earlier papers it appears that the statistical mechanics can be studied as a pure problem of statistics. This study appears to be interesting and instructive.

#### ACKNOWLEDGMENTS

The author expresses his deep gratitude to National Professor S. N. Bose for his keen interest and constant encouragement in this work, and also for the support rendered by him including the work as a part of his research scheme.

#### REFERENCES

- Dirac, O. A. M., 1947, *The principal of Quantum Mechanics* 3rd. Edn., Oxford Univ. Press.
- Dutta, M., 1951, *Proc. Inst. Stat. Cont.* (vide. Bulletin of International Statistical Institute, **32** p. 286).
- 1953, *Proc. Nat. Inst. Sc. (India)*, **19**, 109.
- 1955, *Proc. Nat. Inst. Sc. (India)*, **21**, 373.
- 1959, *Proc. Sum. Inst. of Theor. Phys. at Munsonic (India)*, 291.
- 1960, *Gnan O Vignan*, **13**, 737.
- 1965a, *Zt. f. Phys. Chem.*, **228**, 380.
- 1965b, Communicated.
- 1966, *Statistical Physics* (Foundation), World Press, (in press).
- Epstein, P. S., 1947, *Textbook of Thermodynamics*, J. Wiley & Sons, N.Y.
- Fisher, R. A., 1922, *Phil. Trans. Roy. Soc. London*, **A222**, 30.
- 1925, *Proc. Camb. Phil. Soc.*, **22**, 700.
- Fowler, R. A. 1936, *Statistical Mechanics* (2nd Edn.) Camb. Univ. Press.
- Gibbs, W., 1902, *Elementary Principle in Statistical Mechanics*, Yale Univ. Press, p. 109.
- Giles, R., 1964, *Mathematical Foundation of Thermodynamics*, Pergamon Press, Oxford.
- Goldmann, S., 1953, *Information Theory*, Prentice Hall Inc., N.Y.
- Guggenheim, E. A., 1950, *Thermodynamics*, North Holland Pub., Amsterdam.
- Jaynes, E. T., 1957a, *Phys. Rev.*, **106**, 620; (b), *Phys. Rev.*, **107**, 171.
- Knuth, A. T., 1957, *Mathematical Theory of Information*, Dover Publication, New York.
- Kullback, S., 1959, *Information Theory and Statistics*, John Wiley & Sons, New York.
- Landau, L. D. and Lifschitz, E. M., 1958, *Statistical Physics*, Pergamon Press, Oxford.
- Ludwig, G., 1954, *Die Grundlagen der Quantum Mechanik*, Springer Verlag, Berlin.
- Mandelbrot, Benoit, 1963, *Ann. Math. Stat.*, **33**, 1021.
- Mukherjee, T. K., 1965, *Science and Culture*, **31**, 528.
- Schrodinger, E., 1948, *Statistical Thermodynamics*, Camb. Univ. Press, Cambridge. (1945).
- Shannon, C. and Weaver, Warren, 1949, *The Mathematical Theory of Communication* The University of Illinois Press, Urbana U.S.A.

# Letters to the Editor

*The Board of Editors does not hold itself responsible for opinions expressed in the letters published in this section. The notes containing short reports of original investigations communicated to this section should not contain many figures and should not exceed 500 words in length. The contributions reaching the Secretary by the 15th of any month may be expected to appear in the issue for the next month. No proof will be sent to the author.*

## 3

### X-RAY MEASUREMENTS OF STACKING FAULTS IN $\alpha$ -AgMn ALLOYS

S. P. SEN GUPTA AND K. N. GOSWAMI

INDIAN ASSOCIATION FOR THE CULTIVATION OF SCIENCE, CALCUTTA-32

(Received November 26, 1965)

Since stacking faults exert an important influence on the structural and mechanical properties of face-centred cubic metals and alloys considerable attention has recently been paid to the formation of stacking faults by deformation of certain noble and transition metals, and particularly of binary alloys based on the solvent metals silver and copper. The present note concerns with the determination of the stacking fault probability  $\alpha$  of a series of Ag-Mn alloys in the primary solid solution range at room temperature.

The alloys were prepared from spectrographically standardized silver and manganese supplied by Messrs. Johnson, Matthey and Co. Ltd. London. Accurately weighed quantities of the component metals were melted together in evacuated and sealed quartz capsules; after melting, the alloys were homogenized for a week at 800°C. Weight changes during preparation were negligible.

Cold-working was achieved by hand filing at room temperature ( $28 \pm 1^\circ\text{C}$ ) and out of the filings in each case, one sample was retained in the 'asfiled' condition while the other was annealed at 600°C for 4 hours in pyrex glass capsule sealed under vacuum. The line profiles of the sieved films were recorded using the standard Philips Geiger Counter X-ray diffractometer (PW 1050, 1051) with Ni filtered  $\text{CuK}_\alpha$  radiation from a highly stabilized X-ray Generator (PW 1010). Accurate line profiles of the reflections were obtained by point counting at intervals of  $0.1^\circ$  in  $2\theta$  for the general background, decreasing to  $0.01^\circ$  in  $2\theta$  near the maxima of the peaks, where  $\theta$  is the Bragg angle.

The stacking fault probability  $\alpha$  was obtained from the change in the  $2\theta$  separation of the (111) and (200) peaks due to cold work using the relation (Wagner, 1957) :

$$(2\theta_{hkl}^0 - 2\theta_{h'k'l'}^0)_{CW} - (2\theta_{hkl}^0 - 2\theta_{h'k'l'}^0)_{ANN} = H \cdot \alpha$$

$$\text{and} \quad H = (\langle U \rangle \cdot j \cdot \tan \theta)_{hkl} - (\langle U \rangle \cdot j \cdot \tan \theta)_{h'k'l'}$$

where,  $j$  is the fraction of  $(hkl)$  planes affected by deformation faults,  $U = (\perp) 90\sqrt{3} \cdot h_0/\pi^2 l_0^2$  and  $\langle U \rangle$  is the averaged value for the  $(hkl)$  reflections affected by deformation faults.

The peak positions were obtained by the method of mid-point extrapolation of chords parallel to background level to peak maximum. Elimination of  $\alpha_2$  component in case of cold-worked peaks was not possible since the graphical methods of Rachinger (1948) and of Papoulis (1955) could not be applied for broad, overlapping and asymmetric line profiles. Values of the stacking fault parameter  $\alpha$  for the silver-manganese alloys investigated are given in Table I.

TABLE I  
Stacking fault parameter  $\alpha$  for filings of Silver-manganese  
primary solid solutions

Composition (atomic percent)	$\Delta(2\theta_{200} - 2\theta_{111})$ degrees	$\alpha \times 10^3$
Ag - 5.54 Mn.	-0.015	3.27
Ag-11.03 Mn	-0.017	3.71
Ag-16.20 Mn.	-0.018	3.93
Ag-20.92 Mn	-0.015	3.27

It is apparent from the Table I that concentration of stacking faults in this system is negligibly small compared with that of other elements alloyed with Ag (Davies and Calm, 1962, Adler and Wagner, 1962; Sen Gupta and Quader, 1966) and the values are also less than those obtained for Cu-Mn alloys (Nakajima and Numakura, 1965, Goswami *et al.*, 1966). In Cu-Mn alloys values of  $\alpha$  have been found to increase slowly from  $3.77 \times 10^{-3}$  (for pure Cu) to  $8.72 \times 10^{-3}$  (for Cu-22.34 Mn) reaching a saturation at about 14 at %manganese solute. Thus, it may be inferred that contribution of transition element Mn in silver and copper alloys to stacking fault parameter is very small and is probably due to the interactions between the incomplete 3d shells of the introduced solute atoms which provide an additional contribution to the stacking fault energy of the alloy (Seeger, 1955, 57).

A detailed study on this system will be published elsewhere.

The authors are grateful to Prof. B. N. Srivastava, D.Sc., F.N.I., for his continued interest in the work and to Dr. M. A. Quader for valuable discussions. One of the authors (S. P. S.G.) is thankful to C.S.I.R. (New Delhi) for financial assistance.

# REFERENCES

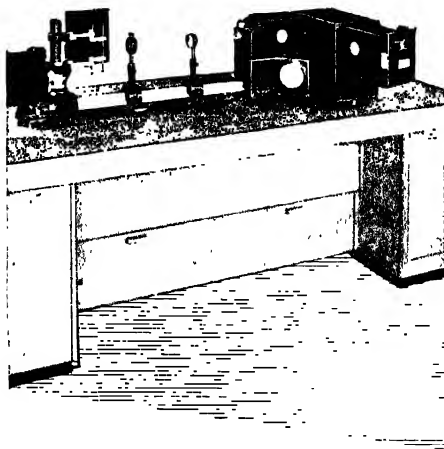
- Adler, R. P. I. and Wagner, C. N. J., 1962, *J. Appl. Phys.*, **33**, 3451
- Davies, R. G. and Cahn, R. W., 1962, *Acta Met.*, **10**, 621.
- Goswami, K. N., Sen Gupta, S. P. and Quader, M. A., 1966 *Acta Met.* (in press)
- Nakajima, K. and Numakura, K., 1965, *Phil. Mag.*, **12**, 361
- Papoulis, A., 1955, *Rev. Sci. Instrum.*, **26**, 423
- Rachinger, W. A., 1948, *J. Sci. Instrum.*, **25**, 251
- Seeger, A., 1955, *Defects in Crystalline Solids* (Report of Bristol Conference 1954) Physical Society (London), p. 328
- — — 1957, *Dislocations and Mechanical Properties of Crystals* (John Wiley, N.Y.) p. 243
- Sen Gupta, S. P. and Quader, M. A., 1966, *Acta Cryst.* (In Press)
- Wagner, C. N. J., 1957, *Acta Met.*, **5**, 427

## BOOK REVIEW

PRINCIPLES OF PHYSICS . by F. Bueche, 1965, Pp 660 Price \$ 9.75  
McGraw Hill Book Company, New York

This a precalculus stage text book on physics which may be very useful to advanced High School, Pre-University of Engineering students. On a superficial glance the book may appear to be just a compendium of the laws, principles, theories of physics, in view of the fact that beginning with elementary mathematical theorems (just trigonometry and vector algebra) practically all the fundamental information on statics, dynamics, general physics, heat, light, electricity, magnetism, acoustics, atomic and nuclear physics have been packed in the compass of about six and half hundred pages. Thus one might causally think that it would be an admirable guide book for a teacher, we has to cover the ever increasing volume of information on physics in a class extending over just one academic year, or again an equally admirable help book for a student who wants to tide over the preuniversity examinations. The author has however repeatedly warned both the teacher and the students that these are certainly not his chief aim and on going more carefully through the book we are of the opinion that the claim of the author that this book may very well serve as lying the fundamental basis of the knowledge of physics for students, is fully justified. The simplicity clarity and conciseness of language with a direct appeal to the mind of the students, while precise statements and explanations of fundamental principles, some of much subsidiary matter will be a great help in developing the independent thinking process and scientific style of expression of the students. The most valuable thing about the book is that each principle of physics is clearly explained and amply exemplified in the form of large number of worked-out exercises and followed up by graduated unsolved problems to test the grasp of the student of the basic principles. This feature of the book immediately raises it from the level of just a help book to a real guide-book or a text book in the modern sense. In such a book as this sacrifice of too many details is obvious and author has been eminently successful in choosing the topics to be retained, including matters from modern physics. The approach is quite unconventional and it is regretted that such a method of teaching basis physics is still lacking in many countries including ours.

A. L



## ZEISS THREE-PRISM SPECTROGRAPH

A glass-type spectrograph with Foresterling set of prisms of high-power and resolving capacity, large dispersion and excellent definition of lines, self-contained construction. Equipment with 3 cameras : Camera  $f = 12$  cm.  $F/2.4$  and camera  $f = 27$  cm.  $F/5.4$  for feeble-light phenomena (Raman effect, fluorescence of flame-spectra, etc.)

Autocollimation camera  $f = 130$  cm.  $F/26$  for taking complex emission spectra in the visible region (special type steel, rare earth etc).

Solves all spectra-chemical problems of organic and inorganic nature.

**VEB Carl Zeiss JENA**

**GERMAN DEMOCRATIC REPUBLIC**

**Birthplace & Centre of Modern Optics.**

*Sole Agents in India :*



**GORDHANDAS DESAI PVT. LTD.**

***Equipment and instruments for all branches of science, technology and industry***

**KERMANI BUILDING • SIR P. M. ROAD • BOMBAY-1 BR**

**NO 22, LINGI CHETTY STREET, • P-7 MISSION ROW EXTENTION, MADRAS-1**

**CALCUTTA**

**4/2 B, JWALA MANSION, ASAF ALI ROAD, NEW DELHI**

# INDIAN JOURNAL OF PHYSICS. VOL. 39, 1965

## Statement about ownership and other particulars about Indian Journal of Physics Vol. 39, 1965,<sup>a</sup>

### FORM IV

1. Place of Publication ... 2 and 3, Raja Subodh Mullick Road, Calcutta -32.
2. Periodicity of its publication Monthly
3. Printer's Name ... Kalipada Mukherjee  
Nationality Indian  
Address ... Eka Press, 204/1, B. T. Road, Calcutta-35.
4. Publisher's Name Samarendra Nath Sen  
Nationality Indian.  
Address Registrar, I.A.C.S., Cal.-32.
5. Editors' Name Prof. K. Banerjee, Prof. S. R. Khastgir,  
Nationality D.Sc., F.N.I. D.Sc., F.N.I.  
Address Indian, Director, (upto 30.9.65) Indian, Head of the  
I. A. C. S., Jadavpur, Cal-32 Dept. of Physics  
Bose Institute  
Dr. G. N. Bhattacharya, 93/1 Acharya Prafulla  
D Sc., F Inst P., M A E I.E.E Ch. Road, Calcutta-9.  
Indian, Department of Prof. D S Kothari,  
Applied Physics, University Ph.D., F.N.I.  
College of Science, 92, Acharya Prafulla Ch Road, Indian, Professor of  
Calcutta-9. Physics, Delhi Univer-  
Prof. D. M Bose, sity, Delhi.  
Ph D., F.N.I. Prof. B. D. Nag Chau-  
Indian, Director, Bose Insti- dhuri, Ph.D.  
tute, 93/1 Acharya Prafulla Indian, Director, Saha  
Ch. Rd., Calcutta-9. Institute of Nuclear  
Physics, 92, Acharya  
Prafulla Ch. Road,  
Calcutta- 9.  
Prof. S. N. Bose, F.R.S. Prof. K. R. Rao,  
Indian, National Professor, D.Sc., F.N.I.  
22, Iswar Mill Lane, Indian, Dept. of Physics,  
Calcutta-6. Andhra University,  
Waltair.  
Prof. S. D Chatterjee, Dr. D. B Sinha, Ph D.  
D.Sc., F.N.I. Indian, Reader Dept. of  
Indian, Head of the Dept. Applied Physics, Univer-  
of Physics, Jadavpur Uni- sity College of Techno-  
versity, Jadavpur, Cal. 32 logic, 92, Acharya Prafulla  
Ch. Road Calcutta-9.  
Prof. P. S. Gill, Prof. S. C. Sukar,  
Ph D., F N I. D Sc., F.N.I.  
Indian, Director, C.S.I O. Indian, Emeritus Profes-  
Chandigarh. Punjab. sor, I.A.C.S., Cal.-32.  
Prof. B. N. Srivastava, Prof. A. Bose,  
D. Sc. F N.I. D.Sc, F.N.I. (Secretary)  
Indian, Director, (From Octo- Indian. Dept. of Magne-  
ber 1, 1965) I. A C.S., Cal. 32 tism, I A.C.S., Cal. 32

6. Names and address of individuals who own the newspaper and partners or shareholders holding more than one per cent of the total capital.

I, Samarendra Nath Sen, hereby declare that the particulars given above are true to the best of my knowledge and belief.

Date, 27-2-65

(Sd) Samarendra Nath Sen,



# STUDIES ON THE DIELECTRIC LOSS AT 7.7 MM. MICROWAVES OF SOME SUBSTITUTED BENZENE AND NAPHTHALENE COMPOUNDS

(Miss) B. SINHA, S. B. ROY AND G. S. KASTHA

OPTICS DEPARTMENT,  
INDIAN ASSOCIATION FOR THE CULTIVATION OF SCIENCE,  
CALCUTTA-32.

(Received January 10, 1966)

**ABSTRACT.** The times of relaxation ( $\tau$ ) of a number of halo-substituted benzene and naphthalene compounds, in solutions in different non-polar solvents at different temperatures have been determined. The results have been compared with the various expressions for the time of relaxation proposed by Hill and Chau *et al* and it has been pointed out that neither of these expressions for  $\tau$  is in agreement with the experimental results. Further, the value of internal viscosity ( $\eta_{int}$ ) obtained from the equation for  $\tau$  derived by Perrin in case of ellipsoidal molecules, has been found to be related with the macroscopic viscosities ( $\eta$ ) of the solutions by the relation  $\eta_{int} = \text{const. } \eta^\gamma$ , where  $\gamma$  is the ratio of molar heats of activation of dielectric relaxation and viscous flow.

## INTRODUCTION

It is well known that the macroscopic viscosity of a medium does not adequately describe the internal friction, opposing the orientation of a polar molecule in that medium under the action of an externally applied R.F. field. Several expressions have since been developed relating the internal friction ( $\eta_{int}$ ) with macroscopic viscosity ( $\eta$ ) (Fischer, 1949, Wirtz, 1954, Hill 1954; Hase, 1953, Chau *et al*, 1957). Fischer (1949) suggested that internal friction  $\eta_{int} = C\eta$  where  $C$  is an adjustable fraction. Hill (1954), from a consideration of the transference of linear and angular momenta at the time of collisions between the solute and the solvent molecules in dilute solutions, concluded that the mutual viscosity between the solvent and the solute molecules should be a better representation of internal friction. Chau *et al* (1957), on the other hand developed an empirical expression for the time of relaxation in terms of the molecular parameters of the solute and physical properties of the solvent. Though all these expressions were found to be of limited applicability either in a particular solvent or at a particular temperature, these were not tested at different temperature regions (where  $\tau$ ,  $\eta_{int}$  and  $\eta$  are expected to vary simultaneously) for want of sufficient data. Recently, Sinha *et al* (1965) have suggested that in the case of dilute solutions of polar molecules in non-polar solvents of viscosity  $\eta$ ,  $\eta^\gamma$  may represent fairly the internal viscosity of the medium. The value of  $\gamma$  is given by the ratio of the molar heats

of activation for dielectric relaxation and viscous flow. The object of the present investigation is to find out how far the values of  $\tau$  obtained experimentally in the case of solutions of some polar compounds having molecules with rigid dipoles in various non-polar solvents at different temperatures are in agreement with various expressions of  $\tau$  and  $\eta_{\text{in}}$  as stated above. The results have been discussed in the following paragraphs.

#### EXPERIMENTAL

The liquids fluoro-, chloro-, bromo- orthodichloro-, metadichlorobenzene and  $\alpha$ -chloronaphthalene studied in the present investigation were of chemically pure quality. These were first fractionated and the proper fractions were repeatedly distilled under reduced pressure and dried before being used in the investigation. The solvents carbon tetrachloride, benzene *n*-hexane and medicinal paraffin were carefully dried by usual methods. The dried solvents showed slight losses in the frequency region of 7.7 mm. which were properly taken into account in determining the overall losses due to various solutions. The experimental arrangements and the method of calculation of loss tangent ( $\tan \delta$ ) were the same as described earlier (Bhattacharyya *et al.*, 1964). The viscosities of paraffin and some of the solutions in carbon tetrachloride and benzene at different temperatures were determined experimentally. The viscosities of the other mixtures and the solvents were taken from the standard literatures.

#### RESULTS AND DISCUSSION

The values of time of relaxation ( $\tau$ ) for the various molecules in solution in non-polar solvents at different temperatures ( $T$ ) were calculated from the experimental  $\tan \delta$  values with the help of the following equation

$$\tan \delta = \frac{(\epsilon' + 2)^2}{\epsilon'} \cdot \frac{4\pi N c \mu^2}{27kT} \cdot \frac{\omega\tau}{1 + \omega^2\tau^2} \quad \dots (1)$$

where the various symbols have their usual significance. The values of dipole moments ( $\mu$ ) of various compounds excepting in a few cases were taken from the standard literatures. The  $\mu$ -values in the case of *m*-dichlorobenzene in benzene and in *n*-hexane and of bromobenzene in *n*-hexane were calculated from the experimental results. The values of  $\epsilon'$  were taken to be equal to the static dielectric constants of the pure solvents taken from the published literature values. The values of  $\tan \delta$ ,  $\tau$  and  $\tau \cdot T / \eta^\gamma$  at different temperatures for different solutions for the various compounds are given in Tables I—VI.

The values of molar heats of activation  $\Delta H\tau$  for dielectric relaxation and  $\Delta H\eta$  for viscous flow have been determined respectively from the plots of  $\log (T \cdot \tau)$  and  $\log \eta$  against  $1/T$ . Some of the plots are shown in Figures 1a, 1b and

1c. The values of  $\Delta H\tau$ ,  $\Delta H\eta$  and their ratio ( $\gamma$ ) for different compounds are given at the foot of respective Tables.

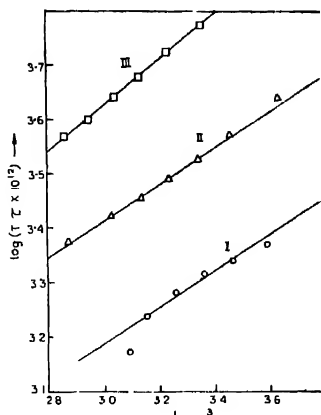


Fig. 1a. Plots of  $\log(\tau T)$  vs  $1/T$  Curve I Solution of bromobenzene in hexane Curve II Solution of bromobenzene in benzene Curve III Solution of bromobenzene in paraffin

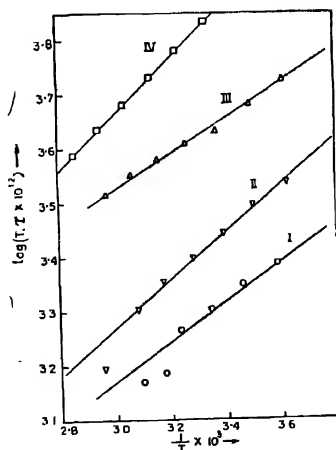


Fig. 1b. Plots of  $\log(\tau T)$  vs  $1/T$  Curve I Solution of metadichlorobenzene in hexane Curve II Solution of metadichlorobenzene in benzene Curve III Solution of metadichlorobenzene in carbon tetrachloride Curve IV Solution of metadichlorobenzene in paraffin

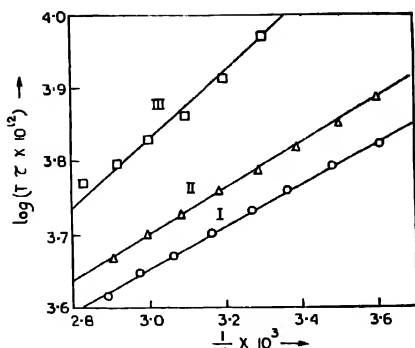


Fig. 1c Plots of  $\log(\tau T)$  vs  $1/T$ . Curve I Solution of  $\alpha$ -chloronaphthalene in benzene  
 Curve II Solution of  $\alpha$ -chloronaphthalene in carbon tetrachloride  
 Curve III Solution of  $\alpha$ -chloronaphthalene in paraffin

a) Comparison of Hill's equation for  $\tau$  with the experimental values

For very dilute solutions of polar molecules in non-polar solvents Hill (1954) deduced the relations,

$$2\tau kT = \zeta = 6g^2\eta_{AB}\sigma_{AB} \text{ with } g^2 = \frac{I_{AB} \cdot I_B}{I_{AB} + I_B} \cdot \frac{m_A + m_B}{m_A m_B} \quad (2)$$

and

$$\eta_m = f_A^2 \eta_A \frac{\sigma_A}{\sigma_m} + f_B^2 \eta_B \frac{\sigma_B}{\sigma_m} + 2f_A f_B \eta_{AB} \frac{\sigma_{AB}}{\sigma_m} \quad \dots \quad (3)$$

$\eta_{AB}$  is the mutual viscosity between the molecules of the solvent (A) and the solute (B) and the other symbols have the meanings given in Hill's paper. The value of viscosity of the mixtures ( $\eta_m$ ) at different concentrations and temperatures were obtained in the case of chlorobenzene + benzene and bromobenzene + benzene systems from International Critical Tables and in other cases they were determined experimentally. The values of  $\sigma_A = \left(\frac{M_A}{Nd_A}\right)^{1/3}$ ,  $\sigma_B = \left(\frac{M_B}{Nd_B}\right)^{1/3}$

and  $\sigma_m = \left[\frac{f_A M_A + f_B M_B}{Nd_m}\right]^{1/3}$  at different temperatures were calculated from

the molecular weights  $M_A$ ,  $M_B$  of the solvent and the solute respectively and the density  $d_A$  of the solvent, the density  $d_B$  of the solute and the density  $d_m$  of the solution. The values of  $\eta_{AB}$  were obtained for two different concentrations and the mean value was used.

TABLE Ia

 $f = 38.8 \text{ K Mc/s}$ 

Chlorobenzene

 $f = 38.8 \text{ K.MC/s}$  $2.93 \times 10^{-4} \text{ mole/cc in Hexane}$  $2.93 \times 10^{-4} \text{ mole/cc in benzene}$ 

T°K	$\tan \delta \times 10^3$	$\tau \times 10^{12} \text{ sec}$	$\frac{\tau T}{\eta \gamma} \times 10^7$	T°K	$\tan \delta \times 10^3$	$\tau \times 10^{12} \text{ sec}$	$\frac{\tau T}{\eta \gamma} \times 10^7$
273	1.71	8.53	14.82	277	12.0	14.13	10.90
287	1.73	7.81	14.66	289	12.8	12.35	16.75
298	1.75	7.10	14.43	299	13.5	11.10	16.54
308	1.78	6.42	13.95	311	14.0	10.10	16.64
321	1.73	6.19	14.63	325	14.3	9.06	16.69
329	1.71	6.01	14.89	336	14.5	8.41	16.76
				348	14.7	7.73	16.93
$\Delta H\tau = 0.63 \text{ K.Cal/Mole}$				$\Delta H\tau = 0.99 \text{ K.Cal/Mole}$			
$\Delta H\eta = 1.84 \text{ K.Cal/Mole}$				$\Delta H\eta = 2.53 \text{ K.Cal/Mole}$			
$\gamma = 0.34$				$\gamma = 0.39$			

TABLE Ib

 $f = 37.9 \text{ K.Mc/s}$  $f = 38.8 \text{ K.Mc/s}$  $2.92 \times 10^{-4} \text{ mole/cc in CCl}_4$  $2.95 \times 10^{-4} \text{ mole/cc in Paraffin}$ 

T°K	$\tan \delta \times 10^3$	$\tau \times 10^{12} \text{ sec}$	$\frac{\tau T}{\eta \gamma} \times 10^7$	T°K	$\tan \delta \times 10^3$	$\tau \times 10^{12} \text{ sec}$	$\frac{\tau T}{\eta \gamma} \times 10^7$
278	11.9	14.27	15.68	297	9.8	16.59	-
290	12.3	13.02	16.14	309	10.0	14.73	11.39
298	12.7	12.07	16.03	319	11.0	13.20	11.72
305	12.9	11.18	16.16	329	11.7	11.83	11.93
315	13.3	10.51	16.03	339	12.3	10.51	11.92
325	13.7	9.06	15.81	339	13.0	9.46	11.41
335	14.1	8.82	15.52				
345	14.3	8.21	15.55				
$\Delta H\tau = 0.90 \text{ K.Cal/Mole}$				$\Delta H\tau = 1.84 \text{ K.Cal/Mole}$			
$\Delta H\eta = 2.11 \text{ K.Cal/Mole}$				$\Delta H\eta = 6.33 \text{ K.Cal/Mole}$			
$\gamma = 0.37$				$\gamma = 0.29$			

TABLE IIa  
Bromobenzene

$f = 38.8 \text{ K.Mc/s}$				$f = 38.8 \text{ K.Mc/s}$			
$2.85 \times 10^{-4} \text{ mole/cc in hexane}$				$2.84 \times 10^{-4} \text{ mole/cc in benzene}$			
T°K	$\tan \delta \times 10^3$	$\tau \times 10^{12} \text{ sec}$	$\frac{\tau T}{\eta \gamma} \times 10^7$	T°K	$\tan \delta \times 10^3$	$\tau \times 10^{12} \text{ sec}$	$\frac{\tau T}{\eta \gamma} \times 10^7$
278	15.0	8.50	7.83	275	9.8	15.81	11.63
288	15.5	7.60	7.93	289	11.1	12.90	11.50
297	16.0	6.96	8.09	299	12.0	11.25	11.37
307	15.9	6.25	8.14	309	12.6	10.03	11.32
317	16.1	5.45	7.99	319	13.3	8.90	11.26
323	16.4	4.62	7.18	330	13.7	8.02	11.34
332	15.9	4.66		348	14.1	6.83	11.57
$\Delta H\tau = 1.54 \text{ K.Cal/Mole}$ $\Delta H\eta = 1.81 \text{ K.Cal/Mole}$ $\gamma = 0.84$				$\Delta H\tau = 1.51 \text{ K.Cal/Mole}$ $\Delta H\eta = 2.53 \text{ K.Cal/Mole}$ $\gamma = 0.61$			

TABLE IIb

$f = 37.9 \text{ K.Mc/s}$				$f = 38.8 \text{ K.Mc/s}$			
$2.83 \times 10^{-4} \text{ mole/cc in CCl}_4$				$2.84 \times 10^{-4} \text{ mole/cc in Paraffin}$			
T°K	$\tan \delta \times 10^3$	$\tau \times 10^{12} \text{ sec}$	$\frac{\tau T}{\eta \gamma} \times 10^7$	T°K	$\tan \delta \times 10^3$	$\tau \times 10^{12} \text{ sec}$	$\frac{\tau T}{\eta \gamma} \times 10^7$
276	7.97	19.75	11.82	298	7.15	19.96	—
286	8.78	16.99	11.70	309	7.79	17.14	12.11
296	9.60	14.74	11.55	319	8.45	15.09	12.31
304	10.20	13.25	11.33	329	9.10	13.33	12.46
314	10.60	12.13	11.61	339	9.75	11.79	12.37
324	11.10	11.08	11.73	349	10.20	10.67	12.47
334	11.40	10.11	11.81				
343	11.85	9.21	11.83				
$\Delta H\tau = 1.46 \text{ K.Cal/Mole}$ $\Delta H\eta = 2.44 \text{ K.Cal/Mole}$ $\gamma = 0.60$				$\Delta H\tau = 1.96 \text{ K.Cal/Mole}$ $\Delta H\eta = 6.33 \text{ K.Cal/Mole}$ $\gamma = 0.41$			

TABLE IIIa  
*m*-Dichlorobenzene $f = 38.8 \text{ K.Mc/s}$  $f = 37.9 \text{ K.Mc/s}$ 

2.62 $\times 10^{-4}$ Mole/cc in hexane				2.61 $\times 10^{-4}$ Mole/cc in benzene			
T°K	$\tan \delta \times 10^3$	$\tau \times 10^{12}$ sec	$\frac{\tau T}{\eta^2} \times 10^{12}$	T°K	$\tan \delta \times 10^3$	$\tau \times 10^{12}$ sec	$\frac{\tau T}{\eta^2} \times 10^{12}$
279	12.00	8.73	7.34	276	10.0	12.51	6.32
289	12.46	7.73	7.38	286	11.0	10.70	6.35
299	12.90	6.73	7.38	295	11.6	9.43	6.50
309	13.14	5.94	7.36	305	12.0	8.20	6.46
315	13.60	4.87	6.50	315	12.7	7.24	656
323	13.38	4.59	6.83	325	13.0	6.23	6.42
331	12.90	3.40		338	13.5	4.58	5.49
				345	13.0	3.44	
$\Delta H_\tau = 1.68 \text{ K Cal/Mole}$				$\Delta H_\tau = 2.61 \text{ K Cal/Mole}$			
$\Delta H_\eta = 1.84 \text{ K Cal/Mole}$				$\Delta H_\eta = 2.53 \text{ K Cal/Mole}$			
$\gamma = 0.91$				$\gamma = 0.79$			

TABLE IIIb

 $f = 38.8 \text{ K Mc/s}$  $f = 38.8 \text{ K Mc/s}$ 

2.62 $\times 10^{-4}$ Mole/cc in CCl <sub>4</sub>				2.61 $\times 10^{-4}$ Mole/cc in paraffin			
T°K	$\tan \delta \times 10^3$	$\tau \times 10^{12}$ sec	$\frac{\tau T}{\eta^2} \times 10^{12}$	T°K	$\tan \delta \times 10^3$	$\tau \times 10^{12}$ sec	$\frac{\tau T}{\eta^2} \times 10^{12}$
277	6.89	19.20	10.96	300	5.42	22.79	
287	7.54	16.73	11.08	310	6.06	19.46	10.49
297	8.19	14.44	10.87	320	6.71	16.78	10.68
307	8.62	13.24	11.13	330	7.36	14.56	10.73
317	9.05	11.97	11.28	340	8.01	12.69	10.69
327	9.50	10.83	11.28	350	8.66	11.06	10.59
337	9.91	9.71	11.22				
$\Delta H_\tau = 1.52 \text{ K Cal/Mole}$				$\Delta H_\tau = 2.35 \text{ K Cal/Mole}$			
$\Delta H_\eta = 2.44 \text{ K Cal/Mole}$				$\Delta H_\eta = 6.33 \text{ K Cal/Mole}$			
$\gamma = 0.62$				$\gamma = 0.37$			

TABLE IVa  
o-Dichlorobenzene $f = 37.9$  K Mc/s $f = 38.8$  K.Mc/s

2.63 $\times 10^{-4}$ Mole/cc in benzene				2.65 $\times 10^{-4}$ Mole/cc in CCl <sub>4</sub>			
T°K	$\tan \delta \times 10^3$	$\tau \times 10^{12}$ sec	$\frac{\tau T}{\eta \gamma} \times 10^7$	T°K	$\tan \delta \times 10^3$	$\tau \times 10^{12}$ sec	$\frac{\tau T}{\eta \gamma} \times 10^7$
275	19.0	16.09	9.44	276	18.3	15.91	10.30
285	21.0	13.62	9.31	290	21.0	13.17	10.31
295	23.2	11.74	9.32	299	22.0	11.74	10.21
305	25.0	10.09	9.08	308	22.6	10.74	10.26
315	26.0	9.11	9.34	319	23.5	9.71	10.38
325	26.0	8.17	9.42	330	24.3	8.75	10.37
335	27.6	7.37	9.45	343	25.2	7.75	10.45
345	28.3	6.46	9.30				
$\Delta H\tau = 1.81$ K.Cal/Mole				$\Delta H\tau = 1.38$ K.Cal/Mole			
$\Delta H\eta = 2.53$ K.Cal/Mole				$\Delta H\eta = 2.41$ K.Cal/Mole			
$\gamma = 0.72$				$\gamma = 0.57$			

TABLE IVb

3.8 K.Mc/s

2.64 $\times 10^{-4}$ mole/cc in Paraffin				
T°K	$\tan \delta \times 10^3$	$\tau \times 10^{12}$ sec	$\frac{\tau T}{\eta \gamma} \times 10^7$	$\eta$ in millipoise
300	16.5	17.91	—	—
310	17.3	16.33	19.71	112.0
320	18.0	14.89	19.94	78.0
330	19.1	13.59	19.97	57.0
340	19.9	12.41	19.88	43.0
349	20.6	11.53	19.87	34.0
$\Delta H\tau = 1.25$ K.Cal/Mole				
$\Delta H\eta = 6.33$ K.Cal/Mole				
$\gamma = 0.20$				



TABLE V  
 $\alpha$ -Chloronaphthalene $f = 38.8$  K.Mc/s $f = 38.8$  K.Mc/s

2.93 $\times 10^{-4}$ mole/cc in benzene				2.93 $\times 10^{-4}$ mole/cc in paraffin			
T°K	$\tan \tau \times 10^3$	$\tau \times 10^{12}$ sec	$\frac{\tau T'}{\eta \gamma} \times 10^7$	T°K	$\tan \delta \times 10^3$	$\tau \times 10^{12}$ sec	$\frac{\tau T'}{\eta \gamma} \times 10^7$
277	6.45	23.98	21.75	303	4.63	30.73	16.46
287	6.89	21.49	22.18	313	5.23	26.19	16.96
297	7.34	19.30	22.42	323	5.84	22.56	17.02
306	7.78	17.55	22.28	333	6.23	20.34	17.41
316	8.20	15.89	22.23	343	6.64	18.25	17.79
326	8.67	14.43	22.28	353	7.00	16.69	18.00
336	9.10	13.11	22.02				
346	9.56	11.91	21.90				
$\Delta H\tau = 1.32$ K.Cal/Mole				$\Delta H\tau = 2.17$ K.Cal/Mole			
$\Delta H\eta = 2.53$ K.Cal/Mole				$\Delta H\eta = 6.33$ K.Cal/Mole			
$\gamma = 0.52$				$\gamma = 0.34$			

TABLE VI  
Solution in Carbon tetrachloride $f = 38.8$  K.Mc/s $f = 38.8$  K.Mc/s

2.93 $\times 10^{-4}$ mole/cc of $\alpha$ -chloro-naphthalene				3.48 $\times 10^{-4}$ mole/cc of fluorobenzene			
T°K	$\tan \delta \times 10^3$	$\tau \times 10^{12}$ sec	$\frac{\tau T'}{\eta \gamma} \times 10^7$	T°K	$\tan \delta \times 10^3$	$\tau \times 10^{12}$ sec	$\frac{\tau T'}{\eta \gamma} \times 10^7$
278	5.60	27.70	17.64	275	12.1	11.87	15.67
286	6.00	24.77	17.54	286	12.5	10.74	15.47
295	6.56	22.34	17.73	299	12.9	9.61	15.39
304	6.89	20.16	17.68	310	13.1	8.91	15.36
314	7.32	18.20	17.80	320	13.4	8.26	15.23
324	7.75	16.51	17.86	333	12.9	7.82	15.63
334	8.19	14.98	17.86	346	12.5	7.76	
344	8.62	13.38	17.62				
$\Delta H\tau = 1.43$ K.Cal/Mole				$\Delta H\tau = 0.70$ K.Cal/Mole			
$\Delta H\eta = 2.44$ K.Cal/Mole				$\Delta H\eta = 2.44$ K.Cal/Mole			
$\gamma = 0.59$				$\gamma = 0.29$			

It is seen from Eqn. (2) that

$$\frac{\tau \cdot T}{\eta_{AB}} = \frac{6g^2\sigma_{AB}}{2k} \quad \dots (4)$$

and since  $g^2\sigma_{AB}$  is expected to remain constant,  $\frac{\tau \cdot T}{\eta_{AB}}$  should not vary with temperatures. The values of  $\tau \cdot T/\eta_{AB}$  at different temperatures for some of the solutions are given in Tables VII to IX.

It is easily seen from the tables that the values of  $\frac{\tau \cdot T}{\eta_{AB}}$  do not remain constant with temperature but increases with increase of temperature which is contrary to the expectation from Hill's equation.

b) *Comparison of Chau, Lefevre and Tardiff's expression for  $\tau$  with the experimental values*

Chau *et al* (1957) proposed the following empirical relation between the time of relaxation and the molecular and physical parameter of the polar solute molecules and the non-polar solvents respectively,

$$\tau = \frac{\pi}{2kT} \eta(AB'') \exp(\Delta)(\epsilon+2)^{-1} \quad \dots (5)$$

where  $\eta$  is the macroscopic viscosity,  $\Delta$  the depolarisation factor and  $\epsilon$  the static dielectric constant of the solvent at the temperature  $T$ .  $A$ ,  $B$  and  $C$  (with  $A \geq B \geq C$ ) are the axial lengths characterising the solute polarisability ellipsoid. It is seen from Eqn (5) that

$$\frac{\tau \cdot T}{\eta'} = \frac{\pi}{2k} ABC = \text{const.} \quad \dots (6a)$$

where

$$\eta' = \eta \exp(\Delta)(\epsilon+2)^{-1} \quad \dots (6b)$$

In order to test the constancy of the values of  $\tau \cdot T/\eta'$  for different polar compounds in solutions in different non-polar solvents at various temperatures, the values of  $\eta'$  have been computed from the macroscopic viscosities ( $\eta$ ), the static dielectric constants ( $\epsilon$ ) of the solvents at different temperatures and the experimental values of depolarisation factor ( $\Delta$ ) at different temperatures reported by Rao (1927, 28) and Krishnan and Rao (1929, 30)

The values of  $\tau \cdot T/\eta'$  at different temperatures for the different solutions are shown in Table X-XII

It is easily seen from the tables that the values of  $\tau \cdot T/\eta'$  instead of remaining constant, increase with the increase of temperatures. From the results presented in the above sections it is clear that neither the Hill's expression nor that of Chau

*et al* for the time of relaxation is in agreement with the conclusion arrived at from the experimentally determined  $\tau$ -values for the various compounds in solutions in the different solvents. In the next section it is proposed to investigate the relation between the  $\tau$ -values and the macroscopic viscosities of the solutions.

(c) *Relation between the time of relaxation ( $\tau$ ), the internal viscosity ( $\eta_{int}$ ) and the macroscopic viscosity ( $\eta$ )*

The Debye relation as modified by Perrin (1934) for ellipsoidal molecules with rigid dipoles lying along one of the principal axes of the ellipsoid is given by

$$\tau = \frac{4\pi abc f \eta_{int}}{kT} \quad \dots (7a)$$

whence

$$\eta_{int} = \frac{\tau kT}{4\pi abc f} \quad \dots (7b)$$

where  $a$ ,  $b$ ,  $c$  are the semi axes of the ellipsoidal molecules,  $f$  is a factor tabulated by Budo *et al* (1939),  $K$  is the Boltzman constant and  $\eta_{int}$  is the internal viscosity of the medium in which the ellipsoidal molecules are rotating under the influence of the applied microwave field. The value of  $a$ ,  $b$  and  $c$  are determined from data on atomic radii (Fischer, 1949) and  $\eta_{int}$  is calculated from the experimental values of  $\tau$  with the help of Eqn. (7b). The molecular parameters are given in Table XIII which also contains the values of ' $f$ ', the molecular volume ( $\frac{4}{3}\pi abc$ ) and the kinetic theory volume wherever available included for the sake of comparison.

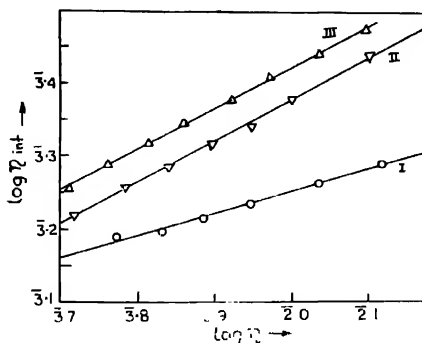


Fig. 2a. Graphs showing variation of  $\log \eta_{int}$  against  $\log \eta$   
 Curve I Fluorobenzene in solution in carbon tetrachloride  
 Curve II Orthodichlorobenzene in solution in carbon tetrachloride  
 Curve III  $\alpha$ -Chloronaphthalene in solution in carbon tetrachloride

TABLE VII  
Chlorobenzene

Solution in benzene				Solution in CCl <sub>4</sub>			
T°K	$\eta_{AB}$ millipoise	$\tau \times 10^{12}$ sec	$\frac{\tau T}{\eta_{AB}} \times 10^7$	T°K	$\eta_{AB}$ millipoise	$\tau \times 10^{12}$ sec	$\frac{\tau T}{\eta_{AB}} \times 10^7$
277	9.04	14.13	4.33	278	11.28	14.27	3.52
289	7.63	12.95	4.68	290	9.13	13.02	4.13
299	6.71	11.10	4.94	298	8.00	12.07	4.50
311	5.82	10.10	5.40	305	7.20	11.48	4.86
325	5.01	9.06	5.88	315	6.22	10.54	5.34
336	4.44	8.44	6.32	325	5.43	9.66	5.78
348	3.98	7.73	6.75	335	4.79	8.82	6.17
				345	4.24	8.21	6.67

TABLE VIII  
Bromobenzene

Solution in benzene				Solution in CCl <sub>4</sub>			
T°K	$\eta_{AB}$ millipoise	$\tau \times 10^{12}$ sec	$\frac{\tau T}{\eta_{AB}} \times 10^7$	T°K	$\eta_{AB}$ millipoise	$\tau \times 10^{12}$ sec	$\frac{\tau T}{\eta_{AB}} \times 10^7$
275	11.83	15.81	3.67	276	14.98	19.75	3.64
289	9.66	12.89	3.86	286	12.59	16.99	3.87
299	8.41	11.25	4.00	296	10.64	14.74	4.10
309	7.45	10.03	4.16	304	9.40	13.25	4.29
319	6.64	8.90	4.28	314	8.13	12.13	4.69
330	5.84	8.02	4.53	324	7.03	11.08	5.11
348	4.81	6.83	4.86	334	6.19	10.11	5.45
				343	5.52	9.24	5.74

TABLE IX  
 $\alpha$ -Chloronaphthalene

Solution in benzene				Solution in $\text{CCl}_4$			
T°K	$\eta_{AB}$ millipoise	$\tau \times 10^{12}$ sec	$\frac{\tau T'}{\eta_{AB}} \times 10^7$	T°K	$\eta_{AB}$ millipoise	$\tau \times 10^{12}$ sec	$\frac{\tau T'}{\eta_{AB}} \times 10^7$
277	11.80	23.98	4.49	278	22.05	27.70	3.49
287	12.28	21.49	5.02	286	18.75	24.77	3.78
297	10.38	19.30	5.52	295	15.78	22.34	4.18
306	8.92	17.55	6.02	304	13.50	20.16	4.54
316	7.72	15.89	6.49	314	11.42	18.20	5.00
326	6.65	14.43	7.08	321	9.78	16.51	5.47
336	5.72	13.11	7.69	334	8.46	14.98	5.91
346	5.07	11.91	8.13	344	7.46	13.38	6.17

TABLE X  
Solution in Carbontetrachloride

Chlorobenzene				Bromobenzene			
T°K	$\eta'$ millipoise	$\tau \times 10^{12}$ sec	$\frac{\tau T'}{\eta'} \times 10^7$	T°K	$\eta'$ millipoise	$\tau \times 10^{12}$ sec	$\frac{\tau T'}{\eta'} \times 10^7$
278	3.11	14.27	12.75	276	3.25	19.75	16.77
298	2.26	12.07	15.89	296	2.34	14.74	18.65
315	1.83	10.51	18.09	314	1.81	12.13	20.70
335	1.46	8.82	20.21	334	1.45	10.11	23.29
345	1.30	8.21	21.78	343	1.32	9.24	24.00

<i>o</i> -Dichlorobenzene				$\alpha$ -Chloronaphthalene			
T°K	$\eta'$ millipoise	$\tau \times 10^{12}$ sec	$\frac{\tau T'}{\eta'} \times 10^7$	T°K	$\eta'$ millipoise	$\tau \times 10^{12}$ sec	$\frac{\tau T'}{\eta'} \times 10^7$
276	3.25	15.91	13.51	278	3.11	27.70	24.74
299	2.25	11.71	15.61	295	2.38	22.34	27.09
319	1.73	9.71	17.91	314	1.84	18.20	31.06
330	1.52	8.75	19.00	331	1.45	14.98	34.49
343	1.32	7.74	20.14	344	1.31	13.38	35.14

TABLE XI  
Solution in benzene

Chlorobenzene				o-Dichlorobenzene			
T°K	$\eta'$ millipoise	$\tau \times 10^{12}$ sec	$\frac{\tau T}{\eta'} \times 10^7$	T°K	$\eta'$ millipoise	$\tau \times 10^{12}$ sec	$\frac{\tau T}{\eta'} \times 10^7$
277	3.06	14.13	12.79	275	3.20	16.09	13.82
299	2.14	11.10	15.47	295	2.27	11.74	15.26
325	1.56	9.06	18.89	315	1.77	9.11	16.21
336	1.39	8.41	20.38	335	1.42	7.37	17.40
348	1.22	7.73	22.04	345	1.26	6.46	17.67

m-Dichlorobenzene				$\alpha$ -Chloronaphthalene			
T°K	$\eta'$ millipoise	$\tau \times 10^{12}$ sec	$\frac{\tau T}{\eta'} \times 10^7$	T°K	$\eta'$ millipoise	$\tau \times 10^{12}$ sec	$\frac{\tau T}{\eta'} \times 10^7$
276	3.13	12.51	11.04	277	3.06	23.98	21.71
295	2.27	9.43	12.26	297	2.21	19.30	25.94
315	1.77	7.23	12.86	316	1.75	15.89	28.64
325	1.56	6.23	12.49	336	1.39	13.11	31.78
345	1.26	3.41	9.33	346	1.25	11.91	32.97

TABLE XII  
Solution in hexane

Bromobenzene				m-Dichlorobenzene			
T°K	$\eta'$ millipoise	$\tau \times 10^{12}$ sec	$\frac{\tau T}{\eta'} \times 10^7$	T°K	$\eta'$ millipoise	$\tau \times 10^{12}$ sec	$\frac{\tau T}{\eta'} \times 10^7$
278	1.07	8.50	22.09	279	1.06	8.73	22.98
288	0.97	7.60	22.70	289	0.96	7.73	23.38
297	0.88	7.96	23.50	299	0.86	6.73	23.40
307	0.80	6.25	24.11	309	0.78	5.94	23.55

TABLE XIII

Compound	Semi-axial length in Å			$f$	$\frac{4}{3} \pi \text{ Å}^3$	Kinetic Theory volume $\text{Å}^3$
	$a$	$b$	$c$			
$\text{C}_6\text{H}_6$	3.11	3.11	1.27	—	51.5	48.0
$\text{C}_6\text{H}_5\text{I}$	3.28	3.11	1.27	1.43	54.3	54.0
$\text{C}_6\text{H}_5\text{Cl}$	3.46	3.11	1.50	1.44	67.6	61.0
$\text{C}_6\text{H}_5\text{Br}$	3.56	3.11	1.70	1.27	78.8	64.0
$\text{o-C}_6\text{H}_4\text{Cl}_2$	3.11	3.01	1.50	1.26	58.8	—
$\text{m-C}_6\text{H}_4\text{Cl}_2$	3.31	3.11	1.50	1.35	64.7	—
$\alpha\text{-V}_{10}\text{H}_7\text{Cl}$	4.04	3.46	1.50	1.35	87.8	—

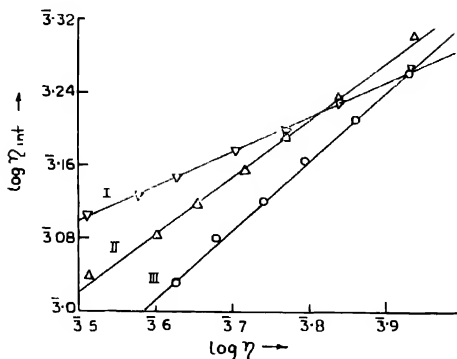


Fig. 2b. Graphs showing variation of  $\log \eta_{int}$  against  $\log \eta$   
 Curve I Chlorobenzene in solution in benzene  
 Curve II Bromobenzene in solution in benzene  
 Curve III Metadichlorobenzene in solution in benzene

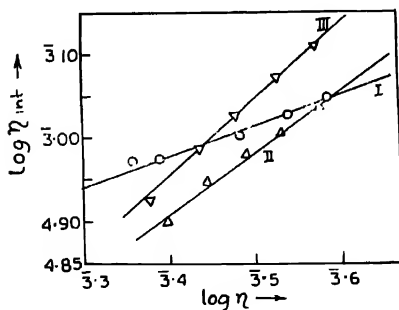


Fig. 2c. Graphs showing variation of  $\log \eta_{int}$  against  $\log \eta$   
 Curve I Chlorobenzene in solution in hexane  
 Curve II Bromobenzene in solution in hexane  
 Curve III Metadichlorobenzene in solution in hexane

In order to find out the relation between the values of  $\eta_{int}$  so calculated and the microscopic viscosities of the solvents, the calculated values of  $\log \eta_{int}$  have been plotted against the values of  $\log \eta$ . Some of these graphs are shown in Figures 2a, 2b, 2c and 2d. It is seen from these graphs that  $\log \eta_{int}$  is connected with the  $\log \eta$  values by the linear relation,

$$\log \eta_{int} = G + \gamma \log \eta \quad (8)$$

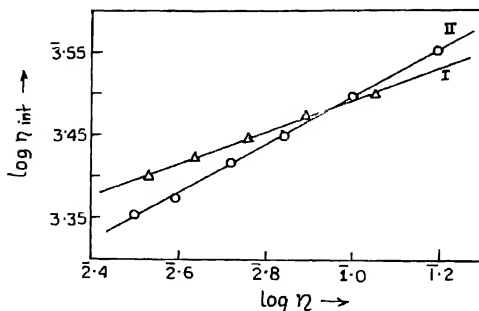


Fig. 2d. Graphs showing variation of  $\log \eta_{int}$  against  $\log \eta$   
 Curve I Orthodichlorobenzene in solution in paraffin  
 Curve II  $\alpha$ -Chloromethylphthalone in solution in paraffin

where  $G$  is a constant and the slope of the straight line is equal to the ratio  $\Delta H\tau/\Delta H\eta$  given at the feet of the Tables (I—IV). From Eqn. (8) is obtained  $\eta_{int} = \text{const } \eta^\gamma$  which in conjunction with Eqn. (7b) gives

$$\frac{\tau \cdot T}{\eta^\gamma} = \text{const.} \quad (9)$$

It is seen from the Tables I-VI, that the values of  $\tau T/\eta^\gamma$  are almost constant for the different compounds in solutions in the various non-polar solvents. This is in conformity with the results obtained previously (Sinha *et al.*, 1965).

The discussions of the experimental results presented in the previous sections, therefore, lead to the conclusion that the internal viscosity ( $\eta_{int}$ ) is a function of the macroscopic viscosity ( $\eta$ ) and may be represented by an equation of the form  $\eta_{int} = \text{const. } \eta^\gamma$ .

#### REFERENCES

- Bhattacharyya, J., Sinha, B., Roy, S. B., Kastha, G. S., (1964), *Indian J. Phys.*, **38**, 413.  
 Budo, A., Fischer, E. and Miyamoto, S., (1939), *Physic. Z.*, **49**, 337.  
 Chau, J. Y. H., Le Fèvre, R. J. W. and Tardif, J., (1957), *J. Chem. Soc.*, 2293.  
 Fischer, E., (1939), *Phys. Z.*, **49**, 645.  
 Fischer, E., (1949), *Z. Naturf.*, **4A**, 707.  
 Hase, H., (1953), *Z. Naturf.*, **8A**, 695.  
 Hill, N. E., (1954), *Proc. Phys. Soc.*, **B 67**, 149.  
 Krishnan, K. S. and Rao, S. R., (1929-30), *Indian J. Phys.*, **4**, 39.  
 Perrin, F., (1934), *J. de Phys.*, (7) **5**, 497.  
 Rao, S. R., (1927-28), *Indian J. Phys.*, **2**, 179.  
 Sinha, B., Roy, S. B. and Kastha, G. S., (1965), *Indian J. Phys.*, **30**, 328.  
 Wirtz, K. and Spornol, A., (1953), *Z. Naturf.*, **8A**, 522.  
 Wirtz, K. and Hierer, A., (1953), *Z. Naturf.*, **8A**, 532.



# DIFFERENT CLASSES OF SOLAR AND SOLAR-TERRESTRIAL EVENTS IN RELATION TO THE PHASE OF THE SOLAR CYCLE

D. BASU AND M. K. DAS GUPTA

INSTITUTE OF RADIO PHYSICS AND ELECTRONICS, CALCUTTA UNIVERSITY, CALCUTTA-9

(Received December 9, 1965)

**ABSTRACT.** The frequency of occurrence of solar and solar-terrestrial events in relation to the phase of the solar cycle has been studied for the period 1956-63. The events include sunspot, Cn-plage, solar flare, solar radio burst at metre wavelengths, geomagnetic storm and short wave fadeout. Each event has been classified into four different groups—viz., small, moderate, large and outstanding depending on its degree of activity. It has been found that solar and solar-terrestrial phenomena show maximum correlation with sunspot cycle when considered as a whole (without classification) as also for small, moderate and large magnitudes of their activities. Outstanding events of all types tend to occur during the ascending and descending phases of the solar cycle, avoiding the peak phase.

## INTRODUCTION

It is now well established that all sorts of solar and solar-terrestrial events are very closely associated with one feature, viz. the sunspot whose number or area actually determines the progress of the solar cycle. Thus when sunspots are numerous, all the different types of solar and associated geophysical phenomena will be more frequent. The frequency of occurrence of all these events follow closely the solar cycle.

Nevertheless, it appears from the analysis of Newton and Milsom (1954) that very big geomagnetic storms occur more frequently few years on either side of the peak phase of the corresponding solar cycle. This behaviour is exhibited by 17 storms of outstanding intensity (average ranges  $2^{\circ}$ - $4^{\circ}$  in  $D$  1180 $\gamma$  in  $H$  and 790 $\gamma$  in  $Z$ ) collected from nine sunspot cycles beginning with the minimum at 1856. However, this peculiar characteristics of avoiding the peak phase was not observed in the case of the distribution of giant sunspots (mean area  $\geq 1500$  millionths of the solar disk) and outstanding solar flares (class 3+).

Again, Kodama (1961) observed that unusual increases in cosmic rays and fast type of polar cap absorption (PCA) events occur only during the ascending and descending phases of the solar cycle avoiding the maximum phase. On the contrary, small increases in cosmic rays and slow type of PCA events were found by him to be concentrated more around the peak period of sunspot cycle. Dependence of the fast type of PCA events as also ground level enhancement (GLE)

of cosmic rays on the phase of the solar cycle can also be inferred from the investigations of Warwick and Haurwitz (1962). They concluded that during the peak solar activity high energy protons rarely reach the earth whilst those producing PCA events suffer maximum delay. It is known that unusual increase in cosmic rays detected on the surface of the earth are almost always associated with highly intense solar eruptions. This led Takakura and Ono (1961) to investigate whether outstanding solar eruptions responsible for cosmic ray increases on the surface of the earth are also absent during the peak period of solar activity or the effect is due to some other reason unfavourable for accelerating particles. Solar flares of importance 3+ and unusually intense radio outbursts on centimetric waves ( $>5 \times 10^3$  flux units for 2800 Mc/s and  $>10^4$  flux units for 3750 and 9400 Mc/s) were considered by them for detecting intense solar eruptions. It was found that intense outbursts on centimetric waves occur in the ascending and descending phases of the solar cycle avoiding the peak phase while the frequency of occurrence of weaker bursts is maximum at the maximum period of the solar cycle. On the contrary, the distribution of frequency of occurrence of class 3- flares as also flares of lower classes follow the sunspot cycle quite closely being most frequent during the peak phase and then decreasing away from it. Japanese workers mentioned above, attributed this peculiar behaviour of the outstanding solar terrestrial events to be exclusively a solar effect. On the contrary, Warwick and Haurwitz suggested that the phenomena as observed by them might be possibly due to the effect of stronger interplanetary magnetic field and high degrees of disorder therein on the movement of particles during the peak phase of the solar activity.

Recently the problem was examined by the present authors (Das Gupta and Basu, 1965) with respect to various other solar and solar-terrestrial events. The former include sunspots, calcium plages, solar flares and metre wave radio bursts (200 Mc/s) while the solar-terrestrial events include short wave radio fade-outs and geomagnetic storms. They found that outstanding classes of all solar and solar-terrestrial events mentioned above mostly tend to avoid the peak phase of solar activity and occur more frequently during the ascending and descending phases. It was concluded by them that the effect in general must be of solar origin rather than any modulation effect in the sun-earth space. It is the purpose of the present paper to describe the details of the work referred to above.

#### METHOD OF ANALYSIS

As has already been mentioned in the previous section, the present analysis has been carried out for events which include sunspots, calcium plages, solar flares, solar radio bursts at 200 Mc/s, short wave radio fade-outs and geomagnetic storms. The period covered is 1956 to 1963 for which fairly continuous data for all these events are available.

Each of the individual events mentioned above was divided into four classes—small, moderate, large and outstanding—depending on the magnitude of its

activity. Thus it is known that activities of sunspots and calcium plages depend on their areas on the solar disk—big centres of activities being formed around large sunspot groups and huge calcium plages. These have therefore been classified according to their areas. Flares of even class 3+ were found by Newton and Milsom as well as Takakura and Ono to obey the sunspot cycle more or less satisfactorily. It was, however, indicated by the latter group that the energy associated with certain 3+ flares might be greater than that for others of the same class. As such  $H\alpha$  line width, also recognised as an index for the intensity of solar flares, was taken as the basis of classification in our analysis. So far as solar radio noise burst at metre wavelength is concerned, the peak flux density in units of watts/sq-metre/cycles per second is the best index for measurement. In the case of short wave radio fadeout, however, the duration of each event, known to vary directly with the intensity of the event, has been considered for the classification. Lastly, the internationally adopted  $K$  index has been taken as a measure of the intensity of geomagnetic storms. The criteria of different classifications are shown in Table I.

TABLE I

Criteria of classification of different solar and solar-terrestrial events

Name of events	Properties to be studied	Unit of measurement	Classifications			
			Small	Moderate	Large	Out-standing
Sunspot group	Area at CMP	$\times 10^{-8} \times$ Area of solar disk.	< 500	500– < 1000	1000– < 2000	> 2000
Calcium plage.	Area at CMP	$\times 10^{-8} \times$ Area of solar disk.	< 1000	1000– < 5000	5000– < 10000	> 10000
Solar flare	$H\alpha$ line width	Angstrom unit	< 5	5– < 10	10– < 15	> 15
Solar radio burst.	Peak flux density.	$\times 10^{-22}$ W/M <sup>2</sup> /CPS.	< 500	500– < 1000	1000– < 5000	> 5000
Short wave fadeout.	Duration	Minutes	< 50	50– < 100	100– < 200	> 200
Geomagnetic storm.	Value of K index.	IAGA classification	< 5	6–7	8	9

Every individual year of the period 1956-63 was divided into two six monthly intervals. The total number of every event, irrespective of classes, occurring during each of these six monthly intervals was first determined for the entire period and histograms were drawn. These are shown in Fig. 1 which also includes six monthly means of final Zurich sunspot numbers. The number of occurrences of each of the different classes for every event were then counted individually for the six monthly intervals over the entire period and the respective histograms, drawn (Figs. 2). From Figs. 1 and 2, the particular half-yearly intervals showing

maximum activity determined by number of occurrences of the different classes as also the total number (irrespective of classes) of each event were obtained.

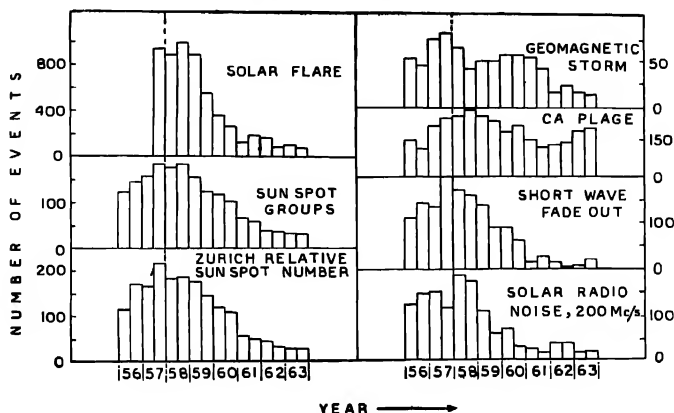


Fig. 1. Variations of the total number of various solar and solar-terrestrial events in course of a solar cycle.

The results are shown in Table II. Correlation coefficients were also determined for each case with respect to corresponding half yearly mean sunspot numbers. These are shown in Table III.

## RESULTS

Results obtained in the present analysis are shown in Figs. 1 and 2 and in Tables II and III. It will be found from Fig. 1 that the half-yearly variations from 1956-1963 of the total number of different events (without classification) take place more or less in accordance with that of sunspot number for the same period. The association with sunspot numbers appears to be very prominent for the events sunspot groups, solar flares, solar radio noise bursts and short wave fade outs the frequency of occurrence falling gradually on either side of the peak period indicated by the dotted line. In case of calcium plages and geomagnetic storms, however, the decrease in frequency of occurrence, as one proceeds away from the peak period, is not so uniform as is expected from sunspot numbers.

Fig. 2 shows the half-yearly intervals indicating the maximum number of occurrences of different classes of each event which have been indicated in Table II. It has been found that all types of solar and solar-terrestrial events considered here and belonging to the outstanding class occur most frequently either in the ascending or in the descending phase or in both of these phases of the solar cycle,

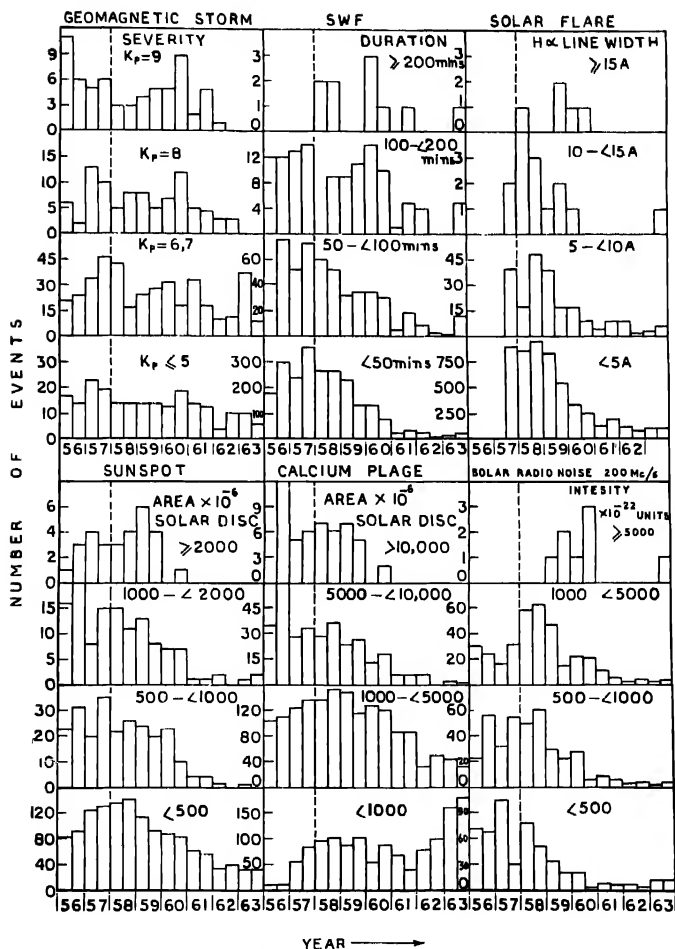


Fig. 2. Variations of different classes of solar and solar-terrestrial events in course of a solar cycle.

TABLE II

Years showing maximum occurrences of different classes of solar and solar-terrestrial events in relation to the phase of the solar cycle.

Events→	Sunspot Group			Ca Plage			Solar Flare		
Classes	Ascend- ing	Peak	Descen- ding	Ascend- ing	Peak	Descen- ding	Ascend- ing	Peak	Descen- ding
Small	—	1958 (II)	—	—	1958 (II)	1963 (II)	—	1958 (II)	—
Moderate	—	1957 (II)	—	—	1958 (II)	—	—	1958 (II)	—
Large	1956 (II)	—	—	1956 (II)	—	—	—	1958 (I)	—
Outstanding	—	—	1959 (I)	1956 (I, II)	—	—	—	—	1959 (II)
Total number of Events	—	1957 (II)	—	—	1958 (II)	—	—	1958 (II)	—

Events→	Solar Radio Burst			Short Wave Fadeout			Geomagnetic Storm		
Classes ↓	Ascend- ing	Peak	Descen- ding	Ascend- ing	Peak	Descen- ding	Ascend- ing	Peak	Descen- ding
Small	—	1957 (I)	—	—	1957 (II)	—	—	1957 (I)	—
Moderate	—	1958 (II)	—	1956 (II)	1957 (II)	—	—	1957 (II)	—
Large	—	1958 (II)	—	—	1957 (II)	1960 (I)	—	1957 (I)	1960 (II)
Outstanding	—	—	1960 (II)	—	—	1960 (I)	1956 (I)	—	1960 (II)
Total number of Events	—	1958 (I)	—	—	1957 (II)	—	—	1957 (II)	—

Note : (1) Ascending phase : 1954-56, Peak Phase : 1957-58 and Descending phase : 1959-63

(2) Suffix (I) indicates first half of the year (January to June), suffix (II) indicates second half (July to December).

TABLE III

Correlation coefficients between half-yearly mean sunspot number and number of occurrences for different classes of various events

Classes	Correlation coefficients for events					
	Sunspot group	Calcium Plage	Solar flare	Solar Radio burst	SWF	Geomagnetic storm
Small	0.9560	0.3534	0.7381	0.6337	0.9587	0.6030
Moderate	0.9358	0.6017	0.6475	0.9005	0.9001	0.4836
Large	0.8321	0.8021	0.6058	0.7861	0.7985	0.5309
Outstanding	0.5548	0.4844	0.2892	-0.2655	-0.2547	0.4134
Total	0.9861	0.6751	0.7378	0.8681	0.9767	0.7471

avoiding the peak phase. The same tendency is also clearly shown by large sunspots and calcium plages. But for all other events, large, intermediate and small classes follow the solar cycle more or less closely-- the number of occurrences in each of these cases being maximum during the peak phase of solar activity. It is found (Table III) that the correlation coefficient with sunspot numbers is least for the outstanding class of all events while it has highest value when total number of events are considered.

#### DISCUSSION

It was shown by previous workers, as has already been mentioned, that unusually high incidents of cosmic ray increase, polar cap absorption and radio outbursts at centimetre wavelengths occur less frequently during the sunspot maximum period. The present analysis shows that outstanding events of sunspot, calcium plage, solar flare, radio outburst at metre wavelengths, short wave radio fadeout and geomagnetic storm tend to concentrate themselves more towards periods of moderate activity. It may be noted that, of these various events, visible solar flare, radio outbursts at all wavelengths and short wave fadeout involves wave radiation of wide range of frequencies from the sun while cosmic ray increase, polar cap absorption and geomagnetic storms recorded on the earth indicate particle radiation therefrom, of various energies. On the other hand, sunspots and calcium plages represent centres of activity on the solar surface. It thus appears that all the outstanding solar and solar-terrestrial events due to both wave and particle radiation from the sun as also centres of activity occur most frequently during the ascending and descending phases of the solar cycle, avoiding the peak phase.

It was indicated by Kodama that solar protons responsible for unusual increase in cosmic rays and fast type PCA are accelerated simultaneously in the same region of the solar atmosphere from where centimetre wave radio outbursts

are also produced. This is the reason, according to him, why these three phenomena, exhibit the same effect of avoiding the maximum period of solar activity. Takakura and Ono, however, suggested that during the peak phase the frequency of disturbance in the solar atmosphere being very high, the time interval between successive triggering actions is too short for much energy to be stored to cause most intense eruptions. During moderate activity, triggers being less frequent outstanding events may occur in the sun due to the possibility of storage of more energy. Thus the Japanese workers investigating on cosmic ray, PCA, and microwave outbursts maintain the view, as was indicated earlier, that this rather peculiar behaviour of the outstanding events of avoiding the peak period of solar activity is exclusively a solar effect. On the other hand, Warwick and Haurwitz working only with cosmic ray and PCA events suggested that the disordered interplanetary magnetic field during the maximum phase might be responsible for preventing particles from reaching the earth. Since it is now evident that the characteristic effect is exhibited by both wave as well as particle radiations from the sun and it being known that the interplanetary magnetic field can have no effect on wave radiation, it is clear that the origin of the peculiar phenomenon is the solar atmosphere itself rather than the sun-earth space. Furthermore, the same phenomenon being shown also by sunspots and calcium plages, it can be concluded that somehow the highly disturbed sun and its atmosphere prevent the formation of very large so-called 'centres of activity' and hence the occurrence of any outstanding event during the peak phases of solar cycles.

Investigations by previous workers showed that unusual events of cosmic ray increase, polar cap absorption and microwave outbursts are concentrated either in the first half of 1956 or in the second half of 1960 or in both. It is found from Fig. 2 and Table II of the present analysis that outstanding occurrence of calcium plage, geomagnetic storms and metro wave radio outburst from the sun have also got the tendency of predominating at the same periods. On the other hand corresponding events of sunspot groups and solar flares are more frequent at the first and second halves of 1959 respectively while those for short wave fadeout are most predominant at the first half of 1960. However, as the international data giving  $H_{\alpha}$  line width of solar flares are insufficient prior to July 1957, it is difficult to assess the situation of intense solar flares at that period. It is rather interesting to note that big flares do not correspond to big spots and plages. It therefore appears that outstanding events of solar flares, sunspots and calcium plages occur more or less independently of each other.

#### CONCLUSION

It may thus be concluded that solar and solar-terrestrial phenomena show maximum correlation with the sunspot cycle when taken as a whole as well as for small, moderate and large magnitudes of their activities. All sorts of outstanding



solar and solar-terrestrial events tend to occur during the ascending and descending phases of the solar cycle, avoiding the maximum phase. Since the same tendency is exhibited by both wave as well as particle phenomena including sunspots and calcium plages, the effect must be of solar origin. It appears that unusually intense centres of activity are much easier to be formed in the solar atmosphere during the period of moderate activity than that during the maximum phase. Outstanding flares are not necessarily associated with outstanding spots or plages.

It should, however, be noted that the present analysis has been carried out over part of one solar cycle for which data are available. Studies of data over several solar cycles in future will be interesting and will establish firmly the phenomenon obtained in this analysis which will definitely reveal many new facts on solar physics in general and on the formation of centres activity in particular.

#### ACKNOWLEDGMENTS

The authors are grateful to Prof. J. N. Bhar for his kind interest. Data used were obtained from CIRPL (Part B) Solar Geophysical Data Books (Sunspot Group, Ca-plage, Solar Flare and Short Wave Fadeout), Geomagnetic and Solar Data published in the Journal of Geophysical Research (Geomagnetic Storm) and the Ionospheric Data Books of the Radio Research Committee of Japan (200 Mc/s Solar Radio Burst)

#### REFERENCES

- Das Gupta, M. K. and Basu, D., 1965, *J. Atmos. Terri. Phys.*, **27**, 1029  
Kodama, M., 1962, *J. Phys. Soc. Japan*, **17**, Suppl. 11-A, 594.  
Newton, H. W. and Milson, A. S., 1954, *J. Geophys. Res.*, **59**, 203  
Takakura, T. and Ono, M., 1962, *J. Phys. Soc. Japan*, **17**, Suppl. 11-A, 207  
Warwick, C. S. and Haurwitz, M. W., 1962, *J. Geophys. Res.*, **67**, 1317

# COVALENCY REDUCTION FACTORS IN THE CASE OF TETRAHEDRAL COMPLEXES

R. RAI AND R. K. MUKHERJEE,

DEPARTMENT OF MAGNETISM,

INDIAN ASSOCIATION FOR THE CULTIVATION OF SCIENCE, CALCUTTA-32, INDIA

(Received November 4, 1965)

**ABSTRACT.** Expressions for the reduction factors associated with the orbital contribution to magnetic moment and with the spin-orbit interaction in the tetrahedral complexes arising from the overlap of the central metal ion  $d$ -orbitals with the ligand  $s$  and  $p$  orbitals, have been deduced and discussed in the light of existing experimental results. It is seen that the ligand  $p$ -orbitals are more effective than  $s$ -orbitals.

## INTRODUCTION

Superiority of the molecular orbital theory over the earlier introduced crystalline electric field theory (Van Vleck, 1932) in many of the compounds of the transition group of elements was first demonstrated by Van Vleck as early as 1935. In contrast to the crystalline field approximations where the basic orbitals are the pure central metal ion orbitals, in molecular orbital theory these are linear combinations of the central metal ion orbitals with the ligand orbitals allowed by symmetry of the complex. Hence the two orbitals have similar transformation properties and the matrix elements for the spin-orbit coupling  $H_{so}$  and the orbital angular momentum  $L$ , in the ligand field approximation can be represented by the old matrix elements multiplied by respective reduction factors arising from the admixtures. In the octahedral complexes, where the  $d_e$  orbitals belonging to the representation  $T_{2g}$  have the proper symmetry to form  $\pi$ -bonds with the ligands whereas  $d_\gamma$  orbitals belonging to the representation  $E_g$  can form  $\sigma$ -bonds with the ligands, the nature and order of the reduction factors have been investigated by Stevens (1953), Owen (1955), Tinkham (1956) and others.

In tetrahedral complexes such calculations are more cumbersome because  $d_e$  orbitals of the central ion have the proper symmetry to form both  $\pi$  and  $\sigma$  bonds with ligands.  $d_\gamma$  orbitals, however, can form only  $\pi$ -bonds. Our aim in this paper is to deduce expressions for these reduction factors and to discuss them in the light of existing experimental results on some tetrahedral complexes.

## MOLECULAR ORBITALS OF COVALENT $XY_4$ TETRAHEDRAL COMPLEXES

The  $d$ -wave functions in a field of tetrahedral symmetry split up into two types  $d_e$  and  $d_\gamma$  spanning the representations  $T_2$  and  $E$  respectively of the point group

$T_d$ . In a molecular orbital scheme the magnetic carriers remain partly in the central  $d$  and  $d\gamma$  orbitals and partly in surrounding ligand  $s$  and  $p$  orbitals. The form of the molecular orbital wavefunctions are as given by Wolfsberg and Helmholtz (1952)

$$\begin{aligned}
 |XY\rangle &= N_t \left[ d_{xy} + \frac{\lambda\sigma}{2} (\sigma_1 + \sigma_4 - \sigma_3 - \sigma_2) + \frac{\lambda\pi t}{2} \left\{ \frac{1}{2} (\pi_{x_1} + \pi_{x_2} - \pi_{x_3} - \pi_{x_4}) + \right. \right. \\
 &\quad \left. \left. + \sqrt{\frac{3}{2}} (\pi_{y_1} + \pi_{y_2} - \pi_{y_3} - \pi_{y_4}) \right\} \right] \\
 |YZ\rangle &= N_t \left[ d_{yz} + \frac{\lambda\sigma}{2} (\sigma_1 + \sigma_3 - \sigma_2 - \sigma_4) + \frac{\lambda\pi t}{2} \left\{ \frac{1}{2} (\pi_{x_1} + \pi_{x_2} - \pi_{x_3} - \pi_{x_4}) + \right. \right. \\
 &\quad \left. \left. + \sqrt{\frac{3}{2}} (\pi_{y_1} + \pi_{y_2} - \pi_{y_3} - \pi_{y_4}) \right\} \right] \\
 |XZ\rangle &= N_t \left[ d_{xz} + \frac{\lambda\sigma}{2} (\sigma_1 + \sigma_2 - \sigma_3 - \sigma_4) + \frac{\lambda\pi t}{2} (\pi_{x_1} + \pi_{x_2} - \pi_{x_3} - \pi_{x_4}) \right] \dots (1) \\
 |X^2-Y^2\rangle &= N_e \left[ d_{x^2-y^2} + \frac{\lambda\pi e}{4} \{ (\pi_{y_1} + \pi_{y_2} - \pi_{y_3} - \pi_{y_4}) \right. \\
 &\quad \left. + \sqrt{3} (\pi_{x_1} + \pi_{x_2} + \pi_{x_3} + \pi_{x_4}) \right] \\
 |3Z^2-r^2\rangle &= N_e \left[ d_{3z^2-r^2} + \frac{\lambda\pi e}{4} \{ (\pi_{x_1} + \pi_{x_2} + \pi_{x_3} + \pi_{x_4}) \right. \\
 &\quad \left. + \sqrt{3} (\pi_{y_1} + \pi_{y_2} + \pi_{y_3} + \pi_{y_4}) \right]
 \end{aligned}$$

where  $N_t$  and  $N_e$  are the normalising constant and  $\lambda$ 's are measure of amount of admixtures of the ligand  $s$  and  $p$  orbitals with the central  $d$ -orbitals

Choice of ligand coordinate axes are such that their  $z$ -axes always point towards the metal atom. All the  $\sigma$ -bonds are described by using  $z$ -coordinates and  $\pi$ -bonds by using  $x$  and  $y$  coordinates.  $\pi_p$  orbitals are perpendicular to the plane formed by the central coordinate  $Y$  axis and the threefold symmetry axes of the point group  $T_d$  at the respective ligand. The direction cosines of  $\pi_{x_1}$ ,  $\pi_{y_1}$  and  $p\sigma_1$  with respect

to the central coordinate system (Fig. 1) are respectively  $\left( \frac{1}{\sqrt{6}}, \frac{1}{\sqrt{3}}, \frac{1}{\sqrt{6}} \right)$ ,  $\left( \frac{1}{\sqrt{2}}, 0, \frac{1}{\sqrt{2}} \right)$  and  $\left( -\frac{1}{\sqrt{3}}, -\frac{1}{\sqrt{3}}, -\frac{1}{\sqrt{3}} \right)$ . Direction cosines of  $\pi$ 's and

$\sigma$ 's for other ligand sites can be obtained from these by making  $180^\circ$  rotations about the cubic axes (i.e. axes of the central coordinate system).

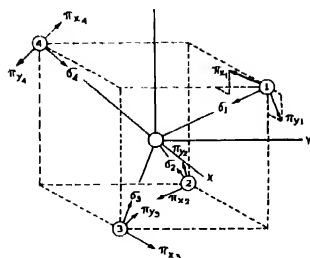


Fig. 1 Orientation of the Orbitals.

Further since both  $s$  and  $p$  orbitals can have  $\sigma$ -bonding with the metal atom, we can write

$$\lambda_o |\sigma_i\rangle = \lambda_{op} |p_{oi}\rangle + \lambda_{os} |s_i\rangle \quad \dots (2)$$

where

$$\lambda_{op}^2 + \lambda_{os}^2 = \lambda_o^2$$

Wavefunctions  $t_2$  and  $e$  in equation (1) can be expressed in a different form also, where  $x, y, z$  coordinate axes at the ligand sites are all parallel to  $X, Y, Z$  axes of the central coordinate system. This is

$$\begin{aligned} |XY\rangle = & N_d [d_{XY} + A\{|px1\rangle + |py1\rangle + |px2\rangle - |py2\rangle + (-|px3\rangle \\ & + |py3\rangle) + (-|px4\rangle - |py4\rangle)\} + B\{|pz1\rangle + |pz2\rangle + |pz3\rangle + |pz4\rangle\} \\ & + \frac{\lambda_{os}}{2} \{|s_1\rangle + |s_2\rangle - |s_3\rangle - |s_4\rangle\}] \quad \dots (3) \end{aligned}$$

$$\begin{aligned} |YZ\rangle = & N_d [d_{YZ} + A\{|py1\rangle + |pz1\rangle + (-|py2\rangle + |pz2\rangle) \\ & + (-|py3\rangle - |pz3\rangle) + |py4\rangle - |pz4\rangle\} \\ & + B\{|px1\rangle + |px2\rangle + |px3\rangle + |px4\rangle\} \\ & + \frac{\lambda_{os}}{2} \{|s_1\rangle + |s_2\rangle - |s_3\rangle - |s_4\rangle\}] \end{aligned}$$

$$\begin{aligned} |XZ\rangle = & N_d [d_{XZ} + A\{|px1\rangle + |pz1\rangle + (-|px2\rangle - |pz2\rangle) + (-|px3\rangle \\ & + |pz3\rangle) + |px4\rangle - |pz4\rangle\} \\ & + B\{|py1\rangle + |py2\rangle + |py3\rangle + |py4\rangle\} \\ & + \frac{\lambda_{os}}{2} \{|s_1\rangle + |s_2\rangle - |s_3\rangle - |s_4\rangle\}] \quad \dots (3) \end{aligned}$$

$$|X^2-Y^2\rangle = N_e \left[ d_{x^2-y^2} + \frac{\lambda\pi_c}{2\sqrt{2}} \{ (|px1\rangle - |py1\rangle) + (-|px2\rangle - |py2\rangle) \right. \\ \left. + (|px3\rangle + |py3\rangle) + (-|px4\rangle + |py4\rangle) \right]$$

where

$$A = \frac{1}{2\sqrt{3}} \left( -\lambda_{np} + \frac{\lambda\pi_t}{\sqrt{2}} \right) \\ B = \frac{1}{2\sqrt{3}} (-\lambda_{np} - \sqrt{2}\lambda\pi_t)$$

Here the notation of Stevens (1953) is followed in which, in each Ket vector the first letter denotes the type of orbit, the second angular dependence and the third the ligand to which it belongs

The new orbitals  $|pxi\rangle$ ,  $|pyi\rangle$  and  $|pzi\rangle$  can easily be related to the old ones  $\pi_{xi}$ ,  $\pi_{yi}$ ,  $p_{zi}$  with the help of usual transformation matrices utilising the direction cosines of  $\pi$ 's and  $\sigma$ 's.

#### CALCULATION OF REDUCTION FACTORS

##### (a) Orbital reduction factors :

There will be two orbital reduction factors occurring

- (i) between a manifold of  $t_2$  orbitals and
- (ii) between a  $t_2$  and  $e$  manifold.

We define them to be

$$\kappa = \langle t_2^+ | L_z | t_2^+ \rangle : \kappa' = -\frac{1}{2i} \langle X^2 - Y^2 | L_z | XY \rangle$$

where

$$t_2^+ = -\frac{i}{\sqrt{2}} [|XZ\rangle + i|YZ\rangle]$$

$$L_z = -i\hbar \left[ X \frac{\partial}{\partial Y} - Y \frac{\partial}{\partial X} \right] \quad \dots (4)$$

$L_z$  is expressed in the central coordinate system but while operating over ligand orbitals, has to be shifted to the ligand sites. Expressed in the new coordinate systems of the ligands (i.e. parallel to the central coordinate system),  $L_z$  is

$$\begin{array}{ll} L_z = l_z^{(1)} + ap_y^{(1)} - ap_x^{(1)} & \text{at ligand site } 1 \\ = l_z^{(2)} - ap_y^{(2)} - ap_x^{(2)} & \text{" " " } 2 \\ = l_z^{(3)} + ap_y^{(3)} + ap_x^{(3)} & \text{" " " } 3 \\ = l_z^{(4)} - ap_y^{(4)} + ap_x^{(4)} & \text{" " " } 4 \end{array}$$

where  $l_z^{(i)}$ ,  $p_x^{(i)} \left( = -i\hbar \frac{\partial}{\partial x} \right)$ ,  $p_y^{(i)} \left( = -i\hbar \frac{\partial}{\partial y} \right)$  are all expressed in the  $i$ -th

ligand new coordinate system and  $2a$  is the edge of the cube in which the tetrahedron is inscribed (Fig. 1).

(i) Substituting for  $t_2^+$  and operating with  $L_z$  we can deduce from eqns (4) and (3).

$$\begin{aligned}\kappa &= \langle t_2^+ | L_z | t_2^+ \rangle \\ &= N_t^2 \left[ 1 + 4A^2 - 4B^2 + 16AS_2 + 8BS_1 + 4\lambda_{os}S_3 + 4\frac{\sqrt{2}}{3} a\lambda_{os}S_4 \right]\end{aligned}$$

$$\begin{aligned}\text{where } S_1 &= \langle d_{xz} | py | \rangle = -\sqrt{\frac{2}{3}} \langle d_{xz} | \pi_{x1} \rangle = -\frac{1}{\sqrt{3}} \langle d_{xz} | p_{01} \rangle \\ &= -\sqrt{\frac{2}{3}} S_{t\pi} = \frac{1}{\sqrt{3}} S_{t\sigma p} \cdot S_{t\pi} = \langle d_{xz} | \pi_{x1} \rangle \text{ and } S_{t\sigma p} = \langle d_{xz} | p_{01} \rangle \\ S_2 &= \frac{1}{2} \{ \langle d_{xz} | px | \rangle + \langle d_{xz} | pz | \rangle \} = \frac{1}{\sqrt{6}} S_{t\pi} = \frac{1}{\sqrt{3}} S_{t\sigma p} \quad (5) \\ S_3 &= \langle d_{xz} | s_1 \rangle = S_{ts} \\ S_4 &= \left\langle s_1 \left| \frac{\partial}{\partial y} | py | \right. \right\rangle = \left\langle s_1 \left| \frac{\partial}{\partial x_1} | \pi_{x1} \right. \right\rangle\end{aligned}$$

$$\text{and } N_t^2 = [1 + \lambda_{\pi}^2 + \lambda_{\pi t}^2 + 4\lambda_{\sigma p}S_{t\sigma p} + 4\lambda_{\pi t}S_{t\pi} + 4\lambda_{os}S_{ts}]$$

In arriving at the result (5), it is found convenient to avoid the operation of the angular momentum operator  $L_z$  upon the ligand orbitals in the integrals of the form  $\langle \psi_d | L_z | \psi_{ligand} \rangle$  by utilizing the Hermitian nature of the integrals (Stevens 1953). The only non-vanishing integrals involving  $a$  are those which involve the overlap integral  $S_4$  also, the rest being monomials of order three and one, change sign with the inversion at the ligand sites and hence vanish. Further we have neglected the overlap between the two ligand orbitals at different sites.

Using eqn (5),  $\kappa$  can be expressed in the usual form as

$$\kappa = 1 - \frac{1}{2} \delta_1 \lambda_{\pi}^2 N_t^2$$

where

$$\delta_1 = \left[ 2 + \frac{3\lambda_{\pi t}^2}{\lambda_{\pi}^2} + \frac{2\sqrt{2}}{\lambda_{\pi}^2} \lambda_{\sigma p} \lambda_{\pi t} + \frac{8\sqrt{2}}{\sqrt{3}} \frac{a\lambda_{os}S_4}{\lambda_{\pi}^2} \right]$$

(ii) For  $\kappa'$ , we proceed in a similar way and obtain

$$\kappa' = \frac{1}{2i} \langle X^2 - Y^2 | L_z | XY \rangle$$

$$\begin{aligned}&= N_t' N_l [1 + \sqrt{2}A\lambda_{\pi o} + \sqrt{2}\lambda_{\pi o}(S_{1x}^2 + S_{1y}^2) + 8AS_2 + \sqrt{2}\lambda_{\sigma p}S_3 \\ &\quad + \sqrt{2}a\lambda_{\pi o}\lambda_{os}S_4] \quad \dots \quad (7)\end{aligned}$$

In the above equation, we define

$$S_{1x}^1 + S_{1y}^1 = \langle d_{x^2-y^2} | px - py | \rangle = \frac{1}{\sqrt{3}} (\sqrt{3} \langle d_{x^2-y^2} | \pi x_1 \rangle + \langle d_{x^2-y^2} | \pi y_1 \rangle) \quad \sqrt{2} S_{e\pi} \quad \dots \quad (8)$$

where

$$S_{e\pi} = \left\langle d_{x^2-y^2} \left| \sqrt{\frac{3}{2}} \pi_{x_1} + \pi_{y_1} \right. \right\rangle$$

and  $S_2$ ,  $S_3$  and  $S_4$  are same as in eqn. (5) and the normalising constant  $N_e^2$  is given by

$$N_e^2 = [1 + 4\lambda_{\pi e} S_{e\pi} + \lambda_{\pi e}^2]$$

and

$$N_t N_e \simeq [1 + 2\lambda_{\pi e} S_{e\pi} + \frac{2}{3} \sqrt{2} \lambda_{\sigma p} S_{t\pi} + \frac{4}{3} \lambda_{\sigma p} S_{t\sigma} + \frac{2}{3} \lambda_{\pi t} S_{t\pi} + \frac{2}{3} \sqrt{2} \lambda_{\pi t} S_{t\sigma} + 2\lambda_{\pi\sigma} S_{t\sigma} \quad \dots \quad (9)$$

$$\frac{1}{3} \lambda_{\pi e}^2 + \frac{1}{2} (\lambda_{\sigma p}^2 + \lambda_{\pi t}^2) + \frac{1}{2} \lambda_{\sigma t}$$

Using (9) and (7),  $\kappa'$  is again expressed in the form

$$\kappa' = 1 - \frac{1}{2} \lambda_{\sigma}^2 \delta_2 (N_t N_e) \quad \dots \quad (10)$$

where

$$\delta_2 = \left[ 1 + 2\sqrt{2}(\sqrt{2} - 1) \frac{\lambda_{\sigma t}}{\lambda_{\sigma}^2} S_{t\sigma} + \frac{\lambda_{\pi t}^2 + \lambda_{\pi\sigma}^2}{\lambda_{\sigma}^2} S_1 \right] \\ \sqrt{\frac{2}{3}} - \frac{\lambda_{\sigma p} \lambda_{\pi\sigma}}{\lambda_{\sigma}^2} - \frac{1}{\sqrt{3}} \left[ \frac{\lambda_{\pi t} \lambda_{\pi\sigma}}{\lambda_{\sigma}^2} + 2\sqrt{2} \frac{\lambda_{\pi\sigma} \lambda_{\sigma t}}{\lambda_{\sigma}^2} S_1 \right]$$

#### (b) Reduction factors for Spin-Orbit coupling

Here again since we are concerned mainly with the ligand atoms with smaller atomic numbers we confine to the approximation made by Owen (1955), originally for octahedral complexes, that the spin-orbit coupling is only effective at the central metal ion and so the reduction factors with  $\langle t_2^+ | \quad | t_2^1 \rangle$  and  $\langle t_2^+ | \quad | e \rangle$  manifold are, respectively

$$R_t = N_t^2 \quad \dots \quad (11) \\ R' = N_t N_e$$

## DISCUSSION

The expressions for reduction factors are quite complicated and involve a number of unknown parameters. However some qualitative results can be easily inferred if we stick to some approximations. Thus in above expressions terms involving  $a$  are small (since  $a$  itself is very small  $\approx 10^{-8}$  cm) and can be neglected. Furthermore the study in molecular bonding in the case of octahedral complexes has shown that usually  $\sigma$ -bonding is more important than  $\pi$ -bonding, in the case of tetrahedral complexes this is not very obvious. However lacking detailed information if for the present, this approximation is made (i.e. if we put  $\lambda_{\pi t} \approx \lambda_{\pi s} \approx 0$ ). Our expressions for  $\kappa$  and  $\kappa'$  reduce to

$$\kappa = 1 - \frac{1}{2} \delta_1 \lambda_o^2 N_t^2 \quad \dots (12)$$

where

$$\delta_1 = 2$$

$$N_t^2 = [1 + \lambda_o^2 + 4\lambda_{op}S_{top} + 4\lambda_{os}S_{tos}]^{-1}$$

and

$$\kappa' = 1 - \frac{1}{2} \delta_2 \lambda_o^2 (N_t N_s)$$

where

$$\delta_2 = \left[ 1 + 2\sqrt{2}(\sqrt{2}-1) \frac{\lambda_{os}}{\lambda_o^2} S_{tos} \right] \quad \dots (13)$$

$$N_t N_s = \left[ 1 + \frac{2\sqrt{2}}{3} \lambda_{op} S_{t\pi} + \frac{4}{3} \lambda_{op} S_{top} + 2\lambda_{os} S_{tos} + \frac{1}{2} \lambda_{op}^2 + \frac{1}{2} \lambda_{os}^2 \right]^{-1}$$

In the tetrahedral complexes of our concern quite often the ligands are either oxygen or chlorine type with  $2s$ ,  $2p$  or  $3s$ ,  $3p$  electrons respectively taking part in bonding. AM O, calculation of the energy spectrum in the case of  $\text{MnO}_4^-$  and  $\text{CrO}_4^{2-}$  complexes has been done by Wolfsberg and Helmholz (1952). They have made a further simplifying assumption that only  $2p$  electrons of oxygen take part in bonding and electrons filling upto  $2s$  orbits form a closed shell. Under this assumption (i.e.  $\lambda_{os} = 0$ ,  $\lambda_{op} = \lambda_o$ ) the equations are further simplified to

$$\delta_1 = 2 \quad \dots (14)$$

$$N_t^2 = [1 + \lambda_o^2 + 4\lambda_{op}S_{top}]^{-1}$$

$$\delta_2 = 1$$

$$N_t N_s = \left[ 1 + \frac{2\sqrt{2}}{3} \lambda_{op} S_{t\pi} + \frac{4}{3} \lambda_{op} S_{top} + \frac{1}{2} \lambda_{op}^2 \right]^{-1} \quad \dots (15)$$

Using the parameters mainly obtained from intensity consideration (Wolfsberg, Helmholz, 1952; Ballhausen and Liehr, 1958; Viste and Gray, 1964)

$$S_{t\pi} = \frac{3 \times .151}{2\sqrt{2} \times 4} ; S_{top} = -\frac{\sqrt{3} \times .167}{2 \times 4} ; \lambda_{os} \approx \lambda_{op} \approx \frac{1}{\sqrt{2}}$$

(Table I) for  $\text{MnO}_4^-$ , we have  $\kappa = .533$ ,  $\kappa' = .678$  and  $R = .476$ ,  $R' = .641$ .



TABLE I

Salt	$\kappa$	$\kappa'$	R	R'	Values of parameters	References
$\text{MnO}_4^-$	.533	.678	.476	.641 (for $\lambda_{\sigma^2}=0$ )	$S_{\sigma^2} = \frac{3 \times 151}{2 \sqrt{2} \times 4}$	Wolfsberg and Helmholz, 1952
					$S_{\sigma^2 p} = -\frac{\sqrt{3} \times 167}{2 \times 4}$	
				.676 (for $\lambda_{\sigma^2}=\lambda_{\sigma p}$ )	$S_{\sigma^2 s} = \frac{246 \times \sqrt{3}}{2 \times 4}$	Ballhausen and Liehr, 1958.
					$\lambda_{\sigma^2} = -\sqrt{(1-\alpha^2)/\alpha} \cdot \alpha = -\frac{1}{\sqrt{2}}$	
$\text{CrO}_4^{2-}$	.551	.693	.691	.633	$\lambda_{\sigma^2 s} = \lambda_{\sigma p} = -\frac{1}{\sqrt{2}}$	Viste and Gray, 1964.
					$S_{\sigma^2 p} = (11 \times \sqrt{3})/(2 \times 4)$	
					$S_{\sigma^2} = (18 \times \sqrt{3})/2 \sqrt{2} \times 4$	Wolfsberg and Helmholz, 1952 Ballhausen and Liehr, 1958
					$\lambda_{\sigma^2} = \lambda_{\sigma p} = -1$	
$\text{Co}^{++}$ in KCl	.799	.891	.775	.877	$\alpha = 1/\sqrt{2}$	Washimiya, 1963
					$S_{\sigma^2 p} = -8.59 \times 10^{-2}/4$	
					$S_{\sigma^2} = 2.25 \times 10^{-2}/4$	Ballhausen and Liehr, 1958
					$\lambda_{\sigma^2} = -0.5$	
$\text{CoCl}_3\text{Cl}_5$	.419	.563	.380	.584	$S_{\sigma^2 p} = -.0947/4$	Washimiya, 1963.
					$S_{\sigma^2} = \text{same as Co}^{++}$ in KCl	
					$\lambda_{\sigma^2} = \lambda_{\sigma p} = \frac{\sqrt{1-\alpha^2}}{\alpha}$	
					$= -1.224$	
					$\therefore \alpha = \sqrt{\frac{4}{10}}$	

Ballhausen and Liehr (1958), however pointed out a serious mistake in the assignment of bands made by Wolfsberg and Helmholz (1952) for  $\text{MnO}_4^-$  and they further undertook more investigation considering also the 2s orbitals as taking part in bonding (i.e.  $\lambda_{ss} \neq 0$ ). If we utilize this parameter, we have for  $\text{MnO}_4^-$

$$\kappa = .502, \kappa' = .678, R = .512 \text{ and } R' = .676 \text{ (Table I)}$$

Thus we see that whatever be the effect on band energy calculation of the approximation that 2s and 3s orbitals do not take part in bonding, for the calculation of reduction factors it is a fairly good approximation.

Results of calculations for several tetrahedral complexes are summed up in Table I.

Our reduction parameters for  $\text{CoCl}_3\text{Cl}_6$  derived semiempirically from susceptibility measurement are  $\kappa' = .92$  and  $R' = .83$  which are appreciably different from the present values  $\kappa' = .653$  and  $R' = .584$  (Table I). The discrepancy may be due to the fact that in tetrahedral complexes  $\pi$ -bonding also play an equally important role as  $\sigma$ -bonding. This is actually so is definitely proved for the cases of  $\text{MnO}_4^-$  and  $\text{CrO}_4^{2-}$  by Wolfsberg and Helmholz (1952). For the present, however, we cannot go to further details due to the insufficient knowledge about the parameters needed.

#### ACKNOWLEDGEMENT

Authors are grateful to Professor A. Bose, D.Sc., F.N.I., for suggesting the problem and kind interest in the work. They are also thankful to Dr M. Chowdhury for helpful discussions. One of us (R. K. M) is also grateful to the authorities of the Patna University for granting him the study leave to work here.

#### REFERENCES

- Ballhausen, C. J. and Liehr, A. D., 1958, *J. Mol. Spect.* **2**, 342.
- , 1960, *G. Mol. Spect.* **4**, 100.
- Owen, J., 1955, *Proc. Roy. Soc.* **A227**, 183.
- Stevens, K. W. H., 1953, *Proc. Roy. Soc.* **A219**, 542.
- Tinkham, M., 1956, *Proc. Roy. Soc.* **A236**, 549.
- Van Vleck, J. H., 1932, *Phys. Rev.* **41**, 208.
- , 1935, *J. Chem. Phys.* **3**, 807.
- Visto, A. and Gray, H. B., 1964, *Inorganic Chemistry* **3**, 1113.
- Washimura, S., 1963, *J. Phys. Soc. Japan*, **18**, 1719.
- Wolfsberg, M. and Helmholz, L., 1952, *J. Chem. Phys.* **20**, 837.

# DYNAMICS OF THE EXTENSIONAL VIBRATION OF A FREE-FREE BAR

S. K. GHOSH AND SUNIL KUMAR BANERJEE

DEPARTMENT OF PHYSICS, JADAVPUR, UNIVERSITY CALCUTTA-32

(Received August 11, 1965)

**ABSTRACT.** The paper discusses the Dynamics of Vibration of a Free-Free Bar excited by an inelastic longitudinal Impact, taking account of the Inertia of Lateral Motion. The problem is worked out using the powerful Operational method. Unlike other theories, this method is free from any assumption, and gives results of higher accuracy. The present problem gives the extension and pressure at the struck-end as functions of time, the other end of the rod being free.

In Section I the nature of vibration and displacement of the struck-end is discussed and in Section II the pressure at the struck-end at different epoch is found out as functions of time.

## INTRODUCTION

The expression for pressure and displacement at the struck-end of a thin rod hammered by elastic load with different end conditions has been worked out by Ghosh (1951). But the present paper proposes to consider all the above phenomena taking account of inertia of lateral motion in the case of a thin rod hammered by an inelastic load at one end the other end remaining free. The equation of motion in such a case is given by,

$$\rho \left( \frac{d^2 \omega}{dt^2} - \sigma^2 k^2 \frac{d^4 \omega}{ds^2 dt^2} \right) = E \left( \frac{d^2 \omega}{ds^2} \right) \quad \dots (1)$$

The second term of the L.H.S. of (1) i.e.  $\rho \sigma^2 k^2 \frac{d^4 \omega}{ds^2 dt^2}$  is due to the Inertia of lateral motion and is the most general equation of vibration of a thin rod. An important contribution due to the second term is that it gives the velocity of wave propagation in the rod with higher accuracy.

*Explanation of the symbols used :*

$E$  = Modulus of elasticity of the bar.

$\sigma$  = Poisson's ratio.

$\gamma$  = Area of cross-section of the bar.

$k$  = Radius of Gyration of a cross-section of the rod about its central line.

$\omega$  = Displacement of any section at any time.

$t$  = Variable time.

$l$  = Length of the rod used.

$s$  = Distance of the particle on the central line from the free-end.

$\rho$  = Volume density of the rod.

$\rho_0$  = Linear density of the rod.

$\omega_l$  = Displacement of a particle at the struck-end.

$m$  = Mass of the load.

$c$  = Velocity of longitudinal wave along the rod.

$t_n = t - n\theta$ , where  $n = 1, 2, 3$ , etc.

$\theta$  = Period of free vibration of the bar.  $= 2l/c$

$v_0$  = velocity of impact.

$J$  = Momentum of impact  $= mv_0$

$P$  = Pressure exerted by the load.

$D$  = Operator  $\frac{d}{dt}$ ,  $\eta = \frac{\sigma^2 k^2}{c^2}$

The differential equation (1) for the extensional vibration of the rod is solved by using operational method of Heaviside instead of using St. Venant's 'Variational method' which is long and laborious.

Now Equation (1) in the operational notations,

$$\frac{d^2 \omega}{ds^2} = \frac{D^2(1+\eta D^2)^{-1}}{c^2} \cdot \omega \quad \dots (1.1)$$

The solution of this equation is given by.

$$\omega = A \cosh \frac{D(1+\eta D^2)^{-1}}{c} s + B \sinh \frac{D(1+\eta D^2)^{-1}}{c} s \quad \dots (2)$$

The end-conditions are at  $s = 0$ ,

$$\frac{d\omega}{ds} = 0 \quad \dots (3.1)$$

and

$$\text{at } s = l, \quad \omega = \omega_l \quad \dots (3.2)$$

From (2), (3.1) and (3.2),

$$\omega = \omega_l \frac{\cosh \frac{D(1+\eta D^2)^{-1}}{c} \cdot s}{\cosh \frac{D(1+\eta D^2)^{-1}}{c} \cdot l} \quad \dots (4)$$

The equation of motion for the striking body is,

$$m \frac{d^2 \omega_l}{dt^2} = -\gamma E \left( \frac{d\omega}{ds} \right)_{s=l} \quad \dots (5)$$

Now substituting the values of  $(d\omega/ds)_{s=l}$  in (5) and imposing the boundary condition, the motion being started by impulse  $J$ , we get

$$mD^2 + \frac{E\gamma}{c} D(1+\eta D^2)^{-1} \tanh \frac{D(1+\eta D^2)^{-1}}{c} \cdot l = DJ \quad \dots (6)$$

The Pressure exerted by the load is,

$$P = m \frac{d^2 \omega_l}{dt^2} \quad \dots (7)$$

From (4), (5) and (7) the expression for  $P$  is,

$$P = - \frac{E\gamma}{c} \omega_l D(1+\eta D^2)^{-\frac{1}{2}} \tanh \frac{D(1+\eta D^2)^{-\frac{1}{2}}}{c} \cdot l \quad \dots (8)$$

$$= - \frac{E\gamma}{c} (1+\eta D^2)^{-\frac{1}{2}} \tanh \frac{D(1+\eta D^2)^{-\frac{1}{2}}}{c} \cdot l \cdot \omega_l \quad \dots (9)$$

Now putting  $m v_0$  for  $J$  in (6) it is found that,

$$\omega_l = \frac{1}{F(D)} \cdot v_0 \quad \dots (10)$$

where,

$$F(D) = D + \frac{E\gamma}{mc} (1+\eta D^2)^{-\frac{1}{2}} \tanh \frac{D(1+\eta D^2)^{-\frac{1}{2}}}{c} \cdot l \quad \dots (11)$$

On substituting the exponential values for hyperbolic tangents in equation (11), neglecting terms containing  $\eta^2$  ( $\eta$  being very small) in the binomial expansion of  $(1+\eta D^2)^{-\frac{1}{2}}$  and writing  $D_1 = D+\alpha$ ,  $D_2 = D+\beta$  we have the final form  $F(D)$  to be,

$$F(D) = \frac{D_1 D_2}{(\alpha+\beta)[1+\exp\{-D(1-\frac{1}{2}\eta D^2)\theta\}]} \times \left[ 1 - \frac{(D-\alpha)(D-\beta)}{D_1 D_2} \exp \left\{ -D \left( 1 - \frac{1}{2} \eta D^2 \right) \theta \right\} \right] \quad \dots (12)$$

$$\text{where, } D_1 D_2 \equiv (D+\alpha)(D+\beta) \equiv D^2 - \frac{2mc}{\gamma E \eta} D - \frac{2}{\eta} \quad \dots (13)$$

$$\text{and } -\alpha, -\beta \text{ are the roots of, } D^2 - \frac{2mc}{\gamma E \eta} D - \frac{2}{\eta} = 0 \quad \dots (14)$$

given by,

$$[\alpha, \beta] = -\frac{1}{2} \left[ \frac{2mc}{\gamma E \eta} \mp \left( \frac{4m^2 c^2}{\gamma^2 E^2 \eta^2} + \frac{8}{\eta} \right)^{\frac{1}{2}} \right] \quad \dots (15)$$

Expanding terms under the radical sign binomially and neglecting higher powers of  $\eta$  other than the first we have from (15),

$$[\alpha, \beta] = \frac{E\gamma}{mc}, -\frac{mc}{\gamma E \eta} \left( 2 + \frac{\gamma^2 E^2 \eta}{m^2 c^2} \right) \quad \dots (16)$$

$$= \frac{\rho_0 c}{m} = \frac{mc}{\rho_0 \sigma^2 k^2} \left( 2 + \frac{\sigma^2 k^2 \rho_0^2}{m^2} \right) \quad \dots \quad (16.a)$$

where,

$$E = \rho c^2, \quad \rho_0 = \rho \gamma, \quad \eta = \frac{\sigma^2 k^2}{c^2}.$$

#### DISPLACEMENT AT THE IMPACT-END

The displacement at the impact-end can now be obtained by the help of equations (10) and (12) as follows :

$$\begin{aligned} v_1 &= \frac{(\alpha + \beta)[1 + \exp\{-D(1 - \frac{1}{2}\eta D^2)\theta\}]}{D_1 D_2} \\ &\times \left[ 1 - \frac{(D - \alpha)(D - \beta)}{D_1 D_2} \exp \left\{ -D \left( 1 - \frac{1}{2}\eta D^2 \right) \theta \right\} \right]^{-1} \cdot v_0 \\ &= \left[ \frac{(\alpha + \beta)}{D_1 D_2} - \left\{ \frac{2(\alpha + \beta)^2 D}{D_1^2 D_2^2} - \frac{2(\alpha + \beta)}{D_1 D_2} \right\} \exp \left\{ -D \left( 1 - \frac{1}{2}\eta D^2 \right) \theta \right\} \right] \\ &+ \left\{ \frac{4(\alpha + \beta)^3 D^2}{D_1^3 D_2^3} - \frac{6(\alpha + \beta)^2 D}{D_1^2 D_2^2} + \frac{2(\alpha + \beta)}{D_1 D_2} \right\} \exp \left\{ -2D \left( 1 - \frac{1}{2}\eta D^2 \right) \theta \right\} \\ &- \left\{ \frac{8(\alpha + \beta)^4 D^3}{D_1^4 D_2^4} - \frac{16(\alpha + \beta)^3 D^2}{D_1^3 D_2^3} + \frac{10(\alpha + \beta)^2 D}{D_1^2 D_2^2} - \frac{2(\alpha + \beta)}{D_1 D_2} \right\} \\ &+ \dots \dots \dots \exp \left\{ -3D \left( 1 - \frac{1}{2}\eta D^2 \right) \theta \right\} \\ &+ (-1)^{n-1} \left\{ \frac{2^n (\alpha + \beta)^{n+1} D^n}{D_1^{n+1} D_2^{n+1}} - \dots - \frac{2(\alpha + \beta)}{D_1 D_2} \right\} \\ &\exp \left\{ -nD \left( 1 - \frac{1}{2}\eta D^2 \right) \theta \right\} + \dots \dots \dots \quad (17) \end{aligned}$$

$$\eta \text{ being } = \frac{\sigma^2 k^2}{c^2}$$

Now writing,

$$f_1(t) = \frac{(\alpha + \beta)}{D_1 D_2} v_0 \quad \dots \quad (17.1)$$

$$f_2(t) = \frac{(\alpha + \beta)^2 D}{D_1^2 D_2^2} \cdot v_0 \quad \dots \quad (17.2)$$

$$f_3(t) = \frac{(\alpha + \beta)^3 D^2}{D_1^3 D_2^3} v_0 \quad \dots \quad (17.3)$$

and so on,

$$f_n(t) = \frac{(\alpha + \frac{1}{2} \eta D)^n D^{n-1}}{D_1^n D_2^n} v_0 \quad (17.4)$$

we get,

$$\begin{aligned} \omega_1 = & [f_1(t) - \{2f_2(t) - 2f_1(t)\} \exp \{ - D(1 - \frac{1}{2} \eta D^2) \theta \} \\ & + \{4f_3(t) - 6f_2(t) + 2f_1(t)\} \exp \{ - 2D(1 - \frac{1}{2} \eta D^2) \theta \} \\ & - \{8f_4(t) - 16f_3(t) + 10f_2(t) - 2f_1(t)\} \exp \{ - 3D(1 - \frac{1}{2} \eta D^2) \theta \} + \dots \\ & + \{2f_1(t) - (4n-2)f_2(t) + (2n-2)^2 f_3(t) - \dots + (-1)^{n-2} f_{n-1}(t)\} \\ & \exp \{ - nD(1 - \frac{1}{2} \eta D^2) \theta \} - \dots ] \quad \dots \quad (18) \end{aligned}$$

Now since,

$$\begin{aligned} \exp \{ - nD(1 - \frac{1}{2} \eta D^2) \theta \} f_n(t) = f_n(t - n\theta) + \frac{1}{2} n \theta \eta f_n''(t - n\theta) \\ f_n(t_n) + \frac{1}{2} n \theta \eta f_n''(t_n) \quad \dots \quad (18.1) \end{aligned}$$

Therefore,

$$\begin{aligned} \omega_1 = & [f_1(t) - \{2f_2(t_1) - 2f_1(t_1)\} + \{4f_3(t_2) - f_2(t_2) + 2f_1(t_2)\} \\ & - \{8f_4(t_3) - 16f_3(t_1) + 10f_2(t_3) - 2f_1(t_3)\} + \dots \\ & + \{2f_1(t_n) - (4n-2)f_2(t_n) + (2n-2)^2 f_3(t_n) - \dots + (-1)^{n-2} f_{n-1}(t_n)\} + \dots \\ & - \frac{1}{2} \theta \eta \{2f_2''(t_1) - 2f_1''(t_1)\} - \frac{5}{2} \theta \eta \{4f_3''(t_2) - 6f_2''(t_2) + 2f_1''(t_2)\} \\ & - \frac{5}{2} \theta \eta \{8f_4''(t_3) - 16f_3''(t_3) + 10f_2''(t_3) - 2f_1''(t_3)\} + \dots \\ & + \frac{1}{2} n \theta \eta \{2f_1''(t_n) - (4n-2)f_2''(t_n) + (2n-2)^2 f_3''(t_n) - \dots \\ & + (-1)^{n-2} f_{n-1}''(t_n)\} + \dots] \quad \dots \quad (19) \end{aligned}$$

Now the functions  $f_1(t)$ ,  $f_2(t)$  etc. can be obtained as follows.

$$f_1(t) = v_0 A \left[ \frac{1}{\alpha} (1-e)^{-\alpha t} - \frac{1}{\beta} (1-e^{-\beta t}) \right] \quad \dots \quad (19.1)$$

$$f_2(t) = v_0 A^2 \left[ \frac{1}{\alpha} (1-A+\alpha t)e^{-\alpha t} + \frac{1}{\beta} (1+A+\beta t)e^{-\beta t} \right] \quad \dots \quad (19.2)$$

$$f_3(t) = v_0 A^3 \left[ \frac{1}{\alpha} \left\{ \frac{3}{2} (A - A^2) + \frac{1}{2} (3A - 1) \alpha t - \frac{\alpha^2 t^2}{2!} \right\} e^{-\alpha t} \right. \\ \left. + \frac{1}{\beta} \left\{ \frac{3}{2} (A + A^2) + \frac{1}{2} (3A + 1) \beta t + \frac{\beta^2 t^2}{2!} \right\} e^{-\beta t} \right] \quad \dots \quad (19.3)$$

etc.,

$$f_n(t) = v_0 A^n \left[ \sum_{r=1}^n (-1)^{r-1} \frac{\Gamma(n+r-1)}{\Gamma(n) \Gamma(r)} B^{r-1} e^{-\alpha t} (D - \alpha)^{n-2} \frac{t^{n-r}}{(n-r)!} \right. \\ \left. + (-1)^n \sum_{r=1}^n \frac{\Gamma(n+r-1)}{\Gamma(n) \Gamma(r)} B^{r-1} e^{-\beta t} (D - \beta)^{n-2} \frac{t^{n-r}}{(n-r)!} \right] \quad \dots \quad (19.4)$$

and so on, where,  $A = (\beta + \alpha)/(\beta - \alpha)$ ,  $B = 1/(\beta - \alpha)$

If we now neglect the term containing the inertia of lateral motion in equation (1) i.e., if,  $\eta = 0$  we must have  $A = 1$ , and  $B = 0$ .

and,

$$f_1(t) = \frac{v_0}{\alpha} (1 - e^{-\alpha t}) = \frac{mv_0}{\rho_0 c} \left( 1 - e^{-\frac{\rho_0 c}{m} t} \right) \quad \dots \quad (19.1a)$$

$$f_2(t) = \frac{v_0}{\alpha} \cdot \alpha t \cdot e^{-\alpha t} = \frac{mv_0}{\rho_0 c} \cdot \frac{\rho_0 c}{m} t e^{-\frac{\rho_0 c}{m} t} \quad \dots \quad (19.2a)$$

$$f_3(t) = \frac{v_0}{\alpha} e^{-\alpha t} \left\{ \alpha t - \frac{\alpha^2 t^2}{2!} \right\} = \frac{mv_0}{\rho_0 c} \left\{ \frac{\rho_0 c}{m} t - \frac{\rho_0^2 c^2}{2m^2} t^2 \right\} e^{-\frac{\rho_0 c}{m} t} \quad \dots \quad (19.3a)$$

and so on. These results of  $f_1(t)$ ,  $f_2(t)$  etc. are found similar to those obtained by Ghosh (1953).

Thus the displacement at the impact-end at any interval of time can be found as a function of time substituting all the values of  $f_1(t)$ ,  $f_2(t)$ , etc. in the above equation (19).

During the interval,  $0 < t < \theta$ ,

$$\omega_I = f_1(t) \quad \dots \quad (19.A)$$

After time  $t = \theta$ , i.e. during,  $\theta < t < 2\theta$ ,

$$\omega_I = f_1(t) - 2\{f_2(t_1) - f_1(t_1)\} + \frac{\theta}{2} \eta \{2f_1''(t_1) - 2f_2''(t_1)\} \quad \dots \quad (19.B)$$



Similarly during,  $2\theta < t < 3\theta$ ,

$$\begin{aligned} \omega_t = & f_1(t) + \{2f_1(t_1) - 2f_2(t_1)\} + \{2f_1(t_2) - 6f_2(t_2) + 4f_3(t_2)\} \\ & + \frac{1}{2} \theta \eta \{2f_1''(t_1) - 2f_2''(t_1)\} \\ & + \frac{2}{3} \theta \eta \{2f_3''(t_2) - 6f_2''(t_2) + 4f_4''(t_2)\} \quad \dots \quad (19C) \end{aligned}$$

and so on.

Equation (19) gives the most general form of displacement at the struck end of the rod. It is found that terms of the right hand side of (19) contain certain number of terms to be positive and some of them to be negative. By a negative term it is understood that waves formed are reflected from the respective ends of the rod. The displacement equation (19) of the struck-end is obtained in the functional form. By putting the functional values of  $f_1(t)$   $f_2(t)$  etc. in (19) the displacement is obtained in terms of known quantities. The pressure at the struck-end is discussed in Section II.

Further, the displacement equation shows, that the wave train does not return after reflection, as shown by the second term of equation (21) below.

*Pressure at the struck end*

The Pressure exerted by the load at the impact end can now be found out taking the help of equation (9) and equation (19) as follows :

$$P = -\frac{E\gamma}{C} (1 + \eta D^2)^{-1/2} \tanh \frac{D(1 + \eta D^2)^{-1/2} \cdot l}{c} \cdot \omega_t'$$

Expanding  $(1 + \eta D^2)^{-1/2}$  binomially as before, neglecting higher powers of  $\eta$  and writing exponential values for hyperbolic tangent the pressure equation becomes,

$$\begin{aligned} P = & -\frac{E\gamma}{C} (1 - \frac{1}{2}\eta D^2) [1 - 2e^{-D(1 - \frac{1}{2}\eta D^2)\theta} - 2e^{-3D(1 - \frac{1}{2}\eta D^2)\theta} \\ & - 2e^{-3D(1 - \frac{1}{2}\eta D^2)\theta} + 2e^{-4D(1 - \frac{1}{2}\eta D^2)\theta} \\ & - \dots \dots + \dots \dots ] \omega_t' \quad \dots \quad (20) \end{aligned}$$

From Equations (19) and (20) the numerical value of pressure at the struck-end can be written as,

$$\begin{aligned} P = \frac{\gamma E}{C} [ & f_1'(t) - 2f_2'(t_1) - \frac{1}{2} \eta \{f_1''(t) - 2f_2''(t_1)\} \\ & + \{4f_3'(t_2) - 2f_2'(t_2)\} - \frac{1}{2} \eta \{4f_3''(t_2) - 2f_2''(t_2)\} \\ & + \eta \{4f_3^{IV}(t_2) - 2f_2^{IV}(t_2) - f_2^{IV}(t_1)\} + \dots ] \quad \dots \quad (21) \end{aligned}$$

Thus during the interval,  $0 < t < \theta$  the pressure is

$$P_1 = \frac{E\gamma}{C} \left[ f_1'(t) - \frac{1}{2} \eta f_1''(t) \right] \quad \dots \quad (21.1)$$

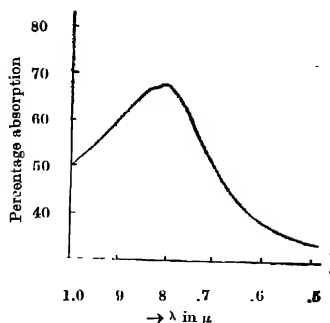


Fig. 1 Absorption curve— $\text{K}_2\text{SO}_4$  (CuZn)  $6\text{H}_2\text{O}$  Crystal.

### DISCUSSIONS

#### a) Crystal field parameters and energy levels

Following Abragam and Pryce (1951) the potential of an electron placed at the point  $(x, y, z)$  in the neighbourhood  $\text{Cu}^{+1}$  ion may be represented by

$$V(x, y, z) = K \left( x^4 + y^4 + z^4 - \frac{3}{5} r^4 \right) + A(3z^2 - r^2) + Q \left[ \frac{5}{2} \left( x^4 + y^4 + z^4 - \frac{3}{5} r^4 \right) - 3(x^2 + y^2 - 6x^2y^2) \right]$$

The stark levels of the ground state of  $\text{Cu}^{+1}$  ion are (Mookherji et al., 1965) taking the lowest as zero,

$$F_5 = 10K - 6A - Q$$

$$F_4 = 10K - 7Q$$

$$F_1 = 0$$

where  $K = \frac{2}{105} K' r^2$ ,  $A = \frac{1}{7} A' r^2$ ,  $Q = \frac{20}{105} Q' r^4$   $\bar{r}$  is the average radial distance

of the 3d electrons,  $K$  is the cubic field coefficient and  $A$  and  $Q$  are those for tetragonal field.

Banerji and Mookherji (1965) have treated  $\text{Cu}^{++}$  ion under a crystal field of above symmetry using Elliot and Stevens method. The field parameters which gave the best fit with the observed values of temperature variation of Bose *et al* (1957) are

$$K = +1460 \text{ cm}^{-1}, Q = -11 \text{ cm}^{-1} \text{ and } A = -90 \text{ cm}^{-1}$$

and hence the energy levels are 0, 14677 and 15151  $\text{cm}^{-1}$

b) *Isotropic Covalency Factor*

In crystalline electric field theory the surrounding ions are considered as point charges or point dipoles; but this will not be exactly true for ions of the iron group as  $d$ -wave functions overlap to some extent with the wave functions of the surrounding ligands. Owen (1955) took account of this effect of partial overlap of 3d-orbitals with  $\sigma$ - and  $\pi$ -orbitals of the surrounding ligands and came to the conclusion that the orbital contribution to magnetic moment is reduced by a factor  $f^2$  called as covalency factor. Hence the stark splitting  $(\Delta E)_m$  deduced from magnetic data will be inclusive of this factor. The stark splitting  $(\Delta E)_0$  as observed from optical absorption data will be then given by  $f^2 = (\Delta E)_0 / (\Delta E)_m$

Representing the overlap factor along the axis of symmetry of the water cluster about  $\text{Cu}^{++}$  ion by  $f_{\parallel}^2$  and that normal to it by  $f_{\perp}^2$  we have

$$f_{\parallel}^2 = \frac{(F_4 - F_3)_0}{(F_4 - F_3)} \quad \text{and} \quad f_{\perp}^2 = \frac{(F_5 - F_3)_0}{(F_5 - F_3)}$$

Using the observed values of  $(F_5 - F_3)_0$  and  $(F_4 - F_3)_0$  and the deduced values of  $(F_5 - F_3)$  and  $(F_4 - F_3)$  we get  $f_{\parallel}^2 = 0.869$  and  $f_{\perp}^2 = 0.868$ . Hence one may take the covalency factor to be almost isotropic and equal to 0.87.

c) *Anisotropy of the water cluster about  $\text{Cu}^{++}$  ion*

Following Bose *et al* (1957) the magnetic anisotropy of  $\text{Cu}^{++}$  ion under a field of symmetry as given by equation (1) is

$$K_{\parallel} - K_{\perp} = \frac{2N\beta^2}{kT} (\lambda + kT) D f^2$$

where  $D = \left( \frac{4}{F_5 - F_3} - \frac{1}{F_4 - F_3} \right)$ ,  $K_{\parallel}$  is the ionic susceptibility along the axis of symmetry of the water cluster about  $\text{Cu}^{++}$  ion and  $K_{\perp}$  that normal to it.

Utilising our observed values of  $(F_5 - F_3)$ ,  $(F_4 - F_3)$  and  $f^2$  we get  $K_{\parallel} - K_{\perp} = 565$  as against 569 at 300°K observed by Mookherji and Lal (1965). This may be compared with the value 572 as deduced from optical absorption in state of solution. Thus it may be concluded that the anisotropy of the water cluster about  $\text{Cu}^{++}$  ion in crystal and in state of solution is almost the same in conformity with our earlier discussion.

d) Spectroscopic splitting factor for directions along and normal to the tetragonal axis of the water cluster surrounding the  $\text{Cu}^{++}$  ion according to Abragam and Pryce (1951) are

$$g_{\parallel} = 2 - \frac{8\lambda f^2}{F_4 - F_3} \quad \text{and} \quad g_{\perp} = \left( 2 + \frac{2\lambda f^2}{F_5 - F_3} \right)$$

using the observed values of  $f^2$ ,  $F_4 - F_2$  and  $F_6 - F_2$  we get  $g_{\parallel} = 2.48$  and  $g_{\perp} = 2.12$ . These may be compared with those (2.45 and 2.05) obtained by paramagnetic resonance for  $\text{CuK}_2(\text{SO}_4)_2 \cdot 6\text{H}_2\text{O}$ .

It may be mentioned here that experimental  $g_{\parallel}$  value gives  $F_4 - F_2 = 14720 \text{ cm}^{-1}$  agreeing with that deduced from susceptibility measurement, but experimental  $g_{\perp}$  value gives  $F_6 - F_2$  more than double as that deduced from susceptibility data.

#### REFERENCES

- Abragam, Q. and Pryce, M. H. L., 1951, *Proc. Roy. Soc.*, **A206**, 165.  
 Bagguley, D. M. S. and Griffiths, J. H. E., 1962, *Proc. Phys. Soc.*, **A265**, 594.  
 Boro, A., Mitra, S. C. and Datta, S. K., 1957, *Proc. Roy. Soc.*, **A239**, 165.  
 Mookherji, A. and Banerji, S., 1965, *Indian J. Phys.*, **39**, 530.  
 Mookherji, A. and Chhonkar, N. S., 1959, *Indian J. Phys.*, **33**, 74.  
 ————, ————, 1960, *Indian J. Phys.*, **34**, 363.  
 ————, ————, 1961, *Indian J. Phys.*, **35**, 437.  
 ————, ————, 1963, *Indian J. Phys.*, **37**, 375.  
 Mookherji, A. and Lal, R. B., 1965, *Ind. J. Pure Appl. & Phys.*, **3**, 288.  
 Owen, J., 1955, *Proc. Roy. Soc.*, **A227**, 183.

## Letters to the Editor

*The Board of Editors does not hold itself responsible for opinions expressed in the letters published in this section. The notes containing short reports of original investigations communicated to this section should not contain many figures and should not exceed 500 words in length. The contributions reaching the Secretary by the 15th of any month may be expected to appear in the issue for the next month. No proof will be sent to the author.*

### 4

## SOME PROBE DATA OF DUOPLASMATRON PLASMA

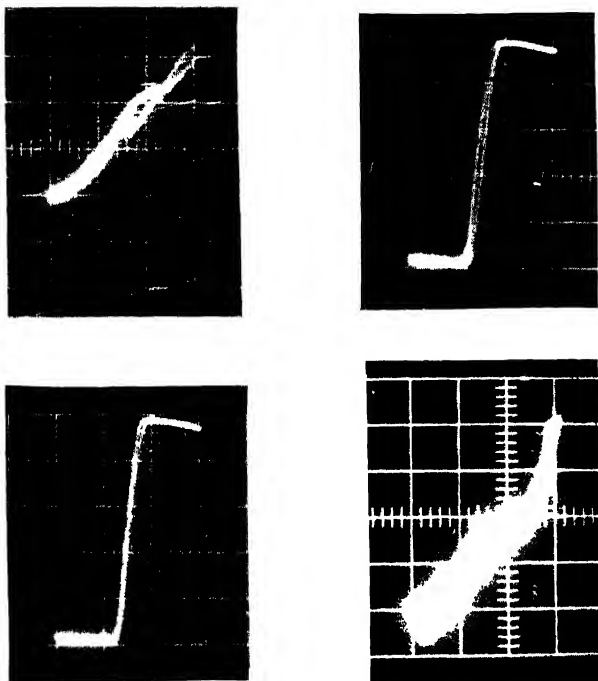
D. K. BOSE, N. K. MAJUMDAR AND S. N. SENGUPTA

Saha Institute of Nuclear Physics, CALCUTTA, INDIA

(Received January 17, 1966)

The high performance of the duoplasmatron source is due to the mechanical and magnetic constraints (Burton, 1961). The magnetic field set in the interspace, intermediate electrode to anode, is so shaped that a magnetic mirror has been supposed to exist in this space (Burton, 1961, Mbak *et al.* 1959) and under that circumstance, electrons have little chance of escape from this region excepting along the axis of the system. The experimental investigation of Popov (1961) on the distribution of magnetic field in this space actually confirms this view. A Langmuir probe (length  $\approx \frac{1}{2}$  mm, diameter = 0.06 mm) has been placed at the mouth of the anode orifice of our duoplasmatron source (Bose, *et al.* 1965) to study the effect of magnetic field on the plasma state in this region under different operating conditions. The probe is operated by electrical pulses (Sengupta). The rising part of triangular pulses was used for the horizontal sweep of an oscilloscope and the other arm was blanked off. Sweep duration was 1/60-th of a second and magnitude was 25 volts. Current voltage characteristics of the probe were recorded by photographs of the oscilloscope traces. The effect of the magnetic field is borne out by these photographs. A stable well developed plasma (Figs. b, c) characterised by absence of any substantial potential gradient and a regular Maxwell-Boltzmann distribution is formed at high arc voltage ( $\approx 150$  V) with the setting of the magnetic field in the interspace. If we consider that trapped electrons enhance the rates of ionisation (Popov, 1961) the mirror action should be noticeable by the setting of a stable plasma tip and hence the role of magnetic field is revealed in the sequence of these photographs (Figs. a, b, c). The electron temperatures have been determined for high arc voltage patterns (the semi-log plots show distinct uniform

slopes) Increase of magnetic field has been accompanied by increase of  $T_e$  signifying increased collisions processes due to the trapped electrons. At low are



Figs. (a, b, c, d). Examples of oscilloscope records of the current-voltage characteristics as obtained by the pulsed probe technique. Each small division of the abscissa represents 1.7 volts and that of the ordinate represents  $37\mu$  A current. (Details of the photos are given in table 1). From the regular patterns of the photographs it becomes evident that the ions of Duoplasmatron have small energy spread.

voltages, equilibrium condition is not observed and the probe pattern shows preponderance of particles not coming from plasma (Ardenne; Chapman, *et al.* 1964). Application of magnetic field is however found to reduce fluctuations and a growth towards a Boltzmann distribution is discernible (Fig. d). The following table presents some features of those probe studies. Some of the photographs taken are shown in Figs. a, b, c, d.

TABLE  
Argon pressure  $1 \times 10^{-3}$  mm of Hg

Sd. No.	Filament current in Amperes	Arc Voltage in Volts	Arc Current in Amperes	Magnet current in Amperes	Floating potential in volts	Plasma potential in Volts	$T_e$ in ev	Remarks	Figure reference
1	15	145	0.7	0	—	—	—	Plasma not formed	a
2	15	145	0.7	0.5	-5.5	-12.0	0.6	Stable plasma	b
3	15	145	0.7	2.0	-5.5	+10.5	0.8	Stable plasma	c
4	17	60	1.42	0	—	—	—	Irregular pattern	
5	17	60	1.40	2.0	—	—	—	Shows admixture of direct electrons	d
6	17	25	0.5	1.0	—	—	—	Instability and Kniks in the pattern	
7	17	25	0.5	2.0	—	—	—	Instability and Kniks in the pattern.	
8	16	80	0.5	2.0	-4.09	-11.9	0.8	Plasma developed.	

Blank spaces in the columns indicate quantities not determinable in view of irregular shapes  
The value of debye length calculated is 0.07 mm

## ACKNOWLEDGEMENT

The authors are grateful to Prof. B. D. Nagchaudhuri, Director, Saha Institute of Nuclear Physics, for guiding the work

## REFERENCES

- Barton, B. S. Jr., 1961, *Electrostatic Propulsion*, Academic Press, New York, London, Ardenne, M. V. *AERE* **232**, (TRANS), Report No. 898.
- Bose, D. K. et al, 1965, *Proc. Nucl. Physics and Solid State Physics, Symposium*, Calcutta, 367.
- Barton, B. S. Jr, 1961, *Electrostatic Propulsion*, Academic Press, New York, London, **21**.
- Chapman, R. A. et al, 1964, *J. Appl. Phys.* **33**, 2813.
- Moak, C. D, 1959, et al, *R S I.* **39**, 694.
- Popov, S. N. (1961), *Pribori i tekhnika eksperimenta* **4**, 20.
- SenGupta, S. N. Saha Institute of Nuclear Physics, Calcutta, Unpublished



# DETERMINATION OF IONIZATION POTENTIAL OF Gd AND Ho BY SURFACE IONIZATION METHOD

S. D. DEY AND S. B. KARMOHAPATRO

Saha Institute of Nuclear Physics, Calcutta-9, India

(Received February 8, 1966)

Several authors (Ionov and Mittsev, 1960, 1961; Alekseev and Kaminskii, 1965) determined the first ionisation potential of a number of rare earth elements by comparing with the known I. P. of some other elements and Dresser *et al* (1965) determined the I.P. of Gd, Er and Yb directly with the help of the surface ionisation process. In the present work we report the values of I.P. of Gd and Ho directly determined by the surface ionisation method with a new and simpler procedure. From the Saha-Langmuir equation, we have

$$\frac{n^+}{n_a} = \frac{g_+}{g_a} e^{(\phi - I)/kT} \quad \dots (1)$$

where  $n^+/n_a$  is the ratio of the number of evaporated ions to neutral atoms from a filament surface of electron workfunction  $\phi$  and maintained at a temperature  $T$ .  $I$  is the ionization potential of the evaporating atoms and  $k$  is the Boltzmann constant.  $g_+$  and  $g_a$  are the statistical weights of the ions and atoms respectively. As  $(I - \phi)$  is greater than  $kT$  over the entire range of variation of  $kT$  in the present case, equation (1) takes the form.

$$n^+ = nG e^{(\phi_{av} - I)/kT} \quad \dots (2)$$

or

$$I^+ = nAGe^{(\phi_{av} - I)/kT} \quad \dots (3)$$

where  $I^+$  is the positive ion current,  $n$  is the sum of  $n^+$  and  $n_a$ ,  $G$  is the ratio  $g_+/g_a$ ,  $A$  is some constant,  $\phi_{av}$  is the average work function of the polycrystalline tungsten filament surface used in this experiment.

From equation (3) it is evident that if  $n$  is maintained constant, the  $\log_{10} I^+ vs \frac{5040}{T}$  plot will be a straight line of negative slope, which determines  $(I - \phi_{av})$ , assuming  $G$  to be constant over the temperature range under consideration. Determining  $\phi_{av}$  from the Richardson plot,  $I$  can be determined.

Experimental set up consisting of a three filament ion source with an ion extraction slit system, electrometer ion detector and method of procedure have already been reported (Dey, 1965) with the results of the measurement of the

I.P. of Li The two side filaments of the ion source are now surrounded by glass capsules with radial holes in them for facilitating the introduction of the volatile rare earth chlorides and also to allow the vapour to come out when heated.

#### RESULTS AND DISCUSSIONS

The ion source chamber is evacuated to a pressure of better than  $10^{-6}$  mm of Hg with a 4" inch oil diffusion pump and liquid oxygen used in a suitable trap. The electron current from the central filament is measured for varying temperature,

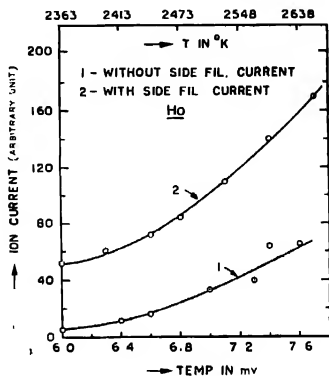


Fig. 1(a). Variation of ion current with temperature for Holmium.

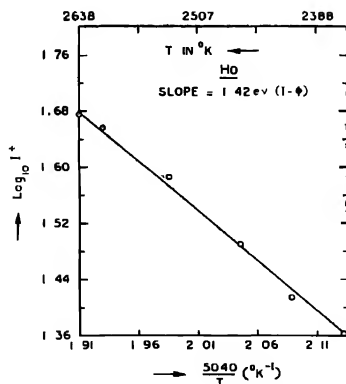


Fig. 1(b). Graphical plot of  $\log_{10} I + 5040/T$  vs  $1/T$  for Holmium.

which is measured by a tungsten-molybdenum thermocouple (Morgan *et al.*, 1950). From the Richardson plot the value obtained for  $\phi_{av}$  is  $4.68 \pm 0.07$  ev.

Chlorides of Gd and Ho are used. The variation of ion current with temperature is noted with and without molecular beam.  $(I - \phi_{av})$  practically remains constant roughly over the temperature range 2200°K-2700°K, the temperature being measured with the W-Mo thermocouple. Mean I.P. for Gd from a set of measurements is found to be  $6.73 \pm 0.09$  ev. in good agreement with the value obtained by Dresser *et al.* (1965).

Fig. 1(a) shows the variation of Ho ion current with temperature with (Curve 2) and without (Curve 1) the molecular beam and in Fig. 1(b) the  $\log I^+ \text{ vs } \frac{5040}{T}$  plot is shown. The mean value of I.P. from sets of four observations is  $6.08 \pm 0.09$  eV comparable with the value (6.19 ev) obtained by Alekseev *et al.* (1965). No spectroscopic data for directly determined value of I.P. of Ho by surface ionisation method is available for comparison with our results.

The spectroscopic value of I.P. for Gd is 6.16 ev (Moore, 1963) which is lower than the present value. This discrepancy may possibly be explained by the fact that the Saha-Langmuir theory needs modifications in case of surface ionization of complicated atoms in beams as indicated by Dresser *et al.* (1965).

Thanks are due to Prof. D. N. Kundu and Prof. B. D. Nagchaudhuri for constant encouragement and to Mr. M. K. Chakravarty for technical assistance.

#### REFERENCES

- Alekseev, N. I. and Kaminskii, D. I., 1965, *Soviet Physics. Technical Physics* **9**, 1177.  
 Dey, S. D., 1965, *Proc. Nucl. Phys. and Solid State Phys. Symposium* held in Calcutta in February, Nucl. Phys. 309.  
 Dresser, M. J. and Hudson, D. E., 1965, *Phys. Rev.* **137**, 2A, A 673.  
 Ionov, N. I. and Mittsev, M. A. 1960, *Soviet Physics—JETP* **11**, 972.  
 ———, 1961, *Soviet Physics—JETP*, **13**, 618.  
 Moore, C. E., 1963, *Applied Optics*, **2**, 665.  
 Morgan, F. H. and Danforth, W. E., 1950, *Jour. App. Phys.* **21**, 112.

## BOOK REVIEW

**ELECTRICITY AND MAGNETISM** · Berkely Physics Course—Volume 2.  
Edward M. Purcell. 459 p Price \$ 5 50. McGraw Hill Book Company,  
New York

Based upon the quite adequate foundations on mechanics and relativity laid down in volume I of the series, the author develops in this book the classical theories of electricity and magnetism. The necessary mathematical tool is developed side by side though not to the extent needed for Honours course. Introduction of spherical harmonics to the solution of general problems would have been appreciated. Approach to the problems is very refreshing and gives a much greater insight into the electromagnetic phenomena than the usual classical mathematical approaches. The exemplifications and many worked out problems are typical of this microscopic method of approach. Fundamental physical concept of treating electric and magnetic phenomenon and the laws guiding them, as manifestations of relativity and invariance of electric charge will bring new enthusiasm to teaching of physics and fresh scope of thinking on the part of the students.

*A. Bose*

## ERRATA

(An Analysis of the J-Phenomenon in Scattered X-rays, Part II)

Vol. 39, No. 3., March 1965.

Page 117 line 9 read  $H_z$  instead of  $I_z$

" 11 read  $H_r =$  instead of  $I_z -$

" 126 foot note read  $x_c$  .. ..  $x_c$

" 127 line 28 read  $(S/P)_{30^\circ}$  .. ..  $(S'/P)_{30^\circ}$

## ERRATA

(An Analysis of the J-Discontinuity in Scattered X-rays,—Part III)

Vol. 39, No. 6, June 1965

Page 283 line 3 affix an asterisk after the author's name.

Page 292 Fig. 1 (a) read along Ordinate-axis  $(S'/P')_{90^\circ} \rightarrow$

(b) read the topmost point of intersection of each graph with the ordinate-axis as 1.0 and the lowest marked sectional point on the same axis for each graph as .9

(c) read along the abscissa-axis  $\rightarrow x$  (No. of Al sheets each .1 mm thick)

(d) read the marked sectional points on the common abscissa-axis as 0, 1, 2, 3, 4, 5, 6, 7, 8

Page 294 last but one line in the text read 'loses' instead of 'losses'.

## ERRATUM

Coupling constant sum rules for the decay of the  $J^P = 2^+$  Nonet in Broken SU(3)

V. P. Gautam and P. Ghose

Vol. 39, No. 9, September 1965.

Read  $G(K^{*+}, \rho K)$ ,  $G(f, K^* \bar{K})$ ,  $G(f', K^* K)$ ,

$G(A_2, K^* \bar{K})$ ,  $G(f, \pi \pi)$ ,  $G(f', \pi \pi)$ ,  $G(f, KK)$ ,

$G(f', K \bar{K})$  and  $G(A_2, \pi \eta)$  with opposite sign.

## An Appeal to the Indian Scientists

Dear Sirs,

Indian Journal of Physics is the pioneer scientific journal in India which has a tradition of its own. With the development of modern science the necessity of quick and regular publication of scientific papers in larger numbers is greatly felt by the scientific workers of this country. Keeping pace with the great demand of the readers for a journal of high standard and in the better interest of the scientific workers of the country, as well as for the further development of the journal, the Board of Editors of the Indian Journal of Physics has resolved as follows :

"It was pointed out by the Secretary, that a large number of important papers in physics by Indian authors, which should normally be communicated to the I.J.P., are sent abroad for publication in foreign journals. In every country with a growing volume of research work carried out in any subject and where a representative journal for publication of such papers exists, it should be a question of national prestige that all such papers be sent to that journal for publication, thereby the standing of the journal as the national medium of publication is recognized both at home and abroad. The Board requested the Secretary to circulate a letter to all research workers in physics requesting them to contribute their important papers in the Indian Journal of Physics and enabling thereby every physicist at home and abroad to recognize the I.J.P. as the important medium for publications in physics in India."

As regards the practical methods that have been adopted to raise the standard of the journal we beg to inform you that we have almost cleared up the arrears in publication of the journal and that from the next year i.e. vol. 40, 1966, the journal is expected to be published more regularly. The time lag in assessing the papers has been considerably reduced and the standard of assessment raised. International practices for good editorship are being adhered to and the number of printed pages are intended to be raised as greater number of contributions are made available. To avoid delay in publication measures have been taken so that it is expected that all papers may be published within three months and the *Letters to the Editors* within one month. We have every hope that you will actively cooperate with us in our attempts to raise the standard of the journal and request you kindly to give serious consideration to the above resolution of the Editorial Board, which is evidently intended to be in the general interest of the progress of science in this country.

Yours faithfully

A. Bose  
*Honorary Secretary*  
Board of Editors  
Indian Journal of Physics

## ON THE THEORY OF SPECIFIC HEAT OF LIQUIDS

S. C. MISRA

FAKIR MOHAN COLLEGE, BALASORE

(Received December 31, 1965)

**ABSTRACT.** Liquid is considered here as a sort of compressed gas in which the inter-molecular forces play a role comparable to translational motion. On this basis the calculation of specific heat of liquids gives reasonable agreement with experimental results of hydrogen, argon, air and carbondioxide.

## INTRODUCTION

Several attempts to explain the specific heat of liquids have been made in the past, but most of them are qualitative. Ghose (1924) had proposed an empirical formula which does not explain the nature of variation of specific heat with temperature. Prigogine and Suzanne (1942) have calculated the specific heat of liquid argon considering the model of Lennard-Jones, but they have not got good agreement with observed values. Later Ookawa (1947) has tried to deduce a relation on the basis that liquid consists of clusters of different sizes the magnitude of which varies with temperature. The final result obtained by him contains an unknown function of temperature and hence the values of specific heat have not been calculated.

When the molecules of a gas are forced to come very close to each other, the intermolecular forces come to operation, the influence of which is taken into account by the addition of a term to the pressure value of the gas equation as is apparent in Vander Waals' equation. This gas equation indicates the energy expression which is found to be modified on account of the potential energy due to intermolecular forces. The specific heat may now be deduced from such an expression. In this paper we have considered the liquid as a sort of compressed gas. So the result of the above deduction can be used to calculate the specific heat in case of liquid argon and liquid hydrogen for which only translatory motion should be considered within the temperature range under consideration. For air whose molecules are diatomic, we are to consider restricted rotations and for carbondioxide in addition vibrations of the atoms inside molecules are to be considered. To explain the specific heat of carbondioxide gas, we take 3 degrees of translation, 3 degrees of rotation and the vibration of atoms inside the molecule. This is also expected from the value of  $\gamma$ , the ratio of specific heats, which is nearly 1.30 at room temperature indicating the number of degrees of freedom to be 6.67 i.e. 3 degrees due to translation, 3 degrees due to rotation and one third of a degree due to vibration. But it is seen that in case of liquid carbondioxide we require

in addition another 6 degrees of freedom for explaining the experimental data. This may be due to some motion caused by the deformation of molecules or may be due to the effect of interaction other than the effect of Vander Waals' forces. The results of our theoretical calculations are in good agreement with experimental findings. At the melting points of argon and air there is, however, some discrepancy.

#### DEDUCTION

If we neglect the extension of the molecules in space; and regard them as point masses Van der Waals' equation becomes

$$\left(P + \frac{a}{V^2}\right) V = RT = NKT$$

We write it as follows :

$$PV = N \left( KT - \frac{a}{VN} \right) \quad \dots (1)$$

The above equation may also be used for liquids; however, the pressure  $P$  caused by the impact of molecules is very small in this case (Partington, 1949)

The constant  $a$  in the above equation, though originally regarded as independent of temperature, is found to depend on temperature when comparison is made with observational results. The exact nature of this function is not known. But it is clear that  $a$  should vanish at high temperatures and at low densities because the gas will become perfect then. At a temperature  $T_m$  where we shall get solid state, the product  $PV$  should be zero because solid does not give rise to any pressure due to impact of molecules. Considering these two limiting cases we suggest that

$$a = VRT e^{-2\theta(T^{1/2} - T_m^{1/2})}$$

where  $\theta$  is a constant independent of temperature. Substituting for  $a$  in (1) we get

$$PV = N[KT - KT e^{-2\theta(T^{1/2} - T_m^{1/2})}]$$

Energy of the system with translatory motion alone is known to be -

$$E = \frac{3}{2}PV = N[\frac{3}{2}kT - \frac{3}{2}kT e^{-2\theta(T^{1/2} - T_m^{1/2})}] \quad \dots (2)$$

Hence 
$$C_v = \frac{dE}{dT} = \frac{3}{2}R[1 - e^{-2\theta(T^{1/2} - T_m^{1/2})}(1 - \theta T^{1/2})]. \quad \dots (3)$$

In equation (2) we find that in case where there is translational energy only the average energy per particle per degree of freedom is

$$\frac{1}{2}kT[1 - e^{-2\theta(T^{1/2} - T_m^{1/2})}]$$



In diatomic and polyatomic molecules we may expect rotation and molecular vibration which will give rise to new degrees of freedom. In case of liquids these motions are not free but restricted due to intermolecular attraction, hence the energy per particle per degree of freedom should not be taken as  $\frac{1}{2}KT$ . Assuming equipartition of energy we shall take the energy per particle for each of these new degrees of freedom also as  $\frac{1}{2}KT[1 - e^{-2\theta(T^{1/2} - T_m^{1/2})}]$ . So the specific heat at constant volume  $C_v$  is given by

$$C_v = \frac{n}{2} R[1 - e^{-2\theta(T^{1/2} - T_m^{1/2})} (1 - \theta T^{1/2})] \quad (4)$$

where  $n$  stands for the number of degrees of freedom.

#### COMPARISON WITH EXPERIMENTAL RESULTS

##### (i) Liquid Hydrogen

Below  $50^\circ$  abs. in case of hydrogen only translatory motion need be considered. So in eqn. (4) we take  $n = 3$  in the temperature range considered and  $\theta = 0.215$  (determined by trial). The calculated values of specific heat are shown against the experimental results obtained by Bartholome and Eucken (1936).

Specific heat of liquid hydrogen

Temp. in abs	$C_v$ (obs) in Cal/degree cent	$C_v$ (Cal) in cal/degree cent
15.33	2.54	2.55
15.86	2.56	2.61
16.23	2.63	2.64
16.87	2.70	2.70
17.22	2.70	2.73
17.88	2.78	2.78
18.92	2.84	2.84
19.50	2.89	2.89
20.00	2.92	2.92
20.50	2.98	2.94

The agreement here is quite satisfactory, the maximum deviation being less than 2%.

##### (ii) Liquid Argon

Argon is monatomic. So we take in equation (4).  $n = 3$  and  $\theta = 0.25$  (determined by trial). The experimental results are taken from Eucken and Hauck (1928).

## Specific heat of Argon

Temp. in abs.	$C_p$ (obs.) in cal/°C	$C_p$ (calculation of Prigogine and Suzanne) in cal/°C	$C_p$ (our calculation) in cal/°C
90	5.5	5.25	6.47
100	5.5		5.94
110	5.5	5.15	5.49
120	5.20		5.13
130	4.90	4.30	4.82
140	4.65		4.54
150	4.35	4.50	4.32
160	4.00	4.30	4.12
170	3.75	4.00	3.97

The agreement in this case is satisfactory beyond 110° abs. The maximum deviation is less than 4%. There is a tendency of deviation after 160° abs. This is expected because critical temperature for argon is only 151° abs. and at this temperature things are not normal.

(iii) *Liquid Air*

Air is a mixture of mostly diatomic molecules. So in equation (4) we are to take  $n = 5$  (for translatory motion 3 and for rotatory motion 2) and  $\theta = 0.33$  (determined by trial). The experimental results are taken from Eucken and Hauck (1928).

## Specific heat of air

Temp in °abs.	$C_v$ (obs.) in cal.°c.	$C_v$ (cal.) in cal /°c.
80	7.8	10.00
90	7.8	8.85
100	7.7	7.90
110	7.35	7.30
120	6.85	6.75
130	6.50	6.40
140	6.10	6.10
150	5.70	5.85
160	5.03	5.70
170	5.55	5.55

The agreement here is satisfactory excepting at the melting point. The maximum deviation is less than 3%.

(iv) *Liquid Carbon dioxide*

In this case we have vibration of atoms in the molecules. The energy due to this vibratory motion is to be calculated using the Einstein function for specific heat. The three characteristic temperatures (abs.) are 3400, 1900 and 960. Out of these three only the last one will have some contribution at the temperature under consideration, the effect of the other two will be negligibly small. We will have only  $N$  oscillators with 960 temperature. The contribution of these for specific heat (given in the second column in the table below) can be obtained in the usual way from the table for Einstein function. To explain the rest of energy we will take  $n = 12$  in equation (4). The experimental results here are taken from Eucken and Hauck (1928).

Specific heat of carbon dioxide

Temp. in °Abs	$C_{vib}$ in cal/°c.	$C$ in cal/°c	$C - C_{vib} - \frac{1}{2}$ in cal/°c	cal/°c
230	0.541	10.116	10.657	10.4
240	0.604	10.38	10.984	10.9
250	0.66	10.620	11.280	11.25
260	0.706	10.836	11.542	11.45
270	0.76	11.028	11.788	11.75
280	0.80	11.244	12.044	12.10
290	0.86	11.292	12.152	12.25
300	0.9	11.892	12.792	12.75
310	0.94	12.024	12.964	13.10
320	0.98	12.156	13.136	13.35

For the last three readings we have taken  $\theta = 0.057$  and for the rest,  $\theta = .055$ . Near the critical temperature a change in the value of  $\theta$  is always expected because things are not normal then, a step anomaly is seen at 300° abs. The maximum deviation in this case is less than 2%.

#### DISCUSSION

It is usually expected that in specific heat measurements at low temperatures, there remains an error of 4%. So the theory suggested above gives very good agreement with experimental results in case of these four liquids. At the melting point and at the critical temperatures abnormal behaviour is always expected. So slight deviation at these points should not be considered as defect of the theory.

Equipartition principle which is deduced for perfect gases can be used, as we have seen, to restricted motions as well.

We may notice that equation (1) can also be written as

$$PV = KT \left( N - \frac{a}{VKT} \right)$$

Substituting for  $a$  in the above equation we notice that a liquid or a real gas can be looked upon as a perfect gas with  $N[1 - e^{-2\theta(T^{1/2} - T_m^{1/2})}]$  moving particles instead of  $N$  molecules and the rest of the particles can be assumed to be at rest. We can get all the above results with this idea also. We will discuss about this idea in our next paper which will deal with the variation of the coefficient of viscosity with temperature both in liquids and gases.

Heuse (1919) has observed a fall in the values of the specific heat of many gases at low temperature. Such a fall has been reported by him even in case of argon which is a monatomic gas. A fall of this type is, however, expected from eqn. (4) and it will be interesting to compare the calculated values of the specific heat from eqn. (4) with the experimental findings.

#### ACKNOWLEDGEMENT

I am thankful to the Board of Scientific and Industrial Research, Orissa, for the financial help in the work. I am grateful to Dr. D. Basu, Professor of Theoretical Physics, and to Dr. N. Sil, Reader in Theoretical Physics, Indian Association for the Cultivation of Science, for helpful discussions.

#### REFERENCES

- Bartholome, E., and Lucken, A. (1936), *Z. Electrochem.*, **42**, 547.  
 Lucken, A. and Hauck R., (1928), *Z. Physik Chem.*, **134**, 161.  
 Ghose, R. N., (1924), *J. Ind. Chem. Soc.*, **1**, 123.  
 Heuse, W. (1919), *Ann. Phys.*, **95**, 86.  
 Ookawa, A. (1947), *J. Phys. Soc. Japan*, **2**, 108.  
 Purlington, J. R., (1940), *Treatise on physical chemistry*, **1**, 683.  
 Prigogine and Suzanne, (1942), *Physics*, **9**, 306.

# RELAXATION METHOD APPLIED TO NETWORK PROBLEM INVOLVED IN ELECTRIC RAILWAY SYSTEM

S. N. DUTTA

DEPARTMENT OF APPLIED PHYSICS, CALCUTTA UNIVERSITY

(Received February 4, 1966)

**ABSTRACT.** In this paper it has been shown how the network problem involving electric railway systems, can be solved using relaxation technique. The present method utilises the set of linear simultaneous equations which are obtained with the help of Kirchhoff's laws of electrical network, and shows how to solve them. The relaxational solution as obtained is seen to be quite useful because it gives the values of the unknown voltages at all the nodal points simultaneously.

## INTRODUCTION

In the electric railway systems (Starr, 1946), a definite electrical problem is difficult to be formulated due to the fluctuating loads. But assuming the loads simulating the typical operating conditions the problem can be solved by different methods, which entail much more labour with the increase of nodal points in the corresponding network. But the method discussed in this paper shows its advantage in the sense that the increase in the number of nodal points does not generally bring about more complication in solving the problem.

In this network system as shown in Fig 1 the supply voltages, resistances of the trolley, feeders and rails, and ampere loads at the designated locations are known. The equivalent circuit diagram can be drawn as in Fig 2. Considering the nodal points of the Fig 2, a set of linear simultaneous equations can be obtained at each of them applying Kirchhoff's laws of networks and these equations are then solved by relaxation method.

## THE METHOD

In this method the following linear simultaneous equations are obtained if the required nodal points of the equivalent circuit diagram are considered.

Hence :

$$\begin{aligned} \text{At } A, & I_A - (V_A - V_B)g_{AB} - (V_A - V_D)g_{AD} - (V_A - V_C)g_{AC} = 0 \\ C, & (V_A - V_C)g_{AC} - (V_C - V_B)g_{CB} - (V_C - V_D)g_{CD} = 0 \\ B, & (V_A - V_B)g_{AB} + (V_C - V_B)g_{CB} - I_{BB'} = 0 \\ D, & (V_A - V_D)g_{AD} + (V_C - V_D)g_{CD} - I_{DD'} = 0 \\ B', & I_{BB'} + (V_C' - V_B')g_{C'B'} - (V_B' - V_A')g_{B'A'} = 0 \\ D', & I_{DD'} - (V_D' - V_C')g_{D'C'} - (V_D' - V_A')g_{D'A'} = 0 \end{aligned} \quad (1)$$

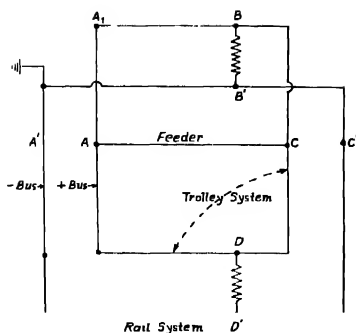


Fig. 1. Diagram for network in Electric Railway System

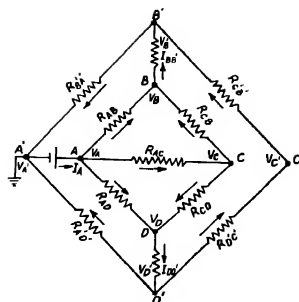


Fig. 2. Equivalent diagram for Network in Electric Railway System.

where

$I_A$  is the current flowing towards A,

$I_{BB'}$  ..... through the branch  $BB'$ ,

$I_{DD'}$  .....  $DD'$ ,

$V_A$  ..... potential at the nodal point A,

$V_B$  ..... B,

$V_C$  ..... C,

$V_D$  ..... D,

$V_{A'}$  .....  $A' = \text{zero (earth point)}$

$V_{B'}$  .....  $B'$

$V_{C'}$  .....  $C'$ ,

$V_{D'}$  .....  $D'$ ,

$g_{AB} = 1/R_{AB}$ , where  $R_{AB}$  is the resistance of the branch AB,

$g_{AC} = 1/R_{AC}$ , .....  $R_{AC}$  ..... AC,

$g_{AD} = 1/R_{AD}$ , .....  $R_{AD}$  ..... AD,

$g_{CB} = 1/R_{CB}$ , .....  $R_{CB}$  ..... CB,

$g_{CD} = 1/R_{CD}$ , .....  $R_{CD}$  ..... CD,

$g_{B'C'} = 1/R_{B'C'}$  .....  $R_{B'C'}$  .....  $B'C'$ ,

$g_{B'A'} = 1/R_{B'A'}$  .....  $R_{B'A'}$  .....  $B'A'$ ,

$g_{D'C'} = 1/R_{D'C'}$  .....  $R_{D'C'}$  .....  $D'C'$ ,

The above set of equations after necessary simplification and rearrangement can be written as shown below :

$$\begin{aligned}
 I_A - V_A(g_{AB} + g_{AD} + g_{AC}) + V_B g_{AB} + V_C g_{AC} + V_D g_{AD} &= 0 = F_1 \\
 V_A g_{AC} + V_B g_{CB} - V_C(g_{AC} + g_{CB} + g_{CD}) + V_D g_{CD} &= 0 = F_2 \\
 V_A g_{AB} - V_B(g_{AB} + g_{CB}) + V_C g_{CB} - I_{BB'} &= 0 = F_3 \\
 V_A g_{AD} + V_C g_{CD} - V_D(g_{AD} + g_{CD}) - I_{DD'} &= 0 = F_4 \\
 I_{BB'} - V_B(g_{CB} + g_{AB}) + V_C g_{CB} &= 0 = F_5 \\
 I_{DD'} - V_D(g_{CD} + g_{AD}) + V_C g_{CD} &= 0 = F_6
 \end{aligned} \tag{2}$$

where  $F_1, F_2, F_3, F_4, F_5$  and  $F_6$  are the residuals. The values of the unknowns shown in the relation (2) can be easily found out when the residuals are liquidated by relaxation method. To liquidate them the basic unit, block and group operations are carried out (Allen, 1954). In basic unit operation (Table I) the changes in the values of the residuals due to unit positive increment of the unknowns are found out. With the help of basic unit operations suitable block and group operations can be performed in which equal simultaneous, and unequal simultaneous increments are given respectively to more than one unknown to bring about the changes in some required residuals without affecting the rest. In the relaxation table (Table II) the use of basic, block and group operations are shown in the liquidation steps, number 2 and 6; 1 and 5, and 3, 4 and 7 respectively. The liquidation is nearly complete in those seven steps yielding the values of the unknowns. The following illustration will clearly show the merit and utility of the method.

#### ILLUSTRATION

This illustrating example described hereafter is solved by Dawes (1952) by conventional method.

In Fig. 1 there is shown a simple railway system with a ring connected trolley and a single feeder connected to the busbars at  $A$  and to the trolley system at  $C$ . The station busbars at  $AA'$  are maintained at 600 volts, busbar  $A$  being positive and  $A'$  being negative and grounded. The resistance of the busbar is negligible. The resistance of the overhead trolley is as follows :  $A_1$  to  $B = 0.30$  ohm,  $B$  to  $C = 0.20$  ohm,  $C$  to  $D = 0.20$  ohm,  $D$  to  $A = 0.28$  ohm. A feeder connected from  $A$  to  $C$  and its resistance is 0.25 ohm. The resistance of the rail and the ground return is as follows :  $A'$  to  $B' = 0.40$  ohm,  $B'$  to  $C' = 0.25$  ohm,  $C'$  to  $D' = 0.25$  ohm,  $D'$  to  $A' = 0.36$  ohm. A trolley car at  $BB'$  takes 70 amps and a car at  $DD'$  takes 80 amps. It was desired to determine (a) Current in each section of trolley and in feeder, (b) Voltages at each car and at feeding point  $CC'$ .

Considering the equivalent circuit diagram shown in Fig. 2 of the railway

system shown in Fig 1, and substituting the numerical values in relation (2) the following set of equations can be written :

$$\begin{array}{rcl}
 3.333 V_B + 4 V_C + 3.571 V_D - 6392.4 & = & 0 = F_1 \\
 5 V_D - 14 V_C + 5 V_D - 2400 & = & 0 = F_2 \\
 -8.333 V_B + 5 V_C + 1930 & = & 0 = F_3 \\
 5 V_C - 8.571 V_D + 2062.6 & = & 0 = F_4 \\
 -6.5 V_D + 4 V_C + 70 & = & 0 = F_5 \\
 4 V_C - 6.778 V_D + 80 & = & 0 = F_6
 \end{array} \quad \left. \vphantom{\begin{array}{rcl} 3.333 V_B + 4 V_C + 3.571 V_D - 6392.4 \\ 5 V_D - 14 V_C + 5 V_D - 2400 \\ -8.333 V_B + 5 V_C + 1930 \\ 5 V_C - 8.571 V_D + 2062.6 \\ -6.5 V_D + 4 V_C + 70 \\ 4 V_C - 6.778 V_D + 80 \end{array}} \right\} \dots (3)$$

On liquidating the residuals of the relation (3) almost completely, the values of the potentials at the said nodal points are obtained correct to the required limit of accuracy. From those values of potentials and the supplied values of different resistances, the currents in the various branches of the network wanted in the illustration can be easily calculated as given below :

$I_{AB}$  = 49.86 amps, where  $I_{AB}$  is the current flowing through  $AB$ ,

$I_{AD}$  = 55.91 ,, .....  $I_{AD}$  .....  $AD$ ,

$I_{B'A'}$  = 70.75 ,, .....  $I_{B'A'}$  .....  $B'A'$

$I_{D'A'}$  = 79.44 ,, .....  $I_{D'A'}$  .....  $D'A'$ ,

$I_{AC}$  = 43.48 ,, ....  $I_{AC}$  .....  $AC$ ,

$I_{CB}$  = 20.44 ,, .....  $I_{CB}$  .....  $CB$ ,

$I_{CD}$  = 23.93 ,, .....  $I_{CD}$  .....  $CD$ ,

$I_{D'C'}$  = 0.60 ,, .....  $I_{D'C'}$  .....  $D'C'$ ,

$I_{C'B'}$  = 0.60 ,, .....  $I_{C'B'}$  .....  $C'B'$ ,

$V_{BB'}$  = 556.74 volts,  $V_{BB'}$  being the voltage at the trolley car at  $BB'$ ,

$V_{DD'}$  = 555.74 ,, ...  $V_{DD'}$  .....  $DD'$ ,

$V_{C'}$  = 28.45 ,, .....  $V_{C'}$  ..... feeding point  $C'$ ,

$V_C$  = 589.13 ,, .....  $V_C$  .....  $C$ ,

The above values as calculated by relaxation method are quite comparable with those found out by the other methods of network analysis (Dawes, 1952), shown in the table below (Table III).

#### DISCUSSION

This method is seen to yield the values of the voltages at different nodal points simultaneously, from which the calculations of the other desired quantities become very quick and easy. Although with the increase of the number of branches



**TABLE I**  
**Basic Unit Operation Table**

$\delta V_B$	$\delta V_C$	$\delta V_D$	$\delta V_{N'}$	$\delta V_{N''}$	$\delta F_1$	$\delta F_2$	$\delta F_3$	$\delta F_4$	$\delta F_5$	$\delta F_6$
1	—	—	—	—	3 333	5 0	-8 333	0	0	0
—	1	—	—	—	4 600	-14 0	5 000	3 0	0	0
—	—	1	—	—	3 571	5 0	0	-9 571	0	0
—	—	—	1	—	0	0	0	0	-6 5	0
—	—	—	—	1	0	0	0	0	4 0	0
—	—	—	—	—	0	0	0	0	0	-6 778

TABLE II  
Relaxation Table

Liquidation steps	$\delta V_B$	$\delta V_C$	$\delta V_D$	$\delta V_B' = V_{B'}$	$\delta V_C' = V_{C'}$	$\delta V_D'$	$F_1$	$F_2$	$F_3$	$F_4$	$F_7$	$F_8$						
	$V_B = V_C$	$\delta V_C$	$\delta V_D = V_D$	$V_B' = V_{B'}$	$V_C' = V_{C'}$	$\delta V_D' = V_{D'}$	-6392	4	2400	1930	2162	6	70	80				
(1)	386	2436	586	2436	556	2436	0	15	0256	-23	9400	-30	8759	70	80			
(2)	—	3	9804	—	—	—	15	7216	0	-4	2979	-11	2230	70	80			
(3)	-0	5156	—	0	5158	—	15	8444	0	0	-15	6448	70	80	0			
(4)	-0	6559	-1	1433	-2	5133	0	0	0	0	0	19609	70	80	0			
(5)	—	—	—	—	—	—	0	0	0	0	0	19609	0	2	216			
(6)	—	—	—	—	—	—	0	0	0	0	0	19609	0	0	0			
(7)	—	0	1	0	1	0	0	7571	-0	9	4	3	-0	1601	-0	15	-0	05
Values of the unliquidated	385	042	589	131	584	344	0	7571	-0	9	0	3	-0	1601	-0	15	-0	65

TABLE III  
Comparison of values

Methods	$I_{AB}$ amps	$I_{AD}$ amps	$I_{B'A'}$ amps	$I_{D'A'}$ amps	$I_{AC}$ amps	$I_{CB}$ amps	$I_{CD}$ amps	$I_{D'C}$ amps	$I_{B'B'}$ volts	$V_{DD'}$ volts	$V_C$ volts
Relaxation method	49.86	55.91	70.75	79.44	43.48	20.44	23.93	0.60	0.60	555.74	589.13
Conventional method	50.00	56.20	70.60	79.40	43.80	20.00	23.80	0.60	0.60	555.60	589.10

or nodal points the network becomes complicated, with some practice this method needs practically no extra labour in solving the problem. In the relaxation table (Table II) the residuals are not liquidated completely and consequently their values are reduced to narrowest possible limits so that the desired limit of accuracy of the values can be achieved.

#### ACKNOWLEDGMENT

The author is highly indebted to Prof. A. K. Sengupta, D.Sc., A.M.I.E.E. (London), Head of the Department of Applied Physics, Calcutta University, for his guidance and help throughout the progress of this work

#### REFERENCES

- Allon, D. N. deG., 1951, *Relaxation Methods*, Chapter 1 and 2. (McGraw-Hill Book Co., Inc., New York).
- Dawson, C. L., 1952, *A Course in Electrical Engineering*, Vol. 1. (McGraw-Hill Book Co., Inc., New York), 76.
- Starr, A. T., 1946, *Generation, Transmission and Utilisation of Electrical Power*, (Sir Isaac Pitman & Sons Ltd, London) 344

# L SUBSHELL RATIOS OF E2 TRANSITIONS IN DEFORMED RARE EARTH NUCLEI\*

W H BRANTLEY\*\*, S C. PANCHOLI\*\*\* AND J H HAMILTON

PHYSICS DEPARTMENT, VANDERBILT UNIVERSITY, NASHVILLE, TENNESSEE, U S A

(Received January 22, 1966)

**ABSTRACT** The  $L$  subshell ratios of the  $2+ \rightarrow 0+$  first excited state to ground state transitions in  $Gd^{151}$ ,  $Yb^{170}$  and  $W^{182}$  have been measured with an ion-bee double-focusing spectrometer. The results indicate that the  $L_1/L_2$  and  $L_1/L_3$  ratios are about 15% or more higher than the theoretical values while  $L_2/L_3$  ratios agree with the theories of Rose, and of Sliv and Band

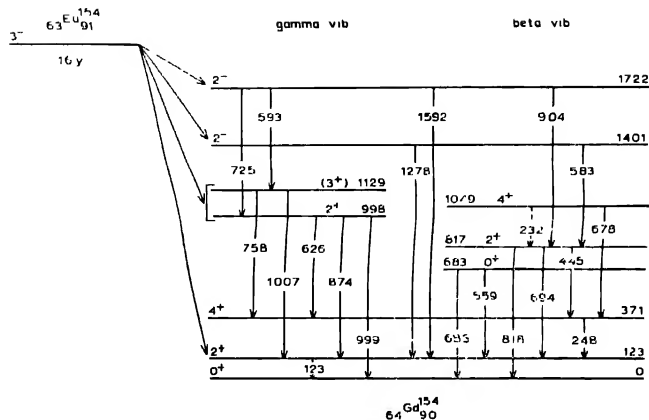
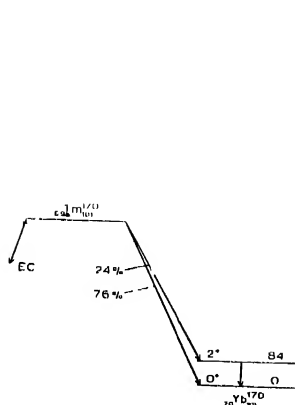
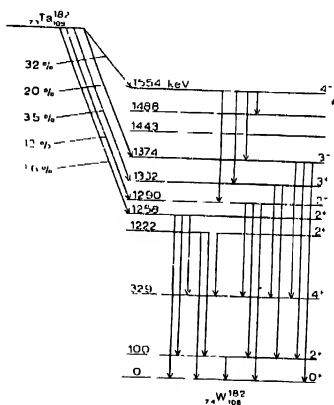
## INTRODUCTION

A powerful tool for the determination of gamma transition-multipolarities is the comparison of experimental and theoretical  $L$ -subshell intensity ratios. The accuracy of the multipolarities and mixing ratios obtained in this manner depends on the validity of the theoretical conversion-coefficient ratios used in the analysis. On a visit to Vanderbilt University in May, 1964, M Mladjenovic communicated some results of studies being carried out in Belgrade on the measurements of  $L$ -subshell ratios of  $2+ \rightarrow 0+$  pure E2 transitions in the deformed rare-earth region. These results did not agree with the theoretical ratios either of Rose (1958) or of Sliv and Band (1956) and Sliv (1961). The  $L_1/L_2$  and  $L_1/L_3$  ratios were found to be ten to thirty percent higher than theory while  $L_2/L_3$  agreed. Following his communication, the present work was begun on the measurements of  $L$ -subshell ratios in the rare-earth region. Later, at the International Conference on the Internal Conversion Process held at Vanderbilt University, May 10-13, 1965, other groups Stopic *et al.*, Novakov *et al.*, and Karlsson *et al.*, presented experimental data on  $L$ -subshell ratios which also disagreed with theoretical results. A brief account of the results of the work described in the present paper were presented at the conference, Brantley *et al.*, (1965). The decay schemes of  $Eu^{154}$ ,  $Tm^{170}$  and  $Ta^{182}$  are shown in figures 1, 2, and 3. The transitions studied were the first excited state to ground state  $2+ \rightarrow 0+$ , transitions in each case.

\*Work supported in part by a grant from the National Science Foundation.

\*\*Present Address, Delft Technical University, Delft, Netherlands

\*\*\*From University of Delhi, Delhi, India; (present address: Oak Ridge National Laboratory)

Fig. 1. Decay scheme of  $\text{Eu}^{154}$  from Reindinger et al (1965) and Brantley et al (1966)Fig. 2. Decay scheme of  $\text{Tm}^{170}$  as given in Nuclear Data SheetsFig. 3. Decay scheme of  $\text{Th}^{182}$  with only the important features as given in the Nuclear Data Sheets and recent literature see for example Daniel et al

#### EXPERIMENTAL TECHNIQUES AND SOURCE PREPARATION

These measurements were done on a 30-cm iron-free, double-focusing spectrometer, Baird *et al.*, (1962). Momentum resolutions better than about 0.10 percent

were required for the present studies. The best previous resolution obtained on the spectrometer was 0.13 percent, which was thought to be near the limit obtainable on the spectrometer. However, the resolution was improved by the use of narrower sources and by better alignment of the source in the spectrometer. A narrow defining slit was placed over the sources. The resolution for the various measurements varied from about 0.06 percent to 0.10 percent. This resolution is near the limit of the control mechanism of the spectrometer and care must be taken to insure that no instrumental distortions enter into the measurements. Several different measurements for each transition were done and care was taken to assure optimum current control in the instrument over the long counting periods of 24-48 hours. A continuous gas-flow G. M. counter with a 0.37-mg/cm<sup>2</sup> aluminum-coated Mylar window was used. The cutoff energy of the window, about 11 keV, was sufficiently low to insure 100 percent transmission at the energies at which the measurements were taken. The lowest energy of the three transitions measured is 84.2 keV for which the L<sub>1</sub> line is found at about 73 keV.

The Eu<sup>154</sup> activity was obtained by irradiation of high-purity Eu<sup>153</sup> in the Materials Testing Reactor at Idaho Falls. The activity was then allowed to decay for nine months so that the short-lived components died out or became negligible. In particular, Eu<sup>156</sup> produced by triple neutron capture in the high flux of the reactor (about  $5.6 \times 10^{14}$  neutrons/cm<sup>2</sup>-sec) has a half life of only fifteen days, so that the amount of it remaining in the sample is negligible. From a consideration of its decay scheme one concludes that the 1.81y Eu<sup>155</sup> can also be neglected. Twenty-five percent of the decay of Eu<sup>156</sup> is to the ground and first excited state of Gd<sup>155</sup>, and since the energy of the first excited state of Gd<sup>155</sup> is only 60 keV this part of the decay can produce no transitions which would interfere with the work on Gd<sup>154</sup>. Almost all of the remainder of the Eu<sup>156</sup> decay is to the second and third excited states of Gd<sup>156</sup> at 87 and 105 keV, so again no transitions of sufficient energy to interfere with the Gd<sup>154</sup> work occur from these decays. Internal-conversion spectra and gamma-ray spectra taken with a solid-state detector by Bedinger *et al* (1965) were used to determine the 13y Eu<sup>152</sup> contamination. The Eu<sup>152</sup> contamination was estimated to be less than one percent. The Eu<sup>151</sup> specific activity was 34.4 milli-curies/milli-gram. The source was prepared by thermal evaporation from the oxide on to a one-mil platinum backing. The dimensions of this source, as well as those of the next two sources discussed, were determined by an aluminum defining slit placed close to the sources. The source had dimensions of  $0.4 \times 18$  mm<sup>2</sup>. The source thickness was estimated to be 2 micro-grams/centimeter from knowledge of the specific activity and the amount used and from the intensity of the L<sub>2</sub> line of the 123 keV transition combined with knowledge of the conversion coefficients and the spectrometer transmission.

Difficulty was encountered in fabrication of the Ta<sup>182</sup> source because of the high melting point of tantalum and the difficulties of electroplating this material. The Ta<sup>182</sup> activity was obtained from Oak Ridge National Laboratory in the

chemical form of tantalate in a KOH solution. Its specific activity was 3.0 milli-curies/milli-gram. Thermal evaporation of the Ta<sup>182</sup> in vacuum was impossible because the boiling point of the tantalum is above the melting point of the crucible. This problem was solved by deposition of the activity in solution (tantalate in KOH) onto a thin strip of platinum. The platinum strip was then placed in vacuum and a current was passed through the strip, so the excess mass of the dried solution evaporated and left behind the Ta<sup>182</sup> activity. The source dimensions were  $0.4 \times 18$  mm<sup>2</sup> and its thickness less than 15 micro-grams/centimeter<sup>2</sup> obtained with the same procedure as for the Eu<sup>154</sup>.

The Tm<sup>170</sup> activity was also obtained from Oak Ridge National Laboratory. Its chemical form was TmCl<sub>3</sub> in weak HCl. Its specific activity was 80.7 milli-curies/milli-grams. The Tm<sup>170</sup> activity was liquid-deposited onto one-tenth mil Mylar which was coated with aluminum on one side. The source thickness was estimated in the same manner as described for Eu<sup>154</sup> to be less than 10 micro-grams/centimeter<sup>2</sup>.

The requirement of good resolution made it necessary that the sources have minimum mass and be 1 mm wide or less. To achieve this narrow width, an aluminum disk with a narrow defining slit was placed over the sources. The dimensions of this defining slit were  $0.4 \times 18$  mm<sup>2</sup>. The counter window was of the same width. This defining slit was found to improve the resolution without distorting the spectrum. Measurements were made with and without the slit and there was no apparent effect on the data other than the improvement in resolution.

## RESULTS AND DISCUSSION

The *L* subshell lines of the 123-keV transition in Gd<sup>154</sup> were measured five times and the results averaged. The resolution for the different runs was varied from 0.06 to 0.10 percent by variation of the spectrometer baffles. In order to separate the *L*<sub>1</sub> line from the *L*<sub>2</sub> line in the analysis, the line shape of the *L*<sub>3</sub> line was used as a standard. It was normalized to the *L*<sub>2</sub> line, and the *L*<sub>1</sub> line was subtracted. A typical measurement is shown in figure 5. The results are presented in Table I. The *L*<sub>1</sub>/*L*<sub>2</sub> and *L*<sub>1</sub>/*L*<sub>3</sub> ratios are higher than theory, while the *L*<sub>2</sub>/*L*<sub>3</sub> ratio agrees with theory. Because the *L*<sub>1</sub>/*L*<sub>2</sub> and *L*<sub>1</sub>/*L*<sub>3</sub> ratios are comparable, a convenient method of showing the results is to average the experimental value of these two quantities and divide this value by the average of the same quantities for the two theories. The mean percentage deviation is obtained by subtracting one from this quotient and multiplying the result by 100. The mean percentage deviation for the Gd<sup>154</sup> case is  $17 \pm 7$  higher than theory.

The *L* subshell lines of the 84 keV transition in Yb<sup>170</sup> were measured two times and the results averaged. The resolution on one run was about 0.06 percent and on the other run about 0.08 percent. In these measurements line tailing due to source thickness was a problem. In order to minimize the errors which are in-

TABLE I  
*L* Subshell ratios for  $2+ \rightarrow 0+$  Pure E2 transitions

Nucleide	$E$ $\gamma$ keV	Exptl. Ratios $\times 10^3$				Rose $\times 10^3$				Shv and Band $/10^3$				Reference
		$L_1/L_2$	$L_1/L_2$	$L_1/L_3$	$L_2/L_3$	$L_1/L_2$	$L_1/L_3$	$L_2/L_3$	$L_1/L_2$	$L_1/L_3$	$L_2/L_3$	$L_1/L_2$	$L_1/L_3$	
$^{64}\text{Gd}^{154}$	123.1	$397 \pm 26$	$415 \pm 27$	$1049 \pm 9$	340	353	1054	336	356	1007	0.99	$(L_1/L_2)_{\text{expt}}$ $(L_1/L_3)_{\text{th av.}}$	$(L_1/L_2 + L_1/L_3)_{\text{expt}}$ $(L_1/L_2 - L_1/L_3)_{\text{th av.}}$	Present work
$^{76}\text{Yb}^{170}$	84.3	$93 \pm 10$ $86 \pm 6$ $89 \pm 8$	$95 \pm 10$ $85 \pm 6$ $88 \pm 7$	$1020 \pm 20$ $983 \pm 11$ $1000 \pm 30$	77	77	994	75	75	993	1.03	$1.24 \pm 0.15$ $1.13 \pm 0.08$ $1.16 \pm 0.09$	$1.24 \pm 0.15$ $1.13 \pm 0.08$ $1.16 \pm 0.09$	Stepic et al. Karls-son et al. Present work
$^{74}\text{W}^{182}$	100.9	$101 \pm 10$ $90 \pm 4$ $98 \pm 7$ $118 \pm 16$	$112 \pm 20$ $96 \pm 4$ $108 \pm 7$ $127 \pm 16$	$1110 \pm 20$ $1090 \pm 20$ $1080 \pm 20$ $1072 \pm 21$	82	80	1080	80	80	1093	1.02	$1.25 \pm 0.15$ $1.09 \pm 0.04$ $1.21 \pm 0.08$ $1.43 \pm 0.18$	$1.25 \pm 0.15$ $1.09 \pm 0.04$ $1.21 \pm 0.08$ $1.43 \pm 0.18$	Stepic et al. Graham et al. Karls-son et al. Present work

volved, the data were analyzed by cutting off the tails at points such that the same percentage of area is contained in each peak. Thus part of the tail is omitted.

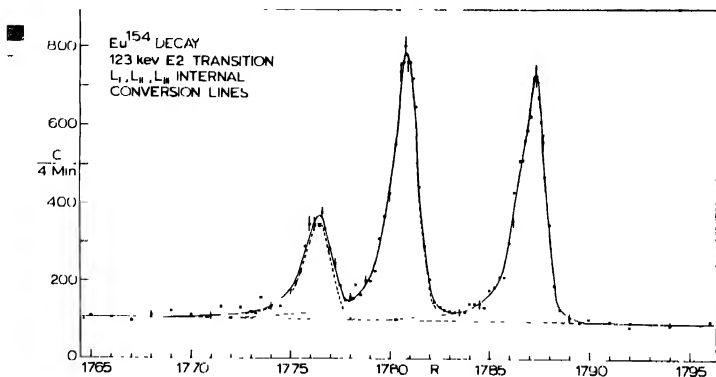


Fig. 4. A typical measurement of the  $L$  subshell lines of the 123 KeV transition in  $Gd^{154}$ .

Various cutoff points below the peaks were used to check on the consistency of the analysis. Ratios obtained from these different cutoff points agreed with each other to within 3.4 percent. One of the measurements is shown in figure 5. As in the case of  $Gd^{154}$  the  $L_3$  line was used as the standard shape in order to separate

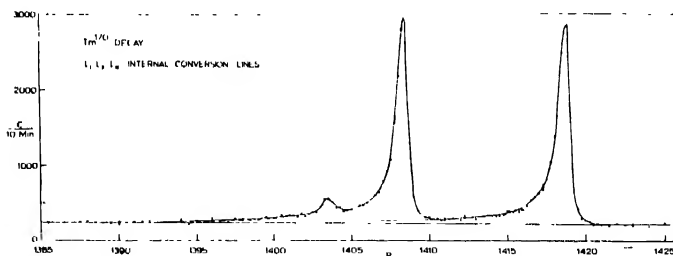


Fig. 5. A typical measurement of the  $L$  subshell lines of the 84 KeV transition in  $Yb^{170}$ .

$L_1$  and  $L_2$ . The result also presented in Table I for the mean percentage deviation compared to theory is  $16 \pm 9$  higher than theory.

The  $L$  subshell lines of the 100-keV transition in  $W^{182}$  were measured three times and the results averaged. The resolution varied from about 0.06 percent to 0.09 percent. Again line tailing was a problem and the same procedure of analysis was used here as was used in the case of  $Yb^{170}$ . In addition it should



be emphasized that the relative errors in this procedure are such that they tend to cancel when one determines ratios. Figure 6 shows one of these measurements. The results were  $43 \pm 18$  higher than theory for the mean percentage deviation.

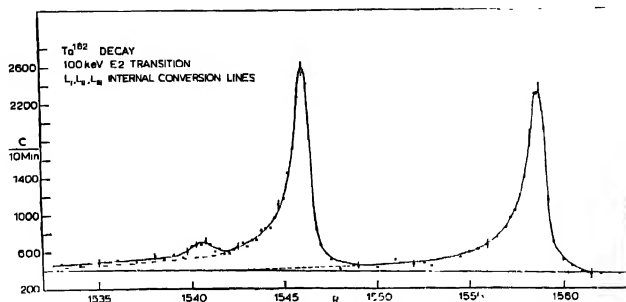


Fig. 6 A typical measurement of the L sub-shell lines of the 100 KeV transition in  $W^{182}$

Figures 4, 5 and 6 do not show the complete energy range that was measured. Part of the background on either side of the peaks is omitted to better illustrate the peaks in the figures

The results are presented in Table I along with the theoretical values of Rose and Sliv and Band. In this Z region, Rose's and Sliv and Band's values agree closely with each other. The results of other measurements in these isotopes are also presented in Table I. The  $L_1/L_2$  ratios for  $Yb^{170}$  and  $W^{182}$  agree with the results of Stepic, Bogdanovic and Mladjenovic and Karlsson *et al* within the limits of experimental error. The results of Graham and Geiger are lower, however

In the time since the International Conference on the Internal Conversion Process at Vanderbilt University there has been more thought and study of the deviations from theory of the L-subshell ratios for E2 transitions in the rare-earth region. Figure 7 shows a plot of experimental measurements which are the sum of  $L_1/L_2$  and  $L_1/L_3$  from experiment divided by the average of this sum for the two theories, versus atomic number. This figure includes results presented at the Vanderbilt Conference by Stepic *et al*, Novakov *et al*, Graham and Geiger, Karlsson *et al*, and Brantley *et al*, and the published data of Herlander and Graham (1964). Lines are shown in Figure 7 and represent  $\pm 6$  percent error in theory which includes the claimed  $\leq 3\%$  uncertainty in the tabulated theoretical coefficients and  $\leq 3\%$  uncertainty in the interpolation. All of the experimental ratios are higher than the corresponding theoretical values. This disagreement is small ( $\leq 5\%$ ) in the heavy, spherical nuclei and within the errors of the theory. But the more deformed nuclei the discrepancies are, with one exception, outside the 6 percent error ascribed to theory and range up to 25 percent.

One notes, however, that the points with the largest discrepancies also have the largest uncertainties. The Chalk River group has considered this fact and

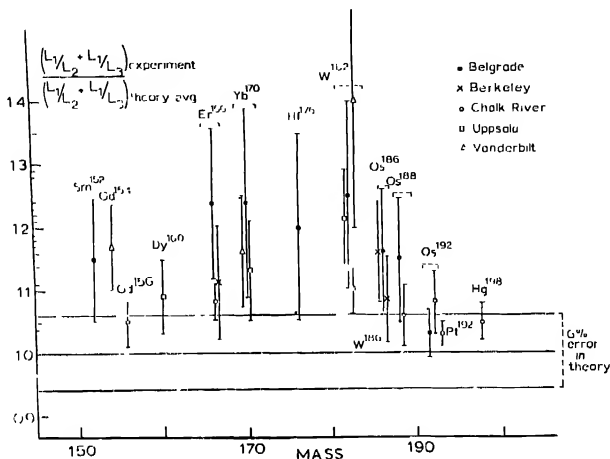


Fig. 7. Experimental values of  $L_1/L_2 + L_1/L_3$  divided by the averages of the theoretical values of Rose and of Sliv and Band. (The laboratories correspond to the following references; Belgrade, Stepić *et al*, 1965; Berkeley, Novakov and Hollander; Chalk River, Graham and Geiger and Herrlander and Graham, 1964; Uppsala, Karlsson *et al*, 1965; Vanderbilt, this paper)

feels that improvements in the accuracies of the measurements will bring theory and experiment into agreement within 6 percent. In order to clarify the differences between different experiments and between theory and experiment additional measurements and a careful study of the techniques of analyses should be made.

Further light is shed on this problem by studies of Hamilton *et al* (1965) on two deformed heavy elements  $\text{Th}^{228}$  and  $\text{Pu}^{240}$ . There the  $L_1/L_2$  and  $L_1/L_3$  results agree well with Sliv and Band but are 10-30% lower than those of Rose. This suggests that these effects may be related to the calculations of the weak  $L_1$  conversion coefficient and not to some nuclear structure effect.

#### REFERENCES

- Bard, Q. L., Nall, J. C., Haynes, S. K. and Hamilton, J. H., 1962, *Nucl. Inst. and Methods*, **16**, 275.  
 Brantley, W. H., Hamilton, J. H., Kotch, T. and Zganjar, E. F., to be published in 1966.  
 Brantley, W. H., Pancholi, S. C. and Hamilton, J. H., 1965, *Internal Conversion Processes*, Hamilton, H. H., editor, Academic Press, New York, 535.

## *L Subshell Ratios of E2 Transitions in Deformed, etc.* 177

- Daniel, H., Haefner, J., Lorenz, Th., Schult, O. W. B. and Gruber, U., (1964) *Nucl. Phys.* **56**, 147
- Graham, R. L. and Geiger, J., *private communication to the Vanderbilt conference and following it.*
- Hamilton, J. H., van Nooijen, B., Ramayya, A. V. and Brantley, W. H., 1965, *Internal Conversion Processes*, Hamilton, J. H., editor, Academic Press, New York, p. 511
- Herrlander, C. J. and Graham, R. L., 1964, *Nucl. Phys.* **58**, 544
- Karlsson, S. E., Anderson, I., Nilsson, O., Malmsten, G. and Aronberg, E., 1965, *private communication to the conference. Internal Conversion Processes*, Hamilton, J. H., editor, Academic Press, New York, p. 513. (An additional measurement was reported following the conference and is included in published proceedings.)
- Novakov, T. and Hollander, J. M., 1965, *private communication to the Vanderbilt conference.*
- Riedinger, L. L., Hamilton, J. H., and Johnson, N. R., 1966, *Bull. Am. Phys. Soc.* **11**
- Rose, M. E., 1958, *Internal conversion coefficients*, North-Holland Publ. Co., Amsterdam.
- Sliv, L. A. and Band, I. M., 1956, *Coefficients of internal conversion of gamma-radiation* (USSR Academy of Sciences, Moscow-Leningrad) Part I. K Shell, Part II. L Shell, *Gammas 1955*, ed. by Sliv, L. A., (1961), (USSR Academy of Sciences, Moscow-Leningrad)
- Stepie, R., Bogdanovic, M., Mladenovic, M., (1965), *Internal Conversion Processes*, Hamilton, J. H., editor, Academic Press, New York, 507

# $\Lambda$ -BINDING ENERGIES OF HYPERNUCLEI. (I)

A. K. DUTTA, D. BANERJEE AND P. GANGULY

UNIVERSITY COLLEGE OF SCIENCE,

92, ACHARYA PRAFULLA CHANDRA ROAD, CALCUTTA-9

(Received March 24, 1966)

**ABSTRACT.** It is considered that the  $\Lambda$ -binding energy of a Hypernucleus is related closely to the maximum binding energy of a nucleus with the same nucleon number as the particle number in the  $\Lambda$ -hypernucleus. The ratio between the  $\Lambda$ -binding energy and the binding energy  $E^*$  of the corresponding nucleus, gives us a smooth curve of the nature of a probability function when drawn against nucleon numbers. The curve may be expressed by the relation:  $\Lambda_{BE} = E^* A^\alpha \exp[-\chi(A)]$ . It is observed, on comparison that the function  $\chi(A)$  is representable in the form  $(\alpha E_n^0(A) - \beta)$ , where  $E_n^0(A)$  is the ground state energy per nucleon, uncorrected by coulomb and asymmetry energies (Dutta et al., 1965). The empirical finding suggests a statistical approach to nucleonic interactions.

The essential properties of hypernuclei have been summarised by Levi-Setti (1965), in a recent communication. It would be noted that  $\Lambda$ -binding energies decrease from a value of the order of 30 Mev. for large hypernuclei, through a range of value of the order of 10 Mev. for light hypernuclei, to the small magnitude  $\sim 0.3$  Mev. for  $\Lambda H^3$ . The hypernuclei  $\Lambda Li^6$ ,  $\Lambda He^4$  have binding energies as  $\sim 3$  and  $\sim 2$  Mev. These values are comparable with the binding energies of the order of 10 Mev for hypernuclei in the range  $\Lambda Li^7$  to  $\Lambda N^{14}$ .

It has been proposed by Dalitz (1958), that the  $\Lambda$ -binding energies may be represented by the relation:

$$\Lambda_{BE} = D - C \cdot A^{-2/3}, \quad \dots (1)$$

where  $D$  is the depth of the nuclear potential well affecting the  $\Lambda$ -hyperon and  $C$  is a constant. The binding energies of light hypernuclei from  $\Lambda Li^7$  to  $\Lambda N^{14}$  conform to the above relation with  $D \cong 26$  Mev and  $C \cong 80$ . The relation, however, gives no binding energies for lighter hypernuclei with 5, 4 and 3 particles. Also, the slowly increasing experimental values (Davies *et al* 1962) for large size hypernuclei are discordant with the equation (1).

It may be conjectured that the potential well to attract the  $\Lambda$ -particle is measured in terms of the maximum binding energy of a nucleus with the same nucleon number as the number of particles in the  $\Lambda$ -hypernucleus. As a consequence one may consider that the  $\Lambda$ -binding energies of a hypernucleus would be directly related to the maximum binding energy  $E^*$ , of a nucleus with the corresponding nucleon number. These  $E^*$  values are obtainable from the nuclear binding energy

tables (König *et al* 1962) The ratio  $\sigma = \Lambda_{B\pi}/E^*$  has been plotted in Fig. 1, for nucleon numbers from 2 to 100. The curve is similar to that expected for a probability function. It should be representable in the form :

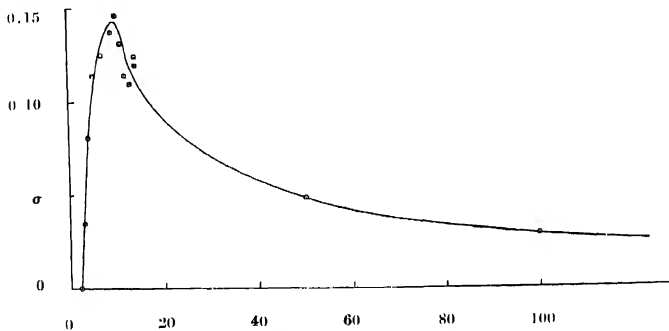


Fig. 1  $\sigma = \Lambda_{B\pi}/E^*$  against nucleon number.

$$\sigma = \Lambda_{B\pi}/E^* = F(A) \exp[-\chi(A)] \quad \dots (2)$$

The exponential function  $\chi(A)$  becomes smooth and regular with  $F(A)$  as  $A^2$ . The function  $\log_{10}(A^3/\sigma)$  has been plotted in Fig. 2, and has been expressed as -

$$\log_{10}(A^3/\sigma) = 7.25 + 7 \times 10^{-3}A - 3.3\{\exp[-2.08 \times 10^{-2}A]\}\{1 + 0.5 \exp[-.5 \times 10^{-3}A^2]\} \quad \dots (3)$$

The curve for  $\log_{10}(A^3/\sigma)$  is very similar to a curve that measures the energy per nucleon for different nucleon numbers in nuclei, without the coulomb and

15

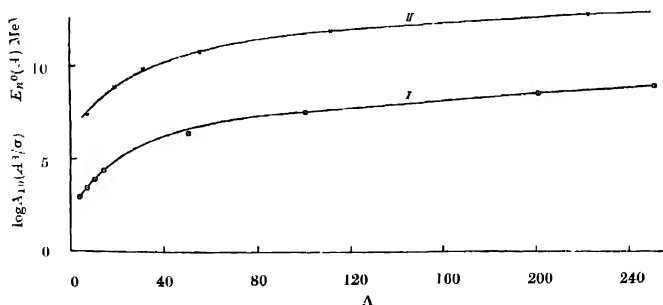


Fig. 2 (I)  $\log_{10}(A^3/\sigma)$  against nucleon number

(II)  $E_n^0(A)$  (binding energy, uncorrected for coulomb and asymmetry energies), against nucleon numbers.

asymmetry energy corrections. Such separations of nuclear binding energies into components  $-f(A)$  dependent only on nucleon number, the coulomb and asymmetry energy correction  $U_c$  and  $U_a$  have been done in a previous communication (Dutta *et al* 1965). It has also been worked out there that the binding energy per nucleon  $f(A)/A$  are 7.74, 8.75, 9.76, 10.80, 11.92 and 12.92 Mev., for nucleon numbers 7, 19, 31, 55, 111 and 222. These values of energies per nucleon have also been plotted in Fig. 2, to demonstrate the strong similarity of the curve for  $E_n(A)$  with the curve for  $\log_{10}(A^3/\sigma)$  although the two relations have been expressed in completely different ways. It implies that we can replace  $2.303 \log_{10}(\sigma/A^3) = \log_{10}(\sigma/A^3) = -\chi(A)$  by  $\{-\alpha E_n(A) + \varphi\}$  where  $E_n(A) = f(A)/A$  is the binding energy per nucleon dependent on nucleon numbers only,  $\alpha \cong 2.303$ ,  $\varphi \cong 2.303 \times d$ , where  $d$  is the displacement between the curves in Fig. 2. The complete expression for the binding energies of hypernuclei is, thus, expressible in the form :

$$\Lambda_{B_i} = E^* A^d \exp [-\alpha E_n(A) + \varphi] \quad \dots (4)$$

where  $\{\alpha E_n(A) - \varphi\}/2.303$  may be calculated by equation (3) and  $E^*$  is the maximum binding energy of a nucleus with its nucleon number equal to the particle number in  $\Lambda$ -hypernucleus. The experimental (Levi Setti, 1965) and calculated values of  $\Lambda_{B_i}$  together with the  $E^*$  values, taken from the binding energy table (Konig *et al* 1962) are given in Table I below

TABLE I  
(Experimental and calculated binding energies of hypernuclei in Mev),

$A$	4	5	7	10	12	14	50	100	200	250
$E^*$	28.3	27.3	39.2	65.0	92.2	105.3	438	863	1580	1870
$\Lambda_{B_i}$ (expt.)	2.3	3.1	5.5	~10	~10.5	~12	~20	~25	~30	~30
$\Lambda_{B_i}$ (calc.)	2.6	3.4	6.3	9.6	11.5	11.0	20.2	25.0	31.8	30.5

It is interesting to note that the exponential function in equation (4) is very similar to the corresponding part in the usual distribution function for particles with different energy values. The observation is of an empirical nature. It should, however, lead us to the formulation of a statistical model of nucleonic interaction in nuclei.

#### REFERENCES

- Levi Setti, R. 1965, *Endeavour*, **24**, 119.  
 Daltz, R. H., 1958, *Phys. Rev.*, **111**, 967.  
 Davies, H., Levi Setti, R., Raymond, M., Koggestad, S. and Tomasini, G., 1962, *Phys. Rev. Lett.*, **9**, 464.  
 Konig, L. A., Muttach, T. H. and Wapstra, A. H., 1962, *Nucl. Phys.*, **31**, 18.  
 Dutta, A. K., Pal, B., Ganguly, P. and Banerjee, D., 1965, *Prog. Theor. Phys.*, **33**, 1129

# NON-DEGENERATE STATISTICAL APPROACH TO THE BINDING ENERGY OF NUCLEI AND OF $\Lambda$ -HYPERNUCLEI (II)

A. K. DUTTA

UNIVERSITY COLLEGE OF SCIENCE,  
92, ACHARYA PRAFULLA CHANDRA ROAD, CALCUTTA-9.

(Received March 24, 1966)

**ABSTRACT.** The binding energy per nucleon of a hypothetical nucleus, without the coulomb and asymmetry energy corrections, is considered to be the mean value of neutron-proton interaction energy between neighbours. The numbers of neutrons and protons in the hypothetical nucleus are considered to be equal (to be modified when coulomb and asymmetry energies are taken into account) and thus the binding energy per nucleon,  $B_0(A)$ , is considered to be approximately constant for all the nucleons in a nucleus. In momentum space these nucleons are considered to be contained in different momentum shells, according to the nucleon numbers in the nucleus. This gives rise to the total number of combination states in different nuclei, which along with the modified non-degenerate Fermi distribution function determines the probable number of occupied states. To correspond to the required values of  $B_0(A)$  (Dutta, et al., 1965) the parameters in the relation are determined. The statistical relation, used as a relation to determine binding energy of neutrons, helps us in finding the relation for the binding energy of  $\Lambda$ -particles, in accordance with the one required empirically.

The binding energies of nuclei, in ground state, consists of a major portion dependent on the total nucleon number " $A$ " and the associated correction terms which are dependent on  $Z$  for coulomb repulsion and on  $(N - Z)$  for asymmetry. The Bethe-Weizsacker relation or its proposed modification (Dutta *et al* 1965), put the binding energies of such nuclei primarily dependent on these three characteristics of nuclear composition. It should be a realisable and comparatively simpler procedure to find an expression for the binding energy of the total nucleon number in a nucleus, without the associated corrections for coulomb repulsion and asymmetry and then to ascertain the corrections.

It may be observed from the empirically fitted Bethe-Weizsacker relation (Green, 1958) or from the modified relation, that the binding energy per nucleon in a nucleus, in ground state, before the aforesaid corrections are made, increases with nucleon numbers. This is presumably on account of the decrease in the proportion of surface nucleons. It would be expected that both the kinetic and the potential energy per nucleon, in ground state, contribute towards this increase in energy per nucleon.

This binding energy per nucleon, might be caused by the interaction between neutrons and protons, when they are neighbours and react by exchange forces. This is in accordance with the view of Bethe and Bacher (1936), as stated on page 150 and 95 of their communication, that "any given nuclear particle interacts essentially with two (neighbouring) particles of the other kind" and that "the nuclear forces have the character of exchange forces between neutrons and protons". On such a basis, when we do not take into account the asymmetry or coulomb energy terms, we have the hypothetical case of nuclei composed of equal or nearly equal numbers of interacting protons and neutrons, such that half the binding energy of a neutron proton pair or rather one fourth the binding energy between two protons and two neutrons, which are neighbours, is regarded as the binding energy per nucleon. The corrections bring down the binding energy of the hypothetical nucleus to the actual value obtaining there

The energy per nucleon of the hypothetical nucleus, thus considered, is expected to be fairly constant for all the nucleons both in respect of their kinetic and potential energy constituents. For nuclei with larger nucleon numbers both the constituents increase, in accordance with our previous observation. Thus, for a particular nucleus, without the corrections, we may take the potential energy per nucleon  $V_n^0(A)$ , as approximately constant, giving us immediately the total potential energy of the nucleus. This eliminates the usual process of potential energy calculation by relations of the form :

$$V = \sum_{i=1}^Z \sum_{k=1}^N \psi_i^*(x_1) \psi_i(x_2) \varphi_k^*(x_2) \varphi_k(x_1) J(r_{12}) d\tau_1 d\tau_2 \quad (B)$$

as suggested by Bethe and Bacher (1936), where  $\psi_i(x_i)$  and  $\varphi_k(x_k)$  refer to the solutions of one particle wave equations for the protons and neutrons and  $J(r_{12})$  is the interaction potential. The kinetic energy  $T_n^0(A)$  per nucleon in the ground state, similarly, is considered to be fairly constant for all the nucleons in a nucleus. It should, however, have a range to accommodate the different energy states of the nucleons, which are exclusive. It would naturally require larger range of energy for nuclei with larger nucleon number. Other possible dispositions of nucleons for any particular nucleus would have less binding energy and the associated kinetic energy. The total energy per nucleon  $E_n^0(A)$ , in a nucleus in the ground state may, however, be considered to be determined by the sum,

$$E_n^0(A) = T_n^0(A) + V_n^0(A). \quad \dots (1)$$

We may, thus, state that if the nucleons are distributed in momentum space, the corresponding values for all the nucleons in the nucleus, in ground state, would lie in a momentum shell  $4\pi(p_n^0)^2 dp$ , rather than be distributed to fill up the momentum space  $\frac{4}{3}\pi p^3$ , with  $p$  varying from 0 to  $p_{max}$ , which is the usually adopted procedure (Fermi 1950)



The number of states for such neutrons and protons in the nucleus, when spin degeneracy is taken into account, would be determined by the expressions,

$$\frac{8\pi\Omega}{h^3} (p_N^2 dp_N)^0 \text{ and } \frac{8\pi\Omega}{h^3} (p_P^2 dp_P)^0,$$

where  $\Omega$  is the enclosing three dimensional space. The neutron-proton combination states in the shell, where each of the neutron states could combine with each of the proton states, would be given by the product as

$$C_j = \left( \frac{8\pi\Omega}{h^3} \right)^2 (p_N^2 dp_N)^0 (p_P^2 dp_P)^0 \quad \dots \quad (2)$$

Such a combination of neutron and proton states is also envisaged in the expression for the potential energy  $V$ , in eqn (B) above, used by Bethe and Bacher

We consider  $\Omega$  as well as  $(p_n^0)^2$ , which increases with  $A$ , to be primarily proportional to  $A$ . In the case of small nuclei with less than about fourteen nucleons, however, the nuclear volume in some nuclei or the binding energy in others, is known to decrease much more slowly than required by the proportionality with  $A$  (Holstadter, 1956). Such irregularity in the range of small nuclei may be taken into account by a term of the form  $f(A) = \{1 + S(A)\}$ , as an additional factor in the converted equation (2) for cell numbers. It is considered that the structure dependent constituent  $S(A)$  establishes itself comparatively slowly, at the dynamically equilibrium condition of the nucleus, in ground state. It gives us the total number of possible combination cells for a nucleus, given by nucleon number as

$$C(A) \propto A^2 f(A) \int_0^{P_N^0} \int_0^{P_P^0} (p_N^2 dp_N) (p_P^2 dp_P) \\ \propto A^5 f(A) \quad \dots \quad (3)$$

Let us now consider the distribution of  $N$  combinations of neutron and protons, with the total energy  $E$ . The combinations may be placed in different energy shells, corresponding to the nuclei of different ' $A$ ' values. The number of cells in a particular shell is  $C(A)$ , with  $N(A)$  nucleons of one type, in each combination that is associated with the energy  $2E_n^0(A)$ , for the shell. The conditions

$$\Sigma N(A) = N ; \Sigma N(A) \cdot 2E_n^0(A) = E$$

and the distribution number satisfying Fermi or Bose distribution,

gives the usual form of most probable distribution function,

$$N(A) = C(A) \left\{ \exp \left( \frac{E_n^0(A) - E_F}{kT} \right) \pm 1 \right\}^{-1} \quad \dots \quad (4)$$

We consider the problem to be nondegenerate for nuclei, with  $A \geq 4$ , on account of the large nucleonic energy and mass. This would give us the simplified nondegenerate statistical relation connecting the number of occupied states and the ground state energy of the nucleons in different nuclei as,

$$N(A) \propto A^4 f(A) \exp \left( -\frac{E_n^0(A) + E_F}{KT} \right) \quad (5)$$

We have considered here that the number of occupied single states is  $A/2$ , with the energy  $E_n^0(A)$ , associated with the occupied combination states  $N(A)$  in a nucleus. If we restrict ourselves to these single states, we have the more explicit form of equation (5) as,

$$A/2 = kA^4 f(A) \exp [-E_n^0(A)/KT] \quad \dots (6)$$

$$1 = 2k \cdot A^4 f(A) \exp [-E_n^0(A)/KT], \quad \dots (6a)$$

where  $\exp E_F/KT$  has been incorporated in the constant of proportionality.

The relation (6) implies that half the occupied single state nucleonic cells equals the probability of occupation of cells with the energy of a single neutron or proton, out of the total cell number. Further since 1/2 unit of occupied single state neutron and proton cells measures 1 unit of occupied neutron or proton cell, we may put the equation (6) also in the form

$$1. (\text{occupied neutron cell}) = kA^4 f(A) \exp [-E_n^0(A)/KT] \quad (6b)$$

The equation (6a) is very suitable to determine the binding energy  $E_n^0(A)$  of a nucleon in ground state, for different nucleon numbers  $A$ . The parameters  $k$ ,  $KT$  and  $f(A)$  have been determined such that the values of  $E_n^0(A)$ , determined from the relation (6a), more or less agree with the values obtained in a previous work (Dutta *et al* 1965) where the values of  $E_n^0(A)$  along with the expected amounts of the coulomb and asymmetry energy contributions, give us the binding energies of nuclei, in close approximation to the observed magnitudes. We, thus, obtain eq. (6a) in explicit form as

$$1 = 2 \times 2.327 \times 10^4 \{1 + S(A)\} A^4 \exp [-E_n^0(A)/0.40] \quad \dots (6c)$$

with  $S(A) = 4.2 \exp [-3.27 \times 10^{-2} A^2]$

The required  $(KT)$  value varies from 6 to 3 per cent of nucleonic energy.

It may be stated that too large coulomb repulsion energy for larger nuclei, with equal proton and neutron numbers, and a consequent too large internucleonic

separation for nucleonic interaction to be effective, introduces the asymmetric nucleons which are not as strongly bound. This brings in the associated corrections. It may also be noted that such non-degenerate statistical approach to the binding energy of the nuclei automatically incorporates the Bethe-Weizsacker relation, from which we started. The numbers of protons and neutrons in a nucleus and the magnitudes of the asymmetry and coulomb energy corrections are to be determined by considering proper functional forms of the two corrections in terms of  $A$  and  $Z$  and finding the particular value of  $Z$  that makes the sum of the corrections a minimum.

The statistical relations discussed so far must necessarily be concerned with the determination of the number of particles occupying different energy states, in the equilibrium condition. One can not extend these statistical relations, as such, to nonequilibrium condition. We may, however, consider these statistical relations in the reverse way, to determine the energy per nucleon in the ground state in terms of a function of the nucleon number  $A$ . Such a consideration may then be extended to include the non-equilibrium states also. It would be seen from eq. (7) below, that the ground state binding energy of a neutron is determinable in units of  $E_N^0(A)$ , by a measure expressed in terms of  $A$ . An appropriate change in the functional form of the measure, would give us the binding energy in the nonequilibrium states also, in units of ground state energy  $E_N^0(A)$ . Thus, we may rewrite eq. (6b) in the equivalent form

$$E_N(A) \cdot \lambda = E_N^0(A) [2.327 \times 10^4 A^{\frac{1}{2}} \{1 + S(A)\} \exp \{-E_N^0(A)/0.40\}] \quad (7)$$

where the values of  $k$  and  $KT$  ascertained in eq. (6c) have been incorporated. The functional form associated with  $E_N^0(A)$ , on the right hand side, is the measure of ground state energy in units of  $E_N^0(A)$ . The binding energy per neutron  $E_N^0(A)$ , in non-equilibrium state, would be determined by the correspondingly changed functional form in the expression for the measure. In the case of the neutral  $\Lambda$ -particles we consider that the comparatively slow structure dependent constituent  $S(A)$  drops out and that the parameter  $(KT)$  is suitably modified. This would give us the binding energy of the  $\Lambda$ -particles in different associations, as

$$\begin{aligned} \Lambda_{B\pi} &= E_N^0(A) [2.327 \times 10^4 A^{\frac{1}{2}} \exp \{-E_N^0(A)/(kT)\Lambda\}] \\ &= 2.327 \times 10^4 E_N^0(A) \cdot A^{\frac{1}{2}} \exp \{-E_N^0(A)/0.42\}, \quad \dots \quad (7a) \end{aligned}$$

where  $E_N^0(A)$  is the uncorrected total binding energy of the nucleus,  $E_N^0(A) \times \Lambda$  and  $(KT)\Lambda$  as 0.42 Mev, has been ascertained by trial. A similar expression on empirical approach, has been found in the previous note (Dutta *et al* 1, 1966), to be suitable for the determination of the binding energies of the  $\Lambda$ -hyperons.

The calculated values of  $E_N^0(A)$  and  $\Lambda_{B\pi}$  by equations (6c) and (7a), along with the previously obtained values (Dutta *et al* 1965) of  $E_N^0(A)$  and the experimental values of  $\Lambda_{B\pi}$  (Levi Sotti 1965), are tabulated below :

TABLE I

$A$	$E_0^n(A)$ eq (6c)	$E_0^n(A)$ (Previous)	$\Delta B_t$ eq.(7a)	$\Delta B_t$ (exp)
4	7.02	—	2.3	2.3
5	7.30	—	3.0	3.1
7	7.66	7.74	5.1	4.9—5.5
8	7.79	7.80	6.5	6.4—6.6
10	8.04	7.83	9.0	8.5—10.0
13	8.41	8.10	11.3	10.6
14	8.52	8.20	11.8	12.0—13.0
19	9.01	8.75	13.2	—
31	9.80	9.76	15.8	—
55	10.71	10.80	19.2	~20
111	11.83	11.92	24.3	~25
222	12.95	12.92	30.2	~30
250	13.14	13.03	31.4	~30

## REFERENCES

- Dutta, A. K., Pal, B., Ganguly, P. and Banerjee, D., 1965, *Prog. Theo. Phys.*, **33**, 1129.  
 Green, A. E. S., 1958, *Rev. Mod. Phys.*, **30**, 569.  
 Bethe, H. A. and Bacher, R. F., 1936, *Rev. Mod. Phys.*, **8**, 82.  
 Fermi, E., 1950, *Nuclear Physics*, Univ. Chicago Press, p. 159.  
 Holstadter, R., 1956, *Rev. Mod. Phys.*, **20**, 214.  
 Dutta, A. K., Banerjee, D. and Ganguly, P., 1966, *Indian J. Phys.*, **40**, 178.  
 Levi Setti, R., 1965, *Endeavour*, **24**, 119.

# DIELECTRIC ABSORPTION OF 3.14 CM MICROWAVES IN SOME POLAR LIQUIDS—PART II. SUBSTITUTED HALO-BENZENES AND NAPHTHALENE

J. BHATTACHARYYA, S. B. ROY AND G. S. KASTHA

(OPTICS DEPARTMENT

INDIAN ASSOCIATION FOR THE CULTIVATION OF SCIENCE,

CALCUTTA-32

(Received December 24, 1965)

**ABSTRACT.** The dielectric losses of chloro-, bromo-, metadichloro and 1, 2, 4-trichlorobenzene and of  $\alpha$ -chloronaphthalene in the liquid state at different temperatures due to absorption of microwaves of wavelength 3.14 cm. have been measured and the values of time of relaxation ( $\tau$ ) of all the compounds have been determined. It has been shown from the results that the viscous forces ( $\zeta$ ) inhibiting the rotations of the molecules of these compounds in the liquid state are functions of the macroscopic viscosities ( $\eta$ ) of the respective liquids and that the internal friction  $\eta_{int}$  may be put in the form  $\eta_{int} = \text{Const. } \eta^\gamma$ , where  $\gamma$  is the ratio of the molar heats of activation for dielectric relaxation and viscous flow. Further, from a comparison of the  $\tau$ -values of chloro-, bromo- and metadichloro-benzene and of  $\alpha$ -chloronaphthalene in the liquid state with the  $\tau$ -values of the respective compounds in solution in non-polar solvents with viscosities equal to or greater than that of the respective pure liquids, it has been concluded that at least in the present case of liquids having molecules with dipole moment about 1.5 D, the dipolar interactions have only minor effect on the times of relaxation of the molecules.

## INTRODUCTION

The time of relaxation of some organic polar molecules with rigid dipoles such as chlorobenzene, bromobenzene,  $\alpha$ -chloronaphthalene etc. in the liquid state and in dilute solution in benzene at different temperature in different radio frequency regions were investigated by many workers (Whiffen and Thompson, 1946, Hennelly *et al.*, 1948, Fischer, 1949, Curtiss *et al.*, 1952, William 1959, Smyth 1955). Smyth (1955) made a comparison of the  $\tau$ -values of a number of organic molecules in the liquid state and in solutions in benzene at a certain temperature and concluded that the larger values of  $\tau$  in the pure liquid compared to those in dilute solutions might be due to dipolar interactions in the liquids which are almost absent in very dilute solutions. In making such conclusion the effect of the difference in the viscosities of the two media on  $\tau$ -values has not been properly taken into account. The object of this investigation was to study how the dipole-dipole interactions influence the  $\tau$ -values of molecules with rigid dipoles in the liquid state and as such a systematic investigation on the  $\tau$ -values of some molecules with rigid dipoles in the liquid state and in solution in non-polar solvents at

different temperatures was undertaken so that the effect of the viscosity, temperature and other parameters could be considered. The results are also expected to throw some light on the dependence of the internal friction on macroscopic viscosity of the medium.

In a previous communication (Bhattacharyya *et al.* 1964) it was shown that in the case of some polar alkyl benzenes in the liquid state composed of molecules with dipole moments about 0.5D, such dipolar interactions are negligible. In the present paper the results of investigation on some substituted benzenes and naphthalene with rigid dipoles having dipole moments about 1.5D have been discussed.

#### EXPERIMENTAL

The compounds studied in the present investigation are chlorobenzene, bromobenzene  $\alpha$ -chloronaphthalene, metadichloro-benzene and 1, 2, 4-trichloro benzene. All the chemicals, obtained from reputed firms, were of chemically pure quality. These were first fractionated and the proper fractions were repeatedly distilled under reduced pressure and dried by usual methods before being used in the investigation. The experimental arrangement for the determination of dielectric loss at 3 cm is as shown in Figure 1.

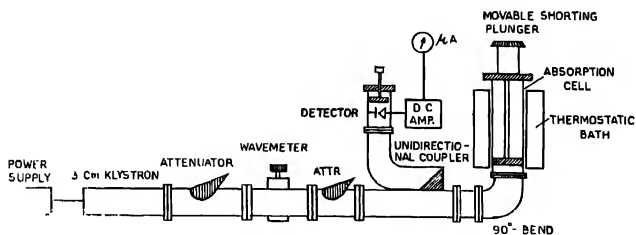


Fig. 1. Schematic diagram of experimental arrangement for determining dielectric loss at 3.14 cm.

$\epsilon'$  and  $\epsilon''$  were calculated from the variations of the reflected power as the shorting plunger is moved in the liquid filled wave guide absorption cell. The magnitudes of the maximum and minimum power and the distance between the successive minima were used for the calculations of  $\epsilon'$  and  $\epsilon''$  following the method due to Surber (1948). The temperature of the absorption cell was maintained constant with the help of a thermostat. The  $\tau$ -values were calculated from  $\epsilon''$ -values by using Debye equation for polar liquids as usual. The values of  $\epsilon_0$  (static dielectric constant) of all the compounds and the macroscopic viscosities ( $\eta$ ) of chloro-bromo- and metadichlorobenzene were taken from standard literatures. The viscosities of 1, 2, 4-trichlorobenzene and  $\alpha$ -chloronaphthalene at different temperatures were determined experimentally.

larger because of the presence of dipolar interaction. So, it may be inferred that dipole-dipole interactions in these liquids have only minor effect on the  $\tau$ -values. This conclusion is also expected to hold in the case of  $\alpha$ -chloronaphthalene molecules having dipole moments almost the same as those of chloro, bromo- or meta-dichlorobenzene. Moreover, because of greater size of the  $\alpha$ -chloronaphthalene molecule and consequently because of greater separation between the dipoles, the dipolar interactions would be less effective than in the above liquids. From these consideration it is expected that the  $\tau$ -values of  $\alpha$ -chloronaphthalene in dilute paraffin solution should be greater or at least equal to those in the pure liquid. But actually, the reverse is the case. This would suggest that the larger values of  $\tau$  in the case of  $\alpha$ -chloronaphthalene in the liquid state may not be due to dipolar interactions in the liquid, but may be due to peculiarity in the arrangement of molecules in the liquid state.

From these it may be concluded that at least in the case of polar liquids composed of rigid molecular dipoles having moderate moments (about 1.5D), the influence of dipolar interactions on the time of relaxation is less important than that of structural hindrances.

#### REFERENCES

- Bhattacharyya, J., Roy, S. B. and Kastha, G. S., 1964, *Indian J. Phys.* **38**, 545.  
 Budo, A., Fischer, E. and Miyamoto, S., 1939, *Physik. Z.* **49**, 337.  
 Curtiss, A. J., McGeer, P. L., Ruhnmann, G. B. and Smyth, C. P., 1952, *J. Am. Chem. Soc.*, **74**, 644.  
 Fischer, E., 1949a, *Z. Electrochem.* **53**, 16.  
 " " 1949b, *Z. Naturf.* **44**, 707.  
 Hennesly, E. J., Heston, W. M. J. and Smyth, C. P., 1949, *J. Am. Chem. Soc.*, **79**, 1102.  
 Peirin, F., 1934, *J. de. Phys.* (7) **5**, 497.  
 Sinha, B. (Miss), Roy, S. B. and Kastha, G. S., 1965, *Indian J. Phys.* **39**, 328.  
 Smyth, C. P., 1955, *Dielectric Behaviour and Structure*, McGraw-Hill Book Company.  
 Surber, W. H. J., 1948, *J. Appl. Phys.* **19**, 574.  
 Williams, G., 1959, *J. Phys. Chem.*, **63**, 534.  
 Whiffen, D. H., and Thompson, H. W., 1946, *Trans. Farad. Soc.* **42**, 114.

# DYNAMICS OF VIBRATION OF A CANTILEVER UNDER LATERAL IMPACT OF AN ELASTIC LOAD

(General Theory—Part I)

B B BANERJEE

PHYSICS DEPARTMENT : UNIVERSITY COLLEGE OF ENGINEERING, BURLA-ORISSA

(Received September 11, 1965)

**ABSTRACT.** In this paper (which forms part I of a series of papers to appear), the writer works out the dynamics of vibration of a cantilever due to lateral impact of an elastic load at the free end as also at its middle. The cantilever is at rest before impact begins and is supposed to behave like a loaded beam so long as the load is in contact with it. The elastic load is taken to be hard load backed by weightless spring. Each of the expressions for displacement of the bar and pressure of impact comes out in forms of respective series involving directly measurable quantities, mass, length, shape and young's modulus of the material of the cantilever and the striking distance as also the striking velocity and the mass of the load. Unlike previous theories, the present theory is built up without assuming any law of force between the load and the beam. The theory is perfectly general and can be easily followed in case of beams with different end conditions. The agreement between the theory and the experiment is remarkable.

## INTRODUCTION

Young (1807), Hodgkinson (1833), Cox (1856), St. Venant (1883), Timoshenko (1956), Hoppman (1948), Ghosh Ray (1955) and others have tried to develop the dynamics of vibration of a beam under lateral impact of a load. H. L. Mason (1936), Hoppman, Timoshenko, have given a partial account of the history of beam-impact problems. The major analytical investigation of the problem started from Cox H., who assumed the deflection of the beam under dynamic condition of impact has the same value as given by statical deflection condition. Further he assumed that the impinging ball moves with the beam until the kinetic energy of the system is completely transformed into potential energy of bending. St Venant (1883), developed a theory on the assumption that the impinging body remains attached with the beam for half the period of vibration. He suggested that the vibration of such a beam can be expressed as a series of normal functions. His case can be looked upon as a loaded beam excited by initial velocity at the point of loading. Experimental observations, made by the writer as also other workers showing existence of multiple contacts within a total period of impact and the load terminating its contact before the maximum deflection is reached, give evidence contrary to these assumptions.

Timoshenko derived the integral equation for the case of the central impact of a load on a simply supported beam. He assumed a definite law of force between



ball and the beam and worked out the problem in line of forced vibration. Further taking into account, the local deformation of the contact region, he considered Hertz's theory of impact which depends on a knowledge of the geometric and elastic properties of materials at contact surface in specific beam-load system to obtain expression for displacement of the beam. Further, as remarked by Hoppman, the procedure consumes much time and so it is not satisfactory. But the solution of the problem as given by Hoppman, on the basis of an assumption of a 'normalised force' of sinusoidal character involve prior determination of some quantities, one of these quantities is co-efficient of restitution for which a formula must be provided in terms of known functions.

Ghosh and Ray considered the problem of lateral impact at the free end of a cantilever. Subsequently Ray applied the same deductions of the problem in case of the load striking at any point of the bar. But such application is not valid and leads to error as he assumed the shearing force to be equal in values with the change in the shearing force, incurred in crossing the struck point, and they could not anticipate correct boundary conditions at the struck point.

Thus, as the force between the load and the beam is not known apriori, these workers had assumed this force as known function of time. The theories are not general.

The present writer develops the dynamics of the problem in a straight forward way. Operational method due to Heaviside has been employed to work out the problem. The main idea upon which the theory is built up is that, the cantilever behaves like a loaded beam so long as the load is in contact with it. Further within limits of elasticity and for a finite and constant area of contact, the pressure exerted by the hammer during impact is proportional to the compression of the hammer. Displacement of the centre of gravity of the hammer at any instant is the displacement of the cantilever together with compression of the load. The shearing force is not continuous near the struck point. The pressure exerted by the hammer is equal to the alteration in the value of the shearing force in the cantilever incurred in crossing the struck point.

#### EXPLANATION OF SYMBOLS

$l$  = length of the cantilever =  $a + b$

$a$  = segment of cantilever towards the fixed end

$b$  = segment of cantilever towards the free end

$t$  = variable time

$x$  = variable measured along the length of cantilever, being fixed at  $x = 0$ , and free at  $x = l$

$y_a$  = displacement of the struck point  $x = a$

$y_1$  = displacement at any point  $x < a$

$y_2$  = displacement at any point,  $a < x$

$M$  = mass of the cantilever

- $E_1$  = Young's modulus of the material of the cantilever  
 $I$  = moment of inertia of cross section about the neutral axis  
 $k$  = radius of gyration of cross section  
 $c$  = velocity of longitudinal waves in the cantilever  
 $m$  = mass of the load (hammer)  
 $v_0$  = velocity of the load before impact  
 $u$  = compression of the load  
 $z$  = displacement of the load =  $y_a + u$   
 $nl = \gamma, \quad na = k_1\gamma, \quad nb = k_2\gamma;$   
 $E_2$  Elastic constant of the load (other than Young's modulus)  
 $\frac{M}{m}$  = 'mass ratio'  
 $D = \frac{d}{dt}$  (operator)  
 $\phi_0$  = duration of impact  
 $J =$  ,  
 $n = \sqrt{\frac{iD}{KC}}$   
 $\frac{E_1 I}{K^2 C^2} = \frac{M}{l}$

The equation of motion of the transverse vibration of the bar is given by

$$\frac{d^2 y}{dt^2} + k^2 c^2 \frac{d^4 y}{dx^4} = 0 \quad \dots (1)$$

which can be written as

$$\frac{d^4 y}{dx^4} + \frac{D^2}{k^2 c^2} y = 0 \quad \dots (2)$$

The solution of this equation is given by

$$y = R_1 \sinh nx + R_2 \cosh nx + R_3 \sin nx + R_4 \cos nx$$

where

$$n = \sqrt{\frac{iD}{kc}}$$

In our problem the load strikes the cantilever at  $x = a$ , and if  $y_a$  is the displacement of the struck point, we have

$$\text{at } x = 0, \quad y = 0, \quad \text{and } \frac{dy}{dx} = 0, \quad \dots (3.1)$$

$$\text{at } x = l, \quad \frac{d^2 y}{dx^2} = 0, \quad \text{and } \frac{d^3 y}{dx^3} = 0, \quad \dots (3.2)$$

is also

$$\text{at } x = a, \quad y_1 = y_a = y_2, \quad (3.3)$$

$$\left( \frac{dy_1}{dx} \right)_{x=a} = \left( \frac{dy_2}{dx} \right)_{x=a} \quad (3.4)$$

$$\left( \frac{d^2y_1}{dx^2} \right)_{x=a} = \left( \frac{d^2y_2}{dx^2} \right)_{x=a} \quad (3.5)$$

With the help of equations (3), we have

$$y_1 = y_a \frac{\Delta_1 (\sinh nx - \sin nx) + \Delta_2 (\cosh nx - \cos nx)}{\Delta_0} \quad (4.1)$$

$$y_2 = y_a \frac{\Delta_3 [\sinh n(l-x) + \sin n(l-x)] + \Delta_4 [\cosh n(l-x) + \cos n(l-x)]}{\Delta_0} \dots \quad (4.2)$$

where

$$\Delta_1 = 2[\sinh nl \sin nb - \cosh nl \cos nb - \sinh nl \sinh nb - \cos nl \cosh nb - \cosh na - \cos na] \dots \quad (5.1)$$

$$\Delta_2 = 2[\sinh nl \cos nb + \sin nl \cosh nb - \cosh nl \sin nb - \cos nl \sinh nb + \sinh na + \sin na] \dots \quad (5.2)$$

$$\Delta_3 = 2[\cosh nl \cos na - \sinh nl \sin na - \sin nl \sinh na - \cos nl \cosh na + \cosh nb - \cosh nb] \dots \quad (5.3)$$

$$\Delta_4 = 2[\cosh nl \sin na - \sinh na \cos nl - \sinh nl \cos na + \sin nl \cosh na - \sin nb + \sinh nb] \dots \quad (5.4)$$

$$\Delta_0 = 4[\cosh na \sin na - \sinh na \cos na + \sinh nb \cos nb - \cosh nb \sin nb + \cosh na \cosh nb \sin nl - \cos na \cos nb \sinh nl] \dots \quad (5.5)$$

since  $nl = \gamma$ , we shall henceforward write  $na = k_1\gamma$ ,  $nb = k_2\gamma$ , as  $k_1 = \frac{a}{l}$ ,

and  $k_2 = \frac{b}{l}$ .

The pressure exerted by the load is given by

$$P = m \frac{d^2z}{dt^2} = -E_2 u \text{ (by Hooke's law)} \dots \quad (6.1)$$

and subsequent motion of the load is represented by the equation

$$m \frac{d^2z}{dt^2} = E_1 I \Delta \left( \frac{d^3y}{dx^3} \right)_{x=a} \dots \quad (6.2)$$

where  $\Delta \frac{d^3y}{dx^3}$  is the alteration in the values of  $\frac{d^3y}{dx^3}$  in crossing the struck point.

and  $E_1 I \Delta \left( \frac{d^3 y}{dx^3} \right)_{x=a}$  can be written from the values of  $y_1$  and  $y_2$  in eqns. (4)

$$\text{as} \quad E_1 I y_a n^3 f(D), \quad \dots (6.3)$$

where, at  $x = a = l$ , i.e., for the struck point at the free end,

$$f(D) = \frac{1 + \cosh \gamma \cos \gamma}{\sinh \gamma \cos \gamma - \cosh \gamma \sin \gamma} \quad \dots (7.1)$$

and at  $x = a = l/2$ , i.e., for the middle point of the bar being struck point,

$$f(D) = \frac{2(1 + \cosh \gamma \cos \gamma)}{\sinh \gamma \cosh^2 \frac{\gamma}{2} - \cosh^2 \frac{\gamma}{2} \sin \gamma} \quad \dots (7.2)$$

With the help of eqn. (6.3), eqn. (6.1) and eqn. (6.2), can be written as

$$m D^2 y_a + m D^2 u - E_1 I y_a n^3 f(D) = D J \quad \dots (8.1)$$

$$m D^2 y_a + m D^2 u + E_2 u = D J \quad \dots (8.2)$$

Now solving these equations for  $y_a$  and  $u$ , we get,

$$\frac{y_a}{v_0} = \frac{F(D)}{F_1(D)} = \frac{D}{D^2 \frac{E_1 I}{m} n^3 \left( 1 - \frac{m}{E_2} D^2 \right) f(D)} \quad \dots (9.1)$$

$$u = - \frac{E_1 I}{E_2} \frac{1}{m} y_a n^3 f(D) \quad \dots (9.2)$$

With the help of Heaviside's expansion theorem

$$\frac{y_a}{v_0} = \frac{F(0)}{F_1(0)} + \sum \frac{F(\alpha_s)}{\alpha_s F_1'(\alpha_s)} e^{\alpha_s t} \quad \dots (10)$$

where summation extends over all roots of  $D = [\alpha_s]$ , ( $s = 1, 2, 3, \dots r$ )

Now  $F(0) = 0$ , putting  $D = 0$ , and  $F_1(0) \neq 0$ ,

$$\text{as for } x = a = l, \quad F_1(0) = \frac{3 E_1 I}{M l^3}$$

For roots of  $D$  from  $F_1(D) = 0$ , we have  $F_1(D) = 0$ , when from eqn. (9), for  $x = a = l$ ,

$$\frac{1 + \cosh \gamma \cos \gamma}{\cosh \gamma \sin \gamma - \sinh \gamma \cos \gamma} = \frac{\frac{m}{M} \gamma}{1 - \frac{E_1 I}{E_2} \cdot \frac{m}{M} \frac{\gamma^4}{l^3}} \quad \dots (11.1)$$

for  $x = a = \frac{l}{2}$ ,

$$\frac{2(1 + \cosh \gamma \cos \gamma)}{\cosh^2 \frac{\gamma}{2} \sin \gamma - \sinh \gamma \cos^2 \frac{\gamma}{2}} = \frac{\frac{m}{M} \gamma}{1 - \frac{E_1 l}{E_2} \cdot \frac{m}{M} \cdot \frac{\gamma^4}{l^3}} \quad \dots \quad (11.2)$$

Eqs. (11.1) and (11.2), can be solved graphically by plotting for  $x = a = l$ ,

$$\eta_1 = \frac{1 + \cosh \gamma \cos \gamma}{\cosh \gamma \sin \gamma - \sinh \gamma \cos \gamma} \quad \dots \quad (11.3)$$

$$\eta_2 = \frac{\frac{m}{M} \gamma}{1 - \frac{E_1 l}{E_2} \cdot \frac{m}{M} \cdot \frac{\gamma^4}{l^3}} \quad \dots \quad (11.4)$$

and for  $x = a = \frac{l}{2}$ ,

$$\eta_1 = \frac{2(1 + \cosh \gamma \cos \gamma)}{\cosh^2 \frac{\gamma}{2} \sin \gamma - \sinh \gamma \cos^2 \frac{\gamma}{2}} \quad \dots \quad (11.5)$$

and

$$\eta_2 = \frac{\frac{m}{M} \gamma}{1 - \frac{E_1 l}{E_2} \cdot \frac{m}{M} \cdot \frac{\gamma^4}{l^3}} \quad \dots \quad (11.6)$$

As  $\eta_2 \sim \gamma_s$  curve exists only in the positive direction, the different values of  $\gamma_s$  are obtained from the intersections of two sets of curves  $\eta_1 \sim \gamma_s$  and  $\eta_2 \sim \gamma$ , lying entirely in positive quadrants. Thus  $\gamma_s$  assumes different sets of values for different struck points.

Therefore  $nl = \gamma_s$ ,  $\gamma_s =$  pure number (for  $s = 1, 2, 3, \dots r$ ) ... (12.1)

Thus  $D = [\alpha_s] = \pm i q_s$ , ... (12.2)

where  $q_s = \gamma_s^2 \cdot \sqrt{\frac{E_1 l}{M l^3}}$ , ... (12.3)

After some mathematical manipulation and with the help of Heaviside's expansion theorem (eqn. 10) we finally get,

for  $x = a = l$ , i.e., at the free end of the bar

$$y_l = \sum_{s=1}^{\infty} \frac{4v_0}{1 + \frac{3m}{E_2} q_s^2} \times \frac{\sin q_s l}{q_s} \dots \quad (13.1)$$

$$+ \frac{M}{1 - \frac{m}{E_2} q_s^2} \left[ 1 - \frac{m}{E_2} q_s^2 \right] + \frac{2\gamma_s}{\cosh \gamma_s - \cot \gamma_s}$$

The same expression was obtained by Ghosh-Ray but their deduction was faulty as stated earlier.

Again at  $x = a = \frac{l}{2}$ , i.e., for centre-struck case,

$$y_{\frac{l}{2}} = 4v_0 \sum \frac{\sin q_s l / q_s}{1 + \frac{3m}{E_2} q_s^2} \dots \quad (13.2)$$

$$+ \gamma_s \frac{\cosh \gamma_s \sin \gamma_s - \sinh \gamma_s \cos \gamma_s}{1 + \cosh \gamma_s \cos \gamma_s}$$

$$+ \gamma_s \frac{\cosh \gamma_s \cos^2 \frac{\gamma_s}{2} - \sinh \gamma_s \sin \gamma_s - \cosh^2 \frac{\gamma_s}{2} \cos \gamma_s}{\sinh \gamma_s \cos^2 \frac{\gamma_s}{2} - \cosh^2 \frac{\gamma_s}{2} \sin \gamma_s} \dots \quad (13.2)$$

For hard load, since  $E_2$  is taken to be infinity,  $3m/E_2$ , and  $m/E_2$  is zero. Finally the expression for displacement of the cantilever at the specific struck points can be represented in some form as

$$y_a = 4v_0 \left[ \frac{A_1}{q_1} \sin q_1 t + \frac{A_2}{q_2} \sin q_2 t + \frac{A_3}{q_3} \sin q_3 t + \dots \right] -$$

where  $A_1, A_2, A_3$ , etc. and  $q_1, q_2$ , etc. have their values as required. Different terms of this series represent, different modes of vibration, excited during impact, whose periods are obtained from eqn. (12.3). Similar type of expression for displacement was shown by Prescott in case of a blow at the free end of a cantilever but amplitudes of different modes etc. in his case are however different from those of ours. Only limited number of terms of the series is required to compute the experimental observations.

## RESULTS

The values of  $\epsilon$ ,  $\epsilon''$ ,  $\tan \delta$  and  $\tau$  along with the macroscopic viscosities ( $\eta$ ) of all the compounds at different temperatures are given in Tables I-V. The  $\tau$ -values of chlorobenzene, bromobenzene and  $\alpha$ -chloronaphthalene at different temperatures along with those reported by Hennolly *et al.* (1948) has been represented graphically in Figure 2 for the sake of comparison. The values of heats

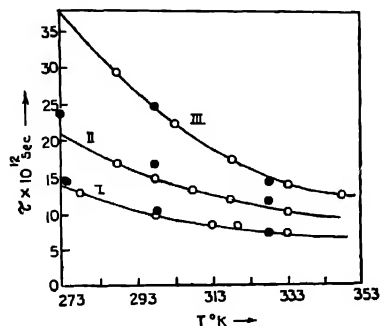


Fig 2 Graphs of  $\tau$  vs  $T$

Curve I—Chlorobenzene, Curve II—Bromobenzene

(curve III -  $\alpha$ -Chloronaphthaleno (The scale for  $\tau$  is to be increased by a factor of two)

Open circles denote the  $\tau$ -values obtained by the authors

Solid circles are those by Hennolly *et al* (1948)

of activation for dielectric relaxation ( $\Delta H_\tau$ ) and viscous flow ( $\Delta H_\eta$ ) have been obtained respectively from the graphs  $\log (\tau \cdot T)$  against  $1/T$  and  $\log \eta$  against  $1/T$  as usual. Some of these curves are shown in Figures 3a, 3b and 3c. The  $\Delta H_\tau$  and  $\Delta H_\eta$  values and their ratios ( $\gamma$ ) are given at the foot of the Tables.

TABLE I

## Chlorobenzene

Wave length ( $\lambda$ ) = 3.14 cm.

Temp °K	$\epsilon'$	$\epsilon''$	$\tan \delta$	$\tau \times 10^{12}$ sec	$\eta$ in millipoise	$\frac{\tau T}{\eta} \times 10^7$
278	4.650	1.770	0.3800	12.69	9.55	9.13
298	4.707	1.400	0.2974	9.80	7.56	8.70
313	4.726	1.226	0.2595	8.51	6.38	8.78
320	4.501	1.058	0.2345	8.08	5.96	8.88
333	4.529	0.953	0.2104	7.20	5.26	8.87

$\Delta H\tau = 1.19 \text{ K Cal/mole}$   
 $\Delta H\eta = 1.99 \text{ K Cal/mole}$

$\gamma = 0.60$

TABLE II

Bromobenzene

Wave length ( $\lambda$ ) = 3.14 cm

Temp °K	$\epsilon'$	$\epsilon''$	$\tan \delta$	$\tau \times 10^{12}$ sec	$\eta$ in millipoise	$\frac{\tau T}{\eta \gamma} \times 10^7$
288	3.852	1.454	0.3773	17.03	11.89	9.21
298	3.976	1.378	0.3465	14.87	10.55	9.02
308	4.075	1.302	0.3195	13.19	9.17	9.09
318	4.137	1.234	0.2983	12.05	8.20	9.25
333	4.230	1.110	0.2624	10.28	7.05	9.15
$\Delta H\tau = 1.49$ K.Cal/mole				$\gamma = 0.68$		
$\Delta H\eta = 2.21$ K.Cal/mole						

TABLE III

Metadichlorobenzene

Wavelength ( $\lambda$ ) = 3.14 cm

Temp °K	$\epsilon'$	$\epsilon''$	$\tan \delta$	$\tau \times 10^{12}$ sec	$\eta$ in millipoise	$\frac{\tau T}{\eta \gamma} \times 10^7$
288	3.546	1.049	0.2959	15.13	11.04	13.53
303	3.601	0.931	0.2585	12.82	9.17	13.20
318	3.86	0.851	0.2374	11.87	7.80	13.89
333	3.630	0.740	0.2039	9.95	6.07	13.15
348	3.620	0.678	0.1874	9.18	5.82	13.55
$\Delta H\tau = 1.02$ K.Cal/mole				$\gamma = 0.49$		
$\Delta H\eta = 2.09$ K.Cal/mole						

## IV

1, 2, 4-trichlorobenzene

Wavelength ( $\lambda$ ) = 3.14 cm

Temp °K	$\epsilon'$	$\epsilon''$	$\tan \delta$	$\tau \times 10^{12}$ sec	$\eta$ in millipoise	$\frac{\tau T}{\eta \gamma} \times 10^7$
288	2.900	0.8143	0.2806	30.48	26.04	30.94
303	2.917	0.7563	0.2593	26.03	18.28	31.13
318	2.983	0.7269	0.2437	22.43	13.65	30.91
333	3.026	0.6905	0.2282	20.16	10.84	31.31
348	3.003	0.6384	0.1775	18.41	9.01	31.72
$\Delta H\tau = 1.11$ K.Cal/mole						
$\Delta H\eta = 3.47$ K.Cal/mole						



TABLE V  
 $\alpha$ -Chloronaphthalene  
 Wavelength ( $\lambda$ ) = 3.14 cm

Temp °K	$\epsilon'$	$\epsilon''$	$\tan \delta$	$\tau \times 10^{12}$ SEC	$\eta$ in millipoise	$\frac{\eta T}{\eta \gamma} \times 10^7$
288	3.096	1.533	0.4950	59.6	42.66	17.19
303	3.215	1.478	0.4506	44.9	29.17	17.19
318	3.150	1.003	0.3184	34.6	20.30	17.37
333	3.170	0.823	0.2596	27.3	14.69	17.50
348	3.215	0.820	0.2551	24.9	11.22	19.07
$\Delta \Pi \tau = 2.71$ K-Cal/mole				$\gamma = 0.61$		
$\Delta \Pi \eta = 4.42$ K-Cal/mole						

TABLE VI

Compound	Semi-axial lengths in Å			$f$	$4\pi abcf$ in Å <sup>3</sup>	$\frac{\tau KT}{3\eta(\eta/\eta_0)^{1-\gamma}}$ in Å <sup>3</sup>	
	$a$	$b$	$c$			$\eta_0 = 1$ mP	$\eta_0 = 0.2$ mP
$C_{10}H_8Cl$	3.46	3.11	1.50	1.44	97.4 (67.6)	40.8	77.9
$C_{10}H_8Br$	3.56	3.11	1.70	1.27	100.0 (78.8)	42.1	70.4
$m-C_{10}H_7Cl_2$	3.31	3.11	1.70	1.35	87.3 (64.7)	61.9	140.7
$\alpha-C_{10}H_7Cl$	4.04	3.46	1.50	1.35	118.6 (87.8)	79.6	149.1

## DISCUSSION

a) *Dependence of time of relaxation ( $\tau$ ) on the macroscopic viscosity ( $\eta$ )*

The Debye relation as modified by Perrin (1934) for ellipsoidal molecules with rigid dipoles is

$$\tau = \zeta / 2KT \quad \dots (1)$$

where

$$\zeta = 8\pi abcf\eta_{int} \quad \dots (2)$$

$\zeta$  being a measure of the viscous force inhibiting the rotation of the dipole lying along one of the axes of the ellipsoid about the other two axes,  $a, b, c$  are the lengths of the semi axes of the ellipsoid,  $f$  is a factor tabulated by Budo *et al.* (1939) and  $\eta_{int}$  is the internal friction of the medium in which ellipsoids are rotating. As

Eqn. (1) shows, the product  $\tau \cdot T$  is a measure of  $\zeta$ . The nature of dependence on the shape and size of molecules and on temperatures can be seen from the plots  $\tau \cdot T$  against  $T$  for all the compounds as shown in Figure 4. It is seen that the values of  $\tau T$  (i.e.  $\zeta$ ) decreases in the order toluene  $\ast$  < chlorobenzene < meta-dichlorobenzene < bromobenzene <  $\alpha$ -chloronaphthalene. The viscosities  $\eta$  of

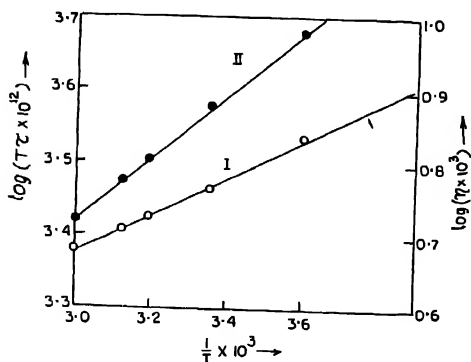


Fig. 3a. Chlorobenzene

Curve I—Plot of  $\log(\tau T)$  vs  $1/T$

Curve II—Plot of  $\log \eta$  vs  $1/T$

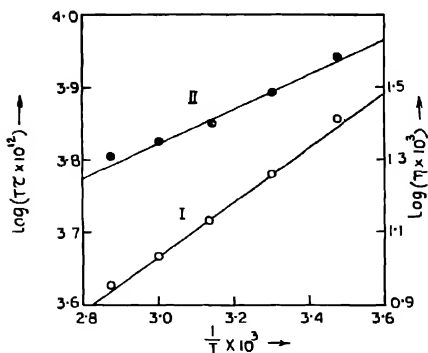
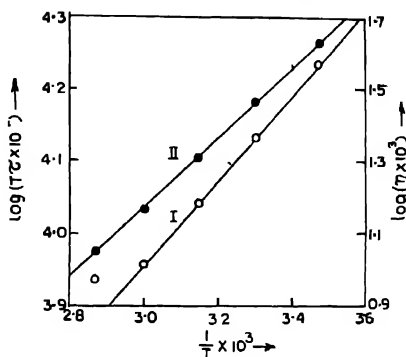
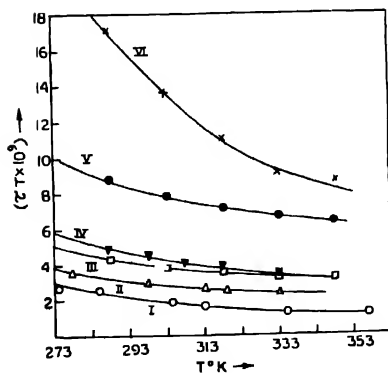


Fig. 3b 1, 2, 4-trichlorobenzene

Curve I—Plot of  $\log(\tau T)$  vs  $1/T$

Curve II—Plot of  $\log \eta$  vs  $1/T$

Fig. 3c.  $\alpha$ -ChloronaphthaleneCurve I—Plot of  $\log(\tau T)$  vs  $1/T$ Curve II Plot of  $\log \eta$  vs  $1/T$ Fig. 4. Graphs showing the variation of  $\tau \cdot T$  against  $T$ 

Curve (i)—Toluene; Curve (ii)—Chlorobenzene;

Curve (iii)—m-dichlorobenzene; Curve (iv)—Bromobenzene;

Curve (v)—1, 2, 4-trichlorobenzene; Curve (vi)— $\alpha$ -Chloronaphthalene.

the compounds also decrease in the same order. The first four compounds have their molecular volume almost equal and so the values of  $\zeta$  in those cases is mainly a function of macroscopic viscosity. The functional relationship between  $\zeta$  and  $\eta$  can be advantageously studied from the plots of  $\log(\tau T)$  vs  $\log \eta$ . Two of

such graphs are shown in Figures 5a and 5b. The linear variation of  $\log(\tau T)$  with  $\log \eta$  can be designated by a relation  $\log(\tau T) = A + \gamma \log \eta \dots (3)$ . The slope of the curve gives the value  $\gamma = \Delta H_\tau / \Delta H_\eta$ . Substitution of Eqn.(3) in Eqn. (1) gives

$$\zeta = D \cdot \eta^\gamma \quad \dots (4)$$

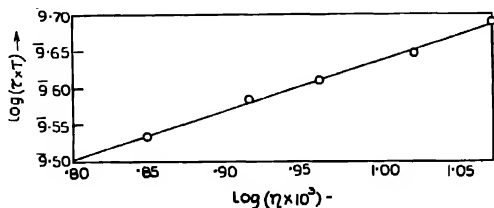


Fig. 5a. Variation of  $\log(\tau T)$  with  $\log \eta$  for Bromobenzene

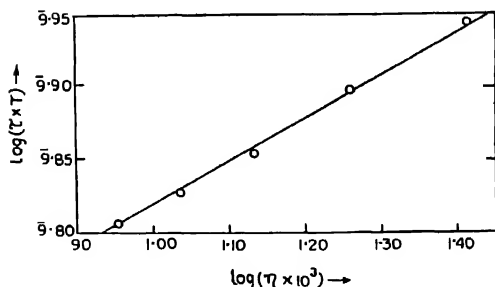


Fig. 5b. Variation of  $\log(\tau T)$  with  $\log \eta$  for 1, 2, 4-trichlorobenzene

which is of the same form as derived in a previous communication (Sinha *et al.* 1965). Following similar arguments as given in that paper  $\zeta$  may be written

$$\zeta = 2\tau KT = C \cdot \left(\frac{\eta_0}{\eta}\right)^{1-\gamma} \cdot \eta. \quad \dots (5)$$

where  $C$  has the dimension of a volume,  $\eta_0$  is a constant having the same dimension as that of  $\eta$  and  $\left(\frac{\eta_0}{\eta}\right)^{1-\gamma} \cdot \eta$  is tentatively identified with  $\eta_{int}$ .

Combining the equations (1), (2) and (5)

$$C = 8\pi abc f \quad \dots (6a)$$

\*The data for toluene is taken from a previous paper by Bhattacharyya *et al.* (1964).

and

$$\frac{\tau kT}{3\eta(\eta_0/\eta)^{1-\gamma}} = \frac{4}{3} \pi abc f \quad \dots (6b)$$

The value of  $\eta_0$  can not be determined, but with certain tentative values of  $\eta_0$  a comparison may be made between the experimentally obtained values of  $\tau kT / 3\eta(\eta_0/\eta)^{1-\gamma}$  and the calculated values of  $4/3 \pi abc f$ . The values of  $a, b, c$  are determined from atomic radii (Fischer, 1946) and those of ' $f$ ' are taken from the Table of Budo *et al.* (1939). All these data are given in Table VI. The value of molecular volume ( $4/3 \pi abc$ ) are given in brackets

It is seen from Table VI that if the value of  $\eta_0$  is properly chosen, some amount of agreement between the experimental values of  $\frac{\tau kT}{3\eta(\eta_0/\eta)^{1-\gamma}}$  and  $\frac{4}{3} \pi abc f$  may be obtained. This may provide some justification for identifying  $\eta \cdot (\eta_0/\eta)^{1-\gamma}$  i.e.  $\eta^\gamma$  for a certain compound as a measure of internal friction as has been suggested earlier (Sinha *et al.* 1965).

#### b) Influence of dipolar interaction on relaxation time

The  $\tau$ -values of the molecules of chlorobenzene, bromobenzene, metadichlorobenzene and  $\alpha$ -chloronaphthalene (having almost identical dipole moments) in the liquid state have been compared with those of the molecules in dilute solutions in suitable non-polar solvents, whose viscosities are either equal to or greater than those of the pure liquids\*. The results are shown graphically in Figures 6a and 6b.

It is seen from the figure 6a that the  $\tau$ -values of chlorobenzene in the liquid state are slightly smaller than those in solutions in  $\text{CCl}_4$  which may presumably be due to the slightly lower values of  $\eta$  in the case of the pure liquid.

In the case of bromobenzene and metadichlorobenzene, however, the  $\tau$ -values in the pure liquid, are almost equal to those in solution in  $\text{CCl}_4$ , the viscosities of the pure liquids and the solvent being almost the same. The behaviour of  $\alpha$ -chloronaphthalene is different from that of the above three compounds. It can be seen from Figure 6b that the  $\tau$ -values of  $\alpha$ -chloronaphthalene in solution in a very viscous solvent paraffin over the range of temperature investigated are much smaller than those in the pure liquid in the same temperature range, although the viscosity of the pure liquid is much smaller than that of paraffin. Curtiss *et al.* (1952) also reported that the value of  $\lambda_{\text{max}}$  ( $= 2\pi c\tau$ ) of  $\alpha$ -chloronaphthalene in the liquid state at 20°C ( $\eta = 33.3$  mp) is 11 cm. which is only slightly smaller than the value of 12 cm. for  $\lambda_{\text{max}}$  in solution in nujol ( $\eta = 1080$  mp) at the same temperature.

The results in the cases of chloro, bromo- and metadichlorobenzene obtained in the present investigation do not show any decrease in the  $\tau$ -values in solution

\*The data on solutions are taken from the works of Sinha *et al.* (to be published soon).

as compared to those in the respective pure liquids. This can not be reconciled with the conclusion made by Smyth (1955) that the  $\tau$ -values of these liquids are

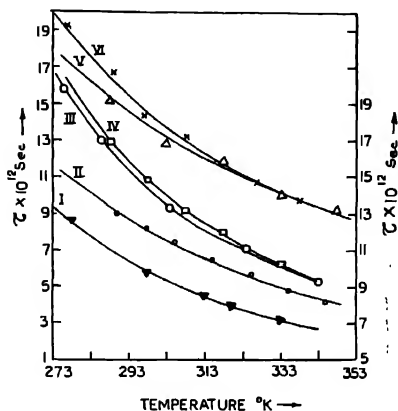


Fig. 6a. Comparison of the  $\tau$ -values at different temperatures  
 Curve (i) - Chlorobenzene-pure liquid;  
 Curve (ii) - Chlorobenzene in solution in  $\text{CCl}_4$   
 Curve (iii) - Bromobenzene-pure liquid  
 Curve (iv) - Bromobenzene in solution in  $\text{CCl}_4$   
 Curve (v) - Metadichlorobenzene-pure liquid  
 Curve (vi) - Metadichlorobenzene in solution in  $\text{CCl}_4$ . The  
 scale for  $\tau$  values is given on the right.

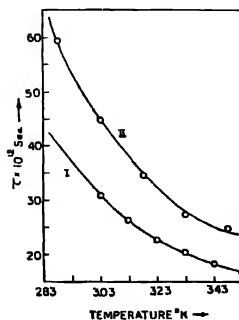
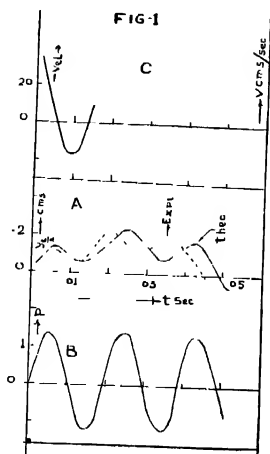


Fig. 6b. Comparison of the  $\tau$ -values at different temperatures  
 Curve (i) -  $\alpha$ -Chloronaphthalene-pure liquid  
 Curve (ii) -  $\alpha$ -Chloronaphthalene in solution in paraffin.

For verification of the theory, the following data are taken from a paper of Banerjee (1964). Length of Cantilever, 90 cms dia 1.27 cms., struck point 45 cms (mid-pt), spherical brass load, 'mass ratio' 3.71 (calculated),  $v_0 = 88.5$  cms. per sec.



The experimental photographic curve for the struck point is projected up to a squared paper by the help of an epidiascope. The curve traced out by the surface of the cantilever during and shortly after impact is drawn upon the paper. The displacement-time curve as calculated from the theory with two terms of the series, is then superimposed upon the experimental curve with same units. These curves are shown in Fig. 1. They are identical upto the time the contact did not cease, i.e. upto about .011 sec (see the said paper). This clearly upholds the validity of the present theory. After this time (.011 sec) also the curves are strikingly similar and very small difference is due to after-impact effects, which has been discussed in Part III of this series.

#### PRESSURE EXERTED BY THE HAMMER

Substituting values of  $y_a$  and  $u$ , of equations (9.1) and (9.2) respectively in eqn. (6.1) we write,

$$= -mv_0 \frac{F(D)}{F_2(D)} \quad \dots \quad (14.1)$$

where, at  $x = a = l$ ,

$$F_2(D) = 1 + \frac{m}{E_2} D^2 + \gamma \frac{m}{M} \frac{\sinh \gamma \cos \gamma - \cosh \gamma \sin \gamma}{1 + \cosh \gamma \cos \gamma} \quad \dots (15.1)$$

and at  $x = a = \frac{l}{2}$ ,

$$F_2(D) = 1 + \frac{m}{E_2} D^2 + \gamma \frac{m}{M} \frac{\cos^2 \frac{\gamma}{2} \sinh \gamma - \cosh^2 \frac{\gamma}{2} \sin \gamma}{2(1 + \cosh \gamma \cos \gamma)} \quad \dots (15.2)$$

For roots of  $D$  from  $F_2(D) = 0$ , we find that  $D = [\alpha_s]$ ,  $= \pm i q_s$ , has same roots as obtained by equations (11), for respective struck points

With the help of Heaviside's expansion theorem

$$P = -mv_0 \left[ \frac{F(0)}{F_2(0)} + \sum_{s=1}^r \frac{F(\alpha_s)}{\alpha_s \cdot F_2'(\alpha_s)} e^{\alpha_s t} \right] \quad \dots (16)$$

Here again  $F(0) = 0$  and  $F_2(0) \neq 0$ , putting  $D = 0$

Finally after some mathematical manipulation and simplification we get,

Pressure at  $x = a = l$ ,

$$P_l = -4mv_0 \sum_{s=1}^r \frac{q_s \sin q_s l}{1 + \frac{3m}{E_2} q_s^2 + \frac{M}{m} \left[ 1 - \frac{m}{E_2} q_s^2 \right] + 2\gamma_s \left[ 1 - \frac{m}{E_2} q_s^2 \right]}{\cosh \gamma_s - \cot \gamma_s} \quad \dots (17.1)$$

This expression is same as obtained by Ghosh and Ray

and Pressure at  $x = a = \frac{l}{2}$ ,

$$P_{\frac{l}{2}} = -4mv_0 \sum_{s=1}^r \frac{q_s \sin q_s l}{1 + \frac{3m}{E_2} q_s^2 + \gamma_s \left[ 1 - \frac{m}{E_2} q_s^2 \right] \frac{\cosh \gamma_s \sin \gamma_s - \sinh \gamma_s \cos \gamma_s}{1 + \cosh \gamma_s \cos \gamma_s}} \\ + \frac{\sinh \gamma_s \sin \gamma_s + \cosh^2 \frac{\gamma_s}{2} \cos \gamma_s - \cos^2 \frac{\gamma_s}{2} \cosh \gamma_s}{2(1 + \cosh \gamma_s \cos \gamma_s)} \quad \dots (17.2)$$

Further velocity of the bar, which is given by  $\frac{dy}{dt}$  can be represented in the form

$$v_t = 4v_0 [A_1 \cos q_1 t + A_2 \cos q_2 t + A_3 \cos q_3 t + \dots] \quad \dots (18)$$

Thus it is possible to directly obtain the velocity of the load from eqn. 18.



ACKNOWLEDGEMENT

My best thanks are due to Prof. M. M. Ghosh, D.Sc., Vice-Principal of City College, Calcutta for his guidance.

REFERENCES

- Banerjee, B. B., 1964, *Indian J. Phys.* **38**, 99  
Cox, H., 1956, *Trans. Camb. Phil. Soc.* **9**, Pt. 1, 73  
Ghosh, M. and Ray, K., 1955, *Ind. Jour. Theo. Phys.* **3**, 77  
Hertz, H., *Mathematical Theory of Elasticity* A. E. H. Love, p. 198  
Hodgkinson, 1833, *Report of the British Assn. for Adv. of Science* Third meeting, 421.  
Hoppman, W. H., 1948, *J. App. Mech.*, **15**, 125  
Mason, H. L., 1936, *J. App. Mech.*, **58**, A-55  
Prescot, John, 'Applied Elasticity' Dover, 227  
Ray, K., 1956, *Ind. Jour. Assn. App. Physicists*, **3**, 2  
Timoshenko, S. P., 1956, *Vibration Problems in Engineering* D. Nostrand Co. Inc. Third Edn. 411-416  
St. Venant, 1883, *Theories de l'élasticité des corps solides de Clebsch*, translated by A. J. St. Venant and A. Flamant  
Young, Thomas, 1807, *Natural Philosophy*, J. Johnson Lond. 2, 50.

# DYNAMICS OF VIBRATION OF A CANTILEVER UNDER LATERAL IMPACT OF AN ELASTIC LOAD—PART II (GENERAL THEORY)

B. B. BANERJEE

PHYSICS DEPARTMENT, UNIVERSITY COLLEGE OF ENGINEERING, BURLA-ORISSA

(Received September 11, 1965)

**ABSTRACT** In Part I, the dynamics of the problem has been worked out for the struck points at the free end and at the middle of the cantilever. In this paper the general case of an elastic load, impinging transversely on any point of the cantilever is rigorously dealt with. The displacement of the cantilever at any point (including the struck point) has been worked out, and a general expression for the same is given. The displacement comes in form of a series and is found to be directly proportional to the striking velocity. Further it involves terms containing easily measurable quantities. The dynamics of the problem is developed without assuming any nature of force between the load and the bar. The theory is perfectly general.

## INTRODUCTION

Symbols used in this part have the same significances as given in part I. Operational method due to Heaviside is employed to work out the problem.

With the help of eqn (4.1) and (4.2) Banerjee, (1966) the displacement at any point of the cantilever can be obtained.

For any point  $x(0 \leq x \leq a)$ , eqn. (4.1) is used

$$y_1 = y_a \frac{\Delta_1(\sinh nx - \sin nx) + \Delta_2(\cosh nx - \cos nx)}{\Delta_0}$$

where the values of  $\Delta_1$ ,  $\Delta_2$ ,  $\Delta_0$ , are given by equation (5.1), (5.2) and (5.3) respectively (Banerjee 1966).

and as per eqn (9.1) (Banerjee 1966)  $y_a = \frac{F(D)}{v_0 F_1(D)}$  where  $F(D)$  stands for  $D$  and

$$F_1(D) = D^2 - \frac{E_1 I}{m} \pi^2 \left( 1 + \frac{m}{E_2} D^2 \right) f(D). \quad \dots (1)$$

Therefore

$$\frac{y_1}{v_0} = \frac{f_0(D)}{F_3(D)} \quad \dots (2)$$

where

$$f_0(D) = D[(\sinh \gamma \sin k_2 \gamma - \cosh \gamma \cos k_2 \gamma - \sinh k_2 \gamma \sin \gamma - \cosh \gamma \cos k_2 \gamma \\ - \cosh k_1 \gamma - \cos k_1 \gamma)(\sinh \gamma x/l - \sin \gamma x/l) + (\sinh \gamma \cos k_2 \gamma - \cosh k_2 \gamma \sin \gamma \\ + \sin k_1 \gamma + \sinh k_1 \gamma - \sinh k_2 \gamma \cos \gamma - \cosh \gamma \sin k_2 \gamma)(\cosh \gamma x/l - \cos \gamma x/l)] \quad \dots (3)$$

and

$$F_3(D) = 2 \left[ D^2 \omega + \frac{E_0 I}{m} n^3 \left( 1 + \frac{m}{E_2} D^2 \right) p \right] \quad \dots (4)$$

where

$$p = 2(1 + \cosh \gamma \cos \gamma) \quad \dots (5.1)$$

and

$$\omega = -[\sinh k_2 \gamma \cos k_2 \gamma + \cosh k_1 \gamma \sin k_1 \gamma + \cosh k_1 \gamma \cosh k_2 \gamma \sin \gamma - \cosh k_2 \gamma \sinh k_2 \gamma \\ - \sinh k_1 \gamma \cos k_1 \gamma - \cos k_1 \gamma \cos k_2 \gamma \sinh \gamma] \quad \dots (5.2)$$

With the help of Heaviside's expansion theorem

$$\frac{y_1}{v_0} = \frac{f_0(0)}{F_3(0)} + \sum \frac{f_0(\alpha_s)}{\alpha_s \cdot F_3'(\alpha_s)} e^{\alpha_s t} \quad \dots (6)$$

Now putting  $D = 0$ ,  $f_0(0) = 0$ , and  $F_3(0) \neq 0$ .

Thus

$$\frac{y_1}{v_0} = \sum \frac{f_0(\alpha_s)}{\alpha_s \cdot F_3'(\alpha_s)} e^{\alpha_s t}$$

where summation extends over all roots of  $D = [\alpha_s]$ , ( $s = 1, 2, 3, \dots, r$ )

For roots of  $D$  from  $F_3(D) = 0$ , in eqn. (4), we have  $F_3(D) = 0$ , whence

$$\frac{p}{\omega} = \frac{\frac{m}{M} \gamma}{1 - \frac{E_1 I}{E_2} \cdot \frac{m}{M} \cdot \frac{\gamma^4}{l^3}} \quad \dots (7)$$

Eqn. (7), can be solved graphically by drawing two sets of curves represented by

$$\eta_1 = \frac{p}{\omega} \quad \dots (8.1)$$

and

$$\eta_2 = \frac{\frac{m}{M} \gamma}{1 - \frac{E_1 I}{E_2} \cdot \frac{m}{M} \cdot \frac{\gamma^4}{l^3}} \quad \dots (8.2)$$

As  $\eta_2 \sim \gamma$  curve exists only in the positive direction, the different values of  $\gamma_s$  of equation (7), are given by the points of intersections of two sets of curves  $\eta_1 \sim \gamma_s$ , and  $\eta_2 \sim \gamma_s$ , lying entirely in positive quadrants. Thus  $\gamma$  assumes different sets of values for different struck points given by the values of  $k_1$  and  $k_2$  etc. in particular beam-load system.

$$\text{Thus } nl = \gamma_s, \gamma_s = \text{pure number, } (s = 1, 2, 3, \dots r) \quad \dots (9)$$

$$D = [\alpha_s] = \pm iq_s, \quad \dots (9.2)$$

$$q_s = \gamma_s^2 \cdot \sqrt{\frac{E_1 I}{M E^3}}, \quad \dots (9.3)$$

We have for equation (6)

$$F_1'(\alpha_s) = 2\omega [F_1'(\alpha_s)] \quad \dots (10.1)$$

and  $F_1(\alpha_s)$  is obtained from  $F_1(D)$  in eqn. (1) and is given by

$$F_1'(\alpha_s) = \frac{\alpha_s}{2} \left\{ 1 - \frac{3m}{E_2} \alpha_s^2 + \gamma_s \frac{\cosh \gamma_s \sin \gamma_s - \sinh \gamma_s \cos \gamma_s}{1 + \cosh \gamma_s \cos \gamma_s} - \gamma_s \cdot \frac{L}{\omega} \right\} \quad \dots (10.2)$$

where  $\omega$  is given by eqn. (5.2) and

$$\begin{aligned} L = & 2[k_2 \sinh k_2 \gamma_s \sin k_2 \gamma_s - k_1 \sinh k_1 \gamma_s \sin k_1 \gamma_s] + \cosh \gamma_s \cos k_1 \gamma \cos k_2 \gamma_s \\ & - \cosh k_1 \gamma_s \cosh k_2 \gamma_s \cos \gamma_s - k_1 [\sin k_1 \gamma_s \cos k_2 \gamma_s \sinh \gamma_s + \sin \gamma_s \sinh k_1 \gamma_s \\ & \cosh k_2 \gamma_s] - k_2 [\sin k_2 \gamma_s \cos k_1 \gamma_s \sinh \gamma_s + \sin \gamma_s \sinh k_2 \gamma_s \cosh k_1 \gamma_s] \dots \end{aligned} \quad (10.3)$$

Further

$$\sum \frac{e^{\alpha_s t}}{\alpha_s} = \sum \frac{2 \sin q_s t}{q_s} \quad \dots (10.4)$$

Thus we have after simplification

$$y_1 = 2v_0 \sum_{s=1}^r \frac{\psi_1(\gamma_s)}{\psi(\gamma_s)} \cdot \frac{\sin q_s t}{q_s} \quad \dots (11)$$

where  $\psi(\gamma_s) = \frac{2F_1'(\alpha_s)}{\alpha_s}$ , where  $F_1'(\alpha_s)$  is given by eqn. (10.2) with  $\alpha_s^2$  being replaced by  $-q_s^2$

and

$$\begin{aligned} & \sinh \gamma_s \sin k_2 \gamma_s - \cosh \gamma_s \cos k_2 \gamma_s - \sinh k_2 \gamma_s \sin \gamma_s - \cosh k_2 \gamma_s \cos \gamma_s \\ & - \cosh k_1 \gamma_s - \cosh k_1 \gamma_s (\sinh \gamma_s x/l - \sin \gamma_s x/l) + (\sinh \gamma_s \cos k_2 \gamma_s \\ & + \cosh k_2 \gamma_s \sin \gamma_s + \sin k_1 \gamma_s + \sinh k_1 \gamma_s - \sinh k_2 \gamma_s \cos \gamma_s - \cosh \gamma_s \end{aligned}$$

$$\psi_1(\gamma_s) = \frac{\sin k_2 \gamma_s}{w} (\cosh \gamma_s x/l - \cos \gamma_s x/l)$$

where  $w$  is given by (5.2) ... (11.1)

Equation (11) for  $y_1$  can be represented in a convenient form as

$$y_1 = 2v_0 \sum q_s \sin q_s t \quad \dots (11.2)$$

where  $q_s$  can be obtained from the quotient  $\frac{\psi_1(\gamma_s)}{\psi_2(\gamma_s)}$  for  $s = 1, 2, 3, \dots$ .

When the observed point at  $x$  is the struck point itself, i.e. for any point,  $x = a$ ,

We have for equation (7),  $f_0(0)$  and

$$F_1(0) = \frac{3E_1 I}{\alpha \alpha^3},$$

putting  $D = 0$ , as usual

$$\frac{f_0(0)}{F_3(0)} = 0, \text{ in eqn. (6)}$$

and we get from eqn. (11)

$$y_a = 4v_0 \sum A_s \sin q_s t$$

where

$$\frac{1}{A_s} = \frac{1 + \frac{3m}{E_2} q_s^2}{1 - \frac{m}{E_2} q_s^2} + \gamma_s \frac{\cosh \gamma_s \sin \gamma_s - \sinh \gamma_s \cos \gamma_s}{1 + \cosh \gamma_s \cos \gamma_s} - \gamma_s \frac{L}{w} \quad (12.1)$$

where  $L$  is given by eqn. (10.3)

The velocity of the load during impact is given by

$$v_t = \frac{dy_a}{dt} = 4v_0 \sum A_s \cos q_s t \quad (13)$$

For hard load since  $B_2$  is taken to be infinity, the  $\eta_2 \sim \gamma$  relation as per eqn. (8.2) is written as

$$\eta_2 = \frac{m}{M} \gamma$$

and the  $\eta_2 \sim \gamma$  curve is a straight line passing through the origin having an inclination such that

$$\tan \theta = \frac{m}{M} = \frac{\text{mass of the load}}{\text{mass of the bar}}$$

From eqn. (11), it is noted that the displacement of the cantilever is expressed in form of a series and is directly proportional to the impinging velocity of the load and since it contains  $\gamma$ , the displacement depends on the striking distance, measured from the fixed end, 'mass ratio', Young's modulus, length, and shape of the bar as also on the and elastic constant of the load. Different terms of the series, given by eqn. (11), represents successive modes of vibration, whose periods are obtained from  $q_s$  of eqn. (9.3) for  $s = 1, 2, 3, \dots, r$ . Further from eqn. (11) it is found that the influence of different modes of vibration in developing the form of the displacement-time curve is not same throughout the length of the bar as it depends on  $\gamma_s$ .

For the struck point at the free end as also at the middle of the cantilever, i.e. for  $x = a = l$ , and for  $x = a = l/2$ , respectively, eqn. (11) which is the general form reduces to eqn. (13.1) and (13.2) (Banerjee, 66)

For any point  $x$  ( $a \leq x \leq l$ ), the displacement of the bar can be obtained from eqn. (4.2) (Banerjee, 66)

$$y_2 = y_a \Delta_3 [\sinh n(l-x) + \sin n(l-x)] + \Delta_4 [\cosh n(l-x) + \cos n(l-x)]$$

where  $\Delta_3, \Delta_4, \Delta_0$ , are respectively given by eqn. (5.3), (5.4) and (5.5) (Banerjee, 66) respectively.

Proceeding in the similar way as was followed in case of determination of  $y_a$ , we get the same roots of  $\gamma_s$  as given by eqn. (7)

Finally after simplification

$$y_2 = 2v_0 \sum_{s=1}^r \frac{\psi_s(\gamma_s)}{\psi'(\gamma_s)} \frac{\sin q_s t}{q_s} \quad \dots \quad (14)$$

where  $\psi(\gamma_s)$  is given by  $\frac{2F_1'(\alpha_s)}{\alpha_s}$  where  $F_1'(\alpha_s)$  is given by (10.2) and  $\alpha_s^2$  in eqn. (10.2) is written as  $-q_s^2$

and

$$\begin{aligned}
 & (\cos k_2 \gamma_s - \cosh k_2 \gamma_s - \sinh \gamma_s \sin k_1 \gamma_s - \sinh k_1 \gamma_s \sin \gamma_s + \cosh \gamma_s \cos k_1 \gamma_s \\
 & - \cosh k_1 \gamma_s \cos \gamma_s) \left\{ \sinh \gamma_s \left( 1 - \frac{x}{l} \right) + \sin \gamma_s \left( 1 - \frac{x}{l} \right) \right\} + (\sinh k_2 \gamma_s + \\
 & \cosh \gamma_s \sin k_1 \gamma_s + \cosh k_1 \gamma_s \sin \gamma_s - \sin k_2 \gamma_s - \sinh \gamma_s \cos k_1 \gamma_s \\
 & - \sinh k_1 \gamma_s \cos \gamma_s) \left\{ \cosh \gamma_s \left( 1 - \frac{x}{l} \right) + \cos \gamma_s \left( 1 - \frac{x}{l} \right) \right\} \\
 \psi_2(\gamma_s) = & \frac{\dots}{\omega}
 \end{aligned}$$

where  $\omega$  is given by (5.2)

It should be noted here that  $E_2$  which occurs in different equations is different from Young's modulus of the material of the load but it depends on the material size and shape of the hammer as also on the area of contact surface.

#### ACKNOWLEDGEMENT

My best thanks are due to Prof. M. M. Ghosh, D.Sc., vice-principal, City College, Calcutta for his lively interest in this work.

#### REFERENCES

- Banerjee, B. B, 1966, *Indian J. Phys.* **40**, 197.  
 Ghosh, M. and Banerjee, B. B. *Ind. Jour. Theo. Phys* (in press).

## BOOK REVIEW

**THEORETICAL PHYSICS IN THE TWENTIETH CENTURY.** A Memorial volume to Wolfgang Pauli. Edited by M. G Fierz and V. F. Weisskopf. Price \$10.00. Interscience Publishers, Inc. N.Y.

By raising a memorial monument to a great man-, we do hero worship, the psychological value of which is unquestionable, though the educative value of which is not often so clear. On the other hand, a memorial volume well contributed is on an altogether different footing. It may sometimes be questioned that such contributions if meant to be expositions of the works of a master are likely to be strongly tinged by the biases of the man, and may not be truly critical of the drawbacks or inadequacies of the teachings. But this can hardly be helped for a time when this is the only light in obscurity. Indeed, Pauli's work brought light and logic in the domain of "classical" quantum theory of the atom which was a strange hybrid between classical electrodynamics and Planck's quantum hypothesis. To quote the words of the other great master Niels Bohr "it was a great comfort when new developments met with his approval. At the same time as the anecdotes around his personality grew into a veritable legend, he more and more became the very conscience of the theoretical physicists". It shows how deeply and widely Pauli's personality and wisdom made themselves felt in the world of Physics and the homages rendered to this great scientist in this volume are never so apt or intrinsic. On the other hand, many of the contributors to this memorial volume are themselves considered to be so many pillars of the grand edifice of modern Quantum Mechanics and thus each article, as one rightly expects, brings fresh thought and exposition to the reader and is delightful and thought-provoking reading.

When we pay homage to a great man we do good to ourselves. We drink at the fountain of knowledge and inspire ourselves to greater efforts. Each article in this volume has a special value in reference to Pauli as well as to the author of the article.

*A. Bose*



# DYNAMICS OF VIBRATION OF A CANTILEVER UNDER LATERAL IMPACT OF AN ELASTIC LOAD. PART III. (GENERAL THEORY)

B. B. BANERJEE

(Received September 11, 1965)

**ABSTRACT.** In part II, the general expression for the displacement of any point of the cantilever, under lateral impact of a load is given. In this paper, the general expression for the pressure exerted by the load on the cantilever is worked out. The duration of contact is the lowest positive root of  $t$ , other than zero, obtained by solving Pressure  $P = 0$ , for the given struck point. This duration of contact can be directly obtained from the expression of pressure. Existence of different modes of vibration governs the magnitude of the duration of contact. Pressure is found to be directly proportional to the striking velocity and depends on all physical constants as appear in the general displacement equation, given in Part II. It has been possible to explain the occurrence of the phenomenon of multiple contacts from the pressure-time and the velocity-time relations. The extension of the general theory in light of Hertz's theory of impact explains fully the dependence of duration of contact on the impinging velocity of the hammer.

## INTRODUCTION

In Part II the general expression for the displacement of any point of the cantilever (including the struck point) is given. In this paper using the same operational method due to Heaviside, the general expression for pressure of impact is worked out. The duration of contact is directly obtained from the pressure equation. Without entering into lengthy mathematical computation to explain the occurrence of the phenomenon of multiple contacts, it has been possible to explain the higher contacts in light of present theory. In previous theories, the physical aspect of the problem was not so much tackled.

## PRESSURE OF IMPACT

Pressure exerted by the hammer is given by eqn. (6.1), (Banerjee, 1966).

$$P = -m \frac{d^2 z}{dt^2} = -E_2 u$$

where

$$z = y_a + u$$

and

$$u = -\frac{E_1}{E_2} y_a v^3 f(D) \text{ from eqn. (9.2) (Banerjee, 1966).}$$

$$v_s = \frac{F(D)}{F_4(D)} \cdot v_0 \text{ from eqn. (9.1) (Banerjee, 1966).}$$

Therefore,

$$P = -mv_0 \frac{F(D)}{F_4(D)}$$

Where  $F(D)$  stands for  $D$  and

$$F_4(D) = 1 + \frac{m}{E_2} D^2 + \gamma \frac{m}{M} \frac{-\cosh k_1 \gamma \sin k_1 \gamma - \cosh k_1 \gamma \cosh k_2 \gamma \sin \gamma}{2(1 + \cos \gamma \cosh \gamma)} \quad \dots (1)$$

Therefore with the help of Heaviside's expansion theorem

$$P = -mv_0 \left[ \frac{F(0)}{F_4(0)} + \sum \frac{F(\alpha_s)}{\alpha_s F_4'(\alpha_s)} e^{\alpha_s t} \right] \quad \dots (2)$$

But putting  $D = 0$ , we get  $F(0) = 0$ , and  $F_4(0) = 1$ ,  
and so

$$\frac{F(0)}{F_4(0)} = 0$$

For roots of  $D$  from  $F_4(D) = 0$ , we have  $F_4(D) = 0$ , whence

$$\frac{2(1 + \cosh \gamma \cos \gamma)}{\sinh k_2 \gamma \cos k_2 \gamma + \cosh k_1 \gamma \sin k_1 \gamma - \cosh k_1 \gamma \cosh k_2 \gamma \sin \gamma - \cos k_1 \gamma \cos k_2 \gamma \sin \gamma} = \frac{\frac{m}{M} \gamma}{1 - \frac{E_1}{E_2} \cdot \frac{m}{M} \cdot \frac{\gamma^4}{l^3}} \quad \dots (3)$$

Equations (3) and (7) (Banerjee, 66) are same and so the roots of  $\gamma$  as obtained from eqn. (24), in case of displacement in Part II (Banerjee, 1966) and eqn. (3) are having same set of values

Thus

$$nl = \gamma_s, \quad (s = 1, 2, 3, 4, \dots r)$$

$$D = [\alpha_s] = \pm i g_s$$

$$g_s = \gamma_s^2, \quad \sqrt{\frac{E_1 l}{M l^3}}$$

and

$$F_4'(\alpha_s) = \frac{1}{2\alpha_s} \left\{ \frac{3m}{E_2} \alpha_s^2 - 1 + \gamma_s \left( 1 + \frac{m}{E_2} \alpha_s^2 \right) \frac{\sinh \gamma_s \cos \gamma_s - \cosh \gamma_s \sin \gamma_s}{1 + \cosh \gamma_s \cos \gamma_s} \right. \\ + 2[k_2 \sinh k_2 \gamma_s \sin k_2 \gamma_s - k_1 \sinh k_1 \gamma_s \sin k_1 \gamma_s] + \cosh \gamma_s \cos k_1 \gamma_s \cosh k_2 \gamma_s \\ - \cosh k_1 \gamma_s \cosh k_2 \gamma_s \cos \gamma_s - k_1 [\sinh \gamma_s \sin k_1 \gamma_s \cosh k_2 \gamma_s + \sinh k_1 \gamma_s \\ \left. + \frac{m}{M} \gamma_s^2 \frac{\cosh k_2 \gamma_s \sin \gamma_s - k_2 [\sinh \gamma_s \sin k_2 \gamma_s \cosh k_1 \gamma_s + \sinh \gamma_s \sinh k_2 \gamma_s \cosh k_1 \gamma_s]}{2(1 + \cosh \gamma_s \cos \gamma_s)} \right\} \quad (4)$$

After simplification we get, with the help of Heaviside's expansion theorem, the pressure exerted by the load as

$$P = -4mv_0 \Sigma B_s q_s \sin q_s t \quad \dots (5)$$

where

$$\frac{1}{B_s} = \left\{ 1 + \frac{3m}{E_2} q_s^2 + \gamma_s \left[ 1 - \frac{m}{E_2} q_s^2 \right] \frac{\cosh \gamma_s \sin \gamma_s - \sinh \gamma_s \cos \gamma_s}{1 + \cosh \gamma_s \cosh \gamma_s} \right. \\ \left. 2[k_1 \sinh k_1 \gamma_s \sin k_1 \gamma_s - k_2 \sinh k_2 \gamma_s \sin k_2 \gamma_s] \right. \\ \left. + \cosh k_1 \gamma_s \cosh k_2 \gamma_s \cos \gamma_s - \cosh \gamma_s \cos k_1 \gamma_s \cos k_2 \gamma_s \right. \\ \left. + k_1 [\sinh \gamma_s \sin k_1 \gamma_s \cos k_2 \gamma_s + \sinh k_1 \gamma_s \cosh k_2 \gamma_s \sin \gamma_s] \right. \\ \left. + \frac{m}{M} \gamma_s^2 + \frac{k_2 [\sinh \gamma_s \sin k_2 \gamma_s \cos k_1 \gamma_s + \sinh k_2 \gamma_s + \sinh k_2 \gamma_s \cosh k_1 \gamma_s \sin \gamma_s]}{2(1 + \cosh \gamma_s \cos \gamma_s)} \right\}$$

Thus the pressure exerted by the hammer during impact is directly proportional to the striking velocity and it involves all the physical constants appearing in the displacement equation (12.1), (Banerjee 1966) for the struck point

#### DURATION OF IMPACT

The duration of contact which plays a very important part in the dynamics of vibration of a cantilever under lateral impact of an elastic load, is the time, measured from the instant the load comes in contact with the bar and maintains its contact till it separates out. There are cases where the phenomenon of multiple contact arises. The hammer or the bar may again overtake each other with a short period of separation and the hammer continues to remain in contact till another separation occurs. This overtaking may take place several times with intervening separations of short intervals until the load is able to leave the region of vibration of the bar. In such cases, the total duration of impact may be the time that elapses between the instant the impact begins and the instant, the hammer finally breaks off with the bar. Thus the duration of impact is obviously the lowest positive root of  $t$ , other than zero, obtained by solving  $P = 0$ , for the given struck point, in the pressure equation (5). This time of collision is used in the expression for velocity (eqn. 13, Banerjee 1966) to obtain the velocity of the hammer at the end of contact. Drawing the pressure-time curve as per equation (5) for pressure with required number of terms of the series we may obtain directly the magnitude of the duration of impact in specific case, of a beam hammer system.

Existence of different modes of vibration of the bar, as given by different terms of the displacement series (eqn. 12.1) (Banerjee 1966) governs the magnitude of the duration of contact. The experiments reported by the writer help to ascertain

the number of terms to be included in the pressure equation (5) in order to calculate the exact value of the duration of impact. Young's rule also holds good. That is if the position of any node of a particular mode of vibration is the struck point, the mode is not excited, and it is found under this condition, that in our pressure equation (5), the terms corresponding to that mode vanishes. Therefore, it is possible to easily obtain the duration of contact, using required number of terms in the expression for pressure (eqn. 5) of the present theory which previous theories failed to do.

#### M U L T I P L E   C O N T A C T S

We proceeded to show that the load and the bar being attached during impact, move with a common velocity (eqn. 13) (Banerjee 1966). But at the instant  $P = 0$ , in our pressure eqn. (5), the contact terminates. The motion of the bar is affected due to detachment of a moving mass and so its equation of motion is modified after impact ceases. The change in the velocity of the bar is in opposite sense to that suffered by the load at the instant separation ensues. This will create a space gap between the load and the bar. At the end of a contact (when  $P = 0$ ), the velocity may have any direction with respect to positive impinging velocity of the load and is determined by the striking distance and the number of modes stimulated into activity during impact. When this velocity, at the end of a contact comes out as positive, the load moves in a forward direction with a uniform velocity as it has no resistance to overcome after impact ceases, and shall meet the cantilever again which would be vibrating with the modified displacement law obtainable at the beginning of separation with load. Thus the second contact in such cases is a fresh contact, compression of the load follows and pressure is built up again to reduce to zero, when another separation occurs. Phenomenon of multiple contacts may be observed in the region, the load reverses its direction where the magnitude of the velocity of the bar shifts towards higher value. So there shall be a sudden set back in the velocity of the bar due to any detachment of the moving load. Overtaking the hammer to make another contact in this region depends on the recovery of this time-lag by the bar by suitably modifying its displacement condition. Thus at the final termination of contact three conditions are satisfied, namely, the pressure between the load and the cantilever is zero, the velocity of the load is negative and the displacement-time curves of the bar and the load do not meet again. The higher contacts other than the first are therefore different from what is given by our general dynamics using pressure equation (5). The higher contacts shall slightly modify the vibration form of the cantilever obtained from the displacement equation (12.1) (Banerjee 1966).

From the general expression for pressure (eqn. 5), it is found that the duration of impact is not altered by the impinging velocity. But considering the effects

of elastic collisions of two bodies. Hertzian impact is superimposed over the general condition of elastic impact, dealt in the previous parts.

#### APPLICATION OF HERTZ'S THEORY OF IMPACT

Ghosh (1940) (in case of struck string) has considered the duration of contact to be divided into three distinct periods. In our problem too, we follow the same arguments. Thus the three periods are named as 'First Hertz', 'Hooke' and 'Second Hertz' periods respectively. During the First Hertz period, the displacement of the bar in our case, is not appreciable, and the pressure of impact obeys Hertz's law of impact until a certain pressure is developed to make the displacement of the cantilever appreciable. As soon as the bar was displaced, the pressure obeys 'Hooke's law and the motion of the hammer is given by displacement eqn. (12.1) (Banerjee 1966) of the present general theory. The duration of contact during this period is calculated by equating the pressure equation (5) to zero as usual. After this 'Hooke' period is over, the extra compression developed in this period is released and the 'Second Hertz' period begins. It is assumed that the 'First Hertz' and the 'Second Hertz' periods have the same durations  $\tau$  (say). Therefore the total duration of contact is  $\phi_0 + 2\tau$ , where  $\phi_0$  is the duration of Hooke's period, as calculated from our general expression of pressure.

Following the method of Ghosh (1940), we write,

The pressure exerted due to Hertzian impact

$$m \frac{d^2 z}{dt^2} = m \frac{d^2 y_a}{dt^2} + m \frac{d^2 u}{dt^2} \quad \dots \quad (6.1)$$

$$= -en^{3/2} \quad \dots \quad (6.2)$$

$$z = y_a + u, \text{ and let } n_1 = \frac{4}{5} \frac{e}{m}, \quad \dots \quad (6.3)$$

where  $e$  is a constant depending on the geometric and elastic properties of the bar and the hammer as also their shapes at the contact surface. Assuming  $y_a = 0$ , during Hertz's periods, and  $v_0 = \frac{du}{dt}$ , at  $t = 0$ , the time to produce compression  $u_0$ , where  $u_0$  is the limiting value of  $u$  at the end of a 'Hertz' period is given by Ghosh (1940) as

$$\tau = \frac{u_0}{v_0} \left[ 1 + \frac{n_1 u_0^{5/2}}{7 v_0^2} + \dots \right] \quad \dots \quad (7)$$

Thus taking the first approximation, i.e. retaining only the first term

$$\phi = \phi_0 + 2\tau \text{ or } \phi - \phi_0 = \frac{2u_0}{v_0} \quad \dots \quad (8)$$

$\phi_0$  is calculated in the usual way from pressure function (eqn 5). The value of  $u_0$  is obtained by selection from a particular set of experimental values of the duration of contact.

#### ACKNOWLEDGEMENT

My best thanks are due to Prof. M. M. Ghosh, D.Sc., vice-principal, City College Calcutta for his helpful guidance.

#### REFERENCES

- Banerjee, B B , 1966, *Indian J Phys*, **40**, 198, 208.  
Ghosh, M. 1940, *Indian J Phys*. **14**. 495.

# DYNAMICS OF VIBRATION OF A CANTILEVER UNDER LATERAL IMPACT OF AN ELASTIC LOAD-PART IV (ENERGY OF THE BAR)

B. B. BANERJEE

UNIVERSITY COLLEGE OF ENGINEERING, BURLA-ORISSA

(Received September 11, 1965).

**ABSTRACT.** In this paper, the energy lost by the hammer, during impact (which is assumed to be the energy of the bar) is deduced, following the deductions of the general theory, as given in Parts I to III of this series of papers. Experiments carried out with a cantilever of length 95 cms., dia. 1.27 cms. and material mild steel is reported. The agreement between the theory and the experiment is excellent.

It is shown by Banerjee (1966-Part II) that the velocity of the load at any instant is given by

$$V_t = \frac{dy_a}{dt} = 4v_0 \Sigma A_s \cos q_s t \quad \dots (1)$$

or

$$\frac{V_t}{v_0} = 4 \Sigma A_s \cos q_s t. \quad \dots (2)$$

Initial energy of the hammer  $\frac{1}{2} m v_0^2$

Equation (2) gives the ratio of the velocity of the hammer at any instant during impact, to the initial impinging velocity of the load. The variable time  $t$  is replaced by the duration of impact, when we require the ratio of the velocity of the hammer at the termination of contact to the initial velocity. The duration of impact is obtained as usual, by equating the expression for pressure (Pt. II Banerjee 1966) to zero for the given struck point.

The ratio of the loss of energy to the initial energy of the load is given by

$$1 - \left( \frac{V_t}{v_0} \right)^2 \quad \dots (3)$$

It is noted here that the velocity of the hammer  $V$ , as calculated from eqn. (5) (Banerjee, 1966) at the termination of first contact is different than the rebound velocity of load in cases of multiple contacts. But in cases, where the influences of multiple contacts are meagre, the energy lost by the hammer, as calculated from eqn. (1) (Banerjee, 1966) will give sensibly accurate results.

The apparatus used is similar to that used by Banerjee in the study of lateral impact on cantilever excepting the photographic recording arrangements. The

rod is struck transversely by the hammer from different distances away to achieve different impinging velocities. The arc along which the hammer swings is measured from the shadow of the outline of the hammer cast on a graduated translucent scale placed very near to it. The length of the hammer (pendulum bob) and its maximum arc of swing in each case help to measure the velocities respectively.

TABLE I

Cantilever mild steel, length 95 cms dia. 1.27 cms.

**Hammers**

- Hammer A** . Brass, weight, 285.5 gms 'mass ratio' 3.29  
radius of curvature at contact surface 2 cms
- Hammer B** mild steel, other specifications same as **Hammer A**
- Hammer C** Aluminum, weight 108 gms rad at contact  
surface 2 cms
- Hammer D** mild steel, weight same as **Hammer C**, radius  
of curvature at contact surface 1 cm

Hammer velocity before impact cm/sec	A 32.75	A 47.36	A 79.21	A 94.73	A 65	B 65	C 65	D 65
Striking distance (cms)	$1 - \left(\frac{v}{v_0}\right)^2$							
95	.6751	.6636	.6519	.6636	.6636	.6975	.9375	.9159
90	.8100	.8151	.8100	.8151	.8151	.7975	.9121	.9395
85	.8701	.8675	.8270	.8319	.8479	.8400	.9444	.9494
80	.9039	.8976	.8775	.8775	.8775	.8556	.9450	.9560
75	.9159	.9100	.8844	.8844	.9010	.8775	.9804	.9676
70	.9405	.9159	.9100	.9040	.9324	.8976	.9919	.9744
65	.9216	.9375	.9160	.9160	.9100	.8911	.9933	.9890
60	.9600	.9572	.8976	.9100	.9100	.8844	.9718	.9639
55	.9900	.9879	.9801	.9831	.9831	.9856	.9600	.9694
50	.9780	.9600	.9600	.9600	.9600	.9744	.9984	.9994
45	.9560	.9159	.9560	.9516	.9448	.9500	.9920	.9980
40	.9350	.9324	.9216	.9324	.9160	.9324	.9600	.9490
35	.8844	.8844	.8811	.8844	.8775	.8775	.9450	.9842
30	—	—	—	—	—	.8140	.9906	.9958
47.5 (mid-pt)	—	—	—	—	—	.9663	—	—

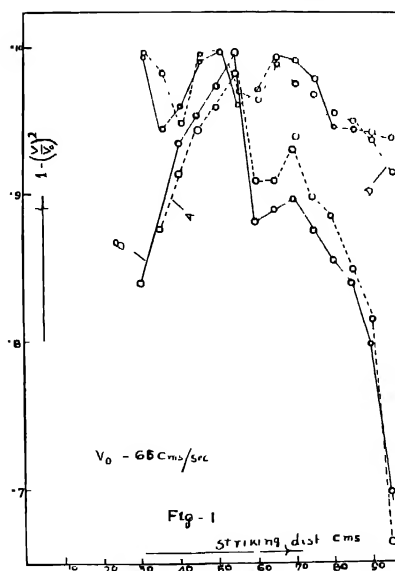


TABLE II

Cantilever : same as given in Table I. struck at free end  
 Hammer : mild steel, velocity before impact 65 cms/sec

Mass ratio	1	1.88	3.29	3.76	8.7
$1 - \left(\frac{v_f}{v_0}\right)^2$	.3916	.5914	.6975	.7286	.9159

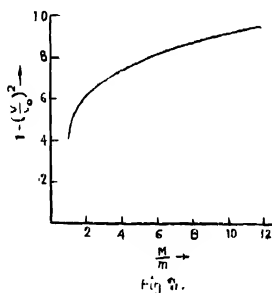
The curves in Fig. 1 are for the same striking velocity and for hammers A, B, C, and D, respectively. It is found that the value of  $1 - \left(\frac{v_f}{v_0}\right)^2$  discontinuously fluctuates with striking distances. The difference in the loss of energy



for particular struck point is very small for hammers of same mass but different elastic constant. Further comparing curves A and B, it is found that the nature of the fluctuation of the ratio of the loss of energy to the initial energy of the hammer with the striking distances appears to be similar. But for hammers C and D, this fluctuation is not similar. This shows that the radius of curvature of the

hammer at the contact surface plays an important part in this nature of fluctuation. Further from curves A and B, we find that the loss of energy is maximum at the particular struck point (55 cms.) this shows that the energy of bending is maximum at this struck point. But from curves C and D, it is found that this point shifts towards shorter length, (50 cms) as the mass of the hammer decreases.

Fig 2 shows the variation of loss of energy to initial energy of the hammer with 'mass ratio' for the same struck point. It is found that the loss of energy tends to a constant maximum value as the 'mass ratio' increases.



For the cantilever, struck by hammer B at 47.5 cms (mid. -pt) the calculated value of the quantity  $1 - \left(\frac{V_t}{V_0}\right)^2$  as per eqn 3, is .9513 and the experimental value (table 1) is .9663. Again for the same hammer, striking at 80 cms., the calculated value of the ratio of loss of energy to initial energy is .8400 and the experimental value is .8556. These are very good agreements.

#### ACKNOWLEDGEMENT

My best thanks are due to Prof. M. M. Ghosh, D Sc., of City College, Calcutta, for his lively interest in this work and to Prof. B. Mahapatra, Principal, University College of Engineering, Burla-Orissa, for extending facilities to perform the experiment.

#### REFERENCES

- Banerjee, B. B., 1966, *Indian J. Phys* **40**, 208, 215  
 ———, 1964, *Indian J. Phys*, **38**, 99-105.

## DIELECTRIC CONSTANT AND INTERATOMIC FORCES

C. M. KACHHAVA AND S. C. SAXENA

PHYSICS DEPARTMENT, RAJASTHAN UNIVERSITY, JAIPUR, INDIA

(Received July 4, 1965, Resubmitted November, 18, 1965)

**ABSTRACT.** The existing classical theory of dielectric constant is improved by considering a more detailed form for the interatomic forces and the corresponding change in the polarisation of the medium. A procedure has been suggested to determine the net polarisation. The theory is finally tested by considering the low and high frequency dielectric constant data of alkali halide crystals.

## INTRODUCTION

The mechanism of polarisation of a dielectric when placed in an electric field is now fairly well understood Debye (1929). In developing such a theory the problem is posed in the calculation of the effective field,  $E_{eff}$ , responsible for the polarisation of each of the atoms or molecules of the medium. Mott and Gurney (1948) discuss a procedure for evaluating  $E_{eff}$  in which the contribution arising from the polarisation due to the overlap of the neighbouring ions is also included. We follow the same general approach and reformulate the theory taking into account a more realistic force-field. We further specialize and confine our discussion to the alkali halide crystals having the sodium chloride type of structure. For such crystals the potential energy when considering only the nearest neighbour interaction is, [Kachhava and Saxena (1963) and Saxena and Kachhava (1964),]

$$\phi(r) = -\frac{e^2}{r} + a \exp(-r/\rho) - \frac{c}{r^6} - \frac{d}{r^{12}}. \quad (1)$$

Here  $r$  is the interionic separation,  $e$  the electronic charge,  $a$  and  $\rho$  are the potential parameters, and  $c$  and  $d$  are the van der Waals constants.

## THEORY

If we represent the polarisation of the medium by  $P$ , when placed in an electric field of intensity  $E$ , the effective field responsible for polarising the molecule is given by

$$E_{eff} = E + \frac{4\pi}{3} P. \quad (2)$$

In many crystals, as in alkali halides, there is considerable overlap between the negative and adjacent positive ions. This causes a reduction in that part of the

effective field which is due to the polarisation of the medium. This necessitates writing equation (2) in the following form,

$$E_{\text{eff}} = E + \frac{4}{3} \pi P(1-\beta) = E + \frac{4}{3} \pi P\gamma. \quad \dots (3)$$

We further suggest that  $\beta$  or  $\gamma$  can be determined if  $\phi(r)$  be known and for the particular form of equation (1) it is

$$\beta = 1 - \gamma = \frac{\left(\frac{r_0}{\rho}\right) e^{-r_0/\rho} - \frac{6c}{r_0^6} - \frac{8d}{r_0^8}}{e^2/r_0} \quad \dots (4)$$

Here  $r_0$  is the equilibrium interionic separation. It may be remarked that  $\gamma = 0$  ( $\beta = 1$ ) corresponds to maximum overlap and  $\gamma = 1$  ( $\beta = 0$ ) to no overlap between the ions.

As shown by Mott and Gurney (1948) the high frequency dielectric constant,  $\epsilon_0$ , is given by

$$\frac{\epsilon_0 - 1}{4\pi} = \frac{N(\alpha_1 + \alpha_2) - (8/3)\pi N^2 \alpha_1 \alpha_2 (1 - \gamma)}{1 - (4/3)\pi N(\alpha_1 + \alpha_2) - (16/9)\pi^2 N^2 \alpha_1 \alpha_2 (1 - \gamma^2)} \quad (5)$$

in which  $N$  is the number of ion pairs per unit volume and  $\alpha_1$  and  $\alpha_2$  are the polarisabilities of the two ions.

Again following Mott and Gurney (1948) it can be shown that the low frequency dielectric constant,  $\epsilon$ , is

$$\frac{\epsilon - 1}{3 + (\epsilon - 1)\gamma} = \frac{\frac{4\pi}{3} N(\alpha_1 + \alpha_2) - \frac{32}{9} \pi^2 N^2 \alpha_1 \alpha_2 (1 - \gamma)}{1 - \frac{4\pi}{3} N(\alpha_1 + \alpha_2)(1 - \gamma) + \frac{16}{9} \pi^2 N^2 \alpha_1 \alpha_2 (1 - \gamma)^2} + \frac{\frac{4\pi}{3} \delta}{1 - \frac{4\pi}{3} \delta(1 - \gamma)}, \quad (6)$$

in which

$$\delta = 2 \frac{Ne^2}{p}, \quad \text{where}$$

$$p = 4 \left[ \omega''(r_0) + \frac{2}{r_0} \omega'(r_0) \right], \quad \dots (7)$$

and

$$\omega(r) = e^{-\gamma r} = \frac{c}{r^6} - \frac{d}{r^8} \quad \dots (8)$$

A much cleaner and physical result is obtained by combining relations (5) and (6) when one gets

$$\frac{\epsilon-1}{3+(c-1)\gamma} = \frac{\epsilon_0-1}{3+(c_0-1)\gamma} + \frac{\frac{4\pi}{3}\delta}{1-\frac{4\pi}{3}\delta(1-\gamma)} \quad \dots \quad (9)$$

### RESULTS

We proceed to check the theory as represented by equations (5), (6) and (9) by considering alkali halide crystals in particular. The potential parameters  $a$  and  $\rho$  were determined by writing equation (1) in the form

$$\Phi(r) = -\frac{\alpha e^2}{r} + 6ac^{-\gamma/\rho} - \frac{c}{r^6} - \frac{D}{r^8}, \quad \dots \quad (10)$$

and using the Born-Mayer conditions viz.,

$$\frac{d\Phi(r)}{dr} = \frac{3VT}{NK} \left( \frac{1}{V} \frac{\partial V}{\partial T} \right)_P \text{ at } r = r_0, \quad \dots \quad (11)$$

and

$$\frac{d^2\Phi(r)}{dr^2} = \frac{9V}{NK} F_{T,P}, \text{ also at } r = r_0 \quad \dots \quad (12)$$

Here  $\alpha$  is the Madelung constant,  $C$  and  $D$  are van der Waals constants and their values as given by Mayer (1933) are used,  $T$  the absolute temperature,  $\left( \frac{1}{V} \frac{\partial V}{\partial T} \right)_P$

the coefficient of thermal expansion,  $F_{T,P}$  is a factor involving  $\left( \frac{1}{V} \frac{\partial V}{\partial T} \right)_P$ ,

$K, \left( \frac{\partial K}{\partial P} \right)_T$  and  $\left( \frac{\partial K}{\partial T} \right)_P$ ,  $P$ ,  $V$  and  $K$  are the pressure, molar volume and the coefficient of compressibility respectively. In the calculations described later the polarisability values wherever needed are those of Pauling (1927). Values of  $r_0$ ,  $K, \left( \frac{1}{V} \frac{\partial V}{\partial T} \right)_P$  and  $F_{T,P}$  as compiled by Saxena (1965) earlier are used.

In Table 1 we report the high frequency dielectric constant of alkali halide crystals. The experimental values are as listed in reference (2). Computed values of  $\epsilon_0$  are according to equation (5) with three different values of  $\gamma$ . These are  $\gamma = 0$ , and 1 being the two extreme values, and  $\gamma$  as calculated from equation (4). The latter  $\gamma$  values are also recorded in the Table I, column 2. It will be seen that  $\epsilon_0$  values are not much dependent on  $\gamma$  indicating thereby, as expected also, feeble dependence of  $\epsilon_0$  on the degree of overlapping between the ions. It is

interesting to note that in general there is a satisfactory agreement between theory and experiment.

In Table II we discuss the low frequency dielectric constant,  $\epsilon$ , which is dependent on overlapping of the neighbouring ions in a much more pronounced fashion. This is substantiated by the computed values of  $\epsilon$  reported in the Table for the two extreme values of  $\gamma$ . The criteria of fixing  $\gamma$  thus is anticipated to have a crucial test in this case. It is encouraging to note that the calculated values according to Equation (6) are in good agreement with the experimental values and specially when one recalls the rather large uncertainty associated with the computed values due to the greater uncertainty in the polarisability data. We personally regard this agreement as evidence of an overall adequacy of the theory of dielectric constant as well as of Equation (4).

A way out of avoiding the uncertainty creeping in the calculation of  $\epsilon$  based on Equation (6) is possible if one utilises the relation of Equation (9). We use this relation in conjunction with the experimental  $\epsilon_0$  and  $\gamma$  values to calculate  $c$ . These are also recorded in Table II, column 7. It is to be noted that the agreement in almost all cases is appreciably improved.

The relation given by Equation (9) can also be utilised to fix the values of  $\gamma$  itself. In such a calculation experimental values of  $\epsilon$  and  $\epsilon_0$  are used. The success of the procedure is therefore related to the accuracy with which these constants can be determined. The  $\gamma$  values obtained according to this procedure are recorded in Table I, column 3.

Within the scope of large uncertainty in the  $\gamma$  values obtained from Equation (9) we feel it reasonable to conclude that the two sets of  $\gamma$  values are in good agreement with each other, again lending confirmation to the procedure suggested for evaluating  $\gamma$ .

So far we have essentially worked within the framework of classical theory of dielectric constant as modified by Mott and Gurney (1948). In this picture the effective charge of the ions is assumed to be unaffected. Szigeti (1949) presented a different theory by considering that overlap causes deformation of the electronic shells so that they are no more spherical, as usually assumed. This approach thus finally makes the reduction in polarization so far considered equivalent to a change in the value of the charge on the ions. According to this latter theory the actual charge  $ze$  on an ion behaves like having an effective value of  $szc$ . Szigeti (1949, 1950) has calculated the value of  $s$  for thirteen alkali halides and eleven of these are reproduced in Table III. If this theory is made equivalent to that of Mott and Gurney (1948)  $s$  and  $\gamma$  should be identifiable. We further confirm this by calculating  $\epsilon_0$  and  $c$  from Eqs. (5) and (9) respectively by using  $s$  values as listed in Table III for  $\gamma$  in them. In this very Table in columns 3 and 5 we report these values and their percentage deviations from the corresponding experimental values in columns 4 and 6 respectively.

These values are seen to be in good agreement and also favourably compared with the findings of Table I and II. The low frequency dielectric constant  $\epsilon$

TABLE I  
Values of  $\gamma$  and  $\epsilon_0$  for alkali halide crystals

Crystal	Calculated $\gamma$ values			$\epsilon_0$			
	Eq. (4)	Eq. (9)	Exptl.	Calculated			
				$\gamma$ variable	% dev.	$\gamma=0$	$\gamma=1$
LiF	0.74	0.49	1.92	2.13	+10.9	2.13	2.16
LiCl	0.68	0.46	2.75	3.53	+28.4	3.51	3.54
LiBr	0.70	0.51	3.16	3.83	+21.2	3.65	3.84
LiI	0.67	0.66	3.80	4.76	+25.3	4.75	4.78
NaF	0.70	0.36	1.74	1.77	+1.7	1.74	1.78
NaCl	0.70	0.70	2.25	2.67	+18.7	2.63	2.70
NaBr	0.70	0.21	2.62	2.90	+14.5	2.83	2.93
NaI	0.69	0.63	2.91	3.45	+16.5	3.31	3.48
KF	0.74	0.79	1.85	1.75	-5.4	1.69	1.78
KCl	0.71	0.41	2.13	2.27	+6.7	2.16	2.31
KBr	0.69	0.49	2.33	2.42	+3.4	2.32	2.48
KI	0.70	0.30	2.69	2.78	+3.3	2.67	2.84
RbF	0.71	0.88	1.93	1.87	-3.1	1.79	1.91
RbCl	0.71	0.64	2.19	2.23	+1.8	2.10	2.29
RbBr	0.69	0.84	2.33	2.34	+0.4	2.21	2.40
RbI	0.70	0.53	2.63	2.63	0.00	2.50	2.71

Av. Abs. % dev. 10.1

TABLE II  
Experimental and calculated  $\epsilon$  values for alkali halide crystals

Crystal	Exptl.	Calculated Eq. (6)				Calculated Eq. (9)			
		$\gamma$ variable	% dev.	$\gamma=0$	$\gamma=1$	$\gamma$ variable	% dev.	$\gamma=0$	$\gamma=1$
LiF	9.27	12.19	+31.5	6.45	20.3	10.50	+13.3	6.24	15.13
LiCl	11.05	14.14	+27.9	5.25	44.3	9.79	-11.4	5.49	17.35
LiBr	12.1	14.45	+19.4	5.03	66.8	10.66	-11.9	5.54	19.67
LiI	11.03	15.69	+42.2	6.76	67.2	11.13	+0.9	5.80	23.81
NaF	6.0	7.10	+18.3	5.19	9.64	7.03	+17.1	5.19	12.00
NaCl	5.62	7.84	+39.5	4.77	11.34	6.37	+13.3	4.36	8.31
NaBr	5.99	8.21	+44.5	4.85	12.49	7.27	+21.4	4.64	10.00
NaI	6.60	8.68	+31.5	4.98	13.80	7.03	+6.5	4.58	9.82
KF	6.05	5.44	-10.8	4.10	6.63	5.79	-4.3	3.99	6.99
KCl	4.68	5.33	+14.6	3.98	7.54	5.46	+16.6	3.95	6.63
KBr	4.78	4.89	+2.3	3.96	7.46	4.47	-6.5	3.96	6.83
KI	4.94	6.66	+32.4	3.26	8.99	6.23	+26.1	4.28	8.25
RbF	5.91	5.18	-12.3	3.84	6.29	5.23	-11.5	3.98	6.39
RbCl	5.0	5.12	+2.4	3.07	6.41	5.06	+1.2	3.76	6.04
RbBr	5.0	5.13	+2.6	3.70	6.57	5.16	+3.2	3.81	6.57
RbI	5.0	5.69	+13.8	3.84	7.20	5.57	+11.4	3.97	6.82

Av. Abs. % dev.

22.2

11.2

TABLE III

Calculated values of  $\epsilon_0$  and  $\epsilon$  from Eqs (5) and (9) respectively using  $s$  values of Szigeti for  $\gamma$

Crystal	$s$	Calculated $\epsilon_0$	% dev	Calculated $\epsilon$	% dev.
LiF	0.83	2.13	10.9	11.7	26.2
NaF	0.93	1.78	2.2	8.63	43.8
NaCl	0.74	2.68	19.1	6.57	15.1
NaBr	0.69	2.86	9.2	7.18	19.9
NaI	0.71	3.46	18.2	7.20	9.1
KCl	0.80	2.32	9.0	5.77	23.3
KBr	0.76	2.46	5.6	5.69	19.0
KI	0.69	2.75	2.2	6.28	27.1
RbCl	0.84	2.25	2.8	5.44	8.8
RbBr	0.82	2.36	1.3	5.57	11.4
RbI	0.79	2.67	1.5	5.84	16.8
Average % dev 7.5					19.9

now on the average is reproduced within a margin of 20 per cent. In Table II we find the reproduction to be relatively superior. The average absolute deviation was 11.2 per cent. This indicates a preference for the use of  $\gamma$  values as obtained here in the theory of Szigeti (1949) for  $s$ . These results further lend confirmation to the picture advanced here for the role played by the overlap forces in the dielectric polarisation.

#### APPENDIX A

While developing the theory of dielectric constant in this paper we have tried to take into account the effect of the overlap on the polarisation of the medium. The reduction is estimated by introducing a factor  $\beta$  (or  $\gamma$ ), which is defined by equation (4). This defining relation was stated more or less on an ad hoc basis and here we present a simple brief proof for the same.

In the absence of overlap the polarisation  $P$  of the medium is entirely due to charge-charge interaction. If the potential energy because of this interaction be  $\phi_0$  we have

$$\phi_0 = -\frac{e^2}{a}. \quad (\text{A1})$$



If  $I_e$  is the corresponding intensity of the electrical field then the force,  $F_e$ , experienced by a charge  $q$  in the polarised medium is

$$F_e = qI_e = -\frac{\partial\phi_e}{\partial r}. \quad \dots \quad (A2)$$

In the presence of overlap the polarisation of the medium is altered, and so are the electrical intensity and the force on a charge. The force  $F_0$  now acting on the same charge  $q$  because of the overlap only is

$$F_0 = qI_0 = -\frac{\partial\phi_0}{\partial r}. \quad \dots \quad (A3)$$

$I_0$  is that part of the total electrical intensity which owes its origin to the overlap force  $F_0$ . The defining relations for  $\phi_0$  for the potential of equation (1) is

$$\phi_0 = a \exp(-1/\rho) - \frac{c}{r^6} - \frac{d}{r^8}. \quad \dots \quad (A4)$$

Obviously

$$\beta = \frac{P_0}{I_e} = \frac{I_0}{I_e} = \frac{\partial\phi_0/\partial r}{\partial\phi_e/\partial r}. \quad \dots \quad (A5)$$

or

$$\beta = 1 - \gamma = \frac{\left(\frac{r_0}{\rho}\right) a e^{-r_0/\rho} - \frac{6c}{r_0^6} - \frac{8d}{r_0^8}}{e^{\gamma}/r_0}. \quad \dots \quad (A6)$$

#### APPENDIX B

In the theory of the dielectric constant discussed in this paper the effect of overlap of the neighbouring ions is regarded to cause the reduction in the polarisation of the medium. In this picture the effective charge of the ions is assumed to be unaffected. Szigeti (1949, 1950) has considered this problem in a different way. He assumes that the reduction in the polarisation is equivalent to a change in the value of the charge on the ions. He introduces a parameters to estimate the refraction in the actual value of the charge. These two pictures can be regarded as equivalent and his  $s$  values can be compared with our values. The two sets of values agree reasonably well. Szigeti's ideas have been further developed (Dick *et al.*, 1958; Hanlon *et al.*, 1959) and some comments in this direction we hope to report in due course.

Johye, P. 1929, *Polar Molecules*, Dover Publications, Inc.  
Dick, B. J. Jr. and Overhauser, A. W., *Phys. Rev.*, **112**, 90  
Huntlon, J. E. and Lawson, A. W., 1959, *Phys. Rev.*, **113**, 472  
Kachhava, C. M. and Saxena, S. C. 1963, *Phil. Mag.* **8**, 1429.  
—————, ————, ————, 1965 *Proc. Natl. Inst. Sci. (India)*, **A31**, 295.  
Mayor, J. E. 1933, *J. Chem. Phys.*, **1**, 270  
Mott, N. F. and Gurney, R. W. (1948), *Electronic Processes in Ionic Crystals*, Clarendon Press, Oxford.  
Pauling, L. 1927, *Proc. Roy Soc.*, **A114**, 191.  
Saxena, S. C. and Kachhava, C. M. 1964, *Ind. J. Pure and App. Phys.*, **2**, 336.  
Szegedi, B. 1949, *Trans. Faraday Soc.* **45**, 155.  
—————, 1950, *Proc. Roy Soc. (London)* **A204**, 51

## ELECTRON COLLISION WITH CAESIUM ATOM

(Mrs) R. BASU AND N. C. SIL

DEPARTMENT OF THEORETICAL PHYSICS

INDIAN ASSOCIATION FOR THE CULTIVATION OF SCIENCE

JADAVPUR, CALCUTTA 32.

(Received December 11, 1965)

**ABSTRACT.** The elastic scattering cross section for slow electron scattering by caesium atom has been calculated by taking the form of Stone and Reitz for the atomic potential and that of Biermann and Harting for the polarization potential. As the exchange effect is negligible in the energy corresponding  $K^2 = 1$  a.u., its consideration has been excluded.

## INTRODUCTION

In the study of the elastic scattering of slow electron by neutral atom we are up against the difficulty of the choice of a suitable potential to represent the field generated by the nucleus and the surrounding electrons of the atom; further we have to consider the distortion of this field induced by the incoming electron. In such a calculation we have to bear in mind the possibility of exchange of roles between the incoming electron and the bound electron when they are close to each other during the impact. Salmona and Seaton (1960) have calculated such a process in Bethe approximation for sodium and caesium atoms and have found that the value of the cross section for Cs. atom reaches a maximum at an energy value  $K^2 = .09$  atomic units, which is nearly the same as has been found experimentally by Brode (1929), but the magnitude of the cross section at that energy is much less than that of Brode. Garrett and Mann (1963) have taken the potential for the atomic field of Cs. atom due to Hartree and for the polarization field due to Biermann and Harting (1942); except for a little increase in the region  $.04 < K^2$

$.06$  a.u. their cross section decreases monotonously with the increase of energy in the range  $.01 < K^2 < 1.96$  a.u. Their calculation fails to show the sharp peak at  $K^2 = .09$  a.u. as observed experimentally by Brode. Stone and Reitz (1963) using an adiabatic model and including exchange effect have calculated the cross section of scattering in the region  $.00025 < K^2 < .065$  a.u. They have found that the influence of exchange is quite considerable below  $K^2 = .02$  a.u. and is small thereafter. The variation of cross section with energy in that range shows a maximum at the value  $K^2 = .02$  a.u. However, the experimental results of Chen and Raether (1962) do not agree with their calculated values. Using a first order perturbation theory in the adiabatic approximation Crown and Russek (1965) have calculated the same problem in the energy range  $.00005 < K^2 < .2$  a.u. They have obtained a minimum value for the scattering cross section

at  $K^2 = .0085$  a.u., whereas Stone and Reitz (1963) have obtained a maximum value near about the same point

In view of the fact that the theoretical results are at variance with each other we have made an attempt to calculate the same problem taking different combination of potentials with a view to obtaining better fit with experimental results, which are also not quite consistent. For our calculation we have chosen the potential field of the Cs. atom as that of Stone and Reitz (1963) and the polarization potential of Biermann and Harting (1942). The value of the scattering cross section in units of  $\pi a_0^2$  at the energy  $K^2 = 1$  a.u. comes to 407 as compared to 160 of Garrett and Mann (1963) and 70 of Crown and Russek (1965), whereas the experimental value due to Brode (1929) is 263

The potential for the screened atomic field of Cs. is split up into two parts. For the region  $0 < r < 2$  a.u. we take the form of Prokofjew which is a modification of the Hartree potential for  $Cs^+$  ion, and which has been tabulated by Stone (1962) for the values of the effective charge  $Z(r)$  of the  $Cs^+$  ion core against  $r$ . We are justified in taking this potential because inner core electrons are insensitive to the state of the valence electron. In the region  $2 < r < \infty$  we choose the values given by Stone and Reitz (1963) who had plotted the logarithm of the potential  $V(r)$  against  $r$ . As this curve is a straight line we choose  $V = Ae^{-br}$ . Our potential is continuous at  $r = 2$ . For the polarization potential we use the form of Biermann and Harting which has also been used by Garrett and Mann in their calculation.

$$Vp = \frac{\alpha}{2r^4} \left[ 1 - \exp \left\{ - \left( \frac{r}{fr_0} \right)^8 \right\} \right]$$

where  $\alpha$  is the polarizability of the atom

As the influence of exchange is not of considerable value at  $K^2 = 1$  a.u. (27.2 e.v.), we have not included it in our present calculation.

#### THEORY

The differential cross section is given by

$$\sigma(\theta) = |f(\theta)|^2 = \frac{1}{K^2} \left| \sum_{l=0}^{\infty} (2l+1)e^{i\eta_l} \sin \eta_l p_l(\cos \theta) \right|^2$$

The total cross section becomes

$$\sigma = \sum_{l=0}^{\infty} \sigma_l$$

where

$$\sigma_l = \frac{4\pi}{K^2} (2l+1) \sin^2 \eta_l$$

To calculate the phase shift  $\eta_l$  we have used WKB method with Langer modification, according to which the phase shift is given by (c.f. Landau and Lifshits, 1959)

$$\eta_l = \int_{r_l}^{\infty} \left[ \frac{1}{\hbar} \left\{ 2m(E-U) - \frac{\hbar^2(l+\frac{1}{2})^2}{r^2} \right\}^{\frac{1}{2}} - K \right] dr + \frac{\pi(l+\frac{1}{2})}{2} - Kr_l$$

where  $r_l$  is the value of  $r$  for which the expression under the radical sign is zero.

## RESULTS AND DISCUSSIONS

The potential term  $U$  consists of two parts; one due to the field of the Cs. atom and the other due to the polarization induced by the incident electron.

$$-U = V(r) + V_p(r).$$

$$V(r) = \frac{Z(r)}{r} \quad \text{for } 0 < r \leq 2$$

$$= 2.2594e^{-3r} \quad \text{for } 2 \leq r < \sigma$$

$$V_p(r) = \frac{\alpha}{2r^4} \left[ 1 - \exp \left\{ - \left( \frac{r}{f_0} \right)^8 \right\} \right]$$

We have taken

$$\alpha = 243 \text{ atomic units}$$

$$r_0 = 6.13 \text{ atomic units}$$

$$f = .8$$

Using the above values of the parameters we have numerically integrated the expression

$$\int_{r_l}^{\infty} \frac{1}{\hbar} \left\{ 2m(E-U) - \frac{\hbar^2(l+\frac{1}{2})^2}{r^2} \right\}^{\frac{1}{2}} - K \right\} dr$$

From Table I it can be seen that at the incident energy  $K^2 = 1$  a.u. quite a large number of phase shifts contribute appreciably to the total cross section. The contribution from such a large number of phase shifts has considerably increased the value of the total cross section  $\sigma$ . The value of the total cross section obtained by us at  $K^2 = 1$  a.u. in units of  $\pi a_0^2$  is 407, the same obtained by Garrett and Mann is 160 and by Crown and Russek is 70; whereas the experimental value due to Brode is 263 at that energy. It may be mentioned here that at our energy the influence of polarization potential is not of much consequence. The value

TABLE I

Calculated phase shifts and partial cross sections at  $K^2 = 1$  a.u.  
(27.2 o.v.)

$l$	$n_l$	$\sigma_l$ in the units of $\pi a_0$
0	18 220	1.36
1	17 955	7 30
2	12 648	0.13
3	6 635	3.32
4	4 505	34 47
5	3 901	20 48
6	3 653	12.46
7	2 824	5.84
8	2 247	41.35
9	1 207	66 38
10	1.009	60.19
11	0 867	53 46
12	0.638	35.52
13	0.491	24.03
14	0.374	15.47
15	0 273	9.04
16	0.269	9.37
17	0.173	4.17
18	0 117	2 03

obtained by Garrett and Mann with Hartree potential is less than the experimental value of Brode, the potential of Stone and Reitz extends further than the Hartree field, as such we felt that the potential of Stone and Reitz would increase the value of the cross section to bring it in better agreement with the experimental value, but the increase is much more than our expectations. It is difficult to judge the suitability of this potential by calculating the cross section at one energy, for proper appraisal it is necessary to see its variation with energy. It is not easy to reconcile our too large value with the too low value of Crown and Russek, who have, in support of their result, compared with the experimental value of Margulis and Korchevoi (1962), which differs considerably from that of Brode (Margulis and Korchevoi have obtained 57 for  $K^2 = .048$  whereas the value of Brode is 300 for nearly the same point).

## ACKNOWLEDGEMENT

The authors wish to thank Prof. D. Basu for his kind interest in the problem and for many helpful discussions during the progress of the work

## REFERENCES

- Biermann, L. and Harting, H. 1942, *Z. Astrophys* **22**, 87.  
Brodie, R. B. 1929, *Phys. Rev.*, **34**, 673.  
Chen, C. L., and Raether, M. 1962, *Phys. Rev.* **128**, 2679  
Crown, J. R. and Russell, A., 1965, *Phys. Rev.*, **138**, A669  
Gurett, W. R. and Mann, R. A. 1963, *Phys. Rev.* **130**, 658  
Landau, L. D. and Lifshitz, E. M., 1959, *Quantum Mechanics Non relativistic Theory* Pergamon Press, London-Paris, p.415.  
Morgulis, N. D. and Korchevov, Yu.P. 1962, *Zh. Tech. Fiz.* **32**, 900 (English transl. 1962, *Soviet Phys. Tech. Phys.* **7**, 655)  
Salmon, A. and Seaton, M. J. 1960, *Proc. Phys. Soc.* **77**, 617  
Stone, P. M. 1962, *Phys. Rev.* **127**, 1151  
Stone, P. M. and Reitz, J. R. 1963, *Phys. Rev.* **131**, 2101.

# INFLUENCE OF LIMITS SET TO LATERAL DISPLACEMENT ON THE DETERMINATION OF MEAN MULTIPLE COULOMB SCATTERING IN NUCLEAR EMULSIONS

PREM K ADITYA

INDIAN INSTITUTE OF TECHNOLOGY  
NEW DELHI-29 (INDIA)

(Received July 27, 1965, Resubmitted December 6, 1965)

**ABSTRACT** Multiple scattering constant has been determined in nuclear emulsions using 8 GeV  $\mu$ -mesons. The influence of limits set on lateral scattering of tracks has been investigated. It has been shown that an underestimation to an extent of upto 25% may be introduced by restricting track displacements to say about 50  $\mu$ m in 10 cm travel. Such limits are generally imposed upon by the requirement of having close pairs of tracks to avoid spurious scattering in relative scattering measurements or due to the limited width of the field of view of the microscopes and due to finite thickness of the emulsion layer.

## INTRODUCTION

In recent years there have been many investigations on multiple Coulomb scattering, particularly the determination of the scattering constant in nuclear emulsions. The scattering constant for a singly charged particle is defined by the relation, (Voyvodic and Pickup, 1952) ·

$$\alpha = \frac{KZt^{\frac{1}{2}}}{p\beta c}$$

where  $\alpha$  is the mean scattering angle in degrees,  $p\beta c$  is momentum times velocity in MeV and  $t$  is the cell length in 100  $\mu$ m units. The scattering constant,  $K$  in MeV deg. (100  $\mu$ m) $^{\frac{1}{2}}$  is known to be about 25 to 30. The determination of  $K$  involves measurement of the mean angle of scattering, the method generally adopted is the coordinate method developed at Bristol (Fowler 1950).

In an investigation carried out recently (Aditya 1964a, 1964b) multiple scattering measurements had been made on tracks of 8 GeV  $\mu$ -mesons. It has been shown that because  $\mu$ -mesons have only electromagnetic interaction, in contrast with protons and  $\pi$ -mesons which have also a finite cross section for inelastic interaction, the multiple scattering is more precisely defined for them.

## STATEMENT OF THE PROBLEM

From the observed multiple scattering for particles of known energy the scattering constant  $K$  should be directly determinable.

Ideally the observed scattering should be entirely genuine. There should be no additional component and there should be no restrictions imposed upon



by the experimental method. In actual practice, however, the emulsion suffers from the presence of spurious scattering (see, for example, Biswas *et al.* 1955, Aditya *et al.* 1963) which severely distorts the frequency distribution of angular scatters and leads to an over-estimation of scattering.

In order to eliminate spurious scattering one of the generally accepted methods has been the relative scattering of "close tracks". It has been shown (Biswas *et al.* 1957) that, spurious scattering increases with increase of mutual separation between two tracks of a pair. Limits are thus generally set to track separation depending upon the magnitude of spurious scattering in the plates. Limits are set sometimes also in order to avoid the inconvenience of realigning a track moving out of the field of view due to large angle scattering and curvature due to genuine scattering. Such a limit is sometimes enforced upon the observer by the finite thickness of emulsion. This phenomena called flat-chamber effect (Monon *et al.* 1951) is severe for low energy particles restricted by limits set on lateral displacement in the vertical plane.

It has been shown (Aditya, 1964a) that the r.m.s. value of displacement  $y_{rms}$  ( $\mu m$ ) of a track of energy  $p\beta c$  (GeV) with respect to original direction in traversing a distance  $x$ (cm) in emulsion is given as :

$$y_{rms} = \frac{50 x^{3/2}}{p\beta c}$$

In deriving this relation it has been assumed that the angular scatters have a normal distribution. Thereby this relation gives the fraction of particles which

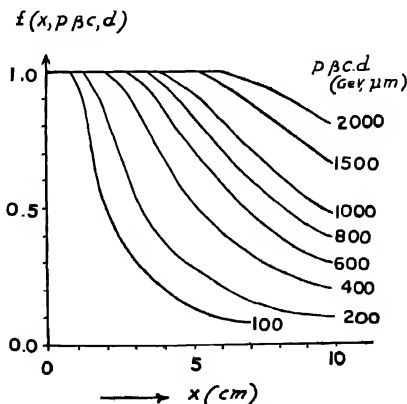


Fig. 1. The probability,  $f(x, p\beta c, d)$  that the track of a particle of energy  $p\beta c$ (GeV) will have a displacement less than  $d$ ( $\mu m$ ) in traversing a distance  $x$ (cm) in emulsion, plotted against  $x$ , for various values of the product  $p\beta c.d$  (GeV  $\mu m$ ), letters attached to the curves.

undergoing genuine scattering will confine themselves to the prescribed limits of lateral displacement. By making use of standard tables for area under the curve of the Gaussian distribution, the fraction of particles that will confine their lateral displacement to several other limits, measured in the units of the standard deviation, has been calculated. The results are plotted in Fig. 1. The ordinate gives here  $f(x, p\beta c, d)$ , the fraction of tracks for which a particle of energy  $p\beta c$  (GeV) is expected to have a displacement less than  $d(\mu_m)$  in traversing a distance  $x(\text{cm})$  in emulsion. For 5 cm traversal and  $f(x, p\beta c, d) = 0.5$ , the product  $p\beta c \cdot d$  is seen to be 400 GeV  $\cdot \mu_m$ . Thus only 50% of particles of energy 10 GeV, undergoing genuine scattering, are expected to have a lateral displacement within 40  $\mu_m$ , measured with respect to the initial direction at  $x = 0$ . A small value of  $f$  indicates that most of the particles (i.e., fraction  $1 - f$ ) will not have their tracks limited to the prescribed lateral displacement. If measurements are made only on such tracks as remain within limits, the observed scattering would be underestimated.

The curves in Fig. 1, can be converted into  $f(x, p\beta c, s)$  for mutual separation  $s(\mu_m)$  between a pair of tracks of equal energy  $p\beta c$  (GeV), starting initially with almost no angle between them. In such a case the probability that the angle will only increase due to scattering is  $\frac{4\pi - \Omega}{4\pi} \sim 1$ , where  $\Omega$  is the solid angle defined by the aperture of the pair. The average separation at small distances may be assumed to be  $\sqrt{2}$  times the individual displacement, (Aditya 1959). Referring to Fig. 1, and the case  $x = 5$  cm,  $f(x, p\beta c, d) = 0.5$  as considered above, the product  $p\beta c \cdot s$  would be  $400/\sqrt{2}$ . Thus for pairs of tracks of 10 GeV particles traversing 5 cm, only half of the total number of pairs will have a separation less than about 30  $\mu_m$  or that only about 35% will have separation to within 50  $\mu_m$ .

In the present work we have determined the underestimation in scattering, due to such restrictions imposed on lateral displacement.

#### EXPERIMENTAL MATERIAL

Multiple scattering measurements on tracks of 8 GeV  $\mu$ -mesons made for the earlier work (Aditya 1964a) have been employed. The momentum of the  $\mu$ -mesons was precisely known in each region. Suitably selected tracks were followed for over 10 cm length.

The overall noise, (personal cum that of the equipment), had been measured from time to time using standard techniques (Biswas *et al.*, 1955); it varied from 0.1  $\mu_m$  to 0.15  $\mu_m$  for different tracks. The observations had been restricted to regions having no measurable distortion, studied in connection with another work (Aditya and Puri 1964) where we have shown that spurious scattering can be understood entirely in terms of distortion. Spurious scattering is estimated to be at most of the same order as the overall noise.

Particular attention had been paid to bias, in the selection of tracks, arising due to limited lateral displacement. From equation (1) above and making allowance for two standard deviations it was known that 95% of particles would restrict themselves to prescribed lateral displacement. On this basis only such tracks were picked up for measurement as were expected to stay within the thickness of emulsion for entire path length in the plate. No limits were set on the displacement in the projected plane. These conditions ensured a bias-free sample of tracks.

### ANALYSIS

The influence of the setting up of limits has been experimentally determined by calculating mean scattering for different arbitrary limits set to the lateral displacement of  $\mu$ -meson tracks with respect to initial direction. Limits have been set at values from  $10\mu$ m to  $150\mu$ m over 5 cm traversal of emulsion, the results on scattering constant for 5 cm cell length are given in table I. The percentage under-estimation is given in column 3,  $K_{err}$  having been taken as 31.0 (Voyvodic and Pickup 1952). The influence of setting arbitrary limits to lateral displacement is seen to be considerable. The data allow an empirical relation to be written as :

$$\text{percentage underestimation} = 30(1 - f_y)$$

where  $f_y$  is the value of the function  $f(x, p/\beta c, d)$  for displacement in the projected plane. This empirical relation is expected to hold upto about 25% underestimation only.

TABLE I

Dependence of  $K$  on Limits Set to Lateral Scattering for 8 GeV  $\mu$ -mesons  
at 5mm Cell Length

Maximum lateral displacement ( $\mu$ m)	K observed [Mov deg. ( $100\mu$ ) <sup>1/2</sup> ]	Underestimation (percentage)	$f(x, p/\beta c, d)$
10	24.0 $\pm$ 1.8	23 $\pm$ 6	0.10
25	25.6 $\pm$ 1.9	17 $\pm$ 6	0.28
50	26.4 $\pm$ 2.0	15 $\pm$ 6	0.52
100	28.7 $\pm$ 2.1	7 $\pm$ 6	0.83
150	30.2 $\pm$ 2.2	2 $\pm$ 6	0.95

The observations in depth were not taken at each successive cell but only at few points along the tracks. However an approximate estimate of the influence

of setting up of limits in the depth direction has been similarly made ; we find empirically:

$$\text{percentage underestimation} = 8(1-f_z)$$

These considerations may now be applied to data available in literature where limits had been set to track separation. The underestimation in  $K$  due to restrictions on lateral scattering has been calculated by using empirical relations given above results are given in table II. It is seen that  $K$  may be underestimated by about 5% to 20% by this type of restricted sampling. The bias for obvious reasons is large in experiments involving larger length per track. It is quite possible that the apparent decrease of scattering constant with cell length (Hossain *et al.* 1961, Pal *et al.* 1963) is partly associated with this effect.

TABLE II

Underestimation of  $K$  calculated for limits set to lateral displacement by other investigators

Reference	Particle	Energy (GeV)	Limits $d$ or $s(\mu\text{m})$	$x(\text{cm})$	Under- estimation (percentage)
Brisbout <i>et al.</i> (1956)	$\pi$	4.5	$s_y = 50$ $s_z = 20$	1 5	0.6 7.2
Biswas <i>et al.</i> (1957)	p	6.2	$s_y = 200$ $s_z = 50$	5 5	3.6 5.6
Aditya <i>et al.</i> (1963)	p	27	$s_y = 100$ $s_z = 50$	8 8	3.0 3.2
Kamal <i>et al.</i> (1964)	p	24	$s_y = 50$ $s_z = 20$	10 10	17.4 6.7
Hossain <i>et al.</i> (1961a)	$\pi$	16.2	$d_y = 50$	10	18
Bozoki <i>et al.</i> (1964)	$\pi$	17.2	$d_y = 50$	10	17.4

The influence of this bias is not felt in the scattering constant values of all the work referred to in Table II, presumably due to different level of spurious scattering. If the level of spurious scattering is low, then the scattering on the whole is underestimated, as in the case of, Brisbout *et al.* (1956) and Hossain *et al.* (1961), leading to underestimation of  $K$ . However, if spurious scattering in the plates is large, as is for other references in Table II, then in spite of best effort it may not be possible to eliminate entirely its influence. The amount of spurious scattering that continues to remain in the result would over-estimate the scattering. It would in the first instance compensate for the underestimation due to bias and eventually increase the observed scattering. A wide variety of results might thus be obtained under different experimental conditions.

# REFERENCES

- Aditya, P. K., 1959, *Indian J. Phys*, **33**, 357
- \_\_\_\_\_ 1964a, *Nuovo Cimento*. **31**. 473.
- \_\_\_\_\_ 1964b, *Indian J. Phys.*, **38**, 326.
- \_\_\_\_\_ Bhatia, V. S and Sood, P M, 1963, *Nuovo Cimento* **29**, 577
- Ahtya, P. K., and Puri, R. K., 1964, *J. Sci. Instrum* **41**, 529
- Biswas, S., Peters, B., and Rama, 1955, *Proc. Ind Acad Sci.* **41**, 154
- Biswas, S., Durgaprasad, N., and Mitra, S., 1957, *Proc Ind Acad. Sci*, **46**, 167.
- Bozoki, G., Gombosi, E, Janik, L., Nagy, E, and Sahni, M., 1964, *Private communication*  
(unpublished )
- Brisbout, F. A., Dahanayake, C, Engler, A, Fowler, P H., and Jones, P. B., 1956,  
*Nuovo Cimento*, **2**, 1400.
- Fowler, P. H., 1950, *Phil Mag*, **41**, 169.
- Hossain, A., Volruba, M F., and Wataghin, A., 1961, *Nuovo Cimento*, **22**, 308.
- Kamal, A A., Rao, G K., and Rao, Y V, 1964, *Nuovo Cimento*. **32**, 863.
- Menon, M G K, O'Ceallaigh, C, and Rochat, O., 1951, *Phil. Mag*, **42**, 932.
- Pal, Y. and Ray, A. K, 1963. *Nuovo Cimento*, **27**, 960.
- Voyvodic, L, and Pickup, E., 1952, *Phys Rev*, **85**, 91

# LOCKING PHENOMENA IN INJECTION SYNCHRONISED PULSED OSCILLATORS

B. N. BISWAS AND G. DATTA

DEPARTMENT OF PHYSICS, UNIVERSITY OF BURDWAN,  
WEST BENGAL, INDIA

(Received January 28, 1966)

**ABSTRACT.** The phenomenon of synchronisation in a pulsed oscillator with a CW reference signal has been studied with particular emphasis on the locking range. The effect of low frequency time-constant of the gain control circuit of the pulsed oscillator on the locking range has been taken into consideration. It has been pointed out that the broadening of the discrete spectral lines which would have otherwise occurred in an incoherent mode of oscillation will be reduced in the case studied. Experimental results have been presented and found to be in good agreement with the conclusions of the analysis.

## INTRODUCTION

A pulsed oscillator, as its name implies, is an oscillator the output of which consists of a series of pulsed sinusoids with a definite duty cycle. A typical circuit diagram of the oscillator is shown in Fig. 1. It is to be noted that the circuit shown is essentially a super-regenerative receiver (Whitehead, J. R., 1950) and as

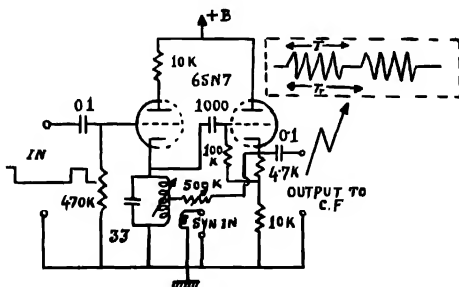


Fig. 1. A typical circuit diagram of a directly synchronised pulsed oscillator. The output waveform of on-period  $T$  and total period  $T_T$  inset in the figure.

such there are two different modes of oscillations so-called logarithmic and linear depending on whether the on-period is such as to enable the oscillations to attain a steady state value in this interval or not. An injection synchronised pulsed oscillator is an oscillator where an oscillation of desired frequency and amplitude is injected into the regenerative circuit. The amplitude and frequency of the injected voltage must be such as to quench the free oscillation, the quenching action being obtained through an instantaneous limiting, due to which there is "strong-

signal capture" and "small-signal rejection" (Chakrabarti, *et al.* 1964). It is to be noted that if there are finite transmissions through the regenerative circuit at other frequencies generated through the process of limiting then the amount of weak signal suppression obtainable is small (Biswas B. N., 1964). The phenomenon of synchronization of a CW oscillator with a CW signal (Van Der pol, B., *et al.*) 1934, or with interrupted sinusoids (Fraser, D. W., 1957) is quite well-known. In this paper the phenomenon of synchronisation of a pulsed oscillator with a CW signal will be studied.

In section 2, the governing equations viz. (i) the equation for the instantaneous amplitude of the pulsed oscillation ( $A$ ) in presence of the external signal and (ii) the equation for instantaneous phase difference ( $\Phi$ ) between the local oscillations and the reference input have been derived. A simple graphical method ( $A-\Phi$  plot) has been illustrated to visualise how the range of frequency entrainment depends on the amplitude of the external signal and as well on the steady state phase difference ( $\Phi_s$ ) between them.

Section 3 deals with derivation of an equation for the locking range of the oscillator. This is followed by a study in section 4 of the effect of low frequency time-constant of the gain control circuit of the oscillator on the locking range of the pulsed oscillator.

Section 5 deals with the spectral analysis of the output waveforms of (i) the coherent mode of oscillations, (ii) incoherent mode of oscillations and (iii) the synchronised mode of oscillations in a pulsed oscillator. It is suggested in this section that the broadening of the discrete spectrum which would have otherwise occurred in an incoherent mode of oscillation will be reduced in the synchronised mode of oscillations.

# DERIVATION OF THE GOVERNING EQUATIONS

Let us consider the equivalent analytical representation of the pulsed oscillator during the on-period as shown in Fig. 2. Let us assume that the non-linearity of the oscillator can be represented by

$$F(x) = a_1 x - a_3 x^3, \quad \dots (2.1)$$

where  $a_1$  and  $a_3$  are constants.

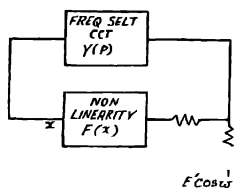


Fig. 2. Equivalent analytical representation of the directly synchronised pulsed-oscillator during the on-period with the external synchronising signal  $E \cos \omega t$ .

Now for the loop shown in Fig. 2, one can write the following equations

$$\cos(\omega_1 t + \Phi) [F(A, E) + E' \cos \Phi] = \frac{A}{Y(p)} - E' \sin \Phi \sin(\omega_1 t + \Phi), \quad (2.2)$$

where  $A$  is the instantaneous amplitude of oscillation in presence of the external signal of amplitude  $E'$  and  $\Phi$  is the phase difference between them and

$$Y(p) = Y_0 \frac{\alpha p}{p^2 + \alpha p + \omega_0^2} \quad \dots (2.3)$$

Now if we put  $p = j\omega_1 + S$  one can write  $Y(P)$  as

$$\frac{1}{Y(P)} \simeq \frac{1}{Y_0} \left( 1 + \frac{2}{\alpha} S + j \frac{\omega_1^2 - \omega_0^2}{\alpha \omega_1} \right), \quad \dots (2.4)$$

where  $S$  represents an operator in a slow time scale and  $1/\alpha = Q_0/\omega_0$ . Hence comparing Eq. (2.2) and (2.4) one can write

$$\frac{2}{\alpha} \frac{dA}{dt} \simeq \frac{3}{4} a_3 Y_0 [A_0^2 - A^2] A + E \cos \Phi, \quad \dots (2.5)$$

and

$$\frac{2}{\alpha} \frac{d\varphi}{dt} \simeq \frac{2}{\alpha} \Omega - \frac{E}{A} \sin \varphi, \quad \dots (2.6)$$

where

$$A_0^2 = \frac{a_1 Y_0 - 1}{3/4 a_3 Y_0}, \quad \dots (2.7)$$

$E$  is the amplitude of the external signal at the input to the limiter and  $\Omega$  is the instantaneous angular difference of frequency between them. From Eq. (2.7) it is quite clear that  $A_0$  would have been the amplitude of the local oscillator if the external input were absent. In Eq. (2.5) it has tacitly been assumed that the strength of the external signal is small compared to that of the local oscillator. This equation also suggests that the oscillations in the on-period build up from and decay to noise in absence of the external signal and in presence of the external signal the oscillations build up from and decay to the reference input signal. From Eq. (2.6) it appears that during the on-period the local pulsed oscillator will be pulled towards synchronism with respect to the reference input if the following condition is satisfied :

$$K \left( = \frac{\omega_0}{2Q_0} \cdot \frac{E}{A_s} \right) \geq \Omega, \quad (2.8)$$



where  $A_s$  is the steady state amplitude of the local oscillator in presence of the external signal. It is to be noted that the value of  $A_s$  depend both on  $E$  and

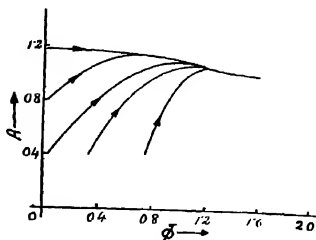


Fig. 3. Amplitude-phase plane trajectories of the directly synchronised oscillator for the case when the amplitude of the local oscillation is small compared to that of the synchronising signal.

$\phi_s = \sin^{-1}(\Omega/K)$ . An idea about the dependence of  $A_s$  on  $E$  and  $\phi_s$  can be had from the  $(A - \phi)$  plot shown in Fig. 3 under the following conditions :

$$\begin{aligned} \frac{3}{4} Y_0(t_0) &= 1.0 \\ A_0 &= 1.0 \\ E &= 0.2 \\ \frac{2}{\alpha} \Omega &= 1.0 \end{aligned} \quad (2.9)$$

Now as the maximum permissible value of  $\phi_0$  is  $90^\circ$  so it is quite clear from the  $(A - \phi)$  plot that the locking range during the on-period depends on the amplitude of free oscillation.

#### FORMULATION FOR THE EQUATION OF LOCKING RANGE

Before attempting to formulate an equation for the locking range it is to be remembered that the locking range is limited by the steady state amplitude of the local oscillator (vide Eq. (2.8)). This is because of the fact that during the building up of the oscillation, the external signal will have better control on the instantaneous phase of the local oscillator than when the local oscillator attains steady state. So in the synchronised condition the phase of the local oscillation will be pulled towards synchronism during the on-period and during the off-period its phase (so to say) will be deviated and the amount of this deviation will depend on the off-period. A pulsed oscillator will, therefore, be said to be in synchronism with reference to input when the local oscillator in the on-period is able to

compensate for the phase deviation incurred during the off-period. That is, the net phase shift between the local oscillator and the reference over a period is zero. Expressed analytically

$$\int_0^{T_r} \left( \frac{d\varphi}{dt} \right) dt = 0 \quad \dots (3.1)$$

Now the phase equation for the on-period is given by

$$\frac{d\varphi}{dt} = \Omega - K \sin \varphi \quad \dots (3.2)$$

and during the off-period it is given by

$$\frac{d\varphi}{dt} = \Omega \quad \dots (3.3)$$

Now at the edge of the band of synchronisation one can assume with a fair degree of accuracy that the phase difference is approximately  $90^\circ$ . With this condition and the condition of Eq. (3.1) in mind and solving Eq. (3.2) and Eq. (3.3) one can easily write the following equation for locking range :

$$\frac{1}{\Omega/K} \sqrt{1 - (\Omega/K)^2} \cdot \frac{\sqrt{1 - \Omega/K} + \tanh(nKT_r)}{1 - \sqrt{1 - \Omega/K} \tanh(nKT_r)} = \frac{1 - \tan(1-n) \Omega T_r / 2}{1 + \tan(1-n) \Omega T_r / 2} \quad \dots (3.4)$$

where  $n$  stands for the duty cycle of the pulse sinusoids. In most of the practical situations the linearised version of the Eq. (3.2) which is achieved by replacing  $\sin \varphi$  by  $\frac{2}{\pi} \varphi$  gives a reasonable estimate of the synchronisation range that is given by

$$\frac{\Omega}{K} \sim \frac{1 - \exp\left(-\frac{2}{\pi} KT\right)}{1 - \exp\left(-\frac{2}{\pi} KT\right) + \frac{4K}{\omega_r}(1-n)} \quad \dots (3.5)$$

where the symbols have their usual significance except  $\omega_r/2\pi$  indicates repetition rate of the pulsed sinusoids.

EFFECT OF LOW FREQUENCY TIME CONSTANT OF  
THE GAIN CONTROL CIRCUIT OF OSCILLATOR  
ON THE LOCKING RANGE

So far we have tacitly assumed that the process of synchronisation is due to instantaneous limiting and thus no filtering other than at r.f. is possible (Chakrabarti 1964). But in most of the practical the gain control is only partly instantaneous. For example, the low-frequency oscillators circuits time constant in the self-bias circuit of the oscillator provides a slow acting gain control circuit. In such a case one can assume that the gain is controlled by the rectified envelope. In such a case it can be shown (op cit.) that there will be nonlinear discrimination of one frequency against the other frequency depending upon the  $R-C$  time constant of the circuit and the governing equation of the oscillator during the on-period is given by

$$\frac{d\phi}{dt} - \Omega = \frac{\omega_0}{2Q_0} \cdot \frac{E}{E_0} \alpha_0 F(p) \sin \psi, \quad \dots (4.1)$$

where  $E_0$  is the non-linear gain controlling voltage,  $\alpha_0$  is a constant that determines the rectified envelope and

$$F(p) = \frac{1}{1 + \tau/p} \quad \dots (4.2)$$

and  $\tau$  is the  $R-C$  time constant of the grid circuit. Therefore in such a case it can be shown (op cit.) that the maximum initial difference of frequency ( $\Omega_{max}/2\pi$ ) upto which the local oscillator can be made to synchronise during the on-period depends essentially on the average value of the network gain ( $\bar{F}(\bar{p})$ ) over the range due to the initial difference of frequency ( $\Omega/2\pi$ ). Thus one concludes from the above discussion that variation of the locking range of a pulsed oscillator for a particular value of the repetition rate and duty cycle of the pulsed sinusoids with  $R-C$  time constant of the local oscillator will be the same as the variation of  $\bar{F}(\bar{p})$  with the  $R-C$  constant.

SPECTRAL ANALYSIS OF THE OUTPUT WAVEFORM  
FOR DIFFERENT MODES OF OSCILLATIONS

From the discussions of the section 2, it is quite clear that the oscillations in each of the blocks of the pulsed sinusoids, (in absence of the external signal), as shown in the diagram inset in Fig. 1, build up from inherent circuit noise and as such the phases of the growing oscillations in the different blocks are completely uncorrelated with respect to the turn-on signal. This is the incoherent mode of oscillation. As a result the discrete spectrum of the output waveform is spread out into a series of broad bands (Edson, 1960). But in a synchronised mode of oscillations in a pulsed oscillator as the oscillations in each block build up from and decay to the synchronising signal so there exists a phase coherency among

the oscillations in different blocks of the pulsed sinusoids in relation to the synchronising signal. It is, therefore, felt that the broadening of the discrete spectral lines which would have otherwise occurred in the incoherent mode of oscillations will be very much reduced.

Now in the coherent-mode of oscillation one can write for the output wave form

$$[e_0(t)]_{COH} = \sum_{n=-\infty}^{n=+\infty} A_c \cos \omega_c t \times U(t - nT_r), \quad n = 0, 1, 2, \text{etc.} \quad \dots (5.1)$$

where  $U(t - nT_r)$  equals step function  $U(t)$ ,  $[nT_r - \frac{1}{2}T \leq t \leq nT_r + \frac{1}{2}T]$  with unity the maximum amplitude and zero elsewhere. Similarly for the synchronised mode the output waveform can be analytically represented as

$$[e_0(t)]_{SYN} \sim \sum_{n=-\infty}^{n=+\infty} A_c [m \cdot U(t - nT_r)] \cos(\omega_c t + \varphi_n), \quad \dots (5.2)$$

where  $\varphi_n$  is the steady state phase difference between the local oscillator and the synchronising signal and 'm' is a quantity that depends on the amount of coupling and the strength of the synchronising signal. In the incoherent mode of oscillations the output waveform can be analytically represented as

$$[e_0(t)]_{INCOH} = \sum_{n=-\infty}^{n=+\infty} A_c \cos(\omega_c t + \varphi_n) \times U(t - nT_r), \quad \dots (5.3)$$

where  $\varphi_{+1}$ ,  $\varphi_{+2}$  etc. are completely uncorrelated with respect to turn-on signal. Spectral analysis of the output waveforms [vide Eqs. (5.1), (5.2) and (5.3)] justifies the statement made elsewhere in the text.

## EXPERIMENTAL RESULTS

In this section experimental results with respect to the variation of locking range of the pulsed oscillator with the frequency of interruption and the low-frequency time-constant of the gain-control circuit of the oscillator will be presented and discussed. Experimental set-up is shown in Fig. 4.

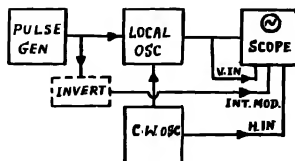


Fig. 4. Experimental set-up for measuring the variation of locking range of the pulsed oscillator with repetition rate of the pulsed oscillation of different duty cycle and low frequency time constant of the gain control circuit.

The  $Q$ -value of the tuned circuit and the coupling coil for the synchronising signal were adjusted in such a way as to have a single-peak response curve of the tuned circuit with a moderate value of  $Q$ . Presence of dip anywhere in the response curve is likely to produce spurious effect and sometimes a type of oscillation

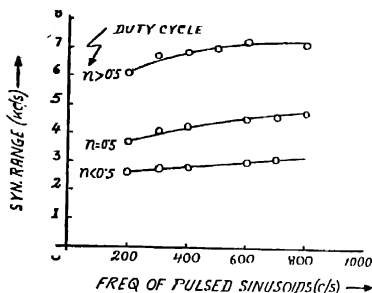


Fig. 5. Pull-in performance of the directly synchronised pulsed oscillator with repetition rate and duty cycle of the pulsed oscillation

tions (Biswas, 1964). Now the amplitude of the external squagging signal is adjusted to a proper value so that the oscillator operates in the logarithmic mode (discussed elsewhere in the text). Further the amplitude of the synchronising signal is set to a minimum value so as to avoid hysteresis effect (Minorsky, 1947). Fig. 5 shows the variation of the locking range with the frequency and duty cycle of the external squagging signal. It will be observed that the results are in quite

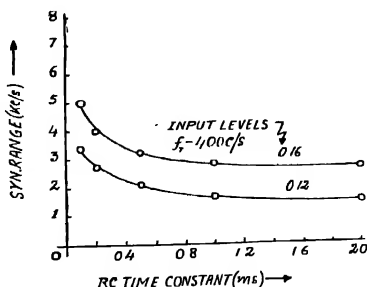


Fig. 6. Locking performance of the directly synchronised pulsed oscillator with the variation of the  $R$ - $C$  time constant of the slow acting gain-control circuit and with two different input strengths.

good agreement with the conclusions of the analysis presented in section 3. Fig. 6 shows the variation of the locking range with  $R$ - $C$  time constant of the grid circuit. These confirm the theoretical findings of section 7.

## CONCLUDING REMARKS

The phenomenon of injection synchronisation of a pulsed oscillator has been analysed for continuous wave synchronising signal with a high value of CNR and its performance studied experimentally. The phenomena of automatic phase control of a pulsed oscillator with respect to a CW input accompanied by an interfering signal and noises will be considered in a future communication.

## ACKNOWLEDGMENT

One of the authors (B.N.B) is greatly indebted to Prof. N. B. Chakrabarti of the Indian Institute of Technology, Kharagpur, for suggesting the problem to the author. The authors take the opportunity of thanking Prof. A. Mookherjee, D Sc, of Burdwan University for his kind interest and constant encouragement in this work. Thanks are also due to Mr. A. K. Datta of the Burdwan University for stimulating discussions.

## REFERENCES

- Biswas, B. N., 1964, *Indian J. Phys.* **38**, 561.  
 Chakrabarti, N. B. and Biswas, B. N., *Indian J. Phys.*, 1964 **38**, 148.  
 Edson, E. A., 1960, *Proc. I.R.E.*, **48**, 1454.  
 Fraser, D. W., 1957, *Proc. I.R.E.*, **45**, 1257.  
 Minorsky, N., 1947, "Introduction to Non-linear Mechanics" J. W. Edwards, Ann. Arbor.  
 Van Der Pol, B., 1934, *Proc. I.R.E.*, **22**, 1051.  
 Whiteloid, J. R., 1950, "Super-Regenerative Receivers" Cambridge, At the University Press.

# DIELECTRIC FUNCTION OF A DEGENERATE ELECTRON GAS IN THE PRESENCE OF A STEADY MAGNETIC FIELD

P. MISRA

DEPARTMENT OF PHYSICS, RAVENSHAW COLLEGE, CUTTACK

(Received November 15, 1965)

**ABSTRACT.** Using Boltzmann—Vlasov equation we derive expressions for the frequency and wave-number dependent dielectric function of a degenerate electron gas in the presence of a steady magnetic field which are valid at and near absolute zero temperatures

## INTRODUCTION

In the presence of a magnetic field, the electron gas becomes anisotropic, the wavenumber and frequency dependent Response function  $\tilde{K}(\vec{k}, \omega)$  of Lindhard is then a tensor. When the wave number vector is parallel to the direction of the external magnetic field,  $\tilde{K}_{11}(\vec{k}, \omega) = \tilde{K}_{22}(\vec{k}, \omega)$ ,  $\tilde{K}_{12}(\vec{k}, \omega) = -\tilde{K}_{21}(\vec{k}, \omega)$  and all other components except these and  $\tilde{K}_{33}(\vec{k}, \omega)$  are identically zero. The last mentioned component is independent of the magnetic field strength. The aim of the present investigations is to obtain explicit expressions for  $\tilde{K}_{11}(\vec{k}, \omega)$  and  $\tilde{K}_{12}(\vec{k}, \omega)$  for a degenerate electron gas at and near absolute zero temperature when the external magnetic field is steady and uniform. The dynamics of the electron gas is described by the Boltzmann- Vlasov equation. The equilibrium distribution function is a Fermi-Dirac distribution. The prescription for integration across the singularity encountered in the expressions for  $\tilde{K}_{\alpha\beta}(\vec{k}, \omega)$  are obtained by invoking causality (Pradhan 1962) as illustrated in our previous work (Misra 1962). For evaluation of integrals over Fermi-Dirac distribution function near absolute zero temperature Sommerfeld's (1928) approximate method has been used.

## DIELECTRIC FUNCTION FROM VLASOV EQUATION

The wave-number and frequency dependent dielectric function is given by

$$\epsilon_{\alpha\beta}(\vec{k}, \omega) = 1 + \frac{4\pi i \tilde{K}_{\alpha\beta}(\vec{k}, \omega)}{\omega} \quad (1)$$

where

$$\tilde{J}_{\alpha}(\vec{k}, \omega) = \tilde{K}_{\alpha\beta}(\vec{k}, \omega) \tilde{E}_{\alpha\beta}(\vec{k}, \omega) \quad (2)$$

The current density  $J(\vec{r}, t)$  resulting from fluctuating electric field  $\vec{E}(\vec{r}, t)$  in a plasma is given by

$$J_a(\vec{r}, t) = -e \int d^3u u_a f_1(\vec{r}, \vec{u}, t) \quad \dots (3)$$

where  $f_1(\vec{r}, \vec{u}, t)$  obeys the linearised Boltzmann-Vlassov equation

$$\frac{\partial f_1}{\partial t} + \vec{u} \cdot \vec{\nabla} f_1 - \frac{e}{m\ell} (\vec{U} \times \vec{B}) \cdot \vec{\nabla} f_1 = \frac{ne}{m} \vec{E}(\vec{r}, t) \cdot \vec{\nabla} f_0 \quad \dots (4)$$

whose space-time Fourier transform, in a cylindrical co-ordinate system  $(u, v, \theta)$  for  $\vec{u}$  with  $\vec{B}$  and  $\vec{k}$  along  $Z$  axis, is given by

$$\begin{aligned} i(ku - \omega) f_1(\vec{k}, u, \omega) + \Omega \frac{\partial f_1(\vec{k}, u, \omega)}{\partial \theta} = \frac{ne}{m} \left[ \frac{\partial f_0}{\partial v} (E_1 \cos \theta + E_2 \sin \theta) \right. \\ \left. + E_2 \frac{\partial f_0}{\partial u} \right] \quad \dots (5) \end{aligned}$$

where  $\Omega = \frac{eB}{m\ell}$

The solution of this equation is immediately seen to be

$$\begin{aligned} \vec{f}_1(\vec{k}, u, \omega) = \frac{ne}{m} \left[ \frac{iku \cos \theta - i\omega \cos \theta + \Omega \sin \theta}{(ku - \omega)^2 - \Omega^2} \left( \frac{\partial f_0}{\partial v} \right) E_1 \right. \\ \left. + \frac{iku \sin \theta - i\omega \sin \theta - \Omega \cos \theta}{(ku - \omega)^2 - \Omega^2} \left( \frac{\partial f_0}{\partial v} \right) E_2 + \frac{i}{ku - \omega} \left( \frac{\partial f_0}{\partial u} \right) E_2 \right] \quad \dots (6) \end{aligned}$$

and which when used in equations (1), (2) and (3) give us

$$\epsilon_{11}(\vec{k}, \omega) = 1 - \frac{4\pi\omega_0^2}{\omega} \int_{-\infty}^{+\infty} du \frac{(ku - \omega) F(u)}{(ku - \omega)^2 - \Omega^2} \quad \dots (7a)$$

$$\epsilon_{12}(\vec{k}, \omega) = 1 - \frac{4\pi\omega_0^2}{\omega} \int_{-\infty}^{+\infty} du \frac{\Omega F(u)}{(ku - \omega)^2 - \Omega^2} \quad \dots (7b)$$

$$\epsilon_{33}(\vec{k}, \omega) = 1 + \frac{4\pi\omega_0^2}{\omega} \int_{-\infty}^{+\infty} du \frac{u \frac{\partial F(u)}{\partial u}}{ku - \omega} \quad \dots (7c)$$



where  $\omega_0^2 = \frac{4\pi ne^2}{m}$  and  $F(u) = \frac{1}{4} \int_0^\infty v^2 dv \frac{\partial f_0}{\partial v} = -\frac{1}{2} \int_0^\infty dv v f_0$

It will be noticed that the integrands in the above expressions are singular at  $u = \frac{\omega + \Omega}{k}$ ,  $u = \frac{\omega - \Omega}{k}$  and  $u = \frac{\omega}{k}$ . The prescription for integration across these poles obtained from causality is to add a small positive imaginary part to  $\omega$  in the integrands

### COMPUTATION OF $\widetilde{K}_{11}$ AND $\widetilde{K}_{12}$ FOR A FERMI DISTRIBUTION

For a Fermi distribution

$$n f_0 = 2 \left( \frac{m}{h} \right)^3 \frac{1}{e^{-v + \frac{1}{2} m \beta (u^2 + v^2)} + 1}$$

and hence

$$F(u) = \frac{1}{4} \int_0^\infty v^2 dv \frac{\partial f_0}{\partial v} = -\frac{1}{m\beta} \left( \frac{m}{h} \right)^3 \log (1 + e^{v - \frac{1}{2} m \beta u^2})$$

Therefore from equations (1) and (7a)

$$\begin{aligned} \vec{k}_{11}(\vec{k}, \omega) &= -\frac{\omega_0^2}{2} \left[ \int_{-\infty}^{\infty} du \frac{F(u)}{\omega - \Omega - ku + i\epsilon} + \int_{-\infty}^{\infty} du \frac{F(u)}{\omega + \Omega - ku + i\epsilon} \right] \\ &= \frac{\omega_0^2}{2ik} \left( \frac{m}{h} \right)^3 \int_{-\infty}^{\infty} du u \frac{\log \frac{(\omega - \Omega + ku)(\omega + \Omega + ku)}{(\omega - \Omega - ku)(\omega + \Omega - ku)}}{1 + e^{-v - \frac{1}{2} m \beta u^2}} \\ &\quad + \frac{\omega_0^2}{2km\beta} \left( \frac{m}{h} \right)^3 \log \left[ 1 + e^{-v - \frac{m\beta}{2k^2} (\omega - \Omega)^2} \right] \left[ 1 + e^{-v - \frac{m\beta}{2k^2} (\omega + \Omega)^2} \right] \quad \dots (8) \end{aligned}$$

The integration over  $u$  cannot be analytically carried out. However for temperatures near absolute zero approximate analytical forms can be obtained by using Sommerfeld's method of integration as is done in the work of Pradhan and Misra (1960) and Misra and Misra (1962). We shall not go into the details but give the final results :

$$\begin{aligned}
{}_m \widetilde{K}_{11}(\vec{k}, \omega) = & \frac{\omega_0^2}{2nk} \left( \frac{m}{h} \right)^3 \left[ 2v_0^2 \omega/k + \frac{1}{2} \log \frac{(\omega - \Omega)(\omega + \Omega) + 2v_0 k \omega + v_0^2 k^2}{(\omega - \Omega)(\omega + \Omega) - 2v_0 k \omega + v_0^2 k^2} \right. \\
& - \frac{1}{2} \frac{(\omega - \Omega)^2}{k^2} \log \frac{\omega - \Omega + v_0 k}{\omega - \Omega - v_0 k} - \frac{1}{2} \frac{(\omega + \Omega)^2}{k^2} \log \frac{\omega + \Omega + v_0 k}{\omega + \Omega - v_0 k} \left. \right] \\
& + \frac{\pi^2 \omega_0^2}{24m^2 \beta^2 v_0^2 nk} \left( \frac{m}{h} \right)^3 \log \frac{(\omega - \Omega)(\omega + \Omega) + 2v_0 k \omega + v_0^2 k^2}{(\omega - \Omega)(\omega + \Omega) - 2v_0 k \omega + v_0^2 k^2} \\
& + \frac{\pi^2 \omega_0^2}{6m^2 \beta^2 n v_0} \left( \frac{m}{h} \right)^3 \left[ \frac{\omega - \Omega}{(\omega - \Omega)^2 - v_0^2 k^2} + \frac{\omega + \Omega}{(\omega + \Omega)^2 - v_0^2 k^2} \right] \quad \dots \quad (9a)
\end{aligned}$$

$$\begin{aligned}
Re \widetilde{K}_{11}(\vec{k}, \omega) = & \frac{\omega_0^2}{8k} \left\{ \frac{2\pi}{n} \left( \frac{m}{h} \right)^3 \left[ v_0^2 - \frac{(\omega - \Omega)^2}{k^2} \right] \right. \\
& + \frac{\pi^2}{16m^2 \beta^2 v_0^5} \left. \right\} \rho \left[ v_0^2 - \frac{(\omega - \Omega)^2}{k^2} \right] + \frac{\omega_0^2}{8k} \left\{ \frac{2\pi}{n} \left( \frac{m}{h} \right)^3 \left[ v_0^2 - \frac{(\omega + \Omega)^2}{k^2} \right] \right. \\
& + \frac{\pi^2}{16m^2 \beta^2 v_0^5} \left. \right\} \rho \left[ v_0^2 - \frac{(\omega + \Omega)^2}{k^2} \right] \quad \dots \quad (9b)
\end{aligned}$$

For the computation of  $\widetilde{K}_{12}(\vec{k}, \omega)$  we proceed in a similar manner and finally obtain

$$\begin{aligned}
Re \widetilde{K}_{12}(\vec{k}, \omega) = & \frac{\omega_0^2}{2nk} \left( \frac{m}{h} \right)^3 \left[ \frac{2v_0 \Omega}{k} + \frac{1}{2} v_0^2 \log \frac{(\omega + \Omega)(\omega - \Omega) - 2v_0 k \Omega - v_0^2 k^2}{(\omega + \Omega)(\omega - \Omega) + 2v_0 k \Omega - v_0^2 k^2} \right. \\
& - \frac{(\omega + \Omega)^2}{2k^2} \log \frac{\omega + \Omega + v_0 k}{\omega + \Omega - v_0 k} + \frac{(\omega - \Omega)^2}{2k^2} \log \frac{\omega - \Omega + v_0 k}{\omega - \Omega - v_0 k} \\
& - \frac{\omega_0^2 \pi^2}{24m^2 \beta^2 v_0^2 nk} \left( \frac{m}{h} \right)^3 \log \frac{(\omega + \Omega)(\omega - \Omega) - 2v_0 k \Omega - v_0^2 k^2}{(\omega + \Omega)(\omega - \Omega) + 2v_0 k \Omega - v_0^2 k^2} \\
& - \frac{\pi^2 \omega_0^2}{6m^2 \beta^2 n v_0} \left( \frac{m}{h} \right)^3 \left[ \frac{\omega + \Omega}{(\omega + \Omega)^2 - v_0^2 k^2} - \frac{\omega - \Omega}{(\omega - \Omega)^2 - v_0^2 k^2} \right] \quad \dots \quad (10a)
\end{aligned}$$

$$\begin{aligned} \text{Im } \widetilde{K}_{12}(\vec{k}, \omega) = & - \frac{\omega_0^2}{8k} \left\{ \frac{2\pi}{n} \left( \frac{m}{h} \right)^3 \left[ v_0^2 - \frac{(\omega + \Omega)^2}{k^2} \right] \right. \\ & \left. + \frac{\pi^2}{16m^2\beta^2v_0^5} \right\} \mathcal{O} \left[ v_0^2 - \frac{(\omega + \Omega)^2}{k^2} \right] + \frac{\omega_0^2}{8k} \left\{ \frac{2\pi}{n} \left( \frac{m}{h} \right)^3 \left[ v_0^2 - \frac{(\omega - \Omega)^2}{k^2} \right] \right. \\ & \left. + \frac{\pi^2}{16m^2\beta^2v_0^5} \right\} \mathcal{O} \left[ v_0^2 - \frac{(\omega - \Omega)^2}{k^2} \right] \quad \dots \quad (10b) \end{aligned}$$

In the limit of vanishing  $B$ , the expression for  $\widetilde{K}_{11}(\vec{k}, \omega)$  coincides with the expression for the same obtained in an earlier paper for the magnetic field free case and the  $\widetilde{K}_{12}(\vec{k}, \omega)$  vanishes identically.

#### ACKNOWLEDGMENTS

We are grateful to Dr. T. Pradhan, Professor, Saha Institute of Nuclear Physics, Calcutta for suggesting the problem and for guidance. We would like to thank Dr. K. Samal, Sri S. Acharya of our Physics Department and Sri B. Dasgupta of Saha Institute for their help and comments while the work was in progress.

#### REFERENCES

- Lindhard, J. 1954, *Kgl. Danske, Videnskab, Selskab, MatK-logs, Medd*, **28** No. 8.  
 Misra, P. and Misra, D. 1962, *Indian J. Phys.* **36**, 549-556  
 Pradhan, T. 1962, *Ann. Phys. (U.S.A.)* **16**, 418.  
 Pradhan, T. and Misra, P. 1960, *Phys. Rev.*, **119**, 1878  
 Sommerfeld, A. 1928, *Z. Physik*, **46**, 1.

# VARIATIONAL TREATMENT OF SLOW ELECTRON SCATTERING BY A HELIUM ATOM

S. N. BANERJEE, R. JHA AND N. C. SIL

DEPARTMENT OF THEORETICAL PHYSICS,  
INDIAN ASSOCIATION FOR THE CULTIVATION OF SCIENCE,

JADAVPUR, CALCUTTA-32.

(Received February 14, 1966)

**ABSTRACT** The scattering of slow electrons by a helium atom has been investigated with allowance for exchange possibility and polarisation effects. Using a two-parameter open shell wave function for the ground state of helium, the  $S$ -wave shifts for several incident electron energies have been calculated by the well-known variational method of Hulthén (1944). The close agreement of our zero-energy cross section with the exact calculations of Williamson and McDowell (1965) shows the correctness of validity of the variational method for this problem. It may be added that our result also agrees well with the experimental values of Bandel and Golden (1965).

## INTRODUCTION

Recently experimental results of Pack, Phelps *et al* (1961, 1964) and of Bandel and Golden (1965) indicate agreement with theoretical findings much closer than what was possible before; in view of this we have tried in this paper to find out whether the same agreement is obtainable with variational method.

The first theoretical investigation of the elastic scattering of electrons by helium atom has been carried out by Massey and Mohr (1931) with the inclusion of exchange possibilities and exclusion of polarisation effects. They found that the exchange effect was quite important below 15 eV incident electron energy. Under the same assumption regarding polarisation and exchange, Allis and Morse (1933) have determined  $S$  and  $P$  wave phase shifts by exact numerical solution of integro-differential equation. Moiseiwitsch (1953) using a closed-shell wave function of helium atom, has calculated the same elastic cross-section using Hulthén's variational method and under the same assumption. Adopting an open-shell wave function of the helium atom, similar calculations have been done numerically by Moiseiwitsch (1961). On the other hand, taking an open-shell wave function, Mukherjee and Sil (1962) have obtained almost the same value of zero-energy cross-section as that of Moiseiwitsch (1961).

LaBahn and Callaway (1964) in their numerical calculation with Hartree-Fock separable ground state wave function have found that the influence of polarisation effect considerably lowers the theoretical zero-energy cross-section towards much better agreement with the experimental value; however, the theoretical

value is somewhat a little less than the experimental one. Williamson and McDowell (1965) have recalculated the same problem numerically with an open-shell wave-function for helium atom. Their findings for the zero-energy cross-section is almost the same as that of LaBahn and Callaway (1964).

In this paper we have applied Hultien's variational method to calculate the *s*-wave phase-shifts for electron-helium atom elastic scattering taking into account both exchange and polarisation effects, we have used the same open-shell wave function as used by Williamson and McDowell (1965). The value of our zero energy cross section is  $16.33 a^2$  as against  $16.10a^2$  and  $16.50a^2$  of LaBahn and Callaway (1964) and Williamson and McDowell (1965) respectively.

### THEORY

The system of helium atom and the incident electron satisfies the wave equation,

$$(H - E) \psi(r_1, r_2, r_3) = 0 \quad \dots (1)$$

where  $H$  and  $E$  are the total Hamiltonian and energy of the system respectively. The Hamiltonian is given by

$$H = -\nabla_1^2 - \nabla_2^2 - \nabla_3^2 - \frac{4}{r_1} - \frac{4}{r_2} - \frac{4}{r_3} + \frac{2}{r_{12}} + \frac{2}{r_{13}} + \frac{2}{r_{23}}, \quad E = K_0^2 + E_0$$

and  $r_1, r_2, r_3$  are the distances of the three electrons from the nucleus of the helium atom,  $r_{12}, r_{23}, r_{13}$  are the distances between the electrons,  $E_0$  being the ground state energy of the atom (in Rydberg units) and  $K_0$  is the wave number of the incident electron (unit of length being the Bohr radius  $a_0$ ).

Let  $\psi(r_1, r_2, r_3)$  be approximated by the following expansion

$$\begin{aligned} \psi(r_1, r_2, r_3) = & F_0(r_1)\psi_0(r_2, r_3)\chi(1, 2, 3) + F_0(r_2)\psi_0(r_1, r_3)\chi(2, 3, 1) \\ & + F_0(r_3)\psi_0(r_1, r_2)\chi(3, 1, 2) \end{aligned} \quad \dots (2)$$

where  $F_0(r)$  is a function describing the free electron,

$\psi_0(r_1, r_2)$  is the singlet ground state wave function of the He atom and is taken equal to  $N(e^{-\lambda r_1 - \mu r_2} + e^{-\mu r_1 - \lambda r_2})$  with  $\lambda = 2.1832$ ,  $\mu = 1.1886$  and  $N = 708991$ .  $\chi(1, 2, 3)$  is a doublet three-electron spin function and is equal to

$$\frac{1}{\sqrt{2}} \alpha_1(\alpha_2\beta_3 - \alpha_3\beta_2), \quad \alpha \text{ and } \beta \text{ being the spin function for an individual electron}$$

The above expansion of  $\psi$  is anti-symmetric with respect to the interchange of any pair of electrons and hence it takes into account the exchange effect.

Substituting (2) in (1) and multiplying by  $1/\sqrt{2}(\alpha_1\beta_2 - \alpha_2\beta_1)\alpha_3$  and summing over the spin co-ordinates and integrating with respect to  $r_1$  and  $r_2$ , we obtain

$$[\nabla_3^2 + K_0^2 - V_{00}(r_3)]F_0(r_3) = \iint F_0(r_1)P_{00}(r_1, r_2, r_3)dr_1dr_2 \quad \dots (3)$$

where  $V_{00}(r_3)$  the static potential and is equal to

$$-g \left( \frac{1}{r_3} + \lambda \right) e^{-2\lambda r_3} - g \left( \frac{1}{r_3} + \mu \right) e^{-2\mu r_3} - 2h \left( \frac{1}{r_3} + \frac{\lambda + \mu}{2} \right) e^{-(\lambda + \mu)r_3}$$

where

$$g = 1.13573 \quad \text{and} \quad h = .864273$$

$$P_{00}(r_1, r_2, r_3) = \psi_0(r_2, r_1) \nabla_1^2 \psi_0(r_1, r_2) + \psi_0(r_1, r_2) \nabla_2^2 \psi_0(r_2, r_3) + \psi_0(r_1, r_2) \nabla_3^2 \psi_0(r_2, r_3) \\ + \psi_0(r_1, r_2) \psi_0(r_2, r_3) \left[ \frac{4}{r_1^2} + \frac{4}{r_2^2} + \frac{4}{r_3^2} - \frac{2}{r_{12}^2} - \frac{2}{r_{23}^2} - \frac{2}{r_{13}^2} + E \right]$$

We expand the wave function of the free-electron in zonal harmonics as

$$F_0(r_3) = \frac{1}{r_3} \sum_{l=0}^{\infty} f_l(r_3) \rho_l(\cos \theta_3) \quad \dots \quad (4)$$

where  $f_l(0) = 0$  and  $f_l(r) \sim \sin \left( Kr - \frac{l\pi}{2} + \eta_l \right)$

$\eta_l$  being the phase-shift.  $r \rightarrow \infty$

Substituting  $F_0(r)$  from (4) into (3) and multiplying both sides by  $P_l(\cos \theta_3)$  sin  $\theta_3 d\theta_3$  and integrating over the space we get finally

$$\left[ \frac{d^2}{dr_1^2} + k_0^2 - V_{00}(r_3) - \frac{l(l+1)}{r_1^2} \right] f_l(r_3) \\ = \int_0^\pi \int_0^\pi Q_{00}(r_1, r_2, r_3) f_l(r_1) dr_1 dr_2 \quad \dots \quad (5)$$

where

$$Q_{00}(r_1, r_2, r_3) = 16\pi^2 r_1 r_2^2 r_3 P_{00}(r_1, r_2, r_3).$$

LaBahn and Callaway (1964) considering the distortion of the atomic wave function induced by the incoming electron, have obtained in addition to the usual static coulomb potential, a term of the type  $-\frac{\alpha(r)}{r^4}$  in the asymptotic region which represents the polarisation effect. For the general case they assume  $\alpha$  to be a function of  $r$  of the form as obtained by Bethe (1943). With that picture in mind, Williamson and McDowell (1965) have taken the total potential as  $V_{00}(r) - \frac{\alpha(r)}{r^4}$  where  $\alpha(r)$  is the same as above, though  $V_{00}(r)$  is different from that of LaBahn and Callaway (1964). In our calculation, we have chosen the same potential as that of Williamson and McDowell (1965). Hence we solve (5) after replacing  $V_{00}(r)$  by  $V_{00}(r) - \frac{\alpha(r)}{r^4}$  where  $\alpha(r)$  as given by Bethe (1943) runs as

$$\alpha(r) = -\frac{9}{\beta^4} \left[ 1 - \frac{2}{3} e^{-4\beta r} (1 + \frac{1}{3} \beta r)^4 - \frac{e^{-2\beta r}}{3} \left( 1 + 2\beta r + 6\beta^2 r^2 + \frac{20}{3} \beta^3 r^3 + \frac{4}{3} \beta^4 r^4 \right) \right]$$

where  $\beta = \left( \frac{9}{\alpha} \right)^{1/4}$  and  $\alpha(r) = \alpha = 1.32a_0^3$

To solve (5) for  $l = 0$  by the variational method of Hulthén (1944), we have used a trial function of the same form as that of Moisewitsch (1953) i.e.  $f_0(r) = \sin K_0 r [1 + (a + be^{-2r})(1 - e^{-2r}) \cos K_0 r]$  where  $Z = 1.6875$ . The phase-shift is given by  $\eta_0 = \tan^{-1} a$ .

The values of the parameters  $a, b$  are found from the simultaneous equations

$$L = 0 \quad \text{and} \quad \frac{\partial L}{\partial b} = 0$$

where

$$L = L_1 + L_2 + L_3$$

with

$$L_1 = \int_0^\infty f_0(r_3) \left[ \frac{d^2}{dr_3^2} + K_0^2 - V_{00}(r_3) \right] f_0(r_3) dr_3$$

$$L_2 = \int_0^\infty f_0(r_3) \left[ -\frac{\alpha(r_3)}{r_3^4} \right] f_0(r_3) dr_3$$

and

$$L_3 = - \int_0^\infty \int_0^\infty \int_0^\infty Q_{00}(r_1, r_2, r_3) f_0(r_1) f_0(r_3) dr_1 dr_2 dr_3$$

The integrals occurring in  $L_1$  are simple and easily evaluated. The integrals occurring in  $L_2$  are of the form

$$I_1 = \int_0^\infty \left[ \frac{p}{\beta^4 r^4} + \frac{q}{\beta^2 r^3} + \frac{s}{\beta^2 r^2} + \frac{t}{\beta r} + u \right] e^{-(vz + 2ik_0)r} dr$$

where

$$p = 6e^{-4\beta r} + 3e^{-2\beta r} - 9$$

$$q = 24e^{-4\beta r} + 6e^{-2\beta r}$$

$$s = 36e^{-4\beta r} + 18e^{-\beta r}$$

$$t = 24e^{-4\beta r} + 20e^{-2\beta r} \quad \text{and} \quad u = 6e^{-4\beta r} + 4e^{-2\beta r}$$

$$v = 0, 1, 2, 3 \text{ or } 4.$$

On simplification we finally got  $I_1$  as the limiting value of the integral  $I_1(c)$  as  $c \rightarrow 0$  where

$$\begin{aligned}
 I_1(c) = & \left[ \left\{ (vz)^3 \left( -\frac{1}{2\beta^4} \right) + (vz) \left( \frac{6K_0^2}{\beta^4} - \frac{12}{\beta^2} \right) - \frac{8}{\beta} \right\} \int_c^\infty \frac{e^{-\eta r}}{r} dr \right. \\
 & \left. + i \left\{ \frac{4K_0^3}{\beta^4} - \frac{24K_0}{\beta^2} - (vz)^2 \frac{3K_0}{\beta^4} \right\} \right. \\
 & + \left[ \left\{ (vz)^4 \left( -\frac{1}{\beta^4} \right) + (vz) \left( \frac{12K_0^2}{\beta^2} + \frac{12}{\beta^2} \right) + \frac{8}{\beta} \right\} \int_c^\infty \frac{e^{-\eta r}}{r} dr \right. \\
 & \left. + i \left\{ \frac{8K_0^3}{\beta^4} + \frac{24K_0}{\beta^2} - (vz)^2 \frac{6K_0}{\beta^4} \right\} \right. \\
 & + \left[ \left\{ (vz)^3 \left( \frac{3}{2\beta^4} \right) - (vz) \left( \frac{18K_0^2}{\beta^4} \right) \right\} \int_c^\infty \frac{e^{-\eta r}}{r} dr \right. \\
 & \left. + i \left\{ (vz)^2 \left( \frac{9K_0}{\beta^4} \right) - \frac{12K_0^3}{\beta^4} \right\} \right. \\
 & \left. + 4 \int_c^\infty e^{-\eta r} dr + 6 \int_c^\infty e^{-\eta r} dr \right.
 \end{aligned}$$

$$\left. + \left\{ (vz)^2 \left( \frac{5}{\beta^3} \right) + (vz) \left( \frac{9}{\beta^2} \right) + \frac{4}{3\beta} + \frac{20}{\beta^3} K_0^2 \right\} + i \left\{ \frac{18K_0}{\beta^2} - (vz) \frac{20K_0}{\beta^3} \right\} \right]$$

with  $\rho = vz + 2iK_0$ ,  $\xi = \rho + 2\beta$ , and  $\eta = \rho + 4\beta$ .

Again  $L_3$  may be written as  $-16\pi^2 N^2 I_2$

where,

$$\begin{aligned}
 I_2 = & \frac{4-8\lambda}{8\mu^3} D_{1,\lambda} D_{2,\lambda} + \frac{4-8\mu}{8\lambda^3} D_{1,\mu} D_{2,\mu} + \frac{4-8\lambda}{(\lambda+\mu)^3} D_{1,\lambda} D_{2,\mu} + \frac{4-8\mu}{(\lambda+\mu)^3} D_{1,\mu} D_{2,\lambda} \\
 & + \frac{4\lambda^2-2\mu^2+8\mu+2E}{8\mu^3} D_{2,\lambda} D_{2,\lambda} + \frac{4\mu^2-2\lambda^2+8\lambda+2E}{8\lambda^3} D_{2,\mu} D_{2,\mu} \\
 & + \frac{4\lambda^2+4\mu^2-4\lambda\mu+8\lambda+8\mu+4E}{(\lambda+\mu)^3} D_{2,\lambda} D_{2,\mu} + \left( \frac{8}{(\lambda+\mu)^3} + \frac{1}{\mu^3} \right) D_{2,\lambda} D_{1,\lambda+2}
 \end{aligned}$$



$$+ \left( \frac{8}{(\lambda + \mu)^3} + \frac{1}{\lambda^2} \right) D_{2,\mu} D_{1,2\lambda+1,\mu} + \left( \frac{4}{(\lambda + \mu)^2} + \frac{1}{\mu^2} \right) D_{2,\lambda} D_{2,\lambda+2,\mu} \\ + \left( \frac{4}{(\lambda + \mu)^2} + \frac{1}{\lambda^2} \right) D_{2,\mu} D_{2,2\lambda+1,\mu} - \frac{1}{2\lambda^3} D_{\mu}^{\mu} - \frac{1}{2\mu^3} D_{\lambda}^{\lambda} - \frac{4}{(\lambda + \mu)^3} (D_{\lambda}^{\mu} + D_{\mu}^{\lambda})$$

with

$$D_{1,\lambda} = \int_0^{\infty} e^{-\lambda r} f_0(r) dr$$

$$D_{2,\lambda} = \int_0^{\infty} r e^{-\lambda r} f_0(r) dr$$

$$\text{and } D_{\lambda}^{\mu} = \int_0^{\infty} e^{-\mu r} f_0(r) \left\{ \int_0^{\infty} (r - r_1) e^{-\lambda r_1} f_0(r_1) dr_1 \right\} dr$$

## RESULTS AND DISCUSSIONS

We have obtained the scattering length  $A$  from our S-wave phase-shifts  $\eta_0(0.025) = 3.1195$  and  $\eta_0(0.01) = 3.0410$  using the modified effective range formula (O'Malley *et al* 1962)

$$k_0 \cot \eta_0(k_0^2) = -\frac{1}{A} + \frac{\pi \alpha k_0^2}{3} - \frac{4 \alpha k_0^2}{3A} \log(1.23 k_0 \alpha^{\frac{1}{2}}) \\ + \left( \frac{1}{2} r_0 + \frac{\pi \alpha^{\frac{1}{2}}}{3} - \frac{\pi \alpha^{3/2}}{3A^2} - \frac{\pi^2 \alpha^2}{9A^3} \right) k_0^2 + \dots$$

This formula yields  $A = 1.1400$  compared with Williamson and McDowell's value of 1.146 and the corresponding value 1.132 of LaBau and Callaway.

TABLE I

Phase-shift values  $\eta_0$  for the low-energy range is tabulated below

Electron wave No. $K_0$	Present Authors	Williamson and McDowell
0.05	3.1195	3.082
0.10	3.0410	3.018
0.50	2.514	2.4935
1.00	2.108	1.963

The zero-energy cross section in our case is  $16.33 a_0^2$ . The recent experimental value by Pack and Phelps (1961) is  $19 a_0^2$ . In most recent experiments by Frost and Phelps (1964), zero-energy cross section is found to be  $17.49 a_0^2$  corresponding

to a scattering length of  $1.18a_0$ . Bandel and Golden (1965) have obtained a scattering length of  $1.15a_0$  corresponding to the cross section of  $16.6a_0^2$ .

In conclusion, we find that taking adiabatic-dipole polarisation effect into consideration, the discrepancy between experimental zero-energy cross section and the corresponding theoretical one is removed to a large extent. The disagreement still left may be mainly due to (i) the adiabatic assumption made in the polarisation potential, (ii) the neglect of higher order terms in the polarisation potential, especially the quadrupole one and (iii) the inaccuracy in the ground-state wave function of the helium atom.

#### ACKNOWLEDGEMENT

The authors are thankful to Prof D. Basu for his kind interest and valuable discussions throughout the progress of the work.

#### REFERENCES

- Bandel, H. and Golden, R., 1965, *Phys. Rev.*, **138**, A 11.  
 Bethe, H. A., 1943, Handb. d. *Phys.* (Ann. Arbor) **24**, 339-349.  
 Frost, L. S., and Phelps, A. V., 1964, *Phys. Rev.*, **36A**, 1538-1545.  
 Hulthén, L., 1944, *K-Fysiska Sällsk. Lund. Förel.*, **14**, No. 21.  
 LaBahn, R. W. and Callaway, J., 1964, *Phys. Rev.*, **135**, A 1539-1549.  
 Massey, H. S. W. and Motor, C. B. O., 1931, *Proc. Roy. Soc.*, **132**, 605-630; 289.  
 Moserwitsch, B. L., 1953, *Proc. Roy. Soc., A*, **219**, 102.  
 ————, 1961, *Proc. Phys. Soc.*, **77**, 721-723.  
 Morse, P. M. and Allis, W. P., 1933, *Phys. Rev.*, **44**, 269.  
 Mukherjee, S. C., and Sil, N. C., 1962, *Indian J. Phys.*, **36**, 283.  
 Pack, J. L., and Phelps, A. V., 1961, *Phys. Rev.*, **121**, 718, 806.  
 Williamson, J. H. and McDowell, M. R. C., 1965, *Proc. Phys. Soc.*, **85**, 719.

# Letters to the Editor

The Board of Editors does not hold itself responsible for opinions expressed in the letters published in this section. The notes containing short reports of original investigations communicated to this section should not contain many figures and should not exceed 500 words in length. The contributions reaching the Secretary by the 15th of any month may be expected to appear in the issue for the next month. No proof will be sent to the author.

6

## WIGNER QUARKS

T. ROY

PHYSICS DEPARTMENT, JADAVPUR UNIVERSITY, CALCUTTA-32

(Received December 29, 1965)

In both SU(6) and  $\widetilde{U}(12)$  there occur redundancies (Beg *et al.* 1964, Salam *et al.* 1965) which are not easy to interpret physically. For many reasons it seems attractive to analyse the case of non-strange baryons and mesons and consequently SU(4) the Wigner group in the static limit or  $\widetilde{U}(8)$  in the dynamic model.

Let us consider SU(4) quarks ( $B = 1/3$ ) then, the baryons are to be described by the (3, 0, 0) representation of dimension 20, exactly accommodating the non-strange baryons which reciprocate in Chew's Bootstrap. These are  $N_4$  and  $N^*_{1/2}$ . The mesons are quark antiquark compounds and are the members of

$$4 \otimes 4^* = 1 \oplus 15$$

The singlet is obviously  $\eta$  and the (31) accommodates  $\pi$ ,  $\rho$  and  $\omega$ . This  $\omega$  may be endowed with the mean mass of  $\omega$  and  $\phi$ . The mass formula can be obtained easily and is for mesons

$$M^2 = M_0^2 + \alpha J(J+1) - \beta T(T+1)$$

which fits nicely with the mass values of the above mesons.

To consider the boot-strap one needs,

$$20 \otimes 15 = 120 \oplus 140 \oplus 20 \ominus 20'$$

$$(300) \quad (31) \quad (511) \quad (421) \quad (300) \quad (21)$$

in which (300) occurs only once and is therefore free from coupling ambiguity (e.g.  $d$ -type,  $f$ -type in SU(3)). Our preliminary calculation (the details of which will be published else where) with Chew's Static model shows that (300) is self resonating (Signs of the elements in  $4 \times 4$  crossing matrix).

The three Casimir operators are responsible for the simultaneous diagonalisation of Spin, Isospin and Magnetic moments of the baryons having wave func-

tions  $\psi^{ABO}$  of (300) representations with  $A = (a, \alpha)$ ,  $B = (b, \beta)$  etc. and  $a = 1, 2$ ;  $\alpha = 1, 2$ . Magnetic moment  $\mu_3 = QS_3$  and

$$\psi_p = \sqrt{\frac{2}{3}} \psi^{11, 11, 22} - \frac{1}{\sqrt{3}} \psi^{11, 21, 12}$$

$$\psi_n = \sqrt{\frac{2}{3}} \psi^{21, 21, 12} - \frac{1}{\sqrt{3}} \psi^{11, 21, 22}$$

One should note that  $\psi^{ABO}$  are eigenvectors of  $\mu_3$  and  $\phi = T_3\sigma_0 + \frac{B}{2}T_0\sigma_0$ . This  $\mu_n/\mu_p = -2/3$  very close to the experimental value.

If one calculates along the line of Rosen and Paksava (1964) one easily finds  $g_A/g_0 = -5/3$ .

Extending this to  $\widetilde{U}(8)$  similar to Salam's  $\widetilde{U}(12)$  (Salam 1965) we find,

$$8 \otimes 8^* = 1 \oplus 63$$

and,

$$8 \otimes 8 \otimes 8 = 56 \oplus 120 \oplus 168 \oplus 168$$

We naturally take the mesons in 63 and baryons in 120. The occurrence of 5 and 10 dimensional Kemmer-Duffin matrices is a must. Also,

$$64 = 63 + 1 = 4 \times 10 + 4 \times 5 + 4$$

The last four being trivial.

One easily finds the contents of 120 as,

$$120 = (4, 20) + (2, 20)$$

and the Bargman-Wigner equations ensure that 4 with fully symmetric iso-indices describes a particle of Spin 3/2 and 2 describes a particle of Spin  $\frac{1}{2}$ . The form factors now come out with relative ease and lead to the expression of the magnetic moments,

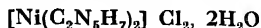
$$\mu_p = \left(1 + \frac{2m}{\mu}\right) \text{ and } \mu_n = -\frac{2}{3} \left(1 + \frac{2m}{\mu}\right)$$

where the numerical values are the same as in Salam (1965) which rest fully on the nonstrange particles.

Lastly the generator of the algebra of  $\widetilde{U}(8)$  satisfy commutation relations which show that there exists a 32-component subalgebra and corresponds to the subgroup  $W(4)$  which again possesses the 16 parameter-subgroup  $U(4)$ .

#### REFERENCES

- Bog, M. and Singh, V. 1964, *Phys. Rev. Lett.*, **13**, 418.  
 Rosen S. P. and Paksava, S. 1964, *Phys. Rev. Lett.* **13**, 773.  
 Salam, A. et al. 1965, *Proc. Roy. Soc.* **284**, 146.

AN X-RAY STUDY OF NICKEL BIGUANIDE<sup>†</sup> CHLORIDE

S. K. RAY AND S. C. CHAKRABORTY

DEPARTMENT OF PHYSICS, THE UNIVERSITY OF BURDWAN,  
WEST BENGAL INDIA

(Received January 27, 1966.)

In our programme to study the crystal structures of some biguanide complexes, the study of the crystal structure of nickel biguanide chloride having a molecular formula  $[\text{Ni}(\text{C}_2\text{N}_5\text{H}_7)_2]\text{Cl}_2, 2\text{H}_2\text{O}$  has been undertaken. Good single crystals were grown by slow evaporation of an aqueous solution of this compound. They were, in general, in the form of pink-red needles.

In absence of a good optical crystal goniometer and polarising microscope at our disposal, the preliminary optical study was carried out with a Unicam S25 universal camera. The approximate interfacial angles were noted. Some crystals showed well-developed (100), (010) and (001) faces. The axial lengths were determined from rotation photographs about the proposed [100], [010], and [001] axes and zero-level Weissenberg photographs were also taken about these axes. From the symmetry of Weissenberg photographs and other consideration, it was seen that the crystal belongs to triclinic system. The positive directions of  $a$ ,  $b$ , and  $c$  axes with the condition  $a < b < c$ , were chosen according to the standard practice in right handed system. The axial angles chosen were also in conformity with the external growth of the faces of the single crystals. All the X-ray photographs were taken using unfiltered Cu-radiation in a cylindrical camera of diameter 57.3mm. Since the crystal is triclinic, the optical study would yield the dihedral angles between the faces (100), (010), (001) i.e.,  $\alpha^*$ ,  $\beta^*$  and  $\gamma^*$ , the angles between the reciprocal axes  $a^*$ ,  $b^*$  and  $c^*$ . The angle  $\beta^*$  could be measured with some accuracy from the optical study. The values of  $\alpha^*$ ,  $\beta^*$  and  $\gamma^*$  which have been used to calculate the axial angles  $\alpha$ ,  $\beta$  and  $\gamma$  using the standard formula, were obtained directly from zero-level Weissenberg photographs taken about [100], [010] and [001] axes respectively.

The axial lengths obtained from rotation photographs and those calculated from Weissenberg photograph were in good agreement. The results may be summarised as follows :

From rotation photographs :

$$a = 6.86 \text{ \AA}$$

$$b = 9.48 \text{ \AA}$$

$$c = 12.30 \text{ \AA}$$

From Weissenberg photographs

$$d_{100} = 6.525 \text{ \AA} \quad \alpha^* = 108^\circ \quad \alpha = 70^\circ 14', \quad a = 6.866 \text{ \AA}$$

$$d_{010} = 8.878 \text{ \AA} \quad \beta^* = 74^\circ \quad \beta = 107^\circ 54', \quad b = 9.458 \text{ \AA}$$

$$d_{001} = 11.11 \text{ \AA} \quad \gamma^* = 87^\circ \quad \gamma = 98^\circ 38', \quad c = 12.28 \text{ \AA}$$

No systematic absence of reflections is possible in triclinic crystals; this was also confirmed from the indices of the spots in Weissenberg photographs. Hence the space group could be either  $P1$  or  $P\bar{1}$ .

The density of the single crystals was determined by floatation method in a mixture of Bromoform and Carbon tetrachloride. The experimentally determined value of the density is  $1.70 \text{ gm cm}^{-3}$  which is also consistent with the value  $1.68 \text{ gm cm}^{-3}$  obtained from X-ray measurements on the basis that there are two molecular units per unit cell.

Further work is in progress.

The work was carried out in the laboratories of the Department of Physics, Burdwan University. Authors wish to express their sincere thanks to Prof. A. Mookherji, D.Sc., Head of the Department of Physics, Burdwan University, for his kind interest in this work and to Dr. R. L. Datta of the Department of Chemistry, Burdwan University, for supplying the specimen.

# STATIONARY SPHERICALLY SYMMETRIC DUST DISTRIBUTION IN A STEADY STATE UNIVERSE

ASIT BANERJEE

JADAVPUR UNIVERSITY, CALCUTTA

(Received February 16, 1966)

As Hoyle and Narlikar (1964) (hereinafter referred to as H N) have shown, one can have, with the field equations of Pyrcie, a stationary spherically symmetric distribution of dust in an outside space which asymptotically approaches the steady state condition. In their solution there is no creation in the stationary region but outside the creation does not vanish. The purpose of the present note is to point out some interesting features of this solution. We show first of all that the conditions of fit at the boundary set a possible upper limit to the dimension of the stationary dust distribution. There is also a lower limit to the value of the density of the matter distribution.

From the boundary relation (equation (83) of H N) one obtains using equation (66) of H N

$$1 - \frac{9}{8}\pi G \rho r_b^2 = \frac{H^2}{8\pi G \rho} \\ = 2f/\rho$$

$$\text{or} \quad r_b = \sqrt{\frac{8}{9\pi G}} \cdot \sqrt{\rho - 2f} \quad (i)$$

The above relation (i) shows that  $\rho \geq 2f$  and further  $r_b$  has a maximum value given by

$$r_{b\max} = \frac{2}{3\sqrt{3}H} \quad \dots \quad (ii)$$

and the maximum occurs at

$$\rho = 4f$$

The exterior solution is formally of the Schwarzschild empty-space type. It is of some interest to investigate whether a Schwarzschild like singularity ( $G_{00} \rightarrow 0$ ) can occur at the boundary for sufficiently large finite concentrations leading to an Oppenheimer-Snyder (1939) cut-off of the light.

From equations (75) and (86) of H.N.

$$g_{00} = e^N = 1 - \frac{\gamma}{R} - H^2 R^2$$

with

$$\gamma = 2G \left\{ \frac{3}{4} M - \frac{27}{128} \left( \frac{H^2}{G} \right) r_b^3 \right\}$$

where

$$M = \frac{4}{3} \pi r_b^3 \rho = \sqrt{\frac{2}{9\pi}} \frac{1}{G^{3/2}} \cdot (\rho - 2f)^{3/2} \quad \dots \quad (\text{ii})$$

so that at the boundary

$$g_{00} = 1 - \frac{GM}{R_b} - H^2 R_b^2 = \frac{27}{64} \frac{H^2 r_b^3}{R_b}$$

Now since  $R_b = 3/4 r_b$  (equation (76) of H.N.)

$$g_{00} = 1 - \frac{2GM}{r_b} - \frac{9}{16} H^2 r_b^3 = \frac{9}{16} H^2 r_b^3 = 1 - \frac{2GM}{r_b}$$

using equations (i) and (iii) one obtains

$$g_{00} = 2f/\rho$$

This is always positive. For the limiting value  $\rho = 2f$ ,  $g_{00} = 1$ ; as  $\rho$  increases  $g_{00}$  monotonically decreases, tending to vanish as  $\rho \rightarrow \infty$ . For any significant condensation  $\rho \gg f$  and  $g_{00} \ll 1$ , so that one has an intense gravitational field at the surface although there is never a Oppenheimer-Snyder type cut-off of light.

The author expresses his gratitude to Professor A. K. Ray-Chowdhuri of Presidency College, Calcutta, for his guidance and valuable suggestions.

#### REFERENCES

- Hoyle, F. and Narlikar, J. V., 1964, *Proc. Roy. Soc. A*, **278**, 465.  
 Oppenheimer, J. R. and Snyder, H., 1939, *Phys. Rev.* **58**, 465.



X-RAY STUDY OF *p*-ANISIDINE

M. Y. KHAN AND Y. MISRA

DEPARTMENT OF PHYSICS, UNIVERSITY OF GORAKHPUR,

GORAKHPUR (INDIA)

(Received April 1, 1966)

The substance *p*-Anisidine (alternative name *p*-amino anisol)  $C_7H_7NO$ , finds an important place in the synthesis of various colorants (Cherniikh, 1935) and drugs (Smith and Burnett, 1949). Good single crystals, of the substance were obtained from its saturated solution in ethanol under controlled evaporation and repeated crystallisation. The crystals are long prismatic in shape with brownish tinge, and show four faces parallel to the needle direction. Goniometric observations from the crystal suggest that it belongs to the monoclinic system. The faces (001) and (100) are very well developed and prominent in all the crystals. The interfacial angles  $(100)\wedge(001)$  and  $(001)\wedge(\bar{1}00)$  are  $74^\circ 18'$  and  $105^\circ 42'$ , are in good agreement with the calculated values of  $74^\circ 17'$  and  $105^\circ 43'$  respectively.

The axial parameters of the unit cell from the oscillation photographs were refined by the method of least squares using high angle spots on the zero layer Weissenberg photographs (Huges, Yakel, and Freeman, 1961). The camera diameter was standardised with the help of aluminum wire powder pattern superimposed on the oscillation and the zero layer Weissenberg photographs. Unfiltered copper radiation from Machelett tube at 25KV, 10mA was used. The monoclinic angle  $\beta$  was determined from the zero layer Weissenberg photograph along the unique axis and was further refined by the method of angular lag from first and second layer equi-inclination Weissenberg photographs (Buerger, 1942).

The density of crystals was measured by flotation method. The observed density is  $D_m = 1.20 \text{ g. cm}^{-3}$  against the reported density  $D = 1.08 \text{ g. cm}^{-3}$ . (Milbrun, and Bunbury, 1934). The number of molecules per unit cell is 4 and the calculated density is  $D_x = 1.21 \text{ g. cm}^{-3}$  which is in good agreement with the observed value. Equi-inclination Weissenberg photographs were taken along the three crystallographic directions and the spots were indexed with the help of lattice row templates (Schnoier, 1928) and checked by direct calculations for the Bragg angles.

From the study of indexed reflections, it is found that all (*hkl*) reflections are present. The systematic extinctions are (*hol*) with *l* odd and (*oko*) with *k* odd.

It shows that the lattice is primitive, the unique axis is a screw axis and the symmetry plane is a glide plane with glide component along  $c$ . These conditions enable us to assign the space group  $C_{2h}^6-P2_1/c$ .

The crystal data as determined from this X-ray study are given below :

$a = 7.78 \pm 0.01 \text{ \AA}.$	$D_m = 1.20 \text{ g.cm}^{-3}$
$b = 5.60 \pm 0.01 \text{ \AA}.$	$D_x = 1.21 \text{ g.cm}^{-3}$
$c = 16.08 \pm 0.02 \text{ \AA}.$	$Z = 4$
$\beta = 105^\circ 22'.$	$F(000) = 264.$
$V_c = 674.44 \text{ \AA}^3.$	
$\mu = 6.69 \text{ cm}.$	

for  $\text{CuK}_\alpha$  radiation ( $\lambda = 1.5418 \text{ \AA}.$ ).

Further work on complete structure determination of  $p$ -anisidine is in progress and will be published shortly.

The authors are indebted to Prof. D. Sharma for his keen interest and Dr. P. Srivastava for his guidance and supervision of the work. Financial assistance from the Council of Scientific and Industrial Research, New Delhi, is also gratefully acknowledged.

#### REFERENCES

- Buerger, M. J., 1942, 'X-ray Crystallography' (Wiley, N. Y.) pp 380.  
 Chotamukh, E. V., 1935 *Russ.*, **41**, 615.  
 Foulton, I., Bunbury, H. M., 1934, 'Dictionary of Organic Compounds', (London)  
 Hugos, E. W., Yakel, H. L., and Freeman, H. C., 1961, *Acta Cryst.* **14**, 345.  
 Schneider, W., 1928, *Zeit. für Kristallogr. (A)*, **69**, 41.  
 Smith, N. C., and Burnett, D., 1949, *Jr. J. Econ. Entomol.* **42**, 439.

# GRÜNEISEN CONSTANT, THERMAL EXPANSION OF CRYSTALS AND THE LAW OF INTERATOMIC FORCES

C. M. KACHHAVA AND S. C. SAXENA

PHYSICS DEPARTMENT, RAJASTHAN UNIVERSITY, JAIPUR, INDIA

(Received April 9, 1965; Resubmitted November, 18, 1965)

In principle it should always be possible to compute the different macroscopic properties of crystals from the reliable knowledge of interatomic forces. Various attempts have been made in this direction from time to time and the purpose of this note is to present such simple and new relations for the Grüneisen constant and the coefficient of thermal expansion

The familiar Grüneisen relation is (Kittel 1956)

$$\gamma = \frac{3\alpha V}{\beta C_v}, \quad \dots (1)$$

where  $\gamma$  is the Grüneisen constant,  $\alpha$  and  $\beta$  the coefficients of thermal expansion and compressibility respectively,  $V$  the molar volume and  $C_v$  the molar specific heat at constant volume. On the basis of the extended Born-Mayer theory of the interatomic forces of ionic crystals we can write for the total energy per cell,  $\Phi(r)$ , as

$$\Phi(r) = -\frac{\alpha e^2}{r} + A \exp(-r/\rho) - \frac{C}{r^6} - \frac{D}{r^8}. \quad (2)$$

Here  $\alpha$  is the Madelung constant,  $e$  the electronic charge,  $r$  the interatomic separation,  $A$  and  $\rho$  the two potential parameters, and  $C$  and  $D$  are the van der Waals constants. The constants  $A$  and  $\rho$  are determined from the familiar conditions of Born and Mayer (1932) but we quote here a simplified version of their second relation which is pertinent for our discussion here viz.,

$$r^2 \frac{d^2\Phi(r)}{dr^2} = \frac{9V}{N\beta}, \quad \dots (3)$$

$N$  being the Avogadro number.

Further if  $\nu$  is the vibrational frequency of the atoms in the crystal we have

$$\gamma = -\frac{d \ln \nu}{d \ln V}. \quad \dots (4)$$

If we make an additional assumption that these atomic vibrations are simple harmonic in nature we have

$$v = 2\pi\sqrt{\frac{f}{m}}, \quad \dots (5)$$

$m$  is the mass of the atom and  $f$  the force constant. Relation (5) leads to

$$\frac{dv}{v} = \frac{df}{2f} \quad \dots (6)$$

We also have  $V = Ncr_0^3$ , where  $r_0$  is the equilibrium interatomic separation, and  $c$  a constant which depends upon the crystal structure. This leads to the relation

$$\frac{dV}{V} = \frac{3}{r} dr. \quad \dots (7)$$

One can also write at  $r = r_0$ ,

$$\frac{d^2\Phi(r)}{dr^2} = -f. \quad \dots (8)$$

Equations (6), (7) and (8) on substitution in Eq. (4) lead to the following desired relation :

$$\gamma = -\frac{r_0}{6} \left( \frac{d^3\Phi(r_0)}{dr^3} \right) \left( \frac{d^2\Phi(r_0)}{dr^2} \right)^{-1}. \quad \dots (9)$$

An interesting relation results if the values of  $\gamma$  and  $\beta$  as given by expressions (9) and (3) respectively are substituted in Eq. (1). We finally get

$$\alpha = -\frac{C_v}{2Nr_0} \left[ \frac{d^3\Phi(r_0)}{dr^3} \right] \left[ \frac{d^2\Phi(r_0)}{dr^2} \right]^{-2}. \quad \dots (10)$$

The relation (10) has also been derived by Saxena and Kachhava (1965) earlier in an entirely different approach based on the simple statistical mechanics result of expressing the average atomic displacement from the equilibrium position in terms of the interatomic potential. That these two results are identical with each other substantiates the various approximations made here in deriving the relation (9). We now check the accuracy of the derived relation (9) by performing calculations on alkali halides where fortunately experimental data are also available.

In the table we list the experimental values of  $\gamma$  for almost all the alkali halides. Also recorded are the calculated values according to Eq. (9). In these computations we have used the  $r_0$  values as compiled by us (1963) earlier, the two potential parameters  $A$  and  $\rho$  needed in connection with evaluation of the various derivatives of  $\Phi(r)$  have also been reported by Kachhava and Saxena (1965),

while  $C$  and  $D$  are given by Mayer (1933). The agreement is satisfactory on the whole while it becomes excellent in some cases.

In order to get an idea of the success of the present theory and consequently of Eq. (9) we also tabulate the values as calculated from the two other approaches. One calculation uses Debye's theory and the knowledge of equation of state (method I), while in the second method we further employ the knowledge of interatomic forces. The values recorded in the table are based on the simpler Born type potential (method II). It is important to note that due to the requirement of the experimental data of a rather complicated and uncertain nature it is not possible to compute  $\gamma$  for all the alkali halides. Wherever the values are reported we find that the second method is definitely not reliable while the present method yields results better than even the first method in most of the cases.

It is also interesting to point out here that calculations of Saxena and Kachhava (1965) based on Eq. (10) for  $\alpha$  of the alkali halide crystals are also satisfactory thereby substantiating the assumptions made in developing the present theory to a large extent. However, the theory developed here is based on the simple Einstein's single frequency model, which is valid only at high temperatures. Although the recent lattice theories are capable of giving relatively more rigorous and accurate results, yet the treatment presented here is useful because it is capable of yielding fairly reliable results in a very straightforward and simple fashion.

Experimental data as well as calculated values of  $\gamma$  for a few alkali halides are available other than shown in the Table. White (1961) found a value of 1.47 for KCl on the basis of the experimental data on  $\alpha$  and other quantities. White (1962), and Rubin *et al.* (1961) report a value of 1.55 for NaCl. Collins (1963) on the other hand has calculated  $\gamma$  theoretically from the observed values of the pressure dependence of the elastic constants. He finds at high temperatures for NaCl and KCl  $\gamma$  values as 1.61 and 1.25 respectively. Barron, Leadbetter and Morrison (1964) have recently reported the values of  $\gamma$  calculated from the experimental values of adiabatic compressibility, specific heat at constant pressure and thermal expansion coefficient. Their values extrapolated to high temperatures for NaCl and KCl are 1.585 and 1.44 respectively. It will be seen that even here the agreement between theory and experiment is roughly of the same order as found in the Table on the basis of equation (9). In view of the simplicity of our approach for calculating  $\gamma$  we refrain comparing further with the values obtained on the basis of more complicated models.

We do not plead on the pretext of the reasonably good agreement obtained on the basis of equations (9) and (10) with the experimental values a great justification for the single frequency model. The underlying idea of the present investigation has been to derive a simple expression and balance out the consequences of the various assumptions in such a way that a good working accuracy may be

achieved. We feel the present investigation achieves this goal in a better way than has been possible so far. This point is specifically made clear by comparing the results also with the two other methods.

TABLE I

Comparison of calculated and experimental values of Gruneisen constant,  $\gamma$

Substance	Experimental values (a)	Calculated $\gamma$ values		
		Eq (9)	Method I (b)	Method II(b)
LiF	1.99	1.80	3.02	1.97
LiCl	1.54	1.70	2.11	2.12
LiBr	—	1.66	2.06	2.16
LiI	—	1.69	—	—
NaF	1.57	1.63	—	—
NaCl	1.43	1.76	1.85	2.27
NaBr	1.55	1.80	1.75	2.33
NaI	1.59	1.87	—	—
KF	1.48	1.73	2.26	2.32
KCl	1.34	1.88	1.59	2.46
KBr	1.43	1.91	1.62	2.47
KI	1.58	1.97	1.54	2.52
RbF	1.28	1.81	—	—
RbCl	1.25	1.93	—	—
RbBr	1.27	1.95	1.46	2.47
RbI	1.50	2.01	1.50	2.56
CsF	1.49	1.82	—	—
CsCl	1.97	2.13	—	—
CsBr	1.93	2.30	—	—
CsI	2.00	2.21	—	—

- (a) BORN, M., and HUANG, K., 1956, *Dynamical Theory of Crystal Lattices* (Oxford: Clarendon Press), p. 52.  
 (b) SLATER, J. C., 1939, *Introduction to Chemical Physics* (London: McGraw-Hill Book Co., Inc.), p. 393.

REFERENCE

- Barron, T. H. K., Leadbetter, A. J., and Morrison J. A., 1964, *Proc Roy. Soc. A* **279**, 62  
 Born, M. and Mayer, J. E., 1932, *Zeit. f.* **75**, 1.  
 Collins, J. G., 1963, *Phil. Mag.* **8**, 323.  
 Kachhava, C. M. and Saxena, 1963, *Phil. Mag.* **8**, 1429  
 ————— 1965, *Proc. Natl. Inst. Sci. (India)*, **A31**, 295.  
 Kittel, C., 1956, *Introduction to Solid State Physics*, 2nd edition (New York · Wiley),  
 p. 154  
 Mayer, J. E., 1933, *J. Chem Phys.* **1**, 270.  
 Rubin, T., Altman, H. W., and Johnston, H. L., 1961, *J. Phys. Chem.* **65**, 65.  
 Saxena, S. C. and Kachhava, C. M., 1965, *Applied Sci. Res.*, **A16**, 1.  
 White, G. K., 1961, *Phil. Mag.* **6**, 1425  
 ————— 1962, *Proc VIII Int Conf Low Temp Phys* (London · Butterworths).

## BOOK REVIEWS

AN INTRODUCTION TO PLASMA PHYSICS—by W. B. Thompson Pergamon Press, Second (revised) impression 1964 Pp. viii+274. Price 70s net.

Thanks to controlled thermonuclear experiments, plasma physics came into prominence in the world of science about a decade ago. The subject has since been developing so fast and in so many directions that students and research workers entering the field need a sound introduction to start with, so that they do not get lost in trying to keep track of the latest developments. In this context the importance of such a book as Prof. Thompson's in elucidating the basic knowledge brought up-to-date cannot be overemphasized.

However, the book, as the author himself points out at the outset, leans—rather heavily, I am afraid,—on the physical phenomena associated with the controlled thermonuclear problem. The author has chosen to omit or to avoid as far as possible a few important aspects of plasma physics, e.g., inelastic collision processes, local inhomogeneities, interaction of a plasma and an electron beam, etc. It appears that treatment of these aspects in a more favourable light would have added to the usefulness of the book as a comprehensive introduction.

The introductory chapter of the book is both informative and interesting. The only important topic one perhaps finds missing pertains to the plasma in solids.

In the chapters that follow, the author deals with the basic properties of the equilibrium plasma, the arc plasma, magnetohydrodynamics, magnetohydrodynamic stability, plasma dynamics and particle motions, and kinetic theory of the plasma.

Almost all the important theoretical approaches for the study of pure plasma dynamics are presented in a precise and lucid manner. It is heartening to find that the book, though essentially theoretical in nature, contains results of relevant experiments and also discussions on various technological applications of plasma, for example, in the propulsion of rockets and in the direct conversion of kinetic energy to electricity.

In comparison the chapters on the basic properties of the equilibrium plasma and the arc plasma seem to be somewhat neglected. In particular, basic experiments such as those involving double probes and microwave interferometers are not referred to. There are also a few mistakes and omissions, mentioned below, which, in part, may however, be ascribed to the printer concerned.

Referring to an experiment by Langmuir, it is written (p. 12), "In arc discharges the electron density is  $10^{11}$ - $10^{12}$  cm<sup>-3</sup> and the plasma frequency  $\sim 100$  Mc/s, ...". For the said electron density the frequency should really be  $\sim 3,000$



10,000 Mc/s. In fact the density in Langmuir's experiment was of the order of  $10^{10}$  cm<sup>-3</sup> and the frequency  $\sim 1,000$  Mc/s

Secondly, it is not quite correct to say (see p. 15) that the resonant form for  $E$  appropriate to a cylindrical cavity of radius  $a$  is  $E \sim J_0(kr)$ , obviously because there may be other resonant forms equally appropriate. The form quoted corresponds to a particular type of modes, one of which (TM<sub>010</sub>) was selected by Adler for his experiment.

Finally,  $c(\text{cm}^{-3})$  in Table 3.1, p. 32 should be replaced by  $n(\text{cm}^{-3})$ .

The book has, however, a number of interesting Tables (see, for example, pp. 11, 20, 51 and 152) and a useful section on problems and their solutions.

The bibliography, though not exhaustive, is presented in a helpful manner.

The book may, by and large, be surely recommended to all those interested in the fourth state of matter, - particularly from the point of view of the study of its dynamics.

*J. Basu*

SEMICONDUCTOR COUNTERS FOR NUCLEAR RADIATIONS by G. Dearnaley and D. C. Northrop, 1963. E and F N Spon Limited, London. 55 Shillings.

In recent years semiconductor counters are playing an important role in experimental nuclear physics for the detection of nuclear radiations. This is because such counters are not only compact and of simple structure but also possess excellent characteristics. In the book under review the authors have first dealt with all the basic principles of nuclear radiation detection as also those of semiconductor physics. They then discussed the problem of application of the latter for the former and the technological aspect. Finally they discussed the damages which might be suffered by such counters by the radiations to be detected. The book also contains an excellent bibliography on the subject. The present volume which is supposed to be the first book in the world on this subject is undoubtedly a very useful one to experimental workers both on nuclear physics and on solid state physics since it is now realised that nuclear radiation can be a powerful tool in the study of semiconductors, just as solid state devices can be useful to nuclear physics.

*A. K. Dutta*

**CLASSICAL CHARGED PARTICLES**—by Rohrlich; published by Addison-Wesley Publishing Company, Inc Massachusetts

It is an excellent text for graduate students. It contains important historical landmarks in the theory of electron. Dirac's  $\lambda$ -limiting process has been written keeping the spirit in tact and showing its importance in future works. Though the name is classical electrons some relevant aspect of quantum electrons have also been discussed. A similar story of electron was written in *Zeit für Physik*, 1928 but a good text was really wanting giving all attempts. Prof Rohrlich's book fills that want.

*T Roy*

**THE STABILITY OF MOTION**—by Chetayev, Published by Pergamon Press, Oxford.

It is an elaboration of Lyapunov's method. The author is bold enough to introduce a chapter on transient motion, a topic which is much less developed compared to the stability of steady motion. The book will undoubtedly be helpful to engineers such as aerodynamic, communication or mechanical engineers. The book indeed contains some of the problems of the above disciplines.

*T Roy*

**TIENSOR CALCULUS AND RELATIVITY**—by D. F Lawden. Publishers Methuen and Co. Ltd, London

The book is a monograph on the subject. Though from a course of lectures the authors has built up the book, it seems difficult to recommend it as a text to graduating students. But that does not mean the book is purposeless. People engaged in researches in other fields or any one who wants to learn general relativity can quickly get the idea reading this lucidly written book. In the opinion of the reviewer the topic of covariant derivative could have been presented more elegantly.

*T. Roy*

**THE FUNDAMENTAL PARTICLES**—by Clifford E. Swartz. Publishers Addison-Wesley Publishing Company, Inc Massachusetts

The book treats the subject in an easily understandable and phenomenological fashion. The author however has kept an eye on the experimental situation all through. Any one having an elementary knowledge of physics e.g., the ideas of conservation, relativity etc., will find the book lucid and instructive. The author has not attempted to give theories like SU(3) or bootstraps though however he has mentioned them taking them with illustrations from *Scientific American* 1964. The book may be used as an introductory course to students of Physics (General).

*T Toy*

# RECIPROCITY EQUATIONS FOR ISOTROPIC OPALESCENT SCATTERING MEDIA

S. P. TEWARSON

DEPARTMENT OF PHYSICS, EWING CHRISTIAN COLLEGE, ALABAMA

(Received May 6, 1965. Resubmitted August 3, 1965 ; September 25, 1965)

**ABSTRACT** Krishnan's reciprocity theorem was found to be restricted to random or vertical orientations of scatterers, and therefore non-general in validity. Perrin extended Krishnan's work to provide a number of reciprocity relations, which were also found to be restricted in validity. S. Subramanian formulated a reciprocity relation concerned with intensity relations and established it experimentally in a much more general form valid for the two cases of orientation in the horizontal plane of observation wherein Krishnan's theorem had previously failed. H. Mueller proposed another general form of reciprocity relation

$$M = M^T,$$

where  $M$  and  $M^T$  are the  $4 \times 4$  matrices of the natural and its corresponding reciprocal optical system involved.

The present paper deals with the formulation of a generalized reciprocity relation, valid for seven types of polarized beams and for all possible orientations and types of scatterers. The equation follows from the Mueller law of reciprocity. Six equations follow from the generalized equation, three of which have been experimentally established through calculations on data from various experimenters available in the published literature. The equations are expected to find usefulness in colloid-optics, gamma-ray polarization studies and allied fields involving electromagnetic beams.

## INTRODUCTION

R. S. Krishnan (1935a), derived the following Reciprocity theorem for Tyndall scattering

$$\rho_u = \frac{1 - 1/\rho_h}{1 + 1/\rho_v} \quad (1)$$

where  $\rho_u$ ,  $\rho_h$  and  $\rho_v$  are depolarization factors for unpolarized, horizontally and vertically polarized incident beams respectively. This relation has been subjected to extensive experimental verifications by Krishnan (1935b), as well as a large number of other workers, mostly for random aggregations of colloidal particles of all shapes and sizes. For specifically oriented non-spherical particles it was experimentally shown by Krishnan (1938), Rao (1945), Subramanya and Rao (1949), etc., that (1) is true for only vertically-oriented particles and fails for particles oriented in the horizontal plane of observation. It was therefore concluded that the law of reciprocity is not a general law of optics, in the original form suggested by Lord Rayleigh (1877)

F. Perrin (1942) extended Krishnan's work to provide a number of additional reciprocity relations which were also found to have restricted validity confined to random orientations only.

In 1948, Muller (1948) reported the formulation of a phenomenological foundation of optics, having only operational bases and founded upon empirical laws of spectral decomposition, polarization, superposition and reciprocity. He gave a new interpretation to the concept of reciprocity based upon the Mueller Phenomenological Algebra (Parke 1949, Muller).

Among the recent workers, Subramanian's (1963) contribution is noteworthy. Under Krishnan's guidance, Subramanian formulated a general reciprocity relation of the form

$$I^A_B = I'^B_A; \quad \dots (2)$$

where  $I^A_B$  is the intensity of the component of the scattered light whose electric vector is inclined at an angle  $B$  to the vertical, with the external orienting field parallel to the incident beam.  $I'^B_A$  is the corresponding intensity component, when the external field is parallel to the scattered beam. The relation (2) was also verified by him experimentally. The reasoning followed in the formulation of (2), is based upon Subramanian's observation that  $\rho_v \times \rho_h$  is a constant for the two cases. However, Subramanian was concerned with intensity only and his result does not deal with the parameters of the optical system constituting the scattering medium.

The present paper deals with certain generalizations of reciprocity relations in light scattering media in terms of Muller's law of reciprocity, valid for all possible orientations of the scattering particles of all shapes and sizes, constituting an isotropic opalescent medium.

Perrin (1942) has defined an isotropic opalescent medium as one whose scattering elements are not very small compared to the wavelength of light, which is more or less turbid or opalescent, and which shows either absolute or statistical isotropy as a whole. Examples of such media are suspensions, colloidal solutions, solutions of large molecules, smokes, fogs, fibrous matter, etc.

#### THE MUELLER LAW OF RECIPROCITY

In the phenomenological Mueller Algebra, an optical system (or instrument), is defined by a  $4 \times 4$  Matrix of the form

$$M = \begin{matrix} & \begin{matrix} 1 & a_1 & a_2 & a_3 \end{matrix} \\ \begin{matrix} b_1 \\ b_2 \\ b_3 \end{matrix} & \begin{matrix} g_{11} & g_{12} & g_{13} \\ g_{21} & g_{22} & g_{23} \\ g_{31} & g_{32} & g_{33} \end{matrix} \end{matrix} \quad \dots (3)$$

where  $t$  is the transmission coefficient,  $a$  and  $b$  are the analyzing and polarizing vectors (3-dimensional), and  $g_{jk}$  ( $j, k = 1, 2, 3$ ) are the matrix elements of an optical Tensor  $G$ .

If  $L$  and  $L'$  are the Stokes' vectors of the incident and the corresponding emergent beams respectively,

$$L' = M \times L; \quad (4)$$

*The reciprocal optical system.*

The reciprocal optical system (or instrument),  $T^\#$ , corresponding to a natural system  $T$ , is defined as one in which the exit aperture is made the entrance aperture and the entrance aperture is made the exit aperture, and wherein the incident and emergent beams are interchanged in their places and reversed in directions. The parameters of the reciprocal system are indicated by superscripting with the sign  $\#$ . The Matrix or the reciprocal system is given by

$$M^\# = t^\# \begin{pmatrix} 1 & b^\#_1 & -b^\#_2 & b^\#_3 \\ a^\#_1 & g^\#_{11} & -g^\#_{21} & g^\#_{31} \\ -a^\#_2 & -g^\#_{12} & g^\#_{22} & -g^\#_{32} \\ a^\#_3 & g^\#_{13} & -g^\#_{23} & g^\#_{33} \end{pmatrix} \quad \dots \quad (5)$$

*The Mueller law of reciprocity*

Starting from the fundamental concepts of reciprocity propounded by Helmholtz and Rayleigh, that, if by any means one point can be seen from the other, the other should also be seen from the first, Mueller's theory states the law of reciprocity in the form

$$M = M^\#; \quad \dots \quad (6)$$

as the most general form of the law.

*Reciprocity conditions*

The following reciprocity conditions follow immediately from (3), (5) and (6).

$$t = t^\# \quad (7)$$

$$a_i^\# = (-)^{i+1} \cdot b_i; \quad (i = 1, 2, 3); \quad (8)$$

$$a_i = (-)^{i+1} b_i^\#; \quad (i = 1, 2, 3); \quad (9)$$

$$\text{and,} \quad g_{jk} = (-)^{j+k} \cdot g^\#_{kj}; \quad (j, k = 1, 2, 3); \quad (10)$$

### III. RECIPROCIITY AND REVERSIBILITY

The horizontal ( $H$ ) and Vertical ( $V$ ) intensity components of the scattered beam, corresponding to horizontally and vertically-polarized incident beams (indicated by subscripting  $H$  and  $V$  by  $h$  and  $v$ ) are given by,

$$H = (I' + M')/2 \quad \dots \quad (11)$$

$$V = (I' - M')/2 \quad \dots \quad (12)$$

where  $I'$  and  $M'$  are Stokes' parameters of the scattered beam. Hence in terms of matrix elements,

$$\begin{aligned} H_h &= (1 + a_1 + b_1 + g_{11})/2 \\ V_h &= (1 + a_1 - b_1 - g_{11})/2 \\ H_v &= (1 - a_1 + b_1 - g_{11})/2 \\ V_v &= (1 - a_1 - b_1 + g_{11})/2 \end{aligned} \quad \dots \quad (13)$$

Krishnan's reciprocity relation  $H_v = V_h$ , yields the relation,

$$b_1 = a_1 \quad \dots \quad (14)$$

This is true only when,

$$a_1^{\neq} = a_1; \text{ and } b_1^{\neq} = b_1; \quad \dots \quad (15)$$

which implies that the system (instrument) is reversible, wherein the reciprocal of the instrument is also the instrument itself and has therefore a Hermitian matrix. The complete requirements of reversibility are expressed by (15) and the additional condition,

$$g_{jk} = (-)^{j+k} \cdot g_{jk}^{\neq}, \quad \dots \quad (16)$$

It can now easily be seen that all reciprocity relations put forth by Perrin (1942) and Krishnan (1935a), follow from the reversibility criteria expressed by (15) and (16). Thus in terms of the new theory, previous reciprocity relations of Perrin and Krishnan appear to be in fact reversibility relations. Since all optical systems cannot be reversible, Krishnan and Perrin's reciprocity relations lack general validity.

#### IV THE RECIPROCITY EQUATIONS

##### A. The scattering experiment

Consider a general scattering experiment with depolarization factors,

$$\rho_u = \frac{H_v + H_h}{V_v + V_h} \quad \dots \quad (17)$$

$$\text{hence,} \quad \rho_u = \frac{1 + b_1}{1 - b_1} \quad \dots \quad (18)$$

$$\rho_h = V_h/H_h = \frac{1 - \left( \frac{b_1 + g_{11}}{1 + a_1} \right)}{\left( 1 + \frac{b_1 + g_{11}}{1 + a_1} \right)} \quad \dots \quad (19)$$

$$\text{and} \quad \rho_v = H_v/V_v - \frac{1 + \left( \frac{b_1 - g_{11}}{1 - a_1} \right)}{1 - \left( \frac{b_1 - g_{11}}{1 - a_1} \right)} \quad \dots (20)$$

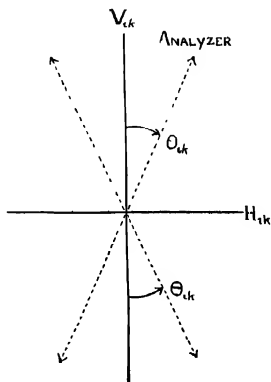
Let the scattering experiment consist of seven types of polarizers and three types of analyzers as under .

*Analyzer*

Plane-Vertical ( $i = 1$ )

Plane at  $45^\circ$  to Vertical ( $i = 2$ )

Circular ( $i = 3$ )



*Polarizer* ,

None (Unpolarized beam)	...(k = 0);
Plane-Vertical	...(k = 1)
Plane-Horizontal	...(k = 1)
Plane at $+45^\circ$ to vertical	...(k = 2)
Plane at $-45^\circ$ to vertical	...(k = 2)
Right circular	...(k = 3)
Left circular	...(k = 3)

Let  $\theta_{ik}$  be the reading of the analyzer for equal intensities of the two halves of the field of view ( $H$  and  $V$ ) which are orthogonally polarized; with the device like a Wollaston prism, etc. From the figure given above we get,

$$V_{ik} \cos^2 \theta_{ik} = H_{ik} \sin^2 \theta_{ik} ; \quad \dots (21)$$

Hence,  $\rho_{ik} = H_{ik}/V_{ik} = \cot^2 \theta_{ik} = (1 + \cos 2\theta_{ik})/(1 - \cos 2\theta_{ik}) \quad \dots \quad (22)$

Using now the abbreviation  $C_{ik} = \cos 2\theta_{ik}$ ; we have from (22),

$$b_i = C_{i0}; \quad (i=1, 2, 3) \quad \dots \quad (23)$$

$$\rho_u = (1 + C_{10})/(1 - C_{10})$$

$$\rho_h = (1 - C_{11})/(1 + C_{11}) \quad \} \quad \dots \quad (24)$$

$$\rho_v = (1 + C_{11}^-)/(1 - C_{11}^-)$$

Also, 
$$C_{ik} = \frac{b_i + g_{ik}}{1 + a_k} \quad (25)$$

$$C_{ik}^- = \frac{b_i - g_{ik}}{1 - a_k}$$

For brevity we express the sum and difference of the above two  $C$  values as,

and, 
$$S_{ik} = C_{ik} + C_{ik}^- \quad \dots \quad (26)$$

$$d_{ik} = C_{ik} - C_{ik}^-$$

Thus we have,

$$a_k = (2b_i - S_{ik})/d_{ik} \quad \dots \quad (27)$$

and, 
$$2g_{ik} = d_{ik} + a_k \cdot S_{ik} \quad \dots \quad (28)$$

### B. The reciprocity equations

Basing our arguments upon Mueller's proposed form of reciprocity law, it is now possible to formulate a generalized reciprocity equation as follows:

From (28) we can write,

$$2g_{jk} = d_{jk} + a_k \cdot S_{jk}$$

and, 
$$2g_{kj}^* = d_{kj}^* + a_j^* \cdot S_{kj}^*$$

hence, 
$$2(g_{jk} - g_{kj}^*) = (d_{jk} - d_{kj}^*) + (a_k \cdot S_{jk} - a_j^* \cdot S_{kj}^*) \quad \dots \quad (29)$$

Substitution of reciprocity conditions (8), (9) and (10) in (29) gives,

$$2[(-)^{j+k} g_{kj}^* - g_{jk}^*] = [d_{jk} - d_{kj}^*] + [(-)^{k+1} \cdot b_k^* \cdot S_{jk} - a_j^* \cdot S_{kj}^*]$$

i.e., 
$$[d_{kj}^* + a_j^* \cdot S_{kj}^*](-)^{j+k} = [d_{jk} + (-)^{k+1} b_k^* \cdot S_{jk}]$$

But 
$$a_j^* = (-)^{j+1} \cdot b_j$$

hence, 
$$\frac{d_{jk} + (-)^{k+1} \cdot b_k^* \cdot S_{jk}}{d_{kj}^* + (-)^{j+1} \cdot b_j \cdot S_{kj}^*} = (-)^{j+k}; \quad \dots \quad (30)$$

In terms of  $C_{jk}$  values from (26) we have,

$$\frac{(C_{jk} - C_{ik}) + (-)^{k+1} \cdot b_k^* (C_{jk} + C_{jk})}{(C_{kj}^* - C_{kj}^*) + (-)^{j+1} b_j (C_{kj}^* + C_{kj}^*)} = (-)^{j+k}; \quad \dots \quad (31)$$



which can finally be written in the form,

$$\frac{[1 - (-)^j C_{jk}^{\omega}] C_{jk} - [1 + (-)^k C_{k0}^{\omega}] C_{j0}}{[1 - (-)^j C_{j0}^{\omega}] C_{k0}^{\omega} - [1 + (-)^j C_{j0}^{\omega}] C_{kj}} = (-)^{j+k}; \quad \dots (32)$$

(where :  $j, k = 1, 2, 3$ )

Equation (32) is the most general form of reciprocity relation existing between the parameters of the natural and its corresponding reciprocal system, measured in terms of  $\cos 2\theta_{jk}$  values. Some special cases of (32) are of great interest, inasmuch as their validity can be tested through available data in literature especially that of Krishnan, Subramanya and Rao, Subramanian, A. Mueller etc. We consider them as follows :

*Case I - ( $j = k = 1, 2, 3$ )*

It follows immediately from the general reciprocity equation (32), that,

(a) For  $j = k = 1$  :

$$\frac{[1 + C_{10}^{\omega}] C_{11} - [1 - C_{10}^{\omega}] C_{11}}{[1 - C_{10}^{\omega}] C_{11} - [1 - C_{10}^{\omega}] C_{11}} = 1 \quad \dots (33)$$

In terms of depolarization factors, (33) can be expressed with the help of (24) and (25) as,

$$\left[ \frac{\rho_u^{\omega} \left( \frac{1 - \rho_h}{1 + \rho_h} \right) + \left( \frac{1 - \rho_v}{1 + \rho_v} \right)}{\rho_u \left( \frac{1 - \rho_h}{1 + \rho_h} \right)^{\omega} + \left( \frac{1 - \rho_v}{1 + \rho_v} \right)^{\omega}} \right] \times \left[ \frac{1 + \rho_u}{1 + \rho_u^{\omega}} \right] = 1, \quad \dots (34)$$

Writing,

$$\left. \begin{aligned} R_u &= \frac{1 - \rho_u}{1 + \rho_u} \\ R_h &= \frac{1 - \rho_h}{1 + \rho_h} \\ \text{and, } R_v &= \frac{1 - \rho_v}{1 + \rho_v} \end{aligned} \right\} \quad \dots (35)$$

Eq. (34) can be reduced to the simple form :

$$\frac{(1 + R_u^{\omega}) R_v + (1 - R_u^{\omega}) R_h}{(1 + R_u) R_v^{\omega} + (1 - R_u) R_h^{\omega}} = 1, \quad \dots (36)$$

(b) For  $j = k = 2, 3$  :

We obtain similarly the following two relations,

$$\frac{[1 + C_{20}^{\omega}] C_{22} - [1 - C_{20}^{\omega}] C_{22}}{[1 + C_{20}^{\omega}] C_{22}^{\omega} - [1 - C_{20}^{\omega}] C_{22}^{\omega}} = 1; \quad (37)$$

and, 
$$\frac{[1+C_{30}^{\pi}]C_{33}-[1-C_{30}^{\pi}]C_{33\pi}}{[1+C_{30}^{\pi}]C_{33}^{\pi}-[1-C_{30}^{\pi}]C_{33}^{\pi}} = 1; \quad \dots \quad (38)$$

Case II

(a)  $j = 1, k = 2$

We have from (32),

$$\frac{[1-C_{20}^{\pi}]C_{12}-[1+C_{20}^{\pi}]C_{12\pi}}{[1+C_{10}^{\pi}]C_{21}^{\pi}-[1-C_{10}^{\pi}]C_{21}^{\pi}} = -1; \quad \dots \quad (39)$$

(b)  $j = 2, k = 1$

$$\frac{[1+C_{10}^{\pi}]C_{21}-[1-C_{10}^{\pi}]C_{21\pi}}{[1-C_{20}^{\pi}]C_{12}^{\pi}-[1+C_{20}^{\pi}]C_{12}^{\pi}} = -1; \quad \dots \quad (40)$$

We can combine (39) and (40) into a single package,

$$\frac{[1-C_{20}^{\pi}]C_{12}}{[1-C_{20}^{\pi}]C_{12}^{\pi}} \cdot \frac{[1+C_{20}^{\pi}]C_{12\pi}}{[1+C_{20}^{\pi}]C_{12\pi}^{\pi}} \times \frac{[1+C_{10}^{\pi}]C_{21}}{[1+C_{10}^{\pi}]C_{21}^{\pi}} \cdot \frac{[1-C_{10}^{\pi}]C_{21\pi}}{[1-C_{10}^{\pi}]C_{21\pi}^{\pi}} = 1; \quad \dots \quad (41)$$

Case III. ( $j = 1, k = 3$ ) and ( $j = 3, k = 1$ )

In the same manner as in (41) the following relation is obtained for this case,

$$\frac{[1-C_{30}^{\pi}]C_{13}}{[1-C_{30}^{\pi}]C_{13}^{\pi}} \cdot \frac{[1+C_{30}^{\pi}]C_{13\pi}}{[1+C_{30}^{\pi}]C_{13\pi}^{\pi}} \times \frac{[1+C_{10}^{\pi}]C_{31}}{[1+C_{10}^{\pi}]C_{31}^{\pi}} \cdot \frac{[1-C_{10}^{\pi}]C_{31\pi}}{[1-C_{10}^{\pi}]C_{31\pi}^{\pi}} = 1; \quad \dots \quad (42)$$

Case IV. ( $j = 2, k = 3$ ) and ( $j = 3, k = 2$ )

$$\frac{[1+C_{30}^{\pi}]C_{23}-[1-C_{30}^{\pi}]C_{23\pi}}{[1+C_{30}^{\pi}]C_{23}^{\pi}-[1-C_{30}^{\pi}]C_{23}^{\pi}} \times \frac{[1-C_{20}^{\pi}]C_{32}}{[1-C_{20}^{\pi}]C_{32}^{\pi}} \cdot \frac{[1+C_{20}^{\pi}]C_{32\pi}}{[1+C_{20}^{\pi}]C_{32\pi}^{\pi}} = 1; \quad \dots \quad (43)$$

Thus, six specific reciprocity relations follow from the general reciprocity equation (32). The experimental verification of all of them requires elaborate and extensive experimental work. Nevertheless, it is possible to verify (34) and (37) with the help of available data in the existing literature.

## V. EXPERIMENTAL VALIDITY

The experimental validity of some cases of the general reciprocity equation (32) is established through available data in the following Tables

a) *Krishnan's (1938) data for Magnetically oriented particles*

Krishnan performed three experiments on graphite sols, using a magnetic orienting field and with incident and emergent beams at right angles in the horizontal plane of observation, as follows.

(i) Particles vertically oriented

- (ii) Particles horizontally oriented and parallel to incident beam
- (iii) Particles horizontally oriented and perpendicular to incident beam and parallel to scattered beam.

In terms of the previous discussion it is easy to see that the system in case (iii) is the reciprocal of the system in case (ii) and vice-versa. The result of calculations for reciprocity Eq.(34) are tabulated below.

TABLE I  
Test of reciprocity Eq. (34) through Krishnan's data

<i>H</i> (Gauss)	Case (ii) Natural Instrument			Case (iii) Reciprocal Instrument			(34) (Left hand side)
	$\rho_h$	$\rho_v$	$\rho_u$	$\rho_h$	$\rho_v$	$\rho_u$	
0	260	045	198	.260	045	198	1.000
1120	410	.086	217	755	045	170	1.010
4060	472	.124	205	1.342	045	.125	1.005
5730	.537	150	.228	2.198	.040	.099	1.030
6860	.537	.163	.238	3.000	037	082	1.050
7620	.537	163	254	3.000	.037	082	1.035

b) *Subramanya and Rao (1949) data for Electrically oriented particles*

The authors repeated Krishnan's experiments with the only difference, that they used an electric field for orienting the particles, given below is their data

TABLE II  
Subramanya and Rao's data  
Concentration of Sols = 0.0008%

<i>H</i> (Volts)	Natural Instrument Case (ii)			Reciprocal Instrument Case (iii)			Rec. Eq. (34) (Left hand side)
	$\rho_v$	$\rho_h$	$\rho_u$	$\rho_v$	$\rho_h$	$\rho_u$	
0	.068	.260	.355	.068	260	355	1.000
60	.102	350	.283	.068	344	.262	0.940
120	.124	.419	.285	.068	476	.255	0.930
180	.131	435	285	.077	.548	.247	1.060

Conc. = 0.0004%

$B$ (Volts)	$\rho_v$	$\rho_h$	$\rho_u$	$\rho_v$	$\rho_h$	$\rho_u$	Rec. Eq. (34) (Left hand side)
0	.070	.236	.331	.070	.236	.331	1.000
60	.078	.255	.331	.074	.390	.312	1.010
120	.092	.307	.328	.079	.394	.305	1.010
180	.108	.350	.315	.083	.448	.295	0.991

The agreement with the proposed reciprocity equation is much more excellent for the lower concentration of 0.0004% than for the higher concentration of 0.0008%. This is because of much better orientation effect and much lower amount of multiple-scattering for lower concentrations.

### 3. Subramanian's data (1963)

Subramanian repeated Krishnan's experiments, using the magnetic field also for verification of his reciprocity relation in terms of Intensities. His data for depolarization factors for the last two cases has been used for verifying the equation (34)

TABLE III

S. Subramanian's Data for oriented particles

$H$ (Gauss)	Field parallel to the incident beam			Field perpendicular to incident beam			Rec. Eq. (34) (Left hand side)
	$\rho_u$	$\rho_v$	$\rho_h$	$\rho_u$	$\rho_v$	$\rho_h$	
0	.20	.09	.69	.20	.09	.69	1.000
3600	.17	.10	.90	.20	.09	.70	0.984
3000	.16	.10	.90	.202	.09	1.00	0.980
2000	—	—	.93	—	.095	1.00	—

Looking at the last column it is apparent, the agreement in this case is also of the order of 98%.

### 4. A. Mueller's data on oriented Nylon fibers

Miss A. Mueller's data is recorded in the present Author's (1964) previous work. She performed a set of extensive experiments using extremely fine parallel nylon fibers as scatterers. The detection technique was developed by H. Mueller utilizing a highly sensitive photoelectric method. Experiments were conducted in an air-conditioned chamber and the angle of scattering was kept at  $41^\circ$ . Table IV gives the result of calculations for the data.

TABLE IV

A Mueller's data on oriented Nylon fibers

Orientation Angle degrees $\Delta$	$C_{10}$	$C\neq_{10}$	$C_{11}$	$C\neq_{11}$	$-C_{11}$	$-C\neq_{11}$	Rec. Eq. (33)
0	.0324	0196	2232	.1898	1552	1826	1 021
30	0256	0239	1286	1192	1205	1184	1.050
60	0399	0544	1855	2043	1211	1234	0 946
90	.0674	0728	4490	4157	3638	3751	1 002
120	0554	0399	3517	2860	.2738	.2367	1 185
150	.0188	0123	1014	1048	0611	0780	1 060
180	.0300	.0175	2000	.1976	1466	1812	0 913

TABLE V

A Mueller's data for verification of Reciprocity Eq.(37)

A Degrees	$C_{20}$	$C\neq_{21}$	$C\neq_{22}$	$C\neq_{20}$	$C_{21}$	$C_{22}$	Rec Eq (37)
0	- 0039	0838	- 0188	- 0008	.0774	- 0148	1 090
30	-.0088	.2124	- 1826	- 0060	2155	-.1883	0 980
60	-.0144	3377	- 3287	- 0366	.3086	- 3065	1 077
90	+ 0035	1741	- 1743	- 0040	1847	- 1468	1 047
120	+.0274	.3067	-.2326	+ 0171	.3075	- 2169	1.035
150	+.0022	2315	- 1753	+ 0019	2331	-.1736	1 001
180	-  0076	0853	- 0585	- 0088	0825	- 0372	1 199

TABLE VI

A. Mueller's data for verification of Reciprocity Eq. (41)

(all  $C$  values are to be multiplied by  $10^{-3}$ )

A (Degrees)	$C_{21}$	$C\neq_{21}$	$C_{22}$	$C\neq_{21}$	$C_{10}$	$C\neq_{10}$	$C_{20}$	$C\neq_{20}$	$C_{12}$	$C\neq_{12}$	$C_{11}$	$C\neq_{11}$	Rev. Eq (41)
0	011	066	015	009	032	020	-001	-001	076	052	-021	-035	1 130
45	031	028	-019	016	022	025	-011	-025	-019	023	061	060	1.090
90	016	010	009	009	067	073	004	-005	159	161	-012	-032	0.890
135	-034	-008	078	041	027	027	016	013	000	-036	055	093	1.175

The agreement of the data with (41), In Table VI, is fairly good considering the number of small parameters involved in the equation and also the greatest

difficulty of maintaining the same experimental conditions over a length of time for the 12 sets of readings involved.

#### *Error Analysis of the Reciprocity Equations*

Consider  $X$  and  $Y$  as the correct values of the numerator and the denominator for the general form of the reciprocity equation

$$X/Y = 1$$

If  $d_x$  and  $d_y$  are the net amounts of error in the experimental values of  $X$  and  $Y$  respectively, it follows that,

$$\begin{aligned} \frac{X \pm d_x}{Y \pm d_y} &= \frac{X(1 \pm d_x/X)}{Y(1 \pm d_y/Y)} \\ &= \frac{X(1 \pm d_x/X)(1 \pm d_y/Y)}{Y} ; \text{ (If } X = Y) \\ &= X/Y \pm (d_x \pm d_y)/Y \end{aligned}$$

Since  $d_x$  and  $d_y$  are bound to be rather small quantities compared to  $X$  and  $Y$ , the error term would be very small. Any consistent and appreciable divergence from the value  $X/Y = 1$  would therefore naturally be due to real significant disparity with the law, and would signify the non-validity of the Mueller's form of the reciprocity law in that case.

#### CONCLUSION

The validity of the proposed reciprocity equation (34) has been conclusively established through the data of Krishnan, Subramanya and Rao, S. Subramanian and A. Muller, as shown in the last columns of tables I to IV. The divergences from the predicted value unity are well within about 5% experimental error limits. Reciprocity Equations (37) and (41) have also been established through the data of A. Mueller in Tables V and VI respectively, though the agreement for these two is not so good as for the previous ones. This is partly because of rather small parameters involved and being for all sorts of arrangements of the scatterers and the apparatus, having been taken over a length of time. It is very difficult to maintain exact experimental conditions over a long period of time, nevertheless the average agreement within about 10% is fairly reasonable. The verification of the equations involving circularly polarized beams is left for further work. The validity of (34), (37) and (41), seems to provide a strong evidence in support of the general reciprocity eq.(32), and as such of Mueller's reciprocity law.

The utility of the proposed form of reciprocity relations is in their efficiency and elegance of providing reliable means of testing the Mueller theory in a straightforward and compact manner. In general matrix elements in ordinary scattering experiments are very small, as such direct comparisons of matrix elements entail

numerous calculations on small quantities yielding inconclusive results. The proposed equations may find usefulness in Colloid-optics and allied fields. Matrix representation of polarized electromagnetic beams is being increasingly used in case of gamma-ray polarization studies as shown by McMaster (1954, 1961) etc.

#### ACKNOWLEDGEMENTS

The author records his gratitude to Prof. Hans Mueller for guidance in the initiation of this work and to Miss. A. Mueller for experimental data. It is a great pleasure to express thankfulness to Prof. K. Banerjee for his encouragement and interest in this work. Thanks are also due to the Danforth Foundation, for financial support in the initial stages of this work at the Massachusetts Institute of Technology, USA.

#### REFERENCES

- Krishnan, R. S. 1935, *Proc. Ind. Acad. Sci.* **1A**, 717, 782.  
——— 1938, *Proc. Ind. Acad. Sci.* **7A**, 91.  
McMaster, W. H. 1954, *Am. J. Phys.* **22**, 351.  
——— 1961, *Revs. Mod. Phys.* **33**, 8.  
Mueller, Hans, 1948, *Opt. Soc. Am. J.* **38**, 661.  
——— 1949, *Foundations of Optics*, (Unpublished text).  
Parke, N. G. 1949, *Tech. Rept. No. 119*, Res. Lab. Electronics, MIT.  
Perrin, T., 1942, *J. Chem. Phys.*, **10**, 415.  
Rao, M. R. A. N. 1945, *Current Science*, **2**, 43.  
Rayleigh, Lord 1877, *Theory of Sound*, Vol I, 92.  
Subramanian, S. 1963, *Kolloid Zests* **189** (2), 135.  
Subramanya, R. and Rao, 1949, *Proc. Ind. Acad. Sci.* **29A**, 442.  
Townson, S. P. 1964, *MIT Graduate thesis, Course VIII*.

## THE 60 MeV GRENOBLE ISOCHRONOUS CYCLOTRON

N. C. SEN

CENTRE DE PHYSIQUE ELECTRONIQUE ET CORPUSCULAIRE  
DE LA U.S.F.—COMPAGNIE GÉNÉRALE DE TÉLÉGRAPHIE SANS FIL  
DOMAINE DE CORDEVILLE PAR ORSAY, FRANCE.

(Received December 27, 1965)

**ABSTRACT.** This article describes the 60 MeV variable energy isochronous Cyclotron designed and constructed by C.S.F. for the University of Grenoble. A general description of the machine along with method of calculations, operational characteristics and the special features are given.

## INTRODUCTION

In a cyclotron the charged particles are submitted to a magnetic induction in a direction perpendicular to their velocity, which forces them to follow circular trajectories at the frequency of rotation  $\omega = eB/m$ . An electric field provides one or several accelerations per turn, which increases their energy and consequently the radius of their trajectory.

But an increase of energy in this way in a cyclotron is limited to 20 to 25 MeV protons due to the increase of mass of the particles with velocity, and the frequency of rotation is no longer constant.

$$\omega = \frac{eB\sqrt{1 - \frac{v^2}{c^2}}}{m_0}$$

In an isochronous cyclotron this limitation is overcome by varying the magnetic field from the centre to the edges. The radial variation of the magnetic induction compensates for the relativistic variation of the mass:

$$B = \frac{B_0}{\sqrt{1 - \omega^2 r^2}}$$

where  $B_0$  is the value of the induction at the center.

The velocity of the rotation is thus maintained constant. It is then possible to obtain a continuous emission of particles, and a beam of much higher average power.

The progressive increase of induction as a function of radius induces a vertical defocussing effect. This is compensated by azimuthal variation of the magnetic field. This azimuthally varying field is created in the median plane by means of



alternate regions of strong (hills) and weak (valleys) fields. This, on the other hand, distorts the circular trajectory of the particle which takes the form of a curvilinear polygon. The effect of focalisation can be further improved by spiralling the sides of the hills in such a way that the angle of entrance into the hill region is increased and that of the angle of departure is decreased.

The index of the magnetic field is expressed by the relation .

$$n = - \frac{\rho}{\beta} \frac{d\beta}{dx}$$

$\rho$  being the radius of curvature of the trajectory and  $x$  the distance measured normally to the trajectory. In an isochronous cyclotron the magnetic field  $B$  as well as  $x$  are functions of  $r$  and  $\theta$  and this leads to the use of the term 'average' index in the theory of these machines and defined by .

$$K = \frac{r}{\langle B \rangle} \cdot \frac{d \langle B \rangle}{dr}$$

where the quantity in the brackets represents average value on the closed orbit. It can be shown that .

$$K = \frac{\frac{\omega^2 r^2}{c^2}}{1 - \frac{\omega^2 r^2}{c^2}}$$

The relation between  $K$  and the energy of the particle is expressed by .

$$E = E_0(\sqrt{K+1}-1)$$

where  $E_0 = m_0 c^2$ , the rest energy.

From this equation the curves of the Figure 1 have been drawn. The values of  $K$  for isochronous field for protons are given below

0.11 for 50 MeV	0.165 for 75 MeV	0.202 for 90 MeV
0.225 for 100 MeV	0.26 for 115 MeV	0.30 for 150 MeV

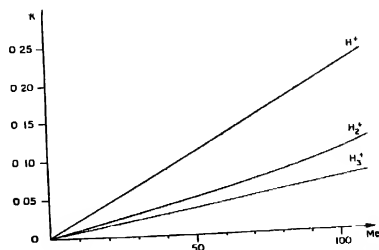


Fig. 1. Variation of the field index with energy for different particles.

The Grenoble machine is a variable energy four sector isochronous cyclotron to give external beams of 60 MeV protons, 30 MeV deuterons, 20 MeV tritons and 60 MeV  $\alpha$ -particles. It has been designed for high performance and is comparable in energy to the cyclotrons of Berkely and Oak-Ridge

### ELECTRO-MAGNET

The electro-magnet of this cyclotron has been designed with enough margin preserved for easy adjustment at all the energies

Consideration for deuteron acceleration led to the choice of 1.52 teslas (Fig 2) as the maximum average field at the radius of extraction which was fixed at 0.86m, having possibility of using 0.9m, if necessary, for extraction purposes. The flux needed at the radius of extraction is therefore  $1.52 \times 0.86^2 = 3.53$  Webers and the model studies show that a total flux of the order of 6.35 Webers is needed to obtain the required field strength

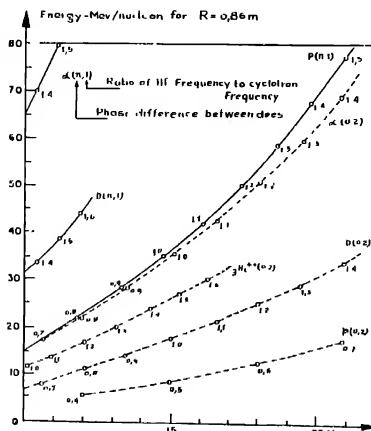


Fig. 2. Operational curves.

A yoke of moulded steel has been chosen. Its maximum permissible induction is 1.7 teslas. Total area of the yoke must therefore be at least  $\frac{6.35}{1.7} = 3.74 \text{ m}^2$ .

The frame was moulded with A48M3 steel of the Société des Forges et Acieries du Creusot (France) and the poles were forged in A11V steel. The composition of these steels are given in table I.

TABLE I

Composition of the metal of the electro-magnet

	Impurity %	<i>Mn</i>		<i>S</i>	<i>Si</i>	<i>Ni</i>	<i>Cr</i>	<i>Cu</i>	<i>Co</i>
A 48 M 3	limit	0 25	0 75	0 03	0 025	0 35	0 15		0 02
	average	0.25	0 63			0 23			
A 11 V	limit	0.07	0.5	0.03	0 03	0.2	0 2	0.2	0 001
	average	0.055	0.45	0 015	0 01	0.15			

The content of Cobalt was specially checked to avoid any danger of activation. The homogeneity was tested by means of ultrasonics

The total gap comprises of 0.166m between the hills and two spaces of 9mm under the hills for returning the auxiliary coils, thus making a total of 0.184m. The ampere turns necessary for a maximum induction of 2 teslas is

$$NI = \frac{2 \times 0.184}{4 \times 10^{-7}} = 307,000 \text{ AT.}$$

The iron of the yoke requires 8000 ampere-turns per meter for an induction of 1.7 teslas. So with average length of 6 meters it needs 48,000 ampere-turns

TABLE II

Characteristics of the Electro-magnet

pole diameter		2,02 m
root diameter		2,15 m
root cross section		3.65 m <sup>2</sup>
yoke cross section	minimum	1.87 m <sup>2</sup>
	maximum	2.0 m <sup>2</sup>
gap between hills		0 166 m
gap between valleys		0.405 m
Maximum flux		7.3 W
yoke induction	minimum	1.82 T (II = 12,000 AT/m)
	maximum	1 95 T (II = 20,000 AT/m)
weight		200 tons
<i>Main coil</i>		
number of turns per coil		180
total number of turns (2 coils)		360
total length of the conductor		2,900 m
weight of the copper		6,800 kg
weight of a coil		4.100 kg
capacity of the power supply		1.100 A
maximum power of the power supply		300 kW
applied voltage		264 V

which is supplied by two coils of five pan-cakes of 36 turns each, making 360 turns in total. The conductor is a copper bar of  $17.6 \times 17.6$  mm with a central hole of 9.7 mm dia. for the circulation of the cooling water. Each coil is moulded in araldite under vacuum and pressure inside a non-magnetic stainless steel casing. The cover-plate along the gap is made of aluminium to suppress any possible modulation of the fringing field by the high frequency harmonics of the supply current. Each pancake is wound with two conductors in parallel to reduce the loss of head into the cooling circuit. All coils are therefore connected electrically in series and hydraulically in parallel.

For the normal intensity of 1000 amperes as envisaged the power consumption is 230 kW with cooling water consumption of  $7.2 \text{ m}^3/\text{h}$ .

The main characteristics of the electromagnet are given in table II.

Four sectors are mounted on the flat pole-face forming the valley floor. During the operation the field shape can be varied by means of 10 circular coils on each pole. There are 4 valley coils, 8 hill coils and 4 harmonic coils on each pole for field corrections and harmonic control.

Power consumption in the auxiliary coils is 140 kW in comparison with 230 kW in the main coil. This is a characteristic of the isochronous cyclotron. In cyclotrons of 100 MeV energy and above, this consumption may exceed the power in the main coils.

The stability of the power supply of the main coils is better than  $10^{-4}$ . The current in the coil is measured by placing a high precision shunt across it. The shunt is cooled by water whose temperature is regulated. The voltage measured across it is compared with a reference voltage of high stability. The difference between these two voltages is chopped to feed an a.c. amplifier. The amplified output is demodulated and it serves to command ballast transistors. The d.c. voltage at the beginning is obtained from a six phase rectifier making use of silicon diodes. The diodes and the transistors are also cooled by water. The stability of the power supply of the correction coils is  $10^{-3}$ . A device consisting of diodes and transistors has been incorporated in the main coil power supply to absorb the stored power in the electro-magnet in case of power failure.

#### R F S Y S T E M

A recent system consisting of two resonant cavities and two accelerating electrodes (dees) has been found most suitable for this cyclotron. The frequency range to be covered has been determined from the energy requirements and the magnetic field according to the fundamental relation  $\omega = \frac{eB}{m}$ . Fig. 3 shows the dispositions of different elements of the Grenoble cyclotron. The great advantage of the two-cavity accelerating system is that two large regions of  $90^\circ$  opening, easily accessible from outside, are available for extraction.

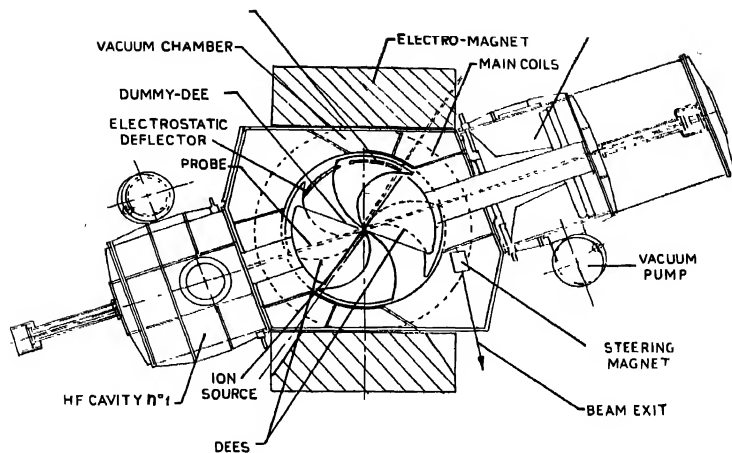


Fig. 3. Top-sectional view of the Grenoble cyclotron

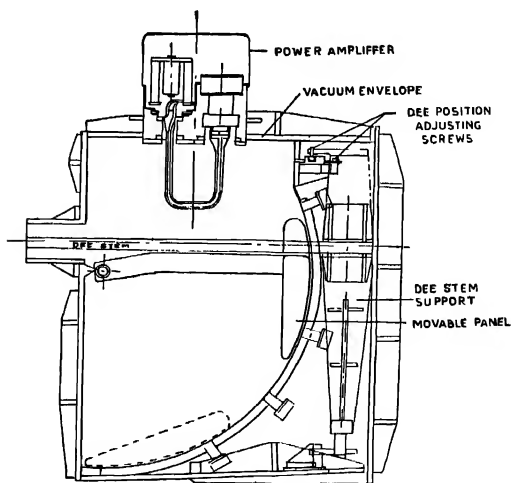


Fig. 4. Side-sectional view of a resonant cavity.

Fig. 2 shows that to satisfy these requirements, the frequency must be adjustable from 10.5 to 21 Mc/s.

Cavity adjustment for change of frequency is done by displacing a contactless capacitive panel inside it (Fig. 4). This structure was chosen after an extensive study of a 1:5 model. The characteristics of one of the cavities are shown in Fig. 5 and 6. The results are particularly satisfactory and they show that this structure avoids the lowering of the  $Q$ -factor at higher frequencies.

Point by point electric field measurements with capacitive probes show that the  $r$ - $f$  high voltage is constant all along the dec in the desired frequency range. The magnetic field measurements along the dec-stem shows that the high frequency current is constant in the lower range. But a small peak appears at high frequency if the arm of the moving panel is not parallel to the dec-stem. At high frequency the currents are equal in the stem and in the arm of the mobile panel.

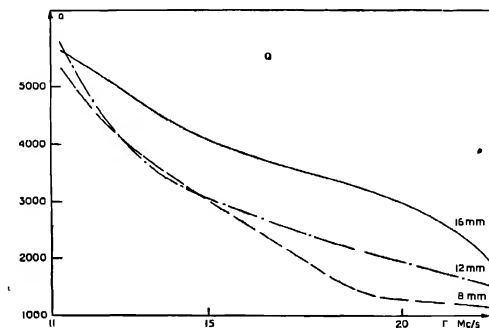


Fig. 5.  $Q$ -factor of the cavity as a function of frequency.

The  $r$ - $f$  drive system consists of a master oscillator and a chain of amplifiers. The power tubes are ceramic metal tetrodes (RS 1082 Siemens) capable of delivering nearly 50 kW up to a frequency of 30 Mc/s. Each tube is mounted directly on its cavity to avoid problems of cable connections. Cooling water for the anodes circulate through the coupling loops thus avoiding problems of high frequency isolation of the water circuit.

These tubes are fed by a distributed amplifier (Marconi HS 113) whose gain and power are constant from 4 to 24 Mc/s without any adjustment. The amplifier itself receives signals from a frequency synthesizer. Actually, besides the frequency adjustment of the pilot and the cavity, the complete chain has only one adjusting point in the grid circuit of the tetrode. The grid is always fed at low impedance, thus avoiding any neutralization of the final stage. A low impedance broad band circuit is under consideration to suppress this adjustment too.

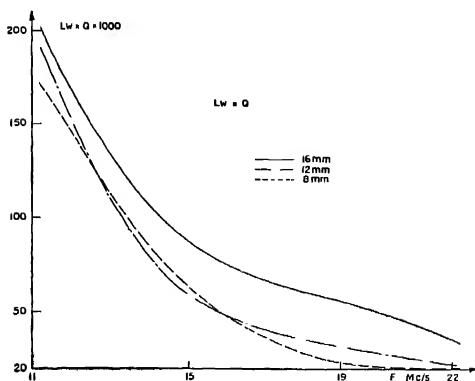


Fig. 6 Impedance of the cavity as a function of frequency

## MAGNETIC FIELD MEASUREMENTS

For precision measurements of the magnetic field the floating wire (hodoscope) method has been adapted, this supplying directly the required information regarding the stability of the particles. Along with it the usual method of taking magnetic field readings and deducing the characteristics of the motion of the particles by means of a computer has also been used for comparison. Details of these techniques have been described by Auecoururier (1964).

## VACUUM

The vacuum is maintained by means of a pumping system whose capacity is 16 000 l/sec. This comprises two diffusion pumps placed on the cavities. The pressure maintained is better than  $10^{-5}$  torr.

## INJECTION

Along with the conventional internal injection, this cyclotron has been designed for an external injection system. A beam of particles may be transmitted axially by a hole on the yoke. A series of electrodes defines the beam injected in the central region to insure the best quality for the accelerated beam. Auxiliary coils taper the magnetic field in the vicinity of the axis for optimum value for best focussing. Axial injection will be used for acceleration of polarized particles, since it is thus possible to avoid pollution by non-polarized ions.

The ion source for the internal injection is of the Livingstone-Jones type where a beam of electrons emitted from a hot tungsten filament ionizes the gas molecules injected into an axial cylindrical chamber. The ion source is extracted by a lateral slit and injected into the cyclotron by the  $r$ - $f$  voltage. The consumption of gas

is at the rate of about  $1 \text{ cm}^3/\text{min}$ . The arc voltage and current are of the order of 200 V and 5 A respectively.

#### EXTRACTION

The extraction system consists of an electrostatic deflector followed by a magnetic channel. A radial disturbance is induced in the region of the outside trajectory to enable the beam to pass into the electrostatic deflector. This deflector displaces the beam from 10 to 15 mm to enter the magnetic channel which is an assembly of steel bars forming a kind of magnetic shield. A coaxial type of extractor as used in Oak-Ridge is also being studied for this purpose.

Centering of trajectories, observed with the help of probes, is adjusted by means of correcting coils. An optical system comprised of focussing triplets and of analysing magnet continues the extraction (Fig. 3).

#### CONCLUSION

Because of the possibility of choosing independently the  $r$ - $f$  frequency, the average magnetic field, and the magnetic field pattern, this cyclotron can be used to accelerate particles of different mass: protons, deuterons, tritons,  $\alpha$ , heavy nuclei and for each one a continuously variable energy output is obtainable.

Tests on the component parts of the machine have been completed and found satisfactory justifying design calculations and model studies. Final installations are being carried out to run the machine next year.

#### ACKNOWLEDGMENTS

The author would like to acknowledge the important contributions made to the work described in this paper by his colleagues, in particular Mme J. Auecuturier and Mr. R. Lacaze. He expresses his gratitude to Prof. J. Teillac, Director, Institut du Radium and to Dr. H. Laboutet for guidance. He is grateful to Dr. R. Jean for constant advice and to Dr. A. Cabrespine of the Faculty of Science, Orsay, for valuable discussion on extraction system design.

He also wishes to thank the Directors of the C.S.F. for permission to publish this paper.

#### REFERENCES

- Auecuturier, J., 1964, *Ann. Radioelectr.*, **19**, 281.
- Jean, R., Laboutet H., Auecuturier J., "Le cyclotron isochrone de la Faculté des Sciences de Grenoble" (to be published in *Annales de Radioélectricité*).
- Khoe Kong Tat, 1960, *The Isochronous Cyclotron*—Thesis Delft.
- Laboutet H., Auecuturier J., Schuuriger J. C., 1963, *International Conference on sector focussed cyclotrons and meson factories*, April, 262.
- Lo Conteur, K. L., 1951, *Proc. Roy. Soc. London*, **13**, 64, 1039.
- Livingood, J. J., 1960, *Principles of cyclic particle Accelerators* Van Nostrand, Princeton.
- Livingstone—Blewett, "Particle Accelerators", Mc Graw-Hill.
- Oak-Ridge National Laboratory, 1963, Report ORNL 3630.
- Sen, N. C., *Internal reports*, 1965 (unpublished).



# ELECTROLYTIC EFFECT ON A CURRENT CARRYING CONDUCTOR

G. P. BHATNAGAR, M. S. GAUR AND V. S. DUBEY

SCHOOL OF STUDIES IN PHYSICS, MADHAV COLLEGE,  
VIKRAM UNIVERSITY, UJJAIN

(Received December 22, 1965)

**ABSTRACT.** Effects due to superimposition of electrolytic current on a current carrying conductor are studied by direct measurement of the potential differences using a high precision potentiometer. The positive terminal of the electrolytic current was connected to (1) the positive end of the heated platinum wire (the electrolytic current adding the heating current) and (2) the negative end of the heated wire (the electrolytic current opposing the heating current). In both the cases the potential differences across the heated platinum wire are calculated by assuming point to point variation of the current along the wire. The agreement between the calculated and measured values is remarkable for small heating currents. However at higher heating currents the measured values are found to be lower than the calculated values. This lowering is due to the increase in the leakage current along the wire in the electrolyte, as the conductivity of the electrolyte increases with the increase of electrolytic current and also with the rise in temperature of the electrolyte in the vicinity of the heated wire.

## INTRODUCTION

Heat transfer in fluids that are subjected to an electric field has been studied by Soufletoben (1931). Similar such problems were then studied by Arajs and Legvold (1958) in different gases and at different pressures. Mixon, Chon and Beatty (1959) reported the changes in heat transfer coefficient from a heated surface due to electrolytic gas evolution. More recently Bhand *et al* (1963, 1963, 1965) have reported the variation in heat transfer coefficient at different ionic currents superimposed upon electrically heated thin platinum wire transferring heat at a small rate in a weak electrolyte. Their contention was that when the so called resistance of the platinum wire decreases, it happens due to the increase in the heat transfer coefficient, whereas the increase in the resistance was due to the decrease in the heat transfer coefficient. Gaur, Bhatnagar and Dubey (1964) using a similar arrangement as that of Bhand *et al* have found that there is no adequate evidence to show any marked change in the heat transfer coefficient. This effect is purely an electrical phenomenon due to the superimposition of heating and electrolytic currents on the platinum wire. The change of resistance attributed by Bhand *et al* is actually the change of potential difference.

The purpose of the present investigation is to measure the potential difference due to the superimposition of electrolytic current on a current carrying

platinum wire, directly by a high precision potentiometer, and to study the effect in greater details.

### EXPERIMENTAL

A schematic diagram of the equipment used in the present investigation is shown in Fig. 1. A fine platinum wire (0.015 cm in diameter and 15.2 cm in length) is dipped horizontally in a weak electrolyte (here tap water) in a large tub

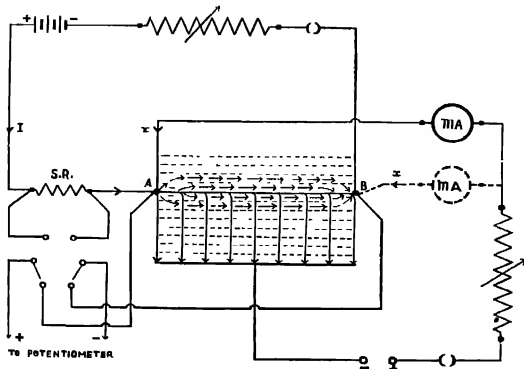


Fig. 1 Circuit Diagram

at 28°C. The platinum wire is surrounded by a co-axial cylinder and the electrolytic current is produced by applying a potential difference between the cylinder and one end of the platinum wire from a D.C. Compound Generator G.E.C. F 2A. The remote temperature of the bath was kept constant within 0.5°C.

A heating current is passed through the platinum wire which is kept constant and is measured by a vernier potentiometer by measuring the potential difference across a standard resistance of 1 ohm in series with the wire. The potential difference developed across the platinum wire is also measured with the same potentiometer.

Firstly, the potential difference across the platinum wire is measured at different heating currents and effective resistance is then found out by dividing the measured potential difference with the respective currents ( $I$ ). A graph is then plotted between effective resistance  $R_e$  and current squared ( $I^2$ ) Fig. 2.

Secondly, the positive end of the platinum wire (as shown at A in Fig. 1) is made the positive electrode for the electrolytic current and at each value of heating current ( $I$ ) the platinum wire is subjected to different electrolytic currents upto 1000 mA. (current densities 1.396 amp./sq.cm.) and the resultant potential difference on the platinum wire is measured keeping  $I$  constant. Fig. 3 solid lines

are the plot of measured potential differences versus electrolytic current ( $x$ ) for different values of heating currents ranging from 0 to 2.0 amps.

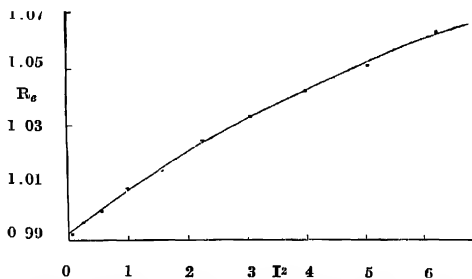


Fig. 2. Plot of Effective resistance  $R_e$  versus heating current squared  $I^2$ .

Thirdly, the electrolytic current was fed from the negative end of the platinum wire (as shown at B in Fig. 1) still keeping it as positive electrode for the electrolytic current. The resultant potential differences were then again measured for the same values of heating and electrolytic currents. Fig. 4 solid lines are the plot of the measured potential differences versus electrolytic current for different values of  $I$ .

#### THEORETICAL CONSIDERATIONS

(1) When the positive end of the heated platinum wire is connected to the positive terminal of electrolytic current, it is quite evident that the electrolytic current varying from  $x$  to 0 will flow along the wire. Taking any length  $dl$  and  $\rho$  as the resistance per unit length of the wire, the potential difference across the element will be

$$\rho dl(I+i)$$

where  $i$  is the electrolytic current in the element  $dl$  and is a function of  $l$ .

that is  $i = 0$  at  $l = 0$  (end B of Fig. 1)

and  $i = x$  at  $l = l$  (end A of Fig. 1)

Hence the total potential difference across the wire will be

$$\begin{aligned} & \int_0^l \rho dl(I+i) \\ &= \int_0^l \rho I dl + \int_0^l \rho i dl \\ &= \rho l I + \rho l \frac{x}{2} \end{aligned}$$

$$= \rho l \left( I + \frac{x}{2} \right)$$

$$= R_e \left( I + \frac{x}{2} \right)$$

where  $\rho l = R_e$

The effective resistance  $R_e$  at any instant will depend upon the heating power  $R_e I^2$  and therefore, it is necessary that to know the effective resistance  $R_e$ , the heating power  $R_e I^2$  must be known. Considering the current flowing in the wire from  $(I+x)$  to  $I$ , the power will be

$$\begin{aligned} & \sum_0^l \rho dl (I+i)^2 \\ &= \sum_0^l \rho I^2 dl + \sum_0^l 2\rho I i dl + \sum_0^l \rho i^2 dl \\ &= \rho l I^2 + \rho l I x + \rho l \frac{x^2}{3} \\ &= \rho l (I^2 + Ix + x^2/3) \\ &= R_e (I^2 + Ix + x^2/3). \end{aligned}$$

Therefore, for a particular electrolytic current  $x$  at a heating current  $I$  the effective resistance  $R_e$  is found out from  $I^2$  versus  $R_e$  graph for  $(I^2 + Ix + x^2/3)$  current squared value and that this value of  $R_e$  is used to calculate the potential difference across the wire viz.  $R_e(I+x/2)$ . The points marked cross (X) and curves represented by dotted lines in Fig 3 represent the calculated potential differences at different electrolytic currents.

(2) Similarly, when the negative end of the platinum wire is made positive terminal for the electrolytic current, the current flowing in the wire varies from  $I$  to  $(I-x)$  and hence the heating power will be

$$\begin{aligned} & \sum_0^l \rho dl (I-i)^2 \\ &= \sum_0^l \rho I^2 dl - \sum_0^l 2\rho I i dl + \sum_0^l \rho i^2 dl \\ &= \rho l I^2 - \rho l I x + \rho l \frac{x^2}{3} \\ &= \rho l (I^2 - Ix + x^2/3) \\ &= R_e (I^2 - Ix + x^2/3). \end{aligned}$$

The effective resistance  $R_e$  is found out from the graph of  $R_e$  and  $I^2$  for  $(I^2 - Ix + x^2/3)$  and this value of  $R_e$  is used for calculating the resultant potential differ-

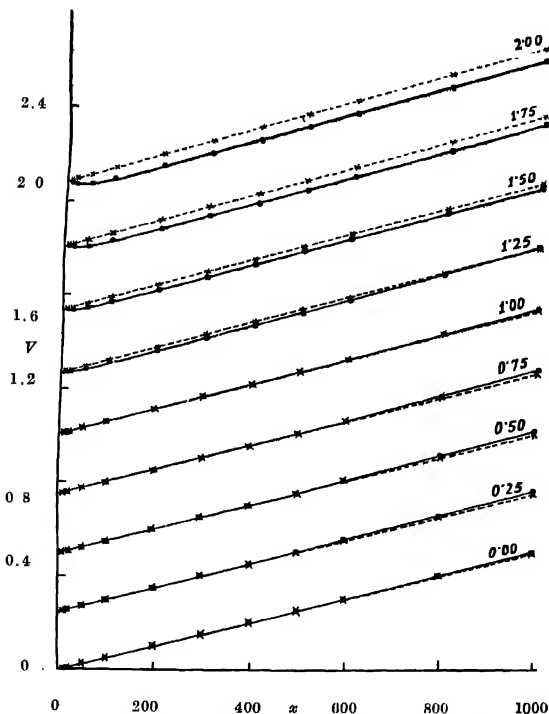


Fig. 3. Plot of calculated and measured potential differences (V) versus electrolytic current ( $x$ ) for electrolytic current adding the heating current.

Since here  $i = x$  at  $l = 0$  (end B of Fig. 1)

and  $i = 0$  at  $l = l$  (end A of Fig. 1)

The resultant potential difference in this case will be

$$\begin{aligned} & \int_0^l \rho i dl (I - i) \\ &= \int_0^l \rho I dl - \int_0^l \rho i dl \end{aligned}$$

$$= \rho l \left( I - \frac{x}{2} \right)$$

$$= R_0(I - x/2).$$

The points marked by cross (X) and curves represented by dotted lines in Fig. 4 represent the calculated potential differences in this case.

Tables (1) and (2) illustrate the examples of calculating the potential differences in the two cases for  $I = 2.0$  amps. The corresponding measured potential differences are also shown for the purpose of comparison.

(3) Whenever a current  $I$  is passed in a conductor (wire) dipped in an electrolyte it is very clear that the whole of the current  $I$  will not pass through the wire, but a portion of it  $i'_\beta$ , in the form of leakage current will pass through the

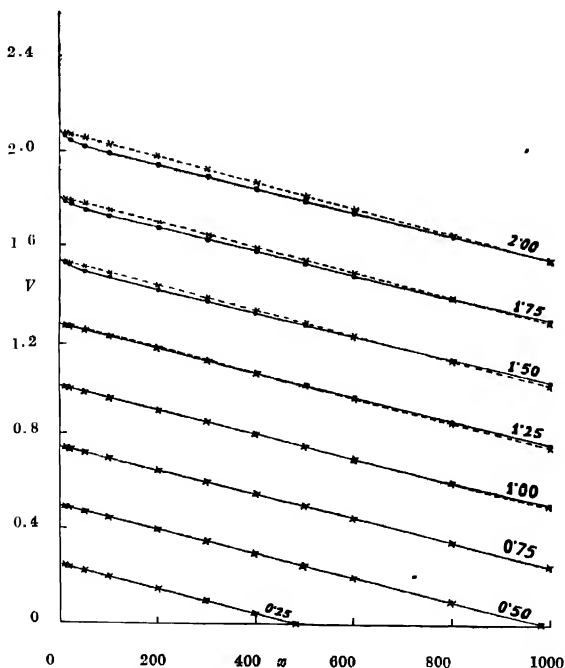


Fig. 4 Plot of calculated and measured potential differences (V) versus electrolytic current ( $x$ ) for electrolytic current opposing the heating current.

electrolyte depending upon its conductivity. Thus if  $R$  is the actual resistance of the wire then

$$R(I - i_\beta) = R_c I$$

When an electrolytic current is passed, the conductivity of the electrolyte increases and after attaining a maximum value becomes constant. Due to this increase in the conductivity of the electrolyte the value of the leakage current increases say by an amount  $i'_\beta$  and hence the net potential difference in the two cases will

$$\text{be } R_c \left( I - i'_\beta + \frac{x}{2} \right) \text{ and } R_c \left( I - i'_\beta - \frac{x}{2} \right).$$

#### INTERPRETATION OF RESULTS

(1) In figures 3 and 4 looking to the calculated and measured values of the potential differences across the platinum wire we find that upto 1.0 ampere of heating current where the increase in the leakage current that is  $i'_\beta$  is very small (which is also evident from the observations of  $dR$  by Gaur, Bhatnagar and Dubey, 1964) the two values are almost identical. However when the increase of  $i'_\beta$  becomes effective, that is above 1.25 amperes of heating current, we find that the calculated values of the potential differences are greater than the measured ones.

TABLE I

Values of potential differences for electrolytic currents adding the heating current. ( $I = 2.0$  amps.)

No.	$x$ mA.	$(I^2 + Ix + x^2/3)$ (Amps) <sup>2</sup>	$R_c$ ohms	$(I + x/2)$ Amps.	Calculated P.D. Volts	Measured P.D. Volts
1.	10	4.020	1.0425	2.005	2.089	2.0764
2.	20	4.040	1.0427	2.010	2.095	2.0700
3.	50	4.100	1.0430	2.025	2.112	2.0738
4.	100	4.203	1.0440	2.050	2.142	2.0968
5.	200	4.413	1.0460	2.100	2.197	2.1508
6.	300	4.630	1.0480	2.150	2.253	2.2076
7.	400	4.850	1.0502	2.200	2.311	2.2580
8.	500	5.080	1.0530	2.250	2.370	2.3194
9.	600	5.320	1.0560	2.300	2.429	2.3764
10.	800	5.810	1.0590	2.400	2.543	2.4972
11.	1000	6.333	1.0650	2.600	2.683	2.6114

TABLE II

Values of potential differences for electrolytic currents opposing the heating current. ( $I = 2.0$  amps.)

No	$a$ mA	$(I^2 - Ix + x^2/3)$ (Amps) <sup>2</sup>	$R$ ohms	$(I - x/2)$ Amps.	Calculated P.D. Volts	Measured P.D. Volts
1	10	3.980	1.0420	1.995	2.078	2.0626
2	20	3.960	1.0417	1.990	2.073	2.0486
3	50	3.900	1.0410	1.975	2.056	2.0226
4	100	3.803	1.0400	1.950	2.028	1.9938
5	200	3.613	1.0382	1.900	1.972	1.9400
6	300	3.430	1.0365	1.850	1.917	1.8880
7	400	3.253	1.0347	1.800	1.862	1.8394
8	500	3.083	1.0310	1.750	1.805	1.7900
9	600	2.920	1.0290	1.700	1.750	1.7398
10	800	2.613	1.0260	1.600	1.642	1.6392
11	1000	2.333	1.0200	1.500	1.531	1.5308

The difference in both the cases should be equal to  $R_e i'_\beta$ . However we find that this difference  $R_e i'_\beta$  in calculated and measured values goes on increasing in the case of  $R_e(I+x/2)$  values whereas it decreases and even becomes zero in the case of  $R_e(I-x/2)$  which requires an explanation. The explanation is not far to find. We know that the conductivity of an electrolyte increases with the rise in temperature (Glasstone 1956).

$$\Delta_t = \Delta_{25}[1 + k(t - 25)]$$

where  $\Delta_t$  and  $\Delta_{25}$  are the equivalent conductivities at  $t^\circ\text{C}$  and  $25^\circ\text{C}$  and  $k$  is a constant for an electrolyte. Therefore in the case of  $R_e(I+x/2)$ , Fig 3 the temperature of the wire and hence the conductivity of the electrolyte goes on increasing and therefore, the difference between calculated and measured values goes on increasing with the electrolytic current. Whereas, in the case of  $R_e(I-x/2)$ , Fig 4 the temperature of the platinum wire goes on decreasing and hence  $i'_\beta$  becomes very small thereby the calculated and measured values almost coincide.

In addition to these we have one more point of interest to consider and that is the electrode heating depending upon the electrolytic current densities. Beck and Putnam (1951) showed that large temperature differences ( $\Delta T$ ) between anode and the electrolyte were observed and therefore, due to the electrode heating also there will be an increase in the value of  $R_e$  and hence the measured values of the potential differences are found slightly higher than the calculated potential differences for the curves for which  $i'_\beta$  is small. In other cases where  $i'_\beta$  is large this effect is masked.



# CONCLUSIONS

From the above discussion it becomes quite clear that when the electrolytic current is superimposed upon a current carrying conductor, point to point variation of the current along the wire should be considered. Thus when the electrolytic current is adding the heating current, the potential difference across the wire is

$$R_e (I + x/2)$$

and when the electrolytic current is opposing the heating current, the potential difference becomes

$$R_e (I - x/2)$$

where  $R_e$  is the effective resistance of the wire at that time

When the electrolytic current is adding the heating current, the difference in the calculated and measured potential differences is due to the increase in the leakage current, as the conductivity of the electrolyte increases with the increase in the electrolytic current as reported earlier by Gaur *et al.* and rise in temperature of the electrolyte in the vicinity of the wire. When the electrolytic current is opposing the heating current the conductivity of the electrolyte decreases with the decrease in the temperature of the electrolyte in the vicinity of the wire.

This difference is certainly not due to the change in the heat transfer coefficient or resistance of the wire, as reported by Bhand *et al.*

With these results it is therefore concluded that in all experiments of heat transfer where a naked wire is dipped in a liquid, the measure of the resistance of the wire is erroneous due to the leakage of current in the liquid. Also when the temperature of the liquid near the wire rises, the molecules of the liquid become mobile, the conductivity of the liquid is bound to increase, which increases the leakage current. Hence the measure of the resistance will not give the correct temperature of the wire.

Therefore, in all such experiments for correct estimation of the resistance and hence the temperature of the wire, a suitable correction will have to be applied for the fraction of the leakage current passing through the liquid.

# ACKNOWLEDGEMENTS

We express our gratitude to Dr. Shiv Mangal Singh 'Suman' Principal, Madhav College, Ujjain for constant encouragement and to Shri P. S. Kale, Asstt. Professor, Department of Physics, Madhav College for providing the facilities to carry out these investigations. We are also grateful to Dr. V. S. Dubey Reader, Head of School of Studies in Physics, Vikram University Ujjain for his constant guidance and suggestions in the theoretical interpretations of the results.

## REFERENCES

- Aarj, S and Logvold, S. 1958, *J. Chem. Phys.* **29**, 531.  
Beck T. R and Putnam G. L., 1951, *Ind. Eng. Chem.* **43**, 1123  
Bhand S C, Gaur. M. S. and Gogate. D. V, 1963, *Indian. J. Phys* **37**, 185.  
Bhand, S C, Patgaonkar, G. V. and Gogate, D V., 1963, *Indian J. Pure Appl. Phys*,  
**1**, 291.  
\_\_\_\_\_, 1965, *Int. J. Heat Mass Trans.*,  
**8**, 111.  
Gaur M. S., Bhatnagar, G P and Dubey, V. S 1964, *Indian J Phys.* **38**, 509.  
Glasstone, S 1956, *Text Book of Physical Chemistry II Edn.* (Mac Millan & Co. Ltd.  
London) 895  
Mixon, F O., Chou, W. Y and Boutty, K. O. 1959, *Chem. Engg. Progr.* **55**, 49.  
Santleben, H. 1931, *Physik Z.* **32**, 550.

# LUMINESCENCE SPECTRA OF BENZYL ACETATE IN THE SOLID STATE AT LOW TEMPERATURES

S. C. BAG

OPTICS DEPARTMENT,  
INDIAN ASSOCIATION FOR THE CULTIVATION OF SCIENCE,  
JADAVPUR, CALCUTTA-32

(Received March 31, 1960).

**ABSTRACT.** The luminescence spectra of benzyl acetate in the solid state and in frozen solutions in  $\text{CCl}_4$ , chloroform and ethyl alcohol at 93°K excited mainly by 3650 Å group of mercury lines, have been investigated. From reasonable assignments of the band system observed under different conditions it has been concluded that  $v_0$  band in the luminescence spectrum of the pure solid at 93°K is at 3972 Å and that this may also correspond to the  $v_0$  band in absorption due to singlet-triplet transition in the molecule of benzyl acetate.

## INTRODUCTION

From a detailed investigation of the phosphorescence emitted by solutions of organic compounds in E.P.A. medium at 77°K under excitation from radiations of a high pressure mercury lamp Lewis and Kasha (1944) concluded that the phosphorescence originates from transitions from the excited triplet levels of the molecules to their respective ground states. Similarly, Biswas (1956a, b, c) who studied the luminescence of some pure substituted benzene compounds in the solid state at 93°K excited mainly by the 3650 Å group of mercury lines pointed out that the luminescence has a life time greater than  $10^{-3}$  sec. and might originate from the metastable triplet states of the molecules. However, he could not detect the absorption due to the reverse transition, i.e., from the singlet to triplet levels and only in the case of methyl benzoate somewhat detailed assignments of the observed luminescence bands were possible. It was, therefore, thought that in the cases where  $S \rightarrow T$  absorptions bands may not be observed easily, a careful investigation of the phosphorescence spectra and the life times of the emitting levels in a number of related substituted benzene compounds might be helpful in identifying as well as obtaining informations about the triplet levels in such molecules. In this short note a preliminary report of the luminescence bands of pure benzyl acetate in the solid state at different temperatures and of its frozen solutions in various solvents at 93°K has been presented.

## EXPERIMENTAL

The sample of benzyl acetate obtained from Société usines Chimiques, France, was first fractionated and the proper fraction was repeatedly distilled under reduced pressure. The solvents used were carbon-tetrachloride, chloroform and ethyl

alcohol. The method of investigation of the luminescence spectra of the pure substance and its solutions in different solvents solidified at about 93°K was the same as that used by Biswas (1956a). A 'Hanovia' type quartz mercury vapour lamp was used as the source of excitation and the Fuess glass spectrograph used has dispersions of 12, 20 and 30° Å/mm in the regions of 4047 Å, 4358 Å and 4916 Å respectively. The width of the slit was kept between .15 mm to .50 mm and the times of exposure varied from one hour for the pure substance to ten hours for the dilute solutions. Iron arc spectrum was photographed along with the luminescence bands as comparison in each case.

Microphotometric records of the luminescence spectra and of the comparison iron arc spectrum were taken with a Kipp and Zonen Moll microphotometer. The record from the iron arc spectrum was carefully calibrated and from comparisons of the records of the luminescence bands with that of the iron arc the position of the bands in Å was determined. Measurements of the band-position for a particular sample were made on the records from at least two different plates for the sample. The positions of the bands were determined within 5 Å for the sharp bands and in the case of very weak and broad bands the error in the measurements was about 10 Å.

The Raman and the infrared spectra of pure benzyl acetate in the liquid state were studied and the ultraviolet absorption spectra of the compound in very dilute solutions in carbon tetrachloride and chloroform in the region 4000 Å—2200 Å were also investigated.

## RESULTS AND DISCUSSIONS

Some of the microphotometric records of the luminescence bands are reproduced in Figures 1(a) to 1(e) in Plate I. The wavelengths of the bands together with their wavenumbers are given in Tables I and II. The relative intensities and the probable assignments of the bands are also given in the Tables.

It is seen from Figures 1(b) and 1(a) respectively that pure benzyl acetate in the solid state at 173°K shows four bands and when the temperature of the solid is lowered to 93°K the number of the bands increases and also the bands become more intense. With a 10% solution of benzyl acetate in CCl<sub>4</sub> solidified at 93°K, the appearance of the band system is almost similar to that due to the pure solid at the same temperature while a frozen 5% solution in CCl<sub>4</sub> [Fig. 1(c)] shows only the stronger bands. Compared to the spectra of the pure solid at 93°K the luminescence band system of a frozen 10% solution of benzyl acetate in chloroform [Fig. 1(d)] at 93°K are definitely shifted towards the shorter wavelength side while in the case of a 5% solution in alcohol [Fig. 1(e)] under similar condition some of the bands are slightly displaced to the higher wavelength.

In order to determine the wavelengths of the radiations effective in producing these luminescence bands, the exciting radiations from the quartz mercury vapour

lamp were filtered through filters of aqueous solution of  $\text{NaNO}_2$  of different thickness and concentrations (Biswas, 1956d).

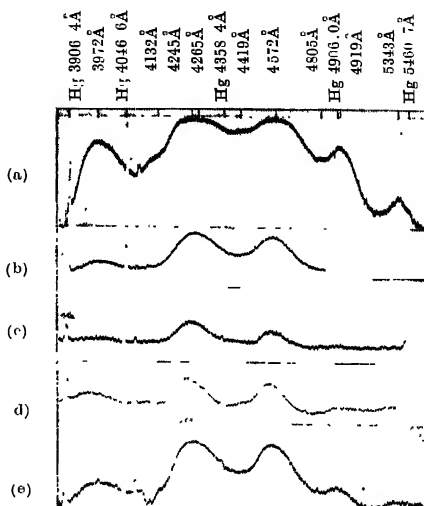


Fig. 1. Luminescence bands of benzyl acetate

- (a) Pure solid at 93°K
- (b) Pure solid at 173°K
- (c) Frozen 5% solution in  $\text{CCl}_4$  at 93°K
- (d) Frozen 10% solution in  $\text{HCCl}_3$  at 93°K
- (e) Frozen 5% solution in  $\text{EtOH}$  at 93°K

The gradual weakening of the intensities of the luminescence bands with increasing concentrations of  $\text{NaNO}_2$  in the filter solutions indicates that mainly the 3650 Å group of mercury lines and other lines of shorter wavelengths are responsible for producing the luminescence bands.

To find out if the region to the longer wavelength side of 3650 Å would show any absorption band which may be connected with the observed luminescence spectra, the ultraviolet absorption of .1% solutions of benzyl acetate in  $\text{CCl}_4$  and in  $\text{HCCl}_3$  at room temperature were investigated throughout the wavelength region from 4000 Å to 2200 Å. Strong absorption bands at 2640 Å and 2650 Å respectively due to solutions in  $\text{CCl}_4$  and  $\text{HCCl}_3$ , probably corresponding to the normal singlet-singlet transition, are observed and the longer wavelength region does not show any appreciable absorption. This inability to detect any absorption band which might be due to  $S \rightarrow T$  transition made the assignment of the luminescence bands difficult.

A careful analysis of the band data presented in Tables I and II were, therefore, carried out in order to find out if there were any regularity in the spacings of the bands which might be helpful in making reasonable assignment of the band system.

TABLE I  
Luminescence bands of benzyl acetate

Substance	Band maxima in Å	$\nu$ in $\text{cm}^{-1}$	Difference from first band in $\text{cm}^{-1}$	Assignment
Pure solid at 173°K	3976 wb	25144		$\nu_0$
	4254 s	23501	1643	$\nu_0 - 1604$
				$\nu_0 - 1730$
	4580 s	21828	3316	$\nu_0 - 1604 - 1730$
	4955 wb	20176	4968	$\nu_0 - 2 \times 1604 - 1730$
5% solution in $\text{CCl}_4$ at 93°K	3974 wb	25157		$\nu_0$
	4247 m	23539	1618	$\nu_0 - 1604$
	4565 m	21899	3258	$\nu_0 - 2 \times 1604$
10% solution in $\text{CCl}_4$ at 93°K	3971 mb	25176		$\nu_0$
	4133 vw	24187	987	$\nu_0 - 1000$
	4250 sb	23523	1656	$\nu_0 - 1604$
				$\nu_0 - 1730$
	4439 w	22521	2655	$\nu_0 - 1000 - 1604$
	4570 sb	21876	3300	$\nu_0 - 2 \times 1604$
				$\nu_0 - 1604 - 1730$
	4944 w	20221	4955	$\nu_0 - 2 \times 1604 - 1730$
	5372 vwb	18610	6566	$\nu_0 - 3 \times 1604 - 1730$
10% solution in $\text{HCCl}_3$ at 93°K	3962 mb	25223		$\nu_0$
	4237 s	23595	1028	$\nu_0 - 1604$
	4550 s	21972	3251	$\nu_0 - 2 \times 1604$
	4912 wb	20353	4870	$\nu_0 - 3 \times 1604$
5% solution in ethyl alcohol at 93°K	3979 mb	25125		$\nu_0$
	4146 w	24113	1014	$\nu_0 - 1000$
	4253 s	23506	1619	$\nu_0 - 1604$
	4560 s	21924	3201	$\nu_0 - 2 \times 1604$
	4920 m	20320	4805	$\nu_0 - 3 \times 1604$
	5356 wb	18666	6459	$\nu_0 - 4 \times 1604$

Intensity: vs—very strong; s—strong; m—medium, w—weak; vw—very weak; b—broad.

The luminescence spectra of the pure solid at 173°K and of the frozen solutions at 93°K show the following characteristics:

i) The shortest wavelength of the luminescence band in each case is at about 3970 Å.

ii) Most of the wavenumber differences between the positions of the band at the shortest wavelength and those of the succeeding bands are found to be such as may be expressed in terms of fundamentals, combinations and overtones mainly of two frequencies—one at about  $1600\text{ cm}^{-1}$  and another at about  $1700\text{ cm}^{-1}$ .

TABLE II

Luminescence spectrum of benzyl acetate in the solid state at  $93^\circ\text{K}$

Position of Band-maxima in Å	$\nu$ in $\text{cm}^{-1}$	Difference from first band in $\text{cm}^{-1}$	Assignment
3972 s	25169		$\nu_0$
4132 m	24195	974	$\nu_0 - 1000$
(4245) (vs)	(23551)	(1618)	$(\nu_0 - 1604)$
4255 vsh	23495	1674	
(4265) (vs)	(23440)	(1729)	$(\nu_0 - 1730)$
4419 m	22623	2546	$\nu_0 - 1000 - 1604$
4572 vsb	21866	3303	$\left. \begin{array}{l} \nu_0 - 2 \times 1604 \\ \nu_0 - 1604 - 1730 \end{array} \right\}$
4805 m	20806	4363	$\nu_0 - 1000 - 1604 - 1730$
4919 s	20324	4845	$\left. \begin{array}{l} \nu_0 - 3 \times 1604 \\ \nu_0 - 2 \times 1604 - 1730 \end{array} \right\}$
5343 m	18711	6458	$\left. \begin{array}{l} \nu_0 - 4 \times 1604 \\ \nu_0 - 3 \times 1604 - 1730 \end{array} \right\}$

Intensity: vs—very strong; s—strong; m—medium; w—weak; vw—very weak, b—broad.

The Raman spectrum of benzyl acetate shows two lines at  $1606$  and  $1750\text{ cm}^{-1}$  and in the infrared spectrum due to the pure liquid two bands at  $1602$  and  $1730\text{ cm}^{-1}$  are observed. These two frequencies obviously correspond to the vibrational modes involving stretching of  $\text{C}=\text{C}$  and  $\text{C}-\text{O}$  bonds in the molecule of benzyl acetate. On the basis of these two frequencies, the probable assignments of the observed luminescence bands are given in column five of Table I. However, the frequencies involved do not exactly agree with those observed in the infrared and Raman spectra of the compound because of inaccuracies in the measurement of the positions of the broad bands. Due to this reason some of the bands in the spectra of the pure solid at  $173^\circ\text{K}$  and of 10% frozen solution in  $\text{CCl}_4$  at  $93^\circ\text{K}$  have been given two different assignments.

From the above assignments it seems fairly reasonable to identify the band at the shortest wavelength as the  $\nu_0$ -band of the luminescence band system. With

3972 Å as the  $\nu_0$ -band in the spectrum due to the pure solid at 93°K, the assignment of the other bands has been made (Table II). It is seen from Figure 1(a) that the first very strong band is broad and has its centre at 4255 Å. If it is assumed to consist of two bands at 4250 Å and 4265 Å, they may tentatively be assigned as  $\nu_0$ —1600  $\text{cm}^{-1}$  and  $\nu_0$ —1750  $\text{cm}^{-1}$  respectively. Similarly, the second very strong band at 4572 Å which is also broad has been assigned both as  $\nu_0$ — $2 \times 1604$   $\text{cm}^{-1}$  and  $\nu_0$ —(1604+1730) $\text{cm}^{-1}$ . Each of the bands of medium intensity at 4130 Å, 4419 Å and 4805 Å are found to involve a frequency roughly 1000  $\text{cm}^{-1}$  corresponding to the breathing carbon vibration of the molecule. This frequency is also found to occur in the luminescence band systems due to the frozen 10% solution of benzyl acetate in  $\text{CCl}_4$  and 5% solution in alcohol (Table I). Lastly, the strong band at 4919 Å and the band at 5343 Å of medium intensity have both been given two different assignments.

Though it has not been possible to observe directly the absorption due to  $S \rightarrow T$  transition, the above analysis suggests that in the case of benzyl acetate in the solid state at 93°K the band at 3972 Å may also correspond to the  $\nu_0$ -band in absorption. This assignment is justified by the fact that with the lowering of the temperature of the solid from 173°K to 93°K the number and intensity of the bands are considerably increased and no other band at shorter wavelength is observed. The ultraviolet absorption spectra of benzyl acetate in different states and particularly in the solid state at 93°K are being studied to obtain further information on the excited singlet and triplet energy levels of the molecule.

#### ACKNOWLEDGEMENT

The author is grateful to Professor G. S. Kastha, D.Sc., for his active interest and continued guidance throughout the progress of the work.

#### REFERENCES

- Biswas, D. C., 1956 a, b, c, d, *Indian J. Phys.*, **30**, 143, 407, 565, 255.  
Lewis, G. N. and Kasha, M., 1944, *J. Am. Chem. Soc.*, **67**, 991.



# MOLECULAR POLARIZABILITY AND ABSOLUTE RAMAN INTENSITIES OF $\Sigma_g^+$ MODES IN MERCURY DICYANIDE AND MEAN AMPLITUDES OF VIBRATION IN SOME LINEAR DICYANIDES

G. NAGARAJAN

DEPARTMENT OF CHEMISTRY, UNIVERSITY OF MARYLAND, COLLEGE PARK,  
MARYLAND, U.S.A.

(Received October 18, 1965, Resubmitted February 4, 1966)

**ABSTRACT** A brief survey of the vibrational and structural data has been made for mercury dicyanide, silver dicyanide ion and gold dicyanide ion possessing a linear symmetrical structure with the symmetry point group  $D_{\infty h}$ . Molecular polarizability has been computed for mercury dicyanide by the Lippincott-Stutman method from a semi-empirical delta-function model of chemical binding using a variational method and delta-function electronic wave functions. The calculated value of the molecular polarizability is in good agreement with the experimental one. The delta-function potential model has been used to obtain an expression for the derivative of the mean molecular polarizability with respect to a change in the internuclear distance at the equilibrium configuration for symmetrical stretching modes in the ground electronic state of a polyatomic system and applied to mercury dicyanide to obtain the polarizability derivatives for the symmetrical  $C\equiv N$  and  $Hg-C$  stretching modes. Mean amplitudes of vibration have also been evaluated by the Cyvin method employing the symmetry coordinates at the temperatures  $T=298^\circ K$  and  $T=500^\circ K$ .

## INTRODUCTION

A linear dicyanide of  $D_{\infty h}$  symmetry is one of the simplest and highly symmetrical molecules for which sufficient number of investigations on the nature of its chemical bonds has not been made. The Raman spectrum of mercury dicyanide was studied and the three Raman lines were assigned by Krishnamurti (1930), Woodward (1930), Petrikaln and Hochberg (1930), Braune and Engellbrecht (1931), Wolkonstein (1937), Francois (1939), Woodward and Owen (1959) and Mathieu (1959). The infrared absorption and Raman spectra of  $Hg(CN)_2$ ,  $KAu(CN)_2$  and  $KAg(CN)_2$  were studied and the fundamentals assigned by Jones (1957, 1963, 1965). The experimental and theoretical investigations by Hassel (1926), Hanawolt, Rin and Frovel (1938), Zhdanov and Shugam (1944), Halford (1946) and Hoard (1933) favour a linear symmetrical structure for mercury dicyanide, silver dicyanide ion and gold dicyanide ion. The fundamental frequencies in  $cm^{-1}$  and internuclear distances in  $\text{\AA}$  for these three dicyanides are given in Table I. It is aimed here on the basis of these recent vibrational and structural data to compute the molecular polarizability and absolute Raman intensities of  $\Sigma_g^+$  modes in mercury dicyanide by the Lippincott and Stutman method (1964) employing the

delta-function model of chemical binding and evaluate the mean amplitudes of vibration for these three dicyanides by the Cyvin method (1959) employing the symmetry coordinates. The importance in undertaking such investigations is that the molecular polarizability, polarizability derivatives and mean amplitudes of vibration obtained here would be much useful for the interpretation of the results of 1) experimental refractive indices i.e. deriving the mean molecular polarizability from measured refractive index through the well-known Lorentz-Lorenz equation and making a comparison with a value obtained from the present study, 2) experimental absolute Raman intensities or polarizability derivatives and 3) electron diffraction studies.

#### MOLECULAR POLARIZABILITY

The polarizabilities for atoms and simple diatomic molecules were calculated by Hasee (1930, 1931), Hirschfelder (1935), Hylleberg (1930), Kirkwood (1932), Mrowka (1932), Steensholt (1935), Buckingham (1937), Bell and Long (1950), Abbott and Bolton (1952, 1953) and Kolker and Karplus (1963) upon different wave functions given by Rosen (1931), Wang (1928) and Guillemin and Zener (1929) and a critical analysis was made by Van Vleck (1932) and Atanasoff (1930). The first use of a delta-function potential model was made by Ruedenberg and Parr (1951) and Ruedenberg and Scherr (1953). Later, Frost (1954, 1955; 1956) applied a delta-function model of chemical binding to the calculation of energies of various systems with introduction of a branching condition and followed by Lippincott (1955, 1957) with a semi-empirical delta-function potential model. Lippincott and Dayhoff (1960) used the semi-empirical delta-function techniques in predicting vibrational frequencies, anharmonicities, bond dissociation energies and equilibrium internuclear distances. Recently, Lippincott and Stutman (1964) applied this semi-empirical model in generating component polarizabilities in order to compute the mean molecular polarizabilities for both diatomic and polyatomic molecules. The same method has been adopted here for mercury dicyanide and one may refer to Lippincott and Stutman (1964) for the detailed theoretical considerations and calculations.

The delta-function strengths  $A$ 's in atomic units, atomic polarizabilities  $\alpha$ 's in  $10^{-25} \text{ cm}^3$  and  $c$ 's in atomic units used here are as follows:  $A_{Hg} = 0.322$ ,  $A_C = 0.757$ ,  $A_N = 0.927$ ,  $\alpha_{H_0} = 178.05$ ,  $\alpha_C = 13.7$ ,  $\alpha_N = 7.43$ ,  $c_{Hg} = 1.675$ ,  $c_C = 3.028$  and  $c_N = 4.146$ . The molecular polarizability is composed mainly of bond parallel components and bond perpendicular components. The contribution to the bond parallel component by the bond region electrons is given as  $\alpha_{||b} = 4nA_{12}(1/a_0)(\langle x^2 \rangle)^2$  where  $n$  is the bond order,  $A_{12}$  the root mean-square delta-function strengths of the two nuclei involved and  $\langle x^2 \rangle$  the mean-square position of a bonding electron expressed as  $\langle x^2 \rangle = (R^2/4) + (1/2c_{R_1})$  where  $R$  is the equilibrium internuclear distance and  $c_{R_1}$  the root mean-square value of  $c_{R_1}$  and  $c_{R_2}$ . The calculated values of polarizability components in  $10^{-25} \text{ cm}^3$

for the  $C \equiv N$  and  $Hg-C$  bonds are 22.245 and 58.926 respectively. In the case that the bond is of heteronuclear type, a polarity correction is introduced using the Pauling's scale of electronegativities (1960) to determine the percent covalent character. The calculated value of the polarizability component for the  $Hg-C$  bond after introducing the polarity correction is  $53.854 \times 10^{-25} \text{ cm}^3$ . Because of greater electronic distribution in the bond region, no polarity correction is introduced for the  $C \equiv N$  bond. The contribution by the nonbond region electrons to the parallel components of the total system is calculated from the remaining electrons in the valence shell of each atom not involved in bonding from the expression  $\Sigma \alpha_{\parallel n} = \Sigma f_j \alpha_j$  where  $f_j$  is the fraction of electrons in the  $j$ -th atom not involved in bonding and  $\alpha_j$  the atomic polarizability of the  $j$ -th atom; and the basis for such calculation is the Lewis-Langmuir octet rule (1916) modified by Linnett (1961) as a double-quartet of electrons. Accordingly, each nitrogen in mercury dicyanide has only two valence electrons which are not involved in bonding while the other atoms have no valence electrons left unshared. Hence,  $\Sigma \alpha_{\parallel n} = (4/5)\alpha_N = 5.944 \times 10^{-25} \text{ cm}^3$ . The perpendicular component of a diatomic molecule is simply the sum of two atomic polarizabilities, i.e.,  $\alpha_{\perp} = 2\alpha_A$  for a nonpolar  $A_2$  molecule and  $\alpha_{\perp} = 2(X_A^2\alpha_A + X_B^2\alpha_B)/(X_A^2 + X_B^2)$  for an  $A-B$  molecule where  $X$  refers to the electronegativity of the atom. Extending this to polyatomic molecule, the sum of all the perpendicular components is given as  $\Sigma 2\alpha_{\perp} = n_{df}(\Sigma X_j^2 \alpha_j)/(X_j^2)$  where  $n_{df}$  is the number of residual atomic polarizability degrees of freedom.  $n_{df}$  is directly obtained from the configuration of a molecule and the assumption that each isolated atom possesses three polarizability degrees of freedom and every bond removes two of these three degrees of freedom with exception that (1) if two bonds are formed from the same atom and exist in a linear configuration, three atomic degrees of freedom are lost and (2) if three bonds are formed from the same atom and exist in a planar configuration, only five atomic degrees of freedom are lost. Accordingly,  $n_{df}$  is 5 for water, 6 for hydrogen cyanide, 7 for methane, 8 for acetylene, 9 for sulphur hexafluoride and 10 for mercury dicyanide (Fig. 1). Hence,  $\Sigma 2\alpha_{\perp} = 277.851 \times 10^{-25} \text{ cm}^3$  for mercury dicyanide. The mean or average molecular polarizability is obtained in terms of the parallel bond, nonbond region electron and perpendicular bond contributions from the following expression:  $\alpha_M = (1/3)(\Sigma \alpha_{\parallel p} + \Sigma \alpha_{\parallel n} + \Sigma 2\alpha_{\perp})$ . The calculated value of the molecular polarizability for mercury dicyanide is given as  $145.331 \times 10^{-25} \text{ cm}^3$ .

Lippincott, Nagarajan and Stutzman (1966) carried out the polarizability calculations for various polyatomic molecules and their values of bond parallel components in  $10^{-25} \text{ cm}^3$  for the  $C \equiv N$  bond are 22.57 in cyanogen, 22.585 in methyl cyanide, 23.272 in methyl isocyanide and 23.183 in fluorine cyanide. These values are well comparable in magnitude with the one obtained here for the  $C \equiv N$  bond. Hence, the bond parallel components could be transferred from one molecular system to another having similar chemical bonds with nearly identi-

cal internuclear distances. The small changes in the values of bond parallel components for the same bond appear above may be due to the slightly different values of the internuclear distances as the bond parallel component is roughly proportional to the fourth power of the internuclear distance. According to Lippincott, Nagarajan and Stutman (1966), the values of bond parallel components in  $10^{-25} \text{ cm}^3$

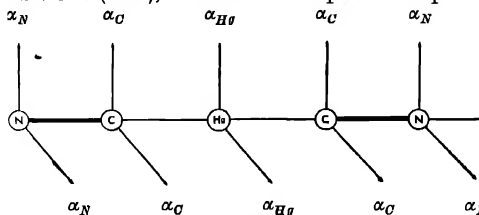


Fig 1. Residual atomic polarizability degrees of freedom for mercury dicyanide.

are 13.899 for the C—N bond in formamide and 18.937 for the C = N bond in hydrogen isocyanate and according to the present investigation it is 22.245 for the  $\text{C} \equiv \text{N}$  bond in mercury dicyanide. The values, as is expected, are in the increasing order with the increase in bond order. The values of bond parallel components for the C—N multiple bonds are in the increasing order roughly in the ratio 14 : 19 : 22. If the  $\pi$  and  $\sigma$  electrons equally contribute to the bond parallel component, the values for the double and triple bonds should be twice and thrice the value for the single bond. Actually the contribution to the bond parallel component by the electrons occupied in the  $\pi$ -orbital is much less than that of the electrons occupied in the  $\sigma$ -orbital. The increment in the bond polarizability from the  $\sigma$  system to the  $\sigma + \pi$  one is greater than that from the  $\sigma + \pi$  system to the  $\sigma + 3\pi$  one. Refractive index for mercury dicyanide is not available either in the gaseous state or in the liquid state but in the crystalline form. Uniaxial crystals have two refractive indices, one of the rays vibrating parallel to the optic axis and another at right angles to this direction. If the extraordinary ray is greater than the ordinary one in a uniaxial substance, the substance is optically positive; if the reverse is true, negative. Uniaxial crystals may be considered simply as a small group of biaxial crystals which have three refractive indices, two lying in one plane and the third in another plane of the particle. These indices are identified by  $\alpha$ ,  $\beta$ ,  $\gamma$  for the least, intermediate and the greatest index respectively of the substance. If  $\beta$  is equal to  $\alpha$ , the crystal is optically positive and to  $\gamma$ , negative. Since mercury dicyanide comes under this category and has a tetragonal system, it has two refractive indices. The experimental values of these two refractive indices have been given by Lange (1952) and their values are 1.645 for the ordinary ray and 1.492 for the extra-ordinary ray. Using 252.646 as the molecular weight and 4 as the density, the molecular polarizability was calculated from the well-known Lorentz-Lorenz equation and its values are given as follows :  $152.67 \times 10^{-25} \text{ cm}^3$  for the ordinary ray and  $95.121 \times 10^{-25} \text{ cm}^3$  for the extraordinary ray. The calculated

value of molecular polarizability is in fairly good agreement with the experimental one for the ordinary ray.

#### ABSOLUTE RAMAN INTENSITIES OF $\Sigma_g^+$ MODES

One of the best applications of the relationships, namely, the  $R^2$ -dependence of the parallel component and the  $R$ -independent form of the perpendicular component of the polarizability in the neighbouring spectroscopic domains immediately appears to the evaluation of the absolute intensity of a Raman line which is proportional to  $(\delta\alpha/\delta Q)^2$ , the square of the change in the polarizability during a vibration. If one could obtain values for the internuclear separations before and after a vibrational transition, one would then be able to calculate the absolute intensity of a Raman line. To a first approximation from the delta-function potential model, only the bond parallel component need be considered to obtain  $(\delta\alpha/\delta Q)$  through well defined transformation  $(\delta\alpha/\delta R)$  where  $Q$  and  $R$  refer to normal mode and internuclear distance at the equilibrium configuration. It is aimed here to obtain  $(\delta\alpha/\delta R)$  for the symmetrical stretching mode of a polyatomic molecule and then apply to the  $\Sigma_g^+$  modes of oscillation in the ground electronic state of mercury dicyanide.

The polarizability derivative may be obtained by differentiating the analytical expression<sup>8</sup> for the parallel component of the polarizability  $\alpha_{\parallel\mu} = 4\pi A_{12}\sigma$

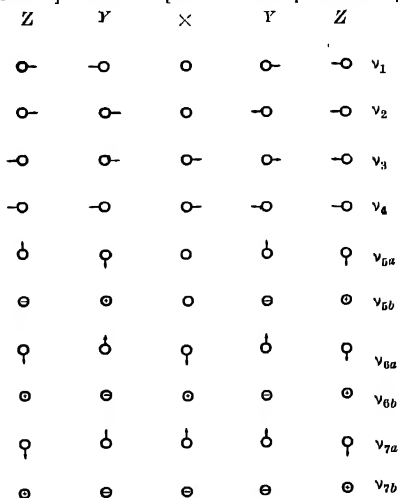


Fig. 2. Schematic representation of the normal modes of oscillation in a linear symmetrical  $X(YZ)_2$  molecule. The positive signs designate the motions in the  $xz$  plane while the negative ones designate the same in the  $yz$  plane or vice versa.

$(1/a_0)\langle x^2 \rangle$  with respect to the internuclear distance  $R$  and neglecting terms of small magnitude and thus the obtained expression is given as  $(\delta\alpha_{\parallel p}/\delta R) = nA_{12}\sigma(1/a_0)(R^3)$ . Here only negligible errors have been introduced by assuming a contribution from only the leading term in the expression for  $\langle x^2 \rangle$ . The molecular polarizability of a diatomic molecule is generally written as a contribution from purely bond parallel and perpendicular components, i.e.,  $\alpha_M = (1/3)(\alpha_{\parallel p} + 2\alpha_{\perp})$ . The necessary desired quantity is the change in molecular polarizability due to the symmetrical stretching of the bond and in obtaining this, the following important features of the delta-function potential model have to be considered: Firstly,  $(\delta\alpha_M/\delta R) = (1/3)(\delta\alpha_{\parallel}/\delta R)$ ; in other words, the change is one-dimensional and secondly  $(\delta\alpha_{\parallel}/\delta R) = (\delta\alpha_{\parallel p}/\delta R)$ ; in other words, there is virtually no contribution from the nonbond region electrons. The quantity  $(\delta\alpha_{\parallel p}/\delta R)^2$  is assumed to be directly proportional to the absolute Raman intensity of the stretching mode in the ground electronic state of a given molecule. Hence the analytical expression for the polarizability derivative with respect to the internuclear distance is given as follows.

$(\delta\alpha/\delta R) = (1/3)(\delta\alpha_{\parallel}/\delta R) = (1/3)(\delta\alpha_{\parallel p}/\delta R) = nA_{12}\sigma(1/3a_0)(R^3)$ . Since the delta-function potential model allows no interaction between neighboring bonds, the analytical expression described above is also applicable for a bond in a polyatomic molecule.

Since the absolute intensities of Raman lines due to the symmetrical C—N and Hg—C stretching vibrations depend on the derivatives of the polarizabilities of the respective bonds, such calculations were made from the above equation using the internuclear distances, delta-function strengths, Bohr radius etc given earlier. The calculated values of the polarizability derivatives in  $\text{\AA}^2$  for the C—N and Hg—C bonds are 2.408 and 3.12, respectively. There is no experimental value of the polarizability derivative for the Hg—C bond but the C—N bond. The experimental value of the polarizability derivative  $2.61 \text{\AA}^2$  reported by Chantry and Plane (1961) for the C $\equiv$ N bond in acetonitrile is in comparable magnitude with calculated one here and thus the polarizability derivatives are in general transferable, as in the cases of bond parallel components, from one molecular system to another having similar chemical bonds with nearly identical internuclear distances. The bond region electrons are alone involved in the calculations of polarizability derivatives but the nonbond region electrons have no influence at all on the polarizability derivatives. The polarizability derivative is a dependent function of the internuclear distance as in the case of the bond parallel component of the polarizability but with third power.

#### MEAN AMPLITUDES OF VIBRATION

A molecule or ion of the  $X(YZ)_2$  type possessing a linear symmetrical structure with the symmetry point group  $D_{\infty h}$  gives rise, according to the relevant symmetry considerations and selection rules, to ten vibrational degrees of freedom consti-

tating only seven fundamental frequencies which are distributed under the various irreducible representations as follows:  $2\Sigma_g^+(R, p) + 3\Sigma_g^+(I, \parallel) + \pi_g(R, dp) + 2\pi_u(I, \perp)$  where  $R, I, p, dp, \parallel$ , and  $\perp$  stand for Raman active, infrared active, polarized, depolarized, parallel and perpendicular, respectively; the subscript  $g$  represents the gerade modes which are symmetric with respect to the centre of symmetry while  $u$  the ungerade ones which are asymmetric with respect to the centre of symmetry. The  $\Sigma$  type vibrations are the nondegenerate while the  $\pi$  type vibrations are the degenerate ones. The frequency  $\nu_1$  corresponds to the  $Y \equiv Z$  stretching vibration,  $\nu_2$  to the  $X-Y$  symmetrical stretching vibration,  $\nu_3$  to the symmetrical  $Y \equiv Z$  symmetrical stretching vibration,  $\nu_4$  to the  $X-Y$  asymmetrical stretching vibration,  $\nu_5$  to the  $X-\hat{Y}-Z$  asymmetrical bending vibration  $\nu_6$  to the  $X-\hat{Y} \equiv Z$  symmetrical bending vibration and  $\nu_7$  to the  $Y-\hat{X}-Y$  symmetrical bending vibration. A schematic representation of the normal modes of oscillation for a linear symmetrical molecule of  $X(YZ)_2$  type has been given in Fig. 2.

Ten internal coordinates have been selected here to describe the ten vibrational degrees of freedom and they are given as follows:  $r_1$  and  $r_2$  are the  $Y-Z$  stretching coordinates,  $d_1$  and  $d_2$  are the  $X-Y$  stretching coordinates;  $\theta_1$  and  $\theta_2$  designate the  $X-\hat{Y} \equiv Z$  bending coordinates in the  $xz$  plane while  $\theta_1'$  and  $\theta_2'$  designate the same in the  $yz$  plane;  $\phi$  designates the  $Y-\hat{X}-Y$  bending coordinate in the  $xz$  plane while  $\phi'$  designates the same in the  $yz$  plane (see Fig. 3). The

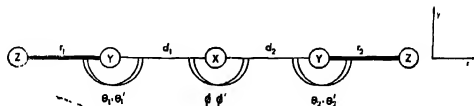


Fig. 3. Geometric illustration of the internal coordinates for a linear symmetrical  $X(YZ)_2$  molecule. The symbols denote the deviations from the values at the equilibrium configuration.  $\theta$  and  $\phi$  designate the changes of the  $\hat{X}-Y \equiv Z$  and  $\hat{Y}-X-Y$  angle bendings in the  $xz$  plane while  $\theta'$  and  $\phi'$  designate the same in the  $yz$  plane or vice versa. The equilibrium  $X-Y$  and  $Y \equiv Z$  internuclear distances are identified by the symbols  $D$  and  $R$ , respectively.

equilibrium internuclear distances  $Y \equiv Z$  and  $X-Y$  are being represented by the symbols  $R$  and  $D$ , respectively. On the basis of the principle postulated by Wilson (1939, 1941), a set of symmetry coordinates satisfying the conditions of normalization, orthogonality and transformations of the concerned irreducible representations has been constructed with help of the internal coordinates described above and given in the following:

$$S_1(\Sigma_g^+) = (2)^{-1/2}(r_1 + r_2)$$

$$S_2(\Sigma_g^+) = (2)^{-1/2}(r_1 - r_2)$$

$$S_d(\Sigma_u^+) = (2)^{-1/2}(d_1 - d_2)$$

$$S_d(\Sigma_u^+) = (2)^{-1/2}(\theta_1 - \theta_2)$$

$$S_{5a}(\pi_g) = RD(2)^{-1/2}(\theta_1' - \theta_2')$$

$$S_{5b}(\pi_g) = RD(2)^{-1/2}(\theta_1 + \theta_2)$$

$$S_{6a}(\pi_u) = RD(2)^{-1/2}(\theta_1 + \theta_2)$$

$$S_{6b}(\pi_u) = RD(2)^{-1/2}(\theta_1' + \theta_2')$$

$$S_{7a}(\pi_u) = D\phi$$

$$S_{7b}(\pi_u) = D\phi'$$

Here the angle displacements are multiplied by the equilibrium internuclear distances  $R(Y-Z)$  and  $D(X-Y)$  in order to keep the dimensions of the mean-square amplitude quantities referring to the angle bending the same as those of the quantities due to the bonded atom pairs.

For a molecule or ion of the present study we will have sixteen mean-square amplitude quantities ( $\sigma$ ) but the symmetry of the molecular or ionic system reduces to ten. The mean-square amplitude quantities due to the interaction between the bonded atom pairs and interbond angles are not at all permitted in this case as the parallel and perpendicular vibrations do not occur in the same symmetry species. Following the principle outlined by Cyvin (1959), the symmetrized mean-square amplitude matrices ( $\Sigma$ ) in terms of the mean-square amplitude quantities ( $\sigma$ ) have been obtained by introducing the symmetry coordinates as follows :

$$\Sigma_{11}(\Sigma_g^+) = \langle S_1^2 \rangle = \sigma_r + \sigma_n$$

$$\Sigma_{22}(\Sigma_g^+) = \langle S_2^2 \rangle = \sigma_d + \sigma_{dd}$$

$$\Sigma_{12}(\Sigma_g^+) = \Sigma_{21}(\Sigma_g^+) = \langle S_1 S_2 \rangle = \sigma_{rd} + \sigma_{rd}$$

$$\Sigma_{33}(\Sigma_u^+) = \langle S_3^2 \rangle = \sigma_r - \sigma_n$$

$$\Sigma_{44}(\Sigma_u^+) = \langle S_4^2 \rangle = \sigma_{dd} - \sigma_{dd}$$

$$\Sigma_{34}(\Sigma_u^+) = \Sigma_{43}(\Sigma_u^+) = \langle S_3 S_4 \rangle = \sigma_{rd} - \sigma_{rd}$$

$$\Sigma_{55}(\pi_g) = \langle S_{5a}^2 \rangle = \langle S_{5b}^2 \rangle = \sigma_\theta - \sigma_{\theta\theta}$$

$$\Sigma_{66}(\pi_u) = \langle S_{6a}^2 \rangle = \langle S_{6b}^2 \rangle = \sigma_\theta + \sigma_{\theta\theta}$$

$$\Sigma_{77}(\pi_u) = \langle S_{7a}^2 \rangle = \langle S_{7b}^2 \rangle = \sigma_\phi$$

$$\Sigma_{67}(\pi_u) = \Sigma_{76}(\pi_u) = \langle S_{6a} S_{7a} \rangle = \langle S_{6b} S_{7b} \rangle = (2)^{1/2} \sigma_{\theta\phi}$$

where the entering quantities may be defined by the mean values given in the following :

$$\sigma_r = \langle r_1^2 \rangle = \langle r_2^2 \rangle$$

$$\sigma_n = \langle r_1 r_2 \rangle$$

$$\sigma_d = \langle d_1^2 \rangle = \langle d_2^2 \rangle$$



$$\sigma_{dd} = \langle d_1 d_2 \rangle$$

$$\sigma_{rd} = \langle r_1 d_1 \rangle = \langle r_2 d_2 \rangle$$

$$\sigma_{rd} = \langle r_1 d_2 \rangle = \langle r_2 d_1 \rangle$$

$$\sigma_0 = RD \langle \theta_1^2 \rangle = RD \langle \theta_2^2 \rangle = RD \langle (\theta_1')^2 \rangle = RD \langle (\theta_2')^2 \rangle$$

$$\sigma_{\theta\theta} = RD \langle \theta_1 \theta_2 \rangle = RD \langle \theta_1' \theta_2' \rangle$$

$$\sigma_\phi = D^2 \langle \phi^2 \rangle = D^2 \langle (\phi')^2 \rangle$$

$$\sigma_{\theta\phi} = (RD^2)^2 \langle \theta_1 \phi \rangle = (RD^2)^2 \langle \theta_2 \phi \rangle = (RD^2)^2 \langle \theta_1' \phi' \rangle = (RD^2)^2 \langle \theta_2' \phi' \rangle$$

TABLE I

Fundamental frequencies in  $\text{cm}^{-1}$  and internuclear distances in  $\text{\AA}$  in some linear dicyanides

Molecule or Ion	$\nu_1(\Sigma_g^+)$	$\nu_2(\Sigma_g^+)$	$\nu_3(\Sigma_u^+)$	$\nu_4(\Sigma_u^+)$	$\nu_5(\pi_g)$	$\nu_6(\pi_u)$	$\nu_7(\pi_u)$	$X-Y$	$Y-Z$
$\text{Ag}(\text{CN})_2$	2141	360	2140	390	250	310	107	2.13	1.16
$\text{Au}(\text{CN})_2$	2164	452	2141	427	304	368	100	2.10	1.16
$\text{Hg}(\text{CN})_2$	2198	412	2194	442	276	341	100	2.20	1.15

The analytical expressions for the mean-square amplitudes of vibration for the nonbonded atom pairs may be obtained in terms of the symmetrized mean-square amplitude matrices as follows.

$$\sigma_{r+dd} = \frac{1}{2}(\Sigma_{11} + \Sigma_{22} + \Sigma_{33} + \Sigma_{44}) + \Sigma_{12} + \Sigma_{34}$$

$$\sigma_{r+2d} = \frac{1}{2}(\Sigma_{11} + 4\Sigma_{22} + \Sigma_{33}) + 2\Sigma_{12}$$

$$\sigma_{2r+2d} = 2\Sigma_{11} + 2\Sigma_{22} + 4\Sigma_{12}$$

$$\sigma_{2d} = 2\Sigma_{22}$$

where  $\sigma_{r+dd}$  is the mean-square amplitude quantity due to the nonbonded atom pair  $Z-X$ ,  $\sigma_{r+2d}$  the quantity due to the nonbonded atom pair  $Z-Y$ ,  $\sigma_{2r+2d}$  the quantity due to the nonbonded atom pair  $Z-Z$  and  $\sigma_{2d}$  the quantity due to the nonbonded atom pair  $Y-Y$ .

On the basis of the principle postulated by Wilson (1939, 1941) and Ferigle and Meister (1951), the  $G$  matrix elements related to the kinetic energy were obtained in terms of the symmetry coordinates given above. In the analysis of the molecular vibrations, Cyvin (1959) was the first to introduce the symmetry coordinates in determining the mean-square amplitudes of vibration. According to his secular equation  $|\Sigma G^{-1} - E\Delta| = 0$ , the following equations for the normal frequencies containing the symmetrized mean-square amplitude matrices have been constructed under the various irreducible representations.

TABLE II

Symmetrized mean-square amplitude matrices in Å<sup>2</sup> in some linear dicyanides

Molecule or ion	Element	Symmetrized mean-square amplitude matrix	
		<i>T</i> = 298°K	<i>T</i> = 500°K
Ag(CN) <sub>2</sub> <sup>-</sup>	Σ <sub>11</sub>	0 0038026	0 0061755
	Σ <sub>22</sub>	0.0008223	0.0007461
	Σ <sub>33</sub>	0.0043439	0.0067080
	Σ <sub>44</sub>	0.0009400	0.0008846
	Σ <sub>55</sub>	0 0252060	0.0392141
	Σ <sub>66</sub>	0.0317268	0 0468469
	Σ <sub>77</sub>	0 0145846	0 0201913
	Σ <sub>87</sub>	0 0063895	0 0082748
Au(CN) <sub>2</sub> <sup>-</sup>	Σ <sub>11</sub>	0 0019492	0 0036935
	Σ <sub>22</sub>	0.0016494	0.0008205
	Σ <sub>33</sub>	0.0031508	0 0050632
	Σ <sub>44</sub>	0 0009583	0 0008516
	Σ <sub>55</sub>	0 0146437	0 0220567
	Σ <sub>66</sub>	0.0226605	0 0342683
	Σ <sub>77</sub>	0 0113754	0.0164755
	Σ <sub>87</sub>	0 0051476	0 0071886
Hg(CN) <sub>2</sub>	Σ <sub>11</sub>	0 0027272	0.0046519
	Σ <sub>22</sub>	0.0009037	0.0007603
	Σ <sub>33</sub>	0 0029152	0.0046504
	Σ <sub>44</sub>	0 0009537	0.0008389
	Σ <sub>55</sub>	0.0171536	0.0264093
	Σ <sub>66</sub>	0.0259675	0.0383644
	Σ <sub>77</sub>	0 0147568	0 0192256
	Σ <sub>87</sub>	0 0069249	0 0086958

For the type Σ<sub>*y*</sub><sup>+</sup> vibrations :

$$\Delta_1 + \Delta_2 = [\Sigma_{11} + \Sigma_{22}(\mu_y + \mu_z)\mu_y^{-1} + 2\Sigma_{12}]\mu_z^{-1}$$

$$\Delta_1 \Delta_2 = (\Sigma_{11}\Sigma_{22} - \Sigma_{12}^2)\mu_y^{-1}\mu_z^{-1}$$

TABLE III

Mean-square amplitude quantities in Å<sup>2</sup> in some linear dicyanides

Quantity	Ag(CN) <sub>2</sub> <sup>-</sup>		Au(CN) <sub>2</sub> <sup>-</sup>		Hg(CN) <sub>2</sub>	
	T = 298°K	T = 500°K	T = 298°K	T = 500°K	T = 298°K	T = 500°K
$\sigma_r$	0.0040733	0.0064418	0.0025500	0.0043784	0.0028212	0.0046512
$\sigma_{rr}$	-0.0002707	-0.0002663	-0.0006008	-0.0006848	-0.0000940	0.0000008
$\sigma_d$	0.0008812	0.0008154	0.0010039	0.0008360	0.0009287	0.0007996
$\sigma_{dd}$	-0.0000589	-0.0000693	0.0000456	0.0000156	-0.0000250	-0.0000393
$\sigma_{\rho}$	0.0284064	0.0430305	0.0187566	0.0281625	0.0215606	0.0323869
$\sigma_{\rho\rho}$	0.0032604	0.0038164	0.0041129	0.0061058	0.0044070	0.0059776
$\sigma_{\phi}$	0.0145846	0.0201943	0.0113754	0.0164755	0.0147568	0.0192250
$\sigma_{\phi\phi}$	0.0063895	0.0083748	0.0051476	0.0071886	0.0069249	0.0086958
$\sigma_{2d}$	0.0018446	0.0014922	0.0020988	0.0016410	0.0018074	0.0015206
$\sigma_{r+d}$	0.0049544	0.0072571	0.0035539	0.0052144	0.0037499	0.0054508
$\sigma_{r+2d}$	0.0057179	0.0079340	0.0040488	0.0060194	0.0046286	0.0061718
$\sigma_{2r+2d}$	0.0092498	0.0038432	0.0059972	0.0090280	0.0072618	0.0108244

For the type  $\Sigma_u^+$  vibrations :

$$\Delta_3 + \Delta_4 = \Sigma_{33}(2\mu_x + \mu_y) + \Sigma_{44}(\mu_y + \mu_z) + 2\Sigma_{34}\mu_y(2\mu_x\mu_y + 2\mu_x\mu_z + \mu_y\mu_z)^{-1}$$

$$\Delta_3\Delta_4 = (\Sigma_{33}\Sigma_{44} - \Sigma_{34}^2)(2\mu_x\mu_y + 2\mu_x\mu_z + \mu_y\mu_z)^{-1}$$

For the type  $\pi_g$  vibration :

$$\Delta_5 = \Sigma_{55}[(\mu_z/R^2) + \mu_y\{(1/R) + (1/D)\}^2]^{-1}$$

For the type  $\pi_u$  vibrations :

$$\Delta_6 + \Delta_7 = \Sigma_{66}K^{-1} + \Sigma_{77}L^{-1} + 2\Sigma_{67}M^{-1}$$

$$\Delta_6\Delta_7 = (\Sigma_{66}\Sigma_{77} - \Sigma_{67}^2)[K^{-1}L^{-1} - (M^{-1})^2]$$

where  $\mu_x$ ,  $\mu_y$  and  $\mu_z$  are the reciprocal masses of the atoms X, Y and Z, respectively;

$$K = \mu_z(1/R^2) + \mu_y\{(1/R) + (1/D)\}^2 + 2\mu_x(1/D^2) ; L = 2(2\mu_x + \mu_y)(1/D^2) \text{ and}$$

$$M = -2[\mu_y(1/D)\{(1/R) + (1/D)\} + 2\mu_x(1/D^2)].$$

In the above equations  $\Delta$  has been related to the normal frequency  $\nu$  as

$$\Delta_i = (\hbar/8\pi^2\nu_i) \coth(\hbar\nu_i/2kT)$$

where  $k$  is the Boltzmann constant and  $T$  the temperature in °K

The secular equations giving the normal frequencies in terms of the mean-square amplitude quantities were constructed with help of the vibrational and structural data given in Table I at the temperatures  $T = 298^\circ\text{K}$  and  $T = 500^\circ\text{K}$ . The off-diagonal elements under the symmetry species  $\Sigma_g^+$  and  $\Sigma_u^+$  were neglected

TABLE IV

Mean amplitudes of vibration in Å in some linear dicyanides

Molecule or ion	Distance	Mean amplitude of vibration	
		$T=298^\circ K$	$T=500^\circ K$
$Ag(CN)_2^-$	C $\equiv$ N	0.0638	0.0803
	Ag-C	0.0297	0.0286
	C - - C	0.0406	0.0386
	Ag - - N	0.0704	0.0852
	C - - N	0.0756	0.0891
	N - - N	0.0962	0.1177
$Au(CN)_2^-$	C $\equiv$ N	0.0505	0.0662
	Au-C	0.0317	0.0289
	C - - C	0.0458	0.0405
	Au - - N	0.0506	0.0722
	C - - N	0.0682	0.0776
	N - - N	0.0774	0.0950
$Hg(CN)_2$	C $\equiv$ N	0.0531	0.0682
	Hg-C	0.0305	0.0283
	C - - C	0.0425	0.0390
	Hg - - N	0.0612	0.0738
	C - - C	0.0680	0.0786
	N - - N	0.0852	0.1040

and only the diagonal elements  $\Sigma_{11}$ ,  $\Sigma_{22}$ ,  $\Sigma_{33}$  and  $\Sigma_{44}$  were evaluated. Since the equation is singular under the species  $\pi_g$ , the symmetrized mean-square amplitude matrix  $\Sigma_{66}$  was directly evaluated. When the off-diagonal element was neglected under the species  $\pi_u$ , the equations resulted to imaginary values for the diagonal elements. Hence the off-diagonal element was taken into consideration and the symmetrized mean-square amplitude matrices  $\Sigma_{66}$ ,  $\Sigma_{77}$  and  $\Sigma_{67}$  were evaluated in the manner described by Torkington (1949, 1951). The computed values of the symmetrized mean-square amplitude matrices in Å<sup>2</sup> for the three dicyanides are given in Table II at the temperatures  $T = 298^\circ K$  and  $T = 500^\circ K$ . The calculated values of the mean-square amplitude quantities in Å<sup>2</sup> are given in Table III at the two temperatures where  $\sigma_r$  is the mean-square amplitude quantity due to the bonded atom pair  $Y \equiv Z$ ,  $\sigma_d$  the quantity due to the bonded atom pair  $X-Y$ ,

$\sigma_\theta$  the quantity due to the bending  $X-\hat{Y} \equiv Z$ ,  $\sigma_\phi$  the quantity due to the bending  $Y-\hat{X}-Y$  and  $\sigma_{rr}$ ,  $\sigma_{dd}$  and  $\sigma_{\theta\theta}$  are the respective interaction quantities. The meaning of the quantities  $\sigma_{2d}$ ,  $\sigma_{r+d}$ ,  $\sigma_{r+2}$  and  $\sigma_{2r+2d}$  has already been explained earlier. The corresponding calculated values of the mean amplitudes of vibration in Å for the bonded as well as nonbonded atom pairs are given in Table IV at the two temperatures for the three dicyanides. Since the interaction quantities between the bonded atom pairs and nonbonded atom pairs are not essential, they are not considered here.

The mean amplitude of vibration for the nonbonded atom pair, as is expected, is much greater than that of the bonded atom pair. The mean-square amplitude quantity due to the bending is in general several times greater than those of the bonded and nonbonded atom pairs. The situation is exactly reversed in the cases of corresponding force constants. The interaction quantities due to the bonded atom pairs are much smaller than that of the quantity due to the interaction of bendings. The mean-square amplitude quantities are in general in the increasing order with increasing temperature except for those due to the metal-carbon and carbon-carbon bonds. The mean amplitude of vibration for the metal-carbon bond is much smaller than that of the carbon-nitrogen bond. Gold dicyanide ion is isoelectronic with mercury dicyanide. The atomic numbers of the central atoms are in the increasing order by one unit while those of the other atoms are fixed in the two systems. The obtained values of the mean amplitudes of vibration for the bonded as well as nonbonded atom pairs are in the increasing order, in contrast to the gaseous molecules and ions, from gold dicyanide ion to mercury dicyanide except for those due to the metal-carbon and carbon-carbon bonds. This shows that the binding force between atoms in mercury dicyanide is greater than that in gold dicyanide ion. In the cases of gaseous molecules and ions the mean amplitudes of vibration will be in the increasing order when we go from a system with lower molecular or ionic weight to the one with higher molecular or ionic weight. In contrast to this, we observe a decrease in the values of mean amplitudes of vibration for the bonded and nonbonded atom pairs from silver dicyanide ion to gold dicyanide ion. This shows in the cases of crystals that the binding force between the atoms in a unit with higher molecular or ionic weight is less than that in the one with lower molecular or ionic weight irrespective of the nature (molecular or ionic) of the two systems concerned. Since experimental values of mean amplitudes of vibration for any of the systems studied here are not available, no comparison could be made at the moment with the results of the present study. However, the values of the present investigation would be very useful for the interpretation of electron diffraction studies in future. The values of the symmetrized mean-square amplitude matrices given in Table II would be readily considered in future for the computations of mean-square parallel amplitudes, mean-square perpendicular amplitudes and mean cross products in order to obtain the shrinkages of chemical bonds for these three systems.

## REFERENCES

- Abbot, J. A. and Bolton, H. C., 1952, *J. Chem. Phys.*, **20**, 762.  
 ———, 1952, *Pro. Roy. Soc. London*, **A216**, 477.  
 Atanasoff, J. V., 1930, *Phys. Rev.*, **36**, 1242.  
 Bell, R. P. and Long, D. A., 1950, *Pro. Roy. Soc. London*, **A203**, 304.  
 Braune, H. and Engelbrecht, G., 1931, *Z. Physik Chem.*, **B11**, 409.  
 Buckingham, R. A., 1937, *Pro. Roy. Soc. London*, **A160**, 93.  
 Chantry, G. W. and Plano, R. A., 1961, *J. Chem. Phys.*, **35**, 1027.  
 Cyvin, S. J., 1959, *Spectrochimica Acta*, **15**, 828.  
 Forigo, S. M. and Meister, A. G., 1951, *J. Chem. Phys.*, **19**, 982.  
 Francois, F., 1939, *C. R. Acad. Sci. Paris*, **208**, 1002.  
 Frost, A. A., 1954, 1955, 1956, *J. Chem. Phys.*, **22**, 1613; **23**, 985; **25**, 1150.  
 Frost, A. A. and Leland, F. E., 1956, *J. Chem. Phys.*, **25**, 1154.  
 Guillemin, V. and Zener, C., 1928, *Pro. Natl. Acad. Sci. USA.*, **15**, 4, 314.  
 Halford, R. S., 1946, *J. Chem. Phys.*, **14**, 8.  
 Hanawalt, R. and Provel, 1938, *Ind. Eng. Chem. Anal. Ed.* **10**, 457.  
 Hase, H. R., 1930, 1931, *Pro. Camb. Phil. Soc.*, **26**, 542; **26**, 66.  
 Hassel, O., 1926, *Z. Krist.*, **64**, 218.  
 Hirschfelder, J. O., 1935, *J. Chem. Phys.*, **3**, 555.  
 Hoard, J. L., 1933, *Z. Krist.*, **84**, 231.  
 Hylleraas, E. A., 1930, *Z. Physik*, **65**, 209.  
 Jones, L. H., 1957, *J. Chem. Phys.*, **26**, 1958; **27**, 468, 665.  
 ———, 1963, *Spectrochimica Acta*, **19**, 1675.  
 ———, 1965, *J. Chem. Phys.*, **43**, 594.  
 Kirkwood, J. G., 1932, *Physik Z.*, **33**, 2, 57.  
 Koller, H. J. and Karplus, M., 1963, *J. Chem. Phys.*, **39**, 2011.  
 Krishnamurti, P., 1930, *Indian J. Phys.*, **5**, 651.  
 Lange, N. A., 1952, *Handbook of Chemistry*, Handbook Publishers, Inc., Sandusky, Ohio.  
 Eighth Edition.  
 Langmuir, I., 1916, *J. Am. Chem. Soc.*, **38**, 2221.  
 Lewis, G. N., 1916, *J. Am. Chem. Soc.*, **38**, 762.  
 Lannett, J. W., 1961, *J. Am. Chem. Soc.*, **83**, 2643.  
 Lippincott, E. R., 1955, 1957, *J. Chem. Phys.*, **23**, 603; **26**, 1678.  
 Lippincott, E. R. and Dayhoff, M. O., *Spectrochimica Acta*, **16**, 807.  
 Lippincott, E. R. and Stutzman, J. M., 1964, *J. Phys. Chem.*, **68**, 2926.  
 Mrowka, B., 1932, *Z. Physik*, **76**, 300.  
 Pauling, L., 1960, *The Nature of the Chemical Bond*, Cornell University Press, Ithaca  
 New York, Third Edition.  
 Petrakou, and Hochberg, 1930, *Z. Physik. Chem.*, **B8**, 440.  
 Poulet, H. and Mathieu, J. P., 1959, *C. R. Acad. Sci. Paris*, **248**, 2079.  
 Rosen, N., 1931, *Phys. Rev.*, **38**, 2099.  
 Ruedenberg, K. and Parr, R. G., 1951, *J. Chem. Phys.*, **19**, 1268.  
 Ruedenberg, K. and Scherr, C. W., 1953, *J. Chem. Phys.*, **21**, 1565.  
 Steensholt, G., 1935, *Z. Physik*, **93**, 620, **94**, 770.  
 Torkington, P., 1949, 1951, *J. Chem. Phys.*, **17**, 357; *Proc. Roy. Soc. London*, **A64**, 32.  
 Van Vleck, J. H., 1932, *Electric and Magnetic Susceptibilities*, Oxford Press, London.  
 Wang, S., 1928, *Phys. Rev.*, **31**, 579.  
 Wilson Jr., E. R., 1939, 1941, *J. Chem. Phys.*, **7**, 1047, **9**, 76.  
 Wolkstein, M., 1937, *Acta Physicochim. URSS.*, **7**, 315.  
 Woodward, L. A., 1930, *Physik. Z.*, **17**, 792.  
 Woodward, L. A. and Owen, H. F., 1959, *J. Chem. Soc.*, 1055.  
 Zhdanov, G. S. and Shugam, E. A., 1944, *C. R. Acad. Sci. URSS.*, **45**, 295.

# LOW-ENERGY SCATTERING OF ELECTRON BY ATOMIC POTENTIAL WITH A LONG-RANGE $r^{-4}$ TAIL

S. B. GUPTA AND N. C. SIL

DEPARTMENT OF THEORETICAL PHYSICS,

INDIAN ASSOCIATION FOR THE CULTIVATION OF SCIENCE,

JADAVPUR, CALCUTTA-32

(Received March 17, 1966).

**ABSTRACT** We have obtained, following Spector (1964), an expression for the  $S$ -matrix in the case of an attractive inverse fourth power potential. An effective range formula for an atomic potential with  $r^{-4}$  tail has also been derived. A general expression for phase shifts  $\eta_l$  for different angular momenta  $l$  is given for an atomic potential which is represented by a screened Coulomb potential of Allis and Morse type when  $r$  is small and the long range  $r^{-4}$  potential when  $r$  is large. Numerical results are presented for  $\eta_0$  for low energy  $e^-$ -He collision. The effect of exchange has been neglected in our work.

## INTRODUCTION

An exact analytical solution of the Schrodinger equation describing the scattering of an electron by a neutral atom is extremely difficult due to the complexity of the atomic potential. The potential surrounding the atom consists of an electrostatic screened field and a polarization field mainly of dipole nature induced by the incoming electron. The form of the latter field is usually taken as  $\alpha(r)r^{-4}$  where  $\alpha(r)$  for small values of  $r$  is a complicated function but for large values of  $r$  reduces to a constant  $\alpha$  the electric polarizability. The Schrodinger equation with a central potential  $\alpha r^{-4}$  can be solved by transforming it to a modified Mathieu equation. O'Malley, Spruch and Rosenberg (1961) have shown that in the case of a long range  $r^{-4}$  potential the expansion of  $k \cot \eta_0$  in the zero energy limit contains a number of terms not present in the usual effective range formula for short range potential. Spector (1964) has made a detailed study of the behaviour of the Mathieu function and its derivative at the transition point where the kinetic energy is equal to the magnitude of the potential energy due to the  $\alpha r^{-4}$  term. He has worked out the scattering matrix for a repulsive potential but in most physical problems the attractive potential comes into play. So we have calculated the scattering relations with an attractive  $r^{-4}$  potential. Further in the zero energy limit  $k = 0$  the expansion of  $k \cot \eta_0$  is influenced by the asymptotic form of the potential i.e.  $\alpha r^{-4}$ , the expansion terms of  $k \cot \eta_0$  agree with those of O'Malley *et al* (1961).

In the potential term in the Schrodinger equation, we have taken for the screened coulomb part the form due to Allis and Morse (1931) when  $r$  is small and

we assume that in this region the polarization potential is negligible. We further maintain that for large values of  $r$  when the latter potential becomes predominant,  $\alpha(r)$  reduces to the electric polarizability  $\alpha$  of the atom. To simplify calculation the exchange effect due to the indistinguishability of the incident and atomic electrons has been neglected. A general expression for low energy phase shift for different angular momenta has been deduced. The phase shifts for zero angular momentum are calculated for  $e^-$ -He scattering in the low energy region 0-1 ev and a comparison with similar calculations of LaBahn and Callaway (1964) shows good agreement.

#### CALCULATION OF S-MATRIX

The Schrodinger equation describing low energy scattering of an electron in presence of an attractive polarization potential  $\beta^2 r^{-4}$  is

$$\left[ \frac{d^2}{dr^2} - \frac{l(l+1)}{r^2} + \frac{\beta^2}{r^4} + k^2 \right] \phi_l = 0 \quad \dots (1)$$

Here  $k$  is the wave number of the incident electron and  $\beta^2 = \alpha$ .

(The atomic units are used throughout our calculations).

The equation (1) can easily be transformed into the Modified Mathieu equation (Spector 1964).

$$\left[ \frac{d^2}{dz^2} - (l + \frac{1}{2})^2 + 2\beta k \cosh 2z \right] M(z) = 0 \quad \dots (2)$$

with the substitutions

$$\begin{aligned} r &= (\beta/k)^{\frac{1}{2}} e^{-z} & \text{when } 0 < r \leq (\beta/k)^{\frac{1}{2}} \\ &= (\beta/k)^{\frac{1}{2}} e^z & \text{when } (\beta/k)^{\frac{1}{2}} < r < \infty \end{aligned} \quad \dots (3)$$

and

$$\phi_l(r) = \sqrt{r} M(z)$$

The solutions of the equation (2) are the various forms of the modified Mathieu functions. It will be convenient to write down those which will be required in our work.

$$M_{e\pm\nu}(z, k) = \sum_{p=-\infty}^{\infty} C_{\nu 2p}^{\nu}(k) e^{\pm(2p+\nu)z} \quad \dots (4)$$

$$M_{\nu}^{(1)}(z, k) = \left[ \sum_{p=-\infty}^{\infty} C_{\nu 2p}^{\nu}(k) \right]^{-1} \sum_{p=-\infty}^{\infty} (-1)^p C_{\nu 2p}^{\nu}(k) J_{\nu+2p}(2\sqrt{\beta k} \cosh z) \quad (5)$$

$$M_{\nu}^{(2)}(z, k) = \left[ \sum_{p=-\infty}^{\infty} C_{\nu 2p}^{\nu}(k) \right]^{-1} \sum_{p=-\infty}^{\infty} (-1)^p C_{\nu 2p}^{\nu}(k) Y_{\nu+2p}(2\sqrt{\beta k} \cosh z) \quad (6)$$

$J_{\nu}$  and  $Y_{\nu}$  are the Bessel functions of the first and second kinds. The order  $\nu$  of the Mathieu functions is a function of  $l$  and  $k$ .



When  $k$  is sufficiently small,  $\nu$  is given by

$$\nu \approx l + \frac{1}{2} - \frac{\beta^2 k^2}{4(l + \frac{3}{2})(l + \frac{1}{2})(l - \frac{1}{2})}$$

the terms involving  $k^4$  and higher powers of  $k$  being neglected. The same coefficients  $C_{2p}^\nu(k)$  which are functions of  $k$  occur in  $M_{e\perp\nu}$  or  $M_\nu^{(1),(2)}$ . These coefficients can be expressed as a continued fraction converging rapidly as  $k \rightarrow 0$ . In fact

$$C_{2p}^\nu \rightarrow C_0^\nu \frac{\Gamma(\nu+1)}{2^{2p} p! \Gamma(\nu+p+1)} (\beta k)^{2|p|} \text{ as } k \rightarrow 0 \quad (8)$$

When  $p$  is negative  $C_{2p}^\nu \rightarrow 0$  as  $k \rightarrow 0$ .

Lastly we may construct the modified Mathieu functions  $\bar{M}_\nu^{(3)}$  and  $\bar{M}_\nu^{(1)}$  from the equations (5) and (6) replacing the Bessel functions  $J_{\nu+2p}$  and  $Y_{\nu+2p}$  by the Hankel functions  $H_{\nu+2p}^{(1)}$  and  $H_{\nu+2p}^{(2)}$ .

The Mathieu functions  $M_\nu^{(1),(2)}$  and hence  $M_\nu^{(3),(4)}$  are continuous functions of  $r$  but their derivatives with respect to  $r$  do not exist at  $r = (\beta/k)^{\frac{1}{2}}$  whereas the functions  $\bar{M}_{e\pm\nu}$  and their derivatives are continuous everywhere. Because of this discontinuity of the derivatives, the general solution of the equation (1) which is a linear combination of the solutions  $M_\nu^{(1)}$ ,  $M_\nu^{(2)}$  or  $M_\nu^{(3)}$ ,  $M_\nu^{(4)}$  (each multiplied by  $\sqrt{r}$ ) should have different coefficients for  $r \leq (\beta/k)^{\frac{1}{2}}$  and  $r > (\beta/k)^{\frac{1}{2}}$ .

So the general solution of the equation (1) may be taken as

$$\phi_l(r) = A\sqrt{r}M_\nu^{(3)}\left(-\ln\left\{\left(\frac{k}{\beta}\right)^{\frac{1}{2}}r\right\}, k\right) + B\sqrt{r}M_\nu^{(4)}\left(-\ln\left\{\left(\frac{k}{\beta}\right)^{\frac{1}{2}}r\right\}, k\right),$$

$$r \leq \left(\frac{\beta}{k}\right)^{\frac{1}{2}} \quad \dots \quad (9)$$

$$\phi_l(r) = A'\sqrt{r}\bar{M}_\nu^{(3)}\left(\ln\left\{\left(\frac{k}{\beta}\right)^{\frac{1}{2}}r\right\}, k\right) + B'\sqrt{r}\bar{M}_\nu^{(4)}\left(\ln\left\{\left(\frac{k}{\beta}\right)^{\frac{1}{2}}r\right\}, k\right)$$

$$r \geq \left(\frac{k}{\beta}\right)^{\frac{1}{2}} \quad \dots \quad (10)$$

It is to be noted that when  $r$  is small,

$$\phi_l \rightarrow A\sqrt{\frac{2}{\pi\beta}} re^{i\left(\frac{\beta}{r} - \frac{\nu\pi}{2} - \frac{\pi}{4}\right)} + B\sqrt{\frac{2}{\pi\beta}} re^{-i\left(\frac{\beta}{r} - \frac{\nu\pi}{2} - \frac{\pi}{4}\right)} \quad \dots \quad (9a)$$

and when  $r$  is large

$$\phi_l \rightarrow A'\sqrt{\frac{2}{\pi k}} e^{i\left(Kr - \frac{\nu\pi}{2} - \frac{\pi}{4}\right)} + B'\sqrt{\frac{2}{\pi k}} e^{-i\left(Kr - \frac{\nu\pi}{2} - \frac{\pi}{4}\right)} \quad \dots \quad (10a)$$

It is evident from (10a) that the  $S$ -matrix for the scattering of a charged particle in the presence of an attractive long range  $\beta^2 r^{-4}$  potential is

$$S(k, l) = i \frac{A'}{B'} e^{-i\nu\pi} e^{i\ell\pi} \quad \dots (11)$$

with  $\nu$  defined in the equation (7)

To evaluate  $A'/B'$  we shall follow the procedures enunciated by Spector (1964) in his development of the  $S$ -matrix for a repulsive  $r^{-4}$  potential. In order to connect the solutions (9) and (10) at the point  $r = (\beta/k)^{\frac{1}{2}}$  where their derivatives do not exist. We shall make use of the Mathieu functions  $M_{e_{\pm\nu}}$  given in equation (4). These latter functions and their derivatives are continuous every where. For some  $r_1$  such that  $0 < r_1 < (\beta/k)^{\frac{1}{2}}$  we may write

$$A M_{\nu}^{(3)} + B M_{\nu}^{(4)} = \alpha M_{e_{\nu}} + \beta M_{e_{-\nu}}$$

and determine the constants  $\alpha$  and  $\beta$  in terms of  $A$  and  $B$  by solving above equation together with the equation

$$A M_{\nu}^{(3)'} + B M_{\nu}^{(4)'} = \alpha M'_{e_{\nu}} + \beta M'_{e_{-\nu}}$$

Similarly for some  $r_2 > (\beta/k)^{\frac{1}{2}}$  we take

$$A' M_{\nu}^{(3)} + B' M_{\nu}^{(4)} = \gamma M_{e_{\nu}} + \delta M_{e_{-\nu}}$$

and determine  $\gamma$  and  $\delta$  in terms of  $A'$  and  $B'$ . The constants  $\gamma$  and  $\delta$  can now be expressed in terms of  $\alpha$  and  $\beta$  by using the conditions for the continuity of the solution and its derivative with respect to  $r$  at  $r = (\beta/k)^{\frac{1}{2}}$  i.e. at  $z = 0$ . With

$z$  as defined in (3) we find that  $\frac{dz}{dr}$  discontinuously changes its sign at this point.

With the help of relation (4) we finally get

$$\gamma = \beta \quad \text{and} \quad \delta = \alpha.$$

Utilizing the various properties of the Mathieu functions as reported in Spector (1964) it is easy to show that

$$\frac{A'}{B'} = \frac{1 - R_l^2 (A - B e^{2i\nu\pi}) / (A - B)}{1 - R_l^2 (A e^{-2i\nu\pi} - B) / (A - B)} \quad (12)$$

where

$$R_l = \frac{M_{\nu}^{(1)}(0)}{M_{-\nu}^{(1)}(0)} \\ \simeq \left( \frac{1}{4} \beta k [\Gamma(1-\nu)/\Gamma(1+\nu)] \times (1 - \frac{1}{4} \nu \beta^2 k^2 / (1-\nu^2)^2) \right) \quad \dots (13)$$

neglecting higher powers of  $k$

For  $l = 0$

$$R_0 \simeq \beta/k \left( 1 + \frac{4}{3} \beta^2 k^2 \ln \frac{\beta k}{4} - \frac{8}{3} \beta^2 k^2 \psi(3/2) + \frac{20}{9} \beta^2 k^2 \right) \quad \dots (13a)$$

$$\psi(3/2) = 0.0365$$

Substituting the value of  $A'/B'$  in (11) one gets an expression for the  $S$ -matrix. If  $A/B$  is known, then in principle one can determine the phaseshifts  $\eta_l$  by virtue

of the relation  $S(k, l) = e^{2i\eta_l}$ . The formula (12) is of great importance in the development of the present work. It will be worth-while to note that since  $B$  is complex conjugate of  $A$ ,  $B'$  is the complex conjugate of  $A'$ .

#### E F F E C T I V E   R A N G E   F O R M U L A

We shall now utilize the formula (12) to develop in a straight forward manner an effective range formula for the scattering of an electron by a central field potential which is assumed to vanish as  $r^{-4}$  with no other long range components. For this purpose it will be convenient to take the solution of the wave equation (1) as a linear combination of  $\sqrt{r}M_\nu^{(1)}$  and  $\sqrt{r}M_\nu^{(2)}$ :

$$\phi_l = c\sqrt{r}(M_\nu^{(1)} + DM_\nu^{(2)}) \quad r \leq \left(\frac{\beta}{k}\right)^{\frac{1}{2}} \quad \dots (14)$$

$$\phi_l = c'\sqrt{r}(M_\nu^{(1)} + D'M_\nu^{(2)}) \quad r \geq \left(\frac{\beta}{k}\right)^{\frac{1}{2}} \quad \dots (15)$$

Where  $C$  and  $C'$  are the normalization constants and  $D$  and  $D'$  are arbitrary constants. It follows from the known properties of  $M_\nu^{(1)}$  and  $M_\nu^{(2)}$  (Spector 1964; Meixner and Schafko 1954) that  $\phi_l$  behaves near the origin as

$$\phi_l \sim \frac{r}{\beta} \left[ \sin \left( \frac{\beta}{r} - \frac{l\pi}{2} + \delta_l \right) - D \cos \left( \frac{\beta}{r} - \frac{l\pi}{2} + \delta_l \right) \right] \text{ for } r < \left(\frac{\beta}{k}\right)^{\frac{1}{2}} \quad \dots (16)$$

$$\delta_l = \frac{\pi \rho^* \kappa^*}{8(l+3/2)(l+1/2)(l-1/2)} \quad \dots (17)$$

In (17), the powers of  $k$  higher than two are neglected.

Now we consider an electron scattered by an atomic potential  $U(r)$  which is supposed to be central. The scattering wave functions  $u_l(r)$  satisfy the radial wave equation

$$\left[ \frac{d^2}{dr^2} - \frac{l(l+1)}{r^2} - U(r) + k^2 \right] u_l(r) = 0 \quad \dots (18)$$

We assume here that  $U(r)$  tends to  $-\beta^2 r^{-4}$  where  $r$  is sufficiently large, and that  $u_l(0) = 0$ . It is to be noticed that when  $r$  is large,  $u_l(r)$  tends to the solutions  $\phi_l(r)$  of the equation (1) to which the equation (18) is reduced when  $r \rightarrow \infty$ .

Taking  $u_l^{(1)}$ ,  $u_l^{(2)}$  and  $\phi_l^{(1)}$ ,  $\phi_l^{(2)}$  as the solutions of the equations (18) and (1) respectively for the wave numbers  $k_1$  and  $k_2$  it is easy to show that (c.f. Bethe 1959)

$$\lim_{r \rightarrow 0} \left| \phi_l^{(1)} \frac{d}{dr} \phi_l^{(2)} - \phi_l^{(2)} \frac{d}{dr} \phi_l^{(1)} \right|_r = (k_2^2 - k_1^2) \int_0^\infty (\phi_l^{(1)} \phi_l^{(2)} - u_l^{(1)} u_l^{(2)}) dr \quad \dots (19)$$

If  $D_1$  and  $D_2$  be the values of  $D$  in the equation (14) and  $\delta_l^{(1)}$  and  $\delta_l^{(2)}$  the values of  $\delta_l$  corresponding to the wave numbers  $k_1$  and  $k_2$ , the equation (19) leads to

$$\left(\frac{D_1 - D_2}{\beta}\right) \cos(\delta_l^{(1)} - \delta_l^{(2)}) - \frac{1 + D_1 D_2}{\beta} \sin(\delta_l^{(1)} - \delta_l^{(2)}) \\ = (k_2^2 - k_1^2) \int_0^\infty (\phi_l^{(1)} \phi_l^{(2)} - u_l^{(1)} u_l^{(2)}) dr$$

so that when  $k_1 = 0$  and  $k_2 = k$  one has

$$\left(\frac{D_0 - D}{\beta}\right) \cos \delta_l + \frac{1 + D_0 D}{\beta} \sin \delta_l = k^2 \int_0^\infty (\phi_l^{(0)} \phi_l - u_l^{(0)} u_l) dr \quad \dots \quad (20)$$

Therefore following Bothe (1949) we have for the effective range formula

$$\frac{D_0 - D}{\beta} + \frac{1 + D_0 D}{\beta} \sin \delta_l \approx \frac{1}{2} r_e k^2 \quad \dots \quad (21)$$

where the effective range

$$r_e = 2 \cdot \int [\{\phi_0^{(0)}\}^2 - \{u_0^{(0)}\}^2] dr \quad \dots \quad (22)$$

Now we propose to determine a formula from which  $D/\beta$  and  $D_0/\beta$  can be calculated.

Substituting the relations

$$M_\nu^{(1)} = \frac{1}{2} [M_\nu^{(3)} + M_\nu^{(4)}]$$

and

$$M_\nu^{(2)} = \frac{1}{2i} [M_\nu^{(3)} - M_\nu^{(4)}]$$

in the equations (14) and (15) we get from the equation (12) on simplification

$$D' = \frac{R_l^2(1 + \cos 4\delta_l + D \sin 4\delta_l)}{2D - R_l^2(D - D \cos 4\delta_l + \sin 4\delta_l)} \quad \dots \quad (23)$$

Again comparing the asymptotic form of  $\phi_l$  in (14) :

$$C' \sqrt{\frac{2}{\pi k}} \left[ \sin \left( kr - \frac{l\pi}{2} + \delta_l \right) - D' \cos \left( kr - \frac{l\pi}{2} + \delta_l \right) \right]$$

with the asymptotic form of the actual wave function  $u_l$  :

$$u_l \rightarrow \text{const.} \times \sin \left( kr - \frac{l\pi}{2} + \eta_l \right),$$

we obtain a relation connecting  $D'$  with the phase shift  $\eta_l$  :

$$\tan \eta_l = \frac{\tan \delta_l - D'}{1 + D' \tan \delta_l}$$

On substitution of the value for  $D'$ , this formula yields

$$\tan \eta_l = \frac{\tan \delta_l (2D - R_l^2(D - D \cos 4\delta_l + \sin 4\delta_l) - R_l^2(1 + \cos 4\delta_l + D \sin 4\delta_l))}{2D - R_l^2(D - D \cos 4\delta_l + \sin 4\delta_l) + R_l^2 \tan \delta_l (1 + \cos 4\delta_l + D \sin 4\delta_l)} \dots (24)$$

Retaining only the relevant terms, we have

$$D \approx - \frac{R_l^2(\cot \eta_l + \delta_l)}{1 - \delta_l \cot \eta_l + 2R_l^2 \delta_l \cot \eta_l} \dots (25)$$

When  $l = 0$  one obtains

$$\begin{aligned} -\frac{D}{\beta} &= k \cot \eta_0 \left( 1 + \frac{4}{3} \beta^2 k^2 l_n \frac{\beta k}{4} - \frac{8}{3} \beta^2 k^2 \psi(3/2) + \frac{20}{9} \beta^2 k^2 \right. \\ &\quad \left. - \frac{\pi \beta^2 k^2}{3} \cos \eta_0 + \frac{2}{3} \pi \beta^3 k^3 \cot \eta_0 + \frac{1}{9} \pi^2 \beta^4 k^4 \cot^2 \eta_0 + \dots \right) \end{aligned} \quad (26)$$

$$\text{and} \quad -\frac{D_0}{\beta} = \lim_{k \rightarrow 0} k \cot \eta_0 = -\frac{1}{A_0}, \quad \dots (27)$$

$A_0$  being the scattering length. Then from the equations (21), (26) and (27) we get the expansion of  $k \cot \eta_0$  in the low energy limit

$$\begin{aligned} k \cot \eta_0 &= -\frac{1}{A_0} + \frac{\pi \beta^2 k}{3A_0^2} + \frac{4\beta^2 k^2 l_n \beta k}{3A_0^2} + \left( \frac{1}{2} r_e - \frac{8\beta^2}{3A_0^2} \psi(3/2) \right. \\ &\quad \left. + \frac{20\beta^2}{9A_0} - \frac{\pi \beta^3}{3A_0^2} - \frac{\pi^2 \beta^4}{9A_0^3} + \frac{\pi \beta}{3} \right) k^2 + \dots \end{aligned} \quad \dots (28)$$

This expansion is identical with that of O'Malley *et al* (1961). Finally in order to obtain an expression for  $\tan \eta_l$  we retain only the leading terms involving  $k^{2l+1}$  in the series for  $R_l^2$  as given by the equation (13). It is not difficult to show from the equation (24) that

$$\tan \eta_l \approx \tan \delta_l - \frac{(2l+1)^2 A_0 (\beta k)^{2l+1}}{[(2l+1)!]^4 \beta} \quad \dots (29)$$

which is again the same as that obtained by O'Malley *et al* (1961).

# PHASE SHIFTS IN ELECTRON-ATOM COLLISION

We shall now deduce an expression for phase shifts for all angular momenta for low energy scattering of an electron by an atom. We shall take for the atomic potential  $U(r)$  a screened coulomb potential of the Allis and Morse type joined smoothly with a long range  $r^{-4}$  potential at some distance  $r_0$ . The solution of the wave function with the Allis and Morse type potential is easily obtainable in terms

of Whittaker's functions. Allis and Morse (1931) assumed that the incoming electron moved in a central attractive coulomb field of the nucleus and the average repulsive coulomb field due to the electrons of the atom. They obtained good results for low energy cross sections for elastic scattering of electrons by light atoms. We have modified their potential with the intention of including the long range potential in the following manner :

$$U(r) = -2z \left( \frac{1}{r} - \frac{1}{a} \right), \quad r \leq r_0 \quad \dots (30)$$

$$= -\frac{\beta^2}{r^4} \quad r \geq r_0 \quad \dots (31)$$

$Z$  being the atomic number.

The potential  $U(r)$  depends upon the two parameters  $a$  and  $r_0$ . The continuity condition at  $r_0$  makes  $a$  dependent on  $r_0$ ; there is thus arbitrariness of the single parameter  $r_0$ . The cut-off distance is so selected that the effect of screening due to the term  $2z/a$  is maximum ;

That is, the selected value of  $r_0$  is that value of  $r_0$  for which  $a$  given by the equation

$$2z \left( \frac{1}{r} - \frac{1}{a} \right) = \frac{\beta^2}{r^4} \text{ is minimum.}$$

$$\text{Then we have } a = \left( \frac{2\beta^2}{z} \right)^{\frac{1}{3}} \quad \dots (32)$$

It will be seen later that the scattering length calculated from  $U(r)$  defined in (30) and (31) with this value of  $r_0$  is very nearly equal to the maximum scattering length obtainable by varying  $r_0$ .

We have completely ignored the effect of exchange of electrons, which is expected to play an important role in low energy scattering

The radial equations we have to solve are

$$\left[ \frac{d^2}{dr^2} - K^2 + \frac{2\eta K}{r} - \frac{l(l+1)}{r^2} \right] u_l(r) = 0 \quad r \leq r_0 \quad \dots (33)$$

$$\text{and} \quad \left[ \frac{d^2}{dr^2} + k^2 + \frac{\beta^2}{r^4} - \frac{l(l+1)}{r^2} \right] u_l(r) = 0 \quad r \geq r_0 \quad \dots (34)$$

Here  $k$  is the wave number of the incident electron

$$K^2 = \frac{2Z}{a} - k^2 \quad \text{and} \quad \eta K = Z \quad (\text{Morse and Feshbach, 1953})$$

To obtain phaseshift  $\eta_l$  we shall join at  $r = r_0$  the solutions of the wave equations for the two regions. The regular solution of the equation (33) is well known (Morse and Feshbach 1953) :

$$u_l(r) = N(2Kr)^l e^{-Kr} F(l+1-\eta; 2l+2, 2Kr) \quad \dots (35)$$

where  $F(l+1-\eta; 2l+2; 2Kr)$  is a confluent hypergeometric series and  $N$  is a constant.

Utilizing the properties of the confluent hyper-geometric series one readily obtains for the logarithmic derivative of the wave function (35) at  $r = r_0$

$$\tan \Phi_l^k = \left( \frac{r}{U_l} \cdot \frac{d}{dr} u_l \right)_{r=0} = \eta - 1 - Kr_0 + (l+1-\eta) \frac{F(l+2-\eta; 2l+2, 2Kr_0)}{F(l+1-\eta; 2l+2, 2Kr_0)} \quad \dots (36)$$

The subscript  $l$  and the superscript  $k$  in  $\Phi_l^k$  are used to indicate its dependence on  $l$  and  $k$ .

Now in the energy range considered by us,  $r_0$  given by the equation (32) is less than  $(\beta/k)^{\frac{1}{2}}$  so for the solution of the equation (34) in the region beyond  $r_0$  we have to consider the ranges,  $r_0 \leq r < (\beta/k)^{\frac{1}{2}}$  and  $(\beta/k)^{\frac{1}{2}} \leq r < \infty$  separately.

When  $r_0 \leq r < (\beta/k)^{\frac{1}{2}}$  the solution of the equation (34) is

$$u_2(r) = \frac{A\sqrt{r}}{1 + \frac{\beta^2 k^2}{4(v+1)}} \left[ H_{\nu}^{(1)} \left( kr + \frac{\beta}{r} \right) - \frac{\beta^2 k^2}{4(v+1)} H_{\nu+2}^{(1)} \left( kr + \frac{\beta}{r} \right) \right] + \frac{B\sqrt{r}}{1 + \frac{\beta^2 k^2}{4(v+1)}} \left[ H_{\nu}^{(2)} \left( kr + \frac{\beta}{r} \right) - \frac{\beta^2 k^2}{4(v+1)} H_{\nu+2}^{(2)} \left( kr + \frac{\beta}{r} \right) \right] \dots (37)$$

We have made use of the formulae (8) and (9) to obtain the equation (37). From the continuity of the logarithmic derivative of the wave function at  $r = r_0$  we have

$$\frac{A}{B} = - \frac{\left( 1 - 2 \tan \Phi_l^k \right) \left( H_{\nu}^{(2)} - \frac{\beta^2 k^2}{4(v+1)} H_{\nu+2}^{(2)} \right)}{\left( 1 - 2 \tan \Phi_l^k \right) \left( H_{\nu}^{(1)} - \frac{\beta^2 k^2}{4(v+1)} H_{\nu+2}^{(1)} \right)} + \frac{2 \left( kr_0 - \frac{\beta}{r_0} \right) \left( H_{\nu}^{(1)'} - \frac{\beta^2 k^2}{4(v+1)} H_{\nu+2}^{(2)'} \right)}{2 \left( kr_0 - \frac{\beta}{r_0} \right) \left( H_{\nu}^{(1)'} - \frac{\beta^2 k^2}{4(v+1)} H_{\nu+2}^{(1)'} \right)} \quad (38)$$

The argument  $kr_0 + \beta/r_0$  of the Hankel functions involved in (38) are suppressed.

On using the formulae connecting the Hankel functions with the Bessel functions (Morse and Feshbach 1953) we obtain

$$\frac{A}{B} = e^{-2i\gamma^k} \quad (39)$$

where  $\cot \gamma_l^k$

$$\begin{aligned} & 2 \left( kr_0 - \frac{\beta}{r_0} \right) \left\{ J'_\nu(z) \cos \nu\pi - J'_{-\nu}(z) - \frac{\beta^2 k^2}{4(\nu+1)} \left( J'_{\nu+2}(z) \cos \nu\pi - J'_{-\nu-2}(z) \right) \right\} \\ & \sin \nu\pi \left( 1 - 2 \tan \Phi_l^k \right) \left( J_\nu(z) - \frac{\beta^2 k^2}{4(\nu+1)} J_{\nu+2}(z) \right) \\ & - \left( (1 - 2 \tan \Phi_l^k) \right) \left\{ J_\nu(z) \cos \nu\pi - J_{-\nu}(z) - \frac{\beta^2 k^2}{4(\nu+1)} \left( J_{\nu+2}(z) \cos \nu\pi - J_{-\nu-2}(z) \right) \right\} \\ & - 2 \left( kr_0 - \frac{\beta}{r_0} \right) \left\{ J'_\nu(z) - \frac{\beta^2 k^2}{4(\nu+1)} J'_{\nu+2}(z) \right\} \left\{ \dots \right\} \quad (40) \end{aligned}$$

$z$  standing for  $kr_0 + \beta/r_0$

For the scattering of a slow electron by a He atom the argument  $kr_0 + \beta/r_0$  is small enough to justify power series expansions of the Bessel functions and their derivatives in (40). If for the scattering by other atoms the argument is large, asymptotic expansions may be used (Watson, 1958)

Now from the equations (12) and (39) one gets

$$\frac{A'}{B'} = e^{-2i\xi_l} \quad \dots \quad (41)$$

$$\text{where } \tan \xi_l = \frac{R_l^2 \operatorname{cosec} \gamma_l^k \sin \nu\pi \sin(\nu\pi + \gamma_l^k)}{1 - R_l^2 \operatorname{cosec} \gamma_l^k \cos \nu\pi \sin(\nu\pi + \gamma_l^k)}.$$

$$\begin{aligned} \text{when } l = 0, \tan \xi_0 = \beta k \left( 1 + \frac{4}{3} \beta^2 k^2 \ln \frac{\beta k}{4} - \frac{4}{3} \beta^2 k^2 \psi(3/2) + \frac{20}{9} \beta^2 k^2 \right) \cot \gamma_0^k \\ - \frac{2}{3} \pi \beta^3 k^3 \quad \dots \quad (42) \end{aligned}$$

where terms containing  $k^4$  and higher powers of  $k$  are neglected. Again using the equations (11) and (41) we get an expression for the phaseshifts for different angular momenta

$$\eta_l = m_l \pi - \xi_l + \frac{\pi \beta^2 k^2}{8(l+3/2)(l+\frac{1}{2})(l-\frac{1}{2})} \quad \dots \quad (43)$$

where  $m_l \pi$  is the zero energy phaseshift for the scattering of an electron by an atom. The value of  $m_l$  can be determined from Swan's conjecture about an extension of Levinson's theorem (P Swan 1955; K Levinson 1949).

We get from the equations (42) and (43)

$$\begin{aligned} \cot \eta_0 = - \frac{1 - \frac{2}{3} \pi \beta^3 k^3}{\beta k \left( 1 + \frac{4}{3} \beta^2 k^2 \ln \frac{\beta k}{4} - \frac{4}{3} \beta^2 k^2 \psi(3/2) + \frac{20}{9} \beta^2 k^2 \right) \cot \gamma_0^k - \frac{2}{3} \pi \beta^3 k^3} \end{aligned}$$

$$\text{whence } \lim_{k \rightarrow 0} k \cot \eta_0 = - \frac{1}{\beta \cot \gamma_0^0}$$



Therefore the scattering length  $A_0$  is given by

$$A_0 = \beta \cot \gamma_0^0 \quad \dots \quad (44)$$

NUMERICAL CALCULATION FOR PHASE SHIFTS  
OF THE ELECTRON HELIUM SCATTERING  
AT LOW ENERGIES

Though we can calculate phaseshifts  $\eta_l$  from the equation (43) for different angular momenta  $l$  and for various light atoms, we shall rest satisfied with the calculation of  $s$ -wave phase shift  $\eta_0$  for  $e$ -He scattering. Taking  $\alpha = 1.376$  (in atomic unit) for helium (Wickner and Das 1957), one gets from the equation (32) the cut-off distance  $r_0 = 1.112$  (a.u.) and the corresponding scattering length  $A_0$  is .844, a result rather low compared with the recent results. The maximum value for the scattering length for the atomic potential as defined in the equations (30) and (31) is .854 corresponding to the cut off distance  $r_0 = 1.200$ . As these values of  $A_0$  and  $r_0$  do not improve  $S$ -wave phaseshifts and as one has to obtain this value of  $r_0$  (i.e.  $r_0 = 1.3$ ) by trial, we shall accept the value  $r_0 = 1.112$  (easily obtainable from the equation (32)) for the calculation of the phase shifts.

In the table below the  $s$ -wave phase shifts in  $e$ -He collisions for various incident energies obtained in this work are compared with the corresponding values of the same calculated by LaBhan and Callaway taking into account both polarization and exchange effects. These authors have followed the method of polarized orbitals used by Tomkin and Lamkin (1961) for a similar calculation on phase shifts in  $e$ -H scattering; the resulting integro differential equations have been solved numerically. Disagreement between our results and their increases with  $k$ . The values of  $\cot \gamma_0^k$  are also shown in the table. The potential used in our calculation is not very exact but its advantage is that it allows a fully analytic treatment.

TABLE

$K$ (a.u.)	Energy e.v.	$\cot \gamma_0^k$	$\eta_0$ (present work)	$\eta_0$ (LaBhan and callaway)
0	0	0.720	(0.844) <sup>a</sup>	(1.132) <sup>a</sup>
0.01	0.00136	0.701	3.1341	3.13016
0.05	0.034	0.6279	3.1015	3.0822
0.10	0.136	0.5409	3.0661	3.0186
0.1917	0.50	0.3986	3.0230	2.8972
0.25	0.85	0.3187	3.0060	2.8189
0.2712	1.00	0.2942	3.0030	2.7904

<sup>a</sup> scattering length in a.u.

## ACKNOWLEDGEMENT

The authors wish to thank Prof. D. Basu for many valuable discussions.

## REFERENCES

- Allis, W. P. and Morse, P. M. 1931, *Z. Physik* **70**, 567.  
 Bethe, H. A. 1949 *Phys. Rev.* **76**, 38.  
 Lu Balm, R. W. and Callaway, J. 1964 *Phys. Rev.* **135A** 1539.  
 Levinson, N., 1949 K. danske vidensk. Selsk., *Mat.-fys. Medd.* **25**, No. 9.  
 Meixner, J. and Schaffke, F. W., 1954 *Mathematische Funktionen und Sphäroid funktionen*, Springer-Verlag., Berlin.  
 Morse, P. M. and Feshbach, H., 1953, *Methods of Theoretical Physics* Vol I p. 624 and Vol. II p. 1682.  
 O'Malley, T. E., Spruch, L. and Rosenberg, L. 1961 *J. Math. Phys.* **2**, 491.  
 Spector, R. M., 1964, *J. Math. Phys.* **5**, 1185.  
 Swan, P. 1955, *Proc. Roy. Soc. (London)* **228A** 10.  
 Tomkin, A. and Lamkin, J. C., 1961, *Phys. Rev.* **121**, 788.  
 Watson, G. N. 1958, *Treatise on the Theory of Bessel Functions* page 194.  
 Wickner, F. G. and Das, T. P. 1957, *Phys. Rev.* **107**, 497.

# ELECTRONIC ENERGY STATES IN ONE DIMENSIONAL CRYSTALS

C. L. ROY

DEPARTMENT OF PHYSICS, INDIAN INSTITUTE OF TECHNOLOGY,  
Kharagpur

(Received March 24, 1966)

**ABSTRACT.** Investigations have been made about the electronic energy state in one dimensional crystals within the frame work of rectangular potential-well model. A matrix method, similar to that of Saxon and Hutner, has been used. The key role in determining the energy band structures under different physical conditions is shown to be played essentially by the trace of a matrix which has been named as  $T$ -matrix in the text. Comparative discussion has been given about the matrix method used here and that used by Luttinger. Both perfect and disordered crystals have been studied and explicit energy band equations have been given for both cases. Results for the disordered case have been given only upto first-order and in a form which is suitable for numerical computation for any type of disorder.

## INTRODUCTION

Quantum-mechanical investigation of the physical properties of solids needs solution of Schroedinger equation for one-electron wave functions with appropriate potential field in which the electrons move inside the solid. For a perfect infinite crystal, the potential energy of electrons inside the solid is assumed to be a periodic function with periodicity equal to that of the lattice. It is well-known that the energy eigen-spectrum of electrons moving in such a periodic potential is divided into allowed and forbidden bands. In reality, one has to solve a three-dimensional problem. However, a lot of insight into the nature of the real three dimensional crystal can be obtained by a study of the one-dimensional case (Fues *et al*, 1952). For a one dimensional solid, the mathematical problem is to find the allowed and regions of the solution of the equation :

$$\frac{d^2\psi}{dx^2} + \frac{2m}{\hbar^2} [E - V(x)]\psi = 0 \quad \dots (1)$$

where  $E$  is the total energy and  $V(x)$  is the P.E of the electron. For a perfect crystal  $V(x)$  is a periodic function with lattice periodicity. For a disordered or amorphous solid  $V(x)$  loses this property of periodicity and one faces difficulty in solving equation (1) to an extent depending on the degree of deviation of  $V(x)$  from periodicity.

In applying equation (1) to the study of a perfect crystal, extensive use has been made of sinusoidal and Kronig-Penney  $\delta$ -potentials. As has been discussed by Allen (1953), the band structures for these models do not show all the characteristics of the band structures for real crystals. Thus for both these models, the band-

structures do not show points of contact between different allowed bands while in actual solids these bands exist and they play an important role in the study of surface states, as has been shown by Shockley (1939). The band structure for Kronig-Penney potential differs from that of the real crystal in another respect. While in the Kronig-Penney case, the size of the forbidden regions approaches a constant nonvanishing value as  $E \rightarrow \infty$ , in the actual case the forbidden ranges of energy approach zero as  $E \rightarrow \infty$ . The band structure for the case of a finite rectangular potential-well, on the other hand, has the proper behaviour as  $E \rightarrow \infty$  and has an infinite no. of points of contact.

What has been said so far points out the importance of the rectangular potential-well model in investigating the electronic energy-band structures in solids. It has been the aim of this paper to make a thorough investigation of the electronic energy states in one-dimensional monoatomic crystal within the framework of the rectangular potential-well model. A matrix method, developed after a work of Saxon and Hutner (1949), has been used. The energy-band structures under different physical conditions are shown to depend essentially upon the trace of a matrix which has been named as '*T*-matrix' (details given later). The general features of this *T*-matrix in connection with energy-band structures have been pointed out. Comparative discussion has been given about the matrix method used here and that of Luttinger (1951). Investigations have been made about perfect and disordered systems. Explicit energy-band equations for both these cases have been given. The effect of disorder on the electronic energy-states has been calculated only upto first order. Although not done in this paper, the first order disorder equation for electronic energy-states is in a form which can be put to numerical computations.

#### MODEL AND THEORY

We consider the motion of an electron in monoatomic one dimensional crystal where the potential energy of the electron is assumed to have the form given by Fig. 1.

Each of the potential energy wells may be considered a rough approximation for the potential in the vicinity of an atom. Schroedinger equations for the motion of the electron are given by the following :

$$\frac{d^2\psi}{dx^2} + \frac{2mE}{\hbar^2}\psi = 0 \quad \dots (2)$$

for regions like  $b < x < a+b$ .

$$\frac{d^2\psi}{dx^2} + \frac{2m}{\hbar^2}(E-V)\psi = 0 \quad \dots (3)$$

for regions like  $0 < x < b$ .

We assume that  $E < V$ . The general solutions of equations (2) and (3) are given respectively by the following equations :

$$\psi(x) = A \exp(i\alpha x) + B \exp(-i\alpha x) \quad \dots \quad (4)$$

$$\psi(x) = C \exp(\beta x) + D \exp(-\beta x) \quad \dots \quad (5)$$

where,

$$\alpha^2 = \frac{2mE}{\hbar^2} \quad \dots \quad (6)$$

$$\beta^2 = \frac{2m(V-E)}{\hbar^2} \quad \dots \quad (7)$$

Considering now an  $x$ -interval equal to one period say from  $x = 0$  to  $x = a + b$ , we can write

$$\begin{pmatrix} A_1 \\ B_1 \end{pmatrix} = T \begin{pmatrix} A_0 \\ B_0 \end{pmatrix} \quad \dots \quad (8)$$

In equation (8),  $T$  is a  $2 \times 2$  matrix and plays a role similar to the scattering matrix of Saxon and Hutner (1949).  $A_1$  and  $B_1$  are the constants for equation (4) at  $x = a+b$  while  $A_0$  and  $B_0$  are the corresponding constants at  $x = 0$ .  $T$  can be written as a product of some other matrices in the following form :

$$T = sRvr \quad \dots \quad (9)$$

$s$  and  $v$  are translational matrices given by the following

$$s = \begin{pmatrix} \exp(i\alpha a) & 0 \\ 0 & \exp(-i\alpha a) \end{pmatrix} \quad \dots \quad (10)$$

$$v = \begin{pmatrix} \exp(\beta b) & 0 \\ 0 & \exp(-\beta b) \end{pmatrix} \quad \dots \quad (11)$$

$R$  and  $r$  are matrices which correlate  $A$  and  $B$  of eqn (4) to  $C$  and  $D$  of eqn (5) at points like  $x = b, a + 2b \dots$  or at points like  $x = 0, a + b \dots$  etc.

Explicitly,

$$\begin{pmatrix} A \\ B \end{pmatrix}_{\text{at } x=b, a+2b \dots \text{etc}} = R \begin{pmatrix} C \\ D \end{pmatrix}_{\text{at } x=b, a+2b \dots \text{etc}} \dots \quad (12)$$

or at  $x=0, a+b \dots$  etc                  or at  $x=0, a+b \dots$  etc

$$\begin{pmatrix} C \\ D \end{pmatrix}_{\text{at } x=b, a+2b \dots \text{etc}} = r \begin{pmatrix} A \\ B \end{pmatrix}_{\text{at } x=b, a+2b \dots \text{etc}} \dots (13)$$

or at  $x=0, a+b \dots$  etc                  or at  $x=0, a+b \dots$  etc

Using the continuity conditions for the wavefunctions and their derivatives, one gets the following results for  $R$  and  $r$

$$R = \frac{1}{2i\alpha} \begin{pmatrix} i\alpha + \beta & i\alpha - \beta \\ i\alpha - \beta & i\alpha + \beta \end{pmatrix} \quad \dots \quad (14)$$

$$r = \frac{1}{2\beta} \begin{pmatrix} i\alpha + \beta & \beta - i\alpha \\ \beta - i\alpha & i\alpha + \beta \end{pmatrix} \quad \dots \quad (15)$$

We notice that the matrix  $T' = Rvr$  correlates the coefficients  $A$  and  $B$  of equation (4) at points  $x = 0$  and  $x = b$  and similar pairs of points at other potential wells through the equation :

$$\begin{pmatrix} A \\ B \end{pmatrix}_{\text{at } x=b, a+2b \dots \text{etc}} = T' \begin{pmatrix} A \\ B \end{pmatrix}_{\text{at } x=0, a+b \dots \text{etc}} \quad \dots \quad (16)$$

When  $b \rightarrow 0$  so that  $bV$  remains finite ( $\delta$ -potential), we find that .

$$T' = \begin{pmatrix} 1 - iP/\alpha & -iP/\alpha \\ iP/\alpha & 1 + iP/\alpha \end{pmatrix} \quad \dots \quad (17)$$

where,

$$P = \frac{mbV}{\hbar^2} \quad \dots \quad (18)$$

The matrix (17) is just the ' $R$ ' matrix for  $\delta$ -potential as obtained by Saxon and Hunter (1949)

Now a straight forward calculation gives the following expressions for the elements of the  $T$ -matrix :

$$T_{11} = \frac{1}{4i\alpha\beta} [(i\alpha + \beta)^2 \exp(\beta b + i\alpha a) - (i\alpha - \beta)^2 \exp(-\beta b + i\alpha a)] \quad \dots \quad (19)$$

$$T_{22} = T_{11}^* \quad \dots \quad (20)$$

$$T_{21} = \frac{1}{4i\alpha\beta} [(i\alpha + \beta)(i\alpha - \beta) \exp(-i\alpha a) \{\exp(\beta b) - \exp(-\beta b)\}] \quad \dots \quad (21)$$

$$T_{12} = T_{21}^* \quad \dots \quad (22)$$

By a straight forward calculation it is also found that  $\det T = 1$ . The  $T$ -matrix here is the same as the  $H$ -matrix derived by a different method by Kerner (1954).

General features of  $T$ -matrix.

(1) Condition for allowed and forbidden bands: We consider a ring of  $n$

atoms. By repeated application of equation (8) from one cell to another, we can write:

$$\begin{pmatrix} A_{n+1} \\ B_{n+1} \end{pmatrix} = T^n \begin{pmatrix} A_1 \\ B_1 \end{pmatrix} \quad (23)$$

But  $(n+1)$  the cell is the same as the first cell. This means

$$T^n \begin{pmatrix} A_1 \\ B_1 \end{pmatrix} = \begin{pmatrix} A_1 \\ B_1 \end{pmatrix} \quad \dots \quad (24)$$

Equ (24) is similar to the one derived by Luttinger (1951). We shall later on present discussions about Luttinger's equation compared to (24). Here we follow his argument to find the connection of the  $T$ -matrix with the energy-band structure. We notice from (24) that the allowed energies correspond to the eigenvalue 1 of the matrix  $T$ . This again shows that the allowed energies correspond to the  $n$ -th roots of unity for the matrix  $T$ . Thus the allowed energy levels are obtained by setting the eigenvalues of  $T$  equal to  $\exp(\pm 2ik\pi/n)$  where  $k$  is an integer satisfying  $0 \leq k \leq (n-1)$ . When  $n$  is very large, the different values of  $k$  gives us for  $k\pi/n$  practically the continuum from zero to  $\pi$ . This is what we mean by an allowed band in a finite crystal. The allowed band is thus determined by those values of the energy which make the eigenvalues of  $T$  complex numbers whose absolute value is unity. Since  $\det T = 1$ , the secular equation for the eigenvalues of  $T$  is given by.

$$\lambda^2 - (\text{Tr } T)\lambda + 1 = 0$$

$$\text{or} \quad \lambda \pm = \frac{\text{Tr } T \pm \sqrt{(\text{Tr } T)^2 - 4}}{2} \quad \dots \quad (25)$$

Now if  $\text{Tr } T \leq 2$ ,  $\lambda_+ = \lambda_-^*$  and  $|\lambda_+|^2 = |\lambda_-|^2 = 1$ ,

so that we have allowed energies. If  $\text{Tr } T > 2$ , both the eigenvalues are real. One of them is of absolute value greater than unity and the other of absolute value less than unity. This means that the condition for the forbidden level is simply  $|\text{Tr } T| > 2$  ... (26)

(2) Properties of  $\text{Tr } T$  in relation to energy bands: we note that  $T$ -matrix is not Hermitian. Had it been so, the eigenvalues would always have been real, which means  $\text{Tr } T > 2$ . All energies would thus have been forbidden. Again if  $\text{Tr } T \leq 2$  always, the eigenvalues are always complex satisfying  $|\lambda_+|^2 = |\lambda_-|^2 = 1$ . In this case all the energies would have been allowed. In either case one does not get a band structure. Thus the occurrence of allowed and forbidden bands of electronic energies in a crystal is equivalent mathematically to saying that  $T$  is neither Hermitian nor  $\text{Tr } T \leq 2$  always. We now examine the circumstances under which  $T$ -matrix assumes these extreme forms.

*Case I.* Suppose  $V = \text{constant}$  and  $E > V$ . We can easily see that in this case  $\beta = i\alpha$ ,  $\alpha^2 = \frac{2m}{\hbar^2} (E - V)$ . From (19) and (20) it then follows that  $\text{Tr } T = 2 \cos \alpha(a+b)$  ... (27)

$$T = \begin{pmatrix} T_{11} & 0 \\ 0 & T_{11}^* \end{pmatrix} \quad \dots (28)$$

$$\lambda_{\pm} = \cos \alpha(a+b) \pm i \sin \alpha(a+b) \quad (29)$$

Thus in this case  $T$  is not Hermitian,  $\text{Tr } T \leq 2$  and  $|\lambda_+|^2 = |\lambda_-|^2 = 1$ , for all values of  $\alpha$ . This means that  $(E - V) = E_k$ , the K.E. of the electron can take all values (no band structure) from 0 to  $\infty$ . This is the well known result for the electronic energy spectrum in the free-electron model.

*Case II.* Suppose  $V = \text{const}$  and  $E < V$ . Then in this case

$$\beta = i\alpha \quad \beta^2 = -\frac{2m}{\hbar^2} (V - E), \quad \text{Tr } T = 2 \cosh \beta(a+b) \quad \dots (30)$$

$$\lambda_{\pm} = \cosh \beta(a+b) \pm i \sin \beta(a+b) \quad \dots (31)$$

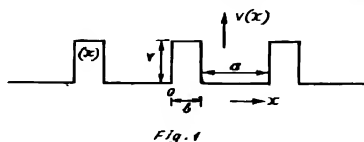
$$T = \begin{pmatrix} \exp \beta(a+b) & 0 \\ 0 & \exp \{-\beta(a+b)\} \end{pmatrix} \quad \dots (32)$$

Thus in this case  $\text{Tr } T > 2$  always,  $|\lambda_+|^2 \neq 1$ ,  $|\lambda_-|^2 \neq 1$  and  $T$  is Hermitian. Hence all the energies below  $V$  are forbidden. This means that there are no electrons inside the crystal with total energy less than the potential energy which is constant throughout the lattice. This conclusion is again consistent with the actual physical situation.

#### EXPLICIT ENERGY EIGENVALUE EQUATIONS

We now use the  $T$ -matrix to derive energy eigenvalues for some special cases.

*Case I.* Perfect infinite crystal. Considering the model of Fig. (1) and noting that



Rectangular potential-well model for a one-dimensional monoatomic perfect crystal.

for such an infinite crystal, Bloch's theorem must hold good, we can write :

$$\begin{pmatrix} A_1 \\ B_1 \end{pmatrix} = \exp i\mu(a+b) \begin{pmatrix} A_0 \\ B_0 \end{pmatrix} \quad \dots (33)$$

From (8) and (33), (using  $\det T = 1$ ), one gets :

$$\cos \mu(a+b) = \frac{1}{2} \text{Tr } T \quad \dots (34)$$



## Electronic Energy States in one Dimensional Crystals 351

Eqn (34) shows that  $|\text{Tr } T| \leq 2$ , which is the same as derived earlier by applying periodic boundary condition to a circular chain. Using  $T_{11}$  and  $T_{22}$  from (19) and (20), we get from (34),

$$\frac{\beta^2 - \alpha^2}{2\alpha\beta} \sinh \beta b \sin \alpha a + \cosh \beta b \cos \alpha a = \cos \mu(a+b) \quad (35)$$

Eqn. (35) is the same as that derived by other workers

*Case II.* One dimensional monoatomic disordered solid. Let us consider the model of the solid as given by Fig. (2) below

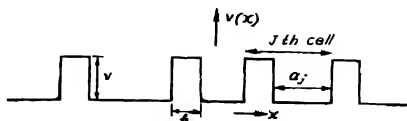


Fig. 2

Rectangular potential well model for a one dimensional monoatomic disordered solid.

Distances such as  $a_j$  for the  $j$ -th cell are arbitrary. They are represented by

$$a_j = a + \epsilon_j \quad \dots (36)$$

where  $a$  is the average of all  $a_j$ 's and  $\epsilon_j$ 's are fluctuations over  $a$ . From eqn (9) we find that the  $T$ -matrix for the  $j$ -th cell is given by

$$T_j = \begin{pmatrix} \exp i\alpha(a + \epsilon_j) & 0 \\ 0 & \exp \{-i\alpha(a + \epsilon_j)\} \end{pmatrix} \quad \dots (37)$$

We note from (37) that  $\det T_j = 1$  for all  $j$ 's. Suppose there are  $n$ -cells in the lattice. By applying periodic boundary condition and following the same argument as used in getting eqn (24) for a perfect lattice, we get the following equation for present case :

$$\begin{pmatrix} j=1 \\ \pi T_j \\ j=n \end{pmatrix} \begin{pmatrix} A_1 \\ B_1 \end{pmatrix} = \begin{pmatrix} A_1 \\ B_1 \end{pmatrix} \quad \dots (38)$$

Thus the eigenvalues of  $(\pi T_j)$  are equal to 1. For the present model, the crystal of  $n$ -cells is one period. Hence the matrix  $(\pi T_j)$  for the present model plays the same role as the matrix  $T$  for Fig. (1). Thus the eigen-values of  $(\pi T_j)$ , like those of  $T$ , are complex numbers with absolute value unity—conforming to eq (38). Since  $\det T_j = 1$  for all  $j$ ,  $\det(\pi T_j) = 1$  and the secular equation for the eigen-values of  $(\pi T_j)$  is given by :

$$\lambda_{\pm} = \frac{\text{Tr}(\pi T_j) \pm \sqrt{(\text{Tr } \pi T_j)^2 - 4}}{2} \quad \dots (39)$$

Thus in the present case, the allowed energies are given by the condition

$$\text{Tr}(\pi T_j) \leq 2 \quad \dots (40)$$

From (37), retaining only the first order term,

$$T_j = (T + K_j T) \quad \dots (41)$$

where,

$$K_j = \begin{pmatrix} i\alpha\epsilon_j & 0 \\ 0 & -i\alpha\epsilon_j \end{pmatrix} \quad \dots (42)$$

With the help of (42), we get by retaining again only the first order terms

$$(\pi T_j) = T^n + \sum_{j=1}^{i=n} T^{n-j} K_j T^j \quad \dots (43)$$

From (40) and (43) equating zero and first order terms separately to zero, we get

$$T_r T^n \leq 2 \quad \dots (44)$$

$$T_r \left( \sum_{j=1}^{i=n} T^{n-j} K_j T^j = 0 \right) \quad \dots (45)$$

Eqn (44) shows that the energy eigen values for the model considered here retain the band structure characteristic of a perfect crystal with periodicity  $na$ . Eqn (45) gives the extra energy-values due to disorder. We now proceed to find explicit forms of equations (44) and (45).

The similarity transformation for diagonalisation of  $T$  matrix is given by

$$X T X^{-1} = \begin{pmatrix} \exp(ic) & 0 \\ 0 & \exp(-ic) \end{pmatrix} \quad \dots (46)$$

$$X = \begin{pmatrix} T_{21} & \exp(ic) - T_{11} \\ T_{21} & \exp(-ic) - T_{11} \end{pmatrix} \quad \dots (47)$$

$$X^{-1} = \frac{1}{\det X} \begin{pmatrix} \exp(-ic) - T_{11} & T_{11} - \exp(ic) \\ -T_{21} & T_{21} \end{pmatrix} \quad \dots (48)$$

$$\cos c = \frac{1}{2} \text{Tr } T \quad \dots (49)$$

Eqn (49) satisfies the requirement that  $\text{Tr } T \leq 2$  and gives  $\exp(ic)$  and  $\exp(-ic)$  as the eigenvalues of  $T$ . Hence the diagonal form (46). From (46), (47) and (48), we can easily show the following:

$$(T^n)_{22}^* = (T^n)_{11} = \frac{1}{\sin c} \{ \sin(n+1)c - T_{11}^* \sin nc \} \quad \dots (50)$$

$$(T^n)_{21} = (T^n)_{12}^* = T_{21} \frac{\sin(nc)}{\sin c} \quad \dots \quad (51)$$

Thus with the help of (50), eqn (44) takes the form :

$$\frac{1}{\sin c} \{ \sin(n+1)c - T_{11r} \sin(nc) \} \leq 1 \quad \dots \quad (52)$$

where,

$$T_{11}^* = T_{11r} + i T_{11} \quad \dots \quad (53)$$

Using eqns (46), (47) and (48) and retaining only the first order terms, eqn (45) can be simplified to the following form .

$$\sum_{j=1}^{j=n} c_j [T_{11r} \cos(n-2j-1)c - 2T'_{11r} T_{11r}] \cdot \cos(n-2j)c + T_{11r} \cos(n-2j+1)c - 2 \left( \sum_{j=1}^{j=n} c_j \right) T_{11r} \cdot \cos(n+1)c - T'_{11} \cos nc] = 0 \quad \dots \quad (54)$$

where,

$$T_{12} = T_{12r} + iT_{12i} \quad \dots \quad (55)$$

If the fluctuations  $c_j$ 's are all random, the different terms in the summation ( $\sum c_j$ ) may cancel one another and the net effect of the second terms in (54) will be practically zero. The extra energy levels due to disorder of system will thus be predominantly determined by the first term of (53) when the fluctuations  $c_j$ 's are all random.

#### DISCUSSIONS

In the work of this paper, we have demonstrated the use of  $T$ -matrix in getting energy-band equations for one dimensional crystals. The critical role in determining the band structure is shown to be governed by  $\text{Tr } T$ . We have shown that for allowed energies  $\text{Tr } T \leq 2$ . Luttinger (1951) has derived a similar condition but his result is expressed through an ' $A$ ' matrix. The elements of  $A$ -matrix are again expressed through  $y$ -solutions of James (1949). Luttinger has discussed some characteristics of energy bands in pure and mixed lattices and for this purpose it is enough to know only some general properties of the  $A$ -matrix (like  $\det A = 1$ ,  $A_{11} = A_{22}$ ). However, for knowing explicitly the energy-eigenvalue equations, one must know exactly the matrix which correlates the co-efficients of the cell-to-cell wave functions. This purpose has been served by the  $T$ -matrix since for the type of potential considered, we have been able to know the exact form of the elements of  $T$ -matrix.

We note here that in deriving eqn (54) for the energy values due to disorder, no assumption other than that of neglecting second and higher order terms—has

been made. Thus equation (54) can be put to numerical computations for any type of fluctuations  $c_j$ . It can also be seen that the method illustrated here can be used to study the energy band structures of mixed lattices. This problem is under author's contemplation and the results will appear in later publications.

#### ACKNOWLEDGEMENT

The author is grateful to Prof. S. Datta Majumdar for many illuminating discussions and for his help in writing the paper. The author is also thankful to Prof. H. N. Bose and Prof. G. Bandopadhyaya for their keen interest and encouragement.

#### REFERENCES

- Allen, G. 1953, *Phys. Rev.* **91**, 531.  
Fues, E. and Statz, H. 1952, *Z. Naturforsch.* **79**, 2.  
James, H. M. 1949, *Phys. Rev.* **76**, 1603.  
Kerner, E. H., 1954, *Phys. Rev.* **95**, 687.  
Luttinger, J. M., 1951, *Philips Res. Rep.*, **6**, 303.  
Saxon, S. D. and Hutner, R. A., 1949, *Philips Res. Rep.* **4**, 82.  
Shockley, W., 1939, *Phys. Rev.* **56**, 317.

# THE INFLUENCE OF $^3\text{He}$ ON THE LAMBDA TEMPERATURE

D. G. KAPADNIS

RAJARAM COLLEGE, KOLHAPUR

(Received September 14, 1965)

**ABSTRACT** The observed change in the lambda transformation temperature with the concentration of  $^3\text{He}$  in  $^4\text{He}$  gives for low concentrations a negative linear shift of 1.48 degrees per mole concentration. The lambda transition is of the second order and there seems to be no appreciable change in the jump in the specific heat at the lambda point.

## INTRODUCTION

The interesting phenomenon of  $^3\text{He}$  not taking part in superfluid flow, observed by Daunt, Probst *et al.*, (1948) in dilute solutions of  $^3\text{He}$  in  $^4\text{He}$ , led to a new method of isotopic separation in the liquid phase by superfluid filtration and also to the conclusion that the lambda temperature of liquid  $^4\text{He}$  would be a function of the concentration of  $^3\text{He}$ . Accordingly the presence of  $^3\text{He}$  has a pronounced effect on the value of the lambda point, which is shifted towards lower temperature as was first shown by Abraham, Wemstock *et al.* (1949) for a mixture with  $^3\text{He}$  concentrations upto 28.2%. Similar experiments were performed by Eselsohn and Lazarev (1950) for a mixture with a concentration of about 1.5% and by Daunt and Heer (1950) for mixtures with high concentrations of 42% to 89%.

The specific heat measurements of the liquid mixtures of  $^3\text{He}$  in  $^4\text{He}$  have been made by the helium group of the Kamerlingh Onnes Laboratory, Leiden. Some of those results have already been published (Dokoupil, Kapadnis *et al.*, 1954 and 1959, Kapadnis and Dokoupil, 1955). In the present investigations the values of the lambda temperature of the mixture for low concentrations of  $^3\text{He}$  in  $^4\text{He}$  have been computed. For the sake of comparison numerical computations of the lambda temperatures have also been made from the theories in vogue. The final check of the exact determination of the composition of the samples of the mixtures and its confirmation delayed appreciably these computations and the discussion of the results. In the mean time the temperature scale in the helium region has been changed. Therefore we have recalculated all our data using the new scale adopted internationally.

## EXPERIMENTAL

As the quantity of  $^3\text{He}$  at the disposal of the Leiden helium group was then very small, the method of a closed capsule completely filled with the condensed

mixture was developed and applied to the calorimetric determination of the specific heat (Dokoupil, Kapadnis *et al.*, 1954 and 1959; Kapadnis and Dokoupil, 1955). Special attention was paid to the accurate determination of the transition temperature. The temperature interval in which the lambda point of the mixture must lie, was first determined by a close scrutiny of the experimental points representing the specific heat of the mixture in the vicinity of the transition temperature. For the determination of its exact value separate runs through the transition point were made with a continuous heat supply, sometimes by the natural warming up only (especially when the bath level was very low). The values for the lambda temperature of the mixture were computed from the resulting discontinuities in the slopes of the corresponding curves of temperature versus time. Figure 1 shows such a typical plot used to compute the lambda temperature of the mixture.

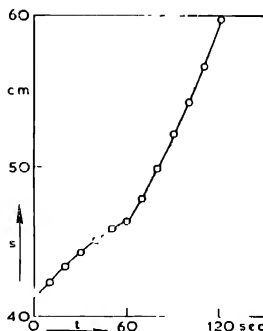


Fig. 1 A typical plot of the Galvanometer reading vs Time ( $X=0.010$ )

## RESULTS AND DISCUSSION

The values of the lambda temperature corresponding to the concentration of  $^3\text{He}$  in  $^4\text{He}$ ,  $X = 1.00, 2.50, 7.13, 21.1$  and  $41.7\%$  are  $T_{\lambda}^m = 2.162, 2.140, 2.072, 1.845$  and  $1.454^\circ\text{K}$  respectively, giving for low concentrations a negative shift of  $1.48$  degrees per mole concentration, which is linear. The lambda transition is of the second order and there seems to be no appreciable change in the jump in the specific heat at the lambda point.

The early experimental observations of the lowering of the lambda point of  $^4\text{He}$  due to an admixture of  $^3\text{He}$ , reported by Abraham *et al.*, (1949) for concentrations upto  $28.2\%$   $^3\text{He}$  by using a superleak formed around a platinum wire, seem to be largely in error, presumably due to the concentration gradient set up in the liquid mixture as a result of the heat flush effect. The value given for the lambda temperature for the concentration of about  $1.5\%$   $^3\text{He}$  by Eselsohn and Lazarev (1950)

is also somewhat low, probably due to the uncertainty of the concentration. They used an apparatus consisting of two reservoirs connected by a narrow capillary and made use of an observation of the supra-surface flow as the criterion for the existence of the lambda temperature. Daunt and Heer (1950) used in their experiments for concentrations from 42% to 89%  $^3\text{He}$ , the same criterion and determined the lambda temperatures at which the heat influx to the reservoir changed abruptly. They expected that their results were not seriously affected by the heat flush effect.

The experimental results of King and Fairbank (1953) using the disappearance of second sound at the lambda point as a criterion, for concentrations below 4.2%  $^3\text{He}$  revealed a linear dependence of the lambda temperature of the mixture on the concentration of  $^3\text{He}$ , giving negative slope of 1.5 degrees per mole concentration. These observations led to the suspicion that the earlier observations were erroneous. It was confirmed by our measurements of the specific heats of liquid mixtures of  $^3\text{He}$  and  $^4\text{He}$  and later on by the oscillating pendulum experiments performed by Dash and Tailor (1955), who obtained from their measurements of the behaviour of a torsion pendulum immersed in the liquids, transition temperatures of the individual solutions by locating the discontinuity in slope of the torsion period versus temperature. This is equivalent to finding the temperature at which the normal fluid density becomes equal to the total density. Their experiments also gave a negative linear shift of  $1.47 \pm 0.03$  degrees per mole concentration for the whole concentration range (upto  $X = 0.092$ ) they studied.

It may be pointed out that in the experiments of King and Fairbank, those of this research and of Dash and Tailor the principles involved in the methods to determine the lowering of the lambda point of liquid  $^4\text{He}$  due to the presence of  $^3\text{He}$  in the mixture, are entirely different from each other. In spite of that the excellent agreement of the results suggests that for low concentrations at least the observed negative shift of 1.48 degrees per mole concentration may be treated as an established fact.

Figure 2 shows the ratio of the lambda temperature of the mixture to that of pure  $^4\text{He}$  as a function of the concentration of  $^3\text{He}$  upto  $X = 0.11$ . The observed data as well as the numerical evaluations made from different theories in vogue have been included in the figure.

It is evident from the work of Stout (1948) that the Gibbs' function written according to the laws for perfect classical solutions leads to the second order lambda transition for liquid  $^4\text{He}$ , the lambda point of liquid  $^4\text{He}$  remaining unaffected by the admixture of  $^3\text{He}$ . In order to account for the experimentally observed change in the lambda transformation temperature with the concentration of  $^3\text{He}$ , using classical thermodynamics it is necessary to inject a reflection of the quantum nature of liquid helium through some experimentally observed phenomenon. It was accounted for, in the theory of de Boer and Gorter (1950) by introducing the

hypothesis put forward by Taconis *et al.* (1949), namely that the  $^3\text{He}$  can be regarded as being in solution with the 'normal' constituent of helium II only. The lambda temperature of the mixture in this case is given by

$$1 - X = \exp [S_\lambda(T - T_\lambda)/RT]$$

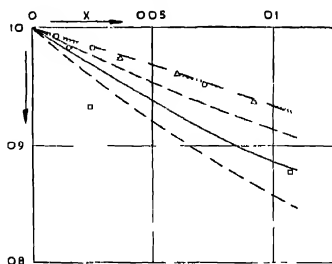


Fig. 2.  $T_\lambda^m$  vs. Concentration of  $^3\text{He}$  is  $^4\text{He}$

○ This Research,

□ Abraham *et. al.*;

△ Dash and Taylor, and

◇ Eselsolm and Lazarev

----- de Boer and Gorter,

———— Heer and Damm;

— · — Mikura,

..... Nanda.

For given  $X$  the value of  $T$  satisfying the above expression corresponds to  $T_\lambda^m$ , the lambda temperature of the mixture. The choice of the Gibbs' function made in this theoretical model does not seem to be the proper one. The expression one gets after making use of the functional dependence of the Gibbs' function for pure  $^4\text{He}$  on the normal fluid fraction gives temperature independent entropy for liquid helium I. This implies that liquid helium I has zero specific heat. Moreover, the Gibbs' function for the  $^4\text{He}$  component as a function of temperature (linear or quadratic in  $T$ ) and the normal fluid fraction of the total number of  $^4\text{He}$  atoms in their theory does not help much in bringing the theoretical  $T_\lambda^m - X$  curve in close agreement with the experimentally observed values. The theory also gives much higher values for the initial slope  $\left(\frac{\partial T_\lambda^m}{\partial X}\right)_{X \rightarrow 0}$  in both the cases of the Gibbs' function for the  $^4\text{He}$  component. The modification of this theory made by Nanda (1955) leads to

$$1 - X = \exp \left[ -\frac{1}{3} \left( \frac{T_\lambda}{T} \right)^{1/6} - \left( \frac{T}{T_\lambda} \right)^{1/6} + \frac{3WX^2}{RT} \right]$$

giving the variation of the lambda temperature with the concentration of  $^3\text{He}$ . This expression, as seen from the figure 2, fails to improve the



situation. An approach to this problem was made by Trikha and Nanda, with the assumption that  $^3\text{He}$  dissolves in  $^4\text{He}$ , normal as well as superfluid. They substituted the experimentally observed value of the initial slope in their expression for the lambda temperature of the solution in order to assign a value to the parameter called the interchange energy. This adjustment did not lead to the desired agreement with the experimental results. An appropriate modification of the form of the Gibbs' function for pure  $^4\text{He}$  or an entirely different approach to introduce the quantum nature of the liquid in the classical thermodynamic treatment is necessary.

Starting from an interpretation of the lambda point in liquid helium as a consequence of the Bose-Einstein condensation, Heer and Daunt (1951) put forward the idea that the behaviour of the mixtures of  $^3\text{He}$  and helium II could be described as an ideal mixture of a degenerate Bose-Einstein gas and a nondegenerate Fermi-Dirac gas. Thus, they assumed the statistical independence of the Bose-Einstein and the Fermi-Dirac systems in solutions of  $^3\text{He}$  and  $^4\text{He}$  and showed that the lambda temperature of the mixture is given by the degeneracy temperature of the Bose-Einstein system. The expression for the lambda temperature of the mixture in this case is

$$\frac{T_{\lambda}^m}{T_{\lambda}} = \left[ \frac{1-X}{1+X\left(\frac{V_3^0}{V_4^0}-1\right)} \right]^{2/5}$$

The agreement with the experimental  $T_{\lambda}^m$  of the mixture improves a bit in this case as seen from figure 2. However the theory was criticized by de Boer and Gorter (1952), who showed that the distribution function  $\frac{C_V}{C_E}$  must have a discontinuity at the lambda point as a consequence of the finite jump in the specific heat of liquid helium at this temperature without regard to the model used, in opposition to the results of Heer and Daunt. Mikura (1954 and 1955) modified this theory by introducing a Bose-Einstein liquid model for liquid helium II in which He II is composed of Bose-Einstein particles in a smoothed potential well. Between the ground state and the first excited state there is an energy gap  $K\Delta$ ,  $k$  being the Boltzmann constant, and the total number of particles are clustered together in groups of atoms. He introduced  $^3\text{He}$  in this system as an ideal Fermi-Dirac gas in a smoothed potential well. It appeared necessary to introduce still another assumption

$$\Delta = \Delta_0 N_4 V_4^0 / (N_3 V_3^0 + N_4 V_4^0)$$

regarding the dependence of  $\Delta$  on  $^3\text{He}$  concentration to get agreement with experimental data on the lambda temperature of the mixtures. The refinement of the treatment made by Mikura leads to a very close, rather a very good fit of his  $T_{\lambda}^m$  vs  $X$  curves with the experimental data, as a result of the adjustment of the

parameters in his theory to that effect. The lambda temperatures of the mixtures are given in this case, by the expression

$$\frac{T_{\lambda}^m}{T_{\lambda}} = \left[ \frac{1-X}{1+X \left( \frac{V_3^0}{V_4^0} - 1 \right)} \right] \cdot \frac{F_{3/2}(\Delta_0/T_{\lambda})}{F_{3/2}(\Delta/T_{\lambda})} \quad \dots$$

One gets according to Ponomarev's model (1949) a negative shift of about 0.8 degrees per mole concentration, by using the effective mass derived from second sound experiments and taking for the lambda point the temperature at which the mass of the excited particles becomes equal to the total mass. (This value is rather too low)

The experimental lambda temperatures are in very good agreement with

$$T_{\lambda}^m = T_{\lambda} (1-X)^{2/3}$$

given by Goldstein (1954) from the asymptotic Bose-Einstein model by neglecting the effect of  $^3\text{He}$  on the total liquid density.

A number of phenomenological and molecular theories are available at present. The phenomenological approach made by de Boer and Gorter does not give any clue to the understanding of the molecular origin of the deviations from the laws of perfect solutions. A different choice of the Gibbs' function and an introduction of a non-ideality parameter make no appreciable improvement in the original theory. The root cause of the disagreement with the experiments seems to lie in the basic assumptions of the theory.

The theories based on the difference in the statistics are also unsatisfactory, though the approach made by Mikura leads to rather very good agreement with the experimental results. The parameters involved in this model render it rather easy to arrive at the desired results by their suitable adjustment. One can also obtain the results in reasonable agreement with the experiments, simply by making  $S_{\lambda}$  and either  $E$  or  $n$  concentration-dependent.

#### ACKNOWLEDGEMENTS

The author expresses his deep gratitude to Dr. C. J. Gorter, Director of the Kamerlingh Onnes Cryogenic Laboratory, Leiden, The Netherlands, for his kind permission to publish this paper.

The observations were taken in the K.O.C. Laboratory, Leiden. The author tenders his indebtedness to Prof. Taconis and Dr. Dokoupil for the facilities, unfailing help and valuable suggestions they gave during the progress of the experimental part of this work. The rest was recasted and carried out in the Physics Department of the Rajaram College, Kolhapur.

REFERENCES

- Abraham B. M.; Weinstock B. and Osborn D. V., 1949, *Phys. Rev.*, **76**, 864  
 Dash J. G. and Taylor R., 1955, *Phys. Rev.*, **99**, 598.  
 Daunt J. G., Probst R. E. and Jonston H. L., 1947, *J. Chem. Phys.*, **15**, 759.  
 ———, 1948, *Phys. Rev.*, **73**, 638.  
 Daunt J. G. and Heer C. V., 1950, *Phys. Rev.*, **79**, 46.  
 de Boer J. and Gorter C. J., 1950, *Physica*, **16**, 225.  
 De Boer J. and Gorter C. J., 1952, *Physica*, **18**, 565  
 Dokoupil Z., Kapadnis D. G., Shroeramurti K. and Taconis K. W., 1959, *Physica*,  
**25**, 567  
 Dokoupil Z., Van Soest G., Wansink D. H. N., Kapadnis D. G., 1954, *Physica*, **20**, 1181.  
 Eselsohn B. N. and Lazarev B. G., 1950, *Dok. Acad. Sc. U.S.S.R.*, **72**, 265.  
 Goldstein L., 1954, *Phys. Rev.*, **95**, 69.  
 Heer C. V. and Daunt J. G., 1951, *Phys. Rev.*, **81**, 447  
 Kapadnis D. G. and Dokoupil Z., 1955, *Rept. Conf. Basses Temp.*, Paris, a, 67, 19.  
 King J. C. and Fairbank H. A., 1953, *Phys. Rev.*, **93**, 21.  
 Mikura Z., 1954, *Prog. Theo. Phys. Japan*, **11**, 25; **14**, 337  
 Nanda V. S., 1955, *Phys. Rev.*, **97**, 571.  
 Pomeranchuk I., 1949, *J. Exp. Theo. Phys. U.S.S.R.*, **19**, 42.  
 Taconis, Boenakker, Nier and Aldrich, 1949, *Phys. Rev.*, **75**, 1966.  
 Stout J. W., 1948, *Phys. Rev.*, **74**, 605.

# Letters to the Editor

The Board of Editors does not hold itself responsible for opinions expressed in the letters published in this section. The notes containing short reports of original investigations communicated to this section should not contain many figures and should not exceed 500 words in length. The contributions reaching the Secretary by the 15th of any month may be expected to appear in the issue for the next month. No proof will be sent to the author.

6

## APPLICATIONS OF THE NON-DEGENERATE STATISTICAL RELATION TO BINDING ENERGY CHARACTERISTICS IN NUCLEI

A. K. DUTTA

UNIVERSITY COLLEGE OF SCIENCE

92, ACHARYYA PRAFULLA CH. ROAD, CALCUTTA-9

(Received June 19, 1966)

We have derived a statistical relation for the number of occupied states in nuclei (Dutta, 1966, eq. 6) which may be stated as,

$$\begin{aligned} A/2 &= \{k_c A^5 f(A)\} \exp(-E_n^0(A) + E_f)/KT \\ &\quad - \{k_c k_f A^5 f(A)\} \exp(-E_n^0(A)/KT) \\ &= 2.327 \times 10^4 A^5 f(A) \exp(-E_n^0(A)/0.40) \end{aligned} \quad \dots (1)$$

where  $f(A) = 1 + 4.2 \exp(-3.27 \times 10^{-2} A^2)$ .

The first factor in the first equation above, gives us the number of cells  $C(A)$  in different nuclei. A slightly modified form of  $f(A)$  as  $1 + 4.32 \exp(-2.29 \times 10^{-2} A^2)$ , with  $k_c = 3.907 \times 10^{-3}$  gives us a more rational mode of increase of cell numbers as  $C(4) = 16$ ;  $C(8) = 16C(4)$ ;  $C(16) = 16C(8)$ ;  $C(32) = 32.C(16)$  and so on for further duplicated nucleon numbers. It gives us  $k_f = 5.955 \times 10^6$  and hence  $E_f = 6.24$  MeV, when  $KT = 0.40$ . With the changed expression for  $f(A)$ , we have also put  $E_f = 6.226$  MeV and  $KT = 0.399$  MeV for better correspondence.  $E_f$  becomes the extrapolated limiting energy per nucleon in a single combination particle, on the basis of  $E_n^0(A)$  values for small nuclei.

We now consider the relations (Dutta, 1966, eq. 7) for nuclear binding energies. It may be expressed as,

$$E_n^0(A) = E_n^0(A) [2k_c A^4 f(A) \exp(-E_n^0(A) + E_f)/KT] \quad \dots (2)$$

The energy of any other form  $e_n^0(A)$ , associated with the nucleons in a nucleus, is expressed by the modified relation

$$e_n^0(A)/E_n^0(A) = [2k_c A^4 f'(A) \exp(-E_n^0(A) + E'_f)/(KT)] \quad \dots (2a)$$

The energy under consideration, may be positive or negative and might be related to a single nucleon as in the case of the  $\Lambda$ -particle or distributed throughout the nucleons in a nucleus. The relationship suggests that the required ratio is primarily determined by the change in the exponential form with respect to  $E_n^0(A)$ . The change in  $(KT)$  and  $E_f$  tells us about the comparative rate of variation of the considered energy in relation to  $E_n^0(A)$  and also about the starting magnitude. We may carry this idea to the minimum values of the total deducted energy,  $U_n^0(A)$ , per nucleon in different nuclei or separately to the coulomb and asymmetry energies per nucleon  $U_{cn}^0(A)$  or  $U_{an}^0(A)$ . The parameters  $E_f'$  and  $(KT)'$  are obtained by trial with the required values. The complete set of relations may be put as follows

$$\begin{aligned}
 E_n^0(A) &= E_n^0(A)[2k_c A^4 f(A) \exp(-E_n^0(A) + 6.226)/0.399] \\
 &= E_n^0(A)[2k_c k_f A^4 \exp(-E_n^0(A)/0.399)] \\
 \Lambda BE &= E_n^0(A)[2k_c k_f A^4 \exp(-E_n^0(A)/0.42)] \quad \dots (2b) \\
 U_n^0(A) &= E_n^0(A)[2k_c A^4 f(A) \exp(-E_n^0(A) + 4.815)/0.4585] \\
 U_{cn}^0(A) &= E_n^0(A)[2k_c A^4 f(A) \exp(-E_n^0(A) + 4.99)/0.443] \\
 U_{an}^0(A) &= E_n^0(A)[2k_c A^4 f(A) \exp(-E_n^0(A) + 0.52/0.643)]
 \end{aligned}$$

One may calculate from the set of relations (2b), above, the optimum binding energy  $E^*$  of a nucleus, the equivalent uniform radius  $R$ , corresponding to the nuclear coulomb energy or the optimum proton number  $Z_0$  in a nucleus. These would be determined by the relations

$$\begin{aligned}
 E^* &= A(E_n^0(A) - U_n^0(A)), \\
 R &= 3/5 \cdot Z(Z-1)e^2/(A \cdot U_{cn}^0(A)).
 \end{aligned} \quad (3)$$

$$A - 2Z_0 = A(U_{an}^0/C)^{\frac{1}{2}}$$

where the parameter ' $C$ ' is taken as 21.3. The calculated as well as the experimental values of  $E^*$  and  $Z_0$  (Konig *et al*, 1962) and of  $R$  (Hofstadter, 1956) are shown in the following tables.

TABLE I  
( $E^*$ , the binding energies of the most strongly bound nuclei)

$\Lambda$	4	5	8	12	14	19	31	55	111	150	222	250
$E^*(\text{Calc})$	26.6	34.3	58.2	99.3	108	151	259	475	949	1239	1705	1868
$E^*(\text{expt})$	28.3	27.3	56.5	97.1	105	148	263	482	948	1240	1708	1870

TABLE II

(R, the equivalent uniform radius of nuclei)

Nucleus	C <sup>12</sup>	Mg <sup>24</sup>	Si <sup>28</sup>	S <sup>32</sup>	Ca <sup>40</sup>	V <sup>51</sup>	Co <sup>59</sup>	In <sup>115</sup>	Sb <sup>122</sup>	Au <sup>197</sup>	Pb <sup>207</sup>	Bi <sup>209</sup>
R (Calc.)	2.90	3.76	4.10	4.35	4.90	4.52	5.02	5.97	5.88	6.84	6.89	7.03
R. Hofstadter	3.04	3.84	3.92	4.12	4.54	4.63	4.94	5.80	5.97	6.87	7.00	7.13

TABLE III

(Z<sub>0</sub>, the optimum proton number in a nucleus)

A	16	32	51	59	111	115	150	208	250
Z <sub>0</sub> (Calc.)	7.8	15.3	23.8	27.3	48.5	50.1	63	82.7	94.5
Z(expt.)	8	16	23	27	48	49	62	82	98

The close agreement between the observed and the calculated values brings out the fundamental nature of  $E_n^0(A)$  in determining all forms of nuclear energy values by modified exponential relations.

## REFERENCES

- Dutta, A. K., 1966, *Indian J. Phys.*, **40**, 181.  
 Hofstadter, R. 1956, *Rev. Mod. Phys.*, **20**, 214.  
 Kong, L. A., Matlack, T. H., and Wapstra, A. H., 1962, *Nucl. Phys.*, **81**, 18.

## BOOK REVIEWS

**ELEMENTARY PARTICLES**—by David H. Frisch and Alan M. Thorndike.  
Publisher—D. Van Nostrand Company, Inc., Princeton, New Jersey

The book is nice description of some of the basic experiments on elementary particles which are the nut-bolts in the structure of theories of elementary particles. The reader of the book need not have extensive familiarity with mathematical physics. The authors however have stressed on the rapidly changing state of knowledge in this field. The book may be used as a rapid reader.

*T. Roy*

**BOUNDARY AND EIGEN VALUE PROBLEMS IN MATHEMATICAL PHYSICS**—by Hans Sagan. Publisher—John Wiley and Sons, Inc, New York, London.

The book does not indulge much on the Technicalities but rather on the general principles by inductive methods. The book emphasises more on the problems. Though instructive, it seems as a text book it only fulfils a partial requirement. It is amusing to see that in Chapter VIII Article 1.2 the author has tried to deduce Schrodinger Equation and his Equation (VIII 18) is not correct though (VIII 20) is. Barring one or two such personal fancies the book is really a good one.

*T. Roy*

**THE PROPAGATION OF ELECTROMAGNETIC WAVES IN PLASMAS**—by V. L. Ginzburg, Translated by J. B. Sykes and R. J. Tayler. Pergamon Press, 1964. Pp. xix + 535. Price £. 7 net.

The theoretical study of the interaction of a plasma and an electromagnetic wave has turned out to be a common factor in many a scientific discipline, namely, ionospheric physics, astrophysics, radio astronomy and physics of laboratory plasmas. Barring a few topics, mentioned in the Preface, the study, in almost all its essential details, is admirably presented by the Soviet author in a single volume. The major topics omitted relate to plasmas with statistical inhomogeneities or with boundary walls and to plasmas in non-equilibrium conditions.

Four distinct types of plasmas are considered in the book—(i) homogeneous isotropic plasma, (ii) homogeneous magnetoactive plasma, (iii) inhomogeneous isotropic plasma and (iv) inhomogeneous magnetoactive plasma. A special emphasis is then laid on the two topics (a) reflection of radio waves from ionospheric layers, and (b) radio wave propagation in cosmic conditions. Finally, the important aspect of the non-linear phenomena in a plasma is considered.

Regarding the theory of wave propagation in plasmas, both the macroscopic and microscopic approaches are dealt with elegantly. The so-called elementary theory and the kinetic theory as well as the hydromagnetic and quasihydrodynamic approximations are presented to deduce plasma properties, such as permittivity,

conductivity, indices of refraction and absorption, etc. Methods for solving wave equations for a plasma are described, and the reflection, penetration, absorption and transmission of electromagnetic waves as well as the change in their polarisation are discussed. (One important omission here pertains to the numerical method of solution on a digital computer). Waves of various kinds—electromagnetic, plasma, hydromagnetic and acoustic—are considered. The special feature in the propagation of pulse signals is explained. Of particular significance are the discussions on spatial dispersion, supplemented by Appendix A, and on energy density and conservation of energy in a dispersive medium, supported by Appendixes B and C.

The problem of the reflection of radio waves by an inhomogeneous layer is discussed in detail mainly from the viewpoint of its applications to the ionosphere. The chapter on cosmic conditions concerns, on the one hand, the ionized atmosphere of the sun, our nearest star, and, on the other, the interstellar medium with particular reference to the absorption of waves owing to motion of electrons in the Coulomb field of a point charge. In the last chapter the author explains nonlinear phenomena in a plasma in terms of its parameters and describes such nonlinear effects as self-interaction, cross-modulation, generation of combination frequencies, etc.

It is worth noting that the author, all throughout the volume, has taken the definite stand of rejecting the Lorentz polarisation term in calculating the effective electric field in a plasma. Although there seems to be stronger evidence against the inclusion of the term than in favour, the issue, according to quite a few, is not yet conclusively settled.

A weak point of the book is its scanty reference to two topics of current interest: the first relating to diagnostics of laboratory plasmas, particularly in controlled thermonuclear experiments, and the second to communication through plasmas surrounding space vehicles during their re-entry into the earth's atmosphere.

The book has, to its credit, a long list of references, but a few well-known names like those of W. H. Eccles and J. Larmor, H. Margenan and W. P. Allis, are, unfortunately, found missing. In addition to the subject index following the list, an author index would have been much welcome.

Nevertheless, the book is really remarkable for the fact that, while it may be regarded as an elaborate work of reference for the research specialist, the expositions of basic phenomena are clear enough to help and satisfy the beginner.

Sykes and Rayler are to be congratulated for their commendable translation of the Russian text. The book incorporates a great deal of results obtained by Soviet physicists, and the English edition is particularly valuable for making the results known to a large number of interested persons who had so long little acquaintance with the work carried out in the USSR.

*J. Basu*



# ON THE ESTIMATION OF ELASTIC SCATTERING CROSS SECTIONS OF GAMMA RAYS FROM DIFFERENT ELEMENTS

M SINGH, S. ANAND AND B S SOOD

PHYSICS DEPT., PUNJABI UNIVERSITY, PATIALA

(Received October 27, 1965)

**ABSTRACT** A method for the estimation of elastic scattering cross sections of low energy gamma rays from different elements at different scattering angles is described. It is based on the use of the exact calculations of Brown and Mayers for mercury and the experimental data on  $Z$  dependence. The estimated values show a good agreement with the available experimental data.

## INTRODUCTION

Rayleigh scattering from atomic electrons and Thomson scattering from nuclear charge are the only processes which make any significant contributions to the elastic scattering of low energy gamma rays. While Thomson scattering from different elements can be accurately calculated, the exact calculations of Rayleigh scattering are available only for  $K$ -electrons of mercury. However, various approximate form factor calculations have been proposed by many workers to estimate Rayleigh scattering from different elements. Unfortunately, these form factor calculations have been found to be in large errors. In a recent communication, we suggested that our experimental studies of  $Z$  dependence of elastic scattering of gamma rays can be combined with the refined calculations of Brown and Mayers (1957) to give reliable estimates of elastic scattering cross sections of gamma rays from different elements at various scattering angles and gamma ray energies (Anand *et al.*, 1964). In the following sections we outline the method of estimation and compare the results so obtained with the available experimental data.

## METHOD OF ESTIMATION

The refined calculations of Brown and Mayers (1957) for Rayleigh scattering are given in terms of  $K$ -shell scattering amplitudes for mercury with and without polarization change. The cross section for Rayleigh scattering is given in the form :

$$(d\sigma/d\Omega)_k = r_0^2 [ |a_{1k} + ib_{1k}|^2 + |a_{2k} + ib_{2k}|^2 ] \quad \dots (1)$$

where subscripts  $1k$  and  $2k$  denote the  $K$ -shell amplitudes with no polarization change and with polarization change respectively, and  $r_0$  is the classical electron

radius. These amplitudes are complex quantities; the contributions of the imaginary part are particularly small at low values of momentum transfer ( $q = \frac{2\hbar v}{mc^2} \sin \frac{\theta}{2}$ ). Neglecting the imaginary parts, Bernstein and Mann (1958) have shown, by plotting the real parts of the scattering amplitudes that these may be written as,

$$\begin{aligned} a_{1k} &= F_{1k}(q) \frac{1+\cos \theta}{2} \\ a_{2k} &= F_{2k}(q) \frac{1-\cos \theta}{2} \end{aligned} \quad \dots (2)$$

$F_{1k}$  and  $F_{2k}$  are smooth functions of  $q$  above  $q = 0.6$  and for all values of  $q$  respectively. Further,  $F_{2k}$  is very nearly equal in magnitude to the Bethe's  $K$ -shell form factor (Bethe 1952), and consistently large than  $F_{1k}$ . Bernstein and Mann (1958) have calculated the contributions of the  $L$  shell electrons to the elastic scattering by assuming that the non-spin flip and spin flip amplitudes for  $L$  shell contribute in the same ratio as the corresponding  $K$  shell amplitudes. However, Brown and Mayers (1957) suggest that this assumption may not be correct at large values of  $q$  and experimental data suggest that it is better to neglect the contribution of non-spin flip amplitude for  $L$  shell electrons for large values of  $q$ . So, in our work we have altogether neglected the contributions of non-spin flip amplitudes for  $L$  shell electrons at values of  $q$  larger than 1. The  $L$  shell amplitudes were taken from the work of Bernstein (1958).

The contributions of nuclear Thomson scattering, which interferes constructively with Rayleigh scattering, are calculated from the well known classical relation

Combining the various contributions, Rayleigh plus nuclear Thomson scattering cross section for mercury at a scattering angle  $\theta$  is given by

$$(\frac{d\sigma}{d\Omega})_{Ray. + Thom.} = r_0^2/4 [(A^2 + B^2)(1 + \cos \theta)^2 + (C^2 + D^2)(1 - \cos \theta)^2] \quad \dots (3)$$

where,

$$A + iB = F_{1k}(q) + F_{1L}(q) + a \quad \dots (4)$$

$$C + iD = F_{2k}(q) + F_{2L}(q) + a$$

and,

$$a = (Z^2 m/M)_e$$

Here  $m$  is the electronic mass,  $M$  the nuclear mass and  $Z$  the atomic number of the scatterer.  $F_{1k}(q)$  and  $F_{2k}(q)$  contain both real and imaginary parts as given in the papers of Brown and Mayers (1957), and

$$F_{1k}(q) = (a_{1k} + ib_{1k})/(1 + \cos \theta)/2 \quad \dots (5)$$

$$F_{2k}(q) = (a_{2k} + ib_{2k})/(1 - \cos \theta)/2$$

The values of  $a_{1k} + ib_{1k}$  and  $a_{2k} + ib_{2k}$  were taken for different scattering angles from the data of Brown and Mayers (1957) for gamma ray energies of 1.28 and 2.56  $mc^2$ , and accordingly  $F_{1k}$  and  $F_{2k}$  calculated as functions of momentum transfer. The values of  $F_{1k}$  and  $F_{2k}$  were taken from the work of Bernstein (1948) for different values of  $q$ . The values of  $A^2 + B^2$  and  $C^2 + D^2$  for mercury, so obtained, are plotted as functions of momentum transfer in Fig. (1). By

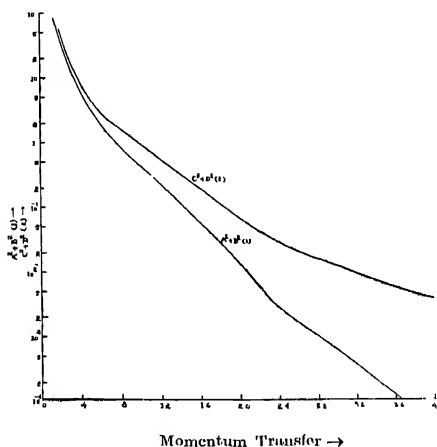


Fig. (1) Plots of  $A^2 + B^2$  and  $C^2 + D^2$  against momentum transfer for mercury.

For definitions reference may be made to text

means of these curves, it is possible to estimate the elastic scattering cross sections for mercury at various gamma ray energies and scattering angles

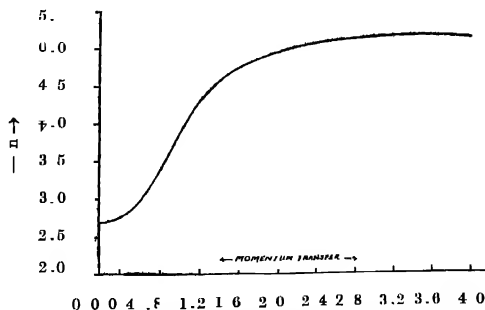


Fig. (2) A Plot of index 'n' of  $Z$  dependence against momentum transfer for elastic scattering of gamma rays

The experimental  $Z$  dependence curve which shows the variation of index  $n$  of  $Z$  dependence is given in Fig (2) for various values of momentum transfer (Anand *et al.*, 1964). This curve has been obtained from a study of the variation of the elastic scattering cross sections with atomic number of the scatterer for 0.280, 0.411 and 0.662 MeV gamma rays scattered from Ag, Sn, W and Pb at different scattering angles.

In order to estimate the scattering cross section from the above data for any desired element ( $Z \geq 47$ ) at particular values of gamma ray energy and scattering angle, the corresponding cross section for mercury was first evaluated from Fig (1), and eqn (3). To convert this cross section for mercury to the desired element of atomic number  $Z$ , the following relation was used,

$$(d\sigma/d\Omega)_{Ray + Thom.}^{Z, q} = (d\sigma/d\Omega)_{Ray + Thom.}^{80, q} (Z/80)^n \quad (6)$$

the index  $n$  was obtained from the experimental curve in Fig (2) corresponding to the particular value of  $q$ .

#### RESULTS AND CONCLUSIONS

The estimated cross sections are compared with the available experimental results in Figs (3-6). Figs. (3a, 3b) show a comparison of estimated cross sections for Pb, Pt, Ta and Sn for 0.662 MeV gamma rays at different angles with the experimental data of Narasimhamurthy *et al.* (1964). Also shown in these Figs are

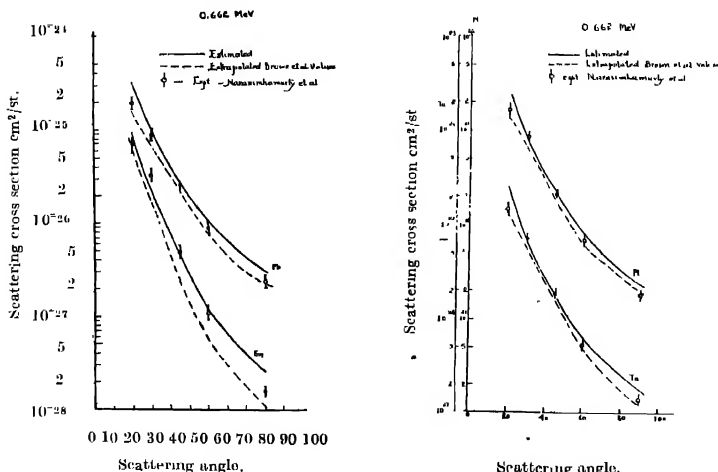
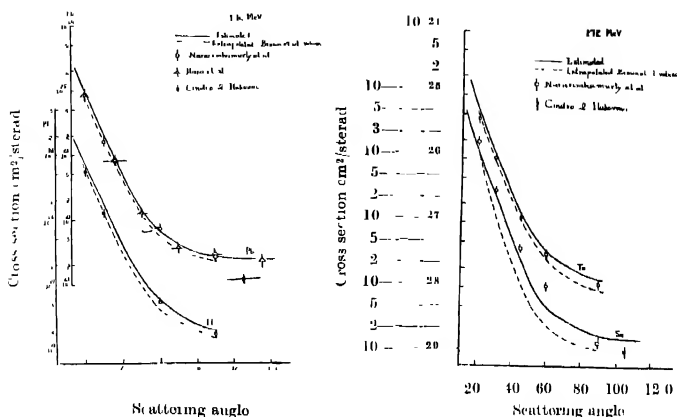


Fig. (3a, 3b) Comparison of the 'estimated' and experimental elastic scattering cross sections for 0.662 MeV gamma rays for Pb, Pt, Ta and Sn.



Figs. (4a, 4b) Comparison of the 'estimated' and experimental elastic scattering cross sections for 1.12 MeV gamma rays for Pb, Pt, Ta and Sn

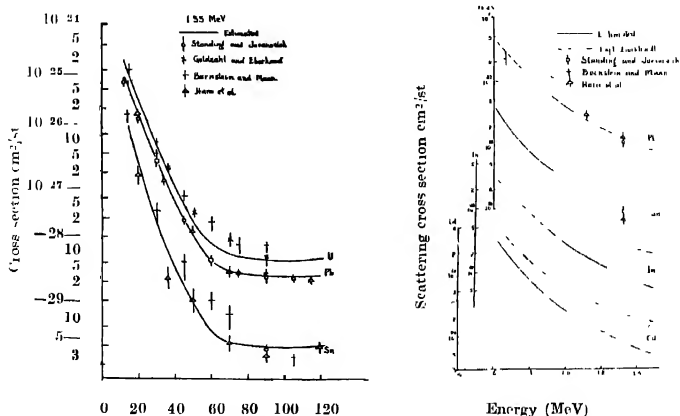


Fig. (5) Comparison of the 'estimated' and experimental elastic scattering cross sections for 1.33 MeV gamma rays for U, Pb, and Sn

Fig. (6) Comparison of 'estimated' and experimental elastic scattering cross sections for Pb, Sn, In and Cd at 90° for different energies.

the extrapolated Brown et al. values of scattering cross sections as reported by Narasimhamurthy *et al* (1964). The agreement is better with our estimates. In Figs (4a) and (4b) a comparison of the estimated cross sections for Pb, Pt Ta

and Sn at 1.12 MeV is made with the experimental results of Hara *et al.* (1958), Cindro and Ilakovac (1958) and Narasimhamurthy *et al.* (1964), and extrapolated theoretical values of calculation of Brown and Mayers (Narasimhamurthy *et al.*, 1964). Again the agreement is quite good with the results of Hara *et al.* and Narasimhamurthy *et al.* while the results of Cindro and Ilakovac are somewhat lower. The extrapolated values are also lower. Fig (5) compares the estimates at 1.33 MeV for U, Ph and Sn with experimental values of Standing and Jovanovich (1962), Goldzahl and Eberhard (1957), Bornstein and Mann (1958) and Hara *et al.* (1958). The results of Hara *et al.* and Standing and Jovanovich agree well with the estimated values while those of Goldzahl and Eberhard and Bornstein and Mann are appreciably higher. This discrepancy is resolved if, as pointed out by Standing and Jovanovich, the experimental results of Bornstein and Mann are assumed to include some contribution of incoherent scattering. In Fig. (6) we have compared our estimates for Pb, Sn, In and Cd at 90° at different gamma ray energies with the experimental results of Burkhardt (1955) and Hara *et al.* (1958). Here, we find that the experimental data of Burkhardt are consistently higher than the latter more reliable data (Hara *et al.*, 1958, Standing and Jovanovich 1962) which are quite scanty. This may be due to the presence of appreciable amounts of incoherent scattering in the measurements of Burkhardt (1955).

Thus there exists an over all agreement between the estimated and reliable experimental values of the differential scattering cross sections for different elements at various scattering angles and gamma ray energies. Moreover, the estimates of the scattering cross sections made by Narasimhamurthy *et al.* (1964) from extrapolation of calculations of Brown *et al.* are lower than our estimates and the experimental values. This is particularly noticeable for tin where any deficiency in the method of extrapolation should be clearly exposed.

The cross sections of non-resonant elastic scattering estimated by the method described above can be used with confidence to determine the cross section of resonant scattering of gamma rays by comparison with non-resonant scattering cross section, especially when the experimental arrangement needed to restore resonance condition is complicated and it is not possible to calculate the solid angles from the geometrical set up (see for example Moon 1951).

#### REFERENCES

- Anand, S ; Singh, M. and Sood, B. S., 1964, *Curr. Sci.* **33**, 333.  
 Bornstein, A and Mann, A. K., 1958, *Phys. Rev.* **110**, 805  
 Bornstein, A., 1958, *Ph. D. Thesis*, Univ. of Pennsylvania  
 Bethe, H. A., 1952, *Private Communication to Levinger, J. S.* 1952. *Phys. Rev.* **87**, 656.  
 Brown, G. E. and Mayer, D. F., 1957, *Proc. Roy. Soc. A* **242**, 89.  
 Burkhardt, J. L. 1955, *Phys. Rev.* **100**, 192.  
 Cindro, N. and Ilakovac, K., 1958, *Nucl. Phys.* **5**, 647  
 Goldzahl, L. and Eberhard, P. 1957, *J. Phys. Radium*, **18**, 33.  
 Hara, E. *et al.* 1958, *J. Phys. Radium*, **19**, 668.  
 Moon, P. B., 1951, *Proc. Phys. Soc.* 1964, **A64**, 76.  
 Narasimhamurthy, V. A. *et al.* *Proc. Nucl. Phys. Symp. Chandigarh*, Page 312, long darh  
 1965, *Nucl. Phys.* **62**, 296  
 Standing, K. G. and Jovanovich, J. V., 1962, *Canad. J. Phys.* **40**, 622.

# EXPERIMENTAL INVESTIGATIONS ON POLARIZATION CHARACTERISTICS, ELECTRON NUMBER DENSITY AND ELECTRON COLLISIONAL FREQUENCY OF DOWN-COMING RADIO-WAVES AT OBLIQUE INCIDENCE

S. R. KHASTGIR AND Y. S. N. MURTY

BOSE INSTITUTE, CALCUTTA

(Received March 3, 1966)

**ABSTRACT.** The paper presents the studies carried out at Banaras on polarization characteristics of the downcoming waves of medium-wavelengths at oblique incidence. The crossed loop-aerial system of Ratcliffe and White was employed. The broadcasting stations were so chosen, that the ground waves from them did not reach Banaras.

The downcoming wave was found to be in general elliptic. It was found that only the ordinary waves with a left-handed sense of rotation were received from the medium-wave stations.

The method of transforming the observed polarization parameters from the set of axes in and at right angles to the plane of incidence, to the set of axes in and at right angles to the magnetic plane has been given.

From the polarization parameters, transformed in the above manner, the values of electron number density and electron collisional frequency have been estimated. The values of electron collisional frequency have been found to be within the expected limits for the E-layer. In the case of electron number density, the values obtained from two stations were found to be in agreement with those obtained from the normal sounding studies of Eckersley and Farmer. The discrepancy in the case of the other stations is discussed.

## INTRODUCTION

The experimental studies of the polarization characteristics of downcoming radio waves were initiated by Appleton and Ratcliffe (1928). They showed that the downcoming medium radio waves were in general, elliptically polarized with a left-handed sense of rotation in the northern hemisphere, as expected from the magneto-ionic theory of Appleton (1932) and Hartree (1929), where the angle between the direction of propagation and the positive direction of the earth's magnetic field was acute. The prediction of Appleton and Ratcliffe from the magneto-ionic theory, that under similar conditions of propagation the downcoming waves should acquire a right-handed sense of rotation in the southern hemisphere, was later verified and confirmed by Green (1934) in Australia. Following these workers,

\*Senior Scientific Officer, Defence Electronics Research Laboratory, Hyderabad—Deccan.

various investigators (Ratcliffe and White, 1933, Martyn and Green, 1935; Eckersley and Millington, 1939, Eckersley, 1950) carried out polarization experiments with different apparatus of their own design. Though all these investigators established the general nature of polarization expected in the southern and northern hemispheres, only Eckersley and Millington undertook a quantitative study in the medium-frequency range, by exactly finding out the ellipticity of the polarization ellipse in the downcoming wave and comparing it with the ellipticity expected from the theory for such a downcoming wave. Though the results of Eckersley and Millington were in general agreement with the nature of polarization expected in the northern hemisphere, they were not able to establish conclusively the agreement of the experimental results with the theoretical values for all the stations employed for this study, excepting in the cases of only two stations. The theoretical values taken by Eckersley and Millington for comparison were based on the Appleton-Hartree formulae which is true for vertical incidence only, whereas the downcoming waves were received at oblique incidence. Budden (1952), however, expressed his view that the applicability of Appleton-Hartree formulae by Eckersley and Millington was not justified for larger angles of incidence, although their results, appeared to show some agreement with the Appleton-Hartree formulae in the cases of two stations. Under these circumstances, it was considered desirable to undertake a systematic study of the polarization of the downcoming waves arriving at large angles of incidence in order to examine how far the experimental results would agree with the theory. Accordingly the present investigation was carried out to determine the experimental values of the polarization characteristics for oblique propagation of radio-waves through the ionosphere, as received at Banaras from the various transmitting stations situated in India and Pakistan and then to obtain the electron number density and electron collisional frequency by using the formulae given by Murty and Khastgir (1959).

The experimental technique in the present investigation was the same as that adopted by Ratcliffe and White (1933). Some advantages of this method of experimental study of the downcoming radio-wave and its suitability for the investigation of rapidly varying polarization, are mentioned below :

(i) This method is free from the assumption that is made in Appleton and Ratcliffe's frequency-change method that the polarization of the downcoming wave should remain sensibly constant for about 15 seconds or more.

(ii) With regard to the method of Eckersley and Millington, it may be mentioned that for the accurate determination of both the ratio of the axes and the tilt-angles of the polarization ellipse, it is essential to choose only those stations for which the ratio of the axes of the projected polarization ellipse lies between 0.3 and 0.6. Since in the present investigation on downcoming radio-waves coming from the different transmitting stations situated at widely different distances, it is expected to have a widely varying polarization, the method of Eckersley and Millington has not been adopted.



(iii) A definite advantage offered by Ratcliffe and White's method over other methods is that the polarization changes, even though rapid, can be followed visually and photographically

In the present investigation the polarization characteristics from five medium-wave transmitting stations were studied. All these stations studied are distant stations from which the ground waves did not reach the receiving station. All the stations with their names, wavelengths and frequencies are given in Table I.

TABLE I

Transmitting station	Wavelength in meters	Frequency Kc/s.	Distance from Benarus (Km)
<i>Medium-wave stations</i>			
1. Calcutta (AIR)	300 0	1000	636
2. Dacca (Radio Pakistan)	257.1	1167	756
3. Delhi-A (AIR)	338.6	886	684
4. Hyderabad-Dorean (AIR)	411 0	730	990
5. Lahore (Radio Pakistan)	276 0	1100	1087

#### METHOD OF RATCLIFFE AND WHITE EXPERIMENTAL

The study of the polarization of the downcoming radio-waves from the different broadcasting stations was made by the method of Ratcliffe and White (1933). In this method a pair of 'crossed' loop-aerials were connected through two separate  $R/F$  amplifier units to the opposite pairs of the deflecting plates of a cathode-ray oscillograph. One of the loop aerials was placed in the direction of arrival of the downcoming wave, and the other at right angles to it. The E.M.F.'s induced in these loop-aerials were then amplified equally by two suitable  $R/F$  amplifier units which were arranged to give linear amplification. If the E.M.F.'s induced in the two loop-aerials were in phase, then the amplified voltages tuned to the frequency of the downcoming wave and applied to the pairs of deflecting plates of the cathode-ray oscillograph were also in phase and a straight line was obtained on the oscillograph screen. When there was a phase-difference between the induced E.M.F.s, an elliptic or circular pattern was obtained. The polarization characteristics of the downcoming wave were studied from the type of the patterns observed on the oscillographic screen.

The details of the equipment employed in this investigation are described below.

#### *'Crossed' loop-aerial system and its associated circuit connections*

For working on medium wavelengths an aerial system consisting of two 'crossed' loop-aerials, 6 ft square, capable of rotation about a common vertical

acis was installed on the roof of the top floor of the Physics Department building (Banaras University). The observation room is of the dimensions of  $11' \times 11' \times 11'$ , with 9" thick walls and with no iron or any metal structure in it. Each loop-aerial could be tuned over a range of frequencies by means of a pair of similar ganged condensers, enclosed in a shielded metal box arranged symmetrically with respect to the loop the common plates of the ganged condensers being earthed. The output terminals from the extreme plates of the two ganged condensers, for each aerial, were connected to the input terminals of the push-pull stage of each of the two identical  $R/F$  amplifier units which will be described later. The connecting wires from each loop to the extreme plates of the two ganged condensers, and then from the latter to the input terminals of each amplifier, were shielded and arranged symmetrically. With symmetrical arrangement and with the push-pull arrangement, the antenna-effect in either loop was practically eliminated.

Since the two loop-aerials were in close proximity, and since both the amplifiers were connected to the same oscillograph, it was necessary to guard against the interaction effects which would be due to the following causes

- (i) Coupling between the two loop-aerials
- (ii) Coupling between the two output circuits by way of electrode capacitances of the deflecting plates of the oscillograph
- (iii) Coupling between the output of one amplifier and the input of the other amplifier.

Since the two loop-aerials were exactly perpendicular to each other and their associated circuits were arranged symmetrically and further since shielded wires were used from the loop-aerials to the ganged condensers and from the condensers to the amplifier units, the coupling between the two loops was eliminated. The coupling between the two output circuits was, however, found to be negligible at these frequencies with the Du Mont Oscillograph, Model 274-A used during the course of this investigation. In order to prevent interaction between the output end of one amplifier and the input end of the other, the original frequency was converted into an intermediate frequency by a local oscillator after the first push-pull stage of the  $R/F$  amplifier unit. It was essential to employ a common oscillator in order to keep the phase relation between the two  $I/F$  output voltages the same as that existing between the voltages before frequency conversion. The use of a common oscillator was also an advantage as the  $I/F$  could be maintained at the same value in both the amplifiers.

#### *Radio-frequency amplifier units*

(i) *Description of the Circuits* The two similar  $R/F$  amplifier units, the purpose of which was to obtain linear amplification, sufficient to produce a good response in the oscillograph, were designed and constructed as follows :

In the first stage of each amplifier two similar pentode valves (6AC7) were used in push-pull, the control grid of each valve being connected through a suitable leak resistance to the earth. The output voltage from each of the two loop-aerials, each of which was tuned by a ganged condenser was applied to the two grids of the push-pull circuit of each amplifier unit. The necessity of employing a ganged condenser with the common plates earthed was due to the push-pull arrangement in the first stage of the amplifier unit. The primary coil of an I/F transformer joined the anodes of the two valves in the push-pull stage in the usual way. The secondary coil was tuned by a variable tuning condenser. The voltage across the tuned secondary was then applied to the grid and the filament of the pentagrid mixer (6L7). Oscillations generated in a separate circuit using a 6J5 triode valve were fed into the mixer tube in the usual way. The same oscillatory voltage was fed into the mixer tube (6L7) of the second R/F amplifier unit. The I/F voltage output in the plate circuit of the mixer tube was fed through an I/F amplifier (6SJ7) to the deflecting plates of the oscillograph. The whole amplifier unit was well shielded. For achieving identical performance of the two amplifiers, care was taken to use similar components in similar circuits of the two amplifier units. The biasing voltage to the control grid of the various valves was obtained by means of self-biasing resistors in the cathode leads of the respective valves as shown in the circuit diagrams (Fig. 1)

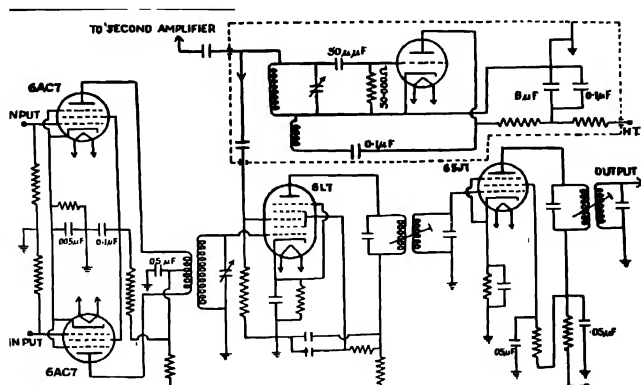


Fig. Circuit diagram of the R/F amplifier with common oscillator.

(ii) *Power Unit*: To avoid any interaction between the two R/F amplifier units through the common power supply, separate power supply units were employed for working the two R/F amplifier units. The power supply units were

of the conventional type used in communication receivers, employing a full-wave rectifier valve of Type 80 and a condenser-choke-filter network to smooth the D.C. output to the desired level. The D.C. output voltage from the power unit was supplied to the various anodes and screen grids of the amplifier valves through suitable dropping resistors and by-passing capacitors.

(iii) *Characteristics Curves*. As the two R/F amplifier units should be identical and their amplifications should be linear, it was necessary to study the gain characteristics of the amplifier units. Employing a signal generator with a calibrated output, the gain of each amplifier unit was determined for various input voltage at required frequencies and found to be satisfactory. It was also found that the two sections of the push-pull circuit were exactly similar.

#### THE OSCILLOGRAPH AND PHOTOGRAPHIC ARRANGEMENTS

A Du Mont oscillograph (Type 274-A) with blue fluorescence was employed for obtaining the elliptical patterns on its fluorescent screen. The deflection sensitivities for the *X* and *Y* deflector plates were 18 rms volts/inch and 16 rms volts/inch respectively. The gains of the two R/F amplifier units were sufficient to produce good elliptic patterns on the oscillograph screen. The patterns were photographed by an Alpha Camera (*f*/1.8 lens) and also by a Cossor Oscillograph Camera (*f*/3.5 lens).

#### THEORY OF THE RECEPTION OF THE DOWNCOMING RADIO-WAVE FROM THE DISTANT BROADCAST STATIONS

For distant transmitting stations the ground waves did not reach the receiving point. Let the downcoming wave be incident at the receiving station at an angle  $i$  in the plane of incidence of the wave. The wave is reflected from the ground at the same angle. The downcoming wave is in general abnormally polarized. Let the component of the magnetic vector at right angles to the plane of incidence be  $H_1$  and the component in the plane of incidence be  $H_2$ , the corresponding electric vectors being  $E_1$  and  $E_2$  respectively. The corresponding vectors for the wave reflected from the ground can be obtained by considering the ground reflection coefficients for the two components.

If  $E_L$  is the E.M.F. induced by the wave in the loop-circuit in the plane of propagation, we have,

$$E_L = \alpha \frac{dH_1}{dt} (1 + K_1) = jp\beta E_1 (1 + K_1) \quad \dots (1)$$

where  $K_1$  is the reflection coefficient of the ground for the normal magnetic component  $H_1$  and  $\alpha$  and  $\beta$  are circuit constants. The value of  $E_L$  at any instant  $t$  is assumed to be of the form  $e^{jpt}$ , where  $p$  is angular frequency of the wave. The current in the loop parallel to the direction of propagation is then given by

$$i_L = jpXE_1(1 + K_1) \quad \dots (2)$$

where  $X$  = a new circuit constant. Considering now the loop-aerial, the plane of which is perpendicular to the plane of propagation of the downcoming wave, the E.M.F. induced in it is given by

$$E_F = \eta \frac{dH_2}{dt} (1 + K_2) \cos i = j\omega \rho E_2 (1 + K_2) \cos i \quad (3)$$

and the current in the perpendicular loop by

$$i = \eta p Z E_2 (1 + K_2) \cos i \quad (4)$$

where  $\eta$ ,  $\rho$  and  $Z$  are circuit constants and  $K_2$ , the ground reflection coefficient for the abnormal magnetic component of the downcoming wave. The ground plan of the fields is shown in Fig. 2.

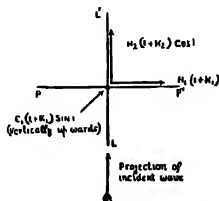


Fig. 2 Ground-plan of fields

Since the amplifiers are arranged to give linear amplifications, the corresponding amplified voltages  $e_1$  and  $e_2$  applied to the deflecting plates of the oscillograph are as follows

$$e_1 = j\omega X' E_1 (1 + K_1) e^{j(\omega - p)t} \quad \dots (5)$$

$$e_2 = j\omega Z' E_2 (1 + K_2) e^{j(\omega - p)t} \quad \dots (6)$$

where  $X'$  and  $Z'$  are new circuit constants, and the factor  $e^{-j(\omega - p)t}$  is due to the frequency change in the amplifier,  $\omega$  being the angular frequency of the local oscillation and  $p$  the angular signal frequency.

As in the experiments, the two loop-aerials were identical and also the two R/F amplifiers,  $X' = Z'$ . Further, as shown in Appendix I,  $\frac{1 + K_1}{1 + K_2} \approx 1$ . Thus the ratio of the voltages would be given by,

$$\frac{e_2}{e_1} = \frac{E_2}{E_1} \cos i \quad \dots (7)$$

The ratio  $e_2/e_1$  and the phase-difference  $\phi$  between the two voltages  $e_2$  and  $e_1$  (which is the same as that between  $E_2$  and  $E_1$ ) were obtained from the elliptic pattern by following the procedure described later.

MEASUREMENT OF THE POLARIZATION  
CHARACTERISTICS FROM THE OSCILLOGRAPHIC  
PATTERN

Let us suppose that the  $Y$ -plates of the oscillograph are connected to the output of the amplifier unit for the loop-aerial in the direction of arrival of the down-coming waves, and the  $X$ -plates to the output of the other amplifiers unit for the other loop-aerial in the perpendicular direction. The voltage  $e_1$  developed across the loop in the plane of incidence will give a vertical line in the  $Y$  direction and the voltage  $e_2$  will give a horizontal line in the  $X$  direction. The resultant pattern on the oscillograph will be elliptic, circular or linear depending on the phase-difference and the amplitude-ratio of  $e_2$  and  $e_1$ . From the elliptic pattern, (i) the ratio  $e_2/e_1$ , (ii) the phase-difference and (iii) the sense of rotation of the ellipse can be determined in the manner described below.

The ratio  $e_2/e_1$  can be easily obtained from the sides of the rectangle which just includes the ellipse as shown in Fig. 3.

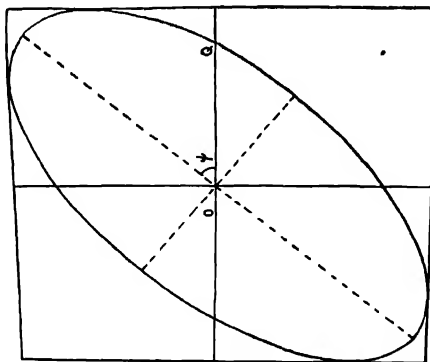


Fig. 3 Diagram of an elliptic pattern inside a rectangle

$$\frac{e_2}{e_1} = \frac{AB}{BC} \quad \dots (8)$$

The sine of the phase-difference can be readily determined as the ratio of the intercept of the  $X$ -axis to the maximum displacement of the spot towards the  $X$ -direction from the origin and hence will be given by

$$\sin \phi = \frac{OQ}{OX} \quad (\text{Fig. 3}) \quad \dots (9)$$

# DETERMINATION OF THE SENSE OF ROTATION

Let  $\phi_1$  and  $\phi_2$  be the phases of the amplified voltages corresponding to  $E_1$  and  $E_2$  at any instant. Then according to our notation, the phase-difference  $\phi = \phi_1 - \phi_2$ . If now the phase  $\phi_1$  of the applied voltage  $e_1$  corresponding to the loop-aerial in the direction of propagation and giving a linear sweep on the oscillograph in the  $Y$ -direction is decreased by increasing the capacity of the tuning condenser  $C_L$  across the parallel loop, the phase-difference  $\phi$  becomes smaller and hence the elliptic pattern approximates more closely to a straight line. The same effect is produced on the elliptic pattern, if the phase  $\phi_2$  of the applied voltage  $e_2$  corresponding to the loop-aerial in the perpendicular direction is increased by decreasing the capacity of the tuning condenser  $C_P$  across the same loop-aerial. This corresponds to the condition,  $0 < \phi_1 - \phi_2 < \pi/2$ , provided the elliptic pattern lies in the calibration quadrant and the downcoming polarized wave has a left-handed sense of rotation (in the northern hemisphere). We have therefore the rule that if an increase of the capacity of the tuning condenser in the parallel loop-aerial or a decrease of the capacity of the tuning condenser in the perpendicular loop-aerial causes the ellipse in the calibration quadrant to approximate more closely to a straight line, the wave is to be considered left-handed and *vice versa*.

## EXPERIMENTAL ADJUSTMENT

The two loop aerials and the two  $R/F$  amplifiers were first tuned to the frequency of the desired station, and the aerial connections were disconnected from the amplifier. An  $R/F$  voltage was then fed to both the amplifiers through an  $R/F$  transformer, the secondary of which was tuned by a ganged condenser. The frequency of the signal generator was adjusted to be the same as that of the desired transmitting station. As the input signal voltage was the same for both the amplifiers and as the amplifiers were already in the tuned position we would expect a straight line on the oscillograph screen. But actually, in practice, a very narrow ellipse was observed on the oscillograph screen. The narrow ellipse was reduced to a straight line by readjusting the amplifier controls. This adjustment indicates that no phase-difference was introduced by the amplifiers during the process of amplification.

The next adjustment was to get equal deflections on the oscillograph along the  $X$  and  $Y$  directions for the same voltage in the two loop-aerials. This was done by adjusting the gain controls in the amplifier units such that the straight line observed on the oscillograph screen made an angle  $45^\circ$  with the  $X$  direction. This  $45^\circ$ -alignment compensated for the unequal deflection sensitivities of the oscillograph plates along with vertical and the horizontal directions.

## EXPERIMENTAL RESULTS ON THE POLARIZATION OF THE DOWNCOMING WAVE FOR OBLIQUE INCIDENCE

The amplifiers were adjusted during the day time to receive the frequency of the station under study. Receiving the signal in the day-time, the loop-aerial

system was also tuned. For about an hour, around sunset, the pattern on the oscillograph was found to be small and looked like a diffused patch of light. A regular polarization pattern, generally, an ellipse, was observed on the oscillograph screen from about an hour after sunset. Observations were taken both visually and photographically. For visual observations, a transparent scale was attached to the oscillographic screen and the coordinates of the ends of the major axis and the intercept of the ellipse on the  $X$ -axis were noted at regular intervals of 10-15 seconds. The elliptic patterns were also photographed at suitable times.

From the observed polarization ellipse, the values of the ratio  $e_2/e_1$  and  $\phi$  the phase-difference were computed by the method described earlier. Some representative polarization patterns recorded photographically after some visual notings from the five medium wave transmitting stations are shown in (Figs 4a-4e). Though the polarization pattern was in general elliptic, there was evidence of linear and circular polarization at times. As the values of  $e_2/e_1$  and  $\phi$  were found to vary with time in a random manner, the most probable values were obtained by drawing in each case a distribution curve showing the number of times the value of  $e_2/e_1$  and  $\phi$ , lying within a small range was found to occur against the mean value over that range, the whole period of observation having been divided into a number of such small ranges. The values of  $E_2/E_1$  were then calculated from the corresponding values of  $e_2/e_1$  and the most probable values of  $E_2/E_1$ ,  $e_2/e_1$  and  $\phi$  are given in Table II.

Following the procedure outlined earlier the sense of rotation of the downcoming waves, from the different transmitting stations as received at Banaras, was determined. The downcoming waves from all the transmitting stations showed left-handed sense of rotation during the whole period of observation which was usually from 1900 to 2300 hrs.

TABLE II  
Most probable values of  $E_2/E_1$  and  $e_2/e_1$

Station	Meters	Distance from Banaras (Km)	Most probable values		
			$e_2/e_1$	$E_2/E_1$	$\phi$
Delhi A	338.6	684	0.7	2.75	55°
Calcutta	330.0	636	0.45	1.94	60°
Hyderabad-Deccan	411.0	990	0.47	2.38	57°30'
Decca	257.1	750	1.07	4.31	42°11'
Lahore	276.0	1087	0.55	3.38	26°36'

In calculating the values of the critical collisional frequency  $\nu_c$  from the expression  $\nu_c = \frac{p_H \sin^2 \theta'}{2 \cos \theta'}$ , we required the earth's magnetic field  $H_h$  at the





Fig 4 (a) DELHI-A (886 Kc/s). Date : 12-11-58. Time : 2034-2036 IST



(b) CALCUTTA (1 Mc/s) Date 7-11-58 Time 2117-2119 IST



(c) HYDERABAD (730 Kc/s). Date : 16-11-58. Time : 2122-2124 IST  
(DECCAN)



(d) Dacca (1107 Kc/s), Date 28.10.58, Time 20.30-20.32 IST  
(PAKISTAN)



(e) LAHORE (1100 Kc/s), Date 30.10.58, Time : 21.13-21.15 IST

TABLE III

Transmitting station	Wave-length in metres	Freq in Kc's	$p$	D	H gauss	$\lambda$	D	$\zeta/\theta'$	$H_h$ (gauss)	$\epsilon$
Delhi	338.6	886	$5.565 \times 10^6$	$37^{\circ}13'$	0.4483	$75^{\circ}15'$	$122^{\circ}24'$	$105^{\circ}$	0.4255	$45^{\circ}53'$
Calcutta	300.0	1000	$6.285 \times 10^6$	$39^{\circ}43'$	0.4384	$74^{\circ}11'$	$93^{\circ}30'$	$59^{\circ}27'$	0.4199	$30^{\circ}11'$
Hyderabad	411.0	730	$1.385 \times 10^6$	$28^{\circ}13'$	0.4222	$78^{\circ}36'$	$28^{\circ}6'$	$31^{\circ}10'$	0.04042	$36^{\circ}45'$
Dacca	257.1	1167	$7.331 \times 10^6$	$34^{\circ}58'$	0.4420	$76^{\circ}36'$	$79^{\circ}45'$	$73^{\circ}45'$	0.4233	$32^{\circ}43'$
Lahore	276.0	1100	$6.01 \times 10^6$	$40^{\circ}0'$	0.4474	$80^{\circ}36'$	$12^{\circ}58'$	$111^{\circ}28'$	0.4285	$40^{\circ}58'$

The values of the gyro-magnetic frequency  $pH$ , the corresponding wavelength  $\lambda_H$  and the critical collisional frequency corresponding to the points midway between the transmitting stations and receiving stations are given in Table IV

TABLE IV

Transmitting station	$pH = \frac{H}{mc}$	$\lambda_H$ (metres)	$r_c$
Calcutta	$7.38 \times 10^6$	258.4	$5.38 \times 10^6$
Dacca	$7.44 \times 10^6$	253.3	$12.26 \times 10^6$
Delhi	$7.48 \times 10^6$	252.0	$13.48 \times 10^6$
Hyderabad—Dacca	$7.11 \times 10^6$	265.3	$1.11 \times 10^6$
Lahore	$7.53 \times 10^6$	250.2	$8.91 \times 10^6$

ionospheric layer and the values of the angle  $\theta'$  between the direction of the downcoming wave and the positive direction of earth's magnetic field at the points midway between the various transmitting stations and the receiving station. The earth's magnetic field at a height  $h$  is given by

$$H_h = H_0 \left( 1 - \frac{3h}{R} \right) \quad \dots (10)$$

where  $H_0$  is the earth's magnetic field at the ground level and  $R$ , the radius of the earth.

The magnetic field  $H_0$  at the ground level is obtained from

$$H_0 = H \sqrt{1 + \tan^2 D} \quad \dots (11)$$

where  $H$  is the horizontal component of the earth's magnetic field at the ground level and  $D$  is the dip-angle

The angle between the direction of the downcoming wave and the positive direction of the earth's magnetic field is calculated from,

$$\cos \theta' = \sin D \cos i + \cos D \sin i \cos \zeta \quad \dots (12)$$

where  $i$  is the angle of incidence of the downcoming wave at the receiving station and  $\zeta$  is the angle between the plane of incidence and the magnetic meridian. In Table III are given the various required values of  $H$  at 90Km and  $\theta'$  along with the values of  $D$ ,  $H_0$ ,  $i$  and  $\zeta$  for the points midway between the transmitting and the receiving stations

TRANSFORMATION OF THE OBSERVED  
POLARIZATION ELLIPSE WHEN THE ORIGINAL  
SET OF AXES LYING IN AND PERPENDICULAR  
TO THE PLANE OF INCIDENCE IS CHANGED TO  
THE SET OF AXES LYING IN AND  
PERPENDICULAR TO THE  
MAGNETIC PLANE

(a) *Evaluation of the angle between the two sets of coordinate axes*

Eckersley and Millington (1939) deduced a formula for the angle  $\epsilon$  between the two sets of coordinate axes: This formula is given by,

$$\tan \epsilon = \tan D \operatorname{cosec} \zeta \sin i - \cot \zeta \cos i \quad \dots (13)$$

where  $D$  is the dip-angle,  $i$  the angle of incidence of the downcoming wave at the receiver and  $\zeta$  the angle between the magnetic meridian and the plane of incidence. The values of this angle calculated for the downcoming waves from the different transmitting stations are entered in Table III, along with the values of  $i$ ,  $D$ ,  $\zeta$  and other parameters.

- (b) *The amplitude-ratio and the phase-difference referred to the axes lying in and perpendicular to the magnetic meridian*

Knowing the values of the angle  $\epsilon$ , the amplitude-ratio and the phase-difference, referred to the new set of axes  $X$  and  $Y$ , have been calculated from the formulae given below :

$$\rho' = \sqrt{\frac{\rho^2 \cos^2 \epsilon + \sin^2 \epsilon + 2\rho \cos \epsilon \sin \epsilon \cos \phi}{\rho^2 \sin^2 \epsilon + \cos^2 \epsilon - 2\rho \cos \epsilon \sin \epsilon \cos \phi}} \quad \dots \quad (14)$$

$$\text{and} \quad \tan \phi' = \frac{2\rho \sin \phi}{(1-\rho^2) \sin 2\epsilon + 2\rho \cos \phi \cos 2\epsilon} \quad \dots \quad (15)$$

where  $\rho$  and  $\phi$  refer to the original set of  $X$  and  $Y$ . The derivation of these formulae is given in Appendix-II.

The calculated values of  $\rho'$  and  $\phi'$  obtained by substituting the experimental values of  $\rho$  and  $\phi$  in the formulae are given in Table V

- (c) *Electron number density and electron collisional frequency calculated from the polarization parameters*

The electron number density  $N$  and the electron collisional frequency  $\nu$  can be calculated from the following expressions (Murty and Khastgir, 1959)

$$p' = \frac{\nu_c}{\sqrt{a'}} \cos \gamma = \frac{\nu_c \cos \gamma \sqrt{-2(\cos 2\phi + \cos 2\gamma)}}{\sin 2\phi} \quad (16)$$

$$\nu = p' \tan \gamma = \frac{\nu_c \sin \gamma \sqrt{-2(\cos 2\phi + \cos 2\gamma)}}{\sin 2\phi} \quad (17)$$

where,  $p' = p(1-p_0^2/p^2)$ ,  $p_0^2 = 4\pi Ne^2/m$ ,  $a' = \frac{\nu_c^2}{\nu_c^2 + n'^2}$

$$\tan \gamma = \frac{\nu}{p'} = \frac{1+p^2}{1-p^2} \cot \phi$$

and  $e$ ,  $m$  = charge and mass of an electron.

The computed values of  $x = \frac{4\pi Ne^2}{mp^2} = \frac{p_0^2}{p^2}$  and also of the electron collisional

frequency  $\nu$  are given in Table V.

TABLE V

Transmitting station	$\rho'$	$\phi'$	$x = \rho^2_0/\rho^2$	$\nu$
Delhi	0.6982	34°6'	0.4141	$2.035 \times 10^6$
Calcutta	0.4888	76°32'	0.0144	$2.395 \times 10^6$
Hyderabad-Deccan	0.5321	45°44'	0.8744	$0.992 \times 10^6$
Dacca	0.4545	21°30'	0.6665	$9.279 \times 10^6$
Lahore	0.7042	15°0'	0.9165	$6.21 \times 10^6$

#### DISCUSSION OF THE EXPERIMENTAL RESULTS

##### *Electron number density from the observed polarization parameters*

(a) From the values of  $\rho'$  and  $\phi'$  obtained from the polarization parameters and given Table V, it can be seen that for the downcoming waves received at Banaras the values of  $x$  for the transmitting stations at Calcutta and Delhi are 0.014 and 0.41 respectively and the corresponding values of the electron number density are  $1.750 \times 10^{12}/\text{cc}$  and  $4.33 \times 10^{13}/\text{cc}$ . These values obtained for oblique-incidence transmissions agree well with the corresponding values obtained earlier by Eckorsley and Farmer (1945) for normal-incidence pulsed transmission. In the case of the downcoming waves from the transmitting stations at Hyderabad (Deccan), Dacca and Lahore, the value of  $x$  varies from 0.67 to 0.92 and the corresponding electron number density ranges from  $1.086 \times 10^{14}/\text{cc}$  to  $1.336 \times 10^{14}/\text{cc}$ . It may be mentioned in this connection that the values of  $x$  obtained by Roy and Verma (1955) were found to be about 0.9.

There are however certain factors which may affect the calculations of  $x$  and  $N$  from the observed polarization parameters. These factors are considered below.

(i) For oblique propagation the angle  $\theta'$  between the direction of propagation and the positive direction of the earth's magnetic field varies continuously along the path of the wave in the ionosphere, while, in the Appleton-Hartree formulae from which the expression for the electron number density had been derived, the angle  $\theta'$  is taken as constant along the path of the wave in the ionosphere. The variation of  $\theta'$  along the ionospheric path is expected to be large for distant transmitting stations.

(ii) In calculating the angles of incidence  $i$  corresponding to the different oblique transmissions received at Banaras, the equivalent height of the  $E$ -layer has been taken to be 90 Km. Any appreciable departure from the value of the equivalent height may cause perceptible variation in the value of the angle of incidence  $i$ . For very distant transmitting stations, even a small variation in the

value of the  $E$ -layer height is likely to produce considerable change in the angle of incidence

(iii) The multiple reflections between the ionosphere and the earth are expected in the case of the transmissions from distant transmitting stations. In our calculations, however, only the single-hop transmission has been considered.

(iv) Though the downcoming wave was found to be predominantly left-handed, the presence of the right-handed component could not altogether be ruled out

(b) *Electron collisional frequency from the observed polarization parameters*

The experimental values of the electron collisional frequency in the  $E$ -layer as given in Table V have been found to be within the limits from  $1 \times 10^6$  to  $10 \times 10^6$ . These values lie within the expected range.

#### ACKNOWLEDGMENTS

We gratefully acknowledge our indebtedness to late Dr. R. Satyanarayana who while working as a Junior Research Assistant in a CSIR-Scheme initiated the experiments on the polarization characteristics of downcoming Radio-waves of medium wavelengths. Our thanks are also due to the Council of Scientific and Industrial Research, New Delhi, for sponsoring a research scheme on the subject.

#### APPENDIX I

##### DETERMINATION OF THE VALUE OF $\frac{1+K_1}{1+K_2}$

The ground-reflection coefficients  $K_1$  and  $K_2$  for the normal and the abnormal components respectively are given by the expressions,

$$K_1 = -\frac{\sqrt{\epsilon} \cos i - \cos r}{\sqrt{\epsilon} \cos i + \cos r} \quad \text{and} \quad K_2 = \frac{\sqrt{\epsilon} \cos r - \cos i}{\sqrt{\epsilon} \cos r + \cos i} \quad \dots \quad (\text{A-1})$$

where  $i$  is the angle of incidence,  $r$  is the (complex) angle of refraction and  $\epsilon$  is the complex dielectric constant of the ground given by  $\epsilon = \epsilon_0 - 2j\sigma/f$ , where  $\epsilon_0$  = true dielectric constant (e.s.u.),  $\sigma$  = conductivity (e.s.u.), and  $f$  = wave-frequency. Thus we have,

$$\frac{1+K_1}{1+K_2} = \frac{\cos i \sec r + \sqrt{\epsilon}}{\sec i \cos r + \sqrt{\epsilon}} \quad \dots \quad (\text{A-2})$$

For the frequencies with which we are concerned the approximate values of  $\epsilon_0$  and  $\sigma$  are known to be  $10$  and  $10^8$  e.s.u. respectively. The disturbing effect of ground increases as the wavelength is decreased, so that if this effect can be shown to be small for a wavelength of  $257.1$  m, the shortest wavelength used in the medium wave experiments, then the effect can be neglected here.

For 257.1 m wavelength,  $\epsilon$  is found to be equal to  $(10-171.4j)$ . Using this value of  $\epsilon$  we get the value of  $\cos r$  as approximately equal to 1 for all values of  $\sin i$ , thus even when  $\sin i = 1$ , it is found that  $\cos r = 0.9999-0.0029j$ . Thus taking  $\cos r = 1$  and putting  $\sqrt{\epsilon} = 9.532-8.991j$ , we find,

$$\frac{1+K_1}{1+K_2} = \frac{\cos i + 9.532-8.991j}{\sec i + 9.532-8.991j} = Re^{-j\delta} \quad \dots (A-3)$$

$$\text{where } R = \sqrt{\frac{(8.991)^2 + (9.532 + \cos i)^2}{(8.991)^2 + (9.532 + \sec i)^2}} \quad \dots (A-4)$$

$$\text{and } \delta = \tan^{-1} \frac{8.991}{9.532 + \cos i} - \tan^{-1} \frac{8.991}{9.532 + \sec i} \quad \dots (A-5)$$

The values of the phase-difference  $\delta$  and the amplitude-ratio  $R$  introduced by the ground reflection for various angles of incidence are shown in Fig 5. It is seen that even with an angle of incidence of  $60^\circ$ , the phase-difference is only

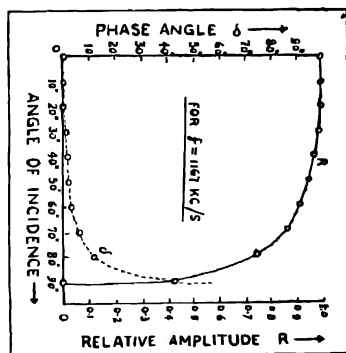


Fig. 5. Effect of ground reflection.

40 and the amplitude-ratio is 0.02 and that for the smaller angles of incidence, which occur in the experiments with the near stations, the phase-difference is less and the amplitude-ratio is more nearly unity, so that we are justified in neglecting completely the effect of the ground and in writing

$$\frac{1+K_1}{1+K} = 1 \quad (A-6)$$



## APPENDIX II

### VALUES OF THE AMPLITUDE-RATIO AND PHASE-DIFFERENCE REFERRED TO THE SET OF AXES IN AND PERPENDICULAR TO THE MAGNETIC PLANE

After calculating the angle  $\epsilon$  between the horizontal direction in the wave-front and the line of intersection of the magnetic plane with the wave-front from the formula given by Eekersley and Millington (1939), it is necessary to transform the experimentally observed amplitude-ratio and the phase-difference with reference to the set of axes in and perpendicular to the plane of incidence to the set of axes in and perpendicular to the magnetic plane

Let  $E_1 \cos(\omega t + \phi)$  and  $E_2 \cos \omega t$  be normal and the abnormal components in and perpendicular to the plane of incidence along  $Y$ - and  $X$ -directions. If we now refer to the set of rectangular axes in and perpendicular to the magnetic plane along  $X$ - and  $Y$ -directions, then the normal and the abnormal electric vectors will have their respective components along the axes  $X$ - and  $Y$ -directions.

The components along  $X$ -are :

$$E_2 \cos \omega t \cos c \text{ and } E_1 \cos(\omega t + \phi) \sin c \quad \dots \quad (\text{A-7})$$

and the components along  $Y$  are

$$-E_2 \cos \omega t \sin \epsilon \text{ and } E_1 \cos(\omega t + \phi) \cos \epsilon \quad \dots \quad (\text{A-8})$$

The resultant electric vectors along  $X$  and  $Y$  directions will be given by

$$E_x = E_2 \cos \omega t \cos c + E_1 \cos(\omega t + \phi) \sin c \quad \dots \quad (\text{A-9})$$

$$\text{and } E_y = -E_2 \cos \omega t \sin c + E_1 \cos(\omega t + \phi) \cos c \quad \dots \quad (\text{A-10})$$

$$\text{Putting } E_x = K \cos(\omega t + \delta) \quad \dots \quad (\text{A-11})$$

$$\text{and } E_y = K' \cos(\omega t + \delta') \quad \dots \quad (\text{A-12})$$

$$\text{we get } K = \sqrt{E_2^2 \cos^2 c + E_1^2 \sin^2 c + 2E_1 E_2 \sin c \cos c \cos \phi} \quad \dots \quad (\text{A-13})$$

$$\text{and } K' = \sqrt{E_2^2 \cos^2 \epsilon + E_1^2 \sin^2 \epsilon - 2E_1 E_2 \sin \epsilon \cos \epsilon \cos \phi} \quad \dots \quad (\text{A-14})$$

$$\text{and } \tan \delta = \frac{E_1 \sin \phi \sin c}{E_2 \cos c + E_1 \sin \epsilon \cos \phi} \quad \dots \quad (\text{A-15})$$

$$\tan \delta' = \frac{E_1 \sin \phi \cos \epsilon}{-E_2 \sin \epsilon + E_1 \cos c \cos \phi} \quad \dots \quad (\text{A-16})$$

The amplitude-ratio  $\rho'$  and the phase-angle  $\phi'$  with reference to the set of axes in and perpendicular to the magnetic plane are then given by

$$\rho' = \frac{K}{K'} = \sqrt{\frac{\sin^2 \epsilon + \rho^2 \cos^2 \epsilon}{\cos^2 \epsilon + \rho^2 \sin^2 \epsilon}} \frac{2\rho \cos \epsilon \sin \epsilon \cos \phi}{-2\rho \cos \epsilon \sin \epsilon \cos \phi} \quad \dots \quad (\text{A-17})$$

and

$$\tan \phi' = \frac{2\rho \sin \phi}{(1-\rho^2) \sin 2\epsilon + 2\rho \cos \phi \cos 2\epsilon} \quad \dots \quad (\text{A-18})$$

#### REFERENCES

- Appleton, E. V. 1932, *J.I.E.E.*, **71**, 642.  
 Appleton, E. V. and Rietveld, J. A. 1928, *Proc. Roy. Soc. A.*, **117**, 576.  
 Budden, K. G., 1952, *Proc. Roy. Soc. A.*, **215**, 215.  
 Eckersley, T. L. 1950, *Proc. Phys. Soc.*, **63 B**, 49.  
 Eckersley, T. L. and Farmer, F. T. 1945, *Proc. Roy. Soc. A.*, **184**, 196.  
 Eckersley, T. L. and Millington, G. 1939, *Proc. Phys. Soc.*, **51**, 110.  
 Green, A. L., 1934, *Proc. I.R.E.*, **22**, No. 3, 324.  
 Martyn, D. F. and Green, A. L. 1935, *Proc. Roy. Soc. A.*, **148**, 104.  
 Murty, Y. S. N. and Khastgir, S. R. 1959, *Proc. Nat. Inst. Sci.*, **25**, A, No. 5, 255.  
 Ratchiff, J. A. and White, E. L. C., 1933, *Phil. Mag.*, **16**, 125.  
 Ratchiff, J. A. and White, F. W. G., 1933, *Phil. Mag.*, **16**, 423.  
 Roy, R. and Verma, J. K. D. 1955, *J. Geophys. Res.*, **60**, 457.

# SCATTERING OF THE RADIATION FIELD OF A LOOP ANTENNA BY A CONDUCTING CYLINDER IMMERSED IN A COLD PLASMA

T. D. SHOCKLEY AND C. R. HADEN

THE UNIVERSITY OF OKLAHOMA NORMAN, OKLAHOMA

(Received March 9, 1966)

**ABSTRACT.** The equations describing the scattered fields of a circular loop antenna and a conducting cylinder immersed in a homogeneous cold plasma are derived. It is assumed that the loop antenna is excited by a one-dimensional, uniform, inphase, sinusoidal current, i.e., a current filament. Solutions of Helmholtz's wave equation are formulated through an integral expansion of the product of cylindrical Hankel functions and transcendental functions. The coefficients in these solutions are evaluated by the application of the problem boundary conditions so that a solution for the scattered electric field is effected.

## INTRODUCTION

Considerable interest has been shown by a number of authors, including Yeh (1964), Seshadri and Hessel (1964), and Seshadri (1964), in the scattering effect of plasmas and perfectly conducting surfaces on the radiation characteristics of various antennas. Seshadri (1964) considered the problem of the scattering of a plane wave due to the presence of a conducting cylinder immersed in a cold plasma. The problem discussed in this paper is the scattering of the radiation field of a circular loop antenna immersed in a cold plasma in the presence of a perfectly conducting cylinder of infinite length (Fig. 1). It is assumed that the thin wire,

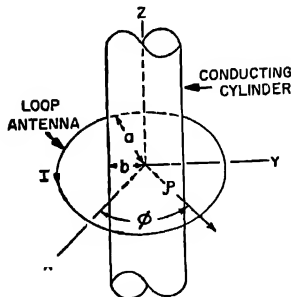


Figure 1.

single turn, loop antenna is located in the  $xy$  plane with its center at the origin and that it is excited by a uniform, inphase sinusoidal current of the form  $I_0 \exp(i\omega t)$

Since the plasma is assumed homogeneous and isotropic, its field characteristics may be described by a complex relative permittivity factor  $K$

The equations governing propagation are Maxwell's equations and the equation of motion of the free charge existing in the plasma. For the sinusoidal steady state case, these equations may be expressed as

$$\nabla \times E = -i\omega\mu_0 H \quad \dots (1)$$

$$\nabla \times H = i\omega c_0 K E \quad \dots (2)$$

$$(i\omega + v)mv = qE \quad \dots (3)$$

where  $E$  is the electric field strength,  $H$  is the magnetic field strength,  $\omega$  is the angular wave frequency,  $\mu_0$  is the permeability of free space,  $c_0$  is the permittivity of free space,  $K$  is the complex relative permittivity factor,  $v$  is the average collisional frequency of electrons with neutral particles,  $q$  is the particle charge,  $m$  is the mass of the charged particles, and  $v$  is the velocity of the charged particles. For the plasma,  $K$  is defined from (3) as

$$K = \left[ \left( 1 - \frac{\alpha^2}{1 + \beta^2} \right) - i \left( \frac{\alpha^2 \beta}{1 + \beta^2} \right) \right] \quad \dots (4)$$

where  $\alpha^2 = (Nq^2/e_0m)/\omega^2$ ,  $\beta^2 = (v/\omega)^2$ , and  $N$  is the number density of charged particles in the plasma.

#### FORMULATION OF THE WAVE POTENTIALS

Maxwell's equations (1) and (2), may be readily combined to yield Helmholtz's vector wave equation in terms of the wave potential  $F$

$$\nabla^2 F + k^2 F = 0 \quad \dots (5)$$

where  $k^2 = \omega^2\mu_0 c_0 K$  is complex. The components of the wave potential  $F$  satisfy Helmholtz's scalar wave equation

$$\nabla^2 \psi + k^2 \psi = 0 \quad \dots (6)$$

Harrington (1961) has shown that the wave potential  $\psi$  may be expressed in the form

$$\psi_{n,k_z,k_\rho} = B_n(k_\rho \rho) g(n\varphi) h(k_z z) \quad \dots (7)$$

where the  $B_n(k_\rho \rho)$  are Bessel or Hankel functions, the  $g(n\varphi)$  and  $h(k_z z)$  are sinusoidal functions, and  $k^2 = k_\rho^2 + k_z^2$ . In general it is possible to formulate solutions to (6) as

$$\psi = \sum_n \int_{k_z} f_n(k_z) B_n(k_\rho \rho) g(n\varphi) h(k_z z) dk_z \quad \dots (8)$$

with the integration over the complex plane and the function  $f_n(k_z)$  to be determined from the boundary conditions.

An examination of Fig. 1 indicates that due to symmetry, there will be no component of  $E$  in the  $z$  direction. The stipulation of a uniform inphase current excitation of the loop antenna requires that  $g(n\varphi)$  be a constant or that  $n = 0$ . Eq (8) may now be rewritten as

$$\psi_1 = \int_{k_z} [AH_0^{(1)}(k_\rho \rho) + BH_0^{(2)}(k_\rho \rho)] e^{ik_z z} dk_z$$

when  $b < \rho < a$  and

$$\psi_2 = \int_{k_z} CH_0^{(2)}(k_\rho \rho) e^{ik_z z} dk_z \quad \text{when } \rho > a \quad \dots (10)$$

Eq (9) represents a standing wave region (region 1) which exists between the conducting cylinder and a mathematical cylindrical surface containing the loop antenna. In region 2,  $\rho > a$ , only travelling waves exist. The constants  $A$ ,  $B$ , and  $C$  are the  $f_0(k_z)$  to be determined from the boundary conditions and the  $H_0^{(1)}(k_\rho \rho)$  and the  $H_0^{(2)}(k_\rho \rho)$  are Hankel functions of zero order of the first and second kind. The electric field  $E$  and the magnetic field  $H$  are given respectively by

$$E = -\nabla \times F \quad (11)$$

$$H = \frac{\nabla \times \nabla \times F}{i\omega\mu_0} \quad (12)$$

where

$$F = a_z \psi$$

#### DERIVATION OF THE SCATTERED FIELD

Application of the boundary conditions over the surface of the perfectly conducting cylinder and the loop of current yields the required  $f_0(k_z)$ . Since the tangential components of the  $E$  field must be zero on the surface of the conducting cylinder ( $\rho = b$ ), application of this boundary condition yields

$$B = - \left\{ \frac{H_1^{(1)}(k_\rho b)}{H_1^{(2)}(k_\rho b)} \right\} A. \quad \dots (13)$$

In addition the tangential components of the  $E$  field must be continuous over the cylindrical surface ( $\rho = a$ ), so setting  $E_{\varphi 1} = E_{\varphi 2}$  at  $\rho = a$  gives

$$C = \left\{ \frac{H_1^{(1)}(k_\rho a)H_1^{(2)}(k_\rho b) - H_1^{(2)}(k_\rho a)H_1^{(1)}(k_\rho b)}{H_1^{(2)}(k_\rho a)H_1^{(2)}(k_\rho b)} \right\} A. \quad \dots (14)$$

Also at  $\rho = a$ ,  $z = 0$ , the magnetic field must change in a discontinuous manner because of the current flowing in the loop antenna. That is

$$H_{z1} - H_{z2} = J_\varphi = \frac{I_\varphi}{a} \delta(z). \quad \dots (15)$$

The delta function may be represented by a complex integral of the form

$$\delta(z) = \frac{1}{2\pi} \int_{k_z} e^{ik_z z} dk_z. \quad \dots \quad (16)$$

Substitution of (16) into (15) allows evaluation of  $A$  as

$$A = \frac{i\omega\mu_0 H_1^{(2)}(k_\rho a) J_\varphi}{2\pi a k_\rho^2 [H_0^{(1)}(k_\rho a) H_1^{(2)}(k_\rho a) - H_1^{(1)}(k_\rho a) H_0^{(2)}(k_\rho a)]} \quad \left( \dots \right) \quad (17)$$

Utilization of the Wronskian for Hankel functions reduces (17) to

$$A = \frac{\omega\mu_0 H_1^{(2)}(k_\rho a) I_\varphi}{8k_\rho} \quad \dots \quad (18)$$

The electric field  $E$  (radiated and scattered) in regions 1 and 2 may now be written as

$$E_{\varphi 1} = -\frac{\omega\mu_0 I_\varphi}{8} \int_{k_z} \left\{ \frac{H_1^{(2)}(k_\rho b) H_1^{(1)}(k_\rho \rho) - H_1^{(1)}(k_\rho b) H_1^{(2)}(k_\rho \rho)}{H_1^{(2)}(k_\rho b)} \right\} H_1^{(2)}(k_\rho a) e^{ik_z z} dk_z \quad \dots \quad (19)$$

$$E_{\varphi 2} = -\frac{\omega\mu_0 I_\varphi}{8} \int_{k_z} \left\{ \frac{H_1^{(1)}(k_\rho a) H_1^{(2)}(k_\rho b) - H_1^{(2)}(k_\rho a) H_1^{(1)}(k_\rho b)}{H_1^{(2)}(k_\rho b)} \right\} H_1^{(2)}(k_\rho \rho) e^{ik_z z} dk_z \quad \dots \quad (20)$$

Since (19) and (20) represent the total field, radiated plus scattered, the field scattered by the cylinder may be found by subtracting the radiation field of the loop from the total field

Correspondingly, the radiation field of the loop antenna may be expressed as

$$E_{\varphi 1} = -\frac{\omega\mu_0 I_\varphi}{4} \int_{k_z} H_1^{(2)}(k_\rho a) J_1(k_\rho \rho) e^{ik_z z} dk_z \quad \dots \quad (21)$$

$$E_{\varphi 2} = -\frac{\omega\mu_0 I_\varphi}{4} \int_{k_z} J_1(k_\rho a) H_1^{(2)}(k_\rho \rho) e^{ik_z z} dk_z \quad \dots \quad (22)$$

Subtracting (21) from (19) and (22) from (20) yields the scattered field produced by the presence of the conducting cylinder. Thus the scattered field in region 2 may be written as

$$E_{\varphi 2}^s = -\frac{\omega\mu_0 I_\varphi}{8} \int_{k_z} \left[ \left\{ \frac{H_1^{(1)}(k_\rho a) H_1^{(2)}(k_\rho b) - H_1^{(2)}(k_\rho a) H_1^{(1)}(k_\rho b)}{H_1^{(2)}(k_\rho b)} \right\} \dots \right] \quad (23)$$

$$-2J_1(k_\rho a) \Big| H_1^{(2)}(k_\rho \rho) e^{ik_z z} dk_z.$$

It is also interesting to note that (23) reduces to a Fourier integral if  $k_z$  is real. For the problem under consideration, this occurs when the plasma collisional frequency  $\nu$  is zero since  $K$  is then real. Integration limits on  $k_z$  in (23) may then be written as  $-\infty$  to  $\infty$ .

#### REFERENCES

- Harrington, R. F. 1961, *Time-Harmonic EM Fields*, McGraw-Hill, 199-201.  
 Seshadri, S. R. 1964, *Canadian J. Phys.* **42**, 860.  
 Seshadri, S. R. and Hessel, A. 1964, *Canadian J. Phys.* **42**, 2153.  
 Yeh, C. 1964, *Canadian J. Phys.* **42**, 1369.

# ON THE MEASUREMENT OF EQUIVALENT FOCAL LENGTH OF TELESCOPE LENSES

J. PRASAD AND M. S. R. S. SARMA

CENTRAL SCIENTIFIC INSTRUMENTS ORGANISATION, CHANDIGARH, INDIA

(Received March 21, 1966)

**ABSTRACT.** A biprism method for rapid measurement of equivalent focal length of telescope lenses is described. It has been shown that precise measurement of focal length is possible even if the biprism is afflicted with small spherical refracting power. The accuracy obtained by the method was found to be within about  $\pm 3$  per cent.

## INTRODUCTION

For the determination of equivalent focal length (e.f.l.) of a lens or lens combination, Indian Standards Specifications (IS 988 : 1959) laid nodal point, Newton's, magnification and focometer methods. The tolerance for nominal focal length is specified as within  $\pm 5$  per cent unless otherwise stated.

Employing a biprism with zero spherical refracting power, Darling (1962) has outlined a method for rapid determination of the e.f.l. of flat field lenses. It was reported that this method permitted a quick check on e.f.l. value of a given lens obtained with the optical bench.

Because of the inherent simplicity and rapidity of Darling's method, an investigation was taken up at this Organisation to ascertain whether it can also be incorporated for e.f.l. measurement in Indian Standards Specifications. The approach adopted had to be, however, a little modified as the available biprism possessed spherical refracting power of  $+0.25$  diopters.

## THEORY

A collimated beam is split with the help of a transmitting biprism, afflicted with spherical refracting power, into two nearly parallel beams inclined at a small angle  $\theta$ . On traversing through the lens  $T$  under test, two images laterally separated by a distance,  $d$ , are formed. It can easily be deduced that focal length,  $f$ , of  $T$  is represented by the equation :

$$f \pm e = Kd \quad \dots (i)$$

where  $e$  is the distance between the image and true focal plane of  $T$  and  $K \equiv \cot \theta$ . Since  $d$ ,  $e$  can be experimentally measured, the constant  $K$  is first evaluated, employing lenses of known focal length, and using equation (i) above. The procedure can then be repeated for determining e.f.l. of unknown lens.



# EXPERIMENTAL

The experimental arrangement used is illustrated in Fig. 1. It was set up on an optical bench, vernier constant 0.05 mm. The slit  $S$  was illuminated with

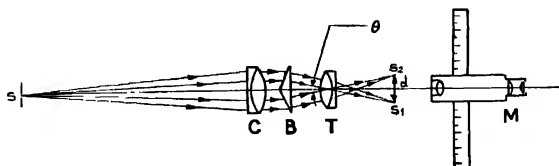


Fig. 1. Experimental set-up.

filtered green light from an incandescent lamp and collimated with the help of an achromatic doublet lens,  $C$ , of 5 cm aperture and 60 cm focal length. The distance between the two slit images  $S_1$  and  $S_2$  formed by  $T$  was measured with the help of a travelling microscope  $M$ , least count 0.01 mm.  $e$  was measured on the bench by sliding the carriage carrying  $M$ .

It was observed that with the available biprism the two slit images did not appear in focus simultaneously indicating thereby that the biprism possessed non-symmetrical refracting power. This observation introduced uncertainties in measurements and hence the following two different procedures were adopted for evaluation of  $d$ ,  $e$  and the results compared.

In procedure I, the optimum position when the two slit images appear in best focus simultaneously is located on the optical bench, and  $d$ ,  $e$  measured.

In procedure II, without  $B$ , the best focus position  $X_0$  for the slit image is first located on the optical bench and the image centred on the cross section of an eyepiece graticule.  $B$  is now introduced and the two slit images are focused in succession moving the carriage carrying  $M$ , noting their positions  $X_1$ ,  $X_2$  and recording from the centre on the ocular micrometer the distances  $d_1$  and  $d_2$  of slit images. ' $d$ ' was taken as  $\overline{d_1 + d_2}$  and ' $e$ ' as  $\overline{X_1 + X_2} - X_0$ .

In both the above cases, measurements were made on same lenses, repeating individual observations five times. As a counter check, the nominal focal length,  $f_n$ , for each lens was also determined independently, with the help of an improvised focometer.

# RESULTS AND DISCUSSION

Following procedures I and II outlined above, the results obtained are given in Tables I and II respectively. The plot between  $d$  vs  $(f_n - e)$  is a straight line passing through origin (Fig. 2). The correlation coefficient is 0.985. On

statistical analysis  $K$  comes out as  $173.3 \pm 1.6$ , which value was used in equation (i) above for computing 'f' by both procedures.

TABLE I  
 $d$ ,  $e$  and  $K$  results as obtained by two procedures\*

Lens No.	$f_n$	Procedure I			Procedure II		
		$d$	$e$	$K$	$d$	$e$	$K$
1	357.97	2.060	13.62	167.16	1.97	14.60	174.65
2	196.21	1.116	3.96	172.26	1.10	5.04	173.79
3	148.15	0.787	3.00	184.43	0.80	2.06	182.61
4	201.83	1.108	4.90	177.73	1.20	4.38	164.54
5	298.54	1.675	9.49	172.56	1.70	8.55	170.58
6	256.85	1.482	6.44	168.96	1.42	8.42	174.65
7	175.41	—	—	—	1.03	2.60	168.74

\* $d$ ,  $e$  and  $f_n$  are in mm.  $K$  is a dimensionless quantity.

TABLE II  
Focal length results as obtained by two procedures

Lens No.	Focal length (mm)		$\frac{f-f_n}{f_n} \times 100$	
	Procedure I	Procedure II	Procedure I	Procedure II
1	370.62	355.31	3.5	-0.7
2	197.36	195.67	0.6	-0.3
3	139.39	140.70	-5.2	-5.0
4	196.92	212.34	-2.4	5.2
5	299.77	303.16	0.4	1.5
6	263.27	252.51	2.5	-1.6
7	—	181.10	—	3.2

It may be seen from Table II that generally the percent difference in focal length from nominal value obtained by any of the two procedures is within the tolerance limit specified in IS 988 : 1959. Small departures from this criterion obtained in case of lens 3 and 4 might be due to uncorrected nature of these doublets, as seen by star test, enabling only approximate measurement of 'd'. Results of the star test (Twyman, 1955) carried out to ascertain the qualitative performance of the lenses used are given in Table III.

TABLE III  
Appearance of star image

Lens No.	At best focus	In-focus	Out-focus	For oblique rays	Remarks
1	circular, first fringe bright and discontinuous	Airy disc expands and pattern fades	outer rings bright, central disc small	comatic flare, two systems of hyperbolae mutually perpendicular at two foci (when the lens is racked to and fro)	Spherically over corrected, presence of coma and astigmatism indicated
2	circular, fringe surrounding Airy disc faint and discontinuous	Airy disc expands and pattern fades	slightly oval shaped-fringe pattern	comatic pattern	spherically corrected, presence of coma
3	oval shaped, right side ring bright and massive	oval shaped	oval shaped, perpendicular to in-focus image	comatic pattern	uncorrected for spherical aberration, coma and astigmatism.
4	circular, first outer ring faint and discontinuous	outer rings fade	outer ring massive and bright	comatic pattern	spherically over corrected, uncorrected for coma
5	circular	outer rings bright and slightly oval shaped	outer rings fade, slightly oval shaped perpendicular to in-focus image	fringes rapidly fade	spherically under-corrected slight astigmatism
6	slightly oval shaped	pattern of rings seen	pattern of rings similar to in-focus image	fringes rapidly fade	spherically corrected, slight astigmatism
7	slightly oval shaped	oval pattern	Airy disc expands and fades	comatic pattern	spherically corrected, presence of coma and astigmatism

Assuming Gauss law to hold good, the error,  $\delta f$ , in measurement of  $f$  can be expressed as

$$\delta f = \pm \left[ \left( \frac{\delta f}{\delta K} \right) \Delta + K^2 \left( \frac{\delta f}{\delta d} \right)^2 \Delta d^2 + \left( \frac{\delta f}{\delta e} \right)^2 \Delta e^2 \right]^{\frac{1}{2}}$$

Substituting the values of partial differential coefficients obtained from equation (1)

$$\delta f = \pm [d^2 \Delta K^2 + K^2 \Delta d^2 + \Delta e^2]^{\frac{1}{2}}$$

TABLE IV  
Error in determination of focal length by two procedures

Lens No	Procedure I				Procedure II			
	2.56 d <sup>2</sup>	$\delta f^2$	$\pm \delta f$	$\pm \delta f\%$	2.56 d <sup>2</sup>	$\delta f^2$	$\pm \delta f$	$\pm \delta f\%$
1	10.86	13.86	3.72	1.04	9.89	12.89	3.57	1.00
2	3.19	6.19	2.48	1.26	3.09	6.09	2.46	1.25
3	1.59	4.59	2.14	1.44	1.64	4.64	2.15	1.45
4	3.14	6.14	2.45	1.22	3.68	6.68	2.58	1.28
5	7.18	10.18	3.19	1.07	7.40	10.40	3.22	1.08
6	5.62	8.62	2.93	1.14	5.16	8.16	2.85	1.10
7	—	—	—	—	2.71	7.71	2.77	1.58

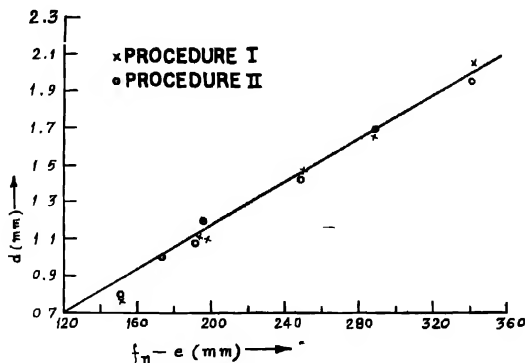


Fig. 2.  $d$  vs  $(f_n - e)$  plot for different lenses.

As reported above the standard error in evaluation of  $K$  is  $\pm 1.6$ . ' $d$ ' and ' $e$ ' can be assumed as accurate to within  $\pm 0.01$  and  $\pm 0.05$  respectively, being the least counts of respective verniers. Hence,

$$\delta f = \pm (3 + 2.56d^2)^{\frac{1}{2}} \quad \dots \text{ (iii)}$$

On this theoretical basis the average percent error in determination of focal length by procedures I and II comes out to be within  $\pm 1.20$  and  $1.26$  respectively (Table IV)

It may be pointed out, however, that from Table II, in case of procedures I and II, the average deviations of measured focal length from nominal value are  $2.9$  and  $3.1$  per cent respectively

It is felt that accuracy in focal length measurement by this method can be further improved upon by employing a biprism producing comparatively large angular deviation, and use of a two directional microscope capable of reading accurate to  $0.01$  mm in mutually perpendicular planes.

#### CONCLUSIONS

1 A method employing a biprism afflicted with small spherical refracting power is described which enables measurement of  $e.f.l$  of telescope lenses accurate to within  $\pm 3$  per cent. It is considered suitable for inclusion in IS 988 : 1959

2  $e.f.l$ . measurements were made following two independent procedures. These yielded results of similar accuracy. Procedure I is more rapid.

3 Accuracy in measurement diminished in case of uncorrected lenses

#### ACKNOWLEDGEMENT

The authors are thankful to Dr. P. S. Gill, Director of the Organisation, for his keen interest in the work and kind permission to publish the paper

#### REFERENCES

- Dwiling, W. R., 1962, *J. Res. Nat. Bur. Std.*, **66C**, 113  
IS 988 : 1959, General requirements for optical components, Indian Standards Institution, New Delhi  
Twyman, F., 1955, *Optical Glassworking*, Hilger & Watts Ltd, London, 156.

# DIMERIZATION IN POLAR GASES

A. N. ROY AND A. DAS GUPTA

INDIAN ASSOCIATION FOR THE CULTIVATION OF SCIENCE,

CALCUTTA-32, INDIA.

(Received April 2, 1966)

**ABSTRACT** The semi-empirical method of Hirschfelder, McClure and Weeks and the statistical approach of calculating the percentage of dimers formed in a polar gas have been compared for several substances. The results indicate the limitation of Hirschfelder et al's approach and also point to the necessity of considering the presence of metastable dimers for the calculation of the equilibrium constant for dimerization.

## INTRODUCTION

The consideration of cluster formation is necessary for representing properly the properties of dense gases (Das Gupta and Barua, 1965). As a first step in this direction it is necessary to consider dimerisation only which is sufficient upto a certain density limit. The dimers consist of bound and metastably bound double molecules. Recently the idea of quasi-dimers has also been introduced (Kim and Ross, 1965). In the present paper we shall confine our consideration to bound double molecules only. The dimers thus formed may be defined as systems whose relative kinetic energy is less than the negative value of the mutual potential energy (Hirschfelder, McClure and Weeks, 1942). The number of dimers is determined by the usual chemical equilibrium constant although the lifetime of these molecules is of the order of the collision time.

The formation of dimers in non-polar gases has been considered by Stogryn and Hirschfelder (1959) for realistic intermolecular potentials. However, for polar gases due to the presence of long-range dipole-dipole forces association plays a much more important part than in non-polar gases. Hirschfelder, McClure and Weeks (1942) suggested a semi-empirical method for calculating the mole fractions of dimers in a polar gas. According to this method, the equilibrium constant for dimerisation is given by,

$$K(T) = b_a - B(T) = n_2 V / n_1^2 \quad \dots (1)$$

where  $n_1, n_2$  are the moles of monomers and dimers respectively and  $V$  is the volume.  $b_a$  is a constant depending on the intermolecular forces and  $B(T)$  is the second virial coefficient at temperature  $T$ .

However, another approach which is more logical and accurate is from the stand point of statistical mechanics. The second virial coefficient  $B(T)$  can be written as follows

$$B(T) = B_f(T) + B_b(T) + B_m(T) \quad \dots (2)$$

where  $B_f(T)$ ,  $B_b(T)$  and  $B_m(T)$  are the contributions of the free, bound and metastably bound double molecules. When metastably bound molecules are neglected the equilibrium constant for dimerisation may be written as,

$$K(T) = b_0 B_b^*(T^*) \quad \dots (3)$$

where

$$b_0 = \frac{z\pi}{3} N\sigma^3$$

Recently Barua, Chakraborti and Saran (1965) have calculated  $B_b^*(T^*)$  for a polar gas by assuming the dipoles to act in the head-to-tail position according to the Stockmayer potential,

$$\phi(r) = 4\epsilon[(\sigma/r)^{12} - (\sigma/r)^6] - \frac{\mu^2}{r^3} (2\cos\theta_1 \cos\theta_2 - \sin\theta_1 \sin\theta_2 \cos\phi), \quad \dots (4)$$

where  $\mu$  is the dipole moment of the interacting molecules,  $\theta_1$ ,  $\theta_2$  are the angles of inclination of the axes of the two dipoles to the line joining the centre of the molecules and  $\phi$  is the azimuthal angle between them,  $\sigma$  and  $\epsilon$  have usual significance.

When the dipoles are in the head-to-tail position Eq. (4) becomes

$$\phi(r) = 4\epsilon[(\sigma/r)^{12} - (\sigma/r)^6] - \frac{2\mu^2}{r^3} \quad (5)$$

The final expression for  $B_b^*(T^*)$  calculated on the basis of Eq. (5) is given by (Barua *et al.*, 1965)

$$B_b^*(T^*) = -\frac{16}{(\pi)^2} \sum_{n=0}^{\infty} \frac{4^n(n+1)!}{(2n+1)!} \times \frac{1}{2n+1} \left[ \frac{4(A + \bar{Y}_n^2 - \bar{Y}_n^6)}{T^*} \right]^n \quad (6)$$

where  $A = \mu^{*2}/2$ ,  $\mu^* = \mu/\sqrt{\epsilon\sigma^3}$  ( $\mu$  being the dipole moment)  $Y = (r/\sigma)^{-3/2}$  and  $T^* = kT/\epsilon$ . The values of  $B_b^*(T^*)$  corresponding to different values of  $A$  and  $T^*$  have been tabulated. It has, however, recently been pointed out by Barua, *et al.* (1966) that it is physically much more realistic to assume an 'effective' relative orientation of the dipoles of the interacting molecules. This means that at any particular temperature and pressure although the different pairs of colliding molecules interact with a different relative orientation, it is possible to assume an 'effective' relative orientation with which all the pairs interact on the

$$A = \frac{\mu^{*2}g_{eff}}{4} ; \quad g = (2\cos\theta_1 \cos\theta_2 - \sin\theta_1 \sin\theta_2 \cos\phi), \quad (7)$$

average. Under this condition. It is possible to utilise the Table  $B_b^*(T^*)$  as obtained by Barua *et al.* (1965) for 'effective' relative orientation of dipoles as given by  $A$  from Eq. (7).

In view of the importance of the problem we thought it necessary to compare the different methods which are at present available for the calculation of the mole-fractions of dimers.

## CALCULATION AND RESULTS

For the purpose of comparison, we have chosen ammonia, chloroform and methyl chloride for which both second virial and viscosity data are available. The force constants  $\sigma$ ,  $\epsilon/k$  and  $A$  used for the calculation of  $B_0^*(T^*)$  are shown in Table I. For ammonia and methylchloride it is not possible to fit the experimental viscosity data for  $g = 2$  (Itcan, Glueck and Sevbla, 1961 and Barua *et al.*, 1966). Consequently we have used only  $\eta_{eff}$  values obtained by fitting viscosity data by using collision integrals calculated by Monchick and Mason. (1961). For the for method suggested by Hirschfelder *et al.* (1942) except for ammonia the value of  $b_a$  was obtained from the relation

$$b_a = 1.75V_c$$

$V_c$  being the critical volume. For ammonia  $b$  was obtained by fitting to experimental data (Hirschfelder, *et al.*, 1942). Results of the sample calculations performed are shown in Table II.

## DISCUSSION OF RESULTS

It may be seen from Table II that for chloroform and methyl chloride the mole fractions of dimers obtained by using the semi-empirical method of Hirschfelder *et al.* is much higher than those obtained by using Eq. (3). For ammonia the agreement between the two methods is fairly good. This is most probably due to the reason that for ammonia the constant  $b_a$  was obtained from experimental data which indirectly shows that  $b_a$  as given by Eq. (8) gives too high value of the mole-fraction of dimers. Another source of discrepancy between the two methods of calculation is the neglect of metastably bound double-molecules in calculating  $K(T)$  from Eq. (3). Therefore, it appears that  $K(T)$  as obtained from Eq. (3) give reliable values of the molefractions of dimers provided metastable double double molecules are also considered.

TABLE I  
Force parameters used for the calculation of  $B_0^*(T^*)$

Substance	$\sigma \text{ \AA}$	$\epsilon/k^\circ\text{K}$	A	Reference
Chloroform	5.513	256.7	0.086	a
Methyl Chloride	4.870	72.4	0.60	Present work
Ammonia	2.733	380	0.25	b

a. Itcan, E. C., Glueck, A. R., and Sevbla, R. A., 1961, Nasa Technical Note D-481.

b. Barua, A. K., Saran, A., and Singh, Y., 1966, To be published.



TABLE II

Molefractions of dimers at different pressures and temperatures

Substance	T°K	P atoms	$x_2$	
			from Eq (1)	From Eq (3)
Chloroform	298	1	0.0598	0.0189
		5	0.2108	0.0826
		10	0.3162	0.1439
		25	0.4721	0.2651
		50	0.6293	0.3788
	348	1	0.0396	0.0121
		5	0.1537	0.0551
		10	0.2447	0.1004
		25	0.3940	0.1900
		50	0.5116	0.3021
	398	1	0.0282	0.0084
		5	0.1168	0.0392
		10	0.1940	0.0730
		25	0.3314	0.1525
		50	0.4506	0.2432
	455	1	0.0387	0.0121
		5	0.1509	0.0554
		10	0.2411	0.1004
		25	0.3897	0.1991
		50	0.5076	0.3043
Methyl Chloride	338	1	0.0194	0.0055
		5	0.0845	0.0265
		10	0.1467	0.0504
		25	0.2691	0.1105
		50	0.3832	0.1853
	450	1	0.0105	0.0029
		5	0.0844	0.0143
		10	0.0886	0.0279
		25	0.1795	0.0645
		50	0.2780	0.1164
	273	1	0.0185	0.0154
		5	0.0992	0.0088
		10	0.1414	0.1224
		25	0.2616	0.2334
		50	0.3749	0.3428
	333	1	0.0094	0.0079
		5	0.0435	0.0374
		10	0.0804	0.0698
		25	0.1654	0.1467
		50	0.2601	0.2357
Ammonia	423	1	0.0048	0.0039
		5	0.0228	0.0188
		10	0.0437	0.0364
		25	0.0973	0.0825
		50	0.1622	0.1438
	523	1	0.0028	0.0021
		5	0.0138	0.0101
		10	0.0281	0.0198
		25	0.0621	0.0468
		50	0.1119	0.0860

## ACKNOWLEDGEMENT

The authors wish to thank Dr A. K. Barua for suggesting the problem and helpful guidance and to Prof B. N. Srivastava, D.Sc., F.N.I., for his kind encouragement and interest in the work.

## REFERENCES

- Barua, A. K., Chakraborty, P. K., and Saran, A., 1965, *Mol. Phys.*, **4**  
Barua, A. K., Saran, A., and Singh, Y., 1966, to be published  
Das Gupta, A., and Barua, A. K., 1965, *J. Chem. Phys.*, **42**, 2849  
Hirschfelder, J. O., McClure, F. T., and Weeks, J. F., 1942, *J. Chem. Phys.*, **10**, 201  
Itcan, E. C., Glueck, A. R., and Svehla, R. A., 1961, *NASA Technical Note* D-481  
Mason, F. A., and Monchuck, L., 1961, *J. Chem. Phys.*, **35**, 1676  
Monchuck, L., and Mason, F. A., 1965, *J. Chem. Phys.*, **42**, 263  
Stogryn, D. E., and Hirschfelder, J. O., 1959, *J. Chem. Phys.*, **31**, 1531.

ON THE RAMAN AND INFRARED SPECTRA OF  
BENZYL ACETATE

S. CHATTOPADHYAY AND D. K. MUKHERJEE

OPTICS DEPARTMENT,

INDIAN ASSOCIATION FOR THE CULTIVATION OF SCIENCE,

CALCUTTA-32

(Received April 27, 1966)

**ABSTRACT.** The Raman spectrum of benzyl acetate in the liquid state and the infrared absorption bands of the pure liquid and its solutions in  $\text{CCl}_4$  and  $\text{HCCl}_3$  have been investigated. A reasonably complete vibrational assignment of the observed frequencies of the molecule of benzyl acetate has been made by treating the vibrations of the phenyl group and the  $-\text{CH}_2\text{OCOCH}_3$  group independently.

## I N T R O D U C T I O N

A large amount of work on the assignment of modes of vibration to various vibrational frequencies in the molecules of benzene and its derivatives have already been carried out (Pitzer and Scott, 1943; Spenser and Kirby-Smith, 1941; Mecke-Kerkhof, 1951; Whiffen, 1956; Stephenson *et al.*, 1961; Sirkar *et al.*, 1964 and others). In most cases the substituent is either a single atom or a single group containing a small number of atoms. However, if the substituent group contains larger number of atoms the Raman and infrared spectra of the compound become more complex and in such cases very little work on the enumeration of the vibrational modes in the molecules seems to have been done.

A systematic programme has been undertaken so that a reasonably complete vibrational assignment of the frequencies of vibrations of molecules of substituted benzene compounds with large substituent groups may be made and in this paper the results obtained with benzyl acetate have been presented.

An incomplete study of the Raman spectrum of this compound was made by Morris (1931) while the infrared absorption bands due to this compound were reported by Lenormant (1948). The Raman and infrared spectra of the compound have been re-investigated in order that as many vibrational frequencies as possible are obtained.

## E X P E R I M E N T A L

The sample of benzyl acetate supplied by Société des Usines Chimiques, France, was first fractionated and the proper fraction was distilled several times under reduced pressure before use. The Raman spectrum of the liquid was investigated in the usual manner and the states of polarisation of some of the Raman

lines were determined qualitatively from the ratio of the intensities of the horizontal and vertical components photographed simultaneously with the double image prism. The Fuoss glass spectrograph used has a dispersion of about  $13 \text{ \AA}/\text{mm}$  and  $19 \text{ \AA}/\text{mm}$  in the  $\text{Hg } 4047 \text{ \AA}$  and  $4358 \text{ \AA}$  regions respectively. The infrared spectra of the compound in dilute solutions in  $\text{CCl}_4$  and  $\text{HCCl}_3$  and also of a thin film of the pure liquid were recorded on a Perkin-Elmer Model 21 double beam infrared spectrophotometer with  $\text{NaCl}$  optics. The absorption due to the pure liquid in a  $0.025 \text{ mm}$  thick cell was investigated carefully so that the existence of very weak bands which might have escaped observation with the dilute solutions and the thin film of pure liquid, could be ascertained. The spectrophotometer was calibrated with the standard absorption bands of atmospheric water vapour, carbon dioxide and of a polystyrene film.

#### RESULTS AND DISCUSSION

The frequency-shifts of the Raman lines ( $\text{in cm}^{-1}$ ) of benzyl acetate together with the estimated relative intensities are given in Table I. The states of polarisation of the lines are denoted by the letters *P* and *D* as usual. The table also contains the wave numbers ( $\text{cm}^{-1}$ ) of the infrared bands due to the pure liquid and its solutions in  $\text{CCl}_4$  and  $\text{HCCl}_3$ . The intensities and the nature of the bands are listed as *s*—strong; *m*—medium, *w*—weak; *b*—broad; *sh*—shoulder and *v*—very. A probable assignment of the various vibrational frequencies is given in the last column of Table I.

The molecule of benzyl acetate contains 21 atoms which give rise to 57 modes of vibration. Since the molecule contains no other symmetry element than the element of identity all these would give rise to 57 frequencies of vibration, all allowed in both the Raman scattering and infrared absorption.

In order to be able to assign the modes of vibration arising from the phenyl group in the molecule of benzyl acetate the observed Raman shifts and infrared absorption frequencies of the compound have been compared with the Raman shifts of a number of benzyl derivatives reported earlier by Reitz and Stockmair (1935). From this comparison it is easily found that the frequencies of certain Raman lines characteristic of the vibration of the phenyl ring vary only slightly from one benzyl compound to another. This indicates that so far as the phenyl group is concerned, the modes of vibration and their frequencies are not sensitive to the variation in the nature of the atoms or group of atoms (denoted by *X*) in the substituent  $-\text{CH}_2\text{X}$ . This simplifies the enumeration of the vibrational modes of the benzyl acetate molecule to the extent that the vibrations arising from the phenyl group and the  $-\text{CH}_2\text{OCOCH}_3$  group may be treated separately.

#### a) Assignments of the vibrations of the phenyl group

If the whole of the  $-\text{CH}_2\text{OCOCH}_3$  group is treated as a single mass point the molecule of benzyl acetate would have to a first approximation, the symmetry

of the point group  $C_{2v}$ . Under this symmetry, the classwise breaking up of the 30 vibrational modes of the monosubstituted benzene compound and the classification of the states of polarisation of the Raman lines arising from the m-plane vibrational modes are well known. The experimentally observed states of the polarisation of some of the easily recognisable Raman lines of benzyl acetate justify the correctness of the assumption.

TABLE I  
Benzyl acetate

Raman shift $\Delta\nu$ cm <sup>-1</sup> liquid	Infra-red frequencies (cm <sup>-1</sup> )				Corresponding modes in benzene
	Pure liquid Thou film	0.025 mm cell*	Solutions in* CCl <sub>4</sub>	CHCl <sub>3</sub>	
178 (5) D					10B
251 (1)					16B
367 (0)					17B
400 ?					10A
182 (1)					6A
559 ?					5
620 (5) D					6B
640 (2)	640 v w.	640 m			bending of O—C=O
692 (o, b)	695 s		692 s	695 s	18B
745 (o, b)	740 s				12
825 (3, b)		824 s			10A, stretching of C—CH bond
	830 m				
	900 w		897 w		
908 (0, b)	915 w		912 w		17A
	960 m		960 m	960 w	?
1002 (10) P	1000 m sh		1000 m sh	1002 m sh	1
1027 (5) P	1025 s		1022 s	1023 m sh	18A
	1040 m sh	1040 s sh		1040 m sh	15
1165 (3)	1060 w sh	1060 s sh			9A
1175 (3)	1180 m sh	1180 s sh			9B
1214 (5) P					7A
	1230 vs, b		1227 vs	1227 vs	C—O stretch
	1260 m sh		1250 s sh	1250 s sh	14 ?
	1362 s		1360 s	1360 m	$\delta$ (CH) <sub>6</sub> in CH <sub>2</sub>
1375 (3, vb)	1380 s		1380 s	1380 m	$\delta$ (CH) <sub>6</sub> in CH <sub>2</sub>
	1440 m sh		1437 m sh		$\delta$ (CH) <sub>6</sub> in CH <sub>2</sub>
1445 (2 vb) D	1457 s		1455 m sh		$\delta$ (CH) <sub>6</sub> in CH <sub>2</sub>
	1485 w sh				19A
	1499 m		1495 m	1495 w	19B
1590 (1)	1590 vw	1590 m			8A
1605 (5) D	1605 m	1605 m			8B
1735 (2, b)	1730 vs		1728 vs	1725 vs	C—O stretch
	2850 w sh				CH sym stretch in CH <sub>2</sub> ?
	2890 m sh	2900 m sh			
2935 (5) P	2965 m	2965 s			CH sym stretch in CH <sub>2</sub>
					CH asym stretch in CH <sub>2</sub>
					CH asym stretch in CH <sub>3</sub>
					CH asym stretch in CH <sub>3</sub>
3037 (8)	3012 m sh	3010 s sh	3015 m	3010	2
	3045 m	3044 s	3045 w sh		13
3060 (6) D	3067 m sh	3067 s sh	3070 s sh	3072 w sh	7B
		3080 s sh		3085 w sh	20 B

\*only prominent bands are tabulated.

The proposed assignments of the vibrational frequencies have been based on the considerations of the intensity and character of polarisation of the Raman lines, the intensity of the corresponding infrared bands, the frequencies of vibration in other benzyl compounds and the assignments made in the case of mono-substituted benzenes.

1) *Modes almost unaffected by substitution*

It is seen from the diagram of the normal modes of benzene (Pitzer and Scott, 1943) that in the case of monosubstituted benzenes the frequencies of vibration of the modes 6B, 7B, 9A, 10A, 16A, 17A and 20B will not be affected by the substitution. Also the modes 8A, 8B, 9B, 18A, 19A and 19B in general give rise to vibrational frequencies in monoderivatives of benzene which are almost the same as in benzene and change slightly from one compound to another. These Raman lines and the infrared bands corresponding to those modes in benzyl acetate are shown in Table I. The weak Raman line  $400\text{ cm}^{-1}$  may correspond to the mode 16A while the other weak Raman line  $908\text{ cm}^{-1}$  is assigned to the mode 17A. The Raman line arising from the mode 10A may be masked by the strong and polarised Raman line  $825\text{ cm}^{-1}$  which originates from a different vibration, discussed later. The strong and polarised Raman line  $1002\text{ cm}^{-1}$  which also appears as an infrared shoulder at  $1000\text{ cm}^{-1}$  and corresponds to a similar Raman line in many monosubstituted benzenes, has been assigned to the mode 1. Similarly, the strong Raman line  $3037\text{ cm}^{-1}$  and the strong infrared band  $3045\text{ cm}^{-1}$  are believed to arise respectively from the modes 2 and 13 of benzene. The  $\phi$  infrared band  $1260\text{ cm}^{-1}$  may originate from the mode 14. Table I contains the proposed assignments. The frequencies arising from the modes 3 and 20A have not been ascertained.

2) *Modes affected by substitution*

Of the remaining eleven normal modes, the frequencies of vibrations, in case of the monoderivative of benzene, arising from the modes 6A, 7A, 10B, 11, 12, 16B, 17B and 18B of benzene would be appreciably changed, while those due to the modes 4, 5 and 15 will be affected to a lesser degree.

The weak Raman line  $482\text{ cm}^{-1}$  is easily identified as arising from the mode 6A while the strong Raman band  $178\text{ cm}^{-1}$  is attributed to the mode 10B. In toluene there are two strong and polarised Raman lines at  $786\text{ cm}^{-1}$  and  $1210\text{ cm}^{-1}$  respectively. In the benzyl derivatives two corresponding moderately strong and polarised Raman lines in the region  $740\text{--}765\text{ cm}^{-1}$  and  $1200\text{--}1210\text{ cm}^{-1}$  respectively are observed. Also, in benzyl acetate there is a weak Raman line  $745\text{ cm}^{-1}$  corresponding to the very strong infrared band  $740\text{ cm}^{-1}$  and a moderately strong and polarised Raman line at  $1214\text{ cm}^{-1}$ . The two Raman lines most probably originate from the modes 12 and 7A respectively of benzene. The strong infrared band  $1230\text{ cm}^{-1}$  is believed to arise from other cause which has been discussed later.

The weak Raman line  $692\text{ cm}^{-1}$  having its counterpart in the very strong infrared band  $695\text{ cm}^{-1}$ , has been assigned to the mode 18B. Since the other benzyl compounds do not show any Raman line corresponding to the Raman line  $640\text{ cm}^{-1}$  (infrared band  $640\text{ cm}^{-1}$ ) of benzyl acetate, this line obviously does not represent a vibration of the phenyl group. On consideration of intensity the very weak Raman lines  $367\text{ cm}^{-1}$  and  $254\text{ cm}^{-1}$  have been attributed to modes 17B and 16B respectively. Moreover, since the frequencies of the modes 15 and 5 are affected slightly on substitution, the weak infrared band  $1040\text{ cm}^{-1}$  and the very weak Raman line  $559\text{ cm}^{-1}$  respectively probably represent these modes. Raman line due to the mode 4 has not been observed. All the proposed assignments are shown in Table I.

b) *Vibrations of the  $\text{CH}_3\text{COOCH}_2$  group.*

If the phenyl group is taken to be a single unit 27 vibrational frequencies would arise from this configuration. From the elaborate Raman and infrared data on the molecule of methyl acetate ( $\text{CH}_3\text{COOCH}_3$ ) reported by Wilmshurst (1957), it is seen that many of the vibrational frequencies of this group except those arising from  $\text{CH}_3$ ,  $\text{CH}_2$  and  $\text{C}-\text{O}$  groups are so close to the frequencies of vibration of the phenyl group, that it has been possible to detect only a few of them. However, the following characteristic group vibrational frequencies are easily recognised. Table I contains the proposed assignments.

1) *Carbonyl frequency*

The weak and broad Raman line at  $1735\text{ cm}^{-1}$  corresponding to the strong infrared band at  $1730\text{ cm}^{-1}$  due to the pure liquid is easily assigned to the vibrational frequency arising from the stretching of the  $\text{C}=\text{O}$  bond.

2) *CH deformation vibrations.*

The Raman spectrum of benzyl acetate shows two very broad lines at  $1375$  and  $1445\text{ cm}^{-1}$  and in the infrared spectrum there are three strong bands at  $1362$ ,  $1380$  and  $1457\text{ cm}^{-1}$ . There will be one symmetric and one asymmetric CH deformation vibrational frequencies arising from the  $\text{CH}_2$  group. A comparison with the spectra due to the other benzyl compounds fixes these frequencies fairly reasonably at  $1360$  and  $1440\text{ cm}^{-1}$  respectively. The very broad Raman line  $1375\text{ cm}^{-1}$  may in part also correspond to the strong infrared band  $1380\text{ cm}^{-1}$ , which is the frequency of the symmetric CH deformation in the methyl group while at least one component of the antisymmetric and doubly degenerate CH deformation in the  $\text{CH}_2$ -group is represented by the strong infrared band at  $1457\text{ cm}^{-1}$ . The Raman line corresponding to this mode may have merged in the broad Raman line  $1445\text{ cm}^{-1}$ .

3) *C-H stretching vibrations:*

In the Raman spectrum of benzyl acetate there is a strong polarised Raman line at  $2935\text{ cm}^{-1}$  while the infrared spectrum shows a strong band at  $2965\text{ cm}^{-1}$

and three medium shoulders at 2850, 2900 and 3010  $\text{cm}^{-1}$ . From a comparison with the Raman shifts of other benzyl compounds the Raman line 2935  $\text{cm}^{-1}$  has been assigned to the symmetric CH stretching vibration in the  $\text{CH}_2$  group and the asymmetric component is most probably represented by the infrared band 2965  $\text{cm}^{-1}$ . This band may also correspond to a component of the doubly degenerate asymmetric CH stretching vibration in the methyl group and the band 3010  $\text{cm}^{-1}$  may represent the other component. The symmetric CH stretching vibration of the  $\text{CH}_3$  group has not been detected in the Raman spectrum but may correspond to the weak infrared band 2850  $\text{cm}^{-1}$ . All the assignments made are in accordance with those proposed by Wilmshurst (1957) in the case of methyl acetate.

Besides these characteristic group frequencies, the strong and polarised Raman line 825  $\text{cm}^{-1}$ , having its counterpart in the strong infrared band 824  $\text{cm}^{-1}$ , the Raman line 640  $\text{cm}^{-1}$  corresponding to a medium infrared band 640  $\text{cm}^{-1}$  and the very strong infrared band 1230  $\text{cm}^{-1}$  probably originate in the vibrations in the acetate group of benzyl acetate. These bands in all probability correspond respectively to the strong and polarised Raman line 844  $\text{cm}^{-1}$  (strong infrared band 843  $\text{cm}^{-1}$ ), the strong and polarised Raman line 640  $\text{cm}^{-1}$  (medium infrared band 640  $\text{cm}^{-1}$ ) and the very strong infrared band 1239  $\text{cm}^{-1}$  in the Raman and infrared spectra of methyl acetate reported by Wilmshurst (1957). Following the assignments proposed by him, in the latter case, the Raman lines and infrared bands in the acetate group have been assigned to the vibrations involving the stretching of the  $\text{C}-\text{CH}_3$  bond, the bending of the  $\text{O}-\text{C}=\text{O}$  angle and the stretching of the  $\text{C}-\text{O}$  bond respectively.

#### ACKNOWLEDGEMENT

The authors are grateful to Professor G. S. Kastha, D.Sc., for his continued guidance throughout the progress of the work.

#### REFERENCES

- Lenormant, H., 1948, *Bull. Soc. Chim., France*, **15**, 53.  
 Morries, C. S., 1931, *Phys. Rev.*, **38**, 131.  
 Mecke-Kerkhof, 1951, *Landolt Börnstein Tables*, Auf. 6, Band I, Teil 2.  
 Pitzer, K. S. and Scott, D. W., 1943, *J. Amer. Chem. Soc.*, **65**, 803.  
 Rietz, A. and Stockmair, W., 1935, *Math-naturwiss. Klasse*, Abt.—IIb, 144 (Series 10), 666.  
 ———, 1935, *Monatshefte für chemie*, **67**, (Series 1 and 2), 92.  
 Sirkar, S. C., Mukherjee, D. K. and Bishui, P. K., 1964, *Indian J. Phys.*, **38**, 610.  
 Sponer, H. and Kirby-Smith, J. S., 1941, *J. Chem. Phys.*, **9**, 667.  
 Stephenson, C. V., Coburn, W. C. Jr. and Wilcox, W. S., 1961, *Spectrochim. Acta.*, **17**, 983.  
 Whiffen, D. H., 1956, *J. Chem. Soc.*, 1350.  
 Wilmshurst, J. K., 1957, *J. Mol. Spect.*, **1**, 201.



# ON THE RAMAN SPECTRA OF DILUTE SOLUTIONS OF PARA- AND METACHLOROTOLUENE

S. K. NANDY

INDIAN ASSOCIATION FOR THE CULTIVATION OF SCIENCE,

CALCUTTA-32.

(Received April 25, 1966)

(Plate 3)

**ABSTRACT.** The Raman spectra of 5% and 20% solutions of para- and metachlorotoluenes in carbon tetrachloride have been studied using a spectrograph of high resolving power and a suitable filter to suppress the continuous background in the spectra and these have been compared with the spectrum of the pure liquid. It has been observed that the Raman frequency  $1092\text{ cm}^{-1}$  of *p*-chlorotoluene increases to  $1098\text{ cm}^{-1}$  in the case of the 5% solution and the Raman lines  $683\text{ cm}^{-1}$  and  $996\text{ cm}^{-1}$  of *m*-chlorotoluene shift to  $688\text{ cm}^{-1}$  and  $1000\text{ cm}^{-1}$  respectively when the strength of the solution is reduced to 5%. It has been concluded that in the 5% solution in both the cases the molecules are monomeric while in the pure liquid they are dimers formed through hydrogen bond.

## INTRODUCTION

Numerous workers studied previously the influence of solvents on the Raman spectra of organic molecules (Gray and Hidalgo; 1952, Feneant, 1952; Puranik, 1952; Bollamy 1959; Rea, 1960 and others). The changes in the spectra observed by most of the previous workers are due to association or formation of hydrogen bond. The strengths of the solution used in some of these investigations are generally not below 20%, because it is difficult to record the Raman spectra of very dilute solutions owing to the presence of strong continuous background in the overexposed spectrum of the light scattered by the solvent. In the investigation on the infra-red spectra of such compounds, however, the strengths of the solutions used range generally from 3 to 5%, but unless a careful comparison of such a spectrum is made with that of the pure liquid slight shifts of the bands which may take place owing to the influence of the solvent may sometimes be overlooked.

Recently, Mukherjee *et al.* (1965) observed by recording the infrared spectra of each of a few substituted toluenes in the vapour and liquid phases on the same chart that the molecules of the meta- and para compounds in the liquid state are dimeric and even in the vapour state certain percentages of these molecules are dimers and the rest are monomers. The shift of certain bands with the formation of the dimers observed by them are small, being of the order of about  $4\text{ cm}^{-1}$ — $10\text{ cm}^{-1}$ . In the case of dilute solution in carbon tetrachloride they observed the

dimers to be broken up into monomers. In order to verify these results by studying the Raman spectra of these compounds it would be necessary to record the spectra due to very dilute solutions. It was therefore thought worthwhile to study the Raman spectra of such dilute solution of meta- and para chlorotoluene of different strengths in carbon tetrachloride in order to find out whether the shifts of some of the bands observed by Mukherjee *et al.* are also observed in the Raman spectra and whether the conclusions drawn by them are corroborated by such results.

### EXPERIMENTAL

The liquids used were taken from the same packing from which Mukherjee *et al.* had taken their samples. Carbon tetrachloride used as solvent was of chemically pure quality and it was redistilled before use. The Raman spectra were photographed using a Hilger two-prism spectrograph provided with medium dispersion camera, the inverse dispersion in the 4358Å region being 18Å/mm. Agfa 'Isopan' films were used to photograph the spectra. The resolving power of this spectrograph being fairly large shifts of the order of  $4\text{ cm}^{-1}$  could be easily detected. A very dilute aqueous solution of  $\text{NaNO}_2$  was used to cut off radiations of wave length shorter than 4046Å in the incident light in order to suppress the continuous background in the spectrum.

### RESULTS AND DISCUSSION

The spectrograms are reproduced in Figs. 1 and 2, Plate 3. The changes observed in the positions of some of the Raman lines are shown in Table I.

TABLE I  
Changes in Raman frequencies

Substance	Raman frequencies in $\text{cm}^{-1}$			Assignment (correspond- ing modes of $\text{C}_6\text{H}_6$ )
	State—			
	Pure	20% Soln. in $\text{CCl}_4$	5% Soln. in $\text{CCl}_4$	
<i>p</i> -Chlorotoluene	1091 (5) p	1092 (s)	1098 (s)	19 A
<i>m</i> -Chlorotoluene	683 (7) p	683 (b)	688 (w)	9 B
	996 (10) p	996 (b)	1000 (s)	1
p-polarised	s-sharp	w-weak	b-broad	

It can be seen from Fig. 1 that the line  $1092\text{ cm}^{-1}$  of pure para chlorotoluene appears unaltered in position and width in the spectrum due to the 20% solution

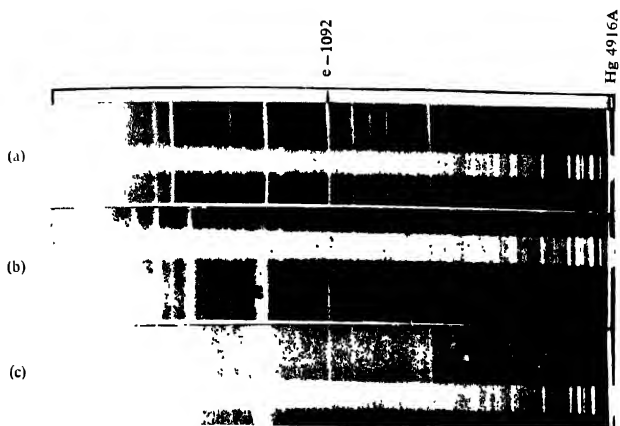


Fig. 1. Raman spectra of *p*-chlorotoluene

(a) Pure liquid (b) 20% Solution in  $\text{CCl}_4$  (c) 5% Solution in  $\text{CCl}_4$

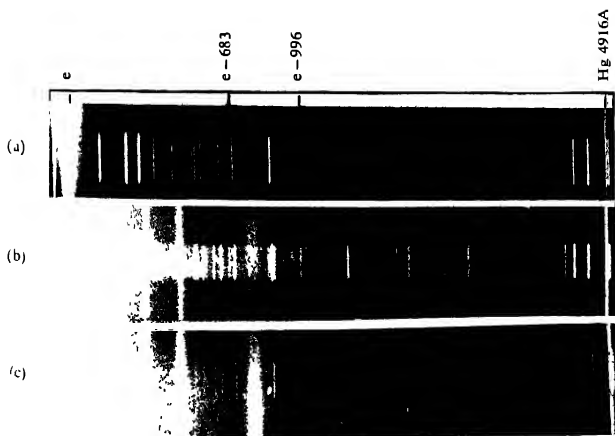


Fig. 2. Raman spectra of *m*-chlorotoluene

(a) Pure liquid (b) 20% Solution in  $\text{CCl}_4$  (c) 5% Solution in  $\text{CCl}_4$



in carbon tetrachloride so that it coincides with a line 4576.2A in the iron arc spectrum as in the spectrum due to the pure liquid, but in the case of the 5% solution the line shifts slightly towards red so that the Raman shift increases to  $1098\text{ cm}^{-1}$ . This can also be seen by measuring the distance of the line from the iron line 4556.13A. In the infrared spectrum of the compound in the vapour phase Mukherjee *et al.* (1965) observed two bands at 1088 and  $1096\text{ cm}^{-1}$  but the liquid was found to give only one band at  $1088\text{ cm}^{-1}$ . Hence the conclusion drawn by them that in the vapour phase some of the molecules are in monomeric state giving the band  $1096\text{ cm}^{-1}$  and the rest are dimers is corroborated by the results mentioned above, because in the 5% solution in carbon tetrachloride all the dimeric molecules are expected to be split up into monomeric ones giving the line  $1098\text{ cm}^{-1}$ . The fact that no change is observed in the case of the 20% solution shows that only at very low concentration the molecules are truly dissolved in the solvent and exist as monomers. Owing to the presence of the strong Raman lines of carbon tetrachloride in the spectrum due to the solution changes in some other Raman lines could not be observed, but the spectra show that the line  $3062\text{ cm}^{-1}$  does not undergo any change probably because in the formation of the hydrogen bond only one of the four hydrogen atoms is involved.

Fig. 2 shows more significant differences between the spectrum due to *m*-chlorotoluene in the liquid and that of the solution. The sharp line  $683\text{ cm}^{-1}$  of the liquid broadens towards red in the spectrum due to the 20% solution and it again becomes sharp but appears at  $688\text{ cm}^{-1}$  in the spectrum due to the 5% solution. Similarly, the line  $996\text{ cm}^{-1}$  becomes broad in the spectrum due to the 20% solution and it appears as a sharp line at  $1000\text{ cm}^{-1}$  in the spectrum due to the 5% solution. Assuming the line  $1000\text{ cm}^{-1}$  to be due to the monomeric molecule, it is concluded that the 20% solution contains a mixture of both monomeric and dimeric molecules. These results further corroborate the conclusions drawn by Mukherjee *et al.*, that the compound in the vapour phase consists of a mixture of monomeric and dimeric molecules.

The results discussed above lead to the conclusion that in both the liquids only dimeric molecules formed through hydrogen bond are present and they persist in the solution unless the strength is reduced to about 5%.

It may be pointed out here that the influence of the solvent observed in the present case is different from that observed by Gray and Hidalgo (1952) in the case of dilute solutions of acetophenone in carbon tetrachloride and cyclohexane. They observed that the  $1684\text{ cm}^{-1}$  line of the C=O group of acetophenone shifts to  $1690\text{ cm}^{-1}$  in the case of a solution containing 5 Mols in 100 Mols of carbon tetrachloride, but in the case of similar solution in cyclohexane the line was found to shift to  $1695\text{ cm}^{-1}$ . They attributed the shift to the breaking up of the anti-parallel alignment of the two C=O groups of the two neighbouring molecules,

but in the present case the breaking up of the hydrogen bond between two molecules is postulated.

#### ACKNOWLEDGMENT

The author's thanks are due to the Authorities of the Indian Association for the Cultivation of Science for providing facilities for the investigation and to Professor S. C. Sirkar, D.Sc., F.N.I., Emeritus Professor and Retired Scientist (under C.S.I.R.) for his kind guidance throughout the progress of the work.

#### REFERENCES

- Bellamy, 1959, *Spectrochim. Acta*, **14**, 192.  
Feneant, S., 1952, *Compt. Rend.*, **235**, 1292.  
Gray, E. and Hidalgo, A., 1952, *Compt. Rend.*, **235**, 152.  
Mukherjee, D. K., Bishui, P. K. and Sirkar, S. C., 1965, *Indian J. Phys.*, **39**, 537.  
Puranik, P. G., 1952, *Proc. Ind. Acad. Sc.*, **37**, 499.  
Ren, D. G., 1960, *J. Mol. Spectro*, **4**, 507.

# DEVELOPMENT OF NEON TUBE HODOSCOPE CHAMBER AS A DETECTOR OF IONISING PARTICLES

B. K. BANDYOPADHYAY, SUBHRA BHATTACHARYA  
AND R. L. SENGUPTA

PHYSICAL LABORATORY, PRESIDENCY COLLEGE, CALCUTTA

(Received December 2, 1965).

**ABSTRACT.** The paper discusses about the construction of a particle detector called the neon tube hodoscope. The details about the processing of the tubes, gas filling and the construction of the chamber as well as the electronics so used has been presented in this paper in a more lucid way. The advantage and disadvantage of this type of detector and the possible cosmic-ray experiments that can be performed with the help of this instrument has also been discussed. A photograph of a single particle, presumably a muon which passes through the chamber and thereby illuminating all the twenty tubes in a column and not the other adjacent tubes has also been presented along with this paper

## INTRODUCTION

The neon tube hodoscope chamber has originally been developed by Conversi *et al.* (1955, 1956). After the publication of this short report this detector has been investigated extensively by many investigators in many countries and now it is used widely in experiments of high-energy and cosmic-ray physics. (Fukui and Miyamoto 1957, Rochester 1960, Coxell and Wolfendale 1961, Hasegawa *et al.* 1963).

This neon tube hodoscope has many advantages such as, it is easy to construct at low cost, very stable in operation and short recovery time (about 0.1 second) as well as the life time of the tubes against failure seems to be very long. Due to these facilities this technic is very suitable for the experiment on large cosmic ray showers as well as in the under ground penetrating shower detection.

The major disadvantage of neon tube hodoscope is its limited resolution due to the finite dimension of the tubes and hence the difficulty in interpreting complex events. We present here a preliminary work along this line.

## CONSTRUCTIONAL FEATURE

In this laboratory a neon tube hodoscope chamber has been constructed with hundred neon flash tubes. This instrument consists of twenty-one aluminium plates placed parallelly and between which a number of glass tubes are inserted. Every second plate being electrically connected. Five such tubes are placed in each row. The arrangement used is shown schematically in Fig. 1.

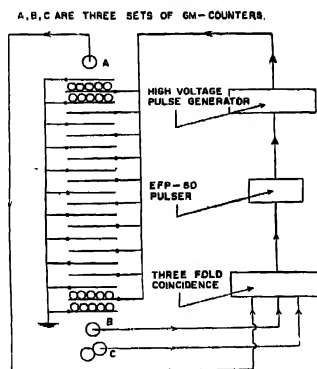


Fig. 1. Schematic diagram of Experimental arrangement.

The tubes are 30 cms long with 1.5 cm in diameter and are made up of Soda

Each tube is filled with neon gas at 35 cm Hg pressure. In this experiment spectroscopically pure neon has been used. All the tubes has been washed properly with the cleaning solution (the chromic and sulphuric acid mixture) and are evacuated in electric furnaces. During the experiment all the tubes has been covered with black paper to keep each tube not being illuminated by the light from other tubes.

#### EXPERIMENTAL ARRANGEMENT AND DISCUSSION

For tests with cosmic rays the chamber is placed between three sets of G. M Counters A, B, and C (as in the diagram shown in Fig. 1). A coincidence between the pulses from the G. M. Counters is made to trigger an EFP60 pulser which in turn fires a 5C22 hydrogen thyatron, applying the high voltage pulse to the chamber. In this test the pulse is derived by discharging a  $0.001\text{-}\mu\text{f}$  condenser through a 100-ohm limiting resistor into the chamber. The condenser is charged to a potential of 8KV from a conventional high voltage power supply.

The electric field thus generated inside the chamber is large enough to accelerate the electrons freed by the ionizing particle and cause a luminous discharge in the neon tubes crossed by the particle and not in the other tubes. Each tube crossed by a particle is set alight and is photographically recorded. A typical photograph of the path of an ionizing particle through the tubes is shown in Fig. 2.

The camera is operated with an  $f/8$  aperture, because enough light is generated by the flash and pictures of tracks taken with this  $f$ -number are quite satisfactory, using Tri-X Pan film.



The spurious discharges which depend partly on the condition of gases filled in the tubes but mainly on the condition of the inner surface of the glass wall

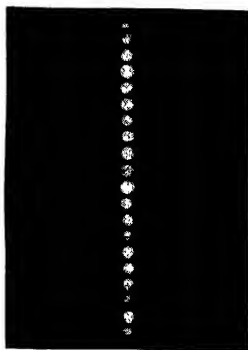


Fig. 2. Photograph of a single penetrating particle.

can be minimised by washing the tubes properly with the cleaning solution and in order to get the best performance it is necessary to get an excellent vacuum before filling.

By the choice of internal diameter of each tube to 2 mm, the spacial resolution of the neon tube hodoscope chamber can be improved to a great extent.

We hope to employ this technic to study an extensive air shower experiment with a larger and more efficient installation.

#### ACKNOWLEDGMENT

Scholarships granted to (B.K.B.) by the Ministry of Education, Government of India and to (S.B.) by Prof. Dr. R. L. Sen gupta have enabled the present work to be undertaken and are gratefully acknowledged. Thanks are also due to the Government of West Bengal for its annual financial grant.

#### REFERENCES

- Conversi, M. and Gozzini, A., 1955, *Nuovo Cimento*, **2**, 189.  
Conversi, M., Focardi, S., Franzinetti, C., Gozzini, A. and Murtas, P., 1956, *Suppl. Nuovo Cimento*, **4**, 234, (Pisa Conf.).  
Coxell, H. and Wolfendale, A. W., 1961, *Proc. Phys. Soc. (London)*, **75**, 378.  
Fukui, S. and Miyamoto, S., 1957, *Contributed to the Air Shower Project*, I.N.S.  
Hasegawa, H., Matano, T., Miura, I. and Shibata, S., 1963, *Proc. of the International Conference on Cosmic-rays*, **4**, 284.  
Rochester, G. D., 1960, *Proc. of the Moscow Cosmic-ray Conference*, **11**, 312.

# ON A NEW DISTRIBUTION FORMULA FOR MOLECULES OF REAL GASES AND FOR IONS OF STRONG ELECTROLYTES IN SOLUTION

M. DUTTA

(A/31, C.I.T., BUILDINGS, SINGHERBAGAN, CALCUTTA-7)

(Received March 20, 1966).

**ABSTRACT.** A distribution formula for molecules of finite size in fields of forces, and of ions of strong electrolytes in solution, which was found to be very useful for development of a new theory of real gases and of strong electrolytes in solutions, was deduced by Dutta (1947, 1948, 1951a, 1951b, 1952, 1959) and by Dutta and Bagchi (1950). In these deductions, the phase-space is split into momental and configurational spaces, the configurational space is divided into layers of different potential energies which are again divided into small cells, and then distributions of image points in momental and configurational spaces are considered separately. Here, over and above all these, the notion of coarse-graining has been introduced for determining distributions in the configurational space. A new distribution-formula, which may be useful in the theory of real gases and of strong electrolytes in solution, is obtained.

## INTRODUCTION

For statistical considerations of an assembly of a large number of particles, the phase-space is conveniently divided into cells of suitably small volume and then the distributions of particles (really, then image-points) in these cells are considered by treating the states of a particle by points in a cell as equivalent (cf., Ehrenfest P. and T., 1959). This procedure is practically the same as the grouping of observational data in statistical analysis. Its significance and justification from information-theoretical and statistical stand-point can be seen in the book of Kullback (1959) and in some recent discussions (Dutta, 1965, 1966a and 1966b).

Before the formulation of Heisenberg's uncertainty principle, the measure of the volume of the small cells was arbitrary. But simple arguments based on this principle (cf. Dutta, 1965, 1966a and 1966b) lead to the value,  $h^3$ , for the volume of the elementary cells,  $h$  being the Planck constant.

In a number of papers (Dutta, 1947, 1948, 1951a, 1951b, 1952, 1959, 1965, 1966a; Dutta and Bagchi, 1950; Dejak, 1959), for the consideration of the volume of exclusion of particles (molecules, ion, etc) supposed to be rigid, i.e., for the consideration of the short-ranged repulsive interactions between particles of the type,

$$F(r_{ij}) = \begin{cases} 0 & \text{for } r_{ij} > r_0 \\ \infty & \text{for } r_{ij} \leq r_0 \end{cases}$$

$r_{ij}$  being the distance between the  $i$ -th and the  $j$ -th particle, and  $r_0$  being a characteristic constant for pair of particles of a particular kind, generally taken as the

sum of the radius of the particles in the pair, the configurational space is divided in small cells of volume,  $b$ , equal to the volume of exclusion of a particle and the particles are assumed to be distributed in such a manner that each cell may either remain vacant or be occupied by a single particle. If there be other forces of some regular types the configurational space is also divided into potential layers, which are again supposed to contain a large number of the above cells, and then, the distributions of particles are to be considered in these cells (Dutta, 1951a, 1951b; Dutta and Bagchi, 1950, Dejak, 1959). By forces of some regular type, it is meant that the gradient of forces is large compared to the dimension of particles and small compared to the volume of the container. Now, when the assembly contains particles of different kinds, the method has been modified suitably by introducing different volumes,  $b_1, b_2, b_{12}$  for pair of different kinds and then by calculating the thermodynamic probability suitably (Dutta 1951b, Dutta and Bagchi, 1950, Dejak, 1959).

Now, in calculations of activity coefficients for strong electrolytes in solution, it is seen that better results are obtained if different values of  $b_+$  and  $b_-$  are chosen suitably in different ranges of concentrations. So, it has appeared that it may be possible to deduce more useful results, if  $b$  is interpreted suitably and slightly differently. Here, it is done simply after the introduction of coarse-grained distribution, as already mentioned earlier (Dutta, 1965).

We shall take  $b$ , the volume of the cell, as a bit arbitrary parameter which is greater than  $b_0$ , the volume of exclusion and is to be chosen suitably to the fit the experimental value.  $b$  is taken to be such a small volume that it is quite sufficient to specify the position of a particle by stating that it is in a particular cell. The equation of an ideal gas can be deduced simply by specifying the position of a particle to be anywhere in the total volume  $V$  of the container, i.e.,  $b = V$  (cf. Falkenhagen, 1950). In denser systems and in the presence of an external external field and or of a field of interactions, more accurate specification is necessary, i.e.,  $b_0 \leq b < V$ . Now, if  $r = [b/b_0]$  the integer just less than  $b/b_0$ , it is easy to see that a cell may be vacant or occupied by utmost  $r$  number of particles. In this respect, it is similar to Gentile statistics. For simplicity, we first consider the case where the forces other than the short-ranged repulsive force for rigid particles are absent. After that, we consider the case where there are other forces of regular type over and above the above short-ranged force. At the end, mixtures of particles of two different types is discussed. Except the introduction of the notion of coarse-grained distribution other notions are similar to those developed earlier by the author.

#### ASSEMBLY OF PARTICLES OF FINITE SIZE

The thermodynamic probability is

$$W = \frac{[V/b]!}{n! N!} \cdot \frac{N!}{n! a_m!} \quad (2.01)$$

where  $V$  is the volume of the container,  $N$  the number of particles,  $N_i$  the number of cells occupied by  $b$  particles, and  $a_m$  the number of particles with kinetic energy,  $\epsilon_i$ .  $[V/v]$  is the integer just less than  $(V/b)$ . As in gases  $(V/b)$  is generally very large, so in future discussion we shall neglect their difference and always write  $(V/b)$ . After using Stirling's formula and taking logarithm, we have

$$\log W = \left( \frac{V}{b} \right) \log \left( \frac{V}{b} \right) - \sum_i N_i \log N_i + N \log N - \sum_i a_m \log a_m \dots \quad (2.02)$$

This is to be maximised subject to the condition that

$$\sum_{i=0}^r N_i = \left( \frac{V}{b} \right) \quad \left| \quad \dots \quad (2.03) \right.$$

$$\sum_{i=1}^r \epsilon_i N_i = N \quad (2.04)$$

$$\sum a_m = N \quad (2.05)$$

$$\sum a_m \epsilon_m = E \quad (2.06)$$

$E$  being the total energy.

Then, by usual variations, we get

$$N_i = e^{-\nu - \nu_1 \epsilon_i} \quad \dots \quad (2.07)$$

and

$$a_m = e^{\lambda - \epsilon_m} \quad \dots \quad (2.08)$$

Therefore,

$$S = k \log W_{max} = k \left[ \left( \frac{V}{b} \right) \log \left( \frac{V}{b} \right) + \nu \left( \frac{V}{b} \right) + \nu_1 N + \lambda N + \mu E \right] \dots \quad (2.09)$$

From well-known thermodynamic relation we have

$$\mu = \frac{1}{k} \left( \frac{\partial S}{\partial E} \right)_{\nu, \nu_1} = \frac{1}{kT} \quad \dots \quad (2.10)$$

$T$  being the temperature.

Then, from (2.05) we have

$$e^{\lambda} = \frac{1}{N} \sum_m e^{-\epsilon_m/kT} = \frac{1}{N} \int \int \int e^{-\frac{p_x^2 + p_y^2 + p_z^2}{kT}} \frac{dp_x dp_y dp_z}{h^3/b} \\ = \frac{b}{N h^3} (2\pi m k T)^{3/2} \quad \dots \quad (2.11)$$

From (2.03), we have

$$e^v = \frac{b}{V} \sum_i e^{-v_i b} = \frac{b}{V} \frac{1 - e^{-(r+1)v_1}}{1 - e^{v_1}} \quad \dots (2.12)$$

From (2.04), we have,

$$e^v = \frac{1}{N} \sum_{l=1}^r l e^{-v_l l}$$

or

$$\begin{aligned} \frac{Nb}{V} &= \frac{\sum l e^{-v_l l}}{\sum e^{-v_l l}} = \frac{\partial}{\partial v_1} \left\{ \log \left( \sum_l e^{-v_l l} \right) \right\} \\ &= \frac{1}{e v_1 - 1} - \frac{(r+1)}{e(r+1)v_1 - 1} \quad \dots (2.13) \end{aligned}$$

Thus, all the parameters (Lagrange's undetermined multipliers), entering in the calculation can be determined. As the case when  $r = 1$ , has already been completely worked out (Dutta, 1957) in actual applications,  $r$  will be two or three and so calculations appear to be not difficult. From (2.09),  $S$  is known in terms of  $V, T$  on substitution of values of  $v, v_1, \lambda, \mu$  and by well-known thermodynamic relations, expressions of other thermodynamic functions can be easily calculated.

#### ASSEMBLY OF PARTICLES OF FINITE SIZE IN PRESENCE OF OTHER FIELDS OF FORCES

As in earlier papers, (Dutta, 1951a, 1952b, 1959), it is assumed that the forces, other than the short-ranged force associated with rigidity, are such that the entire configurational space is divided into potential energy layers of potential energies  $\psi_1, \psi_2, \dots$  of corresponding volumes,  $V_1, V_2, \dots$  which are small compared to the total volume  $V$  but large compared  $b$ . As before the thermodynamic probability can be written as

$$W = \prod_n \frac{(V_n/b)_i}{\prod_l N_{nl}!} \cdot \frac{N!}{\pi_m a_m!} \quad \dots (3.01)$$

where  $N_{nl}$  is the number of cells in the  $n$ -th layer which are occupied by  $l$  particles and other symbols have interpretations, same as in the preceding article.

As usual, after using Stirling formula for factorial, and then taking logarithm, we get,

$$\begin{aligned} \log W &= \left[ \sum_n \left\{ \left( \frac{V_n}{b} \right) \log \left( \frac{V_n}{b} \right) - \sum_{l=0}^r N_{nl} \log N_{nl} \right\} \right. \\ &\quad \left. + N \log N - \sum_m a_m \log a_m \right] \quad \dots (3.02) \end{aligned}$$

This is to be maximised, subject to the condition that

$$\sum_{nl} N_{nl} = \sum_n \left( \frac{V_n}{b} \right) = \left( \frac{V}{b} \right) \quad \dots (3.03)$$

$$\sum_l l N_{nl} = \sum_n l N_n = N \quad \dots (3.04)$$

$$\sum_m a_m = N \quad \dots (3.05)$$

and

$$\sum_m a_m \epsilon_m + \sum_n (\sum_l l N_{nl}) \psi_n = E \quad \dots (3.06)$$

After usual variations, we get

$$\sum_{n,l} N_{nl} (\log N_{nl} + \nu + \nu_1 l + \mu l \psi_n) + \sum_l \Delta a_l (\log a_l + \lambda + \mu \epsilon_l) = 0$$

Then,

$$N_{nl} = e^{-\nu - \nu_1 l - \mu l \psi_n} \quad \dots (3.07)$$

$$a_m = e^{-\lambda - \mu \epsilon_m} \quad \dots (3.08)$$

$$S = k \log W_{max} = k \left[ \sum_n \left( \frac{V_n}{b} \right) \log \left( \frac{V_n}{b} \right) + \nu \left( \frac{V}{b} \right) + \nu_1 N + \lambda N + \mu E \right] \quad \dots (3.09)$$

In the usual way the temperature can be introduced by the thermodynamic relation as

$$\mu = \frac{1}{k} \left( \frac{\partial S}{\partial E} \right)_{V,N} = \frac{1}{kT} \quad \dots (3.10)$$

Then,

$$e^\lambda = \frac{1}{N} \sum_m e^{-\epsilon_m/kT} = \frac{1}{N} \frac{b}{h^3} (2\pi m kT)^{3/2} \quad \dots (3.11)$$

From (3.03), we have

From (3.03), we have

$$e^\nu = \left( \frac{b}{V} \right) \sum_n \frac{1 - e^{-(r+1) \left( \nu_1 + \frac{\psi_n}{kT} \right)}}{1 - e^{-(\nu_1 + \psi_n/kT)}} \quad \dots (3.12)$$

and

$$N_n = \frac{V_n}{b} \left[ \frac{1}{e^{(\nu_1 + \psi_n/kT)} - 1} - \frac{(r+1)}{e^{(r+1)(\nu_1 + \psi_n/kT)} - 1} \right] \quad \dots (3.13)$$

The equation (3.12) gives an expression of  $v$  in terms of  $v_1$ . The equation (3.13) is the new distribution formula. The parameter,  $v_1$ , is determined (at least theoretically) from the restriction (3.04):

### ASSEMBLY OF PARTICLES OF TWO DIFFERENT TYPES

Now we consider an assembly consisting of  $N_1$  and  $N_2$  particles of the first and the second types of masses,  $m_1$  and  $m_2$  respectively. We suppose that the forces are of regular type, so that the configurational space can be divided into potential layers of potential  $-\phi_1, -\phi_2, \dots -\phi_n \dots$  so that the potential energies in the  $n$ -th layer of particles of the first and the second type are  $m_1\phi_n$  and  $m_2\phi_n$  respectively. These layers are again divided into cells of volume  $b$ . If  $b_1$  and  $b_2$  denote the exclusion volume of the first and the second types for particles of the same types and  $b_{12}(=b_{21})$  denote the same for particles of different types and if we write

$$r_1 = \left[ \frac{b}{b_1} \right], r_2 = \left[ \frac{b}{b_2} \right], r_{1j} = \left[ \frac{b - jb_{12}}{b_1} \right], r_{l2} = \left[ \frac{b - lb_{12}}{b_2} \right] \quad \dots \quad (4.01)$$

then a cell may remain vacant or may be occupied utmost by  $r_1$  particles only of the first type, or utmost by  $r_2$  particles only of the second type, or utmost by  $r_1$  particles of the first type when it is already occupied by  $j$  particles of the second type or utmostly  $r$  particles of the second type when it is already occupied by  $l$  particles of the first type.

We write the thermodynamics probability as follows :

$$W = \frac{\Pi (V_n/b)!}{\pi N_{n1}!} \cdot \frac{N_1!}{i! a_{1i}!} \cdot \frac{N_2!}{n! a_{2n}!} \quad \dots \quad (4.02)$$

where  $N_{n1j}$  = the number of cells, in the  $n$ th layers, occupied by  $i$  particles of the first type and  $j$  particles of the second type,

$a_{1m}$  = the number of particles of the first type with the kinetic-energy,  $\epsilon_{1m}$ ,

and  $a_{2m}$  = that of the second type with the kinetic energy,  $\epsilon_{2m}$ .

After using Stirling's approximate formula for factorials and then taking logarithm, we have

$$\begin{aligned} \log W = & \sum_n \left\{ \left( \frac{V_n}{b} \right) \log \left( \frac{V_n}{b} \right) - \sum_{ij} N_{n1j} \log N_{n1j} \right\} \\ & + N_1 \log N_1 + N_2 \log N_2 - \sum_i a_{1i} \log a_{1i} - \sum_n a_{2n} \log a_{2n} \quad \dots \quad (4.03) \end{aligned}$$

This is to be maximised subject to the following conditions :

$$\sum_{n,l,j} N_{nlj} = \sum \frac{V_n}{b} = \frac{V}{b} \quad \dots (4.04)$$

$$\sum_{n,l,j} l N_{nlj} = \sum_n N_{1n} = N_1 \quad \dots (4.05)$$

$$\sum_{n,l,j} j N_{nlj} = \sum_n N_{2n} = N_2 \quad \dots (4.06)$$

$$\sum_l a_{1l} = N_1 \quad \dots (4.07)$$

$$\sum_l a_{2l} = N_2 \quad \dots (4.08)$$

$$\sum_i a_{1i} \epsilon_{1i} + \sum_m a_{2m} \epsilon_{2m} + \sum_{n,l,j} N_{nlj} (im_1 + jm_2) \phi_n = E \quad (4.09)$$

where the volume,  $V$ , of the container, total numbers,  $N_1$  and  $N_2$ , of particles and the total energy  $E$ , are to be taken as constant.

After usual variation, we get

$$N_{nlj} = e^{-\nu - \nu_1 l - \nu_2 j - \mu(m_1 l + m_2 j) \phi_n} \quad \dots (4.10)$$

$$a_{1l} = e^{-\lambda_1 - \mu \epsilon_{1l}} \quad \dots (4.11)$$

$$a_{2m} = e^{-\lambda_2 - \mu \epsilon_{2m}} \quad \dots (4.12)$$

where  $\nu, \nu_1, \nu_2, \lambda_1, \lambda_2, \mu$  are Lagrange's undetermined multipliers to be interpreted suitably. Then by Boltzmann hypothesis after using the relations (4.10, 4.12), we get

$$S = k \log W_{max} = k \left[ \sum_n \left( \frac{V_n}{b} \right) \log \left( \frac{V_n}{b} \right) + \nu \left( \frac{V}{b} \right) + N_1 \log N_1 \right. \\ \left. + N_2 \log N_2 + (\lambda_1 + \nu_1) N_1 + (\lambda_2 + \nu_2) N_2 + \mu E \right] \quad \dots (4.13)$$

As usual, by the well-known thermodynamic relation, we have

$$\mu = \frac{1}{k} \left( \frac{\partial S}{\partial E} \right)_{V, N_1, N_2} = \frac{1}{kT} \quad \dots (4.14)$$

By the equation (4.07) and (4.08), we have

$$e^{\lambda_1} = \frac{1}{N_1} \cdot \frac{b}{N_1} (2\pi m_1 kT)^{3/2} \quad \dots (4.15)$$



$$e^{\lambda_2} = \frac{1}{N_2} \cdot \frac{b}{h^3} (2\pi m_2 kT)^{3/2} \quad \dots \quad (4.16)$$

By the equation (4.04), we have

$$e^{\nu} = \left( \frac{b}{V} \right) \sum_{i,j} e^{-\nu_1 l - \nu_2 j - (2m_1 + jm_2) \frac{\phi_n}{RT}} \quad \dots \quad (4.17)$$

This equation gives  $\nu$  as a function of  $\nu_1$ ,  $\nu_2$ ,  $m_1$ ,  $m_2$  etc. Then, by (4.15) and (4.06)  $\nu_1$  and  $\nu_2$  are to be determined.

Now, also we have

$$\frac{V_n}{b} = e^{-\nu} \sum_{i,j} e^{-\nu_1 l - \nu_2 j - (lm_1 + jm_2) \frac{\phi_n}{RT}} \quad \dots \quad (4.18)$$

$$N_{1n} = e^{-\nu} \sum_{i,j} i e^{-\nu_1 l - \nu_2 j - (lm_1 + jm_2) \frac{\phi_n}{RT}} \quad \dots \quad (4.19)$$

and

$$N_{2n} = e^{-\nu} \sum_{i,j} j e^{-\nu_1 l - \nu_2 j - (lm_1 + jm_2) \frac{\phi_n}{RT}} \quad \dots \quad (4.20)$$

Then, after simple calculations, we get

$$N_{1n} = \frac{V_n}{b} \cdot \frac{\partial}{\partial \nu_1} \log \left\{ \sum_{i,j} e^{-\nu_1 l - \nu_2 j - (lm_1 + jm_2) \frac{\phi_n}{RT}} \right\} \quad \dots \quad (4.21)$$

$$N_{\nu n} = \frac{V_n}{b} \cdot \frac{\partial}{\partial \nu_2} \log \left\{ \sum_{i,j} e^{-\nu_1 l - \nu_2 j - (lm_1 + jm_2) \frac{\phi_n}{RT}} \right\} \quad \dots \quad (4.22)$$

These are the distribution formulæ in a binary mixture in most general form. The evaluation of the series within the logarithms, in a closed form, appears to be very complicated. Moreover, it is also very difficult to express the summation within the logarithms as a symmetric function of the characteristic quantities associated with particles of different quantities, since the summation of  $j$  first and the over  $i$  is apparently different from that of  $i$  first and then over  $j$ . But, the nature of the problems suggests that the expression within logarithms should be symmetric with respect to the characteristic quantities, associated with particles of different types. We postpone the general discussion at present. Here, we consider in details the case which is comparatively much simple to evaluate and also useful for applications.

Case when  $b_{12} = 0$ , i.e.  $b_{12}$  is negligible compared to  $b_1$  and  $b_2$  :

Here,  $r_{1j} = r_1$ , and  $r_{2j} = r_2$ ,

for all  $i$  and  $j$

Now,

$$\sum_{ij} e^{-v \left( 1 + \frac{m_1 \phi_n}{RT} \right) i - \left( v_2 + \frac{m_2 \phi_n}{RT} \right) j} \\ = \left\{ \frac{1 - e^{-\left( v_1 + \frac{m_1 \phi_n}{RT} \right) (r_1 + 1)}}{1 - e^{-\left( v_1 + \frac{m_1 \phi_n}{RT} \right)}} \right\} \left\{ \frac{1 - e^{-\left( v_2 + \frac{m_2 \phi_n}{RT} \right) (r_2 + 1)}}{1 - e^{-\left( v_2 + \frac{m_2 \phi_n}{RT} \right)}} \right\}$$

Then,

$$N_{1n} = \frac{V_n}{b} \left\{ \frac{1}{e^{-v_1 + \frac{m_1 \phi_n}{RT}} - 1} - \frac{(r_1 + 1)}{e^{(r_1 + 1) \left( v_1 + \frac{m_1 \phi_n}{RT} \right)} - 1} \right\} \dots (4.23)$$

$$N_{2n} = \frac{V_n}{b} \left\{ \frac{1}{e^{v_2 + \frac{m_2 \phi_n}{RT}} - 1} - \frac{(r_2 + 1)}{e^{(r_2 + 1) \left( v_2 + \frac{m_2 \phi_n}{RT} \right)} - 1} \right\} \dots (4.24)$$

These are the new distribution formulae in this case for binary mixture. Of course, the discussion can be extended for a mixture of more than two components and the distribution will be similar to those given by (4.23) and (4.24).

#### ASSEMBLY OF IONS OF STRONG ELECTROLYTES IN SOLUTION

In case of ions of strong electrolytes in solution the average minimum approach of ions of opposite charges is always expected to be very small compared to that of ions of opposite charge i.e.  $b_+ \ll b_-$  and  $b_-$ . In actual calculations, (Eigen and Wicke, 1951, Dutta, 1952, 1953; Dutta and Sengupta, 1954)  $b_+$  is taken to be zero. So calculations quite similar to the preceding articles lead to the distribution formulae for ions given by the following expressions :

$$N_{+n} = \frac{V_n}{b} \left\{ \frac{1}{e^{v_+ + \frac{e_+ \phi_n}{RT}} - 1} - \frac{(r_+ + 1)}{e^{(r_+ + 1) \left( v_+ + \frac{e_+ \phi_n}{RT} \right)} - 1} \right\} \dots (5.01)$$

$$N_{-n} = \frac{V_n}{b} \left\{ \frac{1}{e^{v_- + \frac{e_- \phi_n}{RT}} - 1} - \frac{(r_- + 1)}{e^{(r_- + 1) \left( v_- + \frac{e_- \phi_n}{RT} \right)} - 1} \right\} \dots (5.02)$$

where  $N_{+n}$  and  $N_{-n}$  are respectively number of ions of positive and negative charges in the  $n$ -th layer of electric potential,  $-\phi_n$ ,  $e_+$  and  $e_-$  are charges of positive ions and negative ions, and  $w_+$ ,  $w_-$ ,  $r_+$ ,  $r_-$  have interpretations similar to those of the preceding article.

#### CONCLUDING REMARKS

It can be easily seen that all calculations reduce to those made earlier (Dutta, 1947, 1948, etc.), if the volume,  $b$ , of the cell is taken to be equal to the exclusion volume of the particles. From this stand-point the formulae proposed here are generalisation of those proposed earlier.

#### ACKNOWLEDGEMENT

The author expresses his hearty thanks and deep gratitude to National Professor S. N. Bose for his encouragement and for his support in his Research Scheme at the Indian Association of Cultivation of science, Calcutta-32.

#### REFERENCES

- Dejak, C. 1959, *Proceeding of International Symposium in Electrolytes*, Pergamon Press.  
 Dutta, M. 1947, *Proc. Nat. Inst. Sc. (India)*, **13**, 347.  
 ——— 1948, *Proc. Nat. Inst. Sc. (India)*, **13**, 103.  
 ——— 1951, *Proc. Nat. Inst. Sc. (India)*, **16**, 27, 445.  
 ——— 1952, *Proc. Nat. Inst. Sc. (India)*, **17**, 81.  
 ——— 1952, *Naturwiss*, **39**, 108.  
 ——— 1953, *Naturwiss*, **40**, 51.  
 ——— 1959, *Proc. Summer Inst. of Theor. Physics at Mussorie (India)*, p. 297.  
 ——— 1965, *Science and Culture*, **31**, 231.  
 ——— 1966a, *New Statistical Theories of Real Gases and Electrolytes in Solution*, Scientific Book Agency, Calcutta, India.  
 ——— 1966b, *Statistical Physics (Foundation)*, World Press, Calcutta, India.  
 Dutta, M. and Bagchi, S. N. 1950: *Indian J. Phys.*, **24**, 61.  
 Dutta, M. and Sengupta, M. 1954, *Proc. Nat. Inst. Sc. (India)*, **20**, 1.  
 Ehrenfest, P. and Ehrenfest T. 1959, *The conceptual Foundations of the Statistic Approach in Mechanics*, Connell Univ. Press, N.Y.  
 Eigen, M. and Wicke, E. 1951, *Naturwiss*, **38**, 453.  
 Falkenhagen, H. 1959, *Statistik und Quantum Theorie*, S. Hirzel Verlag, Stuttgart.  
 Kullback, S. 1959, *Information Theory and Statistics*, J. Wiley & Sons, N. Y.

# LIFETIMES OF $2^+$ AND $4^+$ STATES OF Dy-160

K. M. M. S. AYYANGAR, V. LAKSHMINARAYANA AND  
SWAMI JNANANANDA

LABORATORIES FOR NUCLEAR RESEARCH, ANDHRA UNIVERSITY, WALTAIR.

(Received January 15, 1965)

**ABSTRACT.** The half-lives of the first and second excited states of Dy-160 are measured by the delayed coincidence method. For this measurement, a time-to-amplitude converter is assembled. With NaI(Tl) crystals on both the photomultipliers, a resolving time of 2.4ns with an intrinsic time resolution of 0.27ns is achieved down to an energy of 200Kev. The life-times of  $2^+$  and  $4^+$  levels of Dy-160 are obtained at  $T(2^+) = 1.94 \pm 0.097$ ns and  $T_1(4^+) = (11.25 \pm 1.13) \times 10^{-11}$  sec. These values confirm those obtained by Li and Schwarzschild. The results of the present investigation are discussed and found to confirm the predictions of the unified nuclear model.

## INTRODUCTION

Recently Li and Schwarzschild (1963) have measured the lifetimes of  $2^+$  and  $4^+$  states in four different isotopes (including Dy-160) which belong to the strongly deformed region. Their results have been found to be in agreement with the predictions of the unified nuclear model (Bohr, 1952). The results obtained by some of the workers, however, show deviations with the predictions of the unified model. These deviations may be ascribed to those arising out of the measured lifetime values. The recent development of the time-to-amplitude converters has enabled the attainment of a better accuracy in the measurement of the lifetimes. These converters enable the attainment of the time spectral data employing a multi-channel analyser. This use naturally reduces the duration of the experiment thereby rendering the minimization of the various systematic errors. The time-to-amplitude converter which is already mentioned, is so modified as to match the characteristics of the NaI(Tl) crystals employed in the present investigations in order to measure the lifetimes of the  $2^+$  and  $4^+$  levels of Dy-160.

## EXPERIMENTAL ARRANGEMENT

The experimental arrangement in the present investigations involve two scintillation heads arranged in triple coincidence. The scintillator-photomultiplier assembly consists of a NaI(Tl) crystal 4.45 cm in diameter and 2.54 cm in height. Whenever the investigation involves the observation of beta-decay, an anthracene scintillator (4.45 cm in diameter and 0.32 cm in thickness) is employed in the beta-channel. The block diagram of the arrangement is shown in Fig. 1. The pulses

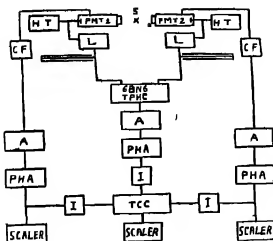


Fig 1. Block diagram of the experimental set-up.

S—Source; H.T.—High Tension; PMT—Photomultiplier, L—Limiter; C.F.—Cathode follower; TPHE—Time-to-pulse height converter; A—Amplifier; PHA—Pulse height analyser; I—Inverter; T.C.C.—Triple coincidence circuit;

from the anodes of the photomultipliers are transmitted to the limiters the outputs of which are so clipped as to obtain pulses of 80ns duration, which in turn are fed to the 6BN6 time-to-amplitude converter of the Green and Bell (1958) type. The output of the converter is connected to the triple coincidence circuit via an amplifier followed by an analyser. It may be pointed out that the pulses from the eighth dynodes of both the photomultipliers are amplified, energy selected and then transmitted to the triple coincidence unit, the output pulses of which are recorded by means of a decade scaler.

The decay time of the NaI(Tl) crystal is approximately 300ns. Hence only a minute part of its pulse is applied to the converter in order to achieve a good time resolution by operating the photomultipliers at voltages upto 2400V. The amplitude of the resulting pulse is of the order of 150V especially in the case of a gamma component with an energy of 511Kev as given out by  $Na^{22}$  annihilation quanta. The arrangement of the fast pulse part of the converter is shown in Fig. 2

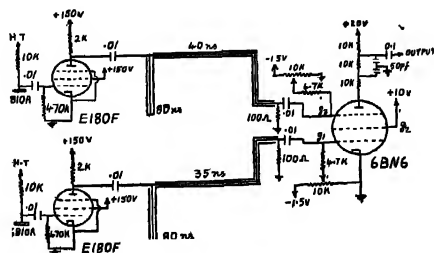


Fig. 2. Fast coincidence arrangement.

in which the converter part is identical with the original one (Green and Bell 1958). In the present arrangement the limiters are of Special Quality Philips E180F tubes operated at a plate potential of 150V. The limiter has a cut-off value less than 2 volts at the operating conditions. The screen potential is so adjusted as to obtain a plate current of 22mA. The clipper in the fast channel is a cable of the type AS48M with an impedance of 100 ohms, a capacitance of 12pf/ft, and a delay of 1.2ns/ft. The distortions which may occur in the rising and falling portions of the shaped pulses are eliminated by employing a fixed delay of 40ns in both the channels of the converter. The valve 6BN6 is operated at potentials of 20V and 10V to the plate and screen respectively. With these operating conditions, the pulses with one volt amplitude can saturate the plate current, as the grids  $g_1$  and  $g_3$ , as shown in Fig 1, are held at negative potentials of 0.7 and 1.0 volt respectively. Since the plate current of the limiter is adjusted at 22mA, and the effective impedance of the clipping stub is 50 ohms (obtained with 100 ohm terminating resistance in parallel), the pulses have a height of 1.1V. It may be mentioned that at these operating conditions of the 6BN6, there is an inherent delay of 5ns arising out of the transit time of electrons from grid  $g_1$  to  $g_3$ . Complete overlap of the pulses at  $g_3$  is effected by inserting 35ns cable in  $g_1$  and 40ns in  $g_3$ . When two simultaneous pulses arrive at the two grids of the 6BN6, a current flows during the time the pulses overlap. Since the plate pulse is integrated, the charge accumulated on the plate is proportional to the overlap time of the pulses so that the amplitude of the pulse obtained from the converter is proportional to the delay between the two pulses.

The introduction of a fixed delay of 40ns in both the channels affords a simultaneous comparison with the prompt coincidence curve. The slopes on the two sides of the coincidence curve arise out of the jitter in the time of arrival of the pulses at the grid of the limiter. When the time jitter is symmetrical, the prompt coincidence curve is symmetrical in shape. With a measurable lifetime, the delayed radiations are detected only in one of the counters hence the distortion of the lifetime is imposed on only one side of the coincidence curve. The plot of the delayed coincidence has a slope as expected for a prompt cascade being of the same energies, whereas the other side has the slope corresponding to the lifetime. With the introduction of a delay of 40ns in both the channels the present arrangement has a useful range of 0.40ns. The negative output of the converter is fed to a high gain linear amplifier through a cathode follower. A single channel analyser which follows the amplifier is used to scan the time spectra. The voltage scale of this analyser is calibrated in terms of time by observing the shift in the centroid of the prompt curve for every 5ns decrease of the cable in one of the channels. The amplifier in the fast channel is kept in one of the two adjusted gain positions corresponding to the calibration values of 0.909ns/volt and 0.425ns/volt for the measurements in the nanosecond and sub-nanosecond regions. The prompt curve has resolving time of 2.4ns with slopes corresponding to half-lives of 0.27ns

for energies down to 200Kev. For energies below 100Kev, the resolution is nearly 3ns. With anthracene-photomultiplier assembly, the operating voltage is only 2000V. This reduction from 2400-2000V enables the limiting of the anode pulse to 6-8% of the amplitude thereby obtaining the best possible resolution, the resolving time in this case being 2.1ns with slopes of 0.26ns. To test the accuracy of the lifetimes of the excited levels in the isotopes under investigation, the lifetimes of the level with an energy of 81Kev of Cs-133 and the level with an energy of 279 Kev of Tl-203 are observed and found to have the values of the half-lives as  $6.09 \pm 0.3ns$  and  $(2.89 \pm 0.14) \times 10^{-10}sec$  respectively. These values are quite in agreement with the results of the previous workers. In other words, the oft measured values of the lifetimes of these isotopes taken as standards are employed for testing the verity of the lifetimes measured with the present equipment

### Determination of lifetime of the $2^+$ state of Dy-160.

The decay scheme of Tb-160 is quite complicated as can be seen from the level diagram (Ewan *et al.*, 1961) given in Fig. 3. The figure indicates most of the intense

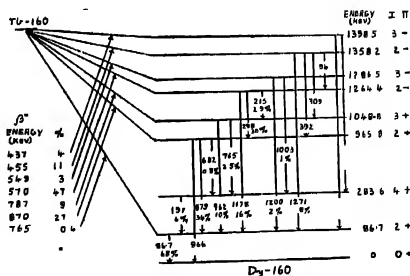


Fig. 3. Decay scheme of Th-160 (Ewan et al.)

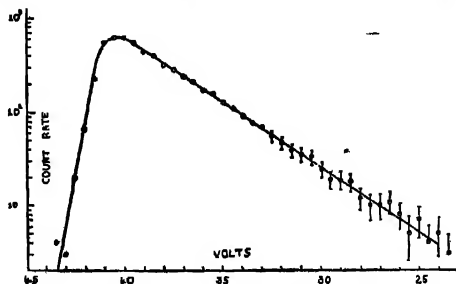
transitions along with the percentage of intensities. It can be seen that there are seven beta groups and nearly twenty gamma transitions, hence the spectroscopic measurements are difficult. It may be pointed out that the  $2^+$  and  $4^+$  states have been identified as members of the  $K = 0$  rotational band, whereas the higher  $2^+$  and  $3^+$  excited states have been identified as those of the  $K = 2$  band resulting from electric quadrupole vibrations. The values of the half-life for the  $2^+$  level obtained by different authors are tabulated as given in Table I.

From this table I it is interesting to find that the values of (1), (4) and (5) are in good agreement within the limits of experimental error; of which those in (4) and (5) are of relatively high precision. On the other hand, the results from (2), (3) and (6) are at variance with one another. The recently measured value<sup>6</sup> 2.059 which is given within a precision of  $\pm 0.016$ ns, is at variance with all the

TABLE I

Author and year	Half-life (ns)	Reference
1. F. K. McGowan (1955)	$1.8 \pm 0.2$	5
2. Berlovich et al. (1962)	$1.6 \pm 0.1$	6
3. Richter and Wiegandt (1962)	$2.25 \pm 0.06$	7
4. Fossan and Herskind (1963)	$1.92 \pm 0.05$	8
5. Li and Schwarzschild (1963)	$1.90 \pm 0.05$	1
6. De Boer et.al. (1963)	$2.059 \pm 0.016$	9
7. Elbok et.al. (1960)	$2.247 \pm 0.14$	10

already mentioned values. Under these circumstances it is considered necessary to reinvestigate the lifetime of the  $2^+$  level using the equipment developed for the purpose. To study the decay scheme, Terbium-160 is obtained in liquid form as Terbium chloride with an intensity of 5.2mC. A small quantity of this liquid is taken in a perspex tube and is mounted on the source mount situated symmetrically between the two scintillation heads. Then the singles spectrum of Tb-160 is recorded. The 87Kev transition being highly populated (nearly 68%), is very intense. Hence a gamma-gamma coincidence study is very desirable for this intense case. The gamma-gamma coincidence involves the record of counts when the detecting units are arranged at right angles to one another and the crystals are covered with 1 mm of lead to cut-off the characteristic X-radiation. The 87Kev gamma component is chosen for observation by one scintillation head, the other being biased at an energy of 600Kev so that those gamma photons feeding the 87Kev level are collected for coincidence. The resulting coincidence spectrum is recorded as shown in Fig. 4. Each experiment is repeated thrice, the total number of separate experiments being four. The resulting average half-life value

Fig. 4. Lifetime measurement of the  $2^+$  level.



obtained by least square fit analysis is  $T_1 = 1.94 \pm 0.035$  ns. This error together with the errors arising out of the instrument, calibration, and those arising out of the measurement of the length of the cables comes to a total value of 5% so that the corrected half-life may be written as  $T_1(2^+) = 1.94 \pm 0.097$  ns which is not in agreement with some of the listed values <sup>6, 7, 8</sup>.

*Determination of the lifetime of the 4<sup>+</sup> level of Dy-160*

The 283 Kev excited level of Dy-160 decays to the 87 Kev level by a transition with an energy of 197 Kev. The 4<sup>+</sup> level is of meagre population being only 5% in the decay of Tb-160. This transition also involves total conversion of nearly 25%. The transitions between the 1264 and 966 Kev levels as well as between 1264 and 1049 Kev levels give rise to conversion electrons of intensity comparable to that of the above transition. If the 765.2 Kev transition be selected in one of the channels and the 215-197 Kev transitions in the other, the lifetime of the 1049 Kev level may influence the value of the lifetime of the 4<sup>+</sup> level. The upper levels have energies of large value and mostly are decaying by E2 transitions. Hence the single particle estimates predict very short lifetimes (of the order of  $10^{-12}$  sec) for these levels. Therefore, they are not expected to influence the lifetime of the 4<sup>+</sup> level. The results of the measurements on the lifetime of the 4<sup>+</sup> level carried out by previous workers are tabulated as given in Table II

TABLE II

Author	Year	Half-life ( $10^{-11}$ sec)	Method	Reference
1. Burde and Rakavy	1961	$7.50 \pm 0.76$	Self comparison	11
2. Berlovich et.al.	1962	$7.10 \pm 0.90$	Centroid shift	6
3. Li and Schwarzschild	1963	$10.7 \pm 0.50$	Slope	1

The first two mentioned values in Table I, though are in fair agreement, differ very much from the last one. The first result in the table is obtained by employing two double lens magnetic spectrometers in coincidence along with a time-to-amplitude converter. The second in the list employed a centroid shift method for measuring the lifetime in the decay of Ho-160 in which the coincidences are measured between the upper gamma components and the conversion electrons. The last mentioned data is obtained by employing a precision time-to-amplitude converter having a slope of  $4 \times 10^{-11}$  sec along with a three crystal spectrometer.

In the present investigations an attempt has been made to measure the lifetime of the same level but with the equipment developed for the purpose. In a certain sense this unit is very sensitive with high efficiency and with a good resolution. In experiments which involve beta-electron or beta-gamma coincidences

the number of prompt coincidences may be very large because of the interference of the upper levels. The scintillation heads as already mentioned, subtend an angle of  $90^\circ$  and the crystals are covered with 1 mm of lead to arrest X-photons. One of the slow channels is set to accept the peak with an energy range of 197-215Kev, the other being biased at about 600Kev. The number of prompt coincidences given out by the 215-765Kev cascade is nearly 20% and as the 1049Kev level lifetime is expected to be very short, the uncertainty in the lifetime is expected to be less than the assigned errors. The gain of the amplifier in the fast channel is set at the position of the higher sensitivity whereas the converter circuit is kept in the 60ns overlapping condition obtained by replacing the cable in the  $g_2$  channel with a cable of length 20ns. After these preliminary arrangements the time spectrum is scanned obtaining a curve, the inverse of which is taken by the interchange of the selection of the gamma components. The two sets of data thus obtained are plotted, after eliminating the errors arising out of chance coincidences, on a semi-logarithmic scale as given in Fig 5. A similar procedure is adopted using

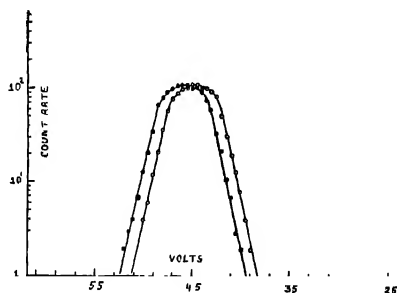


Fig. 5. Lifetime measurement of the  $4^+$  level.

a Co-60 source, with the same energy selections, in order to eliminate the errors due to time-independent and energy-dependent shifts. The resulting spectra thus obtained are shown in Fig. 6. The centroid shifts ( $2\sigma$ ) are determined by numerical integration and are converted to time by comparison with the calibration plot used as standard. The shift for Tb-160 thus determined corresponds to a half-life of  $16 \times 10^{-11}$  sec whereas that for Co-60 corresponds to  $4 \times 10^{-11}$  sec giving the value of the half-life of the  $4^+$  level as  $12 \times 10^{-11}$  sec. The entire experiment is repeated using a different intensity of the source. The result of this repetition is found to have a value of  $10.5 \times 10^{-11}$  sec. Assuming the possibility of 10% error in these measurements, the average value for  $T_{1/2}(4^+)$  is found to be

$$T_{1/2}(4^+) = (11.25 \pm 1.13) \times 10^{-11} \text{ sec.}$$

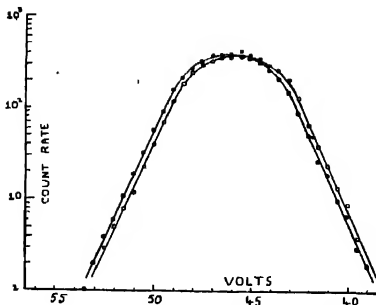


Fig. 6. Experiment with Co-60.

which is indeed in agreement with the latest value listed in the table.

#### DISCUSSION

It is usual that the experimental transition probabilities are compared with the values computed from the theory of single particle model. To obtain the experimental transition rates, the 197 and 86.7 Kev transitions of Dy-160 are considered as having no admixture. It is required that the values of the experimentally determined lifetimes be corrected for internal conversion. The theoretically obtained total internal conversion coefficients<sup>12</sup> are found to be 4.60 and 0.25 for the 86.7 and 197 Kev transitions respectively. Thus after the necessary corrections the experimental transition rates  $T(E2)_{86.7}$  and  $T(E2)_{197}$  are found as

$$T(E2)_{86.7} = 6.392 \times 10^7 \text{ sec}^{-1}$$

$$T(E2)_{11} = 4.939 \times 10^9 \text{ sec}^{-1}$$

The values of the transition rates corresponding to the above are derived from the single particle model and are found to be  $3.148 \times 10^5 \text{ sec}^{-1}$  and  $1.907 \times 10^7 \text{ sec}^{-1}$  respectively. It can be seen that the experimental values are comparatively much higher by an order of 203 and 259 respectively than the theoretically obtained values. This enhancement is expected in the strongly deformed region for E2 transitions within a rotational band. However, the K-forbidden E2 transitions have retardation factors of the order of  $10^3$ .

With a view to see the present experimental transition rates are capable of confirming in a more satisfactory way the predictions of the strong coupling model, the present experimental results for the transition rates are compared with the predictions of the strong coupling model. In this connection it may be

pointed out that the reduced transition probability  $B(E2)$  of an  $E2$  transition from an initial spin state  $I_i$  to the final state  $I_f$  in a rotational band  $K$  is

$$[B(E2); I_i \rightarrow I_f] = \frac{5}{16\pi} e^2 Q_0^2 \langle I_i 2 K 0 | I_f 2 I_f K \rangle^2 \quad \dots (1)$$

where  $Q_0$  is the intrinsic quadrupole moment. Substituting the experimental values in the expression

$$[B(E2)]_{exp} = [1.23 \times 10^{-2} \times E_r^5]^{-1} T(E2) \quad \dots (2)$$

the  $B(E2)_{88.7}$  and  $B(E2)_{197}$  are obtained as

$$B(E2)_{88.7} = 1.061(e^2 10^{-48} \text{ cm}^4)$$

$$B(E2)_{197} = 1.352(<)e^2 10^{-48} \text{ cm}^4)$$

Again substituting the above values of the  $B(E2)$  in the expression (1), the  $Q_0$  values are obtained as

$$Q_0 = 7.302 + 0.18(10^{-24} \text{ cm}^2)$$

$$Q_0 = 6.901 \pm 0.35(10^{-24} \text{ cm}^2)$$

being those determined from the lifetimes of the first and second excited states respectively. It can be seen that the  $Q_0$  values for both the levels are as should be in agreement within the limits of the experiment. From the value of  $Q_0$  given above the deformation parameter  $\beta$  is derived from

$$Q_0 = \frac{3}{\sqrt{5\pi}} ZR^2\beta \quad \dots (3)$$

as  $\beta = 0.3443$ .

The value of the intrinsic quadrupole moment  $Q_0$  may further be tested by employing the result derived from the Asymmetric Rotor Model<sup>13</sup>. Using this model the  $Q_0$  is obtained from

$$[B(E2); 2^+ \rightarrow 0^+] = \frac{e^2 Q_0^2}{16\pi} \frac{1}{2} \left( 1 + \frac{3 - 2 \sin^2 3r}{\sqrt{9 - 8 \sin^2 3r}} \right) \quad \dots (4)$$

where  $r$  is the (shape) parameter of transverse deformation. In the case of Dy-160, from the energies of the first and second excited states, the  $r$  is found to be  $11.85^\circ$  which on substitution in the above expression (4) gives the  $Q_0$  value as  $Q_0 = 7.44 (10^{-24} \text{ cm}^2)$  which is in agreement with that obtained from the unified model. Hence it may be concluded that there is not much difference in the results

obtained from unified and asymmetric rotor models in the strongly deformed region.

The expression (1) gives a value of 1.43 to the ratio of the reduced transition probabilities  $[B(E2); 4^+ \rightarrow 2^+]/[B(E2); 2^+ \rightarrow 0]$ . On the other hand, the experimental value of the same is obtained as  $1.275 \pm 0.2$ . It can be seen that these two values are in a fair agreement. The assigned error 0.2 of the ratio amounts to 16% which naturally as can be seen from the following table is considerably less than those of others.

TABLE III

Authors	Year	$\left[ \frac{B(E2); 4^+ \rightarrow 2^+}{B(E2); 2^+ \rightarrow 0^+} \right]$	Same ratio calculated with $T_{\frac{1}{2}}(87) = 1.94 \text{ ns}$ .
1. Burde and Rakavy	1961	$1.650 \pm 0.33$	$1.897 \pm 0.33$
2. Berlovich et.al.	1962	$1.680 \pm 0.27$	$2.019 \pm 0.27$
3. Li and Schwarzschild	1963	$1.400 \pm 0.22$	$1.341 \pm 0.22$
4. Present investigation		$1.275 \pm 0.20$	$1.275 \pm 0.20$

From the last column of the table it can be seen that with the value obtained by present investigation for the lifetime of the  $2^+$  level, the values of the ratio differ considerably from the theoretical value (1.43) in the case of the results of the authors (1) and (2) mentioned in the table. From the data<sup>1</sup> of four even-even nuclei in the strongly deformed region it can be seen that the values obtained for the same ratio are in good agreement with the theory. Hence the present experimental value for the ratio of the reduced transition probabilities within the  $K = 0$  band confirm the unified model predictions. It can also be seen that the present lifetimes of the  $2^+$  and  $4^+$  levels are accurate within the limits of the experiment.

## ACKNOWLEDGEMENT

The authors wish to express their grateful thanks to the Department of Atomic Energy, Government of India, for having sponsored this scheme of work in this laboratory and for awarding a Senior Scientific Assistantship to one of them (K.M.M.S).

## REFERENCES

- Li, A. C., A. Schwarzschild, 1963, *Phys. Rev.* **129**, 2664.  
 Bohr, A. 1952, *K. Dan. Vid. Selsk. mat-fys. Medd.* **27**, No. 14.  
 Bohr, A., Mottelson, B. R., (1953), *K. Dan. Vid. Selsk. mat-fys. Medd.* **26**, No. 16.  
 Green, R. E., Bell, R. E., (1956), *Nucl. Instr.* **3**, 127.

- Ewan, G. T., Graham, R. L., Geiger, J. S., (1961), *Nucl. Phys.* **22**, 610.  
McGowan, F. K., (1952), *Phys. Rev.* **85**, 142.  
Berlovich, E. E., Gusev, Yu. K. Il'in, V. V., Nikitin, M. K., 1962, *ZETF* **43**, 1625,  
———, 1963, *JETP* **16** 1144.  
Richter, F. W., Wiegandt, D., *Naturforsch.* **Z.**, 1902, **17a**, 636.  
Fossan, D. B., Herskind, B., *Nucl. Phys.* 1963, **40**, 24.  
De Boer, Th. J., Ten Napel, E. W., Blok, J., 1963, *Physica*, **29**, 1013.  
Elbek, K. B., Olesen, M. C., Skilbried, O., 1960, *Nucl. Phys.* **19**, 523.  
Burde, J., Rakavy, M., 1961, *Nucl. Phys.* **28**, 172.  
Shv, L., Band, I., 1956, *Leningrad-Physico-Technical Institute Report*.  
Davydov, A. S., Filippov, G. F., 1958, *Nucl. Phys.* **8**, 237.

# RECTIFIER ACTION OF A GAS DISCHARGE AND ITS DEPENDENCE ON THE V-I CHARACTERISTICS IN THE FORWARD AND THE REVERSE DIRECTION

V. T. CHIPLONKAR AND N. M. A. KUKSHIWALA

ION PHYSICS AND ELECTRONICS LABORATORY  
INSTITUTE OF SCIENCE, BOMBAY.

(Received September 13, 1965; Resubmitted March 3, 1966)

**ABSTRACT.** Observations on the rectification produced in a glow discharge in Hydrogen ( $p=94-275\mu$ ) do not show good correlation with the values to be expected from the d-c  $V-I$  characteristics in the forward and the reverse direction. It is suggested that this may arise because the electrical conduction in the two half cycles may not be independent, which has been confirmed by observations obtained with a transverse magnetic field applied at one of the electrodes.

Gaseous devices for rectification (Gntherschulze, 1927) of low frequency a.c. are well known. They are of several types, of which the two (physically dissimilar) electrode system with a hot or a cold cathode is the most common type. The rectification produced by such a device is based on the asymmetric conductivity of the gas when the first or the second of these electrodes functions as the cathode. The effect can be explained in some cases in terms of the cathode fall at each of the electrodes i.e. to say in terms of the d.c.  $V-I$  characteristics in the forward and the reverse direction. Under these conditions the rectification should be determined by the electrode geometry, the nature of the gas and its pressure etc. (Chiplonkar, 1939 1941). It is clear that whereas the average rectified d.c. output voltage given by the device will be also determined by the ignition potentials in the two half cycles (Talekar, 1956), (which will control the conduction angle of the current), the peak values of the current in the two half cycles will however be determined by the  $V-I$  characteristics only, if one assumes that the electrical conduction in the two half cycles can be considered to be independent of each other. For a given gas the  $V-I$  characteristic of a discharge is controlled by the gas pressure  $p$  and to a limited extent by  $D$ , the interelectrode distance. By a suitable variation of  $p$  and  $D$ , it is possible to vary the nature of the  $V-I$  characteristic so that the discharge changes from the normal, to the abnormal or to the obstructed type, as the case may be. The last type of discharge is obtained when the length of the cathode dark space  $\geq D$ . It may be mentioned that there is no theory available at present (Von Engel, 1965), which is able to account for the different  $V-I$  characteristics observed for these different types of discharges. As a matter of fact these types are specified in terms of their  $V-I$  characteristics. It is also

known that the V-I characteristics of a discharge can be appreciably modified by the application of a magnetic field at a suitable point of the discharge. The object of the present investigation was to examine the correlation between the rectification observed and the corresponding d-c V-I characteristics when these are altered by varying  $p$  and/or  $D$  or by the application of a suitable magnetic field at one of the electrodes. No attempt was however made to investigate the wider problem of the effect of the magnetic field on the nature or form of the characteristic or on the other parameters of the discharge.

The discharge tube used (Pyrex glass, length = 25.0 cm. diameter = 3.0 cm.) was provided with two electrodes of Aluminium (i)  $A$  (dia = 2.9 cm) and (ii)  $B$  (dia = 1.4 cm). The interelectrode distance  $D$  between them could be varied by a magnetic device. No gas streaming was used during the observations. The pressure of the gas in the discharge tube was measured with the help of a thermocouple gauge previously calibrated. The magnetic field was supplied by means of a permanent magnet and had a magnitude  $\approx 150$  Oe as measured with a search coil. The d.c. V-I characteristics with electrode (i)  $A$  as the cathode and (ii)  $B$  as the cathode were taken with the help of a d.c. power-pack (output 20 kV, 20 mA, ripple factor  $< 0.5$  per cent). The circuit arrangement Chiplonkar (1951) shown in Fig. (1) was used, to determine the dynamic rectification. The

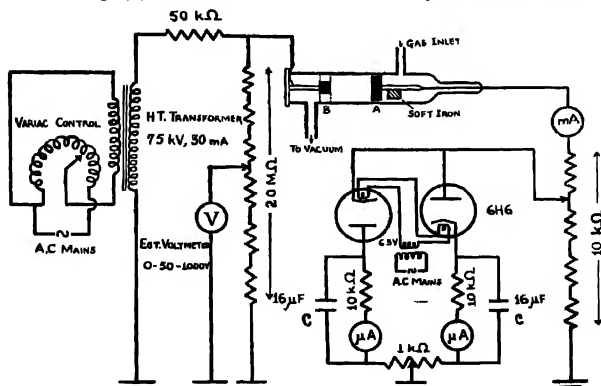


Fig. 1. Discharge tube and electrical connections for measurement of rectification.

use of the condensers  $C'$  enabled the direct measurement of the peak values of the current in the two half cycles for the a.c. operation. If  $\hat{i}_+$  and  $\hat{i}_-$  represent these peak values, the rectification  $\rho$  observed is taken as

$$\rho = \frac{2(\hat{i}_+ - \hat{i}_-)}{\hat{i}_+ + \hat{i}_-}$$



In terms of this notation  $\rho = 2.0$  would correspond to complete rectification. The values of  $\rho$  were determined in this manner as a function of the peak value of the a.c. applied voltage  $\hat{V}_{AC}$  across the tube for different  $p$  and  $D$ . The rectification ratio  $\rho'$  to be expected from the characteristics was calculated from the relation

$$\rho' = \frac{2(i_A - i_B)}{i_A + i_B}$$

where  $i_A$  and  $i_B$  represent respectively the currents observed in the d.c. V-I characteristics corresponding to  $V = \hat{V}_{AC}$  when (i)  $A$  or (ii)  $B$  is used as cathode. In order to bring out clearly the dependence of  $\rho$  on the V-I characteristics, observations were also taken on both these parameters in the presence of a transverse static magnetic field when applied near the electrode  $A$ . The application of the field was found to modify the characteristics to a significant extent. One typical set of these observations with and without this magnetic field are shown in Fig (2). From the characteristics it is clear that the discharge is abnormal (with a positive slope for the V-I characteristic) except in the case of curve I for a small range of currents (0-1.5 mA) where the discharge is obstructed. Fig (3) curves

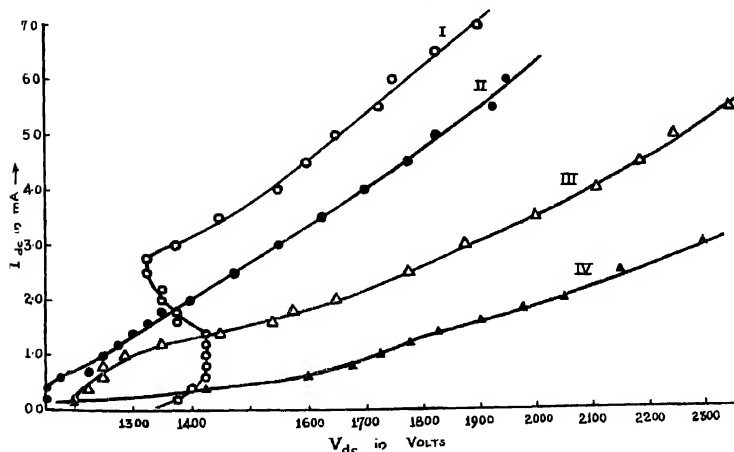


Fig. 2. d.c. V-I characteristics for discharge in hydrogen.

$p = 170$  microns,  $D = 2.0$  cm.

I Electrode A as cathode (without field).

II Electrode A as cathode (with transverse magnetic field at A).

III Electrode B as cathode (without field).

IV Electrode B as cathode (with transverse magnetic field at A).

(I-V) represent the values of  $\rho/\rho'$  as a function of the peak values of the a.c. e.m.f. applied with and without the magnetic field.

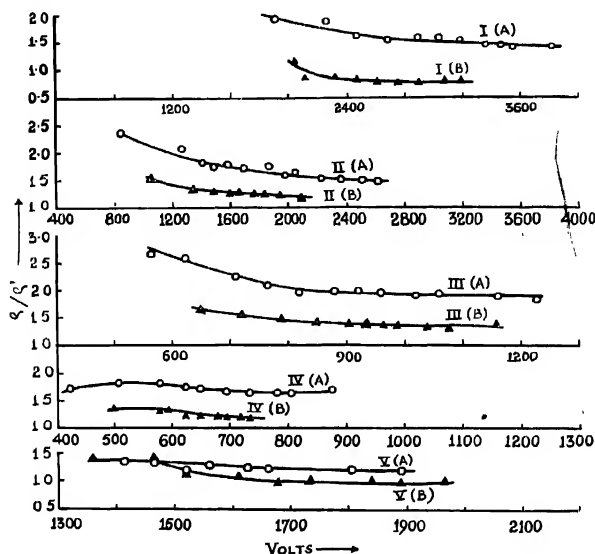


Fig. 3. Variation of  $\rho/\rho'$  with voltage.

$\rho$  = observed rectification ratio

$\rho'$  = calculated rectification ratio

I  $p = 94$  microns,  $D = 4.0$  cm.

A — without magnetic field,

B — with magnetic field.

II  $p = 140\mu$ ,  $D = 4.0$  cm.

A — without magnetic field,

B — with magnetic field.

III  $p = 210\mu$ ,  $D = 4.0$  cm.

A — without magnetic field,

B — with magnetic field.

IV  $p = 275\mu$ ,  $D = 4.0$  cm.

A — without magnetic field,

B — with magnetic field.

V  $p = 170\mu$ ,  $D = 2.0$  cm.

A — without magnetic field,

B — with magnetic field.

Observations were taken for a glow discharge in hydrogen within the pressure range of  $94$ – $275\mu$  for  $D$ , the interelectrode distance, between  $2.0$ – $4.0$  cm. A few

typical curves obtained are shown in Fig. 3 (I-V). The observations obtained for the case where the magnetic field is not present show values for  $\rho/\rho'$  which are very much greater than one, indicating that the actual rectification is always very much higher than the expected. The ratio shows a slow decrease with increasing voltage. The discrepancy between the magnitudes of  $\rho$  and  $\rho'$  may possibly occur because the conduction in the two half a.c. cycles may not be independent of each other as assumed in our analysis. The necessary condition to be satisfied for this to happen is that the quiescent time interval between the quenching of the current in one half cycle and its ignition in the next consecutive half cycle should be less than the deionisation time for the device. Support is given to this view by the observations obtained under the same conditions with a transverse magnetic field. One expects the magnetic field to deflect the discharge channels in the two half cycles in opposite directions and thus help to make them independent of each other. This is in fact shown by our observations that  $\rho$  and  $\rho'$  under those conditions have values which are not very much different from each other. It may be remarked that a gas rectifier with a three electrode system based on the deflection of the discharge channels in opposite directions by a transverse magnetic field has been reported (von Engel and Steenbeck, 1932)

Only in the case of the observations shown in Fig. 3-V which was obtained for an obstructed discharge, that the agreement between  $\rho$  and  $\rho'$  is fairly good even in the absence of the magnetic field. As the magnitude of the plasma region is negligible in this case, the results may be taken to indicate that the deionisation time effects of the plasma region are more important than those of the cathode dark space region.

One can therefore conclude that the dynamic rectification observed in the case of a glow discharge cannot be predicted from its d.c. V-I characteristics, a result in agreement with the observations of Sisodia (1963) for a hollow cathode discharge.

#### REFERENCES

- Chiplonkar, V. T. 1951, *Ind. J. Phys.* **25**, 138-140.  
——— 1939, *Proc. Ind. Acad. Sc.* **10**, 381, (1941), **13**, 323.  
Guntherschulze, A. 1927, *Electric rectifiers and valves*, Chapman & Hall. pp. 28-52 and 153-156.  
Sisodia, M. L. 1963, *Ind. J. Pure Appl. Phys.*, **1**, 270  
Talekar, V. L. 1956, *J. Electronics*, **2**, 205-10.  
Von Engel, A. 1965, *'Ionised gases'*, Clarendon Press pp. 232-236.  
Von Engel A. and Steenbeck, M. 1932, *Elektrische Gasentladungen*, Vol II, 256-284.

## TRANSIENT HEAT CONDUCTION IN A FINITE WEDGE

K. C. SABHERWAL

DEPARTMENT OF APPLIED MATHEMATICS,  
GOVERNMENT ENGINEERING COLLEGE, JABALPUR.

(Received May 14, 1965)

**ABSTRACT.** Inverse and direct problems of transient heat conduction through a cylindrical wedge have been solved with the help of integral transforms

## INTRODUCTION

In most problems in the theory of heat conduction either temperature or heat transfer conditions are prescribed on the surface of a body, and conditions at interior points are to be determined. Such problems are known as "Direct problems". There is another class of problems, (Inverse problems), in which either temperature or heat flux, on some part or whole of the surface of a body, is to be determined from the temperature distribution on suitable interior surfaces, and the remaining portion of the boundary surface. G. Stolz, Jr. (1960) obtained an integral equation, and out-lined a numerical method for solving inverse problems, with special reference to sphere. The problem occurred as a part of quenching programme (G. Stolz Jr. 1956). T. J. Mirsepassi solved the problem by a graphical method. A. V. Maskot and A. C. Vastano (1962) solved similar problems of Mathematical Physics, using Laplace Transform and Separation of variables, and termed these as "Interior Value Problems". O. R. Burggraf (1964) has obtained the solution as a rapidly convergent series, with lumped capacitance approximation, as leading term. Burggraf has taken boundary conditions etc. as a function of time only. E. M. Sparrow, A. Haji Sheikh, and T. S. Lundgren (1964) have also tackled the inverse problems. Inverse problems arise in Quenching studies, the analysis of experimental data, and measurement of aerodynamic heating, etc.

I. *Inverse problem for a cylindrical wedge*  $0 \leq r \leq a$ ;  $0 \leq \theta \leq \theta_0$ ;  $0 \leq z \leq h$ . Temperature on the surface  $\theta = \theta_0$  to be determined from the given temperature distribution on an interior plane  $\theta = \alpha$  and zero temperature on the remaining boundary surfaces. Initial temperature is zero.  $K$  represents the constant thermal diffusivity.  $u(r, \theta, z, t)$  the temperature satisfies:

$$\frac{\partial u}{\partial t} = K \left( \frac{\partial^2 u}{\partial r^2} + \frac{1}{r} \frac{\partial u}{\partial r} + \frac{1}{r^2} \frac{\partial^2 u}{\partial \theta^2} + \frac{\partial^2 u}{\partial z^2} \right);$$

$$0 < r < a; 0 < \theta < \theta_0; 0 < z < h; t > 0 \quad \dots (1)$$

$$u(r, \theta, z, 0) = u(r, \theta, 0, t) = u(r, \theta, h, t) = u(r, 0, z, t) = u(a, \theta, z, t) = 0 \quad \dots (2)$$

$$u(r, \alpha, z, t) = f(r, z, t); \quad 0 < \alpha < \theta_0 \quad (\text{Known}), \quad \dots (3)$$

$$u(r, \theta_0, z, t) = g(r, z, t), \quad \text{say} \quad (\text{unknown}), \quad \dots (4)$$

$u(r, \theta, z, t)$  tends to zero, as  $r$  tends to zero.

Applying to equations (1) through (4) the finite Fourier sine transform, with respect to  $z$ , and the Laplace transform with respect to  $t$ , defined successively as,

$$U(r, \theta, n, t) = \int_0^h u \sin \frac{n\pi z}{h} dz$$

$$\text{and} \quad \bar{U}(r, \theta, n, p) = \int_0^\infty U \exp(-pt) dt$$

We obtain

$$r^2 \frac{\partial^2 \bar{U}}{\partial r^2} + r \frac{\partial \bar{U}}{\partial r} - r^2 q^2 \bar{U} + \frac{\partial^2 \bar{U}}{\partial \theta^2} = 0; \quad \text{where} \quad q^2 = \frac{n^2 \pi^2}{h^2} + \frac{p}{K} \quad \dots (5)$$

$$\bar{U}(r, 0, n, p) = \bar{U}(a, \theta, n, p) = 0 \quad \dots (6)$$

$$\bar{U}(r, \alpha, n, p) = \bar{F}(r, n, p) \quad \dots (7)$$

$$\bar{U}(r, \theta_0, n, p) = \bar{G}(r, n, p). \quad \dots (8)$$

Further applying to equations (5) through (8) the finite Lebedev transform (Naylor, 1963; equation 9) defined as :

$$\bar{U}'(s, \theta, n, p) = \int_0^a [I_s(qa)K_s(qr) - I_s(qr)K_s(qa)] \bar{U} \frac{dr}{r}$$

where  $I_s(qr)$  and  $K_s(qr)$  are the modified Bessel functions of the first and second kind of order  $s$ .

$$\frac{d^2 \bar{U}'}{ds^2} = -s^2 \bar{U}' \quad \dots (9)$$

$$\bar{U}'(s, 0, n, p) = 0$$

$$\bar{U}'(s, \alpha, n, p) = \bar{F}'(s, n, p)$$

$$\bar{U}'(s, \theta_0, n, p) = \bar{G}'(s, n, p).$$

Solution of equation (9), after some simplifications reduces to

$$\bar{G}'(s, n, p) = \bar{F}'(s, n, p) \frac{\sin(s\theta_0)}{\sin(s\alpha)} \quad \dots (10)$$

Applying to equation (10) the inverse finite Lebedev transform (Naylor, 1963; equation 11), the inverse Laplace and the inverse finite Fourier Sine transform (Sneddon, 1951; P. 74, Th. 27), we obtain :

$$g(r, z, t) = - \frac{1}{h\pi^2} \sum_{n=1}^{\infty} \sin \frac{n\pi z}{h} \int_{-i\infty}^{+i\infty} \exp.(pt) \cdot dp \int_L \bar{F}'(s, n, p) \\ \times \frac{\sin(s\theta)}{\sin(s\theta_0)} \cdot \frac{I_s(qr)}{I_s(qa)} \cdot s ds.$$

where  $L$  is the path  $R(s) = C'$ .

II. *A direct problem*: Cooke (1955), Craggs (1945) and Jaeger (1942) have solved direct heat conduction problems for a wedge, with constant surface temperature. Their results can be extended, if in article I,  $g(r, z, t)$  the variable surface temperature is supposed to be known and  $u(r, \theta, z, t)$  the temperature distribution in the wedge, is similarly determined to be :

$$u(r, \theta, z, t) = - \frac{1}{h\pi^2} \sum_{n=1}^{\infty} \sin \frac{n\pi z}{h} \int_{-i\infty}^{+i\infty} \exp(pt) \cdot dp \int_L \bar{G}'(s, n, p) \\ \frac{\sin(s\theta)}{\sin(s\theta_0)} \times \frac{I_s(qr)}{I_s(qa)} \cdot s \cdot ds.$$

This problem can be used for the study of analogous problem of transient flow taking place in earth dams during drawdown.

The author expresses his gratitude to Dr. B. R. Bhonsle, for his guidance during the preparation of this paper. The author's grateful thanks are due to Dr. B. D. Nag Chaudhuri, Director, Saha Institute of Nuclear Physics, Calcutta, for his very kind encouragement.

#### REFERENCES

- Burggraf, O. R., Aug., 1964, *Jour. Heat Transfer, Trans. ASME*, **86C**, 373.  
 Cooke, J. C., 1955, *Amer. Math. Monthly*, **62**, 331.  
 Craggs, J. W., 1945, *Phil. Mag.*, **36**, 220.  
 Jaeger, J. C., 1942, *Phil. Mag.*, **83**, 527.  
 Maekot, A. V., and Vastano, A. C., Oct., 1962, *Amer. Jour. Phys.*, **30**, 796.  
 Mirsepasi, T. J., Mar., 1959, *J. Brit. Chem. Engg*, **1**.  
 Naylor, D. 1963, *Jour. Maths and Mechs.* **12**, 375.  
 Sneddon, I. N., 1951, *Fourier Transforms*, McGraw Hill.  
 Sparrow, E. M., Haji-Sheikh, A., and Lundgren, T., 1964, *Jour. Appl. Mechs. Trans. A.S.M.E.* **31E**, 369.  
 Stolz, G. Jr., 1960, *Jour. Heat Transfer, Trans., ASME*, **82C**, 20.  
 Stolz, G. Jr., and Paschke, V., 1956, *J. of Metals*, **8**, 1074.  
 ————, 1956, *Iron Age*, **178**, No. 21, 95.

# A STUDY OF THERMODYNAMIC BEHAVIOUR OF IMPERFECT GASES ASSUMING ASSOCIATION

S. P. PAL

(DEPARTMENT OF MATHEMATICS AND STATISTICS, NORTH BENGAL UNIVERSITY,  
RAJA RAMMOHANPUR, DIST. — DARJEELING, INDIA).

(Received February 26, 1966; Resubmitted June 15, 1966)

**ABSTRACT.** In this note the thermodynamic behaviour of an assembly of molecules of finite dimension which are associating and forming higher complex, has been investigated. The quasi-lattice theory of Dutta for real gases and ions in solution has been extended for investigating assemblies of associating and dissociating molecules and used here for calculating the isothermal compressibility. The result is in agreement with experience.

## INTRODUCTION

In usual investigations of the properties and behaviour of perfect gases no consideration is taken for association of molecules. But for many real gases, such as  $N_2O_4$ , Iodine vapour, water vapour, sulphur vapour it has been found that association of molecules takes place in various degrees.

According to Fowler's idea (1936), the usual results of the imperfect gases can be obtained very easily by considering dissociation and association of molecules into higher complexes alone. From this idea, the behaviour of an assembly, composed of associating and dissociating molecules complexes like  $X_1, X_2, \dots X_n$ , where  $X$  is the most elementary molecule, is investigated by the method of Fowler (Dutta, 1951). A deviation from the properties of a perfect gas is obtained but this deviation is not in the direction of imperfect gas. The isothermal compressibility, as obtained by Dutta, was greater than that of perfect gas. This result is justified from different considerations. It appears that a behaviour of imperfect gas cannot be obtained purely from association and dissociation if some of the usual causes of imperfection is not introduced. Here, by introduction of finite size of molecules, a deviation towards imperfection is obtained.

The quasilattice theory developed by Dutta (1953) is suitable for the discussion of various properties of gases where association and dissociation take place. Here, this quasi-lattice theory has been extended and used to deduce the equation of state of imperfect gases. After that the isothermal compressibility of the gas is calculated.

Now the imperfections of gases are due to two causes :

- (i) finite size of the gas molecules or particles, and
- (ii) presence of the fields of force. Here only the first cause i.e. the finite size of the particles, is taken into consideration.

*Description of Assembly :*

For the sake of simplicity, gas molecules are assumed to be present in their simplest form and in the form of second complex i.e., the molecules of this complex are formed by the association of two molecules of the gas. Then this system can be looked upon as a binary mixture of gases. In the assembly of the mixture it is assumed that  $N_1$  is the average number of molecules of mass  $m_1$  and  $N_2$  is the average number of molecules of mass  $m_2 = 2m_1$ ,

$$\text{and} \quad N_1 + 2N_2 = N,$$

where  $N$  is the total number of molecules of the gas in the simplest form present in the assembly.

## CALCULATION OF ENTROPY

In case of this binary mixture following quasi-lattice method and the principle of symmetrisation, the thermodynamic probability is given by,

$$W = [W_{12} W_{21}]^{\frac{1}{2}} \quad \dots (1)$$

where

$$W_{12} = \frac{(V/b_1)!}{N_1!(v/b_1 - N_1)!} \cdot \left( \frac{V - N_1 b_{12}}{b_2} \right)! \cdot \frac{N_1!}{\pi a_1!} \cdot \frac{N_2!}{\pi a_2!}$$

and  $W_{21}$  is a similar expression obtained by interchanging the suffices, 1 and 2 in the first two factors.

Here, the symbols have the same interpretation as in the papers of Dutta (1951)

Now, using Starling's approximation formula for factorials and taking usual variation of the logarithm of  $W$ ,

subject to the conditions

$$\left. \begin{aligned} \Sigma_1 \delta a_1 + 2 \Sigma_m \delta a'_m &= \delta N_1 + 2 \delta N_2 = 0, \\ \Sigma \epsilon_i \delta a_i + \Sigma_m \eta_m \delta a'_m + \chi \delta N_2 &= 0 \end{aligned} \right\} \quad \dots (2)$$

where  $\chi$  is the energy of association,

we get,

$$\frac{1}{2} \left\{ \log \left( \frac{v}{b_1} - N_1 \right) + \log \left( \frac{v - N_2 b_{12}}{b_1} - N_1 \right) + \frac{b_{12}}{b_2} \log \left( 1 - \frac{N_2 b_2}{v - N_1 b_{12}} \right) \right\}$$

$$-\log a_i - \lambda - \mu \epsilon_i = 0$$



where  $\lambda$  and  $\mu$  are Lagrange's multipliers.

From this, we have

$$a_i \cdot \frac{b_1}{v} \cdot e^{\frac{N_1 b_1 + N_2 b_{12}}{v}} = e^{-\lambda - \mu \epsilon_i}$$

$$\text{or, } a_i = \frac{v}{b_1} e^{-\lambda - \mu \epsilon_i} \quad \dots (3)$$

(approximately)

and similarly

$$a_m' = \frac{v}{b_2} \cdot e^{-2\lambda - \mu(\epsilon_m + \chi)} \quad \dots (4)$$

According to Boltzmann hypothesis, and by equations (3) and (4) we get

$$\begin{aligned} S &= k \log W_{\text{max}} \\ &= k \left[ \frac{1}{2} \left\{ \frac{v}{b_1} \log \frac{v}{b_1} - \left( \frac{v}{b_1} - N_1 \right) \log \left( \frac{v}{b_1} - N_1 \right) + \frac{v - N_1 b_{12}}{b_2} \log \left( \frac{v - N_1 b_{12}}{b_2} \right) \right. \right. \\ &\quad \left. \left. + \left( \frac{v - N_1 b_{12}}{b_2} - N_2 \right) \log \left( \frac{v - N_1 b_{12}}{b_2} - N_2 \right) + \frac{v}{b_2} \log \frac{v}{b_2} + \left( \frac{v}{b_2} - N_2 \right) \cdot \right. \right. \\ &\quad \left. \left. \log \left( \frac{v}{b_2} - N_2 \right) + \left( \frac{v - N_2 b_{12}}{b_1} \right) \log \left( \frac{v - N_2 b_{12}}{b_1} \right) - \left( \frac{v - N_2 b_{12}}{b_1} - N_1 \right) \right. \right. \\ &\quad \left. \left. \log \left( \frac{v - N_2 b_{12}}{b_1} - N_1 \right) \right\} - N_1 \log v/b_1 - N_2 \log v/b_2 + N\lambda + \mu E \right] \quad \dots (5) \end{aligned}$$

Now from the well known thermodynamic relation

$$\left( \frac{\partial S}{\partial E} \right) = 1/T,$$

$$\text{we get } \frac{1}{T} = \mu k \quad \text{or, } \mu = \frac{1}{kT} \quad \dots (6)$$

Again

$$N = N_1 + 2N_2 = \sum_i a_i + 2 \sum_m a_m'$$

$$= \sum_i \frac{v}{b_1} e^{-\lambda - \mu \epsilon_i} + 2 \sum_m \frac{v}{b_2} e^{-2\lambda - \mu(\epsilon_m + \chi)}$$

$$= \frac{v}{b_1} e^{-\lambda} \frac{b_1}{h^3} \left( \frac{2\pi m_1}{\mu} \right)^{3/2} + \frac{2v}{b_2} e^{-2\lambda - \mu\chi} \frac{b_2}{h^3} \left( \frac{2\pi m_2}{\mu} \right)^{3/2}$$

$$\text{or} \quad \frac{2N}{v} \cdot e^{\lambda} = \left( \frac{2\pi m_1}{\mu h^3} \right)^{3/2} \left[ 1 + \sqrt{1 + 8e^{-\mu\chi} \left( \frac{\mu h^3}{\pi m_1} \right)^{3/2} \frac{N}{v}} \right]$$

$$\text{or} \quad \lambda = \log v + \log \left\{ \frac{1}{N} \left( \frac{2\pi m_1}{\mu h^3} \right)^{3/2} \right\} + \frac{2N}{V} e^{-\mu\chi} \left( \frac{\mu h^3}{\pi m_1} \right)^{3/2} \dots (7)$$

(upto first order).

#### EXPRESSIONS FOR OTHER THERMODYNAMIC FUNCTION

Now, from thermodynamics, we know

$$\psi = E - TS \quad \dots (8)$$

$$\text{and} \quad p = T \left( \frac{\partial \psi}{\partial V} \right)_{T, N} \quad \dots (9)$$

So,

$$\begin{aligned} p = kT \cdot \left[ -\frac{1}{2b_1} \left\{ \log \left( 1 - \frac{N_1 b_1}{V} \right) + \log \left\{ 1 - \frac{N_1 b_1}{V \left( 1 - \frac{N_2 b_{12}}{V} \right)} \right\} \right\} \right. \\ \left. - \frac{1}{2b_2} \left\{ \log \left( 1 - \frac{N_2 b_2}{V} \right) + \log \left\{ 1 - \frac{N_2 b_2}{V \left( 1 - \frac{N_1 b_{12}}{V} \right)} \right\} - \frac{N_1 + N_2}{V} \right. \right. \\ \left. \left. + N \left\{ \frac{1}{V} - \frac{2N}{V^2} e^{-\mu\chi} \left( \frac{\mu h^3}{\pi m_1} \right)^{3/2} \right\} \right] \right] \end{aligned}$$

$$\text{or} \quad p = NkT \left[ \frac{1}{V} + \frac{1}{V^2} \left\{ (x_1^2 \beta_1 + 2x_1 x_2 \beta_{12} + x_2^2 \beta_2) - 2N e^{-\mu\chi} \left( \frac{\mu h^3}{\pi m_1} \right)^{3/2} \right\} \right]$$

where

(upto first order of small quantities)

$$x_1 = \frac{N_1}{N}, \quad x_2 = \frac{N_2}{N}$$

$$\beta_1 = \frac{1}{2} N b_1, \quad \beta_{12} = \frac{1}{2} N b_{12}, \quad \beta_2 = \frac{1}{2} N b_2, \quad \dots (10)$$

$$\text{or} \quad p = \frac{NkT}{V} \left[ 1 + \frac{B}{V} \right] = \frac{NkT}{V-B} \quad \dots (11)$$

$$\text{where} \quad B = \left\{ (x_1^2 \beta_1 + 2x_1 x_2 \beta_{12} + x_2^2 \beta_2) - 2Ne \cdot \frac{1}{RT} \left( \frac{h^2}{\pi mkT} \right)^{\frac{3}{2}} \right\}$$

The expression in the first bracket is same as that obtained by Lorentz (1927) and Dutta (1947), and the other term gives the effect of chemical reaction.

#### *Isothermal compressibility.*

From (11), we have

$$\begin{aligned} \text{isothermal compressibility} &= -\frac{1}{V} \cdot \left( \frac{\partial V}{\partial p} \right)_T \\ &= \frac{1}{p} (1 - B/V). \end{aligned}$$

Now, by using (11), we can write

$$\frac{1}{V} = \frac{p}{NkT} - \frac{Bp^2}{Nk^2T^2}.$$

(upto first order of small quantities)

and, so,

$$-\frac{1}{V} \left( \frac{\partial V}{\partial p} \right)_T = \frac{1}{p} \cdot \left[ 1 - \frac{Bp}{NRT} \right] \left( \leq \frac{1}{p} \right) \quad \dots (12)$$

(upto first order of small quantities),

of course, if  $B \geq 0$ .

Thus, we get the isothermal compressibility of the assembly less than that of perfect gas provided the values of the characteristic constants of molecules like  $m_1, b_1, b_2, b_{12}, \dots$  etc., of temperature and of association energy are suitable. This result is contrary to that obtained by Dutta (1951c) and is entirely due to the effect of exclusion volume.

#### CONCLUDING REMARKS

The investigations of the other thermodynamic behaviour of gas by the present method are interesting and those will be the subject-matter of future papers.

## ACKNOWLEDGMENTS

The author expresses his hearty thanks and gratitude to Professor M. Dutta for the suggestion of the problem and guidance.

## REFERENCES

- Dutta, M. 1951c : *Indian J. Phys.*, **35**, 319.  
——— 1953 : *Proc. Nat. Inst. Sc. Ind.*, **19**, 183.  
Fowler, R. H. 1936 : *Statistical Mechanics*, 2nd Edn., pp. 157-62, and 284-88.  
Lorentz, H. 1927 : *Lectures in Theoretical Physics*, Vol. 2, Macmillan and Co., London.

# A SIMPLE METHOD OF FINDING THE PRINCIPAL IONIC SUSCEPTIBILITIES OF CRYSTALS

J. K. GHOSE

DEPARTMENT OF PHYSICS, ST. JOHN'S COLLEGE, AGRA

(Received August 23, 1965 ; Resubmitted November 30, 1965 and April 12, 1966)

**ABSTRACT.** It is shown that the principal ionic anisotropies in triclinic as well as other crystals can be calculated from just the values of magnetic anisotropy in any two planes and X-ray data regarding the angular orientation of the ions. Slightly less accurate values may be obtained from measurements of anisotropy and the direction of maximum susceptibility in a single plane of the crystal. In case of uniaxial symmetry of the ions, the principal ionic anisotropy can be calculated from a single measurement of magnetic anisotropy in any one plane of the crystal. Additional observation of maximum susceptibility in only one plane, is sufficient for calculating the principal ionic susceptibilities. The probable errors are reduced by choosing a plane of large anisotropy.

## INTRODUCTION

Magnetic susceptibility tensor of a crystal is the resultant of the ionic or molecular susceptibility tensors of the magnetic ions or molecules in the unit cell of the crystal. The ultimate quantity of interest is the ionic or molecular susceptibility tensor because of its use in the investigation of ligand fields. The usual procedure is to first determine the crystalline magnetic susceptibility tensor. Satisfactory methods could not be found easily for triclinic crystals. Krishnan and Mookherjee (1936, 1938) had used a trial and error method of calculation requiring a large number of measurements of anisotropy in different planes. Ghosh and Bagchi (1962) had proposed a method requiring the measurements of both maximum susceptibility and anisotropy in five different planes in addition to the average susceptibility of the crystal. The author (Ghose, 1964) had discussed several alternative methods of calculating the principal susceptibilities and directions of the principal axes using the transformation laws for covariant and contravariant tensor matrices in oblique coordinates. Each method requires just six observations and imposes no restrictions as to the planes of measurement. One of them, in contrast with the method of Ghosh and Bagchi (1962), requires only the values of maximum susceptibility and anisotropy in three different planes. Several other methods designed for greater accuracy of results are being published elsewhere (Ghose, 1966 a, b).

Ghosh and Mitra (1964) pointed out that instead of first determining the susceptibility tensor for the crystal, it is possible to calculate the ionic susceptibility tensor directly from the magnetic measurements and the X-ray data regarding the angular orientations of the magnetic ions or molecules. This brings in a great

economy in the labours of numerical calculation. In most cases the principal ionic susceptibilities can be calculated by solving just one set of simultaneous linear equations.

This elegant method of calculation has two rather subtle drawbacks. Firstly it requires more than the minimum number of observations necessary in principle. The sum of the maximum and the minimum susceptibilities in a plane of the crystal was considered as a single piece of information. Actually it requires the measurements of both maximum susceptibility and anisotropy. Thus for uniaxial symmetry of ions, since only the axial principal susceptibility  $K_{\parallel}$  and the lateral principal susceptibility  $K_{\perp}$  of the ion have to be calculated, just two observations in addition to the data regarding the orientations of the ions should be sufficient. The method of Ghosh and Mitra requires the determination of anisotropy and maximum susceptibility in one plane of the crystal, as well as the average susceptibility of the crystal. The second drawback is a considerable loss of accuracy due to the use of two susceptibility values in the calculations. This is not immediately self-evident from the equations but will be proved here and the cause of this inaccuracy will be traced so that it may be avoided.

An alternative method of calculating the ionic susceptibilities directly from the observations will be presented here. It will be shown that the principal ionic anisotropy ( $K_{\parallel} - K_{\perp}$ ), for axially symmetrical ions can be obtained from only one measurement of magnetic anisotropy in a specified plane, together with X-ray data. In the absence of symmetry the principal ionic anisotropies may be calculated from two anisotropy measurements. In addition to these observations, just one measurement of either maximum susceptibility in a plane or the average susceptibility of the crystal is sufficient for calculating the principal ionic susceptibilities. Not only for triclinic, but for all crystals, this method demands fewer observations and simplifies calculations. Apart from the errors in the measurement of magnetic anisotropy in one case and also absolute susceptibility in the other, the major source of error in the proposed method is the inaccuracy of the X-ray data used. In due course it has been proved that the latter error may be minimised by choosing a plane of measurement such that the observed anisotropy is large. The final error is then expected to be no more than that with the lengthy indirect methods and smaller in some cases.

#### *Ionic and crystalline susceptibilities*

Let the cosines of the angles between the principal ionic axes  $K_1, K_2, K_3$  of any magnetic ion and any set of orthogonal axes  $x, y, z$ , fixed in the crystal, be as follows :

	$x$	$y$	$z$
$K_1$	$\alpha_1$	$\beta_1$	$\gamma_1$
$K_2$	$\alpha_2$	$\beta_2$	$\gamma_2$
$K_3$	$\alpha_3$	$\beta_3$	$\gamma_3$

The direction cosines  $\cos \phi_i^a$ ,  $\cos \phi_i^b$ ,  $\cos \phi_i^c$ , of each ionic axis  $K_i$ , with respect to the crystallographic axes  $a, b, c$ , are known from the X-ray data. Hence  $\alpha_i$ ,  $\beta_i$ , and  $\gamma_i$  may be easily calculated. It has been shown by Ghose (1965) that if the orthogonal axes are so chosen that the  $z$  axis coincides with the  $c$  axis and the  $x$  axis lies in the  $a-c$  plane and close to the  $a$  axis, then  $\alpha_i$ ,  $\beta_i$  and  $\gamma_i$  can be calculated without any ambiguity by the following matrix equation.

$$[\alpha_i \beta_i \gamma_i] = [\cos \phi_i^a \cos \phi_i^b \cos \phi_i^c] \begin{bmatrix} \frac{1}{\sin \beta} & \frac{\cos \alpha \cos \beta - \cos \gamma}{M \sin \beta} & 0 \\ 0 & \frac{\sin \beta}{M} & \\ \frac{\cos \beta}{\sin \beta} & \frac{\cos \beta \cos \gamma - \cos \alpha}{M \sin \beta} \end{bmatrix} \quad (1)$$

where  $\alpha, \beta, \gamma$  are the triclinic angles and  $M$  is the positive square root of  $(1 - \cos^2 \alpha - \cos^2 \beta - \cos^2 \gamma + 2 \cos \alpha \cos \beta \cos \gamma)$ . There is no ambiguity. Similar matrix relations may be obtained if any other set of orthogonal axes is selected.

In most of the actual problems it would be necessary to calculate the values of only  $\gamma_i$ . A shorter method of calculating it for different directions of  $z$  axis will be discussed later.

If in the unit cell there are  $n$  ions of a particular type with different orientations, then the susceptibility matrix for the crystal is  $1/n$  times the sum of the susceptibility matrices for the  $n$  ions. Thus in the  $x, y, z$  coordinate system, the susceptibility matrix is

$$\begin{bmatrix} \chi_{11} & \chi_{12} & \chi_{13} \\ \chi_{12} & \chi_{22} & \chi_{23} \\ \chi_{13} & \chi_{23} & \chi_{33} \end{bmatrix} = \frac{1}{n} \sum \begin{bmatrix} \alpha_1 & \alpha_2 & \alpha_3 \\ \beta_1 & \beta_2 & \beta_3 \\ \gamma_1 & \gamma_2 & \gamma_3 \end{bmatrix} \begin{bmatrix} K_1 \\ K_2 \\ K_3 \end{bmatrix} \begin{bmatrix} \alpha_1 & \beta_1 & \gamma_1 \\ \alpha_2 & \beta_2 & \gamma_2 \\ \alpha_3 & \beta_3 & \gamma_3 \end{bmatrix} \quad \dots \quad (2)$$

#### *Probable errors of existing methods*

The observed values of anisotropy, maximum susceptibility and average susceptibility are subject to errors of the order of 0.1%. The estimated error is smallest for anisotropy and is 0.1% (Krishnan and Banerji, 1935; Datta, 1953, 1954). The error in the values of maximum susceptibility may be about 0.2% (Dutta Roy, 1955) or slightly less (Das, 1963). The error in measuring average susceptibility for powdered samples may be larger still. Thus the estimated errors in the last two quantities is never less than 0.1%.

For uniaxial symmetry of the magnetic ion, i.e.,  $K_1 = K_2 = K_\perp$  and  $K_3 = K_\parallel$ , Ghosh and Mitra proved that

$$K_\parallel \left(1 - \frac{1}{n} \sum \alpha_i^2\right) + K_\perp \left(1 + \frac{1}{n} \sum \alpha_i^2\right) = 2\chi_{\text{max}} - A \quad (3)$$

where  $\chi_{max}$  and  $A$  are the maximum susceptibility and anisotropy in the  $y-z$  plane. Also for the mean susceptibility, we have

$$\bar{\chi} = \frac{1}{3}(2K_{\perp} + K_{\parallel}) \quad \dots (4)$$

Solving equations (3) and (4), we get

$$(K_{\parallel} - K_{\perp}) = \frac{2\chi_{max} - A - 2\bar{\chi}}{\Sigma \alpha_i^2} \quad \dots (5)$$

This is an exact relation without any approximation. If the magnitude of the errors in the values of  $\chi_{max}$ ,  $A$  and  $\bar{\chi}$  be  $\partial\chi_{max}$ ,  $\partial A$  and  $\partial\bar{\chi}$ , then the magnitude of the error in the calculated value of ionic anisotropy is given by

$$\partial(K_{\parallel} - K_{\perp}) = \frac{2\partial\chi_{max} + \partial A + 2\partial\bar{\chi}}{\frac{1}{3} - \frac{\Sigma \alpha_i^2}{n}} + \frac{2\chi_{max} - A - 2\bar{\chi}}{n \cdot \left( \frac{1}{3} - \frac{\Sigma \alpha_i^2}{n} \right)} \partial(\Sigma \alpha_i^2)$$

Neglecting  $\partial A$  the error in anisotropy and the second term on the right hand side which is due to error in X-ray data, the percentage error in ionic anisotropy is equal to

$$\frac{200(\partial\chi_{max} + \partial\bar{\chi})}{2\chi_{max} - 2\bar{\chi} - A}.$$

In any given case this minimum estimated error can be easily calculated because

$\partial\chi_{max} = 0.1\%$  of  $\chi_{max} = \frac{\chi_{max}}{1000}$ , and  $\partial\bar{\chi} = \frac{\bar{\chi}}{1000}$ . Since  $\chi_{max}$  and  $\bar{\chi}$  are large quantities,

the absolute errors  $\partial\chi_{max}$  and  $\partial\bar{\chi}$  are quite large; on the other hand the denominator in the above expression for percentage error is very small. So the accuracy of ionic anisotropy calculated by this method will be necessarily small. Substituting the values of  $\chi_{max}$ ,  $\bar{\chi}$  etc. given by Ghosh and Mitra (1964), the error in principal ionic anisotropy in the case of  $\text{CuSO}_4 \cdot 5\text{H}_2\text{O}$ , is found to be about 25%. Similarly for their determination of the principal ionic anisotropy of  $\text{NiSO}_4 \cdot 7\text{H}_2\text{O}$ , the estimated error is found to range from 20% to 60% for the different sets of observations given by them. Actually the errors must be still larger due to inaccuracies in the X-ray data. The apparently close agreement with previous workers' results, must be due to coincidence. Also the direction cosines of the tetragonal axis of the second copper ion as calculated by them from X-ray data, have an error of about 5%. Proceeding in the same way it can be proved that in the absence of symmetry too, the method of Ghosh and Mitra is likely to give inaccurate results. The only cause of these inaccuracies is the fact that a difference of two large quantities, the maximum susceptibility in a plane and the average



susceptibility, has been used in calculating a small quantity, the principal ionic anisotropy

The same cause may lead to similar large errors in other methods of calculations as well. Thus, following Lonsdale and Krishnan (1936), if  $\chi_a$ ,  $\chi_b$ ,  $\chi_c$  are the observed susceptibilities along the  $a$ ,  $b$  and  $c$  axes of any orthorhombic crystal, then

$$(K_{\perp} - K_{\parallel}) = \frac{\chi_b - \chi_a}{\alpha_a^2 - \beta_a^2}$$

If the quantity  $(\chi_b - \chi_a)$  can be measured directly then the percentage error need not be large. On the other hand if  $\chi_b$  and  $\chi_a$  are measured independently, then

assuming the X-ray data to be correct, the percentage error is  $\frac{100(\partial\chi_b + \partial\chi_a)}{\chi_b - \chi_a}$ ,

and is considerable. As regards the error due to X-ray data, it will be small if the difference in the magnitudes of  $\alpha_a$  and  $\beta_a$  is large

This defect is also common to many methods of determining the magnetic susceptibility tensor for crystals. Ghose (1964, 1966) has shown that if more than one observation of the absolute value of susceptibility have to be used for calculating the elements of the tensor matrix, then large errors are inevitable. Although the percentage error in the value of any of the calculated principal susceptibilities is not much larger than those in the observed values of susceptibilities, the percentage error in the values of the principal anisotropies is much larger and the calculated directions of the principal axes are not accurate. Even if the principal susceptibilities can be directly measured, the error in the calculated principal anisotropies will be large because each is a small difference of two large quantities. On the other hand, the use of several measurements of anisotropy (and also direction cosines of maximum susceptibility in a plane) does not introduce such large errors in the result because the absolute values of the errors are small.

The method of Krishnan and Mookherji (1938) is free of this defect. But the trial and error procedure makes exact calculation so lengthy as to be almost impossible. Moreover, the directions of the  $M$  axes and the principal anisotropies are determined more effectively by those planes for which observed anisotropy is small so that probable error is comparatively large.

#### *Proposed methods*

For the orthogonal coordinate system  $x$ ,  $y$ ,  $z$ , if  $\chi_{max}$  and  $A$  be the observed maximum susceptibility and the anisotropy in  $x$ - $y$  plane and  $\psi$  be the angle which the direction of maximum susceptibility in this plane makes with the  $x$  axis, then the following equations (Ghose, 1964) relating the elements of  $[\chi_{mn}]$ , the susceptibility tensor matrix can be written down.

$$\chi_{11} = \chi_{max} - A \sin^2 \psi \quad \dots \quad (6)$$

$$\chi_{22} = \chi_{max} - A \cos^2 \psi \quad \dots (7)$$

$$\chi_{12} = A \sin \psi \cos \psi \quad \dots (8)$$

Eliminating  $\chi_{max}$  between equations (6) and (7), we get

$$(\chi_{11} - \chi_{22}) = A \cos 2\psi \quad \dots (9)$$

Substituting the values of  $\chi_{11}$  etc. from equation (2) in equations (8) and (9), we get

$$(K_2 - K_1)\Sigma\alpha_2\beta_2 + (K_3 - K_1)\Sigma\alpha_3\beta_3 = nA/2 \cdot \sin 2\psi \quad \dots (10)$$

$$(K_2 - K_1)\Sigma(\alpha_2^2 - \beta_2^2) + (K_3 - K_1)\Sigma(\alpha_3^2 - \beta_3^2) = nA \cdot \cos 2\psi \quad \dots (11)$$

The values of  $\alpha_2$ ,  $\beta_2$ , etc. are known from the X-ray data and either equation (1) or some alternative equation. So if  $A$  and  $\psi$  are measured for the plane  $x-y$ , then the principal ionic anisotropies,  $(K_2 - K_1)$  and  $(K_3 - K_1)$  may be found by solving equations (10) and (11). In case of axial symmetry of the ion, a single equation is sufficient.

$$(K_{\parallel} - K_{\perp}) = \frac{nA}{\Sigma\alpha_2\beta_2} \cdot \frac{\sin 2\psi}{\Sigma(\alpha_2^2 - \beta_2^2)} \quad \dots (12)$$

Thus the principal ionic anisotropies can be calculated from the X-ray data and a single measurement of  $A$  and  $\psi$  in one plane. If the orthogonal coordinates chosen are those corresponding to equation (1), then  $A$  is the anisotropy in a plane perpendicular to the crystallographic  $c$  axis and  $\psi$  is the angle which the direction of maximum susceptibility in this plane makes with the  $a-c$  plane. However it is difficult to determine accurately the value of  $\psi$ . But while measuring the anisotropy  $A$ , the approximate value of  $\psi$  may be easily found for the same plane of observation without requiring any special equipment. Hence the approximate values of the principal ionic anisotropies may be calculated for eliminating ambiguities of results calculated by other methods.

Eliminating  $\psi$  between equations (10) and (11) we get

$$\{(K_2 - K_1)\Sigma(\alpha_2^2 - \beta_2^2) + (K_3 - K_1)\Sigma(\alpha_3^2 - \beta_3^2)\}^2 + 4\{(K_2 - K_1)\Sigma\alpha_2\beta_2 + (K_3 - K_1)\Sigma\alpha_3\beta_3\}^2 = n^2 A^2 \quad (13)$$

The summations are for the  $n$  ions and  $A$  is the anisotropy in  $x-y$  plane. For the coordinates corresponding to equation (1), the  $x-y$  plane is perpendicular to the  $c$  axis and the  $x-z$  plane is identical with the crystallographic  $a-c$  plane. If  $\bar{A}$  be the anisotropy measured in  $x-z$  plane, then

$$\{(K_2 - K_1)\Sigma(\alpha_2^2 - \gamma_2^2) + (K_3 - K_1)\Sigma(\alpha_3^2 - \gamma_3^2)\}^2 + 4\{(K_2 - K_1)\Sigma\alpha_2\gamma_2 + (K_3 - K_1)\Sigma\alpha_3\gamma_3\}^2 = n^2 \bar{A}^2 \quad (14)$$

Equations (13) and (14) are simultaneous quadratic equations in  $(K_2 - K_1)$  and  $(K_3 - K_1)$ . Such equations may be solved without difficulty and the numerical values of the principal ionic anisotropies may be calculated. But in general there will be four alternative sets of solutions of which only one is correct. To resolve this ambiguity it will be necessary to note the approximate value of  $\psi$  in one of the positions for measuring the anisotropy of the crystal and calculate the approximate values of the principal ionic anisotropies by equations (10) and (11). Of the four alternative sets of solutions previously obtained, the one which is closest to this approximate solution, will be the correct one.

In case of axial symmetry of the ions, equation (13) simplifies to

$$(K_{||} - K_1) = \frac{\pm nA}{\{(\Sigma \alpha_3^2 - \Sigma \beta_3^2)^2 + 4(\Sigma \alpha_3 \beta_3)^2\}^{\frac{1}{2}}} \quad (15)$$

Thus the principal ionic anisotropy can be calculated from a single measurement of anisotropy  $A$  in  $x-y$  plane, which may be chosen arbitrarily for experimental convenience. To choose the correct sign in equation (15), we note from equation (12) that the positive sign is to be taken if  $\Sigma \alpha_3 \beta_3$  is positive and at the same time  $\sin 2\psi$  is positive, i.e., if the direction of maximum susceptibility in this plane lies between the positive directions of  $x$  and  $y$  axes.

Some special cases are worth noticing. In orthorhombic crystals, due to the symmetry of orientation of ions in the unit cell,  $(\Sigma \alpha_3 \beta_3)$  is equal to zero, while the squares of  $\alpha$  and  $\beta$  have the same value for each ion. So equation (15) reduces to the relation given by Lonsdale and Krishnan (1936)

On the other hand if all ions are magnetically equivalent, equation (15) simplifies to

$$(K_{||} - K_1) = \frac{\pm A}{\alpha_3^2 + \beta_3^2} = \frac{\pm A}{1 - \gamma_3^2} \quad (16)$$

Again in many triclinic crystals like  $\text{CuSO}_4 \cdot 5\text{H}_2\text{O}$ , there are only two magnetically inequivalent ions with axial symmetry. If the direction cosines of the second ion be distinguished by a dash suffix, then equation (15) reduces to

$$\begin{aligned} (K_{||} - K_1) &= \frac{\pm 2A}{\{(\alpha_3^2 - \beta_3^2 + \alpha_3'^2 - \beta_3'^2)^2 + 4(\alpha_3 \beta_3 + \alpha_3' \beta_3')^2\}^{\frac{1}{2}}} \\ &= \frac{\pm 2A}{\{(\alpha_3^2 + \beta_3^2 - \alpha_3'^2 - \beta_3'^2)^2 + 4(\alpha_3 \alpha_3' + \beta_3 \beta_3')^2\}^{\frac{1}{2}}} \\ &= \frac{\pm 2A}{\{(\gamma_3'^2 - \gamma_3^2)^2 + 4(\cos \phi - \gamma_3 \gamma_3')^2\}^{\frac{1}{2}}} \end{aligned} \quad (17)$$

where  $\phi$  is the angle between the axes of these two ions.

The quantities  $\gamma_3$  and  $\gamma_3'$  are the cosines of the angles between the magnetic axes of the ions and the  $z$  axis or the normal to the plane in which anisotropy

has been measured. So when using equations (16) and (17), it will be more convenient to calculate  $\gamma_3$  and  $\gamma'_3$  directly instead of by equation (1) or its equivalent. For this purpose the unit normal may be expressed as a contravariant vector matrix, as will be illustrated in due course. A unit covariant vector in the direction of the axis of an ion may be expressed by the matrix  $[\cos \phi_3^a \cos \phi_3^b \cos \phi_3^c]$ . So  $\gamma_3$  is the scalar product of these two vectors and is equal to the product of the two matrices.

#### *Probable errors in the proposed methods*

The methods of calculation discussed in the last section, do not involve small differences of large quantities like absolute values of susceptibility. So the percentage errors would be of the same order as in the measurement of anisotropy but for the errors introduced through the X-ray data. The effect of the latter can be reduced by a judicious selection of the plane in which anisotropy is measured.

Consider first the simplest case where all ions in the unit cell are magnetically equivalent, and have axial symmetry. The principal ionic anisotropy is to be calculated by equation (16). If the direction cosine  $\gamma_3$  be equal to  $\cos \theta$ , then the maximum percentage error in the calculated value of the principal ionic anisotropy will be

$$\frac{\partial(K_{\parallel} - K_{\perp})}{(K_{\parallel} - K_{\perp})} \cdot 100 = \frac{\partial A}{A} \cdot 100 + 200 \cdot \frac{\cos \theta}{\sin \theta} \cdot \partial \theta \quad \dots (18)$$

The first term on the right hand side of this equation is the percentage error introduced by magnetic measurement and is no more than that in the measurement of anisotropy. The percentage error due to an error of half a degree in the X-ray

data is  $\frac{200\pi}{360} \cdot \frac{\cos \theta}{\sin \theta}$ , or,  $\frac{200\pi}{360} \cdot \left(\frac{A_1}{A} - 1\right)^{\frac{1}{2}}$ , where  $A$  is the observed anisotropy

and  $A_1$  is the principal ionic anisotropy, which in this case is the maximum observable anisotropy. This error is very large when the observed anisotropy is nearly zero. On the other hand, when the observed anisotropy is maximum, the error is negligible compared to even the 0.1% error due to anisotropy measurement. When  $\gamma_3$  is 0.5, the error is near about 1%. So for greater accuracy, the plane of measurement should be so chosen that the observed anisotropy is large.

In case of two ions in the unit cell, an expression for the maximum error can be obtained from equation (17). Putting  $(\gamma_3'^2 - \gamma_3^2) = R \cos \omega$ ;  $2(\cos \phi - \gamma_3 \gamma_3') = R \sin \omega$ ;  $\gamma_3 = \cos \theta$  and  $\gamma_3' = \cos \theta'$ , we get the following expression for fractional error.

$$\begin{aligned} \frac{\partial(K_{\parallel} - K_{\perp})}{(K_{\parallel} - K_{\perp})} = & \frac{\partial A}{A} + \frac{\cos \omega}{R} \{ \mp \sin 2\theta' \partial \theta' + \sin 2\theta \partial \theta \} \\ & + \frac{2 \sin \omega}{R} \{ \sin \phi \partial \phi \pm \cos \theta \sin \theta' \partial \theta' + \cos \theta' \sin \theta \partial \theta \} \end{aligned}$$

Supposing the maximum errors  $\partial\theta$ ,  $\partial\theta'$  and  $\partial\phi$  due to errors in X-ray data, to be each half degree or  $\pi/360$  radian, the maximum percentage error

$$= \frac{\partial A}{A} \cdot 100 + \frac{100\pi}{360 \cdot R} \{ \cos \omega (\sin 2\theta \mp \sin 2\theta') + 2 \sin \omega (\sin \phi + \sin \theta \pm \theta') \} \quad \dots (19)$$

$$\leq \frac{\partial A}{A} \cdot 100 + \frac{100\pi}{360 \cdot R} \{ 2 \cos \omega + 4 \sin \omega \}$$

$$\leq \frac{\partial A}{A} \cdot 100 + \frac{100\pi 2(5)^{\frac{1}{2}}}{360 \cdot R}$$

The second term represents the maximum limiting value of the percentage error due to X-ray data and is equal to  $3.9/R$ . The value of  $R$ , the denominator in equation (17), lies between 0 and 2. If the observed anisotropy  $A$  is large, then  $R$  is also large and the error is small. The anisotropy  $A$  is maximum when the normal to the plane of measurement bisects the larger angle between the magnetic axes of the two ions. Then  $\theta$  and  $\theta'$  are equal to  $(\pi \pm \phi)/2$  or  $\pm \phi/2$ , according as  $\phi$  is greater than or less than  $\pi/2$ . Substituting these values in equation (19), the maximum error when the observed anisotropy is largest, is found to be

$\frac{400\pi \sin \phi}{360(1+3 \cos \phi)} \%$ , provided that only the numerical value of  $\cos \phi$  be used in this expression. For  $\text{CuSO}_4 \cdot 5\text{H}_2\text{O}$  in particular, this error is rather large, namely about 2.3%, because  $\cos \phi$  has the low value of 0.1633. On the other hand, if the angle between the magnetic axes of two ions be small, then the error introduced by X-ray data can be made negligibly small.

In case of more than two ions or in the absence of axial symmetry of the ions, it is not possible to get a concise algebraic expression for the percentage error. However, equation (15) indicates that firstly the percentage error introduced by magnetic measurements is equal to that in measuring the anisotropy of the crystal in a plane. Secondly, the error due to X-ray data is minimised if the denominator is large which will be the case if the measured anisotropy is near about the maximum observable value.

#### *Example of $\text{CuSO}_4 \cdot 5\text{H}_2\text{O}$*

According to the X-ray data given by Beevers and Lipson (1934), each unit cell of copper sulphate crystal contains two copper ions, each of which is at the centre of an octahedron composed of four oxygen atoms in a plane and belonging to water molecules, and two other oxygen atoms belonging to sulphate groups at the two vertices.

Let the matrix  $[\theta_{mn}] = \begin{bmatrix} 1 & \cos \gamma & \cos \beta \\ \cos \gamma & 1 & \cos \alpha \\ \cos \beta & \cos \alpha & 1 \end{bmatrix}$

where  $\alpha$ ,  $\beta$  and  $\gamma$  are the crystallographic triclinic angles,  $82^\circ 16'$ ,  $107^\circ 26'$  and  $102^\circ 40'$  respectively. Hence the reciprocal matrix is

$$[\rho_{mn}]^{-1} = \begin{bmatrix} 1.1394 & 0.2076 & 0.3135 \\ 0.2076 & 1.0562 & -0.0799 \\ 0.3135 & -0.0799 & 1.1047 \end{bmatrix}$$

Krishnan and Mookherji (1938) have taken the lines joining the sulphate oxygens at the vertices of the octahedrons, as the magnetic axes of the ions. Taking the crystallographic axes  $a$ ,  $b$ ,  $c$ , as the coordinate axes, the oblique cartesian coordinate  $(x, y, z)$  of any atom is found by multiplying the positions given by Beever and Lipson, by  $a$ ,  $b$ ,  $c$  the dimensions of the unit cell. A line joining two atoms in positions  $(x_1, y_1, z_1)$  and  $(x_2, y_2, z_2)$  may be expressed (Ghose, 1964) as a contravariant vector matrix

$$\begin{bmatrix} (x_2 - x_1) \\ (y_2 - y_1) \\ (z_2 - z_1) \end{bmatrix}$$

$$\text{or as a covariant matrix } [U_1 U_2 U_3] = [\rho_{mn}] \begin{bmatrix} (x_2 - x_1) \\ (y_2 - y_1) \\ (z_2 - z_1) \end{bmatrix}$$

On dividing  $U_1$ ,  $U_2$ ,  $U_3$  by the length of the vector, i.e., the square root of the product of the covariant and contravariant matrices, we get the direction cosines of this line. The latter form a unit covariant vector matrix  $[\cos \phi^a \cos \phi^b \cos \phi^c]$ . The calculated values for  $Z_1$  and  $Z_2$ , the axes of the two copper ions agree with those given by Krishnan and Mookherji and are shown in Table 1.

However, the octahedrons are not regular and the water oxygens are closer to the copper ions. So the magnetic axes are likely to be closer to the normals to the planes of water oxygens. The lines joining one of these oxygens with adjacent oxygens may be expressed as before by two contravariant matrices

$$\begin{bmatrix} X \\ Y \\ Z \end{bmatrix} \text{ and } \begin{bmatrix} X' \\ Y' \\ Z' \end{bmatrix}.$$

A normal to the plane containing these two lines is given by (Ghose, 1965) by the covariant vector matrix

$$[V_1 V_2 V_3] = [(YZ - ZY) (ZX - XZ) (XY - YZ)]$$

To get the direction cosines,  $V_1$ ,  $V_2$ ,  $V_3$  are divided by the square root of the matrix product

$$[V_1 V_2 V_3][\rho_{mn}]^{-1} \begin{bmatrix} V_1 \\ V_2 \\ V_3 \end{bmatrix}$$

These values for  $T_1$  and  $T_2$ , the tetragonal axes of the two copper ions are shown in Table I. Those for  $T_2$  differ considerably from the corresponding values calculated by Ghosh and Mitra (1964).

TABLE I

	$\cos \phi^a$	$\cos \phi^b$	$\cos \phi^c$
$Z_1$	0.2026	-0.6479	0.6179
$Z_2$	0.3372	0.7489	0.3567
$T_1$	0.0616	-0.6525	0.6522
$T_2$	0.3664	0.7104	0.3823

To calculate the ionic anisotropy, equation (17) may be used. The angle between the two ionic axes, either  $Z_1$  and  $Z_2$ , or  $T_1$  and  $T_2$ , is obtained easily by forming the scalar product of the two unit vectors, and is given by

$$\cos \phi = [\cos \phi_1^a \cos \phi_1^b \cos \phi_1^c][\rho_{mn}]^{-1} \begin{bmatrix} \cos \phi_2^a \\ \cos \phi_2^b \\ \cos \phi_2^c \end{bmatrix}$$

The value of  $\cos \phi$  is thus found to be -0.1355 for  $Z_1, Z_2$  axes, and -0.1633 for  $T_1, T_2$  axes.

To find the values of  $\gamma_2$  and  $\gamma'_3$ , whatever be the plane in which anisotropy is measured, the unit normal to the plane can be expressed as a contravariant vector matrix with respect to the crystallographic axes (Ghose, 1955). If the plane of

measurement be  $(hkl)$ , then the normal is a covariant vector  $\begin{bmatrix} h & k & l \\ a & b & c \end{bmatrix}$  or a contravariant vector  $[V^1 \ V^2 \ V^3] = \begin{bmatrix} h & k & l \\ a & b & c \end{bmatrix} [\rho_{mn}]^{-1}$ . Dividing each element  $V^1$  etc.,

by the magnitude of the vector, i.e., the square root of  $[V^1 \ V^2 \ V^3][\rho_{mn}] \begin{bmatrix} V^1 \\ V^2 \\ V^3 \end{bmatrix}$ , we

get a unit contravariant vector, say  $\begin{bmatrix} v^1 \\ v^2 \\ v^3 \end{bmatrix}$ .

Again if the plane of measurement be perpendicular to both the planes  $(hkl)$  and  $(h'k'l')$  then the normal is a contravariant vector

$$\begin{bmatrix} V^1 \\ V^2 \\ V^3 \end{bmatrix} = \begin{bmatrix} a(kl' - k'l) \\ b(lh' - l'h) \\ c(hk' - h'k) \end{bmatrix}, \text{ which may be changed to}$$

a unit vector as before. If during measurements, one of the crystallographic axes is the normal, then the unit contravariant matrix has a very simple form.

Thus with the  $c$  axis normal, it is equal to  $\begin{bmatrix} 0 \\ 0 \\ 1 \end{bmatrix}$ .

Now  $\gamma, \gamma'$ , are the matrix products of the contravariant unit matrices in the direction of the normal to the plane of measurement and the covariant unit matrices in the directions of the magnetic axes of the two ions.

Krishnan and Mookherji (1938) have given the observed values of anisotropy in eight different planes of  $\text{CuSO}_4 \cdot 5\text{H}_2\text{O}$  crystal. These are shown in Table II. The principal ionic anisotropy has been calculated in each case. The values obtained by using  $T_1$  and  $T_2$ , the normals to the planes of water oxygens, are shown in the last column, while those obtained by using  $Z_1$  and  $Z_2$ , the directions of octahedron vortices, are shown in the column last but one.

TABLE II

Mode of suspension	Observed Anisotropy	Calculated ionic anisotropy	
		(Z)	(T)
( $\bar{1}11$ ) horiz.	26	180	130
$a$ axis vert.	60	290	303
( $\bar{1}10$ ) horiz.	117	403	412
(100) horiz.	146	435	513
$C$ axis vert.	183	485	421
(110) horiz.	213	572	578
( $\bar{1}00$ ) and ( $\bar{1}11$ ) vert.	263	550	565
( $\bar{1}\bar{1}0$ ) and (111) vert.	204	542	562

It is found that as observed anisotropy increases, the calculated values of ionic anisotropy become more consistent, as was to be expected from the discussion of probable error in the last section. The last three sets indicate a value of 560 with a probable error of magnitude 20, i.e., about 4%. Actually a much higher error should be expected due to the uncertainty regarding the directions of the magnetic axes of the copper ions. From Table I, it is seen that the angle between the direction of the normal to the plane of water oxygens and the direction of the line of the sulphate oxygens at the vertices of the octahedron, is nineteen degrees for the first copper ion and four degrees for the second. Similar variations in the value of ionic anisotropy calculated with the two sets of axes indicate that neither of them may be considered more correct than the other.

Krishnan and Mookherji (1938) obtained a value of 550 for the ionic anisotropy. As a first step they determined the directions of two magnetic axes by trial and error, such that the ratio  $A/(\sin \theta \sin \theta')$  is constant where  $\theta$  and  $\theta'$  are the angles



between the normal to the plane of measurement and the magnetic axes. However, with the best fit that they could obtain, the ratio varied between 273 and 296 or by about 4% indicating a corresponding maximum error in either the measurements of anisotropy or in the suspensions of the crystal. Consequently, the errors in the last three Sets of values in Table II are no more than the maximum errors due to anisotropy measurement.

More satisfactory results can not be expected for the copper sulphate crystal. Firstly, the oxygen octahedrons surrounding the two copper ions are not exactly similar, so that the magnetic susceptibilities of the two ions are probably different. Secondly, the octahedrons are not regular, so that axial symmetry of the ions is only approximate. And lastly greater accuracy can be expected in those crystals where the ionic axes are not so nearly perpendicular to each other.

#### *Principal ionic susceptibilities*

To determine the principal ionic susceptibilities, it is necessary to have one measurement of absolute value of susceptibility, such as the mean susceptibility of the crystal or the maximum susceptibility in one of the coordinate planes. If the average susceptibility  $\bar{\chi}$  is accurately known,  $K_1$  may be calculated by the equation

$$3K_1 + (K_2 - K_1) + (K_3 - K_1) = 3\bar{\chi}$$

Alternatively, the maximum susceptibility in a plane of the crystal may be determined with sufficient accuracy. Adding equations (6) and (7), we get the equation

$$\chi_{11} + \chi_{22} = 2\chi_{max} - A$$

Substituting the value of  $\chi_{11}$  etc. from equation (2), and using the orthogonal properties of  $\alpha_1, \beta_1$ , etc., we get

$$2K_1 + (K_2 - K_1) \left( 1 - \frac{\Sigma \gamma_2^2}{n} \right) + (K_3 - K_1) \left( 1 - \frac{\Sigma \gamma_3^2}{n} \right) = 2\chi_{max} - A$$

Substituting the calculated values of  $(K_2 - K_1)$  and  $(K_3 - K_1)$ , as well as the observed values of  $\chi_{max}$  and  $A$ , the maximum susceptibility and anisotropy in  $x-y$  plane, the value of  $K_1$  may be calculated. In case of axial symmetry of the ions, the same equation reduces to a simpler form,

$$2K_1 + (K_{||} - K_{\perp}) \left( 1 - \frac{\Sigma \gamma_3^2}{n} \right) = 2\chi_{max} - A$$

The error in  $K_1$ , or in  $K_{\perp}$  should be of the same order as the error in determining  $\chi_{max}$ , i.e., 0.2% because the other quantities in the equations are small. The same error will occur in the values of the other principal ionic susceptibilities calculated from the values of principal ionic anisotropies, because the latter quantities being small the absolute magnitudes of their errors will also be small.

## REFERENCES

- Beavers, C. A. and Lipson, H., 1934, *Proc. Roy. Soc. A.*, **140**, 570  
 Dutta, S. K., 1953, *Indian J. Phys.*, **27**, 154;  
 ———, 1954, *Indian J. Phys.*, **28** 239  
 Dutta Roy, S. K., 1955, *Indian J. Phys.*, **29**, 429.  
 Ghose, J. K., 1964, *Ind. J. pure appl. Phys.*, **2**, 94 ;  
 ———, 1965, *Indian J. Phys.*, **39**, 400.  
 ———, 1966a, *Ind. J. pure appl. Phys.*, **4**, 175.  
 ———, 1966b, *Ind. J. pure appl. Phys.*  
 Ghosh, U. S. and Bagchi, R. N., 1962, *Indian J. Phys.*, **36**, 538.  
 Ghosh, U. S. and Mitra, S., 1964, *Indian J. Phys.*, **38**, 19.  
 Krishnan. K. S. and Banerjee, S., 1934-35, *Phil. Trans.*, **234A**, 265.  
 Krishnan, K. S. and Mookherji. A., 1936, *Phys. Rev.*, **50**, 860  
 ———, ———, ———, 1938, *Phys. Rev.*, **54**, 534.  
 Lonsdale, K. and Krishnan. K. S., 1936, *Proc. Roy. Soc. A.*, **156**, 597.

# NON-ANALYTIC SPINOR REPRESENTATION OF 4-DIMENSIONAL LORENTZ TRANSFORMATION

N. N. GHOSH

INDIAN ASSOCIATION FOR THE CULTIVATION OF SCIENCE  
CALCUTTA-32

(Received April 26, 1966)

**ABSTRACT.** This gives a representation of a 4-dimensional Lorentz transformation by utilizing the complex transformation coefficients of a unimodular unitary spinor transformation defined in a non-analytic complex space  $S_2$ . The treatment is similar to that followed in an earlier paper where the spinor representation of 5-dimensional Lorentz transformation was considered.

## INTRODUCTION

In a complex two-dimensional non-analytic space  $S_2$  a special transformation scheme called 'unimodular unitary non-analytic spinor transformation' has been framed. A mixed spinor  $K^\mu_\nu$  undergoing this transformation is then shown to be associated with a real vector  $K_\mu$  undergoing a 4-dimensional Lorentz transformation yielding the connecting relations between the respective transformation coefficients. In a recent paper (Ghosh 1965) the 'analytic spinor representation of 4-dimensional Lorentz transformation has been considered and some general properties of such spinors studied.

1. In an earlier paper (Ghosh, 1962) the general non-analytic spinor transformation scheme in  $S_2$  has been formulated. Referring to § 2 of the next paper (Ghosh, 1964) one can define a unitary non-analytic spinor transformation in  $S_2$  by postulating the invariance of an elementary spinor  $\eta_{\mu\nu}$  with components

$$\eta_{11} = \eta_{22} = i, \quad \eta_{12} = \eta_{21} = 0, \quad \eta_{\alpha\beta} = 0 \quad \dots \quad (1.1)$$

$$\eta_{\alpha\beta} = \text{conj } \eta_{\alpha\dot{\beta}}, \quad \eta_{\alpha\dot{\beta}} = \text{conj } \eta_{\alpha\beta} = 0$$

undergoing the transformation given by (Ghosh, 1962)

$$\eta'_{\mu\nu} = \eta_{\alpha\beta} (\xi'_\mu X^\alpha) (\xi'_\nu X^\beta) (\alpha, \beta = 1, 2, \dot{1}, \dot{2}) \quad \dots \quad (1.2)$$

For the invariance of  $\eta'_\mu$  under unitary non-analytic spinor transformation we put  $\eta'_{\mu\nu} = \eta_{\mu\nu}$  in the above and obtain the set of conditions expressed in the following matrix form :

$$\begin{vmatrix} \alpha & \beta & \lambda & \mu \\ \gamma & \delta & \nu & \sigma \\ \dot{\lambda} & \dot{\mu} & \dot{\alpha} & \dot{\beta} \\ \dot{\nu} & \dot{\sigma} & \dot{\gamma} & \dot{\delta} \end{vmatrix} \begin{vmatrix} \alpha & \gamma & -\lambda & -\dot{\nu} \\ \dot{\beta} & \dot{\delta} & -\mu & -\sigma \\ -\dot{\lambda} & -\dot{\nu} & \alpha & \gamma \\ -\dot{\mu} & -\sigma & \dot{\beta} & \dot{\delta} \end{vmatrix} = \begin{vmatrix} 1 & 0 & 0 & 0 \\ 0 & 1 & 0 & 0 \\ 0 & 0 & 1 & 0 \\ 0 & 0 & 0 & 1 \end{vmatrix} \quad (1.3)$$

In the above  $\alpha, \beta, \gamma, \delta$  denote the transformation coefficients  $\xi'_1 X^1, \xi'_1 X^2, \xi'_2 X^1, \xi'_2 X^2$  respectively and  $\lambda, \mu, \nu, \sigma$  the transformation coefficients  $\xi'_1 X^1, \xi'_1 X^2, \xi'_2 X^1, \xi'_2 X^2$  respectively. Interchanging the order of the matrices in (1.3) we get an alternative set of conditions for unitary non-analytic spinor transformation. The associated contravariant spinor  $\eta^{\mu\nu}$  will be defined by the nonvanishing components

$$\eta^{11} = \eta^{22} = -i, \quad \eta^{12} = \eta^{21} = i$$

so that

$$\eta^{\mu\nu}\eta_{\mu\rho} = \eta^{\nu\mu}\eta_{\nu\sigma} = \delta^\nu_\rho. \quad \dots (1.4)$$

Raising and lowering of spinor indices will be performed under the scheme

$$\eta^{\mu\nu}\psi_\mu = \psi^\nu, \quad \psi^\mu\eta_{\mu\nu} = \psi_\nu.$$

Thus

$$\psi^1 = -i\psi_1, \quad \psi^2 = -i\psi_2, \quad \psi_1 = -i\psi^1, \quad \psi_2 = -i\psi^2 \quad \dots (1.5)$$

It may be noted that the contravariant and the covariant transformation coefficients are connected by the relations

$$\begin{aligned} \xi'_\mu X^\mu &= \xi_\alpha X'^\alpha, \\ \xi'_\mu X^\mu &= -\xi_\alpha X'^\alpha. \end{aligned} \quad \dots (1.6)$$

To obtain the appropriate spinor representation let us impose further restrictions on the unitary spinor field by postulating the invariance of an antisymmetric elementary spinor  $\gamma_{\mu\nu}$  defined by the non-vanishing components

$$\gamma_{12} = -\gamma_{21} = i, \quad \gamma_{12} = -\gamma_{21} = -i. \quad \dots (1.7)$$

This leads to the following set of conditions expressed in matrix form :

$$\begin{bmatrix} \alpha & \beta & \lambda & \mu \\ \gamma & \delta & \nu & \sigma \\ \dot{\lambda} & \dot{\mu} & \dot{\alpha} & \dot{\beta} \\ \nu & \sigma & \dot{\gamma} & \dot{\delta} \end{bmatrix} \begin{bmatrix} \delta & -\beta & -\sigma & \mu \\ -\gamma & \sigma & \dot{\nu} & -\dot{\lambda} \\ -\sigma & \mu & \dot{\delta} & -\dot{\beta} \\ \nu & -\lambda & -\gamma & \alpha \end{bmatrix} = \begin{bmatrix} 1 & 0 & 0 & 0 \\ 0 & 1 & 0 & 0 \\ 0 & 0 & 1 & 0 \\ 0 & 0 & 0 & 1 \end{bmatrix} \quad (1.8)$$

In view of (1.3) this amounts to the additional conditions

$$\alpha = \delta, \quad \beta = -\gamma, \quad \lambda = \sigma, \quad \mu = -\dot{\nu}. \quad \dots (1.9)$$

We shall call the unitary transformation thus modified 'unimodular unitary non-analytic spinor transformation'. Obviously, this set of transformations will possess group property.

2. Consider now a mixed spinor  $K_\nu^\mu$  satisfying the structural equation

$$K_\nu^\mu \eta_{\mu\rho} \eta^{\rho\sigma} = K_\rho^\sigma. \quad \dots (2.1)$$

, that

$$\begin{aligned} K_1^1 &= K_1^1, & K_2^2 &= K_2^2, \\ K_2^1 &= K_1^2, & K_1^2 &= K_2^1, \\ K_1^1 &= 0, & K_2^2 &= 0, \\ K_1^2 &= -K_2^1, & K_2^1 &= -K_1^2. \end{aligned} \quad \dots (2.2)$$

Applying the rule (1.5) of raising and lowering of spinor indices one can see that  $K_{\nu}^{\mu}$  will have the above structure if it is taken in the bilinear form

$$K_{\nu}^{\mu} = \psi^{\mu} \chi_{\nu} - \chi^{\mu} \psi_{\nu}, \quad \dots (2.3)$$

$\psi_{\mu}, \chi_{\nu}$  being arbitrary spinors of rank 1.

Let us now express the components of the mixed spinor  $K_{\nu}^{\mu}$  in terms of four real quantities  $k_i$  in conformity with the structural relation (2.2) in the following way :

$$\begin{aligned} K_1^1 &= k_3, & K_2^2 &= -k_3, \\ K_2^1 &= k_1 + ik_2, & K_1^2 &= k_1 - ik_2, \\ K_1^2 &= ik_0, & K_2^1 &= -ik_0 \end{aligned} \quad \dots (2.4)$$

Here the invariant  $K_{\mu}^{\mu}$  is assumed to be zero.

Let  $K_{\nu}^{\mu}$  undergo a unimodular unitary non-analytic spinor transformation in  $S_2$  given by

$$K'_{\nu}{}^{\mu} = K_{\rho}{}^{\alpha} (\xi_{\alpha} X'^{\mu}) (\xi_{\nu}' X^{\beta}), \quad \dots (2.5)$$

where the coefficients of transformation satisfy (1.3, 7, 9). It can be verified that after the transformation  $K'_{\nu}{}^{\mu}$  will have the same structure as that of  $K_{\nu}^{\mu}$  so that we can express  $K'_{\nu}{}^{\mu}$  in the same way as (2.4),

Rewriting (2.5) in a more compact form as a transformation formula involving

a set of 4 mutually independent components  $K_1^1, K_2^1, K_1^2, K_2^2$  of  $K_{\nu}^{\mu}$  and then converting this into one involving  $k_i$  expressed in the form

$$k_i' = \rho_i^j k_j (i, j = 0, 1, 2, 3) \quad \dots (2.6)$$

the real transformation coefficients  $\rho_i^j$  are obtained as follows :

$$\rho_3^0 = i\alpha\mu - i\alpha\dot{\mu} - i\beta\dot{\lambda} + i\beta\lambda, \quad \rho_0^0 = \alpha\dot{\delta} - \beta\dot{\gamma} + \lambda\dot{\sigma} - \mu\dot{\nu},$$

$$\begin{aligned}
\rho_3^1 &= \dot{\alpha}\beta - \dot{\mu}\lambda + \dot{\beta}\alpha - \dot{\lambda}\mu, & \rho_0^1 &= -i\dot{\alpha}\dot{\sigma} + i\dot{\mu}\dot{\gamma} - i\dot{\beta}\dot{\nu} + i\dot{\lambda}\dot{\delta}, \\
\rho_3^2 &= i\dot{\alpha}\dot{\beta} - i\dot{\mu}\dot{\lambda} - i\dot{\beta}\dot{\alpha} + i\dot{\lambda}\dot{\mu}, & \rho_0^2 &= \dot{\alpha}\dot{\sigma} - \dot{\mu}\dot{\gamma} - \dot{\beta}\dot{\nu} + \dot{\lambda}\dot{\delta}, \\
\rho_3^3 &= \alpha\dot{\alpha} - \beta\dot{\beta} - \lambda\dot{\lambda} + \mu\dot{\mu}, & \rho_0^3 &= -i\dot{\alpha}\dot{\nu} + i\dot{\beta}\dot{\sigma} + i\dot{\gamma}\dot{\lambda} - i\dot{\mu}\dot{\delta}, \\
\rho_1^0 &= \frac{1}{2} (i\dot{\alpha}\dot{\sigma} - i\dot{\alpha}\dot{\sigma} - i\dot{\beta}\dot{\nu} + i\dot{\beta}\dot{\nu} + i\dot{\lambda}\dot{\delta} - i\dot{\lambda}\dot{\delta} - i\dot{\mu}\dot{\gamma} + i\dot{\mu}\dot{\gamma}), \\
\rho_2^0 &= \frac{1}{2} (\dot{\alpha}\dot{\sigma} + \dot{\alpha}\dot{\sigma} - \dot{\beta}\dot{\nu} - \dot{\beta}\dot{\nu} + \dot{\lambda}\dot{\delta} + \dot{\lambda}\dot{\delta} - \dot{\mu}\dot{\gamma} - \dot{\mu}\dot{\gamma}), \\
\rho_1^1 &= \frac{1}{2} (\dot{\alpha}\dot{\delta} + \dot{\alpha}\dot{\delta} - \dot{\mu}\dot{\nu} - \dot{\mu}\dot{\nu} + \dot{\gamma}\dot{\beta} + \dot{\gamma}\dot{\beta} - \dot{\sigma}\dot{\lambda} - \dot{\sigma}\dot{\lambda}), \\
\rho_2^1 &= \frac{1}{2} (-i\dot{\alpha}\dot{\delta} + i\dot{\alpha}\dot{\delta} + i\dot{\mu}\dot{\nu} - i\dot{\mu}\dot{\nu} + i\dot{\gamma}\dot{\beta} - i\dot{\gamma}\dot{\beta} - i\dot{\sigma}\dot{\lambda} + i\dot{\sigma}\dot{\lambda}), \\
\rho_1^2 &= \frac{1}{2} (i\dot{\alpha}\dot{\delta} - i\dot{\alpha}\dot{\delta} - i\dot{\mu}\dot{\nu} + i\dot{\mu}\dot{\nu} + i\dot{\gamma}\dot{\beta} - i\dot{\gamma}\dot{\beta} - i\dot{\sigma}\dot{\lambda} + i\dot{\sigma}\dot{\lambda}), \\
\rho_2^2 &= \frac{1}{2} (\dot{\alpha}\dot{\delta} + \dot{\alpha}\dot{\delta} - \dot{\mu}\dot{\nu} - \dot{\mu}\dot{\nu} - \dot{\gamma}\dot{\beta} - \dot{\gamma}\dot{\beta} + \dot{\sigma}\dot{\lambda} + \dot{\sigma}\dot{\lambda}), \\
\rho_1^3 &= \frac{1}{2} (\dot{\alpha}\dot{\gamma} + \dot{\alpha}\dot{\gamma} - \dot{\beta}\dot{\delta} - \dot{\beta}\dot{\delta} - \dot{\lambda}\dot{\nu} - \dot{\lambda}\dot{\nu} + \dot{\mu}\dot{\sigma} + \dot{\mu}\dot{\sigma}), \\
\rho_2^3 &= \frac{1}{2} (-i\dot{\alpha}\dot{\gamma} + i\dot{\alpha}\dot{\gamma} + i\dot{\beta}\dot{\delta} - i\dot{\beta}\dot{\delta} + i\dot{\lambda}\dot{\nu} - i\dot{\lambda}\dot{\nu} - i\dot{\mu}\dot{\sigma} + i\dot{\mu}\dot{\sigma}),
\end{aligned}$$

Observing now that the invariant corresponding to  $K_\nu{}^\mu$ , namely,

$$K_\nu{}^\mu K_\mu{}^\nu = 4(k_1^2 + k_2^2 + k_3^2 - k_0^2) \quad (2.7)$$

we remark when  $K_\nu{}^\mu$  undergoes a unimodular unitary non-analytic spinor transformation the induced real transformation on  $k_i$  is a 4-dimensional Lorentz transformation. It may be noted that the conditions (1.3, 9) imposed on the transformation coefficients in the representation (2.7) is equivalent to the exact number of conditions required.

On going over to the auxiliary real 4-space  $R_4$  one can frame (Ghosh, 1964) the particular transformation which corresponds to the unimodular unitary non-analytic spinor transformation in  $S_2$ . The mixed tensor which is obtained as 'analogue' of  $K_\nu{}^\mu$  while undergoing this tensor transformation in  $R_4$  will then induce a 4-dimensional Lorentz transformation to a vector, yielding the connection formulae of the representation expressed in real terms.

#### ACKNOWLEDGMENTS

The author wishes to thank Prof. S. N. Bose, F.R.S. for helpful comments.

#### REFERENCES

- Ghosh, N. N., 1962, *Proc. nat. Inst. Sci. India*, **28**, 695.  
 ———, 1964, *Proc. nat. Inst. Sci. India*, **30**, 383.  
 ———, 1965, *Proc. nat. Inst. Sci. India*, **31**, 477.

# A PHOTOCHEMICAL MODEL OF THE MARTIAN ATMOSPHERE

S. N. GHOSH AND A. SHARMA

J. K. INSTITUTE OF APPLIED PHYSICS,  
ALLAHABAD UNIVERSITY ALLAHABAD, INDIA

(Received March 17, 1966)

**ABSTRACT.** On the basis of investigation carried upto now, the constituents of the Martian atmosphere and their relative abundance at the surface has been collected. The altitude distribution of these constituents has been calculated after considering the hydrostatic equilibrium of the atmosphere and assuming the temperature distribution with altitude in the Martian atmosphere given by Goody (1957). The photochemical modifications of the major constituents ( $N_2$  and  $CO_2$ ) are then separately considered. It has been found that  $CO_2$  is completely dissociated above 130 km and  $N_2$  above 250 km. Considering the chemiluminescent reaction between photodissociated products and the main constituents of the Martian atmosphere, it is found that the flame bands of  $CO_2$  and the red and violet systems of CN may be present in the Martian airglow.

## INTRODUCTION

With the great progress of space research achieved in recent years, the necessity of having more information of planets and their atmospheres is felt. One of the methods of investigating the atmospheres of planets, may be to extrapolate the results obtained for the terrestrial atmosphere. For example, on determining the proton flux which is incident on the top of the earth's atmosphere causing thereby either directly or indirectly the aurora, the proton flux incident on the atmosphere of Mars may be estimated. We have considered here the atmosphere of the planet Mars. It is expected that this planet will be the first one to be explored by rockets.

## II VARIATION OF COMPOSITION, TEMPERATURE AND PRESSURE WITH ALTITUDE IN THE ATMOSPHERE OF MARS

The investigation of the Martian atmosphere which has been carried out upto now, (Kuiper, 1952; Urey, 1959; Dollfus, 1951), reveals that  $N_2$ ,  $CO_2$ , Ar and some amount of  $O_2$  and  $H_2O$  vapour are present in its atmosphere.

The table below gives the composition and certain characteristics of the Martian atmosphere at its surface.

TABLE I

N <sub>2</sub>	219.00 gm cm <sup>-2</sup>
CO <sub>2</sub>	5.98 gm cm <sup>-2</sup>
Ar	1.28 gm cm <sup>-2</sup>
O <sub>2</sub> ]	0.35 gm cm <sup>-2</sup>
H <sub>2</sub> O	0.042 gm cm <sup>-2</sup>

---

Total mass of the atmosphere	227.00 gm cm <sup>-2</sup>
Average surface temperature	300°K
Average pressure at the surface	8.87 × 10 <sup>4</sup> dynes cm <sup>-2</sup>
<i>g</i> at the surface	391 cm sec <sup>-2</sup>

From the variation of temperature with altitude in the Martian atmosphere as given by Urey (1959) estimated from Goody's (1957) calculations, the Martian atmosphere can be divided into three regions as follows :

Region (km)	Datum Altitude Z <sub>0</sub> (km)	Temperature at the Datum Altitude T <sub>0</sub> , (°K)	Temperature Gradient (°K. km <sup>-1</sup> )
0-30	0	300	-3.75
30-90	30	187.5	-0.96
90 and above	90	130	+1.05

Assuming complete mixing of the constituents of the Martian atmosphere upto 130 km and neglecting the variation of *g* with altitude, the altitude distribution of the constituents has been calculated after considering the hydrostatic equilibrium. The equation is

$$n_z = n_0 \left( \frac{T_z}{T_0} \right)^{-(mg/k\alpha + 1)} \quad \dots (2)$$

where  $\alpha$  is the rate of increase of *T* with height.

The mean molecular mass *m* has been obtained from the relative abundance given



in the Table 1. The calculated distributions of  $N_2$ ,  $CO_2$ ,  $H_2O$  and  $O_2$  upto 130 km are shown in Fig. 1.

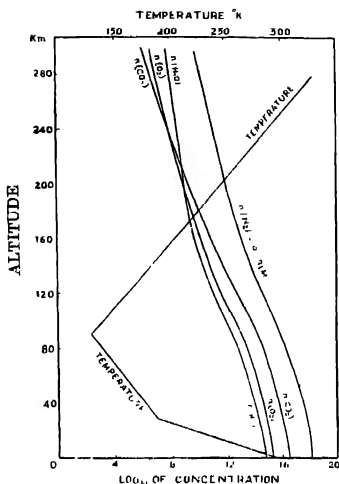


Fig. 1. The calculated distributions of  $N_2$ ,  $CO_2$ ,  $H_2O$  and  $O_2$  upto 300 Km. in the Martian atmosphere.

The distribution of the constituents above 130 km, i.e. in the region of diffusive separation has been calculated from the following equation :

$$\frac{n_{iz}}{n_{i+130}} = \left( \frac{T_z}{T_{130}} \right)^{-\left( \frac{m_i g}{k\alpha} + \alpha \right)} \quad \dots (3)$$

which is obtained after replacing  $\bar{m}$  by the molecular mass  $m_i$  of the  $i$ -th constituent. The distributions of atmospheric constituents of Mars above 130 km and upto 300 km are also shown in Fig. 1.

#### MODIFICATION OF ATMOSPHERIC DISTRIBUTION BY PHOTOCHEMICAL REACTIONS

In this section, we shall consider the distribution of the two main constituents ( $N_2$  and  $CO_2$ ) of the Martian atmosphere as modified by photochemical reactions. Due to solar ultraviolet radiations,  $N_2$  is dissociated into two N atoms and  $CO_2$  into CO and O. As these dissociated products are very reactive, they produce many chemical reactions leading to a complex photochemistry of the Martian atmosphere. We shall now consider separately the dissociation of  $N_2$  and  $CO_2$ .

equation 8 and 12 the distributions of  $\text{CO}_2$  and  $\text{N}_2$  as modified by photochemical reactions and correct to the first approximation is calculated.

In order to obtain the distributions of  $\text{N}_2$  and  $\text{CO}_2$  correct to the second approximation, the transmission coefficients  $K_{\nu}$  are recalculated after assuming the above distributions of  $\text{N}_2$  and  $\text{CO}_2$  correct to the first approximation. The modified distributions of  $\text{N}_2$  and  $\text{CO}_2$  correct to the second approximation are given in Table II and in Fig. 3.

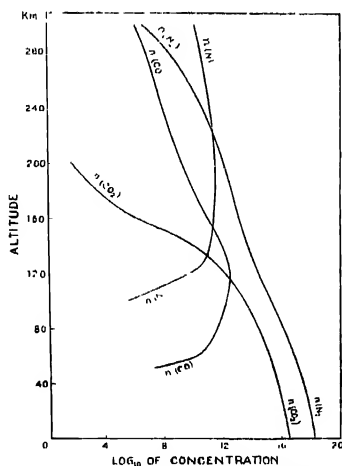


Fig. 3. The distributions of  $\text{N}_2$  and  $\text{CO}_2$  in the Martian atmosphere at modified by photochemical reactions.

## DISCUSSION

The greatest source of error in the determination of the altitude distributions of the constituents in the Martian atmosphere is the uncertainty in the distribution of temperature with altitude. In the present calculation, the temperature distribution given by Goody (1957) has been adopted. If, however, the Martian atmosphere is assumed to be isothermal having the same temperature as at the surface, the distribution of the total particle concentration with altitude is given by

$$n_e = n_0 \exp \left[ - \frac{kT}{mg} Z \right]$$

which gives the distribution as given below.

TABLE I

Altitude	$n_z$ (cm <sup>-3</sup> ) Isothermal	$n_z$ (cm <sup>-3</sup> ) Goody's Temp distribution
0	$2.14 \cdot 10^{18}$	$2.14 \cdot 10^{18}$
100	$2.53 \cdot 10^{16}$	$1.99 \cdot 10^{16}$
200	$2.98 \cdot 10^{14}$	$9.30 \cdot 10^{13}$
300	$3.52 \cdot 10^{12}$	$7.22 \cdot 10^9$

It is to be noted that at 300 km the total particle concentrations obtained from the two temperature distributions differ by about two orders. At lower altitude the difference becomes less.

TABLE II

The distribution of N<sub>2</sub> and CO<sub>2</sub> as modified by photochemical reactions

Altitude Km	$n(\text{CO}_2)$ cm <sup>-3</sup>	$n(\text{CO})$ cm <sup>-3</sup>	$n(\text{N}_2)$ cm <sup>-3</sup>	$n(\text{N})$ cm <sup>-3</sup>
0	$3.64 \times 10^{16}$	—	$2.09 \times 10^{18}$	—
10	$2.58 \times 10^{16}$	—	$1.49 \times 10^{18}$	—
20	$1.74 \times 10^{16}$	—	$1.00 \times 10^{18}$	—
30	$1.09 \times 10^{16}$	—	$6.30 \times 10^{17}$	—
40	$5.54 \times 10^{15}$	—	$3.19 \times 10^{17}$	—
50	$2.71 \times 10^{15}$	$1.93 \times 10^7$	$1.56 \times 10^{17}$	—
60	$1.16 \times 10^{15}$	$5.29 \times 10^{10}$	$6.67 \times 10^{16}$	—
70	$5.68 \times 10^{14}$	$2.02 \times 10^{11}$	$3.27 \times 10^{16}$	—
80	$3.14 \times 10^{14}$	$5.74 \times 10^{11}$	$1.81 \times 10^{16}$	—
90	$9.78 \times 10^{13}$	$1.34 \times 10^{12}$	$5.71 \times 10^{15}$	—
100	$3.18 \times 10^{13}$	$2.22 \times 10^{12}$	$1.96 \times 10^{15}$	$3.28 \times 10^5$
110	$9.60 \times 10^{12}$	$2.93 \times 10^{12}$	$7.23 \times 10^{14}$	$6.44 \times 10^6$
120	$9.00 \times 10^{11}$	$4.08 \times 10^{12}$	$2.87 \times 10^{14}$	$4.33 \times 10^6$
130	$3.00 \times 10^{10}$	$2.00 \times 10^{12}$	$1.20 \times 10^{14}$	$1.24 \times 10^{11}$
140	$7.60 \times 10^9$	$9.13 \times 10^{11}$	$5.30 \times 10^{13}$	$1.90 \times 10^{11}$
150	$2.44 \times 10^7$	$2.85 \times 10^{11}$	$2.46 \times 10^{13}$	$2.22 \times 10^{11}$
160	$9.82 \times 10^5$	$9.49 \times 10^{10}$	$1.19 \times 10^{13}$	$2.64 \times 10^{11}$
170	$5.39 \times 10^4$	$3.33 \times 10^{10}$	$5.92 \times 10^{12}$	$2.64 \times 10^{11}$
180	$3.68 \times 10^3$	$1.23 \times 10^{10}$	$3.02 \times 10^{12}$	$2.65 \times 10^{11}$
190	$2.81 \times 10^2$	$4.70 \times 10^9$	$1.56 \times 10^{12}$	$2.65 \times 10^{11}$
200	$2.47 \times 10^1$	$1.89 \times 10^9$	$8.00 \times 10^{11}$	$2.57 \times 10^{11}$
210	—	$7.91 \times 10^8$	$4.04 \times 10^{11}$	$2.44 \times 10^{11}$
220	—	$3.42 \times 10^8$	$1.62 \times 10^{11}$	$2.22 \times 10^{11}$
230	—	$1.52 \times 10^8$	$8.35 \times 10^{10}$	$1.91 \times 10^{11}$
240	—	$7.00 \times 10^7$	$3.20 \times 10^{10}$	$1.52 \times 10^{11}$
250	—	$3.43 \times 10^7$	$1.13 \times 10^{10}$	$1.11 \times 10^{11}$
260	—	$1.62 \times 10^7$	$1.58 \times 10^9$	$7.92 \times 10^{11}$
270	—	$8.04 \times 10^6$	$8.59 \times 10^8$	$5.06 \times 10^{10}$
280	—	$4.08 \times 10^6$	$2.41 \times 10^8$	$3.36 \times 10^{10}$
290	—	$2.12 \times 10^6$	$6.58 \times 10^7$	$2.17 \times 10^{10}$
300	—	$1.13 \times 10^6$	$1.91 \times 10^6$	$1.44 \times 10^{10}$

TABLE III

The photon flux at the top of the Martian atmosphere and the absorption cross-section of CO<sub>2</sub> between 1750Å—1076Å.

Region × 10 <sup>3</sup> Cm <sup>-3</sup>	A sorption cross-section of CO <sub>2</sub> cm <sup>2</sup>	Photon flux cm <sup>-2</sup> sec <sup>-2</sup>	Region × 10 <sup>3</sup> cm <sup>-1</sup>	Absorption cross-sec. of CO <sub>2</sub> cm <sup>2</sup>	Photon flux cm <sup>-2</sup> sec <sup>-1</sup>
55 — 56	1 × 10 <sup>-21</sup>	6.535 × 10 <sup>11</sup>	74 — 75	9 10 × 10 <sup>-10</sup>	1.055 × 10 <sup>10</sup>
55 — 57	1 × 10 <sup>-21</sup>	4.722 × 10 <sup>11</sup>	75 — 76	9.11 × 10 <sup>-10</sup>	6.034 × 10 <sup>9</sup>
57 — 58	8.52 × 10 <sup>-21</sup>	4.571 × 10 <sup>11</sup>	76 — 77	8.63 × 10 <sup>-10</sup>	9.760 × 10 <sup>9</sup>
58 — 59	1.78 × 10 <sup>-20</sup>	3.905 × 10 <sup>11</sup>	77 — 78	6.24 × 10 <sup>-10</sup>	3.600 × 10 <sup>9</sup>
59 — 60	4.28 × 10 <sup>-20</sup>	1.945 × 10 <sup>11</sup>	78 — 79	4.57 × 10 <sup>-10</sup>	3.491 × 10 <sup>9</sup>
60 — 61	7.04 × 10 <sup>-20</sup>	1.889 × 10 <sup>11</sup>	79 — 80	3.00 × 10 <sup>-10</sup>	1.418 × 10 <sup>9</sup>
61 — 62	1.15 × 10 <sup>-10</sup>	1.821 × 10 <sup>11</sup>	80 — 81	1.70 × 10 <sup>-10</sup>	7.629 × 10 <sup>8</sup>
62 — 63	1.77 × 10 <sup>-10</sup>	1.273 × 10 <sup>11</sup>	81 — 82	0.00 × 10 <sup>-20</sup>	3.254 × 10 <sup>8</sup>
63 — 64	2.60 × 10 <sup>-10</sup>	7.482 × 10 <sup>10</sup>	82 — 83	6.00 × 10 <sup>-20</sup>	8.620 × 10 <sup>7</sup>
64 — 65	3.55 × 10 <sup>-10</sup>	7.241 × 10 <sup>10</sup>	83 — 84	4.00 × 10 <sup>-20</sup>	1.919 × 10 <sup>9</sup>
65 — 66	4.59 × 10 <sup>-10</sup>	7.030 × 10 <sup>10</sup>	84 — 85	5.00 × 10 <sup>-20</sup>	3.017 × 10 <sup>8</sup>
66 — 67	5.46 × 10 <sup>-10</sup>	5.426 × 10 <sup>10</sup>	85 — 86	3.00 × 10 <sup>-10</sup>	1.057 × 10 <sup>9</sup>
67 — 68	5.63 × 10 <sup>-10</sup>	2.454 × 10 <sup>10</sup>	86 — 87	2.71 × 10 <sup>-18</sup>	2.888 × 10 <sup>8</sup>
68 — 69	5.87 × 10 <sup>-10</sup>	2.386 × 10 <sup>10</sup>	87 — 88	9.00 × 10 <sup>-17</sup>	2.801 × 10 <sup>8</sup>
69 — 70	5.97 × 10 <sup>-10</sup>	2.320 × 10 <sup>10</sup>	88 — 89	6.75 × 10 <sup>-17</sup>	2.760 × 10 <sup>8</sup>
70 — 71	6.17 × 10 <sup>-10</sup>	2.308 × 10 <sup>10</sup>	89 — 90	1.03 × 10 <sup>-16</sup>	2.694 × 10 <sup>8</sup>
71 — 72	6.76 × 10 <sup>-10</sup>	1.538 × 10 <sup>10</sup>	90 — 91	1.92 × 10 <sup>-17</sup>	2.487 × 10 <sup>8</sup>
72 — 73	6.35 × 10 <sup>-10</sup>	6.517 × 10 <sup>9</sup>	91 — 92	3.05 × 10 <sup>-17</sup>	1.026 × 10 <sup>8</sup>
73 — 74	7.17 × 10 <sup>-10</sup>	6.370 × 10 <sup>9</sup>	92 — 93	1.02 × 10 <sup>-17</sup>	9.621 × 10 <sup>8</sup>

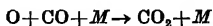
The distribution of the dissociated products may be modified by chemical reactions between N<sub>2</sub>, CO<sub>2</sub>, CO and N. It is apparent from Figs. 3 and 1, that the effect of the dissociation of O<sub>2</sub> (which is neglected in the present calculation) on the distributions of CO<sub>2</sub>, CO and O is negligible below 200 km owing to the low concentration of O<sub>2</sub>, but becomes appreciable above this altitude. Although the concentrations of OH and H (produced by the photodissociation of H<sub>2</sub>O by solar ultraviolet radiation below 1800Å, (see Watanabe *et al.*, 1953) may be very small below 200 km but because of their reactivity the photochemistry of the Martian atmosphere can be altered considerably. Furthermore, the reactions between N, N<sub>2</sub>, O and O<sub>2</sub> can produce the oxides of nitrogen, which are recently reported to be present in the Martia atmosphere (Kieess *et al.*, 1960)

TABLE IV  
Distribution of  $N_2$  molecules in the Martian atmosphere.

Altitude	$n(N)$	$n(N)$ with $n(h\nu)$ $\times K_V = 10^{-10}$	$n(N)$ with $n(h\nu)$ $\times K_V = 10^{-12}$	$n(N_2)$	$n(N_2)$ with $n(h\nu)$ $\times K_V = 10^{-10}$	$n(N)$ with $n(h\nu)$ $\times K_V = 10^{-12}$
0	—	—	—	$2.09 \times 10^{18}$	$2.09 \times 10^{18}$	$2.09 \times 10^{18}$
10	—	—	—	$1.49 \times 10^{18}$	$1.49 \times 10^{18}$	$1.49 \times 10^{18}$
20	—	—	—	$1.00 \times 10^{18}$	$1.00 \times 10^{18}$	$1.00 \times 10^{18}$
30	—	—	—	$6.30 \times 10^{17}$	$6.30 \times 10^{17}$	$6.30 \times 10^{17}$
40	—	—	—	$3.19 \times 10^{17}$	$3.19 \times 10^{17}$	$3.19 \times 10^{17}$
50	—	—	—	$1.56 \times 10^{17}$	$1.56 \times 10^{17}$	$1.56 \times 10^{17}$
60	—	—	—	$6.67 \times 10^{17}$	$6.67 \times 10^{17}$	$6.67 \times 10^{17}$
70	—	—	—	$3.27 \times 10^{16}$	$3.27 \times 10^{16}$	$3.27 \times 10^{16}$
80	—	—	—	$1.81 \times 10^{16}$	$1.81 \times 10^{16}$	$1.81 \times 10^{16}$
90	—	—	—	$5.71 \times 10^{15}$	$5.71 \times 10^{15}$	$5.71 \times 10^{15}$
100	$3.28 \times 10^8$	$1.29 \times 10^{11}$	$1.29 \times 10^{10}$	$1.96 \times 10^{18}$	$1.97 \times 10^{18}$	$1.96 \times 10^{18}$
110	$6.44 \times 10^9$	$1.60 \times 10^{11}$	$1.60 \times 10^{10}$	$7.23 \times 10^{17}$	$7.23 \times 10^{17}$	$7.23 \times 10^{17}$
120	$4.33 \times 10^9$	$1.9 \times 10^{11}$	$1.9 \times 10^{10}$	$2.87 \times 10^{17}$	$2.87 \times 10^{17}$	$2.87 \times 10^{17}$
130	$1.24 \times 10^{11}$	$2.01 \times 10^{11}$	$2.01 \times 10^{10}$	$1.20 \times 10^{17}$	$1.20 \times 10^{17}$	$1.20 \times 10^{17}$
140	$1.90 \times 10^{11}$	$2.94 \times 10^{11}$	$2.94 \times 10^{10}$	$5.30 \times 10^{18}$	$5.30 \times 10^{18}$	$5.31 \times 10^{18}$
150	$2.22 \times 10^{11}$	$3.26 \times 10^{11}$	$3.26 \times 10^{10}$	$2.46 \times 10^{18}$	$2.45 \times 10^{18}$	$2.47 \times 10^{18}$
160	$2.64 \times 10^{11}$	$3.38 \times 10^{11}$	$3.38 \times 10^{10}$	$1.19 \times 10^{18}$	$1.18 \times 10^{18}$	$1.20 \times 10^{18}$
170	$2.64 \times 10^{11}$	$3.41 \times 10^{11}$	$3.46 \times 10^{10}$	$5.92 \times 10^{12}$	$6.48 \times 10^{12}$	$6.84 \times 10^{12}$
180	$2.65 \times 10^{11}$	$3.40 \times 10^{11}$	$3.49 \times 10^{10}$	$3.02 \times 10^{12}$	$1.99 \times 10^{12}$	$3.14 \times 10^{12}$
190	$2.65 \times 10^{11}$	$3.36 \times 10^{11}$	$3.52 \times 10^{10}$	$1.56 \times 10^{12}$	$1.52 \times 10^{12}$	$1.67 \times 10^{12}$
200	$2.57 \times 10^{11}$	$3.24 \times 10^{11}$	$3.54 \times 10^{10}$	$8.00 \times 10^{11}$	$7.66 \times 10^{11}$	$9.10 \times 10^{11}$
210	$2.41 \times 10^{11}$	$1.72 \times 10^{11}$	$3.66 \times 10^{10}$	$4.04 \times 10^{11}$	$4.40 \times 10^{11}$	$5.08 \times 10^{11}$
220	$2.22 \times 10^{11}$	$2.79 \times 10^{11}$	$3.67 \times 10^{10}$	$1.92 \times 10^{11}$	$1.04 \times 10^{11}$	$2.84 \times 10^{11}$
230	$1.91 \times 10^{11}$	$2.34 \times 10^{11}$	$3.76 \times 10^{10}$	$8.35 \times 10^{10}$	$6.34 \times 10^{10}$	$1.60 \times 10^{11}$
240	$1.52 \times 10^{11}$	$2.69 \times 10^{11}$	$3.78 \times 10^{10}$	$3.20 \times 10^{10}$	$2.56 \times 10^{10}$	$9.07 \times 10^{10}$
250	$1.11 \times 10^{11}$	$1.16 \times 10^{11}$	$3.46 \times 10^{10}$	$1.13 \times 10^{10}$	$1.05 \times 10^{10}$	$5.01 \times 10^{10}$
260	$7.92 \times 10^{10}$	$7.86 \times 10^{10}$	$3.21 \times 10^{10}$	$1.58 \times 10^9$	$1.90 \times 10^9$	$2.64 \times 10^{10}$
270	$5.06 \times 10^{10}$	$5.18 \times 10^{10}$	$2.90 \times 10^{10}$	$8.59 \times 10^8$	$2.00 \times 10^8$	$1.12 \times 10^{10}$
280	$3.36 \times 10^{10}$	$3.33 \times 10^{10}$	$2.43 \times 10^{10}$	$2.41 \times 10^8$	$1.50 \times 10^8$	$4.75 \times 10^9$
290	$2.17 \times 10^{10}$	$2.19 \times 10^{10}$	$1.84 \times 10^{10}$	$6.58 \times 10^7$	$1.80 \times 10^8$	$1.69 \times 10^9$
300	$1.44 \times 10^{10}$	$1.45 \times 10^{10}$	$1.32 \times 10^{10}$	$1.91 \times 10^9$	$3.30 \times 10^8$	$6.00 \times 10^9$

It is to be noted from Table II that above 30 km, the atmosphere of Mars is denser than the terrestrial atmosphere (Vaucouleurs has also obtained the same result, 1960). The concentrations of dissociated species ( $CO$ ,  $O$ ,  $N$ ,  $OH$  and  $H$ ) are also much higher. It is known from laboratory experiments that reactions between these constituents produce chemiluminescence and hence an airglow in the Martian atmosphere can be produced. The spectrum of the airglow is expected to contain  $CO_2$  and  $CN$  band systems for the following reasons. It is a well known fact that  $CO_2$  bands are emitted from  $CO-O_2$  flames at ordinary

temperatures. According to Gaydon (1957), such band emission may be caused by the following reaction :



In the martian upper atmosphere where both O and CO are present,  $\text{CO}_2$  band emission is therefore expected. Again, recently Broida and Heath (1957), observed a luminous reaction between CO and N emitting red and violet systems of CN. These bands of CN are also expected to be present in the Martian air glow.

In Table II the N-atom concentration has been calculated by applying equ (13.). In this calculation, it has been assumed that every absorption of photon predissociates  $\text{N}_2$  molecule. This may not happen in reality. In order to obtain the range of concentration of N atom in the Martian atmosphere, two concentrations have been calculated for the limiting lower dissociation probabilities ( $10^{-12}$  sec $^{-1}$  as given by Bates, 1953) and given in Table IV and from  $10^{-9}$  sec $^{-1}$  given in Table III.

#### REFERENCES

- Bates, D. R., 1953, *The Earth As a Planet*, Ed. P. Kuiper The University of Chicago press, p. 584.
- Broida, H. P. and Heath, D. F., 1957, *J. Chem. Phys.* **26**, 1352.
- Dollfus, A., 1951, *C. R Acad. Sci (Paris)* **233**, 467, 1066.
- Gaydon, A. G., 1957, *The Spectroscopy of Flames*, John Wiley and Sons, N. Y.
- Ghosh, S. N. and Shardanand, 1961, *J. Planet Space Sci.* (in press).
- Goody, R. M., 1957, *Weather* **12**, 3.
- Harteck, P. and Dondes, S., 1955, *J. Chem Phys.* **23**, 902.
- Harteck, P., Reeves, R. R. and Mannella, G., 1958, *J. Chem Phys* **29**, 608.
- Herzberg, G. and Herzberg, L., 1948, *Nature* **161**, 283.
- Herzberg, G., 1950, *Molecular Spectra and Molecular Structure I. Spectra of Diatomic Molecules*, D. Van Nostrand Company Inc., Princeton.
- Hinteregger, Inn. E. C. Y., Watanabe, K. and Zelikoff, M., 1953, *J. Chem. Phys.*, **21**, 1648.
- Kiess, C. C., Karrer, S. and Kiess, H. K., 1960, *Publ. Astron. Soc. Pacific (U.S.A.)* **72**, 256.
- Kuiper, G. P., 1952, *The Atmosphere of the Earth and Planets*, Edited by G. P. Kuiper, Chicago University Press.
- Tanaka, Y., 1955, *J. Opt. Soc., Amer.* **45**, 663.
- Urey, H. C., 1959, *Encyclopedia of Physics LII*, Edited by S. Flugge, Springer-Verlag, Berlin.
- Vaucaulours, G. De, 1960, *The Physics and Medicine of the Atmosphere and Space*, John Wiley and Sons, N. Y.
- Watanabe, K., Zelikoff, M. and Inn, E. C. Y., 1953, *Geophysical Research Paper No 21*, AF Geophysical Research Directorate, Cambridge Massachusetts.
- Watanabe, K., 1958, *Advances in Geophysics Vol. 5*, Edited by H. E. Landsberg and J. V. Mueghorn, Academic Press Inc., New York.
- Weissler, G. L., Lee, P. and Mohr, E. I., 1952, *J. Opt. Soc. Amer.* **42**, 84.
- Wilkinson, P. G. and Johnston, H. L., 1950, *J. Chem. Phys.* **18**, 190.
- Wilkinson, P. G., 1961, *J. Mol. Spectr.* **6**, 1.

## Letters to the Editor

The Board of Editors does not hold itself responsible for opinions expressed in the letters published in this section. The notes containing short reports of original investigations communicated to this section should not contain many figures and should not exceed 500 words in length. The contributions reaching the Secretary by the 15th of any month may be expected to appear in the issue for the next month. No proof will be sent to the author.

12

### NOTES ON HIGH VOLTAGE THYRATRON PULSER AND ON FILLING GAS FOR NEON TUBE HODOSCOPE CHAMBER

B K BANDYOPADHYAY AND SUBHRA BHATTACHARYA

PHYSICAL LABORATORY, PRESIDENCY COLLEGE,  
CALCUTTA-12.

(Received July 6, 1966)

Two important considerations for successful operation of neon tube hodoscope chamber recently developed by Bandyopadhyay *et al* (1966) and not reported in the said paper are pointed in this note in brief.

*Thyratron Pulsers* : In order to increase the time resolution of pulsed neon tube hodoscope chamber for particle selection, it is always desired to have a narrow pulse of short rise time under load and the pulse should be applied as soon as after the passage of an ionising particle through the chamber. The value of the applied pulse voltage is denoted by the value of the anode voltage of the thyratron divided by the distance between the plates of the chamber. We have used a 5C22 hydrogen filled thyratron in our experiment.

The thyratron time delay is composed of two parts, the ionisation time of the grid-cathode region and the breakdown of the grid-anode space. The larger delay is in the former and may be reduced by the application of a high input pulse. The second delay is a function of the plate voltage.

Since a large grid drive tends to decrease the delay of the thyratron, a high power EFP60 trigger circuit has been developed for our experiment as shown in Fig. 1. The tube is normally cut off and uses positive feed back from dynode to grid. The output from the dynode may give a large power mainly due to 1500V applied to the plate of the tube and to rather generous cathode emission characteristic of EFP60. Moreover, the dynode surface is very sensitive and emits a copious amount of secondary electrons, on the average about four for each incident primary electron. Other methods to reduce the delay time include the increase of heater current of the thyratron and the application of a positive bias voltage to the grid. The later is significant near the firing potential.

The simplest shape of the high voltage pulse is approximately an RC exponential decay, where C is the output capacitor and R a resistor across the chamber. For our experiment we have selected the value of  $10^{-7}$  sec. for the time constant, i.e.,  $C = 0.001\text{-}\mu\text{F}$  and  $R = 100\text{-ohms}$ , and the condenser is charged to a potential of 8KV from a conventional high voltage power supply.

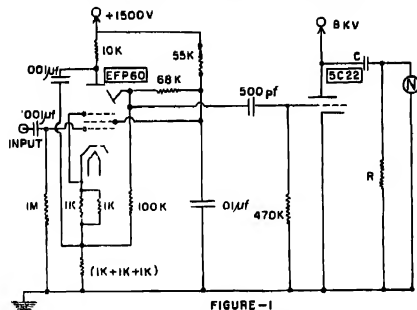


FIGURE-1  
Fig. 1. High Power EFP60 Trigger Circuit.

N--indicates the position of the chamber.

**Filling Gas** In order to get better efficiency the tubes should be filled with the mixture in which a small amount of argon is added to the neon. The addition of argon increases the specific ionisation. One can find data about this in an article by Druyvesteyn and Penning (1940). The main idea is that if one has neon alone, then in course of the avalanche, the electrons produce ionisation which gives rise to a multiplication of the electrons, but more frequently the electrons raise neon to an excited state which then does not improve the reproduction factor of the electrons. In mixture of neon with a small amount of argon the excitation energy is partly used for the ionisation according to the reaction



Excited neon collides with argon and gives ionised argon plus neon, now de-excited, so one gets in this way a much higher efficiency for reproduction of electrons, and the breakdown voltage occurs at much lower values.

We would like to express our appreciation to Professor R. L. Sen Gupta and Dr. M. M. Biswas for their advice and encouragement.

#### REFERENCES

- Bandyopadhyay, B. K. and Bhattacharya, Subhra, 1966, *Indian J. Phys.* **40**, 419;  
Druyvesteyn, M. J. and Penning, F. M., 1940, *Revs. Modern Phys.*, **12**, 87.



# ELASTIC SCATTERING OF ELECTRONS BY HELIUM ATOM IN OCHKUR APPROXIMATION

S. N. BANERJEE, R. JHA AND N. C. SIL

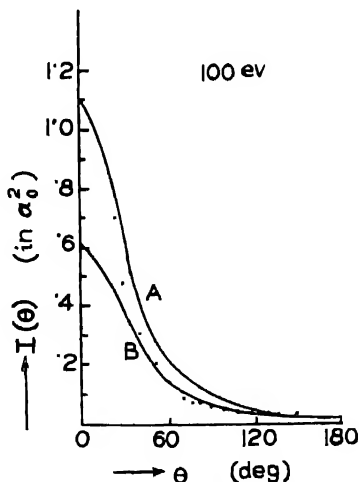
DEPARTMENT OF THEORETICAL PHYSICS,

INDIAN ASSOCIATION FOR THE CULTIVATION OF SCIENCE,

JADAVPUR, CALCUTTA-32

(Received June 15, 1966)

We have applied Ochkur (1964, 1965) approximation to the elastic scattering of electrons by helium atom at the energy 100 ev where Born's approximation is expected not to be valid particularly for differential cross-sections  $I(\theta)$  at very small angles of scattering. We have computed  $I(\theta)$  at 100 ev for angles ranging from  $0^\circ$  to  $180^\circ$ . Here we find that the marked disagreement between the experimental findings of Hughes *et al.*, (1932) and the results of theoretical calculation of Khare and Moiseiwitsch (1965) using static field approximation is removed considerably particularly at forward scattering angles. Moreover, an overall



„Differential cross section  $I(\theta)$  for the elastic scattering of electrons by helium atoms; curve A—present calculation; curve B—calculation of Khare and Moiseiwitsch (1965); 0, experimental points of Hughes *et al.* (1932) normalised to the theoretical curve for 700 ev obtained by employing the Born approximation.

agreement throughout the angular range is obtained, as can be seen from the adjoining figure.

It may be mentioned here that the ground state wavefunction of helium atom we have used is that of Green *et al*, (1954), i.e.

$$\psi_0(r_1, r_2) = \phi(r_1)\phi(r_2)$$

where  $\phi(r) = N(e^{-Zr} + ce^{-2Zr})$

with  $N = 1.48423$

$$C = .60$$

$$Z = 1.4558$$

Further calculations are in progress and will be published soon.

The authors are thankful to Prof. D. Basu for his kind interest and valuable discussions throughout the progress of the work

#### REFERENCES

- Green, L. C., Mulder, M. M., Lewis, M. N., and Woll, J. W. 1954, *Phys. Rev.*, **93**, 757.  
 Hughes, A. L., McMillen, J. H., and Webb, G. M., 1932, *Phys. Rev.*, **41**, 154  
 Khure, S. P. and Morsevitch, B. L., 1965, *Proc. Phys. Soc.*, **85**, 821  
 Oehlku, V. J., 1964, *Soviet Physics JETP*, **18**, 503-8.  
 — — —, 1965, *Soviet Physics JETP*, **20**, 1175.

# ELASTIC AND INELASTIC SCATTERING OF ELECTRONS BY ATOMIC HYDROGEN IN OCHKUR APPROXIMATION

R. JHA, S. N. BANERJEE AND N. C. SIL

DEPARTMENT OF THEORETICAL PHYSICS,  
INDIAN ASSOCIATION FOR THE CULTIVATION OF SCIENCE,  
JADAVPUR, CALCUTTA-32.

(Received June 9, 1966)

For the processes of elastic and inelastic scattering of electrons by atoms, recently Ochkur (1964) has given a formulation which differs from the Born-Oppenheimer approximation by the neglect of certain higher order terms. By doing so, Ochkur obtains for the case of excitation of He atom by an incoming electron, results which agree with experimental findings better than those obtained with other methods. Ochkur (1965) has applied the same method to determine ionisation of hydrogen atom by electron impact and he obtains quite close agreement with experimental results.

We have applied Ochkur's formulation to determine the 1S-1S elastic scattering of the electron by hydrogen at 13.6 eV and also to find the degree of 1S to 2S state excitation of the hydrogen atom when the energy of the incoming electron is 11.7 eV, which is near the threshold energy. The total elastic cross-section (1S-1S) for 13.6 eV turns out to be  $8.83 \pi a_0^2$  ( $a_0$ -Bohr radius) compared with the value  $4.748 \pi a_0^2$  obtained by Burke *et al.*, (1963) from close-coupling approximation; there is no experimental results for this energy, the nearest experimental value is about  $4.8 \pi a_0^2$  at 12.3 eV. The total excitation cross-section (1S-2S) is  $0.292 \pi a_0^2$  obtained by us whereas the corresponding value of Burke *et al.*, (1963) from close-coupling approximation is about  $0.26 \pi a_0^2$ ; the experimental value of Lichten and Schulz (1959) is  $(0.35 \pm 0.05) \pi a_0^2$ . Considering the extreme simplicity of calculation with Ochkur method, the agreement with experimental results is commendable.

We may mention here that Born-Oppenheimer method tends to give misleading result near the threshold energy.

Numerical calculations of elastic scattering for 1S-1S process 1S-2S as well as 1S-2P excitation processes are in progress and will be published soon.

The authors are thankful to Prof. D. Basu for his kind interest and valuable discussions throughout the progress of the work.

## REFERENCES

- Burke, P. G., Seely, H. M., and Smith, K, 1963, *Phys. Rev.* **129**, 1258-74.  
Lichten, W. and Schulz, S., 1959, *Phys. Rev.*; **116**, 1132-9.  
Ochkur, V. I., 1964, *Soviet Physics—JETP*, **18**, 503-8;  
———, 1965, *Soviet Physics—JETP*, **20**, 1175.

## AN X-RAY STUDY OF CHAKSINE IODIDE

S. C. BISWAS AND S. K. TALAPATRA

INDIAN ASSOCIATION FOR THE CULTIVATION OF SCIENCE,  
CALCUTTA-32.

(Received June 25, 1966)

Alkaloid chaksine is not crystallisable, but some of its salts including Chaksine iodide ( $C_{11}H_{20}N_2O_2NI$ ) can be easily crystallised from an aqueous solution of the substance. An X-ray study to elucidate its crystal and molecular structure has been undertaken.

The crystals are very thin, needle shaped and brownish yellow in colour. The unit cell dimensions were obtained from oscillation and Weissenberg photographs along [010] and [001] axes using  $CuK_\alpha$  radiation. The crystals were dusted with aluminium powder in order to standardise the radius of the Camera. From the photographs the crystal was found to belong to the monoclinic system with needle axis as the symmetry axis. The dimensions of the unit cell are given below

$$a = 18.36 \text{ \AA}$$

$$b = 5.26 \text{ \AA}$$

$$c = 17.32 \text{ \AA}$$

$$\beta = 117^\circ 30'$$

Zero, 1st and 2nd layer Weissenberg photographs along [010] and [001] gave the following conditions limiting possible reflections :

$$hkl : h+k = 2n$$

$$hol : (h = 2n)$$

$$oko : (k = 2n)$$

The space group is, therefore,  $C 2/m$ .

The density, as obtained by flotation method in a mixture of benzene and bromoform, was found to be  $1.62 \text{ gm cm}^{-3}$ . The calculated density for four molecules per unit cell is  $1.58 \text{ gm. cm}^{-3}$ . Further work is in progress.

Authors express their sincerest gratitude to Dr. R. K. Sen, D.Sc. for suggesting the problem and guidance, and to Prof. K. Banerjee, D.Sc., F.N.I. for his keen interest in the work.

# MAGNETIC SUSCEPTIBILITY OF GRAPHITE ALONG DIRECTIONS IN THE BASAL PLANE

Miss D. DAS

DEPARTMENT OF MAGNETISM

INDIAN ASSOCIATION FOR THE CULTIVATION OF SCIENCE,

CALCUTTA-32, INDIA,

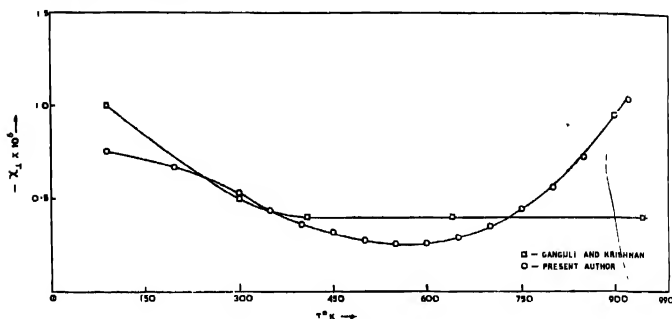
(Received July 21, 1966)

The four electron Brillouin zone in graphite (Dutta 1959; McClure 1957) with a small overlap over only the vertical zone boundary so that the motion of the free carriers are mostly confined in the hexagonal plane, but with a thermal overlap evidently confined in directions perpendicular to the plane, is capable of explaining to a large extent the abnormal anisotropic diamagnetism, the electrical conductivity of the graphite crystals as also the fact observed by Dutta (1953) Ubbelohde and others (1957) that along the  $c$ -axis electrical conductivity increases with temperature, arising from the effect of the thermal excitation

It is then to be expected that the thermally excited electrons responsible for this property, should also contribute towards the magnetic susceptibilities in the basal plane. Krishnan and Ganguli (1939, 1941) gave little importance to the accurate measurement of the small values of  $\chi_{\perp}$ , the susceptibility perpendicular to the  $c$ -axis, and its temperature dependence compared to that of the large value of  $\chi_{\parallel}$ , the susceptibility along directions parallel to the  $c$ -axis. We have therefore carried out a series of very accurate and sensitive measurements of  $\chi_{\perp}$  over a wide range of temperature and the results are graphically represented in fig. 1, wherefrom it is evident that with the rise of temperature  $\chi_{\perp}$  first slowly decreases upto about 550°K remains steady and then finally begins to increase from about 600°K with further rise of temperature. Krishnan and Ganguli's (1939) results are also given in the same graph for comparison.

This increase of  $\chi_{\perp}$  with rise of temperature at higher temperatures observed by us is evidently to be attributed to the increase in the number of carriers, as in case of many other semiconductors, grey tin for example (Busch and Mooser 1953), by the process of thermal excitation across the Brillouin zone boundaries perpendicular to the  $c$ -axis. This excitation may be either intrinsic or extrinsic or combination of these. Ubbelohde's (1960) observation, of a probably positive sign of thermoelectric power along the  $c$ -axis in graphite, seems to indicate more in favour of the extrinsic process, the carriers being positive holes. But before ac-

cepting such a view more accurate investigations on Hall-effect and thermoelectric effect are necessary.



Temperature variation of  $X_1$ , the susceptibility of Graphite along the basal plane.  $X_1$  in C.G.S. e.m.u

The observed decrease of  $\chi_1$  with the rise of temperature at low temperatures is to be ascribed according to the suggestion of Bhattacharya (1965), to the presence of a component of  $\chi_{II}$  (the abnormal part of susceptibility in graphite) due to crystalline derangements, the decrement getting progressively smaller with the rise of temperature. A quantitative estimate of the observed values of  $\chi_1$  according to the above suggestions is in progress and will be published soon.

In conclusion the author wishes to express her best thanks to Shri A. K. Dutta for suggesting the problem and guidance throughout the course of the work.

#### REFERENCES

- Bhattacharya, R., 1965, *Indian J. Phys.* **39**, 53, 300.  
 Busch, G and Mooser, E., 1953, *Helv. Phys. Acta*, **26**, 611.  
 Dutta, A. K., 1953, *Phys. Rev.* **90**, 187.  
 ———, 1959, *Proc. Phys. Soc.* **74**, 604.  
 Krishnan, K. S. and Ganguli, N. 1939, *Z. Kristallogr.* **A100**, 530.  
 ———, 1941, *Proc. Roy. Soc.* **A177**, 168.  
 McClure, J. W., 1957, *Phys. Rev.* **108**, 612.  
 Ubbelohde, A. R., Blackman, L. C. F. and Dundas, P. H., 1960, *Proc. Roy. Soc.* **255**, 203.  
 Ubbelohde, A. R. and Orr, J. 1957, *Nature, Lond.* **179**, 193.

# THE VISIBLE ABSORPTION SPECTRUM OF THE SnS MOLECULE

R. YAMDAGNI AND M. M. JOSHI

DEPARTMENT OF PHYSICS, UNIVERSITY OF ALLAHABAD, ALLAHABAD, INDIA

(Received August 20, 1965)

## Plate IV

**ABSTRACT.** The visible spectrum of the diatomic tin sulphide molecule was known to consist of only one system in the region  $\lambda$  4700-4180. However, on the basis of results obtained by the rotational analysis, Douglas, Howe and Morton (1961) have concluded that more than one excited electronic state should be present in this region. The authors therefore, reinvestigated the visible absorption spectrum of SnS and in fact two systems B $\leftarrow$ X and C $\leftarrow$ X, lying in the region  $\lambda$  5050-4000, have been recognised. The vibrational analyses seem to be in conformity with the rotational work. Following expressions explain the proposed classifications:

$$V\leftarrow X, v = 22756.0 + 325.0(v' + \frac{1}{2}) - 2.50(v' + \frac{1}{2})^2 - 487.7(v'' + \frac{1}{2}) + 1.34(v'' + \frac{1}{2})^2.$$

$$C\leftarrow X, v = 23613.7 + 324.0(v' + \frac{1}{2}) - 1.00(v' + \frac{1}{2})^2 - 487.7(v'' + \frac{1}{2}) + 1.34(v'' + \frac{1}{2})^2$$

Perturbations have been observed in  $v'=2$  level of the B system and in  $v'=1$  level of the C system. Fragments of a third system D have also been recorded.

## INTRODUCTION

The spectrum of the diatomic tin sulphide molecule was for the first time described by Butkow and Tachassowenny (1934). They proposed two systems viz.  $\lambda\lambda 3799-3277$  and  $\lambda\lambda 3764-2580$ . Rochester (1935) extended these two systems considerably and also recognised the new visible system A lying in the region  $\lambda\lambda 4700-4180$ . Shawan (1935) working simultaneously but independently proposed a different analysis for the above system. The rotational analysis of the (0, 0) and the (1, 0) bands of this system was also performed by Shawhan (1936). While Sharma (1945) studied the far ultraviolet system, Barrow and coworkers (1953) investigated the Schumann region also. Hari Mohan (1957) has reported the existence of a new but weak system in the region  $\lambda\lambda 26900-2490$ . Recently Douglas, Howe and Morton (1961) have studied the rotational structure of some prominent bands observed in the visible region. These workers have found that out of the four bands, analysed in the region, one did not contain the Q branch. This evidently led them to conclude that certainly more than one excited electronic states are involved in these transitions and the various vibrational analyses proposed by the low resolution work were incorrect. However they did not suggest any fresh vibrational analysis for this region. It was with an object to

obtain more information regarding the visible systems and the electronic states involved, that the present investigation was undertaken.

### EXPERIMENTAL

The vacuum graphite furnace, described earlier by H. Mohan and K. Majumdar (1961), was used for obtaining the absorption spectrum. A mixture of pure tin and sulphur was placed in a 15 cm. long graphite tube of 1 cm. internal diameter. Temperatures of about 1400°C were best suited for the strong development of bands. In order to avoid rapid diffusion of the vapours, from the experimental graphite tube, nitrogen gas was filled inside the furnace chamber at a pressure of 55 cm of mercury. A 500 watt ribbon filament lamp served as the source of continuum. Jilger E492 large quartz spectrograph was used for photographing the spectrum on Ilford R40 rapid process panchromatic plates. Exposures ranging from two to ten minutes were found enough to record the bands.

### RESULTS

Wavelengths of the band heads along with the visual estimates of their intensities, wavenumbers and the vibrational assignments are given in tables I and II. Table III includes the bands forming two progression (a) and (b) with differences of ground state vibrational frequency. Unassigned bands have been listed in Table IV. Equations for representing the band heads are :

*B System*, ( $\lambda\lambda 5050-4270$ )

$$v = 22756.6 + 325.0(v' + \frac{1}{2}) - 2.50(v' + \frac{1}{2})^2 - 487.7(v'' + \frac{1}{2}) + 1.34(v'' + \frac{1}{2})^2 \dots (1)$$

*C System*, ( $\lambda\lambda 4660-4000$ )

$$v = 23613.7 + 324.0(v' + \frac{1}{2}) - 1.00(v' + \frac{1}{2})^2 - 487.7(v'' + \frac{1}{2}) + 1.34(v'' + \frac{1}{2})^2 \dots (2)$$

The  $v' = 2$  level of the B system was found to be perturbed by about 50  $\text{cm}^{-1}$ . Perturbations of the order of 40  $\text{cm}^{-1}$  were also observed in the  $v' = 1$  level of the C system. The spectrum has reproduced in figure 1,

TABLE I

$\lambda$ air in Å	Int.	$v$ vac Obs.	in $\text{cm}^{-1}$ Calc.	Analysis Authors	Rochester
5048.0	0	19804	19805	(0,6)	
4969.5	1	20117	20125	(1,6)	×
4928.3	2	20285	20277	(0,5)	
4879.3	0	20489	20440	(2,6) p	×
4855.0	3	20592	20597	(1,5)	×
4816.8	1	20765	20761	(0,4)	
4769.4	1	20961	20912	(2,5) p	×



TABLE I (contd.)

$\lambda$ air in Å	Int	$\nu$ van Obs.	in $\text{cm}^{-1}$ Calc.	Authors	Analysis Rochester
4745.0	3	21069	21071	(1,4)	×
4708.9	0	21230	21228	(0,3)	(0,4)
4663.1	0	21439	21386	(2,4) p	×
4639.6	1	21548	21548	(1,3)	×
4605.5	3	21707	21708	(0,2)	(0,3)
4537.8	2	22031	22028	(1,2)	×
4505.3	6	22190	22190	(0,1)	(0,2)
4408.9	4	22675	22675	(0,0)*	(0,1)
4369.0	1	22882	22825	(2,1)p	
4320.3	0	23140	23135	(3,1)	
4279.7	1	23360	23310	(2,0)p	

p — Perturbed.

\* — Rotational analysis performed by Douglas and Coworkers and classified as (y, o).

×

TABLE II

$\lambda$ air in Å	Int.	$\tau$ vac Obs.	in $\text{cm}^{-1}$ Calc.	Authors	Analysis Rohhester
4650.9	1	21495	21450	(1,5)p	(1,5)
4549.4	1	21975	21930	(1,4)p	(1,4)
4526.5	3	22086	22085	(0,3)	(0,3)
4494.0	0	22246	22250	(2,4)	
4453.7	6	22447	22407	(1,3)p	(1,3)
4430.5	7	22565	22565	(0,2)	(0,2)
4398.9	2	22727	22727	(2,3)U	
4360.5	2	22927	22887	(1,2)p	(1,2)
4337.8	9	23047	23047	(0,1)*	(0,1)
4306.3	1	23215	23207	(2,2)	
4248.6	10	23531	23532	(0,0)*	(0,0)
4221.3	2	23683	23689	(2,1)U	
4183.8	10	23895	23854	(1,0)p*	(1,0)
4165.6	2	24000	24007	(3,1)U	
4135.4	4	24175	24174	(2,0)U	
4114.8	1	24296	24297	(7,3)U	
4109.3	3	24328	24323	(4,1)U	
4082.6	4	24487	24492	(3,0)U	
4063.1	1	24605	24605	(8,3)U	
4057.8	3	24637	24637	(5,1)	
4035.2	0	24775	24777	(7,2)	
4029.9	2	24808	24808	(4,0)U	
4018.2	1	24913	24911	(9,3)	

p — Perturbed

\* — Rotational analysis performed by Douglas and coworkers and classified as (x, 1), (x, 0) and (w, 0).

U — Bands left unclassified by Rochester.

TABLE III

(a)	24230 (8)	<sup>(485)</sup> 23745 (1)	<sup>(485)</sup> 23260 (2)	<sup>(461)</sup> 22799 (1)	<sup>(980)</sup> (3)	21819 (1)	<sup>(453)</sup> 21366 (0)	<sup>(943)</sup> (1)	00423 (0)
(b)	<sup>(500)</sup> 24538 (2)	24033 (1)						<sup>(464)</sup> 21644 (0)	21180 (0)

TABLE IV

$\lambda$ air in Å	Int.	$\nu$ vac in cm <sup>-1</sup>
5038.2	0	19843
5006.8	0	19967
4457.2	2	22429
4329.1	4	23093
4293.2	3	23286
4218.0	0	23701

## DISCUSSION

The absorption spectrum lying in the region  $\lambda\lambda 5050-4000$  and attributed to SnS molecule is quite complex and consists of two mutually overlapping systems B ( $\lambda\lambda 5050-4270$ ) and C ( $\lambda\lambda 4660-4000$ ) of which the former is somewhat weaker. It is interesting to compare the results obtained by the authors with those of earlier workers. The authors have been able to record 57 red degraded bands in this region. The systems B and C consist of 18 and 23 bands respectively, 11 appear to fall into progressions showing ground state intervals and the remaining five are unclassified. The vibrational scheme for SnS as drawn by Rochester (1935) consisted of only thirteen sharp and intense bands having only three  $\nu$  progressions. Besides reporting some unclassified bands, he also arranged a few progressions exhibiting the differences of the ground state vibrational frequency. Leaving aside four very faint ones, rest of the above bands have appeared on our plates. Shawhan (1935) had, however, classified only nine bands and failed to observe any vibrational quanta  $\nu'$  greater than unity. He had mentioned the presence of certain unclassified heads most of which he had found to be due to the accidental grouping of rotation lines occurring in the complex structure resulting from overlapping of bands corresponding to the numerous isotopes of tin. It is curious to note that the vibrational assignments of these two workers were mutually inconsistent and while Rochester assigns the origin of band system to be at  $23211\text{ cm}^{-1}$ , Shawhan reports the same at  $23591\text{ cm}^{-1}$ . Although the simple consideration of the Franck Condon principle indicates that Shawhan's analysis is more

R. Vandagni, M. M. Joshi

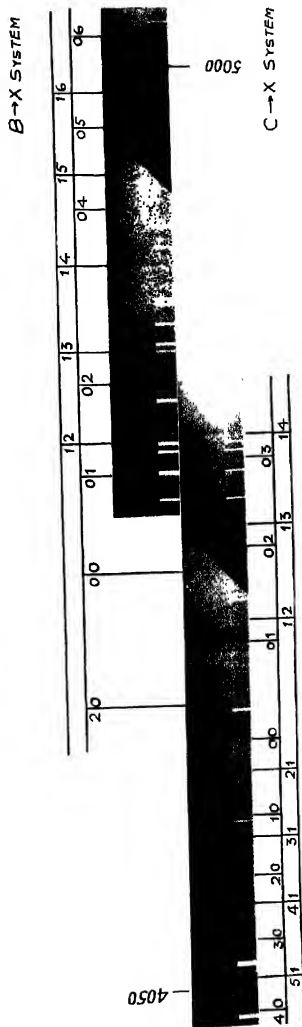


Figure 1 Absorption Spectrum of SnS



plausible, it is, however, unable to explain the 4 bands attributed to  $v' = 0$  progression by Rochester.

The use of somewhat higher temperatures in the present investigation has resulted in the considerable extension of the visible region hitherto known as A, and it is now possible to explain most of the principal bands in terms of two systems, while fragments of a third one are also present.

*System B ( $\lambda\lambda 5050-4270$ )*

The  $487.7 \text{ cm}^{-1}$  value of the ground state vibrational frequency of the SnS molecule is well established. The bands as explained by the equations (1) and (2) have therefore, rightly been attributed to SnS. Leaving aside the (3, 1) band, all the bands attributed to the system B fall into three progressions viz.  $v' = 0$ , 1 and 2. Transitions involving  $v' > 3$  are, however, found to be absent. The  $v' = 0$  progression is well developed and self explanatory. Practically similar situation occurs for the  $v' = 1$  progression. The agreement of the observed and the calculated band head data for these is also satisfactory. Further, the intensity distribution of the bands belonging to these progressions also appears to be reasonable. However, a somewhat different situation arises for the  $v' = 2$  progression. The entire progression is poor in intensity and the observed and the calculated values exhibit a difference of about  $50 \text{ cm}^{-1}$  for each band. This suggests that  $v' = 2$  level might be perturbed by about  $50 \text{ cm}^{-1}$ . Though the (3, 1) band fits in quite well but more information involving higher  $v'$  values is required to make the assignments of  $v' = 2$  progression unambiguous. Attempts to include the progression elsewhere did not succeed and intensity considerations also indicate that its present assignment is quite plausible.

*System C ( $\lambda\lambda 4660-4000$ )*

It can be seen readily that the system C incorporates Shawhan's  $v' = 0$  and  $v' = 1$  progressions as such, but the level  $v' = 1$  is found to be perturbed. The present vibrational assignment extends upto  $v' = 9$  level which has enabled an improved determination of the upper state vibrational constants. The general intensity distribution of the bands is found to be satisfactory and the intense bands lie on a well marked Condon parabola. However, the absence of the (1, 1) band requires some consideration and will be discussed a little later.

Douglas, Howe and Morton (1961) have studied the absorption and emission spectra of SnS in the visible region. They have reported ten absorption bands and designated seven of them as ( $w, 0$ ), ( $x, 0$ ), ( $x, 1$ ), ( $x, 2$ ), ( $y, 0$ ), ( $y, 1$ ) and ( $y, 2$ ) where the letters  $w, x$  and  $y$  are the vibrational levels in certain electronic state and the numbers 0, 1 and 2 are the vibrational levels of the ground state ( $x'\Sigma^+$ ) of the molecule. The rotational structure was measured and analysed for ( $w, 0$ ), ( $x, 0$ ), ( $x, 1$ ) and ( $y, 0$ ) bands. The ( $x, 0$ ), ( $x, 1$ ) and ( $w, 0$ ) bands are found to arise from a  $\pi-\Sigma$  transition while the ( $y, 0$ ) band appeared to have arisen from a  $\Sigma-\Sigma$  transition. This evidently leads to the existence of more than one excited

electric state in the region. It is interesting to note that the  $(y, 0)$ ,  $(y, 1)$  and  $(y, 2)$  bands have been identified as  $B(0, 0)$ ,  $B(0, 1)$  and  $B(0, 2)$  bands and the  $(x, 0)$ ,  $(x, 1)$ ,  $(x, 2)$  and  $(w, 0)$  bands are identical with the  $C(0, 0)$ ,  $C(0, 1)$ ,  $C(0, 2)$  and  $C(1, 0)$  bands of the present classification. Thus the vibrational schemes proposed by the authors are in conformity with the results of the rotational analysis.

Douglas and coworkers (1961) have remarked that while the band  $(w, 1)$  was expected to be quite strong, actually no trace of such a band was found. The absence of the  $(w, 1)$  band has been explained by them on the following lines. The upper state rotational levels are found to be strongly perturbed, the perturbation increasing with higher  $J$  values. Perturbed strong branches were also found to overlap the  $(w, 0)$  band. Thus the effect could reasonably be attributed to the rotational perturbations. It can be seen readily that the  $C(1, 1)$  band would be identical with the  $(w, 1)$  band. The absence of the  $C(1, 1)$  band is therefore explained. In view of the above, it appears that the assignments of the present B and C systems are correct and in all probability they arise from the  $\Sigma-\Sigma$  and  $\pi-\Sigma$  transitions respectively.

#### *Progressions and unclassified bands*

Table III reveals that 11 bands can be grouped into two progressions a and b exhibiting the ground state differences. It can also be noted that the vortical differences of the order of  $300\text{ cm}^{-1}$  are present. It is quite likely that these progressions may from the part of a third system with  $\nu_0$  at  $24230\text{ cm}^{-1}$  and upper state vibrational frequency in the vicinity of  $300\text{ cm}^{-1}$ . However, no definite scheme can be suggested with this meagre data. The remaining 6 bands could not be classified.

It is needless to mention that the visible spectra of SnS and PbS molecules are quite similar in appearance and are characterised by overlapping progressions.

#### ACKNOWLEDGMENT

One of the authors (R.Y.) is grateful to the C.S.I.R., New Delhi, for the grant of a research fellowship to him.

#### REFERENCES

- Barrow, R. F., Drummond, G., and Rowlinson, H. C., 1953, *Proc. Phys. Soc.* **A66**, 885.  
 Butkow, K., and Tschassowenny, W., 1934, *Zeit. f. Phys.* **90**, 53.  
 Douglas, A. E., Howe, L. L., and Morton, J. R., 1961, *J. Mol. Spect.* **7**, 161.  
 Mohan, H., 1957, *D. Phil Thesis*, University of Allahabad.  
 Rochester, G. D., 1935, *Proc. Roy. Soc.* **A150**, 668.  
 Sharma, D., 1945, *Proc. Nat. Acad. Sci. India* **A14**, 217.  
 Shawhan, E. N., 1935, *Phys. Rev.* **48**, 521.  
 1936, *Phys. Rev.* **40**, 810.

# COHERENT RECEPTION USING CARRIER LOCK AND SIDE BAND LOCK TECHNIQUES\*

## PART I

N. B. CHAKRABARTI<sup>+</sup> AND A. K. DATTA<sup>++</sup>

INSTITUTE OF RADIO PHYSICS AND ELECTRONICS, UNIVERSITY OF CALCUTTA

(Received January 15, 1966; Resubmitted May 25, 1966)

**ABSTRACT.** In this paper the design, construction and performances of a receiving system using coherent reception techniques, have been described. The principles of Carrier Lock and Sideband Lock techniques have been discussed. It is pointed out that the reception of different types of modulations (*viz.*, DSB, SSB, conventional AM, Narrowband FM or FM, Binary PSK and VSB) can be made utilising CPL and SRPL techniques. The effects of noise and interference on the locking capability for the system have been studied. The loop phase equations are given in both the cases and modifications that will be caused in presence of noise are also pointed out. This is followed by a description of specific circuits necessary for implementation of the techniques of reception of different modulations mentioned. Experimental results are given with regard to performances of the receiver in the presence of noise, interference and carrier jitter; the minimum bandwidth necessary for the controlling loop for successful tracking of the modulation envelope. Suggestions are given to extend this technique further in reception of narrowband FSK signal.

## INTRODUCTION

The transmission of a message is effected by varying some characteristics of radio frequency wave in accordance with the message or the intelligence to be transmitted. The reception of the signal consists in the recovery of the transmitted message from the received modulated signal i.e. from the received carrier and sideband components in general. The basic idea in reception is to correlate the message or information bearing signal in the received modulated signal and to decorrelate the noise and interference present in the reception band.

A technique of reception is called 'coherent' if specific use is made of the a priori information of all the characteristics of the signals that are not varied in the modulation process for optimum use of the signal energy. In DSB, for example, since the amplitude only of the transmitted signal is modulated, the frequency and the phase of the carrier can be assumed to be constant, the information about these can be stored and used in demodulating (Costas, J. P., 1956). Carrier in the

\* This work has been carried out in the Institute of Radio Physics and Electronics, University of Calcutta.

+ Now with the Department of Electronics and Electrical Communication Engineering, Indian Institute of Technology, Kharagpur.

++ Department of Physics, University of Burdwan, West Bengal.

receiver should have the same frequency and phase as those of the transmitted signal. Similarly, in reception of  $M$ -ary binary keyed signals, use can be made of the information of the expected keying instants and the specific signalling waveforms. Coherent reception is optimum because the fullest possible use is made of the signal energy. It will be realised that coherent reception making use of 'a priori' information stored in the receiver is not practical because the propagation medium is time varying and consequently the characteristics of the transmitted signal even though not modulated, will be subject to unpredictable variations. A practical coherent receiver has therefore to gather these information from the received signal itself, constantly check the stored values with the current information and utilise these for demodulation. The decision process in the demodulator thus involves two steps the first step consists of the 'estimation of the parameters' and the second of 'actual detection'. It is important to realise that such a technique is useful only if the time rate of variation of the 'invariant' parameter is relatively small compared to that of the modulated parameter. In such a case smoothing and filtering of the data is possible enabling reliable extraction of the parameter concerned.

Usefulness of a coherent detection technique arises from the fact that explicit use of the knowledge of the parameters enables one to reject noises and interference which do not have the same character as the signal has.

It would appear that since a coherent receiver is to obtain the estimates of the parameters from the received signal itself, such a receiver is essentially a feedback device. The error signal in the feedback device is a measure of the difference between the present values of the parameters and their past values stored in the system. One can classify the devices in respect of their storage times as (i) feedback detectors if the bandwidth of the control loop ( $B_c$ ) is small compared to the bandwidth of the message ( $B_m$ ) and (ii) feedback demodulators if  $B_c$  is comparable with  $B_m$ . It should be obvious that feedback demodulators are essentially tracking devices incorporating a demodulate-remodulate technique and are therefore useful if the time bandwidth product of the message space is large.

The detectors used in coherent receivers are (or intended to be) necessarily linear. A direct consequence is that there is no threshold effect or suppression of the signal by noise or vice-versa; any reduction of interference and noise results from linear filtering alone. In fact, the principal virtue of a coherent reception technique is that it enables, through exploitation of the distinct characteristics of the signal, reception of relatively weak signals in the presence of strong interference.

The block representation of a Coherent or Homodyne (as it is often called) receiver is shown in fig. (1). The ideal reception condition which is necessary for the operation of such a receiver cannot be achieved in practice, because this requires the incorporation of an oscillator in the receiver which is to be in exact



frequency and phase synchronism with that in the transmitter all the time during which communication is being made. Even with the use of a crystal controlled

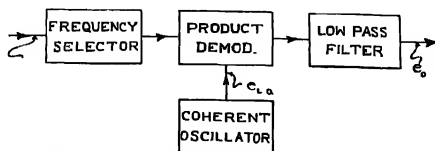


Fig. 1. Block diagram of an ideal coherent reception system.

oscillator with the best engineering attention being given to make their frequencies of oscillation identical, it is not possible to keep their drifts identical. Even if the frequencies of oscillation can be made identical nothing can be reasoned in support of the assumption of the identity in phase of the two oscillations. Apart from the question of frequency and phase synchronism, the time varying character of the propagation media cause received signals to fade randomly in time, both in amplitude and phase and in some cases the received signals undergo large 'Doppler shifts'. These facts introduce further complications and thus increase the unpredictability mentioned earlier.

In a practical version implementing this philosophy of reception, the demodulating carrier is brought in time coherence with the modulated one from the received signal itself. The phenomenon of establishing coherence of the local oscillator is called 'Locking' of the demodulating carrier. For satisfactory reception it is required for the local oscillator to automatically lock in phase with the received signal in presence of additive noise, channel perturbation and 'Doppler shifts'. So what is necessary in the receiver is to incorporate specific circuits to establish coherence and to maintain the synchronism for the period during which transmission and reception of the signal are being effected.

A particularly effective method for doing this is to extract the necessary phase information from a pure carrier component and use this as the input to a phase locked loop of narrow effective bandwidth that controls the local oscillator in the receiving system and the mechanism of locking may accordingly be called 'Carrier Phase Lock' technique in coherent reception.

In the reception of suppressed carrier, Binary PSK, Narrowband PM and FM signals, the received sideband components can also be so utilised as to derive the necessary information for establishing and maintenance of the synchronism. for the demodulating carrier and the mechanism may accordingly be called 'Sideband Phase Lock' technique in coherent reception. Section that immediately follows deals with the principles of the carrier phase lock (CPL) and sideband phase lock (SBPL) techniques.

Section 3 is devoted to a discussion on locking techniques in reception of different types of modulated signals.

The deleterious effects of noise and interference on the locking capability of the phase locked loop have been dealt with in section 4, which also includes a discussion on the deterioration of the SNR due to noise present in the phase locking loop and derivations of loop-phase equations in presence of noise for (i) carrier phase lock and (ii) sideband phase lock cases. The effect of carrier jitter on the demodulated products has also been considered.

In section 6, the basic circuit necessary and the experimental arrangements for studying the applicability of carrier and sideband phase lock techniques in reception of various types of modulated signals are given. The experimental observations with regard to reception of modulated signals like DSB, Binary PSK, Narrowband PM etc. and the results obtained experimentally with DSB signal corrupted with noise and interference are presented in this section. Some remarks in designing a phase locking loop are also included in this section.

#### PRINCIPLES OF CARRIER AND SIDEBAND PHASE LOCKING

In this section we shall discuss the carrier-lock and sideband-lock techniques, the philosophy underlying them and the method of implementation of these techniques in practice. The expressions for the controlling d.c. voltage in a system using a SBPL technique will be derived in case of (i) single tone and (ii) multitone modulations.

*Carrier-Lock*: As mentioned earlier a locked receiver may derive the frequency and phase information from the received modulated wave and make use of these information for demodulating it. A modulated wave consists generally of the carrier and sideband components. The carrier component contains the frequency and phase information and so do the sideband components. In a carrier-lock device the instantaneous phase difference between the received carrier and the local carrier is measured by means of a so-called phase discriminator, the output of the phase discriminator is then used to control the instantaneous phase of the local oscillator in such a way as to reduce and, if possible, eliminate this difference. A reference to fig. (2) will show that the phase equation of phase locking loop is (Chakrabarti, *et al.*, 1964)

$$\frac{d\phi}{dt} = \Omega - Kf(p) \sin \phi \quad (1)$$

where  $\phi$  is the phase difference between the incoming and the local carriers,  $f(p)$  is the transfer function of the filter following the discriminator and the constant  $K$  is proportional to the amplitudes of the two carriers and the sensitivities of the discriminator and the reactance tube and  $\Omega$  is the initial difference in frequency between the two carriers.

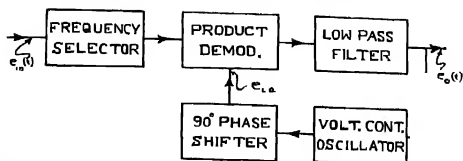


Fig. 2. Block diagram of a carrier phase locked reception system

It follows from the above equation that if the initial difference frequency  $\Omega$  is less than  $Kf(0)$  where  $f(0)$  is the gain of the filter at d.c. a steady state corresponding to  $\frac{d\phi}{dt} = 0$  will be reached and the phase error at steady state will be given by  $\phi = \sin^{-1}[\Omega/Kf(0)]$ . The other important parameters of a carrier-lock device are the locking range and the noise bandwidth which are determined by the filter function  $f(p)$  and the gain constant  $K$ .

The carrier lock technique is obviously applicable in reception of only such modulated waves as contain a carrier. If, however, the carrier component is absent one has to rely on the sideband components for locking the receiver. It should be clear that a phase reference is available from the side-band components only in DSB (Double sideband) systems. A reference is absent in single sideband waves. In double sideband systems even if the carrier is suppressed a phase reference can be obtained from a study of the relations between the sideband components corresponding to a given modulating signal.

**Sideband Lock:** The receiver utilising 'sideband lock' technique (Costas, J. P., 1956) is based on quite different principles from those usual in practice, the frequency and phase synchronisation for the demodulating carrier being established from the received sideband components only. In the receiver the carrier information is ignored even if it is received along with the sideband. The principles of frequency and phase synchronism will be discussed in detail here. An alternative scheme implementing sideband lock technique will also be suggested in this connection.

**Derivation of Phase Information from the Sideband Components:** For the moment we assume that the demodulating carrier frequency is equal to that of the modulated carrier, whether the received signal is a transmitted carrier type or not. In the reception of DSB like signals the information required, is the arithmetic mean position between the sideband components resulting from modulation by a particular modulating frequency. The phase of demodulating carrier should be aligned in such a way as to have this arithmetic mean position. This will ensure coherent addition of the demodulated products of the received sideband components, that is, the modulating frequency outputs resulting from the

upper and lower sideband components will be in phase with each other and the added products will be a maximum. Any departure in phase of the demodulating carrier from the value dictated by the arithmetic mean position will reduce the output (which is the sum of the contribution due to the two sideband components) by a factor  $\cos \phi_e$  where  $\phi_e$  is the phase error mentioned. It is possible to circumvent this difficulty if we instead use a voltage controlled oscillator (VCO) in the receiver where a voltage sensitive capacitor serves as a tuning parameter that controls the oscillation phase of the receiver oscillator. The voltage sensitive capacitor can be actuated by a d.c. controlling voltage in proportion to the phase error talking about. The problem thus is to derive a d.c. controlling voltage in proportion to the phase error  $\phi_e$ .

It can be shown that the demodulated product of the received signal and the demodulating carrier gives the required controlling voltage when multiplied with the demodulated product obtained from the same input but the demodulating carrier in this case being in phase quadrature with the former. The d.c. voltage (slowly varying) thus obtained can be shown to be proportional to the products of the amplitudes of the two sideband (the upper and lower) components and also to  $\sin(2\phi_e)$  where  $\phi_e$  is the phase departure. It is thus seen that the controlling voltage is sinusoidally varying with the phase error  $\phi_e$  and is evidently zero when there is no phase error i.e.  $\phi_e = 0$ . The magnitude of this controlling voltage depends on the amount of phase error  $\phi_e$  and the sense depends on whether  $\phi_e$  is positive or negative. It is, therefore, clear that this error voltage may well be used to vary the capacitance value offered by the voltage sensitive capacitor, thereby controlling the oscillation phase of the VCO. Of course, it must be ascertained that the phase change in oscillation of the VCO caused by the capacitance change does reduce in fact the discrepancy. This depends on the sense of the change of the capacitance values caused by a particular polarity of the controlling voltage which in turn depends on the sign of the error  $\phi_e$ . It may so happen that to obtain the right condition the sense of the controlling voltage is to be reversed and in such a case the VCO automatically comes in lock (synchronism) if the initial phase discrepancy is not greater than  $\pm\pi/4$  radians and synchronism is established. A change in position of the received sideband components causes the arithmetic mean position to have a new value that causes a phase error,  $\phi'_e$ , between the position of the demodulating carrier and the new arithmetic mean position which in turn causes the error voltage to have a new value that again nullifies or minimises the phase error. A little thought will show that such a system in any case cannot be a perfectly coherent device; there will always be a certain amount of phase discrepancy, however small. Under perfectly coherent conditions  $\phi_e$  is equal to zero and the error voltage or the controlling voltage vanishes; in other words, there is no controlling voltage to control the phase of the demodulating carrier under perfectly synchronised condition. Therefore, it seems reasonable to call such a system to be a semicoherent device. The block schematic

diagram for a phase locking arrangement following a SBPL technique is shown in fig. 3.

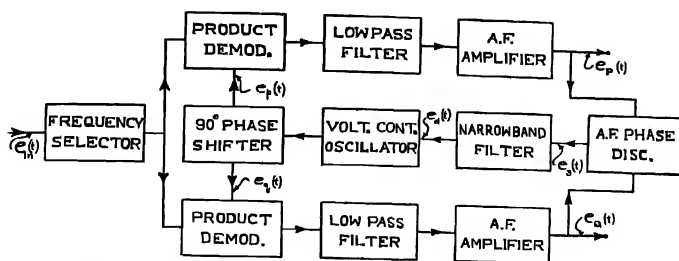


Fig. 3. Block diagram of a sideband phase locked reception system

*Derivation of Frequency Information from the sideband components:* In our previous discussions we devoted our attention to phase coherence with the assumption that frequency coherence already exists. It is of interest to see how frequency synchronism can also be achieved from the information derived purely from the sideband components. We need some controlling voltage which is proportional to the initial frequency discrepancy between the modulated carrier and the frequency of oscillation of the VCO. It is easy to see that the required controlling voltage is obtained from a frequency discriminator, an ideal multiplicative one, if we use the *P* and *Q* channel outputs and their time derivatives.

It can be shown that the difference of the products  $e_p(t) \frac{d}{dt} [e(t)]$  and  $e_q(t) \frac{d}{dt} [e_r(t)]$  gives a slowly varying d.c. voltage which is proportional to the frequency discrepancy  $\Omega$  and may be used to bring down this discrepancy (Refer to fig. 4).

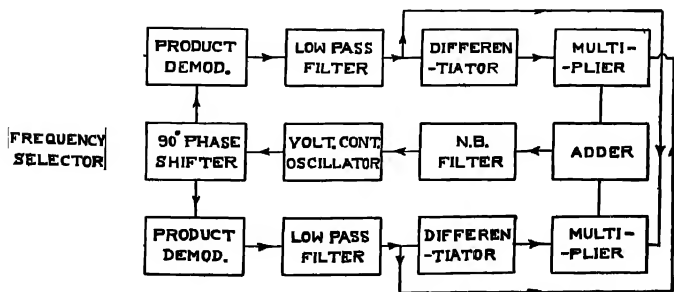


Fig. 4. Block diagram for establishing frequency synchronism from the sideband components

*Sideband-Lock with DSB Signal:* We shall now derive expressions for the controlling d.c. voltage and the inphase and quadrature channel outputs of such a receiving system when the input to the receiver is a DSB signal obtained by modulating a carrier by a single tone modulation. The input to the receiver (refer to fig. 2) in such a case may be written as

$$e_s(t) = A_+ \cos[(\omega_0 + \omega_s)t + \phi_+] + A_- \cos[(\omega_0 - \omega_s)t + \phi_-] \quad (2)$$

where  $A_+$  and  $A_-$  are the received amplitudes,  $\omega_0 + \omega_s$  and  $\omega_0 - \omega_s$  are the frequencies,  $\phi_+$  and  $\phi_-$  are the received phases of the upper and lower sideband components respectively resulting from a carrier  $a \cos(\omega_0 t)$ , and modulating signal  $b \cos(\omega_s t)$ .

The received signal is fed to two product demodulators and gets multiplied by two demodulating carriers  $e_p = B \cos(\omega_0 t + \psi_0)$  and  $e_q = B \sin(\omega_0 t + \psi_0)$  derived from the VCO but in phase quadrature with each other,  $\psi_0$  being the static phase of the oscillator in the receiver.

The modulating frequency components from the output of the product demodulators are accepted by means of an a.f. filter and fed to an audio frequency phase detector. The inputs  $e_1(t)$  and  $e_2(t)$  to the a.f. phase detector may be written to be

$$e_1(t) = \text{D.C.} \frac{B}{2} [A_+ \cos(\omega_s t + \phi_+ - \psi_0) + A_- \cos(\omega_s t - \phi_- + \psi_0)] \quad \dots (3)$$

$$e_2(t) = \text{D.C.} \frac{B}{2} [A_+ \sin(\omega_s t + \phi_+ - \psi_0) - A_- \sin(\omega_s t - \phi_- + \psi_0)] \quad \dots (4)$$

where  $C$  takes account of the constant of the product demodulator and low pass filter.  $D$  stands for the gain of the a.f. amplifier stage.

The output from the a.f. phase detector, an ideal multiplicative one, may be written to be

$$e_3(t) = \frac{D^2 C^2 B^2}{8} \cdot k [A_+^2 \sin 2(\omega_s t + \phi_+ - \psi_0) - 2A_+ A_- \sin(\phi_+ + \phi_- - 2\psi_0) - A_-^2 \sin 2(\omega_s t - \phi_- + \psi_0)]$$

where  $k$  stands for the constant of the a.f. phase detector.

The filter intervening the a.f. phase detector and VCO attenuates the modulating frequency components and components having higher frequencies and allows only the d.c. and slowly varying components to pass through it. The filter output may be written to be

$$e_d(t) = K f(p) A_+ A_- \sin(\phi_+ + \phi_- - 2\psi_0) \quad \dots (6)$$

where  $f(p)$  stands for the filter transfer function and  $K = \frac{D^2 C^2 B^2 k}{4}$  takes account of all the constants including the amplitude of oscillation (B).

When synchronism is established the error voltage vanishes and the condition for coherence may be written to be

$$\phi_+ + \phi_- = 2\psi_0 \quad \text{or} \quad \psi_0 = \frac{\phi_+ + \phi_-}{2} \quad \dots (7)$$

i.e., the phase of the local carrier equals the arithmetic mean of the phase dictated by the received sideband components. A departure in phase by an amount  $\phi_e$

i.e.  $\psi_0 = \frac{\phi_+ + \phi_-}{2} \pm \phi_e$  will cause an error voltage of magnitude  $e_r = \pm Kf(p)$

$A_+A_- \sin 2\phi_e$  to appear. Under perfectly locked condition  $\phi_e = 0$  and  $e_r = 0$ . The outputs  $e_1(t)$  and  $e_2(t)$  change to  $e_Q(t)$  and  $e_P(t)$  and may be given by

$$e_P(t) = G(A_+ + A_-) \cos(\omega_s t + \phi_+ - \psi_0) \quad \dots (8)$$

$$= G(A_+ + A_-) \cos\left(\omega_s t + \frac{\phi_+ - \phi_-}{2}\right) \quad (8a)$$

$$e_Q(t) = G(A_+ - A_-) \sin(\omega_s t + \phi_+ - \psi_0) \quad (9)$$

$$= G(A_+ - A_-) \sin\left(\omega_s t + \frac{\phi_+ - \phi_-}{2}\right) \quad (9a)$$

where  $G$  has been substituted for  $DCB/2$ .

So we see that under locked condition the output  $e_P(t)$  is a maximum and is proportional to the sum of the amplitudes of the received sideband components. On the other hand, the output  $e_Q(t)$  is a minimum and is proportional to the difference of the amplitudes of the received sideband components which is evidently zero when the received amplitudes of the two sideband components are equal. It is interesting to see that the demodulating carrier in the product demodulator which ultimately gives the output, is in phase with the modulated carrier and the demodulated products of this channel may accordingly be called in phase channel or simply  $P$  channel output. The demodulating carrier in the other product demodulator is in phase quadrature and the demodulated products of this channel may accordingly be called quadrature channel or simply  $Q$  channel output.

It has already been pointed out that perfect coherence can never be achieved in such a closed loop error actuated system and there will always be a discrepancy  $\phi_e$  in phase, however small. In such a case  $\psi_0$  may be written to be  $\psi_0 = \frac{\phi_+ + \phi_-}{2} \pm \phi_e$  and the  $P$  and  $Q$  channel outputs may be written as

$$e'_P(t) = G \left[ (A_+ + A_-) \cos\left(\omega_s t + \frac{\phi_+ - \phi_-}{2}\right) \cos \phi_e \right. \\ \left. + (A_+ - A_-) \sin\left(\omega_s t + \frac{\phi_+ - \phi_-}{2}\right) \sin \phi_e \right] \quad (10)$$

$$\simeq G(A_+ + A_-) \cdot \cos \phi_s \cdot \cos \left( \omega_s t + \frac{\phi_+ - \phi_-}{2} \right) \quad (10a)$$

$$e'_Q(t) = G \left[ (A_+ - A_-) \sin \left( \omega_s t + \frac{\phi_+ - \phi_-}{2} \right) \cos \phi_s \right. \\ \left. \mp (A_+ + A_-) \cos \left( \omega_s t + \frac{\phi_+ - \phi_-}{2} \right) \cdot \sin \phi_s \right] \quad (11)$$

$$\simeq \mp G \cdot (A_+ + A_-) \sin \phi_s \cdot \cos \left( \omega_s t + \frac{\phi_+ - \phi_-}{2} \right) \quad (11a)$$

In the following we shall treat the case considered above when the input to the receiver is a DSB signal resulting from multitone modulation.

When the modulating signal is complex, consisting of a large number of tones, the input voltage may be written as

$$e_i(t) = R_s \Sigma A_u \exp j[(\omega_0 + u)t + \phi_u] \quad (12)$$

The output of the product detector can then be represented by

$$e_d(t) = \Sigma \Sigma A_u A_v \sin [(u+v)t + \phi_u + \phi_v - 2\psi_0] \quad (13)$$

where  $A_u$  and  $A_v$  are the amplitudes corresponding to frequency components  $u$  and  $v$  and  $\psi_0$  is the phase of the oscillator voltage. This expression is the same as that results from squaring the input and the L.O. voltage and feeding these to a phase detector.

If the oscillator contains phase modulation (which is indeed the case when it is tracking), the L.O. voltage can be written as

$$e_{L.O}(t) = B_W \exp j[(\omega_0 + w)t + \psi_W] \quad \dots (14)$$

The output of the a.f. phase detector in such a case is

$$e_d(t) = \Sigma_u \Sigma_v \Sigma_w \Sigma_x A_u A_v B_w B_x \sin [(u+v)t - (\omega+x)t + \phi_u + \phi_v - (\psi_w + \psi_x)] \quad (15)$$

Low frequency components of the output in a band  $B_F$  correspond to the condition

$$|u+v-(\omega+x)| \leq B_F$$

It can easily be shown that if the signal input to the receiver and the signal from the local oscillator are squared and mixed one gets the same phase equation as in DSB phase lock. Recognition of this equivalence enables one to simplify the locking procedure in coherent reception of VSB signals. (The normal technique is to establish the phase coherence with the second harmonic component of the local oscillator). When synchronism is established the  $P$  channel in the DSB receiver gives the modulating signal output.



It should be observed that a sideband component  $\omega_0 + u$  say, is effective in producing an error voltage mixing with the sideband component  $\omega_0 + v$  at the output of the filter only when  $u = v$ . If  $u \neq v$  an a-c voltage too appears at the output of the a.f. phase detector of frequency  $(u \sim v)$  which is however attenuated by the filter.

*Domination of the stronger components in phase locking*: The expression for the loop phase equation (Refer eq. 13) shows that the components of signal contribute to the locking voltage in proportion to their powers. Consequently the final equilibrium phases is determined by the stronger components. It follows that if the values of the mean carrier phases demanded by the sideband components in the different parts of the band vary between wide limits, it is only the strong components for which the phase adjustment is correct

A problem that arises in the case of such two loop systems is that of relative phasing between the output in the two bands involved. (In speech modulation this problem is not important). It is easy to see that for a keyed waveform if the relative phases between the different parts of the spectrum are not maintained, the waveform may be distorted without recognition.

*Bandwidth limitation in the locking loop*. It is known that the spectral distribution of the modulated signal is in general non-uniform and the total power in part of the spectrum defined by  $B/2 < |f - f_0|$  is a small fraction of the power contained in the region defined by  $B/2 > |f - f_0|$ , where  $f_0$  is the centre frequency and  $2B$  is the total r.f. bandwidth. Use can be made of this information for improving the signal to noise ratio in the locking loop by restricting the bandwidth of the video or audio filter. This restriction will cause a reduction of the signal power but this is outweighed by the improvement in SNR obtainable, which is given by

$$F = \frac{\text{Signal power density in the reduced band}}{\text{Signal power density in the original band}}$$

*Interference Rejection*: The reception technique discussed with reference to DSB modulation may well be utilised to have a completely interference free demodulated product in case of severe interferences that smudge out the information bearing signal in any one of the two sidebands. The interfering signal may be characterised by

$$e_i(t) = I \cos [(\omega_0 \pm \omega_i)t + \phi_i] \quad \dots (16)$$

according as the interfering signal falls within the upper  $(\omega_0 + \omega_i)$  or lower  $(\omega_0 - \omega_i)$  sideband. It may easily be seen that the  $P$  and  $Q$  channel outputs contain the contribution from the interfering component in addition to the information bearing components. The interfering component in the demodulated products can be annulled if the outputs  $e_P(t)$  and  $e_Q(t)$  are given phase shifts  $\theta_P$  and  $\theta_Q$  such that

$\theta_P \sim \theta_Q$  is equal to  $\pi/2$  radians and the phase shifted outputs are added or subtracted according as the interfering signal is in the lower or upper sideband in the received modulated signal.

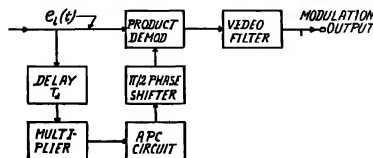


Fig. 5. Block diagram of an alternative scheme suggested for sideband phase locked reception

*An alternative scheme for sideband phase locking:* In this scheme (Refer fig. 5) the incoming signal is fed to a product demodulator where it gets multiplied by the coherent demodulating carrier. The modulation component is accepted by means of a video filter from the products of the demodulator. The filter output gives the modulation or keyed information.

The locking loop consists of a bandpass filter, a multiplier and a CPL circuit. Use is made of a band pass filter to introduce a time delay to the incoming r.f. signal, the amount of delay being equal to that suffered by the modulation components in the video filter. The purpose of the CPL circuit followed by the multiplier is to derive the necessary demodulating carrier out of the products of the multiplier. A little thought will show that the expressions for the controlling d.c. voltage in this case are identical with the equations (6) and (13) for single tone and multitone DSB modulation. When the received signal  $e_i(t) = \pm F(t) \sin(\omega_c t + \phi_0)$  (i.e. Binary PSK modulation) the controlling voltage is given by  $e_d(t) = KF^2(t - T_d) \sin 2(\phi_0 - \psi_0)$ , where  $T_d$  is the time delay mentioned.

#### RECEPTION OF BINARY PSK, CONVENTIONAL AM, SSB AND NARROWBAND FM OR FM SIGNALS FOLLOWING A SBPL TECHNIQUE:

*Binary PSK:* In Binary PSK modulation the phase of the transmitted carrier is altered between two states (either 0 or  $\pi$ ) in accordance with the transmitted message. A binary PSK signal may be generated by modulating the carrier in amplitude by a square wave alternating between the amplitudes  $\pm a$ . The carrier is suppressed as in DSB modulation.

The received signal in this case may be written to be

$$e_i(t) = \pm A \cos(\omega_c t + \phi_0) \quad \dots (17)$$

The demodulating carrier is brought in synchronism with the modulated one following a DSB sideband lock technique. When locking is ensured i.e.

$\psi_0 = \phi_0$  the  $P$  channel gives an output in accordance with the state of the modulating signal i.e. either  $+A$  or  $-A$ .

*Conventional AM* : The received signal in this case may be written to be

$$e_s(t) = A_0 \cos(\omega_0 t + \phi_0) + \Sigma A_u \cos[(\omega_0 + u)t + \phi_u] + \Sigma A_v \cos[(\omega_0 - v)t + \phi_v] \quad (18)$$

Since the carrier component is present, one should make use of the carrier for measurement of the frequency.

The use of an AFC circuit operating on the carrier component would provide an additional facility to maintain the required amount of frequency stability to the VCO. The  $P$  channel in this case gives the modulation frequency input.

*SSB Modulation* : The received sideband in this case may be characterised by either

$$e_i(t) = \Sigma A_u \cos[(\omega_0 + u)t + \phi_u] \quad \dots \quad (19)$$

$$\text{or,} \quad e_i(t) = \Sigma A_v \cos[(\omega_0 - v)t + \phi_v] \quad \dots \quad (19a)$$

The reception of this type of signal may be effected using a crystal controlled oscillator to ensure good frequency stability. In this case both  $P$  and  $Q$  channels contain the modulating signal components and are in phase quadrature. The outputs of both the channels are to be added up after appropriate phasing. The outputs  $e_p(t)$  and  $e_q(t)$  are given phase shifts  $\theta_p$  and  $\theta_q$  such that  $\theta_p \sim \theta_q = \pi/2$  over the audio band and the phase shifted products are added or subtracted to give the modulation output. It should be pointed out in this case that reception can only be effected for signals resulting from speech like modulation. In the case of speech it has been found that intelligibility is not seriously impaired, as long as the local oscillator is within 10 cycles of the correct frequency, even though there may be some loss in naturalness.

*Narrowband PM or FM* : The received signal in this case may be written to be

$$e_i(t) = A \cos(\omega_0 t + m \cos \omega_s t) \quad \dots \quad (20)$$

$$\approx A \cos \omega_0 t - mA \sin \omega_0 t \cdot \cos \omega_s t. \quad \dots \quad (20a)$$

for small values of  $m$ .

We thus have, to a first approximation, a carrier  $A \cos \omega_0 t$  and two sideband components, from a quadrature carrier,  $mA \sin \omega_0 t \cdot \cos \omega_s t$ .

The demodulating carrier in the  $P$  channel in this case is aligned with the arithmetic mean position dictated by the sideband components. The demodulated output is obtained from this channel. If the device be a purely sideband locked type, the  $Q$  channel output will be a minimum. In fact the demodulating carrier in the  $P$  channel is in phase quadrature with the incoming carrier and that of the  $Q$  channel is in phase with it.

*V.S.B. Modulation* : The spectrum of VSB is asymmetric and ordinarily the transmission at carrier frequency is a fraction of the maximum. A VSB wave  $S(t)$  can therefore be resolved into two components, an inphase component  $P(t)$  and a quadrature component  $Q(t)$ . Thus

$$S(t) = P(t) \cos(\omega_0 t + \phi_0) + Q(t) \sin(\omega_0 t + \phi_0) \quad (21)$$

$$= E(t) \cos[\omega_0 t + \phi_0 + \phi(t)] \quad (21a)$$

where  $E(t) = \sqrt{P^2(t) + Q^2(t)}$  is the envelope,  $\phi(t) = \tan^{-1} \frac{Q(t)}{P(t)}$  is the phase and  $\omega_0$  is the angular frequency of the carrier.

In receiving a VSB modulation one has to find the average inphase component in the received signal. For the purpose the input is multiplied by itself and the second harmonic component is selected. This output is given by

$$S_2(t) = [P^2(t) - Q^2(t)] \cos 2(\omega_0 t + \phi_0) + P(t) \cdot Q(t) \sin 2(\omega_0 t + \phi_0) \quad (22)$$

A locally generated carrier  $B \cos(\omega_0 t + \psi_0)$  is locked inphase with the second harmonic component by shifting the voltage by  $\pi/4$  radians, squaring it and mixing the doubled output with  $S_2(t)$ . The phase of the oscillator is controlled by means of an average value of the voltage derived out of mixing. The controlling voltage can be written as

$$e_d(t) = [P^2(t) - Q^2(t)] \sin 2(\phi_0 - \psi_0) + P(t) \cdot Q(t) \cdot \cos 2(\phi_0 - \psi_0) \quad (23)$$

Now the average value of the product  $P(t) \cdot Q(t)$  is zero and the average value of  $Q^2(t)$  is small compared to that of  $P^2(t)$ . The average value of the voltage  $e_d(t)$  is then approximately equal to

$$e_d = KP^2(t) \cdot \sin 2(\phi_0 - \psi_0). \quad \dots (23a)$$

which is identical with that obtained in eq. (6).

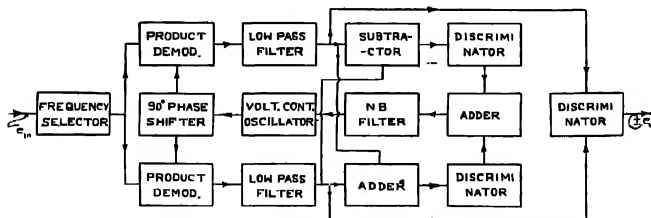


Fig. 6. Block diagram for the reception of Narrowband FSK signals

*Narrowband FSK* : Coherent reception of narrowband FSK signals is possible following SBPL technique. In this case two low frequency discriminators are to be incorporated in the upper sideband and lower sideband channels. The

outputs of these discriminators may be used to maintain the frequency coherence of the local oscillator (Refer fig. 6).

EFFECTS OF NOISE AND INTERFERENCE ON THE  
CAPTURE CAPABILITY OF THE PHASE LOCKED  
LOOP (PLL):

The input signal to a receiver in the presence of an additive noise may be written as

$$e_i(t) = Re \exp(j\omega_0 t) [A_0 \exp(j\phi_0) + \sum A_k \exp j(\omega_k t + \phi_k) + \sum n_l \exp j(\omega_l t + \beta_l)] \quad \dots (24)$$

where  $Re$  stands for the real part of,  $A_0$ ,  $\omega_0$  and  $\phi_0$  denote the amplitude, frequency and phase for the carrier component respectively,  $A_k$  and  $\phi_k$  are the amplitude and phase of the sideband component at an angular frequency  $\omega_0 + \omega_k$  and  $n_l$ ,  $\omega_l$  and  $\beta_l$  are the values of the corresponding quantities for the narrowband noise process.

With reference to DSB modulation reception (Ref. fig. 3) the injected demodulating carriers may be represented by

$$e_p(t) = Re [\exp j(\omega_0 t + \psi_0) + \exp -j(\omega_0 t + \psi_0)] \text{ in the } P \text{ channel} \quad \dots (25)$$

$$e_q(t) = Im [\exp j(\omega_0 t + \psi_0) - \exp -j(\omega_0 t + \psi_0)] \text{ in the } Q \text{ channel} \quad \dots (26)$$

The low frequency outputs of the  $P$  and  $Q$  channel demodulators may be written to be

$$e_P(t) = Re[A_0 \exp j(\phi_0 - \psi_0) + \sum A_k \exp j(\omega_k t + \phi_k - \psi_0) + \sum n_l \exp j(\omega_l t + \beta_l - \psi_0)] \quad \dots (27)$$

$$e_Q(t) = Im[A_0 \exp j(\phi_0 - \psi_0) + \sum A_k \exp j(\omega_k t + \phi_k - \psi_0) + \sum n_l \exp j(\omega_l t + \beta_l - \psi_0)] \quad \dots (28)$$

The phase detector output  $e_d(t) = e_P(t) \cdot e_Q(t)$  is given by

$$\begin{aligned} e_d(t) = & k[A_0^2/2 \sin 2(\phi_0 - \psi_0) + A_0 \sum A_k \sin (\omega_k t + \phi_k + \phi_0 - 2\psi_0) \\ & + \sum \sum A_u A_v \sin (\omega_u t + \phi_u + \phi_v - 2\psi_0) \\ & + \sum \sum A_k n_l \sin (\omega_k t + \phi_k + \beta_l - 2\psi_0) \\ & + A_0 \sum n_l \sin (\omega_l t + \beta_l + \phi_0 - 2\psi_0) + \sum \sum n_w n_x \sin (\omega_w t + \beta_w + \beta_x - 2\psi_0)] \quad \dots (29) \end{aligned}$$

*Phase Equations:* Let us now examine the phase equations in presence of an additive noise in CPL and SBPL cases.

*Case I. Carrier Phase lock:*

Let the received signal be given by

$$e_i(t) = A_0 \cos (\omega_0 t + \phi_0) + n_c \cos (\omega_0 t + \phi_0) + n_s \sin (\omega_0 t + \phi_0) \quad \dots (30)$$

where  $n_e$  and  $n_q$  are the noise components in phase and in quadrature with the carrier  $A_0 \cos(\omega_0 t + \phi_0)$ , white gaussian, independent variables with the highest frequency  $\Delta f$ . Further  $\overline{n_e^2} = \overline{n_q^2} = 2n_0^2 \Delta f$  ... (31)

where  $n_0^2$  is the input noise power density expressed in watts per cycle. The output of the product detector will be (see eq. 29)

$$e_d(t) = k[A_0 \sin \phi + n_e \sin \phi + n_q \cos \phi] \quad \dots (32)$$

If the phase error  $\phi$  is small,

$$e_d(t) = k[(A_0 + n_e)\phi + n_q] \quad \dots (33)$$

If this output be used to control the phase of the oscillator, then

$$\phi(t) = -k_1 f_1(p) e_d(t). \quad \dots (34)$$

$$\text{one derives that } \phi(t) = \frac{k_1 f_1(p) \cdot n_q}{1 + (n_e + A_0) k_1 f_1(p)} \quad \dots (35)$$

$$\text{If } n_e \phi \text{ is small compared to } A_0, \phi \simeq \frac{n_q}{A_0} \quad \dots (36)$$

If, on the other hand, the phase detector output controls the frequency of the oscillator, then

$$\begin{aligned} \frac{d\phi}{dt} &= \Omega - k_1 f_1(p) e_d(t) \\ &= \Omega - k_1 f_1(p) \cdot [(A_0 + n_e) \sin \phi + n_q \cos \phi] \\ &\simeq \Omega - k_1 f_1(p) [(A_0 + n_e) \phi + n_q] \end{aligned} \quad (37)$$

If  $n_e \phi$  is small,

$$\phi = \frac{\Omega - k_1 f_1(p) n_q}{p + k_1 A_0 f_1(p)} \quad (38)$$

### Case II. Sideband phase lock :

Let us consider single tone modulation and restrict attention to noise components around the sidebands. The received signal in this case may be given by

$$\begin{aligned} e_i(t) &= [A_+ \cos \{(\omega_0 + \omega_s)t + \phi_+\} + A_- \cos \{(\omega_0 - \omega_s)t + \phi_-\}] \\ &\quad + n_{e+} \cos \{(\omega_0 + \omega_s)t + \phi_+\} + n_{e-} \cos \{(\omega_0 - \omega_s)t + \phi_-\} \\ &\quad + n_{q+} \sin \{(\omega_0 + \omega_s)t + \phi_+\} + n_{q-} \sin \{(\omega_0 - \omega_s)t + \phi_-\} \end{aligned} \quad \dots (39)$$

where all the noise voltages are white, gaussian, independent and with the highest frequency  $\Delta f$  cycles. Further  $\overline{n_{e+}^2} = \overline{n_{e-}^2} = \overline{n_{q+}^2} = \overline{n_{q-}^2} = 2n_0^2 \Delta f$  ... (40)

## Coherent Reception using Carrier Lock and Sideband, etc. 517

If the phase detector output given by eq. (29) is used to control the frequency of the oscillator, the loop phase equation can be written as

$$e_d(t) = \frac{1}{k_2 f_2(p)} \cdot \frac{d\phi}{dt}$$

$$= [A_+ A_- \sin(\phi_+ + \phi_- - 2\psi_0) + (A_+ n_{q-} + A_- n_{q+}) \cos 2\phi$$

$$+ (n_c n_{e-} + n_{q+} n_{q-}) \sin 2\phi + (n_{c+} n_{q-} - n_{c-} n_{q+}) \cos 2\phi] \quad \dots \quad (41)$$

If  $\phi$  is small one may write to a first order, assuming  $A_+ = A_- = A$  say,

$$e_d(t) = k \left[ \frac{A^2}{2} \phi + \frac{A}{2} (n_{q+} + n_{q-}) + n_{c+} n_{q-} - n_{c-} n_{q+} \right] \quad \dots \quad (41a)$$

The first term is the desired phase control voltage and the remaining terms are the undesired noise voltages. The noise power appearing at the output of the filter can be found thus

$$\bar{e}_d^2 = k^2 [A^2/4 \cdot (n_{q+}^2 + n_{q-}^2) + n_{c+}^2 n_{q-}^2 + n_{c-}^2 n_{q+}^2 + 2(n_{c+} n_{q-} - n_{c-} n_{q+})] \quad \dots \quad (42)$$

*Noise and interference* : It is clear from the expression for the phase locking voltage that in CPL technique the noise and interference components located round the carrier only are responsible in producing the control voltage in the loop. The effects of these components will be to increase the instantaneous phase error between the incoming carrier and the demodulating carrier in the receiver.

When SBPL only is used the components of the noise and interference located round the carrier have no adverse effect as far as the controlling loop is concerned; those affecting the loop are the components which are located round the sideband components arising from the modulation. It will be observed that in this case a part of the output will be produced due to intermodulation between the noise components in the audio band. It will be seen that the appropriate error voltage (proportional to the phase difference between the two carriers) for CPL can be obtained from the quadrature output. Therefore if CPL alone is desired this component after appropriate filtering should only be used for the purpose of locking. It should be mentioned that sometimes the phase of the received carrier may depart substantially from the position indicated by the sidebands. Since the modulation is present essentially in the sidebands the demodulated voltage using the received carrier as the reference is likely to be smaller than that is obtainable by using the sideband reference. In such case it is desirable to use the CPL voltage for adjusting the frequency of the local carrier and the SBPL voltage for adjusting its phase.

The loop phase equation for a loop employing both CPL and SBPL can be written as

$$\begin{aligned} \frac{d\phi}{dt} = & \Omega - k_1 f_1(p) \left[ \frac{A_0^2}{2} \sin 2(\phi_0 - \psi_0) + A_0 \sum A_k \sin (\omega_k t + \phi_k + \phi_0 - 2\psi_0) \right. \\ & + \sum \sum A_u A_v \sin (u t + v t + \phi_u + \phi_v - 2\psi_0) ] \\ & - k_2 f_2(p) [A_0 \sin (\phi_0 - \psi_0) + \sum A_k \sin (\omega_k t + \phi_k - 2\psi_0)] \quad \dots (43) \end{aligned}$$

where  $k_1 f_1(p)$  and  $k_2 f_2(p)$  are the gains associated with the control loops.

*Deterioration of the SNR due to noise present in the PLL :* Any noise present in the input will cause a perturbation of the phase of the VCO. The effect of the phase noise will cause a reduction of the SNR at the output from the corresponding value at the input due to the intermodulation.

Assuming that the phase perturbation caused by the noise is given by  $\phi_{on}$  it is easy to see that the outputs of the  $P$  and  $Q$  channels are respectively

$$\begin{aligned} e_P(t) = & [(A_+ + A_-) \cos (\phi_e + \phi_{on}) \cos (\omega_s t + \psi) \\ & + (A_+ - A_-) \sin (\phi_e + \phi_{on}) \sin (\omega_s t + \psi) \\ & + n_e \sin (\phi_e + \phi_{on}) + n_q \cos (\phi_e + \phi_{on})] \quad \dots (44) \end{aligned}$$

and

$$\begin{aligned} e_Q(t) = & [(A_+ - A_-) \cos (\phi_e + \phi_{on}) \sin (\omega_s t + \psi) \\ & - (A_+ + A_-) \sin (\phi_e + \phi_{on}) \cos (\omega_s t + \psi) \\ & + n_e \cos (\phi_e + \phi_{on}) + n_q \sin (\phi_e + \phi_{on})] \quad \dots (45) \end{aligned}$$

This shows that the modulation output in the  $P$  channel decreases whereas the noise output remains constant, that is to say that the output SNR is smaller than that could have been for perfect locking.

#### EXPERIMENTAL SET-UP, RESULTS AND DISCUSSIONS

A transistorized version of a laboratory model of a receiving system implementing SBPL technique has been constructed and tested. The objective of

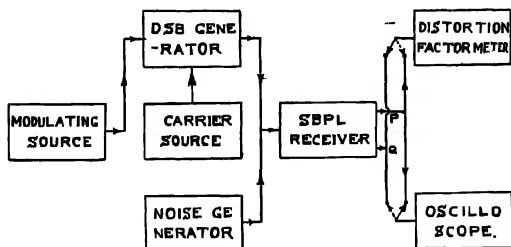


Fig. 7. Block diagram for the experimental arrangements to study the applicability of CPL and SBPL techniques in DSB modulation reception.



the experimental work was to provide experimental verification of some of the conclusions arrived at the previous sections and also to demonstrate the basic principle of operation of the system.

We shall describe here the experimental arrangements for studying CPL and SBPL techniques in reception of different modulations and diversity combination and the results obtained experimentally. A discussion of the experimental results, and some remarks on the design fabrications and performances of such a receiving system, are also given. Studies have been made of the characteristics of the receivers employing sideband phase lock technique in regard to reception of DSB, AM, NBPM and also Binary PSK signals. For these studies complete receivers embodying the techniques mentioned have been constructed. The test equipment constructed include DSB generator, NBPM generator and random fading generator.

*Circuit and Experimental Arrangements:* We shall first describe the auxiliary circuits necessary in the experimental arrangements for studying the applicability of CPL and SBPL techniques in reception of different types of modulated signal and diversity combination. The most important components of any locked receiver are evidently the phase and frequency control circuit incorporating the phase and frequency detector, voltage controlled phase shifters and voltage controlled oscillators. In what follows (the descriptions, performances, circuit diagrams of the units actually used together with typical characteristics obtained experimentally of) some of the circuits will be briefly discussed.

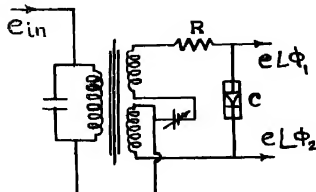


Fig. 8. Circuit diagram of a voltage controlled phase shifter.

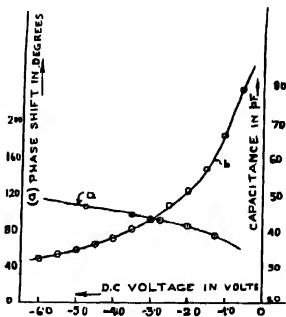


Fig. 9. Figure shows a typical phase voltage characteristic of the voltage controlled phase shifter.

*Voltage Controlled Phase Shifter*—In a voltage controlled phase shifter the amount of phase shifts obtainable is a function of some d.c. voltage. A voltage sensitive diode is used in the phase shifter. The magnitude of the capacitance thrown by such a diode depends on the magnitude of the d.c. potential

across its terminals. fig. (8) shows the circuit diagram for such a phase shifter and fig. (9) is a typical plot showing the variation of phase shifts with d.c. voltage using a diode type V No. 33 in the phase shift network.

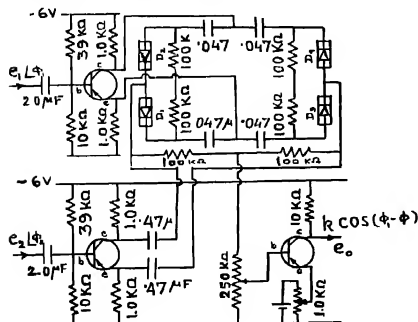


Fig. 10. Circuit diagram of an a.f. phase discriminator in the receiver used to derive the necessary controlling voltage for the VCO's.

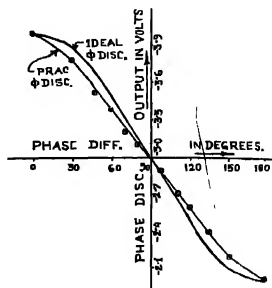


Fig. 11. Figure shows the variation of the d.c. output voltage with phase difference between the two inputs of the audio frequency phase discriminator

**A.F. Phase Discriminator**—The circuit diagram for an audio frequency phase discriminator is shown in fig. (10). When the two inputs  $e_1$  and  $e_2$  are of the same frequency the output for such a system can be shown to be very nearly equal to  $KE_2 \cos \phi$ , where  $E_2$  is the amplitude of  $e_2$ ,  $\phi$  stands for the difference in

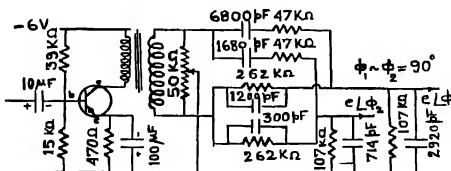


Fig. 12. Circuit diagram of an audio frequency wideband  $90^\circ$  phase shifter.

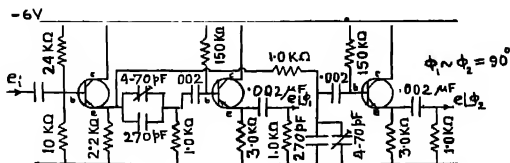


Fig. 13. Circuit diagram of a radio frequency  $90^\circ$  phase shifter.

phase between  $e_1$  and  $e_2$  and  $K$  is a constant for the discriminator under condition that  $E_2 \ll E_1$ , the amplitude of  $e_1$ . fig. (11) shows a set of typical characteristics obtained in an actual experiment which depict the variations of output voltage (d c) with difference of phase ( $\phi$ ), for different amplitude ratios (i.e.  $E_2/E_1$ ).

**Experimental results and discussions :** For any measurement on receiving devices making use of phase lock techniques it must first be ensured that the system has adequate dynamic range both in the locking and demodulating circuits and also satisfactory locking capabilities both in respect of locking range and locking time. One has here to take into consideration the extent and rate of variation of the received input signal and design the control loop accordingly. This aspect of the problem will be discussed later.

Assuming that the loop has been properly designed, one has to test whether the reception technique employed is capable in practice of giving a satisfactory quality of the output signal.

In the receiver employing SBPL technique, measurements have been made with regard to characteristics of reception for DSBAM, NBPM and Binary PSK signals.

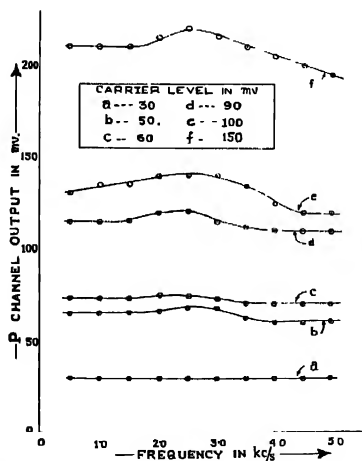


Fig. 14. Figure shows the variation of P channel output with modulating frequency and levels of the modulated input to the receiver for a single tone DSB modulated signal.

Experimental results with single tone modulating signal are presented in fig.(14) where the variations of the output in the P channel with frequency are shown for different levels of the input signal.

Measurements of the output signal and noise components have also been taken in presence of an additive noise at the input to the receiver. Fig 15 shows the variation of the output signal and noise components with different levels of the input noise.

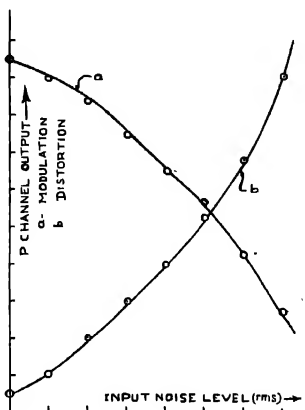


Fig. 15 Figure shows the variations of the output signal and noise levels with input noise level while the input signal level is held constant and that due to a single tone DSB modulation.

The effect of phase jitter caused by the transmission media to the input carrier was also studied in the experimental scheme. The phase jittering was simulated by phase modulating a r.f. carrier (amplitude modulation was balanced out) at a slow rate (of the order of a few tens of cycles), and using this phase modulated signal as the modulated carrier in DSB signal generation. The effect observed in the demodulated product was an amplitude modulation at a rate equal to the frequency of the carrier jitter.

The effect of a CW interfering carrier was also studied. In the experimental scheme using a 1.0 Kc/s modulating signal in DSB modulation, a sudden increase in the channel output was observed when the interfering signal was detuned from the incoming carrier by 1.0 Kc/s on either side of the latter. The fact is in agreement with the analysis in section 4.2.

In receiving Binary PSK signal it was observed that the *P* channel output gives the keyed information and the *Q* channel output remains substantially low so long the system is in lock. From the studies of additive noise in this case it has been confirmed that the reception of a binary PSK signal can be successfully carried out with the DSB receiver if the input SNR is adequate.

In reception of NBPM or NBFM signal it is experienced that the incoming carrier is partly being injected into the demodulating carrier and tries to get it locked with the latter even if the sideband lock voltage is reduced to zero, which causes the ratio of the outputs in the  $P$  and  $Q$  channels to be not as good as in DSB modulation reception. It seems advisable to use APC techniques for reception of such signals.

#### DISCUSSIONS

The following observations with regard to DSB signal reception may be made from the above measurements :

(i) Input r.f. amplitude must lie between certain limits for proper operation. If the input amplitude is too low the system does not lock. If, on the other hand, the input is too high the system also loses lock. This is possibly due to the fact that (since the closed loop bandwidth is larger for larger input amplitude) loop bandwidth at large value of the input amplitude is such as to permit second harmonic of the input modulation to circulate within loop and cause disruption.

(ii) Adequate locking is established if the modulating frequency for the DSB signal lies between 100 cps to 10 Kcps. Both the limits can be extended by controlling the loop parameters (gain etc.).

(iii) When the system is in lock, the output of the inphase channel will be a maximum and that of the quadrature channel will be a minimum. The actual ratio of these two outputs depends on the following :

- (a) Stability of the local oscillator frequency.
- (b) Phasing in the demodulating carriers.
- (c) Phase shift characteristics of the  $P$  and  $Q$  channels.
- (d) Initial difference frequency between the incoming carrier and the local carrier.
- (e) Phase and amplitude relationship between the two sidebands.

Under conditions of correct adjustment and if  $(A_+ = A_-)$ ,  $(\Omega = 0)$ ,  $(\psi_{p,0} = \pi/2, \phi_0 - \psi_0 = 0)$  this ratio is found experimentally to be about 0.05.

It is extremely important to ensure a fair amount of stability of the oscillator frequency when pseudo-static locking as necessary in DSB is to be established, and to have a better stability in the feedback loop. For DSB reception purposes it is expected that a crystal oscillator with frequency controllable within 400 c/s from its centre frequency will serve to remove the instability experienced in the system.

*Considerations in design of the phase locking loop:* In all coherent reception techniques the greatest single requirement is that the system remains

in lock in presence of noises and interferences with the carrier and modulation power available. The effective input power contributed by the carrier and modulation components will in general vary between fairly wide limits. One cause of this variation is the phenomenon of fading in r.f. circuits. Further, the modulation process may be such that the input power varies considerably. For example in linear systems like DSB and SSB the total power is obviously a function of the strength of instantaneous modulation, which for speech-like signals fluctuates by amounts exceeding 30 to 40 db. In amplitude keyed signals or phase or frequency keyed signals also the instantaneous amplitude of the received carrier varies with time.

Considering now the noise and interference powers one notes that these have fairly high peak factors (peak/rms). In the case of fluctuation noise, for example, the peak factor is as high as 4. It is clear then that the r.m.s. values of these interferences do not give an useful and correct estimate of their ability to disturb the circuit.

The choice of the system bandwidth is obviously a matter of compromise. Any design of locked receiver must take these factors into consideration to ensure that the circuit remains usable under the wide range of operating condition likely to prevail at one time or another. There will be two main effects of the noises and interferences present in the system. The first is that the system may lose lock and the second is that although the system remains in lock the SNR at the output is so very low that the system is useless. If the bandwidth of the locking system is small compared with the bandwidth of the modulating frequencies the second phenomenon may occur earlier as the input noise to the system increases. If the bandwidths are of the same order both may occur simultaneously.

It is certainly desirable to keep the noise bandwidth of the control loop as small as possible in order that the noises and interferences present along with the signal do not cause system to lose lock with the desired signal phase. Further large loop bandwidth will increase the probability of faulty locking of the local carrier with the incoming carrier and one sideband component when a fraction of the carrier is also present along with the sidebands. The demodulating carrier frequency may also vary as the modulation varies. A narrower system bandwidth reduces the ability of the receiver to follow such changes. It must however be ensured that the system is able to follow the perturbations of the signal phase caused by the fluctuations of the medium. These two requirements define the upper and lower limits of the closed loop noise bandwidth of the control circuit. As mentioned earlier a further complication arises out of the fact that the signal amplitude varies with time and the closed loop noise bandwidth being dependent on loop gain also varies with this amplitude. It is, therefore, preferable to select only such lowpass filters as do not condition a large change in noise-bandwidth for changes in loop gain and also to incorporate appropriate automatic gain control

circuits. Besides low audio frequency components below 300 c/s should suffer very large attenuation in the AF circuit feeding the phase discriminator in the sideband lock circuit. For otherwise these may circulate in the loop and cause disruption of the control loop.

#### CONCLUDING REMARKS

The results of this paper show that a coherent receiver utilising the information contained in the carrier and sideband components of the transmitted signal for locking the demodulating wave in the receiver is realisable in practice without undue complications provided the signal to noise ratio is adequate. The locking techniques studied have been classified as (a) carrier lock, (b) sideband lock techniques; the former is appropriate for demodulation of CW type signals and the latter for AM like signals. It should be observed that in the carrier lock case initial phase discrepancy between the incoming carrier and the demodulating one should not be greater than  $\pi/2$  rad. i.e.,  $|\phi_0 - \psi_0| \leq \pi/2$  whereas in the sideband lock case this discrepancy is to be within  $\pi/4$  rad. i.e.,  $|(\phi_+ + \phi_-)/2 - \psi_0| \leq \pi/4$ .

It should be emphasised that an efficient and satisfactory locking system should take note of all the apriori information (viz., frequency, phase and time of occurrence) available for the received signal. The nature of medium variations and the knowledge of the waveform of the transmitted message (in reception of keyed signals) should also be utilised to have a satisfactory coherent reception.

It should be obvious that techniques of locking can be utilised only if the average perturbation of the parameters over the modulation period are small. However if the power capacity of the transmitter be small and hence the SNR is low, message intervals will have to be made long in order that energy per symbol may exceed a minimum permissible value necessary for satisfactory reception. It may so happen in such a situation that information about frequency and phase desired to be estimated and stored may undergo large fluctuations over the message period. It is clear that any attempt at coherence worth the name is foredoomed if the correlation time of fluctuation is comparable with the individual message period. In such a case it is advisable to adopt what is called differentially coherent reception, where information embedded in the signal in the immediate past interval only are used as the reference for detection of a currently received signal. The reference is obviously a non-ideal one but that is possibly the best available in the circumstances.

#### ACKNOWLEDGMENTS

The authors wish to thank Prof. J. N. Bhar, D.Sc., F.N.I., for his kind interest and encouragement. Thanks are also due to Messrs. P. Dharbhowmick and B. N. Biswas for helpful suggestions.

## REFERENCES

- Chakrabarti, N. B. and Biswas, B. N., 1964, *Indian J. Phys.*, **38**, 148.  
Costas, J. P., 1956, *Proc. IRE*, **44**, 1713.  
Davonport and Root, 1958, "*Random Signals and Noise*", McGraw-Hill Book Company, Inc.  
Doelz, M. L., Heald, E. T. and Martin, D. L., 1957, *Proc. IRE*, **45**, 686.  
Mazumdar, D., Pal, H. and Datta, A. K., 1963, *M.Tech. Report on "Binary Transmission and Reception"*, Department of Radio Physics and Electronics, University of Calcutta.  
Montgomery, G. F., 1954, *Proc. IRE*, **42**, 447.  
Norgaard, D. E., 1956, *Proc. IRE*, **44**, 1718.  
Smith, R. A., 1951, *Proc. IRE*, **III**, **98**, 401.  
Tuckor, D. G., 1952, *Wireless Engineer*, **29**, 184.



# ON THE MAGNETIC SUSCEPTIBILITY OF PURE AND IMPURE COPPER METAL

A. V. SUBRAHMANYAM

DEPARTMENT OF PHYSICS & METEOROLOGY, INDIAN INSTITUTE OF TECHNOLOGY, Kharagpur

(Received March 24, 1966; Resubmitted June 6, 1966)

**ABSTRACT.** Temperature variation of magnetic susceptibility of copper metal and copper metal with trace of nickel impurity have been measured. An accurate susceptibility balance with an electronic detection system has been described. The mass susceptibility of pure copper is independent of temperature and copper contaminated with nickel shows anomalous temperature variation. A theoretical estimate of the susceptibility of copper has been made.

## INTRODUCTION

The magnetic susceptibility of high purity copper has been the subject of investigation in a number of papers. de Haas and van Alphen (1933) observed a monotonic increase of susceptibility with decreasing temperature. Bitter *et al* (1941) found that the susceptibility first increased by 3% as the temperature was lowered from 300°K to 63°K, but subsequently decreased by about 35% between 63°K and 14°K. Bowers (1956) reexamined the magnetic susceptibility of high purity copper between 300°K and 1.5°K and reported a temperature independent susceptibility. Bower's result confirms the predictions of the free electron model, wherein one would expect the magnetic susceptibility of copper metal to be substantially independent of temperature. Recently van Itterbeek and Du Chateau (1957) have observed that the susceptibility of copper metal decreased by 18% between 17°K and 1.62°K. This decrease has been ascribed to the presence of trace impurities of Ni and Fe. Kaufmann and Starr's (1943) earlier measurement on moderately pure copper metal and dilute Cu-Ni alloys also indicated an anomalous temperature variation of susceptibility both for the pure metal and the alloy. We suspect that the anomalous variation of magnetic susceptibility reported by different workers, is due to the contamination of copper with magnetic impurities. With this in view the measurement of magnetic susceptibility of very pure copper and copper with trace nickel impurity has been undertaken.

## EXPERIMENTAL

The measurements undertaken in this work require very accurate determination of mass susceptibilities of the order of  $10^{-7}$  C.G.S. units; hence a magnetic balance with a cryostat suitable for the purpose was designed and built in this laboratory following the basic design of quartz fibre microbalance of Bose (1947).

The apparatus of Bose was very convenient for accurate single crystal work. But the whole arrangement was very delicate and difficult to handle and because of the manual control it was not free from personal errors and often external disturbing factors and zero shifts made it difficult to have reproducible value. Therefore several modifications were incorporated to increase the sensitivity, stability and robustness of the balance.

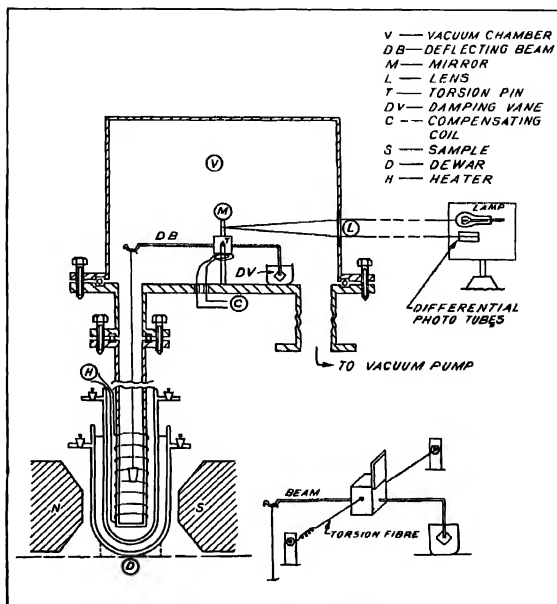


FIG. 1 MAGNETIC MICRO BALANCE

The balance beam was made from quartz rod and (fig. 1) suspended at the middle with horizontally stretched phosphor bronze strips ( $30\text{ mm} \times 0.287\text{ mm} \times 0.022\text{ mm}$ ) cemented to the beam. The other ends of these strips were soldered to the ends of two torsion pins passing horizontally through two upright rectangular brass pieces. The specimen to be studied was suspended to one end of the balance beam with a fine tungsten fibre. In order to protect the balance from spurious vibrations a mica damping vane, dipping in silicone oil, was attached to the other end of the balance beam. The whole assembly was enclosed in a brass case provided with a glass window. Provisions were made to create a vacuum of the order of  $10^{-6}$  mm of Hg in the experimental chamber. This was necessary to avoid convection disturbance and also for excluding the contamination of the sample due to

oxidation. A photoelectric difference amplifier was employed for observing the magnetic force. A spot of light from a stabilised 12 volt lamp was focussed by a lens system and after reflection from the mirror attached to the balance beam was again focussed by another lens system and was allowed to illuminate the cathodes of two photoelectric tubes mounted horizontally one over another. The output from the phototubes was fed to a difference amplifier as shown in Fig. 2. The

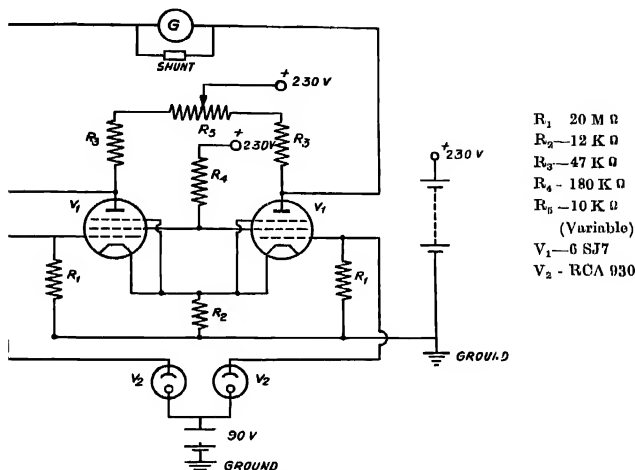


Fig. 2. Schematic diagram of the detecting circuit

difference current was amplified and fed to a shunted galvanometer, and the deflection in the output galvanometer was always made full scale (100 divisions) by adjusting the shunt to the proper value. This was done to maintain a constant deflection sensitivity. The zero drift in the amplifier was appreciable for the first ten minutes, but no further zero drift was observed even when the amplifier was used for 4 to 5 hours.

The restoration of the balance beam to the original position was effected with a compensating coil of 1 cm diameter and 250 turns of insulated copper wire (47 SWG) fixed horizontally to the beam of the balance with its axis passing through the centre of the beam. This follows the method of Neogy and Lal (1962). The current through the coil was regulated by means of five variable resistances in series with the coil. The coil being placed in the stray field  $H$  of the magnet experienced a couple  $(NHIA/10)\text{g-cm}$  where  $N$ , the number of turns of the coil and  $A$ , the area of cross section of the coil and  $I$ , the current through the coil in amperes. If  $I$  was the current required to compensate the torque on the sample

of mass  $m$  and mass susceptibility  $\chi$  and  $I_s$  for the standard sample of mass  $m_s$ , mass susceptibility  $\chi_s$ , (Bose *et al.*, 1963) then  $\chi$  is given by ;

$$\chi = \frac{I}{I_s} \frac{m_s}{m} \left[ \chi_s - \frac{k_a}{\rho_s} \right] + \frac{k_a}{\rho}$$

where  $K_a$  the volume susceptibility of air at a temperature  $T^\circ\text{K}$ ;  $\rho_s$  and  $\rho$  the densities of standard sample and the sample under study, respectively. The current in each case was estimated by measuring the potential drop, across a standard resistance of 10 ohms with a microvolt Kaycee potentiometer. Each measurement was repeated five times and error was found to be less than 0.1%. An air cooled electromagnet of field 10000 gauss with a gap of 5 cm was used.

The temperature of the sample was varied from 1000°K to 90°K. Liquid oxygen cryostat was constructed following the design of Bose *et al.* (1963). In this arrangement any temperature between 300°K to 90°K was kept constant for a long time within 0.5°K. The control was made automatic with the help of a gas-thermometer relay system, which operated a non-inductive electric heater in the experimental chamber. The temperature was read with a calibrated copper constantan thermocouple.

The calibration of the balance was done with conductivity water whose mass susceptibility was taken to be  $-7.214 \times 10^{-7}$  emu/gm at 300°K. Mass susceptibility of five crystals of potassium chloride supplied by Harshaw and Co., U.S.A., was compared with the conductivity water and the mean value was found to be  $-5.179 \times 10^{-7}$  emu/gm at 300°K which was in agreement with the previously reported values to within 0.2%. This crystal was used as a secondary standard in subsequent measurements. For a further check five crystals of sodium chloride were grown in this laboratory and the mass susceptibility was compared with the KCl crystal. The observed mean value was found to be  $-4.995 \times 10^{-7}$  emu/gm at 300°K which agreed with the earlier values (Chowdhury, 1959) to within 0.5%

## RESULTS AND DISCUSSION

The pure copper specimen (A) was supplied by Johnson and Mathey and had the following impurity contents :

Element	Approx. estimate of quantity present
Silver	0.0002%
Lead	0.0004%
Nickel	0.0003%

The mass susceptibility was found to be  $-0.91 \times 10^{-7}$  emu/gm which is higher than the value observed by van Itterbeek and W. Du Chateau (1957) by about 6%. The specimen showed no field dependence even at lower fields. In table I we

have collected the theoretical values which may be compared with our experimental value.  $\chi_s$  is the free electron value for the spin contribution (Korring, 1950). The value of core susceptibility  $\chi_c$  is derived from direct calculations from the electronic wave functions. The orbital contribution  $\chi_0$  used is the Landau-Peierls free electron value.  $\chi_N$  is the nuclear susceptibility which is about 1/5th of the value of  $\chi_S$  (Bowers, 1956). It can be seen that there is no serious disparity between calculated and the experimental value ( $\chi_{Th}$  the  $\chi_{Ex}$ ). The value obtained by van Itterbeek and the present result are in good agreement amongst themselves and closer to the theoretically estimated value

TABLE I

Theoretical estimate of the mass susceptibility of copper in emu/gm, compared to the experimental

	$\chi_{Th}$	$\chi_{Ex}$
$\chi_C$	$-1.91 \times 10^{-7}$	$-0.83 \times 10^{-7}$ (Bowers)
$\chi_S$	$+1.10 \times 10^{-5}$	$-0.87 \times 10^{-7}$ (Van Itterbeek)
$\chi_N$	$+0.22 \times 10^{-7}$	$-0.80 \times 10^{-7}$ (Kaufmann & Starr)
$\chi_0$	$-0.37 \times 10^{-7}$	
Total		
$\chi_{Th}$	$-0.96 \times 10^{-7}$	$-0.91 \times 10^{-7}$ (Present Work)

The temperature dependence of the susceptibility observed by us does not agree with that found by earlier workers. Fig. 3 shows that sample A has temperature independent susceptibility between 600°K to 100°K. This is in good agreement with Bowers' result on copper metal (99.999% purity). A small temperature dependent term observed by Bowers has been ascribed by him to the presence of residual paramagnetic impurity as well as nuclear susceptibility. In the temperature range we have worked the nuclear susceptibility should contribute a temperature dependent term  $\sim 0.3\%$  which is just outside our experimental accuracy. Thus it seems likely that the susceptibility of pure copper is substantially independent of temperature.

The mass susceptibility of specimen B (deliberately contaminated specimen A with nickel) was found to be  $-0.92 \times 10^{-7}$  emu/gm at 295°K. This specimen showed temperature independent susceptibility in the high temperature range (295°K to 600°K) but in the low temperature range (295°K to 100°K) it showed an increase of diamagnetic susceptibility by about 7.5%. This temperature variation is similar to that observed by Bitter *et al.* (1941) on moderately pure copper specimen.

The specimen C was prepared in an induction furnace by melting appropriate quantity of copper and nickel in recrystallized alumina crucible using helium

atmosphere. The details of the method of preparation have already been described by Dutta Roy (1961). The alloy contained 99.9 weight percent of copper and 0.1 weight percent of nickel. The sample was annealed for 24 hours in a vacuum annealing furnace at 500°C. The mass susceptibility of this specimen was found out to be  $-0.758 \times 10^{-7}$  emu/gm at 295°K and was field independent at lower fields. The diamagnetic susceptibility decreased monotonically with the lowering of temperature (600°K to 100°K). This variation (fig. 3) is somewhat

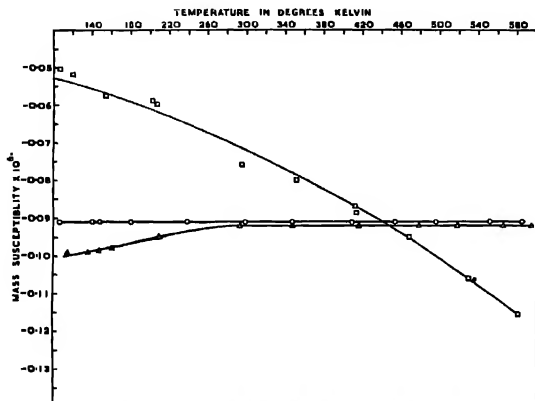


FIG. 3 SUSCEPTIBILITY VARIATION OF PURE AND IMPURE COPPER

O — PURE COPPER (A)  
 Δ — IMPURE COPPER (B)  
 □ — IMPURE COPPER (C)

expected because nickel, if present as trace impurity in copper, contributes a paramagnetic term due to the presence of  $3d$  holes in the alloy. But Curie-Weiss law does not account for this observed temperature variation and only a three constant formula of the type  $AT+B+C/T$  suggested by Kaufmann and Starr (1943) for copper-nickel alloys gives an approximate fit to the experimental temperature susceptibility curve (fig. 3). We have not attempted a rigorous analysis of the experimental results on the basis of the above three constant formula since the origin of the  $AT$  term is obscure and no theory of magnetism suggests such a term. Also the observed temperature variation in specimen B and C can not be connected to the thermal expansion (or contraction), otherwise similar temperature variation of mass susceptibility would have been observed in the case of pure copper (specimen A).

In conclusion the present experimental result on pure copper suggests that the susceptibility is substantially independent of temperature but in impure copper

with nickel as trace impurity susceptibility shows an anomalous temperature variation.

#### ACKNOWLEDGMENTS

The author is deeply indebted to Dr. S. K. Dutta Roy for suggesting the problem and for his guidance throughout the course of this investigation. Grateful thanks are due to Mr. M. L. Mukherjee of the Indian Institute of Technology, Kharagpur, for his help in the experimental set-up.

#### REFERENCES

- Bitter, *et al.*, 1941, *Phys. Rev.*, **60**, 134.  
Bose, A., 1947, *Indian J. Phys.*, **21**, 277.  
Hose, A., Dutta Roy S. K., Ghosh, P. K., and Mitra, S., 1903, *Indian J. Phys.*, **37**, 505  
Bowers, R., 1965, *Phys. Rev.*, **102**, 1486.  
Chowdhury, A., 1959, *Thesis, I I T.*, Kharagpur  
de Haas and van Alphen, 1933, *Leiden Comm* 225b  
Dutta Roy, S. K., 1961, *Thesis, Leeds Univ.*  
Hill, A. V., 1947, *Jour. Sci. Inst.*, **25**, 225.  
Kaufmann, A. R. and Starr, C., 1947, *Phys. Rev* , **63**, 445.  
Korring, C., 1950, *Physica*, **16**, 601.  
Neogy, D. and Lal, R. B., 1962, *Journal of Scientific & Industrial Research* **21B**, 153.  
van Ittorbeck and Du Chateau, W., 1957, *Physica*, **23**, 169.

## COUNTER/FREQUENCY METER

S. S. AGARWAL AND P. S. Gill

CENTRAL SCIENTIFIC INSTRUMENTS ORGANIZATION, CHANDIGARH, INDIA

(Received April 20, 1966)

**ABSTRACT.** A transistorised digital frequency meter capable of operating up to 2 Mc/s has been described. The decade circuit uses 1-2-4-8 weighted working code and nor-transistor resistor logic system has been used for the decimal display.

The counter is the most reliable instrument for an accurate measurement of frequency, period, time interval, frequency ratio of the two applied signals and for the counting of regular or random electrical pulses. It could also be used for the measurement of non-electrical parameters by the use of suitable transducers

The counter consists of four main units.

- (1) Input circuit which amplifies and shapes the incoming signal in order to present pulses of uniform amplitude and rise time to the succeeding circuit.
- (2) The decades with display units which totalize the incoming counts and transform these into numerical display.
- (3) The time base which consists of the crystal oscillator and decades, supplies the precisely known increment of time during which pulses are counted.
- (4) Gate control which starts and stops the counting.

Fig. 1 shows the block diagram for frequency measurement. For other measurements mentioned above the same blocks are used but connected in a slightly different way.

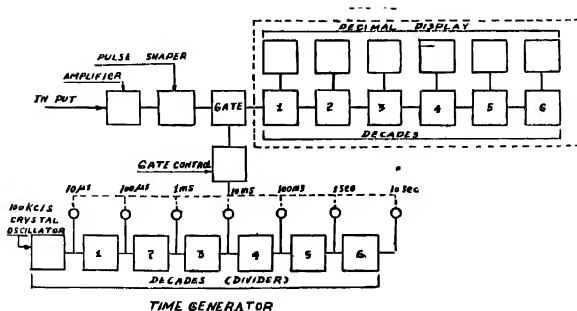


Fig. 1



An accurate measurement of frequency is made by counting the number of pulses for a precisely controlled time interval. The measurement of time or period is made by counting time base pulses for a period controlled by the incoming signal whereas frequency ratio is determined by counting the number of pulses of one signal for a period controlled by the other signal.

Technically, the most important section of a frequency meter is the decade and its associated display unit and these will be described here.

#### DECADE UNIT

Basically, the decade circuit consists of four identical binary stages cascaded in series such that there would be one pulse in the output for every sixteen input pulses. However, the circuit has to be modified suitably in order that the scale of sixteen is reduced to a decade or scale of ten. Broadly speaking, this could be achieved by using either the feedback or the reset technique.

The feedback technique of modifying binary counts, although simple and economical, is not very satisfactory when operating at high frequencies. One reason is that the delay around the feedback loop and its associated decade must be less than the periodic time of the input signal. Secondly, any stage being supplied with feedback pulse in addition to some external input must be capable of resolving the two, in order that it shall not ignore the feedback pulse. These factors limit the operation of the circuit at high frequencies. These disadvantages are overcome by using the 'reset' technique.

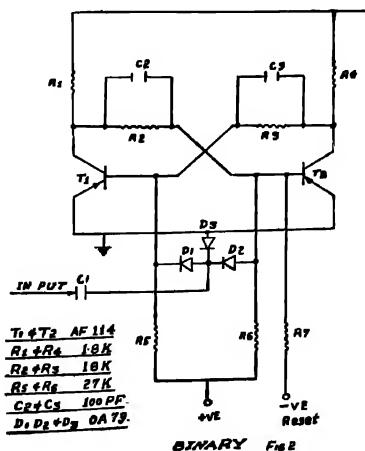


Fig. 2

The reset technique described here employs two Gate circuits such that the code of the resulting decade remains as for the pure binary 1-2-4-8 weighted working.

#### GATE CIRCUIT

The technique used to modify the normal four-binary count of sixteen to ten is simply to allow the circuit to count up to 9 in the normal fashion and make the 10th count reset the binaries into their starting condition. The count of 9 leaves the counter in the binary code condition 1001 and input pulse 10 would normally alter this to 1010. However, the change of state of the fourth binary on the eighth count closes gate  $G_1$  and opens the gate  $G_2$  so that when 10th pulse comes in, it changes over the condition of the fourth binary instead of the second, thus resetting the counter to 0000 condition.

These two gates  $G_1$  and  $G_2$  have been so arranged that when transistor  $T_8$  is in saturation, gate  $G_1$  is open and  $G_2$  closed and vice versa when  $T_8$  goes into cut off.

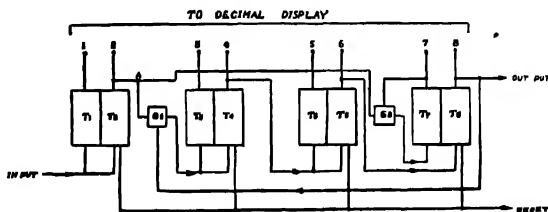


Fig. 3

#### DECADE OPERATION

Consider Fig. 3. Initially the transistors  $T_2$ ,  $T_4$ ,  $T_6$  and  $T_8$  are in saturation and with each successive incoming pulse, the condition of these transistors is as shown in Table I.

Table I shows that all binaries behave conventionally up to 9 input pulses i.e. the incoming pulses at A pass through gate  $G_1$  to the second binary and do not pass through gate  $G_2$  as it is closed, transistor  $T_7$  being in cut-off condition. However, eighth input pulse changes the condition of binary 4, bringing transistor  $T_7$  into saturation and  $T_8$  into cut-off with the result that gate  $G_1$  is closed and  $G_2$  is open. Thus subsequent pulses at A i.e. input pulse 10, will not affect the condition of binary 2 and instead directly changes the condition of the fourth binary, thus bringing transistors  $T_2$ ,  $T_4$ ,  $T_6$  and  $T_8$  in saturation, which is the condition for zero input. Hence zero condition appears once for every ten input pulses i.e. the system is a decade or scale of ten.

• TABLE I

Transistor No. →	Binary I		Binary II		Binary III		Binary IV	
	$T_1$	$T_2$	$T_3$	$T_4$	$T_5$	$T_6$	$T_7$	$T_8$
Pulse No ↓								
0	1	0	1	0	1	0	1	0
1	0	1	1	0	1	0	1	0
2	1	0	0	1	1	0	1	0
3	0	1	0	1	1	0	1	0
4	1	0	1	0	0	1	1	0
5	0	1	1	0	0	1	1	0
6	1	0	0	1	0	1	1	0
7	0	1	0	1	0	1	1	0
8	1	0	1	0	1	0	0	1
9	0	1	1	0	1	0	0	1
10	1	0	1	0	1	0	1	0
Weights	1		2		4		8	

0 = Conduction (Saturation)

1 = Non Conducting (cut off)

The reset count switch enables the counter to be restored to its zero condition manually from any random setting. When the switch is in the reset position, transistors  $T_2$ ,  $T_4$ ,  $T_6$  and  $T_8$  are brought into saturation by the application of external negative pulses to their bases thereby compelling the counter to adopt its zero condition.

## BINARY

Fig. 2 shows a conventional binary circuit capable of operating up to a counting speed of 2Mc/s reliably. The trigger differentiating circuit uses a diode  $D_3$  instead of the conventional resistive load and diodes  $D_1$  and  $D_2$  serve the purpose of steering the trigger pulses to the appropriate points in the circuit.

## DECIMAL DISPLAY

The information contained in a decade circuit can be transformed into a decimal display by various methods, the more popular being the use of meters responding to weighted currents and the use of diodes matrix system with Nixie tubes (for in-line readout) or with Neon indicators. In the circuit described

here, NOR transistor resistor logic system has been used with Neon indicators. This logic system by making use of resistors instead of diodes as in the diode matrix

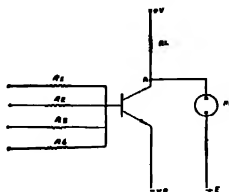


Fig. 4

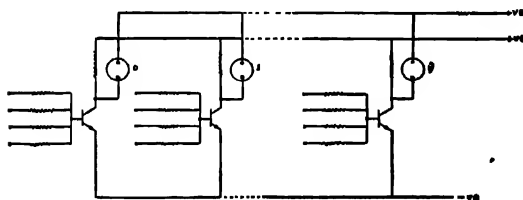


Fig. 5

system, makes it more economical and reliable, too, if the resistors are suitably chosen. This logic system can be used with Nixie tubes also.

Fig. 5 shows the circuit for the numerical display; complete circuit has, however, been shown for digits 0, 1 and 9. It uses ten NPN transistors for driving the ten Neon indicators.—one for each digit. The bases of these transistors are coupled to the collectors of the decade circuit through resistors in such a manner that only one transistor is turned on at a time which instantaneously corresponds

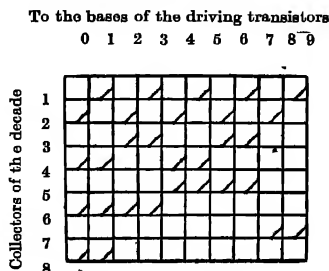


Fig. 6

to the number of counts stored in the decade. In normal fashion 40 coupling resistors have to be used i.e. four resistors for each digit. A few resistors have, however, been eliminated without in any way impairing the working of the circuit. This is shown in Fig. 6.

Let us now consider the operation of the circuit shown in Fig. 4 which is only for one digit. When the inputs of all the resistors are at '0' potential, corresponding transistors in the decade circuit are in saturation indicating the condition for the said digit. The driving transistor will then be turned on and the collector potential will fall towards zero so that the voltage applied across the Neon indicator will be  $E$  volts which is sufficient to strike the neon indicators and the corresponding digit will light up. Now, if the input of even one of the resistors is at a negative potential, not all the corresponding transistors in the decade circuit are in saturation indicating that this is not the condition for the said digit. The driving transistor will therefore be cut off and the collector potential will rise towards supply voltage  $V$  so that the voltage applied across the neon indicator will be  $E-V$  volts which is not sufficient to strike the neon indicator and therefore the neon will not glow. In short, the circuit discussed can be considered as a gating circuit formed by four resistors followed by a transistor inverting amplifier.

#### DESIGN CONSIDERATIONS

To ensure a satisfactory working of the circuit (Fig. 4) two conditions must be fulfilled.

1. When the inputs of all the resistors are at zero potential i.e. no input signal is applied, the transistor should be in saturation. To ensure this, the emitter is kept slightly negative.
2. When there is an input signal on any one of the resistors, the transistor should be in cut-off condition i.e. the amplitude of the input signal should be sufficient to bring the transistor into the said condition.

#### CONCLUSION

The decimal display circuits described earlier (Scollar, 1965; Young, 1965) have used the conventional diode matrix system. T. D. Towers (1964) in his discussion has mentioned that there is hardly any standard cheap and reliable read-out device. The present discussion makes use of only thirty resistors logic system and as such it can be considered to be more economical and reliable. This system could also be used with decades having 1-2-2-4 and 1-2-4-2 code system. In addition, the circuit employed for the decade uses minimum number of components and operates satisfactorily up to 2 Mc/s with a minimum input signal of 100 mV peak.

## ACKNOWLEDGMENT

The authors wish to express their thanks to Mr. B. P. Mital for his active help and work done in the design and development of the circuit throughout and also in the preparation of the manuscript.

## REFERENCES

- Barrow, C. W. M., 1964, *Electronic Engineering*, **36**, 600.  
Scollari, I., 1965, *Electronic Engineering*, **37**, 468  
Towers, T. D., 1964, *Wireless World*, **79**, 569.  
Young, J. F., 1965, *Electronic Engineering*, **37**, 161.

## *Letters to the Editor*

*The Board of Editors does not hold itself responsible for opinions expressed in the letters published in this section. The notes containing short reports of original investigations communicated to this section should not contain many figures and should not exceed 500 words in length. The contributions reaching the Secretary by the 15th of any month may be expected to appear in the issue for the next month. No proof will be sent to the author*

### FLUCTUATIONS AND THERMAL CONDUCTIVITY OF CO<sub>2</sub> IN THE CRITICAL REGION

A. K. BARUA AND T. K. RAI DASTIDAR

INDIAN ASSOCIATION FOR THE CULTIVATION OF SCIENCE, CALCUTTA-32

(Received August 19, 1966)

The measurement of the thermal conductivity of CO<sub>2</sub> in the critical region has recently been receiving considerable attention (Guildner 1958; Michels *et al.*, 1962b). The most interesting feature of these measurements is the appearance of a sharp maximum in the thermal conductivity vs. density curve near the critical density. It has been observed (Michels and Strijland 1952) that the specific heat of CO<sub>2</sub> also shows a similar behaviour in the critical region. This has led Michels *et al.* (1962c) to suggest that the variation of thermal conductivity in the critical region is in some way connected to the variation of specific heat in that region. They have also suggested that due to the formation and the breaking up of the clusters in the critical region additional heat may be transferred as observed in dissociating systems (Hirschfelder 1957, Butler and Brokaw, 1957). The problem of heat transfer in the critical region has been treated along these lines by Barua and Das Gupta (1966) without much success. It, however, appears that a factor which has not yet been considered for explaining the thermal conductivity is the fluctuations in the critical region. Recently, Fixman (1965) has explained the heat capacity of CO<sub>2</sub> in the critical region fairly well by considering density fluctuations given by

$$\langle (\delta n)^2 \rangle = \int \langle n_k n_{k'} \rangle \exp [i(\mathbf{k} + \mathbf{k}') \cdot \mathbf{R}] d\mathbf{k} d\mathbf{k}' \quad (1)$$

where the symbols have their usual meanings.

Michels and Sengers (1962a) made several tests to find whether there was any significant convection effect in their measurement of the thermal conductivity of CO<sub>2</sub> in the critical region. The most important of these tests is the variation

of the temperature difference  $\Delta T$  between the hot and the cold plates of conductivity cell. From the lack of variation of the measured thermal conductivity with  $\Delta T$ , they concluded that their measurements were convection-free. However, density fluctuations in the critical region are not dependent on  $\Delta T$ . Consequently the convection due to this factor will not change effectively with  $\Delta T$ . This means that convection due to density fluctuations is an inherent property of the critical region which cannot be avoided by any modification of the apparatus for thermal conductivity measurement. This effect will be maximum at the critical point as the density fluctuation is also maximum at that point. Very recently an experiment on convection near the critical region has been performed by Hahne (1965). He has observed a very large increase of heat transfer at the critical region which may at least be partially due to density fluctuations.

At present we have no theoretical treatment to calculate the effect of convection due to density fluctuations on the thermal conductivity measurement near the critical region. It is quite possible when this convection effect is accounted for the observed maximum in the thermal conductivity vs. density curve for  $\text{CO}_2$  may disappear.

## REFERENCES

- Baura, A. K. and Das Gupta, A., 1966, *Appl. Sci. Research*, **15**, 313.  
Butler, J. N. and Brakaw, R. S., 1957, *J. Chem. Phys.*, **26**, 1636.  
Fixman, M., 1965, *J. Chem. Phys.*, **42**, 196.  
Guildner, L. A., 1958, *Proc. Nat. Acad. Sciences, U.S.A.*, **44**, 1149.  
Hahne, E. W. P., 1965, *Int. J. Heat & Mass Trans.*, **8**, 481.  
Hirschfelder, J. O., 1957, *J. Chem. Phys.*, **26**, 282.  
Michels, A., and Sengers, J. V., 1962a, *Physica*, **28**, 1238.  
Michels, A., Sengers, J. V. and Van der Gulik, P. S., 1962b, *Physica*, **28**, 1201.  
\_\_\_\_\_, 1962c, *Physica*, **28**, 1210.  
Michels, A. and Strijland, J. C., 1952, *Physica*, **18**, 613.



# EFFECT OF POLARISATION ON THE ELASTIC ELECTRON SCATTERING BY HELIUM ATOM

R. JHA, S. N. BANERJEE AND N. C. SIL

DEPARTMENT OF THEORETICAL PHYSICS, INDIAN ASSOCIATION FOR THE CULTIVATION OF SCIENCE, JADAVPUR, CALCUTTA-32.

(Received May 6, 1966)

**ABSTRACT.** The  $S$ -wave phase-shifts ( $\eta_0$ ) in the elastic  $\bar{e}$ -He scattering have been calculated by Hulthén's (1944) variational method taking into account polarisation effects due to the virtual excitation to  $2^1S$  state, but neglecting exchange. The calculated phase-shift values compare favourably with those of Westin as quoted by Mott and Massey (1965).

## INTRODUCTION

In problems of elastic scattering of electrons by atoms, the inclusion of the influence of exchange and polarisation effects brings in additional complications. Both the effects, due to exchange and polarisation, decrease, though differently, with increasing energy. The exchange issue arises out of the indistinguishability of the incoming and bound electrons and the polarisation effect is due to the distortion of the atomic cloud by the influence of the incoming electron.

The first theoretical attempt to investigate the  $\bar{e}$ -He elastic scattering considering exchange effect has been made by Massey and Mohr (1931). They have concluded that the inclusion of the exchange effect modifies appreciably the phase-shift below 15 eV. McDougall (1932) has computed the  $S$ -wave phase-shifts of elastic scattering of electron by helium atom neglecting exchange and polarisation effects. Using the simple Hylleraas wavefunction for the ground state of the helium atom, Morse and Allis (1933) have taken into account the exchange effect in their calculation of the same problem and have solved the resulting integro-differential equation numerically. Recently LaBahn and Callaway (1964, 1966) have carried out phase-shift computation on elastic  $\bar{e}$ -He collision taking into account both the exchange possibility and the polarisation effect. Williamson and McDowell (1965) also have solved the same problem but with an open-shell wave function. The present authors (1966) have applied the variational method to the same problem. In all these attempts, polarisation effect has been considered by properly modifying the atomic static potential part. This modification manifests itself by the presence of extra polarisation terms in addition to the already existing static potential part.

Here, however, instead of modifying the static potential to include the polarisation effect, we have taken into account the distortion of the original ground-state

wave function of the atom in the presence of the incoming electron, in analogy with our previous work (1965) on  $\bar{e}$ -H scattering to explain the resonance phenomena in the elastic electron scattering experiments of Schulz (1964). We assume that the distortion of the initial  $1S$  state is in the form of a superposition of higher excited states induced temporarily when the incident electron is near the atom but when the electron is far away, the atom comes back to its original  $1S$ -state. For simplicity of calculation we have considered the virtual excitation to the next higher possible state only with the same symmetry (i.e.  $2^1S$  state), as such the exchange effect has not been considered in our formulation.

### THEORY

The wave-function  $\bar{\psi}(r_1, r_2, r_3)$  of the system of three electrons moving in the field of a proton satisfies the wave equation  $(H-E)\bar{\psi}(r_1, r_2, r_3) = 0$

with  $H = -\frac{\nabla_1^2}{2} - \frac{\nabla_2^2}{2} - \frac{\nabla_3^2}{2} - \frac{2}{r_1} - \frac{2}{r_2} - \frac{2}{r_3} + \frac{1}{r_{12}} + \frac{1}{r_{13}} + \frac{1}{r_{23}}$  in atomic units (i.e.

$e = m = \hbar = 1 = a_0$ ); here  $r_1, r_2, r_3$  are the co-ordinates of the three electrons referred to the helium nucleus,  $r_{12}, r_{23}, r_{13}$  are the distances between the two of them,  $E$  is the total energy of the system (in a.u.)

The total wave-function  $\psi(r_1, r_2, r_3)$  is approximated as

$$\psi(r_1, r_2, r_3) = \chi(r_1, r_2, r_3) F(r_3) \quad (1)$$

with  $\chi(r_1, r_2, r_3) = \psi_1(r_1, r_2)(1 - \alpha e^{-\lambda r_3}) + \psi_2(r_1, r_2)\beta e^{-\mu r_3}$

and  $\chi$  satisfies the normalisation condition  $\iint \chi^* \chi dr_1 dr_2 = 1$ ; hence  $2\alpha = \beta^2$  and  $\lambda = 2\mu$  (neglecting higher powers of  $\beta$ )

For convenience of calculation, we have taken  $\lambda = Z$  (i.e. 27/16), the effective charge.

The trial function  $F(r_3)$  is chosen in the form

$$F(r_3) = \left\{ \frac{\sin kr_3}{kr_3} + (a + be^{2r_3})(1 - e^{2r_3}) \frac{\cos kr_3}{kr_3} \right\}$$

$a$  and  $b$  are adjustable variational parameters and  $k$  is the Wave-number of the incoming electron.

The trial wave function has the asymptotic form  $\frac{\sin kr_3}{kr_3} + a \frac{\cos kr_3}{kr_3}$  and is finite at the origin. The  $S$ -wave phase-shift is given by  $\eta_0 = \tan^{-1} a$ .

Calculation of 'L'

The variational integral  $L$  now stands as

$$\begin{aligned} L = & -\frac{1}{2} \int \psi^*(r_1, r_2, r_3) (\nabla_1^2 + \nabla_2^2 + \nabla_3^2) \psi(r_1, r_2, r_3) dr_1 dr_2 dr_3 \\ & -2 \int \left( \frac{1}{r_1} + \frac{1}{r_2} + \frac{1}{r_3} \right) \psi^*(r_1, r_2, r_3) \psi(r_1, r_2, r_3) dr_1 dr_2 dr_3 \\ & + \int \left( \frac{1}{r_{12}} + \frac{1}{r_{13}} + \frac{1}{r_{23}} - E \right) \psi^*(r_1, r_2, r_3) \psi(r_1, r_2, r_3) dr_1 dr_2 dr_3 \end{aligned}$$

the trial wave function  $\psi$  is as given by the expression (1).

Using the eigen-value equations

$$\left( \nabla_1^2 + \nabla_2^2 + \frac{4}{r_1} + \frac{4}{r_2} - \frac{2}{r_{12}} + 2\epsilon_1 \right) \psi_1(r_1, r_2) = 0$$

$$\text{and} \quad \left( \nabla_1^2 + \nabla_2^2 + \frac{4}{r_1} + \frac{4}{r_2} - \frac{2}{r_{12}} + 2\epsilon_2 \right) \psi_2(r_1, r_2) = 0$$

where  $\psi_1, \epsilon_1$  and  $\psi_2, \epsilon_2$  are the wavefunctions and eigen-energies of the atom in the ground state (1S) and excited 2<sup>1</sup>S state (singlet) respectively, we get

$$\begin{aligned} -2L = & \int \left( 1 - \frac{\beta^2}{2} e^{-\mu r_3} \right) F(r_3) \left( \nabla_3^2 + \frac{4}{r_3} + 2E - 2\epsilon_1 \right) \left( 1 - \frac{\beta^2}{2} e^{-\mu r_3} \right) F(r_3) dr_3 \\ & + \beta^2 \int e^{-\mu r_3} F(r_3) \left( \nabla_3^2 + \frac{4}{r_3} + 2E - 2\epsilon_2 \right) e^{-\mu r_3} F(r_3) dr_3 \\ & + 4\beta^2 \int (\psi_1^2 - \psi_2^2) \left( \frac{1}{r_{13}} - 2\mu r_3 \right) F^2(r_3) dr_1 dr_2 dr_3 \\ & - 8\beta \int \psi_1 \psi_2 \frac{1}{r_{12}} e^{-\mu r_3} F^2(r_3) dr_1 dr_2 dr_3 \\ & - 4 \int \psi_1^2 \frac{1}{r_{13}} F^2(r_3) dr_1 dr_2 dr_3 \end{aligned}$$

To evaluate the above explicitly, properly orthogonal analytic (approximate).

functions for the ground state and excited state have been used (Marriott, 1957). They are as follows :

$$\psi_1(r_1, r_2) = \frac{z^3}{\pi} e^{-Z(r_1+r_2)}$$

$$\psi_2(r_1, r_2) = C[e^{-2r_1}(e^{-fr_2} - gr_2e^{-hr_2}) + e^{-2r_2}(e^{-fr_1} - gr_1e^{-hr_1})]$$

where  $C = \frac{2^{1/4} \times .478}{\pi}$  ;  $f = 1.136$ ,  $g = .317$  and  $h = .464$ .

The variational method due to Hulthén starts from the integral  $L = \int \psi^*(H-E)\psi dr_1 dr_2 dr_3$ . The value of the phase-parameter  $a$  is obtained from the following set of equations

$$L(\beta; b, a) = 0$$

$$\frac{\partial L}{\partial \beta} = 0$$

$$\frac{\partial L}{\partial b} = 0$$

It is to be noted that cubes and higher powers of  $\beta$  in  $L$  have been neglected.

The evaluation of  $L$  is now straight forward, though extremely tedious, the numerous integrals occurring therein can finally be reduced to the following three types :

$$A_{v\lambda} = \int_0^\infty (r)^v e^{-\lambda r} dr$$

$$B_{v\lambda} = \int_0^\infty (r)^v e^{-\lambda r} \cos 2kr dr$$

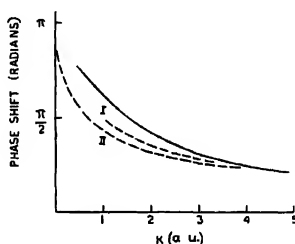
$$C_{v\lambda} = \int_0^\infty (r)^v e^{-\lambda r} \sin 2kr dr$$

In the low energy region we first find the solutions of the quadratic equation  $L = 0$  obtained by putting  $\beta = 0$ . One of the solutions agrees with the results of McDougall (1932). Now to find the required solution of the fourth degree equation at low energy we search for the root in the neighbourhood of the particular solution mentioned above; a root is obtained differing only slightly from the particular solution chosen of the quadratic equation. Once the root has been fixed for a particular low energy, the phase-shifts for higher energies have been obtained by solving the fourth degree equation and using the continuity property of the phase-shift.

# RESULTS AND DISCUSSIONS

We have evaluated the *S*-wave phase-shift values for the case  $b = 0$  in the trial function  $F(r_3)$  for energies ranging from 13.6 eV to 160.6 eV by using only the coupling of 1S and the virtually excited 2'S state.

We have given a plot of  $\eta_0$  against  $K$  in the figure. We find that present values of  $\eta_0$  agree favourably with the experimental values. Recently Schulz (1966) and Kuyatt *et al.* (1965) have observed resonances in the elastic electron scattering by helium at energy  $19.3 \pm 1$  eV. Due to the close coupling of 2'S and 2'S states, it is quite likely that resonance effect cannot be reproduced in this formalism, where we have neglected the contribution due to the exchange effect thus excluding the possibility of virtual excitation to the 2'S state (cf Mott and Massey, 1965).



The *S*-wave phase-shift  $\eta_0$  for elastic scattering of electron by helium atom plotted against  $K$ .

— derived from observed data by Westin as quoted by Mott and Massey (1965);

I—Present Calculation.

II—Calculation from the Hartree field without allowance for exchange as quoted by Mott and Massey (1965).

It may be of interest to compare the present values of  $\eta_0$  with those of LaBahn and Callaway (1964), who took into account the polarisation effect by modifying the static atomic potential. At the energy 54.4 eV,  $\eta_0$  calculated by the present authors is 1.16 radians, whereas the corresponding value of LaBahn and Callaway (1964) is 1.36 radians whereas the experimental value is about 1.24 radians.

# ACKNOWLEDGMENT

The authors are thankful to Prof. D. Basu for his kind interest and valuable discussions throughout the progress of the work.

## REFERENCES

- Banerjee, S. N., Jha, R. and Sil, N. C., 1965, *Indian J. Phys.*, **39**, 455.  
——— 1966, *Indian J. Phys.*, (in press).
- Burke, P. G. and Schey, H. M., 1962, *Phys. Rev.*, **126**, 147.
- Hulthen, L., 1944, *K. fysiogr. Sällsk. Lund. Forh.*, **14**, No. 21.
- Kuyatt, C. E., Simpson, J. A. and Mielezarek, S. R., 1965, *Phys. Rev.*, **138**, 385.
- LaBahn, R. W. and Callaway, J., 1964, *Phys. Rev.*, **135**, 1539.  
——— 1966, (to be published).
- Massey, H. S. W. and Mohr, C. B. O., 1931, *Proc. Roy. Soc.*, **132**, 605.
- McDougall, 1932, *Proc. Roy. Soc., A*, **136**, 549.
- Morse, P. M. and Allis, W. P., 1933, *Phys. Rev.*, **44**, 269.
- Mott, N. F. and Massey, H. S. W., 1965, *The Theory of Atomic Collisions* (3rd Edition).  
The Clarendon Press, Oxford.
- Schulz, G. J., 1964, *Phys. Rev. Letters*, **13**, No. 20.  
——— 1965, *Proceedings of the Fourth International Conference on the Physics of  
Electronic and Atomic Collisions*, Quebec, Canada.
- Williamson, J. H. and McDowell, M. R. C., 1965, *Proc. Phys. Soc.*, **85**, 719.

# LIGAND FIELD THEORY OF TRIGONALLY DISTORTED OCTAHEDRAL $\text{Ni}^{2+}$ SALTS.

B. D. BHATTACHARYYA\* AND MANJU MAJUMDAR\*\*

DEPARTMENT OF MAGNETISM, INDIAN ASSOCIATION FOR THE CULTIVATION OF SCIENCE,  
CALCUTTA-32

(Received May 5, 1966)

**ABSTRACT.** Measurements of the magnetic susceptibility and anisotropy on single crystals of  $\text{NiSiF}_6.6\text{H}_2\text{O}$  and  $\text{NiSnCl}_6.6\text{H}_2\text{O}$  have been made in the temperature range  $300^\circ\text{--}90^\circ\text{K}$  and the results are compared with the ionic expressions. In both these crystals (which belong to the trigonal system with one ion in the unit cell) the anisotropic ligand field parameters as well as the zero field splitting are seen to be temperature dependent, the changes being more pronounced in the fluosilicate. The effect of covalency appears to be high in the chlorostannate.

## INTRODUCTION

The hexahydrated fluosilicate and chlorostannate of  $\text{Ni}^{2+}$  belong to an interesting series of crystals for magnetic, optical, e.s.r. and other studies. The unit cell of the trigonal (rhombohedral) crystals contains only one molecule, the  $\text{Ni}(\text{H}_2\text{O})_6^{2+}$  octahedra being trigonally distorted along the 3-fold axis of the crystals, as evident from the x-ray analysis of the chlorostannate by Pauling (1930) and the recent neutron diffraction studies on the isomorphous ferrous fluosilicate by Hamilton (1962). The  $\text{Ni}^{2+}$  ion is thus under a predominantly octahedral field with a small superposed trigonal component. The ground level of the ion under a cubic field is an orbital singlet  ${}^3\text{A}_{2g}$ , which is split up to a small extent by the combined action of the spin orbit coupling and the non-cubic component of the field into a doublet and a singlet. The magnitude of the separation between these levels, the zero field splitting  $D$ , has been measured from the resonance spectra (Holden, Kittel and Yager, 1949; Penrose and Stevens, 1950). However, the sign of  $D$  cannot be determined from these data and has to be deduced from magnetic susceptibility measurements, as discussed later.

Only the mean susceptibility data for the fluosilicate in the temperature range  $290^\circ\text{--}1.54^\circ\text{K}$  have so far been reported (Hasoda and Date, 1958) which are not enough for evaluating all the theoretical parameters uniquely. In the present paper we have measured the magnetic anisotropy as well as the principal susceptibilities in the range  $300^\circ\text{--}90^\circ\text{K}$ . The study of magnetic anisotropy is of special advantage here, as it is a sensitive function of  $D$  (vide infra). Results on the isomorphous salt,  $\text{NiSnCl}_6.6\text{H}_2\text{O}$ , have also been discussed.

\* Present address: Department of Physics, St. Xavier's College, Calcutta.

\*\* Present address: Department of Physics, Jogamaya Devi College, Calcutta.

## EXPERIMENTAL

Nickel fluosilicate was prepared from nickel carbonate (Schering's Co-free quality) and neutralized with hydrofluoric acid. Zinc fluosilicate (which was required for the diamagnetic correction of the susceptibilities) was prepared in a similar manner. Nickel chlorostannate was prepared from  $\text{NiCl}_2 \cdot 6\text{H}_2\text{O}$  and  $\text{SnCl}_4$  in moderately concentrated hydrochloric acid solution. The fairly large single crystals obtained on crystallization from slightly acid solutions were checked under the polarising microscope.  $\text{NiSiF}_6 \cdot 6\text{H}_2\text{O}$  crystals were ground into cylinders about the axis of suspension to eliminate shape effects on the magnetic anisotropy.  $\text{NiSnCl}_6 \cdot 6\text{H}_2\text{O}$  is very deliquescent and had to be coated with collodion after mounting in the sample holder. Grinding of these crystals was avoided by choosing only those that had as nearly a regular polygonal cross-section as possible about the axis of suspension, so that the shape effects were minimized (Majumdar, 1962).

The magnetic anisotropy was measured in a torsion balance with quartz fibre suspension described in detail by Majumdar and Datta (1965), from which the values of the anisotropy  $\Delta\chi$  in the horizontal plane could be directly obtained. For the measurement of the principal anisotropy ( $\chi_{||} - \chi_{\perp}$ ) (the susceptibility along the trigonal axis,  $\chi_{||}$ , was found to be greater than that normal to this axis,  $\chi_{\perp}$ , for both the salts studied here) the crystal was oriented with a  $\{1\bar{1}0\}$  face horizontal. In order to check if any anisotropy appeared in the plane of trigonal symmetry at low temperatures, the crystals were mounted with the  $[111]$  axis vertical. There was no measurable anisotropy down to  $90^\circ\text{K}$ , showing that the unlike cobalt (Majumdar and Datta, 1965), manganese (Tsujikawa, and Couture, 1955) and copper (Majumdar, unpublished) hexa-aquo fluosilicates, the uniaxial symmetry of the crystal is retained in both the salts in the range of temperature studied.

A sensitive Curie type of torsion balance was used for the measurement of susceptibility (Bose *et al.*, 1963) and one of the principal susceptibilities of the crystal, e.g.,  $\chi_{\perp}$  or the mean susceptibility of the powdered crystal was measured from  $300^\circ$  to  $90^\circ\text{K}$  with its help. Measurement of the mean susceptibility was not possible for the chlorostannate because of the obvious difficulty of powdering and packing the highly deliquescent crystals in an ampoule. The susceptibility values for  $\text{NiSiF}_6 \cdot 6\text{H}_2\text{O}$  were corrected for diamagnetism from the measurements on the isomorphous zinc fluosilicate for which  $K_{||}$  and  $K_{\perp}$  were found to be  $-136.4$  and  $-135.5$  in the usual  $10^{-6}$  e.m. units per mole, respectively. For the chlorostannate no isomorphous diamagnetic salt containing  $\text{SnCl}_6^{2-}$  could be prepared, and the necessary corrections were applied using standard tables\*,  $\chi$  being calculated to be  $-252$ .

\*Tables de constantes et données numériques, 1957, Edited by G. Foex *et al.*, Vol. 7 "Diamagnetisme et Paramagnetisme".



From the corrected susceptibility values the principal and mean effective moments  $\mu_i$  ( $i = \parallel$  or  $\perp$  to the trigonal axis) and  $\mu$ , respectively, were calculated

$$\mu_i^2 = \frac{3k}{N\beta^2} \chi_i \cdot T = 7.995 \chi_i T$$

$$\mu^2 = \frac{1}{3}(\mu_{\parallel}^2 + 2\mu_{\perp}^2)$$

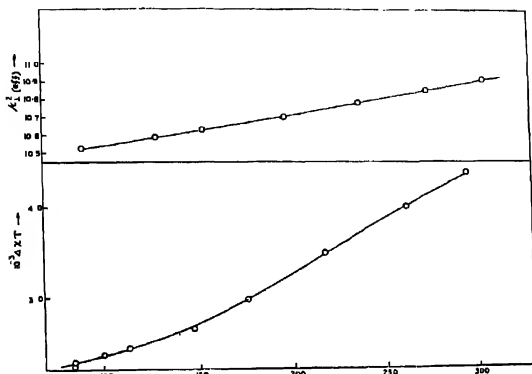


Fig. 1.  $\text{NiSiF}_6 \cdot 6\text{H}_2\text{O}$ . Lower curve—magnetic anisotropy,  $(\chi_{\parallel} - \chi_{\perp})$ , plotted as  $T(\chi_{\parallel} - \chi_{\perp})$ ; Upper curve—squares of the principal moments,  $\mu_i^2$  (eff.)

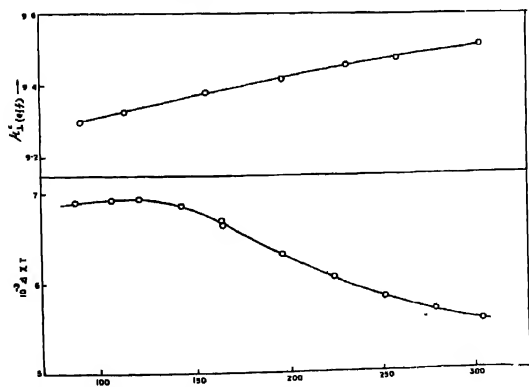


Fig. 2.  $\text{NiSnCl}_6 \cdot 6\text{H}_2\text{O}$ . Lower curve—magnetic anisotropy,  $(\chi_{\parallel} - \chi_{\perp})$ , plotted as  $T(\chi_{\parallel} - \chi_{\perp})$ ; Upper curve—squares of the principal moments,  $\mu_i^2$  (eff.)

using the relationship ( $\chi_i$  being identical with the ionic susceptibility  $K_i$  in the present case) The experimental data for the anisotropy and the susceptibility (or the squares of the principal effective moment  $\mu^2$ ) are shown in figure 1 for the fluosilicate and in figure 2 for the chlorostannate. Graphically interpolated values at regular intervals of temperature are shown in Tables I and II for convenience of comparison with the calculated values. The accuracy of the results is estimated to be  $\pm 0.5\%$ .

TABLE I  
Magnetic anisotropy and susceptibility of  $\text{NiSiF}_6 \cdot 6\text{H}_2\text{O}$   
(interpolated values)

Temp. °K	$10^6 K_{\perp}$	$10^6 (K_{\parallel} - K_{\perp})$	$10^6 \bar{K}$
300	4,530	14.82	4,530
280	4,830	15.00	4,840
260	5,190	15.21	5,200
240	5,610	15.46	5,610
220	6,090	15.80	6,100
200	6,680	16.23	6,680
180	7,400	16.70	7,420
160	8,300	17.40	8,310
140	9,450	18.57	9,460
120	9,990	20.54	10,100
100	13,170	23.63	13,180
90	14,610	25.62	14,610

TABLE II  
Magnetic anisotropy and susceptibility of  $\text{NiSnCl}_6 \cdot 6\text{H}_2\text{O}$   
(interpolated values)

Temp. °K	$10^6 K_{\perp}$	$10^6 (K_{\parallel} - K_{\perp})$	$10^6 \bar{K}$
300	3,963	18.63	3,970
280	4,240	20.20	4,250
260	4,500	22.21	4,570
240	4,930	24.62	4,940
220	5,370	27.71	5,380
200	5,890	31.40	5,910
180	6,540	36.12	6,550
160	7,340	41.90	7,350
140	8,360	49.24	8,380
120	9,730	57.80	9,750
100	11,650	69.21	11,690
90	12,912	76.60	12,950

# THEORY OF TRIGONALLY DISTORTED OCTAHEDRAL Ni<sup>2+</sup> SALTS

Under an octahedral field of symmetry  $O_h$  the  $3d^8$   $^3F$  ground state of the  $Ni^{2+}$  ion splits up into two triplets,  $^3T_{2g}$  and  $^3T_{1g}$ , and a singlet  $^3A_{2g}$  which lies lowest. The appropriate wave functions using the three-fold axis of the octahedron as the axis of quantization are (Bleaney and Stevens, 1953)

Wave functions	Representation
$\frac{\sqrt{2}}{3}(\psi_3 - \psi_{-3}) - \frac{\sqrt{5}}{3}\psi_0$	$A_{2g}$
$\frac{1}{\sqrt{2}}(\psi_3 + \psi_{-3})$	$T_{2g}^0$
$\sqrt{\frac{1}{6}}\psi_2 - \sqrt{\frac{5}{6}}\psi_{-1}$	$T_{2g}^+$
$\sqrt{\frac{5}{6}}\psi_1 + \sqrt{\frac{1}{6}}\psi_{-2}$	$T_{2g}^-$
$\frac{2}{3}\psi_0 + \frac{1}{3}\sqrt{\frac{5}{2}}(\psi_3 - \psi_{-3})$	$T_{1g}^0$
$\sqrt{\frac{5}{6}}\psi_2 + \sqrt{\frac{1}{6}}\psi_{-1}$	$T_{1g}^+$
$\sqrt{\frac{5}{6}}\psi_{-2} - \sqrt{\frac{1}{6}}\psi_1$	$T_{1g}^-$

(1)

The potential for the cubic and trigonal fields may be written as

$$V = D'r^4 \left[ Y_0^4 + \left( \frac{10}{7} \right)^{\frac{1}{2}} (Y_3^4 - Y_4^{-3}) \right] + A'_2 r^2 Y_2^0 + A'_4 r^4 Y_4^0 \quad \dots \quad (2)$$

On applying the corresponding perturbations we arrive at the following wave functions :

$$\begin{aligned} \phi_0 &= a_0 |A_{2g}\rangle + b_0 |T_{1g}^0\rangle \\ \phi_1 &= a_1 |T_{2g}^+\rangle + b_1 |T_{1g}^+\rangle \\ \phi_1' &= a_1 |T_{2g}^-\rangle + b_1 |T_{1g}^-\rangle \\ \phi_2 &= |T_{2g}^0\rangle \\ \phi_3 &= a_1 |T_{1g}^+\rangle - b_1 |T_{2g}^+\rangle \\ \phi_3' &= a_1 |T_{1g}^-\rangle - b_1 |T_{2g}^-\rangle \\ \phi_4 &= a_0 |T_{1g}^0\rangle - b_0 |A_{2g}\rangle \end{aligned} \quad \dots \quad (3)$$

with the corresponding energies (with appropriate subscripts) obtained by solving the secular determinant, given by

$$E_{0,4} = \frac{1}{2} \left[ \left( -6Dq + \frac{3}{10}A_2 + \frac{27}{2}A_4 \mp \left\{ \left( 18Dq + \frac{3}{10}A_2 - \frac{1}{2}A_4 \right)^2 + \frac{4}{5}(3A_2 - 5A_4^2)^{\frac{1}{2}} \right\}^{\frac{1}{2}} \right) \right]$$

$$E_{1,3} = \frac{1}{2} \left[ \left( 4Dq - \frac{9}{10}A_2 - 9A_4 \right) \mp \left\{ \left( 8Dq + \frac{3}{5}A_2 - 8A_4 \right)^2 + \frac{1}{20}(3A_2 - 40A_4)^2 \right\}^{\frac{1}{2}} \right]$$

$$E_2 = -2Dq + \frac{3}{2}A_2 + \frac{9}{2}A_4 \quad \dots \quad (4)$$

where the first and the second subscripts on  $E$  refer to the  $-ve$  or  $+ve$  sign appearing within the square brackets in (4). The coefficients in (3) are given by

$$a_0 = \frac{\sqrt[3]{5} A_2 - \sqrt{5} A_4}{E_0 + 12Dq - 7A_4} b_0$$

$$a_0^3 + b_0^3 = 1;$$

$$a_1 = \frac{\frac{3}{4\sqrt{5}}A_2 - 2\sqrt{5}A_4}{E_1 + 2Dq + \frac{3}{2}A_2 + \frac{1}{2}A_4} b_1 \quad \dots \quad (5)$$

$$a_1^3 + b_1^3 = 1;$$

where the ligand field coefficients are given by

$$A_2 = -eA'_2 \bar{r}^2 \frac{\sqrt{5}}{21\sqrt{\pi}}$$

$$A_4 = -eA'_4 \bar{r}^4 \frac{1}{21\sqrt{\pi}} \quad \dots \quad (6)$$

$$Dq = +eD'\bar{r}^4 \frac{3}{28\sqrt{\pi}}$$

The trigonal field thus splits up the excited orbital triplets into a doublet and a singlet each, the ground level remaining orbitally non-degenerate. Since the excited orbital levels lie  $\sim 10^4 \text{ cm}^{-1}$  higher up we can apply the spin Hamiltonian technique (Pryce, 1950) where we include the effect of spin-orbit interaction and the external magnetic field.

For  $H \parallel z$ , axis of trigonal symmetry of the  $\text{Ni}(\text{H}_2\text{O})_6^{2+}$  complex, the spin Hamiltonian for the system is given by

$$H_s = D\{S_z^2 - \frac{1}{3}S(S+1)\} + \beta g_{\parallel} H_z S_z - \beta^2 \alpha_{\parallel} k_{\parallel}^2 H_z^2 \quad \dots (7)$$

and for  $H \perp z$

$$H_s = D\{S_z^2 - \frac{1}{3}(S+1)S\} + \beta g_{\perp} H_x S_x - \beta^2 \alpha_{\perp} k_{\perp}^2 H_x^2 \quad \dots (8)$$

where

$$D = -(\alpha_{\parallel} \zeta_{\parallel}^2 - \alpha_{\perp} \zeta_{\perp}^2)$$

$$g_{\parallel} = 2(1 - k_{\parallel} \alpha_{\parallel} \zeta_{\parallel})$$

$$g_{\perp} = 2(1 - k_{\perp} \alpha_{\perp} \zeta_{\perp})$$

and

$$\alpha_{\parallel} = \frac{(2a_0 + \sqrt{5}b_0)^2}{E_2 - E_0} \quad \dots (9)$$

$$\alpha_{\perp} = \frac{2\left(\sqrt{2}a_0\alpha_1 - \frac{1}{2}\sqrt{\frac{5}{2}}b_0\alpha_1 + \frac{3}{2\sqrt{2}}b_0b_1\right)^2}{E_1 - E_0} + \frac{2\left(\sqrt{2}a_0b_1 - \frac{1}{2}\sqrt{\frac{5}{2}}b_0b_1 - \frac{3}{2\sqrt{2}}b_0b_1\right)^2}{E_3 - E_0}$$

Here we have introduced the orbital reduction factors  $k_i$  and the spin orbit coupling coefficients  $\zeta_i$  ( $i = \parallel$  or  $\perp$  to the trigonal axis of the complex) reduced from the free ion value and rendered anisotropic due to covalency.

Operating with the spin Hamiltonian  $H_s$  (7) and (8) respectively upon the spin states  $|1\rangle, |0\rangle, |-1\rangle$  we derive the energy expressions as follows :

(a)  $H \parallel z$

$$\left. \begin{aligned} W_1 &= \frac{1}{3}D + g_{\parallel}\beta H_z - \beta^2 k_{\parallel}^2 \alpha_{\parallel} H_z^2 \\ W_0 &= -\frac{2}{3}D - \beta^2 k_{\parallel}^2 \alpha_{\parallel} H_z^2 \\ W_{-1} &= \frac{1}{3}D - g_{\parallel}\beta H_z - \beta^2 k_{\parallel}^2 \alpha_{\parallel} H_z^2 \end{aligned} \right\}$$

(b)  $H \perp z$

$$\left. \begin{aligned} W_1 &= \frac{1}{3}[-\frac{1}{3}D - 2\beta^2 k_{\perp}^2 \alpha_{\perp} H_x^2 + (D^2 + 4g_{\perp}\beta^2 H_x^2)^{\frac{1}{2}}] \\ W_0 &= \frac{1}{3}D - \beta^2 k_{\perp}^2 \alpha_{\perp} H_x^2 \\ W_{-1} &= \frac{1}{3}[-\frac{1}{3}D - 2\beta^2 k_{\perp}^2 \alpha_{\perp} H_x^2 - (D^2 + 4g_{\perp}\beta^2 H_x^2)^{\frac{1}{2}}] \end{aligned} \right\} \quad \dots (10)$$

The expression for the principal gm ionic magnetic susceptibility is given as usual by

$$K_i = - \left[ \frac{N}{H} \frac{\sum_i \frac{\partial W_i^{(i)}}{\partial H} \exp \left( - \frac{W_i^{(i)}}{kT} \right)}{\sum_i \exp \left( - \frac{W_i^{(i)}}{kT} \right)} \right] \quad \dots (11)$$

(i = ||, ⊥)

On substituting the values of  $W_i^{(i)}$  obtained from (10) in the above expression one gets

$$K_{||} = \frac{2N\beta^2 \left[ \frac{g_{||}^2}{kT} e^{-D/3kT} + 2\alpha_{||} k_{||}^2 e^{-D/3kT} + k_{||}^2 \alpha_{||} e^{2D/3kT} \right]}{2e^{-D/3kT} + e^{2D/3kT}}$$

and ... (12a)

$$K_{\perp} = \frac{N\beta^2 \left[ 4k_{\perp}^2 \alpha_{\perp} e^{-D/3kT} + 2\alpha_{\perp}^2 k_{\perp} e^{2D/3kT} + \frac{2g_{\perp}^2}{D} \left( e^{2D/3kT} - e^{-D/3kT} \right) \right]}{2e^{-D/3kT} + e^{2D/3kT}}$$

On the assumption that  $D \ll kT$  the exponentials can be expanded when (12a) reduces to (ignoring terms involving higher powers of  $D$  and  $1/T^2$ ; see also Pryce, 1957)

$$K_{||} = \frac{N\beta^2}{k} \left[ 2k \alpha_{||} k_{||}^2 + \frac{2g_{||}^2}{3T} - \frac{2D g_{||}^2}{9kT^2} \right] \quad \dots (12b)$$

$$K_{\perp} = \frac{N\beta^2}{k} \left[ 2k \alpha_{\perp} k_{\perp}^2 + \frac{2g_{\perp}^2}{3T} + \frac{Dg_{\perp}^2}{9kT^2} \right]$$

For the fluosilicate, since  $D$  is  $\sim 0.5$  cm $^{-1}$  at room temperature and  $\sim 0.1$  cm $^{-1}$  at 14°K (Penrose and Stevens, 1950), it is permissible to use eq. (12b); however, at temperatures of about 1°K,  $D \sim kT$ , and eq. (12a) is more proper to use. For the chlorostannate low temperature data are unavailable and (12b) is adequate for the present purposes.

Since these crystals have an anisotropy of less than 0.5% throughout the temperature range studied and since it has been directly measured in these experiments, it is more convenient to use the expression for the anisotropy

$$\Delta K = K_{||} - K_{\perp}$$

and the mean susceptibility

$\bar{K} = \frac{1}{3}(K_{\parallel} + 2K_{\perp})$ . For  $D \ll kT$  these reduce to

$$K = \frac{N\beta^2}{k} \left[ \frac{2}{3}k(\alpha_{\parallel}k_{\parallel}^2 + 2\alpha_{\perp}k_{\perp}^2) + \frac{2\bar{g}^2}{3T} - \frac{2D}{9kT^2}(g_{\parallel}^2 - g_{\perp}^2) \right]$$

and

... (13)

$$\Delta\bar{K} = \frac{N\beta^2}{k} [2k(\alpha_{\parallel}k_{\parallel}^2 - \alpha_{\perp}k_{\perp}^2) + \frac{2}{3T}(g_{\parallel}^2 - g_{\perp}^2) - \frac{J}{9kT^2}(2g_{\parallel}^2 + g_{\perp}^2)]$$

#### COMPARISON WITH EXPERIMENT

The theoretical parameters involved in the above expressions are the cubic field coefficient  $Dq$ , the second and fourth order trigonal field parameters  $A_2$  and  $A_4$ , respectively, the orbital reduction factors  $k_i$  and the spin orbit coupling coefficients,  $\zeta_i$  ( $i = \parallel, \perp$ ). Recent experiments on the optical spectra of  $\text{NiSiF}_6 \cdot 6\text{H}_2\text{O}$  (in 10% concentration in  $\text{ZnSiF}_6 \cdot 6\text{H}_2\text{O}$ ) by Pryce *et al.* (1964) show a fairly broad band centered around  $9,100 \text{ cm}^{-1}$ , assigned to the transition  ${}^3A_{2g} \rightarrow {}^3T_{2g}$  in the cubic field approximation, which is thus equal to  $10Dq$ . We have consequently accepted the values of  $Dq$  as  $910 \text{ cm}^{-1}$ , since the mean centre of the levels is expected to remain practically unaltered when a small trigonal component is superposed on the cubic levels.

E.s.r. data for  $\text{NiSiF}_6 \cdot 6\text{H}_2\text{O}$  are reported by Holden, Kittel and Yager (1949) who find  $g_{\parallel} = 2.36$  and  $g_{\perp} = 2.29$  at the room temperature with  $D = 0.50 \text{ cm}^{-1}$ , while Penrose and Stevens (1950) obtained, within experimental error, an isotropic  $g$ -value with  $D$  varying with temperature from  $0.32 \text{ cm}^{-1}$  at  $200^\circ\text{K}$  to  $0.12 \text{ cm}^{-1}$  at  $14.6^\circ\text{K}$ . Holden *et al.* ascribed the anisotropy in  $g$ -values to experimental errors.

In correlating the theory with experiment we have found by trial and error a set of values of  $\alpha_i$ ,  $k_i$  and  $\zeta_i$  ( $i = \parallel, \perp$ ) with  $Dq = 910 \text{ cm}^{-1}$  which would give the best fit with the resonance  $D$  and  $g$ -values, as well as our susceptibility and anisotropy data. It was found that a much better agreement with experiment was obtained by taking  $D$  as  $-ve$ . In fitting the results for different temperatures  $k_i$ ,  $\zeta_i$  and  $Dq$  were assumed to remain constant with temperature, as these parameters are associated with strong bindings and hence are expected to change less with temperature. On the other hand, we have assumed that  $\alpha_i$  (which is a function of  $Dq$ ,  $A_2$  and  $A_4$ ; cf eq. 6 and 9) varies with temperature because of a greater likelihood of thermal changes in the anisotropic part of the ligand field, as also observed by earlier workers of this laboratory on many salts of the iron group (Bose *et al.*, 1957, 1958, 1961 *et seq.*). The results are shown in Tables III and IV for the fluosilicate and the chlorostannate, respectively.

#### (a) $\text{NiSiF}_6 \cdot 6\text{H}_2\text{O}$ .

It is seen from table III that the agreement between the calculated and observed values of  $g$ ,  $D$ ,  $k_{\parallel}$  and  $k_{\perp}$  with a suitable and reasonable choice of the parameters  $Dq$ ,  $k_i$  and  $\alpha_i$  ( $i = \parallel, \perp$ ) is very satisfactory particularly in view of the fact

TABLE III

Calculated ligand field parameters for  $\text{NiSiF}_6 \cdot 6\text{H}_2\text{O}$ 

$Dq = 910 \text{ cm}^{-1}$ ;  $k_{\parallel} = 0.786$ ;  $k_{\perp} = 0.825$   
 $\zeta_{\parallel} = -295 \text{ cm}^{-1}$ ;  $\zeta_{\perp} = -309.5 \text{ cm}^{-1}$

Temp. °K	$10^4 \alpha_i$	$g_i$	$-D \text{ cm}^{-1}$	$10^6 \Delta K$	$10^6 \bar{K}$
300	$\alpha_{\parallel} = 6.222$	$g_{\parallel} = 2.289$ (2.36)	0.50 (0.50)*	15.10 (14.82)	4556 (4534)
	$\alpha_{\perp} = 5.600$	$g_{\perp} = 2.286^*$ (2.29)			
200	$\alpha_{\parallel} = 6.159$	$g_{\parallel} = 2.286$ (2.29)†	0.29 (0.32)†	16.00 (16.23)	6720 (6684)
	$\alpha_{\perp} = 5.565$	$g_{\perp} = 2.284$ (2.29)			
140	$\alpha_{\parallel} = 6.025$	$g_{\parallel} = 2.279$	0.214	18.69 (18.57)	9466 (9466)
	$\alpha_{\perp} = 5.451$	$g_{\perp} = 2.278$			
90	$\alpha_{\parallel} = 5.982$	$g_{\parallel} = 2.277$ (2.26)	0.158 (0.17)†	25.90 (25.62)	14597 (14610)
	$\alpha_{\perp} = 5.418$	$g_{\perp} = 2.277$ (2.276)†			
14.6	$\alpha_{\parallel} = 4.705$	$g_{\parallel} = 2.218$	0.034 (0.12)†	136 (—)	84,250 (83,600)§
	$\alpha_{\perp} = 4.271$	$g_{\perp} = 2.218$			
1.54	$\alpha_{\parallel} = 3.450$	$g_{\parallel} = 2.160$	0.014	148 (—)	799,880 (800,000)§
	$\alpha_{\perp} = 3.133$	$g_{\perp} = 2.160$			

\* E.s.r. data of Holden *et al.*, (1949).

† E.s.r. data of Penrose and Stevens (1950).

§ Mean susceptibility data of Hasada and Date (1958).

Figures within parentheses indicate experimental values.

that the anisotropy is very feeble. The change in  $D$  with temperature as observed by the resonance workers is also substantiated by these results, the calculated values being very close to the experimental ones obtained by e.s.r. We note here that the values of  $D$  calculated by Becquerel and Opechowsky (1939) based on the paramagnetic rotation data of Becquerel and van den Handel (1939) at 2°K is numerically higher ( $D = -0.30 \text{ cm}^{-1}$ ) than the resonance value ( $D = -0.12 \text{ cm}^{-1}$ ) reported by Penrose and Stevens (1950), as well as that obtained by Benzie and Cooke (1950) from specific heat measurements at 0.95°K ( $D = -0.15 \text{ cm}^{-1}$ ). This has been ascribed by Ollom and Van Vleck (1951) to the fact that the zero field splitting contains in it an appreciable contribution from exchange interaction between neighbouring paramagnetic ions while the calculations of



Becquerel and Opechowsky include only the crystal field contribution. Since we have chosen the value of  $D$  by trial so as to give the best fit with the experimental susceptibility and anisotropy data it should include both the above effects. The discrepancy between our calculated values and the e.s.r. data below 14°K may arise from the fact that our value is not based on actual measurement of anisotropy at these temperatures but are the extrapolated ones to give close fit with the mean susceptibility data of Haseda and Date (1958). It has also been recently pointed out by Ohtsubo (1965) that exchange effects are small in  $\text{NiSiF}_6 \cdot 6\text{H}_2\text{O}$  which becomes weakly ferromagnetic only below 0.15°K.

TABLE IV

Calculated ligand field parameters for  $\text{NiSnCl}_6 \cdot 6\text{H}_2\text{O}$ .

$$D_q = 910 \text{ cm}^{-1}$$

$$k_{||} = 0.760$$

$$\zeta_{||} = -250.3 \text{ cm}^{-1}$$

$$k_{\perp} = 0.757$$

$$\zeta_{\perp} = -249.6 \text{ cm}^{-1}$$

Temp. °K	$10^4 \alpha_i$	$g_i$	$-D \text{ cm}^{-1}$	$10^6 K$	$10^6 K$
300	$\alpha_{  } = 4.01$	$g_{  } = 2.153$	0.52	18.78	3973
	$\alpha_{\perp} = 3.95$	$g_{\perp} = 2.149$		(18.57)	(3970)
200	$\alpha_{  } = 4.03$	$g_{  } = 2.153$	0.52	31.61	5904
	$\alpha_{\perp} = 3.97$	$g_{\perp} = 2.150$		(31.40)	(5905)
140	$\alpha_{  } = 4.03$	$g_{  } = 2.153$	0.52	50.52	8377
	$\alpha_{\perp} = 3.97$	$g_{\perp} = 2.150$		(49.24)	(8378)
90	$\alpha_{  } = 4.00$	$g_{  } = 2.152$	0.40	75.59	12956
	$\alpha_{\perp} = 3.96$	$g_{\perp} = 2.150$		(76.60)	(12950)

Figures within parentheses are experimental values.

It may be noted here that the contribution of  $D$  to the mean susceptibility,  $\bar{K}$ , (cf. eq. 13) is very small even at helium temperatures, while its effects on the anisotropy  $\Delta K$ , becomes large at low temperatures. Hence anisotropy measurements are desirable at such temperatures for a more reliable estimate of  $D$ .

It is seen from eq. (4), (5) and (9) that  $\alpha_i$  is a function of  $D_q$ ,  $A_2$  and  $A_4$ ; hence it is possible to find the values of  $A_2$  and  $A_4$  ( $D_q$  being assumed to be constant) by trial to obtain agreement with the chosen value of  $\alpha_i$ . Instead of calculating  $A_2$  and  $A_4$  for all the different sets of  $\alpha$ 's ( $i = ||, \perp$ ) which would be very laborious and would not yield any new information we have estimated only

the order of magnitude of these parameters :  $A_2 \sim -70 \text{ cm}^{-1}$  and  $A_4 \sim 160 \text{ cm}^{-1}$  in the range  $300^\circ - 90^\circ \text{K}$ .

(b)  $\text{NiSnCl}_6 \cdot 6\text{H}_2\text{O}$ .

As mentioned earlier, the detailed x-ray structure of this crystal was performed by Pauling (1930). However, no magnetic susceptibility, e.s.r. or optical absorption data have yet been reported. Since the  $\text{Ni}(\text{H}_2\text{O})_6^{2+}$  octahedra in the fluosilicate and this salt are likely to be under very similar octahedral fields, we have assumed  $D_q$  to be the same in both. As before, we have found by trial a set of values of  $\zeta_i$ ,  $k_i$  and  $\alpha_i$  which would give the best fit with the experimental susceptibility and anisotropy data while giving reasonable  $D$  and  $g$ -values (Table IV). We have also assumed, as before,  $D_q$ ,  $k_i$  and  $\zeta_i$  to be independent of temperature  $T$ , while  $\alpha_i$  is assumed to vary with  $T$ .

As in the fluosilicate, it was found impossible to fit the experimental data with fixed values of  $\alpha_{\parallel}$  and  $\alpha_{\perp}$  over the whole range of temperatures; however, the variation in these parameters, and consequently that of  $D$  and  $g_i$  is markedly less than those in the former salts. This points to a smaller change in the ligand field with temperature in the chlorostannate which may be due to greater strength of binding in this complex. It may be noted that both  $k_i$  and  $\zeta_i$  have found to be smaller in this crystal than in the fluosilicate. This means a higher degree of covalency in the  $\text{Ni}(\text{H}_2\text{O})_6^{2+}$  complex, presumably arising from the influence of the  $\text{Cl}^-$  ions, the next nearest neighbours of  $\text{Ni}^{2+}$ ; because of its larger size and hence a smaller charge density than in the  $\text{F}^-$  ions, it is expected to change inductively (Van Vleck, 1939) the metal-ligand charge overlap in the chlorostannate more than in the fluosilicate. Unfortunately, there are no resonance data to compare the calculated  $D$  and  $g$ -values in this case directly.

In the chlorostannate the value of  $A_2$  was found to remain about the same as in the fluosilicate, while that of  $A_4$  changed to  $\sim 90 \text{ cm}^{-1}$ .

#### ACKNOWLEDGMENTS

The authors wish to acknowledge their indebtedness to Professor A. Bose, D.Sc., F.N.I., for suggesting the problem and for his keen interest in this work. They are also grateful to Dr. S. K. Datta, Dr. U. Ghosh and Dr. R. Rai for valuable discussions and help during the experiment and computational work.

#### REFERENCES

- Bequorel, J. and van den Handel, J., 1939, *Physica*, **6**, 1034.  
 Bequorel, J. and Opechowsky, W., 1939, *Physica*, **6**, 1039.  
 Bonnie R. J. and Cooke, A. H., 1950, *Proc. Phys. Soc.*, **A63**, 213.  
 Bleaney, B. and Stevens, K. W. H., 1953, *Rep. Progr. Phys.*, **16**, 108.  
 Bose, A., Mitra, S. and Datta, S. K., 1957, *Proc. Roy. Soc.*, **A230**, 165.  
 ———, ———, ———, 1958, *Proc. Roy. Soc.*, **A248**, 158.  
 Bose, A., Chakravarty, A. S. and Chatterjee, R., 1961, *Proc. Roy. Soc.*, **A261**, 43.

- Bose, A., Dutta Roy, S. K., Ghosh, P. K. and Mitra, S., 1963, *Indian J. Phys.*, **37**, 505.  
Hamilton, W. C., 1962, *Acta Cryst.*, **15**, 353.  
Haseda, T. and Date, M., 1958, *J. Phys. Soc. Japan*, **13**, 175.  
Holden, A. N., Kittel, C. and Yager, W. A., 1949, *Phys. Rev.*, **75**, 1443.  
Majumdar, M., 1962, *Indian J. Phys.*, **36**, 111.  
Majumdar, M. and Datta, S. K., 1965, *J. Chem. Phys.*, **42**, 418.  
Pauling, L., 1930, *Z. Krist.*, **72**, 482.  
Penrose, R. and Stevens, K. W. H., 1950, *Proc. Phys. Soc.*, **A63**, 29.  
Pryce, M. H. L., 1950, *Proc. Phys. Soc.*, **A63**, 29.  
———, 1957, *Nuovo Cimento Suppl.*, **10**, **6**, 817.  
Pryce, M. H. L., Agnetta, G., Carfano, T., Palma-Vittorelli, M. B. and Palma, M. U.,  
1964, *Phil. Mag.*, **10**, 477.  
Tsujikawa, I. and Couture, L., 1955, *J. Phys. Radium*, **16**, 430.  
Van Vleck, J. H., 1939, *J. Chem. Phys.*, **7**, 72.

# VALIDITY OF THE GENERALIZED RECIPROCITY EQUATION INVOLVING CIRCULAR POLARIZATION

S. P. TEWARSON

DEPARTMENT OF PHYSICS, EWING CHRISTIAN COLLEGE UNIVERSITY OF  
ALLAHABAD, ALLAHABAD, U P.

(Received February 12, 1966; Resubmitted May 11, 1966)

**ABSTRACT** A Generalized Reciprocity Equation expressing an algebraic relationship between the parameters of an Optical system and its reciprocal system, was formulated by the author and was verified with the help of data reported by various workers for plane-polarized light beams. This paper establishes within experimental error-limits, the validity of the equation in case of circularly-polarized beams also for light scattering by a set of oriented nylon fibres. Since the Generalized Reciprocity Equation follows from Mueller's Reciprocity Law, this study completes the experimental verification of Mueller's theorem also.

## INTRODUCTION

R. S. Krishnan (1935) derived a reciprocity theorem in the form of an algebraic relation between the depolarization factors for unpolarized, horizontally-polarized and vertically-polarized incident beams of light. It has been experimentally verified by a large number of workers for random aggregation of colloidal particles. In case of oriented particles, it was found by Krishnan (1938) as well as Rao (1945), Subramanya and Rao (1949) and others, that the relation was true only for vertically oriented rod-like particles and failed for orientations in the horizontal plane along and perpendicular to the direction of the incident beams. Krishnan (1939) proposed another reciprocity relation where the electric vector of the incident beam of plane polarized light can assume any angle between the vertical and the horizontal axes. The relation however was found to lack generality because of phase relationship involved therein. Perrin (1942) extended Krishnan's work and proposed six reciprocity relations, which also included Krishnan's theorem. One of these relations involving circularly polarized beams was investigated by Ramanathan (1953) who established a phase reciprocity relation and verified it experimentally for circularly polarized light. Further study of reciprocity relations was undertaken by Krishnan, Narayanan and Sivarajan (1954), and Krishnan and Sivarajan (1956), for various cases. Subramanian (1963) proposed a reciprocity relation existing between the intensities of the scattered beams and verified it experimentally in the case of plane-polarized beams and the scatterers oriented along and perpendicular to the incident beams. Mueller (Parke-1949) trying to explain the cause of non-generality of the reciprocity relations of Krishnan and Perrin, found that these reciprocity relations were in fact reversibility

relations, and as such were valid for only reversible optical systems. He proposed a generalized reciprocity theorem of the form

$$M = M^{\#} \quad \dots (1)$$

where  $M$  and  $M^{\#}$  are the  $4 \times 4$  Mueller matrices (Schuercliff 1962) of an optical system and its corresponding reciprocal system respectively. The reciprocal system being one in which the incident beam is replaced by the emergent beam and vice-versa, the beams being fairly parallel and the entrance and exit apertures being equal in area. The elements of the Mueller matrices are same as the sixteen scattering coefficients of Perrin. The present author (1965) derived a generalized reciprocity equation based on Mueller's theorem (1) and of the form

$$\frac{[1 - (-)^k C_{ko}^{\#}] C_{jk} - [1 + (-)^k C_{ko}^{\#}] C_{jk}}{[1 - (-)^j C_{jo}^{\#}] C_{kj} - [1 + (-)^j C_{jo}^{\#}] C_{kj}} = (-)^{jk} \quad \dots (2)$$

which is an algebraic relation between the parameters of a natural optical system and its reciprocal system, where  $C_{jk} = \cos 2\theta_{jk}$  and  $\theta_{jk}$  is the angle between the vertical component of the electric vector of the scattered beam and the transmission axis of the Analyzer for equal intensity of the resolved components of  $H$  and  $V$  along it. The subscripts  $j, k$  refer to the types of analyzing and polarizing systems respectively, which are specified as follows.

Analyzer ( $j$ )	Polarizer ( $k$ )
1 = Plane horizontal;	0 = Unpolarized;
2 = Plane at $45^\circ$ ;	1 = Plane horizontal;
3 = Right-circular;	$\bar{1}$ = Plane vertical;
$\neq$ = Symbol superscripted on	2 = Plane at $45^\circ$ ;
parameters of the Reciprocal	$\bar{2}$ = Plane at $-45^\circ$
systems.	3 = Right-circular;
	$\bar{3}$ = Left-circular;

The experimental validity of (2) was tested by the author (1965) with the help of data reported by various workers, for all possible cases involving plane polarized beams. This paper provides a test of the generalized equation (2) in case of circularly polarized beams, through a set of data obtained from a light scattering experiment using oriented nylon fibres as scatterers. Mueller's reciprocity theorem is therefore completely verified through this study in conjunction with the previous one (Tewarson 1965), for a set of oriented particles.

# EXPERIMENTAL

The apparatus consisted of a 500 watt projection lamp with a yellow Wratten filter as the source. A set of condensing lenses was used for obtaining a fine parallel beam. The specimen consisted of a set of fine parallel nylon fibres stretched tightly and mounted at the centre of a specially designed holder capable of rotation through known angles in a vertical or horizontal plane. The holder was fitted

into the prism-table shaft of a spectrometer. The collimator arm had a polaroid holder wherein the transmission axis of the polaroid could be set at any desired angle. The telescope arm carried an analyzing polaroid of the same type as the polarizer, having been cut from the same HN-38 sheet polaroid. A lens condensed the scattered beam on a photoelectric cell which was connected to a Leeds and Northrup mirror galvanometer having a sensitivity of  $2.4 \times 10^{-9}$  amp/mm. Adequate protection from stray light was ensured by enclosing the two arms of the spectrometer in blackened tubes, and a small shutter window helped in setting the photocell which was capable of being raised or lowered and also being moved back and forth. Cell biasing and a photomultiplier were not needed, since the cell was of photovoltaic type and provided a maximum deflection of about 20cms. on the scale. A preliminary check showed a linear response of the photocell to intensity variations within the range of the scale. A constant voltage stabilizer with  $\pm 1\%$  stability for 230 volts, 50 cycles A.C. and of 500 watts capacity was used with the lamp. The photocell arm could be set at any desired angle of scattering. Care was taken in cutting down reflected light from entering the photocell arm. The sample holder was enclosed in a blackened cylindrical chamber which had two holes for entrance and exit of the incident beam directly, and another hole for the scattered beam along  $30^\circ$ . All components including the specimen-holder were blackened and all experiments were performed in a dark room.

For the natural optical system the face of the sample was kept normal to the incident beam, while for the reciprocal system, measurements were made after giving a rotation of  $180^\circ$  in the horizontal plane to the sample face and then setting it normally to the direction of the scattered beam. Quarter wave-plates used were also cut out from a single sheet. To avoid errors of centering and slight non-parallelism of the fibres, as well as slight ellipticity of the beams, readings of  $H$  and  $V$  of the scattered beam were taken for fibre orientations on both sides of the vertical, and only mean values were used in calculating the  $C_{jk}$  values by the relation

$$C_{jk} = \frac{H_{jk} - V_{jk}}{H_{jk} + V_{jk}} \quad \dots (3)$$

## RESULTS

The following five equations are obtained from (2) for all cases involving circularly polarized beams :

$$\frac{(1+C_{30}^{\text{pol}})C_{13} - (1-C_{30}^{\text{pol}})C_{1\overline{3}}}{(1+C_{10}^{\text{pol}})C_{31}^{\text{pol}} - (1-C_{10}^{\text{pol}})C_{3\overline{1}}^{\text{pol}}} = 1; (j=1, k=3) \quad \dots (4)$$

$$\frac{(1+C_{10}^{\text{pol}})C_{31} - (1-C_{10}^{\text{pol}})C_{3\overline{1}}}{(1+C_{30}^{\text{pol}})C_{13}^{\text{pol}} - (1-C_{30}^{\text{pol}})C_{1\overline{3}}^{\text{pol}}} = 1; (j=3, k=1) \quad \dots (5)$$

$$\frac{(1+C_{30}^{\alpha})C_{23}-(1-C_{30}^{\alpha})C_{23}}{(1-C_{20})C_{32}^{\alpha}-(1+C_{20})C_{32}^{\alpha}} = -1; (j=2, k=3) \quad \dots (6)$$

$$\frac{(1-C_{20}^{\alpha})C_{32}-(1+C_{20}^{\alpha})C_{32}}{(1+C_{30})C_{23}^{\alpha}-(1-C_{30})C_{23}^{\alpha}} = -1; (j=3, k=2) \quad \dots (7)$$

$$\frac{(1+C_{30}^{\alpha})C_{33}-(1-C_{30}^{\alpha})C_{33}}{(1+C_{30})C_{33}^{\alpha}-(1-C_{30})C_{33}^{\alpha}} = 1; (j=k=3) \quad \dots (8)$$

The following Tables show the results of enumerations of the above equations. The angle  $\alpha^{\circ}$  indicates the orientation of the fibres with respect to vertical, while LHS- implies left hand side of an equation :

TABLE I

$\alpha^{\circ}$	$-C_{30}^{\alpha}$	$-C_{13}$	$-C_{14}$	$-C_{10}$	$-C_{31}^{\alpha}$	$-C_{31}^{\alpha}$	LHS (4)
0	.504	.520	.623	.512	.514	.555	1.005
30	.505	.597	.605	.515	.516	.557	1.019
60	.513	.000	.594	.510	.555	.590	0.985
90	.527	.569	.585	.525	.586	.580	1.005
120	.513	.695	.586	.500	.534	.508	0.945

TABLE II

$\alpha^{\circ}$	$-C_{10}^{\alpha}$	$-C_{31}$	$-C_{31}$	$-C_{30}$	$-C_{13}^{\alpha}$	$-C_{13}^{\alpha}$	LHS (5)
0	.517	.543	.511	.502	.633	.627	0.965
30	.524	.527	.548	.520	.660	.613	0.980
60	.500	.464	.561	.505	.656	.611	1.021
90	.508	.510	.580	.510	.613	.613	0.998
120	.515	.531	.513	.495	.656	.600	0.920

TABLE III

$\alpha^{\circ}$	$-C_{30}^{\alpha}$	$-C_{23}$	$-C_{23}$	$-C_{20}$	$-C_{32}^{\alpha}$	$-C_{32}^{\alpha}$	LHS (6)
0	.504	.791	.805	.829	.500	.522	-0.993
30	.505	.772	.759	.779	.505	.481	-0.992
60	.513	.714	.765	.778	.489	.467	-1.055
90	.527	.765	.785	.855	.485	.530	-1.018
120	.513	.750	.759	.772	.489	.467	-1.036

TABLE IV

$\alpha^{\circ}$	$-C_{20}^{\alpha}$	$-C_{32}$	$-C_{32}$	$-C_{30}$	$-C_{23}^{\alpha}$	$-C_{23}^{\alpha}$	LHS (7)
0	.815	.513	.528	.502	.802	.780	-1.070
30	.810	.496	.482	.520	.807	.781	-1.009
60	.784	.500	.474	.500	.744	.742	-1.060
90	.796	.474	.478	.510	.833	.750	-1.040
120	.813	.520	.460	.495	.734	.818	-1.008

TABLE V

$\alpha^\circ$	$-C_{30}$	$-C_{33}$	$-C_{36}$	$-C_{30}$	$-C_{33}$	$-C_{36}$	LHS (8)
0	.504	.510	.510	.502	.514	.500	1.040
30	.505	.506	.483	.520	.500	.500	0.935
60	.513	.510	.488	.505	.515	.482	1.021
90	.527	.422	.466	.510	.495	.484	1.018
120	.513	.510	.488	.495	.500	.482	1.052

## DISCUSSION

A glance at the last column of Table I through V reveals that the generalized reciprocity equation (2) is valid within about 5% experimental error limits for the cases in which circular polarization is involved, for the various angles of orientation between the vertical and the horizontal planes. Mean deviations of the last columns were also estimated and were found insignificant. The cases for linearly polarized beams having been already verified by the author in the previous paper, Mueller's reciprocity theorem stands completely verified for a set of oriented nylon fibres as the scattering medium. Considering the large volume of the data and the interinvolvement of the C-values, whereby errors would be propagated, the verifications appear fairly reliable. In Table V the C-values appear nearly equal, this being expected when both the analyzing and polarizing systems are alike, the polarizer and analyzer both being circular.

## ACKNOWLEDGMENT

The author expresses his gratitude to Professor Vachaspati for his valuable guidance. He is thankful to Dr. R. W. Nathan and Mr. R. Prasad for their help in the setting of the apparatus.

## REFERENCES

- Krishnan, R. S., 1935, *Proc. Ind. Acad. Sci.*, **1**, 717, 782.  
 ———— 1948, *Proc. Ind. Acad. Sci.*, **1A**, 91.  
 ———— 1939, *Proc. Ind. Acad. Sci.*, **10A**, 395.  
 Krishnan, R. S., Narayanan, P. S. and Sivarajan, S. R., 1954, *Proc. Ind. Acad. Sci.*, **40A**, 140.  
 Krishnan, R. S. and Sivarajan, S. R., 1956, *Proc. Ind. Acad. Sci.*, **44A**, 274.—  
 Parke, N. G., 1949. *Tech. Report No. 119, Res. Lab. Electronics, Massachusetts Institute of Technology, USA.*  
 Portin, F., 1942, *J. Chem. Phys.*, **10**, 415.  
 Ramanathan, N. L., 1953, *Proc. Ind. Acad. Sci.*, **37A**, 385.  
 Rao, M. R. A. N., 1945, *Current Science*, **2**, 43.  
 Shurcliff, W. A., 1962, *Polarized Light*, Harvard University Press, U.S.A.  
 Subramanian, S., 1963, *Kolloid Zeits.*, **189(2)**, 135.  
 Subramanya, R. and Rao, M. R. A. N., 1949, *Proc. Ind. Acad. Sci.*, **29A**, 442.  
 Tewarson, S. P., 1966, *Indian J. Phys.*, **40**, 281.



# SIMPLE PROPERTIES OF CRYSTALS AND RESTSTRAHLEN FREQUENCY

C. M. KACHHAVA AND S. C. SAXENA

PHYSICS DEPARTMENT, RAJASTHAN UNIVERSITY, JAIPUR

(Received January 22, 1966. Resubmitted June 2, 1966)

**ABSTRACT.** Born-Mayer lattice theory has been used to compute the simple bulk properties of alkali halides. For determining the constants of the potential function the Reststrahlen frequency instead of compressibility or molecular data has been used. Properties which have been computed are: cohesive energy, compressibility, thermal expansion, Grüneisen constant and elastic constants. In all cases the success according to the proposed procedure is either of the same order or is better than that obtained by the conventional procedures.

## INTRODUCTION

Born-Mayer theory (1932) has been widely applied and is now fairly well established for discussing the various bulk properties of ionic crystals. The general approach is to assume an analytical form for the interatomic potential function and then exploit the two familiar Born-Mayer conditions (1932) to evaluate the potential parameters. So far, in such approaches, information regarding thermal expansion  $\alpha$ , compressibility  $\beta$ , pressure and temperature derivatives of  $\beta$  are used. In the simplified approach based on this method often only  $\beta$  is used. The purpose of this article is to suggest the use of Reststrahlen frequency in its place. Once the potential energy function is thus completely determined, various bulk properties can be computed according to known procedures. Adopting this procedure we have computed the different properties of the alkali halide crystals. The properties discussed and compared with the experimental predictions are the cohesive energy  $W$ , compressibility  $\beta$ , thermal expansion  $\alpha$ , Grüneisen constant  $\gamma$ , and the different elastic constants. We consider also the simple Born-Mayer potential in which only the coulomb and overlap terms are considered. The reasons for choosing this simplified potential are many. Firstly, the contribution of all of the other types of forces to interaction potential is small and the effect on the calculation of most of the above mentioned properties is invariably negligible. Secondly, the comparison of the properties so computed with the values obtained when compressibility data are used instead of Reststrahlen frequency  $\omega_0$  is possible in a straightway manner. The former type of calculations has been reported earlier by the authors (1964). Thirdly, this investment of computational labour is worth for the underlying idea is to illustrate the replacement of  $\beta$  by  $\omega_0$  even in a sophisticated calculation without any danger of impairing the accuracy.

## INTERATOMIC POTENTIAL

The simplified Born-Mayer potential (1932) which is used in this article is

$$\phi(r) = -\frac{\alpha e^2}{r} + A \exp(-r/\rho). \quad \dots (1)$$

Here  $\phi(r)$  is the interaction energy per atom,  $\alpha$  the Madlung constant,  $e$  the electronic charge,  $r$  the interatomic distance,  $A$  and  $\rho$  the two potential parameters which in the conventional procedure are determined from the Born-Mayer conditions (1932).

$$\left[ \frac{d\phi(r)}{dr} \right]_{r=r_0} = 0, \quad \dots (2)$$

and

$$\left[ \frac{d^2\phi(r)}{dr^2} \right]_{r=r_0} = \frac{9v_a}{\beta r_0^3}. \quad \dots (3)$$

Here  $v_a$  is the volume of the unit cell,  $r_0$  the equilibrium interatomic distance.

Kellermann (1940), and Sharan and Tiwari (1964) have deduced expressions for  $\omega_0$  for NaCl and CsCl-type structures respectively on the assumption that the overlap extends only up to the nearest neighbours. The two relations can be conveniently combined into a single expression viz.,

$$\omega_0^2 = \frac{e^2}{\mu v_a} \left[ \frac{M}{6} (B' + 2A') - \frac{4\pi}{3} \right]. \quad \dots (4)$$

Here  $\mu$  is the reduced mass appropriate to the two kinds of ions in the crystal,  $M$  the coordination number, and  $A'$  and  $B'$  are defined as follows :

$$A' = \frac{2v_a}{e^2 r_0} \left[ \frac{dv(r)}{dr} \right]_{r=r_0} = -\frac{2\alpha v_a}{M r_0^3}, \quad \dots (5)$$

and

$$B' = \frac{2v_a}{e^2} \left[ \frac{d^2v(r)}{dr^2} \right]_{r=r_0} = \frac{2v_a}{M e^2} \left[ \frac{9v_a}{\beta r_0^3} + \frac{2\alpha e^2}{r_0^3} \right]. \quad \dots (6)$$

Here

$$v(r) = \frac{1}{M} A \exp(-r/\rho). \quad \dots (7)$$

Substitution of  $A'$  and  $B'$  from Eqs. (5) and (6) respectively in Eq. (4) leads to the following relation for  $\beta$  :

$$\beta = \frac{9v_a}{[3\mu v_a \omega_0^2 + 4\pi e^2] r_0^3} \quad \dots (8)$$

When  $\beta$  from Eq (8) is substituted in Eq (3) one obtains,

$$\left[ \frac{d^2\phi(r)}{dr^2} \right]_{r=r_0} = 3\mu\omega_0^2 + 4\pi \frac{e^2}{v_a} \quad \dots (9)$$

In the present work we suggest to evaluate the constants  $A$  and  $\rho$  of Eq (1) from Eqs. (2) and (9). We shall refer this as the "proposed procedure" and the one in which use is made of Eqs. (2) and (3) as the "conventional procedure". The present endeavour aims at examining how far a single characteristic frequency is capable of explaining crystal properties. The two parameters  $A$  and  $\rho$  of Eq (1) can thus be calculated from the following explicit expressions obtained by applying conditions given by Eqs. (2) and (9) to Eq. (1) .

$$A = \frac{\alpha e^2}{r_0^3} \exp(-r_0/\rho), \quad \dots (10)$$

and

$$\rho = \frac{\alpha e^2}{3\mu r_0^2 \omega_0^2 + \frac{2r_0^2 e^2}{v_a} \left( 2\pi + \frac{\alpha v_a}{r_0^3} \right)} \quad \dots (11)$$

In this calculation the experimental values of  $\omega_0$  and  $r_0$  are needed  $\omega_0$  values used here are those recorded in Table I, column 2, while  $\gamma_0$  values are those compiled by us earlier (1963) Thus, having determined the potential completely we proceed to calculate the various properties.

#### COHESIVE ENERGY

Cohesive energy per mole,  $W$ , is rather simply related with  $\phi(r_0)$  such that

$$W = -[N\phi(r_0) + c_0]. \quad \dots (12)$$

Here  $N$  is the Avogadro number and  $c_0$  the zero-point energy per mole Values  $c_0$  have also been compiled by us (1963) earlier. Inserting Eq (1) into Eq (12) leads to the following working relation for  $W$  in terms of  $A$  and  $\rho$  .

$$W = - \left[ N \left\{ - \frac{\alpha e^2}{r_0} + A \exp(-r_0/\rho) \right\} + c_0 \right] \quad \dots (13)$$

Computed values of the cohesive energy according to Eqs (10), (11) and (13) are recorded in Table I, column 4.

Experimental values are shown in column 3 of this very Table The agreement is satisfactory. The average absolute deviation is 3.3 percent. According to the conventional procedure used by us (1964) earlier, the average absolute deviation is 2.9. This should be regarded as the first encouraging confirmation for the use of  $\omega_0$  data as an alternative to  $\beta$  suggesting by it the

validity of single frequency model for purposes of computing cohesive energy. A more crucial check is presented in the next section by calculating compressibility itself from  $\omega_0$

TABLE I  
Calculated and experimental values of  $W$ ,  $\beta$ ,  $\alpha$  and  $\gamma$ .

Crystal	$\omega_0$	$W$ (K Cal/mole)		$\beta(10^{-12}\text{dyne}^{-1}\text{cm}^2)$		$\alpha(10^{-6}\text{deg}^{-1})$		$\gamma$	
	$(10^{13}\text{S}^{-1})$								
	(a)	Exptl (b)	Calcd.	Exptl (b)	Calcd.	Exptl (c)	Calcd.	Exptl (d)	Calcd.
LiF	5.73	242.2	245.3	1.43	1.39	34.0	27.9	1.99	1.48
LiCl	3.84	201.5	193.0	3.17	3.60	44.0	42.2	1.51	1.50
LiBr	3.26	191.5	180.2	3.90	4.78	50.0	45.3	..	1.49
LiI	2.71	180.0	164.7	5.30	6.93	59.0	61.0	..	1.76
NaF	4.63	215.4	220.7	2.06	1.83	36.0	31.7	1.57	1.79
NaCl	3.09	184.7	182.2	3.97	3.87	40.0	41.1	1.43	1.83
NaBr	2.54	175.9	172.3	4.75	4.81	43.0	44.5	1.55	1.86
NaI	2.20	166.3	159.5	6.21	6.47	48.3	50.0	1.59	1.88
KF	3.62	190.9	193.3	3.14	3.02	36.7	38.2	1.48	1.88
KCl	2.71	167.8	160.5	5.50	4.94	38.3	45.0	1.34	2.12
KBr	2.18	161.2	159.0	6.45	5.77	40.0	49.1	1.43	2.11
KI	1.94	152.8	149.4	8.07	7.21	45.0	52.1	1.58	2.26
RbF	3.01	185.0	182.8	3.66	5.04	33.33	42.6	1.28	1.85
RbCl	2.24	163.6	159.4	6.16	5.73	36.0	46.9	1.25	2.16
RbBr	1.69	158.0	153.3	7.38	6.55	38.0	49.9	1.27	2.23
RbI	1.41	149.7	142.5	9.00	8.25	43.0	41.0	1.50	1.77
CsF	2.39	176.6	170.0	4.25	3.92	....	..	1.49	1.75
CsCl	1.86	157.8	149.8	5.55	5.50	56.0	45.8	1.97	2.26
CsBr	1.39	152.3	144.6	6.28	6.06	..	..	1.93	2.43
CsI	1.17	145.4	136.6	7.83	7.35	....	....	2.00	2.53

(a) Compiled by Martin, D. H., 1965, *Advances in Phys.*, **14**, 39.

(b) Compiled by Kachhava, C. M. and Saxena, S. C., 1964, *Indian J. Phys.*, **38**, 388.

(c) Compiled by Kachhava, C. M. and Saxena, S. C., 1965, *Indian J. Phys.*, **39**, 145.

(d) Compiled by Born, M. and Huang, K., 1956, *Dynamical Theory of Crystal Lattices*, Clarendon Press, Oxford, 85

#### COMPRESSIBILITY

Compressibility,  $\beta$ , is related with Reststrahlen frequency,  $\omega_0$ , through the relation of Eq. (8). We employ this relation to compute  $\beta$  from the known values of the other quantities involved. The values so obtained are reproduced in column 6 of Table I in which are also listed in column 5 the experimental  $\beta$  values for a direct comparison. It is encouraging to note that the agreement between

the experimental and calculated values is quite satisfactory. The average absolute deviation is 10.4 percent. It is interesting to compare this figure with 15.4 obtained in an earlier effort by us (1964) when molecular data and the relation of Eq. (2) were used to determine the potential parameters. This comparison in fact suggests a relative preference for the procedure suggested in this paper and thereby emphasizes the importance of the Reststrahlen frequency and its capability to predict the various crystal properties.

#### THEMAL EXPANSION

We have (1965a, 1966) recently derived an expression for the coefficient of thermal expansion,  $\alpha$ , in terms of the derivatives of  $\phi(r)$  and other quantities. For the sake of brevity only the final result is quoted here. It is

$$\alpha = - \frac{C_v}{2Nr_0} \frac{\phi'''(r_0)}{[\phi''(r_0)]^2}, \quad \dots (14)$$

in which  $C_v$  is the specific heat per mole at constant volume,  $\phi'''(r_0)$  and  $\phi''(r_0)$  are the third and second derivatives of  $\phi(r)$  at  $r = r_0$ , respectively. Equation (14) has been derived by Kumar (1959) adopting a different approach. For the form has been derived by Kumar (1959) adopting a different approach. For the form of Eq. (1) this gets simplified to the following expression.

$$\alpha = \frac{r_0 C_v}{2N\alpha e^2} \frac{\left(\frac{r_0^2}{\rho^2} - 6\right)}{\left(\frac{r_0}{\rho} - 2\right)^2}. \quad \dots (15)$$

The values of  $\alpha$  are then readily calculated from Eq. (15) as all the other quantities are known and these  $\alpha$  values are recorded in column 8 of Table I, while the experimental values are given in column 7. In the earlier calculation of  $\alpha$  by us, (1966) based on Eq. (14) but where  $\beta$  was used to determine the unknown parameters of  $\phi(r)$  almost similar agreement between theory and experiment was achieved inspite of the fact that the dispersion terms in  $\phi(r)$  were also considered.  $C_v$  values used in the present calculations are the same as compiled in that paper (1966). The average absolute deviations in the present and previous calculations from the experimental data are 13.4 and 14.3 percent respectively. This is again an evidence for the suitability of the proposed method of fixing the interaction potential.

#### GRÜNEISEN CONSTANT

Recently we (1965a) have suggested a method for computing Gruneisen constant,  $\gamma$ , based on a single frequency model. Again we do not reproduce here the details of the derivation but quote only the final result which is,

$$\gamma = - \frac{r_0}{6} \frac{\phi'''(r_0)}{\phi''(r_0)}. \quad \dots (16)$$

For the form of  $\phi(r)$  of Eq. (1), Eq. (7) reduces to

$$\gamma = \frac{1}{6} \frac{\left( \frac{r_0^2}{\rho^2} - 6 \right)}{\left( \frac{r_0}{\rho} - 2 \right)} \quad \dots \quad (17)$$

In the calculation of  $\gamma$  therefore only  $\rho$  and  $r_0$  values are required. When  $\rho$  values obtained from Eq. (11) are employed we get the values of  $\gamma$  recorded in Table I, column 10. The agreement between theory and experiment is not very satisfactory and is also somewhat inferior to that obtained earlier by the authors (1965a). The reason for this lies partly in the use of a simplified potential (the dispersion terms have been neglected) which will affect the computation of  $\gamma$  and  $\alpha$  more than the other properties such as  $\beta$ ,  $W$ , etc. As our idea is more to demonstrate the success of the outlined procedure rather than computing the various properties accurately, we refrain from repeating calculations of  $\alpha$  and  $\gamma$  on a more detailed sophisticated potential.

#### ELASTIC CONSTANTS

The elastic constants can also be computed from the knowledge of the interatomic potential, Kachhava and Saxena (1965b). These calculations are confined to the Kellermann (1940), and Krishnan and Roy (1952) models. Parameters were determined either using the compressibility or molecular data. We reproduce here in brief only the important aspects of the calculation.

Thus, for NaCl-type crystals on the Kellermann potential (1940),

$$\phi(r) = -\frac{\mu\epsilon}{r} + 6v(r), \quad (18)$$

the elastic constant  $C_{11}$  is given by

$$C_{11} = \left[ -2.56 + \frac{B'}{2} \right] \frac{e^2}{2r_0^4},$$

where  $B'$  is defined by Eq. (6) and is given by

$$B' = \frac{2\mu\omega_0^2 r_0^3}{\epsilon} - 6.5169. \quad \dots \quad (19)$$

According to Sharan and Tiwari (1964) the three elastic constants for the CsCl-type crystals on the Kellermann model are given by the following expressions

$$C_{11} = \frac{9e^2}{32r_0^4} \left[ 5.621 + \frac{2}{3} (B' + 2A') \right], \quad \dots \quad (20)$$

$$C_{12} = \frac{9e^2}{32r_0^4} \left[ -5.518 + \frac{2}{3} (B' - 2A') \right], \quad \dots (21)$$

and

$$C_{44} = \frac{9e^2}{32r_0^4} \left[ -2.815 + \frac{2}{3} (B' - 2A') \right], \quad \dots (22)$$

in which again the defining relations for  $A'$  and  $B'$  are the same as given by Eqs (5) and (6) respectively. These lead to finally

$$\left. \begin{aligned} A' &= -\frac{2\alpha}{3}, \\ B' &= \frac{2\mu\omega_0^2 r_0^3}{\sqrt{3}e^2} + 4.4985 \end{aligned} \right\} \quad \dots (23)$$

and

TABLE II

The calculated and experimental values of  $C_{11}$  in units of  $10^{11}$  dyne  $\text{cm}^{-2}$

Crystal	Exptl.	$\alpha$	Calcd	
			Kellermann model	Krishnan and Roy model
LiF	11.35	(u)	11.74	11.82
LiCl	4.94	(a)	4.61	4.64
LiBr	3.94	(a)	3.45	5.64
LiI	2.85	(a)	2.37	2.35
NaF	9.71	(u)	10.55	10.83
NuCl	4.93	(a)	5.19	5.21
NaBr	4.02	(u)	4.22	4.23
NaI	3.035	(a)	3.16	3.17
KF	6.58	(a)	6.77	6.93
KCl	4.08	(a)	4.48	4.49
KBr	3.49	(a)	3.69	3.71
KI	2.775	(a)	3.16	3.17
RbF	5.7	(a)	5.35	5.37
RbCl	3.645	(a)	3.90	3.91
RbBr	3.185	(a)	3.43	3.44
RbI	2.585	(a)	2.74	2.75
CsF	.....		3.62	3.63
CsCl	3.64	(b)	4.05	4.10
CsBr	3.10	(b)	3.55	3.57
CsI	2.45	(b)	2.74	2.90

(a) Spangenberg, K. and Haussühl, S., 1957, *Z. Krist.*, **109**, 422.

(b) Haussühl, S., 1960, *Acta Cryst.*, **13**, 687.

The computed values of  $C_{11}$  on the Kellermann model for all the alkali halides are listed in Table II column 3 along with the experimental values in column 2. The average absolute deviation is 8.5%. This figure competes well with the one of 8.2 obtained when compressibility data are used in place of  $\omega_0$ .

In Table III, column 3, are shown the computed values of  $C_{12}$  obtained from the use of Eq. (21) together with the experimental data in column 2. The average absolute percentage deviation is 18.1 which is a marked improvement over the figure of 25.1 corresponding to the use of  $\beta$ , i.e., the conventional procedure.

The values of  $C_{44}$  for the three CsCl-type crystals obtained according to Eq. (22) are recorded in Table III, column 6, along with the experimental data in column 5. Here the average absolute deviation of theory from experiment is only 7.6 per cent compared to 14.7 obtained from the use of  $\beta$ .

TABLE III

Calculated and experimental values of elastic constants in units of  $10^{11}$  dyne  $\text{cm}^{-2}$

Crystal	$C_{12}$			$C_{44}$		
	Exptl (a)	Calcd		Exptl (a)	Calcd	
		Kellermann model	Krishnan and Roy model		Kellermann model	Krishnan and Roy model
CsCl	0.92	0.69	0.71	0.80	0.690	0.71
CsBr	0.84	0.70	0.75	0.75	0.694	0.75
CsI	0.71	0.62	0.64	0.62	0.61	0.64

(a) Haussühl, S., 1960, *Acta Cryst.*, **13**, 687.

On the model of Krishnan and Roy (1952) for NaCl-type crystals the working Eqs. are

$$C_{11} = [2\alpha(1+\delta) - 6\chi] \frac{e^2}{12r_0^4}, \quad \dots \quad (24)$$

and

$$C_{12} = C_{44} = 3(\chi - \alpha) \frac{e^2}{12r_0^4}, \quad \dots \quad (25)$$

while for CsCl-type these are

$$C_{11} = [2\alpha'(1+\delta) - 18\chi'] \frac{e^2}{16r_0^4}, \quad \dots \quad (26)$$

and

$$C_{12} = C_{44} = [\alpha'(2\delta - 7) + 9\chi'] \frac{e^2}{16r_0^4}. \quad \dots \quad (27)$$



Here  $\delta = r_0/\rho$ ,  $\alpha' = 1.018$ ,  $X = 3.14$  and  $X' = 1.08$ . The values of  $C_{11}$  using Eqs. (24) and (26) are shown in Table II, column 4. The average absolute percentage deviation is 10.8 compared to 8.5 for the conventional approach. The values of  $C_{12}$  and  $C_{44}$  obtained from Eq. (27) are reproduced in columns 4 and 6 of Table III. For  $C_{12}$  the average absolute percentage deviation is 14.5 which is to be compared with the figure of 23.3 found from the conventional procedure. Again for  $C_{44}$  the average absolute deviation is 4.7 only which indicates great improvement over the figure 12.7 obtained previously. Thus we infer that the elastic constants are in general better reproduced through the use of  $\omega_0$  compared to  $\beta$  data or in other words, the proposed procedure is better than the conventional procedure.

### CONCLUSIONS

We now sum up the results obtained on the computation of different bulk crystal properties obtained on the proposed and conventional procedures in particular reference to their success in reproducing the experimental data. The values of cohesive energy of alkali halides are reproduced with almost equal success. In compressibility the proposed method leads to appreciably better results than the conventional procedure. Thermal expansion coefficients are also better reproduced on the basis of proposed method than the conventional approach. The Grüneisen constants on the other hand are well reproduced by the conventional method in comparison to the proposed one. On the other hand, the elastic constants are better reproduced by the proposed than the conventional method. The only exception is  $C_{11}$  where the conventional approach commands a relative superiority over the proposed one.

Thus on the whole we find that the use of Reststrahlen frequency instead of  $\beta$  in determining the potential parameters and then in predicting the properties, is preferable. It leads to a happy conclusion viz. the use of Reststrahlen frequency in interpreting the bulk behaviour of crystals as encompassed in the different properties considered in this paper. Incidentally, this work also brings to light a link between lattice vibrations and the fundamental simple crystal properties through interatomic forces and that too in a very simple way.

### REFERENCES

- Born, M., and Mayer, J. E., 1932, *Z. Physik*, **75**, 1.  
 Kachhava, C. M. and Saxena, S. C., 1963, *Phil. Mag.*, **8**, 1429.  
 ————— 1964, *Indian J. Phys.*, **38**, 388.  
 ————— 1965a, *Indian J. Phys.* (In Press)  
 ————— 1965b, *Indian J. Pure App. Phys.* (In Press).  
 Kollermann, E. W., 1940, *Phil. Trans.*, **A238**, 513  
 Krishnan, K. S. and Roy, S. K., 1962, *Proc. Roy. Soc.*, **A210**, 481  
 Kumar, S., 1959, *Proc. Natl. Inst. (India)*, **A25**, 364  
 Saxena, S. C. and Kachhava, C. M., 1966, *App. Sci. Res. (Netherlands)*, (In Press).  
 Sharan, B. and Tawari, L. M., 1964, *Phys. Stat. Solids*, **7**, 39.

# CRYSTALLOGRAPHIC DATA FOR COMPLEX COPPER LUTIDINE CHLORIDE

T. RATHO AND Mrs. M. KRISHNASWAMY

REGIONAL ENGINEERING COLLEGE, ROURKELA

(Received April 11, 1966; Resubmitted June 1, 1966)

**ABSTRACT.** Debye Scherrer pattern of Copper Lutidine Chloride has been photographed with the help of Rigaku Camera at room temperatures. The Powder diffraction data showed that the complex belonged to the monoclinic system with  $a = 13.75 \text{ \AA}$ ,  $b = 11.56 \text{ \AA}$ ,  $c = 10.91 \text{ \AA}$  and  $\beta = 103^\circ 11'$ . The number of molecules per unit cell is 4. The systematic extinctions observed are consistent with the space group  $P2_1/m - C_{2h}$  or  $P2_1 - C_2$ .

## INTRODUCTION

Copper Lutidine Chloride  $[\text{Cu}(\text{C}_7\text{H}_9\text{N})_2\text{Cl}_2]$  is obtainable in the microcrystalline form, pink in colour, and the diamagnetic properties of such complexes using Lutidine as ligand is of some interest. As it is not possible to grow large crystal powder method has been resorted to, to investigate some of its crystallographic properties.

## EXPERIMENTAL

When Cupric Chloride dissolved in Ethanol is treated with ethanolic solution of Lutidine, a shining pink crystalline substance separates out. This is the microcrystalline complex compound of Copper Lutidine Chloride.

Filtered  $\text{CuK}_\alpha$  radiation was obtained from a Machlett A-2 X-ray diffraction tube running at 15 mA, 30 K.V. and the specimen was contained in a Lindmann glass capillary tube of 0.5 mm. diameter, wall thickness 0.01 mm. The Debye Scherrer pattern of the substance was obtained on a photographic film using the Rigaku Camera of 9 cm. diameter. The time of exposure was about 12 hours.

The interplanar distances were calculated from the measurements on the diffraction pattern with great accuracy. Attempts were made to index the powder lines in terms of cubic, tetragonal and hexagonal systems.

Since the observed data did not fit into any one of these systems of higher symmetry, the Lipson's method (Lipson, 1949) was tried and this also did not give sufficient number of constant differences. This evidently shows that the crystal perhaps belongs to the lower symmetry group of monoclinic or triclinic systems. Therefore it became necessary to apply either De Wolffe's method (De Wolffe, 1957) or Ito's method (Ito, 1950).

### EXPERIMENTAL DATA

The X-ray data obtained are given in Table II. Since all the six unknown parameters are to be determined, the most general method of Ito (Ito, 1950) was applied.

The powder pattern was indexed by Ito's method (Ito's, 1950, Azouaroff and Buerger, 1958). The interplanar spacings and the corresponding  $Q$  values ( $Q_{hkl} = 1/d^2_{hkl}$ ) are listed in Table II.

In Ito's method the expression relating  $\sin^2\theta(Q)$  to the cell constants of a triclinic cell is

$Q_{hkl} = h^2a^{*2} + k^2b^{*2} + l^2c^{*2} + 2hkb^*c^* \cos \alpha^* + 2hlc^*a^* \cos \beta^* + 2hka^*b^* \cos \gamma^*$   
 where  $\alpha^*$ ,  $\beta^*$ ,  $\gamma^*$  and  $a^*$ ,  $b^*$  and  $c^*$  are the reciprocal angles and axes respectively.

The first three lines in Table II were first taken as  $Q_{100}$ ,  $Q_{010}$ , and  $Q_{001}$ . Attempts were made to index the other lines with the above assumption. Since it was not possible, the first three lines were taken again as  $Q_{200}$ ,  $Q_{020}$ , and  $Q_{002}$ . It can be seen from Table I that the observed  $Q$ 's are in good agreement with the calculated  $Q$  values for the other higher orders of reflection.

TABLE I  
Selection of  $Q_{200}$ ,  $Q_{020}$ , and  $Q_{002}$

$Q_{hkl}$	Computed	Observed	Error in $Q$	$Q$ , Corrected
$Q_{200}$		0.0227		
$Q_{400}$	0.0908	0.0891	$\frac{-0.0017}{4} = -0.0004$	0.0223
$Q_{600}$	0.2043	—		
$Q_{020}$		0.0292		
$Q_{040}$	0.1168	0.1106	$+\frac{0.0028}{4} = +0.0007$	0.0299
$Q_{080}$	0.2028	—		
$Q_{002}$		0.03465		
$Q_{004}$	0.1386	0.1418	$+\frac{0.0032}{4} = +0.0008$	0.03545
$Q_{006}$	0.3118	0.3190	$+\frac{0.0072}{9} = +0.0008$	

From Table I one gets the reciprocal cell dimensions as

$$\begin{aligned} a^* &= 0.0747 \\ b^* &= 0.08648 \\ c^* &= 0.09412 \end{aligned}$$

Now considering the  $Q$  values for planes  $hol$  and  $h\bar{o}l$  with  $\beta^* \neq 90^\circ$ , we have

$$Q_{hol} = h^2 a^{*2} + l^2 c^{*2} + 2hl c^* a^* \cos \beta^*$$

$$Q_{h\bar{o}l} = h^2 a^{*2} + l^2 c^{*2} - 2hl c^* a^* \cos \beta^*.$$

It is seen that these quantities are symmetrical with respect to the quantity  $a^{*2} + c^{*2}$ . By giving proper values to  $h$  and  $l$ , the two symmetrically placed lines  $hol$  and  $h\bar{o}l$  were found out. Then  $\beta^*$  was calculated from

$$\cos \beta^* = \frac{(Q_{hol} - Q_{h\bar{o}l})}{4c^* a^* hl}$$

This  $\beta^*$  was found out to be  $76^\circ 49'$ . The other two angles  $\alpha^*$  and  $\gamma^*$  were derived in the same way and they were found to be  $\alpha^* = 90^\circ$ , and  $\gamma^* = 90^\circ$ .

Therefore the six parameters of the reciprocal cells are

$$\begin{aligned} a^* &= 0.0747 & \alpha^* &= 90^\circ \\ b^* &= 0.08648 & \beta^* &= 76^\circ 49' \\ c^* &= 0.09412 & \gamma^* &= 90^\circ \end{aligned}$$

The direct cell dimensions are therefore

$$\begin{aligned} a &= 13.75 \text{ \AA} & \alpha &= 90^\circ \\ b &= 11.56 \text{ \AA} & \beta &= 103^\circ 11' \\ c &= 10.91 \text{ \AA} & \gamma &= 90^\circ. \end{aligned}$$

The Buerger's test for reduced cell dimensions has been applied and the dimensions are found to be the reduced ones.

TABLE II

No. of lines	Intensity	d Å	$Q_{hkl} = 1/d^2$ observed	$Q_{hkl}$ computed	Indices
1.	vs	6.636	0.0227	0.0223	200
2.	w	5.852	0.0292	0.0299 0.0298	020 210
3.	vw	5.371	0.03465	0.03545 0.0355 0.0340	022 120 102
4.	vvw	4.564	0.04799	0.0476 0.0474	121 102
5.	w	4.222	0.0561	0.0569	311
6.	ms	3.773	0.0703	0.0706	202
7.	w	3.538	0.0799	0.0797 0.0794 0.0801	003 321 320
8.	h	3.350	0.0891	0.0892 0.0896	400 230
9.	w	3.181	0.0988	0.0991 0.0986	402 321

TABLE II (contd.)

No. of lines	Intensity	d Å	$Q_{hkl} = 1/d^2$ observed	$Q_{hkl}$ computed	Indices
10.	w	2.892	0.1196	0.1196 0.1192	040 420
11.	ms	2.756	0.1316	0.1311 0.1309	323 141
12.	vw	2.654	0.1418	0.1418 0.1420 0.1420	004 240 114
13.	w	2.605	0.1473	0.1470 0.1471	510 033
14.	ms	2.581	0.1501	0.1503 0.1502 0.1504	402 233 512
15.	vw	2.505	0.1593	0.1588	303
16.	m	2.433	0.1690	0.1684 0.1685 0.1692 0.1694	224 333 341 520
17.	vw	2.353	0.1806	0.1803	422
18.	vw	2.290	0.1907	0.1902 0.1905	242 601
19.	vw	2.261	0.1955	0.1954 0.1959	143 051
20.	vw	2.187	0.2091	0.2091 0.2090 0.2093	034 440 250
21.	vw	2.180	0.2105	0.2111 0.2103	105 532
22.	m	2.104	0.2258	0.2261	333
23.	m	1.998	0.2505	0.2503	443
24.	vw	1.834	0.2972	0.2972 0.2979 0.2977	523 451 334
25.	vw	1.770	0.3190	0.3191 0.3197 0.3195 0.3191 0.3188 0.3194	006 305 360 310 361 551
26.	vw	1.693	0.3486	0.3488 0.3490 0.3487	026 063 535
27.	vvw	1.676	0.3559	0.3567	326
28.	vw	1.642	0.3712	0.3704	363
29.	vw	1.590	0.3956	0.3955	245
30.	vvw	1.544	0.4194	0.4194 0.4190	604 462
31.	vvw	1.429	0.4898	0.4899	256

The crystal therefore belongs to the monoclinic system.

Finally all the  $Q_{hkl}$  values were computed using the above general formula. The powder pattern so indexed showed the following conditions.

$hkl$ —no condition ;

$oko$ —odd absent.

This obviously leads to the probable space group  $P2_1/m-C_{2h}^2$  or  $P2_1-C_2^2$ .

The observed density of 1.412 gms./cc. indicates 4 molecules per unit cell; calculated density is 1.372 gms./cc.

It is however not possible to throw light on the complete structure of this substance. Further work on these lines is in progress.

#### ACKNOWLEDGMENT

Our thanks are due to Dr. D. V. Raman Rao, Head of the Department of Chemistry, for supplying the chemically pure sample used in this work.

#### REFERENCES

- Azroff, L. V. and Buerger, M. J , 1958, *Powder Method*, 150  
Deyo and Wuit, 1960, *X-ray Powder Photography in Inorganic Chemistry*.  
Ito, T , 1950, *X-ray studies in Polymorphism*, Maruzen Tokyo.  
Lipson, H , 1949, *Acta Cryst*, 2, 43

# RELAXATION METHOD OF SOLVING THE CIRCUIT OF AN INDUCTION MOTOR WITH A PHASE ADVANCER

S N. DUTTA

DEPARTMENT OF APPLIED PHYSICS, CALCUTTA UNIVERSITY

(Received May 18, 1966)

**ABSTRACT.** In this paper it has been discussed how the relaxation method can be suitably applied to solve the circuit problem of an induction motor with a phase advancer. For this purpose the relaxational technique of solution of A.C. networks with complex circuit constants is used. It also discusses a method slightly different from the existing ones for obtaining operation groups to liquidate the residuals of linear simultaneous equations in a definite number of steps. The results obtained thereby are compared with those found out by conventional method of solution of A.C. networks which is illustrated with an example.

## INTRODUCTION

The basic idea of having a phase advancer consists in so adding to the rotor induced e.m.f. that there is a phase advancement in the rotor current with a consequent reaction on the stator to advance the phase of the stator current also (Say, 1962). The equivalent circuit of an induction motor with a phase advancer is shown in Fig. 1 (Mem. Staff. Dept. Elect. Engg., M I T., 1953), which can be transformed into a suitable form shown in Fig. 2a. Relaxation method can be conveniently applied to solve this network yielding the values of many desired quantities simultaneously. Southwell and Black (1938) have used the relaxation method to solve the problem of A.C. networks and have shown that the presence of complex circuit constants does not add much difficulty in getting its relaxational solution. The advantages of the method will be indicated by solving the problem represented in the Fig. 2a.

To liquidate the residuals in the solution of linear simultaneous equations a method with some difference from those suggested by Bandyopadhyay and Narshinhan (1956), and Basu (1958) has been developed. In this method the difference lies in the fact that operation groups (Allen, 1954), are found out which will keep only one residual at a time i.e. 1st, 2nd, 3rd etc., successively, unchanged. From this set of group other set of operation groups can be obtained to keep a number of residuals, viz., 1st and 2nd; 1st, 2nd and 3rd and so on, unchanged simultaneously. With the choice of suitable multiples for these groups all the residuals can be liquidated in succession, the maximum number of steps being equal to the number of the residuals.

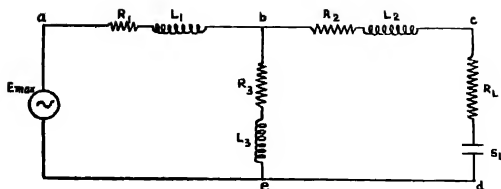


Fig. 1

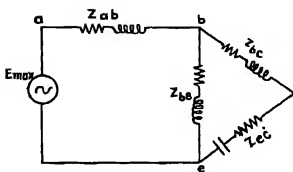


Fig. 2 a

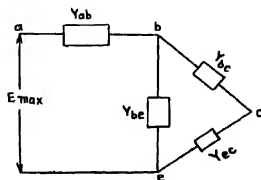


Fig. 2 b

## THE METHOD

Let  $Z_{ab}$ ,  $Z_{bc}$  ... etc., be the impedances and  $Y_{ab}$ ,  $Y_{bc}$  ... etc., be the corresponding admittances of the respective branches of the network shown in Fig. 2b. Considering the admittance of a branch such as  $bc$  it may be written as :

$$Y_{bc} = g_{bc} + j b_{bc} \quad (1)$$

and if the potentials at the nodal points  $b$  and  $c$  be :

$$\left. \begin{aligned} V_b &= v_{x(b)} + j v_{y(b)} \\ V_c &= v_{x(c)} + j v_{y(c)} \end{aligned} \right\} \quad (2)$$

then a current that flows from  $b$  to  $c$  through the branch  $bc$  may be given by :

$$\begin{aligned} I_{bc} &= Y_{bc}(V_b - V_c) \\ &= (g_{bc} + j b_{bc})\{v_{x(b)} + j v_{y(b)} - v_{x(c)} - j v_{y(c)}\} \\ &= [g_{bc}\{v_{x(b)} - v_{x(c)}\} - b_{bc}\{v_{y(b)} - v_{y(c)}\}] \\ &\quad + j [g_{bc}\{v_{y(b)} - v_{y(c)}\} + b_{bc}\{v_{x(b)} - v_{x(c)}\}] \end{aligned}$$

Let the total current flowing into  $b$  from all the branches connected to it be

$$-\sum I_{bc} = I_{b1} = \{i_{x(b)1} + j i_{y(b)1}\}, \text{ so that,}$$

$$-i_{x(b)1} = \sum_b [g_{bc}\{v_{x(b)} - v_{x(c)}\} - b_{bc}\{v_{y(b)} - v_{y(c)}\}] \text{ and} \quad \dots (3)$$

$$-i_{y(b)1} = \sum_b [g_{bc}\{v_{y(b)} - v_{y(c)}\} + b_{bc}\{v_{x(b)} - v_{x(c)}\}]$$



Again if  $I_{b2} = i_{x(b)2} + ji_{y(b)2}$  stands for the current supplied to  $b$  from outside then by Kirchhoff's law,

$$\left. \begin{aligned} i_{x(b)} - i_{x(b)1} + i_{x(b)2} &= 0 \\ i_{y(b)} - i_{y(b)1} + i_{y(b)2} &= 0 \end{aligned} \right\} \quad (4)$$

Assuming the vector potential of  $e$  to be unity and the points  $a$ ,  $b$ , and  $c$  to be at zero potential, the currents flowing from  $e$  to  $b$  and  $e$  to  $c$  along the branches  $eb$  and  $ec$  can be written as

$$\begin{aligned} I_{eb} &= Y_{be} = g_{be} + jb_{be} \\ I_{ec} &= Y_{ce} = g_{ce} + jb_{ce} \end{aligned} \quad (5)$$

and no current will flow in any other branch of the circuit. To have the assumed potentials correct, a current,  $-I_{e2} = -I_{eb} - I_{ec} = i_{x(e)2} + ji_{y(e)2}$  is to be supplied to  $e$  from outside. Then the currents  $I_{eb}$  and  $I_{ec}$  will leave the network at  $b$  and  $c$  respectively. But actually no current flows to or from the network at  $b$  and  $c$ . Hence on the assumed potentials these are to be superposed, which would result if the currents  $I_{b(2)} (= I_{eb})$  and  $I_{c(2)} (-I_{ec})$  were supplied at  $b$  and  $c$  and allowed to leave the network at  $e$  and  $a$ , the latter points being kept at zero potentials. Then it is obtained initially as follows:

$$\begin{aligned} i_{x(b)} &= i_{a(b)2} = g_{be}; & i_{a(e)} &= i_{x(e)2} = g_{ce}; \\ i_{y(b)} &= i_{y(b)2} = b_{be}; & i_{y(e)} &= i_{y(e)2} = b_{ce}; \\ i_{x(a)} &= i_{x(e)2} = -(g_{be} + g_{ce}); \\ i_{y(a)} &= i_{y(e)2} = -(b_{be} + b_{ce}); \end{aligned}$$

with  $i_{x(a)} = i_{y(a)} = 0$ .

To liquidate the residuals i.e. these initial values  $i_{x(b)}$ ,  $i_{y(b)}$ ,  $i_{x(e)}$  and  $i_{y(e)}$  by giving suitable vector potentials at  $b$  and  $c$  only, a standard operation table can be written by the use of the following expression which may be readily obtained from relations (3).

$$\begin{aligned} \frac{\delta i_{x(e)}}{\delta v_{x(b)}} &= g_{be} = \frac{\delta i_{y(e)}}{\delta v_{y(b)}}; \\ - \frac{\delta i_{x(e)}}{\delta v_{y(e)}} &= b_{be} = \frac{\delta i_{y(e)}}{\delta v_{x(b)}}, \quad \dots \quad (6) \end{aligned}$$

$$\begin{aligned} \text{and} \quad \frac{\delta i_{x(b)}}{\delta v_{x(b)}} &= \frac{\delta i_{y(b)}}{\delta v_{y(b)}} = - \sum_b (g_{be}); \\ - \frac{\delta i_{x(b)}}{\delta v_{y(b)}} &= \frac{\delta i_{y(b)}}{\delta v_{x(b)}} = - \sum_b (b_{be}). \end{aligned}$$

After liquidation of the residuals the vector currents at  $a$  and  $e$ , and the vector potentials at  $b$  and  $c$  are obtained, which corresponds to unit potential difference between  $e$  and  $a$ . In liquidating the residuals first of all a set of operation groups can be found out by considering the operation steps of unit operation table in successive pairs to keep only one residual i.e. 1st, 2nd etc., unchanged consecutively. From these groups a second set of operation groups are obtained to keep first two residuals i.e. 1st and 2nd, unchanged at a time. Lastly, another operation group can be written from the second set of groups which will not have any effect on the values of the first three residuals simultaneously. Using these group operations a definite number of liquidation steps can be obtained not exceeding the number of residuals. Although by this method a quick and systematic liquidation is achieved, it imposes no restriction in finding out suitable operation blocks and other groups if required in any particular problem. Hence its flexibility is not affected.

#### ILLUSTRATION

An example (Fig. 1) worked out by different method (Mem. Staff Dept Elect Engg. M.I.T., 1953), has been taken as an illustrating one in which  $E_{max} = 150 \text{ V}$ , frequency = 200 cycles per second,  $R_1 = 12.00 \text{ ohms}$ ,  $L_1 = 0.300 \text{ henry}$ ,  $R_2 = 19.20 \text{ ohms}$ ,  $L_2 = 0.1862 \text{ henry}$ ,  $R_3 = 250.0 \text{ ohms}$ ,  $L_3 = 6.50 \text{ henries}$ ,  $R_L = 200.0 \text{ ohms}$ ,  $S_L = 6.29 \times 10^5 \text{ darafs}$

The effective value of the current delivered by the source, effective value of the voltage across  $cd$  and its phase relative to that of the source are to be calculated.

Considering the different branches of the network shown in Fig. 2b, their corresponding admittances can be calculated from the supplied data as follows :

$$Y_{ab} = (0.8682 - j27.2)10^{-4} \text{ mho}$$

$$Y_{be} = (0.036 - j1.224)10^{-4} \text{ "}$$

$$Y_{bc} = (3.482 - j42.44)10^{-4} \text{ "}$$

$$Y_{ec} = (6.897 + j17.24)10^{-4} \text{ "}$$

In order to simplify the calculation and to have higher accuracy of results the above admittances are multiplied by  $10^4$ , keeping in mind that in finding out the currents, the required quantities are to be multiplied by  $10^{-4}$  and also by the effective value of  $E_{max}$  of the example.

Hence the currents flowing in the branches  $ec$  and  $eb$  can be written as :

$$I_{ec} = 6.897 + j17.24$$

$$I_{eb} = 0.036 - j1.224$$

Then the current of  $-I_{e2}$  that is to be flown to  $e$  from outside comes out to be.

$$-I_{e2} = 6.933 + j16.016$$

So initially it may be obtained as follows :

$$\begin{aligned}i_{x(b)} &= 0.036; \quad i_{x(c)} = 6.897; \quad i_{x(e)} = -6.933; \\i_{y(b)} &= -1.224; \quad i_{y(e)} = 17.24; \quad i_{y(c)} = -16.016.\end{aligned}$$

and

$$i_{x(a)} = i_{y(a)} = 0.$$

Then the unit operation table (Table I) can be written with the help of relations (6) and by multiplying the  $g$  and  $b$  values by  $10^4$  for the reason already stated. The required group operations (Dutta, 1966) can be performed to have no change of  $i_{x(b)}$ ,  $i_{x(c)}$ ,  $i_{y(b)}$ , and  $i_{y(c)}$  successively by using unit operation steps 1 and 2, 2 and 3, 3 and 4, and 4, and 1 of Table I, in pairs shown in group operation steps 5, 6, 7 and 8 in Table II. From these steps (operation steps 5 to 8 in Table II) two other operation groups (operation steps 9 and 10 in Table II) are found out to keep both  $i_{x(b)}$  and  $i_{x(c)}$  unchanged simultaneously. Finally, another group operation step (operation step 11 in Table II) is developed from those steps (operation steps 9 and 10 in Table II) in which  $i_{x(b)}$ ,  $i_{x(c)}$ , and  $i_{y(b)}$  are seen to remain unchanged at a time. The residuals can now be liquidated very easily and systematically in four steps (liquidation steps 12, 13, 14 and 15 in Table II) using the unit and group operation steps (operation step 1 in Table I and 5, 10 and 11 in Table II) without spending much time for finding out other suitable block or group operation by inspecting the unit operation table. The operation and liquidation steps are shown within the brackets ( ) and the actual operation and liquidation are shown within the brackets [ ].

Considering the effective value of  $E_{max}$ , the effective value of the voltage across  $cd$  (Fig. 1) which is the same as that across  $ce$  (Fig. 2b) is given by,

$$\begin{aligned}V_{cd} &= (0.0539 - j2.0961) \times 10.6082 \text{ volts} \\&= 22.2433 \angle -88^\circ 32' \text{ volts} \{ 22.1 \angle -90^\circ \text{ volts} \}\end{aligned}$$

and the required current is given by,

$$\begin{aligned}I_a &= (34.9644 - j14.1152) \times 10.6082 \times 10^{-4} \text{ amp} \\&= 0.0399 \angle -21^\circ 59' \text{ amp} \{ 0.0397 \angle -23^\circ 30' \text{ amp} \}\end{aligned}$$

From the above it is seen that the values of the voltage and the current calculated by other method (Mem. Staff. Dept. Elect. Engg., M. I. T., 1953) shown within brackets { } are in good agreement with those obtained by relaxation method.

#### DISCUSSION

This paper shows clearly how with the help of the method indicated in the paper, values of a number of desired quantities i.e. potentials at the nodal points  $b$  and  $c$ , currents at  $a$  and  $e$ , and the respective phase angles can be obtained simultaneously. This method becomes useful particularly when the number of nodal

points increases in complex networks, where the conventional methods are seen to be laborious.

Also in the method used here to liquidate the residuals, a set of operation groups (operation steps 5 to 8 in Table II) as obtained may be found to be useful in keeping any particular residual unchanged in some operation if required.

Further it is seen that  $V_{ed}$  is greater than the voltage impressed by the source on the circuit. This is due to the fact that in A.C. circuits the impedance of a part may be greater than that of the entire circuit as the imaginary components may be either positive or negative.

#### ACKNOWLEDGMENT

The author is highly indebted to Prof. A. K. Sengupta, D.Sc., A.M.I.E.E. (London), Head of the Department of Applied Physics, Calcutta University, for his help and guidance throughout the progress of this work.

#### REFERENCES

- Allen, D. N. de G., 1954, *Relaxation Methods* (McGraw-Hill Book Co. Inc., New York), 17.
- Bandyopadhyay, G. and Narasimhan, R. K., 1956, *Quart. J. Mech. and Applied Math.*, **9**, 122.
- Basu, R. N., 1958, *Jour. Assn. Applied Physicists*, **30**.
- Black, A. N. and Southwell, R. V., 1938, *Proc. Roy. Soc. (A)* **164**, 447.
- Dutta, S. N., 1966, *Indian J. Phys.*, **40**, 1, 1.
- Members of the Staff of the Department of Electrical Engineering, Massachusetts Institute of Technology, 1953, *Electric Circuits*. The Technology Press, M.I.T., 292.
- Say, M. G., 1962, *The Performance and Design of A.C. Machines*. Sir Isaac Pitman & Sons, Ltd., London, 339.
- Southwell, R. V., 1951, *Relaxation Methods in Engineering Science*, Oxford University Press, London, 114.

## Letters to the Editor

*The Board of Editors does not hold itself responsible for opinions expressed in the letters published in this section. The notes containing short reports of original investigations communicated to this section should not contain many figures and should not exceed 500 words in length. The contributions reaching the Secretary by the 15th of any month may be expected to appear in the issue for the next month. No proof will be sent to the author.*

18

### ON A HOLE THEORY OF LIQUIDS.

S. C. MISRA

PAKIR MOHAN COLLEGE, BALASORE

(Received February 24, 1966; Resubmitted July 12, 1966)

We will consider here the interlattice holes of a crystal as the regular sites of a second lattice and also like Leonard-Jones and Devonshire (1939), assume that each atom of a monatomic crystal is associated with a hole. Upto the fusion point and even at the beginning of the liquid state this is the position. The two lattices coincide at absolute zero and with rise of temperature gradually the two are separated till at the fusion point the two are completely dissociated. After this when the temperature rises, gradually the atoms leave the lattice sites to wander as free particles and the corresponding holes dissolve in the interstitial space. When all the holes will dissolve, we shall get a perfect gas.

All the atoms are at their respective position on the lattice (may be on the minute crystals into which the large crystal has been divided) at the melting point. These atoms cannot produce any impact on the wall of the container and hence can exert no pressure. At any temperature  $T$ , let there be  $N_1$  free atoms and  $N_2$  atoms fixed to the lattice sites. So  $N_1$  holes must have been lost in the interstitial space and only  $N_2$  holes must have remained at the regular lattice sites.

At melting point ( $T_m$ )  $N_2 = L$ , the Avogador's number for one gram. mol. of substance. With increase of temperature  $N_2$  will go on decreasing till at a high temperature it reduces to zero.  $N_1$  will change in a reverse order and will behave as a perfect gas at all temperatures. So the situation is as if a saturated vapour is in contact with its condensed phase. Here  $N_1$  particles belong to one phase space and  $N_2$  to another phase space and with change of temperature, particles pass from one phase space to the other. The  $N_1$  phase space corresponds to the ideal gas and the  $N_2$  phase space corresponds to the ideal solid.

A similar situation we meet when particles come out of a radioactive substance. One type of phase space controls the behaviour of the nuclei and another

controls the behaviour of the particles radiated. It is to be noted that the number of particles passing from one space to the other is found out by a non-mechanical statistics, determined by trial. We will also follow a similar procedure.

Let  $dN$  be the number by which  $N_2$  decreases when temperature increases by  $dT$ .

Let  $dN = -\theta NT^{-1}dT$  where  $N = N_2$

From this we get  $N = Le^{-2\theta(T^1 - T_m^1)} = N_2$  ... (1)

by introducing the condition that at  $T_m$ ,  $N = L$

Now  $N_1 = L - N = L[1 - e^{-2\theta(T^1 - T_m^1)}]$  ... (2)

The picture that we have taken for liquids (and real gases), make it very clear that the only effect of the heat added to the system is to remove the atoms from the lattice sites and to increase the kinetic energy of the particles in the interstitial space. It has, so to say, no other effect on the atoms at the regular lattice sites. So in order to determine the energy-content of a liquid (or of a real gas) we need only consider the effect of the  $N_1$  particles. Since these particles behave like particles of a perfect gas, we are only to write  $L[1 - e^{-2\theta(T^1 - T_m^1)}]$  in place of  $L$  in perfect gas equations. The variation of specific heat with temperature in case of four liquids have been explained successfully by the author (Misra, 1966) on this basis. It has also been shown in another paper (to be published) that the idea can be extended to the case of nonuniform properties like viscosity. Assuming regular distribution of the holes, we can explain X-ray haloes in case of liquids. Attempts are being made to explain other properties of liquids and gases with this idea.

#### REFERENCES

- Lennard-Jones and Devonshire, 1939, *Proc Roy. Soc* **169A**, 317.  
 Misra, S. 1966, *Indian J. Phys.*, **40**, 157,

# RELAXATION TECHNIQUE AS APPLIED TO WHEATSTONE BRIDGE NETWORK PROBLEM

S. N. DUTTA

DEPARTMENT OF APPLIED PHYSICS, CALCUTTA UNIVERSITY

(Received May 18, 1966)

**ABSTRACT.** This paper deals with the relaxation solution of the problem of Wheatstone bridge network. In doing so the heating effects of steady currents flowing in the network have been considered and thereafter the desired quantities are found out easily by relaxation method. It also shows how this method yields a number of useful informations at a time. A comparison of the results obtained by this and other methods has been made.

## INTRODUCTION

Bridges are one of the most widely used circuit arrangement in the field of measurement of circuit parameters, the simplest and important form of which is the Wheatstone bridge. Here a general case of unbalanced Wheatstone bridge (fig. 1), is considered in which the value of the galvanometer current has been found out. The normal methods of analysis of this bridge configuration consisting of three meshes is somewhat complicated for general values of bridge parameters. But here it will be shown that an easy and convenient solution of this problem is possible by relaxation method considering the equivalent circuit diagram (fig. 2) of the network shown in fig. 1

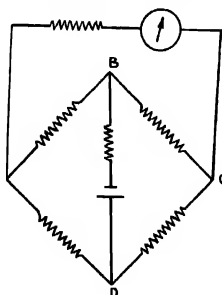


Fig.1.

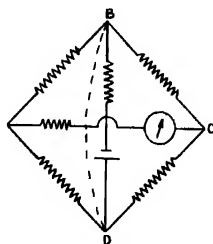


Fig.2.

It was first of all shown by Southwell and Black (1938) and afterwards also by Dutta (1966), how relaxation method can be suitably applied to solve the problem of D.C. network. The underlying principle of this solution will reveal the utility of the technique in solving the network problem shown in fig. 2.

## THE METHOD

The heating effects of steady currents flowing in the network have been considered in this method and an electrical theorem (Southwell and Black, 1938), in this connection has been used which can be stated as follows :

"In a network of conductors to which specified currents are supplied at two or more nodal points, the actual distribution of currents is such that the total generation of heat less twice the energy expended in supplying the specified currents from a source at datum potential has its minimum value consistent with the satisfaction of Kirchhoff's second law".

If the two nodal points  $A$  and  $B$  of the Wheatstone bridge network shown in fig 2, be joined by a conductor of resistance  $R_{AB}$ , then by Ohm's law a current of

$\frac{V_A - V_B}{R_{AB}}$  will flow from  $A$  to  $B$ , where  $V_A$  and  $V_B$  are the potentials at  $A$  and  $B$ .

Let the currents  $I_A$  and  $I_B$  flow towards  $A$  and  $B$  respectively and then,

$$-I_A = I_B = g_{AB}(V_A - V_B), \text{ where } g_{AB} = 1/R_{AB}.$$

Also if all the conductors connected to the nodal point  $A$  be considered it can be written that,

$$\Sigma g_{AB}(V_B - V_A) + I_{AO} = 0 \quad \dots (1)$$

where  $I_{AO}$  means the current supplied to  $A$  from outside. Hence the heat generated in  $AB$  is given by the expression  $g_{AB}(V_A - V_B)^2$ , and thus the total heat generated in the network is represented by

$$2H = \Sigma_m g_{AB}(V_A - V_B)^2 \quad \dots (2)$$

where  $\Sigma_m$  stands for the summation extending to every conductor. Let again a current be supplied to  $A$  from an outside source at datum potential  $V_0$ , so that the rate of expenditure of energy is measured by  $I_{AO}(V_A - V_0)$  and the total expenditure of energy is measured by

$$\Sigma_n \{I_{AO}(V_A - V_0)\} = -E \quad \dots (3)$$

where  $\Sigma_n$  means the summation extending to every nodal point. Thus equation (1) is typical of the conditions for a minimum value of the quantity,

$$Q = H + E = \frac{1}{2} \Sigma_m \{g_{AB}(V_A - V_B)^2\} + \Sigma_n \{I_{AO}(V_A - V_0)\} \quad \dots (4)$$

as it is equivalent to,

$$-\frac{\partial Q}{\partial V_A} = -\frac{\delta}{\delta V_A} (H + E) = 0.$$



In this network problem as the source of e.m.f. (battery) is present it needs some modification in having its relaxational solution. In order to do this the whole e.m.f. of the source may be assumed to be utilized to pass the current to earth through the resistance of its own associated link and then a datum distribution in which the known currents enter and leave the network at the nodal point can be obtained. Thereafter merely the effects of the neutralizing currents are to be calculated and superposed at those points.

Let the nodal points  $B$  and  $D$  be joined by a wire of zero resistance shown by dotted line in fig. 2. Now the current that will pass through the source from  $D$  to  $B$  will return by that wire and so in the datum distribution a current of  $E/R_{BD}$  enters the system at  $D$  and leaves at  $B$ ,  $R_{BD}$  being the resistance in the branch  $BD$ . Next it is required to calculate and superpose the current distribution resulting when the neutralizing currents  $E/R_{BD}$  and  $-E/R_{BD}$  are supplied to the net-work at  $B$  and  $D$  after removing the battery e.m.f.

If all the branches of the network shown in fig. 2, be considered the expression for  $Q$  and the residuals can be written using the equation (4) as follows :

$$2Q = \frac{(V_A - V_B)^2}{R_{AB}} + \frac{(V_A - V_D)^2}{R_{AD}} + \frac{(V_B - V_D)^2}{R_{BD}} + \frac{(V_C - V_B)^2}{R_{CB}} + \frac{(V_C - V_D)^2}{R_{CD}} \\ + \frac{(V_C - V_A)^2}{R_{CA}} + 2 \frac{E}{R_{BD}} \{V_O - V_B - (V_O - V_D)\} \quad \dots (5)$$

Hence,

$$\left. \begin{aligned} -\frac{\partial Q}{\partial V_A} &= -\frac{(V_A - V_B)}{R_{AB}} - \frac{(V_A - V_D)}{R_{AD}} + \frac{(V_C - V_A)}{R_{CA}} = 0 = F_A \\ -\frac{\partial Q}{\partial V_B} &= \frac{(V_A - V_B)}{R_{AB}} - \frac{(V_B - V_D)}{R_{BD}} + \frac{(V_C - V_B)}{R_{CB}} + \frac{E}{R_{BD}} = \frac{E}{R_{BD}} = F_B \\ -\frac{\partial Q}{\partial V_C} &= -\frac{(V_C - V_B)}{R_{CB}} - \frac{(V_C - V_D)}{R_{CD}} - \frac{(V_C - V_A)}{R_{CA}} = 0 = F_C \\ -\frac{\partial Q}{\partial V_D} &= \frac{(V_A - V_D)}{R_{AD}} + \frac{(V_B - V_D)}{R_{BD}} + \frac{(V_C - V_D)}{R_{CD}} - \frac{E}{R_{BD}} = -\frac{E}{R_{BD}} = F_D \end{aligned} \right\} \quad (6)$$

Liquidation of these residuals (Allen, 1954), obtained initially will yield the potentials at the nodal points  $A$ ,  $B$ ,  $C$  and  $D$  (fig. 2) simultaneously.

The method is illustrated by the following example worked out by Frank (1959), using a different method.

In the Wheatstone bridge network shown in Fig. 1,  $E = 28$  volts,  $R_{BD} = 100$  ohms,  $R_{CA} = 200$  ohms,  $R_{AB} = 200$  ohms,  $R_{CB} = 300$  ohms,  $R_{AD} = 100$  ohms and  $R_{CD} = 150$  ohms, when it is balanced. It is required to find out the current flowing through the galvanometer if  $R_{CD}$  is changed by 4%, making the bridge unbalanced.

The value of  $R_{CD}$  is found out to be 156 ohms when the bridge is unbalanced.

Substituting the numerical values in the relations (5) and (6), it is obtained as follows :

$$2Q = \frac{(V_A - V_B)^2}{200} + \frac{(V_A - V_D)^2}{100} + \frac{(V_B - V_D)^2}{100} + \frac{(V_C - V_B)^2}{300} + \frac{(V_C - V_D)^2}{156} \\ + \frac{(V_C - V_A)^2}{200} + 2 \times 0.28(V_D - V_B) \quad \dots (7)$$

$$\left. \begin{aligned} -\frac{\partial Q}{\partial V_A} &= -\frac{(V_A - V_B)}{200} - \frac{(V_A - V_D)}{200} + \frac{(V_C - V_A)}{200} = 0 = F_A \\ -\frac{\partial Q}{\partial V_B} &= \frac{(V_A - V_B)}{200} - \frac{(V_B - V_D)}{100} + \frac{(V_C - V_B)}{300} + 0.28 = 0.28 = F_B \\ -\frac{\partial Q}{\partial V_C} &= -\frac{(V_C - V_B)}{300} - \frac{(V_C - V_D)}{156} - \frac{(V_C - V_A)}{200} = 0 = F_C \\ -\frac{\partial Q}{\partial V_D} &= \frac{(V_A - V_D)}{100} + \frac{(V_B - V_D)}{100} + \frac{(V_C - V_D)}{156} - 0.28 = -0.28 = F_D \end{aligned} \right\} \dots (8)$$

Now using the relations (7) and (8) the basic operation table (Table I) can be written from which the relaxation table (Table II) is easily obtained in order to liquidate the residuals  $F_A$ ,  $F_B$ ,  $F_C$  and  $F_D$ . In Table II the initial values are multiplied by  $10^2$  so that on liquidation of these residuals the potentials at the nodal points  $A$ ,  $B$ ,  $C$  and  $D$  of the unbalanced bridge can be obtained nearest to their values on being divided by  $10^2$ .

The galvanometer current is found out to be 0.428 mA by relaxation method. The corresponding value of the same is calculated to be 0.429 mA by a conventional method (Frank, 1959), which is in very good agreement with that obtained by the relaxation method.

#### DISCUSSION

In the Wheatstone bridge network considered here the resistances are included both in the galvanometer and battery circuits. This does not in any way bring about any complication in the relaxation method described here. But the conventional method of analysis becomes somewhat complicated and more particularly due to the presence of the resistance in the battery circuit, for which this resistance

TABLE I  
Basic operation Table

Operation Step	$\delta V$	$\delta V_B$	$\delta V_C$	$\delta V_D$	$\delta F_A$	$\delta F_B$	$\delta F_C$	$\delta F_D$
(1)	312	—	—	—	-6.24	1.56	1.56	3.12
(2)	—	312	—	—	1.56	-5.72	1.04	3.12
(3)	—	—	312	—	1.56	1.04	-4.60	2.00
(4)	—	—	—	312	3.12	3.12	2.00	-5.24
(5)[(1)+(2)×4.0]	312	1248	—	—	0	-21.32	5.72	15.6
(6)[(2)+(3)×-1.0]	—	312	-312	—	0	-6.76	5.64	1.12
(7)[(5)-(6)×-3.1538]	312	264.0144	983.9856	—	0	0	-12.0676	12.0676

TABLE II  
Relaxation Table

Liquidation Step	$\delta \Gamma_A$	$\delta \Gamma_B$	$\delta \Gamma_C$	$\delta \Gamma_D$	$F_A$	$F_B$	$F_C$	$F_D$
INITIAL VALUES								
(a)[(5)×1.3133]	409.7496	1638.9984	0	0	0	28.0	0	-28.0
(b)[(7)×0.6223]	194.2200	164.3490	612.5310	0	0	0	0	0
	603.9696	1803.3474	612.5310	0	0	0	0	0

is ignored in many cases at the cost of bridge performance, whereas in the relaxation method the resistance in the battery circuit has got to be considered in order to calculate the current in the datum distribution. Also it yields the values of all the potentials at the nodal points simultaneously. Herein lies the advantage of the method described in this paper

#### ACKNOWLEDGMENT

The author is highly indebted to Prof. A. K. Sengupta, D.Sc., A.M.I.E.E. (London), Head of the Department of Applied Physics, Calcutta University, for his help and guidance throughout the progress of this work.

#### REFERENCES

- Allen, D. N. deG., 1954, *Relaxation Methods*. McGraw-Hill Book Co, Inc., New York  
18
- Black, A. N. and Southwell, R. V., 1938, *Proc. Roy. Soc. (A)*, **164**, 447
- Dutta, S. N., 1966, *Indian J. Phys.*, **40**, 1, pp. 7
- Frank, E., 1959, *Electrical Measurement Analysis*. McGraw-Hill Book Co, Inc., New York, 257.
- Southwell, R. V., 1951, *Relaxation Methods in Engineering Science*, Oxford University Press, London, 114.

# MEASUREMENT OF THERMAL CONDUCTIVITY OF GASES USING THERMAL DIFFUSION COLUMN : NEON

V. K. SAXENA, M. P. SAKSENA AND S. C. SAXENA

PHYSICS DEPARTMENT, RAJASTHAN UNIVERSITY, JAIPUR, INDIA

(Received April 14, 1966; Resubmitted June 4, 1966)

**ABSTRACT.** A hot-wire type of thermal diffusion column is employed to measure thermal conductivity of gases. Measurements on neon are reported in the temperature range 323–723°K and for five different values of pressure smaller than an atmosphere. The values agree amongst themselves within a scatter of about 5 per cent and still better with the other existing literature values obtained from established conventional techniques. The success obtained is particularly gratifying when the prospect of thermal conductivity measurements at higher temperatures is recalled.

## INTRODUCTION

Measurements on thermal conductivity of gases and particularly at high temperatures are of great importance to scientists as well as engineers. For the proper understanding of the exchange of energy between external and internal degrees of freedom of polyatomic molecules such an information is basic. A variety of design engineers also very frequently and in an important way need such values.

It has long been known that reliable and accurate measurement of thermal conductivity of gases is probably the most difficult amongst all the transport properties. This is because many complicated corrections are to be considered and the job becomes increasingly difficult as the temperature of measurement is increased. Purely on the grounds of need in the recent years several very impressive efforts have been made for measuring thermal conductivity at high temperatures. Here we report a part of our continuing effort to determine thermal conductivity using thermal diffusion columns.

The use of columns for thermal conductivity measurements was first suggested and employed by Blais and Mann (1960), who reported results on helium and hydrogen in the temperature range 1200–2000°K. The accuracy of these data is doubtful and it is believed that their values are systematically greater than the actual values, Saxena and Agrawal (1961). A few more arguments in favour of this possibility have been advanced by Saksena (1965). In this laboratory we have revived this work and very encouraging preliminary measurements have been reported on helium and air, Saksena (1965). He employed a system of two glass columns completely identical except for length and measured the thermal conductivity in the temperature range 313–413°K. Differential measurements were taken

to avoid the probable losses due to end conduction and these were also theoretically calculated and found to be always less than 0.6 per cent for air and still smaller for helium. These measurements conclusively established the technique in this temperature range because these values were found to be in good agreement with the directly measured values by the conventional thick wire variant of the hot-wire cell, Gambhir (1965). Encouraged by the success of the results obtained we have launched a full range programme to measure thermal conductivity of various pure gases as a function of temperature. This effort has to be preceded by carefully planned sets of crucial runs which may unambiguously establish the technique and provide a clear idea about the precision of measurements. In the present article we report the measurements on neon in the temperature range 323–723°K at five different pressures and compare with the existing data obtained from conventional techniques.

### THEORY

We now present a brief and relevant account of the theory of this method as particularly applicable to our apparatus design. Assuming the wire to be at a uniform temperature, its ends to be at the same temperature as the cold wall, convection to be absent and the heat flow to be radial, we can write the differential equation giving the heat flow as :

$$\pi a^2 K \frac{d^2 \theta}{dz^2} - 2\pi a h_c \theta - Q_r + \frac{I^2 \rho_0 (1 + \alpha \theta)}{J} = 0. \quad \dots (1)$$

Here  $K$  stands for the thermal conductivity of the material of the hot wire of radius  $a$  at a temperature  $\theta$  above the cold wall temperature. The wire material has a temperature coefficient of resistance  $\alpha$  and  $\rho_0$  is its resistance per unit length at  $\theta = 0$ .  $I$  represents the current through the hot wire and  $J$  the mechanical equivalent of heat.  $h_c$  stands for the loss of heat from the wire per unit area per unit temperature difference by conduction through the gas. Similarly  $Q_r$  represents the quantity of heat radiated from a unit length of the wire.

If the column is highly evacuated so that  $h_c = 0$ , eq. (1) reduces to

$$\pi a^2 K \frac{d^2 \theta}{dz^2} - Q_r + \frac{I'^2 \rho_0 (1 + \alpha \theta)}{J} = 0. \quad \dots (2)$$

Here  $I'$  represents that value of the current which maintains a particular element of the hot wire to be at the same temperature in vacuum as a current  $I$  flowing through it does in the presence of the gas.

Subtracting eq. (2) from (1) we get for the power conducted through the gas

$$2\pi a h_c \theta = \frac{(I^2 - I'^2) \rho_0 (1 + \alpha \theta)}{J}, \quad \dots (3)$$

$$\equiv w_g.$$

Now two more reasonable assumptions get associated with equation (3). These are : (a) The temperature distribution along the length of the wire remains practically unchanged with or without the gas, (b) the heat lost by radiation is independent of the nature of surroundings. For a sufficiently long wire the lengths at the two ends where the temperature may be appreciably different from the uniform temperature in the mid region will be relatively small and the first assumption will be reasonable. The second assumption is also valid as under normal operating conditions the gas in the column is invariably transparent to thermal radiations. We therefore get for cylindrical geometry and radial heat flow conditions

$$\begin{aligned} 2\pi a h_c \theta &= -2\pi a \lambda \left( \frac{d\theta}{dr} \right) \\ &= \frac{2\pi \lambda}{\ln(b/a)} \theta. \end{aligned} \quad \dots (4)$$

Here  $\lambda$  is the thermal conductivity of the gas at the wire temperature and  $b$  is the radius of the cold wall. We have consequently,

$$w_c = \frac{2\pi \lambda}{\ln(b/a)} \theta. \quad \dots (5)$$

The eq. (5) leads to

$$\left( \frac{d\omega_c}{d\theta} \right)_{r=a} = \frac{2\pi \lambda}{\ln(b/a)}, \quad \dots (6)$$

and alternatively

$$\lambda = \frac{\ln(b/a)}{2\pi} \left( \frac{d\omega_c}{d\theta} \right)_r, \quad (7)$$

#### EXPERIMENTAL

The principal component of our experimental assembly consisted of a conventional hot wire type thermal diffusion column. In principle it consists of a precision bore tubing, along the axis of which is run a uniform platinum wire. Through suitably designed arrangements the electrical connections to this wire are brought out. A great care is taken to ensure minimisation and constancy of contact and stray resistances and in our arrangement their magnitude never exceeded 0.02 ohms. The outer wall is maintained at a constant temperature by circulating thermostatically controlled water in the surrounding jacket. The relevant constants of the column are given in Table I. The wire is maintained at different temperatures by passing appropriate currents through an arrangement

which is energised by a number of high capacity lead accumulators. The column can be evacuated to high vacuum ( $10^{-6}$  cm of mercury) by means of a metal pumping plant comprising of a two stage rotary and a high capacity oil diffusion pump etc. The potential across the wire and current through it are measured by a sensitive Tinsley vernier potentiometer type 4363D and other accessories. The constants  $A$  and  $B$  of the platinum wire occurring in the relation

$$R_t = R_0(1 + At + Bt^2), \quad \dots \quad (8)$$

are determined by a separate set of experiments. These are also required in the calculation of  $\lambda$  and are reproduced in table I. The detailed description is given by Saksena (1965).

TABLE 1

Geometrical and electrical constants of the conductivity column

Length of the platinum wire	...	..	91.56 cm
Radius of the wire (a)	.	..	0.02463 cm.
Internal diameter of the column tube (2b)	.	..	0.8544 cm.
External diameter of the column tube (2b')	.	..	1.023 cm.
Resistance per unit length of the platinum wire at 0°C ( $R_0$ )	..	...	0.0054477 ohm/cm.
The constant $A$ of the platinum wire	...	..	$38.25 \times 10^{-4}/^\circ\text{C}$
The constant $B$ of the platinum wire	..	...	$-49 \times 10^{-8}/^\circ\text{C}^2$

In nut-shell the procedure amounts to measuring the power required to heat the wire at any arbitrarily chosen temperature with and without the test gas. To achieve this in practice measurements are taken, in vacuum and then with gas, of the resistance of the axial wire when a known current is passed through it. In Table II, we report the computed power at our directly observed points as a functions of temperature for vacuum and for five different pressures. The temperature of the hot wire in each case is identified by its resistance and assuming this variation to be in accordance with relation (8).

To compute  $\lambda$  for each pressure separately,  $W$  and  $W_r$  are plotted on a large graph paper versus temperature and by point to point subtraction a third curve is generated on the same plot for  $W_e$  as a function of temperature. Here  $W$ ,  $W_r$  and  $W_e$  are the powers fed to the wire, with the gas, without the gas and conducted radially through the gas respectively. Next Stirling's formula is employed and the quantity  $\left(\frac{dW_e}{d\theta}\right)$  is computed for equally spaced values of  $\theta$ .



TABLE II

Record of power ( $W$ , Watt) consumed in the wire to maintain it at different temperatures ( $t$ , °C) in vacuum and at different pressures ( $p$ , cm of mercury)

[illegible]

TABLE III

Values of  $10^5 \lambda$  in  $\text{cal cm}^{-1} \text{sec cm}^{-1} \text{deg}^{-1}$  for Neon at different pressures,  $p$ , in cm of Hg as a function of temperature in  $^{\circ}\text{C}$

Temp.	$p = 10.2$	$p = 17.5$	$p = 29.3$	$p^* = 47.4$	$p = 60.5$
50	12.3	12.1	12.7	13.6	12.6
100	13.3	14.0	13.9	14.9	13.7
150	15.0	14.4	14.7	15.9	14.7
200	15.7	15.4	15.8	17.2	16.1
250	16.9	16.9	17.4	17.7	17.9
300	18.1		18.1	18.4	18.2
350	18.8		19.3	19.3	18.7
400	20.1		20.1		19.3
450	20.5				19.6

\* This set is somewhat uncertain due to the instability of the electrical circuit.

The calculation of  $\lambda$  is now straightforward on the basis of relation (7). These values of  $\lambda$  are recorded in Table III and are shown plotted in Fig. (1). It is relevant to point out here that while taking measurements at 47.4 cm of mercury the electrical circuit was somewhat unstable. This, we feel, might have caused uncertainty in the readings of unknown magnitude. We therefore in interpretation of our results do not give any weight to this set of data. Nevertheless, we have shown them plotted even in Fig. (1). It is interesting to note that the obser-

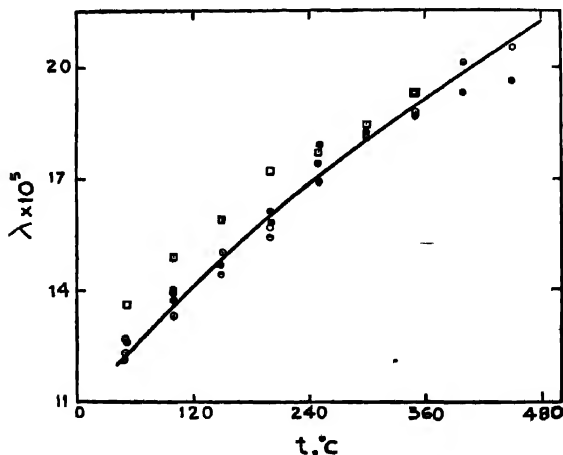


Fig. 1: Plot of  $\lambda \times 10^5$  ( $\text{cal cm}^{-1} \text{sec}^{-1} \text{deg}^{-1}$ ) versus  $t(^{\circ}\text{C})$ . Each set of points refer to a particular value of the pressure (in cm. of mercury). Thus, O,  $\odot$ ,  $\ominus$ ,  $\square$  and  $\bullet$  refer to 10.2, 17.5, 29.3, 47.4 and 60.5 respectively. The continuous curve is obtained as a best compromise plot of all the other existing  $\lambda$  values,

vations even at a pressure higher than this value viz., 60.5 cm of mercury are in accord with the three sets of different observations all at smaller pressures. We hasten to state that all the four sets of  $\lambda$  values show no systematic difference of any particular type relative to each other as a function of temperature. The directly calculated  $\lambda$  values show a scatter of about 5 per cent and at various temperatures it is even smaller. Let us now discuss the important corrections to be applied to these computed  $\lambda$  values.

The corrections likely to be of importance for measurements by this method are : (a) convection, (b) temperature jump, (c) wall and (d) end effects. To discover whether the first two effects are involved in a particular measurement of this type there is an entirely experimental procedure possible. This has been well known to experimentalists of this field and consists in taking measurements as a function of pressure. It was for this reason that we took measurements in the range 10.2 to 60.5 cm of mercury and for five different values of pressure. While taking the measurements it was also kept in mind to detect if there is any systematic variation, howsoever small, with the change in pressure. In the previous measurements pressure dependence was observed only around 2 cm of mercury, Saksena (1965). We thus conclude that for our apparatus and these operating conditions both convection and temperature jump effects are negligible. The calculation of wall effect is fairly well known and is described in detail by Saksena (1965). This effect which arises because of the finite conductivity of the material of the cold wall was found to be fairly small for our measurements. To quote for a numerical estimate it is only 0.3 percent at 50°C and rises slowly with temperature assuming a maximum value of 0.5 percent at 450°C.

The last correction i.e. the end effect is probably the most important of all and unfortunately is least understood. This obviously appears because of the conduction of heat through the two ends of the hot wire and causes a nonuniform temperature distribution along the wire. As it is not simple to rigorously account for this shortcoming a brief discussion regarding its probable consequences will be in order. It may be stated that for a sufficiently long and thin wire this complication is likely to be small and we took the full advantage of this fact and kept the uncertainty on this score to the minimum. The calculations of Saksena (1965) based on the theory of Gregory and Archer (1926) yielded that at 100°C for air the correction is about 0.6 percent and further as the conductivity increases the magnitude of this correction decreases. Thus, for neon it will be still smaller. However, it is not possible to apply this theory as the temperature further increases. Saksena (1965) has further tried to eliminate this effect by taking differential measurements on two columns identical in all respects except length and connected in series. It is believed that under such conditions the measurements taken refer to a small central region of the longer wire at a uniform temperature. His work with helium revealed that till 100°C the effect of end conduction on the

finally calculated  $\lambda$  values is negligible. We propose to consider both these points in our work at still higher temperatures than covered in the present effort. The situation which prompted us to adopt this approach consisted in a comparison of our measured  $\lambda$  values with those existing in the literature from conventional and accepted techniques. Gandhi (1966) has recently pooled together all the available data on rare gases as a function of temperature and recommended a set of best compromised smooth values. In the figure we show these values by a continuous curve. It may be important to mention that there are considerable scatters in the data at different temperatures and a serious guidance is drawn from the measurements taken in this laboratory by a hot-wire cell, Gandhi (1966). It is particularly gratifying to note that the smooth curve passes well through our observed points lending thereby a very good support and reliance in our present measured values. We hope to further extend this work and bring to light the intricacies, if any, by suitably planned programme of work. Thus, this work as well as earlier, Saksena and Saxena (1966), tend to establish this technique and its successful performance only upto the maximum temperature of 713°K. On the basis of this promise we are extending the scope of these measurements to still higher temperatures and will therein take into account all those corrections which may then become appreciable and are negligible in this temperature range. Our present experience based on the work in progress and going upto 1300°K indicate that this technique is capable of yielding sufficiently accurate and reliable values.

#### ACKNOWLEDGMENT

We are thankful to the Department of Atomic Energy, Bombay, and Council of Scientific and Industrial Research, New Delhi, for financial support. One of us (V.K.S.) also acknowledges the award of a research fellowship.

#### REFERENCES

- Blais, N. C. and Mann, J. B., 1960, *J. Chem. Phys.*, **32**, 1459.  
 Gambhir, R. S., 1965, *Ph.D. Thesis*, Rajasthan University, Jaipur, India (unpublished).  
 Gandhi, J. M., 1966, *Ph.D. Thesis*, Rajasthan University, Jaipur, India (unpublished).  
 Gregory, H. and Archer, C. T., 1926, *Proc. Roy. Soc. (London)*, A, **110**, 91.  
 Saksena, M. P., 1965, *Ph.D. Thesis*, Rajasthan University, Jaipur, India (unpublished).  
 Saksena, M. P. and Saxena, S. C., 1966, *Defence Science Journal (in press)*,  
 ————, 1966, *Phys. Fluids*, **9**, 1595.  
 Saxena, S. C. and Agrawal, J. P., 1961, *J. Chem. Phys.*, **34**, 2107.

# LIGHT-SCATTERING STUDIES IN SOLUTIONS OF ACACIA CATECHUIC ACID

J. N. CHAKRAVORTY

PHYSICAL CHEMISTRY LABORATORIES, JADAVPUR UNIVERSITY, CALCUTTA-32 \*

(Received May 30, 1966)

**ABSTRACT** The effects of addition of neutral salts like KCl, NaCl, BaCl<sub>2</sub> and AlCl<sub>3</sub> on the light scattering properties of Acacia Catechuic Acid have been reported. In all cases the cations appeared to have marked influence in reducing the intramolecular repulsion. The behaviour was analogous as observed with the valency rule. The behaviour of aluminum was, however, slightly different probably due to marked hydrolysis of aluminum salt. Although there was variation in the root mean square end to end distance in different cases the molecular weight more or less appeared to remain almost constant, i.e., about  $5 \times 10^6$ .

## INTRODUCTION

Acacia Catechuic Acid (ACA) is a gum acid obtained by the electro dialysis of gum catechu and replacement of the cations by hydrogen ions. Previous investigations (Kubshrestho et al, 1962; Chakraborty et al, 1963), of this gum acid revealed its polyelectrolytic behaviour. In the present communication, this property of ACA has been tested further and its physico-chemical behaviour with respect to the addition of neutral salts having cations of different valencies has been investigated with the help of light-scattering method.

## EXPERIMENTAL

Weighed quantities of ACA were taken and required quantities of NaOH solutions were added to each for their complete neutralisation. They were next dissolved in 0.025N KCl solution by shaking and then allowed to settle for about 24 hours. Both catechuic acid solution and 0.025N KCl solution were made dust free by repeated filtration through G<sub>4</sub> sintered glass filters. Scattering measurements were made at angles  $-45^\circ$ ,  $-90^\circ$ ,  $-135^\circ$  and  $0^\circ$  in a Brice Phoenix Light Scattering Photometer using a semi-octagonal dissymmetry cell.

The net values of turbidity and dissymmetry were calculated after subtracting the values obtained for the solvent in each case. The specific refractive increments were determined by means of a Brice Phoenix Differential Refractometer maintaining a temperature of  $28^\circ\text{C}$ .

All the above mentioned steps were repeated while examining the light scattering behaviour of ACA in presence of 0.025N NaCl, 0.01N BaCl<sub>2</sub> and 0.0039N AlCl<sub>3</sub> respectively.

\* Physics Department, R. K. M. Residential College, Narendrapur (24, Parganas).

## DISCUSSION

The molecular weight  $M$  was calculated from the Debye (1947) equation

$$\frac{HC}{\tau} P(90) = \frac{1}{M} + 2BC \cdot P(90)$$

where

$$H = \frac{32\pi^3 n_0^2 (n - n_0)^2}{3N\lambda^4 C^2}$$

$C$  is the concentration of the solution in  $gm/ml$ ,  $B$ , the interaction constant,  $n$ , the refractive index of the solution  $n_0$ , that of the solvent,  $\lambda$ , the wavelength of the incident light in  $cm$ ,  $N_0$ , the Avogrado number,  $\tau$ , the absolute turbidity of the solution in excess of that of the solvent,  $(n - n_0)$ , the refractive increment of the solution in excess of the solvent and  $P(90)$ , the particle scattering factor at  $90^\circ$  angle.

To examine the effect of monovalent, divalent and trivalent ions on ACA, the light scattering measurements were performed with chlorides of Sodium (and Potassium), Barium and Aluminium. The linear graphs of  $HC/T$  vs.  $C$  (Fig. 1)

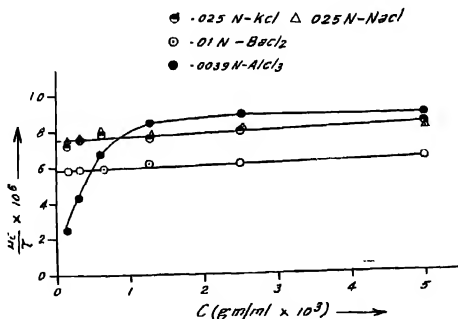


Fig. 1. Variation of  $HC/\tau$  with Concentration

resulted in each case with NaCl, KCl and BaCl<sub>2</sub> solutions. The graphs corresponding to NaCl and KCl solutions overlapped each other showing the identity of the effects of sodium and potassium upon the scattering behaviour of ACA. The slope obtained was very small which indicated negligible interactions between the ACA molecules. The molecular weight from this plot comes out to be  $5.04 \times 10^6$  after making necessary corrections for the dissymmetry of scattering. The depo-

larisation effect in all these experiments were found to be very small and no correction was considered necessary.

The plot of  $\frac{HC}{\tau}$  vs  $C$  with 0.01N  $\text{BaCl}_2$  solution almost ran parallel to that obtained with 0.025N  $\text{NaCl}$  or  $\text{KCl}$  solution which shows that the interaction constants of ACA in presence of these salts are of the same order of magnitude. The molecular weight from this intercept comes out to be  $4.7 \times 10^6$  after making all corrections as usual.

The behaviour of aluminium was slightly different probably due to marked hydrolysis of aluminium salts. The non-linear plot of  $\frac{HC}{\tau}$  vs.  $C$  for  $\text{AlCl}_3$  solution involved a little uncertainty in the determination of the molecular weight. However, if the molecular weight is calculated from the linear portion of the plot neglecting the points in the very dilute region, its value remains almost the same.

Let us now confine our attention to the plots of  $Z$  (dissymmetry) vs  $C$  (Fig. 2) for ACA solutions in presence of the above mentioned salts. It appears that the

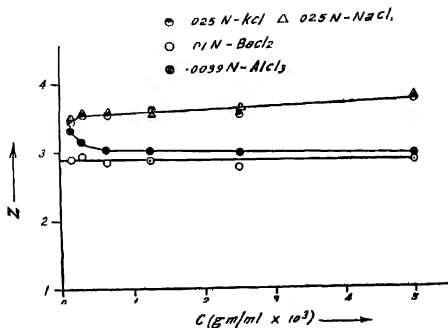


Fig. 2. Variation of Dissymmetry with Concentration.

intrinsic dissymmetry of ACA is 3.5 in 0.025N  $\text{NaCl}$  and  $\text{KCl}$  solution, 2.9 in 0.01 N  $\text{BaCl}_2$  solution and 3.05 in 0.0039N  $\text{AlCl}_3$  solution which refers to a root-mean-square end to end distance of the polymeric coil as 305.2  $\mu$ , 252.9  $\mu$  and 266  $\mu$  respectively as against 327  $\mu$  in pure water. (Chakraborty *et al.* 1963).

The low values of rms end to end distance of ACA, determined from measurements in the salt solutions indicate that a high contraction in the size of the macromolecule takes place in the presence of gegen ions. In the salts, the gegen ions present screen the charged groups and repulsion between them becomes less; under these conditions the molecule undergoes contraction.

It was, however, noted that the barium ion was more effective than Na or K ions in their screening action because the contraction produced by 0.01N  $\text{BaCl}_2$  solution was greater than that produced by 0.025N KCl or NaCl solution. It was interesting to note that although the strength of the  $\text{AlCl}_3$  solution was less than half the strength of  $\text{BaCl}_2$  solution, yet their intrinsic dissymmetry values were only slightly different. Hence it appeared that in all the cases, the cations had marked effects in diminishing the intramolecular coulombic repulsion and the behaviour was almost analogous as observed with valency rule.

The author acknowledges his indebtedness to Prof. S. N. Mukherjee, D Sc., for suggesting the problem and rendering his valuable guidance during the progress of the work. He is also thankful to Dr. D. K. Chatteraj and Dr. M. N. Das for valuable discussions.

#### REFERENCES

- Chakravorty, J. N. and Mukherjee, S. N., 1963, *Jour. Ind Chem Soc.*, **49**, 811-812.  
Debye, P., 1947, *J. Phys. Chem.*, **51**, 18.  
Kulshrestha, V. K., Chatterjee, A. C. and Mukherjee, S. N., 1962, *Die Makromolekulare Chemie*, **54**, 205-217.



# THE STUDY OF THE DYNAMICS OF VIBRATION OF A CANTILEVER UNDER LATERAL IMPACT OF AN ELASTIC LOAD. PART V (Experiment)

B. B. BANERJEE

PHYSICS DEPARTMENT, UNIVERSITY COLLEGE OF ENGINEERING, BURLA—ORISSA

(Received January 27, 1966; Resubmitted May 19, 1966)

**ABSTRACT.** Cantilevers of different materials but of same length and cross section are transversely struck at different points by hammers of different materials and masses, possessing different striking velocities. Photographic method of measurement is adopted. It is found that the duration of impact changes discontinuously with striking distance. Ordinarily, the duration of impact for particular struck point decreases in magnitude as the impinging velocity of the load increases. Soon after impact begins, certain points of the cantilever (other than the struck point) move for a short while along negative direction before it can acquire usual forward motion. Vibration ensues soon after impact begins. The theory developed in parts I to III in this series of papers has been verified with the experimental results. The agreement between the theory and the experiment is remarkable.

## EXPERIMENTAL

Mason (1936), Arnold (1937) and others have reported some experiments on supported beams using electrical method of measurement. Some experiments on cantilever were reported by Banerjee (1966). In this paper, the writer has exhaustively investigated different aspects of the problem systematically.

The experimental set-up is almost similar to that used by Banerjee (1966). The hammer of particular material and mass is released from a distance to ensure a desired impinging velocity as it perpendicularly strikes specified points of the cantilever (including the free end) at regular intervals of 5 cms. Light from carbon arc lamp, facing the narrow slit of a camera box vertically downwards, is obstructed by the pointer of the tuning fork and the point of contact of the hammer and the cantilever to cast their shadows on the running photographic paper, pinned on the photocarrier. The photocarrier slides inside the camera box.

In this way, the effects of the striking distance, 'mass ratio', striking velocity and materials of the cantilever and hammer, on the duration of impact as also on the displacement of the cantilever and hammer are studied. The results of the experiments may be found in different curves and a plate. The displacement of the cantilever at any point other than the struck point is also studied, (vide fig 8B). The slit in this case is brought under the point to be photographed with the arc lamp and the vibrating tuning fork above it.

To reproduce the experimental time-displacement curve for any point of the cantilever during and after impact, to any scale, the corresponding shadowgraph including the waves due to the tuning fork at the top is projected upon a squared paper with the help of an epidiascope. The curve traced out by the surface of the cantilever is drawn upon the paper. The number of waves due to the tuning fork of frequency 100 c.p.s. contained in the portion of the shadowgraph under study and lying within a known length of the time-axis gives the time scale. The depth of the shadow of the bar at rest, towards left of each shadowgraph (taken equivalent to 1.27 cms) helps to fix the displacement scale. For measuring the striking velocity, the method used in part IV (Banerjee, 1966), is adopted. The maximum arc along which the hammer swings to strike the cantilever is measured from the shadow of the particular outline of the hammer on a graduated translucent scale, placed very close and parallel to the path of the hammer. The length of the pendulum bob (hammer) and its arc of swing help calculate the impinging velocity.

#### PARTICULARS OF CANTILEVERS AND HAMMERS

Cantilever A, mild steel rod, length 95 cms, dia. 1.27 cms.

Cantilever B, brass rod, length 95 cms, dia. 1.27 cms.

Hammer C, spherical, mild steel, weight = 285.5 gms., radius at contact surface, 2 cms.

Hammer D, spherical, brass, weight = 285.5 gms., radius at contact surface, 2 cms.

Hammer E, spherical, brass, weight = 108.8 gms., radius at contact surface, 1 cm.

The curves  $e_1$  and  $e_2$  of fig. 1. show variation of the duration of impact (first contact) with striking distances for the same mild steel cantilever A,

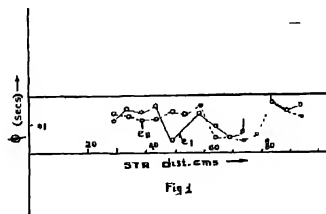


Fig 1

struck by mild steel hammer-C and brass hammer—D respectively. The hammers have equal weight and possess equal striking velocity of 65 cms. per sec. From these curves, we find that the duration of impact fluctuates discontinuously with

striking distance. These curves differ due to a difference in the values of the elastic constant, ( $E_2$ ) of the striking hammers. In most cases of striking distances, this difference is found to be very small, being measured in thousandths of a second, but for such striking distances as 50 and 80 cms. this difference is large. For striking distance of 80 cms. the duration of impact is .08284 sec and is not shown in the curve. The lower magnitude of the duration of impact in these particular cases indicates stimulation of larger number of modes into activity.

The curves in fig. 2, each representing particular struck point, are drawn to show the variation of the duration of impact (first contact) with the striking

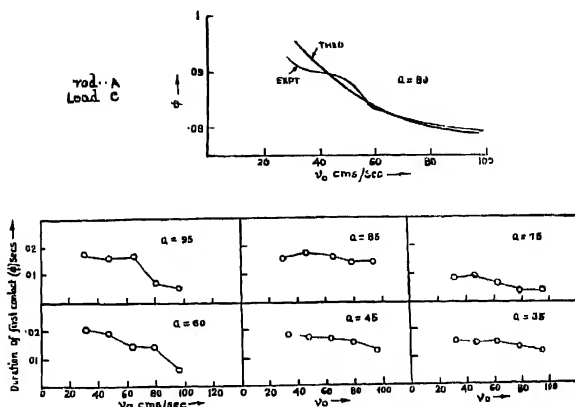


Fig. 2

velocity of the hammer. It is found that ordinarily the duration of impact (first contact) changes with the striking velocity of the hammer. It is found that ordinarily the duration of impact slightly diminishes in magnitude as the striking velocity increases, and for striking distances such as 95 cms. and 60 cms, it appears that beyond a certain limiting velocity (at or around 79.25 cms/sec for 95 cms., and 94.75 cms/sec for 60 cms), the duration of impact abruptly changes. This is due to the higher modes becoming effective at higher velocities.

The curves in fig. 3 show the variation of total duration of impact (measured from the time the load comes in contact to the instant it completely leaves the region of vibration of the rod) with striking distance for different striking velocities of the hammer. It is found that the total duration of impact fluctuates as striking distance, increases, but maintaining the fluctuating character, the total duration of impact increases abruptly from about 55 cms. onward and attains the maximum value at or around 80 cms. of striking distance. Abrupt increases in the magnitude

of the total duration of impact observed from 55 cms. show that, at the instant  $P = 0$  (Banerjee, 1966 ; Part III) and for a specified number of modes being

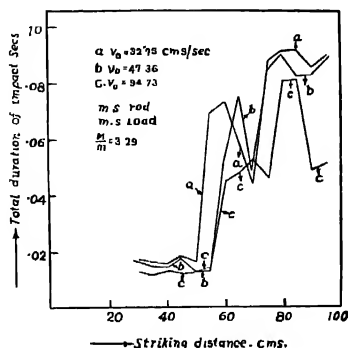
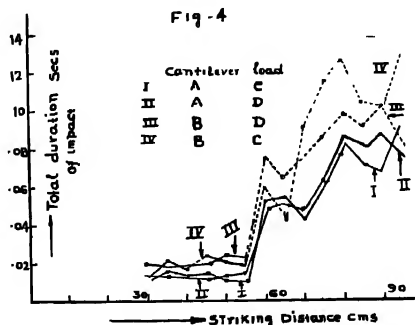


Fig. 3

effective,  $\Sigma A_s \cos q_s t$  (eqn. 13, Pt II) changes sign for a struck point near about 55cms and this change is effected with absorption of maximum energy by the beam (Banerjee, 1966, Pt. IV).

Fig. 4 shows the variation of the total duration of impact with the striking distance for two cantilevers of different materials but of same length and cross section, being struck by two hammers of different materials but of equal mass and possessing equal striking velocity of 65 cms/sec. It is found that the nature of fluctuation of total duration of impact with striking distance depends more or less on the material of the hammer.

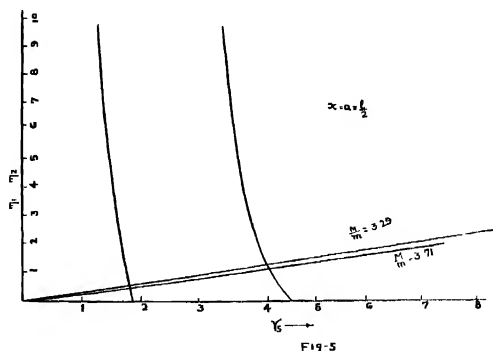


The shadowgraphs (fig. 8) show that the rod begins to vibrate as soon as impact begins. Usually almost for all striking distances, the phenomenon of 'multiple contacts' is observed. For certain struck points (such as 80 cms) the form of time-displacement curve appears to be more or less sinusoidal but for struck points, such as 47.5 cms this curve is more undulating showing importance of the second mode of vibration. Thus stimulation of particular number of modes into activity depends on the striking distance.

It is further found that for a short while from the instant impact begins, the motion of certain points other than the struck point (vide, fig. 8B) is in negative direction with respect to positive impinging velocity of the load. This is also a mode effect. It shows that the rod begins to vibrate soon after impact begins.

#### VERIFICATION OF THE THEORY

The values of  $\gamma_s$ , are required to use different expressions for displacement, pressure etc. (vide. Part I to III, Banerjee, 1966). The hammer is taken to be hard and it does not materially affect the results. The  $\eta_1 \sim \gamma_s$  and  $\eta_2 \sim \gamma_s$ , (vide. Part II, Banerjee, 1966) curves for particular struck points may be drawn as per eqn. 7, Pt. II (Banerjee, 1966) knowing  $k_1$  and  $k_2$  for the struck point. Such a curve for  $x = a = l/2$ , i.e. mid-pt, is shown for 'mass ratios', 3.71 and 3.29. (Fig. 5)



#### Duration of impact

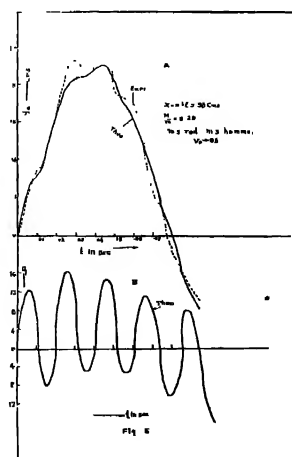
Thus it is found that the difference in the theoretical and experimental values of  $\phi$  is very small and the experimental values are having higher magnitude than the theoretical ones, showing usefulness of the extension of the theory in light of Hertz's theory of impact (vide. Part III, Banerjee, 1966). In applying Hertz's theory of impact, we have considered the case of cantilever A struck by Hammer C at 80 cms from fixed end (vide. fig. 8D). Only the first term of the pressure

cantilever load combination	Mass ratio	striking velocity cms/sec.	striking distance	no. of modes	Duration of impact (secs.)		Difference $\phi_0 - \phi$
					Theo. $\phi_0$	Expt. $\phi$	
A—C	3.29	65	$a = 1$	2	.011	.0154	-.004
A—C	3.29	94.75	$a = 1$	3	.0044	.0045	-.0001
A—C	3.29	65	$a = 1/2$	2	.0105	.0120	-.0015
A—D	3.29	65	$a = 1$	2	.011	.012	-.001
B—C	3.55	32.75	$a = 1$	2	.016	.020	-.004
B—E	8.36	65	$a = 1$	2	.0145	.0175	-.0025

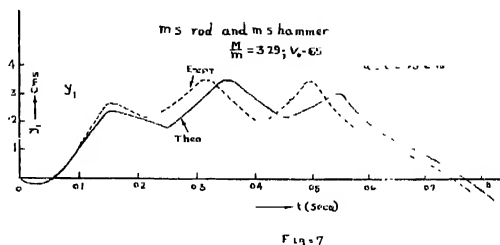
eqn. 5 (pt. III, Banerjee 1966) is considered as in this case the second term is very nearly zero and the higher terms are negligible. The variation of  $\phi$  with  $v_0$  is calculated as per eqn. 8 (part III).  $\phi_0$  is calculated in the usual way from pressure eqn. 37, in Pt. III, for  $P = 0$ , and its value in this case is .0695 sec. Both the experimental and theoretical variation of  $\phi$  with  $v_0$  are shown in Fig. 2,  $u_0$  is taken as .434 cms. It is evident from these curves that the theory put forward (considering Hertz's theory of impact) agrees nicely with experiment.

#### *Displacement of the struck point*

Fig. 6 gives the time-displacement curves (Theo and Expt) for the struck point at the free-end corresponding to the case given by shadowgraph C (fig. 8).



The curves are identical upto about .014 sec. which is nearly the time of duration of impact. This is in agreement with the theory. While the theoretical curve is extended beyond the time of impact (first contact) with the help of corresponding equation upto the time not exceeding half the period of vibration of the cantilever, it is observed that the two curves fit in closely. The undulations



(occurring almost in similar regions in the general body of respective curves) are more pronounced in the experimental curves. The difference between the two curves is due to sudden change in velocity suffered by the rod at the termination of a contact or separation, as anticipated in part III (Banerjee, 1966). In the same Fig. 6, the theoretical pressure-time curve (in arbitrary scale) shows that at about .011 sec. after impact begins, pressure becomes zero. This time is therefore the duration of impact. The experimental value is .015 sec.

For striking distance,  $x = a = 80$  cms (fig 8D), experimentally the time, measured for half the vibration of the bar is about .07 sec. and theoretically it is

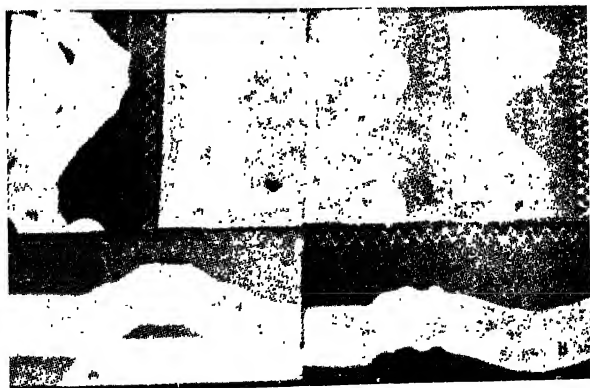


Fig. 7

.0695 sec. This is a remarkable agreement. Further the amplitudes for experimental time-displacement curves for striking velocities of 32.75, 47.36 and 65 cms/sec. bear ratios 5 : 7.1 : 10 respectively, which are nearly the ratios among striking velocities. This is in full agreement of the theory. (Banerjee 1966, Pt. 11).

*Displacement of any point other than the struck point*

Fig. 7 shows the theoretical and experimental time-displacement curves for mid-pt. of the Cantilever-A, being struck by hammer-C at its free end with a velocity of 65 cms/sec (fig. 8B). The two curves are identical upto about .014 sec. which is almost the time of impact (first contact). It is noted that the two curves coincide in the region of negative displacement towards the earliest period of impact. This is in complete agreement with the theory. Here also we have extended the theoretical curve beyond the time of first contact and find that the two curves are strikingly similar. Here also the difference between the two curves is due to after-impact effects, as discussed in Part III. (Banerjee, 1966).

*Velocity of the hammer*

striking distance in cms	Cantilever—hammer	striking velocity cms/sec	Velocity at the end of impact (cms/sec.)		Observation
			Theo	Expt.	
95	A—C	65	+31.68	+30.15	multiple contact
95	B—C	32.75	+10.24	+9.66	—do—
95	B—E	65	+7.5	+5.6	—do—
47.5	A—C	65	—14.5	—13.9	Impact ends

Here also the agreement between the theoretical and experimental values is excellent. Further works on the behaviour of the beam after impact is in progress and will be reported shortly.

My best thanks are due to Dr Mohini Mohon Ghosh, D.Sc., Vice-Principal, City College, Calcutta, for his interest in this work. Thanks are also due to Dr. A. K Sengupta, D.Sc., Head of Applied Physics Department, Calcutta University, and to Dr. S. P. Bhattacharya, D.Phil., of the same Department and to Principal, B Mahapatra, U.C.E., Burla, for their extending facilities for the experiments.

# REFERENCES

- Arnold, R. N., 1937, *Proc. Inst. Mech. Engrs. (Lond.)*, **137**, 217.  
 Banerjee, B. B., 1964, *Indian J. Phys.*, **38**, 2, 99–105.  
 ———— 1966, *Indian J. Phys.*, **40**, 108, 208, 215, 221.  
 Mason, H. L., 1936, *Jour. Appl. Mech.*, **58**, A-55.



## A NEW LABORATORY MODEL HARMONIC ANALYSER

G LAKSHMAN AND SYED ZIAUDDIN

DEPARTMENT OF PHYSICS, CENTRAL COLLEGE

BANGALORE UNIVERSITY, BANGALORE-1

(Received January 22, 1966)

**ABSTRACT.** An Electron Ray Tube (EM 84) popularly known as magic eye has been adapted as a continuous voltage recording device. This note describes the use of this device for the harmonic analysis of complex waveforms. Harmonics with amplitudes of about 5% of the fundamental can be detected, with considerable accuracy. Numerical data obtained with the device are compared with that calculated theoretically. The simplicity of the device should recommend its extensive use.

Several experimental methods are described in literature which are often employed for the harmonic analysis of a complex waveform. Basically these involve tuned circuits tunable over the range of frequencies contained in the harmonics of the waveform. These methods though elaborate give good frequency resolution with a fair accuracy. The method described by Suits (1930), is simple and direct but suffers from lack of accuracy. Graphical methods are laborious and time-consuming and therefore cannot be used for rapid analysis of waveforms.

A continuous voltage recording device using an Electron Ray Tube (EM 84) has been put to use in this laboratory. Using the same device a laboratory model harmonic analyser has been developed which has since given promising results.

The experimental arrangement is shown in fig 1B. The complex voltage to be analysed is fed to the target and a variable frequency oscillator (search oscil-

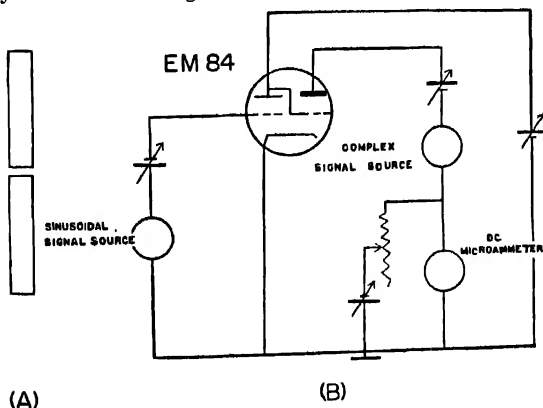


Fig. 1.

lator) is connected to the grid. The plate and target voltages are adjusted to give minimum separation of the strip-images on the fluorescent target, in the absence of any alternating input (fig. 1A). The frequency of the search oscillator is then increased gradually from the minimum. When the fundamental frequency of the complex voltage and that of the search oscillator are far apart, the patterns are steady and the separation between them is constant. But when the frequencies approach each other the patterns oscillate rapidly and when they differ slightly, beat-oscillations are observed. When the frequencies are exactly equal the patterns get locked up with minimum separation and are steady. The dial reading on the search oscillator gives the frequency of the fundamental of the complex wave. The frequency of the search oscillator is then varied to sweep the entire range of the harmonic frequencies involved. When the oscillator frequency is so varied gradually, beat oscillations are observed whenever its frequency approaches the harmonic of the complex wave within a few cycles and the patterns get locked up when the frequencies are exactly equal. The process is repeated to sweep through all the harmonics possibly associated with the complex wave. Using square waves which are rich in harmonics, as many as 37 harmonics have been detected.

When the beat oscillations are observed the corresponding amplitudes can be measured by a DC microammeter connected in the target circuit.

If the grid input signal is  $= E_g \cos \omega_0 t$

And the target input signal is

$$= E_{t1} \cos \omega_1 t + E_{t2} \cos \omega_2 t + \dots + E_{tn} \cos \omega_n t + \dots$$

Then the beat amplitude of the  $n$ -th harmonic and the grid input signal is

$$= K E_g E_{tn} \text{ (see appendix)}$$

where  $K$  is a constant. If  $i_{t0}$  is the observed reading in the microammeter, then  $i_{t0} = 2K E_g E_{tn}$

$E_{tn}$  = amplitude of the  $n$ -th harmonic

$$= \frac{i_{t0}}{2K E_g} \quad \dots \quad (i)$$

If the voltages represent the RMS values, then the amplitude of the  $n$ -th harmonic

$$= \frac{i_{t0}}{4K E_g}$$

The constant  $K$  can be determined by calibration of the microammeter readings with known sinusoidal voltages at the grid and the target. This has been done for various anode and target potentials and also for different input signals.

Before harmonic analysing a waveform,  $K$  is determined for the particular operating voltages, so that the harmonic amplitudes can be directly calculated from the eqn. (i). It is also observed that the value of the constant  $K$  and its

variation with the plate and target voltages vary with individual tubes. Different combinations—feeding the complex voltage input to the anode or to the grid—have also been tried, which generally give satisfactory results.

Square waves and saw tooth waves have been analysed from 3 cps to 100 kcs and its ability to detect harmonics is remarkable considering the simplicity of the procedure. Harmonics with amplitudes to about 5 per cent of the fundamental amplitude can be detected with considerable accuracy. Numerical data given (Table I) are only illustrative and not exhaustive. This method cannot claim the accuracy obtainable from the selective tuned circuits and the Heterodyne wave analysers. However, the simple arrangement involving no tuned circuits speaks in its favour.

One application that suggests itself is the following. In course of any investigation it may be desirable to know when a particular information of known frequency appears on a background noise of complex wave input. With the circuit arrangement shown in fig. 1, the frequency of the search oscillator is fixed at the frequency of the expected information and the input signal (after amplification, if necessary) is fed to the target. The illuminated pattern on the target is sharply focussed into a bright image on a recording film. Whenever the particular frequency occurs in the wave, the film shows up a trace with constant amplitude. With the help of time-markers, the time and duration of occurrence can be read off. This arrangement will perhaps come in handy in certain geophysical instrumentation.

With any disadvantage it may seem to have, this laboratory model of a harmonic analyser strikes to be rugged and easy to adapt for rapid analysis of any waveform.

One of the authors (G.L.) is grateful to the Council of Scientific and Industrial Research, New Delhi, for the award of a Research Fellowship.

## APPENDIX

The instantaneous value of the target current  $i_t$  can generally be given as  $i_t = f(e_g, e_t)$  where  $e_g$  and  $e_t$  are the instantaneous values of the grid and target voltages. If  $e_g$  and  $e_t$  represent the values of the sinusoidal and complex voltages, then the total voltage on the target-grid can be written as

$$e_g = \left( \mu_1 e_g + \frac{e_t}{\mu_2} \right) \quad \dots \quad (i)$$

where  $\mu_1$  and  $\mu_2$  are the amplification factors of the triode and target sections of the tube, respectively. Developing  $i_t$  into an infinite series in  $e_g$ , we have,

$$i_t = a_1 e_g + a_2 e_g^2 + a_3 e_g^3 + \dots + a_n e_g^n + \dots \quad (ii)$$

**TABLE I**  
**Target signal : Square waves. 60 cps**

Search Oscillator Frequency.	Measured amplitude	Calculated amplitude
60 cps.	9.90	9.90
180 cps.	3.30	3.30
300 cps.	1.99	1.98
420 cps.	1.43	1.414
540 cps.	1.10	1.10
660 cps.	0.86	0.90
780 cps.	0.77	0.761
900 cps.	0.65	0.66
1020 cps.	0.57	0.582
1140 cps.	0.53	0.521
1260 cps.	0.48	0.471
1380 cps.	0.44	0.43
1500 cps.	0.40	0.396
1620 cps.	0.36	0.367
1740 cps.	0.33	0.341
1860 cps.	0.32	0.319
1980 cps.	0.29	0.309

Detectable upto 33rd harmonic.

Target Signal: Square Waves 300 cps.

300 cps.	6.20	6.20
900 cps.	2.10	2.066
1500 cps.	1.24	1.24
2100 cps.	0.89	0.85
2700 cps.	0.69	0.688
3300 cps.	0.56	0.563
3900 cps.	0.48	0.476
4500 cps.	0.42	0.413
5100 cps.	0.36	0.364
5700 cps.	0.33	0.326
6300 cps.	not accurate but detectable.	

Detectable upto 21st harmonic.

Target Signal : Square Waves. 10 kcs.

10 kcs.	4.0	4.0
30 kcs.	1.40	1.33
50 kcs.	0.82	0.80
70 kcs.	not accurate but detectable.	

Detectable upto 7th harmonic.

Target Signal : Square Waves. 20 kcs.

20 kcs.	4.8	4.8
60 kcs.	1.4	1.6
100 kcs.	0.92	0.96
140 kcs.	not accurate but detectable.	

Detectable upto 7th harmonic.

Target Signal : Square Waves. 100 kcs.

100 kcs.	6.0	6.0
300 kcs.	not accurate but detectable.	

Detectable upto 3rd harmonic.

\*(Calculated amplitudes are obtained from the Fourier Analysis of the Square Waveform)

Limiting the series to the quadratic terms only which for the most part represent the behaviour of the tube, we get,

$$i_t = a_1 e_g + a_2 e_g^2, \quad \dots \quad (iii)$$

and

$$e_g = E_g \cos \omega_0 t$$

$$e_t = E_{t1} \cos \omega_1 t + E_{t2} \cos \omega_2 t + \dots + E_{tn} \cos \omega_n t + \dots \quad (iv)$$

From (i) and (iii),

$$i_t = a_1 \left( \mu_1 e_g + \frac{e_t}{\mu_2} \right) + a_2 \left( \mu_1 e_g + \frac{e_t}{\mu_2} \right)^2$$

$$= a_1 \mu_1 e_g + a_1 \frac{e_t}{\mu_2} + a_2 \mu_1^2 e_g^2 + a_2 \frac{e_t^2}{\mu_2^2} + 2a_2 \frac{\mu_1}{\mu_2} e_g e_t \quad \dots \quad (v)$$

Only the last term of this expression contains the beat-frequency of the two voltages  $e_g$  and  $e_t$  because,  $e_g e_t = E_g E_{tn} [\cos \omega_0 t \cos \omega_n t]$  if the search oscillator frequency  $\omega_0$  beats with one of the harmonics say, the  $n$ -th, harmonic

$$e_g e_t = \frac{E_g E_{tn}}{2} [\cos (\omega_0 - \omega_n) t + \cos (\omega_0 + \omega_n) t]$$

Since the second term refers to a high frequency component, the beat amplitude is given by  $\frac{E_g E_{tn}}{2} [\cos (\omega_0 - \omega_n) t]$ . If the observed swing of the microammeter needle, between the maximum and minimum values, is denoted by  $i_{t0}$  then from (v)

$$i_{t0} = 2a_2 \frac{\mu_1}{\mu_2} E_g E_{tn} \quad \dots \quad (vi)$$

as it swings twice the 'amplitude'

$$\therefore i_{t0} = 2KE_g E_{tn} \quad \text{where } K = a_2 \frac{\mu_1}{\mu_2}.$$

$E_{tn}$  = Amplitude of the  $n$ -th harmonic

$$= \frac{i_{t0}}{2KE_g} \quad \dots \quad (vii)$$

If RMS values are measured, then

$$E_{tn} = \frac{i_{t0}}{4KE_g}$$

If there is a phase difference between the two voltages  $e_g$  and  $e_t$ , it can be shown that this does not affect the reading obtained as per the Eqn (vii)

## REFERENCES

- Arguimbau, L. B., 1933, *Gen. Rad Expt*, 7, 12.  
Nicholson, M. G., Parkins, W. M. 1934, *Proc. IRE*, 20, 734.  
Scott, H. H., 1938, *Proc. IRE*, 26, 226  
Suits, C. G., 1930, *Proc. IRE*, 18, 178.  
Syed Ziauddin, Lakshman, G. *A Continuous Voltage Recording Device* (In Press).  
Terman, F. E., Pettit, J. M. 1952, *Electronic Measurements*, McGraw Hill Publishing Co., 241.

# S-WAVE NEUTRON STRENGTH FUNCTION AND THE OPTICAL MODEL WITH VOLUME AND SURFACE ABSORPTION

CHHAYA GANGULY AND N. C. SIL

DEPARTMENT OF THEORETICAL PHYSICS,  
INDIAN ASSOCIATION FOR THE CULTIVATION OF SCIENCE,  
JADAVPUR, CALCUTTA-32.

(Received October 17, 1966)

Recently Benczo (1966) has obtained the exact analytical solution of the Schrödinger equation with a complex potential of the form

$$V(r) = - \left[ \frac{V_0 + iW_0}{1 + e^{\frac{r-R}{a}}} + (V_1 + iW_1) \frac{e^{\frac{r-R}{a}}}{\left(1 + e^{\frac{r-R}{a}}\right)^2} \right] \quad \dots (1)$$

for *s*-wave neutrons and has given the explicit expression for the  $S_0$ -matrix element as

$$S_0(k) = e^{-2ikR} \frac{\Gamma(2ika)}{\Gamma(-2ika)} \cdot \frac{AB-C}{D-AE} \quad \dots (2)$$

where

$$A = \left(\frac{b}{1+b}\right)^{2\lambda(1+b)-2ika} \frac{F\left(\lambda+\mu+ika, 1+\lambda-\mu+ika, 1+2\lambda; \frac{b}{1+b}\right)}{F\left(-\lambda+\mu-ika, 1-\lambda-\mu-ika, 1-2\lambda; \frac{b}{1+b}\right)} \quad \dots (3a)$$

$F$  denoting hypergeometric functions and  $k$  being the wave number,

$$B = \frac{\Gamma(1-2\lambda)}{\Gamma(1-\lambda-\mu+ika) \Gamma(-\lambda+\mu+ika)} \quad \dots (3b)$$

$$C = \frac{\Gamma(1+2\lambda)}{\Gamma(\lambda+\mu+ika) \Gamma(1+\lambda-\mu+ika)} \quad \dots (3c)$$

$$D = \frac{\Gamma(1+2\lambda)}{\Gamma(1+\lambda-\mu-ika) \Gamma(\lambda+\mu-ika)} \quad \dots (3d)$$

$$E = \frac{\Gamma(1-2\lambda)}{\Gamma(-\lambda+\mu-ika) \Gamma(1-\lambda-\mu-ika)} \quad \dots (3e)$$

in which

$$\lambda = \pm \left[ 1 + \frac{V_0 + iW_0}{E_n} \right]^{\frac{1}{2}} \cdot ika \quad \dots \quad (4a)$$

$$\mu = \frac{1}{2} \pm \frac{1}{2} \left[ 1 + 4k^2 a^2 \frac{V_1 + iW_1}{E_n} \right]^{\frac{1}{2}} \quad \dots \quad (4b)$$

$E_n$  = neutron energy

In the above potential the first part represents the usual Woods-Saxon potential and the second part corresponds to its derivative. We shall utilise the above results for the calculation of the  $s$ -wave neutron strength function  $\frac{\bar{\Gamma}_n}{D}$  (the ratio of the average neutron width to the average level spacing) and the potential scattering radius  $R'$  using the same form of neutron-nucleus potential with  $V_1 = 0$ .

According to Feshbach, Porter and Weisskopf (1954)

$$\frac{\bar{\Gamma}_n}{D} = \frac{1}{\pi} \operatorname{Re}(1 - S_0(k)) \quad \dots \quad (5)$$

$$kR' = \frac{1}{2} \operatorname{Im}(1 - S_0(k)) \quad \dots \quad (6)$$

for  $kR' < 1$

Since  $\{1 - S_0(k)\}_{k \rightarrow 0} = -K_0 \left( \frac{dS_0(k)}{dk} \right)_{k=0}$

the strength function normalised to 1 ev is given by

$$\frac{\bar{\Gamma}_n^0}{D} = -\frac{1}{\pi} k_0 \operatorname{Re} \left( \frac{dS_0(k)}{dk} \right)_{k=0} \quad \dots \quad (7)$$

and

$$R' = -\frac{1}{2} \operatorname{Im} \left( \frac{dS_0(k)}{dk} \right)_{k=0} \quad \dots \quad (8)$$

where  $k_0$  is the value of  $k$  for 1 ev neutron.

Now

$$\begin{aligned} \frac{dS_0(k)}{dk} = & -2iR \cdot S_0(k) + \left[ \frac{d}{dk} \left\{ \frac{\Gamma(2ika)}{\Gamma(-2ika)} \right\} \right] \cdot \frac{\Gamma(-2ika)}{\Gamma(2ika)} \cdot S_0(k) \\ & + \left[ e^{-2ika} \cdot \frac{\Gamma(2ika)}{\Gamma(-2ika)} \right] \cdot \left[ \frac{(A'B + AB' - C)(D - AE) - (AB - C)(D - A'E - AE')}{(D - AE)^2} \right] \end{aligned} \quad \dots \quad (9)$$



# *S-Wave Neutron Strength Function and the Optical, etc.* 625

where dash denotes differentiation with respect to  $k$ .

We note that  $B_0 = E_0$

$$C_0 = D_0$$

and

$$S_0(0) = 1 \quad \dots (10)$$

where the suffix zero indicates the value of the corresponding quantity at  $k = 0$   
Further we have

$$\left. \frac{dB}{dk} \right|_{k=0} = - \left. \frac{dE}{dk} \right|_{k=0} = -iaB_0 [\psi(1-\lambda-\mu) + \psi(-\lambda+\mu)] \quad \dots (11a)$$

$$\text{and} \quad \left. \frac{dC}{dk} \right|_{k=0} = - \left. \frac{dD}{dk} \right|_{k=0} = -iaC_0 [\psi(\lambda+\mu) + \psi(1+\lambda-\mu)] \quad \dots (11b)$$

where

$$\psi(z) = \frac{d}{dz} \log \Gamma(z)$$

Using (10) and (11) and the relation (1946)

$$\psi(1-z) = \psi(z) + \pi \cot \pi z$$

we get from (9)

$$\left. \frac{dS_0(k)}{dk} \right|_{k=0} = -2iR - 4\gamma a - 2ia \cdot Q \quad \dots (12)$$

where

$$Q = [\psi(\lambda_0 + \mu) + \psi(-\lambda_0 + \mu)] + \pi$$

$$\left[ \left( \frac{b}{1+b} \right)^{\lambda_0} \left( F(\lambda_0 + \mu, 1 + \lambda_0 - \mu, 1 + 2\lambda_0; \frac{b}{1+b}) \frac{\Gamma(1-2\lambda_0)}{\Gamma(1-\lambda_0-\mu) \Gamma(-\lambda_0+\mu)} \cot \{\pi(\lambda_0 + \mu)\} \right. \right. \\ \left. \left. - \left( \frac{b}{1+b} \right)^{-\lambda_0} \left( F(-\lambda_0 + \mu, 1 - \lambda_0 - \mu, 1 - 2\lambda_0; \frac{b}{1+b}) \frac{\Gamma(1+2\lambda_0)}{\Gamma(1+\lambda_0-\mu) \Gamma(\lambda_0+\mu)} \cot \{\pi(-\lambda_0 + \mu)\} \right) \right]$$

$$\left[ \left( \frac{b}{1+b} \right)^{\lambda_0} \left( F(\lambda_0 + \mu, 1 + \lambda_0 - \mu, 1 + 2\lambda_0; \frac{b}{1+b}) \frac{\Gamma(1-2\lambda_0)}{\Gamma(1-\lambda_0-\mu) \Gamma(-\lambda_0+\mu)} \right. \right. \\ \left. \left. - \left( \frac{b}{1+b} \right)^{-\lambda_0} \left( F(-\lambda_0 + \mu, 1 - \lambda_0 - \mu, 1 - 2\lambda_0; \frac{b}{1+b}) \frac{\Gamma(1+2\lambda_0)}{\Gamma(1+\lambda_0-\mu) \Gamma(\lambda_0+\mu)} \right) \right]$$

$\gamma$  = Euler's constant and  $\lambda_0$  is the value of  $\lambda$  at  $k = 0$ . Our expression is symmetric with respect to  $\pm \lambda$  and  $\mu$  and  $1 - \mu$ . Separating (12) into real and imaginary parts we get the expressions  $\frac{\Gamma_0^a}{D}$  and  $R'$  corresponding to a nuclear potential with both volume and surface absorption as follows

$$\frac{\Gamma_0^a}{D} = - \frac{2k_0 a}{\pi} \text{Im}(Q) \quad \dots (13)$$

$$R' = R + 2\gamma a + a \text{Re}(Q) \quad \dots (14)$$

For Woods-Saxon potential without surface absorption we put  $\mu = 0$  in (12). Further taking the limit  $a \rightarrow 0$ , we have for the square well case

$$\frac{dS_0(k)}{dk} \Big|_{k=0} = -2iR + \frac{2i}{p} \tan pR \quad (15)$$

where 
$$p = \left[ \frac{2m}{\hbar^2} (V_0 + iW_0) \right]^{\frac{1}{2}} \quad (16)$$

$$\frac{\Gamma_n^0}{D} = \frac{2K_0 R}{\pi} \cdot \frac{X_1 \sinh 2X_2 - X_2 \sin 2X_1}{(\cos 2X_1 + \cosh 2X_2)(X_1^2 + X_2^2)} \quad \dots \quad (17)$$

where 
$$pR = X_1 + iX_2$$

The expression (17) for  $\frac{\Gamma_n^0}{D}$  is identical with the analytic form given by Feshbach *et al* (1954). The detailed comparison of theoretical and experimental results is in progress.

We are thankful to Professor D. Basu for his helpful discussions.

#### REFERENCES

- Bencze, Gy., 1966, *Commentationes Physico-Mathematicae* (Soc. Scient. Fennica) **81**, 4 (Nordita Publications No. 184)  
 Feshbach, H., Porter, C. E., and Weisskopf, V. F., *Phys. Rev.* **96**, 448.  
 Whittaker, E. T. and Watson, G. N., 1946, *A Course of Modern Analysis*, Cambridge University Press, London, 240

## Letters to the Editor

The Board of Editors does not hold itself responsible for opinions expressed in the letters published in this section. The notes containing short reports of original investigations communicated to this section should not contain many figures and should not exceed 500 words in length. The contributions reaching the Secretary by the 15th of any month may be expected to appear in the issue for the next month. No proof will be sent to the author.

19

### ASYMMETRICAL RAMAN SCATTERING BY WATER AND SULPHURIC ACID

N. RAJESWARA RAO AND K. V. RAMANATHAN

DEPARTMENT OF PHYSICS, OSMANIA UNIVERSITY, HYDERABAD

(Received February 22, 1965; Resubmitted November 20, 1965)

Sokolovskaya and Simova (1963) observed, recently, that in the cases of  $C_6H_6$ ,  $C_6H_5CH_3$ ,  $CS_2$  and  $CCl_4$ , the intensity of the Raman lines asymmetrical, i.e., scattering at an angle  $\theta$  is different from what it is at  $180-\theta$ . This is surprising as Raman scattering is generally considered to be incoherent. A similar observation had been reported much earlier by Pokrowski and Gordon (1930) in the case of water.

Rank (1948) observed another type of asymmetry in the case of  $CCl_4$ ,  $CHCl_3$ ,  $C_6H_6$  and  $CS_2$ . Now, if light is polarised with its electric vector along the axis of the Raman tube ( $H$ ) is incident on the sample tube and the scattered light analysed, the component in the plane of observation and incidence ( $H_p$ ) and the one perpendicular to it ( $H_s$ ) are generally considered to be equal if one considers

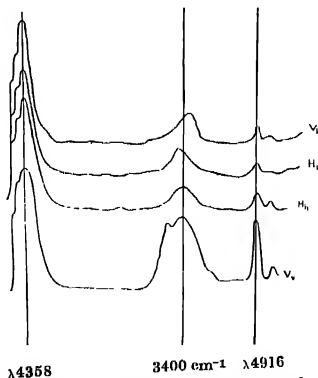


Fig. 1. Microphotometric traces of Raman spectra of water showing the four polarised components.

that Raman scattering is incoherent. Rank observed that in the above cases  $H_h \neq H_v$ .

If incident light is polarised in the vertical plane (V i.e. perpendicular to the plane containing the directions of incidence and observation) and the scattered light analysed one gets  $V_v$  and  $V_h$ . Krishnan (1934) has shown that even in the case of colloidal solutions, for which the Rayleigh scattering is asymmetrical,  $H_v = V_h$ . This is called the reciprocity relation.

Now, we report that for the water band at  $3400\text{ cm}^{-1}$  and the Raman lines  $\delta\nu = 410$  and  $560$  of sulphuric acid, the differently polarised components

show that all the precautions are taken to guard against experimental errors and that the above results are not due to any such errors. A fuller description will be published elsewhere in connection with some other results.

Now, to show that  $H_h \neq H_v \neq V_h$ , for any particular Raman line, very stringent precautions should be taken, and preferably, photo-electric recording should be resorted to. But, in the case of  $\delta\nu = 3400$  of water, the matter is much simplified. It really consists of two components at about  $3200$  and  $3400$ , the former being weaker. According to the present simple theory of Raman scattering by liquids, the three polarisation components should be equal for both the parts  $3200$  and  $3400$ . Hence, the structure of the composite band should retain its shape in all the three spectra. The structural differences demonstrated in the fig. 1 can only be due to the fact that either one of them or both must be violating this requirement. It is very difficult to think of any experimental error that can bring about this differential behaviour of the two parts of the band. Similarly,  $\delta\nu = 410$  and  $560$  of sulphuric acid are also of composite nature, the former due to the splitting of a doubly degenerate line and later due to a triply degenerate mode. Differential behaviour of these lines in the two spectra is seen more conspicuously than in the case of water.

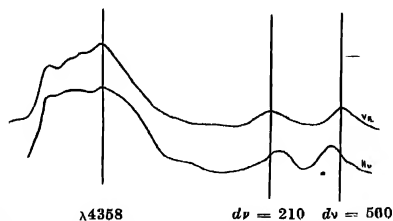


Fig. Microphotometric traces of Raman spectra of  $\text{H}_2\text{SO}_4$  showing structural differences between  $V_h$  and  $H_v$ .

It may be mentioned in this connection, that  $\delta\nu = 3400$  of water as excited by  $\lambda 4046$  is used in this investigation. On this is superposed a very weak band of frequency about  $1600\text{ cm}^{-1}$  which is excited by  $\lambda 4358$ . Its intensity is of the

order of 5% of  $\nu = 3400$ . This does not bring about the structural changes observed as this band also should follow the law that the three differential polarised components are equal. In this investigation a filter with iodine in  $\text{CCl}_4$  is used to reduce the intensity of  $\lambda 4358$  to about  $1/3$ .

## EXPERIMENTAL

Light is allowed to pass through a system of parallel vanes 1 mm apart and one inch long and be incident on a polaroid strip cut in the proper way to allow either  $V$  or  $H$  components. Light, thus rendered parallel and polarised is incident on the Raman tube. Scattered light is analysed by a split polaroid kept almost touching the slit of the spectrograph, so that one part transmits  $h$  and the other the  $v$  component. The pair of photographs  $V_i$  and  $V_h$  and  $H_v$  and  $H_h$  are thus

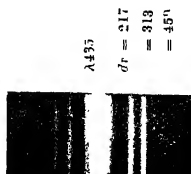


Fig. 3. Raman Spectrum of  $\text{CCl}_4$  with incident light  $H$  polarised, to demonstrate the absence of  $\nu = 459$  which is very sensitive to convergence, leak of the polaroid in the incident light, extraneous light etc.

exposed simultaneously. To eliminate error due to differential transmission of the spectrograph, the arrangement, including the split polaroid is rotated by  $45^\circ$  so that, light is incident on the sample at an angle of  $45^\circ$  to the horizontal plane. A spectrum of  $\text{CCl}_4$  taken under these conditions and showing  $H_h$  and  $H_v$  components shows that  $\nu = 459$  is almost absent (fig. 3). It is about 1% as intense as  $\nu = 313$  while these two are of equal intensity in a spectrum taken with incident light unpolarised. It will show itself prominently, if the arrangement is defective by way of (1) convergence of the incident light (2) convergence of the scattered light (3) leak of the polaroid in the incident light and (4) extraneous light (of unpolarised nature) falling on the sample tube.  $\nu = 217$  and  $313$  appear identical in  $H_h$  and  $H_v$  showing the absence of (1) differential transmission of the spectrograph for  $v$  and  $h$  components and (2) polarisation of scattered light by reflection on the walls of the sample tube.

## REFERENCES

- Bank, D. H. 1948, *Jour. Opt. Soc. Amer.* **38**, 281.  
 ———— 1947, *Jour. Opt. Soc. Amer.* **37**, 798  
 Krishnan, R. S. 1934, *Proc. Ind. Acad. Sci.* **1**, 782  
 Pokrowski, G. I. and Gordon, E. A. 1930, *Ann. d. phys.* **4**, 488  
 Sokolovskaya, A. I. and Simova, P. D., 1963, *Opt. Spectro.* **15**, 338

# INFLUENCE OF INTER-ELECTRODE SEPERATION IN HIGH FREQUENCY TITRATION

J. N. CHAKRAVORTY

DEPARTMENT OF PHYSICS,  
RAMA KRISHNA MISSION RESIDENTIAL COLLEGE,  
NARENDRAPUR

(Received September 14, 1966)

The inter-electrode separation (Mukherjee *et al*, 1963) influences profoundly the response in titrations performed in the high frequency field. A titration of 0.001N HCl with 0.025N NaOH was studied with the help of a high frequency titrimeter working on 8 Mc/s. The electrode distance of the titration cell was gradually varied and the total change in the condenser dial reading pertaining to the end point for each titration was noted. The result was shown in figure 1 whence it is evident that the response is poor at lower electrode distances but is quite satisfactory beyond 3.5 cm. where the variation in the capacitance remains constantly maximum

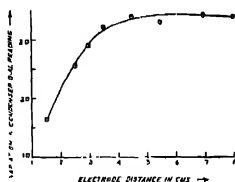


Fig. 1.

This observation can be interpreted from the properties of the circuit as follows. In the present case, the titration cell is connected in parallel with other capacitors. Hence a parallel equivalent circuit is considered as the best representative of the situation whose capacitance (Delahey, 1954) is given by,

$$C_p = \frac{C_1^2 K + \omega^2 C_1 C_2^2 + \omega^2 C_1^2 C_2}{K^2 + \omega^2 (C_1 + C_2)^2} \quad \dots (1)$$

where  $C_p$  is the parallel equivalent capacitance,  $C_1$  is the capacitance due to the dielectric properties of the walls of the container,  $C_2$  that of the solution,  $K$  the

actual low frequency conductance of the solution and  $\omega = 2\pi f$ ,  $f$  being the frequency in cycles/sec.

From the above equation if  $K = 0$ ,  $C_p = \frac{C_1 C_2}{C_1 + C_2}$  and if  $K = \infty$ , the value of  $C_p = C_1$ . Hence the change in  $C$  ( $\Delta C_p$ ) represented by  $C$  in the following is given by  $C = \frac{C_1^2}{C_1 + C_2}$ .

Here  $K = 0$  represents the case of empty well without solution and the other case represents a cell filled with highly conducting electrolyte solution. With the same solution and the same cell the greater the value of this  $C$  with varying electrode distance the deeper will be the titration curve (Mukherjee *et al*, 1963). If we assume this change in  $C$  to be maximum at the optimum electrode separation denoted by  $x$ , then at the point of optimum separation  $\frac{dc}{dx} = 0$  whence,

$$2 \frac{(C_1 + C_2)}{C_1} \cdot \frac{dC_1}{dx} = \frac{d}{dx} (C_1 + C_2) \quad (2)$$

Here we may regard  $C_1$  as the capacitance when the cell is empty and  $(C_1 + C_2)$  the capacitance when the cell contains the solution.

In order to test this relation, the capacitances of the empty cell and the cell with 0.001N NaCl which is the end product of titration was measured at different electrode distance. Results obtained have been shown in figure 2. The slopes

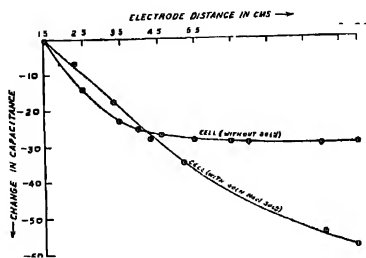


Fig. 2.

$\frac{dc_1}{dx}$  and  $\frac{d(C_1 + C_2)}{dx}$  have been obtained from the respective curves at a given value of  $x$  and the validity of the equation (2) was checked for each electrode distance.

It is interesting to note that the equation fits quite well above a separation of 3.5 cm. Since the equation contains  $C_1$ , the characteristic of the cell wall,  $C_2$  that of the solution and their changes with electrode distance, it is clear that it throws sufficient light to the influence of the electrode distance which appears to depend upon the diameter (Chakravorty *et al*, 1964) of cell, the nature of the glass and that of the solution.

My best thanks are due to Prof. S. N. Mukherjee, D.Sc., Head of the Chemistry Department, Visva Bharati University for valuable discussions. My thanks are also due to the authorities of Jadavpur University and Rama Krishna Mission Residential College for giving me laboratory and other facilities. Financial assistance from University Grants Commission is also gratefully acknowledged.

#### REFERENCES

- Chakravorty, J. N. and Mukherjee, S. N., 1964, *Jour. Indian Chem. Soc.* **41**, 725  
Delahey P., 1954, *New Instrumental Methods in Electrochemistry*, Interscience Publishers Ltd London.  
Mukherjee, S. N. and Chakravorty, J. N., 1963, *Jour. Indian Chem. Soc.* **40**, 643.



# ON A CONDITIONAL ASPECT OF THE J-PHENOMENON IN X-RAYS

H. K. PAL

R. K. M. VIDYAMANDIRA, BELUR MATH, HOWRAH.

(Received July 29, 1966)

While comparing experimentally the ionizations produced by a heterogeneous primary beam of X-rays and its scattered beam in a direction at right angles to the former for different incident wavelengths, Barkla and Khastgir (1927) observed that the graph drawn with the unintercepted ratio of ionizations  $(S/P)_{90^\circ}$  against the mass-absorption coefficient  $(\bar{\mu}/\rho)_{A1}$  of the primary beam transmitted through the scatterer, was a horizontal straight line parallel to  $(\bar{\mu}/\rho)_{A1}$ -axis with a bending down at its harder extremity. This feature was theoretically explained by the writer in a previous paper (Pal 1965, p 119). It was also pointed out in that paper that this was not a general feature of the graph, since it depended on certain experimental conditions.

The author repeated the experiments employing unfiltered radiations with thin and thick scatterers of the same material and with apertures of different sizes for the primary beam. The object of the present communication is to report the results of these experiments and to explain them. Experiments were performed with (i) paraffin wax of thicknesses 3.2 mm. and 18.5 mm. (ii) filter paper of 10, 20 and 50 sheets and (iii) aluminium of thicknesses 0.38 mm. and 0.87 mm. as scatterers and with apertures of different sizes (having diameters ranging from 0.2 mm. to 2.05 mm.) for the primary beam. The results can be stated as follows:

(a) For thin scatterers and narrow apertures, the graph showing  $(S/P)_{90^\circ}$  against the mass-absorption coefficient of the primary beam was found to be horizontal in the proper region (as described above) but with a definite downward slope in the softer region.

(b) For thick scatterers and larger apertures, the same graph was a curve descending steadily towards longer wavelengths.

The results are illustrated by some typical graphs in Figs 1 and 2, where ratio  $(S/P)_{90^\circ}$  is plotted against the exciting peak voltage instead of against  $(\bar{\mu}/\rho)_{A1}$ . It may be noted that all the graphs are reduced to the same scale of reference by taking the maximum value of the ratio  $(S/P)_{90^\circ}$  for each as unity. From these graphs it appears that a smaller scattering thickness (see Fig. 2) or

a narrower primary aperture (see Fig. 1) favours a greater length of the horizontal part of the graph\*.

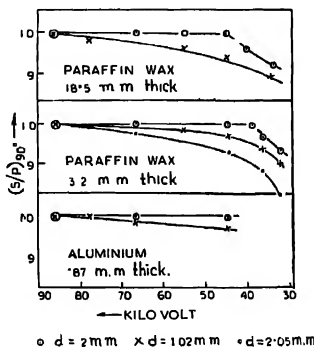


Fig. 1.

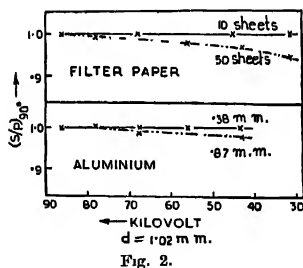


Fig. 2.

To explain the above experimental results, we have to refer to the following equation deduced in the previous paper mentioned before :

$$(S'/P')_{90^\circ} = K' \left[ 1 - 3C_{90^\circ} \left\{ \frac{1}{2} Bx\lambda^3 \left( r_x + \frac{\delta\lambda_{90^\circ}}{\lambda} \right) + \left( \frac{\delta\lambda_{90^\circ}}{\lambda} - r_x \right) \right\} + (A - A')x \right]$$

where  $(S'/P')_{90^\circ}$  denotes the ratio of ionizations when the scattered and the primary beams are each intercepted by a thickness  $x$  of the absorbing material and the other notations are as given in the author's previous paper (Pal, 1965). We shall also take into account the following facts :

- (i) Even though the beams compared are unintercepted in the ordinary sense, they have to pass through a small thickness (.01 cm) of aluminium foil covering the window of the ionization chambers receiving the two beams compared.

\*Graphs of the same nature were obtained also by other workers in the same laboratory.

(ii) The absorbing thicknesses inside the scatterer, for the two beams compared being equal on account of its special setting with respect to the incident beam (method of Barkla and Ayres, 1911), the effect of the thickness of the scattering when considered, may be regarded as equivalent to a small addition to the absorbing thickness  $x$  of the aluminium foil of the ionization chambers in the above equation.

Since  $r_e \approx \frac{\delta\lambda_{90}^\circ}{\lambda}$ , we can rearrange the equation as

$$(S'/P')_{90}^\circ \approx K'[1 - \{3B(C_{90}^\circ \lambda^2) \delta\lambda_{90}^\circ - (A - A')\}x]$$

where  $x$  is the equivalent thickness of aluminium intercepting the two beams compared. It is to be noted that of the three variables (i)  $(C_{90}^\circ \lambda^2)$ , (ii)  $(A - A')$  and (iii)  $x$ , the first increases as the wavelength  $\lambda$  is increased up to a certain maximum value (Backhurst 1934), the second depends on the size of the primary aperture, increasing as the size is diminished (Bachem 1923), the size of the aperture for the scattered beam remaining constant and the third increases as the scattering thickness is increased. The quantity within the curled bracket is usually positive and when this is multiplied by  $x$ , the product represents a general lowering of the graph in question below the horizontal line drawn through the maximum value of  $(S'/P')_{90}^\circ$ . The extent of lowering in any particular case will, however, be determined by the relative magnitudes of the three variables referred to. Thus for very small primary apertures the quantity within the curled bracket may turn out to be vanishingly small, particularly in the harder region of the rays and if, in addition,  $x$  is small too, the lowering of the graph may be trivial, thus accounting for the horizontal course of the same obtained experimentally. With a larger value of  $x$ , of course, the horizontality will cease earlier. If on the contrary, the aperture is large and so also  $x$ , the lowering becomes appreciable even for harder rays. In the case of moderately long wavelengths,  $C_{90}^\circ \lambda^2$  is much greater than  $(A - A')$ , even though the apertures for the primary rays are very narrow, so that the corresponding descent of the graph is very marked despite the smallness of  $x$  (Fig. 1).

The author takes this opportunity of expressing his indebtedness to late Prof. C. G. Barkla, F.R.S., N.L. of the University of Edinburgh for his guidance in the experimental part of this work. His best thanks are also due to Prof. S. R. Khastgir, D.Sc., F.N.I., Head of the department of Physics, Bose Institute, Calcutta, for valuable discussions.

#### REFERENCES

- Bachem, A., 1923, *Principles of X-ray and Radium Dosage* Chicago, p. 152 et seq.  
 Backhurst, I. 1934, *Phil. Mag.* **17**, 321.  
 Barkla, C. G. and Ayres, 1911, *Phil. Mag.* **22**, 187.  
 Barkla, C. G. and Khastgir, S. R., 1927, *Phil. Mag.* **4**, 735.  
 Pal, H. K., 1965, *Indian. J. Phys.* **39**, 108.

## BOOK REVIEWS

"AN INTRODUCTION TO CELESTIAL MECHANICS". By Theodore E. Sterne. Number 9 of Interscience Tracts on Physics and Astronomy, edited by R. E. Marshak. 206 pp. Interscience Publishers Inc. New York, 1960

On going carefully through the book, one is impressed by the learned and persuasive style of this work. There are many books on astronomy or on mechanics and more on geophysics. But a book with such well-chosen topics as are of general and specific interests, is undoubtedly a timely contribution to the literature, and Professor Sterne, who is himself an authority on the subject, has indeed done pioneering work in writing this text.

In recent years with the dawning of the space age and with the great strides that have already been made in this field, the problems of close earth satellites are of great interest to the people of various disciplines. Our impression is that the book is of value for reference to the specialists and will be useful to the advanced students not only of physics, astronomy and engineering (to whom the book is primarily addressed) but also to those of geophysics.

The book is divided into six chapters. The principal aim of the book appears to be to prepare the reader for an understanding of the various problems connected with the artificial earth-satellites which are taken up in the last two chapters. Authors has adequately discussed about his own method as well as those of others for treating the various perturbations involved.

Chapter I discusses gravitation and planetary motions and their orbits. Chapter II is a good account of potential theory for irregular bodies and may be of interest to nuclear physics also, since such gravitational potential is closely analogous to the electrostatic potential of deformed nuclei. In Chapter III the reader is given some glimpses into such complicated topics as the units, orbital elements, time, various precessions and nutations which are primarily the topics of astronomy but have been rendered quite suited to the general readers.

Chapter IV is on classical dynamics dealing with Lagrangian and other equations of motion. This chapter will undoubtedly be the center of interest for many readers. We are however, unable to see the special advantage of the figure 4 over the conventional diagrams generally used to illustrate the Eulerian angles, particularly because the angle  $\psi$  is not indicated in this diagram.

The style of the book is throughout simple, precise and helpful with many examples and hints. Besides, the printed text is kind to the eye.

Finally, it may be mentioned that we have heard about 'printer's devil'. But it appears that the 'binder's devil' can also sometimes do more mischief. The copy of the book given to the reviewer has duplication of the pages from 53

to 84 and unfortunate omission from the pages 85 to 116. Hope this has happened only to the reviewer who did miss those pages.

M. L. G

**PROBLEMS IN QUANTUM MECHANICS**—I. I. Goltzman and V. D. Krivchenkov. Pergamon Press.

The book under review, an English translation from the original Russian, is an excellent contribution which will be undoubtedly highly helpful to the students who like to acquaint themselves with the mathematical techniques of quantum mechanics. As the name suggests, the book contains a large number of worked out problems of preliminary and medium standard, covering almost all the topics of quantum mechanics, usually found in standard textbooks. Although the authors in the preface have stated that the problems are intended for the students who use the book of L. D. Landau and E. M. Lifshitz as their basic text book, the present contribution may also be fruitfully utilized by those who follow other standard textbooks. Of course, the authors have followed the notations similar to those used by Landau and Lifshitz and I think, in some cases more convenient notations would have been preferable. However, the working out of the problems is so logical, methodical and clearly expressed, and the sequence of the chapters and the problems in a chapter are so nicely exposed that even a student having a very preliminary knowledge of quantum mechanics finds no difficulty in going through the worked out examples. A few remarks need mention for an unbiased review of the book. Although the worked out examples extend over a wide range of varieties, the treatment would have been more complete to specialist readers, if it could include some more sophisticated problems, such as those involving the use of time dependent perturbation, permutation of identical particles, the method of second quantization etc. On the whole, the book will undoubtedly benefit those interested in strengthening their basis for handling the intricate mathematical techniques of quantum mechanical calculations.

U. S. Ghosh

**PHYSICS OF COMBUSTION AND EXPLOSION**—by L. N. Khitrin. Pp. 456

Published by the Isreal Program for Scientific Translations, Jerusalem, 1962

Price \$ 12.00 or 84s.

The present book on the physics of combustion has been composed on the basis of lectures, delivered for many years at the Department of Physics of Moscow University. The original book in Russian language has been translated into English by the Isreal Program for Scientific Translations.

Recently, the problems in the theory of combustion have acquired an important field of investigations, since many technological fields including the space-

ships, can not be fruitfully developed without profound knowledge of the nature and laws of combustion of the various combustible substances. A large number of Universities in the U.S.S.R., U.S.A., U.K. Japan and France are now carrying on extensive research work on combustion and explosion. The present book will not only provide a substantial help to those who are engaged in combustion research, but also to the beginners on this subject it will be regarded as a teacher of such qualifications who can make very difficult problems easily understandable to his pupils.

In accordance with the physical and chemical processes involved in combustion of different combustible substances, the science of combustion can be divided into three parts : combustion of gases, combustion of liquid and solid fuels, and explosions. Of those, the combustion of gases has been treated in detail in the present volume. The science of combustion in solid and liquid fuels has occupied the last three chapters of the book. The physics involving explosion has not been included in the book. Starting with the short outline of chemical kinetics, the chapters dealing with the combustion of gases include (i) ignition process, (ii) the process of flame propagation and (iii) the combustion problems in internal combustion engines and gas turbines. At the end eight plates have been presented showing flame propagations under different conditions.

Though a book of advanced study in the physics of combustion, nevertheless, it provides a pleasant reading. It is possibly the best text book on this subject, at the same time it will be treated as a very helpful guidance by those who are interested in combustion research.

*M. M. M.*

## ERRATA

Dielectric absorption of 3.14 cm microwaves in some polar liquids—Part II.  
substituted halo-benzones and naphthalene.

J. Bhattacharyya, S. B Roy and G. S Kastha

Vol 40., No. 4, April, 1966

Page 188 6th line from the bottom read  $\epsilon''$  and  $\epsilon'$  instead of  $\epsilon''$ .  
4th line from the bottom read "Infinite frequency" instead of "static"

Page 191 Table VI

In the 6th. column read the heading as  $\frac{4}{3} \pi abcf...$  instead of  $4\pi abcf$

Page 196, Captions to Fig. 6a- curve (v) and curve- (vi)- "The scale of  $\tau$  values  
given on the right" refer to both the curves.

Page 196 Fig. 6b—The Roman numerals on the curves in the body of the figure  
are to be interchanged.





# ELECTRONIC ENERGY-STATES OF ONE-DIMENSIONAL MIXED CRYSTALS

C. L. ROY

DEPARTMENT OF PHYSICS, INDIAN INSTITUTE OF TECHNOLOGY, KANAGAPUR.

(Received May 10, 1968)

**ABSTRACT.** The electronic energy-states of mixed linear lattices have been investigated by a matrix method which is the same as used by the author in a previous paper (Referred to as I in the text) for studying the electronic energy states of linear monoatomic lattices. As in I, the models in this paper have been constructed in the frame-work of rectangular potential well. Explicit equations for allowed electronic energies have been given for several perfect and disordered cases. The results for the disordered cases have been given only upto first order. Some of the results are in a form suitable for numerical computations.

## INTRODUCTION

By using a matrix method, the author (Roy 1966) has investigated in an earlier paper (Referred to as paper I henceforward) the electronic energy states in one dimensional monoatomic crystals. In this paper, the same method has been used to study the electronic energy-states in one dimensional mixed crystals.

James and Ginzburg (1953) and Landauer and Helland (1954) have studied in a practical way the electronic energy-states of mixed linear lattices in which groups of different species of atoms are connected in a chain with varying degrees of complexity. A theorem of Saxon and Hunter (1949) answers to some extent the question as to what properties of a mixed lattice can be inferred from a knowledge of the separate band-structure of the pure lattices. This theorem states that the common forbidden energies of two pure  $\delta$ -function lattices  $\theta$  and  $\phi$  remain forbidden in any mixture of  $\theta$  and  $\phi$ . A proof of this theorem in a somewhat general way has been given by Luttinger (1954). However, limitations have been pointed out about the validity of the theorem as well as its proof. James and Ginzburg (1953) have analysed the theorem by applying the method of mode counting while Kerner (1954) has used a matrix method. These investigations have brought out that the theorem of Saxon and Hunter is true only for  $\delta$ -potentials. Kerner's analysis has broadened the condition for the persistence of the forbiddenness of any energy simultaneously forbidden in pure  $\theta$  and  $\phi$  crystal. The knowledge of the electronic energy-bands of the  $\theta$  and  $\phi$  crystals can thus supply information only on a limited scale about the electronic energy-states of the mixed  $\theta$ - $\phi$  crystal. The best way to get such information would be to know the equations giving the allowed electronic energies for the particular type of mixing under consideration.

In this paper, investigations have been made about the electronic energy-states in some one-dimensional mixed crystals within the frame work of the rectangular potential-well model. Explicit energy-eigenvalue equations have been derived for various ordered and disordered models. Some of these equations are in a form suitable for numerical computations. A matrix method has been used for investigation of the problems of this paper. This method, as mentioned before, is the same as used in I where a thorough discussion has been given about the importance of rectangular potential well model compared to the  $\delta$ -function model.

### EIGENVALUE EQUATIONS FOR PERFECT INFINITE LATTICES

*Mixed lattice of general type.* we consider the derivation of the energy eigenvalue equation for a mixed lattice as shown in the Fig. 1 below :

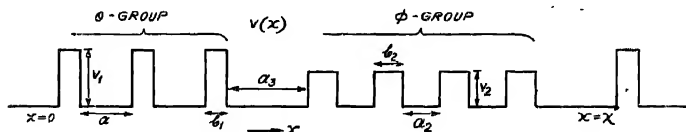


Fig. 1

Rectangular potential-well model for a one-dimensional infinite mixed lattice of a general type.

The model is formulated with an infinite 'no of' two types of atoms  $\theta$  and  $\phi$  producing potentials of rectangular well type. The parameters with suffix 1 refer to the  $\theta$ -atoms while those with suffix 2 refer to the  $\phi$ -atoms. In the model, we suppose that the sequence with  $l$  no of  $\theta$  atoms followed by  $m$  no of  $\phi$ -atoms is repeated infinitely. The distances  $a_1$ ,  $a_2$ ,  $a_3$ , separating respectively two  $\theta$ -atoms, two  $\phi$ -atoms and the groups of  $\theta$  and  $\phi$  atoms are all different. This makes the model somewhat general. The period  $\chi$  of the lattice is obviously given by :

$$\chi = (l-1)a_1 + (m-1)a_2 + lb_1 + mb_2 + 2a_3 \quad \dots (1)$$

Referring to equation (34) of I, we find that the eigenvalues for the present model are given by :

$$\cos \mu\chi = \frac{1}{2} \text{tr } T \quad \dots (2)$$

$T$  is defined through the equation :

$$\begin{pmatrix} A \\ B \end{pmatrix}_{at x = \chi} = T \begin{pmatrix} A \\ B \end{pmatrix}_{at x = 0} \quad (3)$$

$A$  and  $B$  have meanings as in equation (4) of I. As explained in I,  $T$  can be written as a product of some other matrices in the following form :

$$T = \begin{pmatrix} \exp i\alpha(a_3 - a_2) & 0 \\ 0 & \exp -i\alpha(a_3 - a_2) \end{pmatrix} (T_\varphi)^m \begin{pmatrix} \exp i\alpha(a_3 - a_1) & 0 \\ 0 & \exp -i\alpha(a_3 - a_1) \end{pmatrix} (T_\theta)^l \dots \quad (4)$$

In equation (4),  $T_\theta$  and  $T_\varphi$  are the same as  $T$ -matrix of I with appropriate parameters for  $\theta$  and  $\phi$  type atoms. Thus following equations (19) to (22) of I, we find the following expressions for the elements of the  $T_\theta$ -matrix :

$$(T_\theta)_{11} = \frac{1}{4i\alpha\beta_1} \cdot [ (i\alpha + \beta_1)^2 \exp(\beta_1 b_1 + i\alpha a_1) - (i\alpha - \beta_1)^2 \exp(-\beta_1 b_1 - i\alpha a_1) ] \dots \quad (5)$$

$$(T_\theta)_{22} = (T_\theta)_{11}^* \quad (6)$$

$$(T_\theta)_{21} = \frac{1}{4i\alpha\beta_1} [ (i\alpha + \beta_1)(i\alpha - \beta_1) \exp(-i\alpha a_1) \{ \exp(\beta_1 b_1) - \exp(-\beta_1 b_1) \} ] \quad (7)$$

$$(T_\theta)_{12} = (T_\theta)_{21}^*$$

The elements of  $T_\varphi$ -matrix are given by expressions exactly similar to those of (5) to (8) with suffix 1 replaced by suffix 2. Since  $\det T_\theta = \det T_\varphi = 1$ , we notice from (4) that  $\det T = 1$ . Now if  $\frac{1}{2} \text{tr } T_\theta = \cos c_\theta$ , the eigen values of  $T_\theta$  are  $\exp(\pm i c_\theta)$ . Following equations (50) and (51) of I, we then find the following expressions for the elements of  $(T_\theta)^l$  :

$$(T_\theta^l)_{11} = (T_\theta^l)_{22}^* = \frac{1}{\sin c_\theta} \{ \sin(l+1)c_\theta - (T_\theta)_{11}^* \sin c_\theta \} \dots \quad (9)$$

$$(T_\theta^l)_{21} = (T_\theta^l)_{12}^* = (T_\theta)_{21} \frac{\sin l c_\theta}{\sin c_\theta} \dots \quad (10)$$

Exactly similar expressions are obtained for the elements of  $(T_\varphi)^m$  by replacing  $l$  by  $m$  and the suffix  $\theta$  by  $\phi$ . With proper expressions for the elements of  $(T_\theta)^l$  and  $(T_\varphi)^m$ , we get from equations (2) and (4), the following equation for the electronic energy-eigenvalues :

$$\begin{aligned} \cos \mu\chi &= (I_\theta I_\varphi - J_\theta J_\varphi) \cos \alpha(2a_3 - 2a_2 - a_1) - (J_\theta I_\varphi + J_\varphi I_\theta) \\ &\sin \alpha(2a_3 - a_2 - a_1) + (\eta_\theta \eta_\varphi + \zeta_\theta \zeta_\varphi) \cos \alpha(a_1 - a_2) \\ &\quad - (\zeta_\theta \eta_\varphi - \zeta_\varphi \eta_\theta) \sin \alpha(a_1 - a_2) \end{aligned} \quad \dots \quad (11)$$

where,

$$(T_\theta^l)_{11} = I_\theta + iJ_\theta \quad \dots \quad (12)$$

$$(T_\theta^l)_{21} = \eta_\theta + i\zeta_\theta \quad \dots \quad (13)$$

$$I_\theta = \frac{1}{\sin c_\theta} \{ \sin (l+1)c_\theta - (T_\theta)_{11r} \sin lc_\theta \} \quad \dots (14)$$

$$J_\theta = (T_\theta)_{11r} \frac{\sin lc_\theta}{\sin c_\theta} \quad \dots (15)$$

$$(T_\theta)_{11} = (T_\theta)_{11r} + i(T_\theta)_{11i} \quad \dots (16)$$

$$(T_\theta)_{21} = (T_\theta)_{21r} + i(T_\theta)_{21i} \quad \dots (17)$$

The quantities  $I_\theta$ ,  $J_\theta$  . . etc. are given by similar expressions with  $c_\theta$  replaced by  $c_\varphi$  and  $l$  by  $m$ .

Special cases : We can now get some results as special cases of equation (11).

Case I : Let us consider the model as given by Fig. (2) below :

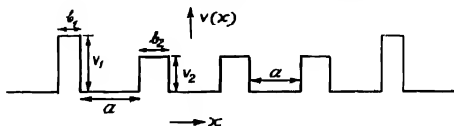


Fig. 2

Rectangular potential-well model of a special type of infinite mixed lattice (Kerner's model).

Here the atoms of one kind say the  $\theta$ -type occur in groups of one and the group to group distances are the same as the interatomic distances of the other group. Thus in this case  $l = 1$ ,  $a_2 = a_1 = a_3 = a$  (say). From (11), we get for the present case :

$$\cos \mu\chi = \frac{1}{\sin c_\varphi} \left\{ \sin (m+1)c_\varphi \cos c_\theta - \sin mc_\varphi \left[ \cos h\beta_1 b_1 \cos h\beta_2 b_2 - \frac{\beta_1^3 + \beta_2^3}{2\beta_1\beta_2} \sin h\beta_1 b_1 \sin h\beta_2 b_2 \right] \right\} \quad \dots (18)$$

Equation (18) is the same as derived by Kerner (1954), starting with the model of Fig. 2.

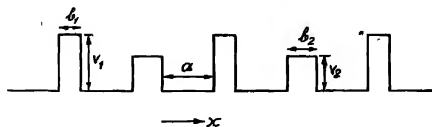


Fig. 3

Rectangular potential-well model, for a one-dimensional infinite perfect diatomic lattice.

Case II : We now consider the model given by Fig. 3 below. This is a model for an ideal diatomic crystal in the framework of rectangular potential-well.

Obviously for this model,  $a_2 = a_3 = a_1 = a$  (say) and  $l = m = 1$ . Thus for this case, we get from (18) :

$$\begin{aligned} \cos \mu(2a+b_1+b_2) &= \frac{(\beta_1^2 - \alpha^2)(\beta_2^2 - \alpha^2)}{4\alpha^2\beta_1\beta_2} \cdot \sin h \beta_1 b_1 \sin h \beta_2 b_2 \\ &- \frac{1}{4\alpha^2\beta_1\beta_2} (\beta_1^2 - \alpha^2)(\beta_2^2 - \alpha^2) \sin h \beta_1 b_1 \sin h \beta_2 b_2 \cos 2\alpha a \\ &+ \frac{1}{2\alpha\beta_1\beta_2} \cdot [\beta_2(\beta_1^2 - \alpha^2) \cosh \beta_2 b_2 \sinh \beta_2 b_2 + \beta_1(\beta_2^2 - \alpha^2) \cosh \beta_1 b_1 \\ &\cdot \sinh \beta_2 b_2] \sin 2\alpha a + \cosh \beta_1 b_1 \cosh \beta_2 b_2 \cos 2\alpha a \quad \dots (19) \end{aligned}$$

Under the conditions  $b_1 \rightarrow 0$ ,  $b_2 \rightarrow 0$ , so that  $b_1 v_1$  and  $b_2 v_2$  remain finite ( $\delta$ -potentials for both  $\theta$  and  $\phi$  atoms), equation (19) reduces to the form given by the present author (Roy 1964) as well as Saxon and Hutner (1949)

#### EIGENVALUE EQUATIONS FOR DISORDERED MIXED LATTICES

Case 1 : Let us consider the model given by Fig. (4) below. The model contains ' $n$ ' no of  $\theta$ -atoms and ' $n$ ' no of  $\phi$ -atoms. The distances between any two potential wells are arbitrary. We suppose that  $a_{j,j} = a + c_{j,j}$  = distance between the  $j$ -th  $\theta$ -atom and  $j$ -th  $\phi$ -atom,  $a_{j,j+1} = a + \epsilon_{j,j+1}$  = distance

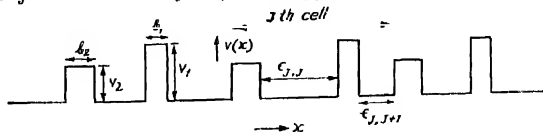


Fig. 4

Rectangular potential-well model for a one-dimensional finite diatomic lattice with a general type of disorder.

between  $j$ -th  $\theta$ -atom and  $(j+1)$ th  $\phi$ -atom. ' $a$ ' is the average of all  $a_{j,j}$ 's. Following equation (4), we find that the  $T$ -matrix  $T_j$  for the  $j$ -th cell in the present case is given by :

$$T_j = \begin{pmatrix} \exp i\alpha(a + \epsilon_{j,j+1}) & 0 \\ 0 & \exp -i\alpha(a + c_{j,j+1}) \end{pmatrix} T_\theta' \begin{pmatrix} \exp i\alpha(a + \epsilon_{j,j}) & 0 \\ 0 & \exp -i\alpha(a + c_{j,j}) \end{pmatrix} T_\theta' \quad (20)$$

where,

$$T_\theta' = (Rvr)_\theta \quad \dots (21)$$

$$T_\theta' = (Rvr)_\theta \quad \dots (22)$$

The matrices  $R, v, r$  have the same meaning as in I and  $(Rv)_\theta$  means that the product has been taken at a  $\theta$  potential well. Now following the same argument as used in deriving equation (40) of (I), we see that for the present case—the allowed energies are given by the condition,

$$\text{tr} \left( \prod_{j=n}^{j-1} T_j \right) \leq 2 \quad \dots (23)$$

Retaining only upto the first order terms, we get from (20),

$$T_j = (T' + K_{j,j+1}T' + T_\theta K_{j,j}T_\theta) \quad \dots (24)$$

where,

$$T_\theta = \begin{pmatrix} \exp i\alpha & 0 \\ 0 & \exp(-i\alpha) \end{pmatrix} T'_\theta \quad \dots (25)$$

$$T'_\theta = \begin{pmatrix} \exp(i\alpha) & 0 \\ 0 & \exp(-i\alpha) \end{pmatrix} T_\theta \quad \dots (26)$$

$$K_{j,j} = \begin{pmatrix} i\alpha e_{j,j} & 0 \\ 0 & -i\alpha e_{j,j} \end{pmatrix} \quad \dots (27)$$

$$T' = T_\theta T_\theta \quad \dots (28)$$

Substituting (24) in (23) and retaining again only upto the first order terms, we get :

$$\text{tr} [T'^{n-1} \cdot \sum_{j=1}^{j-1} (T'^{n-j} K_{j,j+1} T'^j) + \sum_{j=1}^{j-1} (T'^{n-j} T_\theta K_{j,j} T_\theta T'^{j-1})] \leq 2 \quad \dots (29)$$

Equating the zero and first order terms separately to zero, we get from (29) :

$$\text{tr} T'^n \leq 2 \quad \dots (30)$$

$$\text{tr} \left[ \sum_{j=1}^{j=n} (T'^{n-j} K_{j,j+1} T'^j + T'^{n-j} T_\theta \cdot K_{j,j} \cdot T_\theta \cdot T'^{j-1}) \right] = 0 \quad \dots (31)$$

Now if  $\cos c' = \frac{1}{2} \text{tr} T'$ , the eigen values of  $T'$  are  $\exp(\pm ic')$  [ $\therefore \det T' = 1$ ]. The elements of  $T'^n$  are thus given by the same formulae as (9) and (10) with  $c_0$  replace by  $c'$  and  $l$  by  $n$ . With proper expressions for the elements of  $T'^n$ , we get from (30) :

$$\frac{1}{\sin c'} [\sin(n+1)c' - \sin nc'T'_{11r}] \leq 1 \quad \dots (32)$$

where,  $T'_{11} = (T_\theta T_\theta)_{11} = T'_{11r} + iT'_{11i}$

Also using the proper expressions for the elements of  $T'^n$  and retaining again only upto the first order terms, we get from (31) :

$$\begin{aligned} & \sum_{j=1}^{j-1} [e_{j,j+1} \{ (T'^{n-j})_{11r} (T'^j)_{11i} + (T'^{n-j})_{11i} (T'^j)_{11r} \} + \\ & + e_{j,j} \{ P_1 + P_2 + P_3 + P_4 - P_5 - P_6 - P_7 - P_8 \}] = 0 \quad \dots (33) \end{aligned}$$

In equation (33),  $P_1, P_2$  etc. are rather complicated expressions containing the real and imaginary parts of the elements of the matrices  $(T^{n-j})$ ,  $(T^{j-1})$ ,  $T_\theta$  and  $T_\varphi$ . They can be worked out by straightforward multiplication of the matrices in the second term of the bracket [ ] in equation (31). To indicate the general nature of these terms, we write in full only  $P_1$  :

$$P_1 = [(T^{n-j})_{11r}(T_\theta)_{11r} - (T^{n-j})_{11i}(T_\theta)_{11i}] \cdot \\ [(T_\theta^{-1})_{11r}(T^{j-1})_{11r} - (T_\theta^{-1})_{11i}(T^{j-1})_{11i}] \cdot \\ [(T_\varphi)_{11r}(T^{j-1})_{11r} - (T_\varphi)_{11i}(T^{j-1})_{11i}] \cdot \\ [(T^{j-1})_{11i}(T_\theta)_{11r} + (T^{n-j})_{11r}(T_\theta)_{11i}] \quad \dots \quad (34)$$

The connections between  $(T^{n-j})_{12r}$ ,  $(T^{n-j})_{12i}$ ,  $(T_\theta)_{11r}$ ,  $(T_\theta)_{11i}$  etc which are the real and imaginary parts of  $(T^{n-j})_{12}$ ,  $(T_\theta)_{11}$  etc are expressed by the following equations :

$$(T^{n-j})_{11r} = (T^{n-j})_{11}^* = (T^{n-j})_{11r} + i(T^{n-j})_{11i} \quad \dots \quad (35)$$

$$(T^{n-j})_{12} = (T^{n-j})_{12}^* = (T^{n-j})_{12r} + i(T^{n-j})_{12i} \quad \dots \quad (36)$$

$$(T_\theta)_{11} = (T_\theta)_{11}^* = (T_\theta)_{11r} + i(T_\theta)_{11i} \quad \dots \quad (37)$$

$$(T_\theta)_{12} = (T_\theta)_{12}^* = (T_\theta)_{12r} + i(T_\theta)_{12i} \quad \dots \quad (38)$$

$$(T_\varphi)_{11} = (T_\varphi)_{11}^* = (T_\varphi)_{11r} + i(T_\varphi)_{11i} \quad \dots \quad (39)$$

$$(T_\varphi)_{12} = (T_\varphi)_{12}^* = (T_\varphi)_{12r} + i(T_\varphi)_{12i} \quad \dots \quad (40)$$

The full expressions for  $(T_\theta)_{11}$ ,  $(T_\theta)_{12}$  ...etc are given by equations (5) to (8) with  $\beta, v = \beta_1, v_1$  and  $\beta, v = \beta_2, v_2$  for  $\theta$  and  $\phi$  type of atoms respectively and  $a_1 = a_2 = a$ .

Case 2 : Disordered molecular solid . we consider now the model of the solid as given by Fig. (5) below :

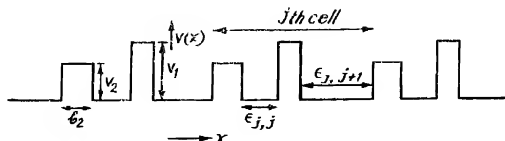


**Fig 5**

Rectangular potential-well model for a one-dimensional finite disordered molecular solid.

This model corresponds to a disordered one-dimensional molecular solid like NaCl where the potential at each molecular site is given by a pair of two different rectangular potential-wells. Thus we see that for the present model,  $c_{j,j} = 0$  for all

$j$ 's. The allowed energies in the present case are given by equation (32) together with another equation given below :

$$\sum_{j=1}^{j=n} [\epsilon_{jj+1} \{ (T'^{n-j})_{11r} (T'^j)_{11l} + (T'^{n-j})_{11l} \cdot (T'^j)_{11r} \}] = 0 \quad \dots (41)$$

Equation (41) follows from (41) with  $\epsilon_{ij} = 0$ . With the full expression for  $(T'^{n-j})_{11r}$ , etc., equation (41) can be further simplified to the following form .

$$\begin{aligned} & \sum_{j=1}^{j=n} c_{jj+1} [T'_{11l} \cos (n-2j-1)c' - 2T'_{11r} T'_{11l} \cdot \\ & \cos (n-2j)c' - T'_{11l} \cos (n-2j+1)c' - 2T'_{11r} \cdot \\ & \sum_{j=1}^{j=n} c_{jj+1} ] [ \cos (n+1)c' - T'_{11r} \cos nc' ] = 0 \quad \dots (42) \end{aligned}$$

## DISCUSSIONS

In the work of this paper, we have used the matrix method of paper I to study the electronic energy-states of mixed crystals within the frame work of the rectangular potential-well model. We have derived the equations for allowed energies of several types of mixed lattices—both perfect and disordered. The allowed energies for the disordered models of Fig. (4) and (5) are given by two equations. One of these [Eqn. (32)] just gives the band structure of a perfect diatomic lattice, with a finite no of atoms ( $n$ ) of both types. The other [Eqn. (42) for Fig. (5) and Eqn. (33) for Fig. (4)] gives additional energy-values due to disorder of the system. The additional energy-states due to disorder of the system affect the electrical conductivity to a great extent. With the help of a Green's function method the author (Roy 1964) has studied the models corresponding to Fig. (4) and (5) in the framework of  $\delta$ -function potentials. As has been discussed in I, the  $\delta$ -function model suffers from several limitations compared to the rectangular potential-well model. Moreover to get the equations for allowed energies for the models of Fig. (4) and (5) using the matrix method, as is done in this paper, we have not used any particular equation connecting the wave functions at any two lattice points. Such an equation has been used in getting equations for allowed energies with the Green's function method. Thus the results obtained by the matrix method are expected to be more general than the results of Green's function method. It would be worthwhile to make numerical computations about the allowed electronic energies for various models, using the equations given by matrix method and Green's function method and compare these computations at least qualitatively with the experimental observations. An investigation in this line is under author's contemplation and the results will appear in later publications.



ACKNOWLEDGMENTS

The author is grateful to Prof S. Datta Majumdar for helpful discussions. He is also thankful to H N. Bose and Prof G. Bandopadhyaya for their keen interest and encouragement.

REFERENCES

- James, H. M. and Ginzburg, A. S., 1953, *J. Phy Chem*, **57**, 810.  
Kerner, E. H., 1951, *Phys. Rev*, **95**, 687  
Landauer, R. and Holland, J. G., 1955, *J Chem Phys*, **22**, 1655.  
Luttinger, J. M., 1951, *Philips Res. Rep.*, **6**, 303  
Roy, U. L., 1964, *Physica*, **39**, 763  
——— 1966, *Indian J Phys.*, **40**, 345).  
Saxon, S. D., and Hutner, R. A., 1949, *Philips Res. Rep.*, **6**, 303

# PHASE FOLLOWING BEHAVIOUR OF AN AUTOMATIC PHASE CONTROL CIRCUIT WITH RESPECT TO A SIGNAL IN PRESENCE OF A RANDOM NOISE\*†

B. N. BISWAS

DEPARTMENT OF PHYSICS, UNIVERSITY OF BURDWAN,  
WEST BENGAL, INDIA.

(Received July 8, 1965, Resubmitted May 30, 1966)

**ABSTRACT.** In this paper the response of an automatic phase control circuit to several different classes of signals has been studied in the presence of noise. The effects of variation of the equivalent gain parameter of the phase locking loop on the system performance for various values of the input signal to noise ratio have also been studied. The concepts of loop noise bandwidth and root-mean-square phase error have been briefly reviewed with particular reference to a band limited noise. Experimental results regarding the performance of the APC circuit in relation to the reception of a FM signal have been presented and found to be in good agreement with the results of the analysis.

$A$  = amplitude of the incoming signal.

$\omega_s$  = angular frequency of the free running local oscillator.

$\omega_i$  = angular frequency of the incoming signal.

$\Omega$  = open loop frequency error in angular measure.

$X(t)$ ,  $Y(t)$  = uncorrelated Gaussian variable of angular bandwidth  $\omega_i$ .

$\tau$  = correlation time.

$\sigma_i^2$  = variance of the input noise.

$m_i$  = index of modulation at the input.

$m_o$  = index of modulation at the output.

$\epsilon(t)$  = phase modulation of the VCO due to noise.

$\beta$  = sensitivity of the VCO.

$K$  = maximum possible synchronisation range in angular measure.

$\sigma^2$  = variance of the noise at the input to phase detector.

$\sigma_p^2$  = variance of the noise at the output of the phase detector.

$B_L$  = loop noise-bandwidth.

$\mu_S$  = equivalent linearised gain of the phase detector for the signal.

$\mu_N$  = equivalent linearised gain of the phase detector for the noise.

## INTRODUCTION

The automatic phase control circuit is essentially an oscillator, the phase of which is locked to an input reference oscillation. It is a narrow-band feedback

\*This work was done at the Institute of Radio Physics and Electronics, Calcutta.

†Part of this paper was presented at the "Symposium on Telecommunication and Electronics, Feb. 26-27, 1963 held at the Institute of Radio Physics and Electronics, Calcutta entitled as "On the Performance of an APC Circuit" (unpublished).

device and consists of a phase detector, a linear filter and a voltage controlled oscillator. The analysis of such a system, even if it is noise-free, is rather difficult because of the inclusion of an error sensing device which is a sinusoidal function of the error itself. But it simplifies considerably if the phase error is small because then the behaviour of the loop can be predicted from a linear analysis of the loop. In such a case it is known that the system can be made to synchronise with respect to the reference input if the open loop frequency error lies within the limits of synchronisation range. But sometimes it has been found that the system may not be synchronised although well within the synchronisation range. This is because of the fact that the 'pull-in' range is different from the 'pull-out' range and this requires a non-linear analysis of the loop to determine almost exactly and completely the performance characteristics of the loop. It is to be further noted that because of the narrow-band feedback process it reduces internally generated noises as well as uncontrolled disturbances that may accompany the input signal to the system. The present purpose of this paper is to develop an analytical method that will help us to know the signal handling capacity of the system as well as to evaluate the output SNR of the system in terms of the input SNR. This, in turn, can be used to find the threshold criterion of the loop. The response of such a circuit to a signal contaminated with stationary random noise has been studied by many authors (Viterbi, A. J. 1963, *et al.*). A convenient approach in such studies is to replace the sinusoidal non-linearity of the phase detector by a linear one whose gain is the equivalent gain of the device, applying quasilinearisation techniques. The other approach employs Fokker-Planck or continuous random walk techniques to find the statistics of random process.

In section 2 a general method for studying the response of an APC circuit to a FM signal contaminated with stationary random noise has been developed. The approach utilised here is to find out the equivalent linearised gains of the phase detector for the signal and noise separately and once the values of the equivalent gains  $\mu_S$  and  $\mu_N$  are known the non-linear system can be analysed as two linear systems—one containing the parameter  $\mu_S$  and the other incorporating the parameter  $\mu_N$ . However, it is to be noted that since the system is a nonlinear one the value of  $\mu_S$  and  $\mu_N$  do depend on the strengths of the signal and noise at the input to the phase detector. Expressions for the equivalent linearised gain of a general type of non-linear element have been developed.

The response of the APC circuit to a FM signal only has been studied in section 3 utilising the concept developed in section 2. An expression for the maximum permissible input modulation index in terms of the modulating frequency, filter parameters and maximum value of the locking range has been developed.

Section 4 deals with the response of the APC circuit to a continuous wave signal which is contaminated with stationary random noise. It also deals with the evaluation of the variance of the noise or the m.s. phase error at the input to the

phase detector when the APC loop is closed through a low-pass filter. This is followed by a discussion in section 5 of the effect of noise on the locking behaviour of the APC circuit. The probability that the system may fall out of lock has been calculated and depicted graphically for different values of the input carrier to noise ratio.

The response of the APC circuit to a FM signal contaminated with stationary random noise has been studied in section 6, particularly when the carrier is in tune with the centre frequency of the voltage controlled oscillator. Due to the difficulty in the analytical computation of the output SNR, in terms of the input SNR, a graphical method for the evaluation of such an expression has been described. The effect of variation of the gain parameter on the performance of such a circuit has also been studied in this section.

In section 7 the concepts of loop noise bandwidth and r.m.s. phase error have been briefly reviewed with particular reference to a bandlimited noise which is common in practice. This is followed by a description of the experimental results with regard to the response of the APC circuit to a FM signal and noise in section 8. These are in good agreement with the results of the analysis presented in the text.

*Response of an APC circuit to signal contaminated with stationary random noise :*

In this section a general method of analysing the response of an automatic phase control circuit to frequency modulated signal that is contaminated with a stationary random noise will be developed. Here the cases of interest are (i) when the centre frequency of the voltage controlled oscillator (VCO) is in tune with the incoming signal and (ii) when the centre frequency of the VCO is slightly out of tune with the incoming signal but the difference of frequency between them is not so high as to cause the system to fall out of lock during the phase following of the modulation cycle by the VCO. In this case, i.e., when the input to the system consists of signal and noise, the presence of the noise will cause a phase jitter at the output of the VCO over and above the so-called slow variation of the output phase of the VCO due to the frequency modulation of the input signal. The amount of phase jitter will depend upon the close loop noise bandwidth, locking range of the system and the amount of initial detuning of the VCO from the incoming signal. These parameters again, on the otherhand, will limit the maximum permissible value of the input modulation index. If the input signal to noise ratio (SNR) is high the amount of phase jitter at the output will almost be the same as that at the input if the noise power be taken equal to that in the close-loop noise bandwidth. This can be found from a straight forward feedback theory. If, however, the noise power is comparable to the signal power, the noise will also cause a change in the equivalent gain of the phase-detector, which is essentially a nonlinear device. The equivalent gain for the noise, in turn, will be affected by the value of signal power.

The nonlinear characteristic exhibited by a phase detector is not a very usual one in the sense that the output is a sinusoidal function of the input. Analysis of such a system is rather difficult and one has to take resort to appropriate approximations. A convenient approach is to replace the sinusoidal nonlinearity by a linear one whose gain is the expected gain of the actual device applying essentially Booton's quasi-linearisation technique

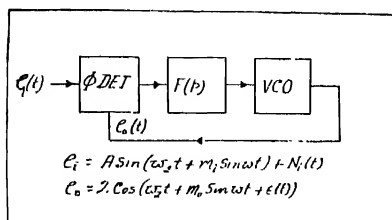


Fig. 1. Block diagram of a typical automatic phase control circuit. The input to the system consists of a FM signal contaminated with a stationary random noise.

Let us consider the automatic phase control circuit as depicted in Fig. 1. The input is a frequency modulated signal which is accompanied by a stationary random noise. The noise possesses a Gaussian amplitude probability distribution with a mean zero and variance  $\sigma^2$  and has power spectral density which is equivalent to that obtained by passing 'white' Gaussian noise through a single tuned IF filter having the centre frequency equal to that of the VCO and angular bandwidth  $\omega_s$ . The net input can, therefore, be written as

$$e(t) = A \sin(\omega_s t + m_i \sin \omega t) + X(t) \sin \omega_s t + Y(t) \cos \omega_s t, \quad (2.1)$$

where  $X(t)$  and  $Y(t)$  are uncorrelated Gaussian variables of angular bandwidth  $\omega_s$ . The auto-correlation function of  $X(t)$  and  $Y(t)$  can be assumed to be given by

$$R_X[X(t)] = R_Y[Y(t)] = \sigma_i^2 \exp(-\omega_s t / \tau), \quad (2.2)$$

where  $\tau$  is the correlation time. Corresponding to this autocorrelation function the power spectral density of the input can be written as

$$G_i(\omega) = 4\sigma_i^2 \frac{\omega_s}{\omega^2 + \omega_s^2} \quad (2.3)$$

Assuming the output of the voltage controlled oscillator to be of the form

$$e_o(t) = 2 \cos[\omega_s t + m_o \sin \omega t + \epsilon(t)], \quad (2.4)$$

where  $m_o$  is the modulation index at the output and  $\epsilon(t)$  is the phase modulation.

of the VCO due to the noise. Therefore the governing equation of the loop is given by (see Appendix A)

$$\frac{d\phi}{dt} = \Omega + \frac{d}{dt} (m_i \sin \omega t) - \beta F(P) [A \sin \phi + N(t)], \quad \dots (2.5)$$

where

$$\begin{aligned} \phi &= \omega_1 - \omega_2 + (m_i - m_0) \sin \omega t - \epsilon(t) \\ \Omega &= \omega_1 - \omega_2 \\ N(t) &= -X(t) \sin [m_0 \sin \omega t + c(t)] \\ &\quad + Y(t) \cos [m_0 \sin \omega t + c(t)] \end{aligned}$$

and  $\beta$  is the sensitivity of the VCO. It can be shown that  $N(t)$  is a stationary process with exactly the same autocorrelation function as  $X(t)$  or  $Y(t)$  (Viterbi, 1963). Eq. (2.5) suggests an analytical equivalent of the APC circuit that is shown in Fig. 2. For the in-tune carrier, the corresponding loop equation is given by

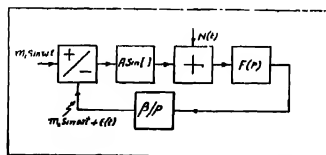


Fig. 2 Equivalent analytical representation of the automatic phase control circuit of Fig. 1.

$$\frac{d\phi}{dt} = \frac{u}{dt} (m_i \sin \omega t) - \beta F(P) [A \sin \phi + N(t)] \quad \dots (2.6)$$

where  $\epsilon = (m_i - m_0) \sin \omega t - \epsilon(t)$  (2.7)

As stated earlier in this case a convenient approach, although approximate, is to find out the equivalent linearised gains of the phase detector for the signal and the noise separately and to break the signal loop into two equivalent analytical loopsone for the signal and the other for the noise (see—Fig. 3d) for studying the signal and noise response of the APC circuit. Now when the system is in lock it was seen that the instantaneous loop error consists of a signal error, a noise error and steady state phase difference that depends on the locking ratio. The noise at the input to the phase detector will again be assumed to a stationary random noise the magnitude of which is normally distributed with a mean zero and variance  $\sigma^2$ . Specifically assuming that the nonlinearity can be represented by

$$F_+(\phi) = \sum a_n(\phi)^{1/n} \quad \text{for } \phi > 0 \quad \dots (2.8)$$

$$F_-(\phi) = \sum b_n(-\phi)^{1/n} \quad \text{for } \phi < 0 \quad \dots (2.9)$$

One can show that the equivalent linearised gains of the phase detector for signal and noise are respectively given by (Sawaragi and Sugai, 1959).

$$\begin{aligned} \mu_s/A = \frac{2}{M} \left[ \frac{1}{2\pi} \int_{\sigma+} F_+(j\omega) I_1(j\omega M) \exp(-\frac{1}{2}\sigma^2\omega^2) d\omega \right. \\ \left. + \frac{1}{2\pi} \int_{\sigma-} F_-(j\omega) I_1(j\omega M) \exp(-\frac{1}{2}\sigma^2\omega^2) d\omega \right] \quad \dots \quad (2.10) \end{aligned}$$

$$\begin{aligned} \mu_N/A = \frac{1}{2} \int_{\sigma+} j\omega F_+(j\omega) J_0(j\omega M) \exp(-\frac{1}{2}\sigma^2\omega^2) d\omega \\ + \frac{1}{2} \int_{\sigma-} j\omega F_-(j\omega) J_0(j\omega M) \exp(-\frac{1}{2}\sigma^2\omega^2) d\omega \quad \dots \quad (2.11) \end{aligned}$$

where  $M$  is the modulation error  $C_+$  and  $C_-$  are integral paths along the straight lines from  $-j\delta-\infty$  to  $-j\delta+\infty$  and from  $j\gamma-\infty$  to  $j\gamma+\infty$  respectively.  $I_1(x)$  is the modified Bessel function of order one and argument  $x$ ,  $F_+(j\omega)$  and  $F_-(j\omega)$  are respectively the Fourier transform of the nonlinearity when  $\phi > 0$  and  $\phi < 0$  and they are given by

$$F_+(j\omega) = \sum_n a_n \frac{\Gamma\left(\frac{1}{n}+1\right)}{(j\omega)^{1+1/n}} \quad \dots \quad (2.11a)$$

$$F_-(j\omega) = \sum_n b_n \frac{\Gamma\left(\frac{1}{n}+1\right)}{(j\omega)^{1+1/n}} \quad \dots \quad (2.11b)$$

At this point one can physically argue that the equivalent linearised gain of the phase detector with respect to the signal in the off-tune case will be smaller than in the in-tune case. Therefore, the probability of loss of lock per cycle for a signal with low modulation index in the off-tuned case will be larger than in the in-tune case.

In the sections to follow we shall discuss in detail the performance of the APC circuit particularly when the incoming signal is in tune with the voltage controlled oscillator.

### *Response of a Frequency Modulated Signal Only.*

A method based on the principle of quasilinearisation technique for analysing the response of the APC circuit to an FM signal is presented here. The method is limited to the case of in-tune carrier only. In this case if the locking range, system bandwidth and the modulation index of the input signal are properly adjusted, it is reasonable to assume that modulation error as well as the distortion

components at the output of the VCO will be small. Therefore the equivalent linearised gain of the phase detector is given by

$$\begin{aligned}\mu_N &= \frac{1}{M} \frac{1}{\pi} \int_0^{2\pi} \sin(M \sin \omega t) d\omega t \\ &= 2A \frac{J_1(M)}{M}\end{aligned}\quad \dots (3.1)$$

where  $A$  is the signal strength  $J_1(M)$  is the Bessel function of order one and index  $M$  and  $M$  is the modulation error. From the equivalent analytical loop for the signal (Fig. 3a) it is easy to show that

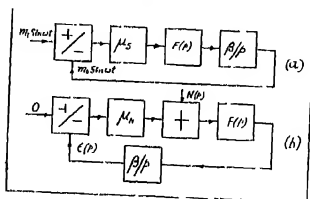


Fig. 3(a) Equivalent analytical representation of the automatic phase control circuit of Fig. 1 for the signal component only. The sinusoidal nonlinearity of the phase detector has been replaced by a linear one whose gain for the signal ( $\mu_N$ ) is the expected gain of the device itself.

Fig. 3(b) Equivalent analytical representation of the automatic phase control circuit of Fig. 1 for the noise component only. The sinusoidal nonlinearity of the phase detector has been replaced by a linear one whose gain for the noise ( $\mu_N$ ) is the expected gain of the device itself.

$$\frac{M}{m_s} = \frac{1}{1 + 2K \frac{J_1(M)}{M} \frac{F(P)}{P}} \quad \dots (3.2)$$

Thus knowing the value of the modulation error  $M$  for a definite value of the input modulation index it is easy to find out a relation between the input modulation index and the output modulation index ( $m_o$ ) in terms of the loop parameters.

The maximum permissible value of the input modulation index can be found from Eq. (3.2) by taking  $M$  to be nearly equal to  $\pi/2$  and one can easily show that

$$[m_i]_{max} \approx \pi/2 \left[ 1 + 0.7K \frac{F(P)}{P} \right] \quad \dots (3.3)$$

It is important to note that the above analysis, although not very accurate as it does not take into account distortion components, gives an idea about the nature of variation of the maximum permissible value of the input modulation



index with modulating frequency. The analysis given above can, however, be extended to the slightly off-tuned carrier depending upon the locking range of the system. In this case it is only to be remembered that the maximum permissible input modulation index will be smaller than that of the in-tune carrier, the amount of which is essentially dependent on the locking ratio and the type of filter used.

*Response of an APC Circuit to a CW Signal Contaminated with Stationary Random Noise .*

In this section a study will be made of the response of the automatic phase control circuit to a CW signal contaminated with stationary random input time function. The amount of phase filter at the output of the VCO caused by the input and the amount of initial detuning of the VCO from the incoming CW signal

The input to the system consists of the signal and random stationary noise, the properties of which have been described elsewhere in the text. Let us assume that the output of the VCO is of the form

$$e_0(t) = 2 \cos [\omega_c t + \epsilon(t)] \quad (4.1)$$

where  $\epsilon(t)$  represents the phase jitter of the VCO output introduced by the noise. It is easy to show that the governing equation of the loop is given by,

$$\frac{d}{dt} [\epsilon(t)] = KF(P) \sin c(t) \quad (4.2)$$

when the noise-phase variation is such that  $c(t)$  remains within the stretch between  $-\pi/2$  and  $+\pi/2$ , one can approximate the sinusoidal nonlinearity by the following relation

$$\sin \phi = F_+(\phi) + F_-(\phi) \quad (4.3)$$

where

$$F_+(\phi) = .04(\phi) + .71(\phi)^{2/3} \text{ for } \phi > 0 \quad \dots (4.4)$$

$$F_-(\phi) = .04(-\phi) + .71(-\phi)^{2/3} \text{ for } \phi < 0 \quad (4.5)$$

It is to be noted that if  $c(t)$  goes beyond the stretch from  $-\pi/2$  to  $+\pi/2$  then one has to find out a suitable relation to approximate the sinusoidal non-linearity. Therefore with this approximation and remembering that

$$|F_+(\phi)| = |F_-(\phi)| \quad \dots (4.6)$$

one can easily show from Eq. (2.11) that the equivalent linearised gain of the phase detector with respect to the noise is given by

$$\mu_N/A = \frac{1}{\pi} \int_{-\pi}^{\pi} j\Lambda \{ F_+(j\omega) \exp \{ - \sigma^2 \omega^2 \} d\omega \quad (4.7)$$

$$= 0.04 + 0.32(\sigma)^{-1} \quad \dots (4.7a)$$

where  $\sigma^2$  is the variance of the noise at the input to the phase detector. The variation of the equivalent linearised gain of the phase detector for noise is shown in Fig. 4. From the equivalent analytical loop of Fig. 3(b) it is easy to show that

$$\sigma^2 = \frac{1}{4\pi A^2} \int_{-\infty}^{+\infty} \left| \frac{KF(j\omega)}{j\omega + K[.04 + .32(\sigma)^{-1/3}F(j\omega)]} \right| G_i(\omega) d\omega, \quad \dots (4.8)$$

and

$$\sigma_\varphi^2 = \frac{1}{4\pi} \int_{-\infty}^{+\infty} \left| \frac{KF(j\omega)}{j\omega + K[.04 + .32(\sigma)^{-1/3}F(j\omega)]} \right| G_i(\omega) d\omega \quad \dots (4.9)$$

where

$$K = A\beta$$

and  $\sigma_\varphi^2$  is the variance of the noise at the output of the phase detector. From above equations it is possible to find the values of  $\sigma^2$  and  $\sigma_\varphi^2$  in terms of the input vari-

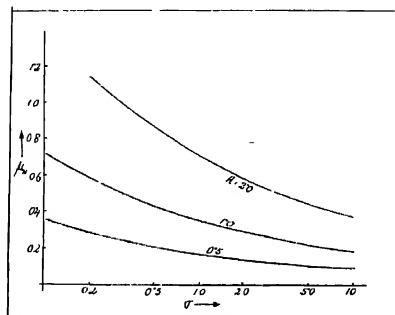


Fig. 4. Variation of the equivalent linearised gain ( $\mu_N$ ) of the phase detector for the noise in presence of a CQW-signal of amplitude A.

ance and loop parameters. For reasons of difficulty in analytical computation of the above parameters it is sometimes advisable to take resort to graphical method of computation.

For example, taking the case of an APC circuit with a low pass filter having the transfer function given by

$$F(j\omega) = \frac{1}{1+j\omega T} \quad \dots (4.10)$$

and comparing Eq. (4.8), (4.9) (4.10) and (2.3) one can easily show that

$$\sigma^2 \cdot \frac{A^2}{\sigma_\varphi^2} = \frac{K}{.04 + .32(\sigma)^{-1/3}} \cdot \frac{1 + \omega_i T}{K[.04 + .32(\sigma)^{-1/3}] + \omega_i(1 + \omega_i T)} \quad \dots (4.11)$$

$$\frac{\sigma_p^2}{\sigma_i^2} = \frac{(1+w_i T)[.04 + 32(\sigma)^{-1/3}]}{[.04 + 32(\sigma)^{-1/3}] + \frac{w_i(1+w_i T)}{K}} \quad \dots (4.12)$$

From the plot of Fig. 5 one can easily find the value of  $\sigma^2$  for a particular loop parameter and hence knowing  $\sigma^2$  it is easy to find the value of  $\sigma_p^2$  from Eq (4.10).

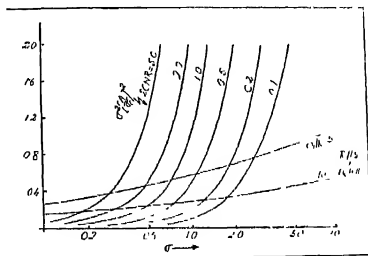


Fig. 5. Illustrates a graphical method for evaluating the value of the variance of the noise ( $\sigma$ ) at the input to the phase detector in terms of the variance of the noise at the input to the system (vide Eq 4.11).

#### Effect of noise on the locking behaviour of an automatic phase control circuit:

If the input to an automatic phase control circuit is corrupted with band-limited white Gaussian noise with mean zero and variance  $\sigma_i^2$ , there will be phase jitter in the output of the voltage controlled oscillator. The amount of phase jitter will, however, depend upon the input signal to noise ratio and the system bandwidth. To understand in physical terms how noise affects the locking behaviour of an APC circuit one may study the nature of the instantaneous variations in phase-difference  $\phi$  between the reference oscillation and the local oscillation. When the input SNR is high and the detuning is small compared to the locking range, the amount of phase jitter will not be large enough to make the system fall out of lock.

If, however, the input SNR is low there are chances of losing lock of the system which will essentially depend upon the locking ratio ( $\Omega/K$ ), system bandwidth and input SNR. In order to investigate the case we will have to study the probability of the phase difference  $\phi$  at the input to sine type nonlinearity of the APC circuit exceeding the phase stretch between  $-\pi/2$  to  $+\pi/2$  i.e. for the phase to be in the unstable region. This means that one has to study cumulative probabilities

$$P_1 = \text{Prob} (+\pi/2 - \phi_0 < \phi < \pi) = \int_{+\pi/2 - \phi_0}^{\pi} P(\phi) d\phi, \quad (5.2)$$

and

$$P_2 = \text{Prob. } (-\pi < -\phi < -\pi/2 - \phi_0) = \int_{-\pi}^{-\pi/2 - \phi_0} p(\phi) d\phi ; \quad \dots \quad (5.2)$$

where  $\phi_0$  is the steady state phase difference and  $P(\phi)$  is the steady state distribution of phase at the input to the phase detector. If, however, the carrier is in tune with the voltage controlled oscillator the above equations reduce to the following simple forms :

$$P_1 = \int_{-\pi/2}^{\pi/2} P(\phi) d\phi \quad \dots \quad (5.3)$$

$$P_2 = \int_{-\pi}^{-\pi/2} P(\phi) d\phi \quad \dots \quad (5.3a)$$

It is to be noted that the relevant SNR is obviously not the input SNR (because of filtering action) but is related to it in a manner that depends upon the filter characteristics and the input SNR.

The probability distribution of the phase when the carrier is in tune with the VCO calculated on the basis of Fokker-plank technique (Viterbi, 1963), for the first order loop is given by

$$P(\phi) = \frac{1}{2\pi I_0(\alpha)} \exp(\alpha \cos \phi) \quad \dots \quad (5.4)$$

where  $I_0(\alpha)$  is the modified Bessel function of order zero and index  $\alpha$ . Where

$$\alpha = 4A/K_1N \quad \dots \quad (5.5)$$

where  $A^2/2$  is the power of the input carrier and  $N$  is the power spectral density of the input 'white' noise and  $K_1$  is the sensitivity of the VCO. Expanding as

$$\exp(\alpha \cos \phi) = I_0(\alpha) + 2 \sum_n I_n(\alpha) \cos n\phi, \quad \dots \quad (5.6)$$

the values of  $P_1$  and  $P_2$  can be easily seen to be given by

$$P_1 = P_2 = \frac{1}{4} - \frac{1}{\pi I_0(\alpha)} \cdot \left[ I_1(\alpha) - \frac{1}{3} I_3(\alpha) + \frac{1}{5} I_5(\alpha) \right] - \dots \quad \dots \quad (5.7)$$

The plot of the cumulative probability  $P$ , is shown in Fig. 6 for different values of input carrier to noise ratio (CNR).

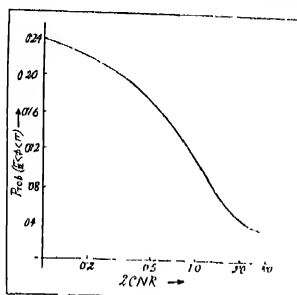


Fig 6 Shows the variation of the cumulative probability ( $P$ ) with different values of the input carrier to noise ratio (CNR)

# *Response of an APC Circuit to a FM signal contaminated with stationary random Noise*

Here the response of an automatic phase control circuit to a FM signal that is contaminated with stationary random noise and is in tune with the centre frequency of the VCO will be considered. The character of the noise has already has already been given elsewhere in the text. Now in this case it is seen that the nonlinear element is a symmetrical one i.e.  $|F_+(\phi)| = |F_-(\phi)|$  and therefore the expressions for the equivalent linearised gains of the phase detector can be written as (see Eq. (2.10) and (2.11)).

$$\frac{\mu_g}{A} = \frac{4}{M} \sum_n \frac{a_n \Gamma\left(\frac{1}{n} + 1\right) \left(\frac{M^2}{2\sigma^2}\right)^{\frac{1}{n}}}{2\Gamma\left(1 - \frac{1-1/n}{2}\right) \left(\frac{\sigma^2}{2}\right)^{\frac{1}{n}}} {}_1F_1\left(\frac{1-1/n}{2}, \frac{1}{2}, -\frac{M^2}{2\sigma^2}\right) \quad (6.1)$$

and

$$\frac{\mu_N}{A} = \sum_n \frac{a_n \Gamma\left(\frac{1}{n} + 1\right)}{\Gamma\left(1 - \frac{1-1/n}{2}\right) \left(\frac{\sigma^2}{2}\right)^{\frac{1}{n}}} {}_1F_1\left(\frac{1-1/n}{2}, n, 1, -\frac{M^2}{2\sigma^2}\right) \quad (6.2)$$

where  ${}_1F_1(x, y, -z)$  is the confluent Hypergeometric function defined as

$${}_1F_1(x, y, -z) = 1 - \frac{x}{y} \cdot \frac{z}{1!} + \frac{x(x-1)}{y(y+1)} \cdot \frac{z^2}{2!} - \dots \quad (6.3)$$

and  $\Gamma(x)$  is the Gamma function. Now in the case when the phase variation does not exceed the stretch from  $-\pi/2$  to  $\pi/2$  we can with reasonable accuracy replace

sinusoidal type of nonlinearity of the phase detector by Eq. (4.3) to Eq. (4.5) and therefore the above Eq. (6.2) and Eq. (6.3) reduce to the following simple forms

$$\mu_s = A \left[ .04 + .32(\sigma)^{-1/3} {}_1F_1 \left( 1/6, 2, -\frac{M^2}{2\sigma^2} \right) \right] \quad \dots (6.4)$$

and

$$\mu_N = A \left[ .04 + .32(\sigma)^{-1/3} {}_1F_1 \left( 1/6, 1, -\frac{M^2}{2\sigma^2} \right) \right] \quad (6.5)$$

The plots of the equivalent linearised gains of the phase detector for the signal and noise are respectively shown in Fig. 7 and Fig. 8. The equivalent analytical loop

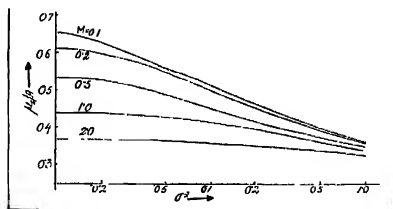


Fig. 7. Variation of the equivalent linearised gain of the phase detector for the signal with the variance of the noise at the input to the phase detector for different values of the modulation error ( $M$ ).

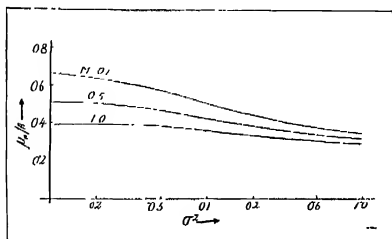


Fig. 8. Variation of the equivalent linearised gain of the phase detector for the noise with the variance of the noise at the input to the phase detector for different values of the modulation error ( $M$ ).

have already been shown in Fig. 3(a) and Fig. 3(b). Now it is a simple matter to show that the modulation error  $M$  is given by

$$M = \frac{m_i}{\left| 1 + K \frac{F(j\omega)}{(j\omega)} \right|} \quad \dots (6.6)$$

where

$$K_S = \beta \mu_S.$$

Denoting the power spectral density of  $N(p)$  as  $G(w)$  (see section 2), the variance of the noise at the input to the phase detector is given by

$$\sigma^2 = \frac{1}{4\pi A^2} \int_{-\infty}^{+\infty} \left| \frac{KF(jw)}{jw + K_N F(jw)} \right|^2 G_i(w) dw, \quad \dots \quad (6.7)$$

where

$$K_N = \beta \mu_N.$$

Therefore the modulation index at the output of the VCO is given by

$$m_0 = m_i \left| \frac{K F(jw)}{jw + K_N F(jw)} \right|. \quad \dots \quad (6.8)$$

Analytical computation of the output SNR in terms of the input SNR is rather difficult because equivalent linearised gains depend both on  $\sigma^2$  and  $M$  in a way given by Eq. (6.4) and Eq. (6.5) and again  $\sigma^2$  and  $M$  depend on  $\sigma_i^2$  and  $m_i$  in a Eq. (6.6) and Eq. (6.7). Therefore it is advisable to employ graphical methods for computation. By way of illustration one may take the example of the APC circuit with a simple lag filter of the form

$$F(jw) = \frac{1}{1+jwT} \quad \dots \quad (6.9)$$

where

$$\begin{aligned} \sigma_i^2 \frac{A^2}{\sigma_i^2} = (1+w_i T) & \left\{ \left[ .04 + .32(\sigma)^{-1/3} {}_1F_1 \left( \frac{1}{6}, 1, -\frac{M^2}{2\sigma^2} \right) \right] \left[ .04 \right. \right. \\ & \left. \left. + .32(\sigma)^{-1/3} {}_1F_1 \left( 1/6, 2 - \frac{M^2}{2\sigma^2} \right) + \frac{\omega_i^2}{K^2} (1+w_i T) \right] \right\} \end{aligned} \quad \dots \quad (6.10)$$

and

$$M^2 = \frac{m_i w^2}{K \left( .04 + .7(\sigma)^{-1/3} {}_1F_1 \left( \frac{1}{6}, 2, -\frac{M^2}{2\sigma^2} \right) \right) - w^2 T^2} + w^2 \quad \dots \quad (6.11)$$

Now taking  $w_i/K = 5$ ,  $w_i T = 1$ ,  $K = 2 \times 400$  rad/sec and  $W = 2.0 \times 400$  rad/sec one can easily show that Eq. (6.11) reduce to

$$\sigma^2 = \frac{A^2}{\sigma_i^2} \frac{2}{\left[ .04 + .32(\sigma)^{-1/3} {}_1F_1 \left( 1/6, 1, -\frac{M^2}{2\sigma^2} \right) \right] \left[ .04 + .32(\sigma)^{-1/3} {}_1F_1 \left( 1/6, 2, \frac{M^2}{2\sigma^2} \right) \right] + 1} \quad \dots \quad (6.10a)$$

and

$$M = \frac{m_i}{\left[ \left\{ .04 + .32(\sigma)^{-1/3}, F_1 \left( 1/6, 2, -\frac{M^2}{2\sigma^2} \right) - 2 \right\} + 1 \right]^4} \quad (6.11a)$$

The plots of Eq. (6.10a) and Eq. (6.11a) are shown respectively in Fig. 9a and Fig. 9b. From these plots it is easy to find the value of  $\sigma_i^2$  and  $m_i^2$  for a particular value of  $\sigma^2$  and  $M^2$  and hence the value of the output SNR can be found out in terms of the input SNR.

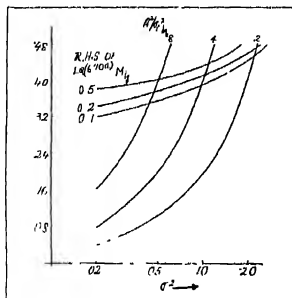


Fig. 9(a) Plots of Eq. (6.10a) and Eq. (6.11a).  
A comparison of Fig. 9(a)

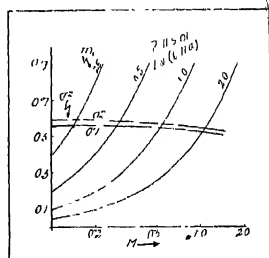


Fig. 9(b) With the plot of Fig. 9(b) yields the values of noise error and the modulation error in terms of variance of input noise and input modulation index.

The analysis of the off-tuned case is not, however, difficult. In this case one will have to take into account the steady state phase difference between the VCO and the incoming signal and it is quite logical to expect that the gain of the phase detector with respect to the signal will be smaller than the in-tuned case. Therefore the probability of loss of lock per cycle for a signal with a definite modulation index in the off-tuned case will be correspondingly larger than the in-tuned case.

Let us now consider the effect of the variation of the gain parameter 'K' with input signal to noise ratio on the system performance. From linear feedback theory it is known that the closed loop bandwidth is always larger than the open loop bandwidth. The closed loop bandwidth is again a function of the gain parameter 'K'. To understand the effect of the variation of the gain parameter on the system performance we may consider what happens if  $K$  is increased from a nominal value  $K_0$ . An increase in  $K$  results in a smaller modulation phase error and a large modulation loop bandwidth. The proportion of the noise phase output to signal phase output will now be smaller than before although the loop bandwidth has increased. This will be clear if we compare the output phase



contributions due to message and noise if their spectral densities in the bandwidth under consideration are the same. In such a case the phase contribution due to noise will be  $1/K$  that due to the message.

The reduction factor will not be as large as the ratio of the gains because the noise power accepted will now be larger because of increase of noise bandwidth. Note that in this case the closed loop bandwidth will have to be kept larger than the message bandwidth to ensure adequate tracking capability.

From the above discussion it appears that it will be possible to limit the maximum value of the input to the VCO. An alternative approach is to control the filter parameters in such a way that the closed loop bandwidth does not vary significantly with signal strength.

#### *Noise-Bandwidth and Root-mean-square Phase Error*

In this section the concepts of noise-bandwidth and root-mean-square phase error of an automatic phase control circuit will be briefly reviewed with a view to designing an optimum system. The concepts of noise bandwidth and r.m.s phase error are important in studying the performance of an automatic phase control circuit particularly when it is tracking a signal that is contaminated with uncontrolled disturbances. The performance of an automatic phase control circuit in tracking a noisy signal will be judged best when the output phase of the voltage controlled oscillator faithfully follows that input phase variations and at the same time ignores the uncontrolled disturbances as far as possible.

When the APC circuit is in lock with the input signal and is tracking a noisy signal it is reasonable, although not very accurate assumption, to consider the phase detector output to be linearly dependent on the phase difference between the signals at the input to the phase detector. This gives the linearised version of the APC circuit.

The concept of loop noise-bandwidth will enable one to have an useful information regarding the propagation of noise through an APC circuit and even to design the required form of the loop filter which will result in Wiener optimum linear system. The loop noise-bandwidth can be defined as

$$B_n = \int_0^\infty G(j\omega)^2 d\omega \quad \dots \quad (7.1)$$

where  $G(j\omega)$  is the normalised closed loop transfer function of the linearised model from the output phase to the input phase of the voltage controlled oscillator. Eq. (7.1) can also be written as

$$B_n = \frac{1}{4\pi j} \int_{-j\infty}^{j\infty} G(p) G(-p) dp \quad \dots \quad (7.2)$$

Thus  $B_n$  is the bandwidth of an ideal square cut-off low-pass filter which produces the same amount of noise power output as does the linear system with transfer function  $G(p)$ . It is to be noted that the very basis of this definition depends on the assumption that noise power spectral density at the input to the linearised model is constant over all frequencies (white noise). White noise cannot occur in practice. The more realistic approach is to consider the bandlimited white noise at the input to the linearised system and the more useful definition for the loop noise bandwidth is given

$$B_L = \frac{1}{4\pi j} \int_0^{jw_c} G(p) G(-p) dp \quad \dots (7.3)$$

where  $w_c/2\pi$  is the cut-off frequency of the input filter to the APC system. Correspondingly the r.m.s. phase error or the variance of the noise at the input to the phase detector can be defined as

$$\sigma^2 = \frac{1}{4\pi A^2} \int_{-\infty}^{\infty} \left| \frac{KFpw}{jw + KF(jw)} \right|^2 G_f(w) dw \quad \dots (7.4)$$

where the symbols have their usual significance as stated elsewhere in the text. The limits of the integration as stated earlier for the most practical case should be taken over the input bandwidth. But if the input bandwidth is large compared to the close loop bandwidth then the limits of integration can be taken from  $-\infty$  to  $+\infty$  without introducing much error to the computed value.

For purpose of comparison the expressions for the noise bandwidth of the APC circuit with the simple lag filter (see Eq. (3.10) of section 3) obtained from the Eqs. (6.2) and (6.3) are given below :

$$B_n = K/4, \quad \dots (7.5)$$

$$B_L = \frac{K}{4} \left[ \frac{1}{2\pi\sqrt{2KT-1}} \log_e \left\{ \frac{\left(\frac{w_c}{K}\right)^2 - \frac{\sqrt{4KT-1}}{KT} \left(\frac{w_c}{K}\right) + \frac{1}{KT}}{\left(\frac{w_c}{K}\right)^2 + \frac{\sqrt{4KT-1}}{KT} \left(\frac{w_c}{K}\right) + \frac{1}{KT}} \right\} \right. \\ \left. + \frac{1}{4} \tan^{-1} \left( \frac{\frac{w_c}{K} \cdot \frac{1}{KT}}{\frac{1}{KT} - \left(\frac{w_c}{K}\right)^2} \right) \right] \quad \dots (7.6)$$

From the above expression it is seen that  $B_L$  tends to  $B_n$  as  $w_c$  tends to an infinitely large value.

For the second order loop, i.e. taking the filter transfer function of the form

$$F(P) = \frac{1+xpT'}{1+(1+x)P'T'} \quad (7.7)$$

the expressions for the noise bandwidth and m.s. phase error are respectively given by

$$B_n = \frac{K}{4} \cdot \frac{[1+x(1+xKT')]}{(1+x)(1+xKT')} \quad (7.8)$$

$$\sigma^2 = \frac{\sigma_i^2}{A^2} \frac{(1+x)KT' + (1+xKT') \frac{K}{w_i} + (xKT')^2}{(1+xKT') \left[ (1+x) \frac{w_i}{K} (KT') + (1+xKT') + \frac{K}{w_i} (1+xKT') \right]} \quad (7.9)$$

The plots of  $B_n$  and  $\sigma^2$  are shown in Fig. 10.

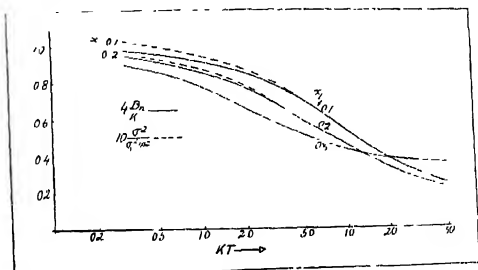


Fig. 10 Variation of the close-loop noise bandwidth and the root-mean-square phase error of an automatic phase control circuit with  $KT$

### Experimental Set-up and results

Fig. 11 shows the experimental set-up for making measurements on the response of the APC circuit to a F.M. signal and the CW signal contaminated with band-limited stationary random noise. The bandlimited noise has been obtained

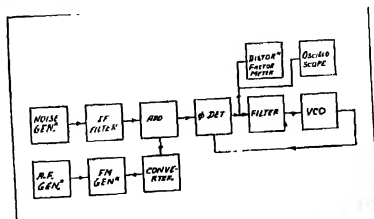


Fig. 11. Experimental set-up.

by passing white Gaussian noise through an I-F filter with the centre frequency of 500 Kc/s. Incidentally it is to be noted that the centre frequency of the IF filter must be equal to the centre frequency of the voltage controlled oscillator. The detailed circuit diagram of the APC circuit has been given in the reference (Chakrabarti, N. B. and Biswas, B. N., 1964). The input amplifier feeding the phase detector should have a flat top response. Presence of dip anywhere in the characteristics, is likely to produce spurious effect and sometimes a type of oscillations (Biswas, B. N. 1964).

Experimental results regarding the performance of the APC circuit in relation to the reception of a FM-signal with different values of input SNR are shown in Figs. 12(a) and 12(b). Fig. 12(a) shows the capability of the APC circuit in

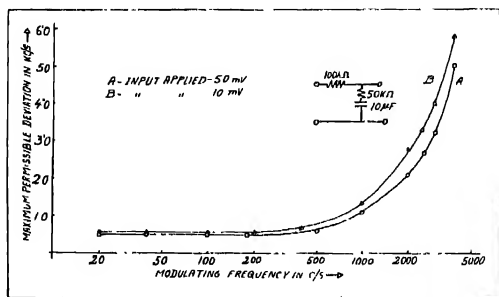


Fig.12(a) Experimental observations regarding the performance of the automatic phase con-

handling a FM signal with maximum permissible input modulation index at different values of the modulating frequency. The variation of the output noise level of the APC system with the input noise level when the system is tracking a low index FM signal contaminated with stationary random noise is shown in Fig 12(b). These experimental results are in good agreement with the results of the analysis.

## CONCLUSIONS

In this paper the response of the automatic phase control circuit to a CW signal contaminated with stationary random noise and a FM signal contaminated with random noise has been studied, and the performance of the APC circuit with respect to such signals has also been studied experimentally. It has been found that the conclusions of the analysis presented in the text give a reasonable estimate regarding the behaviour of the APC circuit with respect to signals corrupted with random noise. The response of an APC circuit preceded by a limiter to a FM signal contaminated with random noise will be taken up in a future communication,

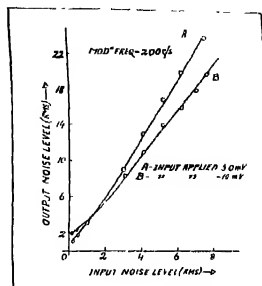


Fig.12(b) APC circuit in respect of reception of a FM signal. Fig. 12(a) shows the variation of maximum permissible value of the input modulation index with modulating frequency and Fig. 12(b) shows the variation of the output noise level with input noise level when the APC circuit is tracking a low index FM signal contaminated with stationary random noise.

#### ACKNOWLEDGMENT

The author takes the opportunity of expressing his gratitude to Prof. N. B. Chakrabarti of the Institute of Radio Physics and Electronics, Calcutta (now at the Indian Institute of Technology, Kharagpur), for suggesting the problem and supervision of the work described. The author is indebted to Prof. J. N. Bhattacharya, D.Sc., F.N.I. of the Institute of Radio Physics and Electronics, Calcutta for his kind interest and providing the author with all the research facilities. The author wishes to thank Prof. A. Mukherjee, D.Sc., of the University of Burdwan, for his kind interest and encouragement. The author also wishes to thank Mr. P. L. Dhar Bhowmick for helpful discussions. Thanks are also due to Messrs. A. N. Chakravarti, A. K. Datta and S. P. Nag for assistance in the experimental work.

#### APPENDIX

##### A.1. Derivation of the Governing of the APC Loop when the Incoming Signal is Contaminated with Stationary Random Noise.

Let us consider the APC circuit as shown in Fig. 1. The input to the system has been assumed to be of the form

$$e_i(t) = A \sin(\omega_1 t + m_1 \sin \omega t) + X(t) \sin \omega_2 t + Y(t) \cos \omega_2 t \quad \dots (A.1)$$

where symbols have their usual significance as stated elsewhere in the text. The output of the voltage controlled oscillator is assumed to be of the form:

$$e(\phi)(t) = 2 \cos(\omega_2 t + m_0 \sin \omega t + \phi(t)) \quad \dots (A.2)$$

Therefore, the output of the phase detector, which is a multiplicative device, is given by

$$\begin{aligned} e\phi(t) = & A \sin [(w_1 t + w_2)t + (m_i + m_0) \sin wt + \epsilon(t)] \\ & + A \sin [(w_1 - w_2)t + (m_i - m_0) \sin wt - \epsilon(t)] \\ & + X(t) \sin [2w_2 t + m_i \sin wt + \epsilon(t)] + Y(t) \cos [2w_2 t + m_i \sin wt + \epsilon(t)] \\ & - X(t) \sin [m_0 \sin wt + \epsilon(t)] + Y(t) \cos [m_0 \sin wt + \epsilon(t)] \quad \dots \quad (A.3) \end{aligned}$$

Since a phase detector is followed by a low pass filter one can easily neglect the high frequency term in Eq. (A.3) and can write the actual output of the phase detector as

$$\begin{aligned} l_p(t) = & A \sin [(w_1 - w_2)t + (m_i - m_0) \sin wt - \epsilon(t)] \\ & - X(t) \sin [m_0 \sin wt + \epsilon(t)] - Y(t) \cos [m_0 \sin wt + \epsilon(t)] \quad \dots \quad (A.4) \end{aligned}$$

Therefore the governing equation of the APC loop is given by

$$\frac{d\phi}{dt} = \Omega - \beta F(p)[A \sin \phi + N(t)] + \frac{d}{dt}(m_i \sin wt) \quad \dots \quad (A.5)$$

where the symbols have their usual significance as stated elsewhere.

#### REFERENCES

- Bootton, R. C. (Jr.), 1953. *Proc. Symp. on Nonlinear Circuit Analysis Polytechnique Institute of Brooklyn*, N. Y., 11.
- Biswas, B. N. 1964. *Indian J. Phys.* **38**, 561
- Chakrabarti, N. B. and Biswas, B. N. 1964. *Indian J. Phys.* **38**, 148
- Davenport, W. B. (Jr) and Root, W. L. 1958 *Random Signals and Noise*, Mc-Graw Hill Book Co., Inc., New York, N. Y.
- Graham, D. and McRuer, D. "Analysis of nonlinear control systems", John Wiley & Sons, Inc., New York.
- Gruen, W. J. 1953. *Proc. I.R.E.*, **53**,
- James, H. M., Nichols, N. B. and Philips, R. J. 1947. *Theory of Servomechanisms*, Mc-Graw Hill Book Co., Inc., New York.
- Middleton, D. "Introduction to statistical communication theory", Mc-Graw Hill Book Co., Inc., New York, N. Y.
- Rice, S. O. 1944. *Bell Syst. Tech. Jour.*, **23**, 282-332
- , 1945. *Bell Syst. Tech. Jour.*, **24**, 46-156.
- , 1948. *Bell Syst. Tech. Jour.*, **27**, 109-157.
- Schilling, D. L. 1963. *Proc. I.E.E.E.*, **51**.
- Sawaragi, Y. and Sugui, N. 1959. *Memoirs of the Faculty of Engineering*, Kyoto University, **21**, Part II
- Viterbi, A. J. 1963. *Proc. I.E.E.E.*, **51**.
- Viterbi, A. J. 1960. *Proc. Symp. on Actual Network and Feedback Systems*, Polytechnique Institute of Brooklyn, N. Y., **10**, April.

## Letters to the Editor

The Board of Editors does not hold itself responsible for opinions expressed in the letters published in this section. The notes contain in short reports of original investigations communicated to this section should not contain many figures and should not exceed 500 words in length. The contributions reaching the Secretary by the 15th of any month may be expected to appear in the issue for the next month. No proof will be sent to the author.

22

### STUDY OF LIGHT ABSORPTION IN 8-HYDROXY-1-METHYL QUINOLINIUM HYDROXIDE ANHYDRO-SALT IN STATE OF SOLUTION

S. P. TANDON\*, K. TANDON\*\* AND J. P. SAXENA\*\*

UNIVERSITY OF JOHNPUR, JOHNPUR, INDIA

(Received October 1 1966)

Though the general features of the spectrum of some of the phenol-betaines have been described (Phillips and Keown, 1951; Saxena *et al.*, 1959), no systematic study of the characteristics and assignments of their absorption bands has been reported so far. The present communication reports probable assignments for the bands of 8-hydroxy-1-methyl quinolinium hydroxide anhydro-salt, observed in the region 185-600m $\mu$  based on characteristics and influence of solvent on them.

Four bands at 18180, 26670, 34480 and 41150 cm<sup>-1</sup> were recorded with an UVISPEK spectrophotometer in the case of 8-hydroxy-1-methyl quinolinium hydroxide anhydro-salt prepared by the method described by Saxena *et al.* (1959) dissolved in chloroform

The intensity (molar extinction coefficient,  $\epsilon \sim 10^2$ , oscillator strength  $f \sim 10^{-3}$ ) coupled with blue-shift of the 18180 cm<sup>-1</sup> band  $\sim 3560$  cm<sup>-1</sup> in changing the solvent from chloroform to ethanol clearly indicates it to be due to a forbidden  $n \rightarrow \pi^*$  transition. The  $n$ -orbital is presumed to be localised predominantly near phenolic oxygen. Hence this transition diminishes electron density near the region of  $n$ -orbital. The presence of hydrogen bonds places a positive charge near oxygen atom making it more difficult to remove the electron from the non-bonding orbital. This explains the blue-shift of the band in hydrogen-bonding-solvents (Strickler and Kasha, 1964; Mookherji and Tandon, 1965).

\*\*Chemical laboratories.

\*Physical laboratories.

The band at 26670 has intensity ( $\epsilon \sim 10^3$ ;  $f \sim 10^{-2}$ ) suggesting it to be due to an allowed transition. The solvent effect is similar to the 18180  $\text{cm}^{-1}$  band. Hence the band may be assigned to an allowed  $n \rightarrow \pi^*$  transition.

The bands at 34480 and 41150  $\text{cm}^{-1}$  are intense ( $\epsilon \sim 10^4$ ;  $f \sim 10^{-1}$ ) and exhibit typical red shift in solvents of increasing polarity and having large hydrogen bonding power (McConnell, 1952). Hence they may be due to allowed  $\pi \rightarrow \pi^*$  transitions.

The study of these bands using polarized light in solid state, and technique of diffuse reflectance in powder state is in progress. An attempt is also being made to evaluate the various molecular orbitals involved.

The authors wish to thank Prof. R. C Kapoor, Head of the Chemistry Department for providing the facilities for the work

#### REFERENCES

- McConnell, H., 1952, *J. Chem. Phys.*, **20**, 700.  
Mookherji, A. and Tandon, S. P., 1965, *Indian J. Phys.*, **39** 137, 396  
Phillips, J. P. and Keown, R. W., 1951, *J. Am. Chem. Soc.*, **73**, 5483.  
Saxena, J. P., Stafford, W. H. and Stafford, W. L., 1959, *J. Chem. Soc.*, 1579  
Strickler, S. J. and Kasha, M., 1964, *Molecular Orbitals in Chemistry, Physics and Biology*, Academic Press, Inc., New York, p. 241.



# A NOTE ON THE ABNORMAL MAGNETIC BEHAVIOUR OF A TETRAHEDRAL COPPER (II) COMPOUND AT LOW TEMPERATURE

S. LAHIRY, D. GHOSH (née GUHA THAKURATA)  
AND D. MUKHOPADHYAY

DEPARTMENT OF MAGNETISM

INDIAN ASSOCIATION FOR THE CULTIVATION  
OF SCIENCE, CALCUTTA-32.

(Received November 29, 1966)

In a previous publication (Bose, Lahiry and Ghosh 1965) we derived the ligand field theory of a flattened tetrahedral copper (II) compound  $\text{Cs}_2\text{CuCl}_4$ , where the complex anion  $[\text{CuCl}_4]^{2-}$  has the symmetry  $D_{2d}$ . We now report the preliminary magnetic studies on a few more tetrahedral copper (II) compounds of the general formula  $M_2^I[\text{CuX}_4]$  (where,  $M^I = \text{Cs}$  or  $(\text{CH}_3)_4\text{N}$ ;  $\text{X} = \text{Cl}$  or  $\text{Br}$ ). The compounds  $[(\text{CH}_3)_4\text{N}]_2\text{CuCl}_4$  and  $\text{Cs}_2\text{CuBr}_4$  have been shown from X-ray analysis (Morosin and Lingafelter, 1960) to belong to the space group  $\text{Pnma}$ , and the coordination tetrahedron is flattened along one of the symmetry axis,  $S_4$ . The other compound  $[(\text{CH}_3)_4\text{N}]_2[\text{CuBr}_4]$  (Morosin and Lawson, 1964) is isomorphous with the others but its complete structural data are not yet available.

The principal crystalline anisotropies and the mean susceptibilities of these compounds have been measured by the method of Guha Thakurata *et al* (1966) and of Bose *et al* (1963) respectively, at a large number of temperatures in the range 300°K to 68°K. Assuming uniaxial symmetry the ionic anisotropies can be calculated from the relation

$$K_{\parallel} - K_{\perp} = \frac{\chi_c - \chi_a}{\gamma^2 - \alpha^2} = \frac{\chi_a - \chi_b}{\alpha^2 - \beta^2} = \frac{\chi_c - \chi_b}{\gamma^2 - \beta^2}, \quad \dots (1)$$

where  $\alpha, \beta, \gamma$  are the direction cosines of the symmetry axis ( $S_4$ ) of the complex anion with respect to the  $a, b, c$  axes of the crystal. However, the ionic anisotropy in this case can be more simply calculated using the equation  $K_{\parallel} - K_{\perp} = (\chi_c - \chi_b) + (\chi_a - \chi_b)$  since  $\beta$  has been found to be zero from X-ray results of the three compounds, so that with only two principal magnetic anisotropy measurements we can determine the value and the sign of  $(K_{\parallel} - K_{\perp})$  without recourse to the values of the direction cosines obtained from X-ray data. For example, we can determine the ionic anisotropy of the compound  $[\text{N}(\text{CH}_3)_4]_2[\text{CuBr}_4]$  whose detailed X-ray structure has not yet been reported. The values of the direction cosines calculated in this manner for the above compound at room temperature are found to

be close to those of the other isomorphous ones mentioned earlier. Further, we can determine the orientation of the ionic axes with respect to the crystallographic axes at all temperatures from the anisotropy measurements only. It may be seen that there is no direct relation of the relative magnitudes of  $K_{\parallel}$  and  $K_{\perp}$  with the elongation or flattening of the tetrahedron.

This particular compound showed some magnetic anomaly at about 238°K in sharp contrast to the others. From 300°K down to just above 238°K, with the crystal suspended in the magnetic field about "b" axis, the value of  $(\chi_c - \chi_a)$  increased from 110.6 to 161.5 units and "c" axis was along the direction of the magnetic field. At 238°K the crystal sharply rotated in the horizontal plane through 90° so that the "a" axis was then along the field and the value of the principal anisotropy i.e.  $(\chi_a - \chi_c)$ , was found to be 80 units. The setting direction did not change any further on cooling down to 68°K. The above change was very sharp and has been found to be reversible with respect to temperature. The thermal variation of the other two principal anisotropies i.e.  $(\chi_c - \chi_b)$  and  $(\chi_a - \chi_b)$  also showed some peculiarities at the same temperature 238°K, though no change in the setting direction of the corresponding suspensions along "a" axis or "c" axis was noted for either (Fig. 1). It is therefore probable that the

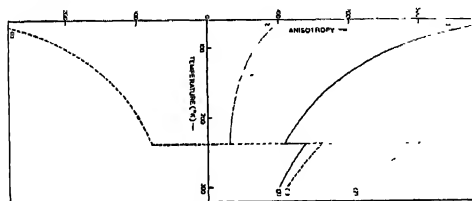


Fig. 1., Principal Crystalline Anisotropies

(1)  $(\chi_a - \chi_c) \times 10^6$ , (2)  $(\chi_b - \chi_c) \times 10^6$  (3)  $(\chi_a - \chi_b) \times 10^6$   
v. s. Temperature (°K) curves of  $[\text{N}(\text{OH}_3)_4]_2 \text{CuBr}_4$ .

sudden reversal of the principal magnetic axes in magnitude is not accompanied by a crystallographic change from orthorhombic system, unless the change over is pseudo-orthorhombic in character. Again, if the  $K_{\parallel}$  axis, i.e., the symmetry axis undergoes rotation with decreasing temperature so that the angles subtended by the  $K_{\parallel}$  axis with the crystallographic "c" and "a" axes respectively change with temperature and cross the value of  $\pi/4$  at about 238°K, then it is easy to show from eqn. (1) that the setting direction will change by  $\pi/2$ , and  $K_{\perp}$  will be greater than  $K_{\parallel}$ . But the angles, made by  $K_{\parallel}$  axis lying in  $ac$  plane with the "c" axis in the temperature range 300°K to 238°K, calculated using the experimental values of anisotropy and eqn. (1), have been found to lie between  $34^{\circ}39'$  to  $34^{\circ}6'$  thus precluding this possibility decisively. The value of the mean susceptibility of this compound was found to remain constant in the temperature region of

240°K to 230°K (Fig. 2). Although at room temperature no detailed X-ray results have been reported as yet, preliminary X-ray study at low temperature carried out in this laboratory showed a marked change in the intensity of spots which may be correlated to shifts in the co-ordinates of some heavy atoms, probably the ligand Br atoms. But we cannot say at this stage, whether the space group of the crystal, or the symmetry of the complex anion undergoes change below 238°K. We are waiting for more detailed X-ray data to elucidate the nature of this change.

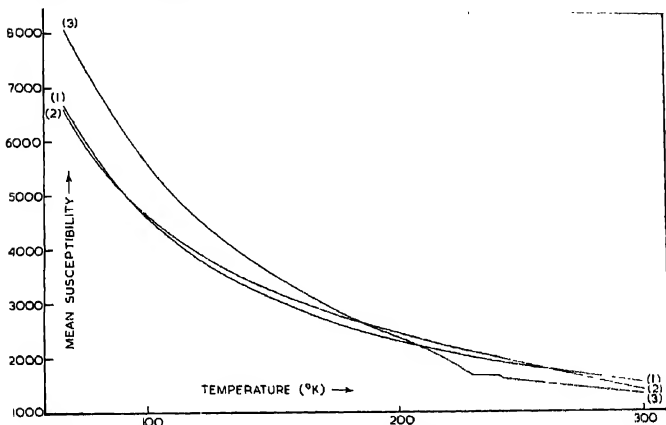


Fig 2.  $\chi_A$  Mean Gram Ionic Susceptibility  $\bar{\chi}_A \times 10^6$ , v. s Temperature (°K) of (1)  $[(CH_3)_4N]_2[CuCl_4]$ , (2)  $Cs_2CuBr_4$ , (3)  $[N(CH_3)_4]_2CuBr_4$

Measurements of anisotropy and mean magnetic moments of the compounds  $[(CH_3)_4N]_2[CuCl_4]$  and  $Cs_2CuBr_4$  did not show any abnormal magnetic behaviour with variation of temperature. However, the ionic anisotropies at 300°K as well as at 68°K for the first compound are found to be small compared to the second compound. These aspects will be discussed in details in a future paper.

Polarised crystal spectra of  $Cs_2CuBr_4$  (Karipides and Piper, 1962) at 77°K and of  $[(CH_3)_4N]_2[CuBr_4]$  in organic solvents (Furlani and Morpurgo, 1963) indicates the presence of an orbital singlet  $^2B_2$  to lie lowest and a doublet  $^2E$  separated by about 5000  $cm^{-1}$  above the singlet. Paramagnetic resonance measurements at 77°K of  $[(CH_3)_4N]_2[CuCl_4]$  in  $[ZnCl_4]^{2-}$  (Sharnoff and Reimann, 1965) give the approximately axial  $g$ -values as  $g_{||} = 2.462$ , and  $g_{\perp} = (2.078, 2.101)$ . No resonance data are yet available for the other two. We have observed resonance signals for  $[(CH_3)_4N]_2[CuBr_4]$  at low temperatures in our laboratory which will be of great help in the further analysis. A preliminary attempt to correlate magne-

tic anisotropy, mean susceptibility and  $g$ -values, where available, appears to indicate a lowest lying orbital singlet  ${}^2B_2$ , including the effects of the anisotropic orbital reduction factor and S-O reduction factors.

Full details of the theory and experimental results for these compounds will be published in due course. The authors express their gratitude to Prof. A. Bose, D.Sc., F.N.I. for helpful criticism and advice.

## REFERENCES

- Bose, A., Dutta Roy, S. K., Ghosh, P. K. and Mitra, S., 1963, *Indian J. Physics*, **37**, 505.  
Bose, A., Lahiry, S. and Ghosh U. S., 1965, *J. Phys. Chem. Solids*, **26**, 1747.  
Guha Thakurta, D. and Mukhopadhyay, D., 1966, *Indian J. Physics*, **40**, 69.  
Furlani, C., and Morpugo, G., 1963, *Theo Chem Acta*, **1**, 102.  
Karpides, A. G. and Pipor, T. S., 1962, *Inorg Chem.*, **1**, 970  
Morosin, B., and Lingafelter, E. C., 1961, *J. Phys. Chem.*, **65**, 50  
—————, 1960, *Acta, Cryst.*, **13**, 807  
Morosin, B. and Lawson, K., 1964, *J Mol Spectroscopy*, **12**, 98  
Sbarnoff, M. and Reimann, C. W., 1965, *J. Chem Phys*, **43**, 2993

# ANOMALOUS MAGNETIC BEHAVIOUR OF COPPER ACETATE MONOHYDRATE

R. N. BAGCHI AND P. SENGUPTA

MAGNETISM DEPARTMENT

INDIAN ASSOCIATION FOR THE CULTIVATION OF SCIENCE, CALCUTTA-32

(Received November 30, 1966)

Recent attempts (Mookherji *et al* 1963, Guba 1965, 1966, Mathur 1965) to explain the observed anisotropy in paramagnetic susceptibility of copper acetate monohydrate by postulating temperature dependent values of  $g$ -tensor and/or the exchange interaction co-efficient have been based on the assumption of  $C_{4v}$  symmetry. It is known from electron spin resonance spectroscopy (Bleaney *et al* 1952, Abe *et al*, 1957) the symmetry is lower and we assume  $C_{2v}$  symmetry (Kokoszka *et al* 1965) to explain the phenomenon more successfully.

The ground state for each half unit of the system can then be written as

$$|a\rangle = \mu\phi_{xz} + \nu\phi_{-y^2xz} \quad \dots (1)$$

where  $\phi_{xz} - y^2$  and  $\phi_{xz}$  are the respective  $d$ -orbitals modified by suitable combination of ligands  $s$  and  $p$  orbitals. The mixing co-efficient  $\mu$  and  $\nu$  will be functions of ligand field parameters. The other higher lying states will be

$$|c\rangle = \phi_{xy}, \quad |d\rangle = \phi_{xz}, \quad |e\rangle = \phi_{yz} \quad \dots (2)$$

and

$$|b\rangle = \nu\phi_{xz} - \mu\phi_{x^2-y^2}$$

The different valence bond configurations will be  $a_1a_2, a_1b_2, a_1b_1, a_2b_1$  etc where the subscripts '1' and '2' refer to the two centres. By operating on the ground

configuration  $a_1a_2$  with  $-Z_{eff} \left( \frac{1}{r_{1B}} + \frac{1}{r_{2A}} \right) \cdot \frac{Z_{eff}}{R} + \frac{1}{r_{12}}$  it can be shown that  $J$

will be a function of one and two electron integrals involving  $\phi_{xz} - y^2, \phi_{xz}$  and the mixing coefficients  $\mu$  and  $\nu$ . Expressing the sum of spin-orbit and magnetic perturbation in the form of spin-Hamiltonian it can be shown that the spectroscopic splitting factors and the principal ionic susceptibilities are given by

$$g_x = 2 \left\{ 1 - \frac{2(\mu\sqrt{3} + \nu)^2 R_{xz} k_{xz} \zeta_d}{E_{ad} - E_{aa}} \right\}$$

$$g_y = 2 \left\{ 1 - \frac{2(\mu\sqrt{3} - \nu)^2 R_{yz} k_{yz} \zeta_d}{E_{ac} - E_{ab}} \right\}$$

$$g_z = 2 \left\{ 1 - \frac{8\nu^2 R_{xz} k_{xz} \zeta_d}{E_{ac} - E_{aa}} \right\}$$

$$K_x = N \frac{1/D g_x^2 \beta^2 e^{-J'/kT} (1 - e^{-D/kT}) - 3\alpha_x e^{-J'/kT} (2e^{-D/kT} + 1) - 1\alpha_x}{1 + e^{-J'/kT} + 2e^{-J' + D/kT}}$$

$$K_y = N \frac{1/D g_y^2 \beta^2 e^{-J'/kT} (1 - e^{-D/kT}) - 3\alpha_y e^{-J'/kT} (2e^{-D/kT} + 1) - 1\alpha_y}{1 + e^{-J'/kT} + 2e^{-J' + D/kT}}$$

$$K_z = N \frac{\frac{g_z^2 \beta^2}{kT} e^{-J' + D/kT} - 3\alpha_z e^{-J'/kT} (1 + 2e^{-D/kT}) - 1\alpha_z}{1 + e^{-J'/kT} + 2e^{-J' + D/kT}}$$

and

$$J' = J + D_x + D_y \quad \dots (3)$$

where  $R_i$ 's and  $k_i$ 's ( $i = x, y, z$ ) are the spin-orbit and the orbital reduction factors respectively,  $\alpha$ 's denote the high frequency terms (the superscripts '1' and '3' indicate whether they originate from the singlet or the triplet levels);  $\zeta_d$  is the  $S=0$  coupling coefficient for the dimer;  $D_i$ 's are the spin Hamiltonian parameters

$$\text{and } D = D_z - \frac{D_x + D_y}{2}.$$

By adjusting the ligand field parameters, the mean susceptibility and the anisotropy data (remeasured by us) in the temperature range 90°K–300°K as also the  $g$ -values and the optical absorption bands at 11000  $\text{cm}^{-1}$  (Garddon, 1961) 14500  $\text{cm}^{-1}$  and 28000  $\text{cm}^{-1}$  (Tonnet *et al* 1964) can all be fitted within an outside limit of 2%. In doing so  $\mu$  and  $\nu$  come out to be 0.124 and 0.984 respectively. Using these values of  $\mu$  and  $\nu$  and the table of integrals calculated by Ross and Yates (1959) one obtains  $J = -138 \text{ cm}^{-1}$ .

It is concluded that :

(1) Mookherji and Mathurs' (1953) magnetic anisotropy data, which is very close to ours, can be made to correspond to the observed e.s.r. data if the effect of orbital reduction is considered in the high frequency term.

(2)  $J$ , calculated theoretically is of the right order of magnitude and sign, considering the rather severe approximations namely, that the integrals involving only the  $d$ -orbitals have been considered through the ligand orbitals may contribute appreciably to  $J$ , that the integrals involving products of  $d_{x^2-y^2}$  and  $d_{z^2}$  have not been considered and that the effect of superoxoexchange interaction, transmitted through the  $\pi$  orbitals of the carbon atoms have not been taken in to account.

(3) The larger value of  $J$  in copper thioacetate is due to the additional orthorhombicity introduced due to the replacement of two of the four oxygen ligands in each half unit by sulphur atoms.

(4) The bonding is neither a pure  $\sigma$ -type or  $\delta$ -type but a mixture of the two.

(5) The band at  $28000\text{ cm}^{-1}$  is of Laporte forbidden type arising from  $^3ab_u \rightarrow ^3aa_u$  and  $^1ab_g \rightarrow ^1aa_g$  transitions (both the levels Span A, representation). The large separation may be attributed to a strongly anisotropic ligand field.

The details will be communicated within a very short period.

## ACKNOWLEDGMENT

The authors are grateful to Prof. A. Bose, D.Sc., F.N.I Dept. of Magnetism, I.A.C.S. for the suggestion and supervision of the work. They are also indebted to Dr. M. Chowdhury, Professor of Chemistry, Presidency College, Calcutta, for many helpful discussions and convey their thanks to their colleague Sri Soumen Mitra, M.Sc., for his co-operation.

## REFERENCES

- Abe H. and Shimada J., 1957, *Nat. Sci. Rep. Okhamonzu Univ.*, **8**, 80  
 Bleaney B. and Bowers K. D., 1952, *Proc. Roy. Soc.* **121A**, 151  
 Figgis B. N. and Martin R. L., 1956, *J. Chem. Soc.* 3837  
 Givelson D. P., 1961, *J. Inorg. Nucl. Chem.*, **17**, 222  
 Guha, B. C., 1951, *Proc. Roy. Soc.* **A206**, 353  
 ———, 1965, *Phil. Mag.* **11**, 175.  
 ———, 1966, *Phil. Mag.* **13**, 619  
 Kokoska, G. F., Allen R. H. C., 1965, *J. Chem. Phys.* **42**, 3693  
 Mookherji A. and Mathur S. Je., 1963, *J. Phys. Soc. Japan*, **18**, 977  
 Mathur S. C., 1965, *Phil. Mag.* **12**, 43  
 Nyholm R. S., 1961, *Proc. Chem. Soc.* 273.  
 Ross I. G. and Yates J., 1959, *Trans. Farad. Soc.* **55**, 1061  
 Tonnet M. L., Tamda S. and Ross I. G., 1964, *Trans. Farad. Soc.* **60**, 810.

# ***r*-CENTROIDS AND FRANCK-CONDON FACTORS FOR THE BANDS OF $A^2\Sigma-X^2\pi$ SYSTEM OF PO MOLECULE**

**S. SANKARANARAYANAN**

DEPARTMENT OF PHYSICS,

INDIAN INSTITUTE OF SCIENCE, BANGALORE 12.

PRESENT ADDRESS P.S.G. COLLEGE OF TECHNOLOGY, COIMBATORE)

(Received June 10, 1966)

In continuation with the work of the author (1963, 1963a) on the *r*. centroids and F C. factors of  $A^1\pi-X^1\Sigma$  system of PN molecule, a study of the  $A^2\Sigma-X^2\pi$  system of PO molecule was taken up. The molecular constants needed for the calculation are taken from the work of Suryanarayana Rao (1958). Both the  $^2\Sigma$  and  $^2\pi$  states were found to obey very closely the Morse potential by calculating the  $\alpha_e$  values from Pekoris relation (1934) and by comparing them with the experimental values.

*r*-centroids. The *r*-centroids were evaluated by the graphical and quadratic equation methods outlined by Nicholls and Jarman (1956). These results are

TABLE I

*r*. centroids (*A*) and wavelengths (*A*) of the bands of ( $A^2\Sigma-X^2\pi$ )  
system of PO

0	1.455 1.455 2477.9	1.401 1.400 2555.05	1.347 1.346 2636.3	1.290 1.290 2721.5		
1	1.517 1.518 2396.3	1.462 1.462 2468.3	1.408 1.407 2543.94	1.356 1.353 2623.42	1.300 1.297 2706.81	
2	1.583 1.584 2320.6	1.524 1.525 2387.94	1.469 1.469 2458.96	1.416 1.414 2533.00	1.364 1.360 2616.7	1.309 1.304 2692.4
3		1.589 1.592 2313.7	1.530 1.533 2379.9			
4			1.596 1.600 2306.9			
5				1.603 1.608 2300.4		



entered in Table I along with the wavelengths of  $P_1$  heads taken from the work of Ghosh and Ball (1931).

First row  $= \bar{r}_{v',v''}$  by graphical method

Second row  $= \bar{r}_{v',v''}$  by quadratic equation method

Third row  $= \lambda_{v',v''}$  wavelengths of the  $P_1$  band heads.

These Morse constants employed in these calculations are

$$\alpha_1 = 2.0915A^{-1}, \quad \alpha_2 = 2.0277A^{-1} \text{ and } \alpha = 2.0596A^{-1}.$$

The quadratic equation method involves the replacement of  $\alpha_1$  and  $\alpha_2$  by a mean  $\alpha$  and an equivalent adjustment of all  $\alpha$ -dependent parameters. The  $r$ -centroids obtained by both the methods compare very favourably for this molecule and are, in fact, identical for the (0, 0) sequence. Slight departures observed in off-diagonal sequences are due to the approximations involved in the quadratic equation method. However, as the maximum deviation is of the order of 0.4% only, the method of  $\alpha$ -averaging of the Morse potential functions is valid for this band system of PO.

*Franck Condon factors.* Further, as  $\left| \frac{d\alpha}{\alpha} \right| = 3.1\%$ , the Franck Condon factors defined by the equation  $q_{v',v''} = \left| \int \psi_{v'} \psi_{v''} dr \right|^2$  were determined by the analytical method of Fraser and Jarman (1953), using the computation technique described by the author (1963a). The Franck Condon factors, thus calculated are given in Table II along with those values in parenthesis as calculated by Bates's method (1952)

TABLE II  
Franck Condon factors

$v' \backslash v''$	0	1	2	3	4
0	.696 (.695)	.244 (.240)	.050 (.049)	.007 (.008)	.003 ..
1	.258 (.255)	.280 (.282)	.318 (.307)	.108 .	..
2	.041 (.042)	.353 (.350)	.185 ..	.235 ..	.027 ..
3	.004 (.004)	.094 ..	..	..	..
4	.000 ..	..	..	..	..

In a plot of  $\bar{r}_{v',v''}$  against  $\lambda_{v',v''}$  all the points are found to lie on a smooth curve and  $\bar{r}_{v',v''}$  decreases with  $\lambda_{v',v''}$ . This is in good agreement with what one should expect for a case where  $r_{e1} < r_{e2}$ . Also  $\bar{r}_{00}$  is only slightly greater than the mean of  $r_{e1}$  and  $r_{e2}$  and the potentials are not very unharmonic as can also be

seen from the magnitudes of the vibrational constants. Table II explains the absence of (0, 4) and (3, 0) bands in the spectrum of this band system.

The author's thanks are due to Prof. R. S. Krishnan and Dr. P. S. Narayanan for their guidance and constant encouragement during this investigation. He also wishes to thank the University Grants Commission for financial assistance and Principal G. R. Damodaran, P.S.G. College of Technology, Coimbatore, for his interest in this work.

#### REFERENCES

- Bates, D. R., 1952, *Mon. Not. Roy. Astr. Soc.* **112**, 614.  
Fraser, P. A. and Jarman W. R., 1953, *Proc. Phys. Soc. Lond.* **66A**, 1145.  
Ghosh, P. N. und Bull G. N., 1931, *Zeit. f. Phys.* **71**, 362.  
Nicholls, R. W. and Jarman, W. R., 1956, *Proc. Phys. Soc. Lond.* **69A**, 253.  
Pekeris, C. L. 1934, *Phys. Rev.* **45**, 98.  
Sankaranarayanan, S. 1963, *Indian, J. Phys.* **37**, 486.  
———, 1963a *Physica*, **29**, 1403.  
Suryanarayana Rao, K. 1958, *Canad. Jour. Phys.* **36**, 1526.

# PRELIMINARY CRYSTAL STRUCTURE DATA OF SOME AMINO ACIDS DERIVATIVES AND METAL COMPLEXES

N. N. SAHA, S. K. MAJUMDAR, S. C. BHATTACHARYA, P. N. ROY,  
R. HANDA AND S. GUHA

MOLECULAR BIOLOGY AND CRYSTALLOGRAPHY DIVISION  
SAHA INSTITUTE OF NUCLEAR PHYSICS  
CALCUTTA UNIVERSITY

(Received October 11, 1966)

The determination of crystal structure by X-ray diffraction methods of the derivatives and metal complexes of amino acids, peptides and of other compounds of biological interest forms a major part of our research programme on the study of the structures and functions of biological molecules by various physico-chemical methods. In this project, we have already undertaken the structure determination of sarcosine hydrochloride, sarcosine hydrobromide, glycocyamine hydrochloride, glycocyamine hydrobromide, ornithine hydrochloride, copper-lysine and calcium EDTA and the present communication reports some of our preliminary structural data, e.g. unit cell dimensions, space groups etc. It may be noted that the structure of sarcosine hydrochloride has already been solved in our laboratory and reported in the Sixth International Congress on Crystallography held in Moscow in July, 1966. The structures of the rest of the above mentioned crystals are at different stages of progress.

Rotation and Weissenberg photographs of these crystals were taken using  $\text{CuK}\alpha$  radiation. Density measurements were made by the method of floatation using a mixture of bromoform and benzene. Morphological studies were made by two-circle goniometer.

## *Sarcosine hydrochloride ( $\text{C}_3\text{H}_7\text{O}_2\text{N} \cdot \text{HCl}$ )*

Single crystals of this compound were obtained by allowing the solution of sarcosine in 40% hydrochloric acid to evaporate slowly at room temperature. The crystals thus obtained were needle shaped, transparent and hygroscopic. For taking X-ray photographs the crystals were sealed in special glass capillaries of 1.5 mm. diameter and 0.02 mm wall thickness. The crystals belong to the monoclinic system and the space group is  $\text{P}2_1$ . Work on the three dimensional refinement of the structure of this crystal is in progress.

## *Sarcosine hydrobromide ( $\text{C}_3\text{H}_7\text{O}_2\text{N} \cdot \text{HBr}$ )*

Single crystals of this compound were prepared in the same manner as sarcosine HCl. In this case also the crystals were found to be transparent, needle shaped and highly hygroscopic. The crystals belong to monoclinic system with space group  $P2_1/c$ .

*Glycocycamine hydrochloride* ( $C_8H_7O_2N_3.HCl$ )

Single crystals were grown from a solution of glycocycamine in 40% hydrochloric acid by the method of slow evaporation at room temperature. Needle shaped, translucent crystals were obtained which belonged to tetragonal system. The space group is either  $I4_2d$  or  $I4_1md$ .

*Glycocycamine hydrobromide* ( $C_8H_7O_2N_3.HBr$ )

Though the method used for growing the crystals was similar to that of glycocycamine HCl, two types of crystals were obtained.

Type I is isomorphous with glycocycamine hydrochloride, i.e. tetragonal with space group  $I4_2d$  or  $I4_1md$ . Most of these crystals were found to be twins.

Type II crystals belong to monoclinic system and the space group is  $P2_1/c$ . Both types are unstable when exposed to air. As before, the crystals were mounted inside sealed glass capillaries for taking X-ray photographs.

*Ornithine hydrochloride* ( $C_6H_{12}O_2N_2.HCl$ )

On evaporating a solution of ornithine hydrochloride in water at room temperature, transparent and needle shaped single crystals were obtained. The crystals belong to the monoclinic system and the space group is  $P2_1$ .

Our grateful thanks are due to Messrs Koehlight Laboratories Ltd., England for making us a free gift of 5 gms of extra pure ornithine hydrochloride for our work.

*Copper lysine Cu* ( $C_6H_{14}O_2N_2$ )<sub>2</sub>  $Cl_2.2H_2O$

The compound was prepared by refluxing a mixture of lysine hydrochloride and cupric carbonate taken in stoichiometric proportions. The crystals were obtained by evaporating a solution of the compound in alcohol and water (50 : 50). The crystals thus obtained were blue and needle shaped. They belong to monoclinic system with space group  $P2_1$ .

*Calcium EDTA* ( $CaC_{10}H_{12}O_8N_2.nH_2O$ )

Calcium—EDTA was prepared by adding ethyl alcohol to a solution containing calcium carbonate and ethylene-diamine-tetra-acetate (EDTA) in equivalent molar proportions. Crystals were grown by slow evaporation of aqueous solution of Ca-EDTA. They were plate shaped and colourless. The crystals belong to triclinic system with space group  $P\bar{1}$ . Values of  $\alpha$ ,  $\beta$  and  $\gamma$  were obtained from zero layer Weissenberg photographs taken about [100], [010] and [001] axes respectively. The positive directions of  $a$ ,  $b$  and  $c$  were chosen according to  $a < b < c$ .

The results are given in tabular form in Table I, which contains the space group, dimensions of the unit cell, number of molecules per unit cell and the morphology of the crystals.

TABLE I

Unit cell dimensions and space group

Compound	Space group	a(Å)	b(Å)	c(Å)	$\alpha$	$\beta$	$\gamma$	Number of Mol. (%)	Morphology-Needle axis along [hkl]
Sarcosine Hydrochloride	P2 <sub>1</sub>	9.00	5.93	5.11	90	96°	90°	2	[010]
Glycocyamine Hydrochloride	I4 <sub>2</sub> d or I4 <sub>2</sub> md	15.70	15.70	11.03	90	90°	90	16	[001]
Glycocyamine Hydrobromide	P2 <sub>1</sub> /c	5.53	13.52	9.24	90°	92°	90°	4	[100]
Ornithine Hydrochloride	P2 <sub>1</sub>	4.99	8.01	10.16	90°	96°33'	90	2	[100]
Cu-lysine	P2 <sub>1</sub>	11.48	16.83	5.21	90°	93°36'	90°	2	[001]
Cu—EDTA	P1	9.88	11.14	13.37	131°58'	114°13'	77°2'	2	[100]

# MAGNETIC PROPERTIES OF $\alpha$ -SILICON CARBIDE CRYSTALS

D. DAS

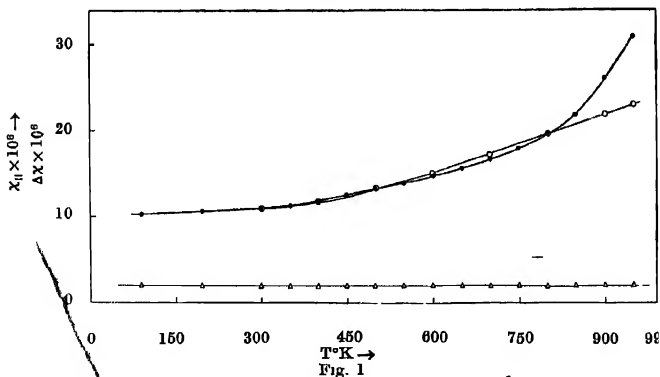
DEPARTMENT OF MAGNETISM

INDIAN ASSOCIATION FOR THE CULTIVATION OF SCIENCE

CALCUTTA-32, INDIA

(Received November 28, 1966)

Silicon carbide is obtained in different polymorphous modifications showing different body colours owing to different impurity contents. Commercial variety of silicon carbide crystals were obtained from Switzerland through the kindness of Prof. G. Busch of E.T.H. Zurich. It has been found that some of the samples are diamagnetic and two varieties are feebly ferromagnetic. For ferromagnetic varieties only magnetic susceptibility of the paramagnetic part has been determined at room temperature. The magnetic susceptibility and anisotropy of all the diamagnetic varieties have been measured at room temperature. Only two varieties of these have been measured from 90°K to about 1000°K. It has been found that the principle susceptibilities for these two samples increase with temperature whereas the anisotropy remains practically the same. The temperature variation of susceptibility upto a certain temperature has been explained with the relation  $\chi = D(kT)^{\alpha} e^{-\frac{\Delta E}{2kT}}$  with  $\alpha = -1/4$ . The room temperature



Temperature variation of susceptibility ( $\chi_{||}$ ) and anisotropy ( $\Delta\chi$ ) of sample — A

● Experimental values of  $\chi_{||} \times 10^5$

○ Theoretically calculated values of  $\chi_{||} \times 10^5$

△ Anisotropy ( $\chi_{||} - \chi_{\perp}$ )  $\times 10^5$

TABLE I

Sample	Colour of the sample	Crystal class of the sample	Orientation of the c-axis w.r. to the field	$\Delta\chi \times 10^6$ per gm.mol.	$\chi_{  } \times 10^6$ per gm.mol.	Anisotropy per cent
A	Pale green transparent	Hexagonal 6H $a = 3.073 \text{ \AA}$ $c = 15.08 \text{ \AA}$	C-axis $\parallel$ to field	0.91621	-10.618	8.1%
F	Light green transparent	Hexagonal 6H $a = 3.073 \text{ \AA}$ $c = 15.08 \text{ \AA}$	C-axis $\parallel$ to field	0.93111	-12.550	7.6%
I	Deep blue transparent	Hexagonal 6H $a = 3.073 \text{ \AA}$ $c = 15.08 \text{ \AA}$	C-axis $\parallel$ to field	0.87140	-10.376	7.9%
C	Black opaque	Hexagonal 6H $a = 3.073 \text{ \AA}$ $c = 15.08 \text{ \AA}$	C-axis $\parallel$ to field	0.90312	-7.331	11.3%
H	Deep green transparent	Hexagonal 6H mixed with Rhombohedral 15R	C-axis $\parallel$ to field	0.7780	-7.321	9.0%
E	Light green transparent	Rhombohedral 21R $a = 3.073 \text{ \AA}$ $c = 52.78 \text{ \AA}$	C-axis $\parallel$ to field	0.93031	-5.739	14.6%
B	Black opaque	Rhombohedral mixture of 15R and 21R	C-axis $\parallel$ to field	0.82279	-4.200	17.3%
D	Yellowish green transparent	Rhombohedral 15R $a = 3.073 \text{ \AA}$ $c = 37.70 \text{ \AA}$	C-axis $\perp$ to field	—	$\chi_{\perp} = 123.744$	—
G	Deep blue transparent	Hexagonal 6H $a = 3.073 \text{ \AA}$ $c = 15.08 \text{ \AA}$	C-axis $\perp$ to field	—	$\chi_{\perp} = 20.035$	—
Sigamony's green Sample				$\Delta\chi$ per gm mol = $0.82 \times 10^{-6}$	mol = $13.1 \times 10^{-3}$	n 40/

values of all the measurements are shown in Table I and temperature variation of two varieties are shown graphically in fig 1 and 2. The values of field independent average susceptibility and anisotropy as found by Sigamony (1944) are also given in Table I.

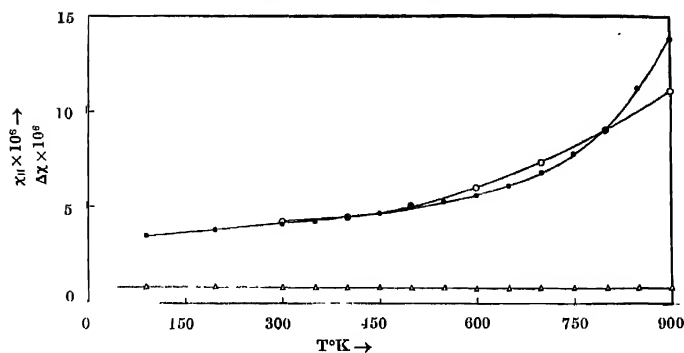


Fig. 2

Temperature variation of susceptibility ( $\chi_{||}$ ) and anisotropy ( $\Delta\chi$ ) of sample -B

- Experimental values of  $\chi_{||} \times 10^6$
- Theoretically calculated values of  $\chi_{||} \times 10^6$
- △ Anisotropy ( $\chi_{||} - \chi_{\perp}$ )  $\times 10^6$

The details of these investigations are in course of publication.

The author wishes to express her sincere thanks to Shri A. K. Dutta for suggesting the problem and guidance throughout the course of the work and to Prof. A Bose, for his kind interest in this work.

#### REFERENCE

Sigamony, A., 1944, *Proc. Indian Acad. Science* **19A**, 377-80.



## BOOK REVIEW

ADVANCES IN UPPER ATMOSPHERE RESEARCH : Edited By B. Landmark and Published by Pergamon Press, on behalf of Agard Price, 80s. net.

The volume consists of nearly twenty papers presented at the NATO Advanced Study Institute at Corfu in July 1960. The subject matter presented covers a sufficiently wide range of topics, such as, the theory of magnetic storms, the geophysical effects of high altitude nuclear detonations, electromagnetic waves in plasma, ionospheric studies, whistler propagation etc. The entire volume is somewhat loosely divided into eight sections, each section dealing with a selected topic. Each section is followed by a summary of discussions on the relevant topic by the participants. Thus in the first section we find two articles by Sydney Chapman on the theory of magnetic storms in the form of an introduction to the subject. The next section contains three papers by Newman, Dyer and Thomas and Taylor on the effect of high altitude nuclear detonations on a number of geophysical phenomena as studied both by the ground-based and satellite techniques. The third section contains only a single paper by A. P. Mitra in which he surveys the various loss-processes which contribute to the effective recombination coefficient in the ionosphere. In the next section we find two purely theoretical papers by Suchi and Napolitan on the electromagnetic wave interactions in plasma. This section also contains a paper by Vassy on the phenomenon of light emission in the atmosphere. The paper gives useful information regarding the nature of emitting particles, their distribution etc.,. The fifth section contains three papers on the  $F$ -region of the ionosphere. The one by Rawer gives an exhaustive account of the  $F_2$ -layer ionization distributions and presents a lot of useful experimental data. Fejer gives a review of the different theories of the  $F$ -layer formation, and there is a small note by Bibl dealing with the fluctuations of ionization in the  $F_2$ -layer. Storey's lone paper on whistler propagation constitutes the next section and is introductory in nature. In the seventh section are included three papers on scatter-problem. Hagfors and Landmark in their paper show how the theory of diffraction from random screens can be used to assess the relative importance of scattering from the irregularities caused by turbulence and that from meteor tails. They also conclude that the continuous signal component is always caused by turbulent scattering. Fejer gives a brief account of "incoherent scattering" as a technique in ionospheric studies. Kavadas deals with auroral back scattering.

The last section contains four papers which deal with solar activity and ionospheric absorption measurements with riometer. Xanthakis shows analytically that the maximum of solar activity as a function of time of rise obeys a parabolic law. Anastassiadis, Ilias and Coroumbalos report some systematic measurements of ionospheric absorption obtained by riometer studies. They also find a high

correlation between solar activity and cosmic noise on 27.6 and 58 Mc/s. Reid's paper concern with polar cap absorption. Hultquist's paper discusses the relation between the riometer measurements and the absorption cross-section of electrons, electron density profile etc.

On the whole, the collection is a mixed fare, some being purely theoretical in nature, some experimental, some reviews and a few in the form of introduction. Perhaps the main distinguishing feature of this volume is that it contains papers dealing with quite advanced researches along with the papers which are somewhat introductory in nature. Thus the volume serves the double purpose of introducing certain topics to young reserchers and of catering to the needs of advanced research students. The presentation and the get up are in a line with the high standards set-up by the Pergamon Press.

*S. R. Khastgir*